SPONSORED BY

Home
Foreword
Conference Sessions
GRI-22

Geosynthetics 2009

We are pleased to present the electronic proceedings of Geosynthetics 2009.

The Geosynthetics 2009 plenary and technical program programs included more than 75 papers assigned to 24 sessions over the three-day conference period.

Geosynthetics 2009 also featured a sold out trade show and impressive participation from our very generous sponsors. We wish to thank them for their generous financial contributions that helped make this show possible. Please be sure to visit their websites by clicking on the logos to the left.

Disclaimer: The opinions expressed and the data provided during Geosynthetics 2009 and the published Proceedings are those of the author(s) and/or presenter(s) and do not necessarily represent the opinions of the Industrial Fabrics Association International (IFAI) or any of its subsidiaries or divisions. Papers contained in these proceedings are the original work of each author. For permission to reprint any paper or presentation materials in these proceedings, please contact the authors directly or the IFAI Bookstore Manager, 1801 County Road B West, Roseville, MN 55113-4061 USA.

Managed by

IFAI | INDUSTRIAL FABRICS Association International

under the auspices of

IGS International Geosynthetics Society

with the support of

GMA nagS GRI GEI GII GSI GAI GCI

CD-ROM produced by X-CD Technologies Inc.

Foreword to Technical Paper Sessions

The technical papers that appear in this CD are the result of a process that commenced with a call for Abstracts in early 2008. The response to the call resulted in over 120 abstracts submitted. The vetting of the abstracts were performed by the Technical Program Committee, with each abstract being reviewed by recognized experts within each abstract's specific subject matter or technology. This vetting process produced 78 papers accepted for the conference.

The papers accepted for presentation at this conference, in general, represent the following:

- For the abstract review, over 100 total hours of review time by the 22 members of the Technical Program Committee.
- Hundreds to several thousands of hours of research for "each" of the 78 papers.
- Many days of writing by each of the 176 authors and co-authors.
- Peer review of each paper by 2 to 3 experts in the specific subject matter or technology, by over 50 experts in the geosynthetic field, representing hundreds of hours of review time.
- Technical knowledge transfer in geosynthetic advancement through the latest pertinent research and/or by leaders of the field with decades of experience.
- All abstracts/papers were peer reviewed under strict criteria set Conference Organizing Committee.

The submission and acceptance of high quality papers for the Geosynthetics 2009 Conference could not occur without the hard work and dedication of the authors and members of the Technical Program Committee. These papers provide a state-of-the-practice in geosynthetics engineering from 14 countries.

I would like to take this opportunity to thank all the members of the Technical Program Committee for their very hard work. Without their effort, this conference Technical Program would not have been possible.

I would also like to acknowledge the team at IFAI headed by Beth Wistrcill who managed the logistics of the conference leaving the technical committee free to focus on the technical paper program. My main contact, and the person who performed an enormous amount of work communicating with the authors and committee members, and keeping me organized, was Barbara Connett. The success of this Technical Program would not be possible without Barbara's extraordinary effort, which is worthy of all of our unending gratitude.

Robert E. Mackey, P.E., BCEE
Chairman, Technical Program Committee

Technical Program Committee Members

Chairman
Robert Mackey, S2L Incorporated

General Members

John Allen, TRI Environmental Inc
Daniel Alzamora, Federal Highway Administration
Ryan Berg, Ryan Berg & Associates, Inc.
Sergio Botero, Syn-Tex
Stan Boyle, Shannon & Wilson, Inc.
Barry Christopher, Consultant
Jim Collin, The COLLIN GROUP LTD
Douglas Gaffney, P.E., Ocean and Coastal Consultants
Gary Kolbasuk, Raven Industries EFD
Craig Lake, Dalhousie University
Robert Lozano, Linear Composites Limited
Michael Mathioudakis Ph.D., PE, New York State DOT
Henry Mock, Golder Associates Inc.
Jim Olsta, CETCO
Ian Peggs, I-Corp
Nicholas Reck, The Tensar Corporation
Kerry Rowe, Queens University
Mark Sieracke, Weaver Boos Consultants
Joel Sprague, TRI Environmental
David Suits, North American Geosynthetics Society
John Workman, Waste Management, Inc.

Managed by IFAI INDUSTRIAL FABRICS Association International

under the auspices of IGS International Geosynthetics Society

with the support of GMA nagS GRI GSI GII GAI GCI

CD-ROM produced by X-CD Technologies Inc.

Conference Sessions

Wednesday, February 25

Long - Term Performance of Landfill Barriers Systems

Water Containment

Drainage

Longevity of Geosynthetics

Floating Covers

Soil Reinforcement - Fabric 1

Soil Reinforcement - Fabric 2

Landfill Applications 1

Landfill Applications 2

Soil Reinforcement - Geogrids 1

Soil Reinforcement - Geogrids 2

Thursday, February 26

Geosynthetic Barriers 1

Geosynthetic Barriers 2

Geotextile Tubes 1

Geotextile Tubes 2

Geotextile Tubes 3

Laboratory Testing 1

Laboratory Testing 2

Laboratory Testing 3

Geogrid Case Histories

Slope / Wall Reinforcements

Erosion Control

Friday, February 27

GRI-22 "It's All in the Details"

Managed by

under the auspices of

with the support of

CD-ROM produced by X-CD Technologies Inc.

GRI-22 "It's All in the Details"

Date: Friday, February 27

Papers

It's in the Details; Specification Issues
P.E. Oliveira

Managed by

under the auspices of

with the support of

CD-ROM produced by X-CD Technologies Inc.

Long - Term Performance of Landfill Barriers Systems

Date: Wednesday, February 25

Papers

Prototype Modeling of GCL Hydration and Shrinkage under Simulated Field Conditions
M.H.T Rayhani , R.K. Rowe, W.A. Take, R.W.I. Brachman, G. Siemens

GCL Shrinkage and the Potential Benefits of Heat-Tacked GCL Seams
R.K. Rowe , L. Bostwick, R. Thiel

Development of X-ray Imaging Techniques to Investigate the Internal Shrinkage Mechanism of GCLs
W.A. Take , R.K. Rowe, H. Munro, A. Kerr, J. Schreiner

Transport of VOCs through a co-extruded Geomembrane with a Nylon Barrier
R.S. McWatters , R.K. Rowe

Managed by IFAI INDUSTRIAL FABRICS Association International
under the auspices of IGS International Geosynthetics Society
with the support of GMA nagS GRI GSI GII GAI GCI

CD-ROM produced by X-CD Technologies Inc.

Water Containment

Date: Wednesday, February 25

Papers

Produced Water Evaporation Ponds
N. Nowak , J. Bradish

Lining of Canals with Flexible HDPE Geomembrane - Successful Case History
M. Venkatraman , S Murugesan

Geomembranes for Canal Lining
T.D. Stark , J.M. Hynes

Challenges and Solutions During the Re-lining of a Concrete Covered Water Reservoir
B.W. Fraser , M.P. Neal

Managed by IFAI | INDUSTRIAL FABRICS Association International

under the auspices of IGS International Geosynthetics Society

with the support of GMA nagS GRI GEI GSI GII GAI GCI

CD-ROM produced by X-CD Technologies Inc.

Drainage

Date: Wednesday, February 25

Papers

Innovative use of a Geocomposite Drainage System in a Clay-Lined Agricultural Waste Storage Pond
B.C. Doerge

Long Term Performance Requirements for HDPE Drainboards
M. Jablonka , E. Blond

Behavior of 'Draintube' Drainage Geocomposites Under High Compression Load
P. Saunier , E. Blond

Evaluation of Perforated Geosynthetic Box to be considered Water Permeability in Waste Landfill Slope
H.Y. Jeon , J.P. Gourc

Managed by IFAI INDUSTRIAL FABRICS Association International
under the auspices of IGS International Geosynthetics Society
with the support of GMA nagS GRI GSI GII GEI GAI GCI

CD-ROM produced by X-CD Technologies Inc.

Longevity of Geosynthetics

Date: Wednesday, February 25

Papers

A Review of the Environmental Factors Influencing the Durability of Polyolefins
M. Koryabina , F. Ceccarani, M. Balow, T. Paff, B. Kozlowski

Long-Term Weathering Stability and Warranty Implications for Thin Film Geomembranes
A. Mills , D. Martin, R. Sati

Hydrolysis Testing of High Tenacity Poly(ethylene terephthalate) - Results from 15 years of Exposure
K.L. Nait-Ali , R.W. Thomas, P.L. Anderson, N. Freitag

Carbon Black and Antioxidant Effect in High Density Polyethylene
W-K. Wong , Y.G. Hsuan

Managed by IFAI INDUSTRIAL FABRICS Association International
under the auspices of IGS International Geosynthetics Society
with the support of GMA nagS GRI GSI GDI GII GAI GCI

CD-ROM produced by X-CD Technologies Inc.

Floating Covers

Date: Wednesday, February 25

Papers

Planning Design and Installation of a Design/Build Gas Collecting Floating Cover System for Excel Meat Solutions
A.A. Harvey

Floating Cover Design & Technology over the past 30 Years
B. Shehane

Geomembrane Cover Systems for Liquids, Quasi-Solids and Gas - An Application Based Comparative
R. K. Frobel , M.A. Sadlier

Managed by IFAI | INDUSTRIAL FABRICS Association International
under the auspices of IGS
with the support of GMA nags GRI GSI GII GAI GCI

CD-ROM produced by X-CD Technologies Inc.

Soil Reinforcement - Fabric 1

Date: Wednesday, February 25

Papers

Raising Cleveland CDF 12 Using Geosynthetic Reinforcement
J.E. Kolber , V.C. Melilli, J.R. Lane, E.N. Lenhardt

Geotextiles in Dams - Forging Federal Guidelines
D.A. Crum

Field Construction and Trafficking of an Unsurfaced Geosynthetic-Stabilized Road
E.V. Cuelho , S.W. Perkins, J. Hauck, M.R. Akin, K. von Maubeuge

"Green" Reinforced Soil Walls Using Geosynthetics: An Alternative For Ecological And Environmental Projects
M.P. Guerra Escobar

Managed by IFAI INDUSTRIAL FABRICS Association International
under the auspices of IGS International Geosynthetics Society
with the support of GMA nagS GRI GSI GII GAI GCI

CD-ROM produced by X-CD Technologies Inc.

Soil Reinforcement - Fabric 2

Date: Wednesday, February 25

Papers

History, Performance and Design of Geotextiles in Levees
M.L. Woodward , J.L. Dendurent

Pore Water Pressure Influence on Geosynthetic Stabilized Subgrade Performance
B.R. Christopher , S.W. Perkins, B.A. Lacina, W.A. Marr

Examination of the Benefits of Enhancing Chip Seal Surface Treatments with Paving Fabric Interlayers
J.L. Dendurent

Stability Analysis of Reinforced Embankments in New Orleans
N.T. Schwanz , N.D. Vroman, R.E. Wahl, M.P. Navin, R.B. Pinner, R.J. Varuso, D.E. Yule

Managed by IFAI INDUSTRIAL FABRICS Association International
under the auspices of IGS International Geosynthetics Society
with the support of GMA nagS GRI GSI GDI GII GAI GCI

CD-ROM produced by X-CD Technologies Inc.

Landfill Applications 1

Date: Wednesday, February 25

Papers

Post-Construction Landfill Liner Failure and Lessons Learned
R. Thiel

Biogas Leakage through Landfill Cap Covers
C. Barral , H. Nunes Pitanga, P. Pierson, I. Djeran-Maigre, O. Monje Vilar, J-P. Gourc

Alternative Lining System Anchorage Using Batten Strips
J.A. McKelvey, III

Innovative Design and Construction of a Landfill Cap: A Case Study of the City of Ottawa's Trail Road Landfill
M.H. Simpson , P.A.S. Benson, D.P. Upton

Managed by IFAI INDUSTRIAL FABRICS Association International
under the auspices of IGS International Geosynthetics Society
with the support of GMA nagS GRI GSI GII GDI GAI GCI

CD-ROM produced by X-CD Technologies Inc.

Landfill Applications 2

Date: Wednesday, February 25

Papers

An Experimental Study of Water and Air Transmissivity of Nonwoven Geotextiles and Geonet Composites
M. Li , B. Ramsey

Geosynthetics as Solution to Geotechnical Problems in a MSW Landfill
S. Veggi , P. Parla

Geotextile use for Landfill Gas Pressure Relief at the Boulevards at South Bay (Former Cal Compact Landfill)
M.L. Leonard, Sr. , J. Deguia, J. Weckmann

Managed by IFAI | INDUSTRIAL FABRICS Association International

under the auspices of IGS International Geosynthetics Society

with the support of GMA nags GRI GSI GII GAI GCI GDI

CD-ROM produced by X-CD Technologies Inc.

Soil Reinforcement - Geogrids 1

Date: Wednesday, February 25

Papers

Influence of the Aspect Ratio on the Mechanical Behavior of a Micro-Reinforced Soil
K.S. Heineck , L. Festugato, N.C. Consoli

Longer Term Monitoring of Strains in MSE Wall
R.L. Parsons , M.C. Pierson, J. Han, C. Vulova, J.J. Brennan

Evaluation of the Zone of Influence of Geogrid Reinforcement in Compacted Base Course using Rotation Measurements
C.C. Schuettpelz , T.B. Edil, D. Fratta

Selecting Reinforced Fill Soil for MSE Retaining Walls
W.A. Marr , R.P. Stulgis

Managed by IFAI INDUSTRIAL FABRICS Association International
under the auspices of IGS International Geosynthetics Society
with the support of GMA nagS GRI GSI GDI GII GAI GCI

CD-ROM produced by X-CD Technologies Inc.

Soil Reinforcement - Geogrids 2

Date: Wednesday, February 25

Papers

Location of Failure Plane within Narrow GRS Wall Systems
K-H Yang , R. Gupta, J.G. Zornberg

Interaction between Geogrid and Lightweight Tire Chips-Sand Mixture: Laboratory and Numerical Investigation
T. Tanchaisawat , D.T. Bergado, K. Shehzad, P. Voottipruex

Comparison of Finite Element and Limit Equilibirium Methods in Stability Analysis of Reinforced and Unreinforced Soil Slope
A. Farhadi

Managed by IFAI INDUSTRIAL FABRICS Association International
under the auspices of IGS International Geosynthetics Society
with the support of GMA nagS GRI GSI GII GAI GCI

CD-ROM produced by X-CD Technologies Inc.

Geosynthetic Barriers 1

Date: Thursday, February 26

Papers

HDPE Geomembranes - Reaching 30 Years, What's Next: or How Much Longer Will My Liner Last?
I.D. Peggs

What IAGI's Approved Installation Contractor and Certified Welding Technician Programs can do for you
L. Honnigford

The Importance of Liner Thickness and CQA Implementation in Landfills
M. Marcotte , A.L. Rollin, C. Charpentier

Managed by IFAI | INDUSTRIAL FABRICS Association International
under the auspices of IGS
with the support of GMA nags GRI GSI GII GAI GCI

CD-ROM produced by X-CD Technologies Inc.

Geosynthetic Barriers 2

Date: Thursday, February 26

Papers

Design of Uranium Mill Facility Liner Systems for the Pinon Ridge Project
K.F. Morrison , J.D. Elliott, J.M. Johnson, R.R. Monok

Rapid Shear Response of a Needle-Punched GCL
P.J. Fox , J.M. Sura, J.D. Ross, J.T. Olsta

Safer Levees with Geosynthetic Clay Liners and Erosion Control Mats
G. Heerten , J. Klompmaker, C. Lesny

High Speed Tear Properties of Geomembranes
G. Kolbasuk , J. Norberg

Managed by IFAI | INDUSTRIAL FABRICS Association International

under the auspices of IGS International Geosynthetics Society

with the support of GMA nagGS GRI GEI GSI GII GAI GCI

CD-ROM produced by X-CD Technologies Inc.

Geotextile Tubes 1

Date: Thursday, February 26

Papers

Shore Line Protection Using Polymer Rope Gabions and Geotextile Tubes
M. Venkatraman

Management of Swine and Dairy Manure with Geotextile Tube Dewatering Containers
B.J. Mastin , G.E. Lebster

Evaluation of Geotextile Tube Dewatering Performance of Tailings using Large and Small Scale Tests
R. Satyamurthy , M.D. Grzelak, T.S. Pullen, S.K. Bhatia, P. Kaye

Managed by IFAI | INDUSTRIAL FABRICS Association International
under the auspices of IGS International Geosynthetics Society
with the support of GMA nagS GRI GEI GSI GII GAI GCI

CD-ROM produced by X-CD Technologies Inc.

Geotextile Tubes 2

Date: Thursday, February 26

Papers

Disposal of Coal Mine Slurry Waste using Geotextile Containers at the North River Mine, Chevron Mining Inc.
M. Watts , E. Trainer

The Use of Geotextile Tube Containers for Dewatering The Restigouche Open Pit Zinc Mine in New Brunswick, Canada.
J. Douhï¿½ret , E. Trainer, A. Lister, S. Hauthier

Tests to Evaluate Dewatering and Filtration Efficiency for Geotextile Tubes Design
N.P.B. de Castro , P. de Mello Martins, T. Stephens, L.C.Q.C. Melo

Managed by IFAI INDUSTRIAL FABRICS Association International
under the auspices of IGS International Geosynthetics Society
with the support of GMA nags GRI GSI GII GAI GCI

CD-ROM produced by X-CD Technologies Inc.

Geotextile Tubes 3

Date: Thursday, February 26

Papers

Experimental Evaluation of Geotextile Dewatering Performance
R. Satyamurthy , S.K. Bhatia

Drainage Characteristics through Geotextiles under Tensile Load
D.A. Gaffney , Y.G. Hsuan, J.R. Weggel, R. Munoz

Geotextile Tube Dewatering Technology Utilized on Massive Scale in Ashtabula River Remediation
W. Cretens

Managed by IFAI | INDUSTRIAL FABRICS Association International

under the auspices of IGS International Geosynthetics Society

with the support of GMA nagS GRI GEI GSI GII GAI GCI

CD-ROM produced by X-CD Technologies Inc.

Laboratory Testing 1

Date: Thursday, February 26

Papers

Geotextile Permeability Testing - A Primer for Technicians and Engineers
R.S. Lacey

Retention Capacity of Geotextile Filters in Cyclic Flow
A. Srikongsri , E.J. Fannin

Geosynthetic Aggregate Drainage Systems: Preliminary Large-Scale Laboratory Test Results for Expanded Recycled Polystyrene
D. Arellano , N.H. Jafari, L.J. Bailey, M. Zarrabi

Permittivity of Geotextiles with Uniaxial Tensile Loads
M. Edwards , J. Kastner, Y.G. Hsuan

Managed by IFAI INDUSTRIAL FABRICS Association International
under the auspices of IGS International Geosynthetics Society
with the support of GMA nagS GRI GSI GII GAI GCI

CD-ROM produced by X-CD Technologies Inc.

Laboratory Testing 2

Date: Thursday, February 26

Papers

A Study to Determine the Causes and Effects of Turbulence in Transmissivity Tests
R.E. Belanger , C.B. Queja, C.V. Zantua

Wide-Width Tensile Testing of High Strength Geotextiles - An Inter-Laboratory Study
C.J. Sprague

Pull Out Tests on a Geosynthetic Composite: Influence of Soil on Shear Resistance
S-H Lajevardi , A. Couradin, D. Dias, A. Herault

Combined Saturated Soil-Geotextile-Geonet Composite Flow Test
G.R. Koerner , A.E. Eith, R.M. Koerner

Managed by IFAI | INDUSTRIAL FABRICS Association International
under the auspices of IGS International Geosynthetics Society
with the support of GMA nagGS GRI GEI GSI GII GAI GCI

CD-ROM produced by X-CD Technologies Inc.

Laboratory Testing 3

Date: Thursday, February 26

Papers

Performance of Using PVD with and without Vacuum Preloading
P. Vootipruex , D.T. Bergado, J. Saowapakpiboon, S. Youwai

Improvement of Pond Ash with Prefabricated Vertical Drain
G. Venkatappa Rao , G.K. Pothal

Managed by IFAI | INDUSTRIAL FABRICS Association International

under the auspices of IGS International Geosynthetics Society

with the support of GMA nagGS GRI GEI GII GSI GAI GCI

CD-ROM produced by X-CD Technologies Inc.

Geogrid Case Histories

Date: Thursday, February 26

Papers

Use of Geosynthetics to Mitigate Frost Heave on Trail Ridge Road
D.E. Alzamora , K. Haramy, S.A. Anderson

Geogrids as Seismic Reinforcement for Earthen Buildings
D. Torrealva

Yeager Airport Runway Extension: Tallest Known 1H:1V Slope in U.S.
J.M. Lostumbo

Earth Dam Project Using Structural Geogrids for a Tailings Ponds
M. de la Torre , B. Torreblanca

Managed by IFAI | INDUSTRIAL FABRICS Association International

under the auspices of IGS International Geosynthetics Society

with the support of GMA nagS GRI GSI GEI GII GAI GCI

CD-ROM produced by X-CD Technologies Inc.

Slope / Wall Reinforcements

Date: Thursday, February 26

Papers

Behaviour of Cellular Reinforced Soil Wall
M.S. Khedkar , J.N. Mandal

Geocell Protection against Shallow Failures on Steep Slopes
S.R. Boyle

Improvement of the Long-Term Trafficability of Container Storage Areas in Harbours with Composite Geogrid Reinforcement
J. Klompmaker , G. Heerten, C. Lesny

Design and Construction of Boulder-Faced MSE Walls (or How Not to Make a Mockery of Rockery)
J.A. Scarborough , S.C. Interlicchia

Managed by IFAI INDUSTRIAL FABRICS Association International
under the auspices of IGS International Geosynthetics Society
with the support of GMA nagGS GRI GEI GSI GII GAI GCI

CD-ROM produced by X-CD Technologies Inc.

Erosion Control

Date: Thursday, February 26

Papers

Evaluation of Vegetated RECPs using ECTC's Bench-Scale Test
J.L. Smith , S.K. Bhatia

Construction of Subsurface Natural Treatment System Using Geosynthetics
R.S. Johnson , S-S Yeo, R. Sundberg

Managed by IFAI | INDUSTRIAL FABRICS Association International

under the auspices of IGS International Geosynthetics Society

with the support of GMA nagS GRI GEI GII GSI GAI GCI

CD-ROM produced by X-CD Technologies Inc.

Geosynthetics 2009
February 25-27 2009, Salt Lake City, Utah

Prototype Modeling of GCL Hydration and Shrinkage under Simulated Field Conditions

M.H.T. Rayhani, GeoEngineering Centre at Queen's-RMC, Queen's University, Kingston, Canada
R.K. Rowe, GeoEngineering Centre at Queen's-RMC, Queen's University, Kingston, Canada
W.A. Take, GeoEngineering Centre at Queen's-RMC, Queen's University, Kingston, Canada
R.W.I. Brachman, GeoEngineering Centre at Queen's-RMC, Queen's University, Kingston, Canada
G. Siemens, GeoEngineering Centre at Queen's-RMC, Royal Military College of Canada, Kingston, Canada

ABSTRACT

Large scale experimental model was designed to investigate the effect of simulated daily thermal cycles on transient suctions for geosynthetic clay liner (GCL) and identify the relationship between initial hydration and subsequent shrinkage. The model container was constructed using rectangular boxes of Plywood, after trying many different materials and configurations. The model set up includes a soil box with dimensions of 600 × 400 × 500 mm, which was placed inside an insulated external box of 1050 × 800 × 600 mm. Rubber membranes were stretched inside the soil box to prevent leakage of water from the container. The soil container was filled with silty sand at a specified moisture content of 17% above which the GCL was placed. Insulation was placed between the two boxes to prevent the heat loss. A heater blanket system was used to apply heat to the surface and the associated changes to water content and temperature were monitored. Soil temperature and moisture content were monitored with depth using TDR system, the temperature and relative humidity of the air space were monitored using RH sensors, and the GCL deformations were monitored using high resolution photography.

1. INTRODUCTION

Geosynthetic clay liners (GCLs) are most typically comprised of a layer of low permeability clay (bentonite) sandwiched between two layers of geotextile (a nonwoven, cover geotextile and a woven, nonwoven or scrim reinforced nonwoven carrier geotextile) with the components being held together by needle-punching. GCLs are often used as part of composite liners with a geomembrane liner (high density polyethylene, HDPE) placed over the GCL. These composite liners have gained widespread acceptance for use in landfill and other liner applications such as heap leach pads.

The composite liner may remain exposed for a period of time (weeks to years depending on landfill operation) before being covered. Field cases have been reported where, after two months to five years exposure to solar radiation, upon removal of part of the geomembrane the GCL panels had been found to have shrunk in the width-wise direction leaving gaps between panels ranging between 200 mm and 1200 mm where there had initially been 150 mm overlaps (Thiel and Richardson, 2005; Koerner and Koerner, 2005, and Thiel et al. 2006).

Thiel et al. (2006) conducted tests on 60cm by 30cm GCL samples placed in aluminum baking pans and clamped at the two ends. The samples were then subjected to up to 40 cycles of heating (to 60^{o}C) and cooling (to room temperature) together with wetting during the cooling cycle. They indicate considerable shrinkage of the GCL as a result of the cyclic wetting and drying. Bostwick et al. (2007) investigated the shrinkage of a non-scrim reinforced GCL with different sizes exposed to a series of applied heating and hydration sequences in a temperature controlled room. They reported that, in comparing samples of a similar aspect ratio but different sizes, size did not play a significant role in either the rate or the magnitude of GCL shrinkage over the period of testing examined. However the question arises as to the effect of potential interaction between the GCL and the subsoil. The objective of the present research is to investigate the effect of simulated daily thermal cycles on transient suctions for the GCL on subsoil and identify the effect of foundation soil on shrinkage of the GCL under simulated field conditions. This paper reports on the test methodology and the first test conducted.

2. MATERIAL PROPERTIES

A nonwoven/nonwoven needle-punched GCL (DN type) containing granular sodium bentonite was used for this testing. This product was selected because it had previously exhibited the largest observed shrinkage in the field and the largest shrinkage in the laboratory tests conducted by Thiel et al. (2006). The initial moisture content of the GCL at the time of testing was about 5% and the mass per unit area of the GCL was 4615 g/m^2.

Soil from the Queen's composite geosynthetic liner experimental field site located in Godfrey Ontario (Brachman et al, 2007) was used as foundation soil to allow future comparison of the laboratory experimental results field data. The particle size distribution of the soil and the granular bentonite (extracted from the GCL) obtained using ASTM D422 are given in Figure 1. This data indicates that the soil is a silty-sand with 40% passing the 0.075 mm sieve. The fines were non-plastic. A series of Standard Proctor compaction tests (ASTM D 698) indicated that the maximum dry density of the soil was about 1.83 g/cm^3 at an optimum water content of 11.4% (Figure 2).

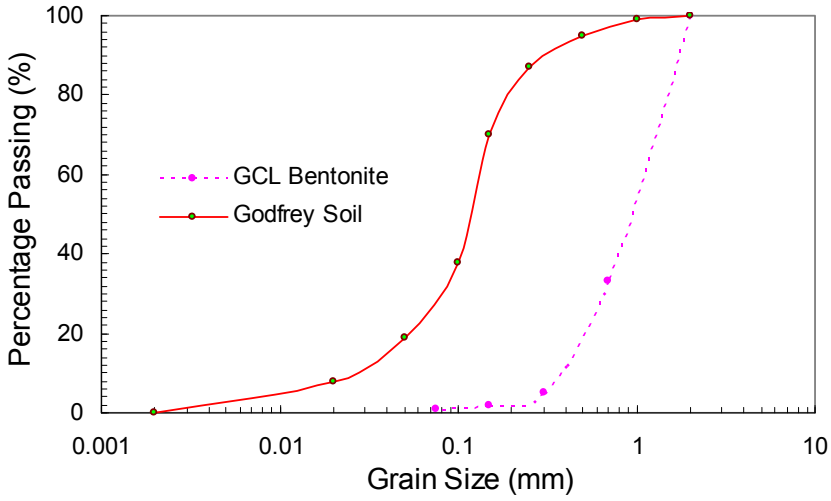

Fig. 1: Grain size distribution of DN GCL and foundation soils

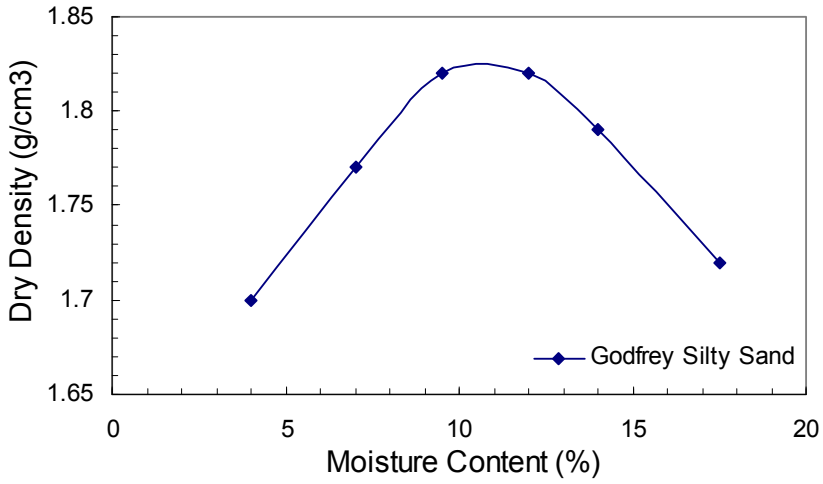

Fig. 2: Compaction curve for Godfrey foundation soil

3. EXPERIMENTAL PROGRAM

3.1 Model Container

The test cell was designed to enable potential 2D shrinkage of the GCL to be observed. The model set up involved a plywood box with dimensions of 550 × 400 × 500 mm, which was placed inside an insulated external box of 1050 × 800 × 600 mm (Fig. 3). Rubber membranes were used to line the inside of the box to prevent leakage of water from the container.

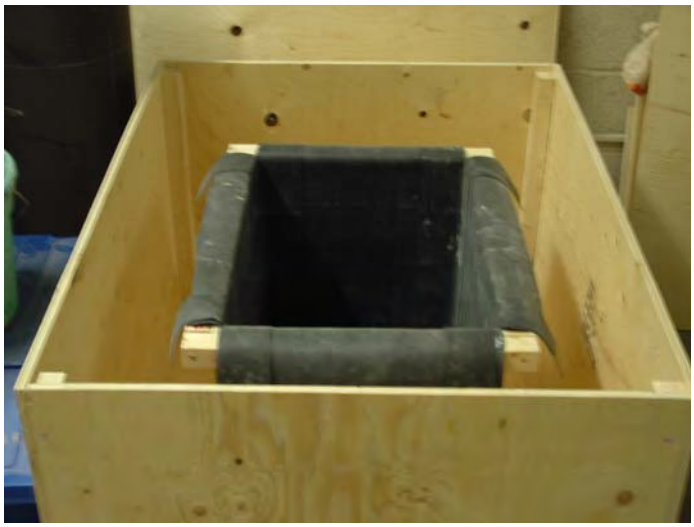

Figure 3: The big-box experimental container

3.2 Model Preparation

Bulk samples of Godfrey site soil were mixed with water to bring its water content to 17%, which corresponds to the average moisture at the Godfrey field test site. After mixing was completed, the mixture was covered with a plastic wrap and allowed to cure for 24 hours. The soil container was filled with the soil which was compacted in nine layers to a dry density of 1.65 g/cm^3, sealed, and allowed to come to moisture equilibrium (Fig. 4).

Figure 4: Sample preparation by tamping of soil layers

The GCL sample was cut to a dimension of 600 mm in the machine direction by 390 mm in the cross-machine direction and hydrated to the moisture content of about 100 % under free swell. To ensure the uniform distribution of moisture content of the GCL the water was sprayed consistently over the sample with the help of hand sprayer. The wet sample was wrapped in a plastic bag for approximately 24 hours at 20ºC to allow for proper hydration and equilibration of moisture content throughout the GCL. Markers were put on the GCL to monitor the changes in dimensions during hydration and shrinkage. To eliminate edge effects, a 25 mm border was drawn around the outside of each sample. The GCL was then, placed on top of the soil and restrained in the "long-direction" using a continuous bar clamp screwed to the container wall (Fig. 5). This clamping is intended to simulate the fact that GCLs are laid out in long panels in the field and most GCL installations include anchorage at both ends. A headspace of 50 mm was imposed on top of the GCL to investigate the role of wrinkles on potential post-hydration shrinkage, and the behaviour of the GCLs observed under thermal cycling.

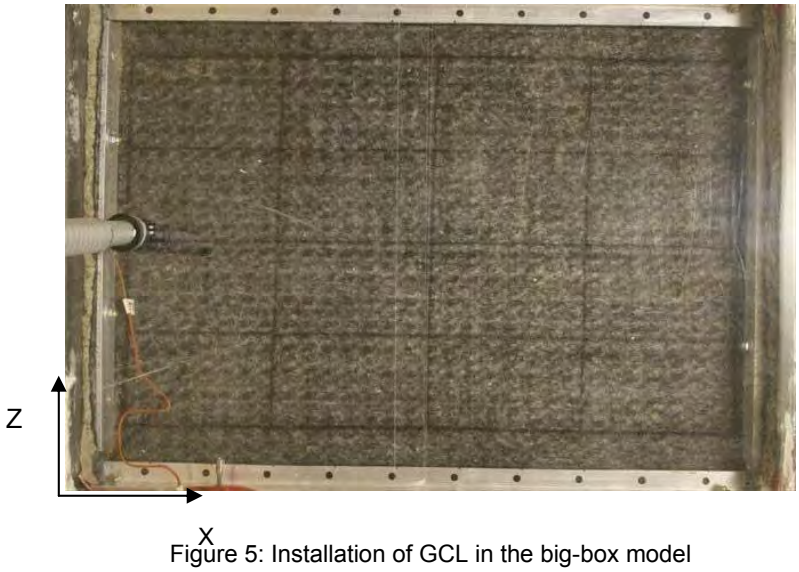

Figure 5: Installation of GCL in the big-box model

Three types of instrumentation were used to monitor the test: (i) Time Domain Reflectometers (TDR) were used for measuring moisture content in the soil, (ii) thermocouples were used for measuring temperature, and (iii) Relative Humidity (RH) sensors were used for monitoring the relative humidity of the air above the GCL. The TDR equipment consisted of a Campbell Scientific CR1000 data logger, TDR100 system, five SDMX50 50Ω coaxial multiplexers, and nine CS635 TDR probes. These waveguide probes consist of three 75mm long rods which were placed within the soil bed at predetermined locations (Table 1). Care was taken to ensure proper contact between the probe rods with the surrounding soil mass during the insertion process, as air filled gaps can have a significant effect on the calibration relationship (e.g. Siddiqui et al, 2000). TDR reading was performed during installation of the probes to verify proper performance of the instruments. The RH sensor (VAISALA HMP45A) was positioned to measure the relative humidity in the headspace on top of the GCL. Figure 6 shows the details of the instrumentation.

Table 1: Location of TDR probes and thermocouples placed within the soil

TDR Probes	X (mm)	Y (mm)	Z (mm)	Thermo-couple	X (mm)	Y (mm)	Z (mm)
TDR1	275	200	25	TC15	250	200	25
TDR2	275	200	50	TC16	250	200	50
TDR3	275	200	75	TC17	250	200	75
TDR4	275	200	100	TC18	250	200	100
TDR5	275	200	150	TC19	250	200	150
TDR6	275	200	225	TC20	250	200	225
TDR7	275	200	325	TC21	250	200	325

TDR8	275	200	425	TC22	250	200	425

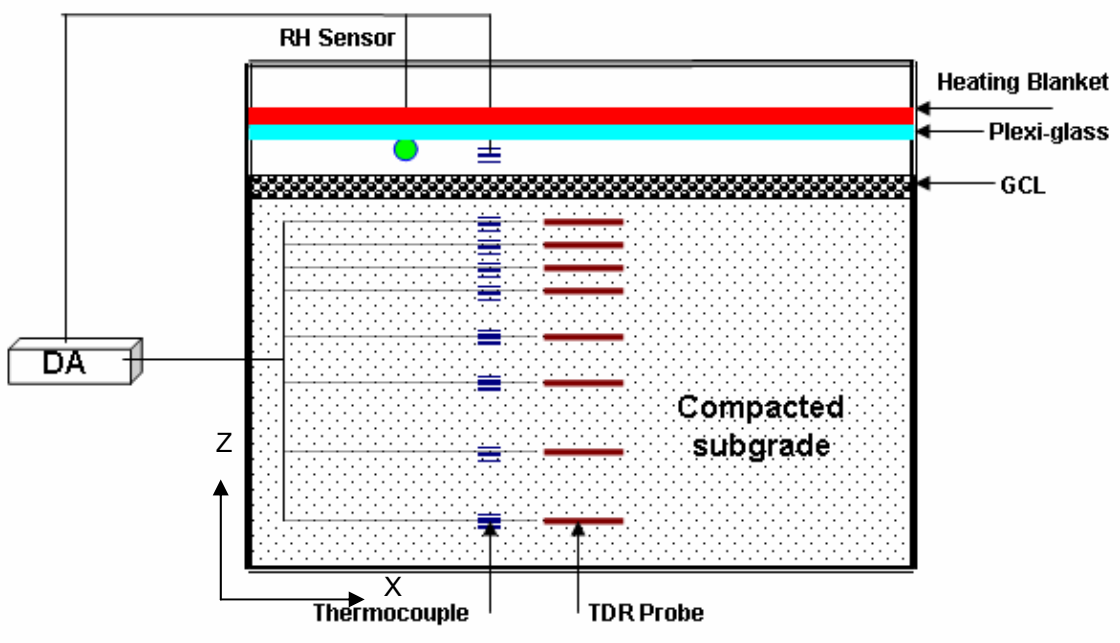

Figure 6: Schematic instrumentation details of the big-box model

To prevent shrinkage of the GCL from exposing the soil along the sides, a plastic cover was placed between the soil and GCL extending 35 mm from each of the sides. The system was sealed with plexi-glass on top of the soil box. Figure 7 shows the Styrofoam insulation around the soil box used to ensure essentially one dimensional heat and moisture flow in the soil. The insulation layer was about 200 mm thick at each side and on top of the soil box. The bottom of the box was placed on a concrete floor with a relatively constant temperature. The model was left at room temperature for about two weeks to allow moisture equilibration prior to the heating cycles.

Figure 7: Insulation details around the soil box in the model

3.3 Testing Procedure

To investigate the effect of daily thermal cycles, the temperature controller was programmed to generate cycles realistic to Canadian landfill construction (20–60ºC), whilst the bottom of the cell was kept at a constant lower temperature to simulate the thermal gradients that develop in the field. Heat was applied to the surface using the heating blanket system. The heater blanket brought the top of the box to about 60^{o}C. Heat was applied for 8 hours and the box was allowed to cool for 16 hours.

3.4 Digital Photogrammetry

Digital photographs were taken using an 8 megapixel digital SLR camera mounted to the top of the big–box (850 mm). A variable focal length lens with the disabled flash setting was employed to create uniform light conditions across the GCL. Photographs were taken at the end of the heating cycle by means of a remote program every day.

Shrinkage calculations were performed using GeoPIV (Particle Image Velocimetry), a digital photogrammetry technique developed by White et al (2003). The measurement system creates a series of “patches” on the images and calculates the displacement of the patches relative to their positions on the initial image. Using GeoPIV, “virtual strain gauges” were created along the length of the GCL and these were used to establish the strain distribution by dividing the width of the sample at each “strain gauge” at given time by the initial width at the same point and expressed as percent shrinkage.

4. RESULTS

4.1 Temperature Profile

Thermocouples were placed at eight different depths in the foundation soil to track the temperature profile in the soil. Figure 8 shows the temperature profile at the end of both the heating and cooling cycle for first, 25th and 50th cycle. The temperature profile appears to move toward higher temperature as the number of cycles increased. The initial temperature was about 23^{o} C. The temperature of the concrete at the bottom of the box appeared to accumulate some heat during the test and thus the temperature of the soil near the bottom of the box increased from 23^{o} C at the start of the test to abut 30^{o} C after 50 heat/cool cycles. During the heating cycle, the temperature at the top of the soil increased to about 60^{o} C. The rate of increase in temperature decreased with depth.

4.2 Moisture Content Profile in Subsoil

Eight TDR probes were installed in subsoil to measure the moisture content of the soil during heat/cool cycles at different depths. The volumetric moisture content profile inferred from the TDR measurements is shown in Figure 9. In general the volumetric moisture content profile moves toward lower water contents as the number of cycles increased. The initial average volumetric water content was about 29%. The average volumetric water content at depths above 150 mm decreased to about 23% after 50 heat/cool cycles. The moisture content at the bottom of the box decreased from 29% to about 26% during heat/cool cycles. There was no cracking or drying evident in the foundation soil.

4.3 Relative Humidity in Air Gap

Relative humidity and temperature in the air gap above the GCL are shown in Figure 10 for all heat/cool cycles. Relative humidity in the air gap appears to decrease with increasing temperature during the heating period, and increases during the cooling time. The peak relative humidity was about 99% at the beginning of first heat/cool cycle, which decreased to about 93% at the end of 50th cooling cycle. at the low point of the relative humidity during the heating periods, decreased from about 29% at first cycle to about 22% at last heating cycle. This indicates that the air above the GCL gradually dried as the number of heat/cool cycles increased.

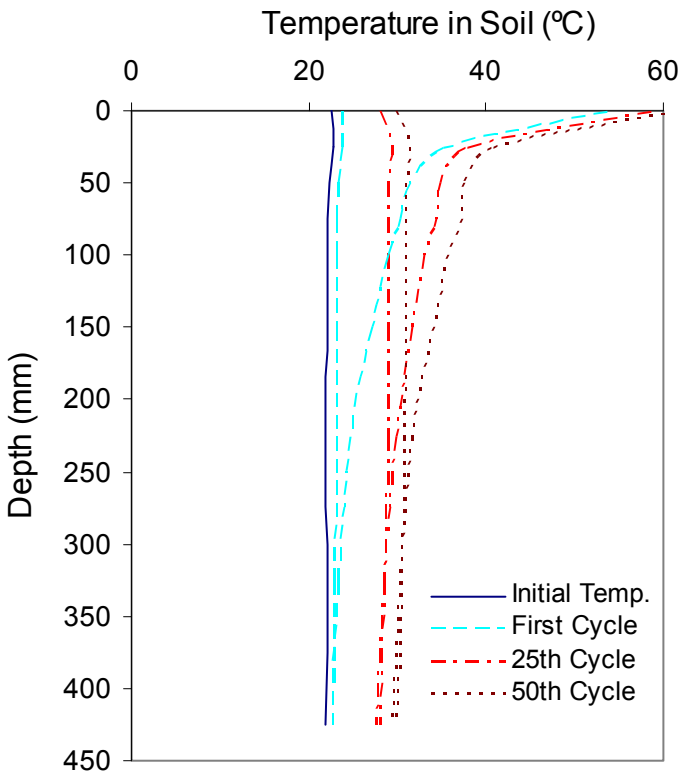

Figure 8: Temperature profile for heat/cool cycles in subsoil

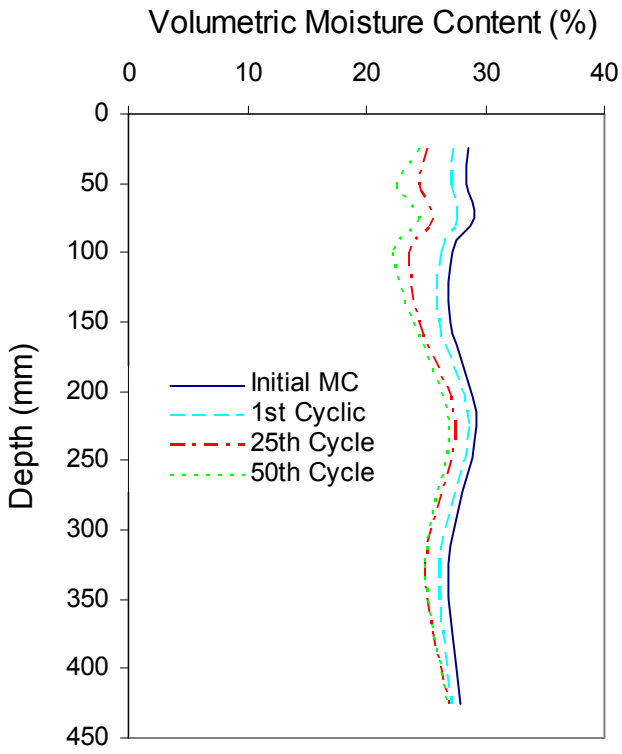

Figure 9: Volumetric moisture content profile in subsoil for heat/cool cycles

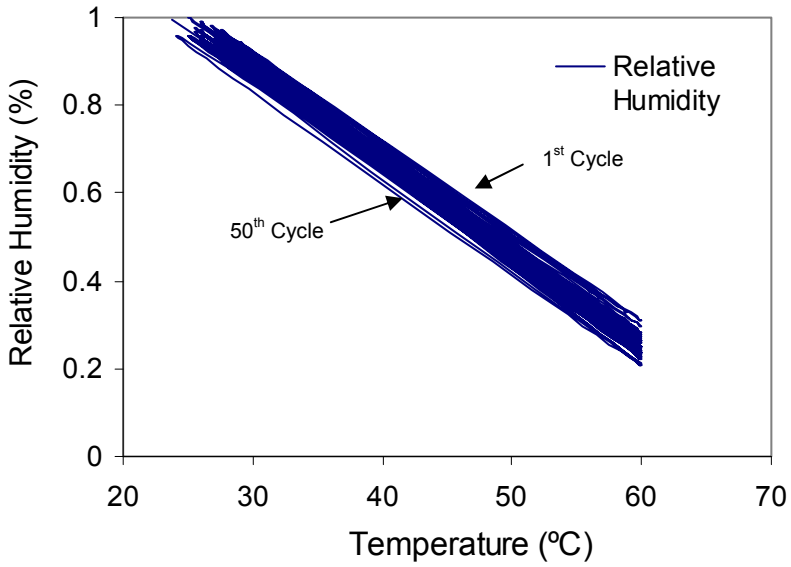

Figure 10: Relative humidity versus temperature on top of the GCL in air gap above the GCL during heat/cool cycles

4.4 GCL Shrinkage

The maximum shrinkage of the GCL occurred near the midpoint of the sample, while the strain at the ends was minimal as clamping prevented the GCL from moving at these locations. As it can be seen from Figure 11, the maximum strain of the GCL was about 4.5% after 50 cycles of heating/cooling, which equates to about 200 mm reduction in panel width for a typical panel width of 4.5 m. The maximum strain reached 4% after 15 heat/cool cycles; the accumulation of shrinkage strain was much slower for the remaining 35 cycles.

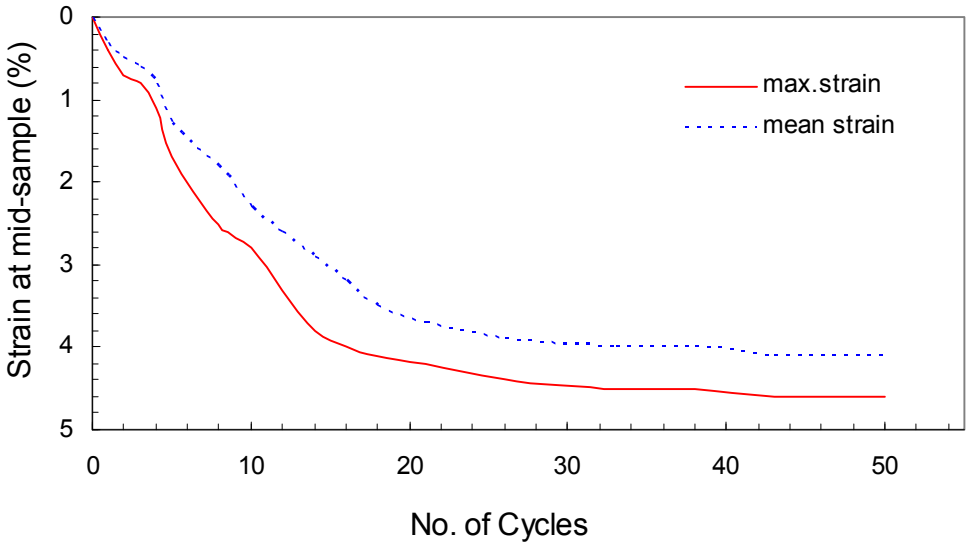

Figure 11: GCL strain at mid-sample at the end of heat/cool cycles

Previous laboratory tests of GCL on a smooth pan exposed to heating cycles of 40ºC (from room temperature to 60°C) reported by Botswick et al. (2007) had a maximum strain about 7% for the same GCL. Thus the frictional forces from soil beneath the GCL may be a factor influencing GCL shrinkage.

5. CONCLUSIONS

The physical model experiment reported in this paper appears to be able to simulate daily thermal cycles similar to the field conditions. TDR probes and RH sensors were shown to provide reasonable data that could be used to evaluate the moisture content profile in the soil and relative humidity and temperature in the air gap above the GCL. Cyclic heating and cooling conditions was found to cause shrinkage in GCL sample. However, the maximum shrinkage of the GCL at mid-sample was much less than what reported by Thiel at al (2006) and Botswick et al. (2007) in pan tests. This difference may be partly due to frictional forces from soil beneath the GCL. However the difference is probably primarily due to the lesser hydration of the GCL that could be achieved during cooling cycles when the only source of water for the GCL was that which could be taken up from the air and subsoil as it cools, as compared to the substantial water added in each cooling cycle in the pan tests. This issue is being investigated in further tests.

ACKNOWLEDGEMENTS

This study was financially supported by the Natural Science and Engineering Research Council of Canada (NSERC), the Ontario Centres of Excellence, and Terrafix Geosynthetics Inc. The authors are grateful to their industrial partners, Solmax International, Terrafix Geosynthetics Inc, Ontario Ministry of Environment, Gartner Lee Ltd, AMEC Earth and Environmental, Golder Associates Ltd., and CTT group.

REFERENCES

Koerner, R.M. and Koerner, G.R. 2005. InSitu separation of GCL panels beneath exposed geomembranes, *Geotechnical Fabrics Report,* June-July 2005: 34-39.

Bostwick, L.E.., Rowe, R.K., Take W.A., and Brachman, R.W.I. 2007. The effect of sample size on shrinkage of a non-scrim reinforced geosynthetic clay liner in laboratory tests, *Canadian Geotechnical Society Proc.*, Ottawa.

Siddiqui, S.I., Drnevich, V.P., and Deschamps, R.J. 2000. Time domain reflectometry development for use in Geotechnical Engineering, *Geotechnical Testing Journal*, 23(1):9–20.

Thiel, R. and Richardson, G. 2005. Concern for GCL shrinkage when installed on slopes, *JGRI-18 at GeoFrontiers*, GII Publications, Folsom, PA, USA, paper 2.31.

Thiel, R., Giroud, J.P., Erickson, R., Criley, K. and Bryk, J. 2006. Laboratory measurements of GCL shrinkage under cyclic changes in temperature and hydration conditions, *8th International Conference on Geosynthetics*, Yokohama, Japan 1: 21-44.

White, D.J., Take, W.A. and Bolton, M.D. 2003. Soil deformation measurement using particle image velocimetry (PIV) and photogrammetry, *Geotechnique*, 53 (7): 619-631.

GCL Shrinkage and the potential benefits of heat-tacked GCL seams

R.K. Rowe, GeoEngineering Centre at Queen's-RMC, Department of Civil Engineering, Queen's University, Kingston, ON, Canada
L. Bostwick, GeoEngineering Centre at Queen's-RMC, Department of Civil Engineering, Queen's University, Kingston, ON, Canada
R. Thiel, Vector Engineering, Grass Valley, CA, USA

ABSTRACT
Shrinkage of GCL panels in composite liners left exposed to solar radiation (i.e with no cover soil/ ballast) has resulted in significant separation between initially overlapped panels in a number of field cases reported in the literature. Separations between panels of 200-450 mm, and in one case of 1200 mm, have been reported. In an attempt to reduce the risk of panel separation, a technique of heat-tacking the overlap between adjacent panels of GCL was employed at a leach pad in Arizona. Exhumation of six mid-slope locations in the field indicated that there was no opening of the panel over-laps at the heat-tacked seams after more than 60 days exposure. This paper reports the results of a laboratory pan shrinkage test as well as tensile tests on seams prepared at this field site. The shrinkage test generated a maximum shrinkage of about 17% in the GCL adjacent to the heat-tacked seam after 40 wet-dry cycles. The same wet-dry cycles generated a tensile stress in the seam corresponding to a 13% tensile strain in the GCL adjacent to the seam. The heat-tacked seam readily withstood this tensile force. The tensile strength of the samples tested was 10-14kN/m. The tensile strength of the sample used in the shrinkage test was controlled by the manufactured groove in the GCL adjacent to the seam and not the seam itself Although additional testing is required to confirm the findings from the tests reported herein, it would appear that the technique of heat-tacking the overlap between GCLs has potential for reducing the risk of shrinkage induced separation at GCL panel overlaps.

1. INTRODUCTION

Thiel and Richardson (2005) first publicly documented the potential problem of shrinkage of geosynthetic clay liners (GCLs) covered by a geomembrane (GM) and left exposed (i.e. with no overlying cover soil). Thiel et al. (2006) summarized six cases where GCL panels, which had reportedly been originally overlapped by 150 mm, had opened up to leave a gap between GCL panels of between 200 and 1200 mm after periods of exposure of between 2 and 36 months. Several laboratory studies (Thiel et al. 2006; Bostwick et al. 2007, 2008) were able to replicate the GCL shrinkage phenomenon and demonstrated that shrinkage of up to 25% could be induced in the laboratory by the application of cyclic wetting and drying. The laboratory work indicated that some products were more susceptible to shrinkage than others. One approach to minimizing the risk of shrinkage is to (a) overlap the panels by 300 mm (as opposed to the previously common 150 mm) and (b) place cover soil on the GM as quickly as possible (within 30 days). However in some large field applications, there is significant cost associated with increasing the amount of GCL in order to double the panel overlap. Also, in these cases, it may be impractical to cover all of the composite liner within less than 30 days. For these situations an alternative approach that would minimize the potential for the opening of the overlap would be highly desirable.

Thiel (2008) recently proposed a novel field approach to addressing the concern regarding separation of GCL panels forming part of a composite liner for a large (60ha) heap leach pad at the Carlota Mine in Arizona, USA (latitude 33^{o}N). The pad was constructed in an alluvium deposit consisting primarily of eroded Pinal Schist, Schultz Granite and Dacite materials. The subgrade upon which the liner was placed was moderately to highly weathered bedrock in the form of a gravelly, silty sand that breaks down during mechanical compaction and surface rolling. The material is of low plasticity and is subject to rapid drying in the local climate. The moisture content (MC) during compaction was 10% to 12% but due to the arid climate, the moisture content dropped off with depth. Depending on the time installed (i.e. proximity to rain events) and the location within the leach pad the subgrade moisture content may have varied between 5% and 20% when the GCL was placed. In some areas a double-nonwoven, needle-punched GCL was used because of its enhanced shear strength, even though this particular GCL experienced the greatest shrinkage in laboratory tests and in field cases where loss of overlap had been observed. In other areas where shear strength was not as critical, a woven-nonwoven, needle-punched GCL (which was slightly less expensive) was used. Each 150 mm GCL panel overlap was heat-tacked with a quick application of a flame torch followed immediately by light pressure (Figure 1). The geomembrane was then placed over the GCL (same day) but it was often 60 days or more before cover soil was placed. To verify that the GCL overlaps had remained intact, the CQA firm cut holes through the geomembrane to exhume the GCL in areas that had been unballasted for more than 60 days. Both the double-nonwoven and the woven-nonwoven GCL products were evaluated. The exhumations were performed at mid-slope in six separate areas of the project

between the months of February and June. The air temperature during this period fluctuated from below 0°C to above 32°C. In every instance there was no evidence of any GCL shrinkage and the heat-tacked GCL seam was intact.

The adoption of heat-tacking as opposed to increasing the panel overlap to 300 mm as a means of addressing concerns regarding potential panel overlap separation provided significant savings at the site. However it is unknown whether the lack of observable shrinkage and the lack of separation is fortuitous (i.e. no shrinkage would have occurred in any event) or because the heat-tacking of the overlaps prevented panel separation. In particular the question arises as to whether the heat-tacking of the GCL panels would have sufficient strength to withstand shrinkage of the GCL. To provide some initial insight into this question a series of laboratory pan shrinkage tests were performed using GCL seams heat-tacked and shipped from the Carlota Mine. The tests were conducted such that the shrinkage was perpendicular to the seam and hence would have placed the seam in tension. This paper reports on the initial shrinkage test and a tensile test on a seam from the site.

Figure 1. Installer heat-tacking GCL edge seam with a 150 mm overlap.

2. TEST SPECIMENS

The nonwoven-nonwoven, needle-punched GCL used in this study consisted of two separate, overlapping pieces of GCL which were heat-tacked in the field. During testing, the GCL was wet with an amount of water equal to 60% of the dry unit weight of the sample. Initial properties of the test specimen are summarized in Table 1.

Table 1. Initial Properties of GCL Specimen tested

Test	Initial W/C* (%)	Water added (g)	Final W/C (%)	Dry mass per unit area – seamed product (g/m^2)
A	5.8	255	65.9	4490

* As received from the site

3. METHODOLOGY

3.1 Sample Preparation

Excess material was first trimmed from around the heat-tacked portion of the GCL, leaving a seamed portion approximately 125 mm wide. The seamed GCL sample was then cut to dimensions of 225 mm in the machine direction (MD) by 420 mm in the cross direction (XD), with the seam located directly in the centre. The sample was placed on a 420 mm x 620 mm aluminum baking pan, where it was secured by means of 25 mm wide bar clamps. The total specimen area between clamps was thus 225 mm by 350 mm. The aspect ratio of the sample was chosen to roughly correspond to that used in previous GCL shrinkage tests (Thiel et al. 2006, Bostwick et al. 2008).

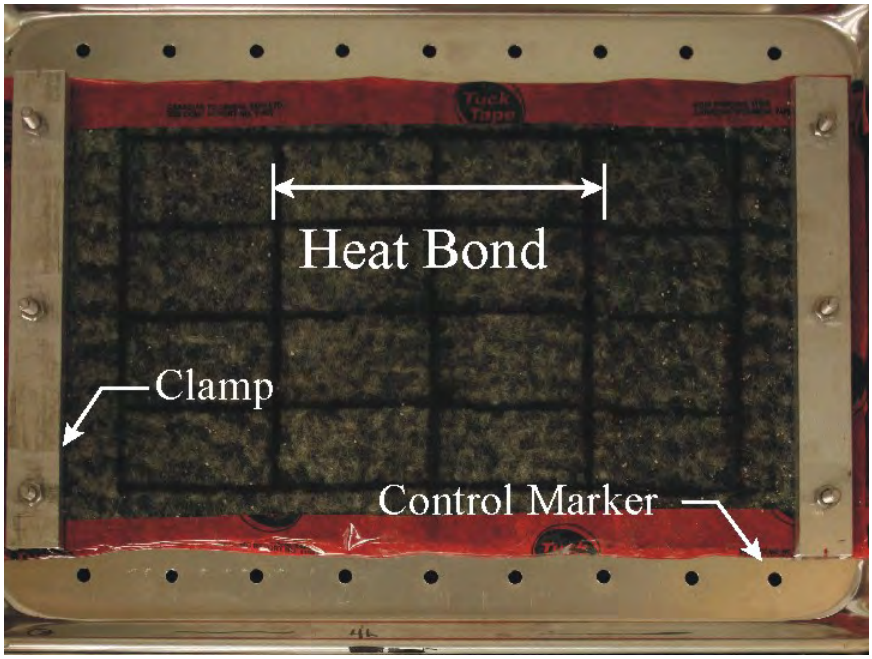

Figure 2. Pan setup immediately before commencement of testing.

Following the methodology of Thiel et al. (2006), a 25 mm border was drawn on all sides of the GCL specimen to enable hand measurements of the dimensions of the sample whilst minimizing edge effects; this resulted in an area of interest of 175 mm by 300 mm. Measurement points were also drawn at quarter points across the sample. All final calculations were based on the distance between border lines, hereafter termed the gauge distance. Moisture barrier tape was used to prevent bentonite loss from the cut edges. Figure 2 shows a pan prior to testing.

Once the sample pan was constructed, initial conditions were recorded. The specimen was then wet, by means of a commercial garden sprayer, with an amount of water equal to 60% of the sample's dry weight. To ensure a uniform spraying technique, the sample was sprayed in a back-and-forth motion, with the nozzle held approximately 50mm from the samples. Following hydration, the sample had a water content of approximately 66%.

Immediately following wetting, the sample was placed in an envelope constructed of moisture barrier tape and clear plastic sheeting to prevent moisture loss. The sample was left in a 20°C room for approximately 8 hours to hydrate. Following this equilibrium period, the sample was placed in an oven at 60ºC and left for 15 hours to dry; this applied heating cycle returned the sample to residual moisture content. This particular drying cycle is based on those used in previous laboratory studies (Thiel et al. 2006, Bostwick et al. 2008).

At the conclusion of the heating cycle, the specimen was removed from the oven and returned to the 20ºC room. Measurements were taken at key locations on the sample; the sample subsequently underwent the wetting process as described above. Handling of the sample required approximately 1 hour, resulting in a 24-hour total cycle length. The testing process was designed such that this wetting/drying cycle was repeated until such time as shrinkage has ceased. The cycle is illustrated in Figure 3.

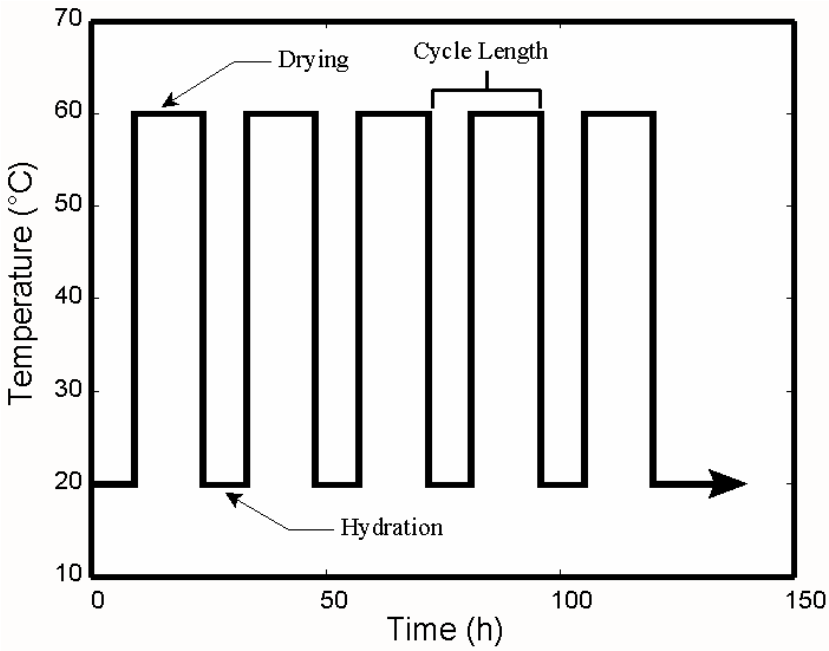

Figure 3. Hydration and Drying Cycles

3.2 Manual Strain Measurement

Initial shrinkage calculations were performed on the basis of daily hand measurements taken immediately following the drying portion of each cycle. The measurements were taken at the quarter points across the width of the sample with only the gauge distance being noted. All measurements were taken to the nearest 1.0 mm and were used to provide an independent check on the more precise measurements obtained using digital image correlation.

3.3 Digital Strain Measurement

Digital image correlation is an image processing technique which enables deformations to be tracked by comparing a series of digital images; in this case, images of the GCL sample at the end of each part of the shrinkage and swelling cycles. Using the GeoPIV code developed by White et. al. (2003), this technique was used to track the cyclic strains of the GCL sample at many locations. Upon completion of testing, fifty-one virtual "patches" measuring 128 x 128 pixels were created along the length of the sample, coincident with the border lines. Using the unique color distribution of each patch (known as the patch "texture"), these locations were then tracked in each subsequent image. By comparing the movement of each patch to that of the one located directly across from it, the cross-sample strain was obtained. This method was also used to approximate the movement of the seam, with patches located at the top edge of the sample and the visible seam edge; this is shown in Figure 4.

Digital photographs were taken with a 10 megapixel digital SLR camera mounted to a specially constructed frame. Photographs were taken twice per cycle: once immediately following the drying phase (but before applying water) and at the end of the hydration period (immediately before the drying phase). To eliminate the effects of small, unavoidable camera or pan movement, the image was calibrated by means of control markers located on the sides of the pan (see Figure 2).

White et al. (2003) have shown that the precision of GeoPIV is typically better than $1/10^{th}$ of a pixel (White et al. 2003). Photographs analyzed in this paper were taken at a resolution of approximately 0.16 mm per pixel. Therefore, the analysis has an approximate error of 0.016 mm. In terms of strain, the error is dependant on the location of analysis. For cross-sample shrinkage, with a gauge length of 175 mm, the average error is 0.009%. Seam movement, which is measured over a distance of 125 mm, has an approximate error of 0.013%.

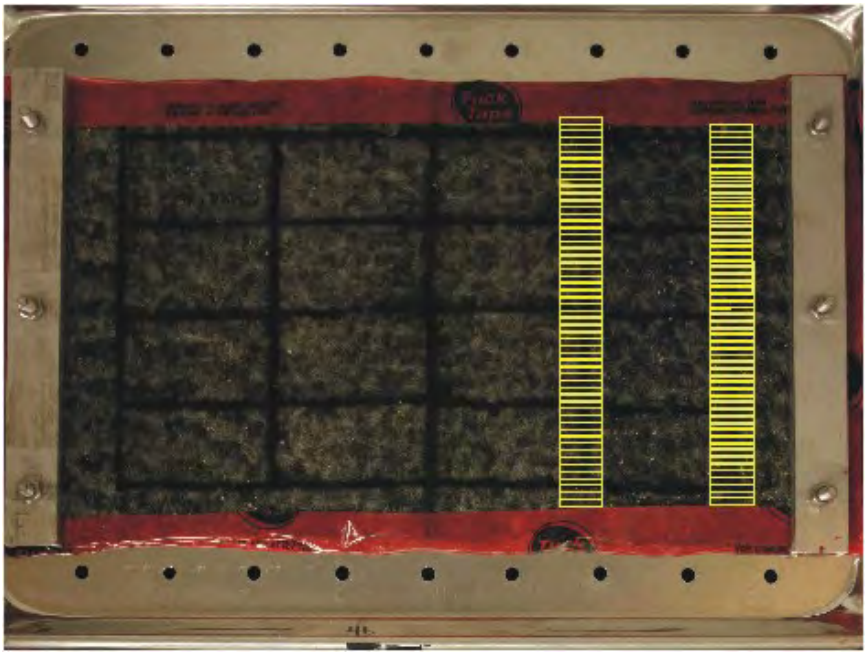

Figure 4. Virtual GeoPIV “patches” used to track seam movement

4. RESULTS

The wet-dry cycling of the testing caused the GCL to shrink across the sample (corresponding to the MD off the roll). As the number of cycles increased, this shrinkage became more pronounced. Figure 5 shows the strain across the middle of the seam versus the number of cycles. As the sample is wetted at the beginning of each cycle the GCL swells, resulting in a positive change in strain. Following drying, however, the sample shrinks, which corresponds to a negative strain. Although each subsequent wetting phase produces a relative positive strain, it is not sufficient to fully counteract the effect of shrinkage; the overall trend is a negative strain. This behavior is consistent with similar studies previously performed (Thiel et. al. 2006, Bostwick et. al. 2007, Bostwick et. al. 2008).

4.1 Location of shrinkage

In previous restrained GCL shrinkage tests, the clamping at each end of the sample caused shrinkage near the middle of the sample, with relatively little shrinkage occurring near the clamps. In this test however, the presence of the seam at the midpoint of the sample restricted strain at that location. The maximum shrinkage strain was observed near the edge of the lower seam – roughly 150mm from the left clamp. This is depicted in Figure 6.

As summarized in Table 2, the shrinkage strain at the centre of the sample was -14.2%, while the shrinkage at the centre seam was found to be 84% of the maximum strain observed on the sample.

Table 2. Summary of absolute maximum and centre strains.

Maximum strain (%)	Strain at centre (%)	Centre strain/ Maximum strain	Location of maximum strain (from left clamp) (mm)
-17.0	-14.2	0.84	150

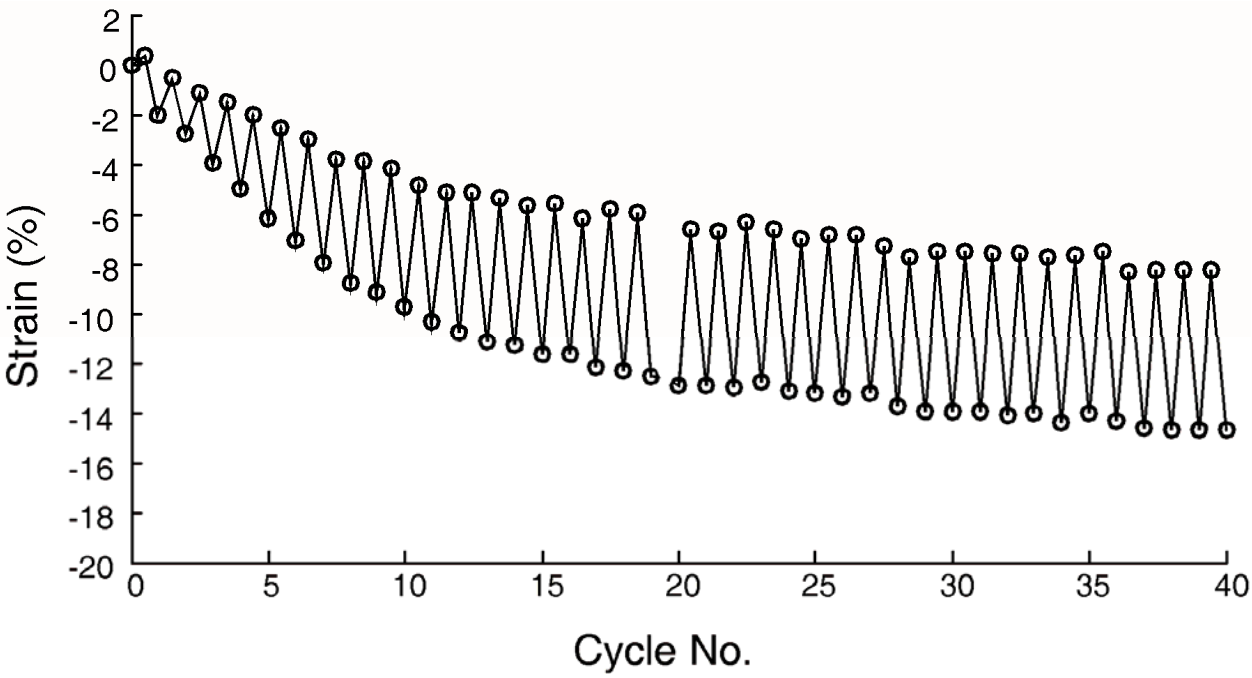

Figure 5. Shrinkage and swelling strain.

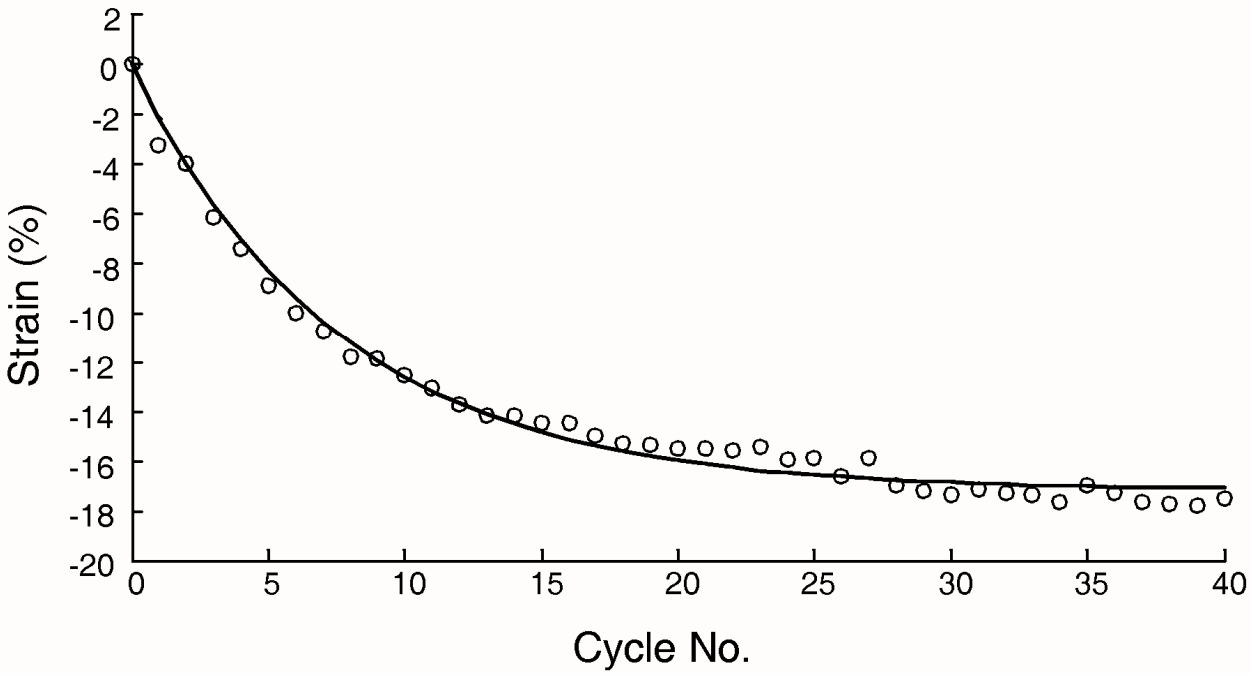

Figure 6. Maximum sample strain.

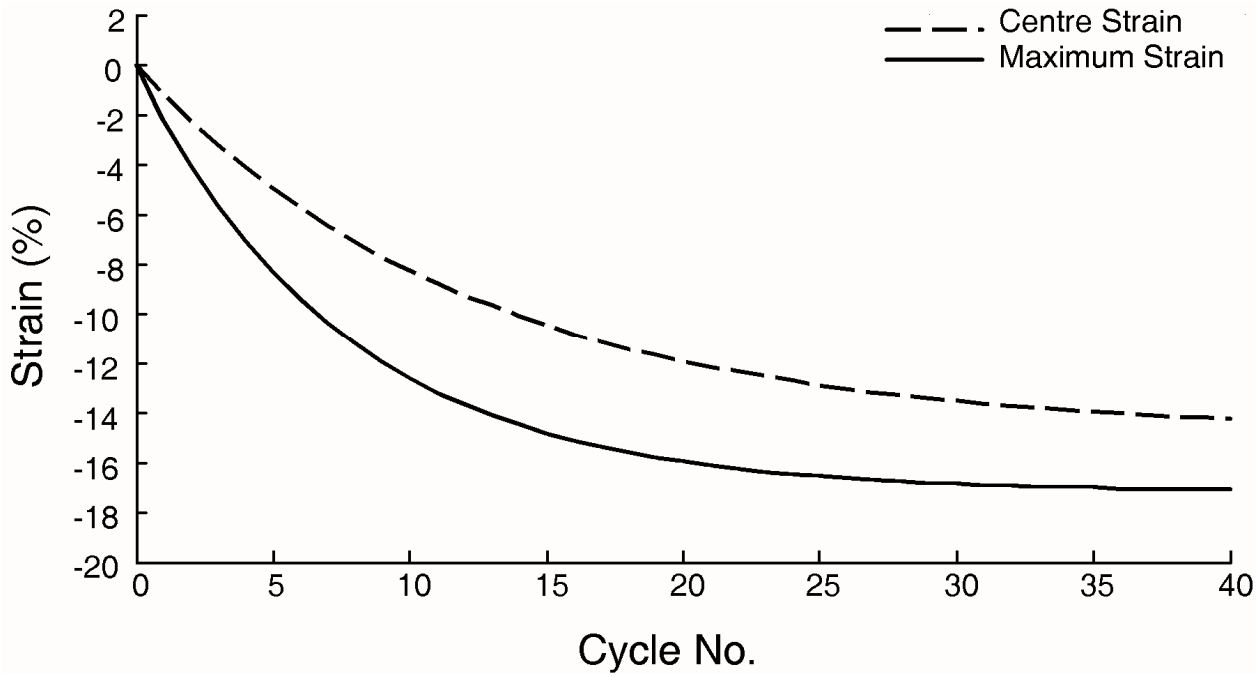

Figure 7. Comparison of maximum shrinkage strain versus that at centre of seam

4.2 Seam performance and strength

Due to the clamping and the arrangement of the samples in the pan, a tensile force was induced perpendicular to the seam as the specimen began to shrink. The tensile strain that developed in the GCL adjacent to the seam, which generated the tensile force on the seam, increased as the number of wet-dry cycles increased. To quantify this strain, the positions of the upper (visible) seam edge and a relatively stationary region near the clamp were compared and expressed as percent strain. These measurement locations are shown above in Figure 4.

As shown in Figure 8, the tensile strain in the GCL adjacent to the seam (which occurs in the cross-machine direction) exhibits similar behavior to the shrinkage between the restrained ends (which represent points of no movement in the GCL such as would, for example, occur at the mid point of each panel in a symmetric panel layout). The degree of shrinkage across the sample and the tensile strain in the GCL adjacent to the GCL seam both increased with the number of cycles.

Following the conclusion of the test at 40 cycles, the sample was removed from the pan and the remaining heat-tack strength was tested as per ASTM D4595. The results (summarized in Table 3) show that the strength of the bond following the wet-dry cycling was greater than the seam strength obtained in two tests on virgin seams. Given the method adopted for forming the seam, some variability in seam strength can be expected and it is not implied that shrinkage necessarily strengthened the seam – but it certainly did not appear to have decreased the seam strength in this case. In the tensile test, the sample failed at the pre-engineered groove at the roll edge (as shown in Figure 9), indicating that the heat-tack had in fact held; hence, it may be inferred that the seam strength was greater than the value indicated in Table 3. In these cases the capacity of the heat-tacking to prevent separation will be controlled by the GCL strength at the groove.

Table 3. Summary of parameters related to seam strength.

Maximum transverse shrinkage (%)	Tensile strain in GCL adjacent to the seam (%)	Tensile strength of sample (kN/m)	Average virgin seam strength (kN/M)	Method of failure
-17.0	13.5	14.0	10.2	Groove

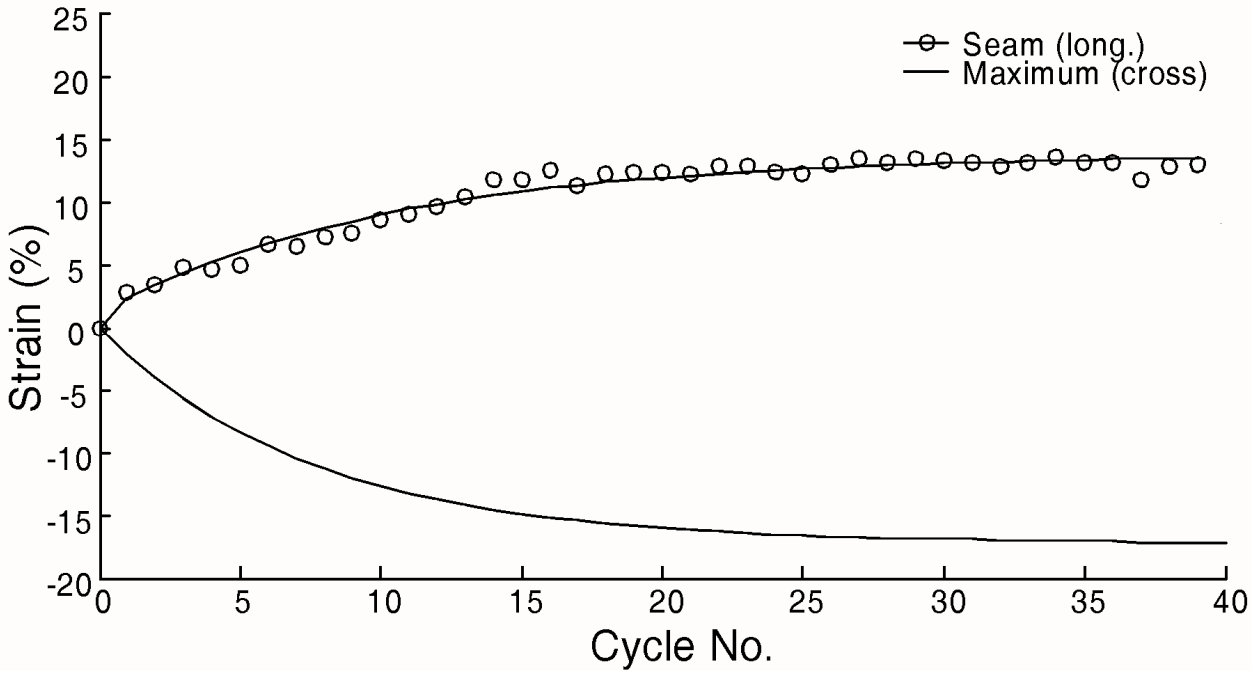

Figure 8. Seam separation as compared to absolute maximum shrinkage.

5. CONCLUSION

A technique for reducing the risk off separation of GCL panels in composite liners left exposed for in excess of 30 days was successfully employed at a leach pad in Arizona. The technique involved heat-tacking of the overlap between adjacent panels of GCL. Exhumation of six mid-slope locations in the field indicated that there was no opening of the panel heat-tacked overlaps after more than 60 days exposure. Samples of the heat-tacked seams from the field site were shipped to the Geoengineering Centre at Queen's-RMC for testing. This paper has reported on the results of a pan shrinkage test on one of these seams as well as the results of two tensile tests on virgin seams and one tensile test conducted on the sample used in the shrinkage test after 40 wet-dry cycles. The shrinkage test was conducted to generate tensile stress on the seam in a small scale simulation of the strain that might develop between the mid-points of GCL panels in a symmetric layout. In the reported tests a maximum shrinkage of about 17% was generated in the GCL adjacent to the heat-tacked seam. The same wet-dry cycles generated a tensile stress in the seam corresponding to a tensile strain of about 13% in the GCL adjacent to the seam. The heat-tacked seam readily withstood the tensile force that was generated. The tensile strength of two virgin seams was about 10kN/m. The tensile strength of the sample used in the shrinkage test (14kN/m) exceeded that of the virgin samples and the tensile failure of this specimen was controlled by the manufactured groove in the GCL adjacent to the seam. Although additional testing is required to confirm the findings from the test reported herein, it would appear that the technique of heat-tacking the overlap between GCLs has considerable potential for reducing the risk of shrinkage induced separation at GCL panel overlaps.

ACKNOWLEDGEMENTS

This study of GCL shrinkage of which the research reported herein forms a part was financially supported by the Natural Science and Engineering Research Council of Canada (NSERC), the Ontario Centres of Excellence, and Terrafix Geosynthetics Inc. The authors are grateful to their industrial partners, Terrafix Geosynthetics Inc, Solmax International, Ontario Ministry of Environment, Gartner Lee Ltd, AMEC Earth and Environmental, Golder Associates Ltd., and CTT group. The authors also gratefully acknowledge the Carlota Copper Company for providing the samples and Dr. A. Take for assistance with the GeoPiv software.

Figure 9. Tensile failure of specimen by pre-engineered groove.

REFERENCES

ASTM D 4595 Standard Test Method for Tensile Properties of Geotextiles by the Wide-Width Strip Method*, American Society for Testing and Materials*, West Conshohocken, Pennsylvania, USA.

Bostwick, L.E., Rowe, R.K., Take, W.A. and Brachman, R.W.I. (2007). The Effect of Sample Size on Shrinkage of a Non Scrim Reinforced Geosynthetic Clay Liner, *60th Canadian Geotechnical Conference*, Ottawa, ON, 2123-2128.

Bostwick, L.E., Rowe, R. K, Take, W. A and Brachman, R.W.I. (2008). Observations of the dimensional stability of four GCL products under combined thermal and moisture cycles, *Geoamericas 2008*, Cancun, Mexico, 435-443.

Thiel R. (2008) GCL Shrinkage - A Possible Solution, submitted for publication in GFR, June 2008

Thiel, R., Giroud, J.P., Erickson, R., Criley, K. and Bryk, J. (2006). Laboratory measurements of GCL shrinkage under cyclic changes in temperature and hydration conditions, *8th International Conference on Geosynthetics*, Yokohama, Japan 1: 21-44.

White, D.J., Take, W.A., and Bolton, M.D. (2003). Soil deformation measurement using particle image velocimetry (PIV) and photogrammetry, *Geotechnique* 53 (7): 619-63.

Development of X-ray Imaging Techniques to Investigate the Internal Shrinkage Mechanism of GCLs

W.A. Take, PhD, Geoengineering Centre at Queen's-RMC, Queen's University, Canada
R.K. Rowe, PhD, Geoengineering Centre at Queen's-RMC, Queen's University, Canada
H. Munro, Geoengineering Centre at Queen's-RMC, Queen's University, Canada
A. Kerr, PhD, Kingston Regional Cancer Centre, Canada
J. Schreiner, PhD, Kingston Regional Cancer Centre, Canada

ABSTRACT
Geosynthetic clay liners (GCLs) are often used in conjunction with a geomembrane to provide a low permeability composite liner in engineered barrier systems. At placement, the bentonite component of the GCL is at a relatively low moisture content and is in either a granular or powdered form depending on the manufacturer. After installation on a foundation soil, the GCL undergoes hydration as moisture is transferred from the subsoil into the bentonite component of the GCL. However, there have been a few reported cases in which field evidence of large strain shrinkage has been recorded when a composite liner has not been covered. One hypothesis is that this separation is cause by shrinkage of the GCL when the composite liner is left exposed to cycles of solar radiation and consequent wetting and drying cycles. This phenomenon was investigated by Thiel et al. (2006) and by Bostwick et al (2008). This paper aims to assess the possibility of using X-ray imaging techniques to provide non-destructive observations of desiccation patterns during the shrinkage to help understand the internal shrinkage behaviour of GCLs.

1. INTRODUCTION

Needle-punched geosynthetic clay liners (GCLs) are often used in conjunction with a geomembrane to provide a low permeability composite liner in engineered barrier systems. At placement, the bentonite component of the GCL is at relatively low moisture content and is in either a granular or powdered form depending on the manufacturer. After installation on a foundation soil, the GCL undergoes hydration as moisture is transferred from the subsoil into the bentonite component of the GCL.

Recently there have been a few reported cases in which field evidence of large strain shrinkage has been recorded when a composite liner has not been covered by ballast for periods ranging from a couple of months to several years (e.g. Thiel and Richardson, 2005; Koerner, and Koerner, 2005; Thiel et al., 2006). One hypothesis is that this separation is cause by shrinkage of the GCL when the composite liner is left exposed to cycles of solar radiation and consequent wetting and drying cycles. This phenomenon was investigated in the laboratory by Thiel et al. (2006) and by Bostwick et al (2008) who both demonstrated that substantial shrinkage can occur. However, despite this recent work on this issue, outstanding questions relating to why some GCL products are more susceptible to dimensional instability under cyclic moisture conditions remain, and explanations for the variation observed in samples of seemingly identical product remain elusive. It is therefore desired to be able to perform dimensional stability tests and take non-destructive images of the hidden bentonite component's cyclic behaviour to further investigate the mechanisms behind the observed behaviour.

Medical imaging techniques such as X-ray tomography have been successfully applied to the non-destructive imaging of geomaterials, with two international research workshops being recently held on this subject (GeoX 2003 and GeoX 2006). For the case of GCL panel shrinkage, X-ray imaging is therefore an excellent candidate technology to provide the non-destructive images required to understand the shrinkage mechanism of these geosynthetic materials.

In order for X-ray imaging to be applied to this experimental application, there needs to be:

- sufficient attenuation of X-rays through the small sub -1cm thickness of the bentonite component of the GCL,
- a method of providing photogrammetric control markers which can be seen in both visible and X-ray images, and
- a preliminary investigation to determine if the resolution of conventional X-ray scanners are sufficient to adequately capture the cracking pattern in GCLs

This paper reports the results of a series of experiments which investigate these factors and describes the suitability of this technique to its application in experiments on dimensional stability of GCLs.

2. ACQUISITION OF X-RAY IMAGES

Projection X-ray images of the samples were acquired using the portal imaging system on a Varian Clinac 2100iX (Varian Medical Systems, Las Vegas, NV). The radiation detector was a Varian aS1000 imaging panel where the active image receptor is based on amorphous silicon technology. The imaging panel measures 22 x 28 cm with 1024x768 pixels, and was positioned 145 cm from the radiation source. The X-ray source has a peak energy of 6 MeV and mean energy of 2 MeV. The Clinac is a radiation therapy machine and the aS1000 is used clinically to take X-ray images of a patient for position verification prior to radiation therapy. The resolution and field of view of this scanner is similar to conventional X-ray scanners, and in the configuration used in this study, the pixel size of the X-ray image is 0.39mm.

The imager measures differences in X-ray intensity reaching the detector plane and displays this as a grayscale picture. It is calibrated so that unattenuated X-rays yield a zero image amplitude (black) and attenuated X-rays yield a non-zero image amplitude (gray to white). Therefore, in an image of a highly cracked bentonite sample, the cracks will appear dark and the solid regions will appear lighter.

3. ASSESSMENT OF X-RAY ATTENUATION THROUGH BENTONITE LAYER

The active image receptor produces a monochrome image in which pixel intensities are represented with a 16 bit integer (i.e. 2^{16} or 65536 gray levels). To assess the use of X-ray imaging techniques to investigate the internal cracking patterns of GCLs, a dry 5.3 mm thick sample of a desiccated GCL was placed on a 1.4 mm thick aluminum pan and placed directly onto the imaging panel. Upon subjecting the sample to X-rays, the image presented in Figure 1a was formed (the grayscale colours were mapped to the range of pixel intensity values shown in Figure 1b, to present this image in a visible form). This X-ray image clearly shows the cracking pattern; however, the background intensity values vary from the top of the image to the bottom with the image of the aluminum pan at the bottom of the image considerably darker than the top. This variation in background intensity makes it more difficult to pick one value of pixel intensity to threshold the image and identify pixels corresponding to either bentonite or cracks. The histogram of pixel intensities is presented in Figure 1b. In this figure, the most frequent pixel value corresponds to the mean value of the background (i.e. the aluminum tray), and pixels of significantly higher intensity correspond to the lighter pixels of the intact bentonite blocks.

The histogram of intensity values indicates that the difference in intensity values between the thin bentonite layer and the background is approximately 20. This is a small difference in pixel intensity compared to X-ray images of bones, for example, and as such additional care is needed to maximize contrast and suppress image artifacts. Since the thickness of the aluminum pan is constant (within the tolerances of the manufacturing process), the intensity of the background region should have a near-zero standard deviation in the absence of image formation artifacts and random noise. As shown in the selected rectangular area of the X-ray image of the aluminum pan in Figure 1a, there is some variation in these pixel intensity values due to calibration artifacts from in the digital X-ray image. The standard deviation of pixel intensity values in this region is 16.1, which is of a similar magnitude to the difference between the background and the bentonite component of the GCL.

In order to eliminate the variation in background intensity and to suppress these image artifacts, an X-ray image was taken without a sample or an aluminum pan on the portal imaging system. The resulting image is included in Figure 2, with the same grayscale colour mapping of Figure 1. This image and histogram clearly shows the variation in background intensity and small variations in signal intensity which are significant due to the low attenuation through the thin bentonite component of the GCL. The standard deviation of the background calculation region of Figure 2 is 15.2.

The background X-ray image was then subtracted from the original X-ray image of the GCL to create a corrected image. To account for the difference in mean intensity of the two images, the mean intensity of the corrected image was set exactly half-way between the intensity values of an 8 bit grayscale image (i.e. pixel intensity 128 of 256 gray levels, where 0 is black and 255 is white). As shown in Figure 3, this image has a flat (i.e. constant) background with lower noise and image artifacts. The standard deviation in the background calculation region has been reduced to 3.5 pixels. To increase the contrast of the image, the pixel intensity values were then stretched to cover a wider portion of the grayscale range (Figure 4). Thus, through the use of background correction image processing techniques, the thin bentonite layer has sufficient X-ray attenuation to clearly identify crack patterns.

4. DEVELOPMENT OF PHOTOGRAMMETRIC CONTROL

The procedure for experiments investigating the dimensional stability of GCLs typically involve the use of ovens to accelerate the drying shrinkage portion of the moisture content cycles to which the GCLs are subjected (e.g. Thiel et al., 2006, and Bostwick et al., 2008). If the shrinkage strain is measured using digital image analysis, photographs of the samples must be taken at the end of every wet and dry cycle for which measurements of strain are desired. Since it is impossible to put the sample in the exact same spatial location with respect to the digital camera every time, a series of photogrammetric control markers is used to produce an accurate and consistent coordinate system for each image.

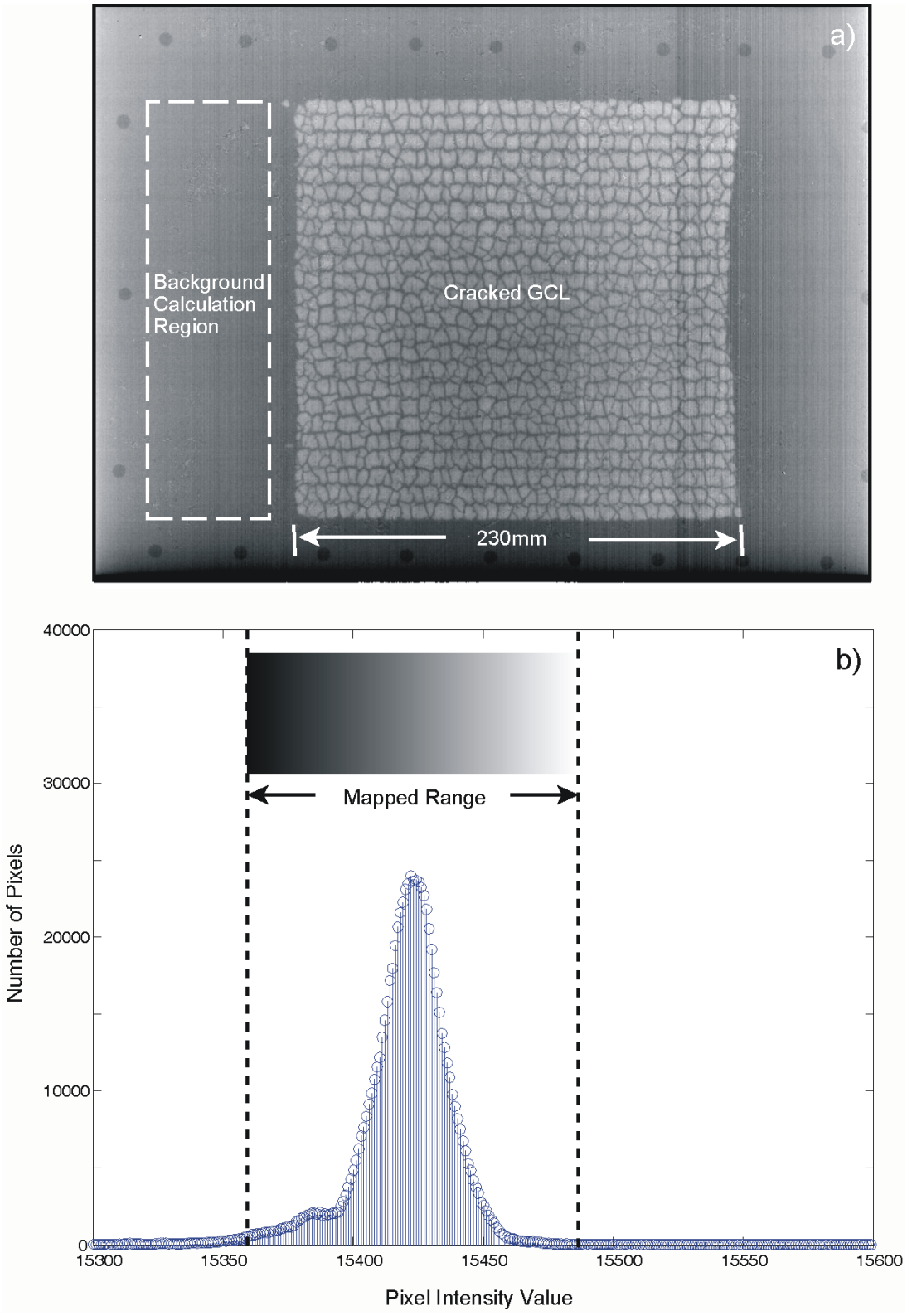

Figure 1. a) Raw X-ray image of GCL sample on aluminum tray, and b) histogram of pixel intensity values

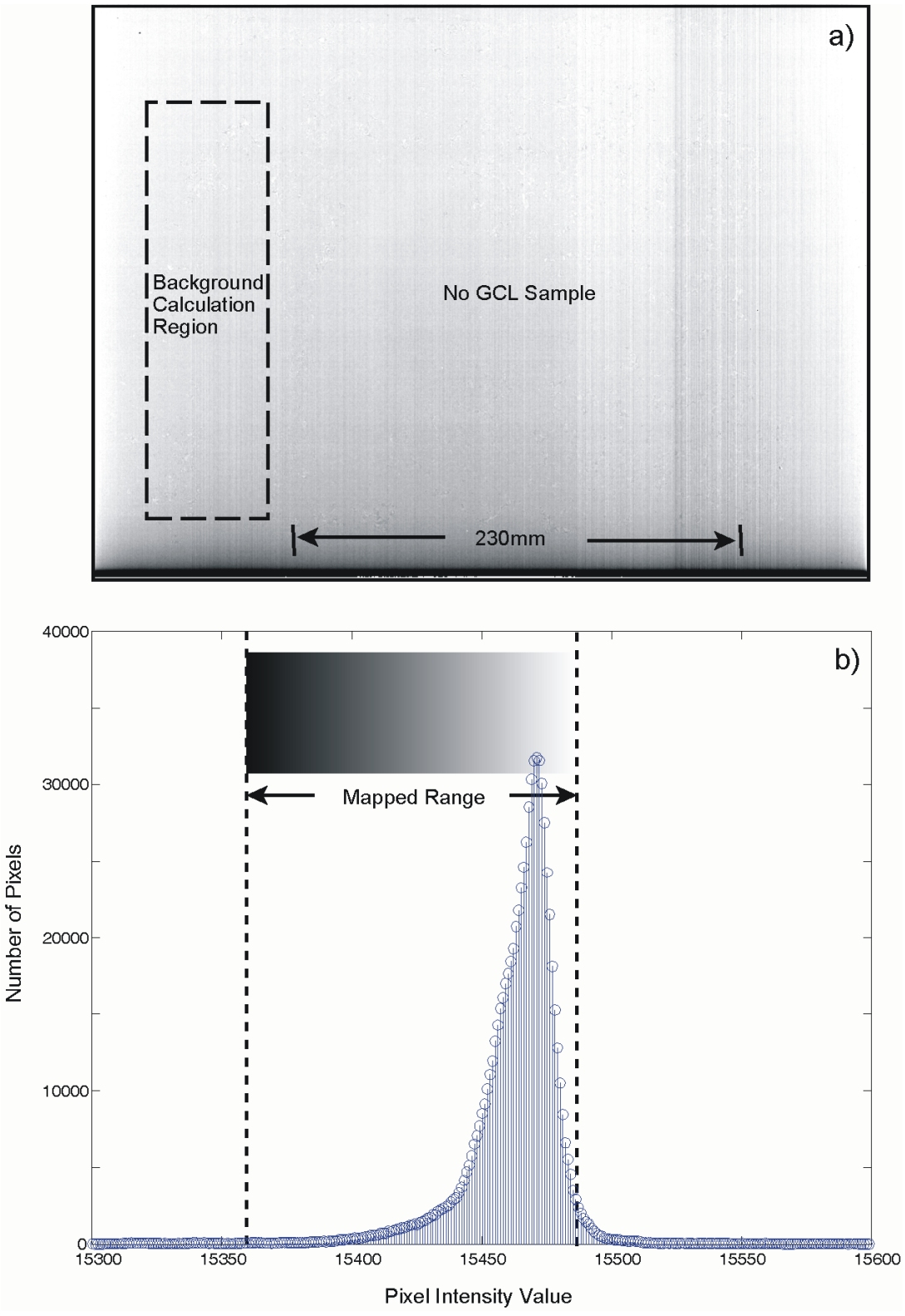

Figure 2. a) X-ray image of empty aluminum tray, and b) histogram of pixel intensity values

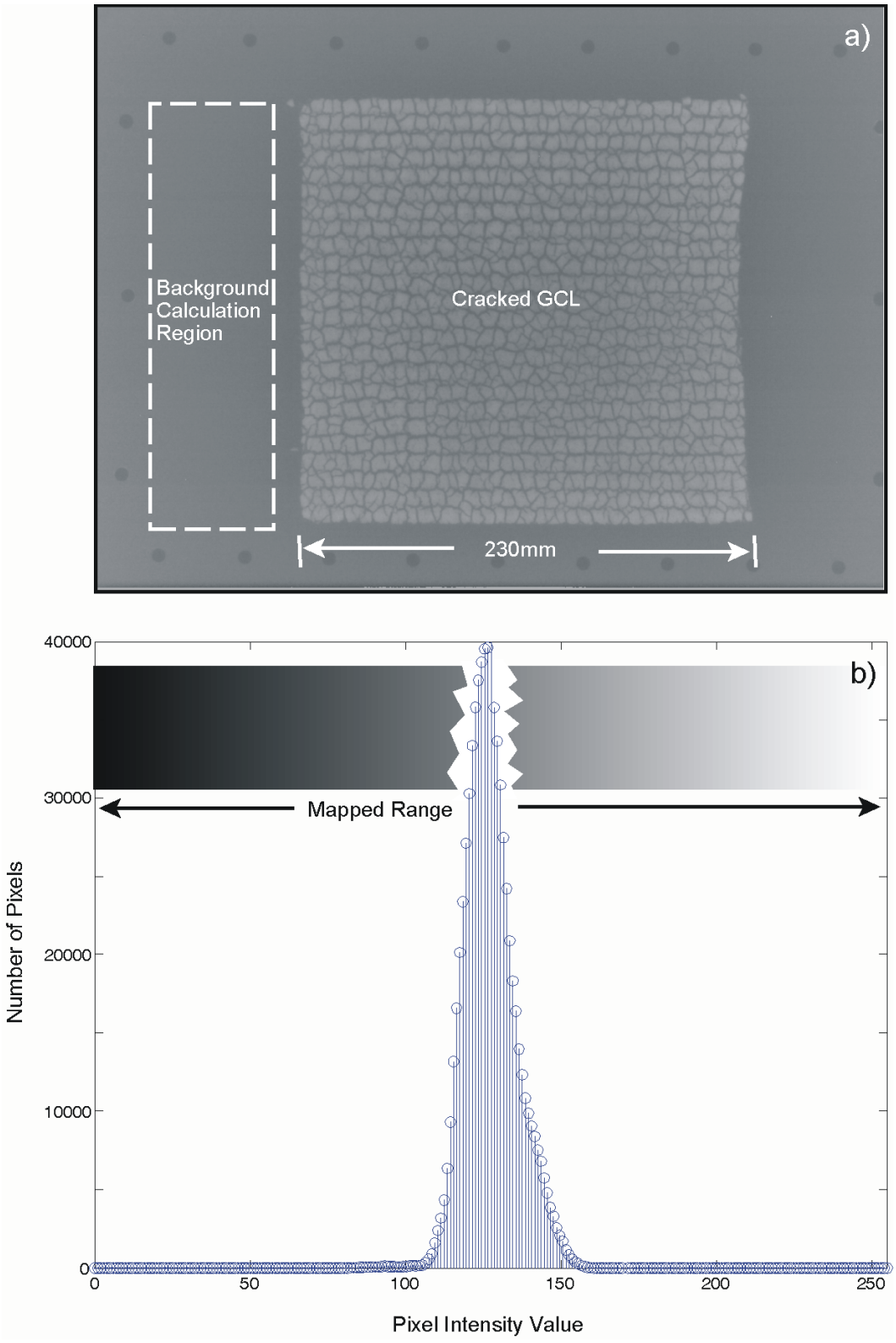

Figure 3. a) Corrected X-ray image and b) histogram of pixel intensity values

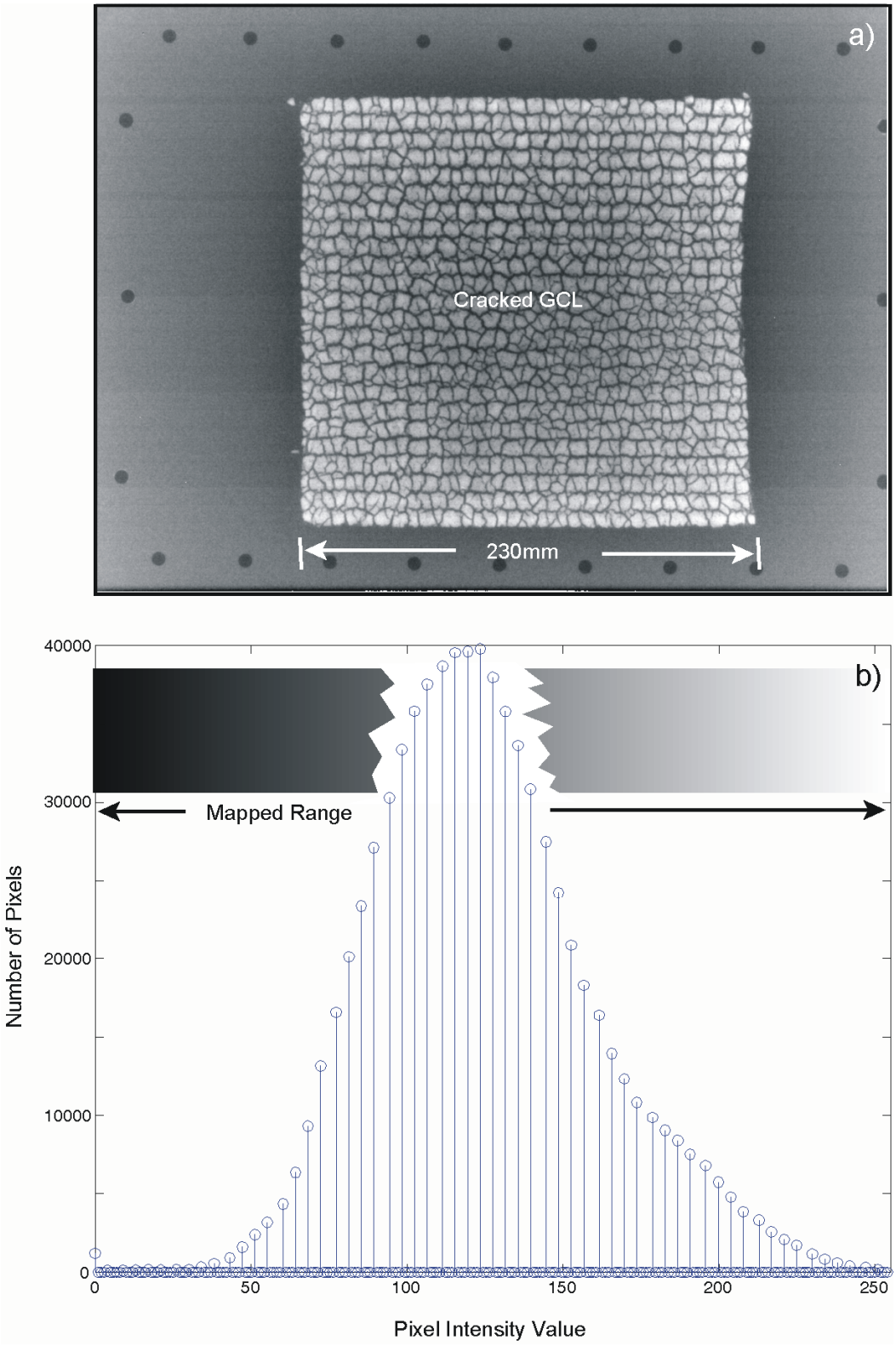

Figure 4. a) Histogram adjusted corrected image, and b) histogram of pixel intensity values

In previous work, these control markers were created on the aluminum pans containing the samples using ink. However, if X-ray techniques are to be used to investigate the internal behaviour of the bentonite component of the GCLs during these dimensional stability experiments, a common photogrammetric control needs to be provided which can be located in both visible and X-ray digital images.

Attempts to provide photogrammetric control by attaching metal washers to the aluminum pans with metal epoxy performed poorly. Although the washers increased the local attenuation of X-rays and were visible in the conventional digital images, they occasionally became debonded due to the temperature cycles the pans were subjected to as part of the dimensional stability experiments.

A second strategy was then adopted in which holes were drilled in the pans housing the GCL samples. When placed above an air gap and with the correct inclination of lighting, these holes appeared black in the visible images (Figure 5a). When subjected to X-rays, these holes appeared darker than the aluminum pan in the resulting X-ray images due to the lack of attenuation through the 1.4 mm thick aluminum pan (Figure 5b). As shown in Figure 5, the magnitude of the intensity differences is sufficient to accurately locate the centre of each dot in both the visible and corrected X-ray images, respectively.

5. COMPARISON WITH VISUAL IMAGE

Whereas visible spectrum digital cameras commonly have pixel arrays greater than 10 megapixels, digital X-ray imaging systems typically do not have the same degree of pixel density. With a required field of view of 270 x 220 mm (i.e. large enough to capture the shrinkage behaviour of a clamped GCL sample), the pixel size of the X-ray images was 0.39mm. This pixel size is potentially significant when compared to the size of cracks which could be encountered in a desiccated GCL. A verification experiment is therefore required to see if this pixel size is sufficient to accurately measure the network of cracks within a desiccated GCL sample. This experiment was performed by carefully removing the cover non-woven geotextile from the top surface of the desiccated GCL sample. This enables a direct comparison of the observed crack network with a high resolution visible spectrum camera with that measured using the amorphous silicon X-ray receptor.

A 125 mm x 125 mm square region has been selected from both X-ray and visible images of this “uncovered” GCL to investigate the effect of the pixel size of the X-ray images. These image regions are presented in Figure 6a and Figure 6c respectively. In the X-ray image, the cracks appear as darkened regions where lower attenuation of X-rays have occurred. As shown in Figure 6a, there exists a clear and well defined network of cracks which indicates that desiccation cracks within GCLs are of a sufficient size to be identified at this pixel resolution.

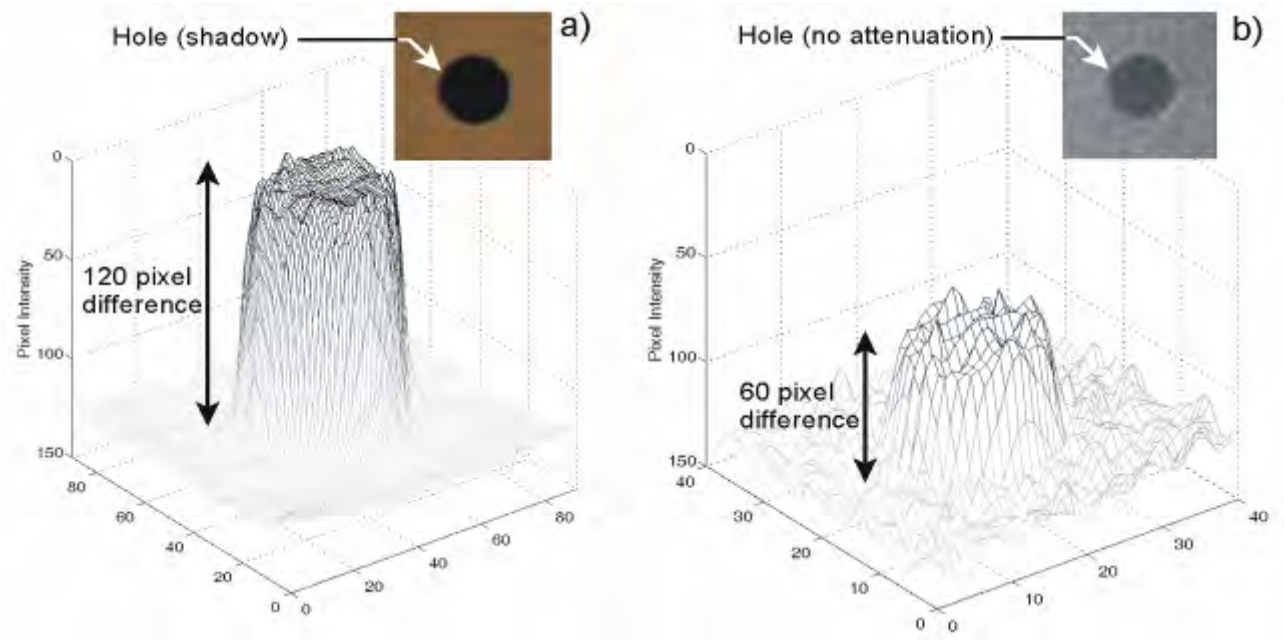

Figure 5. Pixel intensities of photogrammetric control markers in a) visible image, and b) x-ray image

Using the image processing technique of thresholding, this image can be used to differentiate bentonite regions from cracks by using a threshold pixel intensity. In the case of Figure 6b, all pixels lighter than an intensity of 105 were declared to be bentonite. Interestingly, the cracks appear to be aligned preferentially in the horizontal direction as shown on the image. This direction in the image corresponds to the roll direction of the GCL.

The visible image of the same region of the GCL is presented in Figure 6c. This image confirms the shape and distribution of cracks observed in the X-ray image, however the widths of the cracks appear to be less when thresholded at the same intensity level (Figure 6d). As there is no theoretical reason why the threshold intensity values of these two image types must be the same, the sensitivity of the identified crack networks to threshold intensity was investigated in Figure 7. In this figure, the results of the thresholding are presented in terms of the percentage of area of cracks (as identified by a given threshold level) of the total area of the selected region. This figure demonstrates a common problem in all threshold-based image processing analyses – the selection of an appropriate threshold level. If, for example, the threshold level is set too light (i.e. 120), regions that are clearly bentonite are speckled with black dots indicating false-positives for "cracked regions". This is observed in both the visible (Figure 7a) and X-ray images (Figure 7d). The other extreme occurs when the threshold level is set too dark (i.e. 70), and the crack widths are clearly underestimated in Figure 7c and Figure 7f for visible and X-Ray images, respectively.

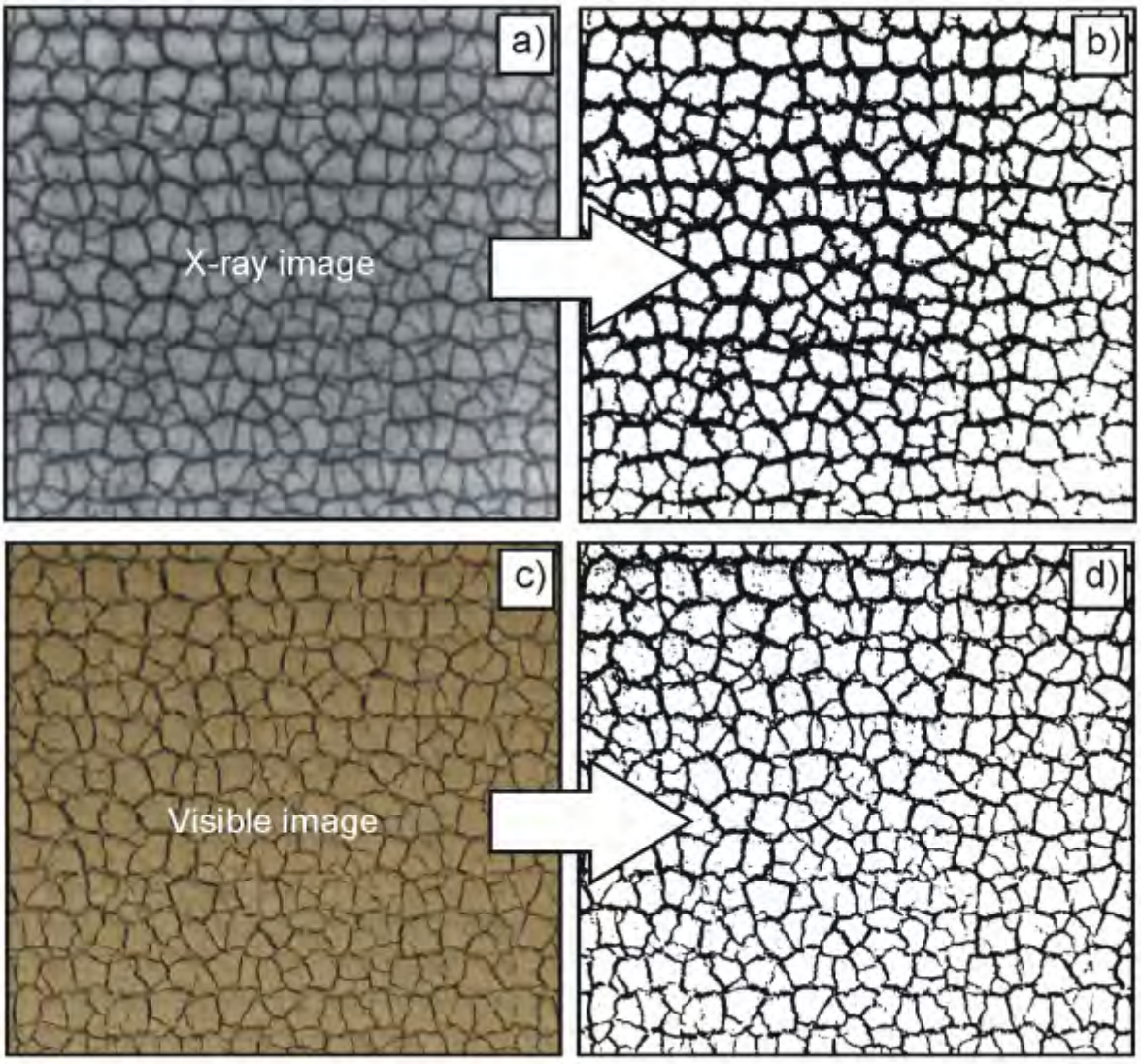

Figure 6. Crack distribution in a) X-ray image, b) thresholded X-ray, c) visible image, and d) thesholded visible image

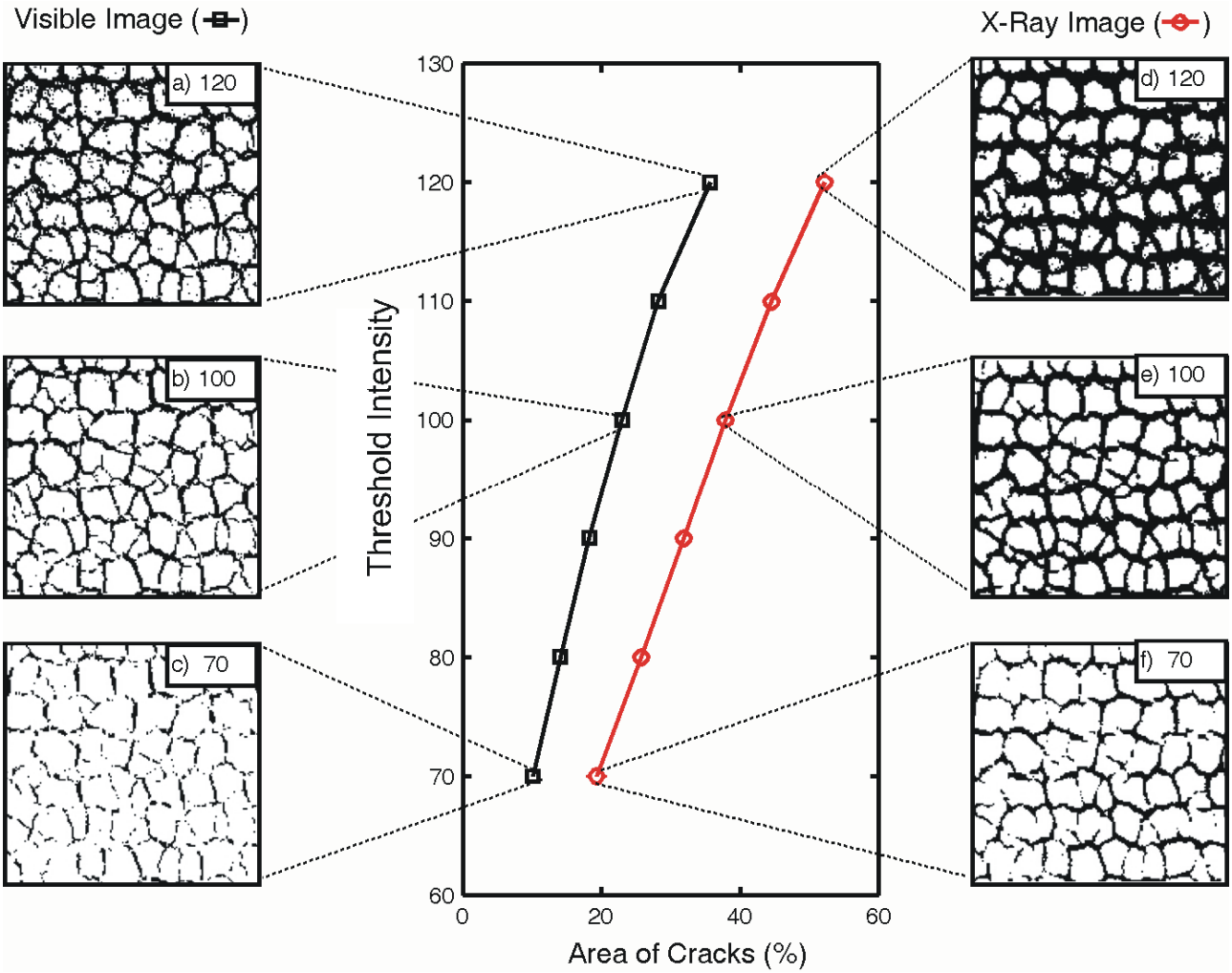

Figure 7. Effect of threshold intensity on apparent crack area on visible (a-c) and X-ray images (d-f).

The optimum threshold level will be intermediate to these two extremes and will be important to identify if a quantitative measure of crack width (or cracked area) is to be made. Image processing methods, such as the nonparametric method of automatic threshold selection of Otsu (1979) and those proposed by other researchers, are therefore required to be investigated. Despite this, it is clear from Figure 7 that the X-ray images predict a larger crack width than the visible images. This difference is likely due to the fact that the X-ray image of a crack is formed by giving the average attenuation through the entire thickness of the sample whereas the visible image of the crack is formed by the casting a shadow from a light source. In other words, the visible image records the position of the cracks at the surface, while the X-ray image will give a slightly wider “apparent crack width” if the surfaces of the cracks are not perfectly orthogonal to the exposed surface of the GCL. An overhead light source such as used in this preliminary study would therefore bias the results towards reduced shadows and lessened apparent crack widths if the cracks were V-shaped. These experimental factors are currently being investigated along with automatic threshold selection methods.

6. CONCLUSIONS

Preliminary experiments have been performed to apply X-ray imaging techniques to investigate the internal shrinkage mechanism of GCLs. In particular, the low attenuation through the small thickness of GCL was seen to require extra attention to the correction of the resulting X-ray image to maximize contrast and suppress image artifacts. Further, photogrammetric control markers consisting of drilled holes in the sample pans were capable of being seen and measured in both visible and X-ray images. Finally, an experiment performed on a sample of desiccated GCL with the cover geotextile removed indicates that the resolution of the X-ray images is sufficient to adequately capture the cracking

pattern of GCLs. This experiment indicated that the X-ray and visible images yield nearly identical crack distribution patterns, but with the X-ray image providing a larger estimate of the width of the cracks. Further research is needed to quantitatively investigate the experimental and analytical reasons behind this observation. However, the preliminary results reported in this study clearly indicate that the application of this non-destructive imaging technology to the problem of dimensional stability of GCLs under cyclic wetting and drying cycles is highly promising. In particular, it is hoped that this technology will address some unanswered questions regarding the phenomena of cracking in the mechanism of cyclic shrinkage in this application. This work is currently ongoing.

ACKNOWLEDGEMENTS

This study was financially supported by the Natural Science and Engineering Research Council of Canada (NSERC), the Ontario Centres of Excellence, and Terrafix Geosynthetics Inc. The authors are grateful to their industrial partners, Terrafix Geosynthetics Inc, Solmax International, Ontario Ministry of Environment, Gartner Lee Ltd, AMEC Earth and Environmental, Golder Associates Ltd., and CTT group.

REFERENCES

Koerner, R.M. and Koerner, G.R. 2005. InSitu separation of GCL panels beneath exposed geomembranes, Geotechnical Fabrics Report, June-July 2005: 34-39.

Bostwick, L.E. Rowe, R. K, Take, W. A and Brachman, R. W. I (2008). Observations of the dimensional stability of four GCL products under combined thermal and moisture cycles, *GEOAMERICAS 2008*, Cancun, Mexico, March, 435-443.

GeoX 2003. X-ray CT for Geomaterials: Soils, Concrete, Rocks -- Otani and Obara (eds.) Swets and Zeitlinger. Lisse. ISBN 90 5809 666 1.

GeoX 2006. Advances in X-ray Tomography for Geomaterials – Desrues, Viggiani, and Bésuelle (eds.). Wiley-ISTE. ISBN: 978-1-905209-60-6

Otsu, N. 1979. A threshold selection method from gray-level histograms IEEE Transactions on Systems, Man, and Cybernetics 9: 62–66. doi:10.1109/TSMC.1979.4310076

Thiel, R. and Richardson, G. 2005. Concern for GCL shrinkage when installed on slopes, JGRI-18 at GeoFrontiers, GII Publications, Folsom, PA, USA, paper 2.31.

Thiel, R., Giroud, J.P., Erickson, R., Criley, K. and Bryk, J. 2006. Laboratory measurements of GCL shrinkage under cyclic changes in temperature and hydration conditions, 8th International Conference on Geosynthetics, Yokohama, Japan 1: 21-44.

Transport of VOCs through a Co-extruded Geomembrane with a Nylon Barrier

R.S. McWatters and R.K. Rowe, GeoEngineering Centre at Queen's-RMC, Department of Civil Engineering, Queen's University, Kingston, Ontario, Canada.

ABSTRACT
Geomembranes are employed in a variety of containment and barrier systems to mitigate the migration of hazardous volatile organic compounds (VOCs) with the potential to contaminate the surrounding environment and air quality. In addition, they are often the primary barriers used in final cover systems of landfills to prevent the release of these contaminants found in leachate and landfill gas. Studying the transport of VOCs through a geomembrane establishes its diffusive and permeation properties and ultimately its performance as a barrier. This paper examines the liquid and gas phase transport of VOCs through a novel co-extruded linear low density polyethylene geomembrane with an inner nylon layer. The 0.38 mm (15 mil) nylon geomembrane showed a 5-15 fold decrease in both the permeation and diffusion coefficients when compared to a standard 0.53 mm (20 mil) LLDPE geomembrane.

1. INTRODUCTION

Geomembranes have been used in the engineering industry for a variety of applications, including containment of waste in landfills and disposal facilities, for surface ponds or reservoirs, and containment basins for fuel and liquid storage. More recently, geomembrane applications have extended to include vapour barriers for buildings, whether as a methane barrier or to prevent harmful vapours from entering through the building foundation. As a vapour barrier, geomembranes also contain landfill gases including, but not limited to, methane, carbon dioxide and volatile organic compounds (VOCs) (Qian *et al.*, 2001). In addition, they have been employed in the remediation of soil piles contaminated by hydrocarbons and to contain gases released during the degradation process in bioreactors (Reinhart *et al.*, 2002; Rowe *et al.*, 2004). As the geotechnical and geoenvironmental industries continue to develop more uses for geomembranes, the types of geomembranes available for use have also grown.

Common polymer types used in barrier systems include high density polyethylene (HDPE), linear low density polyethylene (LLDPE), poly-vinyl chloride (PVC), and polyethylene liners with fluorinated additives (Park and Nibras, 1993). Multilayer geomembranes were first created having higher density polyethylene as the outside layers and a lower density polyethylene as the inner layer (Kolbasuk, 1990). Evolved from multi-layer geomembranes were co-extruded geomembranes with additives, as in a polyamide (nylon) material as the innermost layer. The objective was to create a geomembrane with the flexibility and stability of a standard LLDPE polymer but with a superior resistance to vapour and liquid VOC migration. This paper examines the liquid and gas phase diffusion of VOCs through a novel co-extruded linear low density polyethylene geomembrane with an inner nylon barrier.

2. BACKGROUND

As an effective barrier material in landfill cover systems or hazardous containment systems, geomembranes must be resistant to the migration of VOCs found in landfill gas. For a well constructed and intact geomembrane, there is minimal advective transport of VOCs and diffusion is the dominant mode of transport (Rowe, 1998). The diffusive flux through the geomembrane will depend on polymer type and crystallinity. Crystallinity and polymer orientation have been shown to impact permeability as a tighter packing structure results in a more tortuous path for compounds to navigate, thus reducing the permeability (D'Aniello *et al*. 2000; Aminabhavi *et. al*, 1997). Geomembrane thickness is another important factor as thinner geomembranes have a higher diffusive flux, other things being equal (Sangam, 2001). A polyamide material used in a co-extruded geomembrane could increase the diffusive resistance to VOCs for a thin geomembranes.

Three parameters characterize the potential for diffusive migration of each compound through a geomembrane: diffusion, partitioning and permeation coefficients (Sangam and Rowe, 2001). Diffusion through geomembranes occurs in three steps: adsorption, diffusion and desorption. Initially, the contaminant partitions between the source medium and adjacent surface of the geomembrane. Then the compound diffuses through the geomembrane driven by chemical potential. Finally, the compound partitions between the outer geomembrane surface and the receiving medium (Sangam and Rowe, 2001). Eventually, equilibrium is reached between the concentration in the geomembrane and the

concentration in either the source or receptor media (Rowe, 1998). The equilibrium between geomembrane and the source medium can be related by Henry's law:

$$c_g = S_{gf} c_f , \tag{1}$$

where c_g is the concentration in the geomembrane [ML^{-3}], c_f is the concentration in the source fluid (either gas or liquid) [ML^{-3}], and S_{gf} is the partitioning coefficient [-].

In the second step, the diffusion of the penetrant through the geomembrane is described by Fick's first law:

$$f = -D_g \frac{dc_g}{dz} , \tag{2}$$

where f is the mass flux [$ML^{-2}T^{-1}$]. The diffusion coefficient, D_g [L^2T^{-1}] is specific to the geomembrane and contaminant of interest. c_g is the concentration of the compound in the geomembrane [ML^{-3}] and z represents the distance parallel to the direction of transport. When the diffusion coefficient is constant, the change in penetrant concentration in the geomembrane with time t, is expressed by Fick's second law:

$$\frac{\partial c_g}{\partial t} = D_g \frac{\partial^2 c_g}{\partial z^2} \tag{3}$$

The final step is similar to the first and can also be described by Henry's law with different notation :

$$c_g^{'} = S_{gf}^{'} c_f , \tag{4}$$

where $c_g^{'}$ is contaminant concentration in the receptor medium and $S_{gf}^{'}$ is the partitioning out of the geomembrane. When the source and receptor fluid are the same, the partitioning coefficients into the geomembrane can be assumed to be equal to the partitioning coefficient out of the geomembrane ($S_{gf}=S_{gf}^{'}$) (Sangam and Rowe, 2001).

The concentration of contaminant inside the geomembrane is very difficult to measure; therefore, the change in concentration in the fluid on either side of the geomembrane is measured. The relationship for this change in concentration in the geomembrane when the source and receptor media are alike is given by rearranging Equations 1 and 3. The relationship is as follows:

$$f = -D_g \frac{dc_g}{dz} = -S_{gf} D_g \frac{dc_f}{dz} , \tag{5}$$

Further simplification of this equation in terms of a permeation coefficient, P_g [L^2T^{-1}], which is the coefficient of proportionality for Fickian mass transport for a source to receptor fluid (Sangam and Rowe, 2001), is shown below:

$$P_g = S_{gf} D_g \tag{6}$$

The diffusive properties of a geomembrane (S_{gf}, D_g, P_g) with respect to VOC contaminants in a liquid or vapour phase are established through sorption and diffusion tests. Lower permeation coefficients are indicative of a more effective barrier to the contaminant being investigated.

3. EXPERIMENTAL INVESTIGATIONS

3.1 Material and Methods

This study examined a relatively new co-extruded flexible geomembrane supplied by Raven Industries, Engineered Films Division (Sioux Falls, South Dakota, USA). The geomembrane is marketed as a nylon vapour barrier, trade name VBP15. It is 0.38 mm (15 mil) thick with a five layer structure. The first layer is approximately 42% of the total thickness

and made of low linear density polyethylene (LLDPE) with a 3.5% calcium carbonate inert filler. The second layer, at 6% of the total thickness, is a tie resin made of maleic anhydride modified LLDPE. The innermost layer is only 4% of the thickness and made of nylon. The fourth and fifth layers are identical to the first and second respectively, therefore creating a symmetrically layered geomembrane. The density of the geomembrane is 920 kg/m^3. The coextruded geomembrane was compared with a standard o.53 mm (20 mil) LLDPE geomembrane also manufactured by Raven Industries. The density of this geomembrane was 920 kg/m^3. Table 1 and 2 summarizes the relevant properties of the co-extruded and standard geomembrane tested, respectively. All properties were obtained from the manufacturer.

Table 1. Standard properties of co-extruded LLDPE geomembrane (with an inner nylon barrier) tested.

Properties	Methods (ASTM)	Units	Values
Thickness		mm	0.38
Puncture	D4833	Peak (N)	171.52
Tear resistance	D1004	Peak (N)	39.46 x 39.32
Tensile	D6693	Peak (N)	72.73
Load at break	D6693	N	70.15
Elongation at break	D6693	% (min)	608
Tensile strength	D882	N	298
Impact resistance	1709 Method B	g	3813
Std-OIT		min	23.91
HP-OIT		min	1450

Table 2. Standard properties of LLDPE geomembrane tested.

Properties	Methods (ASTM)	Units	Values
Thickness		mm	0.53
Puncture	D4833	Peak (N)	194.21
Tear resistance	D1004	Peak (N)	53.91 x 55.02
Tensile	D6693	Peak (N)	129.89
Load at break	D6693	(N)	118.28
Elongation at break	D6693	% (min)	955.00
Tensile strength	D882	N	407
Impact resistance	1709 Method B	g	2970
Std-OIT		min	190

The VOCs benzene, toluene, ethylbenzene and xylenes, commonly known as BTEX, were the contaminants examined in this study. These common aromatic hydrocarbons are extremely volatile and often used in VOC migration analysis. They are present in the dissolved and gaseous phase in a range of hazardous settings, including hydrocarbon spills and storage, waste, leachate and landfill gas. Diffusion and sorption tests were performed using BTEX in both a dilute aqueous and vapour phase.

Tests were conducted using purchased BTEX standards and injecting known amounts into vials and cells filled with organic-free distilled deionized water (DD water). In both liquid and vapour sorption tests, liquid samples were taken using gas tight syringes and directly injected into the Purge & Trap syringe filled with distilled deionized water. In the liquid diffusion tests, liquid samples were taken as per the sorption tests. For the vapour diffusion tests, samples were taken from the liquid phase in the cells and directly injected into the P&T syringe. Vapour concentrations were measured from liquid concentration results and then correlating the vapour concentrations in the cells by Henry's Law. Temperatures in the cells were monitored and maintained at 24^{o}C. Surrogates fluorobenzene and 1,4-dichlorobenzene were used as internal standards for quality assurance/quality control. Samples were analyzed by Purge and Trap Gas Chromatography/Mass Spectrometer (P&T)-GC/MS. The procedure used a Hewlett Packard 5890 GC with a P&T unit and 5972 mass selective detector (MS).

3.2 Procedures

3.2.1 Sorption Tests

Single compartment stainless steel cells were secured with a geomembrane sample inside. Liquid sorption tests had cells completely filled with DD water; vapour sorption tests were partially filled with water, leaving an air space. The geomembrane was suspended in the vapour space for these latter tests. BTEX were injected into the liquid phase of all sorption tests. Initial concentrations of the dilute aqueous solution ranged from 0.2-2.0 mg/L (ppm). These concentrations are reflective of typical landfill leachate and landfill gas concentrations (Rowe, 2005; EPA, 2005). Samples were agitated on magnetic stirring plates and maintained at a temperature of 24^{o}C. Contaminant concentrations were evaluated over time until equilibrium was reached. The partitioning coefficient for each contaminant compound was calculated using the following equations derived from the contaminant mass balance at equilibrium:

$$M_{s0} = M_{sF} + M_{gF}, \tag{7}$$

where M_{s0} is the initial mass of the contaminant in solution [M]; M_{sF} is the final mass of the contaminant in solution [M] and M_{gF} is the mass contained in the geomembrane [M]. When Eq. 7 is rearranged in terms of concentrations and volumes, it becomes:

$$c_{f0}V_{f0} = c_{fF}V_{fF} + \frac{M_g}{\rho_g}c_{gF}, \tag{8}$$

where c_{f0} is the initial contaminant concentration in solution [ML^{-3}]; V_{f0} is the initial solution volume [L^3]; c_{fF} is the final contaminant concentration in solution [ML^{-3}]; V_{fF} is the final solution volume [L^3]; M_g is the initial mass of the geomembrane sample [M]; ρ_g is the geomembrane density [ML^{-3}] and c_{gF} is the final concentration of the contaminant in the geomembrane at equilibrium [ML^{-3}]. The partitioning equation can be expressed by substituting Eq. 8 into Eq. 1 to give:

$$S_{gf} = \frac{\left[c_{f0}V_{f0} - c_{fF}V_{fF}\right]\rho_g}{M_g c_{fF}} \tag{9}$$

3.2.2 Liquid Diffusion Tests

In the liquid diffusion tests, a stainless steel double compartment cell (source and receptor) was divided by a geomembrane sample. The receptor cell contained DD water. The source cell contained a dilute aqueous BTEX solution ranging between 0.2 and 2.0 mg/L. The liquid phase was sampled to measure the initial concentration in the source. Diffusion cells were maintained at a constant temperature of 24^{o}C. Samples were taken from the source and receptor at regular time intervals until an equilibrium was established.

3.2.3 Vapour Diffusion Tests

In the vapour diffusion tests, a modified stainless steel double compartment cell (source and receptor) was employed. In both the source and receptor compartments, there was an aqueous phase and a vapour phase. A geomembrane sample was secured between the source and the receptor compartments where it rested entirely in the vapour phase. This ensured that the geomembrane sample was solely exposed to contaminants in the vapour phase. The receptor liquid contained DD water. The source liquid contained a dilute aqueous BTEX solution at concentrations ranging from 0.2 to 2.0 mg/L. The chemicals were allowed to equilibrate between the liquid and vapour phase of the source compartment. The liquid phase was sampled to measure the initial concentration in the source and the vapour phase was related using Henry's Law. Diffusion cells were maintained at a constant temperature of 24^{o}C. Samples were taken from the source and receptor liquid phase at regular time intervals.

3.2.4 Modelling Diffusion Parameters

These experiments used theoretical modelling to establish the diffusion (D_g), partition (S_{gf}) and permeation (P_g) coefficients of contaminants through the geomembranes. The concepts and theory of this approach were developed by Rowe et al. (1998) for clayey soils and by Rowe et al. (1995, 1996) for geomembranes. Analysis of experimental results followed the procedure outlined by Rowe et al. (1995) using the finite layer analysis program POLLUTE© v.7 (Rowe and

Booker, 2004). This procedure was used in previous studies by Sangam and Rowe (2001) and McWatters and Rowe (2007). Further explanation of the procedures can be found in Sangam and Rowe (2001)

4. RESULTS AND DISCUSSION

4.1 Dissolved Phase Diffusion

Throughout sorption and diffusion tests, contaminant concentrations in the cell (source and receptor) were monitored over time until equilibrium was reached. Theoretical curves obtained with POLLUTEv7 were fitted to the experimental data for both the source and receptor. The sorption coefficient, $S_{gf,}$ was measured from the sorption tests. Both the S_{gf} and diffusion coefficient, $D_{g,}$ values were obtained from the diffusion tests. Then the permeation coefficient, P_g, for each contaminant was calculated from these curves.

For the diffusion tests in the dissolved phase, Figures 1 and 2, show the decrease in benzene and *m&p*-xylenes concentrations in the source solution, respectively. Figure 3 and 4 show the increase in benzene and *m&p*-xylenes concentrations in the receptor solution. The changes in concentration are plotted as normalized concentrations relative to the initial concentration. The equilibrium concentration was reached after 60 days for benzene and 40 days for *m&p*-xylenes. Benzene concentrations decreased by 58% of the initial concentration, while the decrease in *m&p*-xylenes was 75%. For benzene, the partitioning coefficient was 120 and the diffusion coefficient ranged from 0.6-0.8 x 10^{-13} m^2s^{-1} with the uncertainty that gives rise to the range being a result of the scatter of the experimental data points. *m&p*-Xylenes has an S_{gf} of 430 and a D_g of 0.5 x 10^{-13} m^2s^{-1}. Toluene, ethylbenzene and *o*-xylene were also monitored. The results for additional BTEX contaminants were: toluene, S_{gf}=220 , D_g= 0.6-0.8 x 10^{-13} m^2s^{-1} ; ethylbenzene, S_{gf}=425 , D_g= 0.5 x 10^{-13} m^2s^{-1} ; *o*-xylene, S_{gf}=400 , D_g= 0.5 x 10^{-13} m^2s^{-1}.

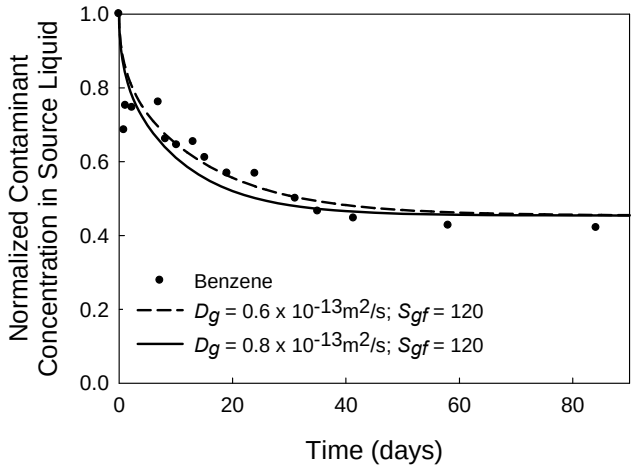

Figure 1. Change in benzene concentration in the source during dissolved phase diffusion tests using co-extruded GM. Experimental data plotted as symbols and theoretical curves plotted as lines.

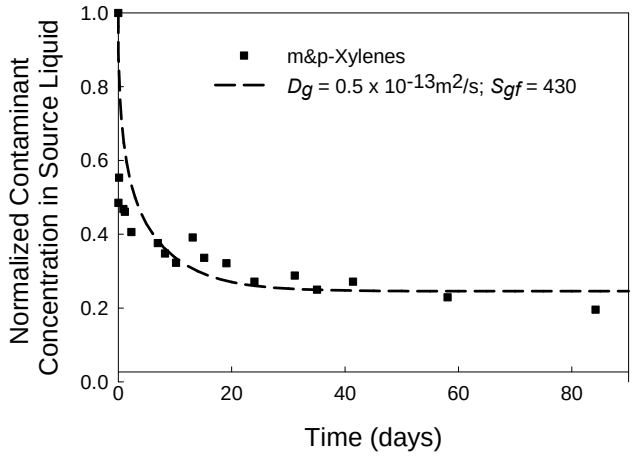

Figure 2. Change in *m&p*-xylenes concentration in source during dissolved phase diffusion tests using co-extruded GM.

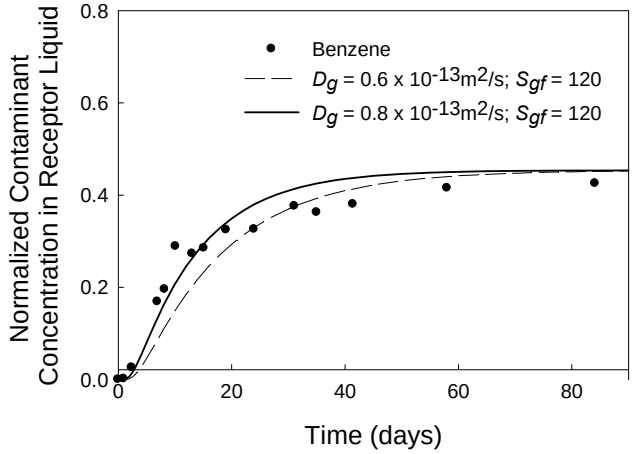

Figure 3. Change in benzene concentration in the receptor during dissolved phase diffusion tests using co-extruded GM.

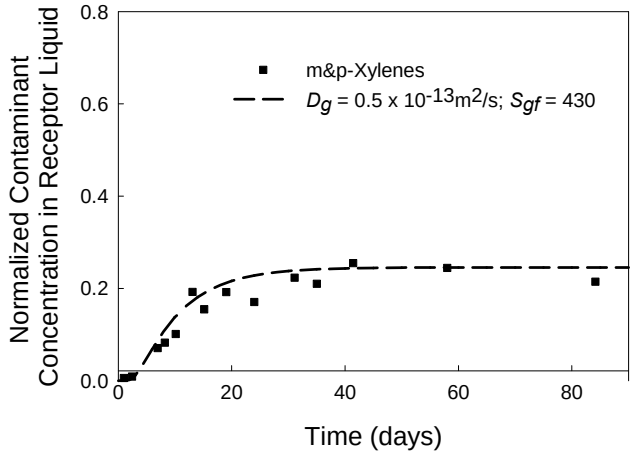

Figure 4. Change in *m&p*-xylenes concentration in receptor during dissolved phase diffusion tests using co-extruded GM.

4.2 Vapour Phase Diffusion

For diffusion tests in the gaseous phase, the concentrations of contaminants were measured in the source and receptor liquid phase. Vapour concentrations were calculated using the Henry's Law correlation at 24°C. Temperature was maintained at 24°C and recorded throughout the tests. Figures 5 and 6 show the decrease in benzene and *m&p*-xylenes concentrations in the source vapour throughout the diffusion testing period. The concentrations were normalized relative to the initial concentration of contaminants in the source reservoir. The concentration decrease for benzene in the source was 82% and for *m&p*-xylenes was 91%.

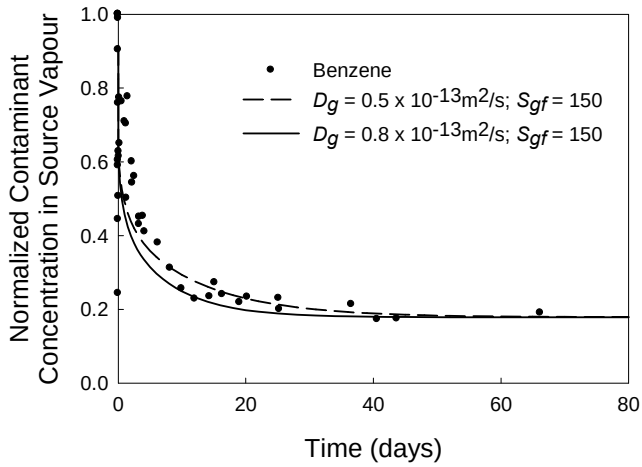

Figure 5. Change in benzene concentration in the source during vapour diffusion tests using co-extruded GM. Experimental data plotted as symbols and theoretical curves plotted as lines.

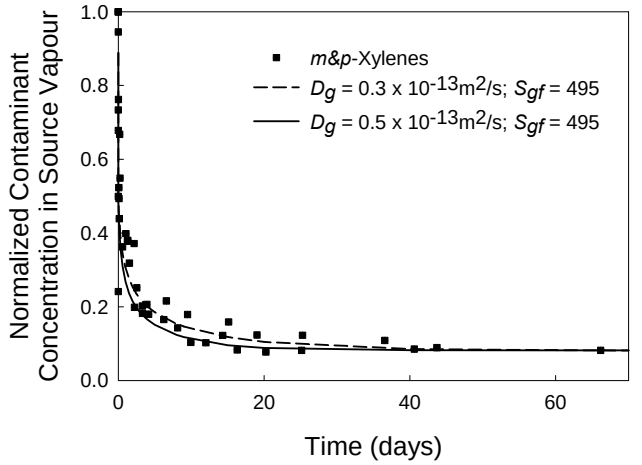

Figure 6. Change in *m&p*-xylenes concentration in the source during vapour diffusion tests using co-extruded GM.

The increase in contaminant concentrations in the receptor are shown in Figure 7 (benzene) and Figure 8 (*m&p*-xylenes). In repeated tests, equilibrium was reached after 55 days for benzene and 40 days for *m&p*-xylenes. For the contaminant benzene, the vapour sorption parameter was 150 and the diffusion coefficient ranged from 0.5-0.8 x 10^{-13} m^2s^{-1}. *m&p*-Xylenes has a sorption parameter of 495 and a diffusion coefficient that ranged from 0.3-0.5 x 10^{-13} m^2s^{-1}.

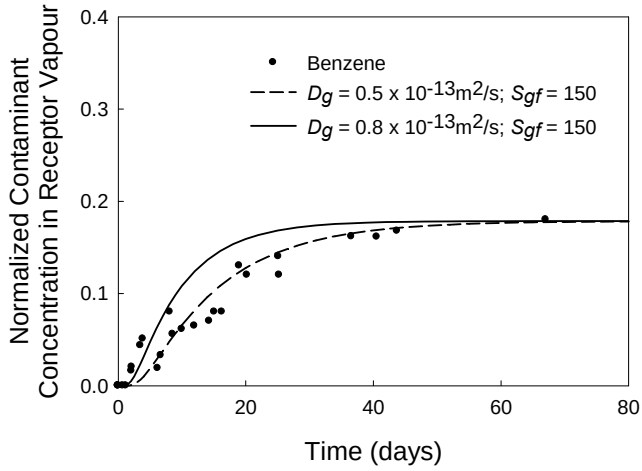

Figure 7. Change in benzene concentration in the receptor during vapour diffusion tests using co-extruded GM.

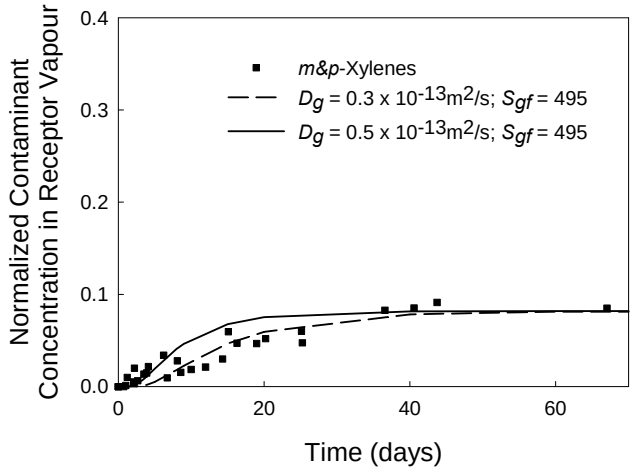

Figure 8. Change in *m&p*-Xylenes concentration in the receptor during vapour diffusion tests using co-extruded GM.

Table 3 presents all three diffusive migration parameters: D_g, S_{gf} and P_g, of all contaminants in both the dissolved and gaseous phase through the co-extruded nylon geomembrane. The partitioning coefficients are slightly higher for the vapour phase than the dissolved phase. The diffusion coefficients for benzene and toluene were similar for both vapour and dissolved phase transport of each contaminant respectively. For the diffusion of ethylbenzene and the xylenes, a diffusion coefficient of 0.5 x10^{-13} m^2s^{-1} fit with the experimental data. For the vapour phase, a D_g range of 0.3-0.5 x10^{-13} m^2s^{-1} was necessary to capture the behavior of the gas phase ethylbenzene and xylenes. This is acceptable, considering fluctuations occur between the vapour and liquid phase concentrations as the equilibrium shifts due to slight temperature changes.

Table 3. Inferred partitioning, diffusion and permeation coefficients of the co-extruded nylon GM from diffusion tests in the liquid and vapour phases.

Contaminants	Co-extruded Nylon Liquid Results			Co-extruded Nylon Vapour Results		
	S_{gf}	D_g	P_g	S_{gf}	D_g	P_g
	(-)	($x10^{-13}$ m^2s^{-1})	($x10^{-10}$ m^2s^{-1})	(-)	($x10^{-13}$ m^2s^{-1})	($x10^{-10}$ m^2s^{-1})
Benzene	120	0.6-0.8	0.07-0.10	150	0.5-0.8	0.08
Toluene	220	0.5-0.8	0.11-0.18	260	0.4-0.7	0.10-0.13
Ethylbenzene	425	0.5	0.21	485	0.3-0.5	0.15-0.24
m&p-Xylenes	430	0.5	0.22	495	0.3-0.5	0.19-0.25
o-Xylenes	400	0.5	0.20	440	0.3-0.5	0.13-0.22

Sorption and diffusion tests in both the dissolve and vapour states were also performed on the standard 0.53mm (20 mil) LLDPE geomembrane. The results for these parameters (S_{gf}, D_g and P_g) are presented in Table 4, below. The LLDPE geomembrane had a D_g range of 2-4 $x10^{-13}$ m^2s^{-1} for both the dissolved phase and vapour phases.

Table 4. Inferred partitioning, diffusion and permeation coefficients of standard LLDPE geomembrane from diffusion tests in the dissolved and vapour phases.

Contaminants	LLDPE Liquid Results			LLDPE Vapour Results		
	S_{gf}	D_g	P_g	S_{gf}	D_g	P_g
	(-)	($x10^{-13}$ m^2s^{-1})	($x10^{-10}$ m^2s^{-1})	(-)	($x10^{-13}$ m^2s^{-1})	($x10^{-10}$ m^2s^{-1})
Benzene	180	4.0	0.7	150	4.0	0.6
Toluene	350	3.0	1.1	300	2.5	0.8
Ethylbenzene	420	2.0	0.8	420	2.5	1.1
m&p-Xylenes	445	2.0	0.9	440	2.0	0.9
o-Xylenes	400	2.0	0.8	375	2.0	0.8

4.3 Permeation Coefficient Comparisons

As shown in Table 4, the standard LLDPE geomembrane has a permeation coefficient that ranges from 0.7-1.1 $x10^{-10}$ m^2s^{-1} for BTEXs contaminants in the dissolved phase and a similar range of 0.6-1.1 $x10^{-10}$ m^2s^{-1} for contaminants in the vapour phase. These permeation coefficients are low, meaning a standard LLDPE geomembrane could provide a reasonable barrier to VOC migration. It would be necessary to perform calculations to establish if the diffusive flux of VOCs through the GM is acceptable for the design purposes of each specific application.

The co-extruded LLDPE with a nylon barrier had a lower permeation coefficient range for both the dissolved phase (0.07-0.22 $x10^{-10}$ m^2s^{-1}) and vapour phase (0.08-0.25 $x10^{-10}$ m^2s^{-1}) than the standard LLDPE geomembrane. This is a 5-15 fold decrease in the P_g and S_{gf} values when compared with the standard geomembrane. Therefore, the co-extruded geomembrane would reduce the mass flux of VOC contaminants significantly, providing a better barrier. However, for engineering designs employing geomembranes, consideration should also be given to other factors such as physical properties, long-term performance and cost of each geomembrane.

5. CONCLUSIONS

Diffusion (D_g), partitioning (S_g) and permeation (P_g) coefficients were established for a relatively new co-extruded LLDPE geomembrane with an inner polyamide barrier and a standard LLDPE geomembrane in the dissolved and gaseous phases. P_g values for the 0.38mm (15 mil) co-extruded geomembrane were 0.07-0.22 x 10^{-10} m^2s^{-1} in the dissolved phase and 0.08-0.25 x 10^{-10} m^2s^{-1} in the vapour phase. P_g values for the LLDPE geomembrane were 0.7-1.1 x 10^{-10} m^2s^{-1} (dissolved phase) and 0.6-1.1 x 10^{-10} m^2s^{-1} (vapour phase). The nylon geomembrane showed a 5-15 fold decrease in

both the permeation and diffusion coefficients when compared to the standard LLDPE geomembrane. The co-extruded geomembrane reduced the mass flux of BTEX contaminants. Results from this study show that a co-extruded geomembranes could provide a better barrier to vapour and dissolved phase diffusive migration of VOCs than traditional LLDPE liners of similar thickness when used in containment and barrier systems.

AKNOWLEDGEMENTS

The authors would like to acknowledge the support of Raven Industries and the value of discussions with Mr. Gary Kolbasuk. The authors are also grateful to the Analytical Services Unit of Queen's University, Kingston, Canada for their support and use of their laboratory facilities.

REFERENCES

Aminabhavi, T.M., Naik, H.G., Donaldson, J. and Siebken, J.R. (1997). Chemical compatibility of geomembranes-sorption, diffusion and swelling phenomena. *Spe/Antec 1997 Proceedings: Plastics Saving Planet Earth,* 1649-1651.

D'Aniello, C., Guadagno, L., Gorrasi, G., and Vittoria, V. (2000). Influence of the crystallinity on the transport properties of isotactic polypropylene. *Polymer*, 41 (7): 2515-2519.

EPA. (2005). "Guidance for evaluating landfill gas emissions from closed or abandoned facilities." EPA-600/R-05/123a. U.S. Environmental Protection Agency, Office of Research and Development, Washington, DC, September.

Kolbasuk, Gary M. (1990). Coextruded HDPE/VLDPE multilayer geomembranes. *Proceedings of 4th GRI Seminar on Landfill Closures: Geosynthetics, Interface Friction & New Developments*, 228-238.

McCourt, M. P., McNally, G. M., Murphy, W. R. and McNally, T. (2000). The effect of fuel components and standard test fuels on the mechanical properties and glass transition temperatures of polymers used in multi-layer fuel line tubing. *Journal of Reinforced Plastics and Composites,* 19 (18): 1504.

McWatters, R. and Rowe R.K. (2007). Diffusive migration of volatile organic compounds through PVC geomembranes, Geosynthetics 2007, Proceedings Environmental Conference*,* Washington, 106-120.

Park, J. K., and Nibras, M. (1993). Mass flux of organic chemicals through polyethylene geomembranes. *Water Environment Research*, (65): 227-237.

Qian, X., Koerner, R.M., and Gray, D.H. (2001). *Geotechnical Aspects of Landfill Design and Construction*, Prentice Hall, New Jersey.

Reinhart, D.R., McCreanor, P.T., and Townsend, T.G. (1997). The bioreactor landfill: Its status and future. *Waste Management & Research* (20): 172-186.

Rowe, R.K. (1998). Geosynthetics and the minimization of contaminant migration through barrier systems beneath solid waste, Geotechnical Research Report GROT-2-98, Geotechnical Research Centre, University of Western Ontario, London, Ontario, Canada.

Rowe, R.K. and Booker, J.R. (2004). POLLUTE v.7- *1D Pollutant Migration Through a Non-Homogeneous Soil*, © 1983, 1990, 1994, 1997, 1998, 2004. Distributed by GAEA Environmental Engineering Ltd.

Rowe, R.K., Hrapovic, L and Kosaric, N., (1995). Diffusion of chloride and DCM through HDPE geomembranes, *Geosynthetics International*, 2 (3): 507-535.

Rowe, R.K., Hrapovic, L., Armstrong, M.D. (1996). Diffusion of organic pollutants through HDPE geomembranes and composite liners and its influence on groundwater quality. Geosynthetics: In: De Groot, DenHoedt, Termaat (Eds.), Applications, Designs and Construction, A.A. Balkema, Rotterdam, The Netherlands, 737-742.

Rowe, R.K., Quigley, R.M., Brachman, R.W.I., and Booker, J.R. (2004) *Barrier Systems for Waste Disposal Facilities*, E & FN Spon, London..

Sangam, H.P. (2001). Performance of HDPE Geomembrane Liners in Landfill Applications. Thesis for Doctor of Engineering Science, University of Western Ontario, London, Ontario, Canada.

Sangam, H. P. and Rowe, R. K. (2001). Migration of dilute aqueous organic pollutants through HDPE geomembranes. *Geotextiles and Geomembranes*, 19 (6): 329-357.

Produced Water Evaporation Ponds

N. Nowak, PE, Weaver Boos Consultants, Denver, Colorado, USA
J. Bradish, Danish Flats Environmental Services, Colorado Springs, Colorado, USA

ABSTRACT
The problem to be solved is the need to dispose of millions of gallons of production water (brine water) generated annually from the Rocky Mountain Region oil and gas industry in an environmentally safe, low cost, and efficient manner. A technology that is effective and safe is the evaporation of the water in lined containment ponds after separation and removal of the sludge component from the production water.

A project near Cisco, Utah was designed and constructed to evaporate production water in a series of lined ponds. The production water from oil and gas wells in the area is trucked to the site for disposal. The water is evaporated in ponds lined with high density polyethylene (HDPE) as the top layer by using a combination of factors that are favorable to the evaporative process, including the following:

- Natural characteristics of the site, including the arid climate, windy conditions, and numerous sunny days,
- The top liner in the ponds is black HDPE, which creates a hot surface, and
- The HDPE liner was used to protect the surface and ground waters of the area and to assist with the evaporation of the water (evaporation is enhanced due to the black color of the liner).

The project is interesting in that the facility provides oil and gas production companies in the area with a single large commercial alternative to production water disposal versus numerous small ponds that may service only one well pad, or expensive re-injection wells. The regulatory agencies like it for centralization and protection of the state's waters. The facility protects surface waters in the area due to the large capacity of the ponds, 2 feet of freeboard, and secondary containment in case of catastrophic failure.

1. INTRODUCTION

1.1 Project Location

The project is located in an arid region of eastern Utah in the area known as Danish Flat, which is situated at approximately 4,610 feet above mean sea level (amsl). The site is located in Grand County approximately 3.5 miles north of Interstate 70 interchange exit number 214, and approximately 43 miles west of the Utah-Colorado state line.

Background and Site Conditions

The ground surface is privately owned land primarily used for stock grazing and oil and gas transmission piping. No residences are located within 10 miles of the site. Access to the site is over unpaved roads used primarily for oil and gas vehicles.

Topography: The topography at the site slopes gradually from elevation 4615 ft amsl to 4600 ft amsl to the southeast. There are no major watercourses on the site.

Geology and Hydrology: The site is located in the Mancos Shale lowland area including the Greater Cisco area. The Mancos Shale Formation is the predominant outcrop in this area. Due to the preponderance of fine-grained sediments and water soluble minerals found in this formation, it does not usually contain any fresh water. Groundwater that comes in contact with the Mancos Shale Formation almost always contains high levels of dissolved solids. Groundwater is usually limited to alluvial deposits along streams and drainages or to sandstone units, some of which are very localized with low recharge rates. Wells in the area are usually drilled with air with little or no water encountered until the Dakota Formation is penetrated (Hunt et al. 1996).

The underlying Mancos shale is a dark grey to black soft shale with sandstone beds at various horizons. The maximum thickness of the Mancos shale is approximately 900 to 1,000 feet. The Mancos shale is considered a confining unit and is a thick barrier to vertical and lateral groundwater flow.

Below the Mancos shale is the lower to upper Cretaceous Dakota Sandstone, which are a yellow-brown and gray friable

to quartzitic sandstone and conglomerate sandstone and interbedded gray to black carbonaceous shale with occasional lenticular coal beds (Cashion et al. Map I-736). The Dakota Sandstone is considered to be the first aquifer in the area.

1.2 Climatological Data

According to the U.S. Department of Agriculture (USDA) Natural Resources Conservation Service (NRCS) map, the average annual precipitation is six inches. The climate survey for Cisco, UT (closest weather station to site) from 1952 to 1967 according to the Western Regional Climate Center (WRCC) is offered in the following table (re-created from WRCC information).

Table 1. Climate Survey

Parameter	Jan	Feb	Mar	Apr	May	Jun	Jul	Aug	Sep	Oct	Nov	Dec	Annual
Avg. Max Temp (F)	37.2	45.7	56.6	68.7	80.3	91.8	98.7	94.3	85.5	72.5	53.4	40.2	68.7
Avg. Min Temp (F)	8.8	17.7	24.0	33.5	43.7	52.1	60.7	58.4	47.3	35.2	22.5	12.5	34.7
Avg. Total Precip. (in.)	0.48	0.50	0.52	0.61	0.61	0.26	0.37	1.03	0.80	0.86	0.63	0.43	7.11
Avg. Total Snow (in.)	4.3	2.1	1.1	0.3	0.0	0.0	0.0	0.0	0.0	0.2	0.9	2.1	11.0

1.3 Design Evaporation Data

The National Weather Service developed an isopleths map of the Free Water Surface Evaporation (shallow lake evaporation) based on 24 years of data. The free water surface evaporation rate is the amount expected to evaporate from the disposal ponds, which is 50 inches per year. Approximately 35 inches of that rate occurs from May to October. The remaining 15 inches would evaporate from November to April. This is based on a water containment that is not lined with black HDPE.

2. PROJECT DETAILS

2.1 Purpose

The purpose of the project is to evaporate the production water as quickly as possible while maintaining environmental controls and containment.

The project was planned and built in order to service the oil and gas industry for the specific purpose of the disposal of production water from oil and gas production in the local area. Several produced water disposal options exist, including reinjection wells, frac injection, treatment for surface discharge, and evaporation. The evaporation technology was chosen for this project due to the ideal site conditions for evaporation, including low precipitation, windy conditions, high ambient temperatures and sun. Other factors that made the project site ideal include the following, no residences within 10 miles of the site, easy access to/from a major highway, long distance to open water at 7 miles, very deep groundwater, and Mancos Shale at 1,000 feet thick.

2.2 Selection of Technology

To enhance the evaporative quality of the project and to adequately contain the brine water, the top layer of the pond lining needs to be a durable long-lasting product that is cost-effective and helps to enhance evaporation while being acceptable to the regulatory agencies involved. Some of the liner technologies considered include compacted clay, geosynthetic clay liner (GCL), polyvinyl chloride (PVC), polypropylene (PPE), and high density polyethylene (HDPE). While several lining technologies exist and are allowed by the regulatory agencies, the HDPE liner was chosen for the top layer for several reasons, including, durability, resistance to ultraviolet degradation, chemical resistance, black color, and ease of construction.

The HDPE is designed to be the top layer of pond and be exposed to the elements (sun, freeze, and physical impact), therefore, the material needs to be resistant to UV degradation and be durable. The addition of the proper amount of high quality carbon black to the geomembrane during manufacturing is universally accepted as being resistant to significant deterioration caused by weathering. In addition to high quality carbon black, highly effective chemical UV

stabilizers further extend the life of the liner. These additives absorb incident radiation and/or terminate free radical production, thus protecting the HDPE against thermal degradation and possible chemical reactions with surrounding materials. Other factors that affect the potential UV resistance of a material include average density, density range or dispersion, chemical stabilizer system, catalyst type and amount of residue, copolymer type, combined chemical exposures, and failure criteria (GSE 2003). HDPE was chosen for this application due to these characteristics.

2.3 Implementation

To enhance the evaporative quality of the facility, and to adequately contain the brine water, high density polyethylene (HDPE) was chosen as the top layer. The liner was designed and constructed with 60-mil thick textured HDPE to help ensure a durable long-lasting containment. The liner was textured to increase the safety factor for personnel using the facility (i.e. the textured surface increases traction and gripping to enable easier egress in case of someone falling into the pond.

The facility was designed in 2007 and constructed in 2008, and consists of the following (refer to Figures 1 and 2 for details):

Access road and truck off-loading pad
Piping and valves
Acceptance Pits (vaults)
Sludge Pond covered with bird control netting
Evaporation ponds (each of 8 ponds at approx. 5 acres and 12 feet deep)

General: The facility plan view is shown on the attached drawings. The operation units include two sets of 14,000 gallon three-stage concrete receiving tanks, a sludge pond, and a series of eight five-acre evaporation ponds. All of the structures are connected via a gravity fed underground piping system.

Pond Inlet: All of the water flows through one of the three-stage concrete settling tank systems and the sludge pond before entering the evaporation ponds. The pre-treatment facilities and the evaporation ponds have been designed to follow the topography, allowing for gravity flow throughout the system. Shut-off valves have been installed on the crossover piping to allow for proper flow management. If necessary, portable gasoline powered pumps will be used to transfer liquid to ponds that are not in the gravity flow line or to empty a pond for maintenance or liner repair.

Slope Design: The sludge pond and evaporation ponds have an interior slope of 3 horizontal to 1 vertical, and a maximum exterior slope of 2 to 1. The HDPE chosen has a textured surface, which will increase the safety characteristics of the facility by making it easier to walk on, especially on the interior slopes.

Berm Design: Surface water will not be allowed to enter the ponds because of the constructed berms and the ditches. The interior berm walls will be covered with a protective layer of 60-mil high density polyethylene (HDPE). The HDPE will provide erosion control. The area between the evaporation ponds has been covered with HDPE to prevent erosion, control dust and enhance evaporation. The exterior sides of the berm have been seeded as necessary.

Leak Detection System: As described in the geology/hydrology section of this report, the site is underlain by approximately 1,200 feet of impermeable shale. The first aquifer is below the shale formation. The geological investigation did not detect perched groundwater. In addition to the ideal natural conditions, a 60-mil HDPE liner has been installed in all of the ponds. The pond floors slope toward a sump that is fitted with a monitoring pipe.

The leak detection system is inspected and data recorded on a weekly basis. A summary of the weekly inspections will be reported to the State of Utah on a quarterly basis. Liquid from the sump can be pumped back into the pond, if excessive amounts accumulate.

Livestock/Wildlife Protection Measures: The entire operations area around Phase 2 has been fenced and gated to help prevent cattle or other animals from entering. Since the sludge pond could have oily material on the surface, netting has been used to deter the entry of birds or other wildlife.

Capacity: The volume of water able to be stored for evaporation in each pond is nearly 240,000 barrels (at 42 gallons per barrel) for a total facility capacity of approximately 2,000,000 barrels.

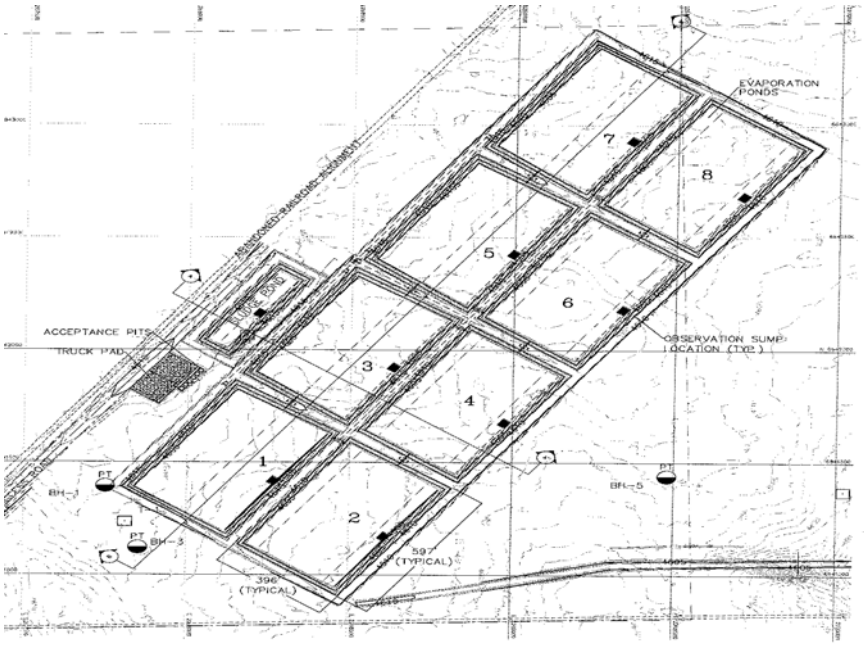

Figure 1 – Pond Facility Design Plan View

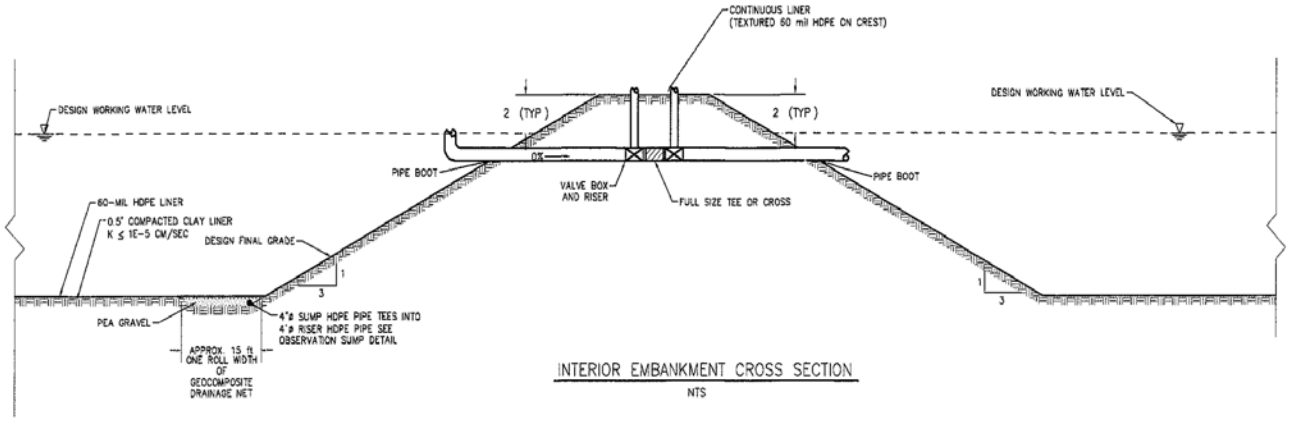

Figure 2 – Pond Liner Details

2.4 Aerial Photo of Completed Project

The completed and partially operation project was photographed from the air on July 22, 2008 and is shown below. The water was distributed from the sludge pond to the Ponds 1 through 4, which are shown in the foreground. The Ponds 5 through 8, shown in the background, were not yet approved for water disposal at the time of the photography, but have since been put into operation. Currently, all 8 evaporation ponds are operational.

2.5 Operational Data

The facility has experienced production water deliveries ranging from 10,000 barrels to 35,000 barrels per day. Each barrel is equal to 42 gallons. The water is moved from the off-loading area through the sludge pond and to the evaporation ponds by gravity. Each pond has a free board requirement of 2 feet.

When an individual evaporation pond was brought on-line, such as Ponds 5 through 8, and the water was allowed to flow into the empty pond lined with HDPE, the water was observed as “disappearing” due to the evaporative nature of the HDPE when in combination with the arid climate in Utah. In July and August the ambient air temperatures often exceeded 100 degrees Fahrenheit and the wind normally blew to some extent. The actual evaporation encountered during the months of July and August 2008 at the site was measured to be 15 inches and 18 inches, respectively. The facility operators are continuing to observe very favorable evaporation of the water in the 8 ponds and anticipate that the total evaporation for the year will exceed the estimate of 50 inches.

3. CONCLUSIONS

The use of HDPE as the primary liner in the ponds appears to be favorably enhancing the evaporation of the water. The estimate of 50 inches of evaporation per year will be far exceeded given the 33 inches of evaporation experienced in July and August 2008, only. The durability and resistance to UV degradation due to the proper amount of carbon black in the geomembrane and other factors as discussed above are the major reasons for the use of the HDPE geomembrane liner as the top layer. The increase with the rate of evaporation due to the black color of the HDPE has been a great benefit. A study was conducted on an HDPE liner installed in Colorado after 20 years of service where the liner was not buried and exposed to weathering, UV light and cooling tower blow-down water. The material was tested for various properties and was found to have no significant reduction in the primary physical properties of the HDPE (Ivy 2002).

ACKNOWLEDGEMENTS

Thank you to Danish Flats Environmental Services for allowing the use of their project in this paper. Also, I'd like to recognize Gerald Knudsen, PE of AgriTech who provided his engineering expertise, during the design.

REFERENCES

Cashion, W. B. *Geologic and Structure Map of the Grand Junction Quadrangle, Colorado and Utah, USGS Miscellaneous Geologic Investigations, Map I-736.*

Gundle/SLT Environmental, Inc. (GSE). (2003). *"Technical Note – HDPE, UV Resistance for GSE Geomembranes."* http://www.truslate.com/grid/techspec.pdf.

Hunt, G. L. (1996). Environmental Handbook, Environmental Regulations for the Oil & Gas Exploration and Production Industry.

Ivy, N (2002). HDPE geomembrane after 20 years of service, *GFR Magazine June/July 2002.*

Lining of Canals with Flexible HDPE Geomembrane – Successful Case History

M. Venkatraman, Geosynthetic Division, Garware-Wall Ropes Ltd., Pune, India
S. Murugesan, Geosynthetic Division, Garware-Wall Ropes Ltd., Pune, India

ABSTRACT
Water, becoming a scarce commodity, there is immediate need to conserve and utilize it effectively for every purpose. It is estimated that nearly 40 to 50% of water distributed through irrigation canals is lost due to percolation which in turn spoils the fertile lands by ponding, salinity of soil etc. Traditional rigid lining system using concrete/ tiles/ brick/stones, have limitations on controlling percolation, longevity etc. This has lead to the development of flexible lining systems using HDPE (High Density Polyethylene) Geomembranes. This paper presents successful case histories in India on lining of canals using HDPE Geomembrane. It was observed that it is very effective with 0% loss of water in the treated portion. This geosynthetics lining system is found to be more economical considering the life cycle cost of the project with benefit cost ratio of 3.5 to 3.7. This paper aims at promoting geosynthetic canal lining throughout India.

1. INTRODUCTION

1.1 Canal Lining

Big irrigation programs have been taken up in India to store and distribute the water for larger areas under cultivation. Such irrigation projects involve conveyance of large quantity of water through canals across various terrains to reach the cultivable land. While transmission of water through canals we encounter loss of water due to evaporation, seepage through canal bed etc. The seepage also leads to deposition of salts on the surface making the soil sterile and there by reducing the productivity of the adjoining agricultural land. In order to prevent seepage losses, a protective layer is provided over the inner surfaces of canal which is called canal lining. Besides minimizing the seepage losses, this lining also ensures the proper cross section of the canal and maintains the sufficient velocity of water in the canal giving optimum discharge. Conventional lining systems like Brick lining, concrete lining have shown loss of water through seepage up to 35-40% of the total discharge. As water is becoming more scare commodity the losses of water in the canal have to be effectively contained by suitable means which are more prone to seepage loss. Irrigation being one of the major consumers of water, the effective utilization of water here will result in tremendous savings in the form of direct cost or extended irrigable area. Hence there is need to find alternate solutions to minimize this seepage loss to maximum possible extent.

1.2 Geosynthetic Liners

In recent year, Geosynthetic products having unique interaction with soil and other earth materials are getting impetus in various construction activities of Civil Engineering works. Geomembrane is one of such products which is very efficient in performing as liquid barrier. They are widely applied as liquid curtains in many applications. Lining of canals with Geomembranes is one of the applications wherein this membrane is laid on the inner surfaces of the canal which will efficiently act as barrier in preventing the water loss through seepage.

Lining of the canals with synthetic planar materials started as early as 1950s as reported by Hickey (1969) where they used plastic films as canal liners for the rehabilitation of the old canals. The use of geosynthetics for lining of new canals started in 1960s as reported by Morrison and Starbuck (1984). Since then it was found that Geomembranes provided effective canal seepage control especially in areas where there are limited construction access, exposure to freeze/thaw cycling, remote construction locations, and cold weather construction etc. (Comer et al. 1996).

Bureau of Reclamation, U.S. Department of the interior compared three types of canal linings viz. concrete, exposed geomembrane, and concrete with geomembrane under liner by assessing the performance of 34 test sections after 1 to 10 years of its service (Jay and Jack 2002). It was concluded that the geomembrane under liner provides the water barrier and the concrete cover protects the geomembrane from mechanical damage and weathering. The system effectiveness is estimated at 95 percent. The irrigation district can readily maintain the concrete cover but does not have to maintain the geomembrane under liner. It was proved that the maintenance costs were relatively low for all the lining alternatives involving geomembranes for the study period of 10 years. Von Maubeuge (2000) has reported the use of needle punched geosynthetic clay liner (GCL) in a navigated waterway in the new turnout Eberswalde, Germany, as a canal liner. Based on the continuous monitoring of the liner they have proved the efficiency of the sealing system.

International Commission on Irrigation and Drainage (ICID) has come out with guidelines for the design aspects for the Use of Flexible Geomembranes for irrigation Canal and Reservoir Lining.

The advantages of using synthetic membranes in canal lining are,

1. Effectively act as barrier for the water loss through seepage.
2. The membrane is highly flexible that it can withstand stresses due to any differential settlement, thermal stresses, high hydraulic pressures etc.
3. The installation of the lining with membrane is simple and easier.
4. This improves canal hydraulics, equity and reliability of water distribution
5. As the water is prevented from reaching the canal bed it reduces water logging and salining the adjoining land when the canal is running full.
6. The membrane covers the inner surface of the canal completely. So there is no possibility of weed growth on the canal surface, which may impede the water flow.
7. Other benefits are prevention of canal erosion and piping through the under channel banks, promoting the movement of sediments rather than deposition, low maintenance and easy cleaning of canal etc.

2. GEOSYNTHETICS IN CANAL LINING

There are varieties of products that can be used as liner material for canals. Some of them are

1. Very Low Density Polyethylene (VLDPE)
2. Composites (geotextile/low density polyethylene (LDPE))
3. High Density Poly Ethylene (HDPE)
4. Geosynthetic Clay Liners (GCL)
5. Unreinforced Poly Propylene (PP)
6. Poly Vinyl Chloride (PVC)
7. Polyurethane Foam with or without coatings,
8. Synthetic Rubber etc.

Among these materials, HDPE membranes have been found to be most effective in acting as liquid barrier. Because of this it is being widely used for lining. High density Polyethylene material with semi-crystalline microstructure with anti-oxidant additives has the following additional benefits when used as membrane for canal lining.

1. It has got high strength to withstand any undue stresses caused due to displacements in the ground.
2. It possesses very good resistance to the degrading effects of ultra-violet light.
3. HDPE is highly inert to most of the chemicals expected in the ground conditions.
4. The coefficient of thermal expansion is very high that it can sustain wide range of temperatures
5. All the seams are made in-situ and tested for their leak proofing.
6. These membranes come under the name Geomembranes among the Geosynthetic family.

2.1 Method of Lining the Canal using the Geomembranes

Koerner (2005) has given some guidelines for the Lining the Canals using Geomembranes. When a geomembrane is used as a liner material, it is generally placed over previously placed geotextile on the prepared ground. On the top of the membrane a soil layer of uniform thickness is laid placed. In order to prevent the scouring of this soil cover and in turn the membranes (particularly the seams) it is not uncommon to cover the liner with concrete, RCC, shotcrete, asphalt etc. Figure 1. shows the schematic of the section illustrating the various layers in the Lining of Canal. The same has been shown in the photograph of Figure2.

2.2 Special Features of Canal Lining with Geomembranes

2.2.1 Cover Soil

A soil cover of 300 to 600 mm thick is required for the following reasons.

a. To hold the liner in place against tractive forces, Protect the liner from the UV radiation, Ozone, wind etc.,
b. To prevent the damage due to animals vandalism, water actions etc.

The soil cover material should be carefully chosen to avoid scouring due to the water movement in the canal.

2.2.2 Seam Joint Overlap

The geomembranes come in rolls and they are laid successively by unfurling the rolls. The successive membranes are joined by one of the following seaming methods.

1. Extrusion welding
2. Thermal fusion or melt bonding
3. Chemical seaming
4. Adhesive seaming.

In general the joints are made with welding process. In canal lining it should be intuitive that the overlaps for the joints should be placed down stream and should be relatively long around 250 to 300 mm.

2.2.3 Concrete Cover

It is recommended to provide a concrete cover over the geomembrane, preferably with a nonwoven geotextile layer intervening in between. This nonwoven geotextile will drain out any water that may seep through the concrete. The concrete is usually reinforced with welded mesh and the thickness of concrete shall be 150 mm.

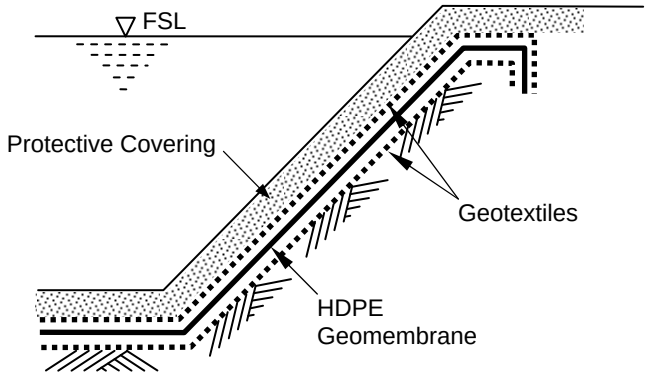

Figure 1. Typical cross section of the Canal Lining with Geomembrane and Geotextiles

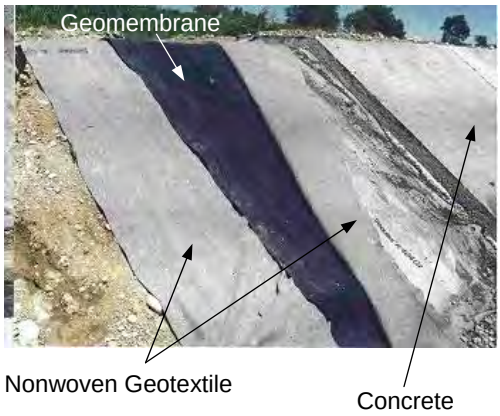

Figure 2. Photograph showing the section of Lining

2.3 Indian Scenario in Canal Lining using Geosynthetics

At the out set, the use of geomembranes for the canal lining is rapidly growing both for the new as well as remediation of the old canals around the world. In India there are lots of evidences of using geomembranes as barriers in land fills but the application in seepage controls for the water bound structures has not been familiarised. There is huge potential for the synthetic lining of canals as the government is planning for interlinking of various rivers. Natesan and Gopalakrishnan (2006) have reported the use of geomembrane for water proofing of the upstream side of the reservoir named Kadamparai dam in Tamil Nadu. Hence there is a great responsibility of the Geosynthetic Engineers in India to proliferate the use of Synthetic lining of canals owing to its efficient performance. This paper describes case histories on the successful implementation of the canal lining projects using Geomembranes in Rajkhat Canal Project in the state of Madhya Pradesh and DoodhGanga canal in Maharastra state in India.

3. CASE HISTORIES ON CANAL LINING IN INDIA

3.1 Rajghat Canal Irrigation Project for Water Resources Department, Dhatia, Madhya Pradesh, India.

This canal forms part of the Rajghat Irrigation Project in the state of Madhya Pradesh in India. The lining work was executed during January 2004 - March 2004. The membrane used was HDPE Geomembrane of Carbofol having 1mm thickness. The nonwoven Geotextile was of 1.8 mm thick and having 220 g/m^2. The quantity of Geomembrane used was around 3200 m^2. The case study is explained in the following sections chronologically.

3.1.1 Problem

Existing Canal Section proposed for the Rajghat Irrigation Project was constructed using LDPE (Low Density Polyethylene) film of 0.1 mm thick and Cement Concrete tiles. It was observed that this was not effective in preventing the seepage of flowing water. The water used for irrigation purposes were seeping through the base and flowing into the nearby creek.

3.1.2 Solution

To prevent the loss of water it was proposed to line the canal with HDPE (High Density Polyethylene) Geomembrane as it has been successfully used worldwide. Two critical sections of 70m lengths each were identified for the above application, with the total width of lining 24m. It was decided to use 1mm thick HDPE Geomembrane on the canal bed and the slopes, along with nonwoven Geotextile. Geomembranes of roll widths larger than 7 m was used. Seaming for the joints were done by Hot Wedge welding and Extrusion welding. Over the nonwoven geotextile M10 grade concrete with 40mm down grade aggregates, was laid cast-in-situ both on the bed and sides. The photographs taken during the installation of geomembrane is shown in Figure 3.

(a) Canal before the Installation of HDPE Lining

(b) Installation of HDPE Lining

(c) Seaming the membranes by extrusion welding

(d) Testing of seams with air pressure

Figure 3. Photographs showing the Installation and testing of HDPE Lining in Rajghat Canal

3.1.3 Current status

HDPE Geomembrane and Nonwoven Geotextile used in the two sections have successfully controlled the seepage which was proved by the nearby creek running dry. Following the success of this the authorities are planning to use this technique for balance stretch lengths of the canal. The performance of the membrane lining is continuously monitored to detect any the seepage for stretches of Geomembrane lined and unlined canals. Piezometers were installed in the locations of lining through pipes at the sides of canal. The pore water pressure was measured at regular intervals i.e. at different discharge levels of canal flow including the peak discharge. Results from the piezometers Monitoring have

shown that the Geomembrane lined stretches had zero leakages as compared to the unlined stretches, where some leakages were reported.

3.2 Doodhganga Canal project, Kohlapur, Maharashtra, India.

This canal flows from the Dhoodhganga Dam in Solankar near Kohlapur in the state of Maharastra, India. Total length of Doodhganga Right Bank Canal is 24 km. Out of this 11 km stretch was lined earlier with concrete and 13 km is unlined portion. The lining was executed for the Doodhganga Canal Irrigation Project by Doodhganga Canal Division, Maharashtra. The work was started since January 2006 and is still in progress.

3.2.1 Problem

The Doodhganga canal traverses along side a hill with valley on the other side which can be observed from the satellite imagery shown in Figure 4. A portion of the canal was lined with concrete earlier but it was observed that the concrete lining has failed completely leading to seepage losses. Seepage was not controlled which was reflected in the adjoining creek as it was always found water logged. The situation is depicted in the photographs given in Figure 5. The seeping water was also creating water ponds in the nearby villages at the base of the hill. The land in and around the villages was always marshy and wet. It was reported that losses of water was around 40% and the 30% is attributed due to seepage.

Figure 4. Satellite imagery showing the canal stretches

(b) Canal before Lining

(c) Canal before Lining

Figure 5. Photographs showing Dhoodhganga canal before Lining

3.2.2 Solution

Initially it was proposed to line the canal using Geosynthetics (geomembrane and geotextiles) for a stretch length of approximately 3.0 kms of concrete lined canal. The lining with HDPE Geomembrane sandwiched between two non-woven Geotextile layers was selected. HDPE membrane of carbofol type1 mm thick and the nonwoven geotextiles having a thickness of 2.2 mm with 250 g/m^2 was used in this project. The membrane lining was done both for the bottom side and the side slopes of the canal. Geomembranes of roll widths greater than 7 m was employed to minimise the joints in the lining. Figure 6 shows the geomembranes being laid and the Figure 6(a) shows the anchoring of the geosynthetic layers at the top of the canal. Seaming for the joints were done by Hot Wedge welding and Extrusion welding.

(a) Laying the Geotextiles

(b) Anchoring at top of the Canal

Figure 6. Photographs showing the Installation of HDPE Lining in Dhoodhganga Canal

Firstly the damaged concrete was repaired and then the HDPE Geomembrane and Nonwoven Geotextile layers were laid. Above the geosynthetic layers a concrete cover of 75 mm thick was laid as a protective layer. This concrete is of M10 grade cast-in-situ with 40mm down grade aggregates laid over the Geotextile both on the bed and the side slope. The total consumption of the geomembrane was 66,000 m^2 and that of Nonwoven Geotextile was around 1,32,000 m^2. The geosynthetic layers are properly anchored at the top of the canal to prevent any sliding along the slope.

3.2.3 Current status

Presently the stretches where the HDPE Geomembrane and Nonwoven Geotextile were installed showed no signs of any seepage /leakage. This was reflected in the nearby creek which was found dry after the lining with Geomembrane. Due to the membrane lining the canal could serve an additional 185 Hectares of land for irrigation.

3.2.4 Cost Benefit Analysis

Though the initial cost of the project with geomembrane lining was higher than that of the conventional methods, the other benefits such as less maintenance, extended land irrigation etc. would lead to over all economy in the project. A detailed const analysis was carried our forecasting all the benefits and the abstract of which is given in the form of flow chart in Figure 7 which is self explanatory.

4. CONCLUSIONS

In recent years as the water is becoming more and more precious and scarce commodity, prevention of all kinds of losses of water is essential. One of the major losses of water is through seepage in the water management structures. Hence lining those structures with suitable barriers to preclude seepage is the need of the hour for water conservation.

Based on the experience world wide, lining of water bodies including canals with geomembranes have been found to be more efficient in nullifying the seepage losses through the bed. Nevertheless in India such a fast development is not taking place due to the higher initial costs. This paper present two successful case histories (One at Rajkhat in the state of Madhya Pradesh and the anther near Kohlapur in Maharastra) on the lining of canals with Geomembranes and demonstrates the benefits thereafter. It is well proved through these case studies that lining the canal with geomembranes bring in lots of other benefits that will lead to overall cost saving. As India is blessed with more rivers and agriculture being one of the most important professions, there is great responsibility for the Civil Engineers to proliferate this technique throughout India.

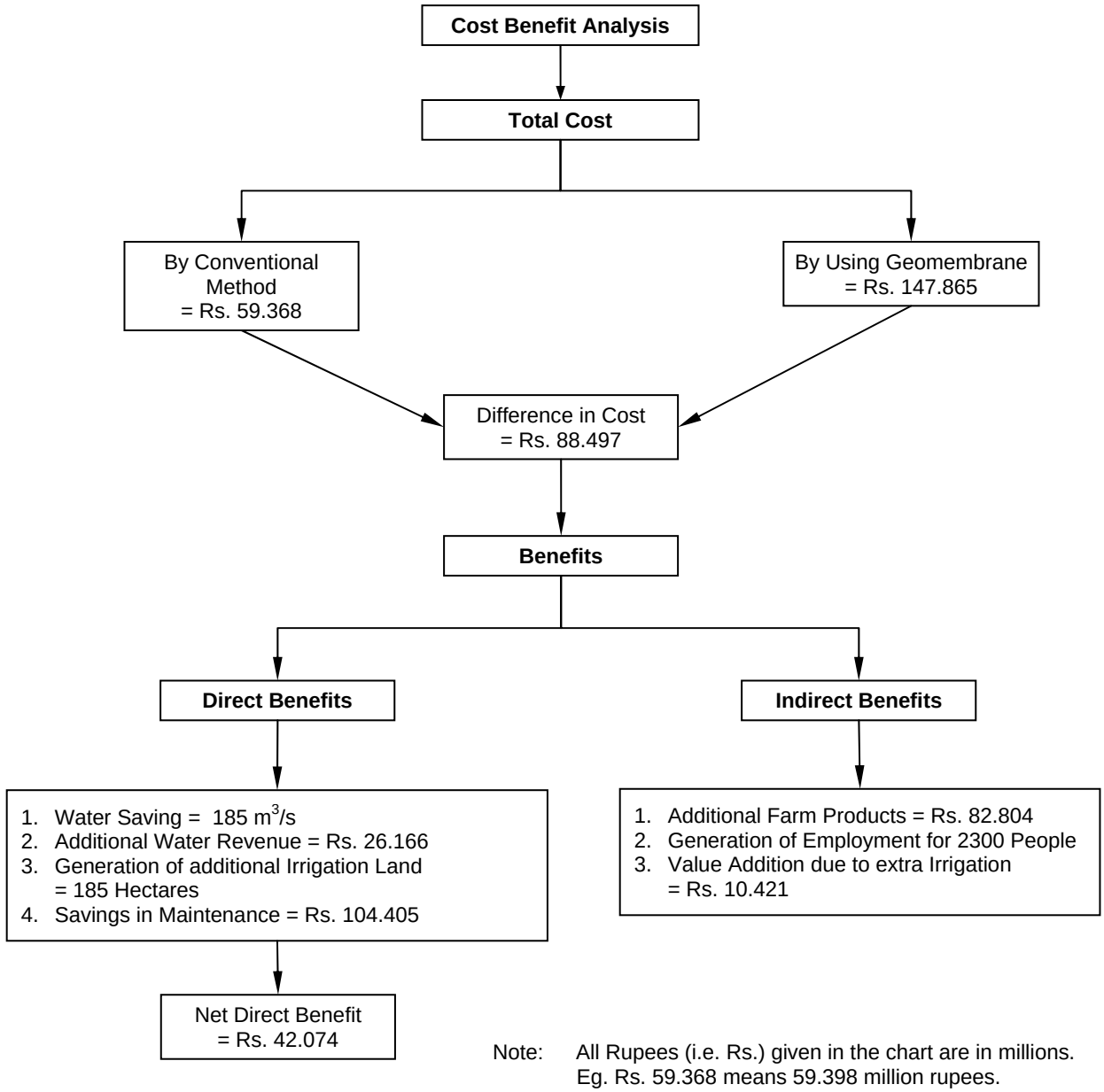

Figure 7. Flow chart showing the Cost Benefits of Geomembrane Lining in Doodhganga Canal.

REFERENCES

Comer, A.I., Kube, M. and Sayer, K. (1996) Remediation of Existing Canal Linings. *Geotextiles and Geomembranes, Elsevier,* Vol.14, pp 313-325.

Hickey, M. E. (1969) Investigations of plastic films for canal linings. Reclamation Research report no. 19, A Water Resources Technical Publication.

Jay, S. and Jack H. (2002) Canal-Lining Demonstration Project Year 10 Final Report. U.S. Department of the Interior Bureau of Reclamation

Koerner, R.M. (2005) Designing with Geosynthetics. *Pearson Printice Hall, Upper Saddle River, New Jersey* – 07458.

lCID GUIDELINE 108 Use of Flexible Geomembranes for lrrigation Canal and Reservoir Lining. *Internatlonal Commission on lrrigation and Drainage.*

Morrison, W.R. and Starbuck, J.G. (1984) Performance of plastic canal linings. *Bureau of Reclamation report REC-ERC-*84-1.

Natesan, K.G. and Gopalakrishnan, V. (2006) Geo-membrane water proofing on the upstream face of Kadamparai Dam. *Geosynthetics – Recent Developments*. pp 179 – 186.

Von Maubeuge, K.P., Witte, J. and Heibaum, M. (2000) Installation and monitoring of a geosyntehtic clay liner as a canal liner in a major waterway. Geotextiles and Geomembranes, Technical note, Vol. 18, pp 263-271

Geomembranes for Canal Lining

T.D. Stark and J.M. Hynes, University of Illinois, Urbana, Illinois, USA

ABSTRACT
Geomembranes are commonly used to control seepage from water canals. There are many types of geomembranes available for this application including PVC, HDPE, LDPE, CSPE, and EPDM geomembranes. Frequently these geomembranes require protection and there are several protection options including compacted soil, concrete, or shotcrete. The U.S. Bureau of Reclamation (USBR) has conducted a number of test programs on canal-lining systems including the Deschutes Canal-Lining Demonstration Project which involves the performance of 34 canal test-sections, many of which utilize geomembranes. Based on USBR and other test programs this paper examines the effectiveness of different types of geomembrane-based canal lining systems in terms of cost, seepage/leakage reduction, and long-term durability. Comparisons are made between the types of geomembrane used as well as the type of protective covering used (if any).

1. INTRODUCTION

Geomembranes have been used as water canal liners to control seepage since the 1950's and are an effective alternative to more traditional lining methods, such as concrete and compacted soil. One of the first uses of a geomembrane for a water canal was in 1954 for a U.S. Bureau of Reclamation (USBR) irrigation canal near Fort Collins, Colorado. The flexibility of geomembranes allows them to conform to the canal subgrade without puncturing and to adapt to subgrade changes with time. Geomembranes are also less pervious than concrete and compacted soil allowing for less loss of water over time. However, geomembranes are susceptible to damage from environmental and mechanical factors so various protective coverings have been used. Mechanical damage means damage to the geomembrane caused by people, animals, and/or equipment, whereas environmental damage refers to ultraviolet, wind, precipitation, etc. damage.

The USBR has extensive experience in the installation and monitoring of geomembranes for canal liners based on field test programs. The first such test program was started with a PVC test section on the Shoshone Project in Wyoming in 1957 (Morrison and Comer 1995). The USBR installed geomembrane linings in other canals and in 1991 began a canal-lining demonstration project on various canals branching from the Deschutes River (Haynes and Swihart 2002). The Deschutes Canal-Lining Demonstration Project is comprised of 34 test sections in Oregon, Idaho, Montana, and Oklahoma and was initiated to evaluate the effectiveness of a range of canal lining alternatives.

Traditionally, PVC geomembranes have been the geomembrane used for canal-lining projects. However, recently polyethylene (PE) based geomembranes (HDPE, LDPE, CSPE and VLDPE) as well as several other types of geomembranes (e.g. EDPM and polypropylene) have been used as canal liners.

All geomembranes are susceptible to damage from sun, wind, wave action, vegetation roots, and animal traffic, and thus must be protected. The most traditional method of protecting a geomembrane is to cover it with compacted soil. Another method is to cover the liner with concrete or shotcrete. The last option is to not protect the geomembrane and leave it exposed. Such exposed geomembranes may require special treatment and consideration to prevent damage.

This paper uses the Deschutes and other canal lining projects to examine the effectiveness of different geomembrane-based canal liners and protective liner systems based on cost, amount of seepage/leakage reduction, and long-term durability.

2. CASE HISTORIES

Tables 1 and 2 present the thickness, type of geomembrane installed, estimated cost (if available), seepage/leakage reduction due to the lining system, long-term durability, as well as references for the case history. The following paragraphs summarize the pertinent information for each of the case histories.

Table 1 – Summary of PVC and Polyethylene (PE) Canal Lining Case Histories

ID No.	Location/Section	Material	Date Installed	Cost (per m^2)	Seepage (m^3/m^2-day) [Reduction]	Status	Reference
PVC-1	Arnold Canal Section A-4	Exposed 0.75 mm PVC w/ geotextile UV cover	Mar-92	$11.30	0.012 [96%] in 1998	2002 - Some stiffening and cracking. Some seams above water table are separated.	Swihart and Haynes (2002)
PVC-2	Arnold Canal Section A-7	1.0 mm PVC w/ 3" grout filled mattress	Nov-91	$27.30	0.015 [95%] in 1998	2002 - A few small holes in mattress. Overall excellent	Swihart and Haynes
PVC-3	Helena Valley Canal	0.25 mm PVC w/ sand and gravel cover	1968	N/A	0.015 in 1983	1989 - Very good performance, some damage from animal hoves. 50% loss in plasticizer	Morrison and Comer (1995)
PVC-4	East Bench Canal	0.25 mm PVC w/ soil cover	1969	N/A	0.015 in 1974	1984 - Shows stiffening and 40% loss in plasticizer	Morrison and Comer
PVC-5	Bugg Lateral	0.25 mm PVC w/ soil cover	1961	N/A	N/A	1980 - Some stiffening and root penetration damage and 40% loss in plasticizer	Morrison and Comer (1995)
PVC-6	Main Canal	0.20 mm PVC w/ soil cover	1959	N/A	N/A	1991 - Significant stiffening has occurred. Field reports indicate still providing satisfactory seepage	Morrison and Comer (1995)
PVC-7	Fivemile Lateral	0.25 mm PVC w/ soil cover	1978	N/A	0.002 in 1983	1985 - Some small mechanical tears and holes. 12-30% plasticizer	Morrison and Comer
PVC-8	Black Sea Canal Section 1	0.25 mm PVC w/ sand and gravel cover	1977	N/A	[60%] in1978	1979 - Some soil sloughing	Timblin et al. (1984)
PVC-9	Black Sea Canal Section 2	0.25 mm PVC w/ concrete cover	1977	N/A	[81%] in 1978	1979 - Minor hairline cracking	Timblin et al. (1984)
PVC-10	Black Sea Canal Section 3	0.25 mm PVC w/ shotcrete cover	1977	N/A	[70%] in 1978	1979 - Some shrinkage cracking	Timblin et al. (1984)
PVC-11	Coachella Canal	0.75 mm PVC w/ concrete cover	1989	N/A	0.003 [98%] in 1994	1994 - No major problems	Kepler and Comer
PE-1	Arnold Canal Section A-1	0.10 mm PE geocomposite liner w/ shotcrete cover	Feb-92	$26.20	0.015 [95%] in 1997	2002 - Some small holes in shotcrete	Swihart and Haynes (2002)
PE-2	Arnold Canal Section A-2	0.75 mm textured VLDPE w/ 540 g/m^2 geotextile cushion	Oct-92	$27.10	0.034 [89%] in 1993	2002 - Only minor cracking found	Swihart and Haynes (2002)
PE-3	Arnold Canal Section A-3	Exposed 2.0 mm textured HDPE	Oct-92	$14.90	0.030 [90%] in 1997	2002 -Moderate stiifening and some small tears.	Swihart and Haynes
PE-4	Arnold Canal Section A-9	Exposed 1.5 mm VLDPE w/ 405 g/m^2 geotextile cushion	Nov-92	$19.30	0.021 [93%] in 1993	1995 - Removed from study due to whales in liner	Swihart and Haynes (2002)
PE-5	Arnold Canal Section A-10	Exposed 1.5 mm HDPE w/ 405 g/m^2 geotextile cushion	Nov-92	$19.30	0.021 [93%] in 1994	1995 - Removed from study due to whales in liner	Swihart and Haynes (2002)
PE-6	Ochoco Main Canal Section O-	Exposed 0.75 mm LLDPE	Nov-99	$8.40	0.003 [99%] in 2001	2002 - A few small tears from animal traffic	Swihart and Haynes
PE-7	Buffalo Rapids Section BU-1	Exposed 1.5 mm textured white HDPE w/ 338 g/m^2 Geotextile cushion	Apr-07	$13.60	N/A	2002 - Minimal problems	Swihart and Haynes (2002)
PE-8	South Canal Belle Fourche	0.75 mm VLDE w/ soil cover	Apr-87	N/A	N/A	1992 - No problems	Morrison and Comer
PE-9	Black Sea Canal Section 4	0.25 mm PE w/soil cover	1977	N/A	[30%] in1978	1979 - Some soil sloughing	Timblin et al. (1984)
PE-10	Black Sea Canal Section 5	0.25 mm PE w/ concrete cover	1977	N/A	[80%] in 1978	1979 - Minor hairline cracking	Timblin et al. (1984)
PE-11	Toshka Canal	1.5 mm textured HDPE w/ concrete	2003	N/A	N/A	2005 - No problems	Yazdani (2005)

Table 2 – Summary of Other Canal Lining Case Histories

ID No.	Location/Section	Material	Date Installed	Cost (per m^2)	Seepage (m^3/m^2-day) [Reduction]	Status	Reference
HYP-1	Arnold Canal Section A-5	Exposed 1.1 mm Hypalon w/ 540 g/m^2 geotextile cushion	Mar-92	$11.90	0.012 [96%] in 1998	2002 - Numerous large L-shaped tears	Swihart and Haynes (2002)
HYP-2	Arnold Canal Section A-6	Exposed 1.1 mm Hypalon w/ 270 g/m^2 geotextile cushion	Mar-92	$11.10	0.012 [96%] in 1999	2002 - Numerous large L-shaped tears	Swihart and Haynes (2002)
SPF-1	North Unit Canal Section NU-1	Spray-applied Polyurethane Foam (SPF) w/ Futura 500/550 Coating	Oct-92	$46.60	N/A	1998 - Half of the foam had washed out. Removed from study	Swihart and Haynes (2002)
SPF-2	North Unit Canal Section NU-2	SPF w/ Geothane 5020 Coating	Oct-92	$42.20	N/A	1998 - Half of the foam had washed out. Removed from study	Swihart and Haynes (2002)
SAG-1	North Unit Canal Section NU-3	Geoxtile w/ Spray-applied Geothane 5020 membrane	Oct-92	$14.90	N/A	Complete failure after first filling	Swihart and Haynes (2002)
SAG-2	North Unit Canal Section NU-4	Geoxtile w/ Spray-applied Geothane 5020 membrane	Oct-92	$19.30	N/A	Complete failure after first filling	Swihart and Haynes (2002)
GCL-1	Ochoco Main Canal Section O-1	Soil Covered Bentomat GCL	Apr-99	$8.83	0.033 [89%] in 2001	2002 - No problems	Swihart and Haynes (2002)
GCL-2	Ochoco Main Canal Section O-2	Exposed Bentomat GCL	Apr-99	$8.18	0.024 [92%] in 2001	2002 - Some crackng above waterline	Swihart and Haynes (2002)
GCL-3	Eberswalde Turnout	Riprap covered GCL	1997	N/A	N/A	2000 - No major problems	von Maubeuge et al. (2000)
EPDM-1	Ochoco Main Canal Section O-3	Exposed 1.1 mm EPDM w/ geotextile cushion on side slopes and soil on invert	Nov-99	$9.15	0.003 [99%] in 2001	2002 - No problems	Swihart and Haynes (2002)
EBG -1	Ochoco Main Canal Section O-5	Exposed 4.0 mm Coletanche NTP 2 ES elasometric bitumen geomembrane	Nov-00	$16.30	0.003 [99%] in 2001	2002 - No problems	Swihart and Haynes (2002)
EBG -2	Lugert-Altus West Canal Section LA-1	Exposed 4.0 mm Teranap elasometric bitumen geomembrane	May-94	$14.70	0.0 [100%] in 2002	2002 - Minor aligator cracking	Swihart and Haynes (2002)
EBG -3	Juniper Flat Main Ditch Section J-1	Exposed 4.0 mm Teranap elasometric bitumen geomembrane	Oct-97	$14.50	N/A	2002 - Minimal alligator cracking, several puntures from cow hooves	Swihart and Haynes (2002)

2.1 Canal Lining Projects

The following section provides background information on some of the larger canal test sections investigated during this study. Because of space constraints of all the test sections cannot be described.

2.1.1 Arnold Irrigation District – Main Canal – Bend, Oregon

The Arnold Main Canal is located several miles south of Bend, OR and diverts water from the Deschutes River about 11 km to the east. On average the canal is 20 m wide, 3 m deep, and has a flow capacity of about 4 m^3/s. The subgrade along the Arnold Canal consists primarily of fractured basaltic rock and a sandy-silty sediment. Subgrade preparation before geomembrane installation included the removal of loose rocks, boulders, and overhangs. Certain sections of the canal were also covered with 2 to 5 cm of soil. Canal-lining systems installed along the Arnold Canal include a 0.10 mm thick polyethylene (PE) geomembrane with a shotcrete cover, a 0.75 mm thick VLDPE geomembrane with a shotcrete cover, an exposed 2.0 mm thick HDPE geomembrane, an exposed 0.25 mm thick PVC geomembrane, a 1.0 mm thick PVC geomembrane with a grout mattress cover, and exposed 1.5 mm thick HDPE and VLDPE geomembranes. In short, a variety of geomembranes were tested in a similar environment which provides for a meaningful comparison of effectiveness and durability which is shown in Table 3. Table 3 shows PVC-1, PE-2, PE-4, PE-5, HYP-1, and HYP-2 are various geomembranes with only a geotextile as a protective cover or cushion. All of the geomembranes with a geotextile cover or cushion exhibit adequate seepage reduction, i.e. greater than 90%, but of these geomembranes only PVC-1 and PE-2 exhibited “good” long-term performance after 10 years of service although at different costs. The performance rating system is described subsequently.

Interestingly, PE-4 and PE-5 are 1.5 mm thick VLDPE and exhibited poor performance after 3 years while PE-2 is only 0.75 mm thick VLDPE and exhibited good performance after 10 years. Thus there may be variability in the performance of VLDPE canal lining systems. In addition, the two hypalon (CSPE) test sections did not perform well because their rating is “fair” after 10 years of service. PVC-2 and PE-1 both exhibited good long-term performance because they were protected with a concrete mattress and shotcrete, respectively.

Table 3 – Arnold Irrigation District Geomembrane Canal Lining Systems

ID No.	Thickness	Material	Cost (per m^2)	Seepage Reduction (%)	Rating at Time of Last Inspection	Service Life at Time of Last Inspection
PVC-1	0.75 mm	PVC w/ geotextile UV cover	$11.30	96%	Good	10 yr
PE-1	0.10 mm	PE geocomposite liner w/ shotcrete cover	$26.20	95%	Good	10 yr
PVC-2	1.0 mm	PVC w/ 3" grout filled mattress	$27.30	95%	Good	10 yr
PE-3	2.0 mm	Textured HDPE	$14.90	90%	Good	10 yr
PE-2	0.75 mm	VLDPE w/ 540 g/m^2 geotextile cushion	$27.10	90%	Good	10 yr
HYP-1	1.1 mm	Hypalon w/ 540 g/m^2 geotextile cushion	$11.90	96%	Fair	10 yr
HYP-2	1.1 mm	Hypalon w/ 270 g/m^2 geotextile cushion	$11.10	96%	Fair	10 yr
PE-4	1.5 mm	VLDPE w/ 405 g/m^2 geotextile cushion	$19.30	93%	Poor	3 yr
PE-5	1.5 mm	VLDPE w/ 405 g/m^2 geotextile cushion	$19.30	93%	Poor	3 yr

2.1.2 Black Sea Canal – Romania

The Black Sea Canal is located in Eastern Romania. These test sections are part of a US – USSR joint study on Plastic Films and Stabilizers. On average the canal is 12 m wide, 2 m deep with 2H:1V side slopes. The test sections installed are a 0.25 mm thick PVC geomembrane with soil, concrete, and shotcrete covers, and a 0.25 mm thick PE geomembrane with soil and shotcrete covers (Timblin et al. 1984).

2.1.3 Toshka Canal – Egypt

The Toshka Canal is located South Valley of Egypt and diverts water from Lake Nasser to the Western Desert. The canal is 30 m wide, 8 m deep with 2H:1V side slopes. The typical flow in the Toshka Canal is about 100 m^3/s. Starting in 2003, as part of the South Valley Project, the Golden Trade Company of Cairo began installing a 1.5 mm thick textured HDPE liner protected by 100 mm of soil-cement mixture and 200 mm of concrete (Yazdani, 2005).

2.1.4 Eberswalde Turnout – Germany

The Eberswalde Turnout is a boat turning basin located near the town of Eberswalde, Germany. The canal is 48 m wide, 4 m deep with 3H:1V side slopes. The canal was lined in 1997 with a needle-punched GCL protected by a sandmat and a 300 mm thick layer of riprap. All installation was performed without dewatering the canal (von Maubeuge et al. 2000).

3. COMPARISON OF CANAL LINING SYSTEMS

Tables 4 through 6 present a comparison of the geomembranes and protective systems collected and studied herein. The geomembrane based liner systems are divided into the following three groups:

1.) Concrete/shotcrete covered geomembranes – Liner systems that incorporate a concrete or shotcrete layer over the geomembrane for environmental and physical protection (see Table 4).

2.) Exposed geomembranes – Liner systems in which the geomembrane is left exposed without any protective cover (see Table 5).

3.) Soil covered – Liner systems where a layer of compacted soil is placed over the geomembrane for environmental and physical protection (see Table 6).

The performance rating for each system describes the condition of the geomembrane at the time of its last inspection. This geomembrane rating is independent of cost, seepage reduction, and time of last inspection. The rating system is as follows:

1.) Good – Geomembrane is still in good to excellent condition. Little maintenance has been required to date and the geomembrane is still of high quality.

2.) Fair – Geomembrane is in adequate condition. Some maintenance has been required to date because the geomembrane has experienced tears, punctures, or signs of significant stiffening.

3.) Poor – Geomembrane is in poor condition. Major repairs have been required to date, or the liner completely failed and/or was taken out of service.

The following paragraphs compare the performance of different geomembrane based lining systems shown in Tables 4 through 6 based on type of geomembrane, protective layer over the geomembrane, cost, seepage/leakage reduction, and long-term durability.

Table 4 - Concrete/Shotcrete Covered Geomembrane Canal Lining Systems

ID No.	Thickness	Material	Cost (per m^2)	Seepage Reduction (%)	Geomembrane Rating at Time of Last Inspection	Service Life at Time of Last Inspection
PE-1	0.10 mm	PE geocomposite liner w/ shotcrete cover	$26.20	95%	Good	10 yr
PVC-9	0.25 mm	PVC w/ concrete cover	N/A	81%	Good	1 yr
PVC-10	0.25 mm	PVC w/ shotcrete cover	N/A	70%	Good	1 yr
PE-10	0.25 mm	PE w/ concrete cover	N/A	80%	Good	1 yr
PE-2	0.75 mm	VLDPE w/ 540 g/m^2 geotextile cushion	$27.10	90%	Good	10 yr
PVC-11	0.75 mm	PVC w/ concrete cover	N/A	98%	Good	5 yr
PVC-2	1.0 mm	PVC w/ 3" grout filled mattress	$27.30	95%	Good	10 yr
PE-11	1.5 mm	PE w/ concrete cover	N/A	N/A	Good	2 yr

Table 5 – Exposed Geomembrane Canal Lining Systems

ID No.	Thickness	Material	Cost (per m^2)	Seepage Reduction (%)	Geomembrane Rating at Time of Last Inspection	Service Life at Time of Last Inspection
PVC-1	0.75 mm	PVC w/ geotextile UV cover	$11.30	96%	Good	10 yr
PE-6	0.75 mm	LLDPE	$8.40	99%	Good	2 yr
HYP-1	1.1 mm	Hypalon w/ 540 g/m^2 geotextile cushion	$11.90	96%	Fair	10 yr
HYP-2	1.1 mm	Hypalon w/ 270 g/m^2 geotextile cushion	$11.10	96%	Fair	10 yr
EPDM-1	1.1 mm	EPDM w/ geotextile cushion on side slopes and soil on	$9.15	99%	Good	3 yr
SPF-1	1.25 mm	SPF w/ Futura 500/550 Coating	$46.60	N/A	Poor	5 yr
SPF-2	1.25 mm	SPF w/ Geothane 5020 Coating	$42.20	N/A	Poor	5 yr
PE-4	1.5 mm	VLDPE w/ 405 g/m^2 geotextile cushion	$19.30	93%	Poor	3 yr
PE-5	1.5 mm	HDPE w/ 405 g/m^2 geotextile cushion	$19.30	93%	Poor	3 yr
PE-7	1.5 mm	Textured white HDPE w/ 338 g/m^2 Geotextile cushion	$13.60	N/A	Good	1 yr
SAG-1	1.5 mm	Geoxtile w/ Spray-applied Geothane 5020 membrane	$14.90	N/A	Poor	1st Filling
SAG-2	1.5 mm	Geoxtile w/ Spray-applied Geothane 5020 membrane	$14.30	N/A	Poor	1st Filling
PE-3	2.0 mm	Textured HDPE	$14.90	90%	Good	10 yr
EBG -1	4.0 mm	Coletanche NTP 2 ES elasometric bitumen geomembrane	$16.30	99%	Good	2 yr
EBG -2	4.0 mm	Teranap elasometric bitumen geomembrane	$14.70	100%	Good	8 yr
EBG -3	4.0 mm	Teranap elasometric bitumen geomembrane	$14.50	N/A	Good	5 yr
GCL-2	N/A	Bentomat GCL	$8.18	92%	Good	3 yr

Table 6 – Soil Covered Geomembrane Canal Lining Systems

ID No.	Thickness	Material	Cost (per m^2)	Seepage Reduction (%)	Geomembrane Rating at Time of Last Inspection	Service Life at Time of Last Inspection
PVC-6	0.20 mm	PVC	N/A	N/A	Fair	21 yr
PVC-4	0.25 mm	PVC	N/A	N/A	Good	14 yr
PVC-5	0.25 mm	PVC	N/A	N/A	Fair	19 yr
PVC-8	0.25 mm	PVC	N/A	60%	Good	1 yr
PE-8	0.25 mm	PE	N/A	30%	Good	1 yr
PVC-7	0.25 mm	PVC	N/A	N/A	Good	15 yr
PE-9	0.75 mm	VLDPE	N/A	N/A	Good	15 yr
GCL-1	N/A	Bentomat GCL	$8.83	89%	Good	3 yr
GCL-3	N/A	GCL w/ Riprap cover	N/A	N/A	Good	3 yr

3.1 Type of Geomembrane

Figures 1 and 2 present the ranges in cost and seepage reduction percentage, respectively, for the exposed geomembranes examined herein. The range in cost for exposed geomembranes is significant because it reflects the installed cost of the geomembrane because no protective layer is used. Figure 1 shows a large cost range for PE geomembranes which reflects the use of different geomembrane thicknesses. Figure 1 also shows the geomembranes with the lowest cost are EPDM and PVC with Hypalon being slightly higher. Figure 2 shows the highest seepage reduction for EPDM and bitumen lining systems. The PE geomembranes show a range in seepage reduction from 90% to 99% while PVC and Hypalon show a similar reduction (~96%) for the cases considered. In summary, all of the geomembranes show a high percentage (≥90%) of seepage reduction.

Figure 3 shows the range of service life for the exposed geomembranes considered herein. The points labeled lower bound (solid triangles) represent the longest service life reported for which the type of geomembrane was rated good. Thus, the lower bound values represent a minimum service life because they are still performing well and the service life is controlled by the length of the study. The points labeled upper bound (solid circles) represent the service life reported at which the geomembrane was rated fair or poor because the geomembrane was already performing fair or poorly at the time. Figure 3 shows that PVC and PE geomembranes have the highest upper bound service lives. However, two of the PE cases examined have a lower bound service life of only three years. EPDM and bitumen geomembranes have upper bound service lives of three and eight years, respectively, but these durations could be greater if the geomembranes continue to perform adequately as the study continues.

In summary, PVC and PE are the two most commonly used geomembranes for canal liners and thus have been in service the longest. The data herein suggest no significant difference between these two materials in terms of leakage reduction (>90%) or durability. For comparison purposes, concrete and shotcrete liners provide a seepage reduction of only about 70% (Swihart and Haynes 2002). PVC geomembranes have shown excellent long-term durability with an exposed service life of 10 years with a good rating for an exposed 0.75 PVC mm thick liner. PE geomembranes have also shown good durability including a 10 year old, 2 mm thick textured HDPE liner in an exposed application. However, the PVC geomembranes generally range in thickness from 0.25 mm to 0.75 mm, whereas the PE geomembranes generally range from 0.75 mm to 2 mm thick for canal linings. An increase in thickness generally results in an increase in durability and cost, but does not result in a reduction of the water seepage/leakage from the canal.

Four cases where spray-applied geomembranes were used as canal liners were also evaluated. In each of these cases, the spray-applied geomembrane was washed out of the canal within five years. Installation of the spray-applied membranes also was more expensive than conventional geomembranes. Thus, spray-applied geomembranes do not appear to be viable for canal linings.

Other geomembranes examined are Hypalon, EPDM, and elasometric bitumen for exposed canal linings. Both Hypalon geomembrane installations developed large L-shaped tears during the first 10 years of service. The Hypalon liners were used in an exposed application which contributed to the decrease in service life. The EPDM geomembrane provided excellent seepage reduction and has exhibited few problems in 3 years of service in an exposed application. The three elasometric bitumen geomembrane showed only minor alligator cracking after 3, 5, and 8 years of exposed service and show a reduction in seepage of 99% and 100% from the pre-liner seepage. In summary, the EPDM and bitumen liners show promise as canal liners but have not been subjected to exposure times as long as PVC and PE geomembranes.

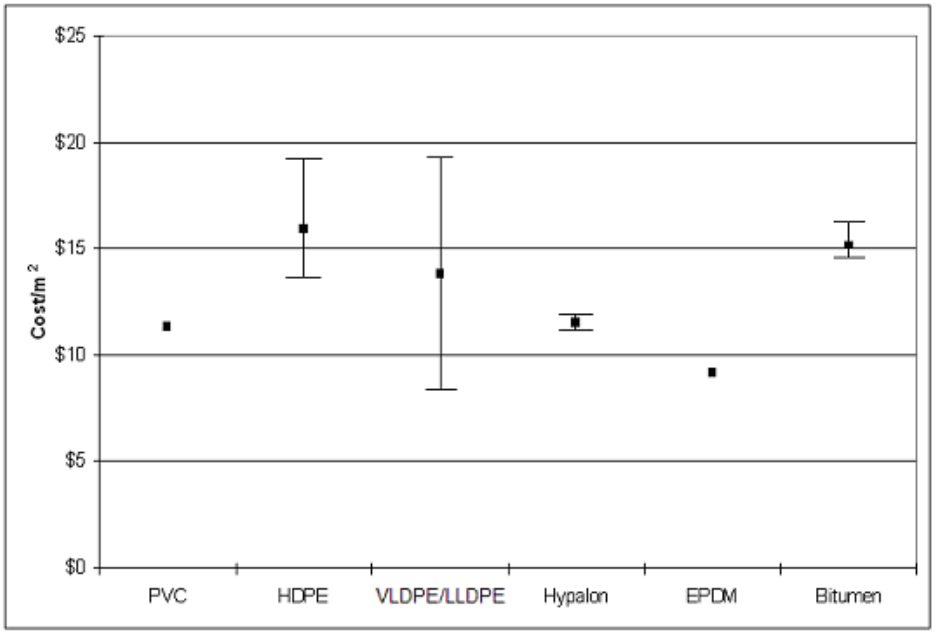

Figure 1 – Range in Cost for Exposed Geomembrane Liners

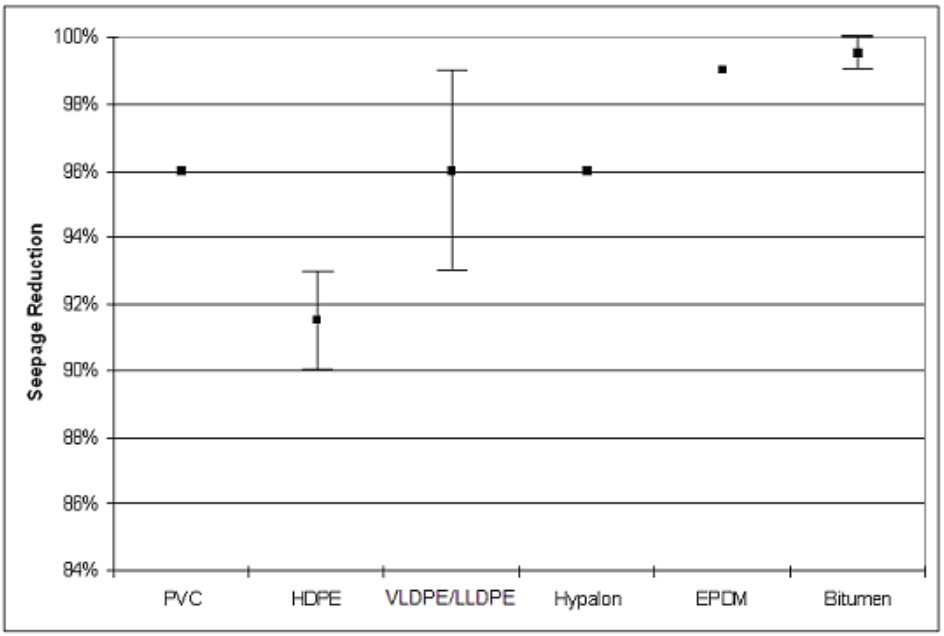

Figure 2. Range in Seepage Reduction for Exposed Geomembrane Liners

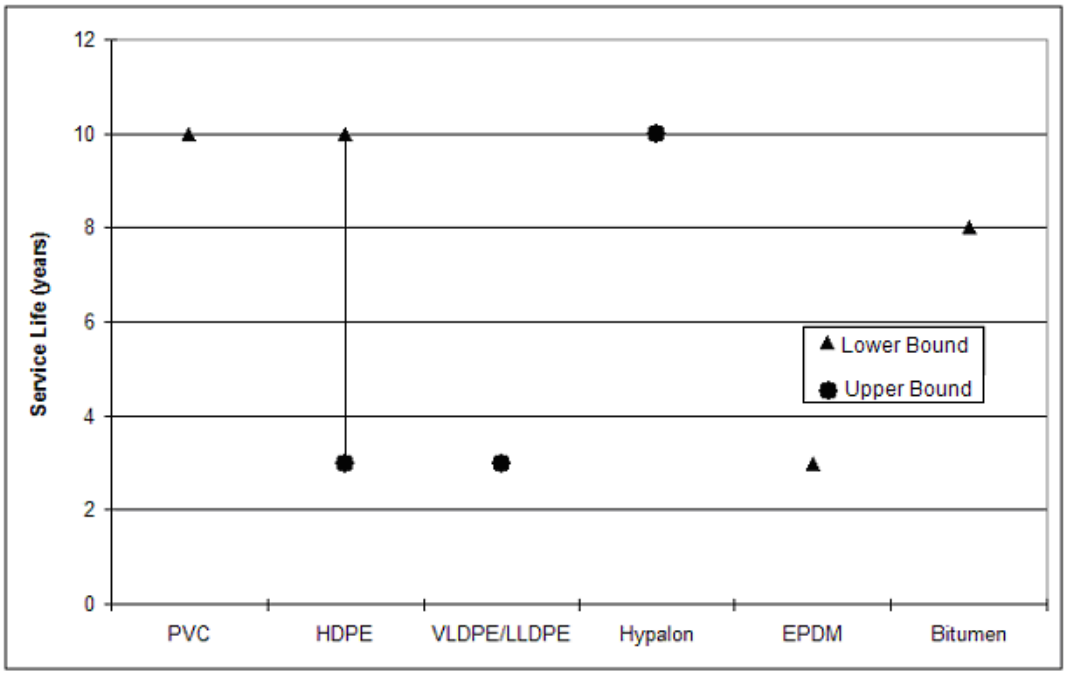

Figure 3. Range in Service Life for Exposed Geomembrane Liners

3.2 Type of Protective Cover

The use of a protective cover for the geomembrane is always an additional cost when compared to an exposed geomembrane. Using a concrete or shotcrete cover for the geomembrane can increase the cost of liner installation by up to 100%. Although no cost data is available for a soil covered liner system, the costs of overexcavating, placing, and compacting soil on top of the geomembrane represents a significant increase over an exposed geomembrane.

A protective cover usually has little effect on the seepage/leakage reduction of a geomembrane-based liner system so the main purpose of the cover is to reduce geomembrane exposure to the environment and physical damage. Concrete/shotcrete covered geomembranes usually exhibit a slightly higher seepage reduction percentage than exposed or soil covered geomembranes, as seen in cases PE-1 and PVC-2.

The use of a concrete/shotcrete cover can greatly extend the expected service life of a geomembrane (Swihart and Haynes 2002). A concrete or shotcrete cover essentially protects the geomembrane from physical and environmental damage. The use of a soil protective cover increases the durability of the liner system but not as much as a concrete/shotcrete cover. Soil covers also frequently have stability problems on side slopes of a canal but are usually less expensive then concrete/shotcrete covers. Generally soil covers are stable with side slopes that are less than or equal to 3H:1V.

By comparison, exposed geomembranes vary in their effectiveness while all covered geomembranes have performed well. All exposed geomembranes have provided adequate seepage reduction while the geomembrane was intact. Six of the exposed geomembranes either failed or were taken out of service due to leakage problems. For comparison, PVC-1 and PE-3 cases are rated good at a service life of 10 years, and PE-6 is rated good at a service life of 2 years even though they are exposed. In contrast, all of the covered geomembranes have not exhibited leakage problems.

4. NEW DEVELOPMENTS

A new alternative non-geomembrane lining system is a bentonite coated aggregate composite (AquaBlok®) which is used extensively for capping contaminated sediments in place, i.e. through a column of water. This material essentially consists of an aggregate core encapsulated with bentonite and proprietary performance enhancers. Bentonite coated aggregate composites are gaining acceptance in a wide range of sealing applications such as, anti-seep collars for piping, sealing dams and ponds, annular seals in wells, and as a canal lining material.

This is a new material for canal lining that does not currently have sufficient installation data for inclusion in the tables and graphs presented herein. However, the material has been extensively tested for Superfund projects and is used in many other sealing related applications. Barriers made of the bentonite coated aggregate are typically applied without draining the water/liquid from the impoundment, can be constructed using conventional equipment, routinely achieves hydraulic conductivities in the 10^{-8} cm/s range, and have been shown to be resistant to stream velocities up to approximately 1.5 m/sec.

5. CONCLUSIONS

This paper summarizes thirty-five case histories in which geomembranes have been used in canal liner system. Based on these cases, the following conclusions can be drawn:

(1) Geomembranes are well suited for use as water canal liners. Lining a canal with a geomembrane reduces the seepage from the canal by at least 90% for the geomembranes considered herein even if the geomembrane is exposed.

(2) There is no evidence herein to suggest a difference in the effectiveness/seepage reduction between PVC and PE; the two most commonly used geomembranes for canal lining systems.

(3) The case histories used herein show that placing a concrete or shotcrete cover over the geomembrane increases the durability of the liner system but also greatly increases the cost. The type of geomembrane is of little importance when a concrete or shotcrete cover is used because the geomembrane is not susceptible to most potential sources of physical and environmental damage. Thus, the geomembrane should be selected solely based on cost when a concrete/shotcrete cover is used because all geomembranes exhibit good seepage leakage control.

(4) Spray-applied geomembranes do not appear to be a viable option for water canal liners because all such test sections failed shortly after installation. In each of these case, the spray-applied material was washed away by the water flow. EDPM and elasometric bitumen geomembranes appear to be well suited for use as canal liners but long-term data is not available for these materials.

(5) Exposed geomembranes can be cost-effective and have performed well in several cases. However, in several cases exposed geomembranes suffered enough physical and/or environmental damage that made them ineffective.

REFERENCES

Kepler, W.K. and Comer, A.I. (1994). *Underwater Lining of Operating Canals,* R-94-15, Bureau of Reclamation, October.

Koerner, R.M., Hsuan, R.M., and Koerner G.R. (2008). “Freshwater and Geosynthetics; a Perfect Marriage”, *The First Pan American Geosynthetics Conference & Exhibition.* March. Cancun, Mexico.

Morrison, W.R. (1990). “Use of Geosynthetics for Underwater Lining of Operating Canals.” *4th International Conference on Geotextiles, Geomembranes and Related Products.*

Morrison, W.R. and Comer, A.I (1995). *Use of Geomembranes in Bureau of Reclamation Canals, Reservoirs, and Dam Rehabilitation,* Rec-95-01, Bureau of Reclamation, December.

Morrison, W.R. and Starbuck J.G. (1984). *Performance of Plastic Canal Linings,* Rec-84-1, Bureau of Reclamation, January.

Suhorukov, P.A., Krupin V.A., Morrison W.R., and Starbuck J.G. (1982). "U.S./U.S.S.R. Joint Studies on Plastic Films and Soil Stabilizers," Interim Report, Vol. 1, Vol. 2, Vol. 3, Vol. 4 Laboratory and Field Studies in Plastic Films, December 18.

Swihart, J.J., and Haynes, J.A. (2002). *Deschutes - Canal-Lining Demonstration Project, Year 10 Final Report,* R-02-03, Bureau of Reclamation, November.

Swihart, J.J. and Haynes, J.A. (2000). *Deschutes - Canal-Lining Demonstration Project, 2000 Supplemental Report,* R-00-01, Bureau of Reclamation, January.

Swihart, J.J and Haynes, J.A. (1999). *Deschutes - Canal-Lining Demonstration Project, Year 7 Durability Report,* R-99-06, Bureau of Reclamation, September.

Swihart, J.J. and Haynes, J.A. (1997). *Deschutes - Canal-Lining Demonstration Project, Year 5 Durability Report,* R-97-01, Bureau of Reclamation, January.
Swihart, J.J., Comer, A.I. and Haynes, J.A. (1994). *Deschutes-Canal-Lining Demonstration Project Durability Report-Year 2,* R-94-14, Bureau of Reclamation, September.

Swihart, J.J., Haynes, J.A., and Comer, A.I. (1994). *Deschutes-Canal-Lining Demonstration Project Construction Report, Upper Deschutes River Basin Water Conservation Program,* R-94-06, Bureau of Reclamation, May.

Timblin, L.O., Starbuck, J.G., Morrison, W.R. (1984). "Joint U.S./U.S.S.R. Field Studies on Canal Linings at Ukrainian Field Test Station, Black Sea Canal U.S.S.R. *International Conference on Geomembranes Denver, U.S.A.*

von Maubeuge, K.P., Witte, J., and Heibaum, M. (2000). "Installation and monitoring of a geosynthetic clay liner as a canal liner in a major waterway", *Geotextiles and Geomembranes* 18, pp. 263-271.

Yazdani, A.M. (2005). "Developing Egypt's South Valley", *GFR Magazine*. Vol. 23 No. 1, Jan/Feb pp. 38-39.

Challenges and Solutions During the Re-lining of a Concrete Covered Water Reservoir

B.W. Fraser, Layfield Group Limited, Edmonton, Alberta, Canada
M.P. Neal, Layfield Environmental Systems Inc., San Diego, California, USA

ABSTRACT
As part of an underground concrete water reservoir re-lining project for the City of Everett, Washington (completed in the fall of 2007) Layfield Environmental Systems fabricated and installed a 45 mil geomembrane containment system for a water treatment facility under some very demanding site conditions. This project included the installation of approximately 15,800 m^2 (170,000 ft^2) of flexible geomembrane in a confined working area around existing piping, concrete columns, and support beams while dealing with difficult water infiltration and structural concrete problems. The project also required tight safety standards, internal lighting, dewatering systems, water surge protection, and repair of damaged concrete. The project had a 55 day completion schedule and was subject to daily financial penalties if not completed on time. This paper discusses the various technical challenges and the innovative solutions that helped to finish the project on schedule.

1. INTRODUCTION

In the fall of 2007 the City of Everett, Washington tendered the re-lining of its Number 3 Reservoir. This was a Type 1 main underground reservoir which contained drinking water for the City of Everett and the surrounding community. This was a highly unique and challenging geomembrane installation project. The scope of work included replacing the existing geomembrane located on the reservoir sloped walls with a new Hypalon® Chlorosulphonated Polyethylene (CSPE) geomembrane and extending the geomembrane to provide a completely lined wetted surface area. This was required as the concrete slope and floor was in poor condition with substantial leakage being detected by the under drain monitoring system. One of the initial requirements for the consulting engineering firm was to determine the geomembrane selection to replace the original geomembrane on the slopes. To address the many site complexities of this difficult lining project, various design criteria needed to be reviewed by the consulting engineer. This included assessing the various geomembrane material alternatives. The project faced some very tight time constraints as the reservoir needed to be completed prior to high demand season as well as the fact that the City of Everett could not completely bypass the Number 3 Reservoir in terms of emergency back up. The City was also required to have several of their staff on site at extra expense for 24/7 monitoring and for adjusting flows to try and maintain water distribution while not flooding the reservoir during construction. At all times during construction the Number 3 Reservoir would need to be available to handle up to 7.7 cubic meters per minute (3 million gallons per day) of back up overflow water surge being directed to the drain sump. In addition to tight time constraints, the project included a number of difficult and unusual challenges in terms of the geomembrane installation. The numerous complexities and constraints involved required a number of highly innovative installation techniques and tight project management.

The City of Everett Number 3 Reservoir was originally an open concrete pond that was covered later in its life with a concrete roof. The original reservoir liner was a 150 mm (6”) thick unreinforced concrete slab with copper waterstops. A number of years ago, leakage was stopped by installing a geomembrane on the slope sections of the reservoir. This geomembrane was mechanically attached at the top and bottom of the slope but did not cover the floor of the reservoir. Over a period of years the erosive force from the water coming in the inlet pipe had worn the surface of the geomembrane until a tear developed. As a result of the tear, the geomembrane on the slope failed and water got underneath the liner and started seeping through the concrete slope panels. Aside from this obvious tear, the remainder of the CSPE geomembrane appeared to be in good condition after approximately 18 years of service. The main purpose of this project was to remove and replace the old slope lining and reline the entire reservoir. To prevent a repeat failure of the geomembrane in the future, a key design feature in this project was to place a substantial splash plate under the main inlet pipe to reduce the erosive forces.

2. GEOMEMBRANE SELECTION

Various project criteria were reviewed regarding the selection of the geomembrane. The first requirement of the geomembrane was the need to be NSF 61 listed for use in potable water containments. The geomembrane also needed to have adequate long-term resistance to chlorine used as a disinfectant. This included resistance to chlorine levels as high as 50 ppm used for disinfecting the geomembrane prior to commissioning of the system (ANSI/AWWA C652

Method #3). The consulting engineering firm was especially concerned with choosing a geomembrane that would not crack when exposed to chlorinated water in long-term service. The geomembrane needed to have the flexibility to be mechanically anchored to inlets, outlet and overflow pipes, a multitude of concrete column footings, 4 unique slope columns and a 100 m (330' lineal foot) seismic beam. Water was going to be present almost constantly during construction so the geomembrane needed to be prefabricated to speed installation and easily welded using various welding and gluing techniques. Finally, the geomembrane needed to be highly flexible, strong in tensile and sufficiently durable to withstand the construction and maintenance. The engineer produced a matrix of desired properties and matched them with various geomembranes available (Cooke, et al.) and concluded that a 45 mil Hypalon® (CSPE) white/black was the right material for this project.

Figure 1. Above Ground view of the City of Everett Number 3 Reservoir

3. CONSTRUCTION CHALLENGES AND SOLUTIONS

This project created some truly unique and difficult challenges in terms of installing the geomembrane system. In addition to the various known complexities there were some unexpected obstacles which added further challenges to the project. The project specifications primarily outlined the requirements for the geomembrane, geotextile, anchoring materials, project schedule, and quality assurance requirements. The remaining project details including: installation methods, design details, and sequencing, were structured more as a design build project with the responsibility placed on the liner contractor. The bidding and construction of this project required some significant innovation. Layfield Environmental Systems Corp. was the successful bidder, and on November 7, 2007 received the notice to proceed with the challenge of relining the City of Everett's Number 3 Reservoir.

3.1 Restricted Access

3.1.1 Challenge

All underground concrete reservoirs have limited access. In this reservoir there were only two 1.2 x 3.6 m (4' x 12') roof hatches on the south side of the reservoir located near the perimeter. One hatch was directly over a concrete stairway and the other was adjacent to it at the top of the slope. Although the staircase was adequate for personnel access, for materials and equipment it was severely limited. It was determined that the limited access would make it very difficult and time consuming to remove the existing geomembrane, geotextiles, and anchor system and replace them with new materials. These hatch locations required that the project materials and equipment be either carried or slid down the narrow stairs into the reservoir. The two existing hatches in the same relative location would also limit air circulation for the workers.

3.1.2 Solution

To address this issue Layfield commission the design and construction of a new equipment hatch that was placed on the opposite side of the reservoir and located over the toe of slope. By locating a hatch over the toe of the slope the materials could be lowered directly to the base of the reservoir. This allowed the heavy materials to be moved in and out of the reservoir with a crane. The new hatch was located so that City water operators had a direct view of the main inlet pipe. This would let them inspect this important pipe in the future without having to place a boat in the reservoir. Another important reason for installing the new hatch entry was to address the requirement for exchange of air under confined access rules. The new entry hatch provided us a point to mount an air circulation fan opposite from the original hatches which allowed for improved cross ventilation.

Figure 2. Main hatch showing restricted entrance to reservoir.

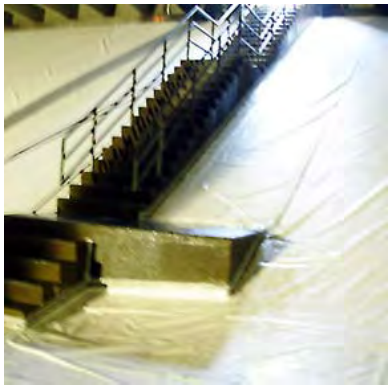

Figure 3. Staircase inside reservoir.

3.2 Unpredictable Surge Water Flows

3.2.1 Challenge

This reservoir acts as a surge reservoir between the water treatment plant and other reservoirs in the system. Whenever a valve closes downstream there is the possibility of a water surge into this reservoir. This surge water could not be shut off during construction as there was no other adequate outlet. This was a major concern as this reservoir could receive, without warning, up to 7.7 cubic meters per minute (3 million gallons per day). This was a major safety and construction concern.

3.2.2 Solution

To address this concern, Layfield fabricated and supplied a 2 m (6.6') layflat bypass tube from reinforced Polypropylene. This tube was attached to the 1.2 m (48") surge in-flow pipe and extended into the primary drain in the bottom of the reservoir. This allowed incoming surge water to be directed to the drain inlet during construction. As a further back up, Layfield had on site two portable coffer dams (Aqua Dams®) that could be filled with water to dam off a section of the reservoir if the surge water tube unexpectedly didn't work. A plan was in place to inflate the two water-filled coffer dams in the event of an emergency using water from an available hydrant. This back-up plan would then allow time to retrieve equipment and to try and shut off the surge water. During the construction of this project we experienced about two to three surges per day, from a small trickle, to significant water flows. The bypass tube worked as designed and was removed after the final liner tie-in at the completion of the project.

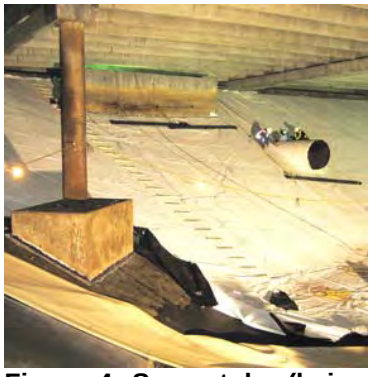

Figure 4. Surge tube (beige tube in foreground) directing surge water to the primary drain. Note the 1.2m (48") pipe boot and sloped column support in the background.

Figure 5. Surge tube leading into a small bypass outlet that connects to the main drain (circular opening on the left)

3.3 Safety

3.3.1 Challenge

The confined space of an underground reservoir can be very challenging. Aside from the typical confined space challenges, the reservoir was cold, dark, with limited access, and could receive surge water at any time.

3.3.2 Solution

This site required a custom designed safety program. This document included site specific requirements to deal with surge water, emergency egress, power failure procedures, and air safety. High output fans were required at the new equipment hatch to create sufficient air turn over to protect workers in the reservoir. This was backed up with air quality monitoring devices within the confined area. An evacuation procedure was developed in the event of a power failure. All personnel on site were trained on this procedure.

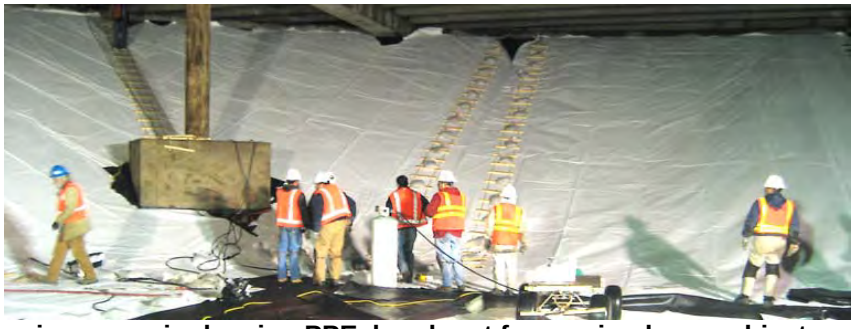

Figure 6. Workers in reservoir showing PPE, hand cart for moving heavy objects, and rope ladders for slope safety.

3.4 Water Infiltration

3.4.1 Challenge

The installation of the liner was further impacted by unexpected water infiltration problems. With the high level of winter rains in the Northwest region, rain water would build up around the site perimeter at a rate faster than the existing storm water removal system could handle. As a result, water constantly found its way through unsealed areas around the perimeter and through leaks in the roofing system construction joints. During numerous rain events, a steady stream of water created additional dewatering requirements and several problems for the welding crews who were required to work around standing water. The south and north side of the reservoir were also affected by high ground water levels. These high water levels created uplift pressures and seepage through floor cracks leading to more liner welding problems.

3.4.2 Solution

Depending on the level of water infiltration and the stage of construction activity various counter measures were required including dewatering by pumping, wet dry vacuums, small mortar dams, squeegees and using elevated welding boards to keep the welding area dry and clean. Filling the concrete construction joints with mortar was a contract requirement and helped to reduce water infiltration as more of the joints were completed.

3.5 Lighting and Power

3.5.1 Challenge

The underground reservoir had no internal lighting system and very little natural light was generated through the hatch openings. Normally liner installations would use portable generators for power; however, the wet environment of this reservoir increased the risk of electrical danger.

3.5.2 Solution

Layfield needed to provide several modular high output flood lights throughout the underground reservoir. As the crews were always working in close proximity to water, ground-fault circuit interrupters (GFCI) were used on all equipment in the reservoir. Four 50 AMP 220 V temporary power cords from temporary power poles with a number of changeable power plug-in boxes provided several 110V circuits.

3.6 Geomembrane Anchorage

3.6.1 Challenge

The original geomembrane had been anchored around the perimeter at both the top and the bottom of the slope. The contract required that the existing anchorage system at the toe of the slope be removed. This required the removal of over 2,500 anchor studs. The studs had to be removed flush to the existing concrete to allow the new geomembrane system to be installed.

3.6.2 Solution

Removing the toe of slope anchor bars was accomplished by first removing the existing nuts from the studs by using battery powered impact wrenches. Some of the nuts were seized on the anchor studs; these were removed by cutting the anchor studs with angle grinders and cutting wheels. After the nuts and washers were removed, the anchor bars were removed from the reservoir. The anchor studs were then cut to floor level and ground flush with the concrete floor. The existing stainless steel anchor bars and bolts in the top anchor system were reused.

Figure 7. Special corner clamp to maintain pressure at the point of the concrete footing.

Figure 8. Attaching the geomembrane to the large seismic beam in the center of the reservoir.

3.7 Penetrations and Attachments

3.7.1 Challenge

Underground reservoirs usually have a great deal of liner attachments due to the roof supports. This reservoir had a few additional challenges. Seven inlet pipes required waterproof pipe boots including sizes up to 1.2 m (48”). There were the expected 32 column footings that required water tight connections, but there were also four column footings located on the slopes requiring a much more complicated attachment. Finally there was a 100 m (300’) long seismic beam in the center of the reservoir that required over 230 m (750’) of water tight attachment. A particular challenge was to attach the liner to the vertical face of the column supports. This is a challenging connection as it is difficult to maintain batten bar pressure around the point of the corner.

3.7.2 Solution

Layfield followed the guidelines of ASTM D6497 for pipe boots and attachments. For attachments on this project, 6 mm x 50 mm (¼” x 2”) 316 stainless steel batten bars and 9.5 mm (3/8”) 316 stainless steel anchor bolts on 150 mm (6”) centers were used. The four slope columns used the same batten system modified to accommodate the slope. The pipe boots followed the standard industry attachment guidelines but were challenged by tight space constraints, concrete remedial work, and dewatering requirements. To address the problem of sealing around concrete corners, Layfield designed and fabricated special compression corner clamps (Figure 7). The complicated penetrations and attachments in this project required a lot of time and detail.

Figure 9. Sealing the liner under multiple small inlet pipes.

Figure 10. A boot on a large 1.2 m (48”) inlet pipe.

3.8 Unexpected Concrete Work

3.8.1 Challenge

The failure of the first geomembrane led to significant damage in two of the reservoir’s concrete slope panels. The original project scope was limited to filling construction joints prior to re-lining. Once the liner system was removed it was observed that two concrete slope panels had shifted and had significant voids underneath. The damaged panels represented 200 m^2 of unreinforced concrete 150 mm thick (2200 ft^2, 6” thick). Removal of this 30 m^3 (1000 ft^3) of

concrete was a significant problem as site and entry access for heavy equipment was extremely difficult. To compound this problem, a large amount of new liner material was already in place adjacent to the problem areas.

3.8.2 Solution

After discussions with the City of Everett and various concrete subcontractors a small remotely controlled hydraulic concrete breaker was sourced that could be lowered into the reservoir through the new equipment hatch. This electric unit did not generate fumes in the reservoir and had tracks so that it was stable on the slopes. The broken concrete and saturated subsurface materials were manually moved to a skip underneath the new equipment hatch and lifted out with a crane. New waterstops were added and then the concrete replaced with a concrete pump. The entire space was filled with concrete as it was not possible to compact any new fill materials with available equipment. Although one panel was located about 12 m (40 ft) horizontally from the new equipment hatch the subcontractor was able to pump the concrete without too much difficulty. The unexpected concrete problems resulted in a major project change order; however, the sequence of the installation was changed to give the subcontractor time to remove and repair the old concrete without affecting the schedule. Even with this change the project was completed within the original 55 day schedule.

Figure 11. Remote controlled concrete breaker working on reservoir slope.

Figure 12. Once the concrete was removed an engineer determined how much of the saturated subgrade to remove.

3.9 Stainless Steel Splash Plate

3.9.1 Challenge

The original liner had failed because the geomembrane had eroded on the slope underneath the inlet pipe. The contract specified that a 2.4 m wide x 6 m long, 6 mm thick (8'x20', ¼") stainless steel splash plate be installed to protect the liner system under the main 48" inlet pipe. The challenge was to place this 2000 pound piece of stainless steel 6 m (20') up the side slope without the use of heavy equipment. Not only was the weight a problem but the concrete on the slope was uneven making it very difficult to make a watertight seal.

3.9.2 Solution

A number of alternative splash pad designs were investigated. Finally a proposal was put forward to build the stainless steel splash plate in sections. Each section would be 1.5 m x 2.4 m (5' by 8'). A strip of stainless steel 6.35 mm (1/4") thick by 10.16 cm (4") wide was welded across the top of each section to form a joint. These joints were shingled in the direction of water flow. The side slope was lined with geomembrane underneath this splash plate and then the plate was placed on top of a protective wear pad on the liner. Neoprene gaskets were placed around the perimeter of the splash plate sections and each section of the plate was secured with a pattern of 12 mm (1/2") stainless steel bolts. Since the splash plate did not need to contain water (the geomembrane is continuous underneath it) it is not sealed between sections.

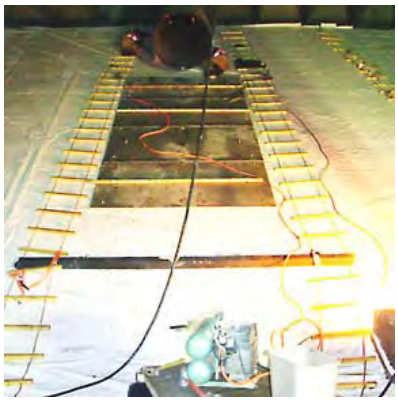

Figure 13. Stainless steel splash plate during installation.

3.10 Unexpected Drain Pipe Cleaning

3.10.1 Challenge

Once the old geomembrane was removed, the entire reservoir was washed using fire hoses. There was an accumulation of silt in the bottom of the reservoir and this was washed down the primary drain. After this washdown the City inspected the drain line with camera and found that a quantity of steel nuts and washers had been washed into the pipe bells. It was determined that the hardware was likely lost in the sediment during the removal of the old geomembrane and had been swept into the drain during the washing of the reservoir. Normally small items in the drain do not cause problems; however, at this site the drain was also connected to the outlet pumps. The loose hardware could cause damage to the pumps if they found their way downstream during high flows.

3.10.2 Solution

Numerous ideas how to clean out this 700 mm (28") drain pipe were proposed. After much debate it was decided that the best option would be to have a person go into the pipe. Because of the extreme nature of this confined space entry we hired a professional diving team. A site specific safety program for this confined space entry was prepared which included plans for the worst case scenario (the possibility of a surge of 3 million gallons of water coming into the reservoir). Part of the drain inlet was a 600 mm (24") stand pipe which was installed prior to the diver going into the pipe. If a surge of water were to occur, this standpipe would prevent water from flowing into the pipe for up to an hour. Even though there would be no water in the pipe at the time, the dive team set up the diver with surface supplied air, a helmet-mounted camera, and two way voice communications. The diver went approximately 36 m (120') down the pipe, collecting the nuts and bolts as he went. When the diver came to a tee in the pipe he was able to turn around which made his exit easier than originally planned. The diver was in the pipe for approximately 40 minutes.

Figure 14. Diving set up at primary drain. Note the bell-shaped standpipe installed on the drain.

Figure 15. Diver preparing to enter the drain pipe.

3.11 Disinfection

3.11.1 Challenge

The final part of the contract was to provide disinfection of the new geomembrane prior to commissioning of the system as per ANSI/AWWA C652 Method #3.

3.11.2 Solution

The disinfection method requires that a 50 ppm sodium hypochlorite solution be applied to the reservoir during initial fill. After working with the City on flow calculations and water quantities it was decided to bring in several 55 gallon drums of 12% sodium hypochlorite. The drums were placed at the new equipment hatch and a chemical feed pump was used to pump the sodium hypochlorite solution into a plastic hose that was placed directly in front of the inlet pipe to allow the mixing of the sodium hypochlorite with the inlet water as it cascaded down the splash pad.

Figure 16. The primary drain after liner installation and disinfection. The bell standpipe is for normal drainage and is designed to exclude silt. The dished section on the right is a small bypass for draining of the reservoir completely.

3.12 Project Time Frame

3.12.1 Challenge

Reservoir 3 needed to be retrofitted and commissioned before peak seasonal flows. Because of this operational requirement, the contract specified that the reservoir be fully accessible 55 days after the project start date in October 2007. There was a penalty clause in the contract that charged the contractor $5,000 for each additional day taken beyond the 55 day schedule.

3.12.2 Solution

Recognizing the importance of meeting the timeline for the City of Everett and the project risk, Layfield ensured this project received a high priority in terms of planning and project management. Even with frequent water intrusions interruptions and the additional time required to remove and replace concrete, the project was completed ahead of schedule. In fact, Layfield was able to apply for bonus money of $5,000 per day for early completion of the work.

Figure 17. Panorama of north side of completed reservoir.

4. GEOMEMBRANE FABRICATION & TESTING

It was a project requirement that the newly installed geomembrane system as part of the overall completed reservoir re-lining pass an allowable specified leak rate. To help achieve this Layfield prefabricated a large portion of the geomembrane system in its El Cajon, California facility. A special 75 mm (3") wide wedge was used for all factory and field welding of the geomembrane. This wider than normal 75 mm (3") wedge welding technique provided increased tensile strengths in the seam and a fully welded top and bottom seam with no lose edges. The wedge welding further reduced the need for chemical solvent welding which can lead to a less safe work environment. Both hot air welding and a specific CSPE adhesive were used in the field to fabricate pipe boots, sumps, corners and other custom fittings. All field or factory cut edges which had an exposed fabric scrim were flood coated with the adhesive to fully encapsulate the scrim. At the start of each day, mid day and the end of work day, peel and shear testing was performed on all factory and field welds. To confirm overall welded seam integrity, all factory and field seams were further probed and then air

lance tested following the guidelines of ASTM D4437-08. Random destructive test samples were sent out for third party testing.

5. CONCLUSION

As stated in Section 5, at the completion of the installation, the reservoir was required to pass a water test to ensure it met an acceptable specified leakage rate. There was also an under drain system which was tested to ensure the system was not leaking. No leakage was found within the reservoir as determined by a static test and no additional water was found in the under drain system. There was also no chlorine residual detected in the groundwater or under drain system.

This project included a large number of difficult challenges that added complexities and time constraints to an already difficult geomembrane installation. It was further impacted by a number of unforeseen external factors related to water infiltration and poor weather conditions. The City of Everett Number 3 Reservoir lining project was completed two days ahead of schedule and met all performance and water test requirements. It is our view that this difficult project was a success due to a number of factors including the quality of the project design provided by the engineer; excellent communications and cooperation between the contractor, owner and engineer; and the project management experience of our installation staff. Without the teamwork of the City of Everett, the design engineers and its sub-consultants in conjunction with the Layfield team, this highly difficult project would not have been completed on time or on budget and certainly would not have included the many system upgrades provided. All parties involved concluded this highly challenging project was well managed and successful.

Figure 18. View of the south side of the completed reservoir.

ACKNOWLEDGEMENTS

The authors would like to thank Mark Sadler P.E. and Al Rosenzweig of the City of Everett for their cooperation and professionalism demonstrated on this project. We would also like to thank MWH Americas Inc. namely Jay Cooke P.E. who worked closely with the us on the project providing design support and recommendations. Bob Pittman from Burke Industries also provided valuable technical and commercial support.

REFERENCES

National Sanitation Foundation, “NSF/ANSI Standard 61 Drinking Water System Components” Ann Arbor MI.

Cooke, J., Harris, G., and Graham. “City of Everett – Reservoir Number 3 Re-Lining Project Design Criteria Summary,” Technical Memorandum by MWH Americas Inc., July 20, 2007, Portland, OR

American Society for Testing and Materials “ASTM D6497 Standard Guide for Mechanical Attachment of Geomembrane to Penetrations or Structures,” West Conshohocken, PA.

American Water Works Association, “AWWA Standard for Disinfection of Water Storage Facilities, ANSI/AWWA C652,” Denver CO.

American Society for Testing and Materials “ASTM D4437-08 – Standard Practice for Non-destructive Testing (NDT) for Determining the Integrity of Seams Used in Joining Flexible Polymeric Sheet Geomembranes,” West Conshohocken, PA.

Innovative use of a Geocomposite Drainage System in a Clay-lined Agricultural Waste Storage Pond

B. C. Doerge, P.E., G.E., USDA-Natural Resources Conservation Service, Fort Worth, Texas, USA

ABSTRACT
A geocomposite drainage system was successfully installed under a compacted clay liner in an agricultural waste storage pond on a western Oregon dairy. The purpose of the system was to provide a safe outlet for seepage flow from an excavated slope on the uphill side of the pond. A geocomposite system was selected over a conventional multi-layer aggregate drain in order to maximize the storage available at the site and provide the minimum storage volume required by the State of Oregon. The site was tightly constrained between a steep hillside on one side and a seasonally inundated floodplain area on the other side.

This paper discusses design considerations, including site geology, determination of design flow capacity, and control of plugging, as well as construction challenges. The featured project may be the first where USDA-Natural Resources Conservation Service has used a geocomposite in conjunction with an agricultural waste storage pond.

1. INTRODUCTION

1.1 Project Background

The USDA-Natural Resources Conservation Service (NRCS) provides technical and financial assistance to private landowners to design and install conservation practices to protect soil, water, and other natural resources. NRCS assists with the installation of hundreds of agricultural waste storage ponds (AWSP) each year. These ponds permit landowners to store manure when conditions for land application are unfavorable. They are sized according to the operation's number of animal units. This paper presents a case history of the design and construction of an AWSP in western Oregon during 2006. The case history will focus on how the inclusion of a geocomposite drainage system in the AWSP design played a critical role in overcoming severe site constraints and making the project both feasible and, ultimately, successful.

The pond site is located on a bench at the base of a terrace slope and is adjacent to the floodplain of Butte Creek, a tributary of the Pudding River and the Willamette River. The pond was formed by constructing a U-shaped embankment that was tied into the slope at each end. Construction was begun in August 2005 by steepening the slope to approximately 1.8(H):1(V) to provide adequate room for the pond. However, the excavation exposed water-bearing sand layers in the slope, and so construction was suspended to allow the original design to be re-evaluated.

At the time construction was suspended, the excavation had reached a level approximately 8.3 m below the top of the slope and 3.7 m above the proposed invert of the pond. The bench at the base of this slope was at approximately the same elevation as the top of the proposed pond embankment. The slope above this bench is referred to in this paper as the "upper slope," and the slope later excavated below this bench is referred to as the "lower slope." The lower slope forms the back slope of the pond.

Further geologic investigations and design analyses were performed during Fall 2005 and Winter 2006 to determine: 1) the stability of the 1.8(H):1(V) slope; and 2) how the original design needed to be modified as a result of the differing foundation conditions. The revised design was completed in July 2006, and construction was completed by October 2006. The AWSP was put into operation immediately following construction as the rainy season was just beginning.

1.2 Site Constraints

Besides the standard NRCS and state requirements related to such things as allowable pond leakage and separation from the seasonal high ground water level, this site was faced with several additional, and mutually opposing, constraints that threatened to kill the project. First, the space available for the pond site was tightly restricted by the steep terrace slope on one side and the seasonally inundated floodplain of Butte Creek on the other. Even with the 2005 steepening of the slope, the area available to construct a pond with the required storage volume (5,700 m^3) was just marginally adequate. Further steepening of the slope was not feasible due to stability concerns, and pushing back the slope was also not possible because of the presence of farm buildings at the top of the slope. Second, the seepage exiting from the slope needed to be collected by a drainage system. But this system would have to occupy some of the limited

storage space. Finally, the storage facility needed to be in operation no later than October 2006 in order for the landowner to comply with the Confined Animal Feeding Operation (CAFO) permit requirements of the State of Oregon. No additional pond sites were available on the landowner's property, and there was no time to pursue permitting for an alternate form of storage, such as a concrete tank.

2. SITE GEOLOGY

2.1 Geologic Investigations

In Fall 2005, geologic investigations were performed by examining the surface of the newly excavated upper slope. A backhoe investigation trench was also excavated below the bench elevation to examine the soils in the lower slope. The bottom slope of the trench was approximately 2.5(H):1(V). The trench revealed a continuation of the alternating layers of fine- and coarse-grained materials observed in the upper slope. The sands exposed in the trench were saturated and released a small amount of seepage, but no instability was observed in the trench during the investigation.

Additional geologic investigations were performed in February 2006. One standard penetration test (SPT) boring was advanced from the top of the slope down to the alluvial sand and gravel layer at the base of the valley. The total depth of the boring was 15.79 m. All SPT samples were collected for index testing. In addition, three undisturbed samples were collected for complex geotechnical testing.

2.2 Soils

The soils in the terrace slope were glacial Lake Missoula flood deposits and consisted of medium to stiff lean clay and silt (CL, ML) interbedded with layers of medium to dense silty sand (SM). These soils were underlain by very dense alluvial silty sand and gravel (SM-GM) at a depth of approximately 15.3 m. The glacial sand layers ranged in thickness from 2.5 to 46 cm. Because of the manner of deposition, the stratigraphy was expected to be uniform throughout the project area. The soil profile data are summarized in Table 1. A schematic view of the slope is shown in Figure 1.

Table 1. Soil profile data

Layer No.	Depth (m)	Consistency/ Relative Density	SPT N (blows/m)	Material
1	0 – 2.23	Stiff	43 - 56	CL

2	2.23 – 5.27	Medium to stiff	20 - 30	CL with SM layers
		---		(10% sand)
3	5.27 – 9.85	Very stiff/	62 - 95	ML with SM layers
		Medium dense		(50% sand)
4	9.85 – 15.33	Hard/	98 - 157	ML with SM layers
		Dense		(50% sand)
5	15.33 –	---	> 328	SM-GM
	(TD = 15.79)	Very dense		

The uppermost sand layer occured at a depth of about 4.4 m below the top of the slope, or 4.0 m above the bench at the base of the upper slope. The top of the bench corresponded to the top of a 60 cm-thick layer of silt.

The fines content of the glacial sands ranged from 19 to 29 percent by dry weight (see Table 2 below). The average fines content in the upper and lower slopes was 27 and 19.5 percent, respectively.

Table 2. Fines content of glacial sands

Depth (m)	Percent < 0.002 mm	Percent < 0.005 mm	Percent < 0.075 mm
Upper slope:			
5.33-5.79	4	4	29
6.40-6.55	6	6	29
7.62-8.08	4	4	23
Lower slope:			
10.67-11.13	3	3	19
12.19-12.65	4	6	20

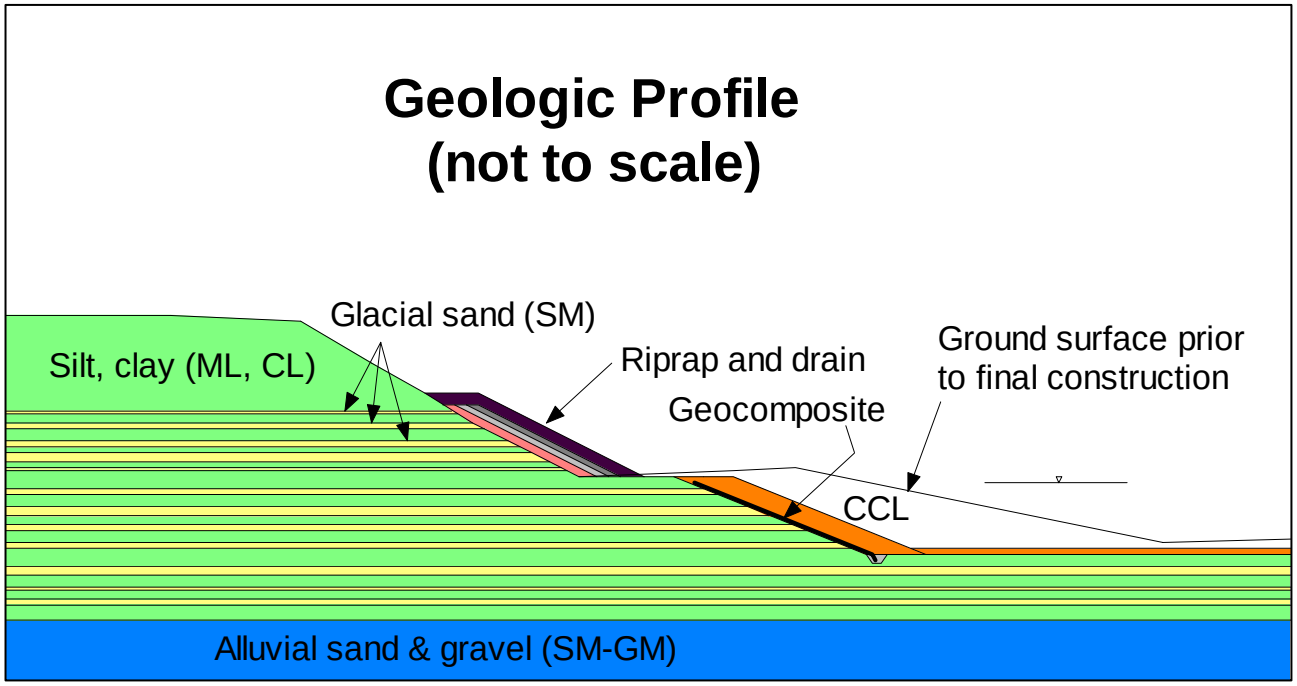

Figure 1. Schematic view of geologic profile.

2.3 Groundwater

Groundwater was observed to exit the 1.8(H):1(V) slope through the sand layers. The rate of seepage varied directly with local precipitation. During periods of higher seepage discharge, sand was observed to sap out from under the individual silt layers. The silt created a “roof” over the resulting void. In some cases, the void under the “roof” became large enough that the “roof” collapsed (see Figure 2). During drier periods, the sand layers exposed in the upper slope continued to bleed some water, but the sapping process slowed to a negligible rate.

During the winter of 2005-06, the rate of seepage from the upper slope was monitored by means of a V-notch weir. The maximum flow rate was 0.50 l/s in early January during a period of prolonged, heavy rain. This flow rate was taken to be the maximum value for design of the drains. The length of the contributing slope was approximately 50 m. Therefore, the maximum flow per linear meter was (0.50 l/s)/(50 m) = 0.010 l/s per m of length. Based on observations during the excavation of the investigation trench on the lower slope, it was concluded that the seepage rate from the lower slope would be less than that from the upper slope.

Figure 2. Void created by sapping of sand from below silt layer (ruler is in inches).

3. DESIGN

3.1 Design Objectives

The objectives of the revised design were: 1) to provide an AWSP of adequate capacity that meets all NRCS and state permit requirements; 2) to provide a safe outlet for seepage from the upper and lower slopes under all environmental and operating conditions; 3) to assure stability of the entire slope for all anticipated conditions, including during construction. Because of the relatively high permeability of the foundation materials, a compacted clay liner (CCL) was required on the sides and bottom of the pond to maintain the seepage from the pond at or below the allowable rate.

3.2 Alternative Selection

The design process for the AWSP consisted of a balancing act between providing the necessary function and stability while providing as much storage volume as possible. Both the upper and lower slopes required drainage systems to collect and discharge the seepage that was expected to exit from them. The upper slope would be left open to the atmosphere while the lower slope would be blanketed by a CCL. Two different designs were used for each of the two slopes. On the upper slope, a multi-layered filter/drainage blanket was installed with a finished slope of 2(H):1(V). This blanket was covered with a protective layer of rock riprap. The lower slope utilized a geocomposite drainage member (geonet with geotextile on top and bottom) between the in-place soils and the overlying CCL. See Figure 1 for a schematic view of both drain systems.

The drainage system used on the upper slope is a very traditional NRCS design in that it utilizes aggregate filter and drain materials instead of geosynthetics. Aggregate materials have typically been preferred within NRCS over geotextiles for critical drainage applications: first, because of long-term familiarity with and confidence in the use of aggregate materials in a wide range of applications; and second, because of concerns over long-term plugging of geotextiles (cf. Crum, 2008). Since NRCS does not maintain ownership of its conservation practices, but leaves the

ownership with the private landowner or sponsoring organization, the risk of future problems requiring additional intervention is typically minimized to the extent practicable. Since proper functioning of the drainage system was critical to the stability of the slope and, therefore, the safety of the farm buildings and the ASWP, the most reliable type of drainage system was desired. Therefore, aggregate filter and drain materials were selected. The configuration used, even with four layers of material, resulted in a greater pond volume than if a geocomposite with an earth cover had been used. The four-layer drain allowed for a steeper slope to be used (2[H]:1[V]) that more than made up for the drain's extra thickness.

For the lower slope, a similar aggregate drainage system was preferred, but such a system would have required two layers of filter material and one layer of drain material, for a combined thickness of about 0.75 m. This volume of material across the back side of the pond was enough to decrease the volume of the pond below the minimum required by the state permit. Therefore, a geocomposite was selected in place of an aggregate drain to cut down on the loss of storage volume. A 1.2 m-thick CCL was placed over the geocomposite to form the 2.5(V):1(H) back slope of the pond. This slope provided adequate stability for the CCL. The thickness of the CCL was selected so that the fill for the liner could be placed and compacted in lifts one equipment-width across. A geomembrane was considered instead of the CCL but was not selected because of cost considerations.

3.3 Drainage System Details

The design flow rate for the geocomposite was conservatively assumed to be the same as that used for the upper slope (0.010 l/s per m of length). The geocomposite was designed for capacity according to the procedure presented by Koerner (1999). The reduction factors listed in Table 4.2 (ibid.) were applied to the flow rate from laboratory tests. The factors for "Retaining walls, seeping rock, and soil slopes" were considered most appropriate for this situation. Mid-range values were used. A geocomposite with a thickness of 5.6 mm (220 mils) would pass the required flow. The material extended up to the maximum water surface in the pond and was 30 cm above the top of the highest sand layer in the lower slope. The geocomposite emptied into a trench filled with drain material meeting the requirements of ASTM Standard Specification for Concrete Aggregates (C 33), Size 89. The trench also contained a slotted plastic pipe to collect the flow and transport it to an outlet point. Therefore, the geocomposite did not need to have additional capacity to carry flow in the cross-slope direction.

The perforated collector pipe on the lower slope formed part of the perimeter drain intended to lower the groundwater level below the CCL as required by NRCS and state criteria. The drain also protects the CCL from excessive uplift pressures when the pond is pumped down. The perimeter drainage system was not intended to provide a means to check for contaminant leakage through the CCL, but it could be used for that purpose, if desired. See Figure 3 for details of the geocomposite drain system.

Because of a significant amount of potentially mobile silt fines in the glacial sands (see Table 2), there was a concern that a geotextile adjacent to these sands could become plugged over time. Therefore, the geocomposite was bedded on a 15 cm-thick layer of filter sand meeting the requirements for ASTM C33 fine aggregate for concrete. This sand had filter compatibility with the glacial sands and would prevent the migration of any fines past the face of the filter material. The filter sand was also filter-compatible with the silt layers in the lower slope. The geotextile on both surfaces of the geocomposite provided filter compatibility with the two adjacent materials, i.e., the filter sand below and the CCL fill above.

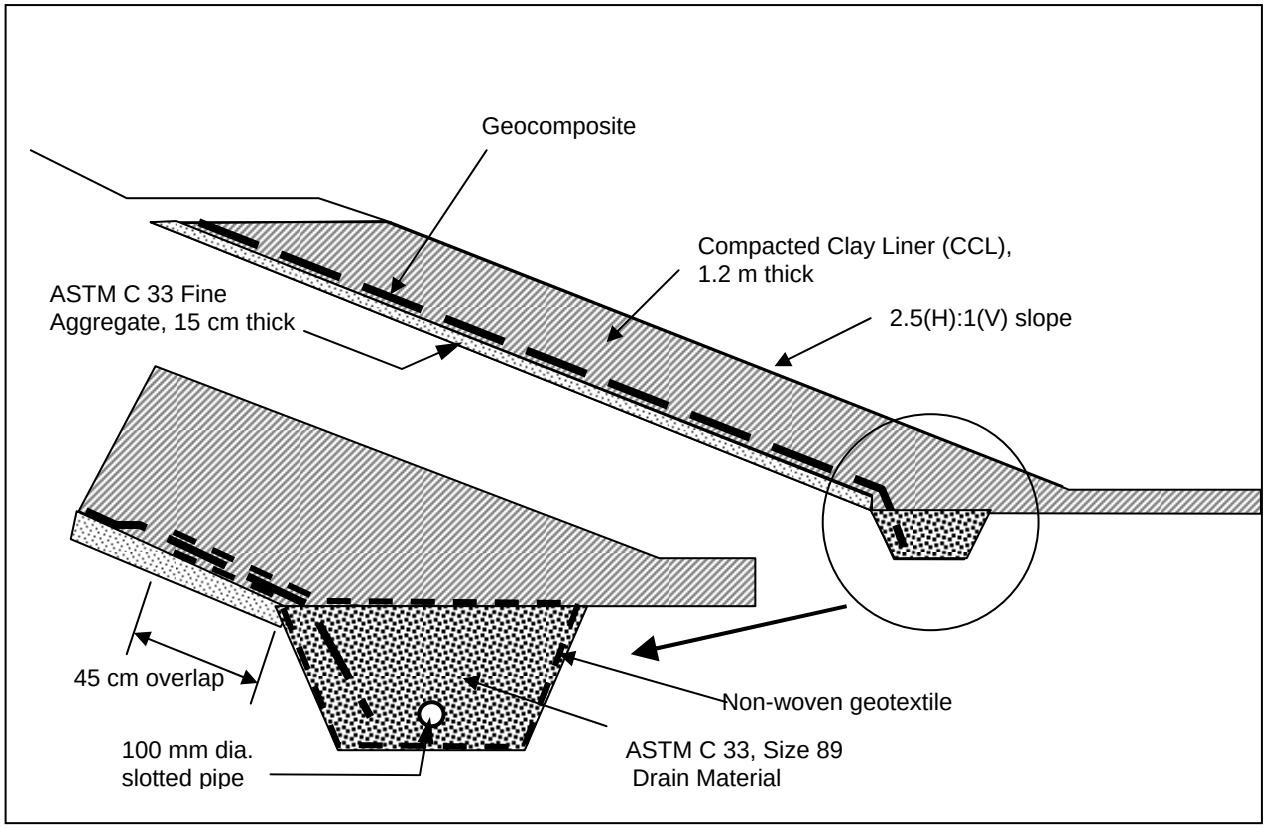

Figure 3. Geocomposite drain details (not to scale).

4. CONSTRUCTION

4.1 Excavation and Sub-grade Preparation

4.1.1 Upper Slope

The contractor elected to complete the work on the upper slope first. No significant problems were encountered, except for dealing with wet conditions on the bench at the base of the upper slope.

4.1.2 Lower Slope

Normally, excavating a 2.5(H):1(V) slope in saturated sands could cause stability problems. However, the excavation of the 2.5(H):1(V) backhoe trench during geologic investigations was completed without instability occurring, and because the construction period fell at the end of the dry summer period, it was decided that the lower slope could be safely excavated without a subsurface dewatering system in place. Because of their high relative density and their appreciable fines content, the glacial sands in the lower slope were anticipated to be of sufficiently low permeability to not slough or flow upon excavation. In support of this judgment was the actual performance of the upper slope during the winter of 2006/2006. Both slopes have similar stratigraphy and would be expected to exhibit the same failure mechanism. Since the upper slope, at 1.8(H):1(V), experienced only slow, small-scale instability during the entire 2005-06 winter rainy season, it was deduced that the lower slope, at only 2.5(H):1(V), would have adequate stability when excavated at the end of the dry season.

Nevertheless, the contractor was concerned about excavating the lower slope without dewatering it first. However, he agreed to excavate several trial trenches to test the stability of the proposed slope. When these trenches experienced no stability problems, the contractor then excavated between the trenches to form the required 2.5(H):1(V) slope. Although the resulting surface was damp and bled a small amount of water, no instability was experienced during the remainder of construction. Figure 4 shows the lower slope immediately prior to placement of the sand bedding and geocomposite.

Figure 4. Lower slope immediately prior to placement of sand bedding and geocomposite.

4.2 Geocomposite Installation

The sand bedding and geocomposite were installed and backfilled without difficulty. Butt joints were used between adjoining sheets of geocomposite. To prevent silt intrusion, all joints and cut edges were covered or wrapped with geotextile, using overlaps of 45 cm. The various components of the geocomposite system are visible in Figure 5.

This is the first NRCS project known to the author in which a geocomposite-based system has been used in conjunction with an AWSP.

Figure 5. Geocomposite installation, showing sand bedding and CCL fill.

5. OPERATION

The AWSP was completed by the required deadline and was put into operation immediately. The facility has been operated continuously since then without any reported problems. The drain on the upper slope has flowed at approximately the same rate as that measured in the V-notch weir prior to the final phase of construction. Flow from the drain on the lower slope has ranged between drips and a trickle. The finished AWSP is shown in Figure 6.

Figure 6. Completed AWSP in operation.

ACKNOWLEDGEMENTS

The assistance of Project Engineer Jan Kem, P.E., is gratefully acknowledged for providing construction photos and details.

REFERENCES

ASTM C 33. Standard Test Specification for Concrete Aggregates, *American Society for Testing and Materials*, West Conshohocken, Pennsylvania, USA.

Crum, D. A. (2008). Geotextiles in dams: Forging federal guidelines, *Geosynthetics*, IFAI, 26(4): 20-29.

Koerner, R. M. (1999). *Designing With Geosynthetics,* 4th ed., Prentice Hall, Upper Saddle River, NJ, USA.

Geosynthetics 2009
February 25-27 2009, Salt Lake City, Utah

Long Term Performance Requirements for HDPE Drainboards

M. Jablonka, Cosella-Dorken, Beamsville, Canada
E. Blond, CTT Group / Sageos, St. Hyacinthe, Canada

ABSTRACT
Drainboards are gaining more and more interest in residential and commercial construction, as well as in the civil engineering industry for their ability to control ground water and protect foundation walls against moisture, reduce/eliminate hydrostatic water pressure on tunnel linings, provide a waterproof membrane as well as either an air gap and/or an open drainage channel on buried structures such as foundation walls. The main objective of these products is to eliminate infiltration of water into the construction, to avoid fungus growth in basements, and to control the humidity of the protected structure's materials in order to decrease their rates of degradation.

In order to provide adequate performance and protection for the construction, the product must maintain its full integrity over the entire design life of the structure. However, it appears that current product specifications completely avoid any reference to durability and long-term performance properties of these products, although many HDPE drainboards available on the market are manufactured with recycled polyethylene, either in part or in whole.

The first section of this paper describes essential advantages and possible concerns associated with the usage and design with dimple sheets and drainboards. In the second section, the common degradation mechanisms associated to HDPE sheets are described. The third section presents two years of laboratory investigations conducted on HDPE dimple sheets, focusing on the aging mechanisms identified in the second section. Details associated twith the test procedures that have been developed to reflect the specific geometrical properties of dimpled sheets are presented as well as the results obtained.

Finally, a summary table presenting recommended product specifications needed to confine the aging properties of drainboards and to design a system that performs adequately throughout the entire lifetime of the structure is provided.

1. INTRODUCTION

Damage to sub-grade building structures ranks high in the damage statistics of buildings (Abel et al., 1991). To a large extent, the – often far-reaching – damages caused by moisture penetration in basements occur due to wrongly assessed underground moisture conditions and water pressure, resulting in the selection of unsuitable protection measures. Having reached the ground in the form of precipitation, water finds its own way as it follows the forces of gravity. If it infiltrates the soil swiftly and without delay, a building will not be exposed to water pressure from surface water. If precipitating water seeps away at a slow rate, however, water pressure will act on a building as long as precipitation continues. An equivalent situation occurs whenever underground water infiltrates permeable subsoil layers and migrates laterally until it reaches a building.

Exposure of a building to hydrostatic pressure increases when the adjacent subsoil layers are impermeable. In clay soils, for instance, water may accumulate in the top layers of soil, causing it to swell and block flow to a footing drain (Rose, 2005). In this case, building walls may be permanently exposed to water pressure. For proper planning of an effective waterproofing, drainage, and protection system, it is important to identify which of these water exposure conditions are present. A careful investigation of the soil-structure, as well as all other relevant factors such as the characteristics of the landscape, is therefore vitally important.

Efficient drainage greatly improves and warrants the reliability of the waterproofing layer by relieving the hydrostatic pressure caused by dammed-up seepage water. A drainboard can also provide effective protection for the waterproofing system against potential damage from mechanical impacts (i.e. from sharp-edged rocks during backfilling) and consequential moisture intrusion.

This paper reflects on the essential advantages of using HDPE dimple sheets and drainboards and on their performance criteria, as well as the possible concerns associated with the usage and design with such products. Furthermore, a general description of potential degradation mechanisms and aging processes of HDPE membranes is given and laboratory investigations conducted on HDPE dimple sheets, focusing on the aging mechanisms are being discussed. Finally, details associated to the test procedures that have been developed to reflect the specific geometrical properties of dimpled sheets are presented, as well as the results that were obtained. A summary table presenting recommended

exhaustive product specifications needed to describe and confine the performance properties of dimple sheets and drainboards and to design a system that performs adequately throughout the lifetime of the structure is provided.

1.1 Essential Advantages of Dimple Sheets and Drainboards

Dimple sheets and drainboards have been gaining increasing interest over the last number of years, and are commonly used in residential and commercial constructions, as well as in the civil engineering industry for their ability to protect foundation walls against moisture, control ground water, and reduce or eliminate hydrostatic water pressure. Dimple sheets are also used in tunnel lining applications to intercept artesian, fissure, and seepage water.

Below grade, the most effective moisture transport mechanism is liquid flow of water. Gravity forces can cause hydrostatic pressure build-up on the outside of sub-grade structures. Even in the absence of hydrostatic pressure moisture can migrate through foundation walls due to capillary conduction. Especially affected by capillary wicking is concrete that shows evidence of voids (i.e. honeycombing).

In addition, fissures and cracks in concrete walls allow adjacent water to migrate through the concrete, either by being pushed through the structure due to hydrostatic pressure build-up on the outside, or by capillary forces occurring within the concrete structure. To eliminate capillary conduction, a capillary breaking layer is required. A 3-dimensional dimple sheet provides a full capillary break with inherent redundancy: the plastic membrane (High Density Polyethylene is commonly used by manufacturers for this type of product) in itself is a capillary break. Additionally, the air-gap, which is being generated between the membrane and the structure also serves as a capillary break.

The main objective of drainboards is to reduce or eliminate hydrostatic pressure against the foundation or below grade structure by providing an effective drainage layer, and to prevent infiltration of water into the construction. Drainboards, generally comprised of a rigid polymer core (dimple sheet) with a geotextile (filter fabric) bonded to the dimpled surface (see Figure 1), make an excellent drain on the backfilled side of retaining walls, basement walls, and plaza decks (Koerner, 1997).

The drainage path for the water is provided by the air gap between the studded polymer core and the geotextile. Figure 1 illustrates how soil-water adjacent to a below-grade structure passes through the geotextile and is safely drained to the footer drain. Hence, the potential for building up hydrostatic pressure against the structure is eliminated.

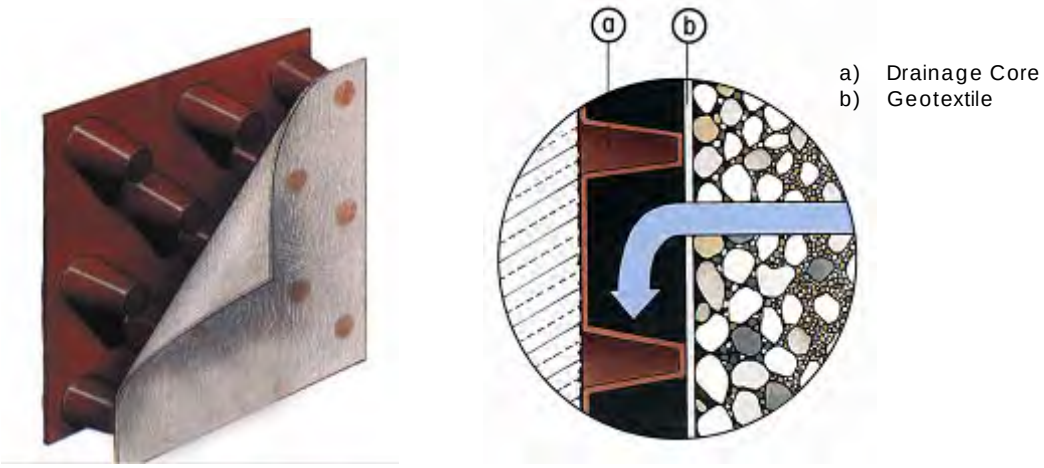

Figure 1: Drainboard comprised of polymer core with geotextile (filter fabric)

Dimple sheets function based on the simple principle of an air gap, formed by a waterproof plastic sheet with a 3-dimensional dimple structure, to keep soil moisture away from foundations. The combination of a waterproof membrane and the air-gap provide a reliable capillary break. Stopping inward moisture migration contributes to controlling the humidity of the protected structure's materials in order to decrease their rates of degradation, and thus helps to avoid mold and fungus growth in basements. An obvious advantage over conventional spray applied dampproofing and waterproofing products is that cracks in the concrete, which occur due to shrinkage and settlement, are bridged by the dimple sheet, ensuring that moisture remains unable to migrate inwards. The function of dimple sheets for foundation wall moisture protection is illustrated in Figure 2.

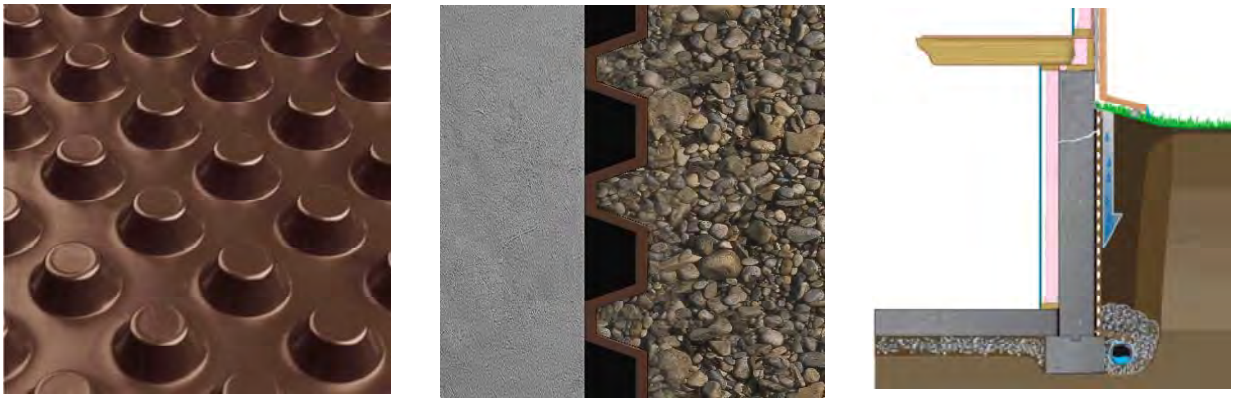

Figure 2: ‘Air gap’ function of dimple sheet

Dimple sheets are also commonly used in civil engineering construction to provide high capacity drainage on deep foundations in vertical or horizontal applications in order to eliminate the destructive forces of hydrostatic pressure. This principle also applies to tunnel construction where dimple sheets are commonly used to intercept artesian, fissure, and seepage water in order to prevent the build-up of hydrostatic pressure against the concrete liner inside the tunnel. Pictures (a) and (b) in Figure 3 illustrate these applications.

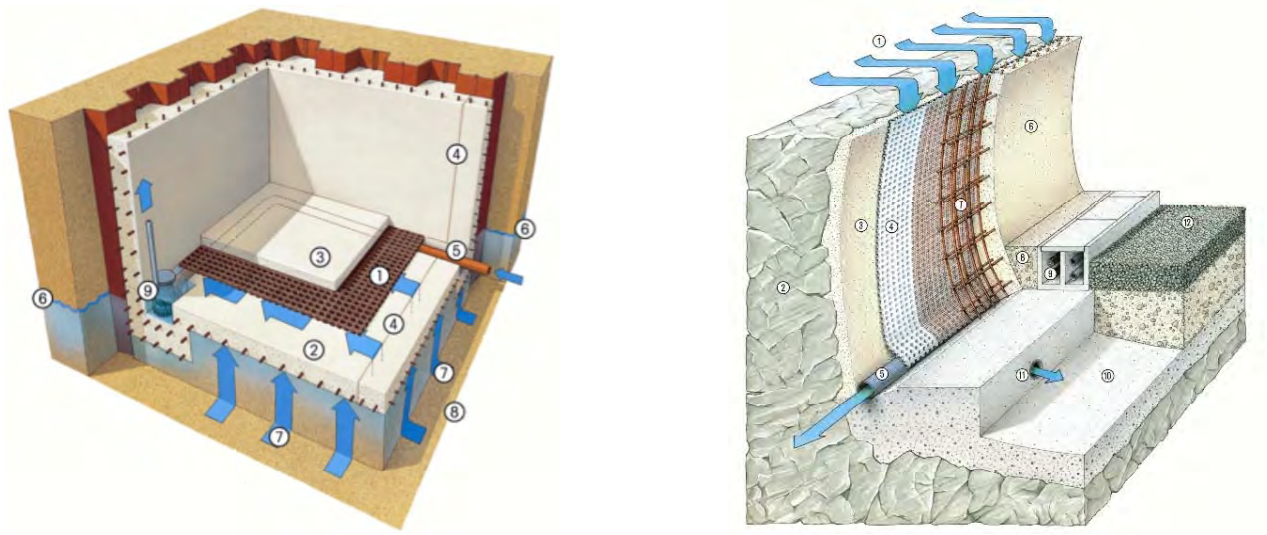

(a) (b)

Figure 3: Dimple sheet for artesian and fissure water drainage

1.2 Performance Criteria for Dimple Sheets and Drainboards

When specifying a dimple sheet or drainboard for a below grade application there are several key performance criteria to consider. For such membranes to function throughout the lifetime of the structure that they are intended to protect, these key performance criteria must be evaluated also with respect to long term durability. Performance criteria for dimple sheets and drainboards can be categorized into mechanical properties, hydraulic properties, and durability. Mechanical properties comprise the compression behavior of the geocomposite (drainboard core with geotextile bonded to its studded side) or the dimple sheet. This material characteristic is fundamentally important since the 3-dimensional membrane will be exposed to soil pressure at varying levels depending on the installation depth, and its functionality, especially with respect to generating and maintaining an air-gap between the foundation wall and the adjacent soil is dependent on its compression resistance. An appropriate test method for determining the short-term compression behavior of the dimple sheet or drainboard is ASTM D6364. While this test standard can give an indication of the

momentary compression behavior of the material, it cannot, by itself, characterize the long term compression behavior of the product.

Other important mechanical properties of such membranes are breaking force and elongation, measurable according to ASTM D5035, as they help to characterize the behavior of the products during the backfill process. It has also been used for determination of the number of anchors per surface area to be applied to ensure stability of the product on a vertical wall. Also of relevance for the characterization of mechanical properties is the static and dynamic puncture resistance of these membranes. Dynamic puncture resistance reflects the product's ability to sustain the shock induced by the fall of a boulder during the backfilling process, which is likely to occur either accidentally or during normal operations. On the other hand, static puncture reflects the ability of the product to sustain a local pressure that would be induced by a boulder in direct contact with the geocomposite or drainboard. Appropriate test standards are readily available, i.e. CGSB 37-GP-56M and CGSB 37-GP-52M.

The characterization of hydraulic properties is especially important for drainboards, as their main function is to safely drain water away from the foundation wall in order to prevent or eliminate hydrostatic pressure. Hence, the hydraulic transmissivity and in-plane flow rate of a geocomposite (drainboard) as determined with ASTM D4716, are vitally important performance characteristics. Since dimple sheets are intended to not only provide protection against liquid water intrusion into foundations, but also to protect against moisture ingress via other transport mechanisms, it is also important to describe the water vapor transmission rates of such materials. An appropriate test method is described in ASTM E96, Procedure A.

In order to characterize the long term durability of dimple sheets and drainboards, a number of standard test methods can be employed. For characterization of aging and oxidation of these membranes, an oven aging test as per ASTM D5721 and an OIT (Oxidative Induction Time) test as per ASTM D3895 are suggested in combination with compression behavior testing at different intervals of aging. This procedure was inspired by the classical aging test used in the polyethylene geomembrane industry. Similar conclusions regarding associated lifetimes and degradation mechanisms can indeed be drawn as both products are using similar base materials (high density polyethylene).

Finally, the last significant degradation mechanism that is likely to develop on HDPE drainboards – as well as on many other polymeric products – is environmental stress-cracking. Although this property is also very well handled in the geomembrane industry, the particular structure of drainboards, the sheet thickness involved and the presence of recycled polyethylene in only the central section of the product (see Figure 4) do not allow the use of one of the common tests addressing this property. These are either ASTM D1693 in most of the plastics industry, ASTM D5397 in the HDPE geomembrane industry, or ASTM F2136 in the HDPE pipe industry. The most significant issue restraining the use of these methods is the fact that some HDPE drainboards are co-extruded sheets involving recycled and non-recycled polyethylene in three separate layers, the two outer – virgin HDPE – layers providing the product its endurance properties, while the central layer, made of recycled HDPE, essentially contributes to the mechanical and other performance properties of the finished product. This particular composition makes it impossible to regrind and re-mold a 3.2 mm thick sheet to conduct ASTM D1693, and also makes irrelevant the use of specimens notched to a depth of 20% of the sheet. This would bring the notch into the recycled polyethylene layer and would thus not adequately reflect the actual product performance. As a consequence, a specific method had to be developed to address this intrinsic material property. It is currently referenced as Sageos GD001 (Stress Cracking Resistance of Dimpled Sheets), until further standardization work at an upper level such as ASTM or ISO. In the meantime, the procedure is further developed in this paper. The aforementioned performance criteria are similarly referred to in the European Standard EN13252, Geotextiles and geotextile-related products – characteristics required for use in drainage systems, Table 1.

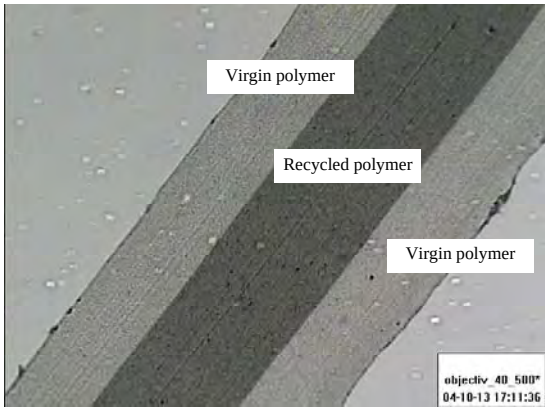

Figure 4: Microscopic section of a HDPE drainboard including a layer of recycled resin

1.3 Possible Durability Concerns associated with the use of HDPE dimple sheets and drainboards

While polymers are being utilized in virtually every area of our life, the volume of polymers used in the above-mentioned applications represents only a small fraction of the entire polymer market worldwide. The use of High Density Polyethylene in foundation protection membranes and drainboards differs from many other applications since these membranes are intended to fulfill their function over long time periods. Where some articles made of HDPE are required to last for short time periods only (i.e. milk bottles), others are intended to last a few years (i.e. kitchen articles). Foundation waterproofing membranes and drainboards are expected to fulfill their function for the lifetime of the structure – typically in the range of at least 50 years.

Durability concerns therefore need to be understood and evaluated. Most situations involving the expertise of a geotechnical engineer are dealt with under the aspect of ground water conditions, seepage, settlement, bearing capacity of soils, etc. Typically the short-term properties of the involved materials are being considered without looking at their durability and potential degradation factors. Important to the durability of foundation protection membranes and drainboards is their raw material formulation, the imposed in-service conditions during their functional lifetime, as well as the environmental conditions to which they will be exposed between manufacturing and the actual service life.

The material formulation deserves special attention when recycled content is used in such membranes, and even more if the membranes are made entirely out of recycled HDPE. In recent years, the utilization of recycled plastic in extrusion of sheet goods, especially in Polyethylene sheets has increased significantly, driven by cost advantages to manufacturers, as recycled material is generally available at a lower cost than virgin material. The rise of environmental concerns has also become influential in the construction industry. A number of green building rating concepts have been generated and implemented, i.e. LEED (Leadership in Energy and Environmental Design), which promote and reward the use of recycled content in the employed construction materials.

The addition of recycled materials to construction products certainly appears responsible under the aspect of environmental concerns. However, it may also raise concerns in regards to the end product's durability and consequential implications, which should be addressed appropriately. This also holds true with respect to adding recycled material into virgin HDPE for the production of plastic sheets. Since the use of recycled content in dimple sheets and drainboards may potentially compromise their long term durability, the intensity of the negative impact must be evaluated and understood in order to ensure that the key performance characteristics of such products are maintained throughout the functional service life of these products. Interestingly, the European Standard EN 13252 even excludes the use of recycled polymers entirely if a drainboard is required to have a service life of up to 25 years.

A designer may be given the choice between different products, of which one may last for the entire lifetime of the structure that it is supposed to protect, while another one – typically cheaper - may have a significantly shorter functional lifespan. Hence, it is critically important that design guidelines are provided, and that the designer has the necessary understanding of the materials and environmental conditions to choose an appropriate product.

In Section 2 the common degradation mechanisms of HDPE sheets are described in order to generate a better understanding of which tests should be performed on such products to assess their long-term performance appropriately.

2. POTENTIAL AGING AND DEGRADATION MECHANISMS RELEVANT TO HDPE SHEETS

Aging and degradation of polymers essentially takes place at the molecular level. Polymers are materials composed of large molecules of very high molecular weight. The cohesive forces of a polymer, which greatly affect the physical and chemical degradation mechanisms that can take place, are determined by the chemical composition of the polymer.

The molecular structure of Polyethylene is shown in Figure 5.

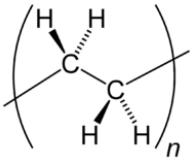

Figure 5: Molecular structure of Polyethylene

The characteristics of the polymer depend on intermolecular forces and are greatly influenced by the chain structure (i.e. chain length, linearity, branching, cross-linking, etc.), morphology (i.e. crystallinity), molecular weight distribution, irregularities (i.e. impurities), additives (i.e. color pigments, Antioxidants, UV stabilizers, flame retardants, antistatic agents, etc.), as well as by the manufacturing process itself, during which the polymer is exposed to thermal and shear stresses that will initiate degradation mechanisms. Process conditions will also determine the effectiveness of mixing additives and stabilizers into the polymer, which can influence the morphology of the end product as well as the degree of stabilization against environmental factors like heat, UV, oxygen, etc.

Polyethylene, the highest-volume polymer in the world (Harper, 1999), offers high toughness, ductility, excellent chemical resistance, low water vapor permeability, low water absorption, excellent processability, and hence is a very versatile and attractive material for many different applications. High Density Polyethylene has a low degree of branching and hence strong intermolecular forces and tensile strength. Since it is non-polar, it provides a very high resistance to chemicals. The permeability of Polyethylene to liquids and gases is extremely low. It is also very resilient to alkaline and acidic agents, as well as salt solutions. Polyethylene copolymers (Ethylene can be copolymerized with many non-olefinic monomers) generally provide improved low-temperature flexibility and increased environmental stress crack resistance. Due to its outstanding characteristics High Density Polyethylene (copolymer) lends itself perfectly for the manufacturing of durable 3-dimensional dimple sheets and drainboards.

Essential aging and degradation mechanisms of polymers commonly used in geosynthetics have been described in depth by Kay et al. (2004). HDPE is generally very resilient against environmental factors, which in fact may initiate degradation mechanisms with many other polymers. Hence HDPE seems to be the ideal polymer to be used for dimple sheets and drainboards in below grade applications. However, when recycled PE is used in the extrusion and forming process of dimple sheets, the resilience to degradation mechanisms under specific conditions may be significantly reduced. During their functional service life the HDPE dimple sheets and drainboards described in this paper are exposed to several relevant degradation mechanisms. These aging mechanisms can, under certain circumstances, influence their properties and even reduce their durability and lifetime expectancy. Hence, the characteristics of the material used as well as the actual exposure conditions must be considered in order to evaluate the potential implication of these degradation mechanisms to the final product and its functional service life.

One of the most relevant degradation mechanisms of High Density Polyethylene is oxidation, which can occur in form of thermo-oxidation, photo-oxidation, and chemical oxidation. The long-term durability and performance of Polyethylene membranes can be ensured through adequate stabilization with antioxidants and UV stabilizers.

In the presence of sensitizing agents, HDPE can become sensitive to Environmental Stress Cracking, which – next to oxidation – is the most relevant degradation mechanism of this polymer. As per the definition in accordance with ASTM D883 stress cracking is “an external or internal crack in a plastic caused by tensile stresses less than its short-term mechanical strength.” This typically describes brittle cracking with little or no ductile drawing from the adjacent failure surfaces of the polymeric material. The occurrence of environmental stress cracking of stressed samples is linked to the presence of surface-active wetting agents such as alcohols and surfactants. The surface-active wetting agents don’t chemically attack the polymer, nor do they produce any effect other than microscopically brittle-appearing fractures. The fractures initiate at microscopic imperfections in the material, and propagate through the crystalline regions of the polymer structure. In the absence of such surface-active wetting agents, these fractures would not occur in any reasonable time period under the same stress conditions.

A polymer’s ability to resist environmental stress cracking is generally known as ESCR (Environmental Stress Crack Resistance). Different polymers exhibit varying levels of ESCR. It is important to know that the stress cracking susceptibility between different types of PE is known to be very different (Hsuan,). Some grades of HDPE have very good resistance against environmental stress cracking, while other grades only show a marginal resilience. The principle variables that affect the ESCR in HDPE include the crystallinity, molecular weight (ESCR improves as molecular weight increases), the molecular weight distribution (generally a narrow molecular weight distribution shows poorer ESCR values than a broader distribution), branch length, and lamellar orientation (Lustiger, 1996). Naturally the ESCR testing conditions (i.e. reagent concentration, testing temperature, applied stress) also have a major influence on the ESCR that the tested sample will exhibit. Recycled content is also known to affect the Environmental Stress-Crack Resistance of polymers. Historically, and practically, recycled materials do not perform as well as virgin polymers when subjected to Environmental Stress-Cracking (Develle et al, 2003).

The pH value of a soil is perhaps the most important factor governing the rate of degradation of foundation protection membranes, drainboards and the attached geotextiles (Corbet et al, 1993). The rate of degradation increases with an increase in ambient temperature. While typical soil temperatures close to foundation walls are in the area of 10°C to 15°C, significantly higher temperatures are usually encountered close to grade surface, as well as behind retaining walls.

3. LABORATORY INVESTIGATIONS

In this section, only the test procedures that are not typically reported in common drainboard specification sheets are introduced. However, Table 4, provided at the end of this document, includes a minimum list of properties that were found to be relevant for most applications of drainboards. Authors thought it would not be appropriate to re-describe those procedures and test results that are very well handled by the common procedures described in the first section of this document.

3.1 Environmental Stress Crack Resistance

3.1.1 Test Procedure

Various test methods have been developed over the years to measure the Environmental Stress Crack Resistance of products. The most widely used and oldest method is ASTM D1693 - Standard Test Method for Environmental Stress-Cracking of Ethylene Plastics (Bent StripTest). Other methods are ASTM D5397 – Standard Test Method for Evaluation of Stress-Crack Resistance of Polyolefin Geomembranes; ASTM F1473 – Standard Test Method for Notch Tensile Test to measure the resistance to slow crack growth of PE pipes and resins or F2136 – Standard Test Method for Notched, Constant Ligament-Stress (NCLS) Test to Determine Slow-Crack-Growth Resistance of HDPE Resins or HDPE Corrugated Pipe. However, as described in 1.3, none of these methods apply to HDPE drainboards in their finished or delivered condition, as the layered structure and geometrical properties of the dimpled sheet make them irrelevant. For that purpose, a specific procedure was first developed in Northern Europe by the Swedish Construction Authorities, and further codified by SAGEOS in “Geodrains Testing Method, Stress-Cracking Resistance of Dimpled Sheets using the ‘Sweden Test’” (2006) to address the stress-cracking resistance issue for dimpled sheets.

In this method, four (4) specimens are placed on a flat concrete surface and covered by a fiber-cement board while immersed in a wetting solution (10% Igepal CO-630 / 90% de-ionized water at 55°C) and stressed using dead loads as described in Figure 6. Periodically, the specimens are unloaded for a visual inspection, and a thickness measurement is taken. A rating of the observed cracking is noted, along with the exposure time. The time required to observe the first crack is finally identified, as well as the time for the dimple to collapse.

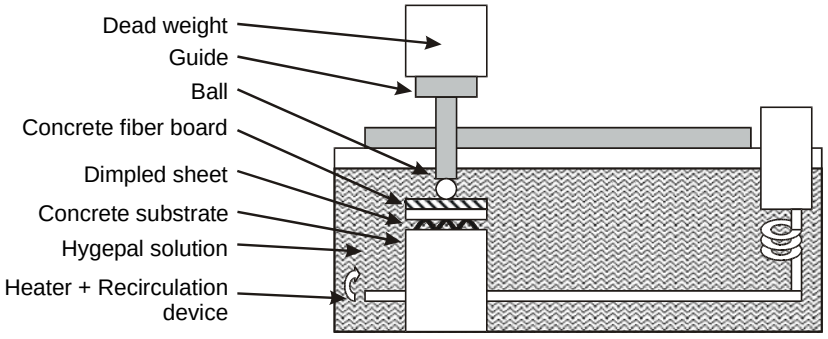

Figure 6: Stress-cracking test for dimple sheets

The visual inspection is done to rate the degradation qualitatively, according to the criteria described in Figure 7.

Rating = 1	Rating = 2	Rating = 3	Rating = 4
No cracking observed	Minor cracks	Severe cracking	Collapsed Dimple

Figure 7: Visual rating for stress-cracking resistance of dimple sheets

3.1.2 Results

Four different products were analyzed using this procedure. Three of them were involving 100% post-consumer recycled resin, and one was co-extruded with two outer layers of pure virgin resin and one central layer of post-consumer recycled resin, as shown in Figure 4. The results are reported in Table 1. They present the observations expressed as the occurrence of the first crack, as well as observation of a severe failure of the product.

(a) No failure (b) Cracking (c) Severe cracking (d) Severe cracking

Figure 8: Observations of the degradation of dimple sheets during a Stress-Cracking test per SAGEOS GD001

Table 1: Time of exposure (hours) for the observation of the first occurrence of a crack and severe failure.

Observation	Co-extruded with virgin and recycled resins	100 % post consumer recycled resin #1	100 % post consumer recycled resin #2	100 % post consumer recycled resin #3
First crack	> 336 hours (2 weeks)	70	70	45
Severe failure		> 336 hours (2 weeks)	70	163
Example picture	Figure 8-a	Figure 8-b	Figure 8-c	Figure 8-d

3.2 Resistance to oxidation

3.2.1 Procedure

Resistance to oxidation was also evaluated on the same four dimpled-sheet products based on ASTM D5721, using temperatures of 40, 50, 60 and 70°C. These temperatures were selected in order to maximize the degradation by oxidation of the product, but minimize the potential influence of other chemicals which could be present (in the recycled fraction), and which would not be active in normal operating conditions. For that reason, test temperatures as high as 85°C were not selected. Aging was monitored using compression resistance, OIT and melt index.

3.2.2 Results

The OIT and compression strength results are presented in Figures 9 and 10 for the reference product (co-extruded virgin & recycled HDPE) and summarized in Tables 2 and 3 for all the tested products. It is shown that OIT varies over time according to the temperature, but that the mechanical properties are not significantly affected by the thermal aging process over the testing period. Similar observations were made for the three other products, that is no significant changes in mechanical properties nor melt index, but a quantifiable decrease of OIT. Results of OIT being the only ones showing some significant variations over time, they were selected to build the Arrhenius model to effectively and objectively compare the relative durability of the products. This durability was defined as the time required to completely consume all the anti-oxidants, calculated for a service temperature of 15°C. This duration was then expressed as a relative value compared to the durability of the reference material, which was arbitrarily selected to be the co-extruded material involving recycled and virgin resins.

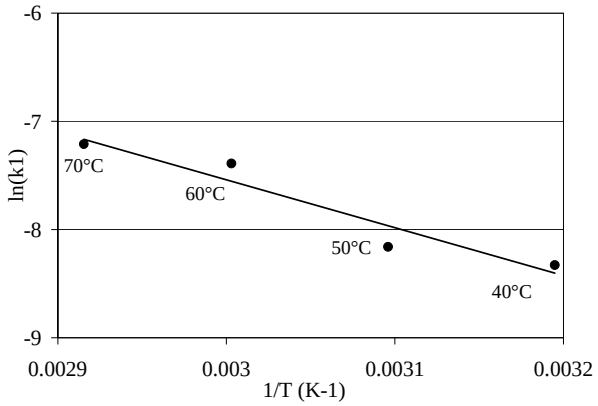

Figure 9: Compilation of OIT results (Arrhenius regression)

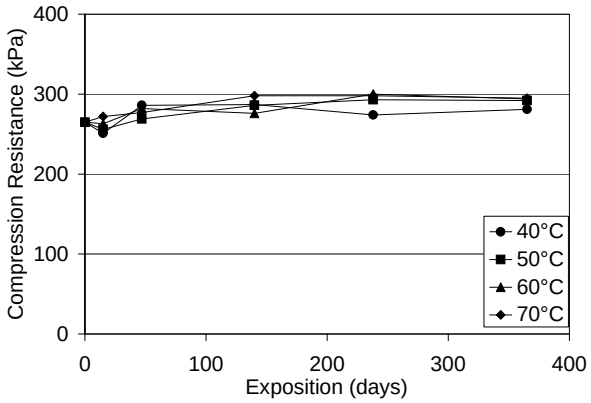

Figure 10: Evolution of the mechanical properties

Table 2: Evolution of the melt index over time at the most critical aging temperature (showing no significant variations)

	Co-extruded with virgin and recycled resins	100 % post consumer recycled resin #1	100 % post consumer recycled resin #2	100 % post consumer recycled resin #3
Initial (g/10min)	0.34	2.35	0.10	0.30
After 365 days at 70°C	0.32	2.34	0.09	0.29

Table 3: Analysis of the OIT and calculation of the relative durability of the tested products

	Co-extruded with virgin and recycled resins	100 % post consumer recycled resin #1	100 % post consumer recycled resin #2	100 % post consumer recycled resin #3
Initial OIT (min)	135	6.9	3.4	15.2
AO depletion rate at 15°C (ln min/day)	0.7×10^{-4}	1.3×10^{-4}	4.8×10^{-4}	1.4×10^{-4}
Relative durability	100% (reference)	15 to 50 %	5 to 10 %	15 to 55 %

Based on these observations it is possible to conclude that the presence of virgin resin on the two outer sides significantly improves the durability of dimpled sheets with respect to oxidation with observed ratios in the range of 2 to 20 depending on the tested materials.

4. RECOMMENDED STRUCTURE FOR THE SPECIFICATION OF DRAINBOARDS

Based on the observations presented above, the specification structure presented in Table 4 was developed. It includes all the testing methods that were found to be relevant either with respect to material performance, survivability, or long term durability.

Table 4: Recommended Specification Structure for drainboards

	Property	Standard	Type
Physical properties	Roll width	/	Typical
	Overall thickness	ASTM D5199	Minimum
Mechanical properties	Dynamic impact resistance	CGSB 37-GP-52	Minimum
	Static puncture	CGSB 37-GP-56	Minimum
	Compression resistance	ASTM D6364	Minimum
	Tensile strength	ASTM D5035	Minimum
Hydraulic properties	Water transmissivity	ASTM D4716	Minimum
	Water vapor transmission	ASTM E96-Proc. A or B	Maximum
Durability	Resistance to heat aging	ASTM D5721 / ASTM D3895	Typical / Minimum

	Stress-cracking resistance	SAGEOS GD-001	Minimum

5. CONCLUSIONS

Analysis of the function of dimple sheets and drainboards used in commercial and residential construction has led to the development of a structure for material specifications, which should be used as a minimum guidance to address most of the concerns typically observed in regards to drainboards. However, it shall be mentioned that Table 4 does not include geotextile filter properties, which shall be treated separately according to the function of the product and its environment. On the other hand, if the usage of recycled resin in drainboard manufacturing presents many benefits with respect to either cost or environmental concerns, the laboratory tests presented in this paper have shown that embedment of the recycled resin between two layers of virgin resin adequately protected against oxidation will tremendously improve the overall durability of the product, with observed improvements of projected life times in the range of 2 to 20 depending on the tested materials.

REFERENCES

Abel, R., Dahmen, G., Lamers, R., Oswald, R., Schnapauff, V. and Wilmes, K. (1991). *Bauschadensschwerpunkte bei Sanierungs- und Instandhaltungsmassnahmen*, Aachener Institut fuer Bauschadensforschung und angewandte Bauphysik.

ASTM D4716-04. In-plane Flow Rate per Unit Width and Hydraulic Transmissivity of a Geosynthetic using a constant head, *American Society for Testing and Materials*, West Conshohocken, Pennsylvania, USA.

ASTM E96/E96M-05, Procedure A. Water Vapor Transmission of Materials, *American Society for Testing and Materials*, West Conshohocken, Pennsylvania, USA.

ASTM D5721-95. Air Oven Aging of Polyolefin Geomembranes, *American Society for Testing and Materials*, West Conshohocken, Pennsylvania, USA.

ASTM D3895-07. Oxidative Induction Time of Polyolefins by Differential Scanning Calorimetry, *American Society for Testing and Materials*, West Conshohocken, Pennsylvania, USA.

ASTM D883. Standard Terminology Relating to Plastics, *American Society for Testing and Materials*, West Conshohocken, Pennsylvania, USA.

ASTM D6364-06. Standard Test Method for Determining the Short-Term Compression Behavior of Geosynthetics, *American Society for Testing and Materials*, West Conshohocken, Pennsylvania, USA.

ASTM D5035-06. Standard Test Method for Determining the Breaking Force and Elongation of Textile Fabrics, *American Society for Testing and Materials*, West Conshohocken, Pennsylvania, USA.

CGSB 37-GP-56M Section 6.4.4. (clause 5.9), *Canadian General Standards Board*, Gatineau, QC, Canada.

CGSB 37-GP-52M Section 6.4.3. (clause 5.12), *Canadian General Standards Board*, Gatineau, QC, Canada.

Corbet, S. and King, J. (1993). *Geotextiles in filtration and drainage*, Thomas Telford Services, London, Great Britain.

EN 13252:2000. Geotextiles and geotextile-related products – Characteristics required for use in drainage systems, B.3.1., *European Committee for Standardization*, Brussels, Belgium

Harper, C.A. (1999). *Modern Plastics Handbook,* McGraw-Hill, Hightstown, NJ, USA.

Hsuan, Y.G. (2000). Data Base of Field Incidents used to establish HDPE Geomembrane stress crack resistance specification, *Geotextiles and Geomembranes*, Vo.18, p. 155.

Kay, D., Blond, E. and Mlynarek, J. (2004). Geosynthetics Durability: A Polymer Chemistry Issue, *57th Canadian Geotechnical Conference*, GeoQuebec 2004.

Koerner, R. M. (1997). *Designing with Geosynthetics*, 4th edition, Prentice-Hall, Inc., Upper Saddle River, NJ, USA

Lustiger, A. (1996). Understanding Environmental Stress Cracking in Polyethylene, *Medical Plastics and Biomaterials Magazine*, p. 8.

N/A (2006). Geodrains Testing Method, Stress-Cracking Resistance of Dimpled Sheets using the “Sweden Test”, *Sageos GD001.*

N/A (2003). Environmental Stress Cracking – A Baseline Study of available recycled materials for land drainage products, ISBN 1844050335.

Rose, W. B. (2005). *Water in Buildings*, John Wiley & Sons, Hoboken, NJ, USA.

Behavior of "Draintube" Drainage Geocomposites under High Compression Load

P. Saunier, Afitex-Texel, Boucherville, Quebec, Canada
E. Blond, SAGEOS / CTT Group, St-Hyacinthe, Quebec, Canada

ABSTRACT
In the late 90's, a new type of drainage geocomposite was developed. This product differs from traditional geocomposites as the drainage core is comprised of multiple corrugated and perforated pipes instead of a planar drainage media. As a result, index and performance properties for this type of structure differ from those commonly used for planar drainage geocomposites.

In this paper, "Draintube" drainage geocomposite is presented along with its key properties and the drainage mechanism associated with its particular structure. The major factors affecting its' engineering properties are also presented. These will show that when adequately confined in soil, the particular structure of this product allows it to sustain extremely large normal loads without significant changes in transmissivity. These observations are further discussed to demonstrate the lack of sensitivity of the product to creep when compared to other conventional drainage geocomposites.

Based on these observations, creep reduction factors to be used in the design of drainage structures involving a 'Draintube' drainage geocomposite confined in soil are suggested. The suggested creep reduction factors for "Draintube" are then compared to those commonly used for conventional drainage geocomposites in similar situations.

1 INTRODUCTION

The design of geosynthetic drainage layers involves the selection of intrinsic material properties including hydraulic transmissivity. However, even when a required performance value is determined for specific site conditions, several safety factors must be applied to allow for the long term degradation mechanisms of geosynthetic products. Among those reduction factors is one for creep.

Creep intensity is a function of the ratio between service load and short term strength. The higher this ratio, the greater the magnitude of creep is. For ratios approaching 1, creep can lead to the complete collapse of the product. For that reason, transmissivity measurements are typically conducted under compressive loads that are multiplied by a safety factor to take into account a creep ratio. Furthermore, an additional creep reduction factor is applied to the measured transmissivity.

This approach is used for products which are susceptible to creep, such as geonet geocomposites. In the case of 'Draintube' drainage geocomposites, the structure of the product makes it difficult to observe this creep phenomenon as it is not possible to measure compressive strength in the same way as a geonet geocomposite or other planar drainage media, i.e. per ASTM D6364. It is thus impossible to define threshold values for creep and long term transmissivity of "Draintube" type products.

This paper intends to define the long term behavior of "Draintube" with respect to creep. To do so, after briefly introducing the key engineering properties of the product, the selected approach proceeds as:

- measure the influence of normal loads on the hydraulic properties of the product;
- determine whether creep can be observed after 100 hours.

It is assumed that if the normal load has only a slight influence on the hydraulic properties and thus the geometric properties of the pipe, then it is not sensitive to creep. Knowing that primary creep occurs during the first minutes or hours of loading, this hypothesis can then be confirmed through observation of the creep behavior for short term duration. It is during this period that the most significant deformations occur (Figure 1).

Based on these results, a threshold value is determined. This becomes the normal load used in the creep test. This threshold value is the actual service load to which "Draintube" can be exposed before creep becomes a consideration as a potential degradation mechanism.

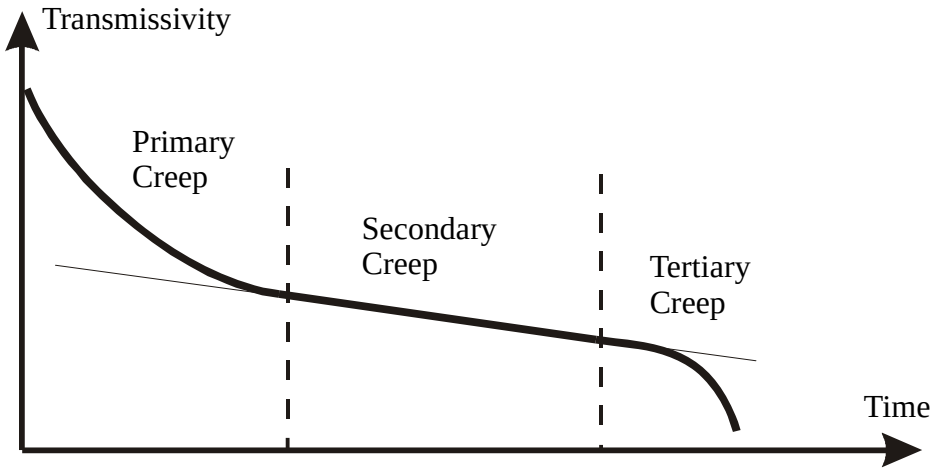

Figure 1: Creep behavior of planar drainage geosynthetics

2 DESCRIPTION OF THE PRODUCT

"Draintube" geocomposite, described in Figure 2, is composed of two layers of non-woven geotextile in a matrix. One acts as a capillary medium, the second as a filter. The two layers are needle-punched to each other. Corrugated polypropylene pipes are then inserted between the capillary layer and filter at regular intervals. These pipes, which provide most of the drainage capability of the product, are perforated in a regular pattern, with two perforations per valley at 180 degree spacing and rotated 90 degrees per valley.

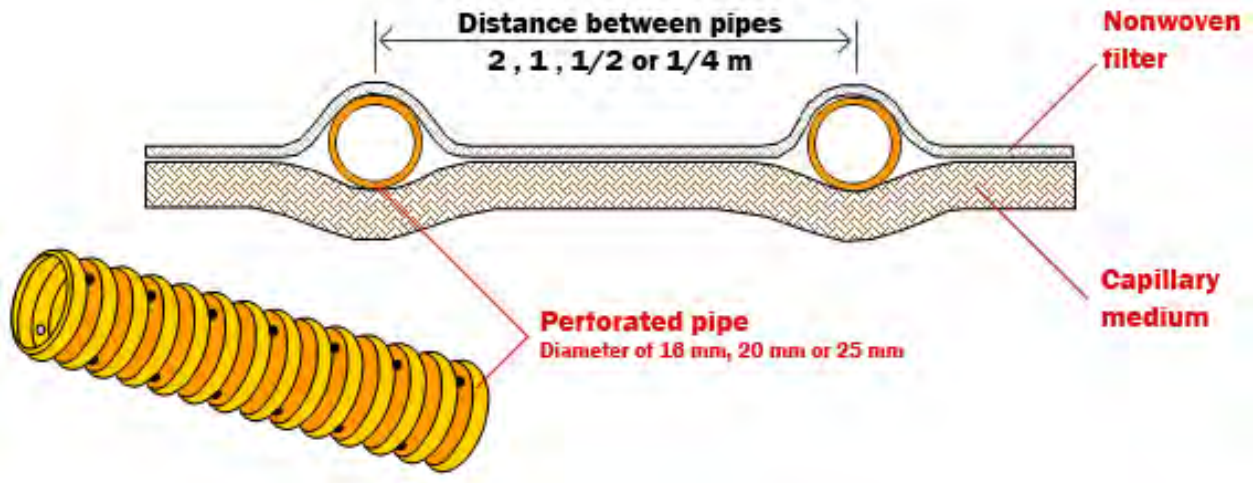

Figure 2 : "Draintube" Product Description

3 FACTORS INFLUENCING THE ENGINEERING PROPERTIES OF THE PRODUCT

3.1 Transmissivity

Unlike other types of geocomposites or granular drainage layers (i.e. sand), water flow from the surrounding environment to "Draintube" is not planar. Drainage design utilizing "Draintube" requires selection of the appropriate spacing for the multiple collector pipes within the granular drainage layer that is typically associated with it.

Given that the calculation of distance and related flow capacity required for these collector pipes is precise, software was developed to help design engineers adapt their design to the particular properties of this product. A full description of this software was previously given by Arab & al (2004).

To identify the specific product properties necessary for an application (e.g. pipe diameter and spacing), the software essentially considers the overall transmissivity of “Draintube”, as measured per ASTM D4716 in a confined soil environment. This is further described in this paper. After this property is determined on a 250 mm wide specimen with a given pipe diameter, the equivalent transmissivity of the entire drainage layer can be determined by calculation given the geometric properties of the product: with one pipe per meter, the actual transmissivity is defined as the measured transmissivity divided by 4, with two pipes per meter, divide by 2 and with four pipes per meter the measured value shall be used as-is.

Another important feature of designing with “Draintube” is determining the appropriate performance criteria necessary to either maintain the drainage pipe in an unsaturated condition or to control the maximum water head in the drainage layer. The definition of transmissivity is thus not a simple laboratory measurement per ASTM D4716, but part of an entire design process that the software facilitates.

It should be noted that because of its particular structure, the product is not influenced by temperature (i.e. thermal expansion facilitating the development of wrinkles) and thus that the overall transmissivity is not likely to be influenced by construction concerns. If appropriate precautions are taken during backfilling operations, the confinement offered by the surrounding soil and the particular shape of the product will ensure preservation of the hydraulic properties after installation without consideration of many of the reduction factors which must be used for traditional drainage geocomposites, e.g. geotextile intrusion.

3.2 Filtration Properties - Filtration Opening Size and Permittivity

As with traditional drainage geocomposites, water enters the drainage core through a filter media. This filter media is selected based on specific filtration engineering properties as with any other filter. These properties typically include permeability and filtration opening size.

Another important feature of filtration design with “Draintube” is the reliability of the engineering properties. Because the filter layer is joined to the capillary medium through needle-punching, with no thermal treatment or bonding and this process is employed only in the areas away from the collection pipe, the actual filtration properties of the delivered product are fully maintained in the area around the pipe. This feature applies to any geotextile filter used since the same methods and equipment set-up are employed.

3.3 Protection of Geomembranes

The geotextile component of “Draintube” provides a minimal contribution to the hydraulic performance of the product. Thus the geotextile is typically selected based upon application requirements. “Draintube” installed between two layers of soil will typically include a light geotextile meeting the filtration requirements described above. When “Draintube” is installed over a geomembrane, a heavier geotextile meeting the engineering requirements for geomembrane protection is selected.

3.4 Interface Friction Properties

The design of drainage geocomposites typically includes consideration of the risk of component delamination under high loads, or interface friction slippage. Since the two layers of geotextile in “Draintube” are intimately bound together through needle-punching, internal delamination is unlikely. Veneer stability and other design issues involving friction characteristics are solely controlled by the interface friction properties of the non-woven geotextile.

4 BEHAVIOR UNDER HIGH LOAD

4.1 Test program

One of the fundamental differences between “Draintube” and other drainage geosynthetics is the structure of the product. This structure consists of two non-woven layers which provide very little to the global drainage capability of the product, and a perforated pipe which provides most, if not all, of its performance. As a result, investigation of the long term hydraulic efficiency of the product must be focused on the behavior of the pipe.

Unlike traditional planar geocomposites, the load transfer mechanism between the overlying and underlying material is only a fraction of the normal load. The pipe component of “Draintube” is confined by the surrounding soil, thus loads are calculated

using traditional flexible pipe design methodologies (Figure 3). The soil arching effect that applies to other flexible pipes applies to “Draintube” as well (Figure 4).

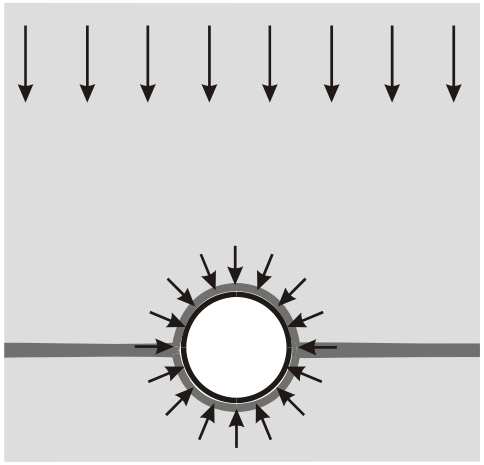

Figure 3: pipe loading mechanism

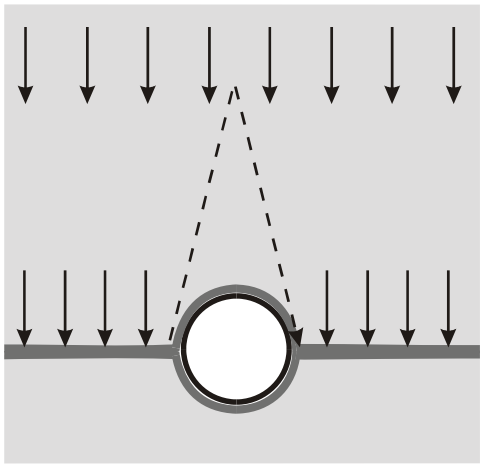

Figure 4: soil arching effect

This loading mechanism is completely different from that used for geocomposites with geonet cores. With those types of geocomposites, loads are applied to the entire surface of the product and are completely transferred into the geonet structure. There is no “shedding” effect afforded through soil arching. Consequently, traditional design approaches for creep, developed specifically for geonet geocomposites, are not relevant.

In order to observe the behavior of “Draintube” drainage geocomposites exposed to high normal loads and to estimate their long term behavior, a research program was developed. Two major aspects were investigated:

1- The influence of normal load on transmissivity, with measurements of transmissivity under 5,000, 10,000, 15,000 and 25,000 psf loads.
2- The influence of time on transmissivity, with measurements of transmissivity after 15 minutes, 1 hour, 24 hours and 100 hours under a 10,000 psf load. The value of 10,000 psf was selected because it is commonly used in drainage geocomposites specifications, and because it exceeds a vast majority of the service conditions met by these products.

The tests were conducted using a 25 mm thick layer of fine sand with a polyethylene sheet as the confining media above and below the “Draintube”. In order to replicate a typical drainage condition in landfill capping applications, a 60 mil HDPE geomembrane was installed below “Draintube”, as shown in Figure 5. The results are presented in Figures 6 and 7 and summarized in Tables 1 and 2.

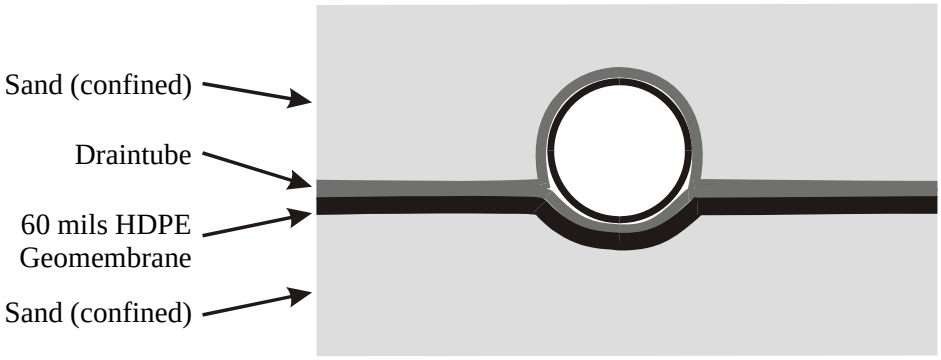

Figure 5: Test configuration

Table 1: Influence of normal load on transmissivity

normal load (psf)	seating time	gradient	Transmissivity (m^2/s)	gradient	Transmissivity (m^2/s)
5 000	0.25	0.1	2.3E-03	1	7.7E-04
10 000	0.25	0.1	2.1E-03	1	6.9E-04
15 000	0.25	0.1	1.8E-03	1	6.0E-04
25 000	0.25	0.1	1.6E-03	1	5.2E-04

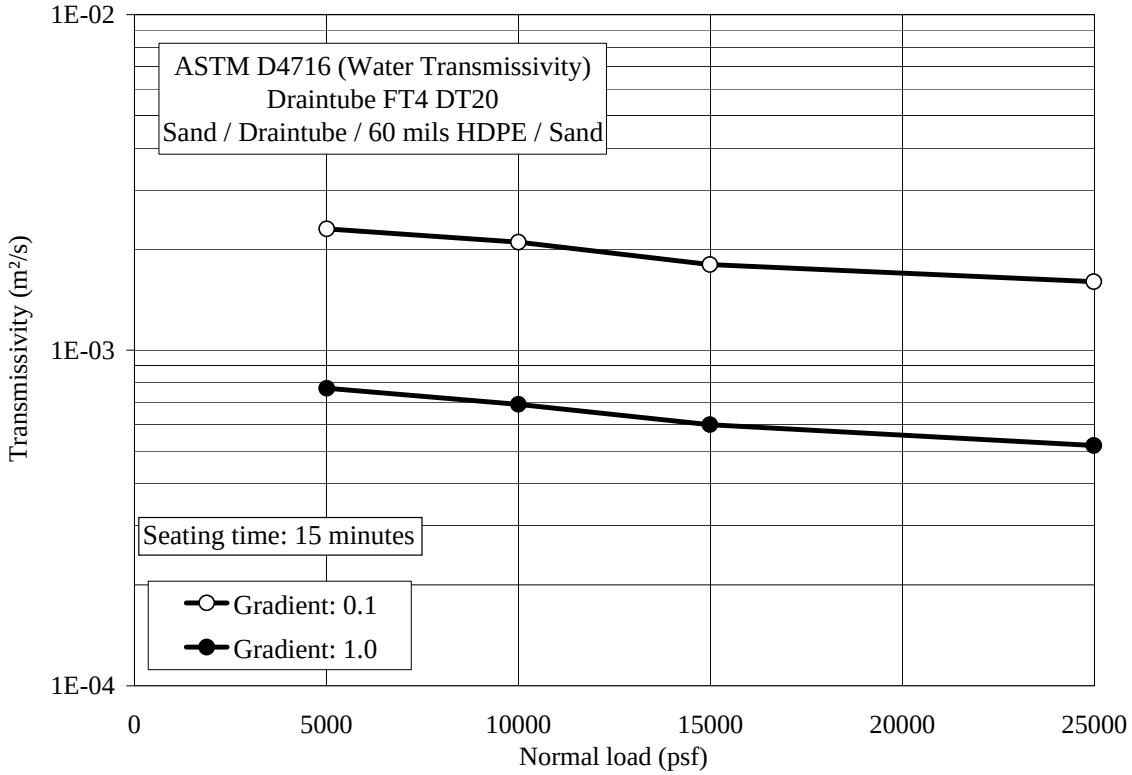

Figure 6: Effect of normal load on the transmissivity of “Draintube” geocomposite

Table 2: Influence of time on transmissivity

seating time	gradient	Transmissivity (m^2/s)	gradient	Transmissivity (m^2/s)
0.25	0.1	2.1E-03	1	6.9E-04
1	0.1	2.1E-03	1	6.9E-04
24	0.1	2.0E-03	1	6.7E-04
100	0.1	2.0E-03	1	6.5E-04

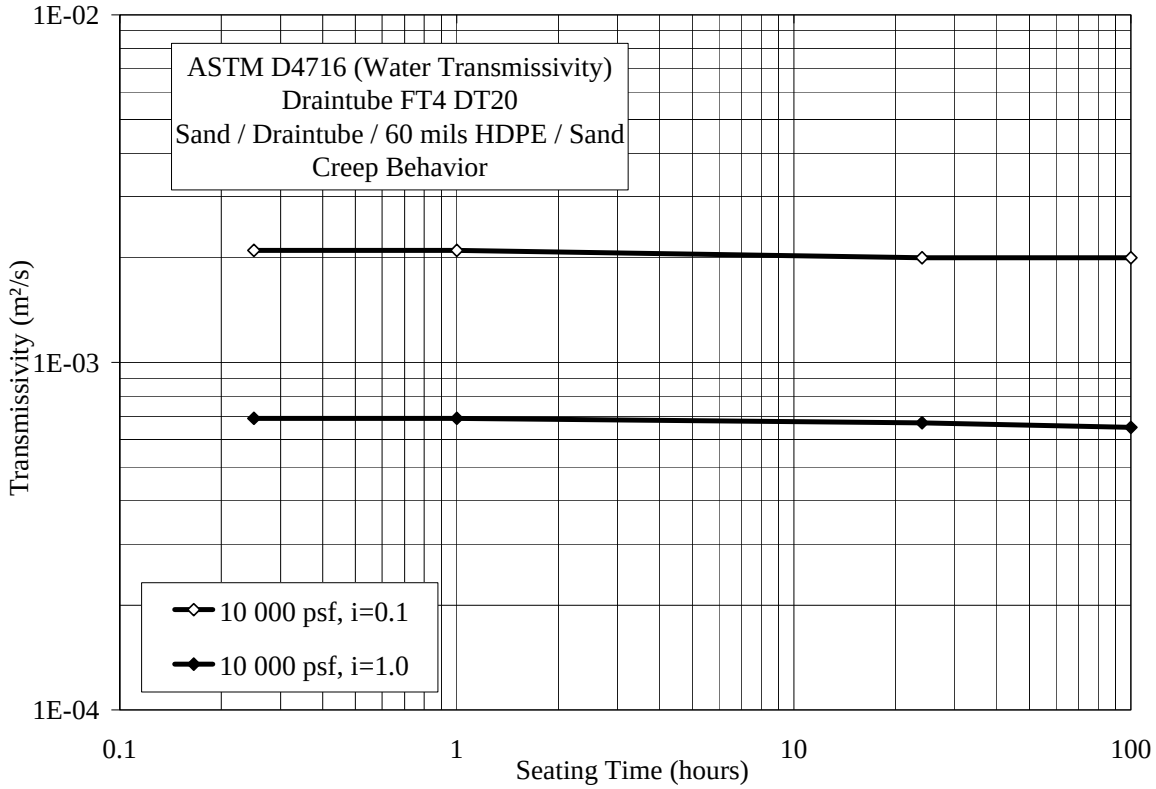

Figure 7: Effect of time on the transmissivity of “Draintube” geocomposite

Figures 6 and 7 show that:

- Normal load had only a minimal effect on the transmissivity of “Draintube” up to 25,000 psf. Overall, the reduction in transmissivity is less than 30% for loads between 5,000 to 25,000 psf.
- Time does not significantly affect transmissivity under a normal load of 10,000 psf for 100 hours.

5 DISCUSSION

The results presented above confirm the hypothesis that normal loads have an insignificant effect on “Draintube’s” transmissivity. Transmissivity is also time independent over the first 100 hours of testing, when primary creep would be expected to occur.

With less than a 30% variation in transmissivity up to loads of 25,000 psf, the influence of normal load on the measured transmissivity was not in line with the hypothesis made at the early stages of the project, nor with the observation of time independence. However, further investigation led to the following observations:

- the presence of a geomembrane under “Draintube” creates a critical condition where there is a “slip” plane under the pipe. When combined with an open void between the pipe and the geomembrane, compression of the pipe can occur. This applies to the application of “Draintube” for capping applications where the geocomposite is installed

above an HDPE geomembrane. However, this approach is conservative with respect to the application of "Draintube" between two layers of granular material, such as in athletic field drainage, some mining applications, etc.

- The test set-up of the transmissivity apparatus does not allow thicker layers of soil to be used for two reasons. The first reason is that there is not sufficient space vertically. The second reason is that as the thickness of the soil layer is increased, friction between the soil and the vertical walls of the apparatus influences the transfer of the normal load. As a result, the soil arching effect described in Figure 4 can not be fully realized. These equipment limitations increase sample compression during testing, resulting in reduced measured values of transmissivity, much smaller than the ones observed in the field.

As a result, the observations made during this project are believed to be conservative when compared to the expected field performance of the product. The minimal reductions in performance observed over the 100 hour test duration, combined with the increased effects of normal load caused by the particular conditions of the test (arching effect minimized due to the limitations of the apparatus) suggest that creep deformation is unlikely to occur in this particular product.

6 CONCLUSION

When confined in soil under a normal load of 10,000 psf, the transmissivity of "Draintube" was not affected by creep over a testing period of 100 hours. Therefore, when designing for the long term transmissivity of a "Draintube" drainage geocomposite, a Factor of Safety for creep (FS_{cr}) of 1.0 can be used for normal loads up to 10,000 psf.

Additional research is needed to confirm the products behavior for normal over 10,000 psf. This should include evaluation of the product in such a way that the soil arching effect that is likely to take place in normal field conditions can be mobilized in the laboratory. This will involve slight improvements or changes to existing testing techniques.

REFERENCES

ASTM D4716. Standard Test Method for Determining the (In-plane) Flow Rate per Unit Width and Hydraulic Transmissivity of a Geosynthetic Using a Constant Head. *American Society for Testing and Materials*, West Conshohocken, Pennsylvania, USA

ASTM D6364. Standard Test Method for Determining Short-Term Compression Behavior of Geosynthetics. *American Society for Testing and Materials*, West Conshohocken, Pennsylvania, USA

Arab R, Faure Y H, Lecendre V, Gendrin P, Douillat M (2004). *Embankment Access Road to A Civil Railway Structure On Soft Soil*, Eurogeo 04, March 1-3 2004, Munich, Germany

Evaluation of Perforated Geosynthetic Box to be Considered Water Permeability in Waste Landfill Slope

H.Y. Jeon, Division of Nano-Systems Engineering, Inha University, Incheon, Korea
J.P. Gourc, Grenoble University, Grenoble Cedex 9, France

ABSTRACT
Geosynthetic separation boxes made from recycled polymeric materials were designed to increase the stability of the steeply sloping sides of waste landfills and improve waste storage efficiencies. The inner sides of the boxes are open and they can be filled with sand, soil, rubble or other materials, in order to fix them to the side slopes of waste landfills. To evaluate the advantages of geosynthetic separation box plates, index tests were conducted, comparing geonet composites and geosynthetic separation boxes. Hydraulic and friction properties of geosynthetic separation box plates were superior to those of geonet composites. Residual tensile strength retention ratios after UV exposure of geosynthetic separation box plates exposed to UV light and to leachate were also better. Finally, the properties of geosynthetic separation boxes as geomembranes were theoretically examined by the requirement values for waste landfill application.

1. INTRODUCTION

Geomembranes which have a water barrier function to waste leachate solutions are the most important materials in waste landfill in the world [1-2]. The general raw materials to make geomembranes are HDPE, PP, PVC and some kind of rubber component resins. Among these materials, HDPE resin is very widely used to make geomembranes in the USA and many European countries because of its excellent waste landfill performance compared to other resins [3]. However, many waste landfills in Korea are constructed between valleys and have very steeply sloping sides (more than 30°). Therefore, large quantities of sand or backfill soils are required to increase the stability of the side slopes and, as a result, the total volume available for waste disposal is decreased by the amount shown by the oblique lines in Figure 1. The resulting reduction in the waste storage volume is one of the main reasons why the construction of waste landfills is often considered to be uneconomic [4]. The use of geosynthetic separation boxes, which are made from recycled high density polyethylene, HDPE(2), can reduce the total cost of constructing waste landfills, because they are cheaper to produce than commercially produced non-recycled HDPE(1). The inner sides of these geosynthetic boxes are open and they can be filled with sand, soil, rubble or other materials, in order to fix them to the slopes of the waste landfills. The use of such filler materials in the geosynthetic boxes allows good drainage performance, as well as increased stability of the side slopes of the waste landfills. In this study, geosynthetic separation boxes composed of recycled high density polyethylene, HDPE(2) plates were designed to improve the waste storage and drainage efficiencies in the steeply sloped sides of waste landfills due to the application of perforated plates as shown in Figure 1 (b). Residual tensile strength retention ratios of geosynthetic separation box (as strength change during waste storage under UV exposure and leachate solutions) were examined and their properties assessed by comparing them to the theoretical values appropriate for waste landfills. The drainage performance of the geosynthetic separation boxes was examined and compared with that of the geonet composites. Finally, the drainage function requirements of the geosynthetic separation boxes were examined through theoretical point of view.

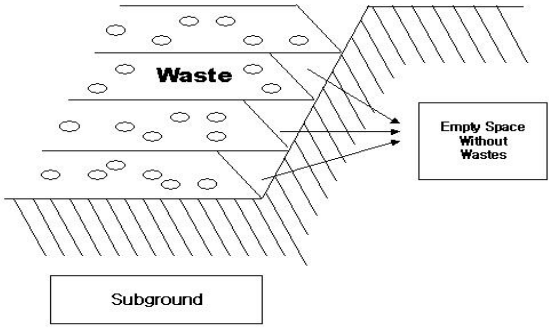

(a) without geosynthetic separation boxes

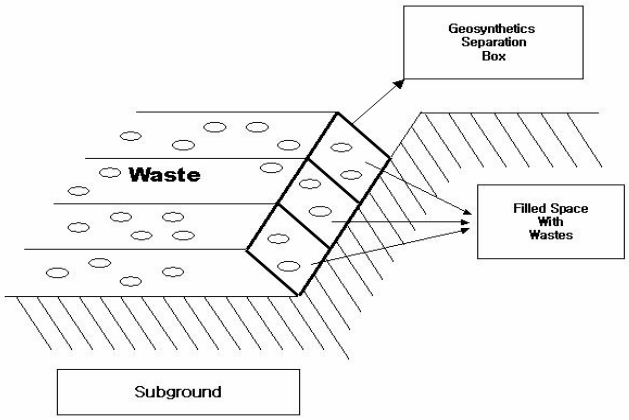

(b) with geosynthetic separation boxes

Figure 1. Schematic diagram of waste landfills with and without geosynthetic separation boxes

2. EXPERIMENTAL

2.1 Manufacture of geosynthetic separation boxes

The geosynthetic separation boxes were made from recycled HDPE(2) plates with a unit size of 1×1 m^2 connected by rods. The plates were made by injection moulding. Boxes upper and lower plates are perforated so that generated gas and leachates are vented and the box exhibits good drainage drainage performance. The boxes were connected to each other continuously, as represented in Figure 2. Sand, gravel and rubble were used as the filler materials between the upper and bottom plates of the boxes. A geonet composite, a nonwoven/geonet/nonwoven structure that is generally applied to the slopes of waste landfills in Korea, was used as a basis for comparison with the HDPE(2) plates of the geosynthetic separation boxes.

Figure 2. Photograph of field installation of geosynthetic separation box of HDPE(2)

2.2 Assessment of performance of geosynthetic separation boxes

To evaluate the advantages of the geosynthetic separation boxes, index tests of the plates were conducted to compare the two cases in which the geonet composites and geosynthetic separation boxes were used in the side slopes of the waste landfills. The tensile, chemical and UV resistance properties of the recycled HDPE(2) plates were examined in accordance with ISO 10319, ISO TR 12960 and ASTM D 4355, respectively. The hydraulic permeability was measured by evaluating the amounts of water loss in accordance with ISO 11058 for both the geonet composite and the plates of the geosynthetic separation boxes. For this test, HDPE(2) plates were prepared as in Figure 3.

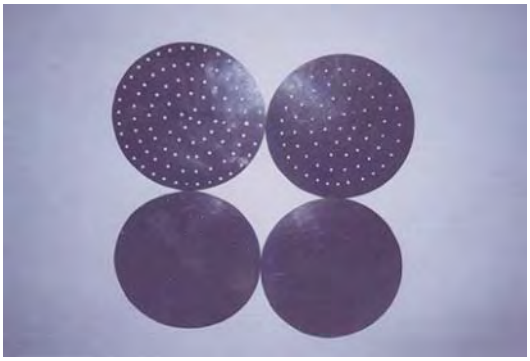

Figure 3. Photograph of HDPE(2) plates for hydraulic test

3. RESULTS AND DISCUSSION

3.1 Engineering Properties

Table 1 shows the tensile properties of the recycled HDPE(2) and normal HDPE(1) plates used in the separation boxes. It is apparent that the recycled HDPE(2) plates have higher tensile strength than the HDPE(1) ones, but exhibit less elongation. This indicates that the former should have good performance for use as separation box plates.

Table 1. Tensile properties of HDPE plates in the machine direction

Tensile Properties / HDPE Plates	Strength (kg/cm^2)	Elongation (%)
HDPE(1)	32.4	603.5
HDPE(2)	36.7	107.4

(1) HDPE plate with a thickness of 3 mm used for geomembranes
(2) Recycled HDPE plate with a thickness of 3 mm used for geosynthetic separation box

Table 2 shows the tensile strength retention ratios of the recycled HDPE plates and geonet composite from durability evaluation measurements.

Table 2. Tensile strength retentions of separation box plate and geonet composite

(a) Chemical resistance

Chemical Resistance / Geosynthetics	Tensile Strength Retention (%)			
	pH 3		pH 12	
	25 °C	50 °C	25 °C	50 °C
HDPE(2)	92.6	88.2	91.2	86.4
Geonet Composite	92.4	88.6	92.6	88.2

(b) UV resistance

UV Resistance / Geosynthetics	Tensile Strength Retention (%)
HDPE(2)	92.4
Geonet Composite	90.6

The chemical resistance of the two HDPE(1), (2) plates was obtained by comparing the tensile strength before and after immersion for zero and 120 days to solutions of pH 3 and 12 in 25ºC and 50ºC, respectively. Their UV resistances were also evaluated by comparing the tensile strength before and after a 500 hours of UV exposure. As shown in Table 2, the tensile strength retention ratios of HDPE(1) and HDPE(2) plates used for the geosynthetic separation boxes were better than those of the geonet composite. In Figure 4, for slope angle β and external load W

in waste landfill, the breaking force of the separation box plate consists of the driving force, W sin β and the resisting force, F against the driving force, respectively.

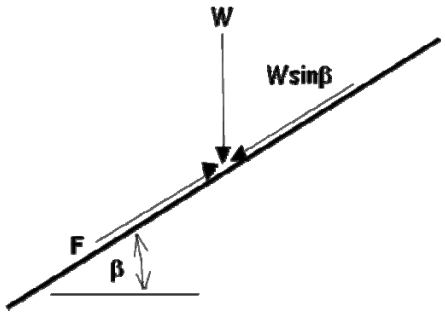

Figure 4. Breaking force of separation box with slope angle in waste landfills

In here, tensile strength of separation box would be dependent on the value of factor of safety. The factor of safety (FS) is defined as:

$$FS = \frac{resisting \cdot force}{driving \cdot force} = \frac{F}{W \sin \beta} \quad [1]$$

If we apply the following installation conditions to Equation (1), then one can calculate the plates' required tensile strength.

* slope angle(β)
  : 15°, 30°, 45°, 50°
* height of waste landfill
  : 3 m, 5 m, 10 m, 20 m, 50 m, 100 m
* density of waste: 1.4 t/m^3
* weight of final covering:
  : vegetation layer + drainage layer = 1 m×1.7 (t/m^3),
  : compaction layer = 0.6 m×2 (t/m^3)
* factor of safety: 1.5
  – driving forces:
    1400 kg/m^3×height of waste landfill + (weights of vegetation and drainage layers) × sin β
  – resistance forces = 1.5×driving forces

Table 3 lists the required tensile strengths of the HDPE(2) plates of the geosynthetic separation boxes for waste landfills with the given slope angles and heights. For example, the minimum tensile strength of the HDPE(2) plates of a geosynthetic separation box must be 1.05 kg/cm^2 if the slope angle is 45°and the height of the waste landfill is 5 m.

Table 3. Tensile strength (kg/cm^2) of separation box plate as a function of the slope angle (β) and height of the waste landfill

		Height of Waste Landfill					
		3m	5m	10m	20m	50m	100m
Slope Angle (β)	15°	0.28	0.38	0.66	1.20	2.83	5.55
	30°	0.53	0.74	1.27	2.32	5.47	10.72
	45°	0.75	1.05	1.79	3.28	7.73	15.16
	50°	0.82	1.14	1.94	3.55	8.38	16.42

3.2 Minimum required strength of separation box under load of filling waste materials

Figure 5 shows the schematic diagram of geosynthetic separation box in waste landfills.

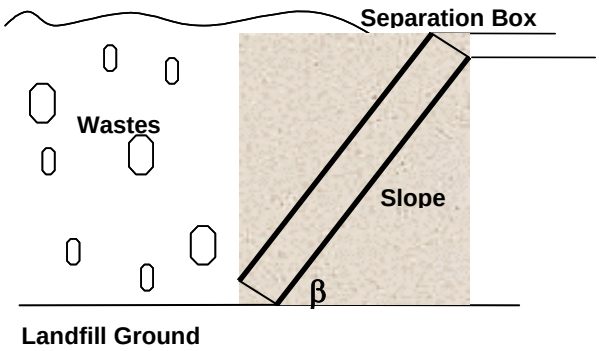

Figure 5. Schematic diagram of waste landfill used geosynthetic separation box with slope angle

The following assumptions were made to calculate the loads resulting from the filler materials.

* filler material: sand
* density of sand: 1.6 ton/m^3 (dry weight)
  - general range of dry-weight density of sand: 1.47 ~ 1.63 ton/m^3
* no water in the drainage layer before landfill
* slope angle of separation box (β): 30°

The minimum required strengths of the unit area of a separation box were determined for the following lengths of slope and slope angles.

* length of slope: 10 m, 30 m, 50 m
* slope angle: 15º, 30º, 45º, 50º
* unit weight of filler materials: sand (1.6 ton/m^3) and gravel (2.0 ton/m^3)

Table 4 shows the minimum required strengths in the case of sand and gravel as a function of the length of the slope and slope angle. For example, in Table 4 (a), the minimum required strength of the unit plate of the separation box should be 6.13 kg/cm^2 for a slope length of 50 m and a slope angle of 50º. In Table 4 (b), the minimum required strength of the unit area of the separation box should be 7.66 kg/cm^2 for a slope length of 50 m and a slope angle of 50º.

Table 4. Minimum required strength (kg/cm^2) as a function of length and angle of the slope for sand and gravel

(a) for sand (1.6 ton/m^3)

Slope Angle (β) \ Slope Length	10 m	30 m	50 m
15°	0.41	1.24	2.07
30°	0.80	2.40	4.00
45°	1.13	3.39	5.66
50°	1.23	3.68	6.13

(b) for gravel (2.0 ton/m^3)

Slope Angle (β) \ Slope Length	10 m	30 m	50 m
15°	0.52	1.55	2.59
30°	1.00	3.00	5.00
45°	1.41	4.24	7.07
50°	1.53	4.60	7.66

3.3 Drainage performance of separation box when applied to waste landfills

The hydraulic conductivity was measured by evaluating the amounts of water loss with and without the filling materials. The permittivity of the HDPE(2) plates with holes was better than that of the geonet composite. The frictional properties

of both the HDPE(2) plates and geonet composite were not good, because of their specified surface structures, but those of HDPE(2) were better than those of the geonet composite. The nonwoven geotextile layer of the geonet composite was damaged by friction and this is the main cause of its reduced frictional properties. However, further performance tests of the geosynthetic separation boxes must be conducted to confirm these results over longer periods of time. Therefore, geosynthetic separation boxes made of HDPE(2) could be installed in the slopes of waste landfills based on the theoretical requirements for tensile strength and coefficient of permeability under waste landfill conditions.

3.4 Numbers of holes in separation box plates for drainage performance

For a geosynthetic separation box to exhibit maximum permeability, it is necessary to maintain the optimum hole size in the plates. The minimum area of the holes was calculated based on the standard permittivity of waste landfills in Korea, which is required to be greater than 1×10^{-2} cm/s. In this study, the minimum required area of the holes per unit area (1m×1m) of the HDPE(2) plate was calculated by considering the following permittivity ranges:

– for sand: 1×10^{0} cm/s ~ 1×10^{-3} cm/s
– for gravel: 1×10^{2} cm/s ~ 1×10^{-1} cm/s

In Figure 7, the thickness, hole diameter, and distance between the separation boxes are designated as A, B and C, respectively. From Darcy's law, the flux of this model can be written as follows.

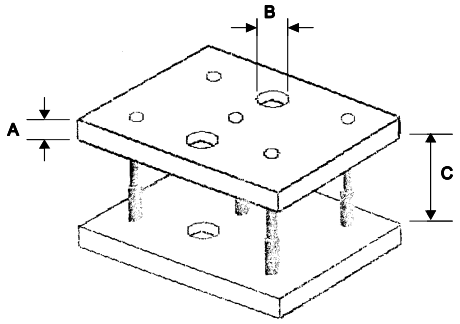

Figure 7. Configuration of separation box with drainage holes
(A) Thickness; 5mm, (B) Diameter; 10mm, (C) Height ; 30cm

$$v = k \cdot i \quad [2]$$

$$Q = v \cdot A \quad [3]$$

$$Q = k \cdot i \cdot A \quad [4]$$

where, v: discharge velocity (cm/s), k: permittivity (cm/s), i: hydraulic gradient, Q: flux (cm^3/s), A: unit area (cm^2)

For hydraulic gradients of two or five with the above conditions, v is constant even if k decreases, because of the increase in i. The minimum numbers and areas of holes are shown in Table 5, as a function of the hole diameter and hydraulic gradient per unit area in the separation box. The minimum numbers of holes per unit area in the separation box are represented in Table 6, as a function of the permittivity and fraction of holes. A factor of safety equal to 2.0 was adopted to take into consideration the clogging of the holes of the plate in the separation box. Based on the data in Table 6, it can be seen that it is possible to maintain the permittivity in the range of 5.0×10^{-2} ~ 1.0×10^{-1} by making 500 ~ 1,132 holes per unit area of the separation box with a hole diameter of 2 cm. It seems reasonable that the fraction of holes in the plate should be in the range of 10 ~ 20% when we consider the permittivity range of sand, which is 5.0×10^{-1} ~ 1.0×10^{-1}.

Table 5. Minimum number and area of holes in the unit plate in the separation box as a function of the diameter of the holes and hydraulic gradient

Hydraulic Gradient	2	5
Area(㎠)	10000	10000
k (㎝/s) - Drainage Layer	1.0E–01	1.0E–01
Acceptable *k*(㎝/s)[1)]	1.0E–02	1.0E–02

Hole Diameter (㎝)	1.0	2.0
Discharge(㎤/s)[2)]	2000.0	5000.0
First *v*(㎝/s)	0.2	0.5
Acceptable Discharge (㎤/s)[3)]	200	500
Minimum Area (㎠)[4)]	1000	1000
Fraction of Holes (%)	10	10
Minimum Numbers of Holes	1273	1273

[1)] standard permittivity
[2)] flux of drainage layer
[3)] flux through separation box
[4)] cross-sectional area of drainage layer with flux through separation box

Table 6. Minimum numbers of holes per unit plate in the separation box as a function of the permittivity and fraction of holes

Permittivity (㎝/s)	0.05	0.11	0.5	1
Fraction of Holes (%)	20	10	2	1
Hole Diameter, 1 ㎝	2547	1273	255	127
Hole Diameter, 1.5 ㎝	1132	566	113	57
Hole Diameter, 2 ㎝	637	318	64	32
Hole Diameter, 3 ㎝	283	141	28	14
Hole Diameter, 5 ㎝	102	51	10	5

4. CONCLUSION

Recycled HDPE showed good tensile strength, chemical and UV resistance, as well as hydraulic and friction properties in comparison to those of HDPE for geomembranes for use in waste landfills. The recycled HDPE plate is an excellent material for geosynthetic separation boxes for stabilizing the side slopes of waste landfills. It is seen that geosynthetic separation boxes could be used instead of geonet composites to very steeply sloping sides of waste landfills, like those encountered in Korea.

REFERENCES

Gourc, J.P. and Villard, P. (2000), Reinforcement by Membrane Effect: Application to Embankments on Soil Liable to Subsidence. Proceedings of 2nd Asian Geosynthetics Conference, Kuala Lumpur, 29–31 May 2000, 1: 55–72.

Jeon, H.Y, et al. (2003), Assessments of long-term filtration performance of degradable prefabricated geotextile drains, Polymer Testing, 22, 7: 779-784.

Koerner, R.M. (2005), Designing with Geosynthetics. 5th ed, Upper Saddle River: Prentice Hall, Chapter 2.

McBean, E.A., Rovers, F.A., and Farquhar, G.J. (1995), Solid Waste Landfill Engineering and Design, Englewood Cliffs, Prentice Hall: 155–206.

A Review of the Environmental Factors Influencing the Durability of Polyolefins

M. Koryabina, F. Ceccarani, M. Balow, T. Paff and B. Kozlowski, LyondellBasell Industries, Lansing, Michigan USA

ABSTRACT
This paper will review the environmental durability of polyolefins, including polyethylene, polypropylene and thermoplastic polyolefin (TPO). Considered will be the effects of heat, light, chemical environment and stress levels known to influence the longevity of these materials.

1. INTRODUCTION

Freedonia, in a 2007 study, indicates that the square footage of installed geosythetics is expected to grow 4.4% per year to reach 870 million square yards through 2010. The study attributes the growth to a rise in population, which will create a demand for materials to contain potable water and both liquid and solid wastes. At the same time, the transportation infrastructure is expected to expand to support population growth, which will also create a demand for geomembranes in this market. There is also a healthy outlook for non-building construction expenditures and mining activity that will help stimulate the increased need for geosynthetics (Bowne, Ferrell and Zielenski, 2007).

With all the changes that are expected to stimulate this market, there will be a need for specifiers and converters to place an increased emphasis on material selection for such membranes. The expansion of today's infrastructure creates pressure on designers to select geosynthetic materials that can be quickly and reliably installed, that perform well in the installed conditions and that are easily repairable. As mining projects continue to expand into geographical locations at high elevations, geomembranes must be able to be installed and to function in the extremes of weather conditions; therefore, material selection for these projects is critical (Menzel and Vaccaro, 2008). Greater consideration by specifiers must be given to the application when deciding on the material that goes into a geosynthetic, thereby minimizing issues both during installation and in use.

This study investigates the properties of polyolefins that are traditionally utilized by converters in the fabrication of geosynthetics, comparing their benefits and weakness against characteristics that may be important to specifiers in proper material selection. This paper will examine a high, medium and linear low density polyethylene; a polypropylene homopolymer and a copolymer; and two types of thermoplastic polyolefins. By relating laboratory testing to puncture resistance, wrinkle formation, and weathering degradation under stress, testing conducted in this study can aid the understanding of how the selected polyolefins would behave in the field.

2. DESCRIPTION OF POLYOLEFINS

2.1 Polyolefin Structures

Polyolefin materials have long been utilized for geosynthetics, due to their combination of unique physical properties with chemical and weather resistance. Table 1 describes the seven polyolefins that were evaluated in this paper. A polypropylene homopolymer (PP HOMO), a polypropylene copolymer (PP HECO), a linear low density polyethylene (LLDPE), a medium density polyethylene (MDPE), a high density polyethylene (HDPE), a reactor-grade thermoplastic olefin (r-TPO), and a post-reactor blend of polypropylene homopolymer and ethylene-propylene rubber (b-TPO).

Table 1. Melt Flow Rate and Density of Polymers used in this study, determined by ASTM D1238.

Characteristics	Units	b-TPO	r-TPO	PP HOMO	PP HECO	HDPE	MDPE	LLDPE
MFR @ 230 ºC, 2.16 kg (ASTM D1238)	g/10 min	4.69	0.60	0.27	1.40	0.65	0.30	2.06
MFI @ 190 ºC, 2.16 kg (ASTM D1238)	g/10 min	-	-	-	-	0.33	0.17	1.0
Density (ISO 1183)	g/cc	0.870	0.880	0.902	0.902	0.949	0.940	0.918

A polyolefin is a polymerized olefin or alkene, which is an unsaturated chemical compound, containing at least one carbon-to-carbon double bond. When an alkene is utilized as a monomer in a polymerization process, a catalyst is introduced to create a reaction that chemically bonds the alkene molecules to form polymer chains. Depending on the type of monomer which is used, on the choice of catalyst, and on the polymerization process employed, different polymers can be produced by chemical reaction.

The three monomers used in making the polyolefins specific to this discussion are ethylene, propylene and hexene. The catalysts chosen for olefin polymerization are Ziegler-Natta, Metallocene or chrome. These catalysts are transitional metal compounds bearing a metal-carbon bond, which in a polymerization reactor is able to carry out a repeated insertion of olefin units (Pasquini 2005). Ethylene and propylene are polymerized to produce polyethylene (PE) and polypropylene (PP), respectively — see Figure 1 for the chemical structures of the monomers and of the polymers after polymerization. The two monomers can also be polymerized together at different molar ratios to produce random polypropylene (0.5 to 7% ethylene), or at nearly equal molar levels to produce ethylene-propylene rubber (EPR).

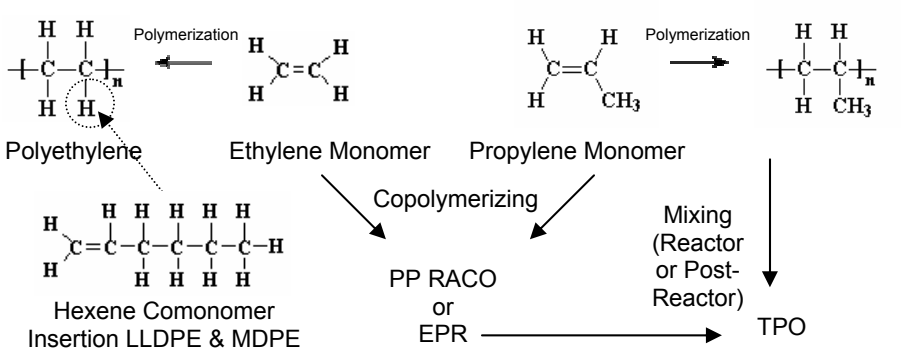

Figure 1. Chemical structures of olefin monomers and their structures after polymerization.

The three types of PE that are traditionally used for geomembranes have different chemical structures and consequently different densities. HDPE resins have densities greater than or equal to 0.941 g/cm^3; MDPE resins have densities in the range of 0.926 to 0.940 g/cm^3; and LLDPE resins have densities in the range of 0.9125 to 0.925 g/cm^3. HDPE consists of chains of repeating carbon atoms, with two hydrogen atoms bonded to each carbon atom, but with no chain branching, meaning that chains do no bond to one another. LLDPE and MDPE are similar to HDPE, with many repeating carbons that form a chain. By copolymerizing the ethylene monomer with an alky-branched comonomer, a copolymer PE is produced, in which hydrocarbon branches replace some of the hydrogen atoms bonded to the carbon atoms. The distinction between LLDPE and MDPE is a result of the degree of copolymerization, ultimately affecting the density of the polymer.

Polypropylene also consists of a carbon chain, but some of the hydrogen atoms are replaced by methyl groups. Depending on the placement of the methyl groups, PP can be isotactic or atactic. The phenomenon that describes the placement of methyl groups is generally referred to as “tacticity.” Isotactic means that the methyl groups are on the same side of the chain, which contributes to a crystalline structure. In atactic PP, the methyl groups are randomly placed on either side of the chain, forming an amorphous solid. PP heterophasic copolymers are two-phase systems that are normally produced in a two-step process: first the main chain is polymerized, then, in a second step, one or more additional monomers are polymerized together, introducing a second phase. These copolymers, therefore, contain both an isotactic crystalline phase and an amorphous rubbery phase. The copolymer being evaluated for this study has a polypropylene crystalline matrix with approximately 12% ethylene-propylene rubber distributed within the matrix.

Thermoplastic olefins are PP based copolymers that contain greater than 40% of a rubbery phase. Two TPOs were selected for evaluation in this study. One TPO was produced in a unique polymerization reactor, known as the *Catalloy* process technology; and one was a post-reactor mechanical blend of PP and an ethylene-propylene rubber (EPR). The *Catalloy* processed resin (r-TPO) that was selected for evaluation has a random copolymer (PP RACO) matrix, with ethylene randomly inserted within the polymer chains, with greater than 65% propylene rich EPR. The post-reactor blend (b-TPO) consists of a PP homopolymer that was compounded with 60% of natural rubber on a Banbury mixer and then pelletized.

2.2 Polyolefin Morphology

The properties of polyolefins are strongly influenced both by their morphology, which includes the structure of a polymer, and by process technique. Figure 2 defines the influencing factors of molecular structure and processing that help to tailor unique polymer morphologies. Effects of polymer processing on morphology will be discussed in section 2.3, Degradation Mechanisms of Polyolefins.

One of the critical factors governing polymeric morphology is the influence of molecular structure on the ability of a polymer to crystallize. The degree of crystallinity is governed primarily by the tacticity of the polymer chain. This tacticity can be altered by the insertion of comonomers, and by the type of comonomer inserted in polyethylene and polypropylene, as discussed above. Inserting a comonomer into the chain essentially alters the backbone, thereby limiting the ability of the polymer to crystallize in an orderly fashion. The crystallinity of a polymer governs such properties as a density and the balance of impact resistance and stiffness that a material demonstrates.

The average molecular weight (MW) of a polymer is related to the average length of polymer chains, which is controlled during the polymerization process and the selection of catalyst. The molecular weight distribution (MWD), which relates to the range of different polymer chain lengths, is also an important factor in morphology and rheology. The average MW of a polymer is strongly linked to the fluidity of the molten polymer. All things being equal, polymers with lower MW will have higher melt flows and easier processability, while MWD can influence properties such as impact resistance and elongation. That is why controlling the MWD has a key role in balancing processability against mechanical properties. MWD also affects the crystallization kinetics. By broadening the MWD the long chains have the ability to give larger crystalline fractions. MWD is also an important factor for orientation in extruded items. This is due to the change of an initially smooth surface into an irregular shape by shrinkage. Shrinkage is caused by the relaxation of stretched (oriented) chains to their original shape as a result of frozen-in stress. A broad MWD increases the orientation and therefore favors warpage (Van Loon 2000). The Results & Discussion section of this paper will attempt to link morphology to properties and their subsequent importance to specifiers in raw material selection for geomembranes.

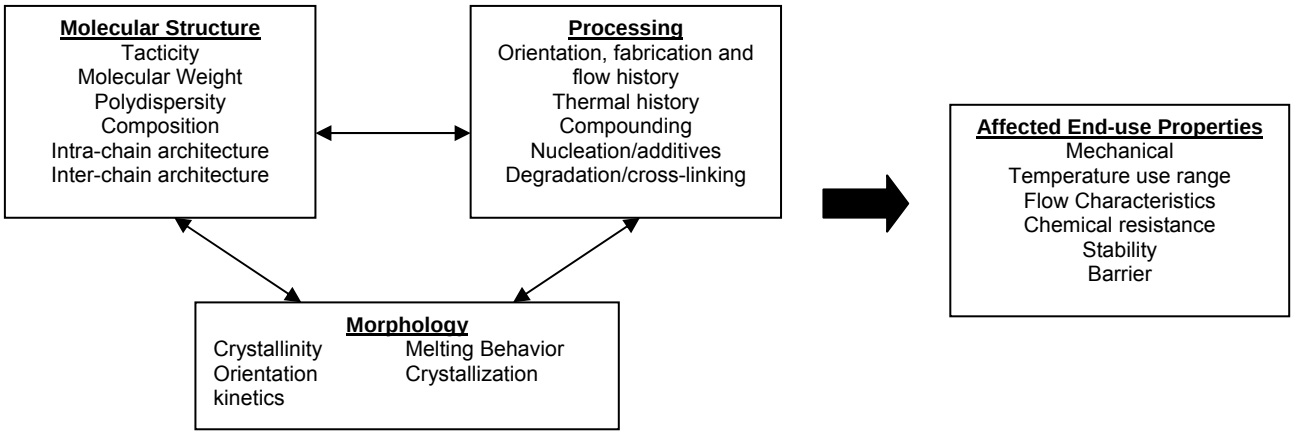

Figure 2. Factors influencing polyolefin morphology (Pasquini 2005).

Figures 3a-3c compare transmission electron microscope (TEM) micrographs of different morphologies, ranging from the highly crystalline to semi-crystalline structures with a high degree of an amorphous phase. Figure 3a represents the morphology of an HDPE: the micrograph demonstrates a lamellae structure, indicating a high degree of crystallinity. Figures 3b and 3c are polypropylenes: the PP HOMO examined also demonstrates a crystalline structure, whereas Figure 3c shows a clear phase distinction between the homopolymer matrix (light region) and the EPR (dark region). Figures 3d-e are micrographs of the phase morphology of the r-TPO and b-TPO. One key to the unique physical properties of the r-TPO is the fact that it is produced in the reactor, thus providing a polymer with a higher rubber content excellently dispersed in the matrix; another key is the uniqueness of the composition of the rubbery phase, compared with post-reactor blends of polypropylene and rubber. Dark areas in the image represent soft, amorphous rubber phases; light areas represent the harder matrix phase, mainly random PP. A diffuse boundary is apparent in the r-TPO at the interface between the rubber and PP phases as a result of their partial miscibility. The b-TPO shows similar phase morphology to the TEM in Figure 3c, but with much higher concentrations of rubber. Here, as before, the rubber domains (dark colored) are clearly discrete within the continuous polypropylene phase (light colored) but are poorly dispersed. The rubber-domain size and distribution are dependent on compounding conditions, blending ratio and structure of the individual components. The very finely dispersed rubber particles in the matrix of the reactor-produced TPO contribute to the enhancement in physical properties compared with the blended TPO. This characteristic is key to

understanding the mechanical properties of these unique resins, which will be discussed later in the Results & Discussion section.

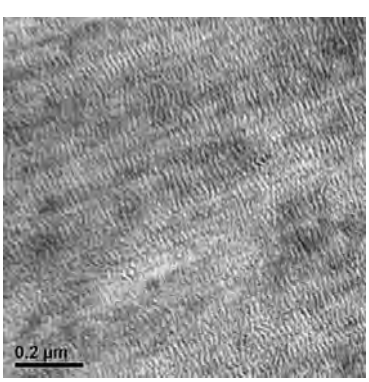

(a) HDPE

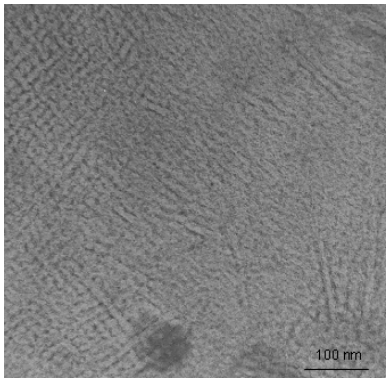

(b) PP HOMO

(c) PP HECO

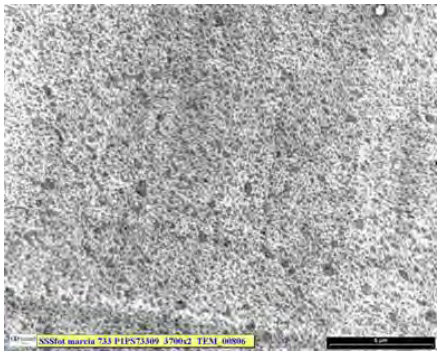

(d) r-TPO

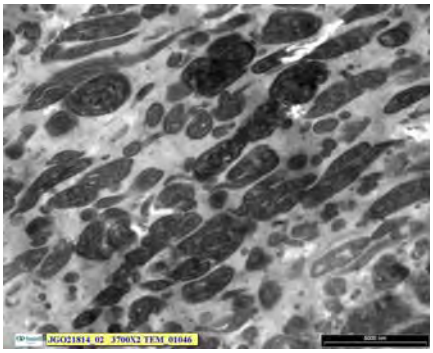

(e) b-TPO

Figure 3. Micrographs demonstrating unique polyolefin morphology by type.

2.2 Degradation Mechanisms of Polyolefins

Polyolefins are affected by two types of oxidative degradation that are relevant to geosynthetics in service: thermal oxidation, which would occur at elevated temperatures; and photo-oxidation, mainly caused by exposure to ultraviolet light. These two conditions may also occur simultaneously (Gächter and Muller, 1990). The oxidative process is dependent on many factors, which include: oxygen availability, impurities, residual catalyst form, crystallinity, storage temperature, air pollutants, radiation exposure, metal exposure, chemical exposure, part thickness, stress in the part, co-monomer content and other additives present (Pasquini, 2005). Typical manifestations of oxidation can affect the appearance of the polymer (such as a color or gloss shift), chalking or surface cracking and a loss of mechanical properties. The effects of thermal and photo-oxidation can be mitigated by the proper use and selection of additives, such as antioxidants, hindered amines and UV absorbers.

2.2.1 Thermal Oxidation of Polyolefins

In the presence of oxygen, the main initiator of oxidation in polyolefins is the generation of free radicals, which may lead to the propagation, branching and termination of polymer chains, thereby affecting the morphology of the polymer. The initiation of thermal oxidation in polyolefins is still not thoroughly understood; it is believed that mechanical stresses and/or heat during processing may lead to the formation of radicals through the dissociation of the carbon-hydrogen or carbon-carbon bonds. The direct interaction of the polymer with molecular oxygen or catalyst residues may also contribute to the formation of free radicals.

Physical changes in PP resulting from thermal oxidation are primarily a consequence of main chain scissions. The termination of these chains results in a decrease of the polymer's molecular weight, which consequently leads to an alteration of mechanical properties over time (Gächter and Muller, 1990). One theory holds that the root cause of this chain termination is the molecular breakdown of radical formations.

In PE, physical changes resulting from thermal oxidation are not due to chain scissions, as they are in PP, rather the dominating reactions in PE are long-chain branching and cross-linking, which affect the morphology of the polymer and therefore its physical properties. Two sources for the initiation of cross-linking in PE are free-radical combinations and radical reactions to form double bonds (Gächter and Muller, 1990).

2.2.2 Photodegradation of Polyolefins

Incident light falling on a polyolefin can be reflected from the surface, scattered or absorbed in the bulk of a polymer. The first law of photochemistry would indicate that only that part of the light that is effectively absorbed leads to photochemical transformations and degradation, which lead to a loss of mechanical properties. The presence of catalyst residues and radicals formed during polymer manufacturing, processing or storage are the main cause of photodegradation, because all these species absorb UV light above 290 nm and then participate in photochemical reactions. Polyolefins are sensitive to particular wavelengths that may induce degradation: PE to wavelengths above 300 nm, and PP to wavelengths above 370 nm (Lodi, Bueno, Costa and Zornberg, 2008).

UV light alters the physical characteristics of PP and PE by breaking the carbon and hydrogen bonds, creating free radicals, which, in turn, break the polymer chains, thus decreasing the molecular weight, and resulting in a more brittle polymer (Gächter and Muller, 1990). Effectively, UV light creates a higher melt index polyolefin, especially on the exposed surface area, which has the tendency to reduce elongation at break and to degrade impact resistance. The subsequent attachment of oxygen at these broken sites further accelerates degradation and the formation of oxidized species such as carbonyl and carboxyl structures, which are often used as analytical indicators of UV degradation (Gächter and Muller, 1990).

2.3 The Effects of Chemicals on Polyolefins

The performance of a polymeric material during chemical exposure is influenced by a number of parameters including, but not limited to, time of exposure, temperature, stress on the polymeric material during the exposure, the specific chemical itself and how it interacts with the polymeric structure.

There are at least two common ways various chemicals can interact with polymers. The most common way is when a liquid or gas material interacts with a polymer to behave as a kind of solvent or plasticizer. Solvents have the ability to penetrate the polymer to varying degrees, depending on the polyolefin type and the solvent. Generally this is a reversible process; and other than slight morphology changes, the polymer's molecular weight remains relatively unchanged. The second kind of interaction is one in which the polymer is chemically altered. In polyethylene materials the molecular weight can either decrease or increase. In the case of polypropylene, the result of chemical interactions, with few exceptions, is a reduction in molecular weight. The most common of these chemical interactions is with air or oxygen, whereby oxidation occurs. Ethylene-propylene rubber can undergo chain scission and crosslinking simultaneously, depending on the composition.

Strong oxidizing agents including peroxides, chlorine, hydrochloric acid, chromic/sulfuric acid and other free-radical generators can cause chain scission, which is a permanent change in the polymer structure and/or molecular weight. These interactions in conjunction with temperature, mechanical stress or other environmental stress can act to accelerate the effects. Stabilization against these environments can frequently but not always mitigate these changes in molecular weight. Some of the stabilizers used in these materials are, in fact, directly affected in some of these chemical environments and are rendered ineffective. Normal indicators of these effects include reduced elongation, cracking upon bending, loss of tensile properties and embrittlement. As stated above, this phenomenon can be rapidly accelerated in areas of high stress.

3. EXPERIMENTAL

3.1 Sample Fabrication

3.1.1 Polymer Polymerization

The r-TPO that was examined in this study was produced in a LyondellBasell Industries plant employing the *Catalloy* process, which consists of three independent gas-phase reactors in series. This technology allows the production of alloys of polypropylene and ethylene-propylene-butene rubber while in the reactor, thereby evenly dispersing very high levels of rubber throughout the polypropylene matrix. The PP HOMO and the PP HECO evaluated in this study were produced in a plant employing the *Spheripol* process, which consists of two liquid-phase loop reactors and one or two gas phase reactors in series. Ethylene and butene are typically used as comonomers.

The HDPE and the MDPE were produced in a slurry plant (Phillips Loop). The linear low density polyethylene (LLDPE) was produced in a low pressure gas-phase plant using the Unipol technology. Comonomers, such as butene, hexene or octene are added with ethylene to create linear polymer chains with short chain branches and low densities.

3.1.2 Polymer Compounding

The blended Thermoplastic Olefin (b-TPO) was compounded of ethylene-propylene rubber and homopolymer polypropylene using a Banbury mixer.

3.1.3 Fabrication of Test Samples

Samples for laboratory testing were injection molded on a 120-ton Van Dorn press under the conditions called out in ASTM D3641 and ISO 294.

3.2 Mechanical Property Characterization

ISO test methods were used for determining the tensile strength and elongation at yield and at break, as well as for measuring the flexural modulus and tear resistance. Multi-axial impact data was generated using ASTM standards.

3.3 Thermal Properties

Thermo-mechanical analysis (ASTM method E831) was utilized for measuring the coefficient of thermal expansion. The melting characteristics were analyzed by the ISO method of differential scanning calorimetry (DSC).

3.4 Light Resistance

The accelerated weathering data was obtained via Ultraviolet Florescent Tube device, using ASTM methods (Koerner, Hsuan and Koerner, 2008).

4. RESULTS

4.1 Physical Property Comparison
4.1.1 Density

Table 1 demonstrates that TPO materials have significantly lower densities than PP materials and, in particular, than PE materials. Density reductions can translate into lighter membranes of equivalent thickness, with consequent reductions in the costs of raw materials and in transportation costs.

4.2 Mechanical Properties
4.2.1 Flexibility

Flexural modulus is a measure of the resistance of a specimen to bending, and can be used, therefore, as an indication of a material's stiffness. This property can be important in this market because it affects the ability to prefabricate large sections. If the polymer is sufficiently flexible, large adjoining sections up to an acre in size can be prefabricated in a controlled manufacturing environment prior to shipping to an installation site. Prefabrication of large sections helps minimize the need for on-site joints that result in longer installations time and may require inspection.

As expected, PP materials are very stiff compared to PE and TPO materials (see figure 4a). PP HOMO is in fact the stiffest material compared, with a flexural modulus of approximately 1,600 MPa. Note that the flexural modulus of the PP HECO is approximately 600 MPa lower than that of the PP HOMO, due to the presence of a certain amount of EPR in the polymer. The stiffness of PE increases with an increase in density and hence in crystallinity. Therefore, HDPE has a higher flexural modulus than either LLDPE or MDPE. Chain branching decreases a polymer's crystallinity; therefore LLDPE, the most highly branched PE in this study, has the lowest flexural modulus among the polyethylenes. The r-TPO has the highest flexibility, with a flexural modulus below 90 MPa. Compare this to the b-TPO, which has a flexural modulus greater than 200 MPa. The lower flexural modulus is a direct consequence of the morphology of the material. The fact that the rubbery amorphous phase of the r-TPO is more evenly distributed throughout the matrix leads to a lower flexural modulus versus the b-TPO. The r-TPO material shows increased flexibility even when compared with LLDPE, which is considered a flexible material for geomembranes due to its high level of short-chain branching, contributed by the incorporation of a comonomer.

4.2.2 Tensile Properties

The tensile properties of a membrane material are important because they provide practical indications about the behavior of the material in the field, where it is stretched during installation or in its service life. Tensile elongation is also linked to puncture resistance and, therefore, to the ability of a material to plastically deform without rupture, hence avoiding tears and holes in a membrane.

Polymer stress-strain curves are produced by stretching a sample at a constant rate through the application of a tensile force. Figure 4b indicates that the PP materials have higher tensile strength compared to the PE materials and the TPOs; but the PPs exhibit considerable less plastic deformation and, therefore, will fracture shortly beyond the polymer's yield point. On the other hand, both the TPO materials and the LLDPE yield at a much lower tensile strength, but they are able to be stretched, or plastically deformed, much more prior to rupture than the polymers with higher degrees of crystallinity. For the r-TPO, the optimal dispersion of the ethylene-propylene rubber incorporated in the material enhances the ability of the polymer to be stretched and gives a value above 700% for the elongation at break. In fact the amorphous fraction is plastically deformed when the load is applied, and the rubber domains are oriented in the direction of the applied force. In the case of LLDPE, the combination of low crystallinity with the reduced level of long-chain branching and the narrow molecular weight distribution contributes to the outstanding result of 800% elongation at break. Stress-strain curves confirm the behavior differences between the highly crystalline materials and the materials with low crystallinity. Again the r-TPO material and LLDPE do not have clearly defined yield points and seem to behave more like elastomers than plastomers.

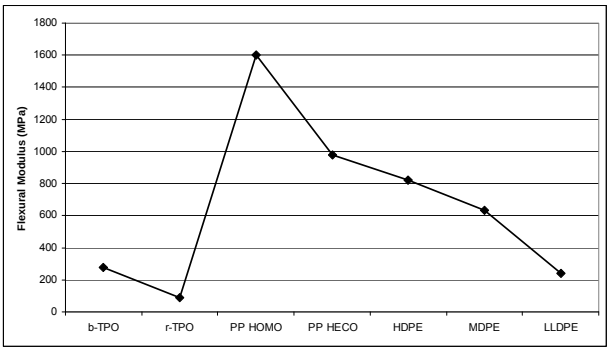

(a) Flexural (Chord) Modulus (ISO 178).

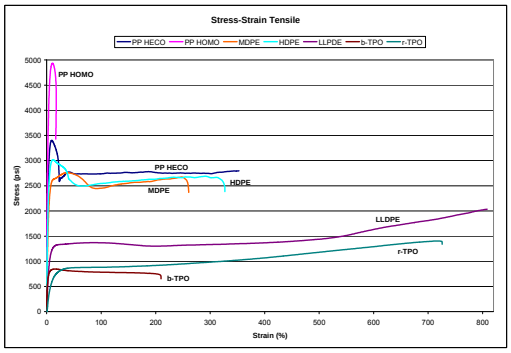

(b) Tensile Properties (ISO 527-1, 2).

Figure 4. Mechanical Properties tested by an Instron.

4.2.3 Impact Properties

High-speed Multi-axial Instrumented Impact testing is useful in determining a material's toughness, in generating load-deflection curves and in understanding energy absorption of impact events and failure modes. The data generated by such testing can be useful in understanding a material's resistance to impact and puncture. This testing can also be used to evaluate the effects of secondary operations or other environmental factors on plastic impact properties.

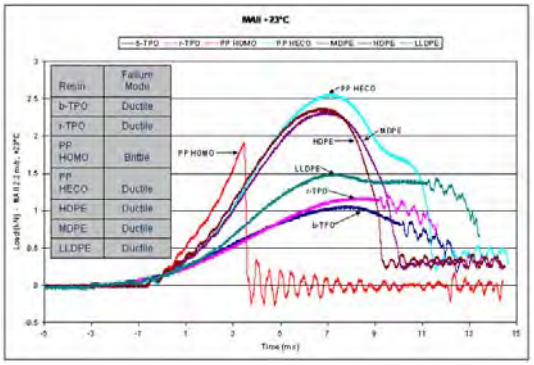

(a) MAII at 23 ºC

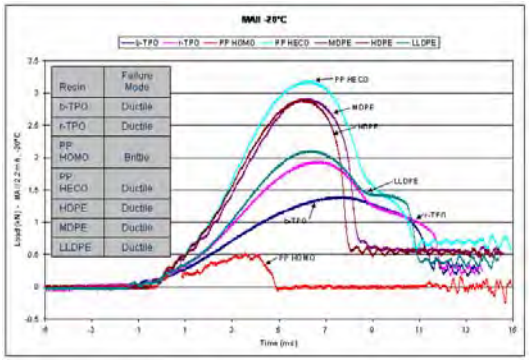

(b) MAII at −20 ºC

Figure 5. Multi-Axial Instrumented Impact Results at 2.2 m/s (ASTM D3763).

Since many materials exhibit lower impact strength at reduced temperatures, and geomembranes in use are exposed to extreme weather conditions, it is appropriate to test materials at lower than ambient temperature. In this study, MAII tests were performed at +23 ºC and −20 ºC in order to understand the impact performance of the polymers at low temperatures. As expected, PP HOMO is very brittle and has low energy values (see figure 5), while the polyethylene types are quite similar to one another and also similar to PP HECO. The TPO materials show lower energies, due to the presence of high amounts of amorphous materials, which require less energy to be punctured. Still, ductile failures occur at −20 ºC.

4.2.4 Tear Strength

Inevitably geosynthetics will encounter tear forces during service life. A laboratory tear test can be useful to predict a material's ability to resist these forces. Figure 6 compares the tear strengths of the polyolefins examined in this study on a side-by-side basis. The test results show that tear resistance is higher when the polymer has a higher degree of crystallinity, indicated by high tear strengths exhibited by the PP HOMO and HDPE. The TPO materials have significantly less tear strength compared with the PP and PE polymers, due to the presence of rubber particles that deform and promote crazing under an external load. The results also show that the r-TPO demonstrates higher resistance to tear than the than b-TPO with the same rubber level, which is due to the better adhesion between the EPR and the PP matrix. The rubber particles with poor adhesion are "expelled" from the matrix creating voids that can propagate a fracture.

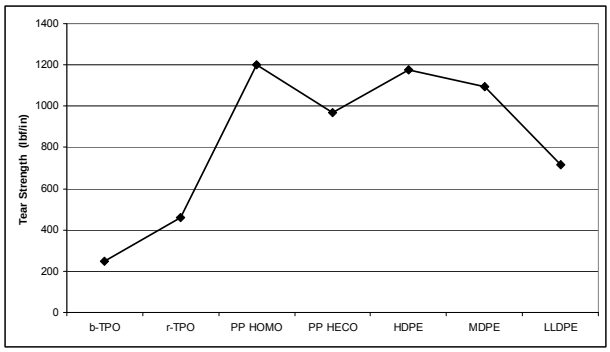

Figure 6. Tear Strength Properties (ASTM D624, Die C).

4.3 Thermal Properties

4.3.1 Coefficient of Thermal Expansion

The coefficient of linear thermal expansion (CLTE) indicates the rate at which a material expands as a function of temperature. The test can be used for design purposes, to determine if failure by thermal stress may occur, to understand the relative expansion/contraction characteristics of two materials in contact with each other or simply to evaluate how much a material might change in size when installed outdoors. Thermal excursions can, in fact, be significant between day and night or between summer and winter; and the expansion/contraction of the material will cause stress on the polymer, which can result in the formation of wrinkles in large sheets. The lower a material's coefficient of linear thermal expansion, the greater it's dimensional stability.

The thermal expansion curves in figure 7a have been generated using Thermo-Mechanical Analysis (TMA) from −30 ºC to 100 ºC at a rate of 3 ºC/minute. In this technique, dimensional changes in a sample are measured while the sample is heated or cooled within the desired temperature range.

In the range between −30 ºC and +60 ºC (which can probably be considered the broadest range of temperatures at which a polymeric membrane will be exposed when installed outdoors) the dimensional change of PE materials increases almost linearly up to values well above 150 µm, while the dimensional change of PP and TPO materials stays below 60 µm. Between −30 ºC and +30 ºC in particular, PE materials have a dimensional change that is approximately 90 µm for HDPE, approximately 110 µm for LLDPE, and approximately 150 µm for LDPE; while PP HOMO and PP HECO have a much smaller dimensional change of approximately 30 µm. TPO materials have very low dimensional change also, which is approximately 50 µm. Indeed PP and TPO exhibit significantly higher dimensional stability than PE materials, which translates to less stress and less wrinkling in an installed liner.

4.3.2 Melting Behavior of Polyolefins

Due to the size of most geomembrane projects, field seams are normally required. Since installations occur all year round in varying weather conditions, it is important that membranes are able to be seamed together efficiently with high levels of integrity. Heat-welding seams using hot-air gun is considered to be a fast and reliable method for joining two sections of membrane. Therefore a material's ability to be heat-welded is extremely important; and the wider the acceptable temperature window for the welding operation, the more flexibility is given to the installer to install the membrane at varying conditions. Figure 7b demonstrates the melting behaviors of the polyolefins tested in this study by DSC. The sharp slopes and peaks of the curves for the PE and PP HOMO indicate that the welding window is limited to 10 to 20 ºC. The TPO materials begin softening between 120 and 130 ºC, due to the EPR incorporated into the matrix, but are not fully melted until approximately 160 ºC, therefore creating a very wide processing window for seaming TPO. This data would indicate that TPO materials can be installed under a wider range of weather conditions and that the integrity of the seam is not as sensitive to the temperatures generated by the hot-air gun as is the case for PE.

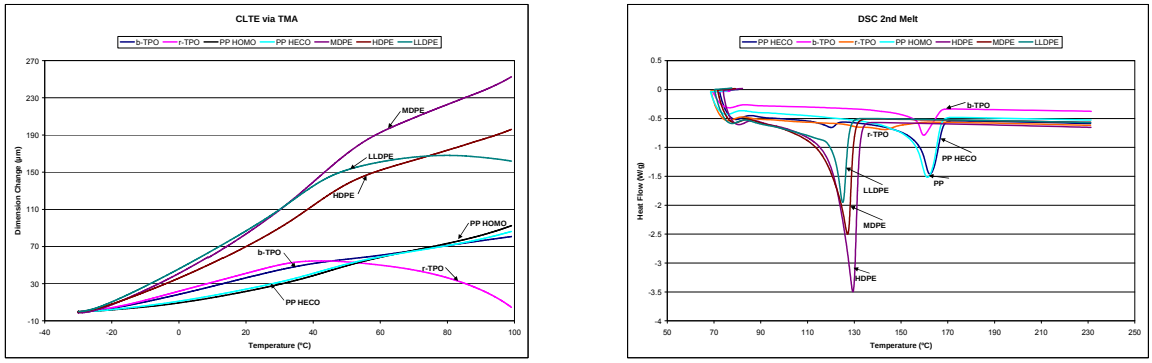

(a) CLTE via TMA (ASTM E831) (b) DSC (ISO 1183-1)

Figure 7. Graphs of Thermal Characteristics of Polyolefins.

4.4 Accelerated Weathering

Weathering resistance is an extremely important characteristic of materials utilized for geosynthetics. Membranes can either be buried, which limits their contact with factors known to degrade polymers. The other extreme would be membranes that are continuously exposed in service to harmful UV rays that can initiate photo-oxidation. As we learned in the proceeding sections of this paper, the morphology of a polymer dictates its mechanical and thermal properties, and those are sometimes compromised by photo-oxidation, which is why it is important to understand the retention of properties over time to help predict a reasonable service life. Koerner, Hsuan and Koerner (2008) attempt to predict the service life of fPP and PE membranes by evaluating UV florescent accelerated weathering data (fPP is an industry term to indicate flexible polypropylene, generally a TPO. The definition for fPP is called out in ASTM D4439, Standard Terminology for Geosynthetics, and in summary is defined as a PP with rubber having a 2% secant flexural modulus less than 300 MPa). In their study they expose a series of TPOs, HDPE and LLDPE to light-hours under ASTM D7238 (figures 8a and b) and measure the percent retention of tensile elongation.

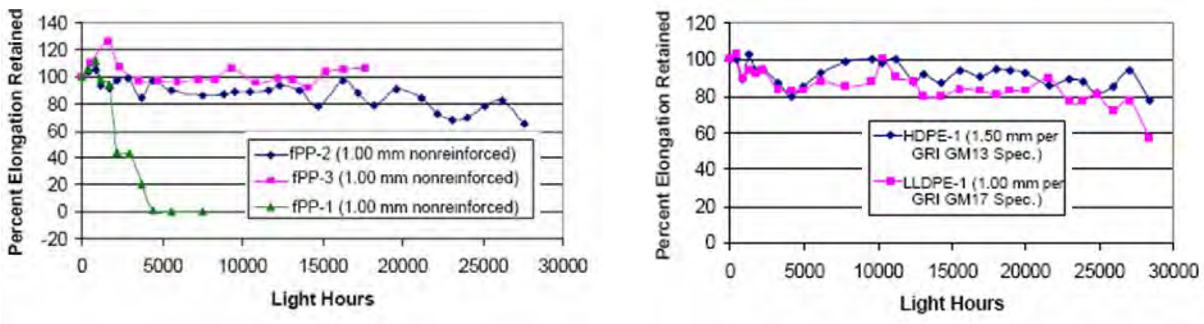

(a) r-TPO (fPP: "flexible polypropylene" industry terminology). (b) HDPE and LLDPE.

Figure 8. UV Florescent Accelerated Weathering Results (ASTM D7238 [Koerner, Hsuan and Koerner, 2008]).

The graphs in figure 8 indicate that after 25,000 light-hours fPP-2, fPP-3, HDPE and LLDPE retain greater than 50% of their original tensile elongation. On the other hand, fPP-1loses most of its original tensile elongation at 5,000 light-hours (Koerner, Hsuan and Koerner, 2008). This is a good indication that similar polymers can perform differently, which could depend on a polymer's morphology and its stabilization system to mitigate degradation.

5. SUMMARY

In summary, this paper has outlined the differences among traditional polyolefins that are utilized by converters to fabricate geosynthetics and evaluated their benefits and weaknesses against characteristics that are important in proper material selection. The goal of this paper is to provide the reader a general understanding of polyolefins, summarizing the differences between PE types, PP HOMO, PP HECO, reactor and blended TPOs. It has been discussed that these polymers all have different chemical structures and morphology, which translates into unique, characteristic mechanical and thermal properties, as well as weathering and chemical resistance. Proper stabilization of these polyolefins is critical to mitigating degradation in order to retain important properties during the service life. The paper was also intended to give fabricators and specifiers a way to link laboratory testing to performance criteria, such as puncture resistance, wrinkle formation, tear resistance, weld integrity, welding window, applied stresses, the ability to prefabricate large sections and property retention after exposure to heat and UV light. Material selection by specifers and converters is critical for minimizing possible installation issues and field failures.

REFERENCES

ASTM D 624-00. Standard Test Method for Tear Strength of Conventional Vulcanized Rubber and Thermoplastic Elastomers, *American Society for Testing and Materials*, West Conshohocken, Pennsylvania, USA.

ASTM D1238, Standard Test Method for Melt Flow Rates of Thermoplastics by Extrusion Plastometer, *American Society for Testing and Materials*, West Conshohocken, Pennsylvania, USA.

ASTM D3641-02, Standard Practice for Injection Molding Test Specimens of Thermoplastic Molding and Extrusion Materials, *American Society for Testing and Materials*, West Conshohocken, Pennsylvania, USA.

ASTM D3763-06, Standard Test Method for High Speed Puncture Properties of Plastics Using Load and Displacement Sensors, *American Society for Testing and Materials*, West Conshohocken, Pennsylvania, USA.

ASTM D4439, Standard Terminology for Geosynthetics, *Society for Testing and Materials*, West Conshohocken, Pennsylvania, USA.

ASTM D7238, Standard Test Method for Ultraviolet Florescent Tube device, *American Society for Testing and Materials*, West Conshohocken, Pennsylvania, USA.

Bowne, T.R., Ferrell, T.P. and Zielenski. M. (2007) *Industry Study 2153 Geosynthetics*, The Freedonia Group, Inc. Cleveland, Ohio, USA.

Gächter, R. and Muller, H. (1990). *Plastics Additives, 3rd ed*., Hanser Publishers, Munich, Germany.

ISO 178, International Standard, Plastics-Determination of flexural properties, *ISO*, Geneva, Switzerland.

ISO 294-1,2,3,4, International Standard, Plastics-Injection moulding of test specimens of thermoplastic materials, *ISO*, Geneva, Switzerland.

ISO 527-1,2, International Standard, Plastics-Determination of tensile properties, *ISO*, Geneva, Switzerland.

ISO 1183-1, International Standard, Plastics-Methods for determining the density of non-cellular plastics, *ISO*, Geneva, Switzerland.

ISO 11357-1, International Standard, Plastics-Differential scanning calorimetry (DSC), *ISO*, Geneva, Switzerland.

Koerner, R.M., Hsuan, Y.G. and Koerner, G.R. (2008), *Freshwater and Geosynthetics; A Perfect Marriage*, The first Pan American Geosynthetics Conference & Exhibition, IFAI, Cancun, Mexico: 4-28.

Lodi, P.C., Bueno, B.S., Costa, C.L. M. and Zornberg, J.G. (2008), *Degradation of Geomembrane after Weathering*

Exposure, The first Pan American Geosynthetics Conference & Exhibition, IFAI, Cancun, Mexico: 681-689.

Menzel. C and Vaccaro. (2008), *Installation of Geomembranes in Zones Located at Geographic Altitudes over 3,000 M.A.S.L.*, The first Pan American Geosynthetics Conference & Exhibition, IFAI, Cancun, Mexico: 1492-1501.

Pasquini, N. (2005). *Polypropylene Handbook, 2nd ed.*, Hanser Publishers, Munich, Germany.

Long-Term Weathering Stability and Warranty Implications for Thin Film Geomembranes

A. Mills, C.E.T., Layfield Environmental Systems Ltd, Edmonton, AB, Canada.
D. Martin, P. Eng, Layfield Geosynthetics and Industrial Fabrics Ltd, Edmonton, AB, Canada.
R. Sati, Layfield Geosynthetics and Industrial Fabrics Ltd, Edmonton, AB, Canada.

ABSTRACT
The decision to issue warranties on a geomembrane is one that needs to balance risk with science. This paper summarizes the testing that our company performed to establish a model that could be used to evaluate warranties. Three UV testing studies were completed including a natural weathering study, a 20,000 hour accelerated testing study, and a 30,000 hour accelerated testing study. The results of these UV studies are outlined and the implications of these studies on our decision to issue warranties are discussed.

1. INTRODUCTION

Establishing warranty criteria for long-lived products used in exposed environments is always a challenge. When our company started manufacturing geomembranes in 2000 we were faced with the need to evaluate the ultra violet light (UV) stability of our geomembranes and to set warranty guidelines for those products. We were aware of long-term research that had been completed on thicker HDPE films (cite ref) and had first hand experience with coated fabric type geomembranes but were not aware of information on the extended UV stability of thin film geomembranes.

We are a specialty manufacturer of geomembranes concentrating on materials with thicknesses between 0.5 and 1.0 mm (20 to 40 mil). These thin film geomembranes are used by our fabrication facilities to produce small specialty containments in our market areas. In many cases, small size containments do not economically allow a full installation crew to perform a geomembrane installation so we have a specialized business where fabricated liners are supplied to end-users for self-installation. Our goal was to create a geomembrane that could be fabricated but that had the UV stability of thicker geomembrane materials.

Our first hand experience with coated fabric geomembranes indicated that it was possible to adequately UV stabilize thinner films. A typical 1.0 mm (40 mil) coated fabric geomembrane uses two layers of 0.4 mm (16 mil) polymeric coatings to protect an inner layer of fabric. Our experience showed that properly stabilized coated fabrics could function as exposed geomembranes for well over 20 years. We had examples of 0.75 mm to 1.14 mm (30 to 45 mil) geomembranes that had performed for more than 20 years in exposed conditions. These coated fabrics included PVC alloy materials (XR-5®) and CSPE coated materials (Hypalon®). Knowing that the UV stabilization of thin films could be accomplished, we set out to improve the stability of our thin film geomembranes to match that of 60 mil HDPE.

Our initial research showed that UV stabilization is pretty fuzzy science. Geomembranes could be installed in varieties of climate, geography, orientations to the sun, and other variables. Every time we asked the question, “how long will it last” we got the answer, “it depends.” In order to establish realistic warranty criteria we needed concrete data that would give us a realistic and conservative estimate of longevity.

2. INITIAL UV RESISTANCE STUDIES

2.1 Natural Weathering Study

In 1996, one of the authors placed a series of geomembrane samples on racks on the roof of our fabrication plant to see how a wide variety of geomembranes (and other plastic sheet samples) would react to local sunlight. These racks were oriented to face directly south and were raised to the sun at an angle of 3 V to 1 H. Our plant was located in Edmonton at 54 degrees N latitude. Since Edmonton has one of the highest levels of incident sunlight of any city in Canada this was a good choice for an initial study.

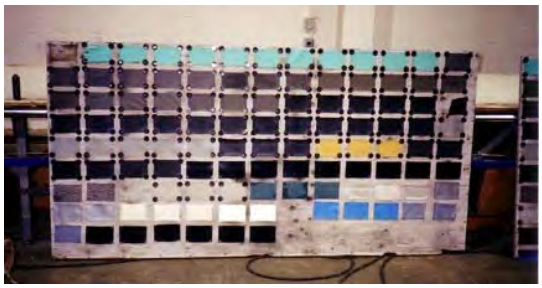

Figure 1 One of three natural weathering sample racks after 6 years of exposure.

Shortly after we began manufacturing geomembranes we saw the need to conduct a UV study. Shortly after the study was started, we retrieved the sample racks from the roof for comparison. The sample racks and their contents were used to help us relate our accelerated UV study with natural weathering data. The samples that had been exposed for six years were compared to the original specifications for the materials.

2.2 Initial Accelerated UV Study

Since an easy answer to the UV stability question was not available for our new geomembranes, we embarked on an accelerated UV testing program. We evaluated a number of accelerated UV test systems and decided to purchase a QUV/SE model fluorescent-tube accelerated UV tester from QUV. Although we reviewed a Xenon arc testing machine our testing budget did not allow consideration of the Xenon arc machine. Once the tester was obtained, we needed to determine the testing conditions. Research found that the most damaging wavelength of light for polyethylene was 300 nm and that the most damaging wavelength for PVC was 320 nm. In looking at the types of UV bulbs available we settled on UVB bulbs as the most aggressive. The second setting was the UV cycle. The equipment supplier recommended that the most aggressive settings would be an irradiance of 0.80 W/m2/nm (at 313 nm) and to include a short condensation cycle. We used these settings and an initial cycle of eight hours of UV at 60C followed by four hours of condensation at 50C.

Our initial study included many of the same materials that had been exposed in the natural weathering trial in an attempt to establish a reasonable correlation. The results of this study are contained in the paper, “UV Resistance In Thin Film Geomembranes: Accelerated and Natural Weathering Studies” (Martin, 2005) published in the proceedings of Geo-Frontiers 2005.

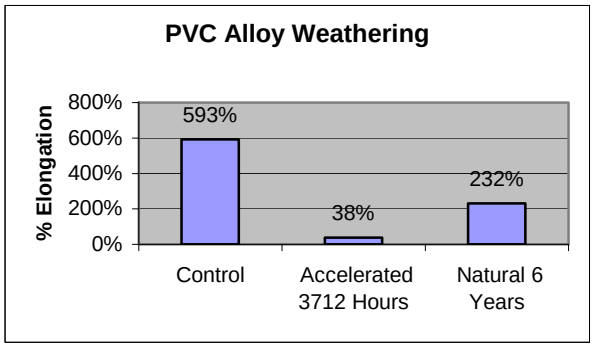

Figure 2 Comparison of PVC Alloy Elongation (Reprinted from Martin, 2005)

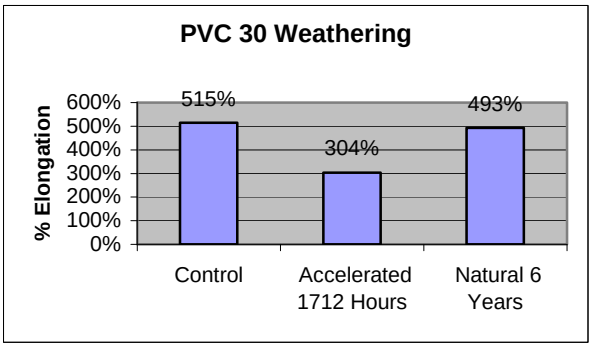

Figure 3 Comparison of PVC 30 Elongation (Reprinted from Martin, 2005)

The initial UV study looked at materials that were affected by both the natural weathering and the accelerated weathering. Figure 2 and Figure 3 show two of the PVC material types where the elongation properties had changed significantly. Neither material contained significant UV stabilizers and both materials were 0.75 mm (30 mil) unsupported film samples. Elongation in flexible materials was one of the first properties to be affected by UV degradation. The initial comparison of natural to accelerated UV testing was used to create an initial correlation.

2.3 Establishing a Correlation

A search of the literature found that an energy equivalency approach would likely suit our needs for calculating the relationship between natural and accelerated UV exposures. Since we now had examples of natural UV exposure and accelerated weathering testing we needed to establish the equivalent energy between the two tests.

From the literature (see Martin, 2005), we estimated that the total irradiance between 300 and 320 nm, which was received in a natural exposure by our geomembrane samples, could be conservatively estimated at between 4.64 and 27.9 MJ/m^2/year. Since our samples had been mounted at a 3 to 1 slope angle, this energy estimate was considered conservative. Based on the irradiance curve for fluorescent UVB bulbs (ASTM G154) and our irradiance setting of 0.80 W/m^2/nm measured at the peak emitted wavelength of 313 nm, we made an estimate of the area under the irradiance curve to determine the total irradiance between 300 and 320 nm. Based on this rough estimate, the samples in our accelerated weathering study received approximately 0.0429 MJ/m^2/hour in total energy between 300 and 320 nm.

These two calculated values gave us the following relationship:

$$\frac{\text{4.64 to 27.9 MJ/m}^2\text{/year}}{\text{0.0429 MJ/m}^2\text{/hour}} = \frac{\text{108 to 650 Hours of Accelerated UV exposure}}{\text{Year of Natural Exposure}}$$

Our initial accelerated exposure was 16 hours per day so the values of the multipliers increase to 162 to 975 hours of accelerated testing to years of natural exposure (650 hours/year x 1.5 = 975 hours/year). Because we are attempting to establish a conservative correlation we rounded up the higher term in the relationship to 1000 hours per year of natural exposure.

When we compared this correlation number with our observed results we found that this relationship was quite conservative. Looking at Figures 2 and 3, the correlation relationship would predict that the properties of the materials would be the same after 6000 hours of exposure. Since the properties were lower after a shorter period of QUV exposure, the relationship appeared to be very conservative. A final check of the literature showed that a relationship of 1000 accelerated hours to 1 year of natural weathering was a reasonable estimation and was supported by other studies (Martin, 2005).

3. LONG-TERM UV STUDY

3.1 First Long-Term UV Study

After our success with the initial UV studies we sat down to determine what kind of testing plan would provide us with the best data for a warranty evaluation. In the literature the longest UV testing period that we found on geomembranes was 16,000 hours (Wagner and Ramsey, 2003) on HDPE. Since our goal was to match the UV performance of existing HDPE materials we established our exposure time at 20,000 hours. Since a 20,000 hour running time is 2.26 years of actual machine time, we went in to this testing knowing that it would be a long time before we had any results. With additional delays and setbacks along the way, this first long-term study took over three years to complete.

The purpose of this long-term UV study was to evaluate our new Enviro Liner® proprietary polyolefin geomembrane. In this study we included three variants of this material and one control sample of 1.5 mm HDPE. The polyolefin geomembranes were stabilized with a proprietary UV stabilization package. We established two loading levels for this package; a high and a low level. The high level was twice the loading of the low level. The study included a black and a white sample with high level UV loading and a white sample with a low UV loading. The HDPE material was obtained from our supplier at the time.

Halfway through this test, at the 10,000 hour mark, we changed the machine cycle. We increased the UV exposure time from an 8 hour UV exposure and 4 hour condensation cycle to a 10 hour UV and 2 hour condensation cycle. This was done to make the conditions more aggressive and to make our correlation between accelerated UV testing and natural testing more conservative.

Sufficient specimens were included in the study so that we could perform intermediate testing. Tests were performed at 2000; 6000; 10,000 and 20,000 hours (tensile tests at break, method appropriate to the material, see Martin 2005 for details). The results are plotted in Figure 4. See the previous paper (Martin 2005) for a more complete description of this testing.

The results of this first long-term UV study were very encouraging. We learned that we could stabilize a 0.75 mm (30 mil) polyolefin geomembrane to match the performance of a standard HDPE 1.5 mm (60 mil) material. With a high loading of

the UV additive we could even stabilize a white material to give similar performance. Our conclusions from this first study were that we could conservatively expect our 0.75 mm (30 mil) stabilized geomembrane to retain over 80% of its properties after 20 years of exposed service.

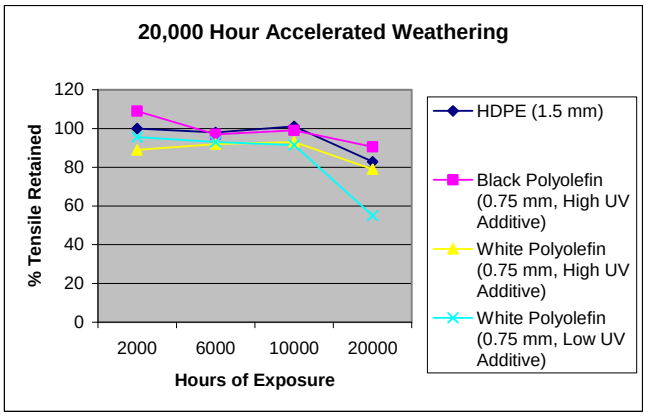

Figure 4 First Long-Term UV Test Results
(Reprinted from Martin, 2005)

4. WARRANTY IMPLICATIONS

4.1 Relating UV Testing to Real Life

With the first long-term UV study in hand we set out to evaluate a level of acceptable warranty risk. On the one hand, our UV study had shown that our stabilized polyolefin geomembrane had performed as well or better than a similar sample of HDPE. On the other hand, we needed confidence that the 20,000 hour performance of the HDPE could be related to a real life exposure. In order to convince senior management that the risk was acceptable we needed to connect real life HDPE exposures to our accelerated weathering testing.

Fortunately we had been monitoring one of our first HDPE installations. As described in the paper by Mills (1998) samples had been removed from a 1987 HDPE installation and tested. The results of that testing had shown that the HDPE was holding up well and should easily last 20 years. Additional maintenance visits in 2002 and 2007 showed that this early type of HDPE has easily stood up to 20 years of service. Measurements of the anti-oxidant level (OIT testing) have shown that the antioxidant is mostly depleted; however, the tensile strength of the material is still holding up at 20 years. Having this real life example to make comparisons with was an important input to our evaluation of warranty risk.

4.2 What Risk is Acceptable?

At this point we had a quantity of test data that gave us some confidence that our material would easily last for 20 years in an exposed condition in our region. We felt that our data was conservative since we had purposely chosen the most conservative values throughout our evaluation. The next step was to evaluate the level of risk.

The most common type of warranty in the geomembrane market is a straight line warranty. In this type of warranty the value decreases by 1/period each year until you reach the end of the period. There is also another type of warranty that is used by at least one geomembrane manufacturer where the retained value is multiplied by a factor for each year in the period (Year A Value x Factor = Year B Value; Year B Value x factor = Year C Value; etc.). This declining balance type of warranty does not reach a zero value at the end of the term. These two types of warranty are illustrated in Figure 5.

Since this is an evaluation of risk, the key is to look at the retained value near the end of the warranty term. In the case of a 20-year straight line warranty, the retained value of a $100,000 geomembrane at year 19 is $5,000. By way of comparison when we set the factor in the declining balance warranty to 0.86 we were able to duplicate a retained value of $5,000 at year 19. Comparing these two types of warranty in Figure 5 shows that the declining balance type presents the least risk to the geomembrane manufacturer but that the straight line warranty provides the most protection to the project owner.

It takes a remarkable amount of discussion to establish an extended warranty program in a company that has not previously issued product warranties. That discussion is especially difficult when the term of the warranty is significantly higher than the current warranties available in the market place. The longest warranty term available at the time for unsupported thin film geomembranes was a 5-year straight line type. We were proposing a 20-year warranty. The issue of the warranty type was settled in favor of the type most advantageous to the customer. We chose the straight line warranty as being more common in the industry and of most advantage to our customers. Our goal was to set the standard of 20-year warranties on 0.75 mm (30 mil) geomembranes and after much discussion we achieved that goal. Our company now provides 20-year straight line warranties to our customers.

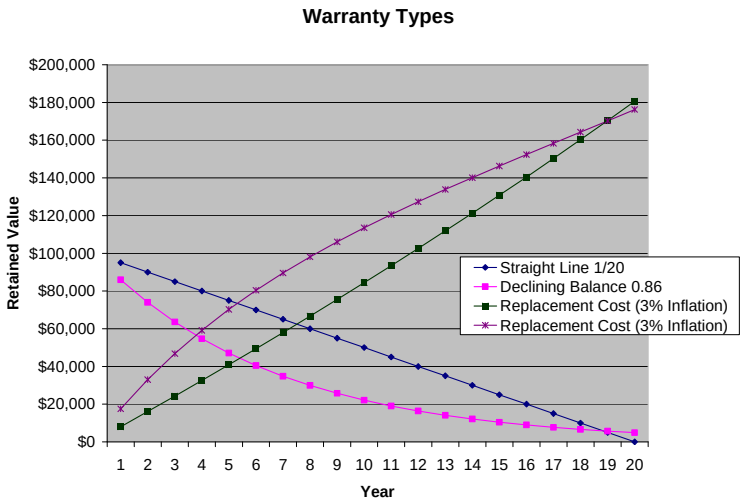

Figure 5 Possible warranties applied to a $100,000 Geomembrane showing replacement costs

5. SECOND UV STUDY

5.1 Confirmation of Production Material Properties

Some people will have noticed in the discussion to this point that in the first long-term UV study we had not tested our black polyolefin geomembrane with the lower UV loading level. This was a result of problems during sample preparation and was identified early on as a deficiency of the first extended UV test. The first samples had been prepared on lab equipment since we had not yet started full geomembrane production. During that first UV study we added additional samples as they became available. The paper on the first long-term study (Martin 2007) was published before these production samples were tested at the 20,000 hour mark.

By the time the first long-term UV test had reached the 10,000 hour mark, our production of geomembrane was well established. We added production samples of our black polyolefin geomembrane to the UV tester with the low level of UV additive with the specific intention of testing that formulation at 20,000 hours. A second control sample of HDPE was also added to the UV tester to match the exposure of this specific sample. This second long-term UV test then, was to confirm that our black 0.75 mm (30 mil) polyolefin geomembrane with the lower level of UV stabilizer, would provide equivalent performance to 1.5 mm (60 mil) HDPE.

Since this particular test was being carried out at the same time as the first UV test (offset by 10,000 hours) the first results were available for our discussion on warranties. For example, the 20,000 hour portion of this test was completed before the final decision was made on warranties. Having the results from this production sample allowed us to establish our warranties based on actual production material with an economical loading of the UV stabilizer.

5.2 Moving the Goal Posts Again

So, with warranties in place, and 20,000 hour UV testing completed on production samples, we were prepared to wrap up our UV testing. But we still had three specimens of each material in the weather tester. We decided at this point to push the UV testing out to 30,000 hours. This additional exposure would solidify our decision on 20-year warranties, allow us to make reasonable warranty decisions in regions with higher incident sunlight, and would allow us to consider extending warranties beyond 20 years.

This extended long term UV test tested a sample of our 0.75 mm (30 mil) black polyolefin material and a 1.5 mm (60 mil) HDPE material out to 30,000 hours. The exposure for these samples was 10 hours of UV light at 60C followed by a 2 hour condensation cycle at 50C. UVB bulbs were used with an irradiance of 0.80 W/m2/nm (at 313 nm). This exposure level was set when these samples were added to the weather tester and were not changed over the period of this test.

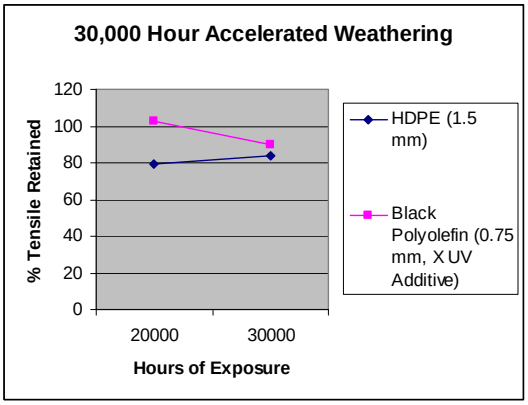

Figure 6 Tensile Results from 30,000 UV Test

The samples were tested for retained tensile strength. The 0.75 mm (30 mil) black polyolefin geomembrane was tested according to ASTM D882 using 6 mm (0.25") wide specimens. Using this small specimen size allowed us to cut 15 test coupons from the exposed area of the sample. Identical test coupons were cut from the same relative location on retained samples for comparison. The HDPE tensile samples were cut with an ASTM D638 type VI die. This die is smaller than what is used in normal HDPE tensile testing but allowed us to cut 10 test coupons out of the exposed sample. The same size test coupons were cut from the same relative location on a retained sample. Figure 6 summarizes the tensile test results. The HDPE maintained about 80% strength retained at both 20,000 and 30,000 hours. The 0.75 mm (30 mil) polyolefin sample retained 100% at 20,000 hours and 90% at 30,000 hours.

Another key indicator of longevity is the retained stabilizer content of the polymer. We measured the content of anti-oxidant stabilizers in the samples using the HP OIT test (ASTM D5885). We compared the stabilizer content in the sample after 30,000 hours of exposure with the content measured in the retained sample. The 1.5 mm (60 mil) HDPE retained 44% of its HP OIT value while the 0.75 mm (30 mil) polyolefin retained 69% of its original HP OIT value. Figure 7 illustrates this result. The GRI-GM13 specification for HDPE specifies an HPOIT value of 400 minutes for new material so this sample is still very close to specification after 30,000 hours. You can see by these results that the 0.75 mm (30 mil) polyolefin material is highly stabilized and is retaining its properties very well at 30,000 hours of exposure.

HP OIT Results	Retained Sample	30,000 Hour Sample	% Retained
0.75 mm Black Polyolefin	4410 min	3056 min	69%
1.5 mm HDPE	899 min	396 min	44%

Figure 7 HPOIT Retained Values

6. WARRANTY IMPLICATIONS 2

The implications of the 30,000 hour test on our warranties are important. First of all, the purpose of all this testing was to give us confidence in the longevity of our product so that we could establish industry-leading warranties. We are now comfortable with our results and are able to offer a 20-year straight line warranty in most regions. We also have sufficient information now to evaluate warranties in regions with more intense UV exposure. We recognize that our initial relationship between accelerated UV testing and natural exposure was done at temperate latitudes. By taking the testing to the extreme of 30,000 hours we have a better guideline to help us make reasoned choices about whether to provide a warranty in higher UV locations.

Finally, we are beginning the discussions about whether we can extend our warranties even further than 20 years. The data from this latest test seems to support a longer warranty term. What we have to decide is whether a warranty longer

than 20 years is in the interests of our company, whether it will provide commercial advantage, and whether setting a standard warranty on this product will have an adverse affect on other products. Those discussions are just beginning.

7. CONCLUSION

The decision to issue product warranties on geomembranes is a difficult decision for a company. The best way to approach that decision is to test the product in a way that most closely replicates conditions of use and then make a conservative estimation of how your testing and actual use will compare. Over the past number of years we have taken UV testing on our material far beyond normal industry practice and have obtained excellent results. That testing has influenced our decisions regarding warranties and continues to shape how we apply our product to our customer's applications.

REFERENCES

ASTM G154, Standard Practice for Operating Flourescent Light Apparatus for UV Exposure of Nonmetallic Materials. American Society for Testing and Materials, West Conshohocken, Pennsylvania, USA.

ASTM D638. Standard Test Method for Tensile Properties of Plastics, American Society for Testing and Materials, West Conshohocken, Pennsylvania, USA.

ASTM D882. Standard Test Method for Tensile Properties of Thin Plastic Sheeting, American Society for Testing and Materials, West Conshohocken, Pennsylvania, USA.

ASTM D5885. Standard Test Method for Oxidative Induction Time of Polyolefin Geosynthetics by High Pressure Differential Scanning Calorimetry, American Society for Testing and Materials, West Conshohocken, Pennsylvania, USA.

GRI-GM13, Test Properties, Testing Frequency and Recommended Warranty for High Density Polyethylene (HDPE) Smooth and Textured Geomembranes. Geosynthetic Research Institute, Folsom, PA, USA.

Hsuan, Y.G., and Koerner, R.M., (1993). Can outdoor degradation be predicted by Laboratory Acceleration Weathering? Geotechnical Fabrics Report,11(8), 12-16

Martin, D (2005). UV Resistance in Thin Film Geomembranes, Accelerated and Natural Weathering Studies, GeoFrontiers 2005, IFAI, Austin, TX, USA.

Mills, A., "Performance of an Exposed HDPE Pulp Mill Pond Liners After 10 Years" , Proceedings of the 51st Canadian Geotechnical Conference, 1998, Edmonton AB.

Wagner, N., and Ramsey, B., (2003) QUV Accelerated Weathering Study: Analysis of Polyethylene Film and Sheet Samples. GSE Lining Technology Inc. Houston, TX, USA.

Hydrolysis Testing of High Tenacity Poly(ethylene terephthalate) – Results from 15 Years of Exposure

K.L. Nait-Ali, Terre Armée Internationale, Velizy, FRANCE
R.W. Thomas, TRI/Environmental, Austin, Texas, USA
P.L. Anderson, The Reinforced Earth Company, North Reading, Massachusetts, USA
N. Freitag, Terre Armée Internationale, Velizy, FRANCE

ABSTRACT
There has long been an interest in the performance of poly(ethylene terephthalate) (PET) products that may be exposed to aqueous environments during their service lifetimes. A study was initiated in 1993 to determine the hydrolysis resistance of high tenacity polyester yarns over 15 years time. The samples were exposed to three levels of pH (1, 7,12) and two temperatures (23, 50°C). The changes observed in the strength in the first ten years have been recently reported (JM. Jailloux et.al, 2008). This paper will add the 15 year results and focus on other properties of the samples such as molecular weight, carboxyl end group concentration and percentage crystallinity. These results will provide important information concerning the mechanisms of hydrolysis as a function of pH and exposure time and temperature.

1. INTRODUCTION

Polyethylene terephthalate (PET) geosynthetic materials are widely used in reinforced soil structures, generally in the form of high-tenacity fibers. This polyester is obtained by a reversible polycondensation reaction of a diacid (terephthalic acid) and a dialcohol (ethylene glycol). Condensation/hydrolysis reactions lead to structural changes which can be considered as reversible providing that water concentration is well controlled. Generally, if the polymer moisture content is higher than 0.02 %wt (J. Scheirs, 1998), ester hydrolysis leads to the increase of carboxylic acid and alcohol end-chains content, and the molecular weight decreases significantly with time and temperature.

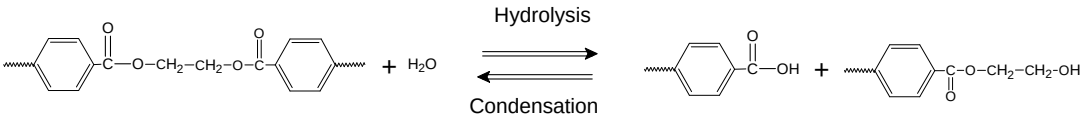

Figure 1. Condensation/hydrolysis of PET.

An important part of the current research is devoted to the improvement of the knowledge of high-tenacity PET lifetime by accelerated testing procedures. Currently there are many lifetime prediction models that are not linked with real conditions of degradation.

In 1993, a specific program was launched by Terre Armée Internationale (TAI) at TRI Environmental (TRI) to study the hydrolytic degradation of high-tenacity PET yarns during 15 years of exposure. Polyester fibers used in geosynthetic's manufacturing were exposed in different media (acidic, alkaline, neutral and/or saline) and temperature. A previous paper has presented the 10 years results and a kinetic model was developed by processing the abundant data (J-M. Jailloux et al., 2008). This paper is focused on the analysis of molecular chain hydrolysis to understand its impact on structural and macroscopic long-term behavior in real conditions.

2. EXPERIMENTAL

2.1 Material

The high-tenacity PET which was selected is in accordance with the recent report ISO/TR 20432 on yarns for durable reinforcing geotextile applications. Its main properties are detailed in Table 1.

Table 1. Main properties of PET yarns.

Properties	Value	Unity
Molecular weight	28000	g/mol
Carboxyl end group	25	mmol/Kg
Linear density	1000	den
Tenacity	790	mN/tex
Elongation at break	13.2	%

2.2 Long-term Exposure

Samples were exposed for 15 years in four different media, at 23°C and 50°C:

- Deionized water (H_2O, pH = 7)
- Hydrochloric acid (HCl, pH = 1)
- Sodium Hydroxide (NaOH, pH = 12)
- Calcium Hydroxide ($CaOH_2$, pH = 13)

Containers were sealed with RTV silicone and an aluminum lid. The containers were opened at the end of each exposure time. Samples were evaluated at 0.5, 1, 2, 5, 10 and 15 years.

2.3 Breaking Strength

All the samples were tested for breaking strength, with the use of horn grips at a crosshead speed of 12.7 cm/min (5"/min) and a grip separation of 10 cm. Twenty replicates were tested whenever possible. A set of baseline samples was tested along-side each set of samples from the exposures. The baseline material was kept in a sealed container in the dark for the 15 year period.

2.4 Melting Profile by Differential Scanning Calorimetry

DSC experiments were carried out on a TA Instruments Model Q2000 DSC at 10°C/min, under a nitrogen atmosphere. The heat of fusion was determined from 200 to 270°C. The percentage crystallinity was calculated from the heat of fusion of 100% crystalline PET (140 J/g). The samples evaluated were all from the water exposures.

2.5 CEG and Molecular Weight

CEG (Carboxyl End Group) and molecular weight were determined in accordance with the Geosyntetic Institute's (GSI) Methods GG7 and GG8. The CEG is found by titration of a sample dissolved in o-cresol at 80°C with a standard solution of KOH in methanol. The basis of the molecular weight determination is the intrinsic viscosity determined in a 60/40 blend of 1,1,2,2-tetrachloroethane and phenol at 25°C. The samples evaluated were from the deionized water exposures.

3. RESULTS AND DISCUSSION

3.1 Solution pH

The pH values measured in the solutions after 15 years of exposure were:

H_2O - 23°C, 6.0
50°C, 8.2
HCl - 23°C, 1.6
50°C, 1.5
NaOH - 23°C, 10.4
50°C, 11.0

These results show that the solutions were fairly stable, in terms of pH over the 15 years of exposure. Remarkably, the maximum amount of liquid loss from the 3.8L containers was only about 200 mL. Most of the containers lost less than 200 mL.

3.2 Breaking Strength

The evolution of PET strength with temperature and pH during 15 years is presented Figure 2.

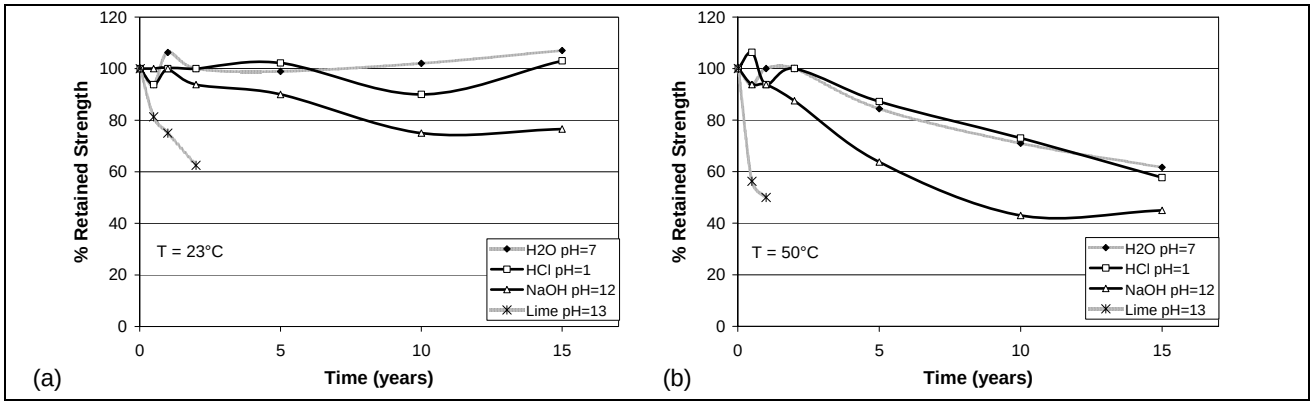

Figure 2. Hydrolytic degradation of PET yarns in various media (1<pH<13) at (a) 23°C and (b) 50°C during 15 years.

The curves show a significant increase of degradation rate with temperature and a high importance of pH level in the evolution of strength loss, even at low temperature. The average loss of strength in water and hydrochloric acid is the same so low pH seems to have no catalytic effect on PET hydrolysis. Concerning high pH, the average evolution of strength is the same during the first two years and then diverges. The degradation process in caustic soda and lime is a catalyzed hydrolysis coupled with surface erosion that leads to the material embrittlement. The erosion of the fiber surface is the consequence of its dielectric properties modification by hydroxide ions attack. This phenomenon is more manifest in lime where the impact of degradation on PET fiber service life is significant even at 23°C. One can see from the results that the samples were degraded beyond the ability to test them at 1 year and 2 years for 50°C and 23°C, respectively.

Considering the previous curves, hydrolysis over time can be described in 3 parts, as shown in Figure 3:

- *Phase 1 (time-lag)*: the polymer tensile strength is stable or sometimes increases slightly because of chemicrystallization (N.S. Allen *et al.*, 1991). This last phenomenon can be explained by chain-scission (due to hydrolysis in the amorphous phase of the polymer) that leads to the disentanglement of chain segments. The rearrangement of these short molecules induces an increase of crystallization rate (chemicrystallization) hence a slight increase of the tenacity.
- *Phase 2*: the hydrolytic degradation rate is stable until about 50% of strength loss.
- *Phase 3:* beyond approximately 50% strength loss, we do not observe a dramatic increase of the degradation rate as it was anticipated by an autocatalytic scheme. On the contrary, the degradation rate decreases. That can be attributed to the fact that degradation in the crystalline phase is slower than in the amorphous phase and that during the degradation process, the proportion of the crystalline phase increases in the total matter as the amorphous phase is almost totally degraded in phase 1 and 2.

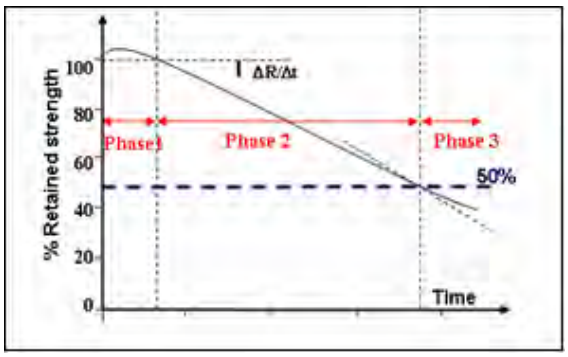

Figure 3. General hydrolytic degradation evolution with an incubation period followed by a constant rate.

As shown in Figure 2, it seems that at 23°C and after 15 years, the material is not yet in the second phase of the hydrolysis process. At 50°C, the yarn is still in the second phase, except in alkaline media where it seems to be in the third phase.

In a previous paper (J.-M. Jailloux et al., 2008), a new model on the hydrolysis of PET fibers in water (pH=7) has been presented. Arrhenius equations have been applied both to time-lag (phase 1) and degradation rate (phase 2). The respective expressions of induction time and degradation rate are:

$$I_t\,(\text{days}) = 1/e^{(26.6 - 21350 / 2\,T_K)} \qquad \text{and} \qquad R_{deg}\,(\%/\text{day}) = e^{(28.5 - 21350 / 2\,T_K)}$$

With 2 being the value of R (= 2 cal/mol.K), the perfect gas constant, and T_k is the absolute temperature. We observe that both activation energies are similar since both phases of PET yarn hydrolysis have the same degradation process: chain-scission. The average value we suggest is 21 350 cal/mole, which is significantly lower than the value generally retained, around 25 000 cal/mole. At 23°C, the time-lag is 35 years; this is the reason why at this temperature no degradation of the macroscopic properties is observed. At 50°C, time-lag is about 20 months and our model propose a degradation rate of about 3.9%/year for this temperature. Figure 4 present a comparison between experimental and simulated results.

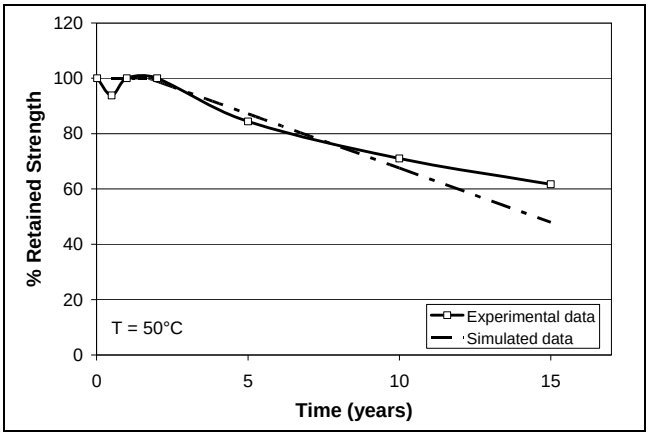

Figure 4. Comparison between experimental and simulated results for HTPET exposed to deionized water at 50°C.

The simulated curve is in good agreement with the experimental one. Around 60% of retained strength, we observe a slight decrease of the degradation rate. This is the beginning of phase 3, exposed previously and not modeled. The induction time is perfectly simulated and so is the first part of degradation until 10 years. The apparition of this 3rd phase could be due to:

- A total consumption of the amorphous phase and a decrease of the rate of molecular weight loss (slow diffusion of water into the crystalline fraction that induces a decrease of the degradation rate)
- A high increase of crystallinity that induces a slow down of strength loss with time of degradation.

In both cases, the evolution of the fiber morphology and not the evolution of its molecular weight govern the rate of strength loss.

To verify these hypotheses, a chemical study of the aged samples has been launched in order to understand the evolution of degradation rate during the 15 year exposure period. Our investigations are focused on degraded yarns in deionized water at 50°C and 23°C.

3.3 DSC Results

Figure 5 presents the percentage crystallinity and Figure 6 the melting profiles with degradation time for the samples aged in water at 50°C

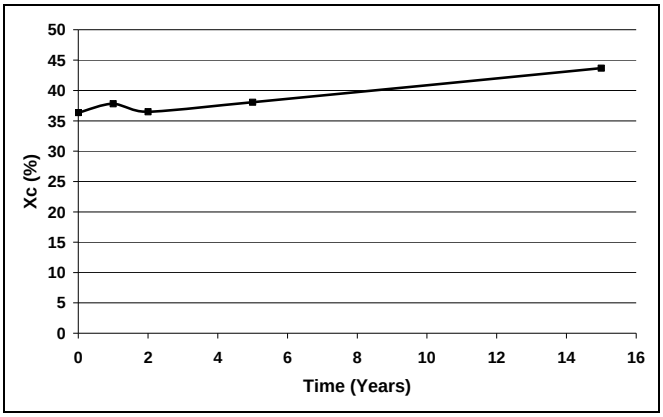

Figure 5. Evolution of crystallinity with time exposure for PET yarn exposed to deionized water at 50°C.

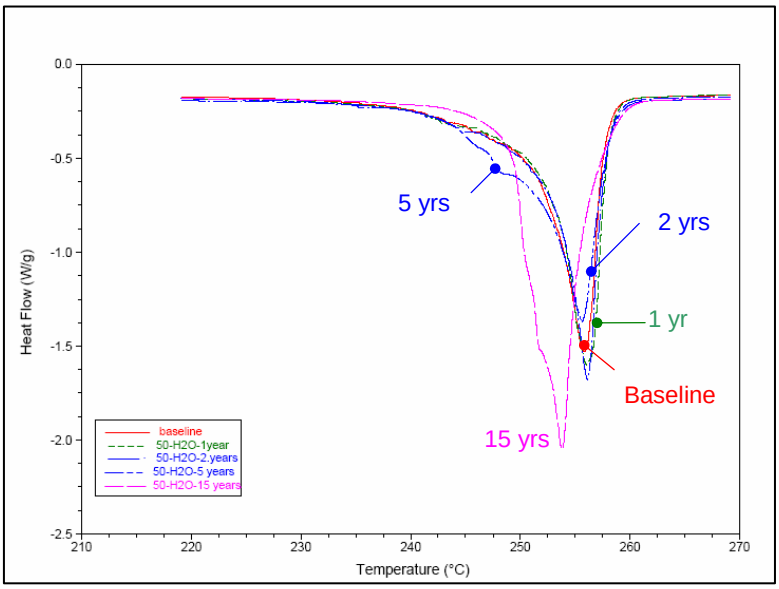

Figure 6. Evolution of heat flow with temperature and time exposure for PET yarn exposed to deionized water at 50°C.

The 2 previous curves show an increase of crystalline content in the material with exposure time. The first part of the curve presented in Figure 5 is associated with 'chemicrystallization'. Chain cleavage enhanced the mobility of the polymer chains and thus their crystallization ability. The crystallization of the yarn seems to be constant during the second phase of hydrolysis. Concerning the melting temperature (T_m), we observe a shift of the transition peak to lower temperature and a widening of the curve after 5 years. According to the Gibbs-Thomson relation, a decrease of melting temperature can be assigned either to a decrease of the lamellar thickness or to a change in amorphous-crystal surface energy, both being likely to occur simultaneously. So the observed evolution of T_m can be attributed to the degradation of amorphous phase and/or to the crystallization of imperfect or thinner crystallites that melt at lower temperature. These crystallites are generally created between two crystalline phases during the degradation of amorphous intercrystalline phase.

So, during water exposure at 50°C, chain-scission induces an increase of chain mobility and the development of small, imperfect crystallites, as obtained during the material annealing at highest temperature. The increase of crystallinity has no direct influence on the macroscopic properties of the yarn in the second phase of degradation: chain-scission has a predominant effect on the loss of mechanical strength. After 15 years of exposure, the observed decrease of strength loss rate could be due to the polymer high crystallinity content (about 45%). So these results reveal that DSC analysis of aged yarns confirms the degradation of PET in successive phases.

3.4 CEG and Molecular Weight

The CEG content and molecular weight evolution with time are presented in Figures 7 and 8

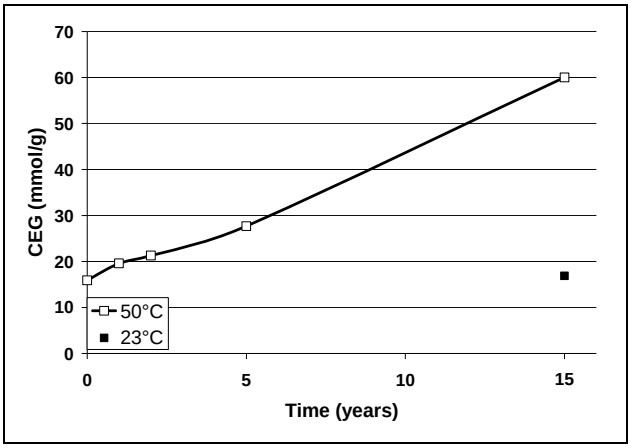

Figure 7. CEG content evolution with time for PET yarns exposed to deionized water at 50°C and 23°C during 15 years.

The evolution of CEG content is almost constant with exposure time at 50°C. So, there is no catalytic effect in these specific conditions. After 15 years and at 23°C, it is surprising to observe that CEG content has not increased at all. Hydrolysis is not chemically measured at this temperature after 15 years. The increase in carboxyl end-groups during long term exposure is characteristic of a situation where the water molecules are distributed evenly throughout the bulk of the yarn.

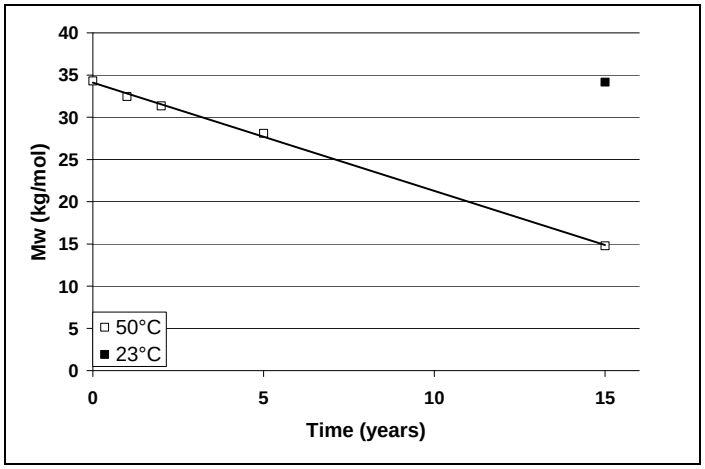

Figure 8. Molecular weight evolution with time for PET yarns exposed to deionized water at 50°C and 23°C during 15 years.

Molecular weight (Mw) has been obtained by intrinsic viscosity measurement. The dissolved molecules are characterized by their hydrodynamic volume, that is to say their linear length. So, the decrease of PET molecular weight exposed to water at 50°C and presented in figure 8, is the consequence of random chain-scission. As the hydrolysis process did not reach the third phase under these conditions (water, pH=7, 50°C, 15 years), the evolution of molecular weight seems linear. But we suppose that for a higher temperature or longer time, if the 3rd phase is reached, the evolution of molecular weight would present an asymptote corresponding to the molecular weight of the crystalline fraction that is insensitive to hydrolysis (A. Launay et al., 1999). So, after 15 years of hydrolysis at 50°C, this critical value, corresponding to the 3rd phase of hydrolysis, was not met.

The increase of crystallinity did not affect the change in molecular weight with time. It is assumed then, that the crystallites created during long-term exposure are effectively thin or imperfect.

Concerning PET yarns exposed 15 years at 23°C, they do not seem to have been degraded during the test.

In the first phase of degradation the effect of crystallization is predominant on the PET yarns macroscopic properties. During the second phase, random chain-scission is the main cause of tensile strength loss. From these results, one can deduce that PET hydrolysis is chemically homogeneous at least at low conversions. The heterogeneity observed in microscopic measurement (crystallinity) is due to the presence of nonreactive crystalline segments and on the evolution of spherulitic morphology during chemicrystallization, depending on environmental parameters.

The strength and Mw as a function of time are shown for the samples exposed in water at 50°C in Figure 9.

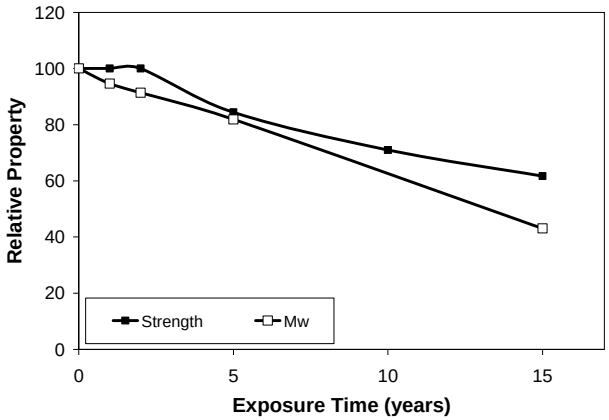

Figure 9. The relative change in Breaking Strength and Mw in H2O at 50°C.

Notice that the slopes are similar between 2 and 10 years of exposure but the Mw does not have an induction period and a decrease of degradation rate after 15 years of exposure like the strength results. The strength is dependent on a number of factors such as draw ratio, and the amount and type of crystals present. The Mw is not affected by these and is a fundamental property that is sensitive to the effects of aging. Therefore, in the case of water exposure, where the hydrolysis reaction occurs uniformly throughout the sample, following change in Mw with time can result in the determination of hydrolysis rates more quickly than changes in strength.

3.5 Application of Results

The results demonstrate that it may be possible to characterize the hydrolysis of high tenacity PET yarns early in the degradation process by monitoring the evolution of molecular weight. As shown by our hydrolysis model, it is not possible to determine the yarn degradation by measurement of loss of strength at 23°C because the time-lag for loss of strength at this temperature is about 35 years. So, use of simple chemical tests may be an alternative to tensile tests on durability samples extracted from in-service structures. The evolution of the mechanical properties of PET fibers depends on its morphology (crystalline content and chains orientation), and the morphology of the fiber depends on the evolution of molecular weight, on the applied load and on the temperature. On the other hand, we have shown that it may be possible to correlate the loss of molecular weight and the evolution of strength if the in-service temperature and initial properties of the yarn are known. Additional investigation on durability samples is needed and underway to confirm our hypothesis.

If we confirm the existence of this correlation, it could be a useful tool to determine the true evolution of PET yarn degradation and to monitor soil reinforcements in actual structures for early detection and prevention of rupture due to accelerated degradation.

4. CONCLUSIONS

The results of the 15 year aging study on the hydrolysis of PET yarns have led to the following conclusions:

a. The hydrolysis rates in HC1 (pH=1) and deionized water were essentially identical, which confirms the belief that lower pH values do not accelerate the hydrolysis rate.

b. High pH environments accelerate PET hydrolysis dramatically.

c. No measurable loss of strength was seen in the samples aged at 23°C in water, even after 15 years of exposure, confirming a long time-lag for the on-set of strength loss at 23°C.

d. A 3-step model for hydrolysis has been proposed with an induction period, a linear region, and a slowing down of the hydrolysis rate due to the increase in crystallinity of the exposed materials as chain scission occurs mainly in the amorphous regions.

e. Additional investigations are needed to confirm a correlation between loss of molecular weight and the evolution of loss of strength in order to develop a new method for early detection of PET degradation in reinforced soil structures.

REFERENCES

J-M. Jailloux, K.L. Nait-Ali, N. Freitag (2008), Exhaustive long term study on hydrolysis of high-tenacity polyester – 10 year results, Eurogeo 4, Edinburgh, UK

J. Scheirs, Polymer recycling: Science, Technology and Application, John Wiley & Sons, 1998, England, chapter 4.

Allen, N.S., Edge, M., Mohammadian, M. 1991. Hydrolytic degradation of poly(ethylene terephthalate): importance of chain scission versus crystallinity. European Polymer Journal, 27, 1373-1378.

Launay, A., Thominette, F., Verdu, J. 1999. Hydrolysis of poly(ethylene terephthalate). A steric exclusion chromatography study. Polymer Degradation and Stability, 63, 385-389.

Carbon Black and Antioxidant Effect in High Density Polyethylene

W-K. Wong, Drexel University, Department of Civil, Architectural and Environmental Engineering, Philadelphia, PA, USA
Y. G. Hsuan, Drexel University, Department of Civil, Architectural and Environmental Engineering, Philadelphia, PA, USA

ABSTRACT
All high density polyethylene (HDPE) geosynthetics contain 2 to 3% of carbon black (CB) to protect products from ultraviolet (UV) degradation. This paper presents the effects of carbon black on the depletion of antioxidants (AOs) in HDPE. A constant amount of 2.5% of CB with particle size of 75 μm was used in this study. Five AO formulations consisting of different concentrations of Irganox® 1010 and Irgafos® 168 were evaluated.

The effects of CB on the depletion of AOs were evaluated by incubating HDPE samples in forced air ovens at temperatures of 65, 75, and 85°C. The amount of AOs remained in the incubated sample was monitored using oxidative induction time (OIT) test. Regardless the type or concentration of AOs, a significantly higher OIT decreasing rate was detected in samples with CB than without CB, indicating the chemical interaction between CB and AOs. Also the effect of different AOs on the OIT depletion rate was observed among samples without CB.

1. INTRODUCTION

Most of the polymeric products contain additives. Carbon black (CB) and antioxidant (AO) are two of the most commonly used additives for UV protection and for prolonging service life time in geosynthetic products.

Carbon black is well known for functioning as a UV protector and as a mild thermo-oxidation stabilizer (Watson, 1955, Hawkins et al., 1959, Pleshanovet et al., 1982, Mwila et al., 1994). The effectiveness as a protector and stabilizer is not only based on the particle size and dispersion of carbon black but is also based on oxygen functional groups that are on the surface of CB. Chemical groups and structures attached on the surface of CB are mainly dependent upon the manufacturers, processing condition, and additional treatments such as liquid phase oxidation, chemical method and plasma treatment (Wypych, 2000). The surface chemistry of oxygen functional groups on CB is particularly important as a contributing stabilizer because the groups can interact with free radicals and delay degradation of the polymer. This was proven by Kovacs, E and Wolkober, Z, (1976). They found that by increasing oxygen contained surface groups and the surface area of CB, the function of AO against thermo oxidation increased.

Antioxidants are known for protecting polymer from oxidation degradation. Even though both AO and CB protect polymer, sometimes when combined, they may have a negative effect on each other's protective capabilities. Results of research studies showed to have either positive or negative effects. Phease et al. (2000) show that CB with both phenolic and phosphite based AO increases the initial oxidative induction time (OIT) value. Gilroy and Chan (1984) blended polyethylene (PE) with different combinations of CB with four types of AO, including amine, hindered phenol, thiobisphenol, and a second sulfur bridge phenol, to demonstrate the effects of suppressing the onset of the oxidation for each combination. Their findings confirmed the positive effects AO and CB have on polymer. On the other hand, Hawkins et al. (1959) found that CB combined with certain types of phenol antioxidant or secondary amines can greatly reduce the effectiveness of AO function. This loss of effectiveness might be due to the decreased AO mobility which was restricted by the absorption on CB particles and/or due to the reaction of AO with free sulfur on CB surfaces. Kovacs and Wolkober (1976) found that the acidic nature of CB could reduce the effectiveness of AO performance in thermo-oxidation. This finding might be explained by the quinine type oxygen on the acidic CB surface reacting with the hydrogen on AO rather than a free radical resulting in an antagonistic effect. Pena et al. (2001) used flow micro-calorimetry to measure the heat of adsorption/desorption of Irgafos 168, Irgafos P-EPQ, and Alkanox TNPP. Four types of CB were blended with these three AOs and both synergistic and antagonistic effects were found. They concluded that the adsorption/desorption activity were not only dependent upon the particle size but also influenced by oxygen content, neighboring surface functional groups, CB surface structure, and porosity.

Although the initial effects of the reaction between AO and CB have been well studied by researchers, their long term interaction was often overlooked. This paper examined the interaction between CB and AO under elevated temperatures. The purpose is to gain a further understanding of CB and AO behavior in terms of long term performance of geosynthetics. In this study, OIT test was used to measure the retaining AOs in the HDPE samples to determine the AO depletion behavior of different formulations.

2. EXPERIMENT

2.1. Test Materials

HDPE pipe grade resin with density of 0.953 g/cm^3 was blended with two AOs, Irganox® 1010 (I-1010) and Irgafos® 168 (I-168), in five formulations. In addition, 2.5% furnace black with 75μm particle size was used in each formulation. The carbon black master batch, which consists of 50% carbon black and 50% linear low density PE, was first ground into powder. The appropriate amount of carbon black powder, PE fluff, and AOs were fed into the laboratory scale single screw extruder to produce pellets. A total of ten formulations were made, as shown in Table 1. The test samples were compressive molded plaques prepared according to ASTM D4703, A1 at a cooling rate of 15^{o}C/min. The thickness of the plaques ranges from 1.8 mm (0.071 inch) to 2.1 mm (0.083 inch). Small coupons with dimensions of 75mm (3 inch) x 90 mm (3 ½ inch) were cut from the plaques for incubation.

Table 1. Formulation in each of the blend samples

Formulation	**0% Carbon Black**	**2.5% Carbon Black**
I-1010: 0 ppm I-168: 0 ppm	Blend 1 (B1)	Blend 2 (B2)
I-1010: 500 ppm I-168: 0 ppm	Blend 3 (B3)	Blend 4 (B4)
I-1010: 500 ppm I-168: 1000 ppm	Blend 5 (B5)	Blend 6 (B6)
I-1010: 1000 ppm I-168: 0 ppm	Blend 7 (B7)	Blend 8 (B8)
I-1010: 1000 ppm I-168: 1000 ppm	Blend 9 (B9)	Blend 10 (B10)

2.2. Incubation Conditions

Forced air ovens at 65, 75, and 85^{o}C were used to accelerate the thermo-oxidation process. Coupons were hung in the oven with 1" spacing and taken out at different time intervals to measure the loss of antioxidants.

2.3. Test Methods

The depletion of AOs was monitored by the standard oxidative induction time (OIT) test followed the ASTM D3895 procedure using Differential Scanning Calorimeter (DSC).

The concentration of AOs in the original un-incubated samples were analyzed using High Performance Liquid Chromatography (HPLC) according to the ASTM D6953 using cyclohexane as solvent for extraction.

3. RESULTS AND DISCUSSIONS

3.1. Depletion of Antioxidants

The OIT depletion of four blends without CB was evaluated. The original OIT of these blends are shown in Table 2 along with the remaining AO concentrations in the sample measured by HPLC. It shows that the addition of I-168 greatly increases the OIT value.

Table 2. Original OIT values of four blends without CB

Blend	Antioxidant				Original OIT (min.)
	Added I-1010 (ppm)	Added I-168 (ppm)	Detected* I-1010 (ppm)	Detected* I-168 (ppm)	
B3	500	--	355	--	19.4
B5	500	1000	199	537	33.3
B7	1000	--	749	--	34.0
B9	1000	1000	836	718	58.7

*The detected concentration referred to AO concentrations in the extruded resin pellets.

Depending on the AO formulations, two OIT depletion trends were observed among the four blends, as shown in Figure 2(a). For B3 and B7, which consist of only I-1010, the OIT remains almost unchanged throughout the 1000 days of incubation. On the other hand OIT decreases steadily with time from the beginning of the incubation in B5 and B9 which contain I-1010 and I-168. The steadily decreasing OIT trends are believed to be due to the loss of I-168. As indicated in Figure 2(b), the OIT value of B9 decreases exponentially with time until it approaches to the value of B7, after that the OIT values of both blends deplete at similar rates. Similar result was also obtained by Dörner and Lang (1998); they found that the remaining content of I-168 decreased much faster than I-1010 in oven incubated HDPE samples using HPLC.

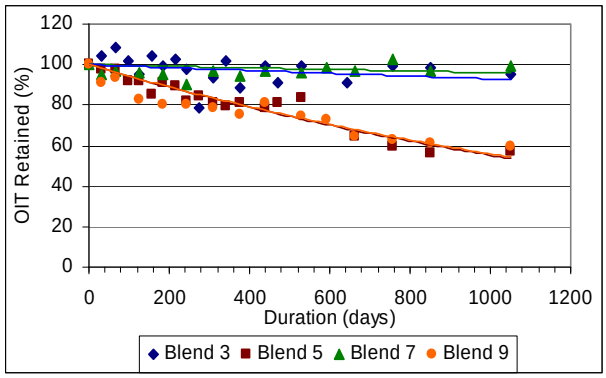

(a)

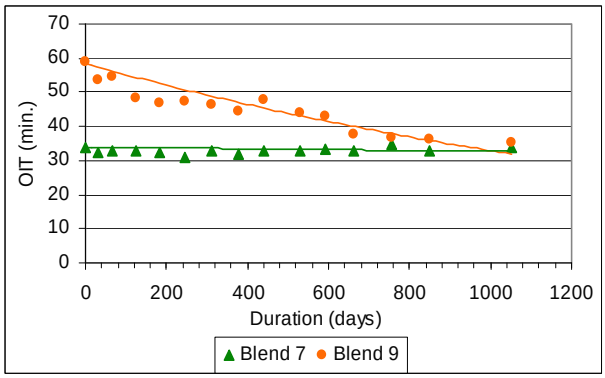

(b)

Figure 2. (a) OIT retained versus time of blends without CB at 85°C,
(b) OIT versus time of B7 and B9 at 85°C

The test data of these four blends suggest that the initial OIT value and its depletion rate are governed by the type of AOs in the polymer. Adding I-168 to I-1010 increases the initial OIT value while the OIT depletion rate is accordingly faster in comparison. In addition, I-1010 outperforms I-168 in terms of OIT retention in the oven incubation condition.

3.2. Interaction between Carbon Black and Antioxidant

Besides providing UV protection, CB is also believed to function as a mild antioxidant against thermo-oxidation. The sample B1 contained no AOs, while sample B2 was blended with 2.5% CB. Dispersion of CB was examined on all CB blends using the ASTM D5596 slicing the sample into a thin layer. Figure 1 reveals the dispersion condition of CB in the microtome specimens.

Blend 2 Blend 4 Blend 6 Blend 8 Blend 10

Figure 1. Photos of microtome sliced of original samples with CB

Table 3 shows the original OIT values of all ten blends. In general, blends with CB exhibit a slightly higher OIT values, except for B10. Even for B1 and B2 which are unstabilized blends, the original OIT value of B2 is slightly higher than B1. Thus, based on the original OIT value, the CB used in this study seems to delay the onset of oxidation as observed by other researchers (Watson, 1955, Hawkins et al., 1959, Pleshanovet et al., 1982).

Table 3. Comparing the original OIT values for blends with and without CB

Blend	CB (%)	Original OIT (min)	Blend	CB (%)	Original OIT (min.)
B1	0	0.5	B2	2.5	1.2
B3	0	19.4	B4	2.5	21.0
B5	0	33.3	B6	2.5	39.1
B7	0	34.0	B8	2.5	37.2
B9	0	58.7	B10	2.5	56.4

Table 4 shows the original OIT values of four CB blended samples along with the remaining AO concentrations in the sample. Similar to blends without CB, the additional of I-168 substantially increases the OIT value.

Table 4. Original OIT values of four blends with CB

Blend	CB (%)	Antioxidant				Original OIT (min.)
		Added I-1010 (ppm)	Added I-168 (ppm)	Remained I-1010 (ppm)	Remained I-168 (ppm)	
B4	2.5	500	--	368	--	21.0
B6	2.5	500	1000	342	745	39.1
B8	2.5	1000	--	762	--	37.2
B10	2.5	1000	1000	799	718	56.4

The changing of OIT retention with incubation time at 85°C of these four CB blends can be seen in Figure 3(a). All blends undergo a similar depletion behavior regardless of the type and concentration of AOs. The only difference among them is the initial OIT value, as depicted in Figure 3(b). In addition, the depletion rates of the CB blends are significantly faster than the corresponding blends without CB, as illustrated in Figure 4. The results clearly demonstrate a strong interaction between CB and AO during the oven aging. Since only one type of CB is used in this study, it is uncertain whether similar interaction would take place in other types of CB. Evaluation of different types of CB will be carried in the next phase of the study.

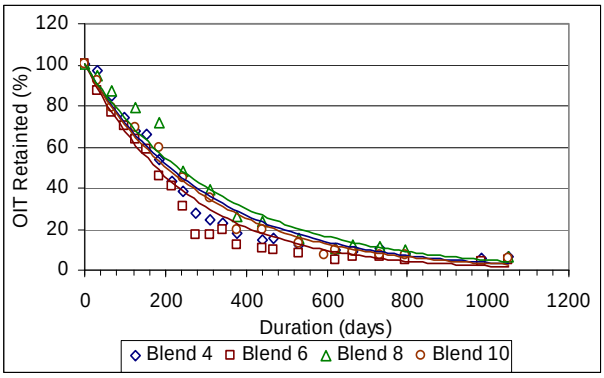

(a)

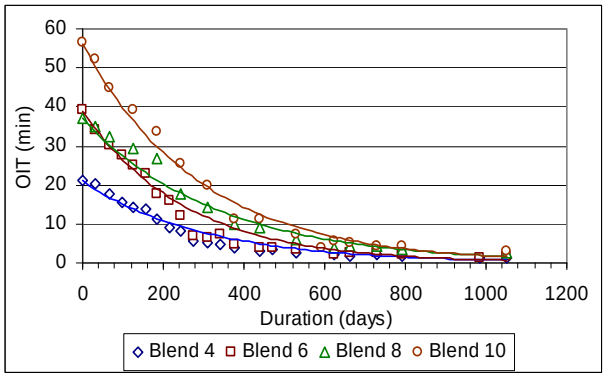

(b)

Figure 3. (a) Changing of OIT retained versus time of blends with CB at 85°C oven
(b) OIT versus time of blends with CB at 85°C oven

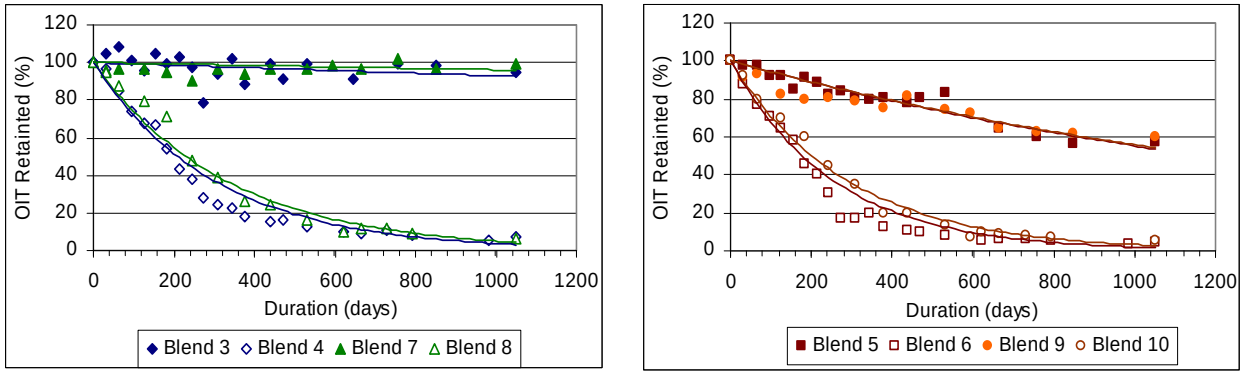

(a) (b)

Figure 4. (a) OIT retained versus time of blends contained I-1010 with and without CB at 85°C oven (b) OIT versus time of blends contained I-1010 and I-168 with and without CB at 85°C oven

3.3 Antioxidant Distribution Within The Material

To understand the consumption and migration of AOs within the incubated samples at different incubation durations, the AO distribution in terms of OIT across the thickness was examined. OIT test was performed on thin sections that were sliced parallel to the thickness of the incubated sample. Figure 5 shows the OIT profiles of 0-, 30-, and 310-day of incubation at 85°C. The OIT values are relatively constant across the thickness at different incubation durations in B3. Similarly, the OIT values across the thickness of B4, which contains CB, are also fairly consistent. On the other hand Viebke et al. (1996) have found a parabolic OIT profile across the HDPE pipe wall; OIT values were lower at two exposed surfaces than at the center. They explained that the depletion of AO at the surface due to chemical reactions and evaporation was faster than the migration of AO within the polymer. Therefore results obtained from B3 and B4 suggest that the surface evaporation is not a major phenomenon for samples contained I-1010, with or without CB. The consumption of AO took place evenly across the thickness of the sample.

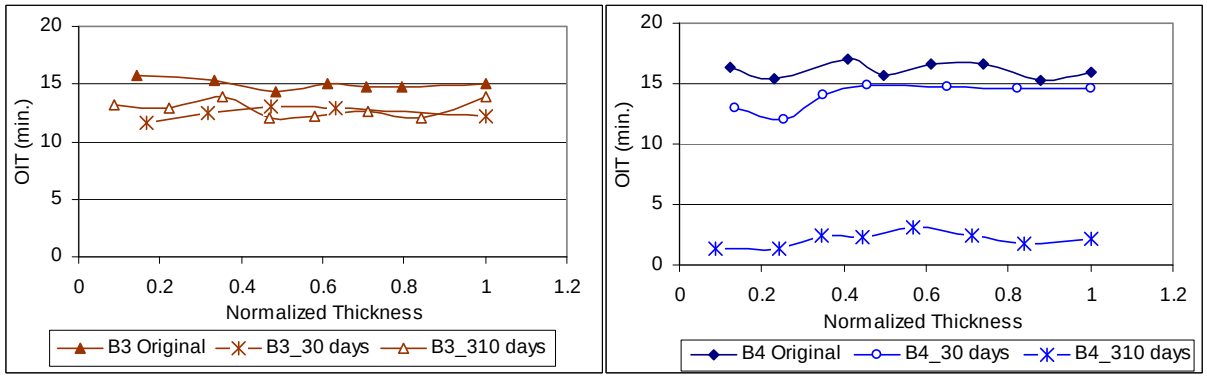

(a) (b)

Figure 5. OIT profiles of B3 and B4 at 85°C incubation temperature

For blends with both I-1010 and I-168, different OIT profiles were detected. Figure 6(a) shows a higher OIT value at the surface of B5, which may be caused by the dissimilar solubility of the two AOs. During the cooling of plaques, the solubility of AO decreased and created an over-saturation state at room temperature. After equilibrium state has been reached, the stabilizers bloomed to the surfaces (Haider and Karlsson, 2002). Due to the small molecular structure of I-168, the migration/diffusion rate of I-168 was faster than I-1010; thus, a higher OIT was measured. However, the booming effect did not take place symmetrically on both surfaces. This may be caused by the discrepancy in the temperature and cooling rate on two sides of the mold. Apart from the surface booming, the OIT values are fairly consistent across the thickness of B5. This suggests that the depletion of AO took place evenly throughout the thickness. The loss of AO due to surface evaporation is promptly balance by the migration of AO within the sample.

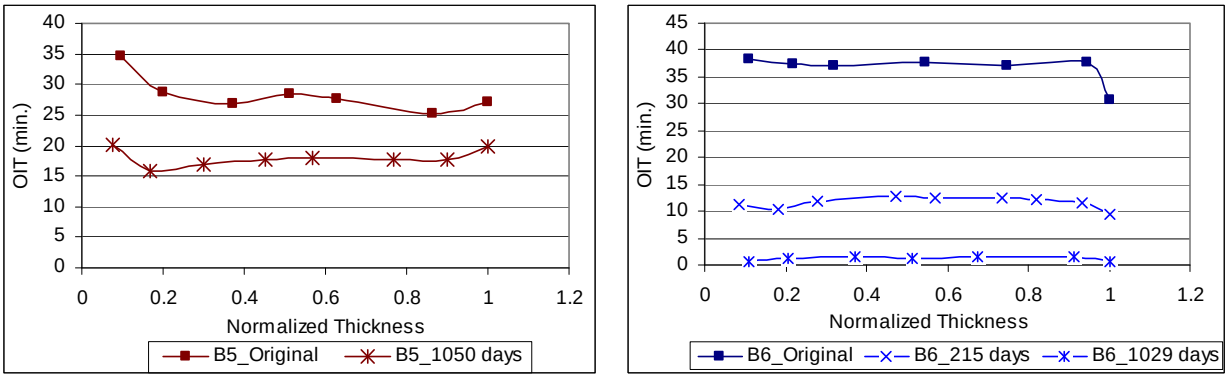

(a) (b)

Figure 6. OIT profiles of B5 and B6 at 85°C incubation temperature

For B6 (Figure 6(b), the added CB exhibits a strong interaction with AO and minimizes the surface booming. The depletion of AO across the thickness seems to be consistent throughout the incubation. However, it is uncertain the cause for the drop in OIT on one of surfaces.

3.4. Antioxidant Lifetime Prediction

The AO lifetime which is critical to the long-performance of the geosynthetics is predicted using Arrhenius equation, as shown in Eq. (1). The activation energy (E) is determined for each blend and the service lifetime at ambient temperature (20°C) is extrapolated. Since most geosynthetics contain CB, the lifetime prediction was performed on B4, B6, B8, and B10. The Arrhenius plot of the four blends is shown in Figure 7.

$$k = A * \exp\left(-\frac{E}{RT}\right) \quad (1)$$

where k is the reaction rate constant at each incubation temperature, A is a constant, E is the activation Energy (kJ/mol), R is the gas constant (8.314J/mol) and T is the incubation temperature (K).

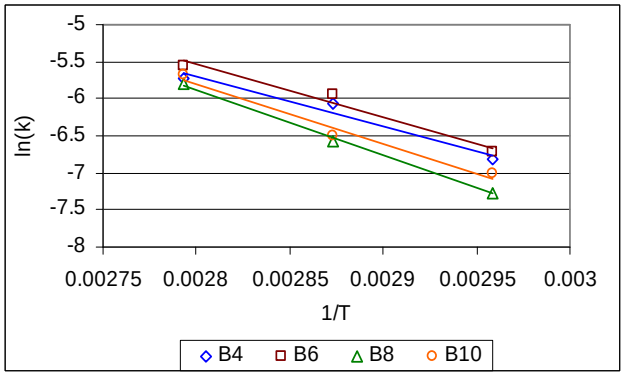

Figure 7. Arrhenius Plot of blends with CB

Based on the original OIT value of B2, the lowest OIT limit is assumed to be 1.2 minutes. The results of the activation energy and predicted AO lifetime are shown in Table 5. There is no correlation between the predicted lifetime and the original OIT value. The effect of I-168 on the predicted lifetime is inconsistent in B6 and B10, while increase the concentration of I-1010 does enhance the lifetime, particularly without I-168.

Table 5. Predicted service lifetime of the blends with CB

Blend	AO in Plaque I-1010 (ppm) / I-168 (ppm)	Initial OIT (min)	Activation Energy (kJ/mol)	AO lifetime (years)
B4	368 / 0	21.0	52.6	130
B6	342 / 745	39.1	57.9	190
B8	762 / 0	37.2	58.9	235
B10	799 / 718	56.4	55.5	211

4. CONCLUSIONS

From the results of this study, following conclusions are drawn:

- The initial value of OIT is governed by the types and amount of AOs, particularly I-168.
- The evaporation/consumption rate of I-168 is much faster than I-1010.
- The OIT depletion rate is significantly slower for I-1010 alone than the combination of I-1010 and I-168, implying that I-1010 performed more effectively than I-168 in the forced air oven incubation.
- The CB used in this study exhibited a strong interaction with AOs during the oven incubation.
- The predicted AO lifetime of blends with CB ranges from 130 to 235 years. The I-1010 has greater effect on the predict lifetime than I-168.

ACKNOWLEGEMENT

The project is funded by the Florida Department of Transportation. Miss Wai-Kuen Wong is supported by GSI Fellowship. Appreciation is given to GSI for using their laboratory facility. The sample plaques used in this study were supplied by Dr. Shuya Cheng of Exxon-Mobil Chemical Company, together with HPLC analysis of the antioxidants.

REFERENCE

Dörner, G., and Lang, R. W. (1998). "Influence of various stabilizer systems on the ageing behavior of PE–MD—II. Ageing of pipe specimens in air and water at elevated temperatures." *Polymer Degradation and Stability,* 62(3), 431-440.

Gilroy, H. M., and Chan, M. G. (1984). "Effect of Pigments on the Aging Characteristics of Polyolefins." *Polymer Science and Technology,* 26 273.

Haider, Nadejzda , Karlsson, and Sigbritt (2002). “Loss and transformation products of the aromatic antioxidants in MDPE film under long-term exposure to biotic and abiotic conditions.” *Journal of Applied Polymer Science*, 85, 974-988

Hawkins, W. L., Hansen, R. H., Matreyek, W., and Winslow, F. H. (1959). "The effect of carbon black on thermal antioxidants for polyethylene." *J Appl Polym Sci,* 1(1), 37-42.

Kovacs, E., and Wolkober, Z. (1976). "The Effect Of The Chemical and Physical Properties Of Carbon Black On The Thermal And Photooxidation Of Polyethylene." *Journal of Polymer Science,* Symposium No. 57 171.

Mwila, J., Miraftab, M., and Horrocks, A. R. (1994). "Effect of carbon black on the oxidation of polyolefins—An overview." *Polymer Degradation and Stability,* 44(3), 351-356.

Peña, J. M., Allen, N. S., Edge, M., Liauw, C. M., and Valange, B. (2001). "Factors affecting the adsorption of stabilizers on to carbon black (flow micro-calorimetry studies) 4. Secondary antioxidants." *Polymer Degradation and Stability,* 72(1), 31-45.

Phease, T. L., Billingham, N. C., and Bigger, S. W. (2000). "The effect of carbon black on the oxidative induction time of medium-density polyethylene." *Polymer,* 41(26), 9123-9130.

Pleshanov, V. P., Berlyant, S. M., and Burukhina, G. A. (1982). "Study of kinetics of inhibition of thermo-oxidation of polyethylene by carbon black." *Polymer Science U.S.S.R.,* 24(6), 1462-1468

Viebke, J., Elble, E., and Gedde, U. W. (1996). "Degradation of polyolefin pipes in hot water applications: Simulation of the degradation process." *Polymer Engineering & Science,* 36(4), 458-466.

Watson, W. F. (1955). "Combination of Rubber and Carbon Black on Cold Milling." *Ind. Eng. Chem.,* 47(6), 1281-1286.

Wypych, G. (2000). Handbook of Fillers - A Definitive User's Guide and Databook (2nd Edition). ChemTec Publishing,

Planning Design and Installation of a Design/Build Gas Collecting Floating Cover System for Cargill Meat Solutions

A.A. Harvey Spring Valley, CA United States

ABSTRACT
In May of 2004 CLI-Clearwater Construction completed the installation of a 17,315 square meter floating cover system for Cargill Meat Solutions. The application was gas collection over a pork processing and rendering operations anaerobic digestion lagoon located in Beardstown, Illinois.

The area that was covered measured 160 m x 108 m. The lagoon was in service at the time of installation and featured a 2.5 mm thickness High Density Polyethylene or "HDPE" liner membrane that a 2 mm thickness gas collecting HDPE floating cover membrane was welded to via extrusion welding process.

1. TYPICAL HDPE GAS COLLETING COVER INSTALLATIONS

Because of the material's inherent stiffness, HDPE membrane covers are suitable for use over reservoirs that have fixed operating levels. In general, HDPE covers are ill suited in applications where lagoons have liquid levels subject to fluctuation more than 1m. In gas collecting applications HDPE tends to be the most commonly used material. This is largely due to durability, relative ease in repair in floating cover environments and chemical resistance. Many gas collecting cover systems are installed in rendering plant applications where plant waste is fermented anaerobically. Rendering plant waste has high concentrations of fatty acids and oils that can permeate and destroy other types of membranes such as polypropylene or Hypalon®.

Typical HDPE gas collecting covers are built on-site by wedge welding one manufacturer's roll width (usually 6.86 m minus seam overlap) of material at a time and incrementally pulling the cover as its being built over a full lagoon until the required cover area is complete. Pulling a cover over a reservoir usually involves deployment of aircraft style wire ropes placed on strategic centers along a buoyant, semi-rigid leading edge detail that helps spread loading forces to prevent the cover from wadding-up into a mess or sinking in a rain event. This process requires synchronization of heavy loader type machines deployed to tug the cables at equal rates. Once covers are pulled into place the leading edges are cut away and typically re-used on other projects. The perimeters of these covers may be secured into earthen anchor trenches, mechanically fastened to a purpose engineered perimeter concrete curb detail or welded onto the surface of an existing lagoon lining membrane of compatible resin type and suitable thickness.

Large scale gas collecting floating covers must be fitted with ballast grid details to help provide stability against wind forces while also providing a means of directing storm water to convenient collection and removal points with explosion proof mobile and/or fixed pump systems. One of the most prevalent methods to achieve cover ballast and storm water management is to design covers with ballast grids consisting of continuous flexible grout filled pipes of 2 or more sizes running in opposing directions. In this approach, typical covers will feature one large diameter HDPE grout filled pipe (i.e. 200 mm or 300 mm diameter) that will be installed upon the centerline of the cover's long axis. Smaller diameter HDPE grout filled pipes (i.e. 150 mm diameter) are typically installed in a perpendicular direction on 12 m – 15 m center spacing. With this type of ballast system layout most storm water collects along the single larger diameter ballast pipe and concentrates at the edges of the lagoon cover where it is easy to remove. The smaller diameter ballast pipe details on parallel centers are referred to as "laterals". The single larger diameter ballast pipe is referred to as a "bisector". Gas collecting covers are subjected to some degree of inflation from the internal pressure of biogas that percolates out of the waste water as part of the anaerobic digestion process. Gas generation is often not uniform within a covered lagoon. Waste stream flow and many other factors within the lagoon can result in uneven biogas production causing uneven cover inflation. Because of these factors and the interaction of wind and rain, it is necessary to strap ballast pipes to the cover membrane preferably in a fusible link type fashion to avoid cover damage in extreme wind conditions. Without designed restraint, ballast pipe systems cannot remain in-situ and perform effectively.

Gas extraction is usually achieved by provision of a blower and a full lagoon perimeter perforated pipe located at the top of slope between the floating cover membrane and secured to the sub surface where liquid (other than vapor) cannot enter the pipe and fowl downstream systems. Blowers are selected to be of appropriate size and type to maintain covers in low wind profiles and of sufficient force to safely fuel a fare system, generator or boiler.

2. THE BEARDSTOWN CHALLENGE

Although this cover featured the usual design elements associated with HDPE floating covers, there was a special circumstance that made this a unique project to design and install. The challenge was the presence of a concrete valve vault tower that was placed 13.5 m into the interior of the lagoon roughly in the middle of the160m dimension (see Figure 1. Anaerobic Lagoon Layout). The valve vault had a rectangular plan view section measuring roughly 3 m x 3.35 m. Compounding this was the presence of a permanent 1.5 m wide steel catwalk structure extending from the bank of the reservoir to the valve vault tower. There was 1m of vertical clearance between the catwalk and the lagoon's operating water level.

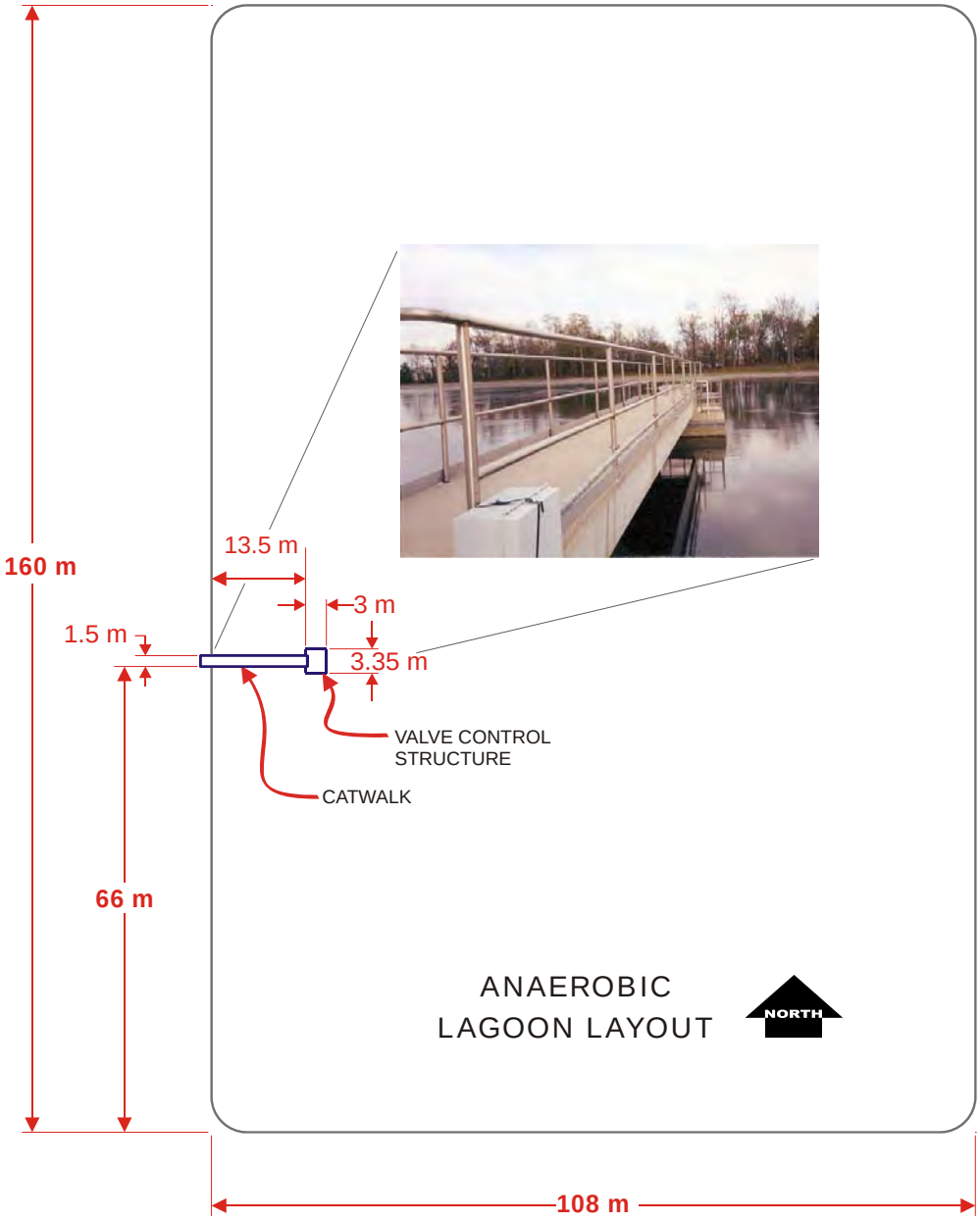

Figure 1. Anaerobic Lagoon Layout

3. THE DESIGN AND INSTALLATION RESPONSE

The catwalk and valve structure location required that the 2 mm thickness HDPE floating cover membrane be constructed in two “halves” for installation around the vertical valve structure. The two “halves” necessity further required that two leading edges were to be deployed and permanently be left in-situ at the completion of work. The cover halves were designed for pulling into place parallel to the long/160 m axis in opposing directions to meet at the structures.

One of the leading edges was designed with a notch feature that was dimensioned to envelop the tower on 3 sides while providing .75 m of clearance on those sides and further extending beyond the tower a distance of .75 m. The second “half” once both leading edges were abutted around the tower. Pulling the cover halves into place from opposing directions required that special rigging plans be developed as to avoid the 7 each 9.5 mm diameter vinyl coated pull-on cables from making destructive contact with the cover half that was already in place.

The leading edges featured removable longitudinal galvanized steel tubing in hems on the top side and encapsulated 10 cm thick x 1.22 m wide x 2.74 m length Expanded Polystyrene (or “EPS”) foam planks on the bottom sides. Plank encapsulation material was 1.5 mm thickness HDPE. Planks were placed under the frontal/leading edges of the cover membrane “halves” and welded in-situ via extrusion welding process.

Where the leading edges met/wrapped around the tower, Dow Ethafoam, a HDPE type closed cell foam of 35 kg/m^3 density was deployed for enhanced durability (see Figure 2. Foam Plank Detail at Concrete Structure).

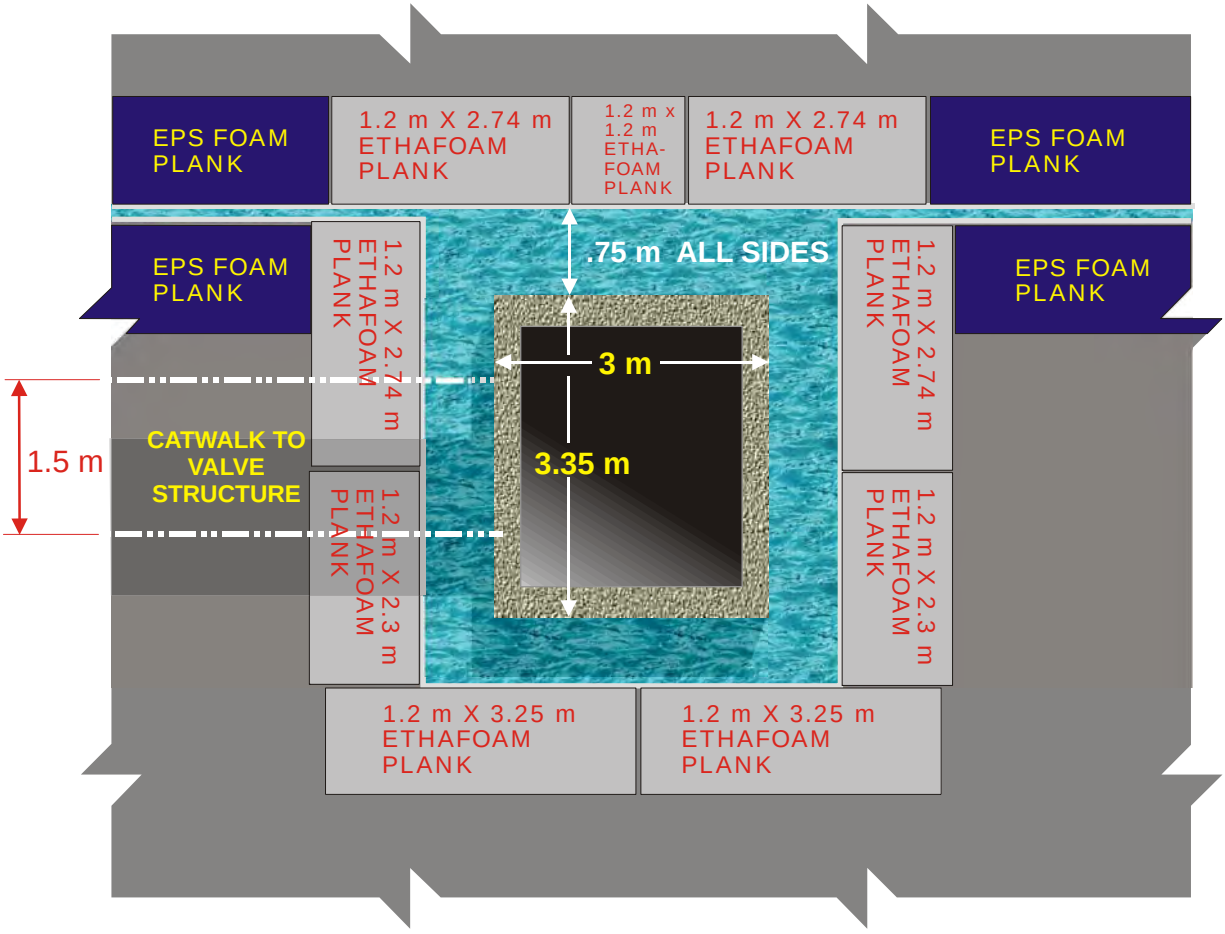

Figure 2. Foam Plank Detail at Concrete Structure

In execution, each “half” of the floating cover system was installed in separate events starting with the north side first which featured the straight leading edge. Once positioned, this cover half was ballasted in-situ around the perimeter with sandbags and the longitudinal galvanized tube detail was removed. Following this, the south cover “half” was deployed and temporarily ballasted in-situ and the longitudinal galvanized tube detail was removed. The two “halves” of

the cover were joined at the leading edge locations by installation of a 2 mm thickness HDPE cap strip welded via extrusion welding. Once both "halves" of the cover system were joined, the perimeter of the cover system was attached to the liner system via continuous extrusion welding.

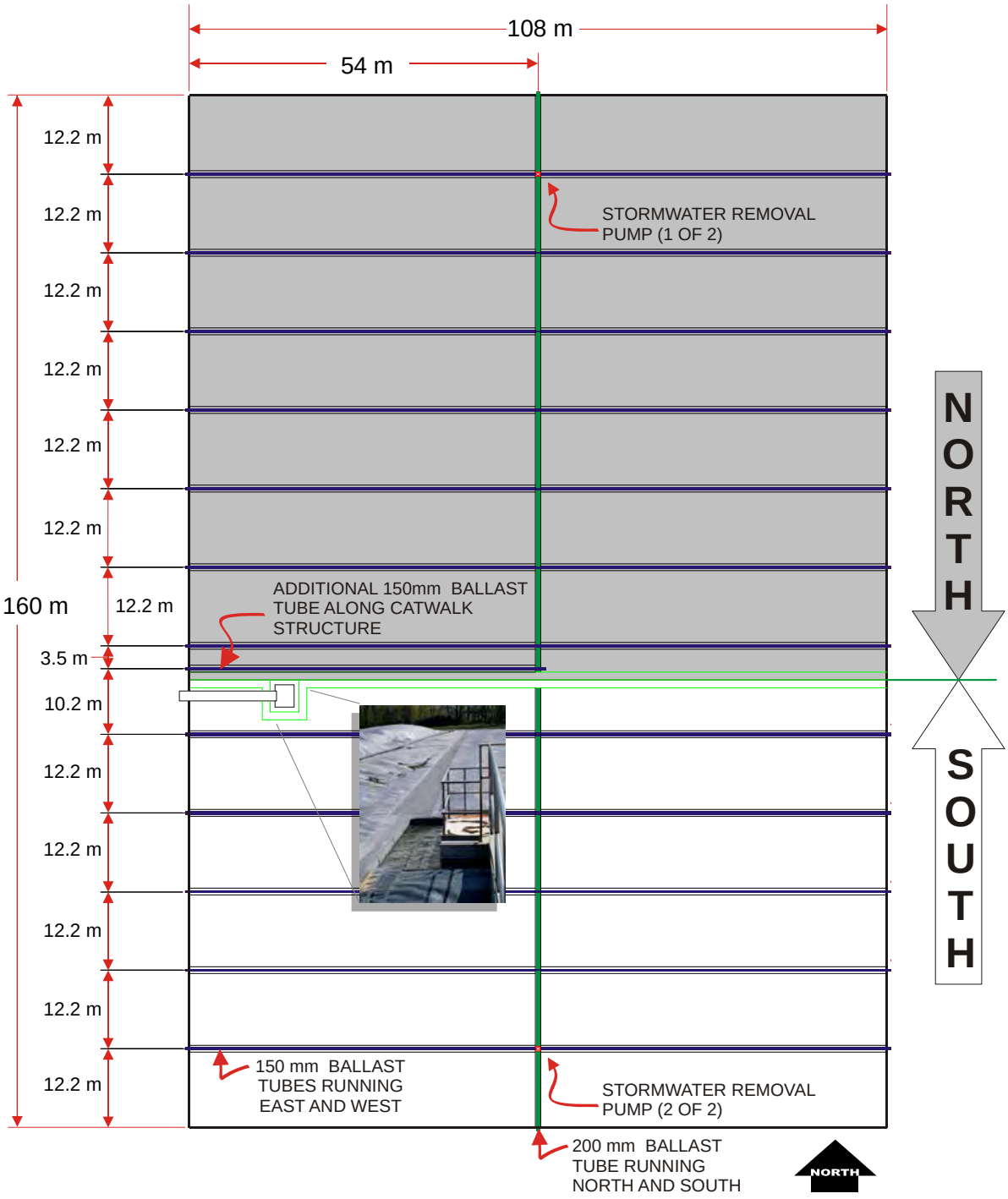

Figure 3. Floating Cover Layout Plan

To prevent biogas from migrating under the cover to the opening around the valve tower, a weighted impervious curtain was installed on the cover at this location that extended a vertical distance of 2 m (see Figure 4. Gas Trapping Curtain Section Detail at Valve Structure).

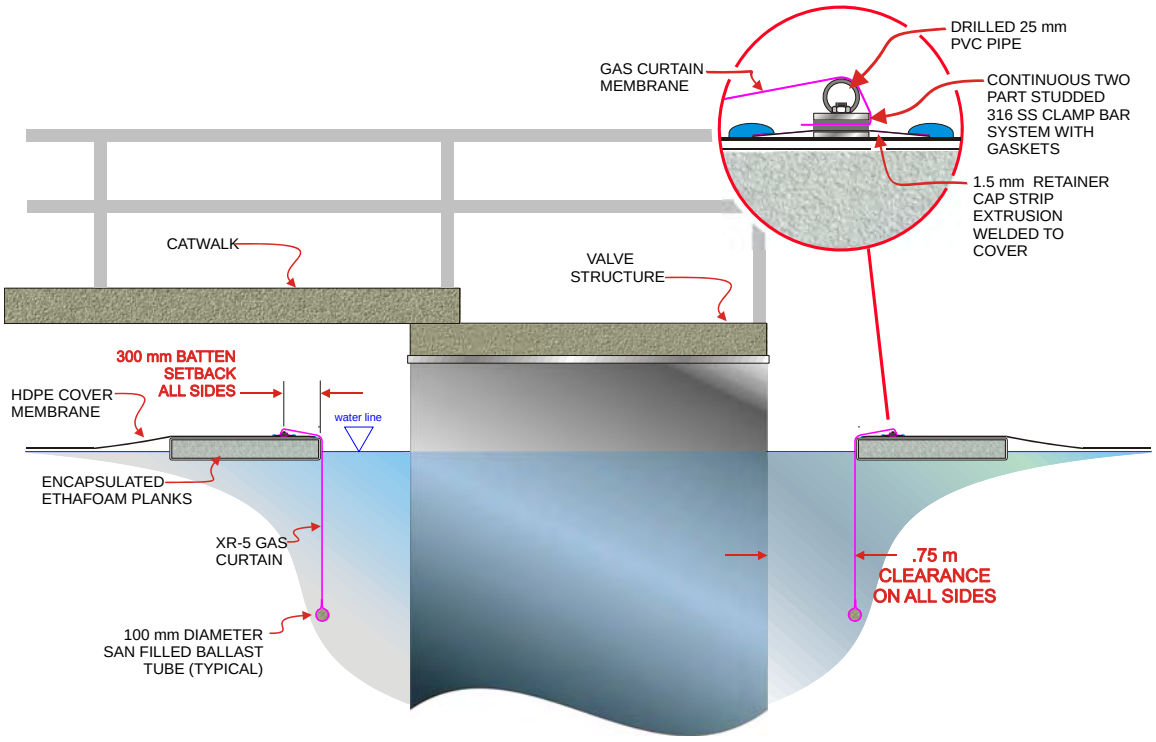

Figure 4. Gas Trapping Curtain Section Detail at Valve Structure

The curtain was affixed to the floating cover using a stainless steel dual clamp batten detail with gas-tight Buna N rubber seals for biogas resistance. 8130 XR-5 was selected as the curtain material. The curtain was fabricated into a gas tight ring around the tower and then secured into the perimeter batten detail. The curtain also featured ports like the cylinder of a two stroke engine (see Figure XR-5 Gas Trapping Curtain Plan). The ports were set 45 cm below the water level with the intent being if the cover inflates from biogas pressure then the ports will relieve pressure once the cover lifts 45 cm.

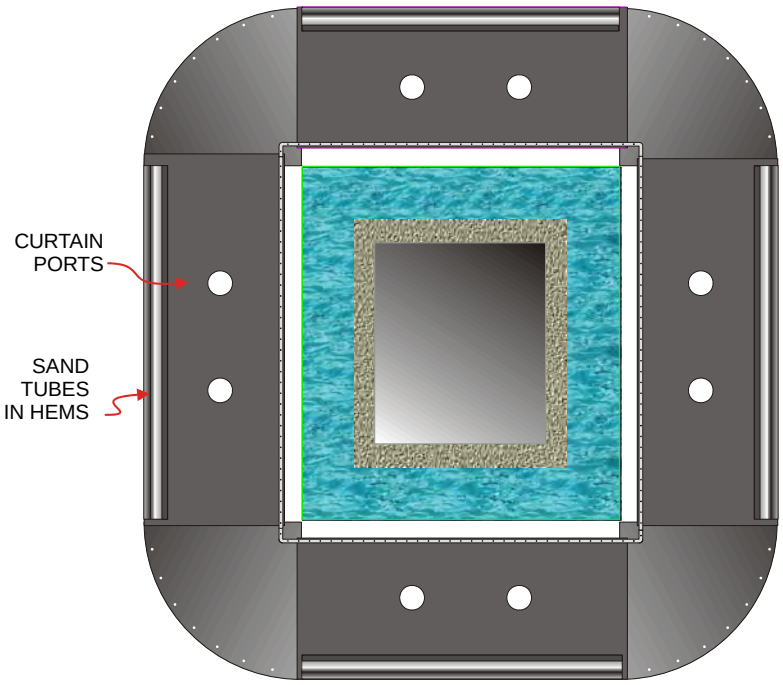

Figure 5. XR-5 Gas Trapping Curtain Plan

Curtain corners were set with grommets, pleated and hemmed with industrial grade zip ties threaded through the grommets (see Figure 6. Gas Trapping Curtain Corner Pleating for Installation).

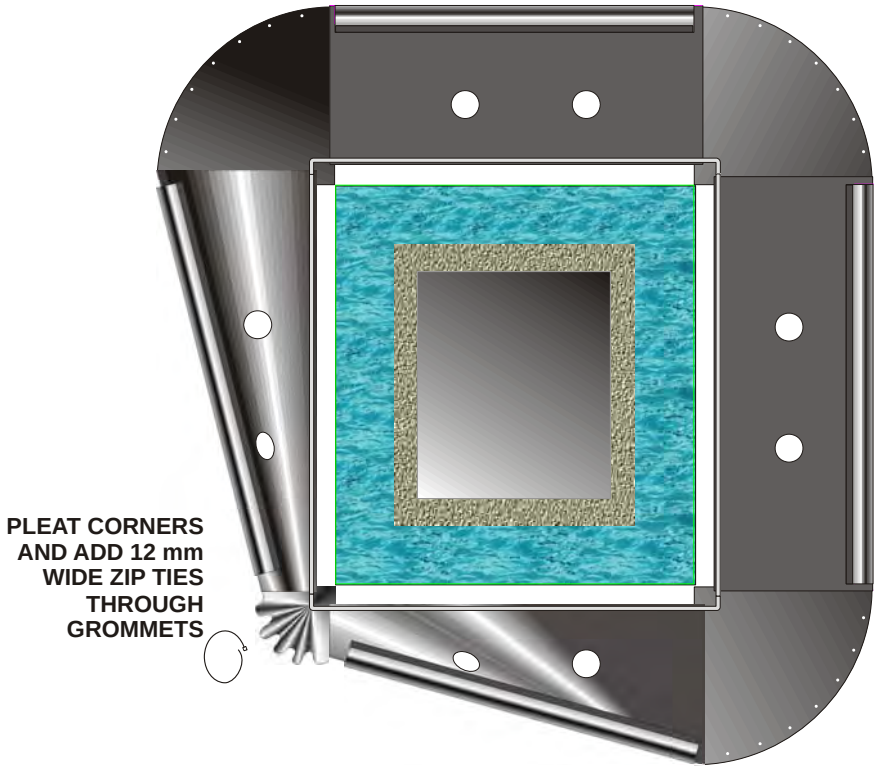

Figure 6. Gas Trapping Curtain Corner Pleating for Installation

Anaerobic digestion lagoon covers are continuously subject to inflation up to several meters vertically if there's a mechanical failure with the biogas scavenging system. The amount of uplifting force can be enormous even within the ½ million kg range over large lagoons. These potential conditions mandated that very special attention be paid to the floating cover system around the catwalk as there was a risk of severe damage to it and the cover membrane at that location. The design response was to locate an additional cover ballast pipe detail parallel and adjacent to the catwalk and to place a cluster of 5 each passive gas relief vents with 200 mm diameter openings around the structures. The passive vents were installed in such a manner as to not activate until the cover system lifted off of the water surface by 45 cm or more and automatically close off once the cover descends below this height. This passive feature helps mitigate against continuous biogas release under normal operating conditions while protecting the cover and catwalk structure (see Figure 7. Vent Tube Plan around Structures).

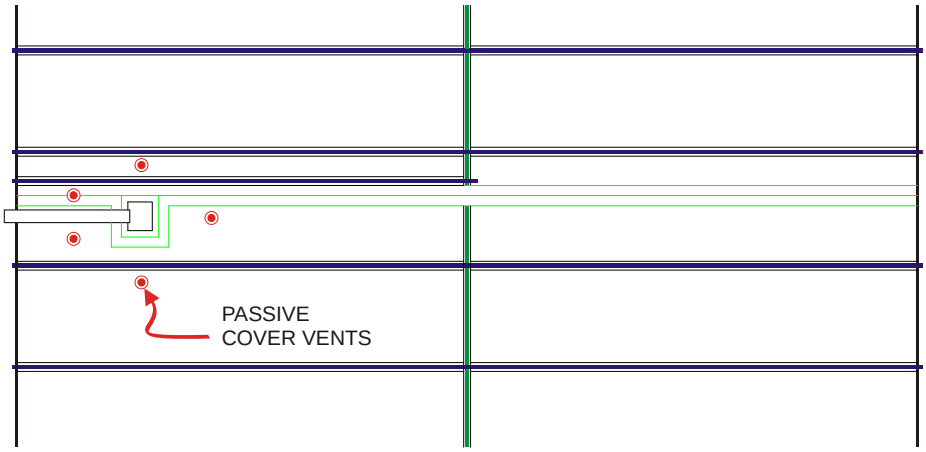

Figure 7. Vent Tube Plan around Structures

4. OUTCOME

The installation of this cover system immediately transformed the local community as the permeating odor from their wastewater lagoon was eliminated. It was also a “green” project in that methane is captured and used to fire boilers saving the owner significant energy expenditures.

This project represented a most challenging biogas cover installation and was a hugely successful keynote installation.

Geosynthetics 2009
February 25-27 2009, Salt Lake City, Utah

Floating Cover Design & Technology over the Past 30 Years

B. Shehane, P.E., Seaman Corporation, Wooster, OH, USA

ABSTRACT
Geomembrane floating covers have been used for over 30 years now in applications such as potable water systems, anaerobic digesters, deicing fluid covers at airports and odor control. The actual design of floating cover systems has changed dramatically in the past 30 years. Some of the first floating cover designs did not tie down to the lagoon/tank perimeter and therefore rainwater was not diverted. This increased the treatment costs in both anaerobic and potable water systems. Current floating cover design can incorporated rainwater collection systems, active pumping and discharge collection systems, maintenance walkways and access hatches. Also, with renewable energy a current hot topic, most of the newer anaerobic floating covers use methane collection systems to be blended with natural gas, etc. to create electricity and sold back to the electric grid. As a result, many of these floating cover systems can pay for themselves within 4 or 5 years.

Figure 1. Anaerobic cover system in Harnes, France (1981)

1. INTRODUCTION

According to some, floating covers were first introduced back in the 1960's. However, decent records of floating cover case histories go back to late 70's and early 80's. Many of the first floating covers were installed with minimal or no actual design. Todays properly designed cover systems can improve water quality, lower evaporation rates, capture organic gases and reduce biological oxygen demand (BOD). This paper will look at early designs of cover systems leading up to current technology in several types of floating cover systems.

Some of the earlier designs in floating covers used a central float grid which was stiff enough to maintain its structure as the reservoir filled with liquid. Figure 1 shows a centrally floated, untensioned peripheral sump reservoir cover system. It can be seen that all of the slack in the cover is forced to the sides where rainwater and snow collects. This is eventually pumped away when the channels are full of water. Some of the disadvantages of this type design are (1) it is unsafe to walk on the cover in the peripheral area, (2) wind can push the central float section to one side of the cover leaving no slack on the other side, (3) snow, ice and debris can accumulate in certain areas of the central float section. (Koerner, 2005).

Figure 2. Wastewater covers in Memphis, TN - 90,000 sm (1988)

Other early floating covers were designed to not attach to the perimeter directly (i.e., anchored into soil or battened to concrete). Figure 2 is an example of this type of design. A 1 to 2 meter wide perimeter of liquid surface was left exposed in the lagoon or tank and the cover was tethered in place with cables. Floats and gas evacuation troughs or raceways were built into the cover and some inflation of the cover was allowed. Stormwater runoff was shed by either draining through the cover into the lagoon by open ended vertical pipes laid on the cover surface. Surface pipes were attached to a pumping system, which were normally activated manually. Unfortunately, this design led to higher maintenance costs due to standing water, trapped gases and limited service life.

Figure 3. Clarifier Cover in Madison, WI (1992)

Current technology in floating covers provides a cost-effective solution for odor control, gas containment/recovery, heat loss and chlorine/water evaporation. In general, typical geomembrane covers are at least one quarter and up to one-eighth the cost of alternative metal or concrete cover systems. Geomembrane covers also offer longer material warranties and can be used in large areas where rigid structures are impractical.

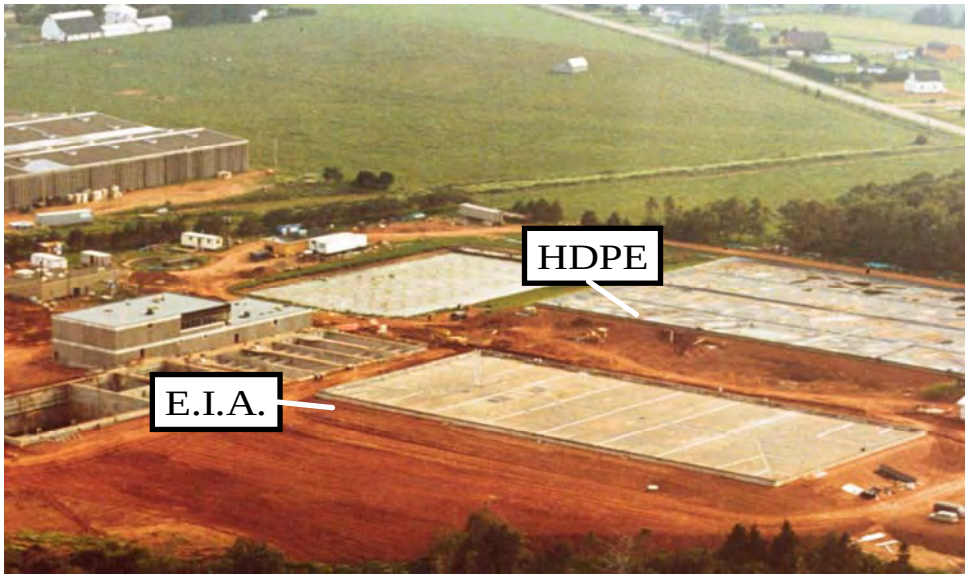

Figure 4. Cavinish Farms, Canada

Three basic types of floating covers are in use today – single geomembrane covers, modular cover systems and thermally insulated three-layer composite cover systems.

2. TYPES OF FLOATING COVERS

2.1 Single Geomembrane Cover

Several technical points need to be addressed before designing a single geomembrane cover system – wet or dry installation, required service life, chemical compatibility of contained liquid with geomembrane, fluctuation of liquid level during service life, gas collection system, surface water collection system, service hatches and perimeter geomembrane connection details.

Figure 5. Single Layer Cover in Washington

A single geomembrane cover normally uses attached closed cell foam floats and/or sand tube ballasts. This is used to create drainage sumps that can collect and carry rain water to either submersible pumps or gravity drains for water removal into a drainage system. Examples of weight tensioned floating cover layouts are shown in Figures 6 and 7. This “defined sump reservoir cover” is now a preferred design over the older “centrally floated reservoir cover”. If the reservoir liquid level

falls, the slack in the geomembrane cover lessens as the defined folds reduce and then deepen as the liquid level rises again. Active gas collection can be achieved using a perforated extraction pipe beneath the cover under negative pressure. (Source: FLI Environmental)

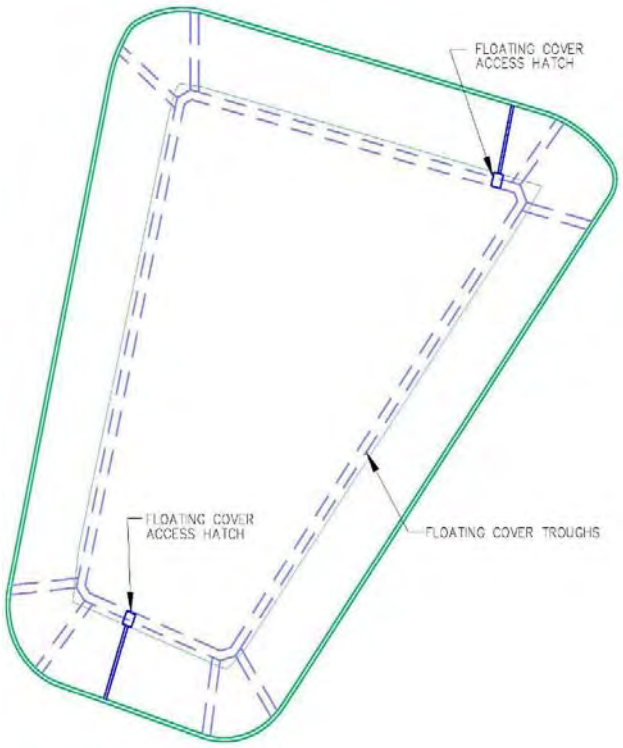

Figure 6. Perimeter Trough

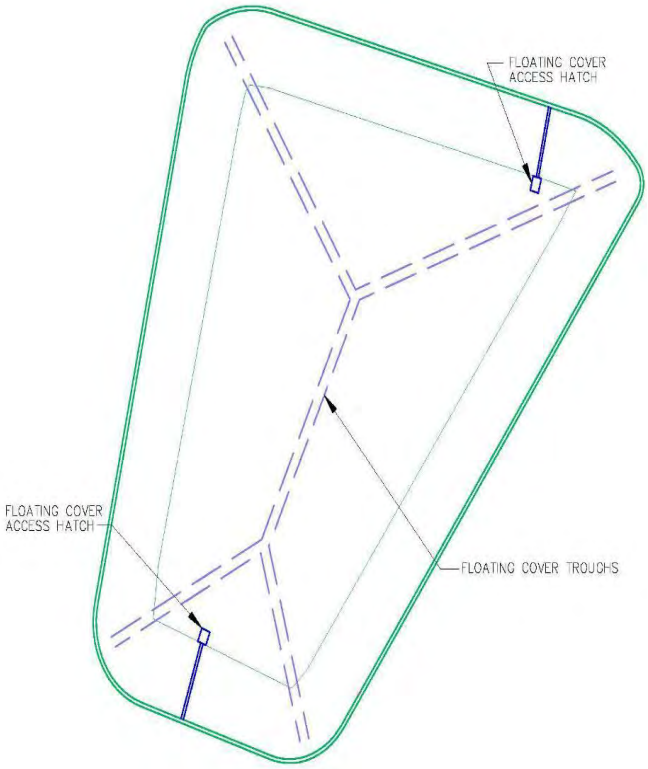

Figure 7. Double-Y Trough

Figure 8. Salt Lake City Airport Deicing Covers (2000) with Double-Y Channels

Another form of single layer cover is the mechanically tensioned (REVOC® style). This type of cover uses spring or weight-loaded cable tension to achieve definition and stability. The mechanically tensioned portion of the cover is held into place and becomes a defined plate that is protected from wind uplift and drifting. The outer perimeter is relaxed and forms a sump where storm water can be diverted off of the cover through a drainage system. (Source: Layfield Plastics)

2.2 Modular Geomembrane Covers

Modular cover systems have been in use since 1983. A modular cover system consists of individual casings that are laced together during installation to form a complete cover over the liquid in the basin. Each casing is made of closed cell polystyrene insulation sealed between two sheets of geomembrane and is anchored to the perimeter with PVC coated cables. This design allows rainwater to pass between the individual casings while also allowing gases to escape. As a result, water collection systems are not needed. This type of cover system can offer insulation R-factors ranging up to 30. (Source: Lemna Technologies Inc.)

2.3 Insulated Three-Layer Composite Cover Systems

This type of cover system has 2 separate layers of geomembrane, which can be different materials. For example, a reinforced geomembrane can be used as the top layer exposed to sunlight and a film geomembrane on bottom providing an underskin layer. In between the 2 geomembranes is poly-foam insulation which can vary in thickness depending on the R-value needed and also provides buoyancy. In most cases, the poly-foam insulation is welded directly to the underskin layer while the top geomembrane layer is independent from the insulation.

This type of cover is primarily used for biogas collection and control and is specifically designed to store biogas under the cover. Most often the owner/operator will collect the biogas produced and generate electricity to be used at the plant. This three-layer cover system provides a lightweight but durable structural integrity to the cover system. It also allows buoyant access for periodic maintenance and inspection. Lower permeability geomembranes for methane recovery are especially important in this type of system.

- Ethylene Copolymer (EIA) has denser compound, SG 1.3 vs. 0.94 for HDPE
- Very Low Methane Permeability

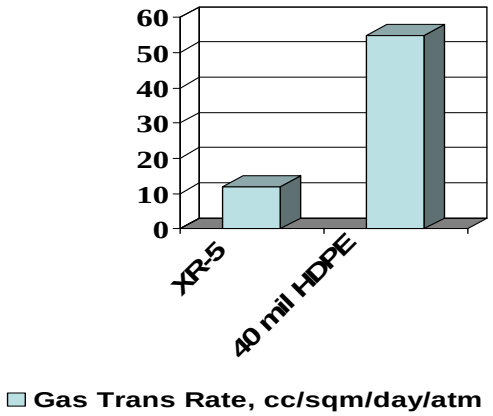

Figure 9. Methane Permeability Comparison

Biogas is allowed to migrate between the 2 geomembranes through orifices normally located along the perimeter. When biogas storage is required, the pressure beneath the cover is allowed to go positive and biogas is forced between the cover layers. This design allows the underskin layer to remain in contact with the liquid surface, which helps prevent mounding of the scum layer.

A three-layer composite cover system normally has no folds in the design for collection of rainwater. Since there are no folds, there are fewer wear areas in the cover that would require periodic maintenance. Also, this design allows the designer to use the entire walled perimeter of the lagoon as a transmission zone for biogas. (DeGarie, 2000)

3. PATENTED TECHNOLOGY IN FLOATING COVERS

Listed below are several patents that have been implemented over the years primarily in the design of floating cover systems.
(Source: www.freepatentsonline.com)

3.1 Floating cover for large liquid reservoir (patent #6338169)

The floating cover has a floating grid anchored to the perimeter walls of the reservoir, and floats over the liquid level inside the reservoir. The floating grid comprises a flexible keel member and an array of flexible buoyant beams affixed to the keel member. A flexible impermeable membrane is affixed to the perimeter wall and is loosely laid over the floating grid. An array of flexible weight lines is anchored to the perimeter walls and is loosely laid over the impermeable membrane. Each weight line is laid at about halfway between an adjacent pair of buoyant beams. The floating grid, the impermeable membrane and the array of weight lines constitute three separate layers that are movable relative to each other without generating destructive stress in the impermeable membrane.

3.2 Tensioned reservoir cover, rainwater runoff enhancement system (patent #4603790)

A rainwater run-off enhancement system for flexible reservoir covers which have substantial portions which are horizontal and in two way tension forming large flat areas. Elongated weights are placed on the flat areas forming depressions which collect and channel rainwater which flows into sumps formed in the cover.

Figure 10. Potable water cover in Staunton, VA (2003)

3.3 Covering systems and venting methods (patent #7374059)

A covering system that includes a first membrane, a first flotation member coupled to the first membrane. The first flotation member includes a first float and a first float compartment membrane, and the first float compartment membrane is coupled to the first membrane. The covering system also includes a first plurality of gas-relief passageways positioned either within the first float compartment membrane, or within the first membrane and adjacent to the first flotation member. And at least one of the gas-relief passageways within the first plurality is structured so that gas flows unobstructed through it when the system is used. Gas-relief openings formed between overlapping membranes may also be utilized as avenues through which gas may escape to atmosphere from beneath the covers and covering systems. Venting methods are also disclosed. The covering systems and methods may be applied to control odor, algae growth, and heat loss associated with the retaining various liquids, while permitting for the controlled release of gases that are produced.

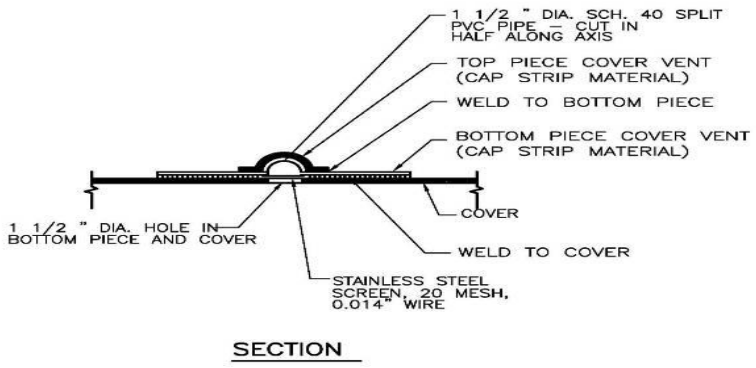

Figure 11. Perimeter Vent Detail

3.4 Tensing a flexible floating cover (patent #6893005)

Apparatus comprising a tensing element connected at one end thereof to a supporting structure and at another end thereof to a cover, wherein movement of the cover imparts a force on the tensing element, an actuator adapted to move the tensing element, and a sensing device adapted to sense an equilibrium force position of the tensing element, wherein if the force changes the equilibrium force position the sensing device instructs the actuator to change a tension imparted by the tensing element on the cover.

3.5 Insulated removable pond cover (patent #5400549)

An insulated removable pond cover for settling ponds. The pond cover comprises a plurality of sealed panel units containing insulation. The panel units are linked together by means of a system of cables which pass through grommets in the panel units.

3.6 Membrane-covered reservoir having a hatchway therein (patent #7430834)

The membrane cover has fold lines therein intersecting the walls of the reservoir at intersection points. A geometric chord or secant joins two intersection points, and defines, with a portion of the walls of the reservoir, a static segment in the membrane cover. The membrane cover in the static segment is tensioned along lines of force that are parallel to or that make acute angles, with the aforesaid chord or secant. The membrane cover in the static segment remains substantially planar and stationary, thus static, despite the rising and lowering of the remaining portion of the cover in response to variations in the level of the content of the reservoir. A hatchway is mounted in the static segment of the cover. In another aspect of the invention, the hatchway has an airtight compartment extending between the membrane cover and a point below the level of the material inside the reservoir.

4. CONCLUSION

Floating cover design has improved dramatically over the past three decades. This improvement has primarily been in the details of the design itself and is still constantly evolving. Some examples are better rainwater collection systems and pumping systems plus better design of hatches for access and venting. In addition, safety measures have improved in keeping drinking water safe from pollution. As a result, state health departments are now much more receptive to floating cover technology for drinking water reservoirs.

With so many types of potential floating cover systems available, a site specific design is imperative to assure longevity and maintenance-free performance. In general, floating covers can be an economical alternative to other methods of protecting drinking water or controlling odors and gases. One of the most important factors in a successful cover system is using an experience and reputable fabricator/installer. If needed, a qualified engineering firm can also be used to develop the appropriate design and specifications in order to solicit competitive bids.

REFERENCES

DeGarie, C.J. (2000). Floating geomembrane covers for odour control and biogas collection and utilization in municipal lagoons, *Water Science and Technology* Vol XLII.

Koerner, R.M. (2005). *Designing with Geosynthetics*, 5th ed., Pearson Prentice Hall, Upper Saddle River, NJ, USA.

Geomembrane Cover Systems for Liquids, Quasi-Solids and Gas – An Application Based Comparative

R.K. Frobel, MSCE, P.E., R.K. Frobel & Associates, Evergreen, Colorado, USA
M.A. Sadlier, MIE Aust, CP Eng., Geosynthetic Consultants Australia, Brighton, Victoria, Australia

ABSTRACT
Over the past 30 years, polymeric geomembranes have been used as cover systems over liquids, quasi-solids and gas for numerous types of applications, sometimes with little regard for ultimate performance and lifetime or with little regard for proper design. Major applications of polymeric geomembranes in floating and inflatable cover systems include: potable water supply, waste storage odor control, industrial tanks, anaerobic digesters, mine/mineral processing, food processing waste lagoons and as thermal covers. This paper will provide an overview and technical comparison of the polymeric geomembranes available for use today in open liquid, quasi-solid and gas cover applications as well as basic design considerations that must be implemented to provide a workable and durable long term cover system. Geomembrane polymers as well as reinforced and non-reinforced polymer geomembranes will be briefly discussed for each application with reference to both durability and design considerations.

1. INTRODUCTION

Geomembranes are by definition “an essentially impermeable geosynthetic composed of one or more synthetic sheets” (ASTM, 2008) whose primary function is that of a “hydraulic barrier”. As such, polymeric geomembrane materials have been in use for over 60 years in the prevention of liquid migration from one area to another in a man made project usually associated with a geotechnical application such as embankment dams, water containment reservoirs and canals, landfill bottom liners and caps and industrial liquid storage. Geomembrane materials have been “redesigned” and “reformulated” to meet demanding hydraulic barrier applications. Civil Engineers are most familiar with these types of applications based on historical use but what about the specialty applications area of covers or barriers over liquid, quasi-solids and gas? Do we simply throw any available geomembrane (or polymeric sheet material) on a body of liquid (water or waste)? Are there special engineering design methods to consider? What about the environment? Durability? Should this be a specialty discipline (geo-covers)? Non-landfill covers are addressed in the literature and most notably in the book “Designing with Geosynthetics” by R.M. Koerner (R. M. Koerner, 2005) where a 10 page section is devoted to this application under Chapter 5 – Designing with Geomembranes. Additionally, a number of technical papers have been devoted to this subject, usually by application. But are all geomembrane polymer materials and structural types suitable for any cover application over liquid, quasi-solids and gas? What are the general design considerations specific to each type of cover application?

2. WHY ARE COVER SYSTEMS CONSIDERED?

There are a number of viable reasons for specifying a floating or inflated polymeric geomembrane as a cover system over liquid, quasi-solid and gas generation ponds and facilities. The principal design considerations for specifying a cover include but are not limited to the following:

- Protection of potable water supplies from pollution (airborne, birds, industrial)
- Protection of potable water supplies from acts of Terrorism
- Economical alternative to rigid column supported roofs
- Evaporation reduction for water supplies
- Chemical additive evaporation control – chlorine and other disinfectant additivies to control biological growth
- Control of aquatic growth (weeds, algae, other biological growth)
- Odor control for waste containment and industrial ponds in close proximity to the general population
- Reduced greenhouse gas emissions
- Reduction in lagoon or pond maintenance
- Safety (public access potential for drowning)
- Temperature control for anaerobic digesters or mineral processing (insulated covers)
- Elimination of wave action and damage on large containments
- Gas collection and storage/regulation of gas generation – anaerobic digesters
- Enhanced mine mineral solution processing
- Protection from rainwater infiltration (mineral processing, digesters, high quality water containment)

3. POTENTIAL LOADS, STRESSES AND ENVIORMENTAL IMPACTS THAT ARE APPLIED TO COVER SYSTEMS AND SHOULD BE USED IN DESIGN CONSIDERATIONS

All of the types of applications for covers systems over liquid, quasi-solid and gas must be designed for mechanical loading and stress to provide for an effective long term operation. Mechanical loads that should be considered when designing an exposed floating or inflated cover system include the following:

- Dynamic movement and flexural fatigue
- Edge restraint and tensile pullout forces
- Cover installation, access, removal and inflation
- Tearing (edges, hatches, holes, attachments)
- Wind uplift – static
- Wind uplift and buffeting – dynamic
- Ice (floating covers northern climates)
- Tensile forces (edge attachment, ballast loading)
- Multiaxial (multidirectional) stress due to gas pressure, maintenance inflation, water load on fixed covers
- Puncture – due to ballast tubes, falling objects, maintenance traffic, access)
- Impact resistance (hail, wind blown debris)
- Abrasion (sumps, edge restraints, slopes, structures, access points)
- Seam tensile stress – static and dynamic
- Expansion/Contraction in temperature changes

Additionally, the following general physical / chemical / biological attack mechanisms must be considered in final design:

- Ultraviolet / Ozone
- Heat (especially digesters and arid desert climates)
- Cold (northern climates)
- Waste water and sludge contaminants
- Animal waste contaminants
- Chlorine and chemical attack
- Aqueous methane and H2S (under covers for gas control)
- Birds and bird excrement
- Industrial mine processing liquor and solid contaminants
- Mine processing radiation
- Algae accumulation (floating covers)

4. PREDOMINANT TYPES OF POLYMERIC GEOMEMBRANES USED IN DESIGN OF COVER SYSTEMS

There are several types of polymeric geomembranes that have and are being used in the various application based cover systems for floating, supported and inflated covers. Table 1 lists the most prominent types in use. A thorough description of each type can be found in the book Designing with Geosynthetics (Koerner, 2005). Comparisons of the various types based on attributes and design considerations can be found in the paper “Geomembrane Properties – A Comparative Perspective” (Frobel and Sadlier, 1997).

Table 1. Cover System Geomembranes

Polymer Type	Thickness Range (mm)
HDPE	1.00 – 2.50
LLDPE Alloy	1.00 – 2.50
LLDPE-R	0.50 – 1.00
EPDM	1.14 – 1.50
CSPE-R or Hypalon	1.14 – 1.50
fPP-R	1.14 – 1.50
LDPE coated woven fabric	0.30 – 0.50
EIA-R	0.75 – 1.00
Composites	10.0 – 50.00

5. MAJOR APPLICATION AREAS FOR GEOMEMBRANE FLOATING AND INFLATED COVERS

The engineering community is primarily familiar with floating covers for potable water storage reservoirs. However, there are a number of other specialty application end uses for polymeric geomembrane materials which include the following:

- Potable water supply – floating defined sump tensioned
- Potable water supply – floating / cable tensioned
- Potable water supply and industrial tanks – floating non attached
- Anaerobic Digesters – Floating over liquid and quasi-solid
- Anaerobic Digesters – expanding / restrained over gas (lagoon or tank)
- Odor control – floating over liquid and quasi-solid
- Mine processing liquid and quasi-solid containments
- Tanks and small area lagoons – fixed, floating and expanding
- Modular – floating sectional (partial cover systems)
- Composite Layers – floating, insulated or dual purpose polymers

5.1 Potable Water Supply Covers – Floating / Defined Sump Tensioned

Potable water containment reservoirs are usually much larger than most facilities requiring a floating cover and are also municipal projects that require long life durability, proven historical use and an economically viable alternative to rigid column supported roofs. Gerber (1984) and Koerner (2005) details several types of defined sump ballast / float designs that are in use today. The design considerations most important to this type of cover are the following;

- High UV/Ozone resistance
- High chlorine resistance (stressed and unstressed)
- High tensile strength
- High tear strength
- High puncture and impact resistance
- High flexural fatigue resistance

This type of cover requires a high tensile strength, highly flexible geomembrane (especially for the flexure areas at ballast/sump locations) as well as a geomembrane that will accommodate large changes in water level. It will have a defined network of ballast with associated tensioning floats (hence defined sump/tensioned). Ballast will create trenches which take up the slack material as the water level rises and provide a collection point for surface water which is then pumped off the cover.

Because of the constant flexure required at the trench and hinge zones, these covers need a highly flexible geomembrane such as flexible reinforced polypropylene (fPP-R) or reinforced Hypalon (CSPE-R). Historically, these two materials have been the design choice for defined sump tensioned covers in potable water reservoirs. Figures 1 and 2 illustrate this type of cover system.

5.2 Potable Water Supply Covers – Floating / Cable Tensioned

Although not as popular in design as the defined sump floating cover systems, this type of cover requires high tensile strength, especially at the perimeter attachments to the cable supports. All of the design considerations noted for defined sump covers apply to cable tensioned covers. The key element is the use of a cable tensioning system at the entire perimeter to take up the slack in the cover material as the water level rises. It should be noted that these covers normally use the highly flexible scrim reinforced materials fPP-R, Hypalon or CSPE-R or XR-5, again due to the fact that tensile strength (both point load and wide width) and flexural fatigue resistance is critical.

5.3 Floating (non attached) Tank Covers

Floating tank covers differ from other covers in that the walls of the tank are vertical and the tank is most probably circular in plan. A system of rolling ballast is used to create a trench against the tank wall that will take up the slack as the water level rises. Due to the fact that tank covers are relatively small in size (area) and are for the most part protected by the tank walls from wind, any one of the geomembrane materials listed in section 4 can be used. In many cases, insulated composite covers are used that incorporate EPS foam for floatation and insulation. Specialty

tank covers such as foamed EPDM rubber with a closed cell structure and low density have been used (Dedrick, 1984).

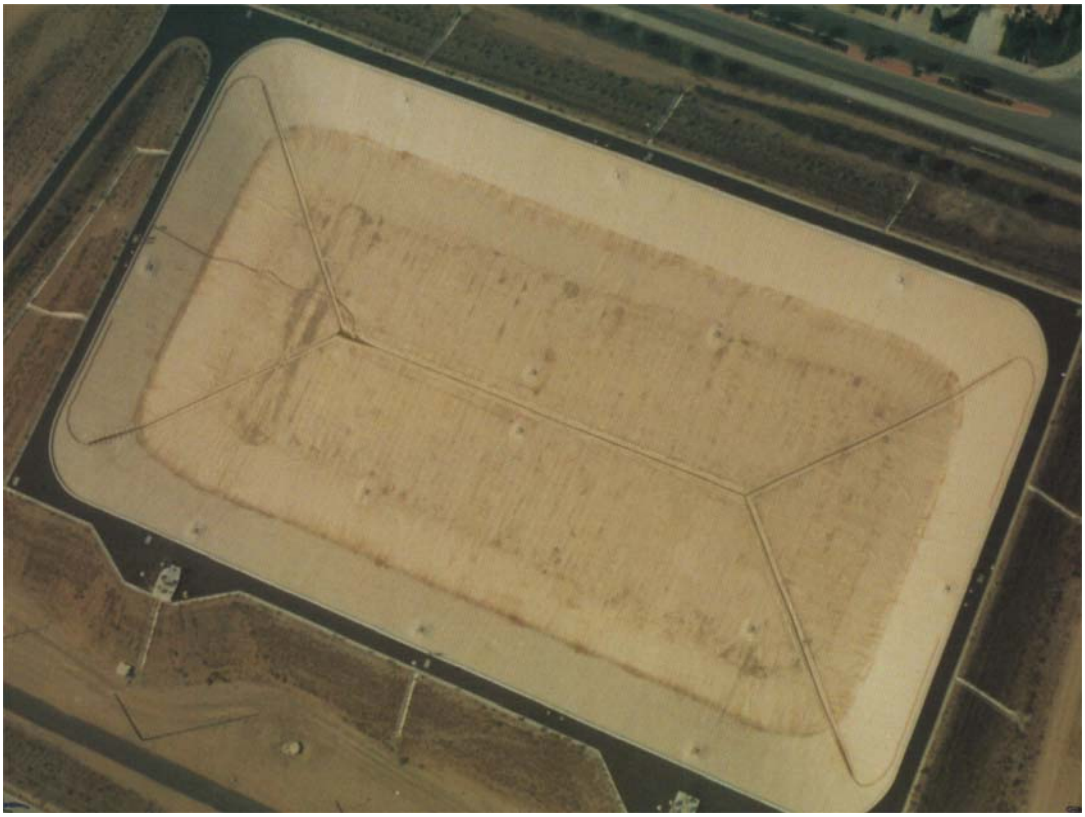

Figure 1 – Overhead view of a ballast and float defined sump tensioned cover system

Figure 2. Ballasted trenches and floats – fPP-R defined sump floating cover

5.4 Anaerobic Digester Covers - Floating

The simplest anaerobic covers are fixed level covers with the water level controlled by an overflow weir. However these covered lagoons generate large volumes of gas and require an extensive system of ballasting and floats to harvest the gas at the perimeter. They are usually constructed from a pontoon or by launching with water already in the lagoon. HDPE and HDPE-R have been predominant in this type of cover, primarily due to the low density and easy floatation. Figure 3 illustrates this type of floating cover over a large waste lagoon.

A further category of this type of cover occurs when the cover has to be built over a dry lagoon and yet provide the functions of an anaerobic gas collection cover when in service once the animal waste is pumped into the lagoon. This requires a primary ballasting and tensioning system similar to a defined sump cover as well as a secondary ballasting and floatation system for gas management and harvesting. Figure 4 shows this type of cover system in operation.

5.5 Anaerobic Digester Covers – Expanding / Restrained

Many anaerobic gas collection covers are required to regulate gas storage or allow the cover to lift from the surface so that mechanical equipment can operate. Once inflated these covers are similar to inflatable structures but there is a transition from floating to inflated when they can be very unpredictable, especially in strong winds. Smaller anaerobic digesters are designed with lagoon cross cables or supports that allow the geomembrane to be supported above the waste during low gas generation. The primary geomembrane types for inflated anaerobic covers are fPP-R, XR-5 (scrim reinforced) and EPDM (non reinforced). EPDM that is used in tank and lagoon digesters is often restrained from expansion by the use of high strength netting. Figure 5 illustrates a large fPP-R white inflated cover and figure 6 illustrates the use of highly extensible EPDM rubber that is restrained by net to accommodate higher internal working pressure. Some of the design considerations important to Anaerobic Digesters are the following (Frobel, 2003):

- Chemical Resistance (animal waste, aqueous methane)
- Low gas vapor transmission
- High tensile, tear, puncture resistance
- High elasticity (expansion and contraction)
- High resistance to flexural fatigue

- Large prefabricated panels
- Repairable by the owner
- UV/Ozone resistance

5.6 Odor Control Covers

Odor control covers are common to the waste water and other process industries and they are often covers to small tanks such that they can be fixed to operate only at the top level of the tank. Often they are fixed at the top of the tank with some kind of cable support for the geomembrane if the water level drops. Sometimes they are floating and not fixed to the tank and have some kind of perimeter skirt arrangement intended to control odor escape. Although any of the geomembrane types could be used just for odor control, large area lagoon covers are sometimes fabricated of more economical materials such as LDPE coated woven fabric. Odor control covers do not require the same technical design requirements as more demanding applications and are often designed for short term life spans where the cover is to be replaced every 5 years or less. Odor control cover systems can also be a composite of fabrics and odor absorbing synthetic or natural components.

Figure 3. A fixed level floating HDPE cover for gas collection from an anaerobic lagoon

Figure 4. A combined defined sump and gas harvesting cover – HDPE

Figure 5. Inflatable Gas Cover – Flexible fPP-R Scrim Reinforced

Figure 6. Inflatable / Expanding EPDM Rubber Gas Cover with Restraining Net

5.7 Mine Processing Liquid / Quasi-Solid covers

Water is a very precious commodity for many mining operations and in many places the water loss by evaporation can be significant. This gives rise to an incentive to cover not only water storages but process lagoons as well. Mine process water storages are not significantly different to potable water storages but process liquid storages can and do present some interesting and different challenges, especially as regards chemical resistance, radiation and temperature. Figure 7 illustrates a mine processing floating cover system. Primary types of geomembranes for mining covers are HDPE, LLDPE-R, fPP-R. However, in many instances, life expectancy can be less of a consideration due to the fact that many mines and mine processing facilities are designed for only a 10 year (or less) life span. In many cases the covers are white in color to resist the attack by UV and temperature. The covers must be designed to accommodate large and small diameter pipes used to move process water or sludge. Primary technical considerations for design are:

- High chemical resistance to sludges and liquors
- High temperatures (processing and climate)
- High tensile, tear, impact, abrasion and puncture resistance
- High UV/Ozone resistance

Figure 7. Cover to PLS pond with twin 750 mm diameter inlet pipes floating under cover.

5.8 Modular Cover Systems

Most covers are anchored or fixed to the perimeter of the lagoon or reservoir but it is possible to use floating perimeter elements such as plastic pipe to create a cover edge that is not fixed. With these covers only part of the surface is covered and there may be odor escape. A cover may have this kind of fixing on all sides to create a cover based on modules or a series of modules. A very common application is to only cover the front portion of a lagoon such that the upstream portion is anaerobic and the downstream portion is aerobic. Modular covers must be tied off or tethered to resist wind movement.

5.9 Composite Cover Systems

Composite covers are constructed or fabricated in layers and utilize 2, 3 or 4 types of geomembranes, natural fiber, EPS foam (floatation), or reinforcing fabric. These types of covers ranage from highly porous odor control covers (allowing rainfall to penetrate) to layered insulated covers to provide temperature control, especially in northern climates. These types of covers may incorporate 3 layers – a lower geomembrane resistant to process chemicals (ie., HDPE), a mid section of EPS foam for floatation and insulation and a top geomembrane for UV/weathering resistance as well as composite structural stability (ie., fPP-R). Improtant design considerations include:

- High chemical resistance
- Interface adhesion and attachment of layers
- Stability of panels during installation and long term
- Low temperature / ice accumulation (northern climates)
- High wind uplift resistance
- Low shear resistance to quasi-solids (ie., fat, grease, agglomerates)

6. SUMMARY

Geomembranes of various polymer types, structures and combinations have proven to be a viable construction material for use in floating and inflated cover systems for over 30 years. There has been a steadily increasing use of these types of covers worldwide. However, the strengths and weaknesses of each type of material must be recognized and carefully considered in the design, installation and construction quality control (CQC) as well as requisite operation and maintenance procedures. Properly designed and selected for the specific application, currently available geomembrane materials will provide durable, long lasting cover systems for many decades to come.

REFERENCES

ASTM D 4439. Standard Terminology for Geosynthetics, American Society for Testing and Materials, West Conshohocken, PA, USA

Dedrick, A.R. (1984). Foam Rubber Covers for Evaporation Control, *Proceedings International Conference on Geomembranes*, IFAI Publishers, Denver, CO, USA

Frobel, R.K. and Sadlier, M.A. (1997). Geomembrane Properties – A Comparative Perspective, *Proceedings GeoEnvironment 97 Conference*, Melbourne, Australia

Frobel, R.K. (2003). Animal Waste Containment and Anaerobic Digesters, *Proceedings 17th GRI Conference*, GII Publishers, Folsom, PA, USA

Gerber, D.H. (1984). Floating Reservoir Cover Designs, *Proceedings International Conference on Geomembranes*, IFAI Publishers, Denver, CO, USA

Koerner, R.M. (2005). *Designing with Geosynthetics,* 5th Edition, Prentice Hall, Saddle River, NJ, USA

Raising Cleveland CDF 12 using Geosynthetic Reinforcement

J.E. Kolber, P.E., U.S. Army Corps of Engineers, Buffalo, USA
V.C. Melilli, P.E., U.S. Army Corps of Engineers, Buffalo, USA
J.R. Lane, P.E., U.S. Army Corps of Engineers, New England, USA
E.N. Lenhardt, E.I.T., U.S. Army Corps of Engineers, Buffalo, USA

ABSTRACT
The United States Army Corps of Engineers (USACE), Buffalo District will design and construct a new Confined Disposal Facility (CDF) in Cleveland Harbor, Cleveland, Ohio. The existing CDF in Cleveland Harbor is almost at its design capacity and the new CDF that is estimated to cost from $250M to $370M will not be on-line until 2015. Interim capacity was created by raising the previously filled CDF 12 by incorporating geosynthetic reinforcement in selected reaches to achieve a design elevation of +18 LWD (Low Water Datum). Construction was completed in 2007, with the first placement of dredged material in the summer of 2008. The Buffalo District plans to design and construct another raised embankment within the adjacent CDF 9 in 2009 as the current CDF12 is being filled to provide additional interim dredged material storage capacity. CDF 12 will be raised another 6 feet to a +24 LWD in 2010 to provide additional capacity. All lessons learned from the efforts in the CDF 12 berm raising project will be applied to the design of the upcoming CDF 9 project.

1. SITE HISTORY:

The Buffalo District, USACE faces a significant challenge over the next decade to provide sufficient interim dredged material disposal capacity to support future dredging contracts in Cleveland Harbor which will keep navigation viable, especially to steel mills on the Cuyahoga River. Because the sediments in Cleveland Harbor are polluted and unsuitable for open lake disposal in Lake Erie, they must be placed and securely stored in CDF's. The first CDF's in Cleveland Harbor, CDF's 9, 13 and 12, were constructed around Burke Lakefront Airport. After these were filled to their design capacities, CDF 14 was constructed in the late 1970's near the eastern end of Cleveland Harbor, at a cost of about $35 million. CDF 14 was turned over to the City of Cleveland in 1996-97, with some remaining capacity. It now serves as a premier bird sanctuary and is not available for dredged material disposal. CDF 10B, located near the northwest corner of Burke Lakefront Airport, was constructed in 1997 to replace CDF 14. CDF 10B was nearly full in 2006. In light of the difficulties presented by constructing a new CDF in Cleveland Harbor, a fill management plan was initiated to create interim capacity at existing CDF's. By raising previously filled, currently inactive CDF's in Cleveland Harbor, sufficient interim dredged material capacity could be created to accommodate the harbor's dredging requirements over the upcoming years until a new site and funding becomes available for a new CDF. CDF 12 was selected for the first raising project because it is located furthest from Burke Lakefront Airport than the other candidate sites (CDF 9 and 13). While raising formerly filled CDF's is not a preferred alternative, considering the engineering challenges of building over inferior foundation soils, it was the only viable alternative.

2. SITE GEOLOGY:

Cleveland Harbor is comprised predominantly of glacial lake deposits consisting of silts and clays over preconsolidated clay. Bedrock consisting of shale is located at consistently at a considerable depth and therefore not a significant factor on this project. The soil composition relative to placing embankments or berms in CDF 12 is comprised of redeposited material dredged hydraulically by either a trailing arm hopper dredge or a hydraulic dredge retro-fitted with a snorkel to pump out hopper scows. This method has been used to fill this site to design capacity. The two predominant soil types are a medium granular sands and a silty-clayey fine sand mixture. Hydraulic deposition of the dredged material placed in CDF 12 (Figure 1) created a complex surficial geology consisting of both types of sediment interspersed across the extent and depth of the facility. This is primarily due to the hydraulic placement of the dredged material. Heavier granular material is deposited at the point of deposition while the lighter and finer particulates are transported alluvially into the facility. Containment of the hydraulically discharged slurry is held in the CDF until the total suspended solids have decreased sufficiently to allow decanting of the water into the lake. Typically the material is pumped into the facility at the north side of the CDF, thus allowing the granular

fraction of the material to be readily deposited while depositing the finer fraction towards the south side of the CDF for ultimate discharge in the southeast corner. This deposition method has yielded significant stratification of materials that have created some interesting situations to address in the design. The south side contained lush vegetation to the point whereby a roadway was constructed to provide vehicular support for traffic and to mitigate plant growth to allow the USCG access to their navigation aids. This non-homogeneous material served not only as the foundation for the raised berm, but as the sole borrow site to construct the embankments or berms in the facility. All of the listed items above are interdependent and critical factors for design and construction.

…

Figure 1- Hydraulic deposition of dredged material Into CDF 12

3. SUBSURFACE EXPLORATIONS AND LAB TESTING:

Four test borings were advanced along the perimeter of CDF 12 in 2004 to characterize the existing foundation soils. These were taken at the four corners of the proposed footprint extending to depths of about twenty feet below existing ground surface. Access to intermediate locations along the perimeter was limited due to soft, pumpable and wet conditions. Also, eleven test pits were excavated within the interior of the facility to a maximum depth of 10 feet. These test pits helped to characterize the soils as potential borrow areas. Laboratory testing classified most of the fine-grained soils as OH in the Unified Soil Classification System (organic silts and clays of high plasticity). Both laboratory triaxial and field vane shear tests were performed to provide additional data for the design team.

4. DESIGN ANALYSIS:

The design of the raised berm was based on available subsurface and lab testing information from the 2004 CDF 12 program as well as from other previous related studies. Figure 2 is a plan of the raised berm design. Figure 3 is a typical design cross section of the raised berm where geosynthetic reinforcement was used. The primary factor controlling dike stability is the shear strength of the foundation soil. This was estimated as 160 PSF, which is a relatively weak soil. A portion of the perimeter, approximately one-quarter of the total length of raised berm, had an inferior foundation condition which required the use of geosynthetic reinforcement to enable a stable design. Consequently, this area was also the lowest part of the CDF, about 2 to 3 feet above the water table. The design cross section for this special condition design reach includes a semi-compacted center berm section built to elevation +18 LWD with a 12 foot wide crest and 1 Vertical on 3 Horizontal side slopes, built over a woven geotextile reinforcement layer. The woven geotextile reinforcement specifications for this design included: 3000 LB/FT minimum tensile strength at 5% strain (ASTM D 4595); 7000 LB/FT ultimate tensile strength (ASTM D 4595); and a coefficient of friction with sand of 0.7 (ASTM D 5321). On either side of the center berm section, semi-compacted stability berms extend 55-60 feet to either side, constructed to +10 LWD. This raised berm was designed to “float” over the existing CDF surface, supported by the stability berms and the geosynthetic reinforcement. This is considered to be a relatively high-risk design, due mainly to the nature of the site, the variability in foundation soil types and the funding constraints.

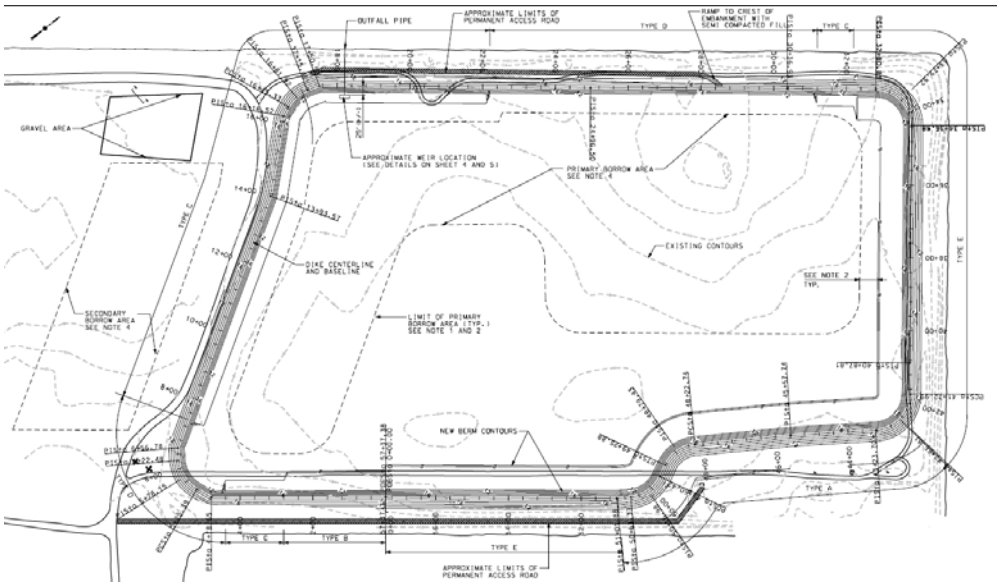

Figure 2 - Plan of Cleveland CDF 12 raised berm design

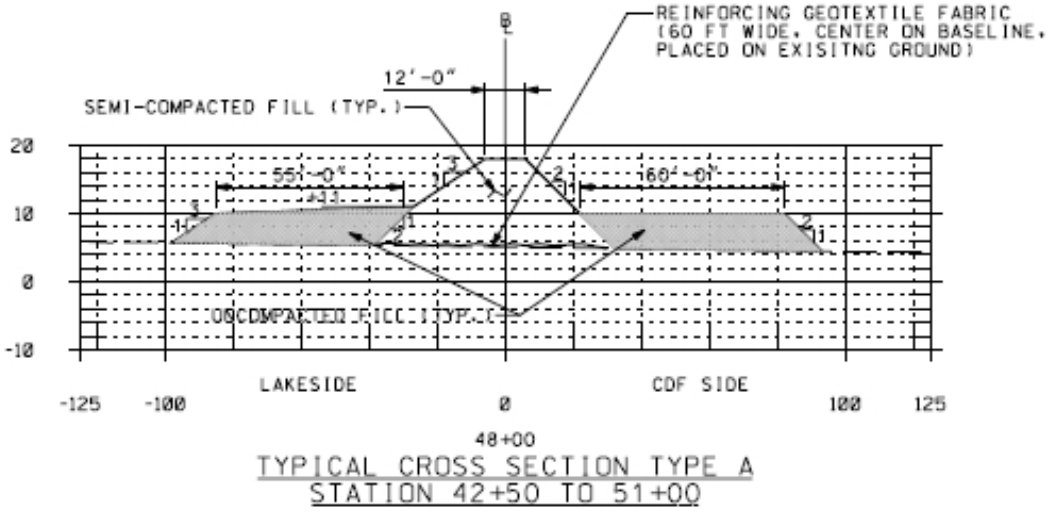

Figure 3 Typical design cross section of Cleveland CDF 12 raised berm where geosynthetic reinforcement was used

5. SOIL BORROW CONSIDERATIONS

Soil type, characteristics and performance considerations played a large role in selecting the most suitable borrow area to harvest material for this berm raising project. Soil was saturated up to +5 to +6 LWD (three to four feet above lake level). The extent of the borrow area within the interior of CDF 12 was limited to allow a buffer of 50 feet from the inner toe of the raised berm for stability reasons. The sand sediment was the only practical borrow material for use on this project since the fine-grained silts and clays were far too wet to be useful/practical for construction. Borrow soil of sufficient quality (sand) and quantity was required to make this project succeed. Financial constraints and local city coordination issues limited the harvesting of borrow to on-site locations.

6. ISSUES RELATING TO CONSTRUCTION NEXT TO AN ACTIVE AIRPORT

One major constraint to this project involved its proximity to the adjacent Burke Lakefront Airport. FAA regulations, mainly involving required height clearances for planes approaching the airport, limited not only the geometry of the raised berm both horizontally and vertically, but the construction means and methods, i.e., equipment height restrictions. In addition to the FAA regulations, the stability of the raised berm is important to avoid disruption of the airport by berm failure and release of the impounded dredged material. In the event of a breach, approximately 140,400,000 gallons (810,000 cubic yards) of dredge material slurry could flow onto the airport runway and facilities. Additional considerations included avian deterrence and animal control that is a threat to safe airport operations. Avian and animal control matters are under the control of the U.S. Department of Agriculture and sponsored in part by the USACE. Given the limited choices of locations to increase or enhance capacity, these considerations were embraced in the design since they are unavoidable and would put the local sponsors at risk for safe airport operations. It was not possible to avoid this situation, but not building next to an active airport would have made this project much less complex.

7. CONSTRUCTION

Construction of the raised CDF 12 began in the spring of 2007 and was approximately 85 percent completed by the fall. The construction was strictly defined in the specifications in an effort to avoid inducing failures in the soil foundation material, which if allowed would have prevented the berms from ever being constructed. Initial placement of the geotextile reinforcement layer was along the center of the proposed berm alignment. Soil borrow was excavated from the interior of the CDF and trucked around the perimeter and dumped. The material was then pushed onto the fabric in lifts to insure an even ground pressure on the subbase. The sand borrow was at a workable natural moisture content and was easily excavated, handled and compacted. A special small low ground pressure (LGP) dozer spread and compacted the deposited material. The project specifications limited heavy equipment traffic over the alignment until a minimum thickness of excavated material had been placed (two feet). The cross section gradually grew evenly until the entire perimeter was raised to the full design elevation of +18 LWD, except for a 1000 LF reach along the south side of the alignment. This area is the lowest point in the entire site. This reach continued to consolidate and settle more than anticipated as the berm was raised. In order to assure that the berm would not fail in this location, it was left constructed to +12 LWD, 6 feet lower than planned, and allowed to “rest” over the winter. During this time a monitoring program was initiated to determine how much movement was occurring and where it was happening. In a subsequent construction contract in the spring of 2008, prior to the first placement of dredged material, this reach was built up to +16 LWD to create sufficient capacity to accept dredge material.

8. FABRIC PLACEMENT:

The following series of photos illustrates some of the steps involved in the placement of geofabric reinforcement on this project, from beginning to end.

Figure 4 - The sewing process begins

Figure 5 - Ensuring a straight seam and even edges

Figure 6 - Folding the completed unit - two sections sewed together to allow the connecting seam to be completed on location.

Figure 7 - Stockpile of completed segments folded and ready for use.

.

Figure 8 - Fabric units in placed and a field seam installed

Figure 9 - Pie-shaped sections going around a curve

Figure 10 - Placement of harvested material in lifts to not exceed bearing capacity of the sub-soil

Figure 11- Placing fabric and sewing ahead of material placement.

Figure 12 - Aerial view of operation, note interior haul road constructed to provide ORT access to berm construction. Note pile of material in the right side of the picture ready to be pushed onto the fabric. Dewatering pump in the top right of the picture.

9. POST-CONSTRUCTION ASSESSMENT

Following the completion of construction of the raised berm in the fall of 2008, an assessment was made along the 1000 LF south reach that had been terminated prematurely and not constructed to final grade due to foundation problems. Several parallel rows of cracks had appeared before construction was completed, just beyond the outside toe of the raised berm (Figure 13). The exact meaning of these cracks was unknown/unclear since all operations were conducted from the interior of the facility; no cracks or settlement were noted. To provide some performance data, a monitoring program, consisting of survey measurements (horizontal and lateral) was immediately initiated. This continued until the onset of winter. The work on the project was suspended for the winter, which allowed the soil to consolidate with the benefit that an increase in foundation strength would be gained. In the spring of 2008, the survey was revisited. The survey indicated not only increased settlement along the 1000 LF reach of concern but also that the raised berm, in locations where measurements were taken, had moved inward approximately two feet. This confirmed that the formation of the rows of parallel cracks along the outer toe of the raised berm were a result of possible lateral displacement. The exact geometry of this movement was not clear. It was clear, however, that the raised berm behaved differently and more dramatically than around the rest of the CDF perimeter. It was also noted that the crest of the berm had settled more on the interior than on the outside portion of the crest. To provide further evidence, three test trenches (Figure 14) were excavated through the inner slope of the raised berm with a backhoe, each reaching the geotextile reinforcement layer. Existing pre-construction elevations had been taken and provided a basis as to where the fabric should be located. The test pits located the fabric so exact measurements could be taken. Since the geotextile moved with the berm as it settled, its location provided an exact measure of the settlement/subsidence that the berm had undergone. Settlement or subsidence ranged between 2.5 and 4.5 feet at the three locations, with the largest value corresponding to where the cracks in the surface outside the CDF berm were the largest. The geotextile was intact and highly stressed when uncovered by the backhoe. The ability of the fabric to carry and transmit the earthen loads into the sub-soil is rather dramatic and allowed a second possible failure method. The fabric acted as a diaphragm to transmit the loads causing a rotation about the outside toe of the fabric/berm system. The block rotation (fabric and soil) would have caused the cracks on the exterior of the berm and a significant subsidence or compression load on the interior toe of the berm (a minimum distance of 60 feet). Note that the settlement along the CDF perimeter had been estimated in the design to be approximately two feet. It is evident that these excessive settlement/subsidence readings in the 1000 LF south reach provided proof that something had happened here of significance. It was not known how significant it might be for the design life of the structure – approximately three years.

Figure 13 – Parallel cracks developed at the base, as the berm settled and shifted inward

Figure 14 - Excavation of test trenches to reveal location of geofabric reinforcement

10. FIRST FILLING

In the summer of 2008, 185,000 CY (approximately 740,000 cubic yards of slurry) of dredged material was placed into the raised CDF 12 facility. Since this was not a very deep basin, and with the invert of the weir set somewhat higher than optimal for future design integration, the raised CDF filled quickly. To expedite continued productivity, the weir was allowed to flow freely without placement of weir boards. This was permissible because the effluent quality stayed below the maximum allowable value (100 PPM) throughout the dredging contract by controlling the placement locations and therefore the hydraulics. However, the raised CDF was impounded with dredged material throughout the contract. The main concern during this first filling was widespread seepage and softening of the silty-clayey subsoils. Seepage was noted and persisted along various reaches of the perimeter, not restricted to the 1000 LF south reach of concern, but along the northeast and eastern reach of the facility. The seepage was closely monitored, with daily SITREPS (situational reports) prepared and distributed. Action was taken on the seepage issue by carefully choreographing the deposition of material dredged in locations where seepage was noted. By placing additional material on the interior of the AOC's (Areas of Concern) it provided a longer flow path through the berm structure and provided material to bolster the berm retention system. It is critical to realize that given the only material available to incorporate into the work was sand. Seepage was inevitable and expected. As the filling proceeded, the worst seepage areas were mitigated and the entire facility performed extremely well through the design efforts and the incorporation of fabric reinforcement for the first filling operation.

11. SUCCESSES AND FAILURES

Raising CDF 12 had its shares of successes as well as some failures, which is to be expected from a project with relatively high associated risk associated. The raised CDF survived its first filling, with nothing more than seepage mitigation. The troublesome 1000 LF reach of concern along the southern side appeared to maintain its integrity throughout the dredging contract. Monitoring will continue to insure a proactive approach to resolving any issues that may arise. The contractor was responsive to not only the project construction but also to monitoring the project and adapting to changing conditions as directed by the Government. Despite the project's limitations of building on an inferior foundation and limited funding, it appears that the raised CDF has performed as designed and as well as can be expected. The primary failures or shortcomings include the foundation problems along the 1000 LF south berm reach and their potential impact on the future raising of CDF 12 to +24 LWD, a lack of operational flexibility during the first filling due to the (high) invert elevation of the weir, and the seepage, which is a product of the pervious nature of the borrow material. While the geotextile reinforcement maintained its integrity within the raised berm, the excessive amount of settlement/subsidence along the reach of concern indicates it may not have had enough strength to properly resist the imposed stresses. This project provides a realistic opportunity to assess these successes and failures for use in future similar projects.

12. LESSONS LEARNED

The lessons learned from the Cleveland CDF berm-raising project include:

- It is feasible to create interim dredged material storage capacity in Cleveland Harbor by building over a previously filled CDF using onsite borrow exclusively. Strategic placement of the dredge discharge pipe can greatly aid in future berm construction operations.

- The geotextile reinforcing layer performed as well as it was capable of. However, specifying stronger geotextile reinforcement might help to reduce excessive settlement or subsidence issues and prevent slope failure or lateral translation.

- Insufficient site characterization was conducted for this project. There were no intermediate borings taken between the corners, including along the 1000 LF south berm reach. The borings were spaced at over 1000 LF apart. More concentrated subsurface explorations are recommended for future similar projects to improve the likelihood for a better design.

- It is important to assess the project as it proceeds through the construction phase and after the completion of construction. This includes monitoring programs, regular visual observations, and, as needed, special forensic tests, such as excavating to expose the geotextile.

Geotextiles in Dams – Forging Federal Guidelines[1]

D. A. Crum, P. E., U. S. Army Corps of Engineers, Kansas City, Missouri, USA

ABSTRACT
The major dam building era for large dams in the United States during the 1940's to the 1970's ended about the time geotextiles were becoming popular. For the last 40+ years, geotextiles have been used in many dams worldwide for various applications. During this period, federal agencies have resisted experimentation with geotextiles in critical applications, agency policy has been to generally restrict use, and there have been minimal criteria governing use in federally funded water resource projects. Geotextiles have been used for various purposes on levees and dams, sometimes (by some interpretations) against agency policy. Geotextiles are often recognized to provide economical solutions. In some cases, geotextiles have been reported to provide the only viable solution, which can be especially useful in remediation of existing structures. Current projections are for increasing, perhaps explosive growth in rehabilitation of levees and dams. With the current geosynthetic industry experience, it is increasingly compelling to formulate criteria that encourage general use of geotextiles while preventing misuse. Even within high hazard structures, there exist non-critical applications such as landscaping fabrics or those that promote longevity of pavements. On the other spectrum, internal filters for large dams are a critical application and a controversial issue. The federal approach for utilization of geotextiles should not condone use through absence of criteria. Compromise solutions based on technical merit alone are not adequate to resolve restrictions governing geotextile use. For critical applications, criteria must be based on design resiliency and risk tolerance. A perspective will be offered concerning pragmatic use of geotextiles for water resource projects, especially in critical applications and high hazard structures.

1 INTRODUCTION

The purpose of this paper is to promote establishment of criteria concerning use of geotextiles in dams. Criteria establishment has a dual purpose: to both increase use of geotextiles where acceptable, and to avoid misuse of geotextiles where unacceptable.

2.1 Example Uses

There is a variety of potential applications for geotextiles in dams. The most common uses of geotextiles in embankment dams in the Unites States are as a riprap filter placed on the upstream slope or in a downstream discharge area, a riprap filter used to line watercourses, or a filter in a downstream trench drain (often remedial work after construction). Less common embankment dam applications include a protective layer and drain placed in contact with an upstream waterproofing geomembrane, as an internal filter, and as an internal drain. Internal drains and filters are the most controversial. The applications shown in Figure 1 are not intended to define acceptable use, but rather to describe some of the potential uses that are contemplated for the purposes of this paper (most of these have been used and are in existence).

2.2 Performance Requirements for Dams

Misuse of geotextiles primary focuses on the potential problems associated with using a geotextile as a critical and non-redundant design element deeply buried in a dam. It is the position of the National Dam Safety Review Board that geotextiles should not be used within a dam where they are both critical for dam safety and inaccessible for repair or replacement. This view was formulated during a workshop in October 2000 where the participants reached a consensus that a) geotextiles should not be used in applications that are both critical to safety and inaccessible for replacement, and b) geotextiles can possibly be used in locations that are critical for safety but accessible for replacement. However, the workshop participants qualified the second case with the caveat that the engineer must assess the potential hazard posed by failure of the geotextile and the time available to respond and repair or replace the geotextile.

[1] *This paper, with minor modifications, has previously been published in USSD 2008, United States Society on Dams, Portland, OR, 29 – 30 April 2008 and in Geosynthetics, August/September 2008.*

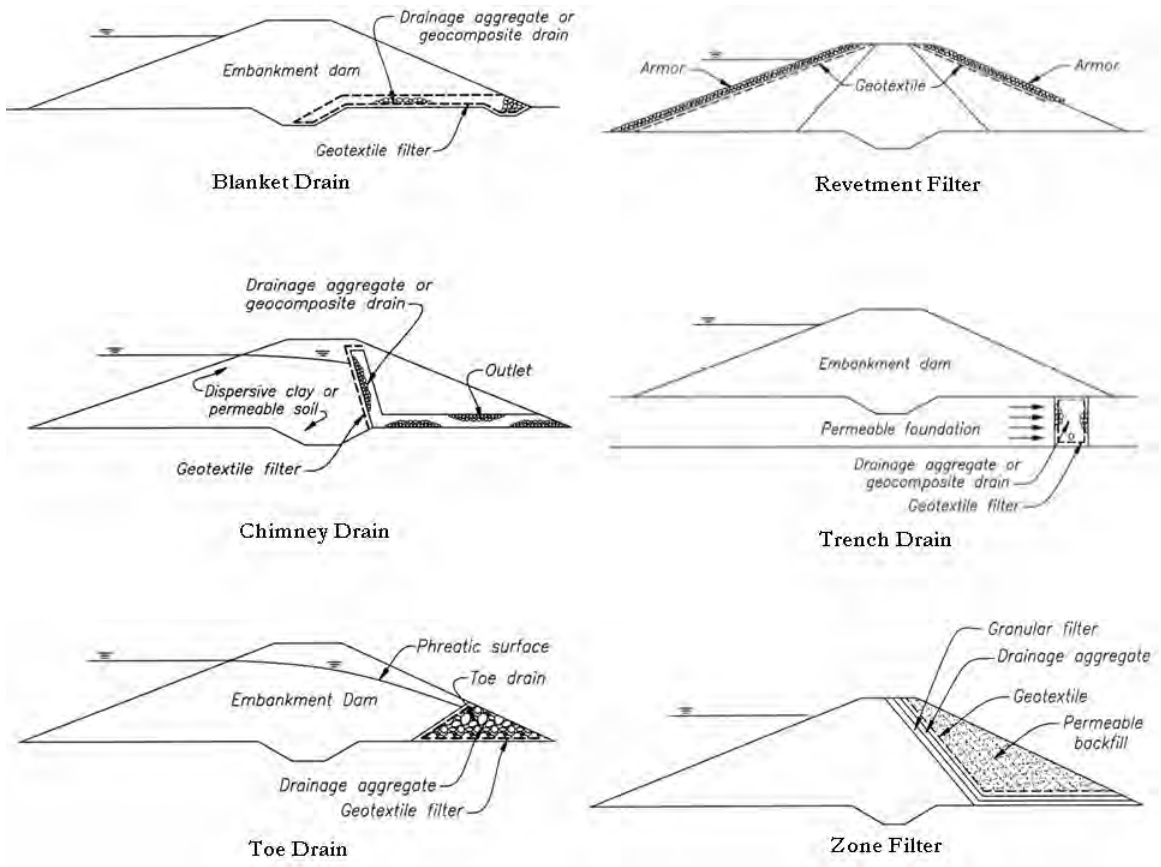

Figure 1. Examples of Potential Geotextile Applications in Embankment Dams (after FEMA draft document)

2.3 Case Histories

In 1986, the International Conference on Large Dams prepared a special publication to address use of geotextiles in dams (ICOLD 55). They concluded: "The cautious adoption of geotextiles in dam engineering properly reflects the uncertainties involved in using a new and novel material." Also, "Successful performance of geotextile filters in non-critical locations cannot be used to validate use in more highly stressed locations where behavior mechanisms may be different. It has not yet been demonstrated that geotextiles can provide an equivalent to properly designed granular filters for this purpose, particularly when protection against cracking or the effects of earthquakes is required." Although this document is somewhat dated, and that there have been some pioneering efforts in both research and construction toward breaking this barrier, these concerns are still relevant.

There is a study awaiting publication (FEMA, draft document) that includes a literature review of geotextile applications in dams. The use of geotextiles for embankment filtration and drainage is mainly evident in France, Germany, China, and South Africa. A common factor in foreign practice regarding the use of geotextiles as filters and drains is the requirement that design must include rigorous performance testing to evaluate filtration and permeability using the proposed geotextile materials and actual soils from the project site. The findings evident in the literature are almost entirely positive, where geotextiles appear to be functioning adequately.

While the apparent successful use of geotextiles in constructed dams cited in published literature would suggest acceptance of geotextiles, the conclusions derived from this need to be taken cautiously. Often, technical publications are submitted within a few years of construction, and clogging may occur over much longer periods of time. Bad experiences are much less likely to be published for various reasons connected with litigation or designers reputations. Undocumented experience from the grapevine often alludes to bad experiences. The past success stories alone do not define a threshold of acceptable use. Failure analyses are often more informative, but they too have shortcomings. Failed designs are difficult to obtain and designers are understandably reluctant to advertise their mistakes. If the findings from post mortem analysis are that the geotextile was used with little or no testing & analysis, then the conclusions are trivial and may not help to define the threshold envelope. While the geotextile industry criteria and experience may be substantial for conventional applications,

the reviewed case histories are not substantial enough to defend a higher degree of confidence desired for high hazard structures.

Concerns regarding long term performance of materials, products, or innovative construction methods are not attributable to geosynthetics alone. As an example, drain pipes embedded within embankments have proven to be problematic. Corrosion of the pipes can lead to loss of embankment and sink holes. Clogging can lead to elevated water levels. The liability for these risks is not fully appreciated until performance assessments identify increased risks from low probability but high consequence failure events. Interim risk reduction measures imposed as mitigation to these concerns can be very costly. Also, the time to verify unsatisfactory performance, plan/design repairs, obtain funding appropriations, and construct the repairs can unacceptable.

3. EXISTING AGENCY CRITERIA

The status of existing criteria at some agencies with missions in design, construction and operation of dams was reviewed in a recent FEMA funded study (FEMA draft document). A summary of the findings is included below:

3.1 Bureau of Reclamation

Geotextiles can be used in embankment dams, but not as a sole element in a critical application. (Bureau of Reclamation, 1992)

3.2 Corps of Engineers

There many separate documents that provide a brief mention of geotextiles, but sometimes lead to conflicting criteria. The most representative excerpt pertinent to dams is: “Since long-term experience is limited, geotextiles should not be used as a substitute for granular filters within or on the upstream face of earth dams or within any inaccessible portion of the dam embankment. Geotextiles have been used in toe drains of embankments where they are easily accessible if maintenance is required and where malfunction can be detected.”(TM 5-818-8)

3.3 Natural Resources Conservation Service

The use of geosynthetics is interpreted as a variance to design policy since it is not explicitly allowed; so use in dams is deferred to agency review by national technical staff. Unwritten policy does not permit the use of geosynthetics as an internal design component of a dam, particularly as a filtering/drainage function. Geotextiles have been used extensively as a separator function placed between rock riprap and soil in rock-lined plunge pool basins and outlet channels downstream of concrete stilling basins. Geotextiles have also been permitted beneath riprap on the upstream slope of dams for wave protection.

3.4 Federal Energy Regulatory Commission

Unwritten policy that geotextiles are not allowed in inaccessible areas of embankment dams, and are not accepted as a filter for riprap. Geotextiles have been permitted in trench drains that are accessible for repairs.

3.5 State dam safety programs

In a poll of state dam safety engineers, only 8 of 40 respondents indicated that their states had implemented standards or guidelines that prescribe the use(s) of geo-synthetics in the design or construction of earthen embankment dams. There were 14 respondents who expressed reservations against using geosynthetics in the design and construction of earthen dams. The respondents ranked their reluctance based on (1) absence of design standards, (2) poor performance, (3) too few examples, (4) lack of experience, or (5) insufficient support. This showed a wide dispersion of answers, leading to the interpretation that all of the above are considered to be valid concerns.

3.6 Private Practice

Based on a poll of design firms, the consensus is that geotextiles should not be used for critical applications such as filtration and drainage where their failure could affect the integrity of the dam. Liability is a primary concern to consultants.

3.7 Discussion

It is concluded that the only federal agency that has a comprehensive policy on use of geotextiles in dams is the USBR, but that document was last updated in 1992 and does not reflect current practice. Currently, both the USBR and the Corps of Engineers have work in progress to update criteria.

In the non-federal sector, it is noted that reliance on professional judgment creates a conflict of interest situation. While large established engineering firms may take liability very seriously, small design firms with limited assets and history can afford considerably more risk. Without state policy on the use of geotextiles in dams, the regulating criteria depend heavily on ethical conduct for professional practice. Ethical conduct intertwined with innovative technologies leads to subjective design details without the hindsight of a failure. The liability to the consultant is not necessarily linked with the liability to the public.

4. PERFORMANCE CONCERNS

Performance issues with geotextile products fall into 3 common categories: (1) Limitations that can be accommodated by design, conservative assumption of material properties, and use of safety factors; (2) Harsh environments that may be recognized and avoided; and (3) Inherently high-risk applications. Geotextiles have numerous potential applications in civil works. Some applications in water retaining structures have high consequences if they should fail, and should be avoided or used with caution and full understanding of the risks.

Under the first category, uncertainties may include ultraviolet degradation, installation damage, and design methods for using geotextile products. These concerns are normally addressed in design conservatism and construction quality control. These common performance issues are relevant to all applications of geotextiles in civil engineering and construction.

Harsh environments have contributed to documented failures of geotextiles. However, these conditions can usually be recognized through site investigation and experience gained from past performance problems. Environmental degradation includes the effects of ultraviolet light, high temperatures, hydrolysis, chemicals, radioactive materials, and biological organisms. Degradation of the polymers used in geotextiles has been shown to be inconsequential for typical soils. Difficult applications may also contribute to geotextile failures. Filtration in dispersive soils and filtration in flow reversal are applications that can cause clogging. These issues require increased attention to detail, and in some cases high-risk environments can be avoided by early recognition.

The first two categories require attention to detail, but do not preclude use of geotextiles for classes of applications, such as in dams. The last category does. Perhaps the highest concern is use of geotextile filters for drainage in portions of a dam that are not readily accessible for removal and replacement. Failure of an internal feature of a large dam is not only very expensive to repair; it could jeopardize the safety of the dam. Designers are cautioned to evaluate the consequences of failure during the design process and decide if the risks are worth taking.

4.1 Clogging Potential for Granular and Geotextile Filters

The advantages of geotextiles in conventional civil engineering practice typically outweigh the risks associated with clogging. In critical applications however, it is a cause for concern. It is generally known from experience that geotextile filters have on occasion experienced significant clogging problems. It has also been determined that generally these failures could have been avoided by increased attention to detail and design rigor. However, there are some concerns that suggest geotextiles are inherently more susceptible to clogging than granular filters:

4.1.1 Blinding and Particle Deposition

There are two competing requirements for design of granular filters: retention and permeability. The filter must be sufficiently large to pass flow, but sufficiently small to retain the base soil. There are three requirements for design of geotextile filters: retention, permeability, and clogging. Particulate clogging of granular filters is generally limited to screening for problematic conditions such as internally unstable soils (gap graded), dispersive soils, or mixed/stratified zones of variable soil types. These same issues are also problematic for geotextiles, but geotextile design additionally includes explicit clogging criteria in the design process. The retention at a plane (or sheet) in the soil concentrates particles that migrate in the soil but are retained on the filter. To avoid particle clogging, the number and size of openings in the filter are increased to pass the small particles not necessary to retain the skeletal structure of the base soil. When the design criteria for clogging is more stringent than for permeability, then the design sensitivity (range of admissible sizes) is tighter and the construction tolerances are tighter. It is a physical limitation that controlling the opening size for geotextile filters will always have tighter tolerances than granular filters. Conversely, geotextiles are manufactured products with better control of parameters than natural materials. The impacts of this on filter reliability have been debated in the geosynthetics industry with no clear consensus.

4.1.2 Intimate Contact at the Discharge Face

It has been shown that fabrics that are not confined (i.e. those that move within large pore spaces due to water pressure fluctuations) are more susceptible to clogging. Presumably, this is because a moving fabric does not form a natural filter, so over time suspended particles eventually find a hole to become lodged in, contributing to blinding or particle deposition within the fabric. If the fabric is confined, and if the AOS is appropriately sized, the fabric replicates the soil structure close enough that a natural filter forms.

4.1.3 Growth Medium

In addition to particle clogging, the polymer sheets can provide a medium for chemical precipitation or biological growth. Experience suggests chemical and biological fouling may be the dominant concern for drain clogging in dams. Drainage systems in dams located near the toe or galleries typically have persistent drainage with discharge water rich in minerals. Ochre is common at many projects, which is an iron deposit of gelatinous mass associated with bacterial slimes. Lined wells in soils and unlined wells in rock commonly require regular rejuvenation programs to remove biologic fouling and chemical precipitates. Well rejuvenation methods have included chloride tablets and other chemical treatments, bleach and other cleaning agents, steam and hot water, high pressure water jets, boring with drill tools, and scrubbing with wire brushes. Even with such aggressive treatments, some wells are eventually abandoned and replaced. Drainage systems in dams commonly have a very harsh environment conducive to chemical and biologic fouling.

4.2 Integrity

There are some applications when 100% integrity of the geotextile is important. Internal zoning of embankments (e.g. impervious cores, rockfill, chimney drains) require a high confidence of filter integrity, which is difficult to assure with geotextiles. Generally, flaws fall into two categories:

4.2.1 Installation Damage

Constructed features with flaws from installation damage have a potential to propagate or expand over time, causing a crisis or failure. To a degree, the QA/QC can be commensurate with the risk from installation damage. However, there is a practical limit for the intensity of QA/QC that is productive or effective. The practical limit of QA/QC may be governed by cost effectiveness, destructive sampling, or sampling theory that an infinite number of samples are required to achieve 100% confidence. For high hazard structures, the practical limit may occur before the acceptable risk is achieved.

4.2.2 Post Construction Damage

Internal filters in earth embankment dams are to a limited degree, self healing. This resiliency has an important benefit when considering consequences from low probability events but high risk consequences. Granular filters may be resilient if they were to be penetrated by displacement from slope instability, seismic events, hydraulic fracturing, root or animal penetration, or some other circumstance.

4.3 Accessibility

The ability to access portions of a structure is relative. Accessibility should be determined on the basis of a plan that shows access for replacement is practical under the basis of cost and normal operating budgets. Given unlimited time and funding, almost everything is accessible. However, the practicality of repairing features that are difficult to access must be considered. If the cost to complete the repair exceeds budget available for routine operations and maintenance, then it might not get accomplished. If the time for planning, design & construction exceeds the interval between when the problem is recognized and when a design loading event occurs, then it is too late. If the performance is first recognized as distress to other portions of the facility that are more costly and to which the feature is ancillary, then it is too late. Deeper than 20 feet is generally not accessible for removal and replacement.

Replacement may not be possible during certain loading conditions. Work that is intrusive sometimes requires pool restrictions. Since performance limitations are most noticeable during record pool levels, this is a particular concern for dams with storage allocated to flood control.

5. RESTRICTIONS AND CRITERIA

There are some primary concerns where use is cautioned:

- Geotextiles used within any inaccessible portion of dam embankments, because of residual risk for clogging.

- Geotextiles used in toe drains of embankments may be related to the embankment stability, but they are easily accessible if maintenance is required. This assumes that malfunction can be detected before unusual (flood or seismic) events.

- The preceding sections allude to the necessity of providing restrictions and criteria, but do not provide the exact terms. There is reason for difference in the criteria between agencies, depending on size and purpose of dams, hazards presented by typical dams, risk tolerance, and post construction rehabilitation needs. Criteria can be prescriptive based, performance based, or a combination.

5.1 Prescriptive Criteria

Some of the possible applications for geotextiles in dams include ancillary and temporary features. These applications are generally more acceptable since they do not generally lead to high consequence failure scenarios.

5.1.1 Ancillary features

Features that do not affect the dam performance are acceptable use. Such features may include:

- Drains for ground maintenance
- Pavement applications
- Landscaping

5.1.2 Temporary works

Caution is advised, as large cofferdams may be in place for several years and can incur significant damages. Temporary works may include:

- Cofferdams
- Construction Dewatering
- Construction Access Roads
- Inverted Filters
- Sandbags

5.1.3 Rehabilitation of Existing Dams

There are cases where alternatives for rehabilitation of existing dams using geotextiles have been presented as the only feasible alternative. The only technically feasible alternative would be difficult to justify for new projects. In structural repair or rehabilitation, there are cases where funding limitations merge economic alternative issues into technical feasibility issues. A granular filter zone and a geotextile filter are generally economic alternatives that are compared using life-cycle cost analysis. But if a granular aggregate source is not locally available, and the cost to import materials renders the project unfeasible or delays it indefinitely, then the technical alternatives are to compromise the design parameters by reducing the filter zone or layer thickness, or using an alternative approach such as geotextile filters. From a risk based approach, it may become justified to use geotextile filters, even in critical applications.

Risk methodology should not be used to lower standards, or circumvent codes, regulations, or criteria. However, risk assessment is highly useful for prioritizing remediation activities in a resource-constrained environment. Allowance of geotextile filters in critical applications is perspective dependent, bearing on competing goals of maximizing use of resources or maintaining high standards. If the risk minimization goal is favored, then allowing geotextile filters in critical applications should only apply to existing projects, where the do-nothing and decommissioning alternatives are not acceptable.

5.1.4 Low hazard dams and agricultural levees

Low hazard structures (FEMA 333) that do not impose a health and safety risk are not a primary concern.

5.1.5 Crack Stoppers

Transverse embankment cracking is a concern in arid climates. Geotextiles have been proposed as a membrane to prevent soil erosion through open cracks. The issue of embankment cracking is a concern for existing dams constructed with natural materials, so use of geotextiles for mitigation is not a substitution for a standard design using other materials and methods.

5.2 Performance Criteria

Because of the vast alternatives for incorporating geotextiles into dams in various geometries and functions, the prescriptive criteria may not always apply or will be subject to interpretation. The hazard of a geotextile in a dam can be identified in an analogy to the Fracture Critical Member concept in structural steel design. If failure of a certain component can lead to the collapse or failure of the structure, then it should be labeled as a Failure Critical Component (FCC). For example, if a drain is installed for landscaping or grounds maintenance concerns, and if the embankment stability meets all factors for safety with the drain 0% effective, then the drain would be non-FCC. However, if a drain is installed for the purpose of reducing the phreatic surface and the design computations for the structures stability relies on this drain, then the drain is a FCC. If there are 100% integrity concerns (where holes, flaws or imperfections in the component may render it ineffective) then it is probably a FCC. If engineering analysis is not required by regulation, code, or funding authority, then it is probably not FCC.

6. CONCLUSIONS

While it is acknowledged that geotextile filters have been used in critical applications, particularly in projects outside the United States, this should not directly lead to acceptable industry practice. The amount of risk imposed by such projects has not been substantiated; and endeavors by industry experts do not justify common practice for all practitioners.

Guidance regulating use of geotextiles in dams is currently lagging behind the industry knowledge base and technical capabilities. Agencies that design, operate, or regulate high hazard dams should establish explicit written criteria for use of geotextiles.

Clogging of geotextile filters is a paramount concern governing use in dams. The implications regarding the use geotextiles as filters and drains in embankment dams needs to be fully considered. In some applications, the zero-defects concern may be paramount.

While a properly designed geotextile filter is preferred over an inadequately designed or improperly applied granular filter, increased emphasis on design does not change the limits of what is obtainable. Granular filters have a longer history suggesting a more reliable design than geotextile filters, given a similar level of design effort, expertise, and quality control/assurance.

Risk management in dam safety delves into consideration of low frequency – high hazard events. Such considerations lead to standards that favor very conservative design and are not tolerant of innovative technologies. It should not come as a surprise that regulators will impose some restrictions on use of geotextiles in dams.

There are many applications associated with dams with varying implications to dam safety. Some applications are appurtenant to the dam stability, some are redundant, and some are amenable to monitoring and maintenance. Criteria for use of geotextiles in dams should be formulated in consideration of critical and non-critical applications.

7. REFERENCES

Bureau of Reclamation, (1992) *Design Standards, No. 13 – Embankment Dams, Chapter 19 – Geotextiles*. U.S. Department of the Interior, Bureau of Reclamation, Denver, Colorado.

FEMA 333, (1998) *Federal Guidelines for Dam Safety: Hazard Potential Classification Systems for Dams*.

FEMA (draft document), *Geotextiles in Embankment Dams: Status Report on the Use of Geotextiles in Embankment Dam Construction and Rehabilitation*, (pending publication).

ICOLD 55, (1986) *Geotextiles as filters and transitions in fill dams*, International Commission on Large Dams Bulletin 55.

TM 5-818-8, (1995) *Engineering Use of Geotextiles*, U. S. Army Corps of Engineers.

Field Construction and Trafficking of an Unsurfaced Geosynthetic-Stabilized Road

E.V. Cuelho, Western Transportation Institute, Montana State University, Bozeman, Montana, USA
S.W. Perkins, Civil Engineering Department, Montana State University, Bozeman, Montana, USA
J. Hauck, Western Transportation Institute, Montana State University, Bozeman, Montana, USA
M.R. Akin, Western Transportation Institute, Montana State University, Bozeman, Montana, USA
K. von Maubeuge, NAUE GmbH & Co. KG, Espelkamp-Fiestel, Germany

ABSTRACT
The use of reinforcement geosynthetics in unsurfaced roads built upon a soft subgrade is known to provide benefit by allowing a better distribution of applied loads and increased bearing capacity. This paper describes a research project where field test sections were constructed to evaluate the performance of several geosynthetics commonly used for subgrade stabilization. A sandy clay subgrade was prepared to a CBR strength of approximately 1.7 and an aggregate layer of 20 cm thickness was compacted over the geosynthetics. Trafficking was provided by a fully-loaded tandem axle dump truck. Rut depth was monitored throughout the trafficking period. Post trafficking excavations were performed to facilitate future evaluations of damage to the geosynthetic, base contamination and deformation of the layers. The construction and monitoring techniques employed during the course of this project help create a test bed of relatively equal conditions across all of the test sections.

1. INTRODUCTION

At times it is necessary to construct roads in areas that have weak native soil deposits. When excavation and replacement of these soils is not cost effective, soil stabilization may be necessary to provide a working platform so that the base course gravel layer can be properly constructed and overall rutting reduced. Geosynthetics are planar polymeric materials that have been extensively used in these situations (i.e., subgrade stabilization) to reinforce or separate the surrounding soils. Separation is typically attributed to geotextiles, while reinforcement may be derived from geotextiles and geogrids; however, under the right circumstances, geogrids may also offer separation. Subgrade stabilization is typically applicable for unpaved temporary roads such as haul roads, or construction platforms to support permanent roads. These roads are generally characterized by low volumes of heavy vehicles that can tolerate deeper ruts. Historically, geotextiles were first used in these applications; however, geogrids have also been commonly used in more recent years.

Montana Department of Transportation (MDT) has used both geotextiles and geogrids for subgrade stabilization. MDT helped instigate this research because currently there is a lack of: 1) a universally accepted standard design technique that incorporates non-proprietary material properties of geosynthetics when used as subgrade stabilization, and 2) agreement as to which geosynthetic properties are most relevant in these cases. Therefore, this research was initiated to begin to understand which properties are most relevant as they seek to update their specifications to more broadly encompass materials with which they have had good experience, as well as open up the application to other suitable materials. This is particularly important since new geosynthetics and manufacturing processes are regularly being introduced into the market. Field sections were constructed at a transportation research facility to avoid having dissimilar conditions across the test site which tend to obscure the true reasons for differences in performance between different geosynthetic products. A similar methodology was used by Hufenus et al. (2006) to evaluate geosynthetic reinforcement of unpaved roads built on weak sub-soils. This paper describes the design, construction, trafficking and preliminary results of this research project.

2. DESIGN AND MATERIALS

Many test trials for geosynthetics have been constructed on native soil deposits as part of existing highway construction jobs. While this is generally more efficient and less costly, variations in the subgrade strength, depth and consistency are oftentimes significant enough to make it difficult to clearly distinguish differences between different products or construction practices. Therefore, construction of these test sections was done in a way to minimize these differences. To do this, the research project was constructed at the TRANSCEND research facility in Lewistown, Montana on a decommissioned taxiway. Most importantly, an artificial subgrade material was prepared, placed and compacted the same along the entire test site to ensure that underlying soil strength did not vary significantly. Moisture and shear strength were continuously monitored for all layers of the artificial subgrade. The driving surface consisted of a compacted, crushed base course approximately 20 cm thick. The experiment was designed to evaluate how many truck passes were necessary to cause 10 cm of rutting in each of the test sections, and to evaluate pertinent characteristics of the geosynthetics relative to this application.

2.1 Artificial Subgrade

The natural soils at the TRANSCEND test site consisted mainly of large-stoned dense gravels topped by a layer of base course and asphalt. The existing soils and pavement were excavated so that an artificial subgrade could be constructed. It was desired to construct the artificial subgrade out of materials that were weak when wet, in relatively close proximity to the test site, and were commonly encountered in Montana construction projects. A suitable subgrade soil, which consisted of overburden material, was purchased from a nearby gravel pit and delivered to the test site. This soil classified as A-6 according to the AASHTO classification system (AASHTO M-145) or SC (clayey sand) according to the USCS classification system (ASTM D 2487). Other relevant properties of the artificial subgrade material include the following parameters: liquid limit = 32, plasticity index = 13 and percent passing the #200 sieve = 31%. Laboratory tests were conducted to determine the appropriate method to prepare the subgrade soil so that it had the desired strength characteristics (i.e., CBR strength of 1.7 ±0.1). A hand-held vane shear device was chosen as the primary method to monitor in-place shear strength of the subgrade as it was being constructed because it was: 1) simple to operate, 2) able to provide a rapid assessment of strength, and 3) was more precise than other devices. A dynamic cone penetrometer (DCP) was also used as a comparison to monitor subgrade strength before and after trafficking. Unsaturated CBR tests were conducted in the lab prior to construction to determine a relationship between soil strength and moisture content. Vane shear tests were also conducted on the laboratory CBR samples to relate CBR to vane shear strength. The linear relationship that was developed in the lab using both of these tests was generally good, as shown in Figure 1. According to this data, the shear strength as determined using the vane shear device must be between roughly 52 and 62 kPa to achieve the desired CBR strength (1.7 ±0.1) in the field. Attempts to relate moisture content and density to CBR in the laboratory did not yield satisfactory results (R^2 values = 0.1071 and 0.0374, respectively).

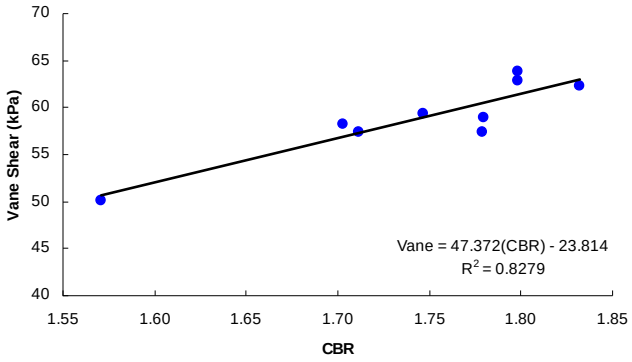

Figure 1. Relationship between California Bearing Ratio and the hand-held vane shear device.

2.2 Base Course Aggregate

The base course aggregate for this project was a crushed gravel Grade “6A” according to Montana Department of Transportation standard material specifications, having the gradation shown in Figure 2a. It classified as A-1-a according to the AASHTO classification system (AASHTO M-145) or GW-GM (well-graded gravel with silt with sand) according to the USCS classification system (ASTM D 2487). The optimum moisture content and maximum dry density were 5% and 2310 kg/m^3 (Figure 2b), respectively, as determined using the modified Proctor procedure (AASHTO T-180). The base aggregate satisfied the natural filter gradation requirements as specified in Holtz et al. (2008), so a geotextile separation layer is not recommended to prevent contamination of the gravel layer.

The thickness of the base course was determined using the Federal Highway Administration design methodology (FHWA, 1995), which is based on the U.S. Forest Service method (Steward et al., 1977). The design process begins by selecting an appropriate bearing capacity factor, N_c, which depends on 1) presence of geosynthetics, 2) allowable rutting, and 3) traffic levels. Bearing capacity factors for a matrix of these conditions are listed in Table 1. It was assumed that test sections which utilized geosynthetics for subgrade stabilization would have less rutting and would therefore fail less rapidly as compared to sections that did not use geosynthetics (i.e., the control test sections). Consequently, bearing capacity factors of 5.0 and 3.3 were selected for sections with and without geosynthetic stabilization, respectively. The thickness of the base course was then determined using the design curve for tandem (dual)-wheel loads (assumes 550 kPa tire pressure and each axle carries 40 kN of load). From this analysis a relationship of CBR to base course thickness was created (Figure 3). An average base course thickness of 20 cm was specified for a CBR of 1.7 to minimize rutting in the control sections and to maximize rutting in the geosynthetic stabilized sections. Using the aforementioned design methodology and input values, it was anticipated that the control test sections would reach 10 cm of rut at approximately 33 truck passes (~100 traffic passes – one passage of the truck equals three traffic passes, also known as axle passes) and that the majority of the geosynthetic-stabilized test sections would reach 10 cm of rut at approximately 333 truck passes (~1000 traffic passes).

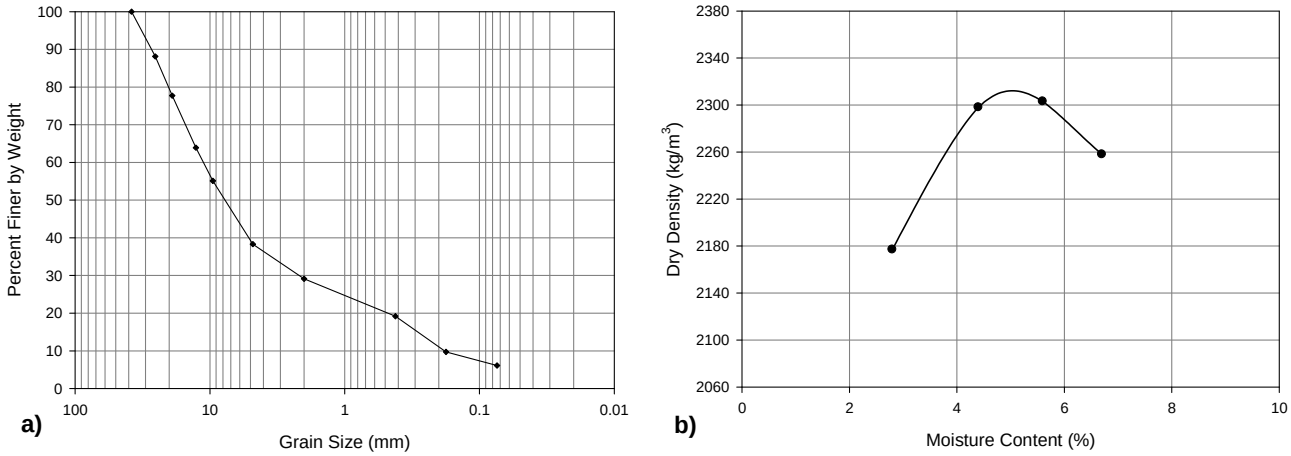

Figure 2. Base course material properties: a) grain-size distribution, b) compaction curve.

Table 1. Bearing Capacity Factors

	Allowable Rut (mm)	No. of Traffic Passes	Bearing Capacity Factor, N_c
Without Geosynthetic	< 50	> 1000	2.8
	> 100	< 100	3.3
With Geosynthetic	< 50	> 1000	5.0
	> 100	< 100	6.0

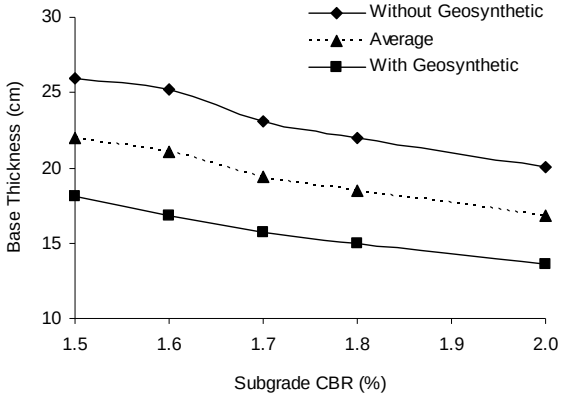

Figure 3. Relationship of CBR to base course thickness

2.3 Geosynthetics

Ten geosynthetic products were used in this research project to evaluate their relative performance under the conditions presented herein. Pertinent information for each of these products is listed in Table 2. The general layout of the test sections and the direction of traffic are illustrated in Figure 4. Each geosynthetic test section was 15 meters long, with the exception of the two control sections (C1 and C2) and section A, which were 20 meters long. The geosynthetic in adjacent test sections overlapped one another by approximately 1 meter such that “upstream” geosynthetics overlapped “downstream” geosynthetics (i.e., geosynthetic A was on top of B, B was on top of C, etc.).

Table 2. Summary of Geosynthetic Properties

Test Section	Structure	Polymer[a]	Roll Width (m)	Mass per unit area (g/m^2)	Aperture Size (mm)	Strength[c] @ 2% (kN/m)		Strength[c] @ 5% (kN/m)		Ultimate[c] Strength (kN/m)	
						MD	XMD	MD	XMD	MD	XMD
A	biaxial welded geogrid	PP	5.00	240	44 x 40	11	NP	22	NP	30	NP
B	vibratory-welded geogrid	PP	4.75	155	32 x 32	8	8	16	16	20	20
C	integrally-formed biaxial geogrid	PP	4.88	NP	25 x 33	6.0	9.0	11.8	19.6	19.2	28.8
D[†]	composite vibratory-welded geogrid with integrated non-woven geotextile	PP	4.75	200	32 x 32	12	12	24	24	30	30
				150	N/A	N/A		N/A		6	10
E	integrally-formed biaxial geogrid	PP	4.00	NP	25 x 33	4.1	6.6	8.5	13.4	12.4	19.0
F	vibratory-welded geogrid	PP	4.75	200	32 x 32	12	12	24	24	30	30
G	PVC coated woven geogrid	PMY	4.00	308.5	25.4 x 25.4	7.3	7.3	13.4	13.4	29.2	29.2
H	polymer coated woven geogrid	PMY	3.66	NP	25.4 x 25.4	7.7	8.4	11.5	15.2	34.9	56.5
I	woven geotextile	PPY	3.81	342	0.425[b]	8.8	8.8	21.9	21.9	52.5	47.3
J	non-woven needle-punched geotextile	PP	4.57	NP	0.18[b]	NP		NP		912[d]	

[†] Material D is a composite; the top row of values is for the grid component and the bottom row is for the non-woven textile

[a] PP = polypropylene, PMY = polyester multifilament yarn, PPY = polypropylene yarn

[b] Apparent Opening Size (AOS), ASTM D 4751

[c] MD = machine direction, XMD = cross-machine direction

[d] Grab strength in Newtons

NP – information was not provided by the manufacturer; N/A – information not applicable

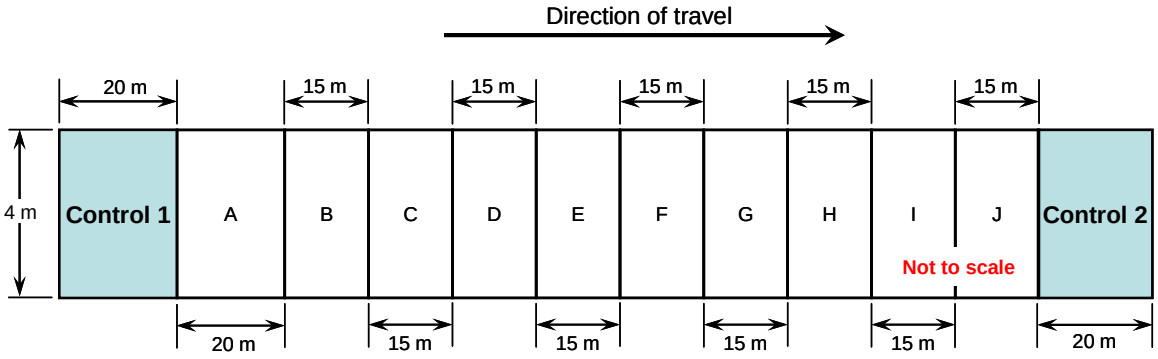

Figure 4. General layout of test sections.

2.4 Instrumentation

Displacement and pore pressure were measured in each test section. Three linearly variable displacement transducers (LVDTs) were used to measure displacements near the rut bowl, and a single stainless steel pressure transducer was used to measure pore pressure. Both dynamic and static measurements of displacement and pore pressure were collected during testing. Static measurements were made every 15 minutes and dynamic measures were made during all of the truck passes while trafficking.

3. CONSTRUCTION

Four main steps were followed to construct the test sections, which are described in more detail in the subsections below:

1. excavation of existing roadbed to make a trench and installation of a plastic liner,
2. preparation and placement of the artificial subgrade soil,
3. installation of the geosynthetics and instrumentation, and
4. construction of the base course aggregate.

3.1 Excavation and lining of trench

Because this experiment was conducted at the TRANSCEND test facility in Lewistown, Montana on a decommissioned taxiway, the existing pavement, base course and sub soils were excavated to a depth of 1 meter to facilitate construction of the weak subgrade. Final grading of the test pit that would later contain the artificial subgrade is shown in Figure 5a. The entire length of the test pit was lined with a 6 mil plastic liner to help maintain uniform moisture conditions in the artificial subgrade over the course of the experiment (Figure 5b).

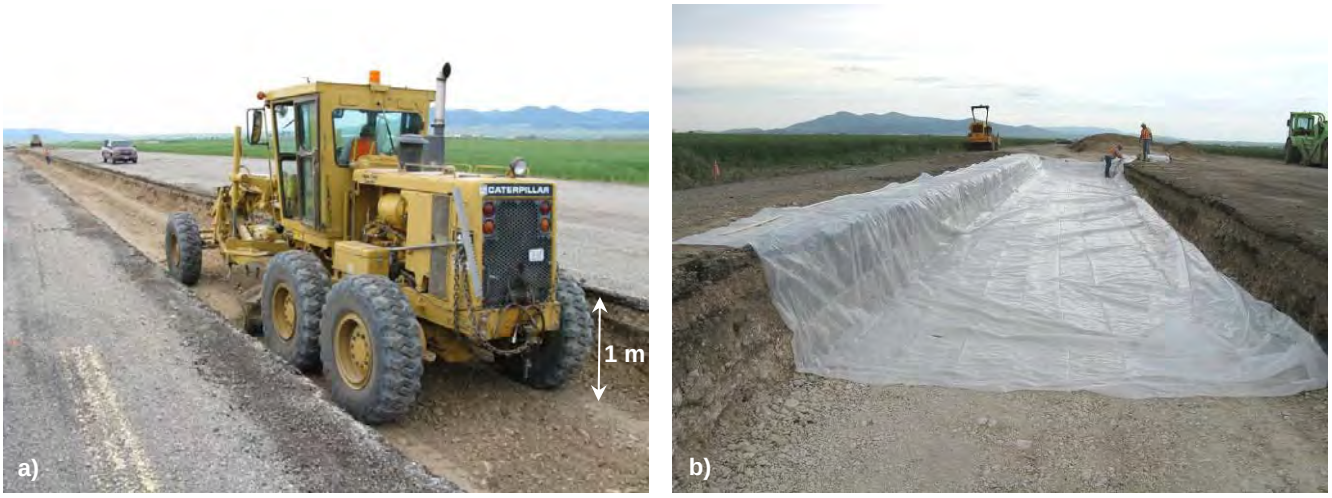

Figure 5. Construction of the test pit: a) final grading, b) installation of liner.

3.2 Preparation and Placement of the Artificial Subgrade

The subgrade was constructed by first wetting the stockpile and tilling the surface to ensure uniform conditions. The subgrade soil was then brought to the trench where a track-driven, skid-steer tractor was used to distribute it evenly into a layer approximately 15 cm thick. Once a significant area was covered in this way, a large roto-tiller was used to even out the surface and further mix the soil mass (Figure 6a). After tilling, soil samples were taken to determine the average moisture content of the layer. Water was then added using a large water truck (if too low) or the tilled surface was allowed to dry (if too wet). Compaction was done using a single cylinder, smooth-drum, vibratory roller (Figure 6b). Immediately after compaction, the vane shear device was used to determine in-place shear strength. If the shear strength of the artificial subgrade was not relatively close to the specified limits, two basic remedies were used: 1) shear strength too low – re-till the layer, allow soil to dry, and recompact the soil layer, or 2) shear strength too high – re-till the layer, add water, allow the water to penetrate the tilled soil mass, re-till the soil again, and recompact the soil layer. Altogether, seven layers were necessary to fill the trench (one layer at a time along the entire length of the trench) until the top surface of the subgrade was approximately equal to the original level of the existing pavement. A slight crown was set into the surface of the subgrade so that water from rain or the water truck would not accumulate on the surface.

Figure 6. Subgrade construction: a) tilling, b) compacting.

The quality and consistency of the artificially constructed subgrade was mainly monitored using a hand-held vane shear device and moisture content. On average, four strength measurements were randomly taken within each of the test sections on each layer during construction using the vane shear device (shown in Figure 7a). Moisture content was mainly used to ensure uniform conditions in the subgrade prior to compaction while vane shear was used to monitor subgrade strength after compaction. In general, there was more variability in earlier (i.e., lower) layers of the subgrade and less in the upper layers. Average strength values during construction ranged from 57.9 kPa (layer 7) to 71.3 kPa (layer 5), which corresponds to CBR strengths of 1.72 and 2.01, respectively (calculated using the regression equation in Figure 1). The DCP device was also used to evaluate the strength of the subgrade after it had been fully constructed, despite that the DCP device was not necessarily well suited to evaluate very small differences in soil strength. One to three DCP measurements were made within each test section to get a general idea of the strength of the soil using this method. Overall, strength characteristics were generally similar between test sections (Figure 7b), especially in the upper layers.

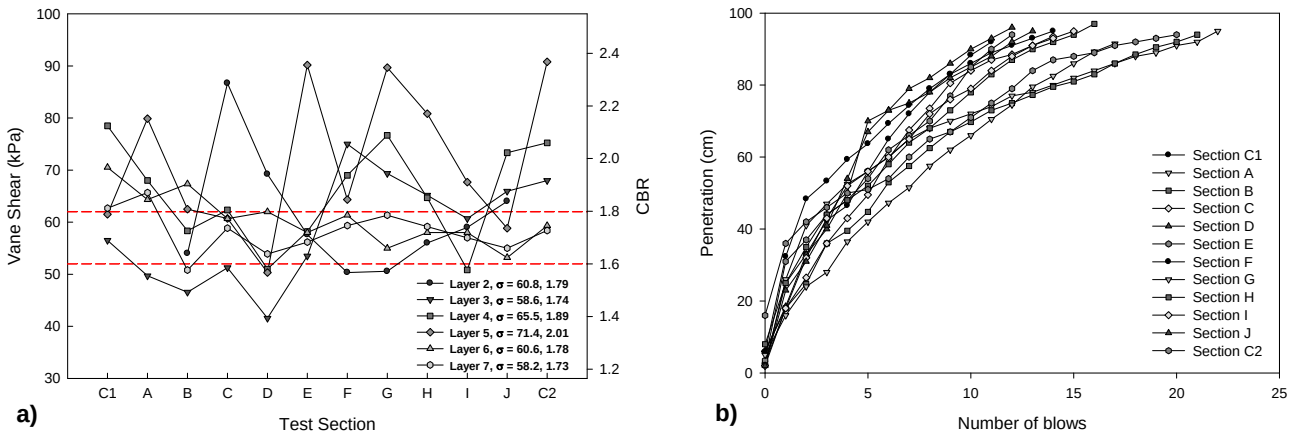

Figure 7. Average strength of artificial subgrade during construction: a) vane shear results, b) DCP results.

3.3 Installation of Geosynthetics and Instrumentation

Geosynthetics were installed by carefully rolling them out in the direction of traffic. Any wrinkles were removed by gently pulling on the end of the material. The edges of the geosynthetic were not staked in place. As indicated in Table 2, the widths of the geosynthetics varied between manufacturers; therefore, they were centered on the subgrade so that the vehicle would be centered on the material during trafficking and properly positioned in relation to the displacement and pore pressure sensors. The LVDTs were mounted in a box that was rigidly attached to the existing pavement away from the edge of the test pit. Lead wires were attached to the geosynthetic using the methodology outlined in Cuelho et al. (2008) to bring the point of measurement on the geosynthetic back to the sensor. An illustration of where the lead wires were attached is provided in Figure 8a. Individual lead wires were housed in small diameter brass tubes inside rigid, 13 mm, schedule 80 PVC pipes(Figure 8b), which were plumbed into the side of the sensor box. Data from the LVDTs is used to estimate strain in the

geosynthetic caused by rutting. A single measure of pore pressure was made within each test section to evaluate pore pressure development in the wheel path during trafficking. Pore pressure sensors were housed in the same box as the LVDTs, and 3 meters of rigid tubing was used to extend the point of measurement to a position 15 cm below the top surface of the subgrade directly in the wheel path. Porous ceramic stone tips were attached to the end of the tube and the entire system was fully saturated with de-aired water. Saturated subgrade soil was carefully packed around each stone during installation to keep air from entering the sensor and tubing arrangement. The same rigid 13 mm, schedule 80 PVC pipes were used to protect the pressure tubing from damage during construction and trafficking. Using these methodologies, all sensors were active and in good working condition after construction.

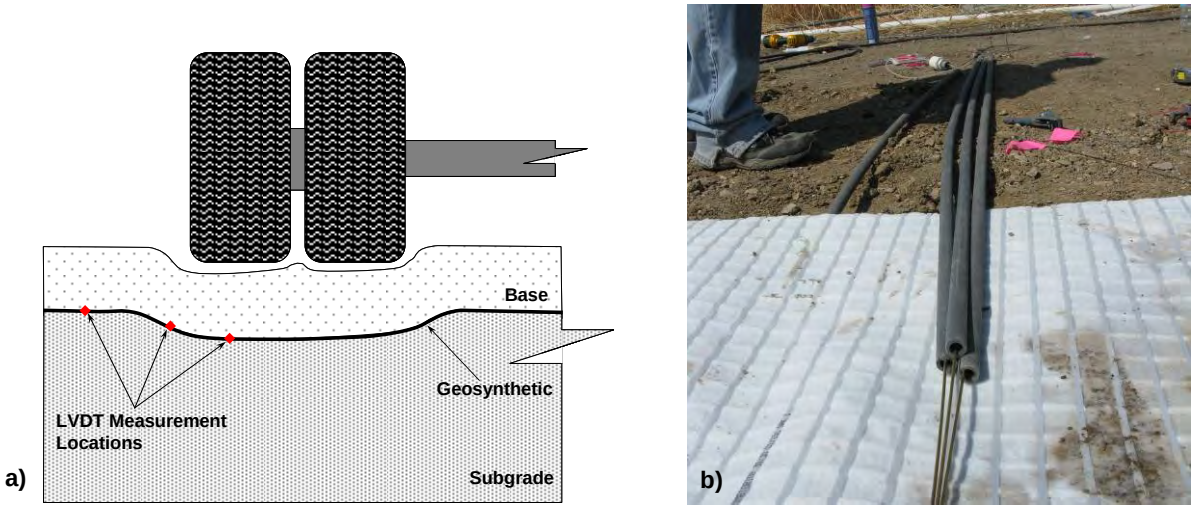

Figure 8. Displacement measurements: a) lead wire measurement locations, b) protective tubing.

Power to the sensors and data acquisition systems were provided by solar panels and batteries installed adjacent to the site. All wires to and from the sensors were run through PVC conduit to one of three centrally-located metal cabinets to protect them from damage during construction, as well as water and varmints.

3.4 Construction of the Base Course Layer

The base course aggregate was delivered directly adjacent to the test sections so that water could be mixed into it prior to compaction. After placement of the geosynthetics, installation of the instrumentation and preparation of the base course (Figure 9a), a single layer of base course aggregate 20 cm thick was placed on top of the geosynthetics from the side using a track-driven, skid-steer tractor (Figure 9b). The Installation of the base course aggregate was carefully monitored to prevent damage to the geosynthetics during construction. Final grading of the surface of the base course was done from the side using a road grader with an extended blade attachment so that the test sections would be in a virgin state prior to trafficking. A slight crown was put into the base course so that water did not accumulate on the finished surface. The same single-drum vibratory roller used to construct the artificial subgrade was used to compact the base aggregate. Three passes of the compactor were necessary to reach at least 90 percent of the maximum dry density (determined according to ASTM D 1557) along the entire length of the test section as measured using a nuclear densometer.

4. TRAFFICKING

Trafficking was accomplished using a fully loaded three-axle dump truck. A photo of the truck and the associated weights and dimensions of the vehicle are shown in Figure 10. The bed of the truck was filled with concrete blocks which were carefully loaded to ensure similar applied loads on each tire (tire pressures were approximately 690 kPa). Lines were painted on the gravel surface prior to loading so that the truck was properly positioned on the test sections. The truck traversed the test sections at approximately 15 kph.

Figure 9. Construction of base course: a) prior to placement of aggregate, b) during placement of aggregate.

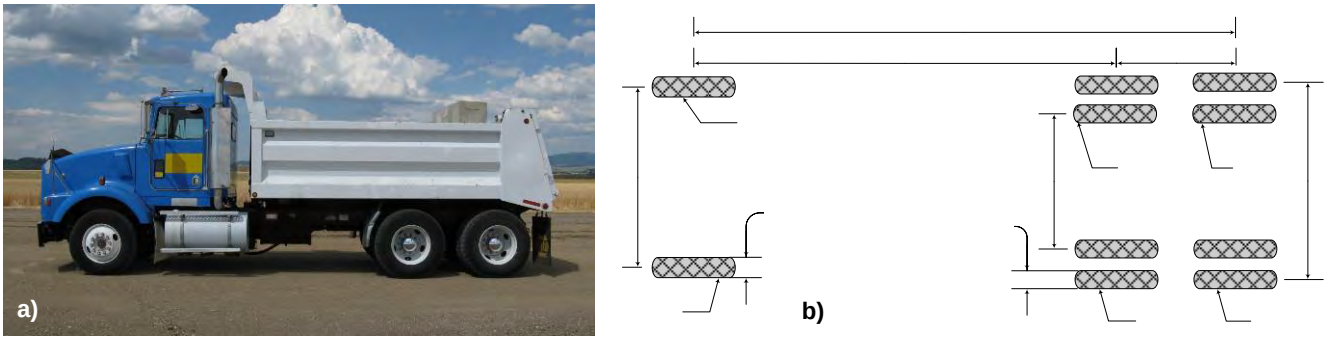

Figure 10. Three-axle dump truck used for trafficking: a) side view of vehicle, b) axle dimensions and associated weights.

5. DATA COLLECTION

The analysis of respective performance of each of the test sections will be based largely on rut depth. Therefore, rut depth was measured in each of the test sections at regularly scheduled intervals during the trafficking (more frequently in the beginning and less frequently toward the end) to capture rutting as a function of truck passes. The depth of the rut was measured in the two outermost wheel tracks of the rear wheels at one-meter intervals along the length of each test section using a digital level with ±1 mm accuracy. In this case, rut was a function of the difference in the elevation of the measurement points over time. Total rut, therefore, was determined by comparing current measurements to a baseline measurement which was made before trafficking. This type of rut may be referred to as “elevation rut”, as illustrated in Figure 11. The “apparent rut”, however, is typically greater and can be defined as the vertical distance from the upper crest of the rut bowl to the bottom of the rut bowl (Figure 11). The apparent rut is generally greater than the elevation rut because bearing failure in the soil beneath the wheel load is shoved outward and upward adjacent to the wheel path. Measurement of the transverse surface contour was also made during trafficking to attempt to quantify the apparent rut at a single location in each test section.

6. PRELIMINARY RESULTS

A maximum of 40 truck passes (120 axle passes) was necessary to cause an average of 10 cm rutting (elevation rutting) in the strongest test sections. As expected, the control sections on both ends of the test bed failed first. Even though the elevation rut in these areas was only 10 cm, the apparent rut was much greater which made it necessary to fill them with gravel so that the test vehicle could pass over without dragging or getting stuck. This procedure was also used on any of the other test sections that reached an average of 10 cm of elevation rutting. Sections C1, C2, J, E and I failed earliest (in that order), making it necessary to fill in the ruts in those sections to support further trafficking. After trafficking, forensic investigations were conducted to evaluate damage to the geosynthetic from trafficking as well as re-evaluate pertinent soil strength characteristics.

2.00 m

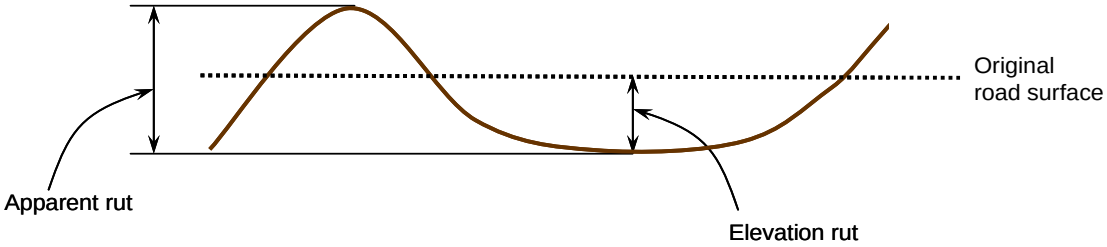

Figure 11. Illustration of rut measurements

6.1 Post-Trafficking Forensic Excavations

Forensic evaluations were located in areas that had experienced approximately the same rutting since a major component of this research was to evaluate damage to the geosynthetic due to trafficking. Therefore, elevation rut data was evaluated to find an area within each test section that had experienced approximately 10 cm average rut. Three of the eleven geosynthetic-stabilized test sections failed earlier than the rest which made it necessary to fill in the ruts with gravel to facilitate trafficking. In those cases, areas that had experienced an average of 10 cm of rut prior to filling were selected for forensic investigation. An area 1.5 meters wide (in the direction of traffic) and 4 meters long was selected in each of the test sections, including the control test sections. Transverse profiles of the edges of these areas were taken prior to and during excavation to evaluate rut shapes and layer thicknesses.

Excavation of the base course was accomplished using a large vacuum truck and a high-flow compressed air nozzle to minimize disturbance and damage of the geosynthetic (Figure 12a). After exposing the entire area of geosynthetics, they were carefully removed for future analysis which will include overall damage, junction survivability, junction strength, and tensile strength. Three DCP measurements were taken in the excavated area prior to removal of the subgrade. The subgrade was then removed from these areas (Figure 12b) to comprehensively evaluate soil mixing between the subgrade and base course in the rutted areas, soil shear strength using the vane shear, soil moisture contents and a general evaluation of the rutted area.

Figure 12. Forensic investigations: a) air and vacuum removal of base course, b) excavation of subgrade.

Horizontal vane shear measurements were taken at 10, 20, 40 and 60 cm below the subgrade/base course interface in each of the wheel paths and the center on each side of the excavated trench for a total of six measurements at each depth. In general, the upper layers (i.e., 10 cm and 20 cm depths) were within the specified range (average values of 58.4 and 58.7

kPa, respectively), as shown in Figure 13a. Lower layers were only slightly stronger making the overall range of predicted CBR strengths 1.74 to 1.92. Overall, subgrade strengths were relatively close to the specified ranges, thus making differences between test sections relatively small. DCP measurements were taken in each of the wheel paths and the center for a total of three measurements in each test section. The wheel path measurements were averaged together and the relationship of penetration to number of blows is shown in Figure 13b. Post-trafficking DCP measurements were very similar between all of the test sections.

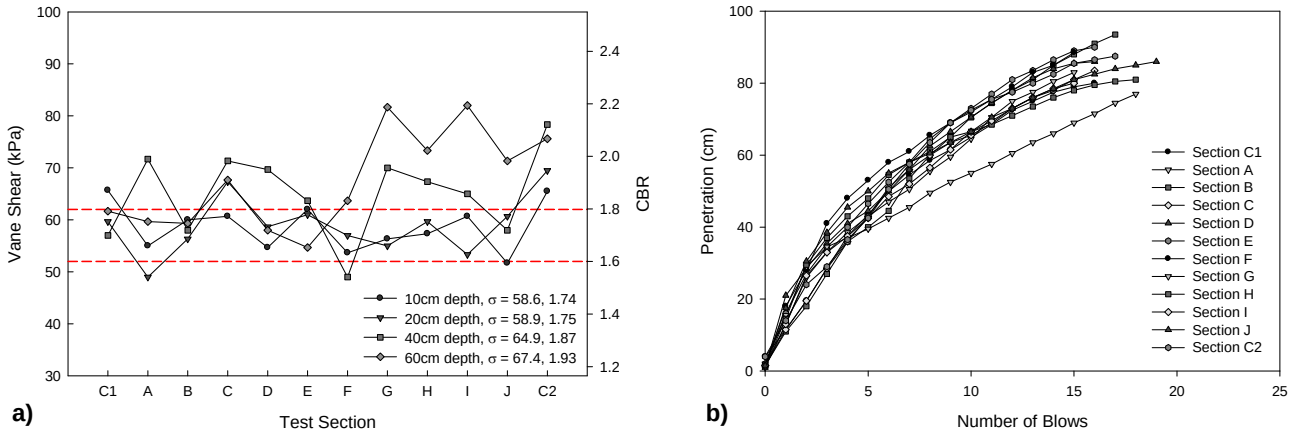

Figure 13. Average strength of artificial subgrade after trafficking: a) vane shear, b) DCP.

7. SUMMARY AND CONCLUSIONS

A full-scale test bed to evaluate the performance of ten different geosynthetics was constructed during the summer of 2008. Existing pavement and base materials were excavated to create a trench where an artificial subgrade was placed in a weak condition (CBR = 1.7 ±0.1). Vane shear, moisture content and DCP measurements were primarily used to monitor subgrade strength during construction and after trafficking. Results from these tests showed that the subgrade soil was indeed weak and generally similar between test sections, especially for the upper layers. Twenty centimeters of base course was placed on top of the geosynthetics as a structural layer and driving surface. The depth of the base course was determined using the FHWA U.S. Forest Service method. Other subgrade stabilization design methods will later be used to evaluate potential differences in design outputs. Failure (i.e., 10 cm of elevation rut) occurred in each of the test sections at or before 40 passes (120 axle passes) of a fully-loaded, three-axle dump truck, which was much less than the 1000 design axle passes expected from the geosynthetic-stabilized sections. The two control sections failed earliest, followed successively by sections J, E and I. The ruts in these sections were filled in to facilitate future traffic on the remaining test sections. Post-trafficking forensic excavations were conducted in areas containing similar rut at failure to facilitate a future assessment of damage to the geosynthetics during trafficking, junction survivability, junction strength, and tensile strength. Vane shear and DCP measurements were also taken to evaluate soil strength in the excavated areas after trafficking. A comprehensive analysis of the displacement data from the LVDTs, pore pressure data from pressure sensors, rut data and forensic excavations is still ongoing.

ACKNOWLEDGEMENTS

The authors would like to acknowledge the generous financial support for this project from NAUE GmbH & Co. KG, Montana Department of Transportation, and Western Transportation Institute University Transportation Center at Montana State University – Bozeman.

REFERENCES

Cuelho, E.V., Christopher, B.R., Perkins, S.W. (2008), Small Strain and Displacement Monitoring Methods for Geosynthetics under Monotonic and Cyclic Loading, *Geoamericas 2008 Conference*, IFAI, Cancun, Mexico.

FHWA (1995), Geosynthetic Design and Construction Guidelines, FHWA-HI-95-038, 417p.

Holtz, R.D., Christopher, B.R. and Berg, R.R. (2008) Geosynthetic Design and Construction Guidelines, U.S. Department of Transportation, Federal Highway Administration, Washington DC, Report No. FHWA-NHI-07-092, 592 p.

Hufenus, R., Rueegger, R., Banjac, R., Mayor, P., Springman, S.M., and Bronnimann, R., (2006), Full-Scale Field Tests on Geosynthetic Reinforced Unpaved Roads on Soft Subgrade, *Geotextiles and Geomembrane 24 (1)*, pp. 21–37.

Steward, J., Williamson, R. and Nohney, J. (1977), Guidelines for Use of Fabrics in Construction and Maintenance of Low-Volume Roads, USDA, Forest Service, Portland, OR.

Geosynthetics 2009
February 25-27 2009, Salt Lake City, Utah

"Green" Reinforced Soil Walls Using Geosynthetics: An Alternative For Ecological And Environmental Projects

M.P.Guerra Escobar, AMANCO-PAVCO. Geosistemas Pavco S.A., San José, Costa Rica.

ABSTRACT
For some projects the environmental and landscaping requirements have obliged the engineers and architects to look for novel methods of constructing retaining walls and slopes. The "Green" walls and slopes are constructed from soil reinforced with geosynthetics and facades made from UV-degradable sacks filled with organic material and vegetation to have a natural appearance This article provides a detailed description of the designs of the "Green" reinforced soil walls and slopes. These designs incorporate the use of various geosynthetics, including woven geotextiles to reinforce the soil, geodrains for the drainage both behind and within the walls, and permanent Turf Reinforcement Mats (TRMs) to protect the wall facade from erosion. Also presented are details of the construction process needed to ensure the stability of the wall. The article concludes with an analysis of the "green" reinforced soil walls highlighting the economic, technical and environmental advantages.

1. INTRODUCTION

Retaining soil walls and slopes reinforced with Geosynthetics present an alternative to traditional retaining wall solutions, such as walls of reinforced concrete or soil embankments in their natural angle of repose. Reinforced soil walls are challenging the more traditional constructions due to their economic competitiveness and their green environmental credentials. Additionally, the introduction of soil walls or slopes has permitted the construction of retaining walls in places where the load capacity of the foundation soil is not sufficient for rigid walls, or where there are space restrictions preventing the construction of soil fills or soil embankments at their natural angle of repose.

Geosynthetic reinforced soil walls or slopes are also attractive solutions because of the flexibility they provide, as their design can be adapted to suit a wide range of different loads, solicitations, geometries, landscape features and environments. Increasingly urban housing complexes and new tourist developments are emphasizing ecological awareness and care for the environment in their construction, and Geosynthetic reinforced soil walls are used as they meet the construction goals. For these types of projects we have developed a system for building "green" walls or slopes, which are geotextile reinforced soil slopes which have a uniform covering of vegetation on their facade to give a natural appearance. The resulting slope is attractive and as strong and robust as the traditional solutions which use concrete, block or stone facades.

The facades, of the so-called "green" walls, are made from UV-degradable sacks filled with organic soil and vegetation. Once the facade is finished, these sacks are covered with a permanent erosion control mat (Turf Reinforcement Mat) to guarantee the growth and development of the vegetation on the wall facade. The facade inclination for this type of structure must be no more than 80 degrees with respect to the horizontal, to guarantee the development of the vegetation on the wall facade. When the inclination is 70 degrees or less, the structure is analyzed as a reinforced soil slope and for inclinations between 70 degrees and 80 degrees, the structure is calculated as a reinforced soil wall.

The maximum height recommended for the "Green" reinforced wall or slope is 12 m in one block. If the height is greater than 12 m, it is recommended to design a wall or slope with different terraces, and a berm of 1m minimum between terraces. For example, for a 18 m wall, it is recommended to design 3 terraces each one of 6 m height with a 1 m berm between each terrace.

2. DESIGN METHODOLOGY

2.1 Overview

Soils have a high resistance to compressive forces but they give way easily under the application of tensile forces. However, soils may be reinforced with other materials, such as Geotextiles, which are specially designed to absorb tensile forces. Therefore, where we have a soil wall needing to resist both compressive and tensile stresses we can

obtain a structure of much greater resistance by including a suitable Geotextile within the soil mass. The extra strength provided is principally due to shear stresses produced by the friction between the Geosynthetic material and the adjacent layers of soil.

Various design methodologies exist for the reinforcement of soil walls using Geosynthetics. In our case, we use the methodology proposed by Robert M. Koerner (in "Designing with Geosynthetics", 4th Ed) and by Robert D. Holtz, Barry R. Christopher, Ryan R. Berg (in "Geosynthetic Engineering"). Fundamental to this methodology are the design principles of Whitcomb y Bell (1979), which state that you don't consider hydrostatic pressure in the design calculations and the active failure surface should be a plane surface defined by the Ranking methodology.

2.2 Stages of the Design Methodology

The design methodology for soil walls or slopes reinforced with Geosynthetics consists of three stages:

- Stage 1: Internal stability. In this stage the vertical space between layers is calculated as well as the correct length of reinforcing required to achieve the necessary resistance. The calculations must be based on the technical specifications of the Geosynthetic being used.

- Stage 2: External stability. In this stage the design must be reviewed to ensure adequate external stability. This stage analyses the overall structure using the Limit Equilibrium approach to verify the safety factors of Base Sliding, Overturning and Bearing Capacity.

- Stage 3: External conditions. In this stage the type of wall facade is specified and the conditions of drainage and sub-drainage analysed.

3. DESIGN FOR A "GREEN" REINFORCED SOIL WALL OR SLOPE

In order to describe the process of design for a Geosynthetic reinforced soil retaining wall or slope we will use the example of a slope designed and constructed in Costa Rica in January 2008. This slope was designed to have an erosion resistant facade of vegetation and for this it is referred to as a "green" reinforced soil slope.

3.1 Initial conditions

For the example of the reinforced soil slope that is described in this document, a stability failure of the initial slope occurred in October 2007 (October being the rainiest month in Costa Rica). Because of the failure, part of the road collapsed and some of the areas of the project had no access.

The failure was a landslide, typical of the soils of this region, which are a lateritic type, with a red color. When pore pressure increases the tear strength of this type of soils reduces, and it produces movement of the soil mass. The landslide was produced because of the saturation of the soils, due to the intense and almost constant rain of the previous months.

As a solution to the landslide, it was proposed to construct a Geotextile reinforced soil slope with a facade of vegetation, using the "Green" wall methodology. It was also important to construct a drainage system at the base and the rear of the slope. For this drainage we used a Gecomposite Drain as is described in section 3.5.

A superficial drainage system was necessary over the retaining slope and the terrain beside the slope, to control and avoid infiltration of water in the slope.

3.2 Design considerations

<u>Geometry dimensions:</u>

- Variable heights = 3.30m, 4.00m y 6.00m.
- Maximum height = 6.00m. (This is the height critical for the design.)
- Base = 0.8H (80% of the height) = 4.80 m.
- Total length = 80 m
- Facade inclination = 70 degrees (with respect to the horizontal)

<u>Loads:</u>

- Surcharge Load = 2.00 ton/m^2
- Vehicle loads on the wall were considered

Fill Material: reinforced soil

The fill material must meet or exceed these conditions:

- Properties of fill material (reinforced soil):
    - Cohesion : c = 0.1 Ton/m^2
    - Friction Angle : ϕ = 28°
    - Unit weight: γ_T = 1.70 Ton/m^3
- Minimum requirements for fill material (reinforced soil):
    - Plasticity Index < 10
    - Maximum particle size 75mm
    - Passing sieve #200 < 25% in weight
    - Laboratory CBR > 10%
    - Tested CBR expansion 0%
    - Organic material content 0%
- Minimum requirements for the compaction of the fill material:
    - Determined optimum humidity ω_{opt} y unit weight γ_{dmax} using the Modified Proctor
    - Compaction minimum 95% of the Modified Proctor
- Seismic acceleration in order to analyse pseudo-static = 0.20g
- Reduction factors and Overall Safety factors:
    - FR_{DI} = 1.5 for installation damages
    - FR_{CR} = 2.2 for creep
    - FR_{QD} = 1.0 for chemical degradation
    - FR_{BD} = 1.0 for biological degradation
    - FS_G = 1.3 factor of overall safety
- Reinforcement Woven Geotextiles used in design:
    - **Woven Geotextile T2400: Class 1 – Standard Specification AASHTO M288-05**
        - Wide – Width resistance (ASTM D-4595) = 41 kN/m
        - Tensile Grab strength (ASTM D-4632) = 1560 N
        - Tensile Grab elongation (ASTM D-4632) = 20%
        - Tear strength (ASTM D-4533) = 570 N
        - CBR Puncture strength (ASTM D-6241) = 6.2 kN
    - **Woven Geotextile TR4000: Class 1 – Standard Specification AASHTO M288-05**
        - Wide – Width resistance (ASTM D-4595) = 64 kN/m
        - Grab strength (ASTM D-4632) = 2570 N
        - Grab elongation (ASTM D-4632) = 22%
        - Tear strength (ASTM D-4533) = 810 N
        - CBR Puncture strength (ASTM D-6241) = 10 kN

3.3 Analysis results for internal stability

The internal stability analysis is made using in-house software for the design of soil reinforced walls. In this analysis the space between layers is defined as well as the type of Geotextile to be used and the length of Geotextile necessary for each layer. The results for the exemplar wall are shown in Table 1.

Table 1. Results for "Green" reinforced soil slope : Internal Stability

Layer #	Depth (m)	Space between layers (m)	Type of Woven Geotextile	Geotextile Wide -Width Resistance (kN/m)	Total Length of Geotextile (m)
	0.00				
26	0.40	0.40	T2400	41.00	4.80
25	0.80	0.40	T2400	41.00	4.80
24	1.20	0.40	T2400	41.00	4.80
23	1.60	0.40	T2400	41.00	4.80
22	1.80	0.20	T2400	41.00	4.80
21	2.00	0.20	T2400	41.00	4.80
20	2.20	0.20	T2400	41.00	4.80
19	2.40	0.20	T2400	41.00	4.80
18	2.60	0.20	T2400	41.00	4.80
17	2.80	0.20	T2400	41.00	4.80
16	3.00	0.20	T2400	41.00	4.80
15	3.20	0.20	T2400	41.00	4.80
14	3.40	0.20	T2400	41.00	4.80
13	3.60	0.20	TR4000	64.00	4.80
12	3.80	0.20	TR4000	64.00	4.80
11	4.00	0.20	TR4000	64.00	4.80
10	4.20	0.20	TR4000	64.00	4.80
9	4.40	0.20	TR4000	64.00	4.80
8	4.60	0.20	TR4000	64.00	4.80
7	4.80	0.20	TR4000	64.00	4.80
6	5.00	0.20	TR4000	64.00	4.80
5	5.20	0.20	TR4000	64.00	4.80
4	5.40	0.20	TR4000	64.00	4.80
3	5.60	0.20	TR4000	64.00	4.80
2	5.80	0.20	TR4000	64.00	4.80
1	6.00	0.20	TR4000	64.00	4.80

3.4 Analysis for external stability

For the analysis for external stability a number of factors must be taken into account. These factors include the, geotechnical characteristics of the foundation, backfill and reinforced soils as well as the static and dynamic conditions of the wall. For the purposes of this article, which is to highlight the overall design and construction process, the details of this stage are not important and so they are not included here.

3.5 Wall drainage and sub-drainage systems

- Wall drainage at the base and rear

  Adequate wall drainage can be achieved using a Geodrain at the rear of the wall and a drainage trench at the base. The trench should have a transverse section of 0.40 m x 0.30 m, with a perforated drainage tube of 4 inches in diameter. The Geodrain should be hung in strips 2 m wide, with 1 m spacings between the strips to prevent a failure surface at the rear. The 2 m wide strips of Geodrain should cover the full height of the wall.

  - Drainage Geocomposite used in design:

- **Geodrain:**
  - Non Woven Geotextile: Class 2 – AASHTO M288-05
    - Tensile Grab strength (ASTM D-4632) = 770 N
    - Tensile Grab elongation (ASTM D-4632) > 50%
    - Tear strength (ASTM D-4533) = 340 N
    - CBR Puncture strength (ASTM D-6241) = 2.4 kN
  - Geonet:
    - Density Polymer - HDPE (ASTM D-1505) = 0.94 g/cm^3
    - Compressive resistance (ASTM D-1621) = 1250 kPa
    - Thickness (ASTM D-5199) = 5 mm
  - Geodrain: Geocomposite
    - Hydraulic Transmissivity (ASTM D-4716) (i=1, 10kPa) = 2.5x10^{-4} m^3/s.m
    - Adhesion strength (ASTM D-413) = 1.4 pounds-force/in
    - Thickness (ASTM D-5199) = 6.5 mm

- Internal wall drains

  As with other types of wall it is recommended to include internal drains in order to remove any water that infiltrates the wall. One option for the internal drains is to use strips 0.5 m wide of Geodrain, with a length that is 2/3 that of the wall base. The drains should be put each 1.50 m (both horizontally and vertically).

3.6 Facade of UV degradable sacks, vegetation and turf reinforcement mat

In order to achieve a wall facade of uniform vegetation the following steps need to be followed:

Polypropylene sacks filled with organic rich soil are used as the base for the final covering of vegetation. The placement of these sacks in the wall facade should be carried out at the same time as the compaction of each layer of soil. This option is the most economic and represents a major construction benefit as it means that it is not necessary to use formwork at any stage in the construction process.

The sacks should only be filled to a third of their volume so that the soil filled part of the sack is 0.20 m in height, 0.35 m in width and 0.30 m in depth. The quantity of organic rich soil in each sack should be 0.021 m^3 (0.20x0.35x0.20 m^3).The sacks however need to be larger than this so that there is approximately 0.50 m of sack length at one end without filling which can be used as an anchorage when the soil is compacted over it. The connection between the Geotextile and the sacks is provided by gravity, and which is guaranteed by the soil compacted over the empty part of the sack.

To use this method of construction successfully it is very important that the vegetation is installed as soon as the wall construction is complete. Sacks must not be left exposed (without the benefit of a vegetative covering) for any more than a week. To ensure the correct growth of the vegetative covering a permanent erosion control mat (Turf Reinforcement Mat) must be placed on the outer surface of the wall. The principal functions of this mat are to improve the growing conditions for the vegetation and prevent the erosion of the organic material in the sacks.

- Permanent erosion control mat (TRM) used in design:

  - **Erosion control Mat TRM435: EPA – Turf Reinforcement Mat**
    - Tensile Strength (ASTM D-6818) = 2.6 kN/m
    - Tensile elongation (ASTM D-6818) = 50%
    - Thickness (ASTM D-6525) = 8.9 mm
    - Color = Green
    - Light penetration (%passing) (ASTM D-6567) = 40%
    - UV Resistance @ 1000 hrs (ASTM D-4355) = 80%
    - Flexibility (ASTM D-6575) = 16000 mg-cm

4. CONSTRUCTION PROCESS

The following photos show the details of the construction process for our “green” retaining soil wall, reinforced with a woven Geotextile.

Figure 1. Initial state: Failure of the existing soil and road

Figure 2. Preparation of the site for the construction of the wall

a) Strips of Geodrain at the rear of the wall

b) Drainage trench at the base of the wall

Figure 3. Wall Drainage Systems

Figure 4. Installation of sacks (filled to a 1/3 of their volume with organic soil) in the façade

Figure 5. Installation of the woven Geotextile and spread of the fill soil

a) Compaction of the fill soil with a standard roller compactor

b) Compaction of the soil in the face with a light vibrating plate

Figure 6. Compaction of the soil: density greater than 95% of Modified Proctor

Figure 7. Facade of the wall with sacks filled with organic soil

Figure 8. Vegetation seeds installed in each sack

Figure 9. Installation of the permanent erosion control mat: TRM435


Figure 10. Vegetative state of the facade two months after construction

Figure 11. Another example of a “Green” Reinforced Soil Wall four months after construction was finished

5. CONCLUSIONS

We have shown how “green” reinforced soil walls can be constructed from soil reinforced with Geosynthetics. An attractive vegetative facade is created by the use of UV-degradable sacks filled with organic rich soil and a permanent erosion control mat to protect the wall facade. These “green” walls are technically and economically attractive solutions for all retaining walls, but particularly for projects where the landscaping and the natural appearance of the walls is important.

From an economic perspective the walls are attractive as the cost of a reinforced soil wall is generally lower in comparison with traditional structures. Natural fill soil walls or embankments use a large amount of material in their construction but reinforced soil walls can be constructed with steeper slopes substantially reducing the amount of material needed, and so the wall cost. Whereas, when compared to rigid structure walls, the reinforced soil walls are usually cheaper due to the relative cheapness of the materials being used.

From a technical perspective the walls are attractive as all the construction materials are easily obtainable and the construction techniques used do not need any highly specialized equipment or workforce. Following the steps outlined in this article a “green” reinforced wall may be built by anyone with basic construction skills. Additionally, the reinforcement of the soil with Geosynthetics guarantees an improvement of the wall safety factor, in static and dynamic conditions, over that of a natural fill soil wall or embankment.

REFERENCES

PAVCO, Departamento de Ingeniería. *Manual de Diseño*. Sexta Edición.

AASHTO, American Association of State Highway and Transportation Officials, *Guide for Design of Pavement Structures*, 1993.

KOERNER Robert, *Designing with Geosynthetics*, Forth Edition.

AASHTO, *Geotextile Specification for HighwayApplications, AASHTO Designation: M 288-00*, American Association of State Highway andTransportation Officials, Washington, D.C (2000).

Holtz, R.D., Kovacs, W.D., *An Introduction to Geotehcnical Engineering*. Prentice – Hall , (1981).

Holtz, R.D., Christopher, B.R. and Berg, R.R.,*Geosynthetic Engineering*. BiTech Publishers Ltd., (1997).

IFAI, *A Design Primer: Geotextiles and Related Materials*. Industrial Fabrics Association International, USA (1992).

EPA, Storm Water Management for Construction Activities, USA (1992).

History, Performance and Design of Geotextiles in Levees

M.L. Woodward, P.E., New Orleans District, USACE, New Orleans, Louisiana, USA
J.L. Dendurent, P.E., TenCate Geosynthetics, Wichita, Kansas, USA

ABSTRACT
Geotextiles are a key element in building levees that will survive catastrophic storms. The geotextile-reinforced earthen levees in New Orleans performed remarkably well during Hurricane Katrina. With the current focus on updating their levee system to protect New Orleans from a 100-year storm event, the United States Corps of Engineers (USACE) may rely heavily upon geotextiles in their designs.

In addition to reinforcing levees and allowing existing levees to be built taller and more robust, geotextiles help reduce construction costs and reduce the size of or even eliminate stability berms. Geotextiles are also being used in innovative ways for recovery and immediate repair of damaged levees.

This paper will focus on the history, performance and future use of geotextiles in levees. It will include a review of literature and design methods, an examination of the performance of the geotextile-reinforced levees that survived Hurricane Katrina, and USACE design improvements.

1. INTRODUCTION

Most of the engineering focus in the aftermath of Hurricane Katrina has been on the failed levees, the causes of failure and how to improve levee design so that we do not experience similar calamities in the future. Little attention from the media, technical investigators and the general public has been focused to the levees that successfully withstood the similar storm surges and conditions as the levees that failed. For example, 9 miles (14.5 km) of the St. Charles levee and 7 miles (11.3 km) of the Jefferson Lakefront levee on the south shore of Lake Pontchartrain are reinforced with geosynthetics (Figure 1).

In a press release from the Industrial Fabrics Association International (IFAI) in April, 2008, the United States Army Corps of Engineers (USACE)-New Orleans District (NOD), stated that “both the St. Charles and Jefferson levees were loaded (filled by the storm) during Katrina and performed exceptionally. They were stable and the geosynthetic was inherent to their strength.” (Aho, 2008b)

USACE engineers have been among the pioneers in levee design who saw the merits of utilizing high-strength geotextiles to improve the stability of the levees and in the process save billions of dollars in construction costs, thousands of acres in land and years of construction time. USACE has continuously been at the forefront of innovation in the design of geosynthetic-reinforced embankments and levees on soft soils. As the USACE works to update the New Orleans levee system to withstand design storm events, they will continue using geotextiles as part of their routine design methods, and they are still partnering with industry leaders to improve public safety and refine the design of reinforced levees.

2. HISTORY OF GEOTEXTILES IN LEVEES

In the 1980s, the geosynthetics industry was small but established. Forward-thinking design engineers were looking at conventional designs in many areas of civil engineering and starting to see where geosynthetics could be used to improve such things as public safety, project lifecycles, constructability, feasibility and construction costs.

USACE engineers were among the first to use geosynthetics in a soft-soil embankment project. They designed and built a 26 ft (8 m) high embankment at the USACE’s dredged disposal site Pinto Pass in Mobile Harbor, Alabama in 1980 (Holtz, 2004). The foundation soils under the embankment had cohesions ranging from 50 psf (2.4 kPa) to 150 psf (7.2 kPa) (Fowler, 1981). As per Holtz (2004) this is an important case history because USACE documented and verified their design assumptions and procedures. They also emphasized that proper construction methods are absolutely crucial for successful construction of embankments on soft soils.

The USACE-NOD is credited with working with the geosynthetics industry to develop the high-strength geotextiles that USACE now routinely uses to reinforce hurricane levees. These geotextiles were first proposed for use on the New Orleans to Venice Hurricane Protection Project which “was stalemated because they could not raise the levee by

conventional methods. Raising would have made the levee fail into a drainage canal and they would have been forced to ruin a whole lot of wetlands". (Hall, 2003). Prior to beginning work on the 13 miles (21 km) of geotextile-reinforced

Figure 1 – Geotextile-Reinforced Levees in New Orleans area

hurricane levee, USACE-NOD constructed the first full-scale test section of a geotextile-reinforced hurricane levee to test the performance of the proposed design. The test section performed better than expected (Duarte et al., 1989) and the levee has performed well to date.

Since this first test section, USACE-NOD has been constructing and monitoring levee test sections and stretches of geotextile-reinforced levees. They use what they have learned to improve their design methodology and construction techniques.

2.1 USACE-NOD Test Sections

In order to better understand and improve the performance of geosynthetic-reinforced levees, USACE-NOD designed and monitored four major levee test sections, three of which are examined in this article.

2.1.1 "Reach A" Test Section

The "Reach A" geotextile-reinforced levee test section was constructed in 1986 between the towns of Nairn and Empire in Lower Plaquemines Parish in southern Louisiana as a prototype for a proposed 13 mile (21 km) enlargement of an existing levee between City Price and Tropical Bend. This levee is part of the New Orleans to Venice Hurricane Protection project mentioned above and is typically called "Reach A." (Figure 1). The geotextile-reinforced alternative was considered because raising the levee, by conventional methods, to the design storm height would have required a very large footprint and relocating the levee 120 ft (46.6 m) toward the Gulf side and into the marsh (Bakeer et al., 1988).

The geotextile-reinforced design showed that such a levee could be built by degrading and raising the levee on its existing alignment; saving time, money and land (Duarte et al, 1989).

Prior to this test section, it was well known that geotextiles could reinforce a levee embankment, reduce its footprint, control deformation and increase its stability. However, the actual design methods for geotextile-reinforced embankments still consisted mostly of conventional concepts of earth pressure and slope stability with minor modifications for the effect of the geosynthetic. They had also not been sufficiently field verified to give USACE-NOD the confidence they needed to build a large reinforced hurricane protection levee (Bakeer et al., 1988).

The potential benefits of buiding and monitoring the performance of a geotextile-reinforced embankment were significant enough to justify the expense of such a test section. The Reach A test section was successfully instrumented with inclinometers, settlement plates, piezometers and foil strain gauges. The instrumentation monitoring continued for two years after construction began and verified the assumption that this geotextile-reinforced levee design was feasible, safe and economical (Duarte et al., 1989).

The economic benefits of the geotextile-reinforced design on the 13-miles (21 km) of raised levee were (Bakeer et al., 1988):

- A 35% savings on the overall cost compared to the original design ($30.8 million savings)
- Reduction in construction time from 13 to 6 years (resulting in significant insurance savings to residents)
- A 97% reduction in marshland used for the levee (original estimates of 4,000 acres (1,619 ha) were reduced to 100 acres (41 ha)
- A 60% reduction in required construction materials

The contributions of the test section to ongoing reinforced soft-soil embankment design research were:

- The measured (mobilized) strains in the geotextile were less than half of the design strains (Bakeer et al., 1988)
- The reinforced levee design resulted in a smaller cross section which reduced the destabilizing (driving) forces and reduced vertical settlements (Bakeer et al., 1988)
- The observed maximum stresses as captured by the field instrumentation were not in the same location as the postulated failure plane during design (Duarte et al., 1989)
- A well thought instrumentation installation is essential for capturing and presenting meaningful (reliable and realistic) displacement and deformation profiles (Duarte et al., 1989)
- Provided data that helped refine and calibrate finite element analysis of geotextile-reinforced embankments (Bakeer et al., 1988)
- Provided data that were used in the development of new guidelines for future reinforced embankment design
- The settlement and deformation pattern at the fabric level followed that of the generation and dissipation of the observed pore water pressures (Bakeer et al., 1988)

After USACE-NOD completed the Reach A test section, the Plaquemines Parish Government reported that “The Plaquemines Parish Government wholeheartedly supports the U.S. Army Corps of Engineers in the use of the geotextile fabric to bring the New Orleans to Venice Hurricane Protection Levee up to grade and feels that the cost and time saved to complete this portion of the project (Reach A) was excellent.” (Petrovich, 1987)

2.1.2 Bonnet Carre Test Section (Chiu et al., 1988)

The Bonnet Carre Spillway test section was constructed in 1988-89 in St. Charles Parish prior to the construction of 7 miles (11.3 km) of the Jefferson Parish Lakefront Levee. The goal of this test section was to verify USACE's newly revised geotextile-reinforced levee design procedures. Similar to the Reach A levee, weak foundation soils and right of way concerns made the cost of constructing an unreinforced levee prohibitive. The cost savings already realized in Reach A and the potential cost savings in the Jefferson Parish Lakefront, St. Charles parish and West Bank levee projects provided justification for further full-scale research.

This test section consisted of an all earthen unreinforced section of levee (UI), a reinforced levee section with one layer of geotextile (RI) and a reinforced levee section with two layers of geotextile (RII), all built to a typical earthen levee height of 19 ft (5.6m) National Geodectic Vertical Datum (NGVD). Full-scale field pullout tests were also conducted at the test site using the borrow fill that would be used to construct the St. Charles and Jefferson Parish Lakefront Levees. USACE-NOD wanted to push all three test sections to failure, which they tried to do by excavating immediately adjacent to the levee toe. Table 1 summarizes the design geotextile strengths and the failures of the three sections.

Table 1. Bonnet Carre Spillway Test Sections

Section	Geotextile Strength Required at 5% Strain (lbs/inch / kN/m)	Failure Elevation (ft/m) (NGVD)	Failure Mode
UI - Unreinforced	NA	-7/-2.1	Catastrophic stability failure
RI - One layer of reinforcement	1250/219	-10/-3.1	Large widespread cracks with no displacement*
RII - Two layers of reinforcement	900/158 (Bottom layer) 400/70 (Top layer)	-10/-3.1	Very small cracks with no displacement**

*The strain in the geotextile in RI was less than 3% at failure. There was a concern about whether the geotextile reinforcement was stretched and tightened correctly.
**After small cracks appeared at Elevation -10 ft, the levee was repaired by dressing it up to full grade and section. It was excavated again down to Elevation -10 ft with no signs of failure.

Chiu et al (1988) observed and Napolitano (1994) stated that the "analyses indicate that these two levees (RI and RII) may have experienced a bearing capacity failure, or excessive lateral movement, and not the conventional rotational shear failure." This is important because it reinforced that all failure modes should be analyzed very carefully.

The economic savings and benefits realized from the Bonnet Carre test section for the mainline St. Charles Parish and Jefferson Parish Lakefront levees were similar to the benefits realized on Reach A.

The contributions of the Bonnet Carre test section to ongoing reinforced soft-soil embankment design research were:

- Two layers of reinforcement appear to be a more efficient "reinforcing pattern" than one layer
- Levees with two layers of geotextile can be easily and effectively repaired
- Often the assumed failure mode may not be the most critical one
- Failures of reinforced levees involve less significant consequences than failures of unreinforced ones under similar conditions
- Particular attention must be paid to the stress-strain characteristics of the soil and the geotextile to ensure that the two materials are compatible, as large movements in the soil may cause failures at correspondingly small strains in the geotextile

2.1.3 Westminster East-West Test Section (Varuso et al., 2005)

The Westminster East-West test section was constructed south of the Mississippi River between the towns of Westwego and Harvey, Louisiana to help USACE-NOD determine how to efficiently utilize geosynthetic reinforcement in earthen levee embankment design and construction. This test section was part of a levee project approximately one mile (1.61 km) long. An unreinforced section for this levee was analyzed in design but was determined to be expensive and difficult to construct.

USACE-NOD wanted to use monitoring data from this test section to derive a new design methodology that would account for the anticipated gains in shear strength of the foundation soil due to consolidation during and immediately following construction. USACE-NOD had observed in the past that consolidation, and thus subsequent shear strength gains, were more uniform underneath reinforced test sections. This shear strength gain was attributed to the rapid consolidation of upper strata resulting in less tensile force being transferred to the geotextile. USACE-NOD wanted to verify all their design assumptions using the field instrumentation data.

The test section had the same cross-section as the mainline reinforced levee but used reinforcement with a five percent (5%) strain strength of 5,822 lbs/ft (85 kN/m) instead of the 11,644 lb/ft (170 kN/m) reinforcement that was used in the mainline levee. The test section included geogrids and geotextiles, but since the focus of this article is on geotextiles and since a geotextile was proven to be the most cost-effective solution for the test section, all references in this article will pertain to the geotextile reinforcement.

Instrumentation for this test section was designed to provide data needed to develop a design methodology that would result in optimizing the use of the geotextile reinforcement's tensile strength. Soil samples were also taken 6 months after construction to further analyze gain in shear strength.

The economic savings and benefits realized from this test section were very similar to past geotextile-reinforced levees.

Its main impact to ongoing reinforced soft-soil embankment design was:

- Quantification of the magnitude of shear strength increase in the foundation of this test section and formulation of a method to account for it in design

- Verification that the increase in cohesive shear strength resulted in an increased factor of safety from 1.0 to greater than 2.0
- Verification that second lift construction costs could be reduced by up to 75% if the geotextile reinforcement is initially designed to support the loading conditions.

2.2 Design Guidance

As in other areas of civil engineering, design concepts using geosynthetics are still not included as standard design topics in many foundation and soft-soil embankment textbooks or design manuals. Likewise, USACE issued engineering manual, EM 1110-2-1913 Design and Construction of Levees (2000), does not include any discussion on designing or constructing levees with geosynthetics.

Like other agencies, such as the Federal Highway Administration (FHWA), USACE references a separate design manual, the Unified Facilities Critieria (UFC) Engineering Use of Geotextiles (USACE et al., 2004). The UFC Engineering Use of Geotextiles manual (2004) has one chapter dedicated solely to the design of geotextile reinforced embankments on soft foundations, following the basic design methodology of Holtz et al., (1997) and other industry-accepted geotextile-reinforced embankment design procedures. The following topics are addressed in the UFC Engineering Use of Geotextiles manual (USACE et al., 2004):

- Overall bearing capacity
- Slope stability
- Sliding wedge analysis for embankment spreading/splitting
- Analysis to limit geotextile deformation
- Determine geotextile strength parallel to the centerline of the levee
- Analysis of embankment settlements due to primary consolidation and plastic flow

The UFC Engineering Use of Geotextiles manual (USACE et al., 2004) is currently under revision and is scheduled to be published shortly. It is the authors' understanding that the basic design methodology on geotextile-reinforced embankment on soft soil foundations has not been significantly modified, but it has rather been updated to reflect more current constructability criteria.

Since 1995 (the date of the most recent technical changes to the UFC Engineering Use of Geotextiles manual), USACE-NOD has refined and improved the analysis, design and construction of geotextile-reinforced levees. They currently use a design procedure for reinforced levees similar to design methodologies of the UFC 3-220-08FA manual (USACE et al., 2004) with updates based on technology advances, improvements to industry-accepted design procedures, experience accumulated from test section monitoring data analyses and advances in construction methods.

The most significant design development that USACE-NOD has implemented is incorporating (or quantifying) the foundation shear strength gain during construction of a new geotextile-reinforced levee. This development is not yet included in any of their technical manuals. This reality will increase the calculated stability factor of safety of a levee (Varuso et al., 2005) and will reduce the required geotextile tensile strength, the size of the levee stability berms and right of way requirements.

Other design procedures that USACE-NOD has incorporated into their levee designs as a result of lessons learned from Katrina and the intense reviews that followed, are:

- Designing the geosynthetic reinforcement to support subsequent lifts that sometimes have to be constructed to reach long-term elevations. This has significantly reduced the cost, construction time and settlement of the subsequent lifts.
- Performing the design procedures using a number of different analytical methods to determine the possible failure modes of a reinforced levee and the needed geotextile modulus. This has increased the confidence in newly designed geotextile-reinforced levees by ensuring that possible failure modes are recognized and the geotextile is designed to withstand loading associated with critical failure planes.

3. PERFORMANCE OF GEOTEXTILE-REINFORCED LEVEES IN HURRICANE KATRINA

As stated in the introduction, the geotextile-reinforced levees all performed exceptionally well through hurricane Katrina. Both the Jefferson Parish Lakefront and the St. Charles Parish levees were inundated with storm surges but were not breached, while other parts of the greater New Orleans storm and damage reduction system failed. The only breach in a geotextile-reinforced levee was in the Plaquemines Parish Reach A levee due to erosion from overtopping and close proximity of a perpendicular canal. The failure was not attributed to a bearing capacity, slope stability or geotextile failure, and it is quite possible that the presence of the geotextile layer prevented deeper scour.

3.1 Plaquemines Parish Levee

3.1.1 Design

Reach A begins at the Buras Levee District MR&T Mainline Levee near City Price LA and extends to the B-1 hurricane levee in the vicinity of Tropical Bend, LA (Figure 1). The levee height ranges from elevation 11.0 ft (3.4 m) North American Vertical Datum (NAVD) to 14.5 ft (4.4 m) NAVD. The levee was built in two lifts on top of soils with cohesions as low as 150 psf. The typical levee enlargement cross section for Reach A consisted of a marsh side embankment with a wave berm. Floodwalls were constructed at the pumping stations. The base of the levee was constructed on one or two separated layers of geotextiles of varying strengths that were anchored in to the existing levee. A sand blanket was placed on the geotextile and covered with at least 2 ft (0.6 m) of clay. The additional layer of geotextile was used at structural locations, such as pipelines, where a 1.5 global stability factor of safety was required by USACE-NOD . The geotextile tensile strengths (at 5% strain) ranged from 1,070 lbs/in (187 kN/m) to 2,420 lbs/in (424 kN/m) on the protected side and 140 lbs/in (25 kN/m) to 1,860 lbs/in (326 kN/m) on the flood side of the levee. Figure 2 shows a typical geotextile-reinforced earthen levee section for Reach A. (USACE, 1987a)

3.1.2 Performance in Hurricane Katrina

During hurricane Katrina along Reach A, there was movement of the transition walls between the reinforced levee and the Hayes and Gainard Woods Pump Stations and a breach at Nairn at a floodwall which allowed a pipeline penetration. The only area where USACE- NOD had to replace a section of geotextile was at Homeplace, LA.

The hurricane protection levee at Homeplace, LA was significantly scoured during Hurricane Katrina and parish workers tenuously reconstructed the section shortly afterward. The levee section was damaged further after Hurricane Rita and the levee crown and slopes were replaced utilizing material from the adjacent levee crown. The as-built, geotextile-reinforced levee system was damaged in the area of the scour. In addition, the compaction and moisture control during the initial repairs was questionable and therefore the stability of the section was of concern. The permanent repair of the levee section entailed degrading the levee section on either side of the scoured area to the elevation of the geotextile. The geotextile was then replaced for that entire degraded section and the full levee embankment was reconstructed to include stability and wave berms.

It is the opinion of USACE-NOD that the geotextile did not fail to serve its purpose. The scoured down to the geotextile area (which was overtopped) was adjacent to a flood-side perpendicular canal. It is quite possible that the geotextile prevented scour beneath the base of the levee.

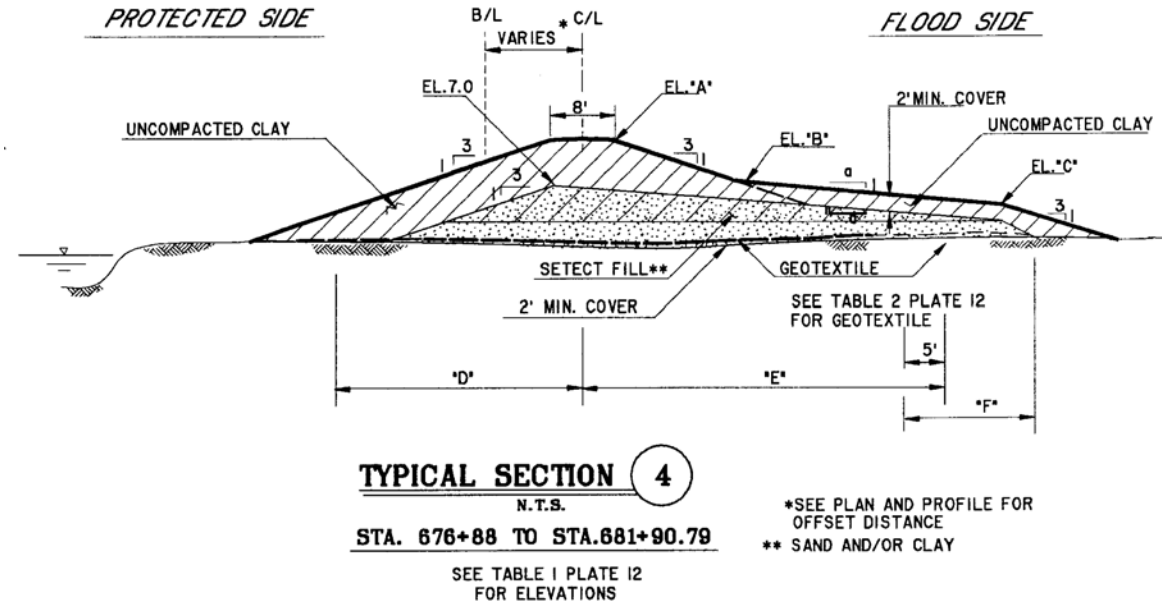

Figure 2 Typical Section of Reach A (USACE, 1987)

3.2 St. Charles Parish Levee, North of Airline Highway

3.2.1 Design (USACE, 1989)

The St. Charles Parish north of Airline Highway levee is located in St. Charles Parish on the east bank of the Mississippi river (Figure 1). It separates approximately 26,000 acres (10,522 ha) of wetlands from the developed areas of St. Charles Parish. The geotextile-reinforced levee was constructed of semi-compacted haul clay fill on a sand bed and reinforced by one layer of high strength geotextile (varying from 300 lbs/in (53 kN/m) to 700 lbs/in (123 kN/m) at 5% strain). The net levee grade elevation varies from 12.0 ft (3.7 m) NAVD to 13.0 ft (4.0 m) NAVD. The levee was built in two lifts over 15 years.

The design of the St. Charles levee utilized the results and advancements of the USACE-NOD test sections. The original levee design was revised to reflect knowledge gained from the Bonnet Carre test section, which demonstrated that the initial design was conservative. The new design accounted for foundation shear strength gain during construction. Shear strength testing after subsequent lift construction of the mainline levee validated assumed shear strength gains. Figure 2 shows a typical design section of this levee.

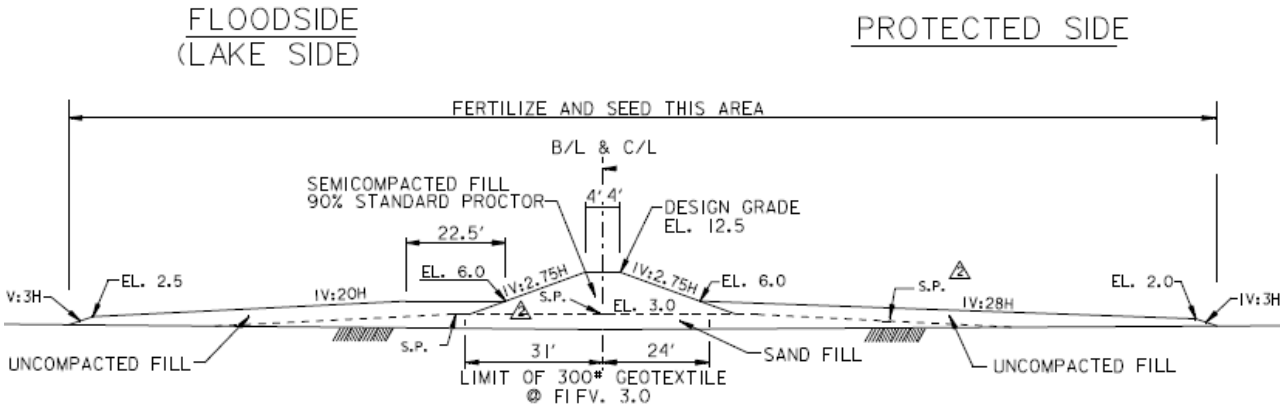

Figure 3 Typical Section St. Charles Parish Levee (USACE, 1989)

3.2.2 Performance in Hurricane Katrina

The St. Charles Parish levee experienced a storm surge during Hurricane Katrina lower than the surges along the south shore of Lake Pontchartrain where other types of levees failed. The St. Charles Parish levee was not breached or damaged during Hurricane Katrina.

3.2.3 Future

The St. Charles Parish levee is currently being raised to Elevation +14 ft (4.3 m) NAVD. A straddle enlargement is planned to raise the protection to Elevation +16.5 ft (5.0 m) NAVD mainly through the use of stability berms. The tensile strength of the existing geotextile is typically not high to provide additional benefit in the enlarged section or failure planes circumvent the existing geotextile.

3.3 Jefferson Parish Lakefront Levee

3.3.1 Design (USACE, 1987b)

The Jefferson Parish Lakefront Levee is located on the east bank of the Mississippi River. It is approximately 10.4 miles (16.4 km) in length and is bounded on the north by Lake Pontchartrain. The geotextile-reinforced portion of the levee is an enlargement of 9.4 miles (15.1 km) of the existing earthen levee to raise it to elevation +17 ft (5.2 m) NAVD. The high-strength geotextile (1,000 lbs/in (175 kN/m) to 2,010 lbs/in (352 kN/m) at 5% strain) was used to reinforce the soil foundation so that the levee could be brought to grade and section using the minimum amount of fill and no additional rights-of-way. The existing levee was degraded, the geotextile was installed and the levee was built up to final grade. Figure 4 shows a typical section of the Jefferson Parish Lakefront Levee.

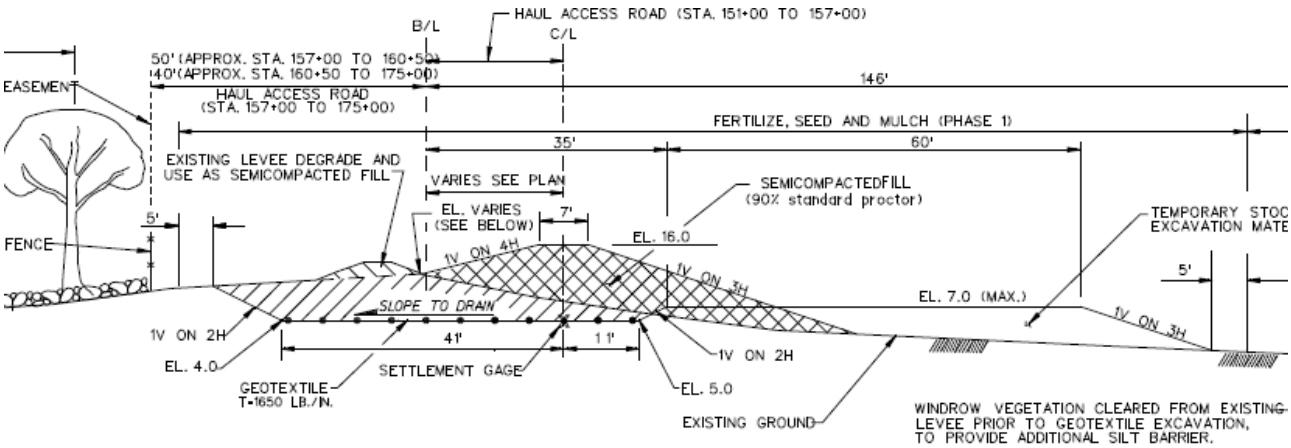

Figure 4 Typical Section Jefferson Parish Lakefront Levee (USACE, Nov 1987)

3.3.2 Performance in Hurricane Katrina

The Jefferson Parish Lakefront levee experienced a surge during Hurricane Katrina similar to the surges along the eastern south shore of Lake Pontchartrain where other types of levees did fail. The Jefferson Parish Lakefront levee was not breached or damaged during Hurricane Katrina.

3.3.3 Future

The Jefferson Parish Lakefront levee is currently being analyzed hoping that the existing geotextile will still provide some benefit and the levee can be raised using a straddle enlargement. An alternative under consideration is to move the levee centerline slightly towards Lake Pontchartrain.

3.4 Performances in Hurricanes Gustave and Ike

Damage assessments made after Hurricanes Gustave and Ike revealed no damage to the Reach A levee even though both storms loaded the entire 13 mile (4.0 km) stretch of levee. Damage assessments of both the St. Charles Parish and Jefferson Lakefront geosynthetic reinforced levees also revealed no damage to either levee subsequent to loading from both Hurricanes Gustav and Ike.

4. FUTURE DESIGN AND USE OF GEOTEXTILES IN LEVEES

In the USACE-NOD's efforts to bring the Greater New Orleans Hurricane and Storm Damage Risk Reduction System to design storm event flood elevations, geotextiles may incorporated into many of the enlarged and new levees in order to strengthen designs, reduce berm widths, save on fill material and subsequent lifts, reduce vertical settlement and reduce the amount of real estate needed for the levees.

4.1 Existing Design Methods

The design methodology used by the USACE-NOD for geotextile-reinforced levees analyzes several modes of failure including inadequate bearing capacity, slope stability failure, inadequate embedment/anchorage length of the geotextile, lateral embankment sliding/spreading, creep of geotextile, service life of geotextile, and inadequate seam strength and/or field overlap requirement of the geotextile. The design methodology also outlines potential for foundation strength gains and use of noncircular slope stability failure surfaces using limit equilibrium methods. These design improvements have not yet been incorporated into published USACE or UFC manuals. Numerical analysis of geotextile-reinforced sections and strength reduction over the time and life of geotextiles are being researched for future inclusion into design criteria.

4.2 Raising Levees Already Reinforced with Geotextiles

The basic alternatives for enlarging existing geotextile-reinforced levees include

- Degrading the existing levee down to its base, installing a new geotextile and rebuilding the levee to the design elevation. Due to construction durations and a June to December hurricane season, USACE-NOD prefers not to degrade long stretches of existing levee protection, thus limiting this option.

- Building directly on top of the existing levee with long berms for stability in lieu of a new geotextile
- Building a new levee on a different alignment

4.3 Raising Unreinforced Levees with Geotextiles

There are two viable scenarios for raising the elevation of existing unreinforced earthen levees using geotextiles without degrading the existing levee. Both alternatives are new reinforced levees constructed on the protected side of the existing levees, one behind an existing unreinforced earthen levee and the other behind an I-wall levee (Figure 5).

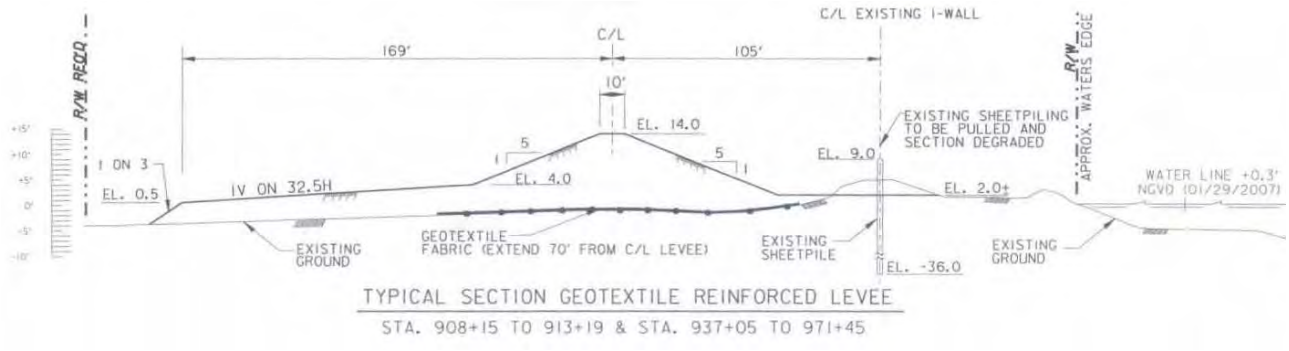

Figure 5 Typical Section of Reinforced Levee behind Existing I-Wall

4.4 Design Improvements

As discussed throughout this article, USACE-NOD has recently made the following design improvements for geotextile-reinforced levees:

- Higher factors of safety
- Incorporating (or quantifying) the foundation shear strength gain during construction
- Evaluation of more complex failure surfaces than previously used wedge or circular failure surfaces
- Designing the geotextile for the ultimate elevation of that levee and the loading required in the year 2057
- Setting an upper limit on the permissible geotextile tensile strength consistent with standard geotextile products

4.5 Construction Innovations

There have not been any major construction innovations on geotextile reinforcement placement as a result of Hurricane Katrina. USACE-NOD continues to specify and enforce strict construction standards to ensure that the benefits of the geotextiles are fully realized.

4.6 Research

The USACE and the geosynthetic industry have identified the following areas of research and testing as priorities that are relevant to geotextile-reinforced levee design and performance:

- The long term design properties of geotextiles used in levees
- Measurement of settlement of geotextile-reinforced levees
- Measurement of lateral spreading of the base of geotextile-reinforced levees
- A design methodology accounting for foundation shear strength gain during construction in geotextile-reinforced levees
- Numerical analysis and field verification of the actual failure modes and failure surfaces of geotextile-reinforced levees
- The use of geotextiles for prevention of piping damage
- The use of geotextiles for scour protection
- The use of geotubes in levees

Language authorizing the USACE Engineering Research and Development Center (ERDC) to conduct studies, testing and demonstration in some of these areas has been submitted in the Water Resources Development Act 2008 in the United States Congress. (Aho, 2008b)

5. CONCLUSION

Sprague et al. (1993) summarize the evolution of basic soft-soil embankment design and significant projects that demonstrated the acceptance of and major lessons learned from the use of high strength, high modulus geotextiles in this application to that time. Since then, the fundamental design approach has not changed significantly, but USACE-NOD has refined and advanced the design and state-of-practice of geotextile-reinforced levees considerably. These advancements could be beneficial to other entities (public and private) involved in levee design and embankment over soft-soil foundation applications.

The substantial influence of the USACE-NOD test section monitoring results analysis and the performance of the geotextile-reinforced levees through hurricanes Katrina, Gustave and Ike, as well as the lessons learned from Katrina, provide further evidence that geotextiles have greatly contributed in sustaining our infrastructure and protecting the public.

REFERENCES

Aho, A (2008b), *Language specifying use of geosynthetics submitted for water resources development act 2008*, Industrial Fabrics Association News Release.

Aho, A. (2008a), *Levees reinforced with geosynthetics perform exceptionally well*, Industrial Fabrics Association International, News Release.

Bakeer, R.M., Hadj-Hamou, T.A., Duarte, F.M., Satterlee, G.S. (1988), Field test of a geotextile-reinforced levee, *Journal of Geotechnical Engineering*, 26: 90-101.

Chiu, S.K., Napolitano, P.J., Duarte, F.M., (1988), Bonnet Carre spillway geotextile-reinforced test section and pullout tests report, United States Army Corps of Engineers-New Orleans District, 1-16.

Duarte, F.M., Satterlee, G.S. (1989), Case Study of a Geotextile Reinforced levee on a Soft Clay Foundation, *Geosynthetics '89 Conference*, San Diego, USA: 160-171.

Fowler, J. (1981), Design, Construction and Analysis of Fabric-Reinforced Embankment Test Section at Pinto Pass, Mobile, Albama, *Technical Report EL-81-7*, U.S. Army Engineer District, Mobile Alabama and Office, Chief of Engineers, U.S. Army, Washington D .C.

Haliburton, T.A., Fowler, J., Langan, J.P. (1980), Design and Construction of Fabric-Reinforced Embankment Test Section at Pinto Pass, Mobile, Alabama, *Transportation Research Board*, Transportation Research Record 749: 27-34.

Hall, J. (2003), Satterlee: Corps must rise to challenges, *Riverside Magazine*, United States Army Corps of Engineers (USACE), New Orleans District (NOD), January-February 2003: 3, 7.

Holtz, R.D. (2004), Geosynthetics R&D-The “Early” Days (1960s to Circa 1985), *Proceedings of the Koerner Research Symposium*, Drexel University, Philadelphia, Pennsylvania.

Holtz, R.D., Christopher, B.R. and Berg R.R. (1997), *Geosynthetic Engineering,* BiTech Publishers Ltd., Richmond, British Columbia, Canda.

Mylleville, B.L.J. and Rowe, R.K. (1991), On the design of reinforced embankments on soft brittle clays, *Geotechnical Fabrics Report*, May/June 12-24.

Napolitano, P.J. (1994) Levees Constructed on Soft Soils Using High Strength Geotextiles, *Proceedings of REMR Workshop on Levee Rehabilitation*, USACE, 105-129.

Petrovich, L.A. (1987), *Letter to the United States Army Corps of Engineers*, July, 1987.

Pinner, R.P. (1993), *St. Charles parish geotextile-reinforced levee instrumented section*, USACE New Orleans District, 2-14.

Nicolon Mirafi Group (1989), *“Reach A” Hurricane Protection Levee*, Case study.

Sprague, C.J. and Koutsourais, M. (1993), The Evolution of Geotextile Reinforced Embankments, *Proceeding from Grouting, Soil Improvement and Geosynthetics*, ASCE Geotechnical Specialty Conference, New Orleans, LA 1129-1141.

USACE, Naval Facilities Engineering Command, Air Force Civil Engineer Support Agency (2004), *United Facilities Criteria (UFC) 3-220-08FA Engineering Use of Geotextiles*.

USACE (1989), Design Memorandum No. 18 St. Charles Parish North of Airline Highway, *Serial No. 23*, Volume I.

USACE (1987a), Design Memorandum No. 1 Reach A City Price to Tropical Bend.

USACE (1987b), Design Memorandum No. 17 Jefferson Parish Lakefront Levee, Volume I.

USACE (2000), *Design and Construction of Levees, EM 110-2-1913*.

Varuso, R.J., Grieshaber, J.B., Nataraj, M.S. (2005), Geosynthetic reinforced levee test section on soft normally consolidated clays, *Geotextiles and Geomembranes 23,* Elsevier Ltd.: 362-383.

Pore Water Pressure Influence on Geosynthetic Stabilized Subgrade Performance

B.R. Christopher, Ph.D., P.E., Christopher Consultants, Roswell, Georgia, USA
S.W. Perkins, Ph.D., P.E., Montana State University, Bozeman, Montana, USA
B.A. Lacina, P.E., TenCate Geosynthetics, Pendergrass, Pendergrass, Georgia, USA
W.A. Marr, Ph.D., P.E., Geocomp Corporation, Boxborough, MA, USA

ABSTRACT
Surfaced and unsurfaced roadways underlain by weak subgrade typically experience distress in the form of rutting. Geosynthetics are commonly used for base reinforcement and subgrade stabilization to reduce rutting, thereby improving roadway performance. Weak subgrades are typically wet, nearly saturated fine-grained soils. Traffic loads produce a pore pressure increase in the subgrade that grows with traffic repetitions. Development of pore pressure reduces the effective stress in the subgrade and thereby reduces the subgrade stiffness and strength. The reduction of stiffness and strength can have a dramatic impact on the performance of the roadway as expressed in terms of rutting. The purpose of this paper is to display results from pavement box test sections where a weak, nearly saturated subgrade was used and instrumented with pore pressure transducers. The results show a significant increase in pore water pressure, which is influenced by the type of geosynthetic used for base reinforcement and/or stabilization. In most cases, the pore pressure developed was found to directly correspond to the surface deformation measurements in terms of both the rate and magnitude of rutting. Results from mechanistic-modeling are shown to illustrate how the effect of pore pressure might be accounted for in existing pavement modeling principles.

1. INTRODUCTION

Most of the current empirical design models for geosynthetics in roadway stabilization are based on bearing capacity theory with modifications for inclusion of the geosynthetic (e.g., Barenberg, 1975; Steward et al., 1977; Giroud and Noiray, 1981; and, Giroud and Han, 2004). In each of those methods, the subgrade soil is assumed to be saturated and exhibit undrained behavior under traffic loading. The design charts or the input values to computer programs contain a property of the subgrade (resilient modulus, undrained shear strength and/or CBR). This property represents a measure of the in-place subgrade prior to construction or trafficking of the roadway. However, field measurements of this property are likely to be made on partially saturated soil in a pre-trafficking condition. Thus, this initial value of stiffness or strength may not be the same after roadway construction or trafficking, as the soil could change in volume and thus water content due to compression. In addition, the soil may become saturated, again due to compression, and develop pore water pressure during repeated loadings, which will result in a reduction of subgrade stiffness/strength. The development of pore water pressure can thus occur in both saturated and unsaturated soil, but is most likely more pronounced in a saturated soil. As a result, the deformation response measured in the field or in full scale lab models may not match the design charts as has been reported in the literature (e.g., see Christopher et al., 2001). Measurement of excess pore water pressure during trafficking can be used to adjust and more accurately model the strength of the soil during trafficking.

In full scale box tests performed to evaluate geosynthetics used in both stabilization and base reinforcement, the authors have observed the development and increase in pore water pressure during cyclic loading (Perkins et al., 2004; Christopher and Lacina, 2008; Christopher and Perkins, 2008). As indicated in these references, the pore water pressure measurements in most of the tests were found to directly correspond to the performance of the geosynthetic with the largest amount of deformation per cycle occurring in the tests with the highest developed pore pressure (e.g., the control tests) and the best performing tests (least amount of rutting under the same number of cycles) showing the lowest amount of pore pressure. These results indicate that the performance of the geosynthetics vary with both the subgrade type and conditions (i.e., a geosynthetic may perform well in one condition and not so well under other conditions). Geosynthetics could influence the development and magnitude of pore water pressure through: 1) a reduction in stress in the subgrade (Berg et al., 2000); 2) separation, which would reduce point stress and corresponding pore pressure developed from gravel penetration into subgrade layers (Christopher and Lacina, 2008); and/or, 3) pore pressure dissipation in the plane of some geosynthetics when the in plane permeability is greater than the permeability of the base layer (e.g., poorly draining base layers containing fine grained soils) (Holtz et al., 2008).

In this paper, an example of pore water pressure developed during stabilization tests with and without geosynthetics is presented. Effective stress principles are then used to evaluate the influence of the pore pressure on the strength of the soil. The strength of the soil is then incorporated into a design model using mechanistic modeling to illustrating how the effect of pore pressure might be accounted for in design using existing pavement modeling principles.

2. EXAMPLE OF PORE WATER PRESSURE INFLUENCE ON STABILIZATION PERFORMANCE

Figure 1 shows example results from full scale laboratory stabilization tests with and without a geosynthetic. Figure 1a shows the response to cyclic loading in terms of the permanent surface deformation plotted against number of load cycles to log scale. Figure 1b shows the dynamic deformation plotted against log of load cycle and Figure 1c gives the excess pore pressure in the upper portion of the subgrade beneath the load plate as reported by Perkins et al., 2008. The geosynthetic was a polypropylene fibrillated filament woven geotextile, $GT_{w\text{-}f}$. The subgrade soil was brown sandy silt (ML-MH). The subgrade has a standard Proctor maximum dry unit weight of 97 lb/ft^3 and an optimum moisture content of 22 %. The material was placed at a moisture content of approximately 36 %, which produced an in-place CBR of 1. Vane shear tests on in-place material produced a strength of 30 kPa (620 psf) in both sections. The in-place unit dry weight and moisture content was approximately 85 lb/ft^3 and 36 %, respectively. The base course aggregate was a graded aggregate meeting the Georgia Department of Transportation specifications. The material has a maximum dry unit weight of 145 lb/ft^3, an optimum moisture content of 5.4 %, and a drained friction angle of 43 degrees. The material was placed at a moisture content of 6 % and at an average dry unit weight of 136 lb/ft^3. The complete details of the test program are reported by Christopher and Lacina, 2008. As can be seen from Figure 1c, the pore water pressure measured in the control test section was significantly higher than in the geotextile test section. These measurements indicate that strength of the soil, although the same in both sections at the beginning of the test, was reduced during repeated loading, with a much greater strength loss occurring in the control section.

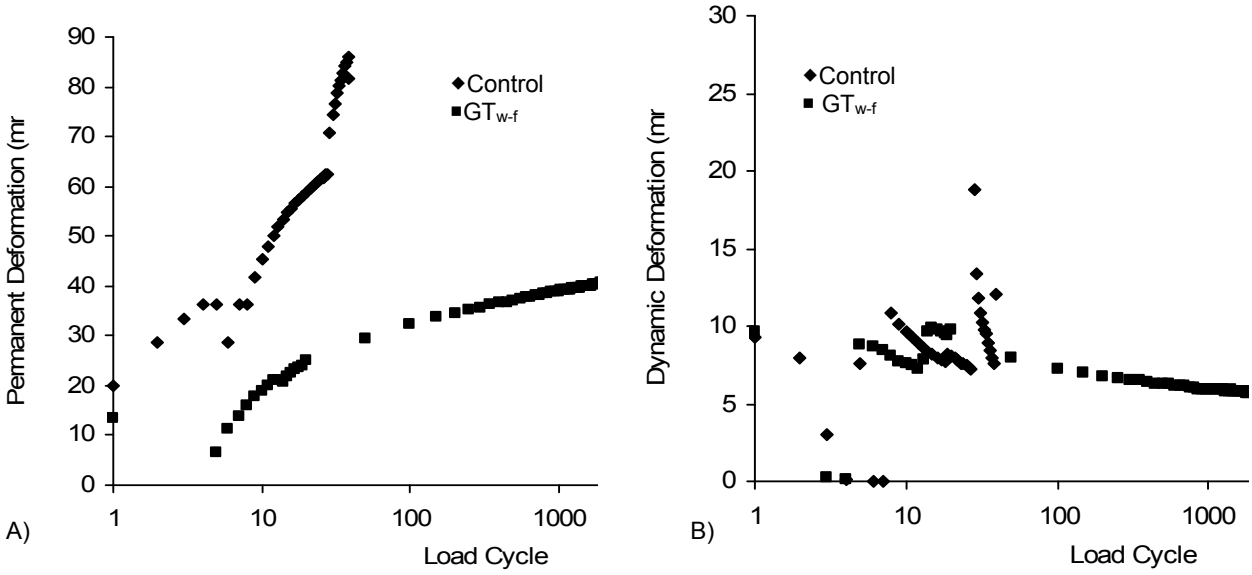

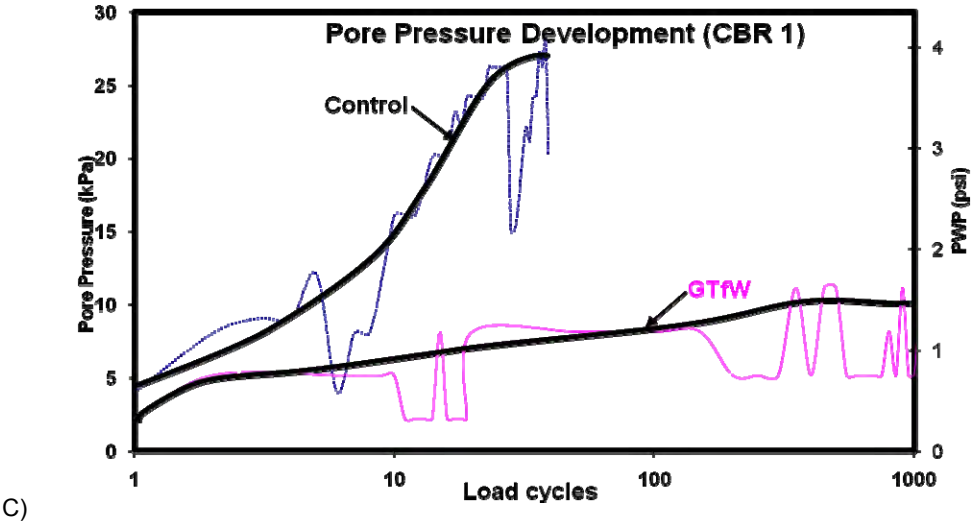

Figure 1. Representative Large Scale Box Test Results for control and a woven geotextile showing the load cycles versus a) Permanent Surface Deformation b) the dynamic deformation, and c) the excess pore pressure in the top of the subgrade

3. SOIL STRENGTH IN RELATION TO PORE WATER PRESSURE

The influence of pore water pressure on the strength of the soil can be computed from well established soil mechanics effective stress principles (e.g., Lambe and Whitman, 1969). Figure 2 shows a Mohr-Coulomb diagram for a normally-consolidated clay having an effective cohesion of zero and an effective friction angle of ϕ'. An element of the subgrade soil prior to roadway construction can be characterized by an initial state of stress with zero pore water pressure. This state of stress is represented by point *i* in Figure 2 having total and effective stresses given by $\sigma'_{1i} = \sigma_{1i}$ and $\sigma'_{3i} = \sigma_{3i}$. If this sample was sheared in an unconsolidated-undrained conventional triaxial compression test, it would result in an undrained shear strength given by S_{ui}, and with total and effective stresses as given in Figure 2 and where the additional subscript *f* denotes failure. The pore water pressure developed during undrained shear is given by u_{ti} and is equal to:

[1] $$u_{ti} = \sigma'_{3i} - \sigma'_{3i-f}$$

Skempton's pore water pressure equation can be used to relate the excess pore water pressure, u_{ti}, to the increase in total stresses during triaxial loading:

[2] $$u_{ti} = B\Delta\sigma_3 + A_f(\Delta\sigma_1 - \Delta\sigma_3)$$

where A_f denotes the pore water pressure parameter *A* at failure. For triaxial loading, $\Delta\sigma_3 = 0$ and equation 2 reduces to:

[3] $$u_{ti} = A_f \Delta\sigma_1$$

Furthermore, in a triaxial test, $\Delta\sigma_1$ is equal to the diameter of the total stress Mohr's circle, which can be expressed in terms of the total major and minor principal stresses, which in turn is equal to two times the undrained shear strength:

[4] $$\Delta\sigma_1 = \sigma_{1i-f} - \sigma_{3i} = 2S_{ui}$$

The effective stress equation can be used to relate the minor principal stresses to the excess pore water pressure:

(5) $$\sigma'_{3i-f} = \sigma'_{3i} - u_{ti}$$

Substitution of equation 3 and 4 into 5 results in:

(6) $$\sigma'_{3i-f} = \sigma'_{3i} - 2A_f S_{ui}$$

The undrained shear strength is by definition:

(7) $$S_{ui} = \frac{\sigma'_{1i-f} - \sigma'_{3i-f}}{2}$$

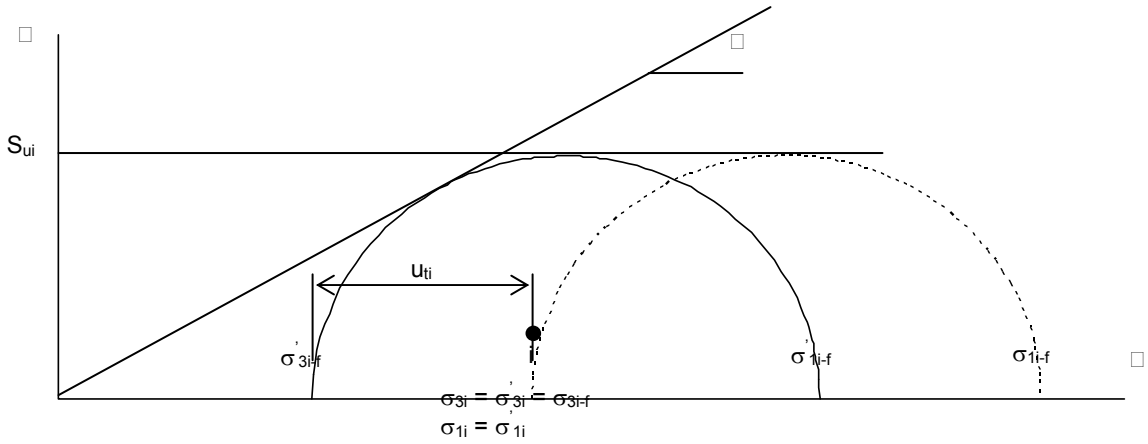

Figure 2. States of stress and undrained shear strength for pre-construction subgrade

The major and minor effective principal stresses at failure can be related to the friction angle by the equation:

(8) $$\sigma'_{1i-f} = \sigma'_{3i-f} \tan^2(45 + \phi/2)$$

Substitution of equation 8 and 6 into 7 and solving for σ'_{3i} gives:

(9)
$$\sigma'_{3i} = S_{ui}\left[\frac{2}{\tan^2(45+\phi/2)-1}+2A_f\right]$$

After roadway construction and trafficking, an excess pore water pressure (u_e) is developed, which is the excess pore water pressure in an unloaded state that develops after repeated trafficking. For the same element of subgrade as examined above, if the total stresses of the post-trafficked sample are unchanged, the effective stresses are reduced by u_e. This sample now has a state of stress given in Figure 3, with u_e given by:

(10)
$$u_e = \sigma'_{3i} - \sigma'_{3f}$$

If this sample is now sheared in an unconsolidated-undrained conventional triaxial compression test, lower undrained shear strength (S_{uf}) will result. By following the same procedure as detailed above, it can be shown:

(11)
$$\sigma'_{3f} = S_{uf}\left[\frac{2}{\tan^2(45+\phi/2)-1}+2A_f\right]$$

Substitution of equations 9 and 11 into 10 results in:

(12)
$$u_e = (S_{ui} - S_{uf})\left[\frac{2}{\tan 2(45+\phi/2)-1}+2A_f\right]$$

Based on consolidated undrained triaxial tests with pore pressure measurements, the subgrade soil has an effective friction angle of 30 degrees and a typical value of A_f of 0.7. Thus, for this subgrade equation 12 reduces to:

(13)
$$u_e = 1.4(S_{ui} - S_{uf})$$

This overly simplified example illustrates the important role that build up of pore pressure from the repeated loading has on the undrained shear strength of the subgrade material. Actual performance is complicated by the facts that A_f for the soil may change with repeated loading and the excess pore pressure may dissipate if the repeated loading is spread out over time so that excess pore pressures can drain away.

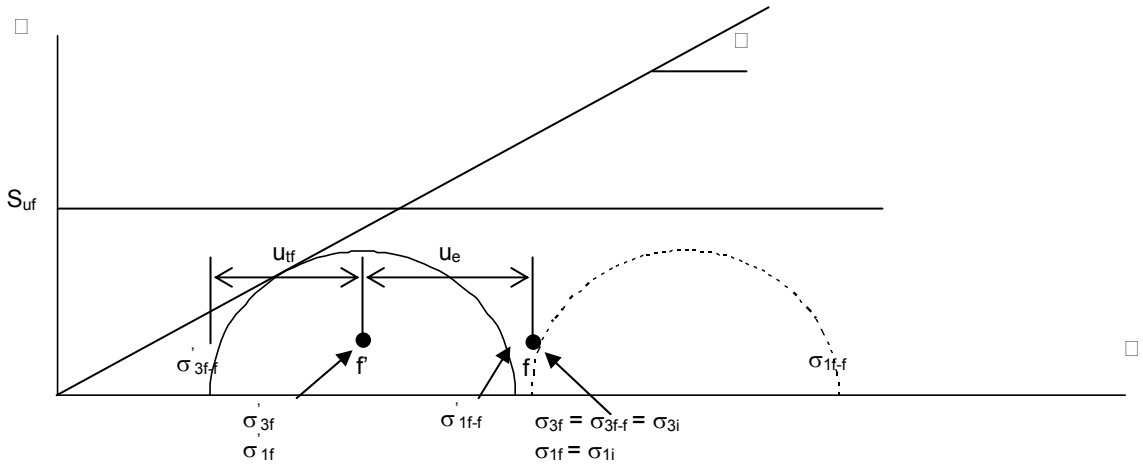

Figure 3. States of stress and undrained shear strength for post-construction and trafficking subgrade

4. ACCOUNTING FOR PORE WATER PRESSURE IN DESIGN

After construction, the subgrade had an undrained shear strength of 30 kPa (4.4 psi) as measured from a vane shear test. In the unreinforced test section, the excess pore water pressure is seen in Figure 1c to increase by an average value of approximately 28 kPa (4.0 psi). This reduces the effective stresses in the subgrade and results in a lower value

of undrained shear strength and stiffness. Using Equation 13, an increase in pore water pressure of 28 kPa results in an undrained shear strength of 10 kPa (1.4 psi).

Resilient modulus and permanent deformation testing on the subgrade material showed that the subgrade has an elastic modulus between 5.5 to 6.9 MPa (800 to 1000 psi) prior to testing. The pore-water pressure build-up in the subgrade layer of the unreinforced test section results in a reduction of both strength and stiffness of the subgrade. If the decrease in undrained shear strength is assumed to be proportional to the decrease in elastic modulus, then the material will have a new modulus of 1860 kPa (270 psi).

The authors used this lower subgrade modulus as an input value in a mechanistic design model for the subgrade (Perkins et al., 2008). The response model results in terms of dynamic deflection were found to match the observed value of approximately 8 mm shown in Figure 1b, while use of the initial modulus of the subgrade (0 pore water pressure) resulted in an overly stiff response with a dynamic deflection that was much less than the observed average value. Reinforced response model modules corresponding to compaction, traffic 1, traffic 2 and traffic 3 modules were created, where these modules were described by Perkins et al. (2004). The compaction module describes the increase in lateral confining stress in the base aggregate during the compaction of the aggregate. The traffic 1, 2 and 3 modules are used to define the build-up of lateral stress in the aggregate during traffic loading of the section. From the unreinforced and reinforced response models, the distribution of dynamic vertical strain with depth through the base aggregate and subgrade layers was determined and used in a damage model for rutting, as described in the paper by Perkins et al. (2008). For the reinforced test section, the excess pore water pressure was approximately 7 kPa (1.0 psi). Using the same approach described above, the elastic modulus of the subgrade for the reinforced test section was 4600 kPa (667 psi). Following guidelines established by Perkins et al. (2004), the cyclic elastic modulus of the geotextile in the machine and cross-machine directions and the material's Poisson's ratio was used to determine an equivalent isotropic elastic modulus of 790 MPa (115 ksi). Figure 4 shows the predicted results of the unreinforced and reinforced section as compared to the test results. The steps taken to account for the reduced excess pore water pressure in the reinforced test section as compared to the unreinforced section accounted for approximately 80 % of the reduced rutting. An additional 20 % is accounted for by the effects of the reinforcement. Overall, the predicted rutting using the reinforced model is greater than that seen in the reinforced test section but shows considerable improvement as compared to the unreinforced section and is regarded as a favorable and successful prediction.

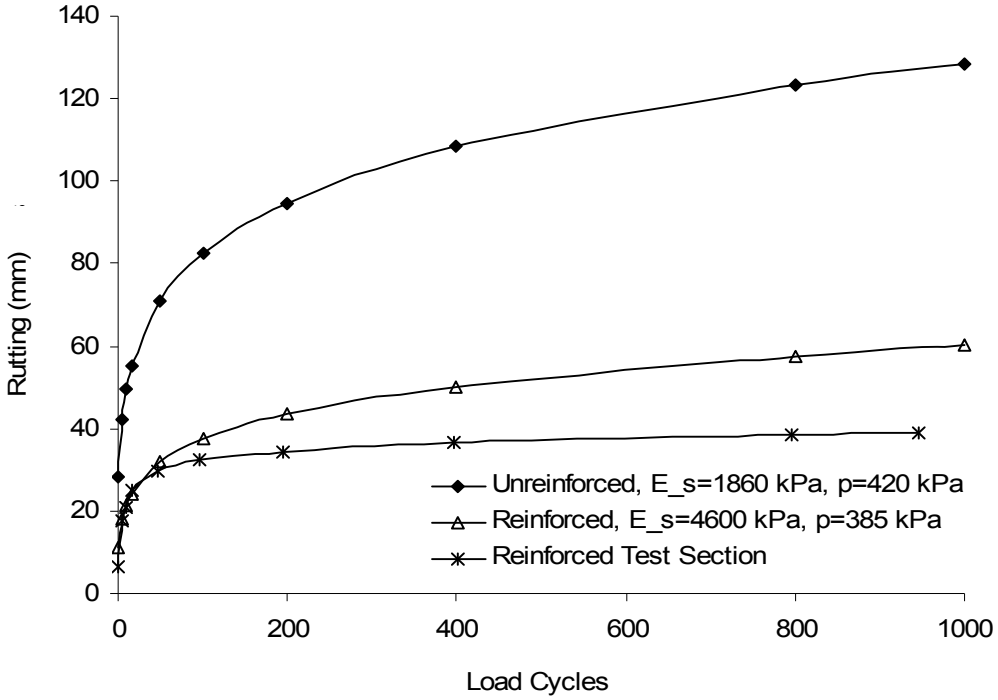

Figure 4. Unreinforced and Reinforced rutting predictions and comparisons

5. DEVELOPMENT OF DESIGN CHARTS WITH CONSIDERATION FOR PORE WATER PRESSURE

Traditional design charts can be modified to account for specific subgrade conditions to include the effect of pore water pressure build up during trafficking though the use of mechanistic-empirical design as discussed in the previous section. As an example, unreinforced design curves were developed for the silt type subgrade used in the example test section shown in Figure 1 (see Perkins et al., 2008 for complete details and input parameters for the mechanistic design model). The base line charts used for comparison were the design charts by Barenberg, 1975 and United States Forest, USFS, curves (Steward et al., 1977). Models of four cross sections having an aggregate thickness of 1000 mm, 760 mm, 500 mm, and 300 mm (40, 30, 20 and 12 in.) were created and analyzed. For simplicity, the stiffness value in the model is taken to be the subgrade resilient modulus at the end of trafficking when the pore water pressure build up is the greatest. Equation 13 was used to determine what u_e needed to be for each of the four model runs to gives an S_{ui} matching the traditional design curves for the S_{uf} used in the model. This results in values for u_e shown below in Table 1.

The four unreinforced models were analyzed by varying the subgrade resilient modulus until 75 mm (3 in.) of rut were developed in 1000 passes of the 45 kN (9000 lb) wheel load inflated to 550 kPa (80 psi). Figure 5 shows the design chart with values of subgrade CBR and resilient modulus plotted against the aggregate thickness for these four sections as compared to the original Barenberg design chart and the USFS design curve. In the evaluation of these cross-sections, the permanent deformation properties of the subgrade were varied as the resilient modulus varied. Principles contained in El-Basyouny et al. (2005) were used to adjust the subgrade permanent deformation properties. The difference in the subgrade CBR between the mechanistic-empirical model and the traditional design curves is due to the effect of pore water pressure build up during trafficking. The adopted approach was to assume that the initial subgrade CBR should lie on the traditional unreinforced design curves and that the difference between the final (model value) and initial (traditional design curve) undrained shear strength was due to the increase in pore water pressure during trafficking.

The authors are currently creating the reinforced design charts using both the data from the tests sections and the mechanistic-empirical model approach described previously in section 4. The result for the singular data point described in the previous section for a cross section with 12 inches of gravel is shown on Figure 1. Traffic loads on these sections were modeled identically to that for the unreinforced cross sections. Additional cross sections will be evaluated and the complete charts published in a future paper.

Table1: Initial and final shear strength and excess pore water pressure for unreinforced model cross-sections

Model Aggregate Thickness (in)	Initial Undrained Shear Strength, S_{ui} (kPa)	Final Undrained Shear Strength, S_{uf} (kPa)	Excess Pore Water Pressure, u_e (kPa)
40	6.80	6.08	1.01
30	14.70	10.53	5.84
20	26.30	17.83	11.86
12	55.00	39.43	21.80

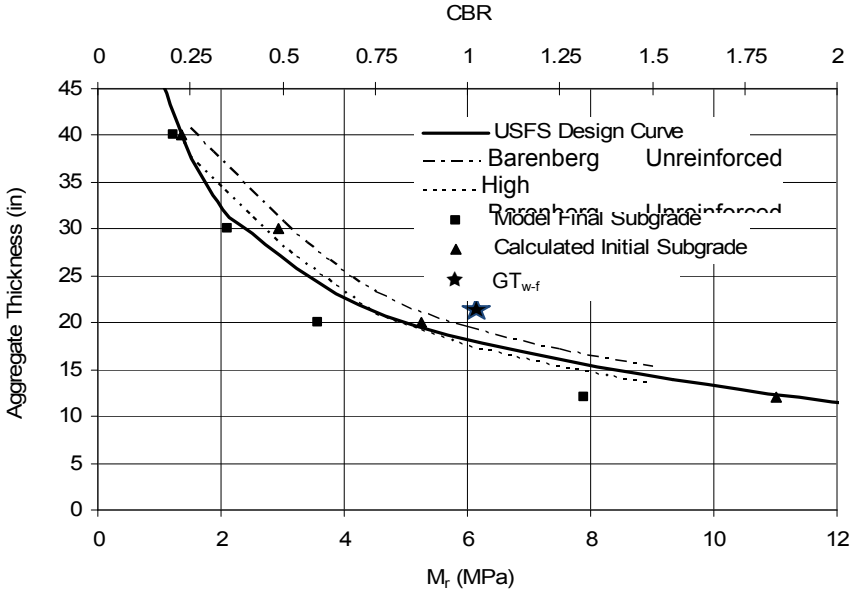

Figure 5: Model final subgrade CBR versus aggregate thickness with consideration for pore water pressure.

6. CONCLUSION

The laboratory test sections indicated that pore water pressure development played a significant role in the rutting behavior of the test sections. In the mechanistic-empirical modeling, pore water pressure development can be accounted for by adjusting the shear strength of the soil based on the effective stress principle of soil mechanics. Pore water pressure can be empirically included in design charts by matching unreinforced results to previously established design curves and then extending these results to reinforced sections using a reduced pore pressure development consistent with that observed in test sections. The mechanistic-empirical technique appears to work well for unpaved roads experiencing on the order of 1000 wheel passes for 75 mm of rutting, as long as the influence of pore water pressure is included in the analysis.

REFERENCES

Barenberg, E.J., Hales, J., and Dowland, J. (1975). Evaluation of Soil-Aggregate Systems with MIRAFI Fabrics, UILU-ENG-75-2020 Report for Celanese Fibers Marketing Company, University of Illinois, Urbana.

Berg, R.B., Christopher, B. R. and Perkins, S., Geosynthetic Reinforcement of the Aggregate Base/Subbase Courses of Pavement Structures, prepared for American Association of Highway and Transportation Officials Committee 4E, Prepared by the Geosynthetic Materials Association, 2000, 176 p.

Christopher, B.R., Berg, R.R., Perkins, S.W. (2001) Geosynthetic Reinforcements in Roadway Sections National Cooperative Highway Research Program, NCHRP Project 20-7, Task 112, FY2000, Transportation Research Board, National Academy Press, Washington, D.C., 2001.

Christopher, B.R. and Lacina, B., "Roadway Subgrade Stabilization Study", Proceedings of GeoAmericas 2008, Cancun, Mexico, 2008, International Geosynthetic Society, pp. 1013–1021.

Christopher, B.R. and Perkins, S.W. (2008) "Full Scale Testing of Geogrids to Evaluate Junction Strength Requirements for Reinforced Roadway Base Design," Proceedings of the Fourth European Geosynthetics Conference, Edinburgh, United Kingdom, International Geosynthetics Society.

El-Basyouny, M.M., Witczak, M. and Kaloush, K. (2005), "Development of Permanent Deformation Models for the 2002 Design Guide", *Transportation Research Board 2005 Annual Meeting Preprint*, 23p.

Giroud, J.P. and Noiray, L. (1981). *Geotextile-Reinforced Unpaved Roads*, Journal of the Geotechnical Engineering Division, American Society of Civil Engineers, Vol. 107, No GT 9, pp. 1233-1254.

Giroud, J.P. and Han, J. (2004a). *Design Method for Geogrid-Reinforced Unpaved Roads: I Development of Design Method*, Journal of Geotechnical and GeoEnvironmental Engineering, Vol. 130, No. 8, pp. 775- 786.

Holtz, R.D., Christopher, B.R. and Berg, R.R. (2008). *Geosynthetic Design and Construction Guidelines*, U.S. Department of Transportation, Federal Highway Administration, Washington DC, Report No. HI-95-038, 1995 (revised 1998 and 2008), 396 p.

Lamb. T.W. and Whitman, R.V. (1969), Soil Mechanics, John Wiley and Sons, Inc.

Perkins, S.W., Christopher, B.R., Cuelho, E.L., Eiksund, G.R., Hoff, I., Schwartz, C.W., Svanø, G., and Watn, A. (2004). *Development of Design Methods for Geosynthetic Reinforced Flexible Pavements*, U.S. Department of Transportation, Federal Highway Administration, Washington, DC, FHWA Report Reference Number DTFH61-01-X-00068, 263p.

Perkins, S.W., Christopher, B.R. and Lacina, B. (2008). "Mechanistic-Empirical Design Method for Unpaved Roads Using Geosynthetics," Proceedings of the Fourth European Geosynthetics Conference, Edinburgh, United Kingdom, International Geosynthetics Society.

Steward, J., Williamson, R. and Nohney, J. (1977), *Guidelines for Use of Fabrics in Construction and Maintenance of Low-Volume Roads*, USDA, Forest Service, FHWA-TS-78-205.

Examination of the Benefits of Enhancing Chip Seal Surface Treatments with Paving Fabric Interlayers

J.L. Dendurent, P.E., TenCate Geosynthetics, Wichita, Kansas, USA

ABSTRACT
Paving fabric interlayers have been used in the United States (U.S.) to mitigate reflective cracking in hot mix asphalt (HMA) overlays for decades. Chip seal surface treatments (or simply chip seals) have been used to seal roads for over a century. Combining paving fabric interlayers with chip seals is a hybrid system that has been successfully used in the U.S. and elsewhere abroad for reflective cracking control and extending pavement's service life for more than 25 years. Besides this application field, it has also been widely used in several other countries for reducing sub-grade moisture content and stabilizing roadways built on expansive clay sub-grades.

This paper will examine the exploding use of paving fabrics under chip seal systems in the U.S. through literature review, it will update the reader on the systems' current use and it will pay some emphasis on using the system to stabilize roadways over expansive clay subgrades.

1. INTRODUCTION

Geosynthetics are used to improve the performance and/or life cycle cost in many civil engineering applications. Geosynthetics are still relatively new when compared to materials like rock, asphalt, concrete, steel and lime. The acceptance and use of geosynthetics in civil engineering is most similar to the acceptance and use of reinforcing steel in concrete. Because geosynthetics are still relatively new, many federal, state and academic entities still separate designs with geosynthetics from standard design methodologies. For example, the Federal Highway Administration (FHWA) has recently incorporated geosynthetics into some of their standard design guides, but they still have a separate manual for designing with geosynthetics. FHWA also did not consider geosynthetics as a standard construction material in the Long Term Pavement Performance Project (LTPP) and in the development of the Mechanistic-Empirical Pavement Design Guide (MEPDG). They are currently integrating geosynthetics into the MEPDG. The United States Army Corps of Engineer's (USACE) manual Design and Construction of Levees (USACE, 2000) does not include design methods for geotextile-reinforced levees although geotextiles are commonly used in levee construction. USACE has a separate geosynthetics design manual, Engineering Use of Geotextiles (USACE et al., 2004), with a chapter dedicated to the design of geotextile-reinforced levees. Geosynthetics design is still taught as a separate and/or elective course at many universities instead of being incorporated as a regular part of basic design courses, despite the fact that many civil engineering professors are knowledgeable to varying degrees about geosynthetics design. The excellent multifaceted performance of geosynthetics has enabled engineers to build structures which were not possible prior to geosynthetics' existence. However, geosynthetics performance and manufacturing complexities may make the incorporation of geosynthetics into standard designs more difficult.

This complexity and struggle for acceptance is very apparent in the paving fabric market. Billions of dollars worth of paving fabrics have been successfully installed and numerous case studies have been published on performance and life-cycle benefits. Some cities even include paving fabric in every hot-mix asphalt (HMA) street they own. There have also been pavements with paving fabrics that have failed for different reasons, and there is good documentation on these failures. Most failures associated with installed paving fabric systems can be traced to the paving fabric being the wrong treatment for the problem at hand or an improper installation. Industry experts, good paving fabric installers and frequent end users of paving fabrics know that when utilizing paving fabrics is the right treatment for a certain pavement and when fabrics are installed properly and at the right time, their benefits are fully realized.

Most states, counties and cities in the U.S. can not afford to properly maintain the rapidly deteriorating transportation infrastructure system. Entities that do not have a pavement preservation or maintenance program have a large percentage of pavements that need to be seriously rehabilitated or completely replaced. It is now well known that every dollar spent on preservation, before rapid deterioration of the pavement structure begins, saves four to ten dollars in the future. FHWA is strongly encouraging states, counties and cities to focus on and spend a significant portion of their transportation budget on pavement preservation.

FHWA and other agencies are evaluating the use of paving fabrics under chip seals as a standard pavement preservation treatment option. It has been proven that the application of paving fabrics under chip seals can

significantly decrease the life-cycle cost of pavements when it is used in the right place at the right time. Agencies that have successfully incorporated paving fabrics into their chip seal program report considerable savings.

2. DESCRIPTION

2.1 Paving Fabric under Chip Seal System

The “paving fabric under chip seal” system is constructed by installing a paving fabric on a properly prepared existing pavement followed by a conventional single (Figure 1) or double chip seal over the fabric. Proper installation of a paving fabric for use under a chip seal is slightly different and more critical than proper installation of a paving fabric for use under an HMA overlay. Guidance on the proper installation of paving fabrics under a chip seal can be found in the recently published (Davis et al., 2008), in installation guidelines published by major U.S. manufacturers of paving fabrics, in Brown (2003) and Sprague et al. (1993).

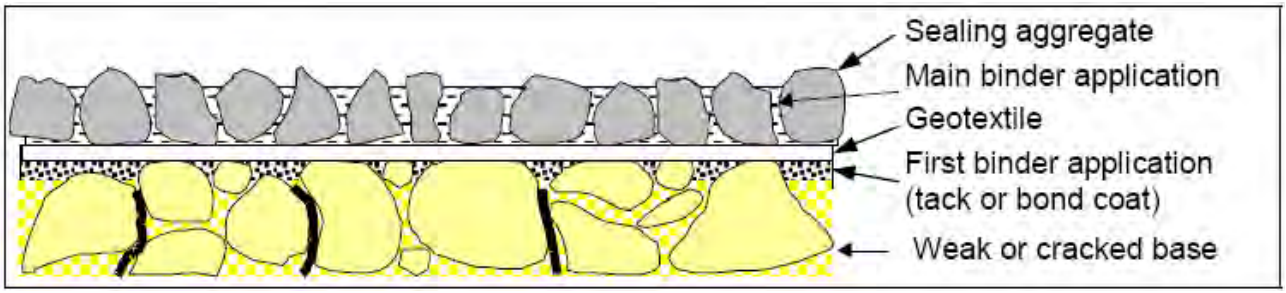

Figure 1 Paving Fabric Under Single Chip Seal (Alderson, 2006)

2.2 Benefits of Paving Fabric under Chip Seals

The benefits of using paving fabrics under chip seals are (Brown, 2003):

- Reflective cracking control: the saturated paving fabric bridges cracks and allows for the movement of the blocks of pavement beneath without directly affecting the chip seal matrix on the surface
- An extension of the pavement life that is directly attributable to the complete blockage of sunlight, air and water that typically age and cause deterioration of asphalt pavements
- Prevention of surface water infiltration,
- Stabilization of subgrade moisture content
- Allowing wet, weak subgrades to regain strength and load-carrying capacity

2.3 Successful Site Selection for Paving Fabric under Chip Seals

Paving fabrics are typically used under chip seals on low- to high-volume rural roads and low volume municipal roads. They are best suited for:

- Straight or gradually curving roads
- Sections of roadway with few driveways or intersections
- Vertical grades up to about eight percent
- Pavements that would have a sound structural section under optimum subgrade moisture conditions

For subgrade moisture control, the system has been successfully used as a surface treatment on existing asphalt pavements as well as directly on the clay subgrades of remote, light traffic roads.

For reflective cracking control, the “paving fabric under the chip seal” system performs well on pavements with extensive age-induced alligator or block cracking and oxidation.

Experienced users of the system have used paving fabric under chip seals in extreme conditions with outstanding results. However, it is highly recommended that new users be conservative with site selection to ensure success.

3. USE OF PAVING FABRICS UNDER CHIP SEALS

3.1 Current Use in the United States

In the U.S., the "paving fabric under the chip seal" system has been a standard treatment option in San Diego County's, CA annual chip seal program for over 20 years. Successful applications of this system in Northern California have been reported in the literature (Brown, 2003). Some fabric under chip seal projects in the U.S. have resulted in maintenance-free pavement life-cycles of over 20 years with little to no reflective cracking. Figures 2 and 3 are two sections of the same pavement in northern California (Brown, 2003). The section in Figure 2 was treated with an HMA overlay. The section in Figure 3 was treated with a double chip seal over paving fabric. When these photographs were taken both sections were at least 20 years old and had received no maintenance.

Figure 2 Aerojet Facility, Northern California
20-year old 2-inch hot mix asphalt overlay (Brown, 2003)

Figure 3 Aerojet Facility, North California
20-year old double chip seal over fabric (Brown, 2003)

The County of San Diego, CA first started using paving fabric under chip seals as a standard treatment option in the 1980s after installing and evaluating different chip seal methods. By incorporating paving fabrics into their chip seal program they estimate annual savings of about $100,000 a year. On pavements with fabric under a chip seal, maintenance costs are decreased and crack sealing is eliminated once the paving fabric is in place. Details of the San Diego County, CA program have been reported in a TRR Circular (Davis, 2005).

Currently, Texas DOT and FHWA, as well as several other transportation agencies throughout the U.S., have installed and continue monitoring and evaluating several paving fabric under chip seal test sections.

3.2 Current Use in Other Countries

Paving fabric under chip seal is a standard pavement preservation treatment option in France, South Africa, New Zealand and Australia. It is commonly described regionally as a geotextile-reinforced sprayed seal or GRS.

Australia is a strong proponent and user of GRSs and all Australian states have been using some form of GRS. Single chip seal GRSs are used as stress-absorbing membrane interlayers (SAMI) under other surface treatments. Australian practice seldom exposes a single chip seal over paving fabric to traffic. In Victoria, NSW, double chip seals over paving fabric are applied over a variety of surfaces, most of which are in poor condition. In some cases, the GRS yields 12 to 15 years of pavement life. VicRoads, the state road authority in Victoria, NSW also uses a GRS on some roadways in advanced states of deterioration. They aim in keeping the roadway in service until they can plan, design, arrange funding or relocate services for a more permanent pavement treatment. Used in this context, even 5 years of addtional service life is considered a successful treatment as those additional 5 years of performance could not have been reasonably achieved by other means (Esnouf, 2008).

Vicroads uses GRS both in stress alleviating membrane (SAM) and SAMI applications as de facto rehabilitation treatments. GRSs are occasionally used as the sealed riding surface directly on formed but unpaved pavements in remote locations. In metropolitan regions, GRSs are increasingly used in composite treatments such as under ultra thin asphalts and as a waterproofing membrane under new asphalt overlays (Esnouf, 2008).

Vicroads and other Australian road agencies also use GRSs to control pavement shrinkage cracks built over expansive clay subgrades. Field studies and literature findings demonstrate that moisture contents in expansive clay subgrades below a GRS remain consistent and, as a result, the subgrade remains firm. Deutschbein et al. (1987) conclude that “the geotextile reinforced seal is effective as a moisture control tool.” Gordon et al. (1984) conclude that water ingress into the pavement occurs at the edge of the sealed section if vertical moisture barriers are not installed. Thus, the seal is extended well beyond the trafficked zone to maintain the desired stiffness of the pavement or vertical moisture barriers are installed.

4. LITERATURE REVIEW

4.1 Pavement Preservation Technology

FHWA and the National Cooperative Highway Research Program (NCHRP) jointly sponsored the Pavement Preservation International Scanning Study (FHWA, 2002). The objective of the scanning study was to review and document innovative techniques, materials, procedures and equipment used in the host countries (France, South Africa, and Australia) for pavement preservation and to evaluate these elements for potential application in the U.S. The scanning team traveled to the host countries and met with government agencies and private-sector organizations involved with pavement preservation. They also visited project sites to observe the results of successful pavement preservation techniques and strategies.

The scanning team reported that these countries emphasize pavement preservation, use only quality materials and have rigorous specifications that they firmly enforce.

Two of the scanning team's key findings are:

- All the countries visited have made a commitment to design and build long lasting structural pavement sections on their national roadway networks. This initiative has shifted focus of maintenance activities on surface courses in order to preserve the large investment made in the underlying layers. This, in turn, promotes the use of relatively low cost seals and thin overlays as the primary maintenance techniques, instead of more costly types of rehabilitation.
- By providing initial high structural capacity sections, emphasis is placed on maintaining the structure using relatively low cost seals and thin overlays on set, repeatable maintenance cycles. For the most part, rehabilitation is a minor portion of the agency maintenance programs. Consequently, pavement preservation techniques are emphasized.

The scanning team developed eleven recommendations with implementation potential in the U.S. One of these eleven recommendations was to “test and evaluate geotextile-reinforced chip seals in both freeze and no-freeze environments.”

The scanning team also recommends that individual entities partner with sponsor agencies to develop “research statements to evaluate the use of better aggregates, geotextiles, and binder application procedures in preventive maintenance treatments."

4.2 Chip Seal Best Practices

The most common pavement preservation treatment in use today is the chip seal. NCHRP Synthesis 342, “Chip Seal Best Practices,” (Gransberg et al., 2005) contains an international survey and summary of chip seal best practices. Ninety two entities responded to the survey. The survey revealed almost 610,000 lane miles of chip seals have been installed in Canada, Australia, New Zealand, South Africa and the United Kingdom while another 140,000 lane miles have been installed in the U.S.

Gransberg et al. (2005) gave special consideration “to the highly technical process used to design and build chip seals in Australia, South Africa and the United Kingdom”. As per Gransberg et al. (2005), "the average chip seal life-cycle in the U.S. is 5.75 years. The average chip seal life-cycle in Australia is 10 years, in South Africa is12 years and in the United Kingdom is 10 years. Each of these countries “indicated that they consistently achieve chip sealing performance excellence on both low- and high-volume roads.” GSRs are also a standard treatment chip seal in all three countries. These “international respondents unanimously believe that geotextile-reinforced seals are effective for treating badly cracked, oxidized or structurally distressed pavements”. Gransberg et al. (2005) also report that these other countries have a standardized chip seal design method, they demand and they are willing to pay for higher quality materials and they have strictly-enforced installation procedures. San Diego County, CA and several state authorities in the U.S. have reported excellent chip seal performance. It is the opinion of the author that these states could easily incorporate paving fabrics into their chip seal programs.

Gransberg et al. (2005) also concluded that “it appears that the use of geotextile-reinforced chip seal is promising and should be considered for those roads that have more than normal surface distress and for which an overlay is not warranted.”

4.3 FHWA, Texas DOT Research

In an effort to implement the findings of the Pavement Preservation Technology Study (FHWA, 2002), FHWA partnered with Texas DOT to evaluate the use of paving fabric under chip seals. The research was conducted from 2004 to 2008. “The project objective is to assess as to what extent non-woven geotextile fabric underneath chip seal surface treatments will reduce reflective cracking, reduce moisture penetration through the pavement structure, affect ride quality and increase the pavement life.” In 2004, TXDOT Waco District constructed single chip seals over paving fabric at six sites using different combinations of tack coat, seal coat binder and aggregate materials. Each test section was at least 0.5 miles long and covered at least two travel lanes. The traffic volumes at the sites varied from an average daily traffic (ADT) of 330 up to 31,000. (Rodriguez, 2007) Each section also had a control section consisting of just the chip seal treatment (no fabric) used in the “paving fabric under chip seal section”. A visual evaluation./survey and several standard pavement condition surveys of the test sites were completed annually and are now available from FHWA.

The following key observations are in FHWA's 2007 Annual Pavement Condition Survey (Rodriguez, 2007):

- The chip seal sections with geotextile fabric are doing a better job of controlling reflective cracking
- Most of the noted pavement surface problems in the chip seal over geotextile fabric sections are a result of poor geotextile fabric placement practices
- The rate of deterioration is higher in the control sections than in the ones including the geotextile fabric.

It is the opinion of the author that the benefits of using paving fabric under chip seals will be apparent at the end of the study. However, due to the fact that proper placement practices have not being meticulously implemented and documented and due to the wide variation in the asphalt and aggregate materials properties, the author also believes that the results of the study may not show the benefits of the system to the extent that it has been realized among users such as San Diego County, CA and the Australian transportation agencies.

4.4 Vicroads Geotextile Reinforced Seals Technical Note (Vicroads, 2008)

Vicroads (2008) reports that “since being introduced into Australia in the 1970s, Geotextile-Reinforced Seals have found particular application in the rehabilitation of cracked and weak pavements by reducing the incidence of reflection cracking and provision of a high level of performance as a waterproofing membrane.” On SAM treatments, Vicroads (2008) states that “GRS treatments may be used to provide more robust waterproofing and resistance to reflection cracking on pavements that are cracked due to ageing of asphalt or sprayed seal surfaces, shrinkage of cemented base materials or high deflections on weak pavements.”

Australian road agencies use a double chip seal over paving fabric for SAMs. Vicroads (2008) recommends that “expert advice should be sought before using a single coat seal” over a paving fabric under direct traffic loading. Vicroads (2008) and Brown (2003) both assert that double chip seals over paving fabric provide a robust treatment with good resistance to turning traffic.

Vicroads uses a GRS as a SAMI where there is a risk of “reflection cracking from shrinkage of cemented base materials, or excessive embedment and/or high deflections on weak base materials” but a GRS may not be the preferred riding surface.

4.5 Other Literature

Once Australia and other countries made long-term budget goals, they also placed heavy emphasis on pavement preservation and life-cycle cost instead of initial construction cost (FHWA, 2002). Austroads (2006), Vicroads (1995) and Austroads (2004b) refer to the system as a common treatment when a durable, highly waterproof seal is needed. The U.S. is still in the process of shifting care of infrastructure from rehabilitation and replacement to preservation. Some agencies that have made that paradigm shift are beginning to realize the benefits of incorporating paving fabrics into their chip seal programs.

The author recommends the following reference sources for detailed information on site selection, design, installation, performance and cost savings of the “paving fabric under chip seal” system: Davis et al., 2008; Brown, 2003; Sprague, 1993; Austroads, 2003, Austroads, 2004a, Austroads 2004b, Austroads, 2005 and Austroads, 2006.

5. PAVING FABRIC UNDER CHIP SEALS OVER EXPANSIVE CLAY SUBGRADES

As mentioned in previous sections, a specific use of the “paving fabric under chip seal” system is to control pavement cracks created by the shrinking and swelling of underlying (subgrade) expansive clay soils. Such subgrade conditions are encountered in many areas around the U.S. Most of the US research, technology and treatments addressing this issue involve modifying and stabilizing clay soils prior to building a pavement. Some significant research has also been reported on encapsulating expansive soils with impermeable membranes in order to stabilize the subgrade moisture content. Texas DOT and the Colorado Department of Transportation (CDOT) have invested significant resources in researching and looking for solutions to this problem. A significant drawback to the current practice for controlling surface cracking caused by expansive clay soils is the expense, time and effort of modifying or encapsulating the expansive clay subgrade soil. This may be a practical option for new roads, but rather a very expensive proposition for existing ones, where removing and replacing existing pavements is very expensive.

The use of a paving fabric under chip seal is a viable solution for many existing roads with shrinkage cracks and premature deterioration caused by expansive clay subgrades. Most of the surface water landing on a cracked asphalt pavement infiltrates into the pavement section. The paving fabric under the chip seal system prevents surface water from entering the subgrade through the pavement surface. This minimizes moisture fluctuations and reduces swelling and contracting potential of subgrade soils which cause shrinkage cracks in a pavement surface. A paving fabric under a chip seal will not eliminate surface cracking, but if it is designed and installed properly, it can reduce the size and movement of the surface cracks. Deutschbein et al. (1987) state that in clay underlain pavements sealed with a GRS, the role of the asphalt saturated geotextile is to bridge the cracks caused by shrinkage in the clay and prevent their reflection into the seal so that the clay is in turn protected from downward moisture ingress. Deutschbein et al. (1987) also conclude that the pavement beneath a GRS remains firm and well dry of optimum moisture. In comparison, the same material beneath the shoulder was spongy and well above optimum moisture.

Research and field studies, as early as 1965, have demonstrated the benefits of surface seals for controlling subgrade moisture content fluctuations (Gordon et al., 1984). The reader can also view the Austroads and Vicroads web sites (www.austroads.com.au and www.vicroads.gov.au, respectively) for information on the use of GRS for controlling expansive clay subgrades.

6. INCORPORATING PAVING FABRIC UNDER CHIP SEALS INTO AN EXISTING PROGRAM

To successfully incorporate the “paving fabric under chip seal” system into a pavement preservation program, transportation agencies must:

- Understand the benefits and limitations of the system
- Understand the importance of proper site selection
- Use a rational design methodology, and
- Establish and enforce thorough material and installation specifications

It is the recommendation of the author that any agency interested in incorporating this system into their pavement preservation program must:

1. Study the site selection criteria, design methodologies and installation practices of the agencies and owners who have been successfully using this system
2. Partner with a paving fabric installer, chip seal contractor and/or paving fabric manufacturer experienced with the “paving fabric under chip seal” system
3. Perform and document field trials to determine the design methodology, specifications, materials and installation method most suited to their needs, location and available resources
4. Create guidance documents and specifications particular to their agency

7. CONCLUSIONS

Most of the work being performed on the U.S. transportation infrastructure is on existing pavements. Yet, due to budgetary constraints and rapid infrastructure deterioration, many agencies can not afford to rebuild, rehabilitate or sometimes even maintain their roads. FHWA is encouraging agencies at all levels to implement pavement preservation programs. As a result, larger portions of transportation budgets are being dedicated to pavement preservation.

Increased pavement life and decreased life-cycle costs are core elements of any pavement preservation effort. The keys to realize increased pavement life and decreased life-cycle cost with paving fabric under chip seals are the same as any other pavement preservation treatment; correctly installing the right treatment on the right pavement at the right time.

Australia, the United Kingdom, France, and San Diego County, CA have all reported successful applications of the "paving fabric under chip seal" system to increase average life-cycle and decrease life-cycle cost of pavements. There are detailed design methodologies for installing paving fabrics under chip seals. FHWA is encouraging agencies to research and test paving fabrics under chip seals. FHWA is also providing strong incentives for pavement preservation to qualifying agencies. The author strongly believes that US transportation agencies could increase the average life of their chip seals and pavements by properly incorporating paving fabrics into chip seal programs.

REFERENCES

Austroads (2003), *Guide to the Selection of Road Surfacings*, Austroads, Incorporated, Sydeny, NSW, Australia, August, 2003

Austroads (2004a), *Sprayed Seal Design*, Austroads, Incorporated, Sydeny, NSW, Australia, January, 2004

Austroads (200b), *Sprayed Sealing Guide*, Austroads, Incorporated, Sydeny, NSW, Australia, January, 2004

Austroads (2005), Technical Report AP-T37/05 *Geotextile Reinforced Seals,* Austroads, Incorporated, Sydney, NSW, Australia, 2005

Austroads (2006) *Update of the Austroads Sprayed Seal Design Methods*, Austroads Incorporated, Sydney, NSW, Australia.

Brown, N.R. (2003), Solution for Distressed Pavements and Crack Reflection, *Transportation Research Record 1819*, Paper No. LVR8-1169, 313-317.

Davis, L. (2005), Chip Sealing over Fabric in Borrego Springs, California, *First National Conference on Pavement Preservation,* Kansas City, MO, Transportation Research Board, Washington D.C., 42-52.

Davis, L. and Dendurent, J. (2008). Proper Installation of Paving Fabric Interlayers When Placed Prior to Chip Sealing, *Sixth **RILEM** International Conference on Cracking in Pavements*, CRC Press, Chicago, IL, USA, 703-712.

Deutschbein, E.A. and Sutherland, M.R. (1987), Geotextile Reinforced Bitumen Seal on an Expansive Clay Road Pavement, *engineering Conference Darwin,* May, 1987, 15-19.

Esnouf, J. (2008) Personal communication.

Gordon, R.G. and Waters, T.J. (1984), A Case Study of Performance of Pavements on an Expansive Soil Subgrade, *Fifth International Conference on Expansive Soils,* Adelaide, South Australia, May 1984, 263-269

Gransberg, D. and James, D. (2005), NCHRP Synthesis 342 Chip Seal Best Practices, A Synthesis of Highway Practice, *Transportation Research Board*, Washington D.C.

Federal Highway Administration (2002). Pavement Preservation Technology In France, South Africa and Australia, International Technology Exchange Program, Publication No. FHWA-PL-03-001 HPIP/10-02(5M)EW.

Petry, T.M. and Little, D.N. (2002), Review of Stabilization of Clays and Expansive Soils in Pavements and Lightly Loaded Structures-History, Practice and Future, *Journal of Materials in Civil Engineering*, ASCE, November/ December, 447-460

Polk County, Polk County Natural Hazards Mitigation Plan: Expansive Soils, Section 12

Rodriguez, L. (2007). TxDOT Chip Seal over Geotextile Fabric Project Research Study, 2007 Progress Report. FHWA Resource Center, Atlanta, GA, USA.

Sprague, C.J., Campbell, D.M., Kuck, P.J. (1993), Fabric Reinforced Chip Seal Surfacing and Resurfacing, *Reflective Cracking in Pavements RILEM,* E&FN Spon., London, 323 -333.

Sutherland, M. and Phillips, P. (1990), Geotextile reinforced sprayed seal roads in Australia, *Geotextiles, Geomembranes and Related Products, Den Hoedt (ed.)*, Balkema: 209-212.

Vicroads (1995) Technical Note 13 *Vertical Moisture Barriers,* October 1995

Vicroads (2008) Technical Note 14 *Geotextile Reinforced Seals*, March 2008

Stability Analysis of Reinforced Embankments in New Orleans

N.T. Schwanz, P.E., U.S. Army Corps of Engineers, St. Paul District, St. Paul MN
N.D. Vroman, P.E., U.S. Army Corps of Engineers, Engineer Research and Development Center, Vicksburg, MS
R.E. Wahl, P.E., U.S. Army Corps of Engineers, Engineer Research and Development Center, Vicksburg, MS
M.P. Navin, PhD, P.E., U.S. Army Corps of Engineers, St. Louis District, St. Louis, MO
R.B. Pinner, P.E., U.S. Army Corps of Engineers, New Orleans District, New Orleans, LA
R.J. Varuso, P.E., U.S. Army Corps of Engineers, New Orleans District, New Orleans, LA
D.E. Yule, P.E., Geotechnical Engineer, U.S. Army Corps of Engineers, Engineer Research and Development Center, Vicksburg, MS

ABSTRACT
The stability of geotextile reinforced levees constructed on soft foundations was investigated for the New Orleans Hurricane and Storm Damage Risk Reduction System. Limit equilibrium analyses performed to evaluate preliminary design sections of levee raises indicated that potential failure mechanisms during hurricane storm surges may extend around the reinforcement on the flood side. The critical failure surface defining these failure mechanisms sometimes contains non-classic concave and convex portions. Numerical analyses were performed to determine if these failure mechanisms (non-classic shaped surfaces) are kinematically admissible. The numerical analysis includes separate interfaces to allow slip above and below the geotextile. Full scale pullout tests are referenced to assign interface properties. Results from the numerical analysis validate the non-classic failure surface shapes found in the limit equilibrium analyses. Design requirements resulting from these non-classic shaped failure surfaces are now being considered for the design of geotextile reinforced levees.

This paper presents results of full scale pullout load tests and a discussion of the non-classic shape of the failure surface during loading for geotextile reinforced levees. Limit equilibrium analyses are compared to numerical model results at two levee alternative design sections.

1. INTRODUCTION

The U.S. Army Corps of Engineers, New Orleans District (MVN) has successfully used geotextile as reinforcement in the construction of levees founded on soft soils in the Hurricane and Storm Damage Risk Reduction System (HSDRRS). Based on research and years of experience, MVN has adopted a design procedure for geotextile reinforced levees. This design procedure evaluates the global stability of the reinforced levee embankment, bearing capacity of the foundation beneath the levee, the required embedment/anchorage length, lateral embankment sliding/spreading along the top of the geotextile, creep and long term embankment stability, and consolidation and settlement. The MVN design procedure considers potential failure surfaces both through and around the geotextile reinforcement. This paper presents an evaluation of the global stability aspect of design accounting for the hurricane storm surge loading.

Since Hurricane Katrina, stability criteria for levees in the HSDRRS have been updated in terms of factors of safety and stability method. The updated criteria require higher factors of safety and require evaluating non-circular failure surfaces that are more complex than the traditionally used three-part wedge or circular failure surfaces. Reinforced, as well as unreinforced, levees are required to meet updated criteria, which has resulted in larger levee sections that require more fill material and additional real estate. Through the use of non-circular failure surfaces, critical failure surfaces are found that extend around the reinforcement on the flood side (or active zone) that could lead to lower factors of safety than failure surfaces passing through the fabric. This type of critical failure surface sometimes includes unexpected non-classic concave and convex portions leading to questions of whether these are kinematically admissible failure mechanisms.

The validity of these non-classic shaped failure surfaces that extend around the end of the reinforcement was evaluated using numerical analyses of two preliminary alternative levee design sections where alternative designs were evaluated to include raising the levee in one large lift to the required 2011 top of barrier elevation which included significant overbuild for anticipated settlement. These sections include a section from the Jefferson Lakefront levees where the existing levee was originally constructed using geotextile reinforcement and a section from the Lake Cataouatche levees where the existing levee is not reinforced but geotextile reinforcement is being considered for one design alternative. The locations of these levees are shown on Figure 1. Numerical modeling was completed using FLAC (Fast Lagrangian Analysis of Continua, Itasca, Consulting Group, Inc., 2006a) with separate interfaces to allow slip above and below the

geotextile. Interface properties were selected from full scale pullout tests performed at the Bonnet Carre' Spillway in New Orleans, LA (USACE 1989)

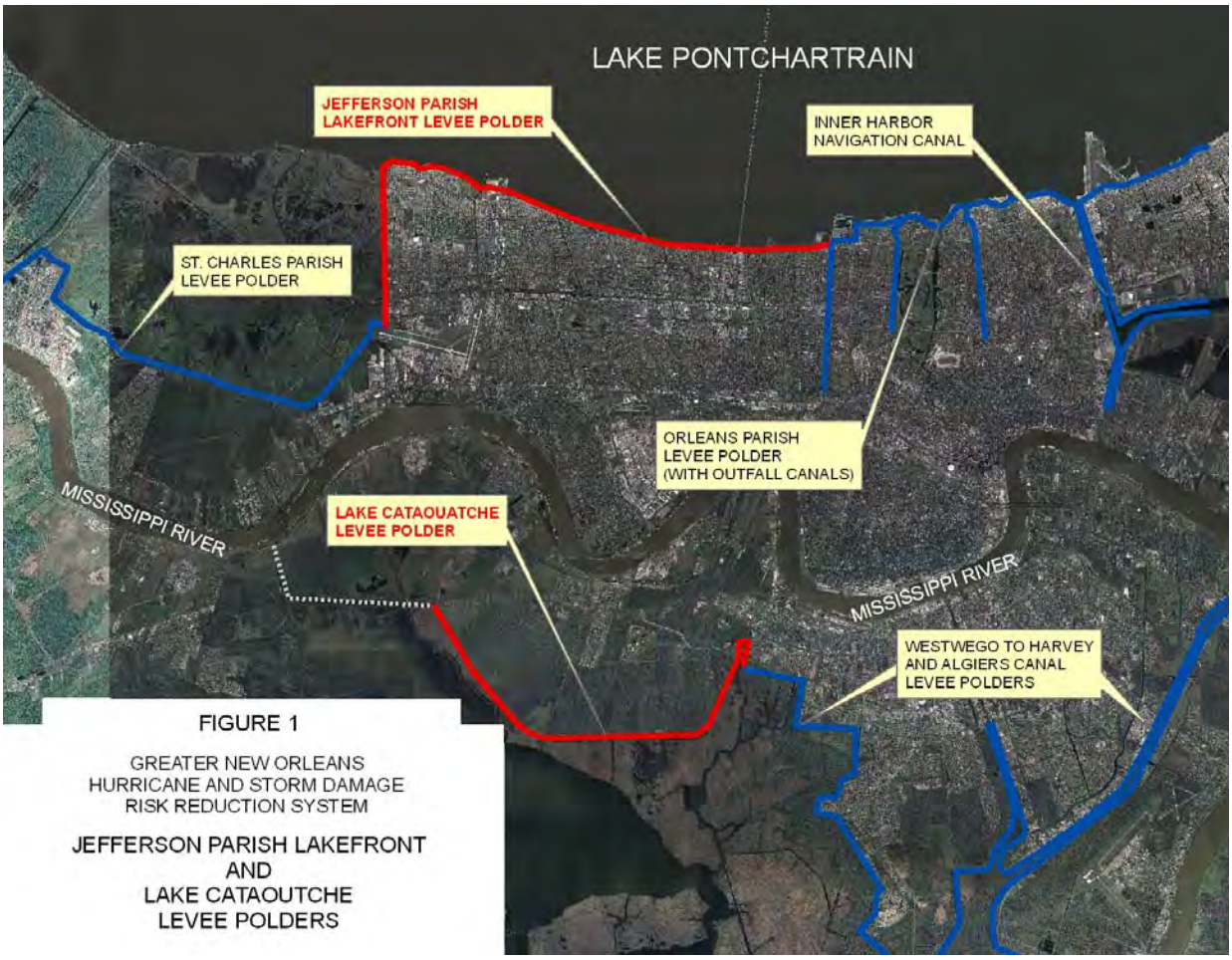

Figure 1. Jefferson Lakefront and Lake Cataouatche levee locations.

2. DESIGN STABILITY ANALYSIS

The current slope stability design criteria for the HSDRRS (USACE 2008, USACE 2007) was adapted from the criteria presented for new embankment dams in the USACE slope stability manual EM 1110-2-1902 (USACE 2003), Several load cases (including the end of construction case and hurricane storm surge loading) are checked to satisfy the slope stability design criteria. Due to the rapid loading conditions from levee construction and/or hurricane storm surge, design stability analyses are performed using drained strengths for free-draining materials and undrained strengths for slow draining materials. Where foundations soils have marginal strengths, stability berms, geotextile reinforcements, soil improvements or other similar features are considered in order to satisfy the required factors of safety.

Slope stability analysis is performed to determine the required geotextile tensile capacity and total length needed to meet the required factors of safety for stability. Originally, the reinforcement tensile force and total length required to satisfy criteria for failure through the embankment and foundation was estimated using the MVN Method of Planes stability software (horizontal force equilibrium) in conjunction with conventional limit equilibrium slope stability analysis to check force and moment equilibrium. For these stability analyses the following assumptions were made:

- Soil shear strength and reinforcement tensile strength are mobilized simultaneously.
- The critical slip surfaces or circles at all elevations throughout the foundation will be the same for both the geotextile-reinforced and non-reinforced embankments.
- Required length of the geotextile reinforcement was determined through pullout calculations and ensuring all failure surfaces around the reinforcement had adequate factors of safety at all elevations throughout the foundation.
- Shapes of the active and passive wedges within the failure surfaces were assumed to be fixed at 45 +/- ϕ/2 deg.

The initial assumption stated is generally met by requiring reinforcement strength at 5% axial strain, which approximately corresponds to the strain at peak soil strengths. The second assumption is one that is commonly made for reinforced embankment design and is based on the design intent to improve the most critical slip surfaces. When coupled with the design of the geotextile anchorage length, beyond the intersection of the critical slip surface and the reinforcement, it is envisioned that levee stability will be adequately improved, as discussed in the third assumption. However, non-classic potential failure surfaces may develop in the slope stability analyses when hurricane storm surge loading is added on the flood side of the levee. This loading creates an asymmetric loading condition on the embankment, and through rigorous non-circular search procedures using UTexas4 (Shinoak Software) and Slope/W (version 7.1, Geo-Slope International, Ltd) limit equilibrium slope stability analysis programs revealed non-classic shaped critical slip surfaces that can extend beyond the flood side end of the reinforcement. The MVN design procedure requires checking the stability of slip surfaces extending beyond the flood side reinforcement and the current use of software with rigorous search techniques indicated that these slip surfaces can be just as critical as those extending through the reinforcement.

3. NUMERICAL MODELING

Numerical modeling was completed using FLAC. This two-dimensional code for modeling soil, rock, and structural behavior was used at two different levee sections to model high strength geotextile as reinforcement for embankments constructed on soft foundations. Each model required embankment and foundation soil properties, geotextile properties, and soil to geotextile interface properties.

The numerical analyses were based on the Mohr-Coulomb constitutive model (linearly elastic-perfectly plastic soil behavior). Only undrained analysis was performed to match the loading conditions considered in the design stability analysis and provide a consistent comparison to the limit equilibrium analysis. Unit weight and shear strength parameters were selected from recent subsurface investigation and testing. Soil modulus values were determined using pressuremeter test values (Schnabel Engineering South, LLC 2006) relating shear modulus to undrained shear strength (G/S_u) with an assumed Poisson's ratio. Shear strength reduction technique (SSR) was used in numerical analyses to calculate the factor of safety and determine the critical failure surface.

The geotextile was incorporated in the models as structural beam elements with zero moment of inertia and no strength in compression. In this way the geotextile was included with only tensile capacity characterized by a tensile modulus and yield strength.

There are several ways that beam elements can be attached to the mesh. For all models, the beams were connected using interface elements that were set to allow slip and separation. This was important to try to capture the behavior near the ends of the geotextile where the reinforcement may tend to pullout or where sliding along the reinforcement could occur. Interface elements were used to connect the geotextile (beam) to the soil (mesh) on both the upper and lower contact surfaces.

4. GEOTEXTILE AND INTERFACE PROPERTIES

4.1 Geotextile

Often the geotextile used on the HSDRRS reinforced levee projects have strengths of 8400 lbs/ft to 24,000 lbs/ft at 5% strain. For both the Jefferson Lakefront and Lake Cataouatche alternative sections in this study, Mirifi HS 1715 was used with a wide width tensile strength of 8400 lbs/ft at 5% strain. Product data on this material were provided from the manufacturer. Using an average geotextile thickness of 65 mils the geotextile modulus (E) was computed to be $3.1x10^7$psf. The tensile strength of the geotextile was based on the fabric strength at 5% strain to maintain strain compatibility between to the soil and the geotextile. For hurricane storm surge loading, the ultimate fabric strength factored by 1.21 for biological and construction considerations was used for numerical factor of safety computations as this is a short term load condition with minimal potential for creep. Typically, HSDRRS reinforced levees are designed for maximum geotextile strength of 50% of the ultimate strength (when utilizing polyester geosynthetics) to minimize creep at service state conditions (i.e. construction of levee embankment). Following each analysis in this study, the computed axial force/ft was checked for overstress and rupture as well as interface slippage and fabric pullout.

4.2 Interfaces

The boundary between the geotextile and the soil is a plane of weakness where sliding or separation can potentially occur. The numerical analysis software provides interfaces that have the properties of friction, cohesion, dilation, normal and shear stiffness, and tensile strength (Itasca Consulting Group, Inc 2006). In this analysis, the properties that are of

primary concern are friction, cohesion, shear stiffness, and normal stiffness for the boundary with soil both immediately above and below the geotextile. The interface is considered to have no tensile strength for these analyses.

The cohesion and friction properties of the interface were determined from full scale field pullout tests and laboratory pullout tests. Full scale field pullout tests were conducted at the Bonnet Carre' Spillway in 1989 (UACE 1989). Bonnet Carre' Spillway is located 26 miles northwest of New Orleans and the pullout tests performed there used fill from local borrow sources typically representative of levee embankment fill for reinforced levee sections. The field pullout tests were originally undertaken because of concerns with values from smaller laboratory tests, which may suffer from laboratory boundary effects. The field pullout tests were performed using a 24 ft long by 6.75 ft wide high strength woven polyester geotextile with confining fill heights of 3 ft, 4.5 ft and 6 ft. Two types of interface soils were used to match conditions that maybe experienced during construction of reinforced sections. These interface soils include (1) clay above and below the geotextile, and (2) clay above and sand the below the geotextile. The results of the full scale tests, plotted in terms of pullout resistance versus normal load, indicated a linear trend and pullout resistance for the clay/clay interface could be defined by the following equation.

$$\text{Pullout Resistance (psf)} = 265 + [\tan(19°) \times \text{effective normal stress (psf)}] \quad [1]$$

Note that this resistance applies to top and bottom interface separately

.

Gilbert et al. (1992) performed laboratory pullout tests to evaluate the performance of three geotextiles with four soils from the Bonnet Carre' Spillway area in support of levee design work being performed by MVN Geotechnical Branch in the early 1990's. The laboratory work supplemented the full scale field pullout tests described earlier in this paper. The laboratory testing program was set up recognizing that geotextile pullout resistance is affected by water content, compaction, normal pressure between soil and fabric, rate of pullout, and submergence conditions. Two types of laboratory tests reported by Gilbert et al (1992) include soil to fabric friction test and the fabric pull out tests. Both tests were run in a specially fabricated direct shear box with dimensions of 24 inches x 24 inches and each half of the shear box is 6-inches high. These laboratory tests indicated good agreement with the full scale pullout test, but noted that water content of the soil adjacent to the geotextile and geotextile submergence have significant impacts on the pullout resistance. Gilbert also reported that post-test excavation in the soil show that there was no slippage at the soil-geotextile interface rather shearing and displacements were occurring in the soil mass away from the interface.

The interface shear and normal stiffness was determined by adhering to some basic guidelines provided in the software manual (Itasca Consulting Group, Inc. 2006a). These guidelines indicate that the interface stiffness should be slightly stiffer than the lowest stiffness adjacent to the interface. A rule of thumb is given here suggesting the interface stiffness to be 10 times the lowest adjacent stiffness or the equivalent stiffness of the stiffest adjacent zone defined by:

$$\text{Equivalent Stiffness} = \max[(K+1.33G)/Zmin] \quad [2]$$

Where K and G are the bulk and shear modulus respectively and Zmin is the smallest width of the adjacent zone in the direction normal to the interface.

A sensitivity analysis of the interface stiffness (both shear and normal) was performed for the numerical analysis of the Jefferson Lakefront section. The interface stiffness had very little to no effect on the factor of safety values and location of the critical failure surface. In addition, interface stiffness had little impact on the calculated displacement.

5. ANALYSIS

5.1 Jefferson Lakefront

The Jefferson Lakefront levees are located in Jefferson Parish on the south shore of Lake Pontchartrain. The levees extend westward from the west side of the 17th Street Canal to the northern end of the West Return Levee that runs north and south between Lake Pontchartrain and the Louis Armstrong International Airport. The location of the Jefferson Lakefront alternative section used in the analysis is presented on Figure 1.

5.1.1 Subsurface Conditions

The soil stratigraphy including density and strength properties were determined from geotechnical investigations and laboratory testing. This data typically characterized the foundation having lower undrained shear strength and lower saturated density beyond the existing embankment and higher values beneath the embankment where settlement and consolidation have occurred. The both the numerical and the limit equilibrium analyses divided the foundation into five vertical regions to model the variation of foundation material properties. These vertical regions were separated by

vertical planes termed “verticals”. The stratigraphy and locations of verticals are shown in Figure 2. Although the numerical model ends at the vertical 1 location the material properties to the left of vertical 1 and to the right of vertical 5 are constant. Between the verticals, the material properties (unit weight; shear strength; modulus) vary linearly within each soil layer (only lateral variation at this section). In the numerical model, the soil is discretized into 2 ft square zones and each soil zone between verticals is assigned properties associated with a horizontal location at the center of the zone. The soil shear strengths did not vary with depth so the modulus values were also constant with depth as shown in Table 1. For all clay soils a G/S_u ratio of 100 was used with a high Poisson’s ratio of 0.47 for saturated soils.

5.1.2 Limit Equilibrium Analysis

Limit equilibrium analysis was completed using UTexas4 (Spencer procedure) with varying unit weights and interpolated shear strengths. For these analyses, stability was checked using the geotextile strength at 5% strain (8400 lbs/ft). Using the pullout resistance equation of Equation 1, an anchorage length of 16 ft was needed to develop the geotextile strength of 8400lbs/ft.

The reinforcement strength was varied linearly from 0 lbs/ft at the end of the reinforcement to 8400 lbs/ft at the anchorage length. Stability was checked with and without water load for the no geotextile condition and with water loading for the with geotextile reinforcement condition. The critical slip surfaces and factor of safety results are shown on Figure 3. Note that in the limit equilibrium analyses there is a very small increase in factor of safety for the full water load condition without and with the geotextile reinforcement. This difference is slightly greater in the numerical analyses.

5.1.3 Numerical Analysis

The numerical model was constructed in several steps. Initial stresses were computed for the near horizontal ground surface condition expected to exist prior to constructing the embankment. Next, displacements and velocities were reset to zero and the geotextile was installed and embankment fill was added. Deformations computed at this stage represent only displacement from shape changes as there is essentially no volume change in the saturated soil and no consolidation effects were modeled. Strains, displacements, and forces developed in the geotextile may represent lower than expected axial forces in the geotextile. This is not expected to affect the failure mechanism for global stability as long as the fabric does not rupture. Storm surge effects are included as mechanical pressure. Water pressures were added in five load increments, each representing 3 or less feet of water.

Factor of safety results from the numerical SSR analyses are 1% to 6% higher than those found using the limit equilibrium procedures. A simplification was made regarding the use of a tension crack. Adding a tension crack is difficult in the numerical model as this would require inserting an interface to allow separation. Instead, the Mohr-Coulomb models were set with a tensile strength of zero, which mimics the use of a tension crack without water filling (note that the limit equilibrium analyses included tension cracks as need to eliminate negative forces on the slices and were not filled with water). Figures 4 through 7 present the critical failure surface locations by plotting the accumulated shear strain. These analyses were performed for the same load conditions used in the limit equilibrium analyses plus an analysis of the stability of the reinforced levee without any storm surcharge load.

It is interesting that Figures 4 and 6 (no geotextile) show a developing slip surface at a lower elevation than the critical failure surface. The introduction of water load in Figure 6 (no geotextile model with water load) induces greater displacement at depth. The slip surface shown in Figure 5 substantiates the assumption that it is reasonable to design reinforcement to improve the most critical slip surface since the critical failure surface is practically the same for the no geotextile condition. The reinforcement in Figure 5 ruptured at a calculated factor of safety of 1.51, which exceeded original design criteria.

The results shown in Figure 7 represent the reinforced embankment under full storm surge loading. The introduction of the reinforcement is sufficient to force the critical failure surface around the geotextile, which increases the factor of safety. Figure 7 shows that the deeper failure surface has fully developed when the geotextile is added with the full water load as compared to Figure 6. The fully developed slip surface with geotextile trends along the developing, deeper slip surface found in the no-geotextile condition.

The axial loads in the geotextile were not changed significantly by the addition of the storm surge loading. The magnitude of axial force increases slightly at the flood side end but generally decreases the maximum axial force in the fabric. Thus, the analysis indicates that the maximum axial force occurs in the fabric during the no water load condition. This is due to the impacts of the storm surge loading of the embankment and foundation deformations. The critical failure surface shown in Figure 7 indicates little relative displacement of the geotextile to the embankment/foundation as the entire geotextile is within the failure mass. Initially, the embankment construction induced lateral spreading about the centerline of the levee. This behavior is best depicted in Figures 8a and 8b, which show the displacement of the

geotextile with and without water load. It is also important to note that very little to no interface slippage occurred in any of the load conditions analyzed.

Table 1. Jefferson Lakefront material properties

Material Classification	unit wt. (pcf)	unit wt/g	Su (psf)		Material Classification	unit wt. (pcf)	unit wt/g	Su (psf)
Material 1a	115	3.575	600		Mat 8 vert 1,5	104	3.233	320
Material 2	115	3.575	600		Mat 8 vert 2,4	100	3.108	450
Mat 3 vert 1,5	108	3.357	300		Mat 8 vert 3	82	2.549	500
Mat 3 vert 2,4	99	3.077	400		Mat 9 vert 1,5	104	3.233	320
Mat 3 vert 3	118	3.668	800		Mat 9 vert 2,4	100	3.108	450
Mat 4 vert 1,5	108	3.357	300		Mat 9 vert 3	111	3.450	500
Mat 4 vert 2,4	99	3.077	310		Mat 10 vert 1,5	100	3.108	570
Mat 4 vert 3	116	3.606	500		Mat 10 vert 2,4	100	3.108	650
Mat 5 vert 1,5	83	2.580	450		Mat 10 vert 3	103	3.202	650
Mat 5 vert 2,4	90	2.798	450		Mat 11 vert 1,5	102	3.171	400
Mat 5 vert 3	116	3.606	500		Mat 11 vert 2,4	105	3.264	420
Mat 6 vert 1,5	83	2.580	450		Mat 11 vert 3	108	3.357	600
Mat 6 vert 2,4	90	2.798	450		Mat 12 vert 1,5	102	3.171	800
Mat 6 vert 3	82	2.549	500		Mat 12 vert 2,4	105	3.264	800
Mat 7 vert 1,5	104	3.233	320		Mat 12 vert 3	108	3.357	1000
Mat 7 vert 2,4	90	2.798	450		Mat 13 vert 1,5	120	3.730	1200
Mat 7 vert 3	82	2.549	500		Mat 13 vert 2,4	120	3.730	1200
					Mat 13 vert 3	117	3.637	1200

Note: Poisson ratio of 0.47 and shear modulus (G) to undrained strength (Su) ratio of 100 was used for all materials.

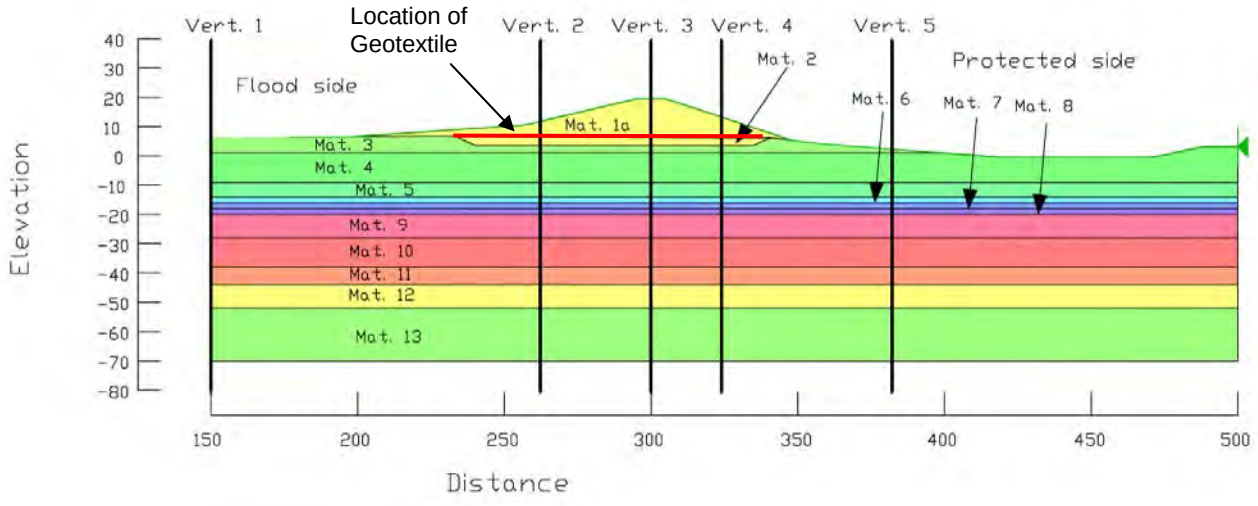

Figure 2. Stratigraphy and material types with vertical locations for the Jefferson Lakefront Section.

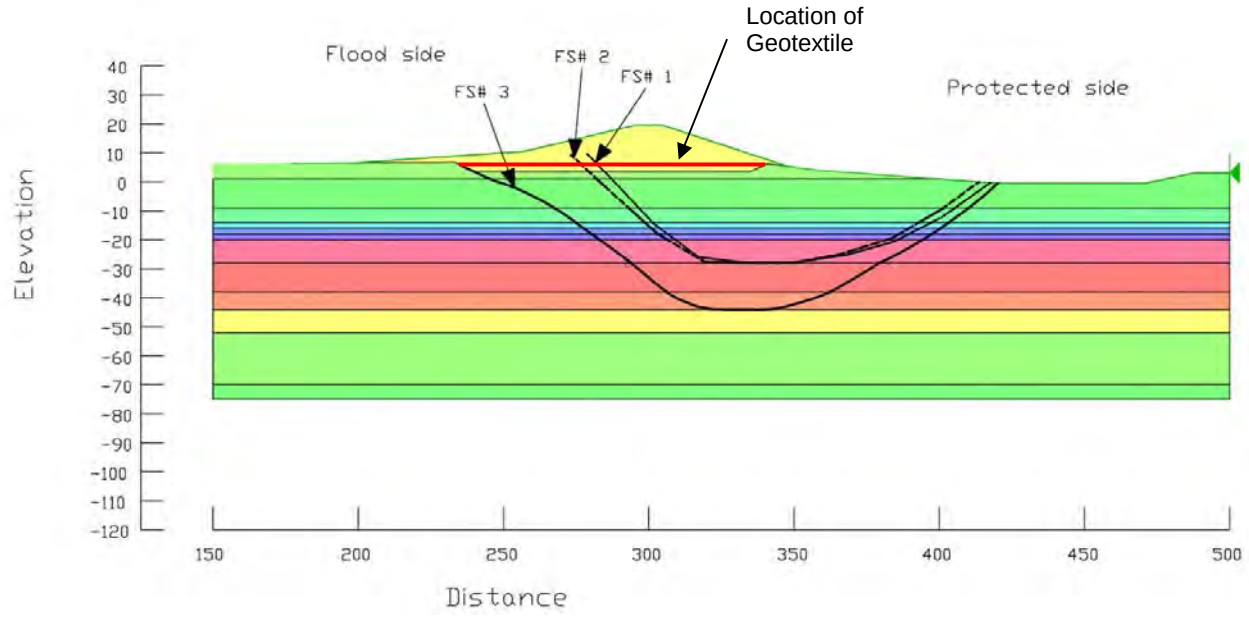

Figure 3. Limit equilibrium failure surfaces. FS# 1 = failure surface without geotextile and without water, FOS = 1.26. FS# 2 = failure surface without geotextile with WL = 19.5 ft, FOS = 1.22. FS# 3 = failure surface with geotextile with WL = 19.5 ft, FOS = 1.23.

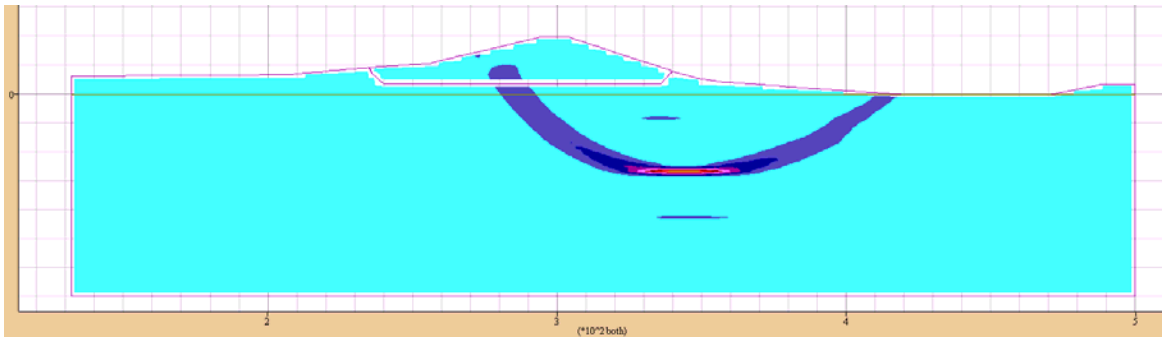

Figure 4. Failure surface without geotextile and without water. FOS = 1.33.

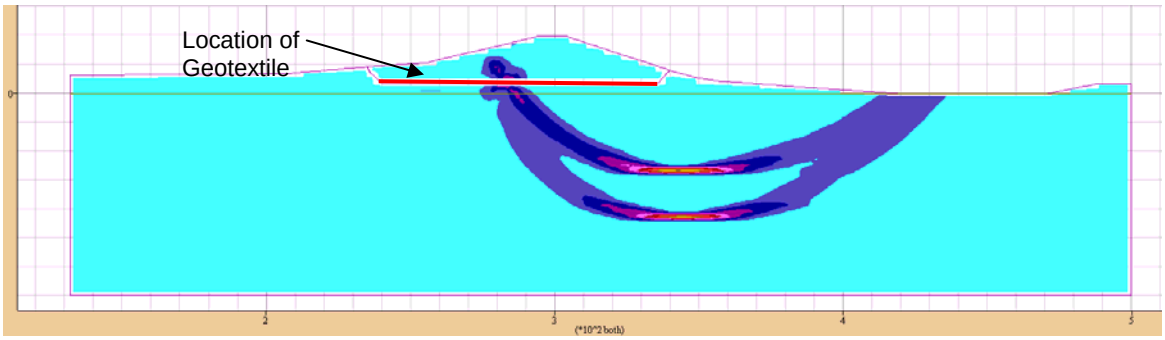

Figure 5. Failure surface with geotextile and without water. FOS = 1.51 at geotextile rupture.

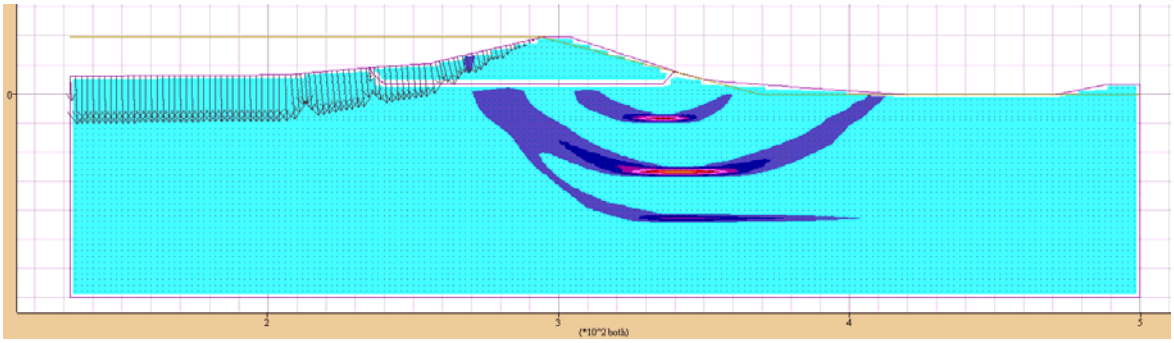

Figure 6. Failure surface without geotextile with WL = 19.5 ft. FOS = 1.20.

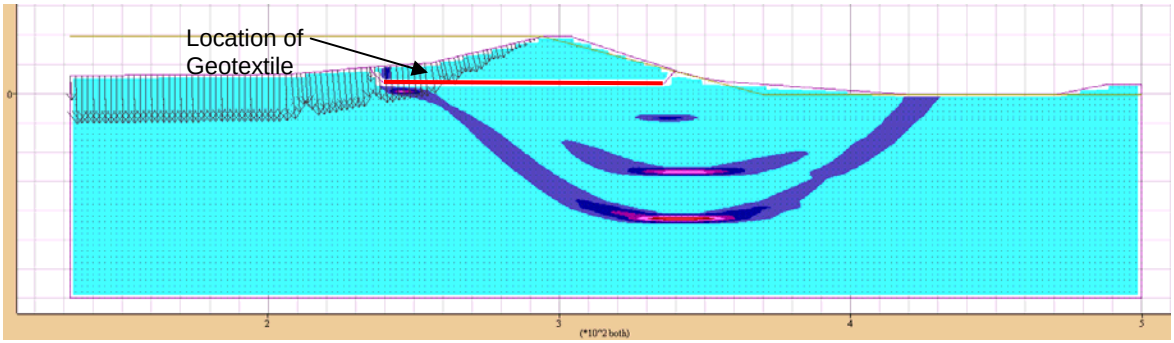

Figure 7. Failure surface with geotextile with WL = 19.5 ft. FOS = 1.30.

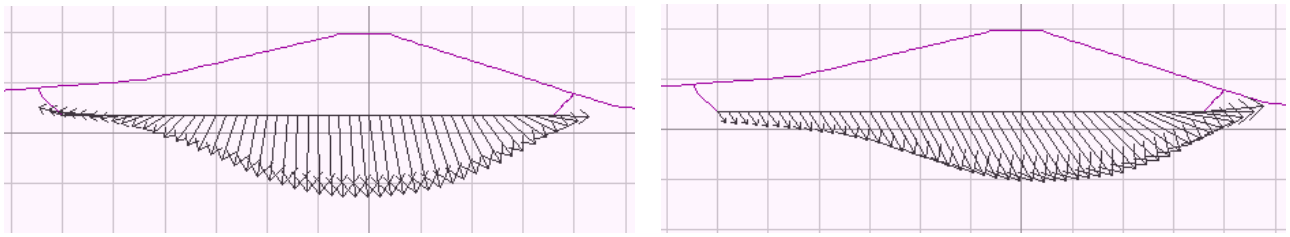

a) Embankment loading only. b) Embankment and water loading.

Figure 8. Geotextile displacement showing effect of storm surge water loading.

5.2 Lake Cataouatche

The Lake Cataouatche levees are just south of the Jefferson Lakefront levees as shown in Figure 1. Due to limits on the size of this paper, only a brief overview of the analysis and results are presented. A limit equilibrium and numerical analysis similar to the Jefferson Lakefront levee section was performed for a Lake Cataouatche preliminary alternative levee section. A cross section of the Lake Cataouatche levee is shown in Figure 9. The geometry of the Lake Cataouatche section is much wider than the Jefferson Lakefront section and contains berms on both the protected side and flood side. The soils strengths in the foundation are generally lower at the Lake Cataouatche section than the Jefferson Lakefront section by about 35%.

Similar to the Jefferson Lakefront section, the limit equilibrium analysis indicated a failure surface that extends around the geotextile on the flood side for the storm surge loading condition. A numerical analysis of the same loading condition was performed and indicated the same non-classic shaped potential failure surface. Comparison of the failure surface from the limit equilibrium analysis (using UTexas4) and numerical analysis are shown in Figure 10 by plotting the accumulated shear strains from the numerical analysis and overlaying the limit equilibrium failure surface (shown in blue). The factor of safety from both the limit equilibrium and numerical analyses were 1.58 for this loading condition.

While the majority of the details of the analysis are not provided for the Lake Cataouatche section, it is important to note that the non-classic shaped failure mechanism found in the Jefferson Lakefront section is similar. Furthermore,

geotextile displacement for the Lake Cataouatche section followed the same trend shown in Figure 8 for the Jefferson Lakefront section.

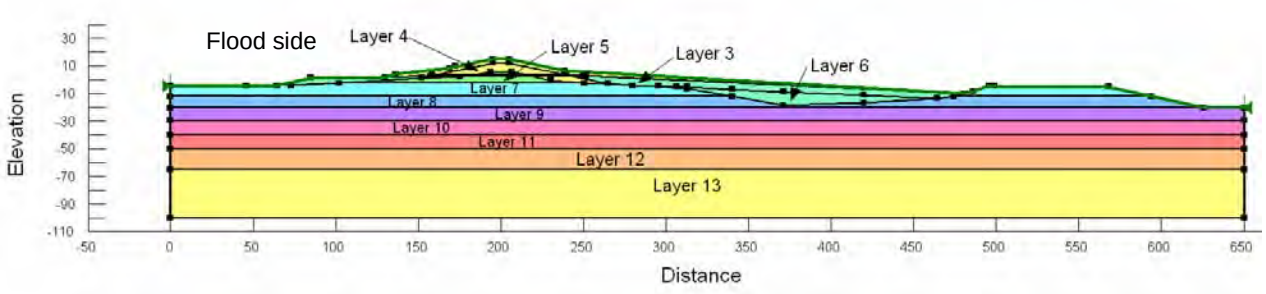

Figure 9. Geometry and stratigraphy of the Lake Cataouatche section.

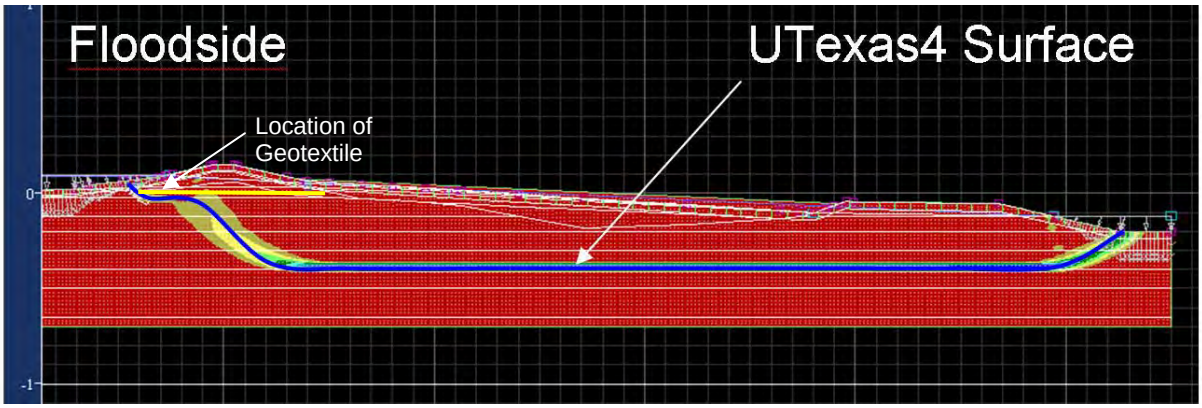

Figure 10. Comparison of the limit equilibrium failure surface (shown in blue) with numerical analysis accumulated shear strains for Lake Cataouatche section.

6. CONCLUSIONS

Critical non-classic shaped slip surfaces that extend around the geotextile in limit equilibrium slope stability analyses of levees are credible failure mechanisms that should be checked in the design process. It is reasonable for the presence of the geotextile to alter the location of the critical failure surface. Although embankments constructed on geotextile generally tend to spread laterally in both directions in an end of construction case, the short term case including hurricane surge loading can result in a different response. The asymmetric loading due to the surge tends to cause the embankment and foundation to displace more toward the protected side.

The effectiveness of the geotextile can be reduced where the critical failure surface extends beyond the flood side end of the reinforcement and the entire geotextile is within the failure mass. For the load cases considered, a properly designed geotextile capacity would allow the same factor of safety for the critical failure surface that extends around the geotextile and for the critical failure surface through the geotextile. Thus, for global stability criteria designers should evaluate the critical failure surface through the geotextile to determine the geotextile strength, determine pullout requirement, and evaluate critical non-classic shaped failure surfaces extending around the geotextile for a properly designed reinforced levee. This general design process (with the exception of the discovery of the non-classic shaped failure surfaces discussed here) has been utilized by the New Orleans District for a number of years and has proven to be an appropriate design procedure.

Locations of the critical slip surfaces found from the numerical analyses closely correspond with those found using limit equilibrium analyses. Factor of safety results from all analyses are summarized in Table 2. A comparison of the results indicates that there are minor differences between the limit equilibrium and numerical analyses, but generally the

different analyses from the three differing software packages support each other. Analysis of the Lake Cataouatche section indicated good comparisons between numerical and limit equilibrium analysis for both the factor of safety and critical failure surface.

Very little to no interface slippage occurred along the geotextile for both levee sections analyzed. This is similar to what was found in the laboratory pullout tests which indicated virtually no slippage between the soil and geotextile. Actual displacements and shearing during the laboratory pullout test occurred within the soil mass away from the fabric.

Table 2. Summary of computed factors of safety

Analysis Case	UTexas4 Factor of Safety	FLAC Factor of Safety
Jefferson Lakefront Section -		
No geotextile; no storm surge	1.26	1.33
Geotextile; no storm surge	-	1.51
No geotextile; full storm surge	1.22	1.20
Geotextile; full storm surge	1.23	1.30
Lake Cataouatche Section -		
Geotextile; design storm surge	1.58	1.58

7. SUMMARY

The stability of geotextile reinforced levees constructed on soft foundations is investigated for the New Orleans Hurricane and Storm Damage Risk Reduction System. Limit equilibrium analyses were performed for reinforced levees on soft soils within the HSDRRS. These analyses indicated that non-classic shaped failure mechanisms during hurricane storm surges may extend around the reinforcement on the flood side. A numerical analysis was used to verify the limit equilibrium results and indicated these failure mechanisms are kinematically admissible.

ACKNOWLEDGEMENTS

The authors would like to acknowledge the New Orleans District and Task Force Hope, New Orleans, LA of the U.S. Army Corps of Engineers for funding this work and the assistance provided by the MVN Geotechnical Branch in providing the background and specific project information.

REFERENCES

Gilbert, Paul A., Oldham, Jesse C. and Coffing, L. Rodgers, Jr. (1992) Laboratory *Measurement of Pullout Resistance of Geotextiles Against Cohesive Soils,* Technical Report GL-92-96. US Army Engineer Waterways Experiment Station, Vicksburg, MS 39180.

Itasca Consulting Group, Inc (2006a), *FLAC – User's Guide,* software version 5.0, Minneapolis, Minnesota.

Itasca Consulting Group, Inc (2006b), *FLAC/SLOPE – User's Guide,* software version 5.0, Minneapolis, Minnesota.

Schnabel Engineering South, LLC (2006), Final Geotechnical Data Report Self-Boring Pressuremeter Testing 17th Street, Orleans and London Street Canals New Orleans, LA, March 2006.

US Army Corps of Engineers (1989). *Bonnet Carre' Spillway Geotextile Reinforced Test Section and Pullout Tests,* New Orleans District, September 1989.

US Army Corps of Engineers (2003). *Slope Stability Engineer Manual,* EM 1110-2-1902, October 2003.

US Army Corps of Engineers (2007). *Hurricane and Storm Damage Reduction System Design Guidelines,* New Orleans District Engineering Division, October 2007.

US Army Corps of Engineers (2008). *Hurricane and Storm Damage Reduction System Interim Geotechnical Design Guidelines (Section 3),* New Orleans District Engineering Division, June 2008.

Post-Construction Landfill Liner Failure and Lessons Learned

R. Thiel, P.E., Vector Engineering, Inc, Grass Valley, CA, USA

ABSTRACT
A relatively small rural landfill was designed with a PVC/GCL composite liner system overlain by 300 mm of gravel. One end of the project contained a slope having an inclination at 4(H):1(V) for a length of approximately 58 m. Three months after construction the PVC liner had ripped along the crest of the slope, and the gravel and PVC had slid on top of the GCL along the entire slope length. The GCL was exposed about half way down the slope. The failing interface was clearly between the PVC and the GCL. The lessons learned from this project were (a) to conduct slope stability testing and analyses for interim and construction conditions in addition to final fill conditions, and (b) interface direct shear testing should have interfaces sprayed with water during the setup, and not just count on flooded conditions to allow water to travel to the interface. Neither of these lessons is particularly new to the industry, showing the value of having a project peer-reviewed by designers experienced with the nuances of geosynthetics design and construction.

1. INTRODUCTION

A relatively small rural landfill was designed with a composite liner system to be constructed well in advance of waste placement. The landfill expansion was designed to tie into a previous landfill cell. The lining system consisted of the following elements, from bottom to top:

- Prepared subgrade on firm well-graded native soils
- Needle-punched fabric-supported GCL, with a nonwoven geotextile on its upper side facing the overlying geomembrane
- 1 mm thick smooth PVC geomembrane
- 300 mm of granular drainage soil

The geometry of the landfill was very simple: a relatively flat bottom area, and at one end of the project there was a slope having an inclination at 4(H):1(V) for a length of approximately 58 m.

Because of the low waste volumes received at this rural landfill, the completed construction would be expected to remain exposed for a period of several years. Being in a northern climate, the site could expect snow and freezing conditions every winter.

Landfill construction was performed using conventional methods of subgrade preparation, smoothing, geosythetics deployment and seaming, and placement of gravel with thickened roads and spreading with an LGP dozer (D6). At one point during gravel hauling, dumping, and spreading on the floor some slippage and tearing of the geomembrane was noted. The incident was attributed to the haul trucks operating on a ridge line, and turning too tightly. The damaged area was repaired, the haul roads were rerouted to the valleys, and all spreading was pushed in an uphill direction, even on the relatively gentle 4% and 8% flanks of the bottom ridge-and-swale pattern.

After experiencing that small failure, for which the Contractor took full responsibility, the Contractor decided to take extra caution when placing gravel on the 4:1 slope. Instead of placing and spreading gravel in the traditional manner of dumping at the toe and pushing upslope with a dozer, the Contractor elected to place all of the gravel using a “telebelt” (Figure 1). The telebelt could extend approximately 36 m, and place the desired gravel thickness relatively precisely at all slope locations using a cantilevered conveyor belt using a remote control joystick. By using the telebelt from both the bottom and the top of the slope, no piece of construction equipment was ever required to get on the slope, and the exact thickness of gravel (300 mm) was able to accurately be placed everywhere in a gentle manner. Note that this method of placement, while not extremely rare, is not common because it is substantially more expensive than the traditional method of dumping and dozer-spreading. The Contractor decided to absorb the extra cost of doing the work in this manner rather than take a chance of creating any potential slippage after his experience in the more gently sloping bottom area.

The project was completed at the end of November. Just over three months later, in March, it was noted that from one day to the next the PVC liner had ripped a few hundred feet along the crest of the slope. The gravel and PVC had slid and exposed the GCL about half way down the slope. It had snowed and then rained that previous day and evening.

The failing interface was clearly between the PVC and the GCL. The exposed GCL appeared unstressed and undamaged.

Figure 1. Placing gravel onto PVC with telebelt on 4:1 slope.

The author was consulted by the Contractor after the failure to help ascertain why the slope had failed. The author had very limited design information available, and had not been involved during construction. During this investigation the author was only able to make one site visit, and conduct only a limited amount of testing before the parties were satisfied with the results discussed in this paper. Thus, while this case history is not fully comprehensive in its investigation, the limited amount of information that was gathered may prove useful to others designing veneer systems.

2. FIELD VISIT AND LABORATORY INVESTIGATION

The engineer had originally performed shear strength testing for the PVC/GCL interface. The normal loads used in the test program, however, were directed to evaluate the stability of the filled landfill, and were much too high to use for an evaluation of the veneer condition that existed at the time of construction or immediately after.

After consultation with the author, the engineer performed additional testing using samples of the exhumed GCL with fresh pieces of PVC. The GCL samples were carefully cut out, wrapped on a plastic pipe core, wrapped with plastic, and placed in sealed bags to preserve their moisture content. In the laboratory, the GCL samples were sandwiched against the PVC, and this was placed between native subgrade soils and gravel to simulated field conditions. The sandwich was hydrated under 4.8 kPa (100 pounds per square foot [psf]) below water for 24 hrs, and sheared at 0.1 mm/min. The tests were performed with a 30 cm by 30 cm square direct-shear box designed specifically for low-normal loads, and the boxes were calibrated to account for machine-friction. The resulting frictional shear strength of approximately 36 degrees peak and 35 degrees post-peak was much too high to be able to predict the failure (Figure 2).

Another sample was similarly prepared, and then froze to see if perhaps the freezing condition would affect the shear strength. After freezing, the sample was quickly placed in the shear box and sheared at 5.0 mm/min. Similar results were achieved, which again would not have predicted the failure.

In June the author was requested by the Contractor to visit the site. The failed slope was fully visible, with exposed GCL on the upper half. The exposed GCL was dry because of the arid site conditions. It was clear that the slope had failed from crest-to-toe as evidenced by the presence of bunched-up wrinkles in the PVC at the toe (Figure 3), and bulging and open cracks is the soil cover at the toe (Figure 4). The author shoveled through some of the gravel at the edge of the failed PVC, and lifted the edge of the PVC to observe how the interface looked where it had been protected from meteoric conditions. The surface condition of the exposed un-ripped PVC appeared to be excellent in all cases. The GCL was observed to be normally hydrated (defined by the author as softened to the point that it could be deformed with thumb pressure, but was in no way very soft or oozing), as one would expect from extended contact with the subgrade.

Very little bentonite was observed on the top of the GCL's upper NW geotextile. The bottom side of the PVC was observed to have a thin film of moisture (Figure 5).

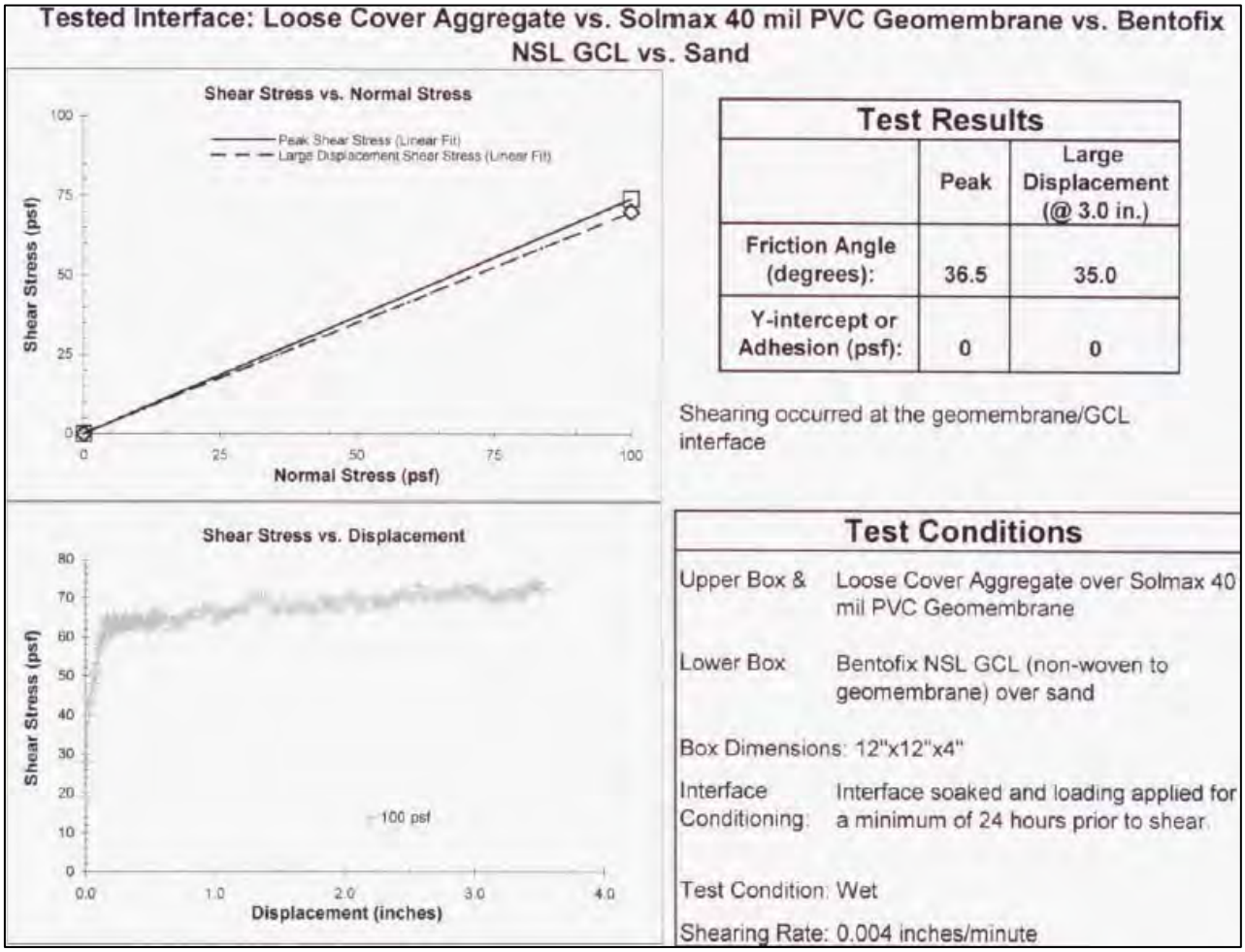

Figure 2. Direct shear test: Interface dry for test assembly, and then submerged after assembly.

Figure 3. Bunched-up wrinkles in PVC at toe of 4:1 slope.

Figure 4. Deformed and cracked cover soils near toe of slope.

Figure 5. Standing on exposed GCL (obscured with sandy gravel cover) and lifting edge of torn PVC. Clean white GCL can be seen been raised edge of torn PVC. Condensation water was noted on bottom side of PVC.

The last observation led the author to immediately commission the same laboratory used by the designer to perform a single-point shear test at 4.8 kPa (100 psf) normal load where the interface was sprayed with water immediately prior to shearing (a very common procedure when performing interface shear testing during the design phase). Using the same laboratory, equipment, and technician would remove inter-laboratory variations in test values. The test was performed with virgin materials with insignificant pre-hydration or consolidation, and sheared at 5.0 mm/min. Although other test parameters could have been used, these were the parameters chosen by the author given that he only had this single test opportunity on this project. The measured shear strength was a peak secant friction angle of 15.9 degrees and a post-peak angle of 13.5 degrees (Figure 6). These results, showing peak and post-peak frictional strength parameters straddling the slope angle, are indicative of a high probability of failure. These results also show what a large difference there is between a dry PVC/geotextile interface versus a wet one.

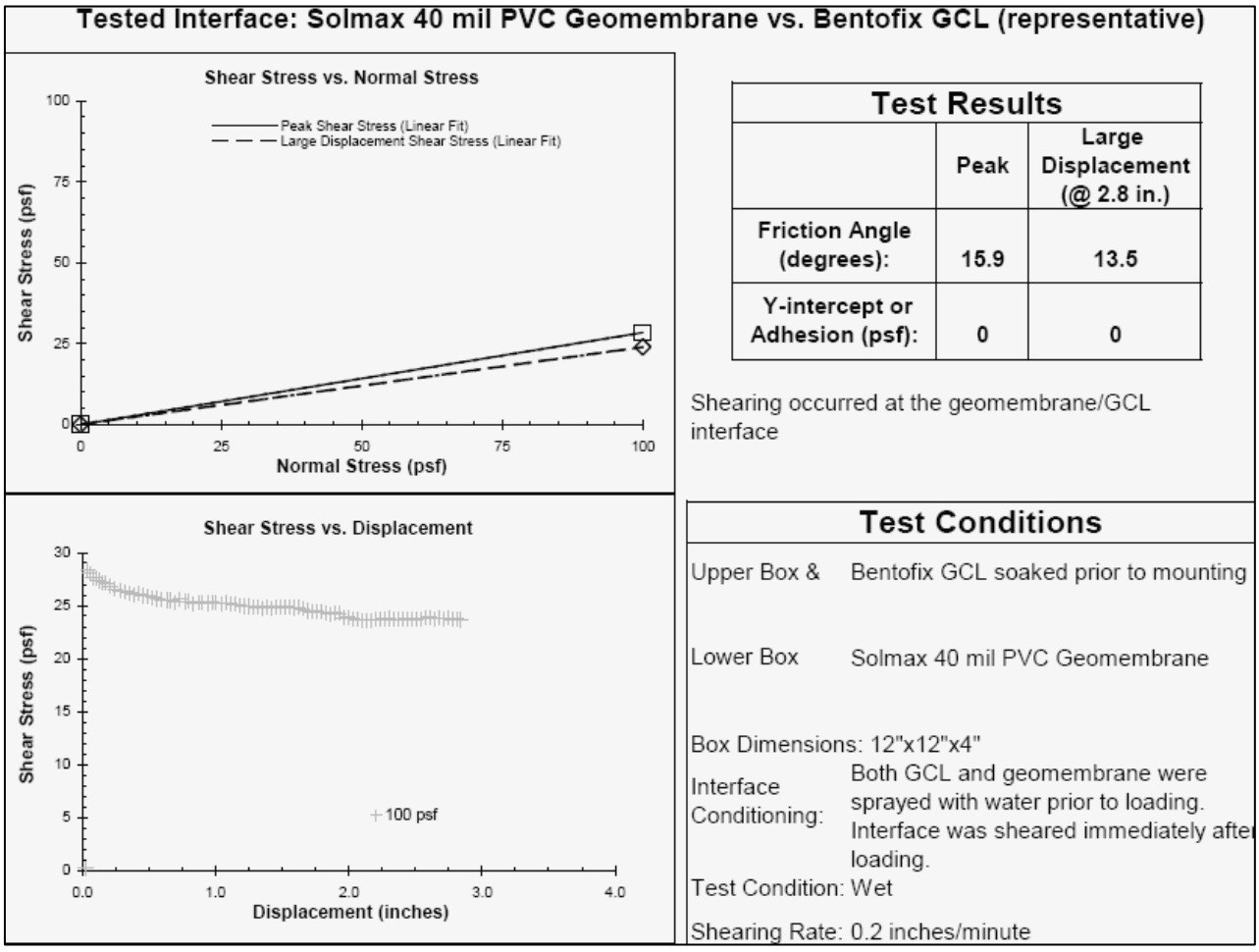

Figure 6. Direct shear test results: Interface sprayed with water before test assembly.

3. DISCUSSION

The relatively high friction angles achieved in the first round of forensic testing by the engineer were undoubtedly due to the presence of a dry interface between the PVC and the GCL. This condition existed even through the GCL from the field was pre-hydrated through months of subgrade contact, and in spite of having the test sandwich submerged under load for 24 hours. This suggests that even though a GCL may become largely hydrated, it may also preclude free water from getting to the interface in a direct shear test.

Common observation shows how quickly free-water condensation occurs on the underside of a piece of plastic that is placed on the ground. This is even more true if the plastic is exposed through a day-night cycle. Almost every geomembrane placed in the landfill industry is exposed for at least one day-night cycle. It is extremely rare that a

deployed geomembrane is covered with soil the same day that it is deployed. And thus designers, installers, and contractors accept it as a fact that virtually any time a geomembrane is deployed on earthen materials, free moisture will occur at the interface between a deployed geomembrane and its underlying subgrade.

When performing direct shear testing, it is essential that the test set-up reflects field conditions as closely as practical. The two preceding paragraphs lead to the following conclusions:

- The presence of free water is almost guaranteed in the field conditions at the geomembrane interface with underlying earthen subgrades.
- Sandwiching a GCL against a geomembrane in a dry state, loading, and then hydrating may have a very low likelihood of allowing any free water to reach the geomembrane interface.
- Laboratory direct shear testing with geomembranes against surfaces that will have access to soil moisture should always be sprayed with water before assembling them in the shear box.

The limited amount of field observation and laboratory testing performed for this case study suggests how critical the difference between wetting and not wetting the interface can be in a test program. This same lesson was learned in the 1988 failure of the Kettleman Hills hazardous waste repository (author's personal discussions with designers).

4. LESSONS LEARNED

There were two main lessons learned in this project for people who regularly practice in this industry.

1. Projects need to evaluate stability for construction conditions; not just final operational conditions. In this case, this would have meant evaluating the slope stability for the veneer system by performing interface shear strength testing at the appropriate low normal loads.
2. Direct shear tests involving clays or GCLs against geomembranes need to have the geomembrane interface sprayed with water before the test materials are assembled. Simply flooding the assembled test "sandwich" may never allow the interface to become wet. Under field conditions a deployed geomembrane will have condensation water on its bottom surface within a matter of hours, and thus spraying the interface with water is representative of field conditions. There can be a large difference in shear strengths between a dry interface and a wet one.

Neither of the two lessons described above are unusual or new in the geosynthetics and landfill lining industry. For designers who do not regularly practice in this field, it is useful to engage the peer-review services of someone who regularly practices in this field. In fact, this principle applies to any area of professional practice.

Biogas Leakage through Landfill Cap Covers

C. Barral, LTHE, University Joseph Fourier Grenoble, France, LGCIE, INSA Lyon, France.
H. Nunes PITANGA, EESC, University of São Paulo, Brazil.
P. Pierson, LTHE, University Joseph Fourier Grenoble, France.
I. Djeran-Maigre, LGCIE, INSA Lyon, France.
O. Monje Vilar, EESC, University of São Paulo, Brazil.
J-P. GOURC, LTHE, University Joseph Fourier Grenoble, France.

ABSTRACT
This paper presents a simple laboratory method to measure the gas permeability of porous materials with the method of the falling-pressure test. The experimental set consists in a chamber filled with a specific gas at a specific pressure. The specimen of the material tested is placed at one side of the chamber with a gastight seal. Once the chamber is isolated from the gas supply, the gas pressure in the chamber decreases because of the gas leakage through the material tested. This is registered and the analysis of the response shows that it can be approached by an exponential law with only one time constant, under some experimental conditions. It is possible to characterize the gas permeability of the specimen by this time constant and to deduce its gas permeability coefficient. This method is applied to laboratory tests to compare different cover liners: compacted clay liners and geosynthetic clay liners.

1. INTRODUCTION

In municipal solid waste landfills, the cover barrier must minimize the biogas leakage to the atmosphere, during all the lifespan of the site and under mechanical (relative settlements), climatic (cycles of freezing-thaw and drying-moistering) and chemical (strong capacity of cation exchange of clayey materials) stresses. The materials constituting the layer of sealing are natural (site clay alone or bentonite added) or composite (geomembrane, geosynthetic clay liner) and their hydraulic efficiency must be maintained during the lifetime of the cover system.

Gas emissions generated in waste containment facilities and released into the atmosphere have become a very sensitive issue in recent years given that carbon dioxide and methane, the main gases resulting from waste decomposition, have been recognized for their significant contribution to the process of global warming (Grantham et al., 1997). Furthermore, gases can induce explosions within landfill and can migrate to adjacent areas hence resulting in extensive property damage and loss of life as exemplified by the incidents in Loscoe, England (Williams and Aitkenhead, 1991), Skellingsted, Denmark (Kjeldsen and Fisher, 1995) and in Masserano, Italy (Jarre et al., 1997).

In this context, the efficiency of clay barriers in controlling gas emissions is a major issue in landfill cover-layer designs and an assessment of their effectiveness as a barrier to gases continues little investigated up to the present time.

This paper presents a simple method to characterize the gas permeability of porous materials with an imposed deformation, and with the method of the falling pressure test. The main principles of the method are presented in section 3. It is applied to a laboratory test (section 4) on CCL and GCL special experimental devices.

2. GAS PERMEABILITY OF CCL AND GCL

The traditional method for determination of porous materials gas permeability essentially consists in measuring the gas flow through the material under steady-state flow. Tests are generally conducted on unsaturated soils (Eischens and Swanson, 1996; Samingam et al., 2003), rocks (Cosse, 1996), geosynthetic clay liners (Didier et al., 2000; Shan and Yao, 2000; Bouazza and Vangpaisal, 2003; Vangpaisal and Bouazza, 2004) or cement based materials (Gallé and Daian, 2000; Loosveldt et al., 2002). Moreover, the measure of very low permeability values presents special problems for which the standards of measurement techniques are generally not very practical and are difficult to be implemented (Roy, 1988). In the case of very low permeability, it takes a significant period of time to establish the steady-state flow condition.

Therefore, low permeabilities in porous media can be determined in an unsteady state (Selvadurai and Carnaffan, 1997). Figg (1973) proposes an unsteady state method to determine the air permeability of concrete: the initial pressure in a chamber in contact with the specimen tested is lowered by a vacuum pump. The time necessary to obtain a given pressure increase in the chamber characterizes the air permeability of this specimen. Calogovic (1995), Yssorche et al. (1995) and Claisse et al. (2003) propose to determine an air permeability coefficient from Figg's experiment by applying Darcy's law.

Recently, Li et al. (2004) proposed an analytical solution for estimating air permeability of asphalt layers using the data obtained by applying the falling-pressure method in laboratory. In this method, air under pressure is introduced into a chamber in contact with the specimen tested. Once this upstream chamber is isolated, the reduction in the air

pressure P(t), due to air migration through the specimen, is recorded. An analytical solution of the simplified equation describing the variations over time of the air chamber pressure allows the determination of the effective permeability coefficient (k):

$$P(t) = P_{atm} \frac{\left[\alpha + e^{\left(-\frac{t}{\tau}\right)}\right]}{\left[\alpha - e^{\left(-\frac{t}{\tau}\right)}\right]} \quad [1]$$

$$\text{where } \alpha = \frac{\left[P_c(0) + P_{atm}\right]}{\left[P_c(0) - P_{atm}\right]} \quad [2]$$

$$\text{and } \tau = \frac{V_0 L \mu}{A_0 P_{atm} k} \quad [3]$$

P_{atm} is the atmospheric pressure (Pa), V_o is the air chamber volume (m^3), A_o is the specimen area (m^2), L is the sample thickness (m), μ is the gas dynamic viscosity (Pa.s) and k the effective permeability coefficient (m^2).

3. THE FALLING PRESSURE TEST

The principle of the gas permeability test based on the falling-pressure method is the following (Figure 1.): the specimen of the material tested of thickness Z is placed with a lateral gas tight seal, at one side of a chamber of known volume (V_0) which is filled with air at a specific pressure.

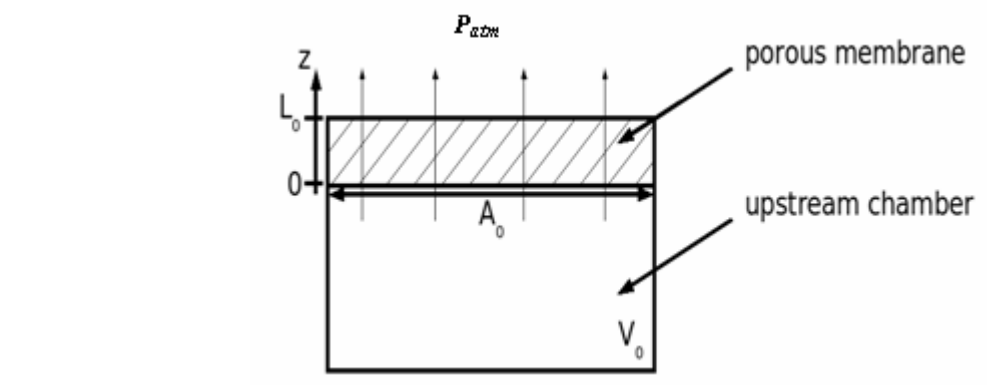

Figure 1. Lay out of gas permeability test based on the falling-pressure method.

Once the chamber is isolated from the air supply, the gas pressure in the chamber [P_c(t)] decreases until equilibrium with the atmospheric pressure (P_{atm}) is reached because of the air leakage through the material tested. If during the test P_c(t) is closed to P_{atm}, an analytical solution of the simplified equation describing the variations with time of the air chamber pressure allows the determination of the intrinsic permeability coefficient k (Barral et al., 2008):

$$P_c(t) = P_{atm} + \left(P_c(0) - P_{atm}\right)\exp\left(-\frac{t}{\tau}\right) \quad [4]$$

where τ is as shown in Equation 3.

This method can be easily applied to measure the biogas permeability of compacted clay liners (CCL) (Barral et al., 2008) or geosynthetic clay liners (GCL) (Pitanga et al., 2008) in laboratory. It may also be applied on geomembranes as shown by Barroso et al. (2006).

4. EXPERIMENTAL PROGRAM

4.1 Tests on Compacted Clay Sample

This test was conducted at the laboratory LTHE in Grenoble. In order to take into account the mechanical stress which may be observed on site, the specimen of CCL (rectangular shape) is subjected to a 4 point bending test as shown on Figure 2. The primary chamber below the specimen is filled with the gas tested (i.e. nitrogen or other) and the pressure decrease of this gas is recorded during the experiment time. The advantage of such a method is to allow to test deformed specimens as well as material characterized by a very low gas permeability. The aptian clay samples have a uniform porosity equals to 30 % and are saturated about 90 % (w_{opt} = 16,25 % for an energy of compaction of 100 %).

Figure 2. Gas permeability test on a compacted clay liner specimen subjected to a 4 point bending test (Barral et al., 2008).

The gas pressure relaxation to the atmospheric pressure is presented in Figure 3. Several independent tests have been conducted on the same non deformed CCL specimen under different initial pressure. Even if the measurement noise appears to be sensitive, the accordance between the different tests is satisfactory. Then a fitting procedure is used to calculate the time constant τ from Equation 4 using the first 1,3 seconds of the experiment (corresponding to 70 measurement points). Finally, the gas permeability coefficient (k) of the specimen is calculated from Equation 3 using the geometrical characteristics of the apparatus. It leads to the permeability coefficient with nitrogen: k = $3{,}0\times10^{-12}$ m^2 for a CCL with moisture content w = 17%.
The test was repeated until 6 times to see if what we measure corresponds to the gas permeability of the sample and if we do not measure partially the effect of the gas absorption by the clay. The constancy of the measures and the importance of the quantity of gas having crossed the sample during these successive tests show that the absorbed part is very negligible in front of the quantity of gas having crossed the sample.

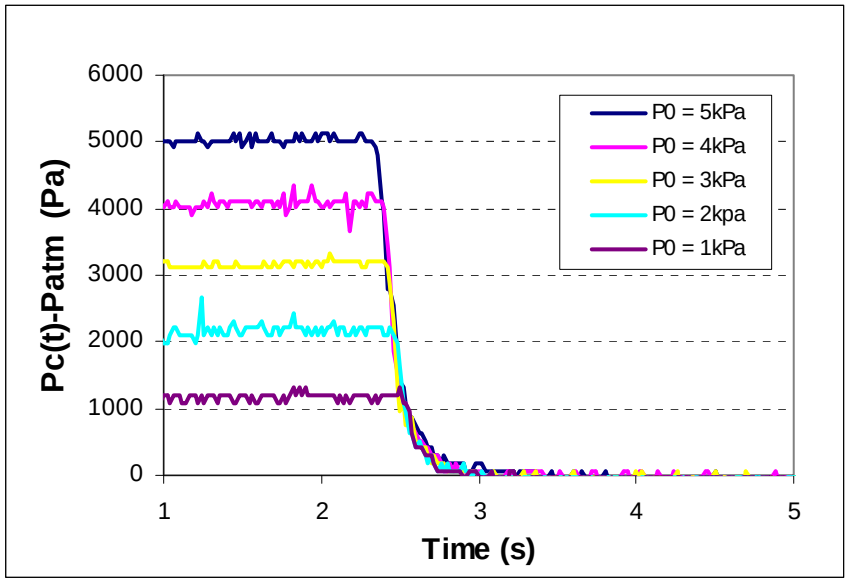

Figure 3. Results obtained on a non deformed CCL specimen under different pressure gradients (Barral et al., 2008).

4.2 Tests on Geosynthetic Clay Liner

The tests on the deformed GCL are carried out in a cylindrical cell with a deformed base (diameter Ø= 46 cm).The GCL sample (Figure 4.) is placed on it and is deformed (with a final shape imposed by the base of the cell) by application of a water pressure (Pitanga et al., 2008). Because of the small gas permeability of GCLs, the permeability gas test is carried out in unsteady state on the deformed sample. Indeed, below the sample, the mould is porous and constitutes a volume (V_o) filled by gas under pressure. The lower face of the sample is in direct contact with gas and the upper face is opened with the ambient air. The gas in the cell can escape only through GCL. GCL samples consisting of dry powdered sodium bentonite sandwiched between a non-woven and a woven geotextiles, held together by needle punching, with a mass per unit area corresponding to 5.7 kg/m^2, were used for the tests.

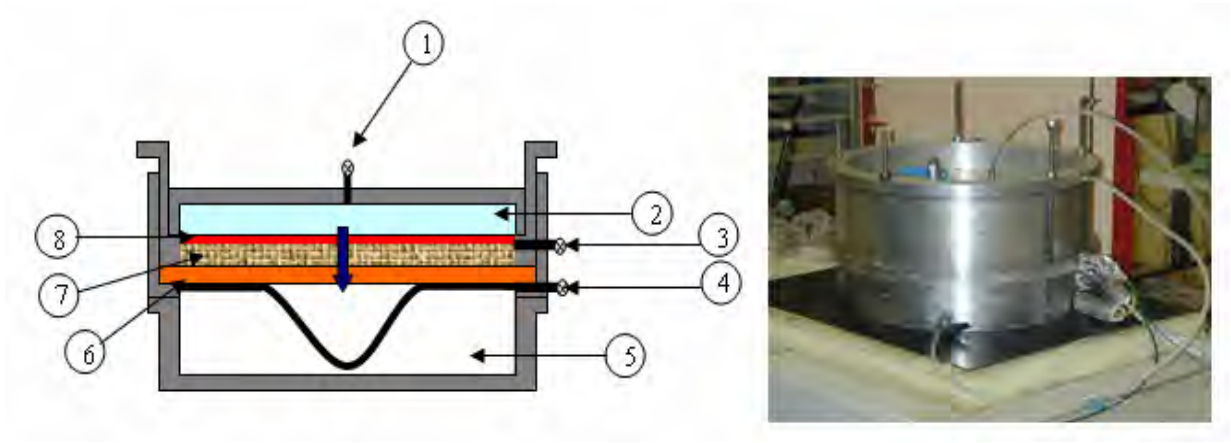

Figure4. Cell with a deformed base: 1 Water inflow; 2 Water pressure; 3 Gas outflow; 4 Gas inflow; 5 Porous mould; 6 GCL; 7 Sand; 8 Membrane (Pitanga et al., 2008).

Different hydration conditions and moisture content of the samples were obtained after immersion at different times (5 to 60 minutes). After the immersion time, the samples were placed in plastic bags, sealed to prevent moisture loss and then the samples were left to swell under zero confinement for 15 days, time deemed necessary to obtain uniform moisture (Didier et al., 2000; Bouazza and Vangpaisal, 2003).
Once the test assembly was completed, a normal stress of 20 kPa was applied to the GCL sample to deform it and settle it to the surface of the porous plate. The imposed relative gas pressures were on the order of 2,5 to 3,6 kPa. Each sample was tested 8 to 9 times to check the repeatability of test results.

Figure 5. shows two typical curves of the gas pressure variation [P(t)-P_{atm}] over the duration of the test (t) corresponding to the non deformed GCL samples with moisture content of 68% (Fig. 5a) and 99,7% (Figure 5b.). It is worthy to notice the difference between the duration of the tests, as the drier sample demands less time for completion of the test thanks to its larger permeability as compared to the wetter sample.

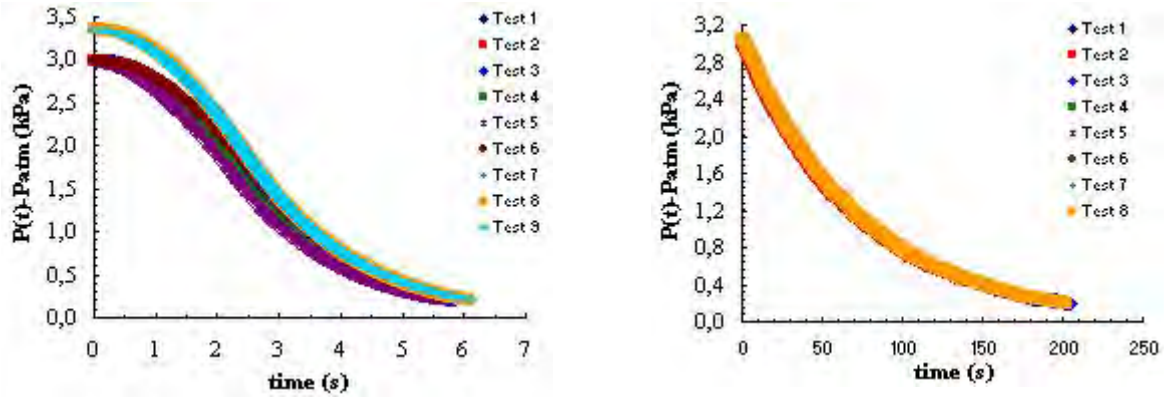

(a) w=68% (b) w=99,7%

Figure 5.Variation of the gas pressure with time for the GCL samples (Pitanga et al., 2008).

Test results from Figure 5. were used to calculate the permeability coefficient k of the specimens from Equation 3 using the geometrical characteristics of the apparatus. It leads to the permeability coefficient with nitrogen: k = 2,9×10^{-14} m^2 for a GCL with w = 68% and k = 6,85×10^{-16} m^2 for a GCL with w = 99,7%.

5. CONCLUSION

The experimental results obtained in this work attest to the interest in and the validity of the falling-pressure method aimed at determining the gas permeability of CCL and GCL. This method provides results in a faster and simpler way. Furthermore, the repeatability of the falling-pressure curves and the results obtained for the same sample test demonstrate better reliability of the proposed method. It should be observed that the method is still valid at high water content, contrary to many steady state methods generally used to measure the gas permeability of porous media, because of the very small gas pressure gradient applied. Steady state methods require high pressure gradients to make the gas flow measurement possible, which generate uncontrolled water movements inside the material, with a possible drying effect.
This study, which is still going on, should give useful informations about the biogas leakage through landfill covers. The falling-pressure test allows the comparison of all the materials used in landfill cover barriers (CCLs, GCLs) concerning their gas permeability in laboratory or on site. Additional research should be carried out aiming to study the effect of other variables of the test, such as the effect of bending stress.

REFERENCES

Barral, C., Oxarango, L., Pierson, P. (2008). Characterizing the gas permeability of natural and synthetic materials. To be published in *Transport in Porous Media*.

Barroso, M., Pierson, P., Lopes, L.G. (2006). A non destructive method for testing non flexible dual geomembrane seams using gas permeation. *Geosynthetics International*, 13(1), pp.15-22.

Bouazza, A., Vangpaisal, T. (2003). An apparatus to measure gas permeability of geosynthetic clay liners. *Geotextiles and Geomembranes*, 21, pp 85-101.

Calogovic, V. (1995). Gas permeability Measurement of porous Materials (Concrete) by time-variable Pressure Difference method. *Cement and Concrete Research*, 25(5), pp. 1054-1062.

Claisse, P.A., Ganjian, E., Adham, T.A. (2003). A Vacuum-Air Permeability Test for in situ Assessment of Cover Concrete. *Cement and Concrete Research*, 33, pp.47-53.

Cosse, R. (1996). Basics of Reservoir Engineering: Oil and Gas field development techniques. *Institut Français du*

Pétrole Publications, Edition Technip, pp 44-46.

Didier, G., Bouazza, A., Cazaux, D. (2000). Gas permeability of geosynthetic clay liners. *Geotextiles and Geomembranes,* 18, pp 235-250.

Eischens, G., Swanson, A. (1996). Proposed standard test method for measurement of pneumatic permeability of partially saturated porous materials by flowing air. *Geotechnical Testing Journal,* 19(2), pp 232-238.

Figg, J.W. (1973). Methods of measuring the air and water permeability of concrete. *Magasine of Concrete Research*, 25 (85), pp 213-219.

Gallé, C., Daian, J.F. (2000). Gas permeability of unsaturated cement-based materials: application of a multi-scale network model. *Magasine of Concerte Research*, 52 (4), pp 251-263.

Grantham, G., Latham, B., Callen, G., (1997). Landffil contribution to “greenhouse gas emission”. Proc. *6th Int. Landffil Symposium*, Cagliari, Italy, 1, pp 17-34.

Jarre, P., Mezzalama, R., Luridiana, A. (1997). Lessons to be learned from a fatal landfill gas explosion. Proc. *6th Int. Landfill Symposium*, Cagliari, Italy, pp 497-506.

Kjeldsen, P., Fisher, E.V. (1995). Landfill gas migration – field investigations at Skellingsted landfill, Denmark. *Journal Waste Manag. Res.,* 13, pp 467-484.

Li, H., Jiao, J.J., Luk, M. (2004). A falling-pressure method for measuring air permeability of asphalt in laboratory. *Journal of Hydrology*, 286, pp 69-77.

Loosveldt, H., Lafhaj, Z., Skoczylas, F. (2002). Experimental Study of Gas and Liquid Permeability of a Mortar. *Cement and Concrete Research,* 32, pp. 1357-1363.

Pitanga, H.N. , Pierson, P., Monje Vilar, O. (2008). Gas permeability of geosynthetic clay liner under transient flow regime. Send to *Geotextiles and Geomembranes*.

Roy, D.M. (1988). Relationships Between Permeability, Porosity, Diffusion and Microstructure of Cement Pastes, Mortar and Concrete at Different Temperatures. *Materials Research Society Symposium*, MRS Press, Pittsburgh.

Samingam, A.S., Leong, E.C., Rahardjo, H., (2003). A flexible Wall Permeameter for Measurements of Water and Air Coefficients of Permeability of residual Soils. *Can. Geotech. J.,* 40, pp. 559-574.

Selvadurai, A.P.S., Carnaffan, P. (1997). A transient pressure pulse method for the measurement of permeability of a cement grout. *Canadian Journal of Civil Engineering*, 24, pp 489-502.

Shan, H.Y., Yao, J.T. (2000). Measurement of air permeability of Geosynthetic Clay Liners. *Geotextiles and Geomembranes*, 18, pp 251-261.

Vangpaisal, T., Bouazza, A. (2004). Gas permeability of partially hydrated geosynthetic clay liners. *Journal of Geotechnical and Geoenvironmental Engng.*, ASCE, 130 (5), pp 93-102.

Wiliams, G.M., Aitkenhead, N. (1991). Lessons from Loscoe : the uncontrolled migration of landffil gas. Quarterly *Journal of Engineering Geology*, 24, pp 191-207.

Yssorche, M.P., Bigas, J.P., Ollivier, J.P. (1995). Mesure de la perméabilité à l'air des bétons au moyen d'un perméamètre à charge variable. *Materials and Structures*, 28, pp 401-405.

Geosynthetics 2009
February 25-27 2009, Salt Lake City, Utah

Alternative Lining System Anchorage using Batten Strips

J.A. McKelvey, III, Earth Engineering Incorporated, East Norriton, Pennsylvania, USA

ABSTRACT
At a landfill in Southern California, a temporary concrete drainage channel was required along the limits of the first phase of the lining system. During the subsequent phase of landfill development, the drainage channel was to be removed and relocated. Once the drainage channel was removed, the lining system would be extended to the final limits of the subsequent phase. Due to construction sequencing, it was desired to construct the drainage channel prior to installing the first phase lining system. This sequence would preclude anchorage of the lining system in a conventional anchor trench due to the geometric constraints at the limits of the first phase. Accordingly, an alternative anchorage system for the lining system would be required. A batten strip anchorage system was considered the most appropriate means to provide the necessary anchorage for the lining system. In order to develop the appropriate anchorage capacity, veneer stability and wind uplift analyses were performed for the lining system. The lining system would be supported by placing the geosynthetics between two timbers, which would then be bolted to the concrete drainage channel at regular intervals. The distance between bolts was maximized by modeling the system as a beam on an elastic foundation. This paper will present the design methodology used in development of the batten strip anchorage system, and discuss construction of the system. The subsequent dismantlement of the batten strip anchorage system during lining system expansion will also be discussed.

1. INTRODUCTION

At a landfill located within a canyon in Southern California, development of the landfill was to be performed in phases to accommodate massive earthworks activities necessary to carve out landfill airspace within the canyon, while allowing revenue from waste acceptance to begin as soon as practical. The phased development required construction of a concrete-lined drainage channel along the perimeter of the first phase of development. The perimeter drainage channel was required to collect the substantial amount of surface water during the rainy season that would otherwise flow into the landfill, creating additional leachate. Subsequent development of the landfill would extend the lining system to the final limits of the landfill, which would require the drainage channel to be relocated to the permanent perimeter. The first phase of the landfill had slope inclinations as steep as 1.5H:1V (Horizontal:Vertical) with slope heights as high as 12m. The lining system on the side slopes is shown in Figure 1, consisting from bottom to top of a geosynthetic clay liner overlain by a high density polyethylene geomembrane with a textured surface on the bottom and a smooth surface on the top, overlain by a geonet, that is overlain by a nonwoven geotextile. The protective cover soils for the lining system were 600mm thick, and were to be placed in 6m vertical intervals, once during initial construction of the phase, the remaining to be placed by landfill operations personnel once waste reached 6m thick.

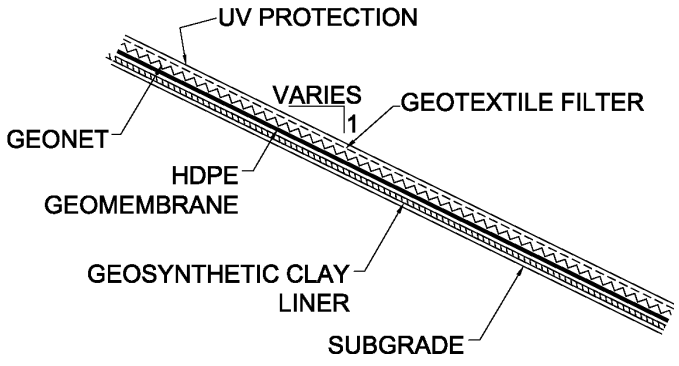

Figure 1. Side slope lining system

The lining system was to be supported at the top of the slope by embedding the lining system components in a standard anchor trench. Due to the volume and velocity of stormwater flowing at the limits of the first phase lining system during the rainy seasons, a concrete trapezoidal channel was required. Figure 2 shows the anchor trench and perimeter drainage channel initially proposed for the first phase of construction. To minimize stormwater flow into the excavations

required for the first phase of development, the drainage channel was constructed prior to installing the first phase lining system. This sequence would preclude anchorage of the lining system in a conventional anchor trench due to the geometric constraints at the limits of the first phase. An alternative anchorage system for the lining system needed to be provided to secure the lining system during the filling of the first phase of the landfill.

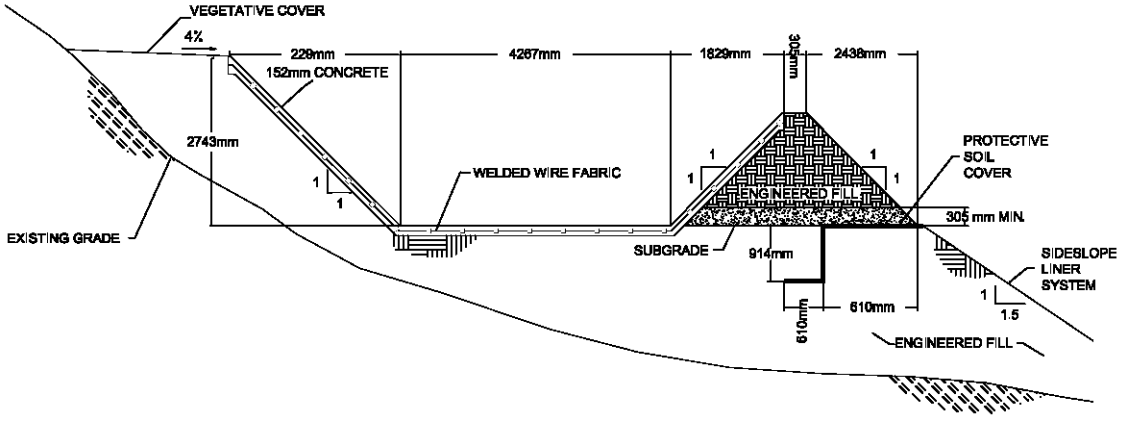

Figure 2. Initially proposed anchor trench

The lining system would be supported by placing the geosynthetics between two timbers, which would then be bolted to the concrete drainage channel at regular intervals. As the anchorage was to be constructed at the top of the concrete channel, seepage beneath the lining system was anticipated to be nominal. The geosynthetic clay liner was protected from hydration by placing between two geomembranes which were welded together as shown in Figure 3. To develop the alternative anchorage system, the tensile load anticipated on the lining system needed to be understood.

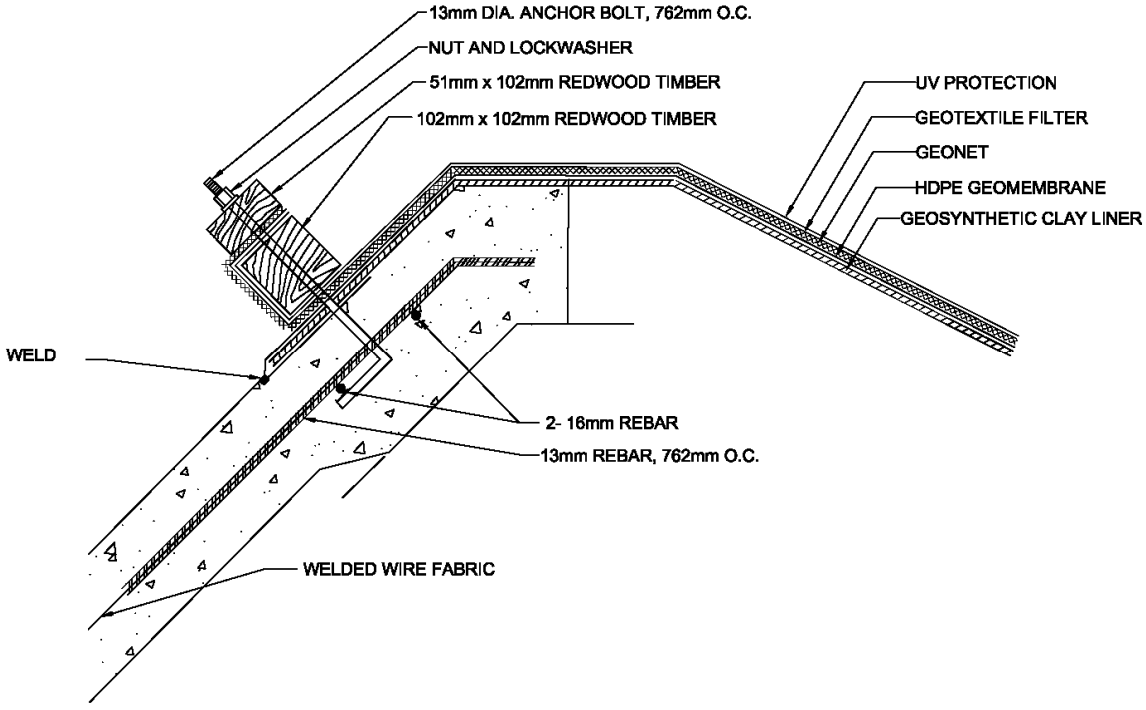

Figure 3. Batten strip anchorage system.

2. ANTICIPATED TENSILE LOADS

Tensile loads anticipated for the lining system included tension of lining system components associated with down drag due to cover soil placement, and wind uplift on exposed portions of the lining system. As the landfill is located in a significantly active seismic area, a slip plane was intentionally introduced to preclude the geomembrane from being stressed during the design earthquake. The slip plane was the smooth surface on the upper surface of the geomembrane and the overlying geonet. As the inclination proposed for the side slope was 1.5H:1V (horizontal:vertical), staged construction of the first phase of the lining system was anticipated. Veneer stability analyses were performed to ascertain the optimum height of protective cover soil placement for each stage of protective cover soil placement.

2.1 Veneer Stability

It was anticipated that the lining system components above the slip plane would be subjected to tensile loadings as the angle of slope far exceeded the interface friction angle governing the lining system (i.e., the smooth geomembrane to geonet interface). Using the analysis methods developed by McKelvey (1994), the largest equipment that could be used to place the protective cover soils was determined to be a bulldozer having a gross operating weight no more than 17,510kg and an applied ground pressure not exceeding 58kPa. The gross operating weight and ground pressure limitations allowed use of small and medium size bulldozers. To maximize the amount of protective cover soil that could be placed, the thickness of protective cover was tapered, which increased toe buttressing of the protective cover soils (McKelvey and Deutsch, 1991). It was found through analysis iteration that the cover soils would need to placed in stages, with a maximum height of slope of 6m, with the upper surface of the protective cover soils inclined at 1.95H:1V.

As the veneer stability analyses dictated the need for staged construction of the landfill side slopes, a thin-film geomembrane was required to be placed over the top of the lining system to protect the upper geotextile from ultraviolet degradation. As the thin-film geomembrane would be exposed to the elements, the geomembrane would subjected to tensile loadings associated with wind uplift.

2.2 Wind Uplift

Results of the veneer stability analyses dictated the need for staged construction, which left as much as 6m of the landfill side slopes exposed to the elements. The greatest wind velocities measured at the landfill during operations approached 80km/hr. Leeward slopes would experience a suction over their entire length, with the most pronounced suction occurring along the upper third of the slope (Giroud, et. al., 1995). For this application, it was assumed that the most pronounced suction occurred along the entire length of the exposed thin-film geomembrane. Using equations developed by Giroud, et.al, (1995), the peak suction on the exposed lining system was calculated to be 250Pa, over the maximum exposed slope length of 11m.

The thin-film geomembrane that was used for ultraviolet protection of the top geotextile had a nominal thickness of 0.76mm, and an estimate modulus of elasticity of 227MPa. The geomembrane stiffness (J) of the thin-film geomembrane was calculated as the product of the thickness and modulus of elasticity (Giroud, et. al., 1995), equal to 173kN/m. Using the appropriate table in Giroud, et. al, (1995), the resulting geomembrane tension induced by wind uplift was calculated to be 3.87kN/m. As the veneer stability analyses developed a protective cover soil geometry that would not include tension in the lining system, only the tension induced by wind uplift would need to be resisted by the batten strip anchor system.

3. BATTEN STRIP ANCHORAGE DESIGN

To transfer the tensile load to the batten strip anchorage, the geosynthetics were to be placed under the lower board, and the geonet and upper geotextile placed between the two boards, which were then to be secured together using nails. Spacing of the nails was then determined using the method of beams on an elastic foundation. This analytical model was initially developed by Winkler in 1867 to analyze stresses and deflections in railroad track (Cook and Young, 1985). The stiffness of the beam foundation is called the Winkler foundation modulus (k, kN/m/m), which is equal to the product of the foundation beam's elastic modulus (kN/m^2) and the width (m) of the beam.

For this application, the top board was considered as an infinitely long beam having concentrated loads at uniform spacing. The lower board was to serve as the foundation for the upper board, which has the same elastic modulus as the upper board. The nails would constitute a point load on the boards. The deflection at the midpoint between two adjacent nails (ω_p, m) is determined using the following relationship from Cook and Young (1985):

$$\omega_p = \frac{\beta P_0}{k}\left(e^{-\beta x}\right)\left(\cos(\beta x) + \sin(\beta x)\right) \quad [1]$$

Where: P_o is the equal point loading of the nails (kN), x is the distance to the midpoint between the two nails (m). The term βx is measured in radians in the trigonometric relations. The term β is defined by Cook and Young (1985) by the following relationship:

$$\beta = \left[\frac{k}{4EI}\right]^{0.25} \quad [2]$$

Where: E is the modulus of elasticity of the upper board (kN/m^2), and I is the moment inertia of the upper board (m^4), which is defined by $wt^3/3$ for bending at it's base. The terms w and t are the width (m) and thickness (m) of the board, respectively. In the application, the elastic modulus is the same for the upper board as for the foundation board. Accordingly, Equation 2 reduces to:

$$\beta = \left[\frac{3}{4t^3}\right]^{0.25} \quad [3]$$

If the upper board is uniformly loaded over the distance between the two nails, the deflection of the upper board at the midpoint between two adjacent nails (ω_q, m) is determined using the following relationship from Cook and Young (1985):

$$\omega_q = \frac{q_0}{k}\left(1 - e^{-\beta x}\cos(\beta x)\right) \quad [4]$$

Where: q_o is the uniformly distributed load (kN/m). By setting Equations 1 and 4 equal to each other and solving for the term q_o yields the following relationship:

$$q_0 = \beta P_0\left(\frac{e^{-\beta x}\left(\cos(\beta x) + \sin(\beta x)\right)}{1 - e^{-\beta x}\cos(\beta x)}\right) \quad [5]$$

Equation 5 is the equivalent uniformly distributed loading resulting from the two concentrated loads P_o. For this application, the uniformly distributed load needs to be equal to the geosynthetic tension previously discussed. Additional resistance can be obtained by partially wrapping the geosynthetics around the lower board. The amount of resistance offer by wrapping the geosynthetics around the lower board can be determined using the following relationship (McKelvey and Cushing, 1995):

$$\ln\left(\frac{T}{q_o}\right) = \mu_s \chi n \quad [6]$$

Where: T is the load on the thin-film geomembrane (kN/m), q_o is the resistance provided by the batten strip (kN/m), μ_s is the coefficient of static friction, which is equal to the tangent of the interface friction angle (dimensionless), χ is the contact area of one wrap (equal to 2π radians), and n is the number of wraps.

Using Equations 5 and 6 with typical values of nail resistance, it was determined to satisfactorily offset the tension induced by the wind uplift, spacing of the nails would need to be 102mm, and the geosynthetics partially wrapped around the lower board as shown in Figure 3. Using similar calculations, it was determined that the lower board needed to be bolted to the underlying concrete at a spacing of 760mm.

4. CONSTRUCTION AND DISMANTLEMENT OF SYSTEM

While obviously more difficult to construct than conventional anchor trenches, construction of the batten strip anchorage system went relatively smoothly. Placement of the anchor bolts within the concrete channel involved typical concrete

construction practices, and therefore no problems were encountered. Layout of the lower timber was only problematic in the areas where the anchorage system was in one of the tighter curves. Wrapping the geosynthetics around the upper board was initially trying, but the contractor was able to increase production as construction proceeded. Once the initial anchor bolts were tightened down, it was visually recognized that the anchor bolts were going to significantly deflect the upper beam, leading to enhanced tensile resistance. After a back analysis of the deflected beam, it was decided not to nail the upper board to the lower. This decision led to increased productivity of the anchorage system.

During the next phase of landfill expansion, the batten strip anchorage for the first phase was dismantled and the lining system extended into the next phase. The landfill operator understood that landfill waste within the first phase needed to be filled to within 1m from the top of slope, such that sufficient buttressing of the lining system would exist. As wind uplift would no longer be a concern, and the anchorage system could be dismantled as the lining system components would be free of tension.

Without the nails in place, dismantlement of the batten strip anchorage occurred rapidly. Once the timber boards were removed, the contractor cut the anchor bolts flush with the surface of the concrete channel. A thick geotextile was then placed over the anchor bolts to act as a cushion for the new lining system components as shown on Figure 4. Once the geotextile cushion was placed, the remaining components of construction were simply a transition from a side slope lining system in the first phase of landfill development to a landfill floor lining system within the subsequent development phase.

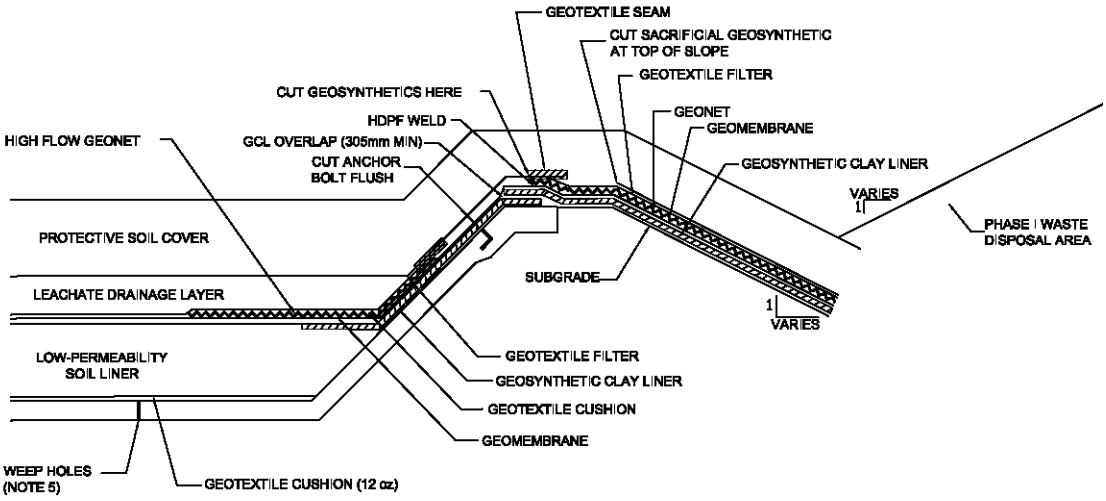

Figure 4. Lining system after dismantlement of batten strip anchor.

5. SUMMARY

By modeling the batten strip anchorage as a beam on an elastic foundation, the capacity of the anchorage system and distance between anchor bolts was determined. Construction of the batten strip anchorage system went relatively smoothly. The system was able to withstand the tensile loads induced on the lining system without incident. Dismantlement of the batten strip anchorage and extension of the lining system into the next phase of landfill expansion also went smoothly. While it is recognized that the batten strip anchorage system developed is more complex and more costly than the standard anchor trench counterpart, the system did prove effective in overcoming the obstacles faced on this project. Accordingly, the batten strip anchorage system can be considered an effective anchorage system where project constraints limit geometry for standard anchor trenches or in areas where obstructions such as building foundations or similar are encountered.

REFERENCES

Cook, R.D. and Young, W.C. (1985). *Advanced Mechanics of Materials*, Macmillian Publishing Company, New York, New York, USA.

Giroud, J.P., Pelte, T. and Bathurst, R.J. (1995). Uplift of geomembranes by wind, *Geosynthetics International*, IFAI, 2: 897-952.

McKelvey, J.A. and Deutsch, W.L. (1991). The effect of equipment loading and tapered cover soil layers on geosynthetic lined landfill slopes, *14th Annual Madison Waste Conference*, University of Wisconsin, Madison, Madison, Wisconsin, USA, 1: 395-411.

McKelvey, J.A. (1994). Consideration of equipment loading in geosynthetic lined slope designs, *8th International Conference of the International Association for Computer Methods and Advances in Geomechanics*, Balkema, Morgantown, West Virginia, USA, 2: 1371-1377.

McKelvey, J.A. and S.S. Cushing (1995) “Brick Flat Pit: a demand for geosynthetic design innovation, *Geosynthetics '95*, IFAI, 2: 597-610.

Innovative Design and Construction of a Landfill Cap: A Case Study of the City of Ottawa's Trail Road Landfill

M.H. Simpson, Layfield Group Ltd., Canada
P.A.S. Benson, Golder Associates Ltd., Canada
D.P. Upton, J.L. Richards & Associates Limited, Canada

ABSTRACT
As part of the interim closure of Stages 3 and 4 for the Trail Road Landfill site, the City of Ottawa decided to install a low-permeability geosynthetic cap in order to minimize infiltration and leachate generation. The design service life for the interim cap was required to be a minimum of 15 years. This is the estimated time before operations in these stages would resume, in accordance with the plans for vertical expansion of the landfill as granted by the Ontario Ministry of the Environment. Various interim cap options were considered at the conceptual design stage, ultimately leading to the selection of an exposed geomembrane cover. This paper discusses the interim cap system selection process as well as associated design and construction challenges such as the creation of the wind uplift countermeasures to prevent excessive vertical and lateral movement of this 320,000 m^2 (32 hectare) cap as well as the challenges associated with landfill gas and stormwater management. The project was completed in October, 2008 and this paper reflects on the challenges faced by the project team.

1. INTRODUCTION

The Trail Road Landfill is the City of Ottawa's primary landfill site and has been operated by the local municipal government since it was opened in May of 1980. The landfill footprint covers a total area of approximately 65 hectares and was developed in four stages. Stages 1 and 2 are unlined landfill cells and Stages 3 and 4 are engineered landfill cells underlain by a low-permeability liner and leachate collection system. Early in 2000, the City of Ottawa undertook an Environmental Assessment (EA) for an expansion of the site given that the last stage was fast approaching its approved limit. Site expansion plans were approved by the Ministry of the Environment in 2005 for the vertical increase of Stages 1 through 4. Although Stage 4 was the active landfilling area at the time, City staff decided to complete the vertical expansion of Stages 1 and 2 in anticipation of potential future urban growth immediately to the east of the landfill site. Providing a temporary cap on top of Stages 3 and 4 would significantly reduce leachate generation at the site and the need for off-site haulage while Stages 1 and 2 were being vertically expanded. The minimum service life of the temporary cap is estimated to be 15 years.

2. DESIGN OF GEOSYNTHETIC CAP SYSTEM

2.1 Design Objectives

Overall objectives for choosing the interim cap included selecting a cost effective low-permeability interim cap for Stages 3 and 4 that would result in the reduction of leachate generation at the site for a period of at least 15 years. The interim cap was also required to be compatible with the newly installed gas extraction well network that supplies gas to an on-site power generation facility. The cap was designed to provide access routes for all terrain vehicles to service the gas extraction wells that are located on top of Stages 3 and 4. Other design considerations included upgrading the existing site drainage network and the ability to easily remove the cap upon re-opening Stages 3 and 4 to continue with the vertical expansion plan in these Stages. Figure 1 shows the partially completed landfill cap with Stage 3 nearing completion.

Figure 1 Landfill Cap Under Construction

2.2 Conceptual Design

During the site expansion Environmental Assessment process, it was determined that limited quantities of clay were available in the area for the construction of a low-permeability soil cap. As such, the conceptual design considered either a buried geosynthetic barrier layer or an exposed geosynthetic cap. An exposed geosynthetic cap offered several advantages over a buried barrier layer including: no concern for slope stability of materials overlying the barrier layer; minimized maintenance requirements (i.e., no concern for erosion of surficial cap materials and no care of vegetated cap); and, lower costs for removal of the interim cap (i.e., no cover soils to be excavated). As with any low-permeability cap design, the conceptual design needed to consider the potential for significant and differential waste settlement due to decomposition of heterogeneous waste materials, variable compaction rates, etc. For these reasons, a relatively flexible cap material was desirable. With an exposed geomembrane interim cap, wind uplift was identified as a critical design element. Given the design objective to provide access routes to the landfill gas extraction wells, the conceptual design included the use of pathways for both travel routes and for ballast against wind uplift.

2.3 Geomembrane Selection

Proposals were received from four proponents for the geosynthetic cap. Layfield proposed two alternative geomembrane products: 0.75mm thick (30 mil) High Density Polyethylene (HDPE 30) and a proprietary 30 mil Flexible Membrane Liner named Enviro Liner 6030 (referred to in this paper as FML). Layfield recommended HDPE 30 as the lowest cost geomembrane that met the Owner's minimum specified performance requirements in the Request For Proposal. HDPE 30 has an approximate service life of 15 years in exposed conditions as was specified, however, an extended 15-year warranty was not available in the 30 mil thickness. The FML was found to be a superior choice for this landfill cap as it exceeded the provisional requirement for an extended 15 year exposed weathering warranty. For this project, the material warranty was extended to 20 years. For exposed use, the FML was found to be the most durable flexible liner of equal thickness due to a special additive package of UV stabilizers and antioxidants. The FML's other important qualities for this project are its flexibility and ability to remain intact through excessive elongation. FML's have a number of advantages over stiffer products like HDPE. Firstly, many FML's can be factory prefabricated into large panels and folded without damaging the membrane. HDPE cannot be folded and must be entirely field fabricated, increasing risk to quality, safety, and productivity. Also an FML's flexibility makes it immune to environmental stress cracking, a failure pattern associated with highly crystalline materials like HDPE. With elongation at break of more than 800%, and actual measured values often exceeding 1000%, the FML used has significant ability to accommodate subgrade settlement. Finally, studies of realistic puncture mechanisms (such as truncated cone testing) repeatedly show than an FML's high elongation properties make it tougher to puncture than higher tensile, but stiffer materials.

2.4 Design of Ballast System

The design of the ballast system, which consisted of a series of granular-filled ballast trenches, anchor trenches and landfill gas well access paths, was based on uplift predictions using equations in Giroud et al. (1995). The design wind speed was in excess of 90 km/h. The elastic properties of the FML were viewed as favourable from a durability perspective (e.g., in accommodating differential settlement, etc.), however they also contributed to relatively large potential uplift values. At the design wind speed it was predicted that the geomembrane could lift by between about 5.5 to 7.5 metres at a spacing between anchor/ballast trenches of between 25 metres and 35 metres. With this relatively close spacing for ballast requirements, the ballast network was simplified on the side slope portions of the waste mound by designing only a few across-slope ballast trenches instead of multiple trenches running up and down the side slopes. On the top portion of the waste mound, the number of required ballast trenches was decreased by designing the landfill gas well access paths (Figures 2&3) to also provide adequate ballast.

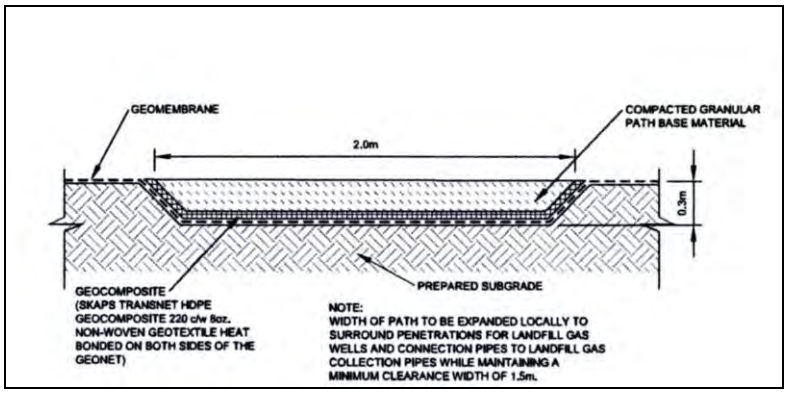

Figure 2 Access Path Detail

Figure 3 Access Path at Gas Well Junction

2.5 Site Drainage Network

The site drainage network was originally sized for a final cap placement over Stages 3 and 4 that would incorporate a vegetated cover. Therefore, the site drainage network needed to be re-sized to accommodate the significant additional storm runoff generated by the exposed low-permeability interim cap. Culvert crossings in the existing outside perimeter ditch were replaced with larger concrete box culverts. The existing perimeter ditch grades at the north end of the landfill site were virtually flat and there was no opportunity to increase the grade due to existing infrastructure already in place. Therefore, this portion of the ditch was lined with the FML material due to the low roughness coefficient thereby minimizing the size of ditch required to convey the additional flows from the capped portion of the site. Lining the ditches with the FML material also helped to protect the drainage ditches from erosion during severe storm events and the spring thaw (See Figure 4). The site stormwater management pond was also fitted with an outlet control structure to limit the amount of runoff leaving the site during the interim cap condition.

Another unique design feature included the use of granular-filled ballast tubes in the portions of the drainage ditches that were lined with FML to maintain conformity to the ditch geometry. In addition, careful consideration was needed in extending the geomembrane cap around and past existing leachate collection system access pads.

Figure 4 Drainage Ditch Showing Ballast Tubes

3. CONSTRUCTION OF CAP SYSTEM

3.1 Landfill Gas Pressure

During the design of the interim cap, neutral conditions were assumed with regards to underlying landfill gas pressures. That is, it was assumed that the active landfill gas collection system was not creating negative pressures through the cover soils and that the system was 100% effective in preventing passive migration of landfill gas out through the cover soils. As such, the wind uplift ballast system design was conservative in that it didn't rely on negative pressure beneath the cap to assist in preventing wind uplift.

During installation, portions of the cap were observed to be lifting up from the subgrade, even under very low wind conditions. The ballast system was observed to be effective in containing lifted areas to within the perimeter of adjacent ballast trenches and/or travel paths. It was determined that the lifted areas were due to inflation forces by landfill gas venting through the underlying waste and sandy bedding soils. It was later considered that upper portions of the waste mound may be isolated from the influence zone of the landfill gas extraction wells due to perched leachate resulting from past leachate recirculation practices in these Stages of the landfill.

In some areas, the underlying landfill gas pressures, possibly combined with some wind uplift, resulted in lifting of the geomembrane interim cap by up to almost 5 metres in height. This became a concern as the magnitude of uplift approached the wind uplift predicted under the maximum design wind speed. In particular, exceeding the maximum predicted wind uplift could result in tension within the geomembrane that could result in permanent deformation or could pull the geomembrane out from beneath the travel paths or ballast trenches.

The design team worked with the designers of the landfill gas extraction system to devise a means to extract accumulated landfill gas from beneath the cap in inflated areas and convey the extracted gas into the landfill gas collection system. A trial exercise was carried out which involved perforating the geomembrane cap in an inflated area and inserting a hose connected to an adjacent landfill gas extraction well. It was observed that the landfill gas extraction well was able to provide sufficient negative pressure to remove all of the accumulated landfill gas in an inflated area in less than 12 hours. Figure 5 shows one of the trial landfill gas extraction connections. In the background of Figure 5, an adjacent inflated portion of the cap is visible.

Figure 5 Inflated Area and Trial Landfill Gas Extraction Connection

Based on the success of the field trial, permanent landfill gas extraction ports were designed and installed in areas of the cap that had been observed inflating and in provisional areas adjacent to landfill gas extraction wells. The extraction ports were designed to facilitate easy connection to the landfill gas collection system on an as-required basis.

3.2 Verification of Elastic Properties

The first area of the geomembrane interim cap that was observed lifting due to underlying landfill gas pressures occurred near the end of the first construction season in late 2007. Geomembrane installation activities were suspended during the winter months and re-commenced in May 2008. Between November 2007 and May 2008 portions of the geomembrane remained inflated with the magnitude of uplift reaching as high as 4 metres. Following deflation of these inflated areas a micrometer was used to measure the thickness of the geomembrane. No notable change in geomembrane thickness was observed compared to measurements taken as part of the construction quality assurance testing during installation. In addition, no signs of permanent deformation could be observed. This was considered to be positive verification of the elastic properties of the EL 6030 material under sustained uplift forces within the predicted maximum range of wind uplift.

3.3 Modification of Ballast Details at Leachate wells

It was observed that the geomembrane was being stressed at the connection to the leachate wells. The original design incorporated the use of a ballast tube surrounding the penetration through the liner. It was found that this ballast tube could move with a significant wind event and allow the liner to shift at the rigid connection to the well. The revised detail, illustrated in Figures 6 and 7 provided the required extra mass at the well to prevent movement of the liner in this area. The new detail also incorporated additional slack in the geomembrane to accommodate some movement.

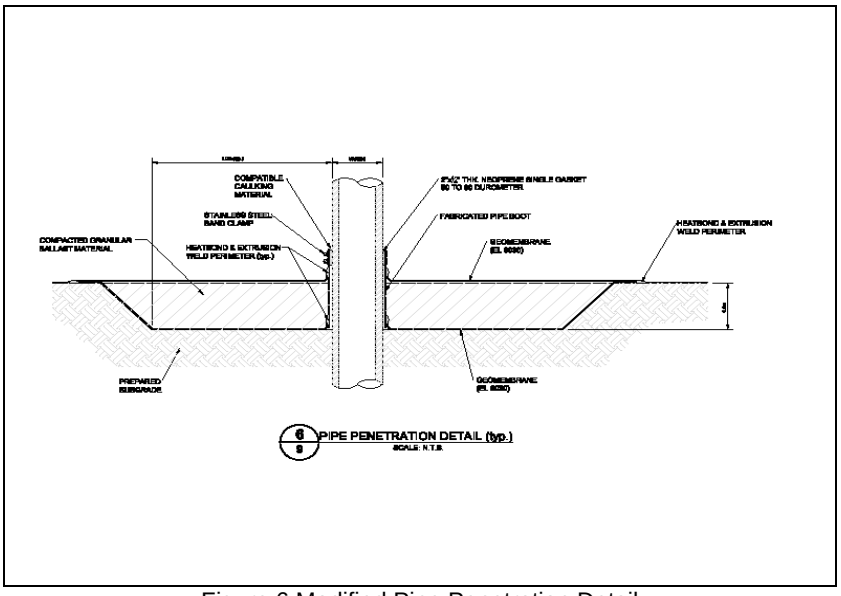

Figure 6 Modified Pipe Penetration Detail

Figure 7 Photo of Pipe Penetration

3.4 Panel Layout and Co-ordination of Liner Placement

The geomembrane panel layout was a complex undertaking that went through numerous iterations due to the highly irregular shape, grade changes and numerous trenches. A panel layout was determined using three standard panel sizes. This would minimize time spent in the field sorting individual panels, as well as eliminate the need to carefully coordinate fabrication and shipping of particular panels to meet the field placement plan. The general layout involved lining the ballast trenches with a long narrow strip of liner. Once the strip was placed, the earthworks contractor placed and compacted granular backfill in the trench. The strip was then folded over the backfill and sealed to a larger panel that connected the area between the two ballast trenches. This proved challenging due to the non-parallel nature of the landfill gas well access paths and adjacent ballast trenches. Figure 8 shows a typical design detail for the ballast trench and Figure 9 shows a ballast trench under construction.

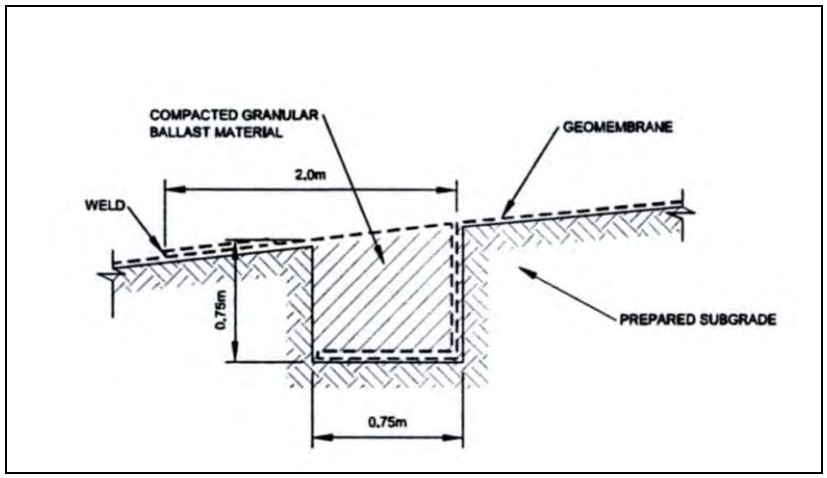

Figure 8 Primary Wind Uplift Ballast Trench


Figure 9 Ballast Trench Under Construction

An additional challenge was accommodating the landfill gas wells that were installed in a random nature across the top of the landfill, long in advance of the cap system. Future gas well designs for sites considering the use of an exposed geomembrane cap should consider a more grid-like alignment to more easily accommodate geomembrane installation.

3.5 Site Drainage Design and Construction Challenges

There were many design challenges associated with site drainage. Installation of the liner commenced in Stage 3 during the late summer months of 2007. Stage 4 continued to receive waste during this period while preparations to re-open Stage 1 were underway. Stage 4 stopped receiving waste during the fall of 2007 and Stage 1 opened. Initial design grades were provided which would allow for uniform and positive sheet flow drainage over the entire capped surface of Stages 3 and 4. Once filling operations in Stage 4 stopped, a field survey of the top of the existing fill pile was conducted to review and adjust grades as required to better reflect existing conditions. The re-grading exercise helped to reduce the amount of fill required to provide positive drainage toward the existing side slopes and perimeter ditches surrounding the base of Stage 4.

Due to the variability of the fill placed on top of Stage 4, low spots were utilized as drainage channels on the top portion of the landfill to convey surface runoff toward the steeper side slopes. This resulted in concentrated discharge points located along the top portion of the side slopes surrounding Stage 4. The area located below and beyond the toe of the

side slopes was kept relatively flat to reduce the velocity of surface runoff leaving the steep side slopes prior to entering the perimeter ditches. In addition, diversion berms were constructed beneath the FML cap material at select locations along the lower sections of the landfill footprint to help re-direct and disburse surface flows prior to entering perimeter ditches. The finished "ripple" effect of the FML cap material (due to slack and folds in the ballast anchor trenches) also helped to reduce the velocity of storm water runoff and disperse flow along the side slopes and lower flat sections of the capped landfill prior to entering the perimeter ditches.

Other site drainage design challenges included re-sizing the existing perimeter ditches to convey storm runoff from extreme storm events. Existing conditions provided limited grades and a confined area in which to construct the new perimeter ditches as a result of existing landfill infrastructure and established site access routes.

The contract to install the interim cap spanned over an entire year, while receiving near record snowfall accumulation in the winter of 2007/2008 and near record precipitation in the summer months of 2008. As a result, management of surface water runoff during the spring melt and wet summer days was a challenge. Installation of the liner sections on the steep side slopes down to the perimeter collection ditch were scheduled to be completed during dry weather events. Areas where the sand subgrade base had been prepared in advance of the liner placement experienced washout during intense summer rain events. The spring melt also resulted in washout of the granular base material placed beneath the access travel paths already constructed on the north face of Stage 3. Therefore, the design of the travel paths located on the side slopes needed to be revisited. The travel paths placed on steeper slopes incorporated a textured FML geomembrane material into the design which was placed above a non-woven geotextile and extrusion welded to the top of the FML liner cap material (Figure 10).

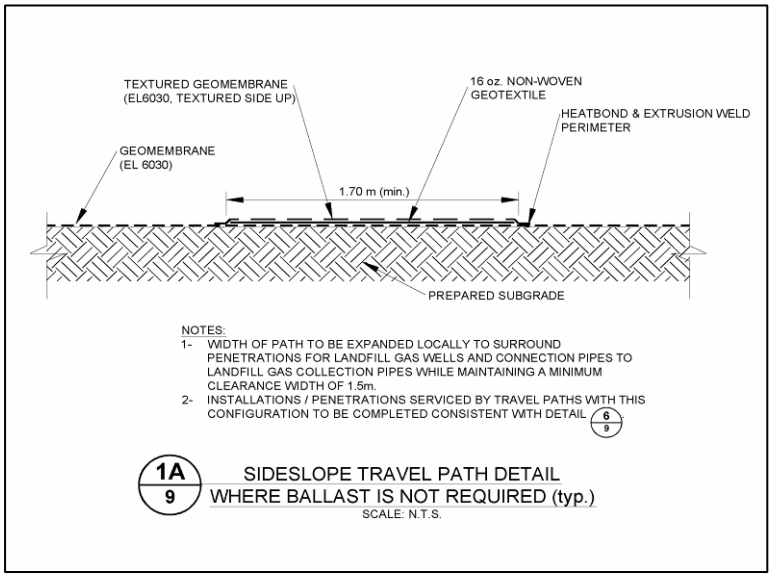

Figure 10 Sideslope Travel Path Detail

4. SUMMARY

This application of an exposed FML geomembrane interim landfill cap is expected to significantly reduce leachate generation at the site and the need for off-site haulage and treatment, as per the original design goals. In addition, it was demonstrated during installation that the interim cap is effective at providing a barrier to the passive venting of landfill gas through the surface of the waste mound that is not captured by the active landfill gas collection system. By adopting a means to capture landfill gas collected beneath the interim cap and convey the extracted gas into the landfill gas collection system, the volume of landfill gas collected and resulting electrical generation capacity has been increased, while fugitive landfill gas emissions to the atmosphere have been reduced. While the application of an exposed geomembrane posed various design challenges, including increased stormwater runoff and susceptibility to wind uplift and inflation by underlying landfill gas pressures, it offered several advantages over a buried barrier layer including no concern for slope stability of materials overlying the barrier layer; minimized maintenance requirements (i.e., no concern for erosion of surficial cap materials and no care of vegetated cap); and, lower costs for removal of the interim cap (i.e., no cover soils to be excavated).

This complex and unique geomembrane installation relied on close co-operation of the entire project team. Successful management of the challenges posed by site drainage, landfill gas, construction co-ordination, and geomembrane installation over the two year construction timeline led to a successful project delivery to the City of Ottawa in the fall of 2008.

ACKNOWLEDGEMENTS

The writers would like to acknowledge the contribution of the following individuals to the paper.

Ted Woytowich, P.Eng Senior Project Manager, City of Ottawa.

Chris Rowson Field Supervisor, Layfield Group Ltd.

REFERENCES

Giroud, J.P., Pelte, T. and Bathurst, R.J., 1995. Uplift of Geomembranes by Wind. *Geosynthetics International,* 1995, Vol. 2, No. 6.

Geosynthetics 2009
February 25-27 2009, Salt Lake City, Utah

An Experimental Study of Water and Air Transmissivity of Nonwoven Geotextiles and Geonet Composites

M. Li, GSE Lining Technology, Inc., Houston, Texas
B. Ramsey, GSE Lining Technology, Inc., Houston, Texas

ABSTRACT
In this paper, a laboratory study was carried out to determine the water and/or air transmissivities of four types of typical landfill gas transmission geosynthetic materials: three nonwoven geotextiles (270 g/m^2, 540 g/m^2, and 1080 g/m^2), and a 6 mm geonet composite with both sides heat-bonded to 200 g/m^2 nonwoven geotextiles. Two experimental methods, a linear-flow transmissivity test device (ASTM D4716) and a radial-flow transmissivity test device (ASTM D6574), were used to obtain the material flow data. The resulting transmissivity data were analyzed to assess the validity of Darcy's law and intrinsic permeability theory for the sample geotextiles and geocomposite. Water and air flowing through all three nonwoven geotextiles remained within the laminar flow regimes over the test pressure gradient ranges. Nevertheless, flow data of both air and water in geocomposite linear-flow tests showed behaviors of laminar, transient and turbulent regimes at very low pressure gradients. Instead of the transition Reynolds number range, it is proposed to use the critical pressure gradient to experimentally define the fluid flow regime status.

1. INTRODUCTION

Nonwoven geotextiles and geonet composites have been frequently designed and installed as the gas relief layer underneath the landfill cover geomembrane. As an important part of the landfill gas control system, the primary design goal of such a gas relief layer is to provide enough in-plane landfill gas (LFG) flow capacity to reduce the gas pressure to a safe level to avoid potential geomembrane uplifting or slope stability failures. Thiel (1998, 1999a and 1999b) developed a three-step design methodology for such geosynthetic gas relief layers:

I. Estimate the maximum flux of gas below the landfill final cover that may need to be removed
II. Perform slope stability analyses to estimate the maximum allowable gas pressure under the landfill cover system
III. Under conditions of Step 1 and in Step 2, design a passive vent system with adequate gas flow capacity to remove gas flux efficiently and avoid gas pressure over the safety limit

The landfill gas flux and slope stability analysis are beyond the discussion in this paper. This study is focused on the evaluation of the gas flow capacity of selected geosynthetic gas transmission materials. Very limited gas transmissivity test data of geosynthetics have been published before. Also very few laboratories in US geosynthetic industry have the necessary equipments to perform such tests. Thiel (1998, 1999a and 1999b) and Bouazza (2004) reported gas transmissivity test results of some nonwoven geotextiles under wet and dry conditions. Both showed that geotextiles could be an appropriate option for some landfill cover gas relief layer design systems provided that proper design approach and testing protocol are applied.

In this paper, both air and water transmissivity tests were performed on three nonwoven geotextiles and a geocomposite using the standard radial-flow and/or linear-flow transmissivity test devices.

2. DARCY'S LAW AND THE INTRINSIC PERMEABILITY OF POROUS MEDIA

To determine the flow capacity of a water/gas transmission material, the simple form of Darcy's law is commonly applied in estimating flow rate through porous media

$$Q = k\, i\, A \qquad [1]$$

where Q = volumetric flow rate (m^3/s)
k = hydraulic conductivity (m/s)
i = dimensionless hydraulic gradient, i.e. head loss Δh divided by flow distance L
A = gross cross-sectional area (m^2)

This equation shows a linear relationship between the volumetric flow rate through a porous media and the flow area. The proportionality constant k is called the hydraulic conductivity, which is dependent on the properties of both the porous medium (such as its effective pore diameter) and the flowing fluid (such as its dynamic viscosity and density), but independent of the hydraulic gradient. Darcy's law was based primarily on observations made by Darcy on the water flowing through clean sands, but it was proven to be valid for most soil types and drainage geosynthetic materials like nonwoven geotextile and geonet/composites provided that the flow remains in a laminar flow regime.

When the hydraulic gradient is gradually increased, the flow becomes turbulent. Usually there is a transition zone between the laminar flow zone and the turbulent flow zone. In the transient and turbulent flow regime, the linear relationship of Darcy's law no long holds valid and the ratio of the flux q=Q/A to the hydraulic gradient i would be lower than the hydraulic conductivity k measured in the laminar flow regime. It would be unwise to apply the hydraulic conductivity or transmissivity test values obtained from the laminar flow in lab if the turbulent flow condition is expected on site. Thus, it is an imperative task to determine the flow regimes of the gas or liquid flow at the site conditions, and in laboratory tests, to verify the flow capacity of a candidate porous geosynthetic material within the same flow regime.

Below is a more generalized form of Darcy's Law, which expands its applicability to the gaseous fluid phase. This form incorporates the concept of the intrinsic permeability of porous media.

$$Q = (K_i / \mu)\, A\, \nabla P \qquad [2]$$

where K_i = intrinsic permeability (m^2) of the porous medium
∇P = pressure gradient (kPa/m or kN/m^3), which is equal to the fluid pressure loss ΔP divided by flow distance L
μ = dynamic viscosity of fluid

Intrinsic permeability is representative of the properties of the porous medium alone and independent of the transmitting fluid. It is a function of size of the openings that the fluid moves through. $K_i = Cd^2$ [C = dimensionless constant, d = mean pore diameter] Intrinsic permeability of a porous media is a constant value as long as the fluid flow remains in laminar zone. Intrinsic permeability ranges from 10^{-17} to 10^{-7} m^2 for most common soil/gravel types. Note that the intrinsic permeabilities of a clean graded sand or sand & gravel are between ~10^{-10} and ~10^{-9} m^2 and that of a well graded gravel between ~10^{-7} and ~10^{-8} m^2.

The relationships between the hydraulic conductivity (also called permeability coefficient) k, the transmissivity θ and the intrinsic permeability K_i are

$$k = K_i\, (\gamma/\mu) \qquad [3]$$
$$\theta = kt = K_i\, t(\gamma/\mu)$$

where μ = dynamic viscosity of fluid ($N\text{-}s/m^2$)
γ = specific weight of fluid (N/m^3)
t = specimen thickness (m) under the test conditions

Ideally, the intrinsic permeability of a porous media is the same regardless of the fluids. Thus, one may predict the transmissivity of one fluid, from the measurement of a second with equation [3]. For example, with the constant intrinsic permeability in a laminar flow regime, the ratio of the air transmissivity θ_g to the water transmissivity θ_w of a porous media can be expressed in Equation 4 (Thiel, 1998)

$$\theta_g / \theta_w = (k_g t) / (k_w t) = (\gamma_g/\mu_g) / (\gamma_w/\mu_w) \qquad [4]$$

where μ_g and μ_w = dynamic viscosity ($N\text{-}s/m^2$)of air and water, respectively
γ_g and γ_w = specific weight (N/m^3)of air and water, respectively

The objectives of this paper are to investigate the correlation between the gas transmissivity and the water transmissivity of various porous geosynthetic media, and to assess the validity of the constant intrinsic permeability assumption which is the basis for the inter-conversion of the transmissivity data obtained with various fluids, and to find the critical conditions under which the flow in geosynthetic transmission media starts to transition from a laminar regime to a turbulent regime.

3. EXPERIMENTAL

3.1 Test materials

This laboratory transmissivity test program was carried out to determine the air transmissivity of four types of geosynthetic materials: three polypropylene nonwoven geotextiles (270 g/m^2, 540 g/m^2, and 1080 g/m^2), and a 6 mm geonet composites with both sides heat-bonded to 200 g/m^2 polypropylene nonwoven geotextiles. The material physical properties related to this study are listed in Table 1 and Table 2 for the three geotextiles and the geocomposite, respectively. It should be noted that all three geotextiles tested were manufactured using same type of polypropylene staple fiber properties.

Table 1 Geotextile material physical properties

Geotextile Types		***GT1***	***GT2***	***GT3***
Polymer		Polypropylene	Polypropylene	Polypropylene
Mass (g/m^2)		270 g/m^2	540 g/m^2	1080 g/m^2
Thickness (m)	@ 2 kPa	0.0027	0.0054	0.0103
	@14.4kPa	0.0022	0.0046	0.0091
	@28.8kPa	0.0020	0.0042	0.0084
Denier	avg.	6.6	6.6	6.6
Fiber Diameter	(m)	3.20E-05	3.20E-05	3.20E-05

Table 2 Geocomposite materials physical properties

Geocomposite Type	***GC***
Geonet Polymer	HDPE
Bonded Geotextile	Double-sided 200 g/m^2 polypropylene nonwoven
Composite Thickness (mm)	7.5 @28.8KPa
Geonet Density (g/cm^3)	0.940
Strand Thickness (mm)	3.0±0.5
Strand Spacing (mm)	12.0±0.5
Strand Structure	Biplanar with strands in ~30^o to machine direction

3.2 Test devices and test program

Two experimental methods, utilizing a regular transmissivity test device (suitable for use in compliance with ASTM D 4716) or radial transmissivity test device (suitable for use in compliance with ASTM D 6574), were performed on specimens of the geotextile and geocomposite samples. Transmissivity tests in this study were performed using both air and water as the substitute test fluids for the landfill gas. For geotextile specimens, only the radial-flow device was used because materials with relatively low transmissivity like geotextiles are more sensitive to side leakage commonly encountered in linear transmissivity apparatus. Also, the radial-flow device is better for geotextiles with the isotropic flow behavior. The radial-flow device was not used for the biplanar geocomposite specimen due to its oriented flow behavior. The latter was only tested with linear-flow device in the geonet machine direction.

Figure 1 Radial Transmissivity Testing Device – ASTM D 6574
(Courtesy of TRI/Environmental, Inc.)

ASTM D 6574 radial-flow transmissivity box

The photograph of a radial-flow transmissivity test apparatus is shown in Figure 1, which is in conformance with ASTM D 6574 requirements, and also applicable to testing with both liquids and gases. During the test, a circular specimen of the geotextile is placed in the test chamber which has an inner diameter of 5.08 cm and an outer diameter of 30.48 cm. Radial transmissivity is calculated per an equation (provided in ASTM D 6574) using the measured values of the pressure drop of the fluid, the fluid density, and the fluid radial-flow rate.

ASTM D 4716 linear-flow transmissivity box

The linear-flow transmissivity test apparatus (not shown here) and procedures used in this study are in conformance with ASTM D 4716 requirements. The test specimen has the length of L = 305 mm and the width of w = 305 mm. A modified linear-flow transmissivity test apparatus with a special gas flow meter and sealing plates was used for measuring transmissivity of gases.

The test program for the four material types is listed in Table 2. To match the typical landfill cover conditions, the highest normal load used was 28.8 kPa. For geotextiles, a pressure of 14.4 kPa was also evaluated. For GT2 and GC, both air and water were used as test fluids in order for a more direct comparison.

Table 3 Testing Program

Geotextile Types	***GT1***	***GT2***	***GT3***	***GC***
Transmissivity device	Radial-flow	Radial-flow	Radial-flow	Linear-flow
Fluid Type	Air	Water and Air	Air	Water and Air
Normal Load σ (kPa)	14.4 and 28.8	14.4 and 28.8	14.4 and 28.8	28.8
Boundary condition	Between steel plates			
Seat time	15 minutes			

3.3 Equivalent pressure gradient

For a horizontal fluid flow moving through the porous media, the hydraulic gradient i (in water test), the pressure loss ΔP (in both water and gas tests) and the pressure gradient ∇P follows the relationships as show in equation group [5]

$$\nabla P = \Delta P/L = \Delta h/L = \gamma_w i, \text{ or}$$
$$\Delta P = \nabla P L, \text{ or} \qquad [5]$$
$$i = \nabla P/\gamma_w$$

By applying equations [5], the straight lines in chart a) and chart b) of Figure 2 illustrate the equivalency between the hydraulic gradient, the pressure drop, and the pressure gradient for ASTM D 4716 linear-flow device and ASTM D 6574 radial-flow device, respectively.

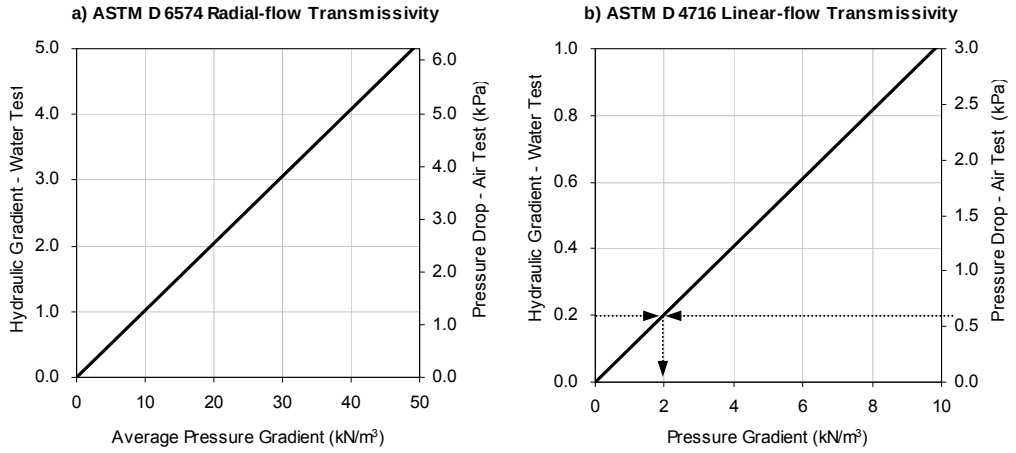

Figure 2 Equivalent Pressure Gradient Charts for Transmissivity Tests

Example: On Chart b), for a hydraulic gradient i = 0.2 in water test, one can find the equivalent pressure drop ΔP = 0.60 kPa in the air test, and both are equivalent to a pressure gradient P_G = 2.0 kN/m^3.

The flow distance L was = 0.305m for D 4716 linear-flow device and L= 0.127m for D 6574 radial-flow device. It should be noted that the gradient calculated for the radial device are average value over the entire flow distance. The actual pressure/hydraulic gradients are not constant along the radial flow path due to the varying cross-sectional area.

All flow rate and permeability results generated from the air and water tests in this study are plotted against the pressure gradient to show the correlations between the flow properties of the two fluids under the same basic testing conditions.

4. TEST RESULTS AND DISCUSSIONS

4.1 Geotextile radial-flow tests

Figure 3 shows that the geotextile air radial-flow rate bears a linear relationship to the pressure gradients for three tested geotextile materials, GT1, GT2, and GT3, at the pressure levels of 14.4 kPa and 28.8 kPa,. This implies that Darcy's law holds valid in all these six test groups. The scatter of some data points at the beginning part of each curve in Figure 3 should be attributed to the device precision at the very low flow rates and in-flow pressure levels. The linear part of each curve intersects with the origin of the coordinate system. This demonstrates that the laminar flow exists throughout the test pressure gradient ranges.

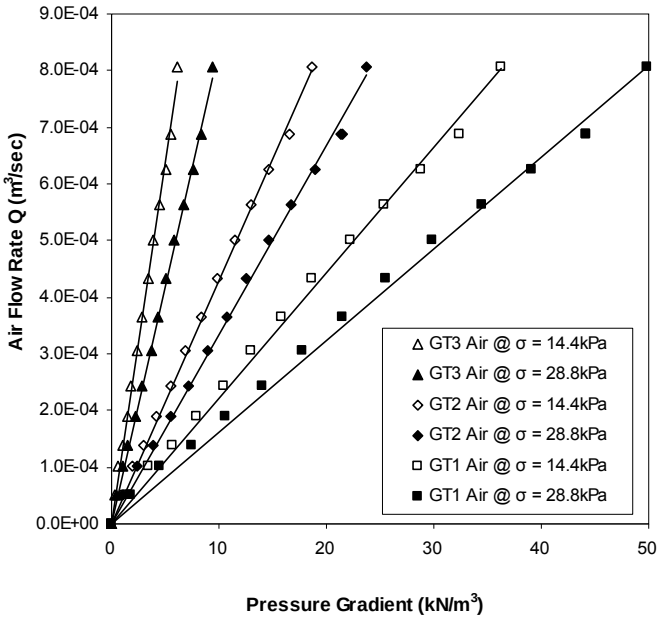

Figure 3 Geotextile air radial flow rate versus pressure gradient

Same linear patterns can also be observed for test data points of water radial-flow rate versus pressure gradients shown in Figure 4. This group of tests was performed on GT2 geotextile material only. Same test pressure gradient range was applied for GT2 water and air radial-flow tests. The pressure gradient range was from 1 kN/m^3 to 22 kN/m^3 in the GT2 air radial-flow test. To match that range, the hydraulic gradients were selected to be 0.28, 0.55, 1.1, 1.7 and 2.2 for water radial-flow test, per Figure 2a.

For each data point in Figure 3 and Figure 4, the transmissivity value can be calculated by the ASTM D 6574 radial transmissivity equation. They are then plotted against the pressure gradients in Figure 5. Except for the scattered data points at the low gradients, the transmissivity resulting from each test condition is basically independent of the pressure gradients and remain constant. Again, this is the feature of the laminar flow regime. Figure 5-a) compares the three GT samples at two pressure levels. As expected, the transmissivity tends to increase with the increasing geotextile mass/unit area (MUA) and tends to decrease with the increasing pressure levels. Figure 5-b) shows that over the pressure gradient range 0-22 kN/m^3, GT2 geotextile has nearly constant transmissivity values in both air and water tests. Apparently, the ratio between air and water transmissivities will be close to constant too. The question is, does this validate the intrinsic permeability theory behind the Equation 4?

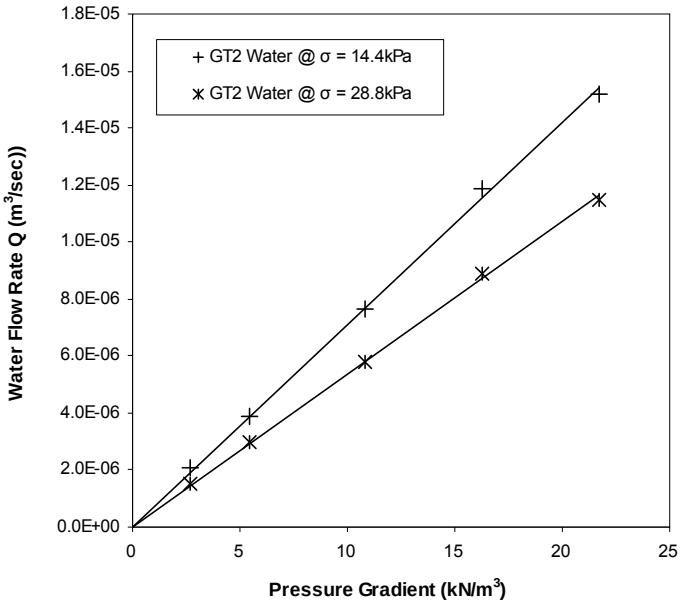

Figure 4 Geotextile water radial flow rate versus pressure gradient

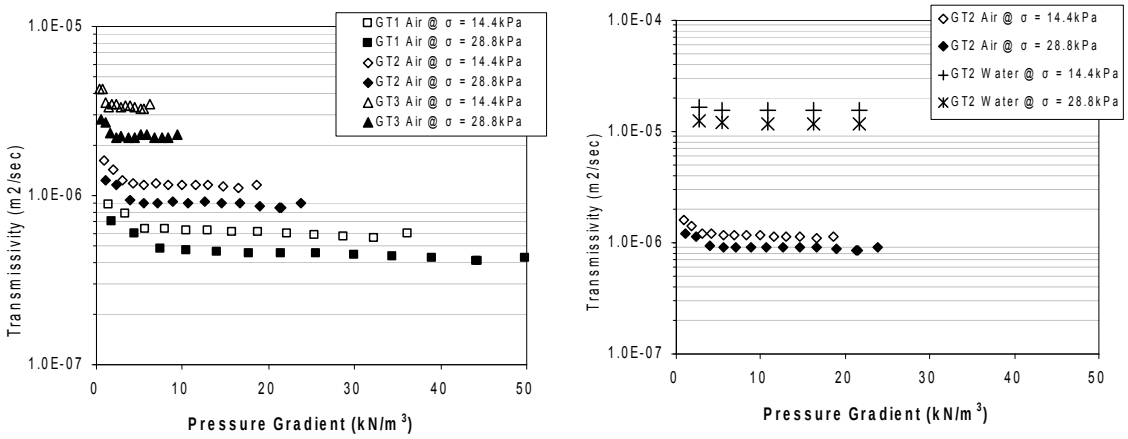

a) Air tests for three GT types

b) Air and Water tests for GT2

Figure 5 Radial transmissivity of geotextiles vs. pressure gradient

By applying Equation 3 and using the geotextile thickness data (at the testing pressure levels) provided in Table 1, the transmissivity in Figure 5 can be directly converted to the intrinsic permeability, which is presented graphically in Figure 6.

Figure 6-b) compares the intrinsic permeabilities from water tests and air tests from GT2 at two pressure levels. This graph leads to the following finding: the water data and air data of GT2 yield very close intrinsic permeability results; only around 10% variation exists between the air and water results. The author believes that this was caused by the different temperature sensitivity of air and water within the range of temperature variation within the laboratory. Thus, the inter-conversion of the air transmissivity and water transmissivity is applicable by using Equation 3 or Equation 4. This conclusion is only valid for GT2 material over the pressure gradient range 0-22 kN/m^3.

In Figure 6-a), the intrinsic permeability values are calculated from the air transmissivity data for the three GT samples at two pressure levels. The intrinsic permeabilities of the three geotextiles fall into a range of $3x10^{-10}$ to $6x10^{-10}$ m^2, which is comparable to that of a clean graded sand or sandy gravel. However, some slight difference exists between the test

groups. Intrinsic permeability is a function of size of the openings through which the fluid moves. Geotextile thickness and porosity decrease with the increasing stress level applied, thus the effective pore diameter decreases as well. That is why the intrinsic permeability at 28.8 kPa is always lower than that at 14.4 kPa for each geotextile. Nevertheless, although the fiber type is exactly same, the three geotextiles with different mass/unit area (MUA) do not share same intrinsic permeability. The K_i results of the three geotextiles are close but observable differences still exist between them. The different needlepunching intensity, calendaring and/or heat-setting process during their production could generate different porosity and opening size, which in turn can affect their intrinsic permeability. It is strongly recommended that the flow property analysis be performed on a material-by-material basis.

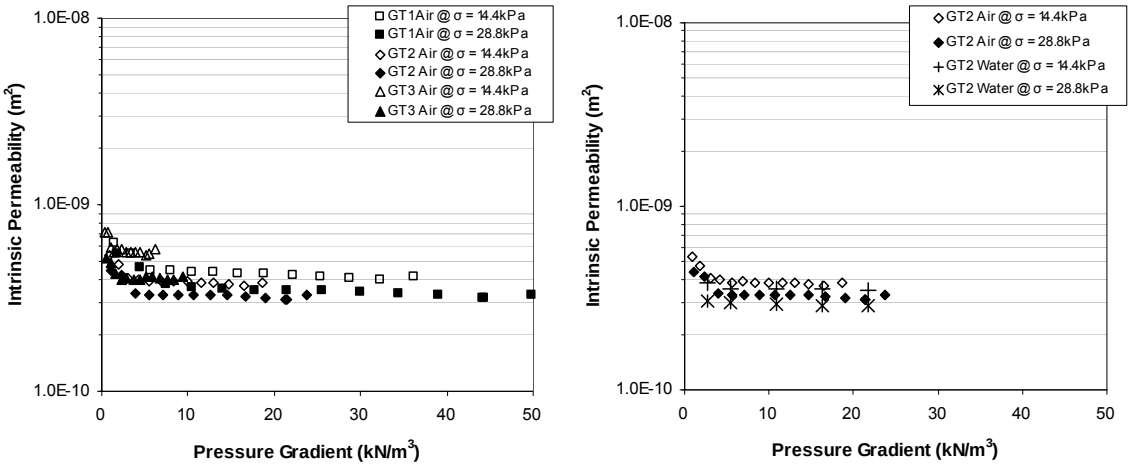

a) Air tests for three GT types

b) Air and Water tests for GT2

Figure 6 Radial-flow intrinsic permeability of geotextiles vs. pressure gradient

4.2 Geonet composite linear-flow test

The curves of water and air linear-flow rate versus pressure gradient for the biplanar geocomposite GC are shown in Figure 7a and Figure 7b, respectively. Unlike the geotextile behavior, both water and air flowing through the GC sample start to become turbulent at very low pressure gradients. By observing the trends, it could be approximated that water flow has a transition flow zone within a critical pressure gradient range from 0.5 kN^3/m to 3.0 kN^3/m. For air flow, transition zone takes place at even lower critical pressure gradient range, which is estimated at 0.2 kN^3/m to 0.4 kN^3/m. Linear relationships in Equation 1 and Equation 2 (Darcy's law) are generally valid when pressure gradients are below the low limits of these critical ranges.

The flow rates in Figure 7 can be converted to transmissivity data as shown in Figure 8a. As expected, for both air and water, the transmissivity curves follow a decreasing trend as the pressure gradient increases, except for the data points at the gradients lower than the critical ranges.

Equation 3 is applied to convert the transmissivity data to the intrinsic permeability of the geocomposite (GC). Results are shown in Figure 8b. Technically, the calculated intrinsic permeability values in transition and turbulent zones are not "real" intrinsic permeabilities. They should be regarded as sort of "quasi-intrinsic permeabilities" and should only be used for data analysis purposes. The intrinsic permeability of a give porous medium must be calculated with the laminar flow data and it should be used as a material constant. The calculated intrinsic permeability of the sample geocomposite (GC) is about $5x10^{-8}$ m^2 in laminar flow regime, which is two orders of magnitude higher than that of the best nonwoven geotextile of this study and falls into the permeability range of well graded gravels.

Note that Figure 8 has a secondary x-axis on the top of the chart which shows the hydraulic gradients equivalent to the pressure gradients in primary x-axis. To match the critical pressure gradient of 0.2 kN^3/m for air flow, one must use a hydraulic gradient equal to or lower than 0.02 in water flow tests in order to make certain that the flow regimes of both fluids are laminar at this gradient level. Only in the laminar regime, theoretically, one can use the intrinsic permeability theory for inter-conversion of the flow transmissivity of different fluids.

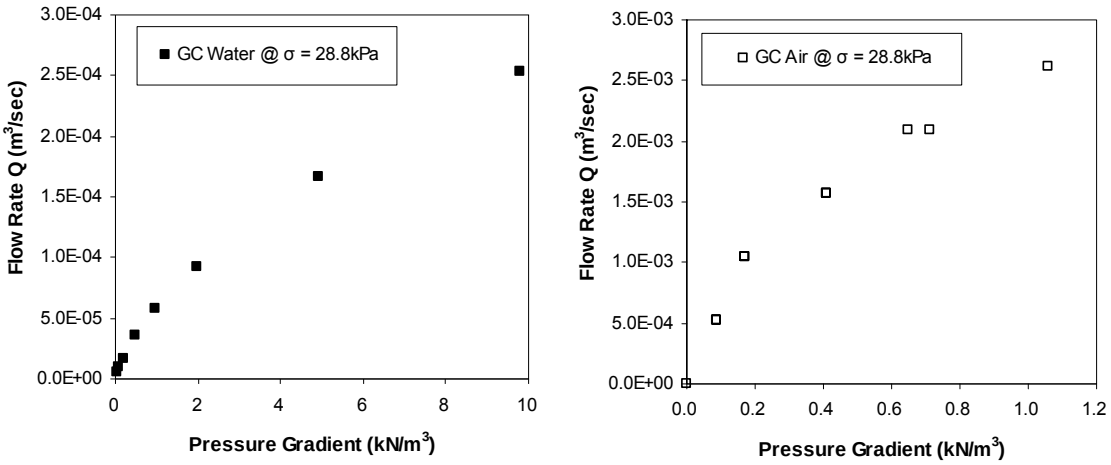

a) Water tests b) Air tests

Figure 7 Linear-flow rate of geocomposite vs. pressure gradient

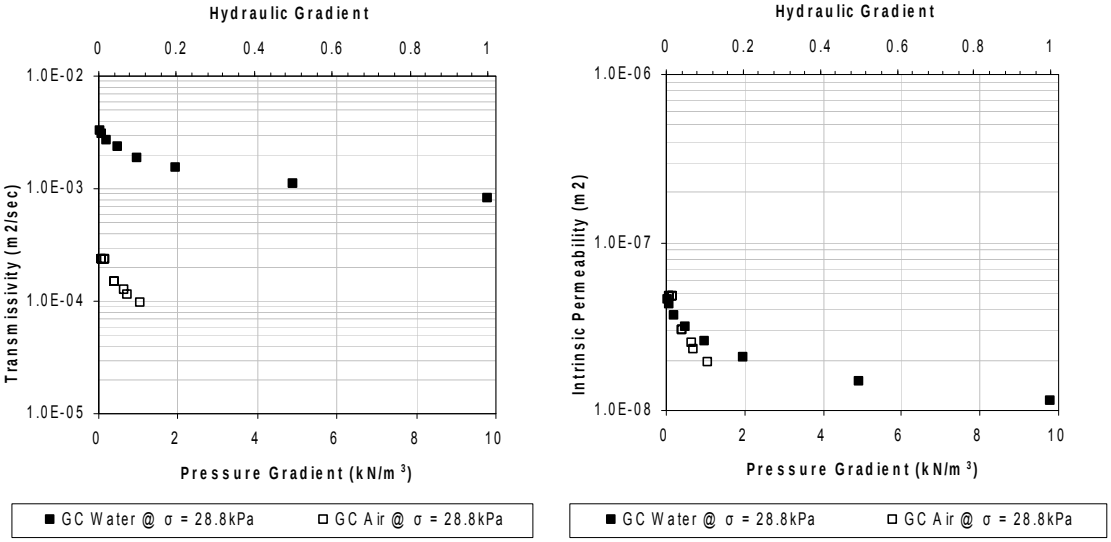

a) Transmissivity b) Intrinsic permeability

Figure 8 Linear-flow transmissivity and intrinsic permeability of geocomposite vs. pressure gradient

However, for a specific material tested with two fluids at a certain same pressure gradient, Equation 4 will be valid as long as the calculated K_i values from the two fluid flows are approximately equal, even if either one or both of the fluids already exits the laminar flow regime. K_i does not need to be a constant. K_i could be a function of the gradient. As long as this function is identical for both fluids, Equation 4 will still be correct. This is the case for GC data presented in Figure 8b. The K_i vs. ∇P curves for air and water have an overlapping range for the low gradient range, in which the K_i start to decrease with ∇P.

That being said, Equation 4 would hold valid until the pressure gradient reaches a certain level, at which the two Ki vs. ∇P curves for air and water start to diverge. This pressure gradient level can be determined on a material-specific basis. For GC material in this study, Figure 8b shows that this critical level is around a 0.7 kN^3/m pressure gradient for air tests or a 0.07 hydraulic gradient for water tests. In other words, any water transmissivity data obtained under a hydraulic gradient lower than 0.07 can be safely converted to air transmissivity under an equivalent pressure gradient lower than a 0.7 kN^3/m using Equation 4, and vice versa. It should be noted that at ∇P=0.7 kN^3/m, the air flow rate/width Q/w =

(2.1×10^{-3} m^3/sec) / 0.305 m = 7 liter/sec-meter width, which is much higher than any landfill gas flux design need. Thus, the air transmissivity converted from water test results of GC material with any hydraulic gradient greater than 0.07 should be conservative for landfill cover gas relief layer design.

4.3 Discussions - Reynolds number and critical pressure gradient

As stated in Section 2, Darcy's Law is only valid when a fluid flow is laminar. In fluid mechanics, whether a flow regime is laminar, transient or turbulent is determined by the Reynolds number, R_e (dimensionless)

$$R_e = (\rho v d)/\mu \quad [6]$$

where,
ρ = fluid density
μ = fluid viscosity
d = average pore diameter of the porous medium
v = average flow velocity

Theoretically, a transition Reynolds number range can be defined for every flow medium. The fluid flow remains laminar when R_e is below the low limit of this range and it becomes turbulent when R_e is greater than the high limit. However, this range could vary broadly for different flow media. For instance, the transition Reynolds number range is between 2000 and 4000 for pipes; and it could be between 1 and 10 for porous media like soils. It becomes more difficult to identify such a transition Reynolds number range for geosynthetic drainage media. Average pore diameter (d) in Equation [6] is a porous medium property, which unfortunately has not been fully understood or well defined for most geosynthetic fluid transmission materials, especially for biplanar and triplanar geonets. This makes it impossible to precisely calculate their Reynolds numbers, let alone finding the transition Reynolds number range. However, instead of using Reynolds number, one can use flow tests to find the critical pressure gradients at which the flow starts to exit the laminar regime.

Average flow velocity v=Q/A is a measured value during the flow testing. In a laminar flow regime, v can be expressed as a function of the pressure gradient by rewriting Equation 2 as

$$v = Q/A = (K_i/\mu)\,\nabla P \quad [7]$$

Substitution of Equation [7] into [6] yields

$$R_e = (\rho v d)/\mu = (\rho d)\cdot(K_i/\mu)\,\nabla P/\mu = (\rho K_i d/\mu^2)\nabla P \quad [8]$$

where, density ρ and viscosity μ are fluid properties while K_i and d are porous medium properties. Thus, for a certain fluid type flowing through a certain medium type, the ∇P is linearly proportional to R_e,

Transition Reynolds number range is an intrinsic property of the porous medium itself, it doesn't change with fluid types. Assuming, for a certain medium, the critical R_e = C for both air and water, when the transition flow regime starts;

If the fluid is water, critical pressure gradient $\nabla P_{critical\text{-}water} = C/(\rho_w K_i d/\mu_w^2)$
If the fluid is air, critical pressure gradient $\nabla P_{critical\text{-}air} = C/(\rho_a K_i d/\mu_a^2)$

Take a ratio of the two equations above and use the fluid constants: ρ_a = 1.2 kg/m^3, $\mu_a = 1.79 \times 10^{-5}$ N-s/m^2, ρ_w= 1000 kg/m^3, $\mu_w = 1.01 \times 10^{-3}$ N-s/m^2

$$\nabla P_{critical\text{-}water}/\nabla P_{critical\text{-}air} = (\rho_a/\mu_a^2)/(\rho_w/\mu_w^2) = 3.74 \quad [9]$$

Note: Equation 8 and Equation 9 are only valid when both fluids are laminar at the certain ∇P of concern.

Equation 9 indicates that the air, water or any other fluid shall have a unique critical pressure gradient range corresponding to the transition Reynolds number range. The critical pressure gradients of different fluids are not equal but can be converted to each other by certain ratios determined by fluid properties using Equation 9. This may also explain why the critical pressure gradient of air is much lower than that of water in GC tests shown in Figure 7. There is, however, no need to determine the critical gradient for geotextiles since they all remained in laminar flow regime over the test pressure gradient range up to 10-50 kPa/m, which should be greater than most landfill gas relief layer design needs.

5. CONCLUSIONS

In this paper, the intrinsic permeabilities of three geotextiles and one biplanar geocomposite were calculated from the air and/or water transmissivity test results of these materials. The intrinsic permeability theory was verified for these flow media at certain test pressure gradient ranges. The authors believe that the same testing procedures and computational methods can be effectively applied to obtain intrinsic permeabilities of other types of geosynthetic drainage media.

Water and air flows in radial-flow tests of all three tested nonwoven geotextiles remained within the laminar flow regime over the tested pressure gradient range. Within this range, the intrinsic permeability theory was proven to be valid.

In the geocomposite linear-flow tests, the water flow has a transition flow regime within a critical pressure gradient range from 0.5 kN/m^3 to 3.0 kN/m^3, and for the air flow, the transition regime takes place within a range about 0.2 kN/m^3 to 0.4 kN/m^3. Flows become turbulent at pressure gradients beyond these ranges.

Under typical normal loading conditions for landfill cover systems, the intrinsic permeabilities of the three geotextiles fall into a range of $5x10^{-10}$ to $1x10^{-9}$ m^2, which is comparable to that of the well graded sand or sandy gravel, and the calculated intrinsic permeability of the geocomposite (GC) is about $5x10^{-8}$ m^2 in laminar flow regime, which falls into the permeability range of well sorted gravels.

The intrinsic permeability of a geotextile material varies with the slight changes of its flow channel micro-matrix, which is affected by geotextile thickness, porosity and mass per unit area, even though the fiber types are exactly same.

For geocomposite (GC), at a certain pressure gradient, transmissivity inter-conversion of two fluids will be valid as long as the calculated K_i values from the two fluid flows are equal, even if either one or both of the fluids already exits the laminar flow regime. This was found to be true for the geocomposite GC tested in this study until a pressure gradient level much higher than the critical pressure gradient.

Instead of using Reynolds number, one can use the critical pressure gradients to define the flow regime status transmitted by a geosynthetic material. The critical pressure gradient can be experimentally determined for one fluid and then be converted to a second fluid type.

Lastly, the authors suggest that similar air and water flow tests be performed to other candidate geosynthetic drainage materials for gas transmission function, since each geosynthetic drainage material type has its unique intrinsic permeability and other flow properties. In order to use the water transmissivity of a material for calculating its gas relief capacity, the patterns similar to Figure 6 and Figure 8 in this paper should be experimentally generated.

REFERENCES

ASTM D 4716 Test Method for determining the (In-plane) Flow Rate per Unit Width and Hydraulic Transmissivity of a Geosynthetic Using a Constant Head, American Society for Testing and Materials, West Conshohocken, Pennsylvania, USA.

ASTM D6574 Standard Test Method for Determining the (In-Plane) Hydraulic Transmissivity of a Geosynthetic by Radial Flow, American Society for Testing and Materials, West Conshohocken, Pennsylvania, USA.

Bouazza, A. (2004) “Effect of wetting on gas transmissivity of non-woven geotextiles.” *Geotextiles and Geomembranes,* Volume 22, Issue 6, December 2004, Pages 531-541

Thiel, R. (1998) “Design Methodology for a Gas Pressure Relief Layer below a Geomembrane Landfill Cover to Improve Slope Stability.” *Geosynthetics International,* Vol. 5, No. 6, pp. 589-616.

Thiel, R.S. (1999a) “Design of Gas Pressure Relief Layer below a Geomembrane Cover to Improve Slope Stability.” Proceedings to Geosynthetics '99 conference held in Boston, MA in April 1999, pp. 235-252.

Thiel, R. (1999b) “Design and Testing of a NWNP Geotextile Gas Pressure Relief Layer Below a Geomembrane Cover to Improve Slope Stability.” Proceedings for Sardinia ’99 Seventh International Landfill Symposium, Vol. III, pp. 343-350, Oct. 1999.

Geosynthetics as Solution to Geotechnical Problems in a MSW Landfill

S. Veggi, Studio Geotecnico Italiano s.r.l., Milano, Italy
P. Parla, Studio Geotecnico Italiano s.r.l., Milano, Italy

ABSTRACT
Scarpino landfill is the biggest mountain-located landfill in Italy, and the second one for waste material placed (about 9,000,000 m^3). Recently, due to some changes in environmental regulations and to allow the expansion of the landfill in its central part, some stabilization works, together with the definitive closure at the toe of the landfill, have become necessary. The authors are involved in the design and in the work direction of the stabilization works, up to date almost finished, and of the capping, now in execution.
The article describes the applications of geotextiles and geomembranes in the stabilization works (that is reinforced earth), in the replacement of the old bottom lining system and in the final capping, focusing on the problems related to the particular morphology and topography of the site, that have required the use of geosynthetic materials instead of earth materials.

1. INTRODUCTION

Scarpino landfill is the major waste disposal site in the northern part of Italy; waste materials are conveyed from the whole Region Liguria, besides from the town of Genova, in which territory is located. Due to the particular morphology of the Region (i.e. mountains very close to the sea, and basically the whole seaboards and flattish areas urbanized), it is very difficult to find area suitable for new waste disposal site location. As a consequence, lots of waste disposal site are in mountain areas and many of them have been enlarged respect their predicted dimensions.
Scarpino landfill is located over Genova, in a valley with lateral slopes very steep, and it is virtually invisible from the town. In the upper part, which altitudes range from about 410 m to about 570 m above sea level, waste disposal operations started in 1968 and ended in 1995; in the lower part (about 350 m-410 m above sea level) waste disposal operations started in 1995 and ended in 2001. Nowadays, waste placement is going on in the central part of the landfill, and the whole landfill covers an area of about 490,000 m^2; since 1968, about 9,000,000 m^3 of waste materials have been placed (see fig. 1).
With the purpose to allow a further enlargement in the central part and to close definitely the lowest part (toe) of the landfill (see fig.2), some stabilization works have become necessary to provide the stability factor of safety requested by Italian regulations. These works include structural, geotechnical and hydraulic works, new profiling of the lower part of the landfill and the execution of the final cover, together with the replacement of part of the old bottom lining system.
Because of the site conditions (very steep lateral slopes and very narrow operational space, see fig. 3) and other unpredictable events (like meteoric events, lack of appropriate earth materials in the requested amount), realization of the works has been rendered very difficult in some circumstances; some problems could have been overcome only thanks to the usage of geosynthetics materials, as described in the present paper.

2. LANDFILL MAIN FEATURES

As said, the whole landfill covers an area of about 490,000 m^2, comprised between the altitudes of 350 and 570 m above sea level. At the bottom and at the slopes of the landfill, the subsoil is constituted of rock materials (mostly serpentines and slates, weathered) in the upper meters. The slope at the sides can reach the inclination of 50° and more, and the mean inclination of the bottom, in the longitudinal axis, can vary from 5° to 10°.
The oldest part of the landfill has been cultivated before the first Italian regulations in the field of waste materials and disposal site had become effective (that is prior to 1982 and 1984); then, the whole landfill bottom system has been completed before the European and last Italian regulations had become effective (2003). So, the lining systems can be different from one part to another part of the landfill and can be different from what the current regulation requires.
Prior to 2003, the bottom and lateral lining system of a MSW disposal site must comprehend at least a mineral layer (thickness not less than 1 m and permeability not exceeding 10^{-6} cm/s) and – but only where the natural subsoil it was not sufficiently impervious – a geomembrane.
At the toe of Scarpino, the bottom lining system consists of a clay layer, a smooth HDPE geomembrane, a geotextile and a mineral drainage layer; at the sides of the landfill (that is on the slopes of the valley), according to the local needs, three different types of lining system have been placed, comprising a GCL composite and an HDPE geomembrane (smooth, textured on one side or textured on both sides). Before the starting of the stabilization works, at the lowest part

of the landfill two rows of gabions were placed. Under the toe, there are the basins for the leachate treatment and raising (about 25 m x 60 m and 7.5 m high).
The height of wastes in the central part of the landfill is more than 80 m.

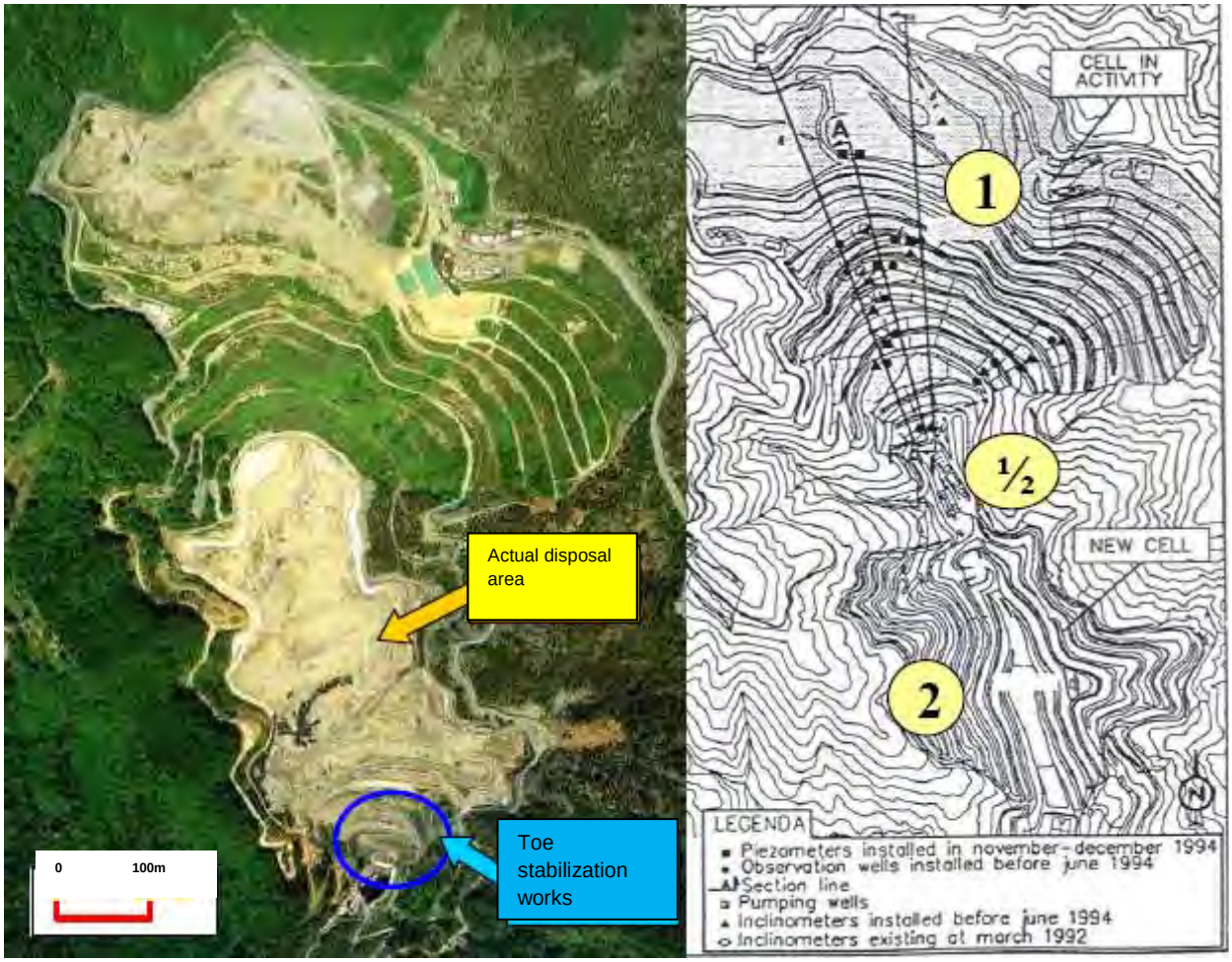

Figure 1 Scarpino landfill plant. The aerial view on the left is taken before the stabilization works begun. The picture on the right shows a plant of the disposal site in 1994.

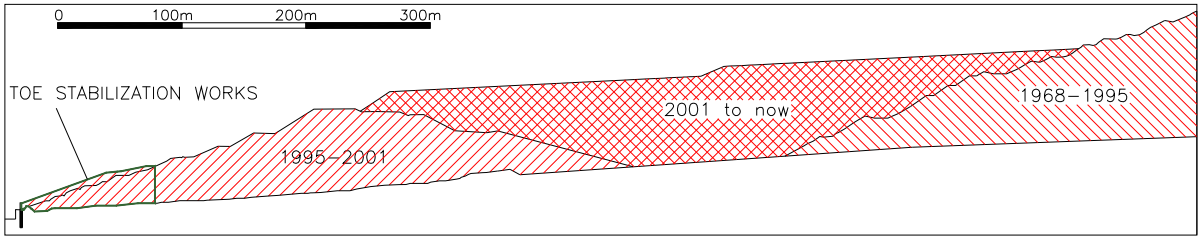

Figure 2 Longitudinal section

Figure 3 Picture of the toe of Scarpino before the beginning of the stabilization works

3. STABILIZATION WORKS

Scopes of the stabilization works are: to provide an adequate factor of safety to the stability of the landfill slopes (referred to the maximum volume technically available), to protect the basins for the leachate collection and treatment, to renew and improve the drainage systems and the final closure of the toe, avoiding any possible damage to the existing containment system. The major stabilization works contemplate: wells to extract the leachate (first phase), a jet-grouting soil treatment to improve the soil properties, a wall of 5 m height founded on a diaphragm of drilled piles with anchor, embankments, new drainage and containment systems and the final closure at the toe (second phase).
Apart from the leachate extraction wells, already completed before the beginning of all the others, so many works in a particular and delicate environment required the careful study of the operative phases. Attention must be paid to the fact that Scarpino toe is a natural impluvium where both leachate and surface waters are conveyed; the operative phases sequence take into account that any leachate escape must be avoided during the works, especially when the existing bottom lining system has to be discovered and joined to the new one.
Figure 4a shows a typical section at the landfill toe, while fig. 4b shows a typical section of the structural works to be done, taken from the detailed design: bored piles, ground anchors, concrete wall, jet grouting columns and the stabilizing embankment. On both sides, the wall finishes against the slopes of the valley, thus forming a sort of dam. The figure also shows lining system and the final capping; both the bottom lining system and the final cover respect the Italian regulation (D.Lgs. 36/2003).
Operative phases can be summarized as follows:

1. demolition of some existing structures and site preparation;
2. drilled piles;
3. micropiles with ground anchor function;
4. reinforced concrete wall;
5. backfilling of the wall;
6. jet grouting columns (from the top of the backfilling);
7. excavation behind the wall (from a distance of about 5m to a distance of about 15-17m) to discover the bottom HDPE geomembrane;
8. adaptation of the bottom drainage and lining system;
9. embankment construction;
10. final cover construction.

Jet grouting columns are designed in a square pattern; their scope is to improve the geotechnical characteristics of the first soil stratum. According to the original design (that is according to the operative phases mentioned above), columns had to be realized from the top of the embankments behind the wall, with grouting only up to the wall base. It was reputed essential to realize the wall and the backfilling before starting to excavate in the wastes and to discover the

bottom HDPE geomembrane, because it was expected to have some leachate collected on the bottom of the landfill, and the existing culvert had been demolished to realize the piles and the wall. Thus, the wall, the backfilling and the jet grouting columns could prevent any leachate escaping.
Indeed it can be seen that the last row of columns reach the top of the surface and that the columns are at an angle to the vertical. This because the last row, besides to form a barrier of low permeability, might have supported the wall of the excavations during the operation for the replacement of the bottom lining system; in fact, it must be observed that, in the downhill direction, the working space are limited by the basins for the leachate collection, and so it was not possible to keep smaller inclinations of the backfilling during the works.

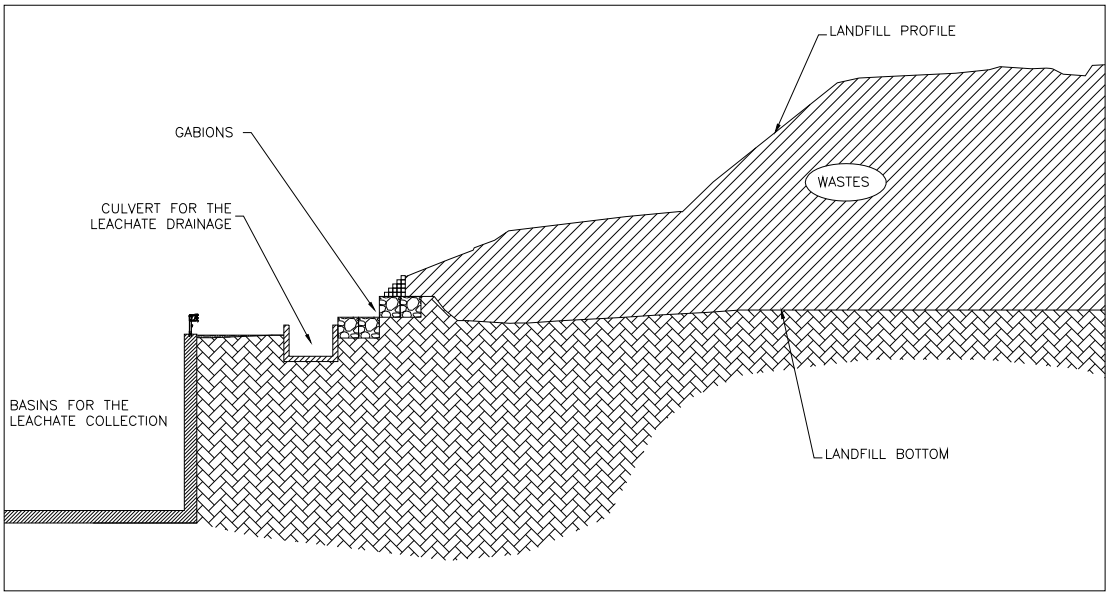

Figure 4a Section at the toe of Scarpino, before the beginning of the stabilization works

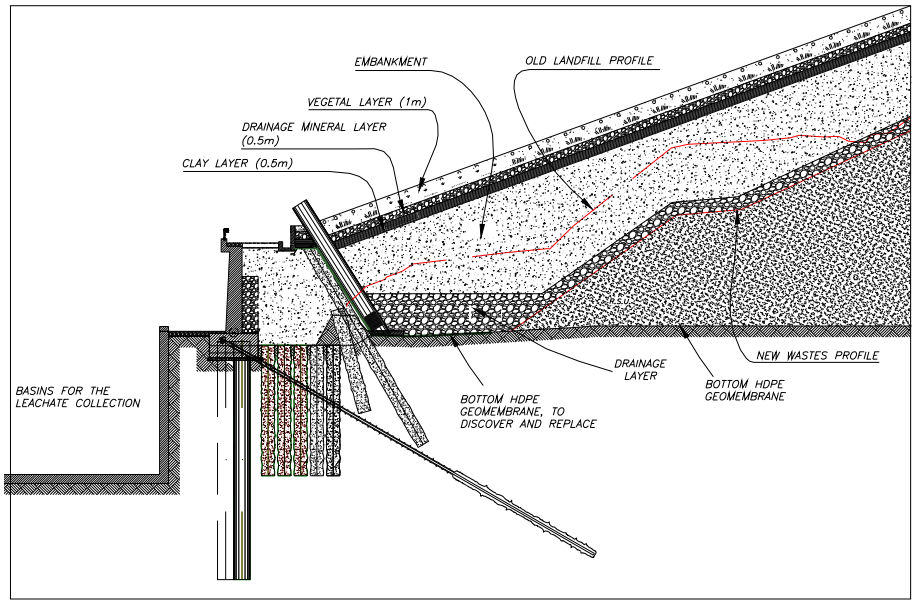

Figure 4b Section of the stabilization works at the toe of Scarpino

4. REINFORCED EARTH TO GUARANTEE TEMPORARY STABILITY

During the realization of the drilled piles, together with the client and the contractor, it was decided to execute the jet grouting treatment after the piles and ground anchors, before the wall and prior to backfill; referring to the operative phases listed in Chapter 3, it means anticipate phase 6 between phases 3 and 4. This could lead to some advantages, both economical and functional: the execution of the jet grouting could have made directly from the soil surface (easier operativeness, easier quality control, lesser costs). The finding to keep a high inclination of the backfilling (about 60°) during the operations related to the connection to the existing bottom lining system was obtained by a reinforced earth embankment.
So doing, besides the temporary result, also a permanent result has been achieved, that is the improving quality of the backfilling (smaller pressures transferred on the internal face of the wall due to the friction developed between the soil and the reinforcement). Fig. 5 shows the reinforced earth embankment behind the wall and the connection between the old and the new bottom lining system.

Figure 5 Reinforced earth embankment behind the wall and connection to the old lining system

Because any escape of the leachate collected on the bottom of the landfill had to be prevented, a fabric-encased GCL in a reinforced configuration (that is the two geotextiles needlepunched together) with one side laminated with an HDPE geomembrane was incorporated to the geogrids (fig. 6).

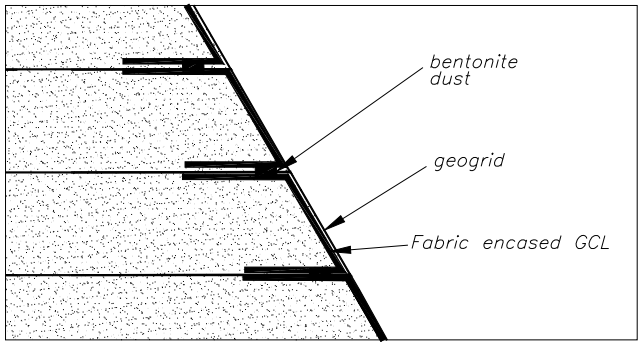

Figure 6 Particular of the reinforced earth embankment

The sealing between the reinforced earth layers, so to obtain a perfect water proofing face, was obtained by the interposition of bentonite dust, as shown in figure 6.
It must be noted that the fabric encased GCL can substitute the mineral clay liner foreseen by the Italian regulation for the lateral containment barrier. In fact, it is said that particular solutions can be adopted in the realization of the lateral containment barrier provided they guarantee a performance equivalent to that one of the mineral layer of 1 m. The CGL has been already used at Scarpino, because the lateral slopes of the landfill are so steep that the mineral clay liner could hardly be placed.

Equivalence between the clay liner and the GCL liner can be easily demonstrate through the Darcy equation, which leads to the following:

$$k_{GCL} \times \frac{H+T_{GCL}}{T_{GCL}} = k_{CCL} \times \frac{H+T_{CCL}}{T_{CCL}} \quad [1]$$

where k_{GCL} and k_{CCL} are respectively the permeability of the geocomposite clay liner and mineral clay liner, T are their thicknesses and H is the height of the leachate above the liners (Koerner and Daniel, 1993).

5. EXECUTION OF THE CONTAINMENT SYSTEM (BOTTOM)

According to the original design, the containment system at the bottom (added to the existing) would have been constituted by the following layers (from bottom to top): GCL, HDPE geomembrane and a protection geotextile (areic mass of 1500 g/m^2), connected to the existing ones and extended to the top of the reinforced earth embankment (anchored under the culvert at the top of the wall, see fig. 4b); geotextile (areic mass of 125 g/cm^2), drainage layer (0,8 m thick) and a GCL between the bottom lining system and the embankment.
During the work, problems were encountered to find a surface of the existing geomembrane adequate to be connected to the new one. To well execute the welding, you need to have a dry and polished surface, without holes, larger than the overlapping width between the two geomembrane; to find a suitable surface, it was necessary to enlarge the excavation much more than the design foresaw. Because it was impossible to go behind at the top of the excavations with the same amount, this leaded to have a steeper excavated slopes than those designed. As a consequence, the placing (and the stability) of the drainage mineral layer could be very difficult. To make easier the placing and to improve the stability of the drainage mineral layer two different types of drainage materials were selected: one, with rounded grains and one with angular grains (like ballast). While rounded grains can be better as drainage layer, angular grains can have higher internal friction angle and so can easily stand firm where the slope are steeper.
Figure 7 sketches a definitive section of the bottom containment system.

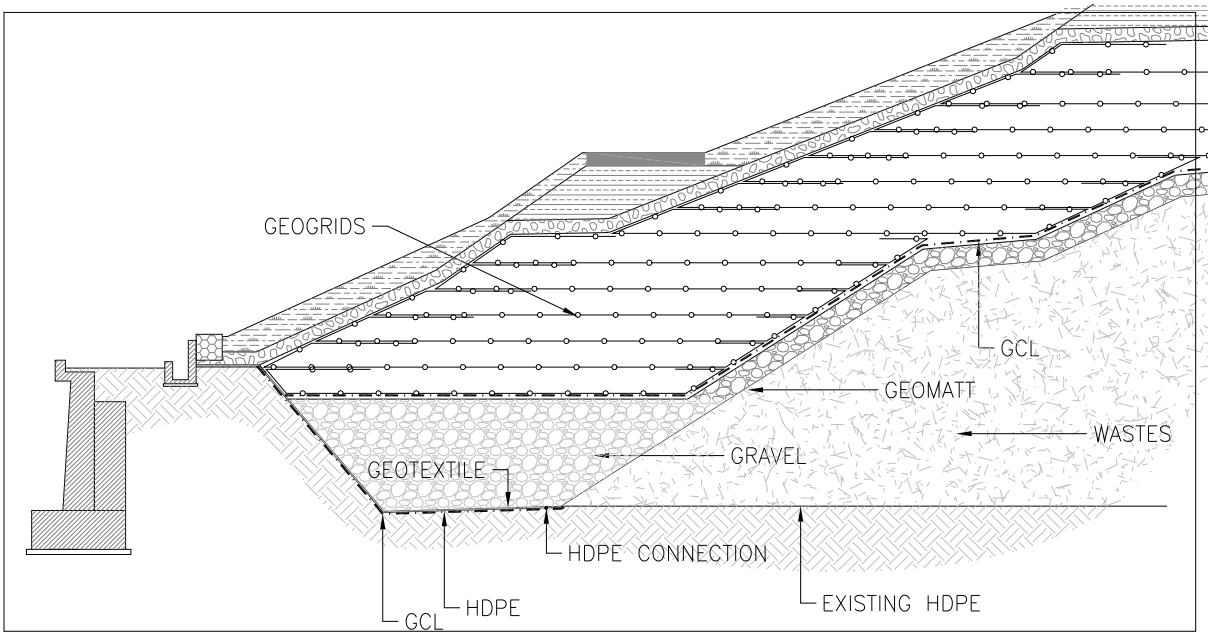

Figure 7 Bottom containment system

A geomatt was placed between the waste and the drainage layer; the aim of the geomatt is to avoid the occlusion of the drainage layer pores that leachate filtering could cause, and, at the same time, to accommodate the placing of the draining mineral, with the new sloping angle, better than a common geotextile can do.

6. EMBANKMENT

The embankment between the drainage layer and the clay layer is of basic importance to give stability to the landfill. Many stability analyses were performed according both limit equilibrium methods (2D) and finite elements (3D),

searching the most critical surfaces, both within the landfill and through the landfill and the sub-layer. Various hypotheses were assumed regarding the leachate, based on the piezometers and wells data collected through the years, because it is known that leachate plays an important role in the stability of slope. As often happens (Mitchell and Mitchell, 1991; Oweis, 1993, Dixon et al., 2006) the 2D analyses showed that the most critical surfaces are those in which a slip of the wastes over the bottom lining system occurs along the line of maximum gradient. To take into account that there are different sorts of containment barriers at the bottom and at the sides of the landfill (and then different friction), a weighted average (where the weights are the respective surfaces) has been calculated to obtain the strength parameters of the equivalent lining system. Shear tests on big scale specimens were made, to assess the interface strength parameters (friction angle and cohesion) to be used in the analyses. More details are given in Fratalocchi et al. (2003).
The stability analyses showed that some weighting at the toe, together with a proper leachate extraction system, were needed to obtain the factor of safety for the critical surfaces requested by the Italian regulations. So, the embankment between the drainage layer and the clay layer was designed. Strength parameters of the embankment are assumed in the stability analyses, and so the material selection and quality control become critical.
Due to some unpredictable factors, after the works had begun it was impossible to find the earth with the proper granular and geotechnical characteristics (A3, A-2-4 or A-2-5 according the AASHTO M 145-82 classification) in the amount calculated (it must be noted that a quantity of about 65,500 m^3 was calculated to be necessary). To guarantee the internal stability of the embankment using materials coming from excavations or other building sites (with inferior geotechnical properties respect to those requested), it was so necessary its reinforcement (fig. 7). Stability analyses were again performed to find the right reinforcements given the strength parameters of the fill materials supplied.
References on the stability analyses are given in Ghionna and Olivetta (2005) and in Ghionna and Veggi (2007).
Three different types of geogrids were selected; in particular, a draining geogrid was selected for the lower part of the embankment. The utilization of a draining geogrid can permit to use of cohesive soil as a filling material in a reinforced earth embankment.
In situ and laboratory tests on the embankment and on the reinforcements (Proctor standard tests, Plate Load Tests, in situ density tests, pullout tests) were performed to ascertain if the final properties of the embankment could match the design specifications. For reasons of shortness, the description of the tests conducted and the discussion of the results obtained are not included in the present paper, but they could be presented in the future.
Figure 8 shows the embankment at its actual stage of construction (September 2008).

Figure 8 Embankment construction

7. FINAL CAPPING

The layer sequence of the final capping, from the embankment surface to the final surface, is the same requested by Italian regulation, that is: a clay layer of 0.5 m thickness, a drainage mineral layer of 0.5 m thickness, a geotextile to prevent fine particles being carried in from the upper layer (areic mass 125 g/m^2) and a vegetal earth layer (1 m thickness).
Another problem appeared in finding the about 6000 m^3 of clay with the requested performance (a maximum k of 5 x 10^{-7} cm/s from laboratory tests and of 10^{-6} cm/s from in situ tests). It must be noted that only local suppliers can be considered by the contractor, because, in the case of Scarpino, transportation costs affects the general costs in a very serious manner.
So, again the solution was to use a GCL as a substitute of the clay as impervious layer in the final capping. To achieve the same elevations foreseen by the design, as the GCL is obviously thicker (about 0.5-0.6 cm before hydration takes place) than the clay layer (50 cm), the thickness of the embankment was increased.

8. CONCLUSIONS

Controlled landfill design is based the national regulation, in which guidelines for the bottom lining system and for the capping are provided. Generally, the regulations give prescriptive standards, obtaining three main advantages (Manassero et al., 1998): minimizing the burden of approval by the regulator, facilitating the receipt of regulatory approval by the proponent and to assure a minimum protection of the environment. The Italian regulation prescribes, for the bottom and the sides of a controlled landfill, a geological (mineral) layer of minimum thickness and maximum permeability, that must be integrated by an artificial material (i.e. a geosynthetic) to place over the mineral layer. The regulation explicitly says that the geosynthetic alone can never be considered as an adequate barrier, but only an accomplishment to that, provided an equivalent protection level is demonstrated. Besides, the regulation recognizes that particular solutions can be approved for the sides of the landfill, mainly because, in cases where the sides are too steep, it can be difficult (and no economic) to place a well compacted clay layer. What must be kept in mind is that some unpredictable factors can takeover at certain stages of construction that constrains the designer to change its design (lack of adequate materials, excessive increase of materials costs, etc.); in this cases, performance standards as an alternative to the prescriptive standards can permit the construction to proceed without costs increasing (or with little cost increasing) and, most of all, preserving the design requirements.
In this paper, some examples have been presented, virtually involving every part of the design (lining systems and structural works). Reinforced earth is a practical and cost effective solution when the stability with high slope angle must be guaranteed or when no good materials from a geotechnical point of view can be found. In particular, the adoption of draining reinforcements can enable the usage of materials with high fine contents as fill materials.
Clay of adequate geotechnical characteristics is becoming difficult to find is some parts of Italy, especially, like in the controlled landfills, high performance in terms of hydraulic conductivity are prescribed and big quantities are requested. In this case, it is very important that an equivalence criterion is admitted by the regulations, which leave the designer the possibility to adopt a solution without costs increasing.

REFERENCES

Dixon, N., Jones, D.R.V. and Fowmes, G.J. (2006). *Interface Shear Strength Variability and Its Use in Reliability-Based Landfill Stability Analysis,* Geosynthetics International, **13**, No 1, pp.1-14.

Fratalocchi, E., Pasqualini, E., Patacchini, C., Stella, M. and Veggi, S. (2003). *Stabilità delle Discariche Controllate per Rifiuti Solidi Urbani,* (in italian), Proc. of XIX Turin Geotechnical Conference (CGT), Technical University of Turin.

Ghionna, V.N. and Olivetta, M. (2005). *La progettazione Geotecnica delle Opere in Terra Rinforzata con l'Approccio degli Eurocodici,* (in italian), Proc. of XX Turin Geotechnical Conference (CGT), Technical University of Turin.

Ghionna, V.N. and Veggi, S. (2007). *Stabilizzazione e Rinforzo delle Discariche,* (in italian), Proc. of XXI Turin Geotechnical Conference (CGT), Technical University of Turin.

Koerner, R.M. and Daniel, D.E. (1993). *Technical Equivalency Assessment of GCLs to CCLs,* Proc. Seventh Annual GRI Seminar, Geosynthetic Research Institute, Philadelphia, PA, USA.

Manassero, M., Parker, R., Pasqualini, E., Szabò, I., Almeida, M.S.S., Bouazza, A., Daniel, D.E. and Rowe, R.K. (1988). *Controlled Landfill Design (Geotechnical aspects)*, Environmental Geotechnics, Sêco e Pinto ed., Balkema, Rotterdam.

Mitchell, J.K. and Mitchell, R.A. (1991). *Stability of Landfills,* Proc. of XV Turin Geotechnical Conference (CGT), Technical University of Turin.

Oweis, I.S. (1993). *Stability of Landfills,* Geotechnical Practice for Waste Disposal, Daniel Ed., Chapman & Hall, London.

Geotextile use for Landfill Gas Pressure Relief at the Boulevards at South Bay (Former Cal Compact Landfill)

M.L. Leonard, Sr., P.E., Bryan A. Stirrat & Associates (BAS), Diamond Bar, California, USA
J. Deguia, Bryan A. Stirrat & Associates (BAS), Diamond Bar, California, USA
J. Weckmann, Tetra Tech, Inc., San Bernardino, California, USA

ABSTRACT
BAS has been the primary gas system designer for a multi-use development (commercial, retail, office, and residential development) to be constructed over a large closed landfill containing mostly municipal solid waste (MSW), located in the City of Carson, California. Structures are to be supported on piles to avoid landfill settlement-related distress. Deep dynamic compaction was completed to reduce settlement that could impact parking, walkways, small slabs on grade, and other surface features. The landfill will have a geomembrane cap (with overlying soil) or a low permeability soil cover installed to prevent infiltration of liquids and control gas emissions. Landfill gas migration will be controlled with a multi-component system composed of vertical and horizontal gas extraction wells, a geotextile placed beneath the geomembrane cap, the geomembrane, a building protection system consisting of passive vents and a secondary geomembrane attached to all building floor slabs. This paper describes the selection of the geotextile located below the main landfill cap geomembrane to meet two requirements:

1) To prevent geomembrane “ballooning”; and
2) To provide continued flow of the landfill gas during failure of the gas collection system.

The methodology is described and the calculations presented. Calculations utilized a published technique based on the assumptions presented.

1. INTRODUCTION AND BACKGROUND

The future development area is composed of approximately 168 acres, including: 157 acres of the former Cal Compact Landfill, and 11 acres of undeveloped (non landfill) property. The currently-proposed redevelopment of the Site includes construction of mixed-use commercial and residential units.

In 1959, Cal Compact, Inc., a California Corporation, was issued an industrial waste disposal permit to operate a Class II landfill on the Site. The facility operated from approximately 1959 to 1964, with an approximate closing date of February 1965. The Cal Compact Landfill was permitted to accept both municipal solid waste and specified industrial liquid wastes.

The landfill accepted approximately 6 million cubic yards of municipal solid waste and 6.3 million gallons of industrial liquid waste. The liquid waste was predominately water and clay mixtures. Other wastes received included solvents, oils, sludges, heavy metals, paint sludges, and inorganic salts. The landfill is comprised of five separate cells, divided by haul roads, and is currently separated by Lenardo Drive and Stamps Drive. A soil cover which varies in thickness overlies all five cells.

The California Environmental Protection Agency, Department of Toxic Substances Control (DTSC) approved a Remedial Action Plan (RAP) in 1995 which permits Site development provided that an engineered landfill cap is installed to protect human health and the environment. In accordance with the approved RAP, remedial action improvements include an engineered landfill cap, a LFG collection and treatment system, a building gas protection system and a groundwater containment system. Deep dynamic compaction was completed to reduce settlement that could impact parking, walkways, small slabs on grade, and other surface features. The landfill will have a geomembrane cap (with overlying soil) or a prescriptive soil cover installed to prevent infiltration of liquids and control gas emissions. Landfill gas migration will be controlled with a multi-component system consisting of vertical and horizontal gas extraction wells, a geotextile placed beneath the geomembrane cap, the geomembrane, and a building protection system composed of passive vents and a secondary geomembrane attached to all building floor slabs.

An aerial photograph showing the site boundaries is provided as Figure 1.

Figure 1: Site vicinity plan

Figure 2: Cross section showing LFG collection

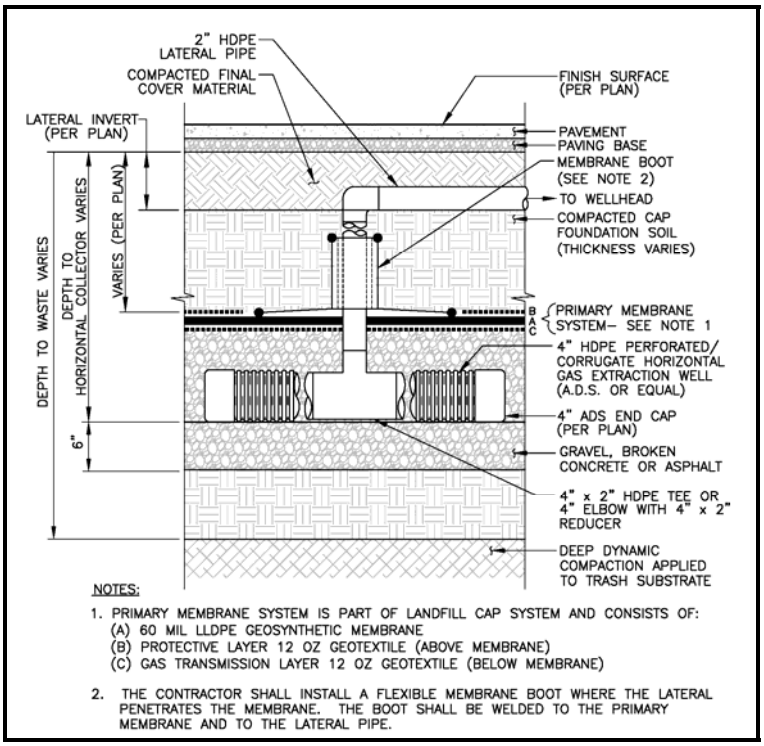

2. PURPOSE

The purpose of the calculation described herein was to evaluate the gas flow through the non-woven geotextile located immediately beneath the LLDPE geomembrane landfill cap, to confirm that it is adequate to provide passive flow of landfill gas should a reasonable portion of the LFG collection system fail to operate for a short period of time until repairs can be made. The non-woven geotextile beneath the LLDPE geomembrane is typically provided on landfill closure caps to protect the geomembrane from damage by puncturing if the subgrade inadvertently contains angular rocky material. A typical cross-section of the landfill cap with geomembrane and with the geotextile shown is presented as Figure 2. A 3-D model of the estimated radii of vacuum influence from the horizontal and vertical LFG extraction wells for a typical portion of the landfill is presented as Figure 3. The analysis of zones of vacuum influence does not incorporate any influence from the geotextile layer which will be placed under vacuum, as the methods used do not accommodate that type of a gas collector, rather only slotted pipe type collectors. The geotextile layer is provided as an extra measure to control landfill gas emissions and migration should the gas collection system be shut down for an extended period of time (but not beyond the permit constraint time period) for repairs or a portion of the collection system.

Figure 3: 3D model of estimated radii of vacuum influence from the horizontal and vertical LFG extraction wells

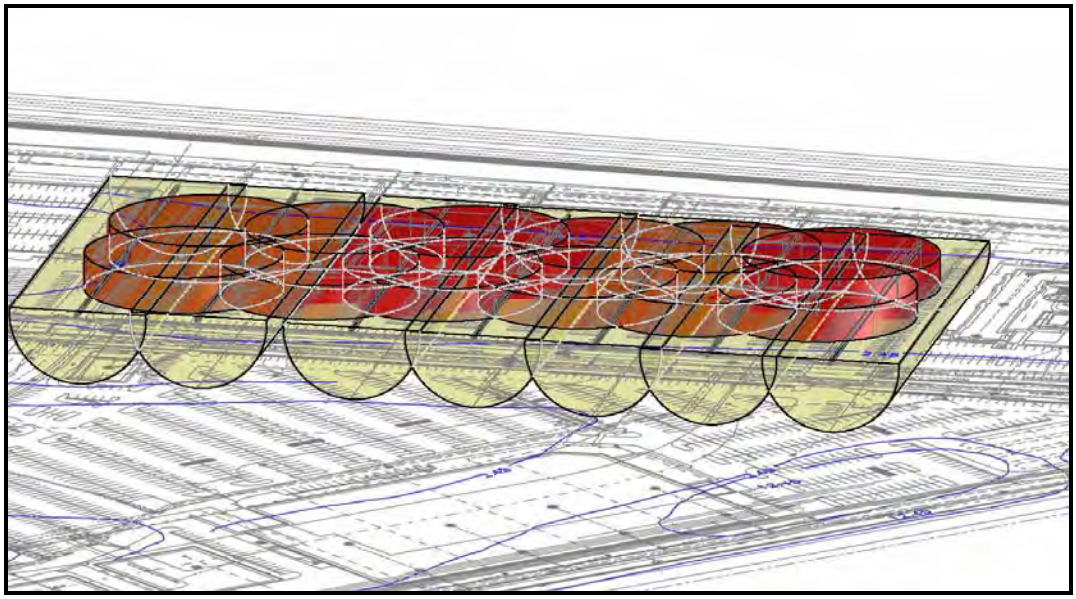

3. METHODOLOGY

Two methods were used to calculate the required LFG transmissivity and compare the values to published data on the measured transmissivity for non-woven 12 oz/yd^2 geotextile under similar overburden and gas mass flux conditions:

Advanced Geotechnical Systems (AGS) Method

The method is fully described in the reference and only summarized here.

- LFG Mass Flux equation used for each surface area:

$$\Phi_{LFG} = \frac{flow_{LFG}}{Area_{surface}} \left[\frac{m^3/s}{m^2}\right]$$

- Required LFG Relief Layer Transmissivity Design Equation rearranged to solve for Maximum LFG pressure values:

$$\mu_{g\,\max} = \frac{\Phi_{LFG}\,\gamma_{LFG}}{\theta_{reqLFG}} \left(\frac{L^2}{8}\right) [kPa]$$

- Required LFG Relief Layer Transmissivity equation used to solve for various LFG pressure values:

$$\theta_{reqLFG} = \frac{\Phi_{LFG}\gamma_{LFG}}{\mu_{g\max}}\left(\frac{L^2}{8}\right)\left[\frac{m^2}{s}\right]$$

- The landfill gas mass flux is calculated for a reasonable area of the landfill assuming two adjacent vertical and horizontal collectors fail for some reason, i.e. 150 x 150 sf by pro-rating the total flow from the landfill of 700 scfm over the 150 x 150 sf area and rounding to 2.5 scfm.

Giroud *et al* Method

The following presents the basic equations and assumptions published Giroud et al. More detail of the method is presented in the referenced paper.

- LFG Mass Flux equation:

$$Q_{gas} = \frac{Weight_{Waste}\, x0.1scf/lb/yr}{Area_{FinalCover}\left(1\,ft^2\right)}$$

- Required LFG Relief Layer or Geotextile Required Transmissivity equation:

$$\theta_{reqLFG} = \frac{Q_{gas}\gamma_{gas}}{\mu_{\max}}\left(\frac{L^2}{8}\right)$$

- Recommends use of a Long-Term Service Reduction Factor for LFG Relief Layer of 6 to be applied to determine the safe value of transmissivity to select for design.

The computed values of transmissivity were then compared to an average value from published data on the geotextile transmissivity testing to confirm that the 12 oz/yd^2 geotextile provides adequate gas flux for the short term period of possible gas collection system non-operation.

4. ASSUMPTIONS AND INPUTS

The following assumptions and input values were used in the computations:

- It is assumed that the geotextile remains largely unplugged. This is the likely condition as the geotextile is placed on a compacted and prepared foundation layer and water that could carry soil fines into the geotextile is highly unlikely to penetrate the LLDPE geomembrane located continuously over the geotextile in any significant volumes.
- The geotextile will be continuous, but the equations require a set spacing of geotextile strips, thus a very close spacing of 0.1 m was assumed.
- Gas flow from the surface in the subject area will be about 2.5 standard cubic feet per minute (scfm) or less. This assumes a 700 scfm design flow from the entire landfill surface pro-rated for a 150 x 150 sf area. This area was based on one vertical and one horizontal collector failing at the same time.
- Parameters used:

LFG Generation Rate	0.1 scf/yr/lb
LFG Unit Weight	0.00128 kN/m^3
Surface Area	1 sf
Spacing between Strip Drains (assumed, but geotextile is continuous)	0.1 m
Long-term Service Reduction Factor (for plugging)	6
Waste Depth (ranges from 10 to 40 ft, conservative value used)	40 ft
Waste Density	55 pcf
Average Spacing of Horizontal Collector Pipes	125 ft
GeotextileTransmissivity (Based on Published Test Data—see references)	0.0002 to 0.75 m^2/s

5. CALCULATIONS AND RESULTS

Results of the analysis included:

- Tables 1 and 2 present the results of the calculations for the two methodologies.

- The 12 oz/yd^2 geotextile has more than adequate transmissivity to vent all the gas that may flux from the landfill, i.e., 0.0002 to 0.75 m^2/s transmissivity of geotextile vs. 2.30 x 10^{-05} to 1.16 x 10^{-04} m^2/s minimum required (with long-term service reduction factor of 6 applied) to vent expected LFG flux from the landfill.
- Also, if required on slopes, and gas wells fail, the geotextile will eliminate the pressure that could build up below the cover; thus, not impacting the cap/cover stability on slopes.

Also, many closed landfills located throughout the United States have a geotextile in the cap beneath the geomembrane or geotextile in the leachate collection and recovery system (LCRS), and there have been reported in the literature cases of landfill gas flowing through the geotextile and being detected at the perimeter cap anchor trench (see McCready *et al* and Sullivan *et al*). Mitigation for this issue has included placing gas collection wells or horizontal collectors in a trench along the perimeter to capture the gas (passive or active with vacuum applied) and route it to the treatment plant. The key to avoidance of these gas migration issues is to have the liner and closure cap designer work with a landfill gas system designer as a team.

Table 1: Required Transmissivity – AGS Method

					Average
Range of LFG Transmissivity Per Published Test Data [1]	m^2/s	θ_{reqLFG} =	1.5	2.000E-04	7.50E-01
LFG Unit Weight	kN/m^3	γ_{LFG} =	0.00128		

@ Surface Area = 150*150 [sf]

Mass Flux	m^3/s/m^2	$\Phi_{LFG} = \frac{(\text{Flow Rate/Surface Area}_{Landfill}) \times \text{Area}_{150x150}}{SF} = \frac{2.46\ [scfm]}{1\ [sf]} = \frac{0.0012\ [m^3/s]}{0.09\ [m^2]} =$		1.25E-02
Spacing Between Strip Drain (assumed to simulate continuous geotextile)	m	L = 0.10		
			θ_{reqLFG} = 1.5	θ_{reqLFG} = 0.0002
Maximum LFG Pressure	kPa	u_{gmax} = 1.3E-08		1.0E-04
	psi	u_{gmax} = 1.9E-09		1.4E-05

Required LFG Transmissivity	m^2/s	θ_{reqLFG} =	4.60E-08	=	3 psi	
	m^2/s	θ_{reqLFG} =	2.76E-08	=	5 psi	
	m^2/s	θ_{reqLFG} =	3.83E-06	=	0.036 psi	Per 1 inWC
Req'd LFG Transmissivity Adjusted for Long-Term Service Reduction Factor of 6[2]	m^2/s	θ_{reqLFG} =	2.30E-05	=	0.036 psi	Per 1 inWC

Table 2: Required Transmissivity (Giroud *et al* Method)

						Average
Range of LFG Transmissivity Per Published Test Data	m^2/s	θ_{reqLFG}	=	1.5	2.000E-04	7.50E-01
Waste Depth	40	ft				
Waste Density	55	pcf				
LFG Generation	0.1	scf/yr/lb				
Spacing	125	ft				
LFG Density	0.0815	pcf				
Maximum Pressure	1	inWC	=	5.2	psf	
Q_{gas} = $Depth_{waste}$ x $Density_{waste}$ x LFG Generation	220	scf/ft^2/yr	=	4.19E-04	scf/ft^2/min	
Req Transmissivity = Qgas x $Density_{gas}$/Max Pressure x L^2/8	1.28E-02	ft^3/min-ft				
Adjust for Long-term service factor =	6					
Adjusted Required Transmissivity =	7.69E-02	ft^3/min-ft				
	1.16E-04	m^3/sec-m		m^2/s		

REFERENCES

Advanced Geotech Systems, “Landfill Gas Pressure Relief Layer – Design Calculator.” http://www.landfilldesign.com/cgi-bin/gaspressure.pl.

Propex, Inc., “Gas and Water Transmissivity Testing of Non woven Geotextiles.” http://www.sedimentremediation.com/TechRef/Dredge/GPD-SM-110.pdf.

Richardson, G.K., Giroud, J.P., and Zhao, A. Design of Lateral Drainage Systems for Landfills. PG 46. Published 2000.

McCready, A.A., Stearns, R.P., and Leonard, M.L. Liner Design and Landfill Gas Migration. Presented at SWANA Landfill Conference, June 2004.

Sullivan, P.S., Huff, R.H., and Leonard, M.L. Unique Solutions to Complex Landfill Gas Migration Problems. Presented at SWANA Landfill Gas Symposium, 2005.

Geosynthetics 2009
February 25-27 2009, Salt Lake City, Utah

Influence of the Aspect Ratio on the Mechanical Behavior of a Micro-Reinforced Soil

K.S. Heineck, L. Festugato, N.C. Consoli, Federal University of Rio Grande do Sul, Porto Alegre, Brazil

ABSTRACT
The study of the mechanical behavior of a soil micro-reinforced with fibers with distinct aspect ratios is the purpose of this investigation. Thus, drained standard triaxial tests on 100mm diameter and 200mm high specimens were carried out. A uniform fine sand, was reinforced with 24mm length polypropylene fibers with different diameters: 0.023 and 0.100mm, and consequently with distinct aspect ratios: 1043 and 240, respectively. The results showed the effectiveness of fiber reinforcement in the strength increase of the samples, compared to the non-reinforced material. The values of the friction angles were not influenced by the aspect ratio of the fibers. However, the values of cohesive intercept of the composites were strongly influenced by the aspect ratio. Finally, the measurement of the fibers length before and after the tests showed that the reinforcement do not break in tension. The failure is a combination of slippage and yielding of fibers.

1. INTRODUCTION

Randomly distributed monofilament discrete fibers incorporated into sands improve their mechanical behavior by interacting with the soil particles through surface friction and also by interlocking. The role of friction and interlock is to transfer the stress from the soil to the tensile inclusions, and to mobilize their tensile strength and impart this resisting force to the sand, thus reducing the strains induced in reinforced sand which lead to the improvement in load carrying capacity of the material. The general characteristics of granular soils reinforced with discrete fibers have been reported in previous studies by several investigators (e.g. Gray and Ohashi 1983, Gray and Al Refeai 1986, Maher and Gray 1990, Ranjan et al. 1994, Santoni et al. 2001, Zornberg 2002, Heineck et al. 2005 and Consoli et al. 1998, 2002, 2003, 2005, 2007a, 2007b).

The study of the mechanical behavior of a soil micro-reinforced with fibers with distinct aspect ratios is the purpose of this investigation. The ratio between the fibers length and diameter was considered the aspect ratio. Through the results of a series of triaxial tests conducted on uniform sand reinforced with polypropylene fibers, the influence of fiber inclusion on the mechanical behavior as well as the specific significance of the fiber characteristics in determining the triaxial strength envelope of the fiber-reinforced soil were investigated.

2. EXPERIMENTAL PROGRAM

Triaxial tests were carried out in this experimental program using fully saturated samples, at effective confining pressures ranging from 20 to 200kPa. Standard triaxial tests were used in the present study, considering one fiber length, 24mm, two diameters, 3.3dtex (0.023mm – very thin) and 100dtex (0.1mm – thin), and consequently two different values of aspect ratios, 1043 and 240 respectively.

2.1 Materials

Uniform quartzitic sand, Osorio Sand, from southern Brazil was tested in this experimental program. The Osorio Sand was sampled from the region of Osorio near Porto Alegre. The soil is classified as non-plastic uniform fine sand (SP) and the specific gravity of the solids is 2.62. The grain size distribution is entirely fine sand (0.075 mm < diameter < 0.42 mm), with an effective diameter of 0.09 mm and uniformity and curvature coefficients of 2.1 and 1.0, respectively. Mineralogical analysis showed that sand particles are predominantly quartz. The minimum and maximum void ratios are 0.6 and 0.9 respectively.

Monofilament polypropylene fibers were used throughout this investigation to reinforce the soil. Their average dimensions were 24mm in length and 0.023mm (dtex=3.3) and 0.1mm (dtex=100) in diameter, with a specific gravity of 0.91, tensile strength of 120MPa, elastic modulus of 3GPa and linear strain at failure of 80%. The values of the studied fibers aspect ratios were 1043 and 240 respectively. The fiber content used in the experiments was 0.5% by weight of soil. The density of filaments in mixtures with the higher aspect ratio fibers was about 825 millions per cubic meter, and in mixtures with the lower aspect ratio fibers was about 44 millions per cubic meter.

2.2 Testing Methodology

The compacted soil and fiber-reinforced specimens used in the triaxial tests were prepared by hand-mixing dry soil, water and polypropylene fibers, when used. During the mixing process, it was found to be important to add the water prior to adding the fibers, to prevent floating of the fibers. Visual and microscope examination of exhumed specimens showed the mixtures to be satisfactorily uniform. The undercompaction process (Ladd 1978) was used to produce homogeneous specimens that could be used for a parametric study in the laboratory-testing program. The specimens were statically compacted in three layers into a 100mm diameter by 200mm high split mould, to a moisture content of 10.0% and dry unit weight of 15.0kN/m^3, equivalent to a relative density of 50%. Each sample was compacted in a mould on the triaxial pedestal by applying a static load via the loading platen. The final height of the sample was controlled to ensure a relative density of 50%. Such relative density was selected because it was efficiently achieved for all inclusions used.

The triaxial tests were conducted using a computer controlled large triaxial cell. This apparatus allowed the tests to be conducted with constant radial stress. The samples were saturated under back pressure and saturation was monitored in each test, ensuring B values of at least 0.98 for all specimens. The axial strains were monitored inside the triaxial cell using a Hall effect sensor type of local strain transducer (Clayton and Khatrush 1986) and outside the cell using a standard type of displacement transducer. The volumetric strain was measured by an Imperial College volume gauge (Maswoswe 1985) connected to the drainage outlet. The triaxial tests were run at a sufficiently low axial strain rate to ensure full drainage within the sample, 0.015% per minute. Drainage was also monitored by measuring the excess pore pressure at the opposite end of the specimen to the drainage. The membrane and area corrections followed recommendations proposed by La Rochelle et al. (1988).

3. RESULTS AND ANALYSIS

3.1 Stress Strain Behavior

The behavior of non-reinforced and fiber-reinforced sand with 0.5% monofilament polypropylene fibers by weight of sand (fiber length of 24mm - fiber diameters of 0.023 and 0.1 mm) was examined through the drained standard triaxial tests results and its typical deviator stress [*q*, $\left(\sigma'_{axial} - \sigma'_{radial}\right)$] : shear strain [$\varepsilon_s$, $\frac{2}{3}(\varepsilon_{axial} - \varepsilon_{radial})$]: volumetric strain [ε_v] curves. The results are grouped for effective confining stresses of 200, 100 and 20kPa, and presented in Figures 1, 2 and 3 respectively.

The analysis of Figures 2, 3 and 4 shows, as expected, the increase of materials strength with the increased of effective confining stress. It is also indicated the higher strength of fiber reinforced matrices. The largest gains in strength, according to the same figures, compared to the non-reinforced material, are found in mixtures reinforced with fibers of index point 1043.

The volumetric strain : shear strain curves suggest that fibers inclusion do not significantly alter the initially compressive and latter expansive behavior of sand.

It can be seen in the same figures the strain hardening behavior of matrices reinforced with 1043 aspect ratio fibers, which is not clearly observed for non-reinforced and 240 aspect ratio fiber reinforced sand.

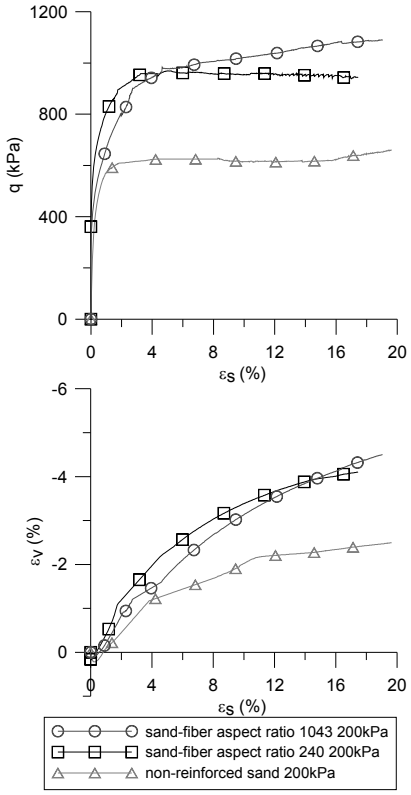

Figure 1. Stress-strain-volumetric response of the studied mixtures for a confining stress of 200kPa.

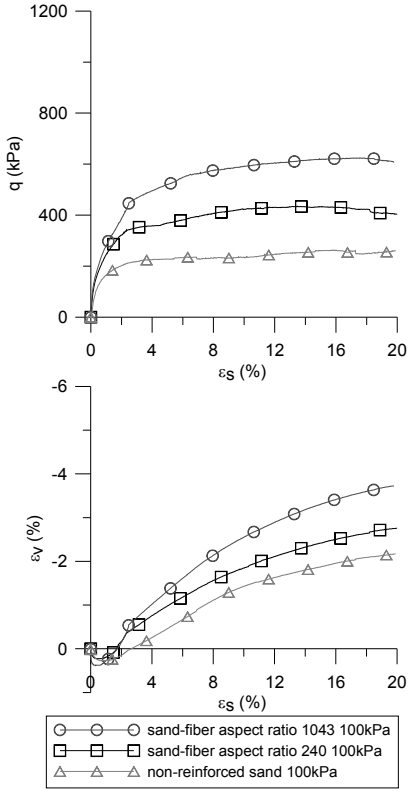

Figure 2. Stress-strain-volumetric response of the studied mixtures for a confining stress of 100kPa.

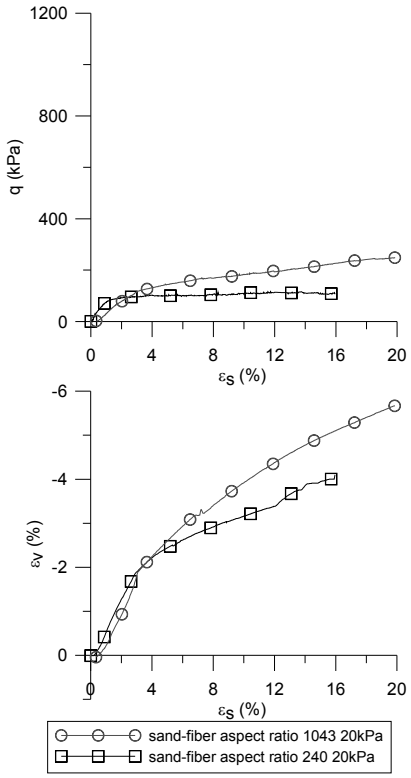

Figure 3. Stress-strain-volumetric response of the studied mixtures for a confining stress of 20kPa.

3.2 Strength Parameters

The shear strength envelopes obtained from triaxial tests with polypropylene fibre-reinforced and non-reinforced samples of Osorio sand are shown in Figure 4, where the deviator stress [*q*] is plotted against the corresponding mean effective stress [*p'*]. The shear strength envelope for the fibre-reinforced sand was taken at 17% shear strain. This was important because several test results on the fibre-reinforced sand were generally strain hardening until the maximum strain that the apparatus could reach, as can be seen in the stress: strain data in Figures 1, 2 and 3, so that a "strength" had to be defined at an arbitrary strain.

The strength increase from the fibers inclusion is also observed through shear strength envelopes and their corresponding strength parameters. According to Figure 4, the non-reinforced matrix friction angle [φ'] was 37.0° and its cohesive intercept [*c'*] was nil. Whereas the strength parameters *c'*=4.8kPa and φ'=43.4° was observed for the 240 aspect ratio fiber reinforced matrix, and *c'*=30.9kPa and φ'=44.6° for the 1043 aspect ratio fiber reinforced matrix.

The parallelism of reinforced materials strength envelopes highlights the small influence of fibers aspect ratio over the values of mixtures internal friction angle. However, in the highest aspect ratio fiber reinforced mixture, the cohesive intercept is at least six times higher than in the lowest aspect ratio fiber reinforced mixture.

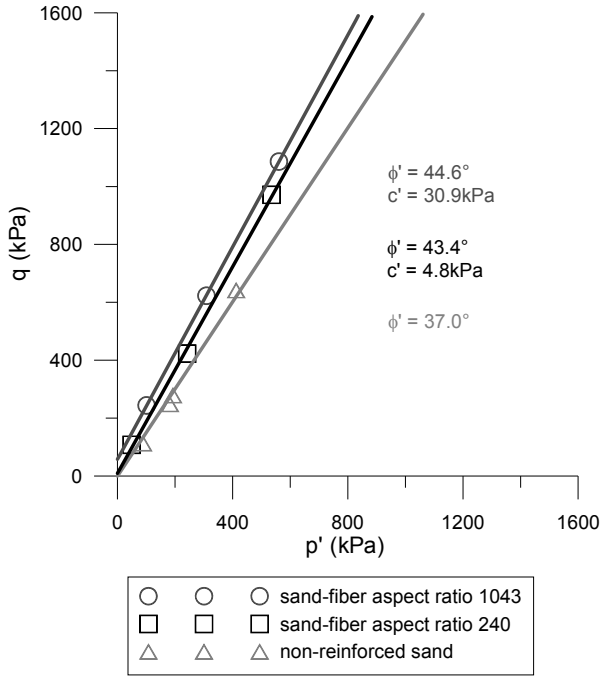

Figure 4. Shear strength envelopes of non-reinforced Osorio sand and fiber-reinforced Osorio sand.

3.3 Fiber Measurement

After completing the standard drained triaxial tests on the fiber-reinforced specimens, the fibers were recovered from the specimens and their final lengths measured. Around 180 fibres were measured after each test. These data indicate that none of the fibers checked in the present study broke in tension. It could be suggested that the failure is a composite of slippage and yielding of fibers, as the fibers show only limited stretching, and so there is possibly slipping occurring between the fibers and the soil particles because of the low confining stress. Possibly, the fibers have not broken because they are highly extensible with a fiber strain at failure of 80%, and the necessary strain to cause fiber breakage had not been reached under triaxial conditions at these strains.

4. CONCLUSIONS

Through the drained standard triaxial tests deviator stress [*q*] : shear strain [ε_s] : volumetric strain [ε_v] curves, some conclusions can be drawn:

- The reinforced matrices presented strength gains, compared to the non-reinforced sand, for both types of fibers added;
- The value of the fibers aspect ratio influences the mixtures behavior. The higher the aspect ratio value, the higher the number of filaments per cubic meter, the higher the strength gain of mixtures;
- High aspect ratio fibers, about 1000 in this study, provide the soil of a hardening behavior, which is not found in mixtures reinforced with fibers of low aspect ratio, about 200 in this study;
- The inclusion of fibers does not significantly alter the initially compressive and latter expansive behavior of sand.

Based on the shear strength envelopes obtained from triaxial tests, the following conclusions are defined:

- There was an appreciable improvement of the strength parameters of the reinforced materials, compared to the non-reinforced sand, for both types of fibers added;
- The mixtures internal friction angle values were not influenced by the fibers aspect ratio. The shear strength envelopes are parallel. In contrast, the values of mixtures cohesive intercept were strongly influenced by fibers aspect ratio. The higher the aspect ratio, the greater the intercept cohesive.

According to the fiber measuring data, it can be indicated that none of the fibers checked in the present study broke in tension. The failure was a composite of slippage and yielding of fibers, as the fibers shown only limited stretching.

ACKNOWLEDGEMENTS

The authors wish to express their gratitude to MCT/CNPq for their financial support to the research group.

REFERENCES

Clayton, C.R.I and Khatrush, S.A. (1986). A new device for measuring local axial strain on triaxial specimens, *Géotechnique*, 25: 657-670.

Consoli, N.C., Casagrande, M.D.T. and Coop, M.R. (2007a). Performance of fibre-reinforced sand at large shear strains, *Géotechnique*, 57(9): 751-756.

Consoli, N.C., Heineck, K.S, Casagrande, M.D.T. and Coop, M.R. (2007b). Shear strength behavior of fiber-reinforced sand considering triaxial tests under distinct stress paths, *Journal of Geotechnical and Geoenvironmental Engineering*, 133(11): 1466-1469.

Consoli, N.C., Casagrande, M.D.T. and Coop, M.R. (2005). The effect of fiber-reinforcement on the isotropic compression behavior of a sand, *Journal of Geotechnical and Geoenvironmental Engineering*, 131(11): 1434-1436.

Consoli, N.C., Casagrande, M.D.T., Prietto, P.D.M. and Thomé, A. (2003). Plate load test on fiber-reinforced soil, *Journal of Geotechnical and Geoenvironmental Engineering*,129(10): 951-955.

Consoli, N.C., Montardo, J.P., Prietto, P.D.M. and Pasa, G.S. (2002). Engineering behavior of a sand reinforced with plastic waste, *Journal of Geotechnical and Geoenvironmental Engineering*, 128(6): 462-472.

Gray, D.H. and Al-Refeai, T. (1986). Behavior of fabric versus fiber-reinforced sand, *Journal of Geotechnical Engineering*, ASCE, 112(8): 804-820.

Gray, D.H. and Ohashi, H. (1983). Mechanics of fiber reinforcement in sand, *Journal of Geotechnical Engineering*, ASCE, 109(3): 335-353.

Ladd, R.S. (1978). Preparing test specimens using undercompaction, *Geotechnical Testing Journal*, ASTM, 1(1): 16-23.

La Rochelle, P., Leroueil, S., Trak, B., Blais-Leroux, L. and Tavenas, F. (1988). Observational approach to membrane and area corrections in triaxial tests, *Proc., Symposium on Advanced Triaxial Testing of Soil and Rock*, ASTM, Louisville, 715-731.

Maher, M.H. and Gray, D.H. (1990). Static response of sands reinforced with randomly distributed fibers, *Journal of Geotechnical Engineering*, ASCE, 116(11): 1661-1677.

Ranjan, G., Vasan, R.M. and Charan, H.D. (1994). Behaviour of plastic fibre-reinforced sand, *Geotextiles and Geomembranes*, 13: 555-565.

Santoni, R.L., Tingle, J.S. and Webster, S.L. (2001). Engineering properties of sand-fiber mixtures for road construction, *Journal of Geotechnical and Geoenvironmental Engineering*, 127(3): 258-268.

Zornberg, J.G. (2002). Discrete framework for limit equilibrium analysis of fibre-reinforced soil, *Géotechnique*, 52 (8): 593-604.

Longer Term Monitoring of Strains In MSE Wall

R.L. Parsons, Ph.D., P.E., The University of Kansas, USA
M.C. Pierson, The University of Kansas, USA
J. Han, Ph.D., P.E. The University of Kansas, USA
C. Vulova, P.E., Tensar International, USA
J.J. Brennan, P.E. Kansas Department of Transportation, USA

ABSTRACT
Interest is growing in the construction of mechanically stabilized earth (MSE) walls with deep foundations included within the reinforced mass to minimize space requirements for bridge abutments, sound walls, and similar structures. The Kansas Department of Transportation currently has multiple projects designed with drilled shafts installed through the geosynthetic reinforcement of MSE block walls for the support of sound walls. To evaluate the lateral capacity of these MSE block walls, a test wall 43 m in length and 6.1 m in height was constructed with 8 test shafts behind the wall facing. The shafts were loaded laterally to failure in the direction of the wall facing. This loading resulted in significant deformation at the top of the wall facing and localized deformation of the geogrid.

This paper contains a discussion of the lateral capacity of the wall and the performance of a control section of the wall during the six months after testing. Wall deflections were also monitored. It was observed that little additional movement of the wall occurred after testing was completed.

1. INTRODUCTION

Conservative design practices related to laterally loaded shafts contained in an MSE mass prompted the initiation of a research project to determine the lateral load response of concrete shafts contained within and solely supported by an MSE mass. The Kansas Department of Transportation (KDOT) and The University of Kansas (KU) developed the project which eliminated a traditional rock socket at the base of the laterally loaded shaft. The MSE wall and shafts were heavily instrumented and yielded results that are potentially applicable to a variety of wall/foundation configurations. This paper describes the monitoring of strain gages that were attached to four different layers of geogrid.

2. CONSTRUCTION

The test site was located in Wyandotte County, Kansas, on the west side of the Kansas City metropolitan area. The soil was excavated to bedrock for a distance of 12 m behind the wall location to eliminate settlement and lateral pressures from the natural soils. The wall was designed and constructed in accordance with FHWA procedures (FHWA, 1997). At each shaft location a 0.9m diameter corrugated metal pipe (CMP) was placed to act as a form for the concrete and to prevent aggregate from entering the shaft area. The reinforcement layers consisted of uniaxial high density polyethylene geogrid with an ultimate tensile strength of 114 kN/m for the lower reinforcement layers and an ultimate tensile strength of 70 kN/m for the upper layers when tested in accordance with ASTM D 6637 (layers referred to as G1 and G2 in this paper). Reinforcement was spaced vertically every 0.61 m of elevation. The lower four layers consisted of G1 and the upper six layers consisted of G2. The geogrid was cut to fit around the CMP as shown in Figure 1. Backfill material consisted of a clean crushed limestone rock whose specifications were established by KDOT as CA-5 (Figure 2). The CA-5 specification consists of 19mm maximum size and more then 95% of particles retained on the U.S. # 8 sieve. The CA-5 used in the project had a peak friction angle of 51˚based on large diameter triaxial cell testing for confining stresses within the range of the wall (34.5 – 138 kPa). A 20 cm low permeability cover was placed above the aggregate fill. Vertical slip joints were located in between test sections in an attempt to isolate the test sections from each other. For each slip joint the geogrid and facing blocks were cut such that forces could only be transmitted across the slip joint through aggregate interlock.

After the wall was constructed, the steel reinforcement cages were lowered into the CMP forms. The cages consisted of 12 evenly spaced #11 bars for longitudinal reinforcement and #5 hoops for transverse reinforcement spaced every 152 mm for the first 0.9 m and every 305 mm for the remainder. High (229 mm) slump concrete was poured having an average compressive strength of 45 MPa.

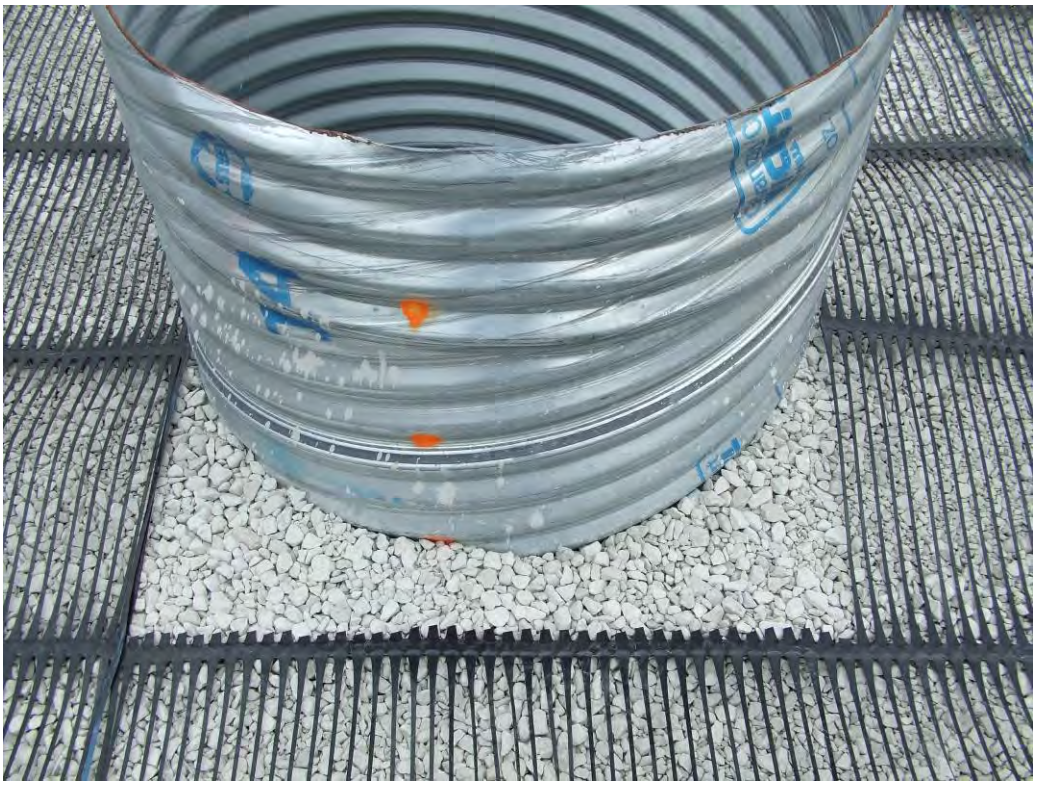

Figure 1 Cut geogrid around CMP metal forms.

Figure 2 Backfill and general construction profile.

Instrumentation consisted of three systems. Monitoring of the shaft top utilized five LVDTs, a hydraulic pressure gage, and a load cell attached to a data acquisition system. Each test shaft and reaction shaft had two LVDTs attached and the hydraulic ram also had an LVDT to serve as a check of the shaft LVDTs. The hydraulic pressure gage served as a check for the load cell. Inclinometers were used as a second check of the LVDTs and to determine the magnitude of any

of shaft bending. A second data acquisition system was used to monitor performance of the MSE wall using earth pressure cells and strain gages. Movements of tell tales installed within the fill and attached to the geogrid, as well as targets attached to the wall facing, were monitored using a digital camera and a photogrammetric process. Additional details on construction and instrumentation are located in Pierson (2008).

The photogrammetric process used to monitor movements of the wall facing and telltales consisted of mounting 84 PVC targets with a 0.152 m scale on each target in addition to the telltales which passed through notches in the wall facing. Images of the wall, including the targets and telltales, were taken using a high-quality digital SLR camera before and during each test. These images were then downloaded into AutoCAD and used to determine wall or telltale displacement at each measurement location. A more detailed discussion of this use of photogrammetry is discussed in Pierson et al. (2009).

Tensar and KU attached many strain gages to the geogrid in 5 locations (Table 1), and 4 different courses of grid. Kyowa 120 ohm strain gages were used with a length of 5.5 mm. The gages were attached using the Vishay M-Bond adhesive kit. Pairs of strain gages were located on the top and on the bottom of the geogrid at up to six different distances from the wall facing. For protection the wires were run away from the grid locations in small flexible tubing toward each slip joint. From the slip joint the wires were encased in PVC pipe and run from the slip joint to the data logger.

Table 1 Geogrid Instrumentation

	Instrumented Geogrid Layers at Shafts A, B, BG-1, BG-2		Instrumented Geogrid Layers at CONTROL Section				Distance between Gage Location and Back of Wall Facing	
Layer Elevation	El. 6.7	El. 14.7	El. 2.7	El. 6.7	El. 10.7	El. 14.7	(m)	(ft)
Strain Gage Location								
	Aperture 1	Aperture 1	Aperture 1	Aperture 1	Aperture 1	Aperture 1	.178	0.6
	CMD Bar 2	CMD Bar 2	CMD Bar 2	CMD Bar 2	CMD Bar 2	CMD Bar 2	.406	1.3
	Aperture 3		Aperture 3	Aperture 3			1.143	3.8
	CMD Bar 4		CMD Bar 4	CMD Bar 4			1.32	4.3
			Aperture 4		Aperture 4	Aperture 4	1.55	5.1
			Aperture 5	Aperture 5	Aperture 5		2.01	6.6
		Aperture 6			Aperture 6	Aperture 6	2.46	8.1
		CMD Bar 7			CMD Bar 7	CMD Bar 7	2.69	8.8
				Aperture 7			2.92	9.6
						Aperture 9	3.84	12.6
Strain Gages Per Layer	8	8	12	12	12	12		

3. LOADING

Each single shaft test used a single 667 kN capacity 1.2 meter stroke hydraulic cylinder (Figure 3). Testing was displacement controlled. Hydraulic pressure was increased and movement was initiated until the desired displacement was achieved. The hydraulic cylinder valves were then closed to prevent any further movement and remained closed for the greater of 5 minutes or until the inclinometer measurements were completed. During the holding time, deflection was nearly constant and load decreased. Due to the stress release behavior three values of load and deflection were reported; a peak value for each step, a value at 2.5 minutes after the peak, and the final load before initiation of the following step (Figure 1). Additional results can be found in Pierson (2008).

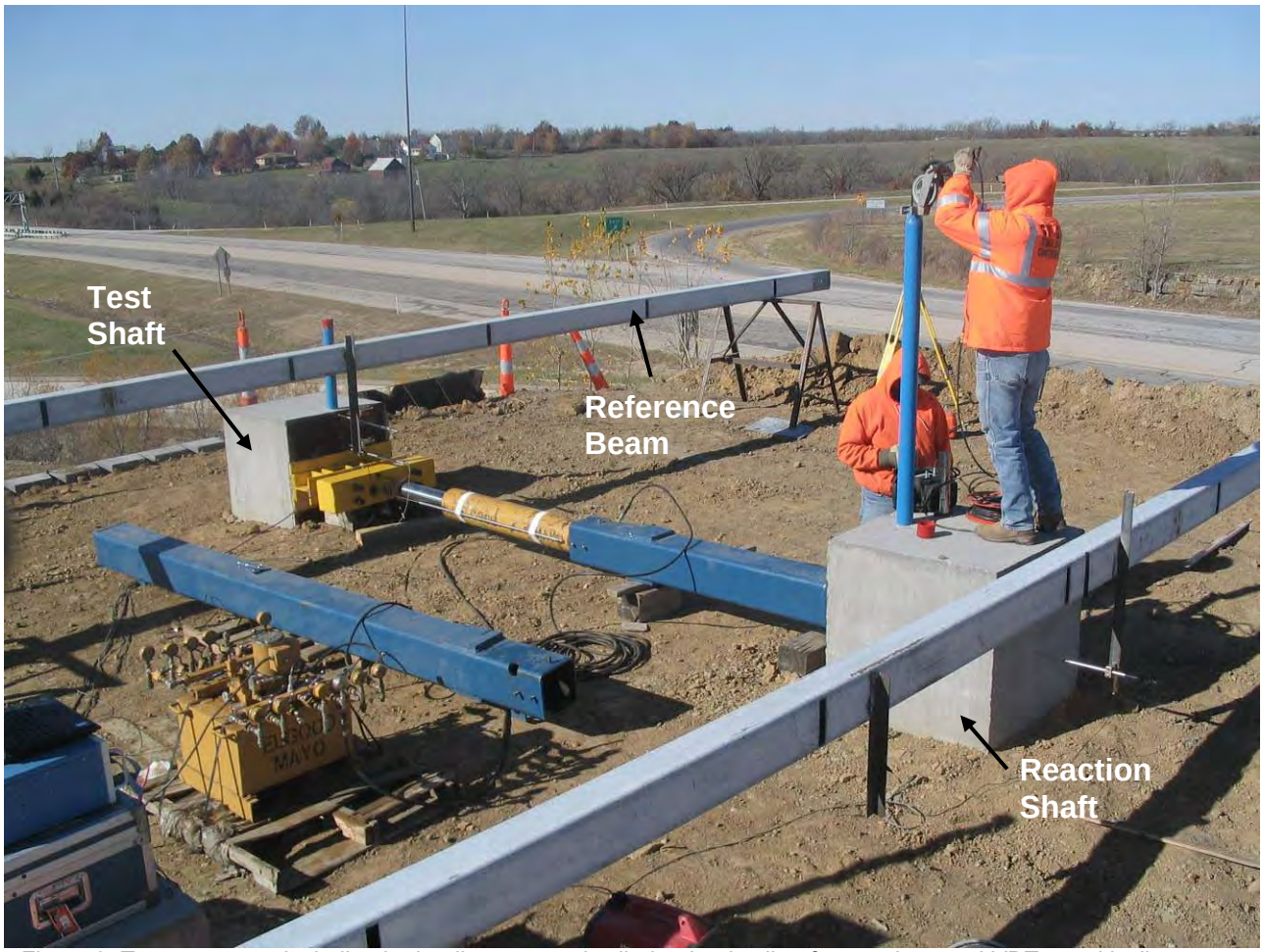

Figure 3 Test apparatus including hydraulic pump and cylinder, load cell, reference beams, LVDTs, and inclinometer.

4. DEFORMATION

Significant deformations occurred during testing. The soil surface at all single shafts had cracks form behind the shafts due to caving and from the sides at a diagonal toward the wall facing as a result of shaft movement. During the group test a large crack developed at a distance of between 4.1 m and 4.4 m from the back of the wall that ran parallel to the wall face. This is the same location as the end of the reinforced zone. It is believed that this crack was a result of sliding along one or more layers of geogrid (Figure 4).

After testing of each shaft was performed, a section of geogrid 2.1 m to either side of selected shafts were exhumed (Figure 5). This geogrid was then measured to determine the elongation of the grid. Strains in excess of 3 percent were observed next to the shaft, with strains rapidly decreasing to near zero five feet from the shaft.

Analyses of wall facing movements were conducted using photogrammetric analysis of targets attached to the wall facing. The results of this analysis produced wall facing displacements that are discussed in Parsons et al (2009).

Strains in the geogrid directly next to the shaft were recorded at four distances from the back of the wall facing (Figure 6). Very distinct steps are present which illustrates that stress was transferred from the shaft through the fill and to the reinforcement and was measured by the strain gages used for this project.

Figure 4 Cracks developed at the back of the reinforced soil mass.

Figure 5 Exhumed section of geogrid showing elongation and tension in the reinforcement.

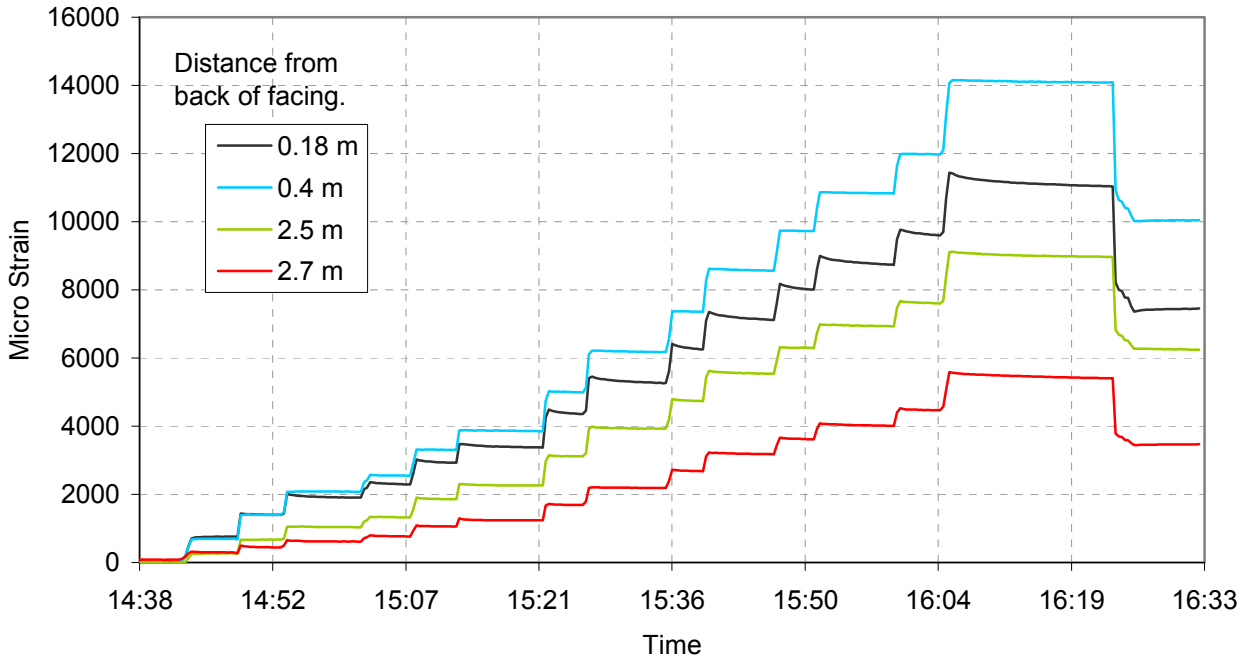

Figure 6 Strain measured in geogrid at elevation 14.4 feet next to the shaft spaced two diameters from the wall facing.

5. LONG TERM STRAIN DATA

During construction (ends September 19th, 2007) a portable "Strain Indicator" box was used to measure each gage several times a week at generally the same time of day. This data is combined with hourly strain measurements or gages in the control section that began nearly a month before testing. Load testing was performed and one month after the load testing was complete hourly measurements of the gages in the control section were resumed (Figure 7). Figure 7 clearly shows the strains that developed during construction of the wall. Analysis of the control section yielded two trends among active strain gages, a sampling of which are reported in Figures 7 and 8. One group of strain gages followed temperature almost exactly while others showed little change over the time period studied. This difference may be the result of different localized stress levels in different elements of the grid. A closer analysis of the data collected during April of 2008 (Figure 8) shows the same two trends. Daily fluctuations were observed in both trends.

Several observations can be made based on the data in Figures 7 and 8. The early readings clearly reflect the strains that occurred during construction. The strains in the bottom of the fill were greater than those near the surface, and the maximum magnitude of the strains observed was less than 0.4 percent. After construction, both daily trends and seasonal trends driven by temperature are visible in the strain data, but no significant permanent creep was observed.

When ambient temperature versus strain is plotted, the gages that correlate well with temperature yield a tight cluster of points (Figure 9) and the gages that do not correlate with temperature yielded a less distinct pattern, although an underlying trend of increasing strain with increasing temperature is still visible (Figure 10).

When strain at a particular temperature was isolated and then all strains at that temperature were plotted over time, little correlation could be found for either set of trends. Generally more change was found for gages that correlate well with temperature than gages that do not correlate well.

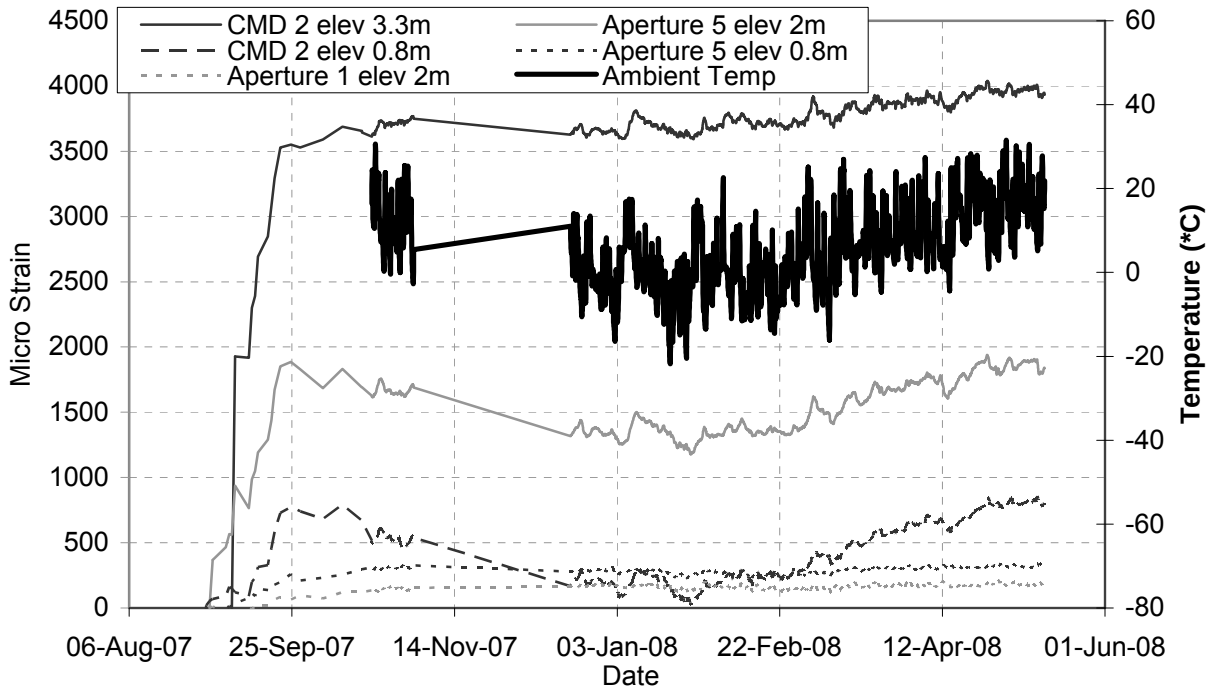

Figure 7 Shows temperature and all strain measurements over the period of study for three gages that correlate with ambient temperature and two that do not correlate.

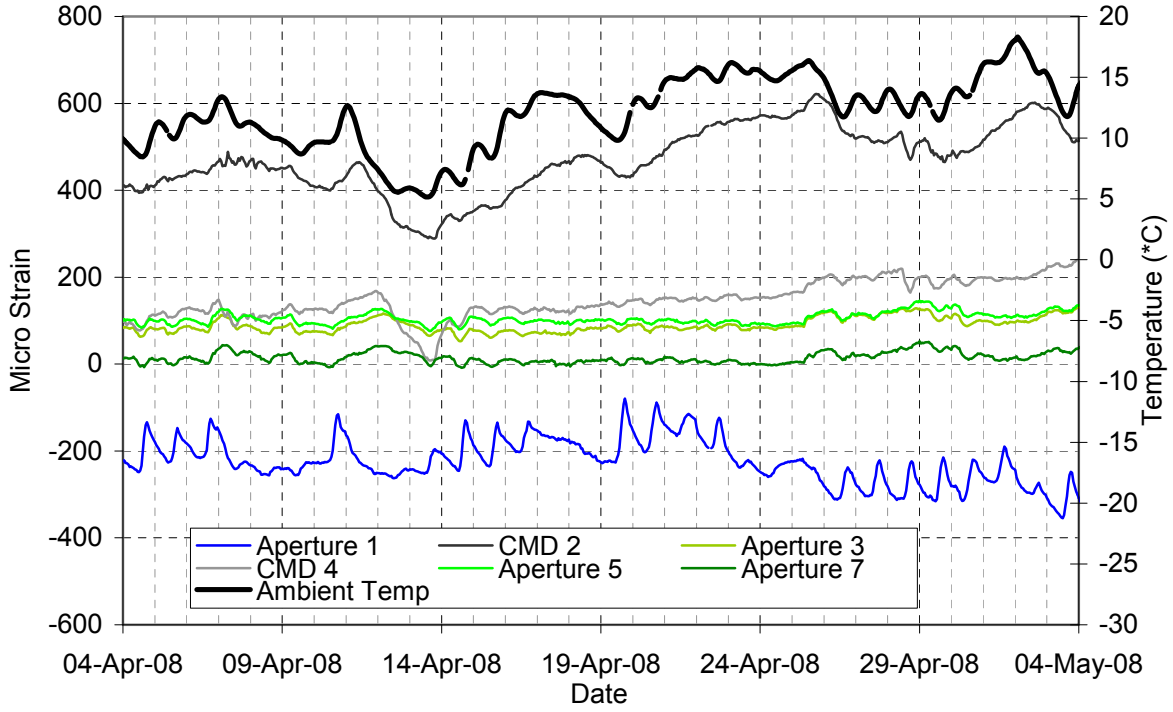

Figure 8 Shows temperature and all strain measurements at elevation 6.7 ft over a period of one month for four gages that correlate with ambient temperature and two that do not correlate.

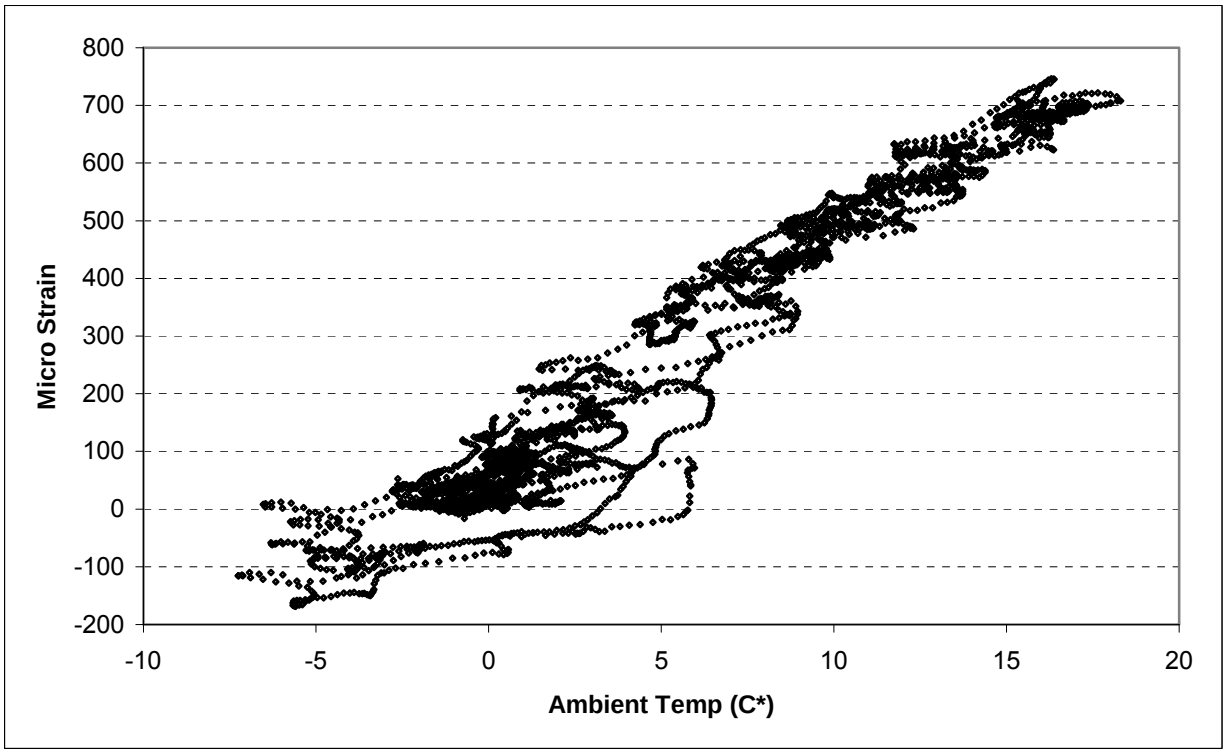

Figure 9 Data from strain gages that correlated well with ambient temperature.

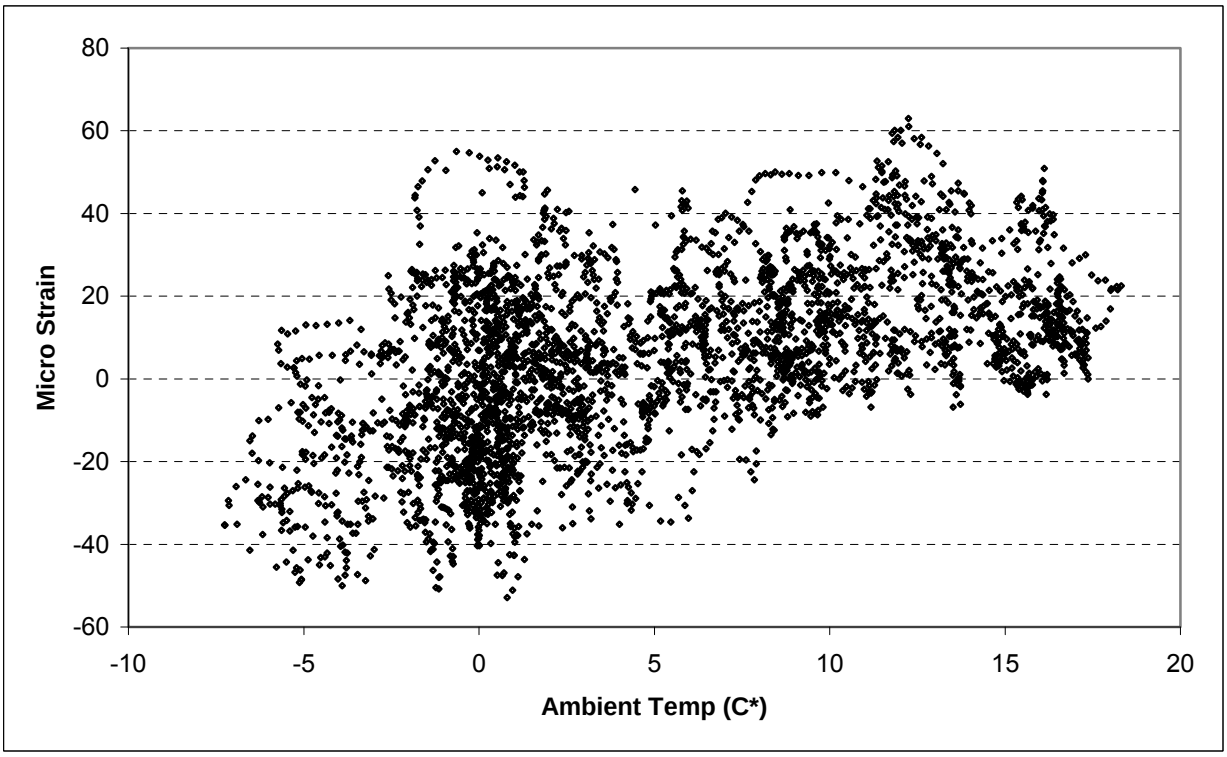

Figure 10 Weaker correlation for strain gages that did not correlate as well with ambient temperature.

6. CONCLUSIONS

Laterally loaded drilled shafts installed within an MSE mass successfully transferred their loads to the reinforcement. Large strains in the reinforcement were measured near the shafts after lateral load testing was completed. Strains were also measured in a control section of an MSE mass and only small strains were observed. The small strains measured in the control section occurred primarily during the construction phase. Monitoring of the control section continued for eight months after construction, and during this period daily and seasonal fluctuations in strain were observed. These fluctuations were much smaller than the strains that occurred during construction, and appeared to be reversible as no significant permanent strain (creep) was observed.

ACKNOWLEDGEMENTS

The authors wish to acknowledge the financial and logistical support of the Kansas Department of Transportation, and particularly KDOT Maintenance and the Geotechnical Unit for their time and efforts in constructing and testing the wall. The authors also thank Tensar, International for their financial and logistical assistance, and the authors also wish to acknowledge the contributions of Applied Foundation Testing and Dan Brown and Associates in testing the wall and designing the shafts.

REFERENCES

Pierson, M.C. (2008*). Behavior of Laterally Loaded Shafts Constructed Behind the Face of a Mechanically Stabilized Earth Block Wall.* MS Thesis, The University of Kansas, 89 pages.

Pierson, M.C., Parsons, R.L., Han, J., Brennan, J.J., and Vulova, C. (2009). Instrumentation of MSE Wall Containing Laterally Loaded Drilled Shafts. *Foundation Engineering Congress & Equipment Expo (IFCEE'09),* March 2009, Orlando, FL

Parsons, Robert L.,Pierson M.C., Han, Jie, Brennan J. J, Brown D.A. (2009). "Lateral Load Capacity of Cast-in-Place Shafts behind an MSE Wall." *Submitted to Foundation Engineering Congress and Equipment Expo* (IFCEE'09), March 2009, Orland FL.

Geosynthetics 2009
February 25-27 2009, Salt Lake City, Utah

Evaluation of the Zone of Influence of Geogrid Reinforcement in Compacted Base Course using Rotation Measurements

C.C. Schuettpelz, Golder Associates, Denver, USA
T.B. Edil, Civil and Environmental Engineering, University of Wisconsin-Madison, USA
D. Fratta, Geological Engineering Program, University of Wisconsin-Madison, USA

ABSTRACT
Geogrid reinforced base enhances the load carrying capacity of pavement systems, reduces excessive deformation of the road surface, and enhances the stiffness of the material next to the geogrid. Previous research has examined and demonstrated the benefits of geosynthetic reinforcement; however, the interaction between base course soils and the geogrid is less well understood for quantitative incorporation in the design process under service loads. In other words, the determination of stiffness increase and thickness of the influence zone remains elusive. This research deploys MEMS accelerometers in modeled soil-geogrid systems to monitor soil rotation and determine the thickness of the zone. Laboratory results are compared to finite elements solutions to determine differences between the model and the laboratory tests. Rotation angles are highest directly beneath the edge of a 150 mm-diameter plate and diminish in close proximity to the geogrid, with the influence zone of the geogrid depending on the depth of reinforcement. This zone of influence is around 50-mm thick as indicated by internal rotation measurements.

1. INTRODUCTION

Flexible pavement systems typically consist of several components including asphalt surface layers, aggregate base course, sometimes a lower quality aggregate or sand subbase, and subgrade. Subgrade is often a weak material that is compacted from surficial soils. The function of the several stiff layers in the pavement structure is to reduce the wheel load stresses reaching the subgrade and to minimize deformations in the pavement surface. The performance of the stiff layer can be greatly improved with the installation of geosynthetic reinforcement. In particular, geogrids have been engineered to increase lateral resistance to shear stresses and improve load carrying capacity and stiffness of the pavement system susceptible to cyclic traffic loads (Bender and Barenberg 1978; Steward et al. 1977; Perkins et al. 2005).

The increase in lateral resistance is due to the interlocking between the granular material and the geogrid (Huntington and Ksaibati 2000; Haas et al. 1989). Interlocking provides tensile strength to granular soils that do not naturally have resistance to tensile forces and increases confinement of soil near the geogrid layer. Lateral confinement of soil above and below the geogrid increases the compressive force between grains, generates more interlock between the soil and geogrid and, increases the soil stiffness (Perkins et al. 2005; Kim et al. 2005). When particle movement is reduced, the ability of particles to rotate against one another is also expected to decrease.

The volume of soil affected by reinforcement is an important design consideration in the mechanistic-empirical pavement design, but quantification of modified physical soil properties after the insertion of a geogrid is yet to be completely understood. McDowell et al. (2006) used a discrete element model (DEM) to identify a “zone of influence” computationally. They determined it to be no more than 100 mm on either side of a geogrid reinforcement layer. Perkins et al. (2004) used large scale resilient modulus testing with lateral strain measurements to identify a zone of influence on the order of 150 mm. Edil et al. (2007) supported this thickness by backcalculation from a large-scale model experiment. The motivation of this paper is to document the development of a laboratory testing scheme that can be used to directly measure the “zone of influence” of the geogrid layer in the surrounding base course.

2. METHODS AND MATERIALS

2.1. Numerical Methods

PLAXIS is a finite element code that can be used for stress/strain analysis of soils. It contains features that allow for the evaluation of the dependence of soil stiffness on confining stress. Soil is represented as a hardening material where it becomes stiffer with higher applied effective stresses. Geogrids can also be input into PLAXIS modeling as tensile elements with an interaction coefficient to determine the effects of these reinforcement elements on stress and strain characteristics of underlying soil. The output from each simulation can then be used to estimate the rotation of individual nodes within the model. Numerical simulations in PLAXIS are used to evaluate the shear stresses induced

in a granular soil in a container loaded by a plate simulating wheel loads on the surface. The effect of the geogrid is incorporated into the numerical simulations to determine the effectiveness with which the program can estimate the rotations in the soil measured in the laboratory.

To estimate the amount of rotation in numerical simulations, relative displacements are measured with respect to the horizontal (x) and vertical (y) coordinates. The rotation tensor (ω_{xy}) can be expressed as:

$$\omega_{xy} = \frac{1}{2}\left(\frac{\partial u_x}{\partial_y} - \frac{\partial u_y}{\partial x} \right) \quad (1)$$

where $\delta u_x/\delta y$ is the partial derivative of the displacement in the x-direction with respect to y and $\delta u_y/\delta x$ is the partial derivative of the displacement in the y-direction with respect to x (Achenbach 1975). Figure 1 shows the parameters used for the computation of the rotation tensor. This figure shows the basic solution of calculating the rotation tensor using a rectangular coordinate system, but since PLAXIS uses polygonal grid elements, the calculation of the rotation tensor becomes more difficult. To simplify the calculation, the average rotation of four nodes is analyzed.

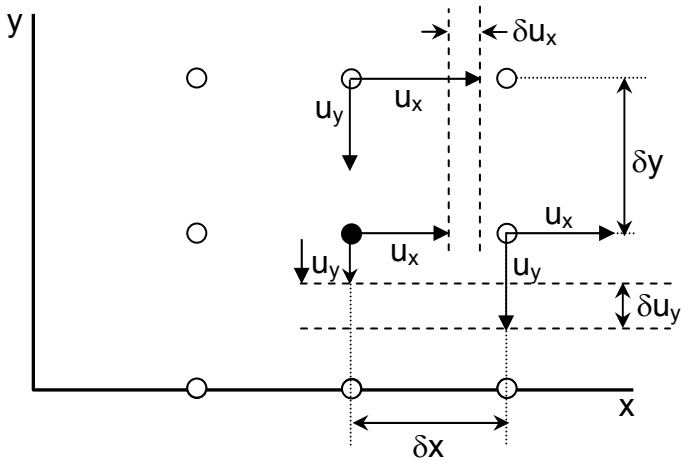

Figure 1. Relative displacement and rotation of particle in two dimensions with respect to x and y axes.

As shown in Figure 2, four independent elements defined with numbers 1, 2, 3, and 4 are used to calculate the rotations. Each coordinate has an x and y position in the 2D finite element space. Each of the four coordinates also has a corresponding displacement in both the x-direction (u_x) and y-direction (u_y). The average node where the rotation will be calculated has coordinates x_{ave} and y_{ave} where:

$$x_{ave} = \frac{x_1 + x_2 + x_3 + x_4}{4} \quad (2)$$

$$y_{ave} = \frac{y_1 + y_2 + y_3 + y_4}{4} \quad (3)$$

The first part of the rotation tensor is calculated using the PLAXIS output:

$$\frac{\partial u_x}{\partial y} = \frac{\frac{u_{x1} + u_{x2}}{2} - \frac{u_{x3} + u_{x4}}{2}}{\frac{y_1 + y_2}{2} - \frac{y_3 + y_4}{2}} \quad (4)$$

The derivative of u_y with respect to x can be written in a similar manner:

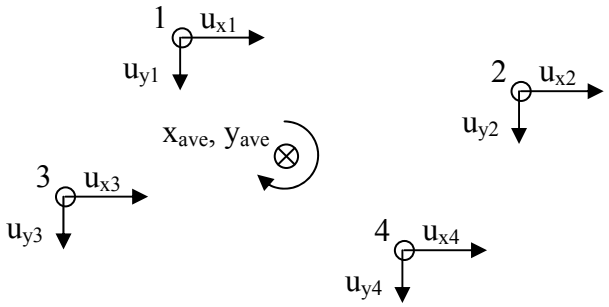

Figure 2. Coordinate system and displacement vectors used to calculate the average rotation between particles.

$$\frac{\partial u_y}{\partial x} = \frac{\frac{u_{y1} + u_{y3}}{2} - \frac{u_{y2} + u_{y4}}{2}}{\frac{x_1 + x_3}{2} - \frac{x_2 + y_4}{2}} \qquad 5$$

Once equations 4 and 5 have been calculated as a function of depth, Equation 1 can be solved for the rotation tensor, ω_{xy}. The rotation tensor can then be plotted from x_{ave} and y_{ave} for the desired location within the soil and compared to laboratory results.

2.2 Laboratory Methods

The internal response of soils in the physical soil-geogrid model were monitored with Analog Devices Miniature Electromechanical System (MEMS) ADXL 203CE dual axis accelerometers. Selected properties of accelerometers are given in Table 1. Static acceleration caused by the gravity field is measured by monitoring the DC output of accelerometers. When an accelerometer axis is aligned parallel to the direction of gravity, the accelerometer response is a maximum. The accelerometer response is minimum when the axis is aligned opposite to the direction of gravity. At inclined angles, the accelerometer response follows a sine function and rotation angle can be measured by applying trigonometry to the measured output voltages:

$$V(\theta) = A\text{-}Sens \cdot g \cdot \sin(\theta) \qquad 6$$

where g=9.81 m/s^2 is the acceleration of gravity, A=2.5V is the accelerometer response at 0 g, the Sens=1 V/g is the accelerometer sensitivity, and θ is the accelerometer axis angle measured from the horizontal. Since accelerometers are not originally oriented perpendicular to gravity after soil is compacted, the difference between the original rotation angle and new rotation angle is required to obtain the rotation of soil as a function of depth during loading. The angle change reported by the accelerometer due to an applied load can be expressed as the difference between angles θ_2 and θ_1 (Figure 3).

Accelerometer resolution is maximized when aligned parallel to earth's surface and least sensitive when perpendicular. The maximum resolution of the MEMS accelerometers for tilt measurements is 0.06° based on manufacturer specifications. Resolution also depends on the accuracy of voltage measurements used to compute rotation angles. However, the voltmeter used in this research has a resolution of 0.1 mV and therefore provides a calculated tilt resolution of 0.0057°, so the accelerometer itself limits the resolution of the system.

Table 1. Analog devices ADXL203CE accelerometer specifications (after: Analog Devices 2007)

Accelerometer	Range (g)	Frequency range (Hz)	Input voltage (V)	Sensitivity (mV/g)	Noise Density (μg/√Hz rms)	Approx. dimensions
203CE	±1.7	DC-1 kHz	3-6	1000	110	25 mm wide, 25 mm long, 12 mm high

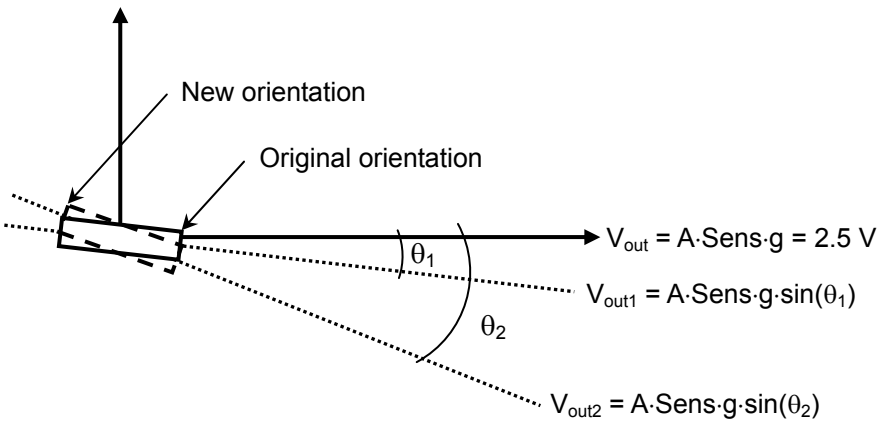

Figure 3. Calculating rotation of accelerometers with respects to horizontal.

2.3 Materials

The influence of geogrid reinforcement on granular base course materials was tested using Wisconsin grade 2 gravel (19 mm - ¾" crushed limestone road base gravel), a common aggregate used as base course. Specifications for grade 2 gravel are given in Wisconsin Department of Transportation (WisDOT) section 304 (Standard Specifications for Highway and Structure Construction 1996). Physical properties of the Wisconsin grade 2 gravel are shown in Table 2.

A stiff geogrid with square 38-mm apertures and elastic in-plane modulus of 534 kN/m was used in this study. This geogrid was chosen in an attempt to maximize the stiffening benefits of the geogrid and to explore the usefulness of rotation measurements on a reinforced base course material. Sarsby (1985) suggested that geogrid apertures be greater than 3.5 times larger than the D_{50} particle size for sufficient interlocking to occur between the reinforcement and soil. Geogrid aperture is 12.7 times larger than the mean particle size of grade 2 gravel. .

Table 2. Physical properties of grade 2 gravel aggregate tested in laboratory experiments.

Soil Name	C_u	C_c	Gravel (%)	Fines (%)	Void Ratio	D_{50} (mm)	γ_{dmax} (kN/m^3)	γ_d (test) (kN/m^3)	USCS symbol
Grade 2 gravel	217	1.4	40	18	0.40	3.0	22.6	18.5	SW

Notes: C_u = coefficient of uniformity, C_c = coefficient of gradation, e = void ratio, D_{50} = mean particle size, γ_{dmax} = maximum unit weight, SW = well-graded gravelly sand

2.4 Test Procedures

A large test container, 0.61 m wide, 0.91 m long, and 0.61 m deep, was constructed from wood. The test material was tamped in 75 to 100 mm lifts in an attempt to produce a uniform density throughout the test mass. MEMS accelerometers and a geogrid were placed concurrently while filling the test container with the aggregate and the distance between accelerometers was measured with a string secured below the load cell. Accelerometers were secured vertically beneath the edge of the 150-mm diameter load plate at separations of approximately 20 mm above the geogrid to 25 mm below the geogrid (Figure 4). All tests were run with the geogrid pre-stressed at 0.26 kN/m to secure the interaction between aggregate particles and the geogrid. The geogrid was secured at a depth of 100 mm.

The testing scheme used for monitoring rotation involves application of a series of surface static loads. Rotation angles were calculated as a function of surface deflections.

3. RESULTS AND ANALYSIS

Each test performed in grade 2 gravel was modeled using PLAXIS. The model parameters (i.e., soil properties, geogrid stiffness, "virtual thickness", etc.) were based on laboratory test results. The "virtual thickness" specified in PLAXIS changes for each geogrid reinforcement position based on accelerometer information. The virtual thickness

is the soil volume where particle-geogrid interlock occurs and where the soil deformation remains elastic. The strength reduction factor (R_{int} – the ratio of interface strength to soil strength - Brinkgreve 2002) is set equal to 1 for geogrid. Figure 5 shows PLAXIS analysis results of changes of shear strain in the aggregate base that was reinforced with geogrid at a depth of 100 mm. The effect of the geogrid is shown as the difference between the shear strains in the base system with and without geogrid reinforcement. The results show the reduction of shear strains below the load plate and below the geogrid location.

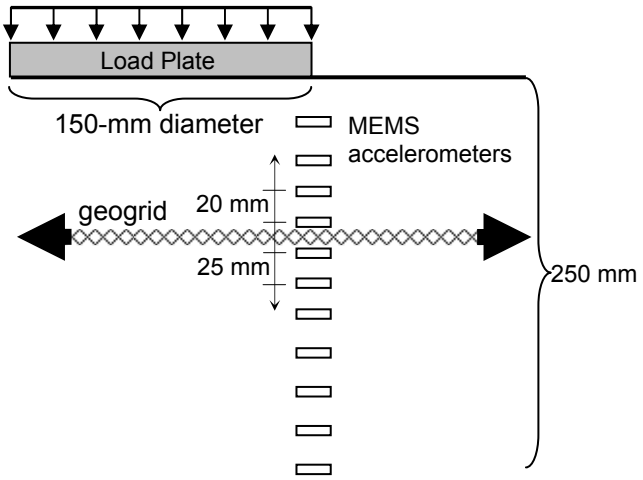

Figure 4. Test schematic for monitoring rotation. MEMS accelerometers were spaced 20 mm apart (center to center) near the geogrid and 25 mm apart further from the geogrid.

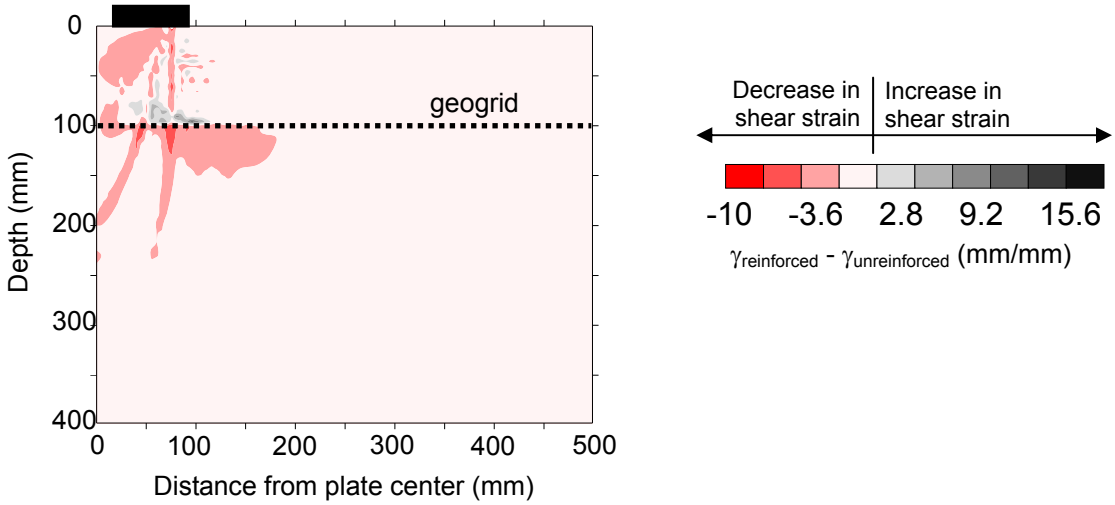

Figure 5. Difference in shear strains between reinforced and unreinforced sections for geogrid at a depth of 100 mm.

Figure 6 shows the horizontal displacement (u_x) of soil calculated using the PLAXIS model. The horizontal displacement may be the best method of examining the confinement of soil since horizontal movement of soil is an indication that particles are compressing and unable to move freely. Without the presence of geogrid (Figure 6a), the maximum u_x is approximately 1.5 mm and displacements propagate to a depth of about 200 mm, beyond which horizontal displacements are nearly zero. Figure 6b shows horizontal displacements when geogrid is placed at 100 mm deep. The maximum horizontal displacement is 1.8 mm. Therefore, when geogrid is placed at a depth of 100 mm, the soil appears to displace more laterally in the uppermost 50 – 70 mm of material. The greater displacements may be an indication that soil rotation is confined to shallow depths when geogrid is secured 100 mm deep. Furthermore, the influence area of the geogrid appears relatively small (~10 mm) on either side of the geogrid, the geogrid reduces the horizontal movement of particles near the reinforcement, forcing displacement of particles above and below the geogrid.

The numerical results presented in Figures 5 and 6 provide insight about the mechanics and the volume of the interlock between geogrid and particles. However, the parameters can not be easily quantified using physical models as the internal displacements and shear strains cannot be directly measured. For this reason, the internal particle rotations were measured in the physical model to evaluate the thickness of the zone of influence..

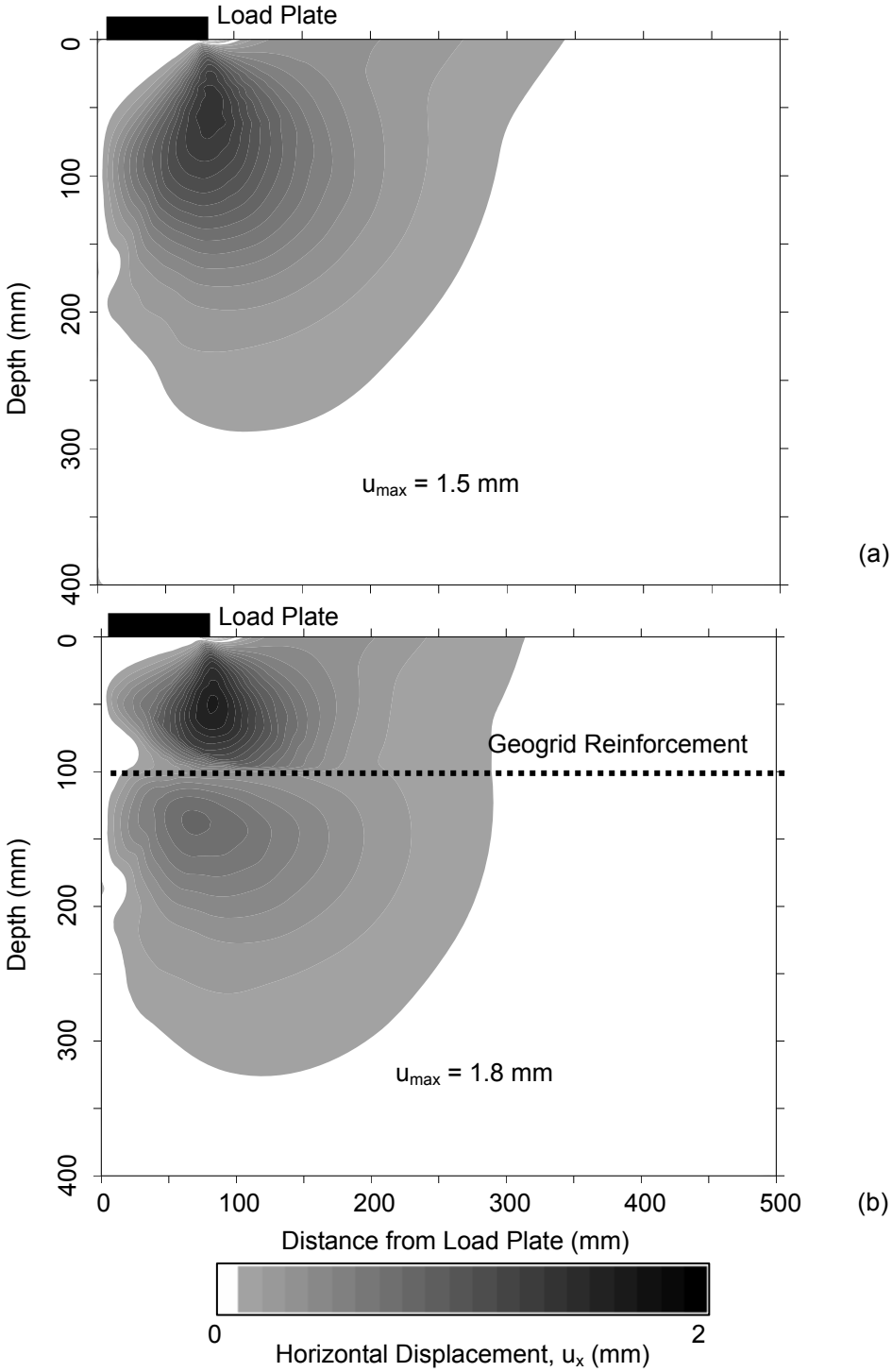

Figure 6. Horizontal displacement from PLAXIS analysis below a circularly loaded plate when (a) no geogrid is present, (b) geogrid is buried at 100 mm depth

Internal particle rotation results are summarized in Figures 7 through 9. Without the geogrid present, the rotation angle as a function of depth and surface deflection are shown in Figure 7. Measured rotation angles are typically lower than PLAXIS analyses at shallow depths, but the measured rotations show similar trends as those shown in the numerical simulation. The maximum rotation angle is measured to be approximately 2° at 50 mm depth and a surface deflection of about 6 mm.

Rotation results with a geogrid reinforcement layer at 100 mm depth are presented in Figure 8. At 50 mm depth, the rotation angle is about 3°. Laboratory tests and PLAXIS models predict an increased rotation angle at around 170 mm depth and rotations that extend to greater depths once again as shearing is spread over larger depths than in the rotations in the unreinforced case. Furthermore, rotation angle results indicate a deeper zone of shearing, as the laboratory test and PLAXIS results have measurable rotations at greater depths indicating that shearing is spread over a larger area of soil when geogrid is present.

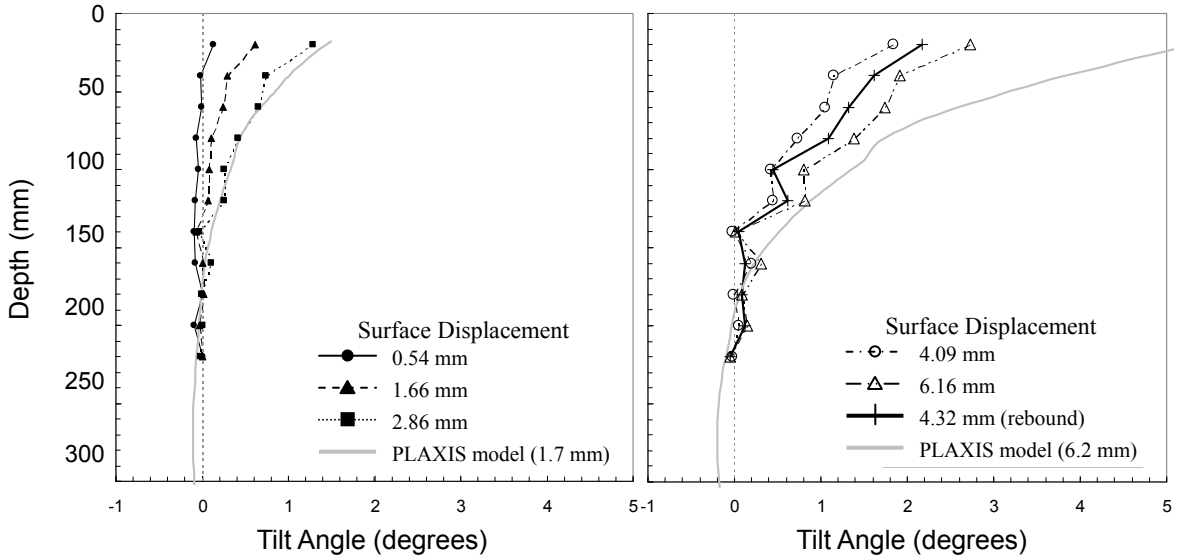

Figure 7. Rotation angle at the plate edge as a function of depth and applied surface displacement without geogrid reinforcement. PLAXIS modeling results are shown at two surface displacement levels for comparison.

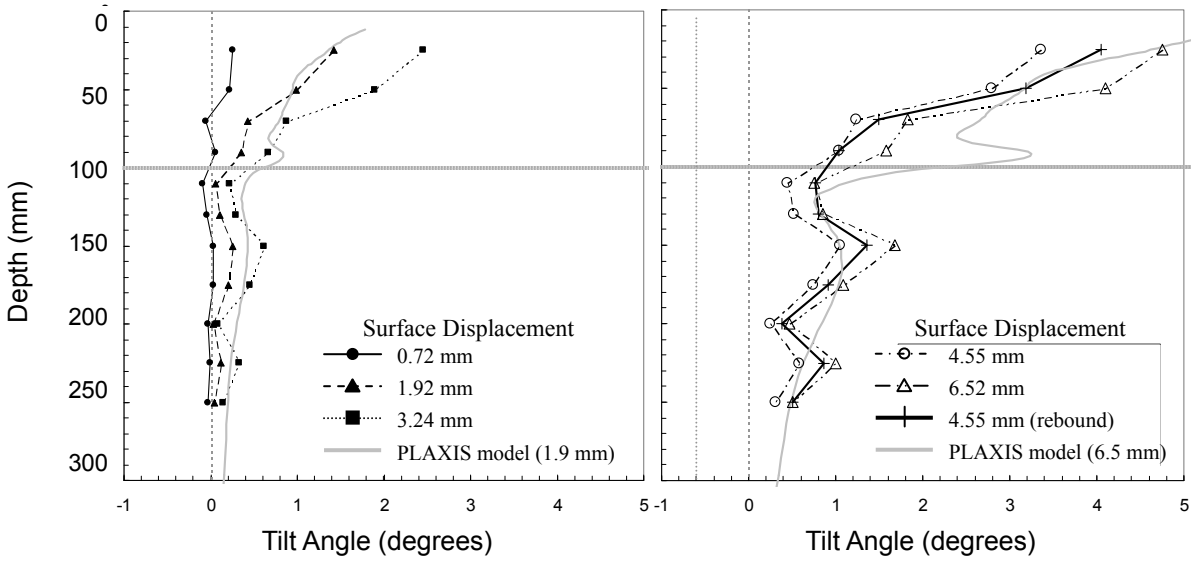

Figure 8. Rotation angle at the plate edge as a function of depth and applied surface displacement with geogrid reinforcement at 100 mm depth. PLAXIS modeling results are shown at two displacement levels for comparison.

The “zone of influence” specified for the reinforcement position at a depth of 100 mm is shown in Figure 9. Differences in rotation angles as a function of depth with and without geogrid best show the influence zone of the geogrid, as the changes in rotation are minimized in the area around the geogrid that is confined.

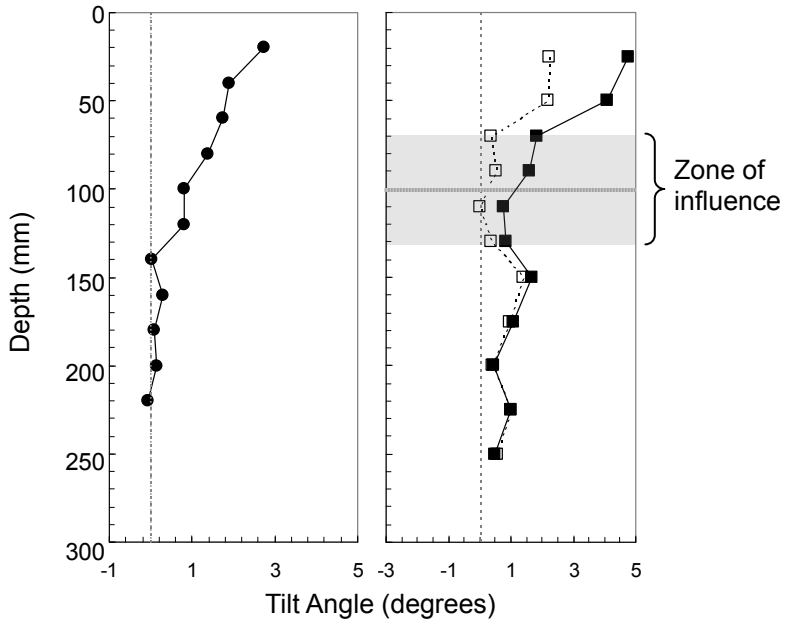

Figure 9. “Zone of influence” (shaded area) determined using rotation angle test results: (a) no geogrid and (b) geogrid at 100-mm depth. The solid symbols represent the rotation angles at maximum surface displacement and the open symbols represent the difference between the rotation angles with and without reinforcement ($\Delta\theta=\theta_{reinforced}-\theta_{unreinforced}$).

4. CONCLUSIONS

Soil rotations were monitored to determine the “zone of influence” of a geogrid reinforcement layer on surrounding base course material. The effective depth of influence from a loaded 150 mm diameter load plate extends to 180 mm without reinforcement and 200 – 250 mm with reinforcement, agreeing closely with PLAXIS modeling.

Soil rotation is greatest at the plate edge and is typically between 2.5 and 5° at 50 mm depth. Furthermore, soil rotations are higher at shallow depth when geogrid is secured at 100 mm.

Measured rotations agree well with PLAXIS modeling results in terms of the expected rotation behavior; however, PLAXIS typically limits soil rotation to a smaller area around the geogrid and overestimates rotation angles when compared with the laboratory tests on aggregate. The influence of accelerometers on results and the inability of the finite element model to represent individual grains in a similar way to a DEM model (McDowell et al. 2006) are two potential areas of future study. Different geogrid/soil combinations should be tested with the geogrid at various depths to effectively evaluate the “zone of influence” of the geogrid on a particular material and the influence of the geogrid depth.

5. ACKNOWLEDGEMENTS

This research was funded by the Wisconsin Highway Research Program (WHRP - Project ID# 0092-07-05) and the Midwest Regional University Transportation Center (MRUTC).

REFERENCES

Achenbach, J.D. (1975). *Wave Propagation in Elastic Solids*. Elsevier Science Publishers B.V., Amsterdam, Netherlands.

Analog Devices (2007). Analog Devices, Inc. Web Site. http://www.analog.com

Bender, D.A. and Barenberg, E.J. (1978). Design and Behavior of Soil-Fabric-Aggregate Systems. *Transportation Research Record 671*: 64-75.

Brinkgreve, R.B.J., ed. (2002). *PLAXIS Version 8 Manual*. A.A. Balkema Publishers, Lisse, NL.

Edil, T.B., Kim, W.H., Benson, C.H., and Tanyu, B.F. (2007) "Contribution of Geosynthetic Reinforcement to Granular Layer Stiffness," *GeoDenver2007,* American Society of Civil Engineers, CD-ROM

Haas, R., Walls, J., and Carroll, R.G. (1989). Geogrid Reinforcement of Granular Bases in Flexible Pavements. *Transportation Research Record* 1188: 19-27.

Huntington, G. and Ksaibati, K. (2000). Evaluation of Geogrid-Reinforced Granular Base. *Geotechnical Fabrics Report*. January/February: 22-26, 28.

Kim, W.H., Edil, T.B., Benson, C.H., and Tanyu, B.F. (2005). Structural Contribution of Geosynthetic-Reinforced Working Platforms in Flexible Pavement. *Transportation Research Board. 84th Annual Meeting*.

McDowell, G. R. Harireche, O., Konietzky, H., Brown, S.F. and Thom, N.H. (2006). Discrete Element Modeling of Geogrid-Reinforced Aggregates, *Geotechnical Engineering*, 159(GE1): 35–48.

Perkins, S.W., Christopher, B.R., Cuelho, E.L., Eiksund, G.R., Hoff, I., Schwartz, C.W., Svanø, G., and Watn, A., Perkins, S. (2004). *Development of Design Methods for Geosynthetic Reinforced Flexible Pavements, U.S. Department of Transportation*. Federal Highway Administration, Washington, DC, FHWA Report Reference Number DTFH61-01-X-00068, 263p.

Perkins, S.W., Christopher, B.R., Eiksund, G.R., Schwartz, C.S., and Svano, G. (2005). Modeling Effects of Reinforcement on Lateral Confinement of Roadway Aggregate. *Proceedings of the Sessions of the Geo-Frontiers 2005 Conference, Austin, TX, USA.*

Sarsby, R. W. (1985). The Influence of Apperture Size/Particle Size on Efficiency of Geogrid Reinforcement. *Proceedings of the Second Canadian Symposium on Geotextiles and Geomembranes*, Edmonton, Canada, Geotechnical Society of Edmonton: 7-12.

Steward, J.E., Williamson, R., and Mohney, J. (1977). Guidelines for Use of Fabrics in Construction and Maintenance of Low-Volume Roads. *USDA, Forest Service report PB-276972*, Portland, Oregon, 172 p.

Wisconsin (1996). Standard Specification for Highway and Structure Construction, Wisconsin Department of Transportation, Madison, WI.

Geosynthetics 2009
February 25-27 2009, Salt Lake City, Utah

Selecting Reinforced Fill Soil for MSE Retaining Walls

W.A. Marr, P.E., Geocomp Corporation, Boxborough, MA, USA
R.P. Stulgis, P.E., Geocomp Corporation, Boxborough, MA, USA

ABSTRACT
Mechanically Stabilized Earth (MSE) retaining walls on transportation projects are generally conservatively designed, using “low fines” reinforced soils. Four full-scale field tests were conducted, in order to establish properties for “high fines” reinforced soils and associated design controls that give acceptable MSE wall performance. The walls were constructed with wire basket face elements and polyester geogrid reinforcement, except that one wall used geotextile reinforcement. The field tests included provisions to demonstrate the role of pore water pressure in the reinforced fill and the importance of including a positive drainage system to obtaining good wall performance.

The full-scale field test program is funded by the Transportation Research Board, under National Cooperative Highway Research Project (NCHRP) HR 24-22. The objective of the Project is to develop selection guidelines, soil parameters, testing methods, and construction specifications that will allow the use of a wider range of reinforced fill materials within the reinforced zone of mechanically stabilized earth (MSE) walls. The estimated potential savings from replacing AASHTO reinforced fill materials with “higher fines” reinforced fill materials could be in the range of 20 to 30% of current MSE wall costs.

This paper presents some of the results of the field tests on four full-scale test walls and documents the basis for our conclusions that MSE retaining walls on transportation projects using backfills with fines up to 25% with a plasticity index less than 6% will deliver acceptable performance provided positive drainage measures are included at the back of the reinforcement and provisions are made to prevent surface water from entering the backfill.

1. PURPOSE OF FULL-SCALE FIELD TEST

Mechanically Stabilized Earth (MSE) retaining walls on transportation projects are generally conservatively designed with “low fines” reinforced soils. Private MSE walls are less conservatively designed, and use a variety of reinforced soils (National Concrete Masonry Association) allows up to 35% < 0.075mm). From cases in the literature, reinforced soil consisting of fine-grained soils (either “high” fines or “high” plasticity) and pore pressure resulting from lack of drainage in the reinforced zone have created serviceability problems (excessive deformation) or failure (collapse).

However, a higher quantity of fines can be safely allowed in the reinforced fill, provided the properties of the materials are well defined and controls are established to address the performance issues. The potential savings from replacing AASHTO reinforced fill materials with “higher fines” reinforced fill materials could be in the range of 20 to 30% of current MSE wall costs.

A full-scale field test was conducted to demonstrate that MSE structures with “high fines” backfills can be successfully used and to establish properties for “high fines” reinforced soils and associated design controls that give acceptable MSE wall performance. The field test included provisions to demonstrate the role of pore water pressure in the reinforced fill and the importance of including a positive drainage system to obtaining good wall performance. Based on the survey of the literature, full-scale test or experimental MSE walls have not rigorously evaluated this important aspect.

The full-scale field test is funded by the Transportation Research Board, under National Cooperative Highway Research Project (NCHRP) HR 24-22. The objective of NCHRP Project 24-22 is to develop selection guidelines, soil parameters, testing methods, and construction specifications that will allow the use of a wider range of reinforced fill materials within the reinforced zone of mechanically stabilized earth (MSE) walls.

The project originally included provisions for testing three full-scale sections. At a September 2004 review meeting, the Reviewing Panel voted to recommend additional funds from NCHRP for construction of a fourth test section as part of the full-scale field test and those funds were obtained.

2. WORK PLAN

NCHRP Project 24-22 includes four full-scale test wall sections. One section uses an A-1-a reinforced fill to provide a baseline of performance for current AASHTO standards. A second section used an A-2-4 reinforced fill to demonstrate that non-plastic, silty sand materials with up to 35% fines (of no plasticity) can provide suitable reinforced fill for MSE

walls. The third and fourth sections incorporated an A-4 material consisting of non-plastic silty soils (50% fines). Welded wire was used for the wall face system. Polyester geogrid was used for the reinforcement in all sections, with the exception of one section where geotextile reinforcement was used. The wall sections were designed so that they demonstrated acceptable performance for the normal design conditions, but show distress when subjected to extreme conditions of a surcharge load combined with high pore water pressures in the reinforced fill.

We did not include a clay reinforced fill. Available information and responses from a survey of state DOT engineers indicated that clay soils used as MSE reinforced fill have the potential to cause too many construction difficulties, which can otherwise negate the economic benefit of using on-site soils. Furthermore, clay soils have routinely contributed to excessive MSE wall deformations and wall collapses.

We also proposed to take advantage of the project time scale to subject the walls to two seasons of winter conditions, to document the effects of freeze-thaw conditions on the performance of different reinforced soils. Reinforced soils containing higher fines may be more susceptible to damage from freezing conditions.

2.1 Layout of Field Test

Field tests of four full-scale MSE wall sections were conducted at a private site presently occupied by an active sand and gravel borrow and rock quarry operation, located approximately 7 km from the Geocomp headquarters. A relatively flat location in a “played out” area of the gravel pit, away from any active operations, was provided by the P.J. Keating Co.

Geocomp personnel supervised the construction. We retained the services of the gravel pit operator to provide earth moving equipment, borrow materials and construction labor. Our instrumentation technicians provided and installed the instrumentation and monitoring system. As many instruments as possible were electronically connected to a real-time WEB-based data acquisition system to allow us to detect any problems at an early stage and to facilitate the dissemination of results among our team members in an efficient and effective way.

Figure 1 shows the field test layout that fits within the site constraints and meets the project objectives. This layout permitted the simultaneous and efficient testing of four test sections. Each test section is 20 ft (6 m) high and 60 ft (18 m) long. The width of fill behind the reinforced fill was established by analysis to minimize boundary effects on the test sections.

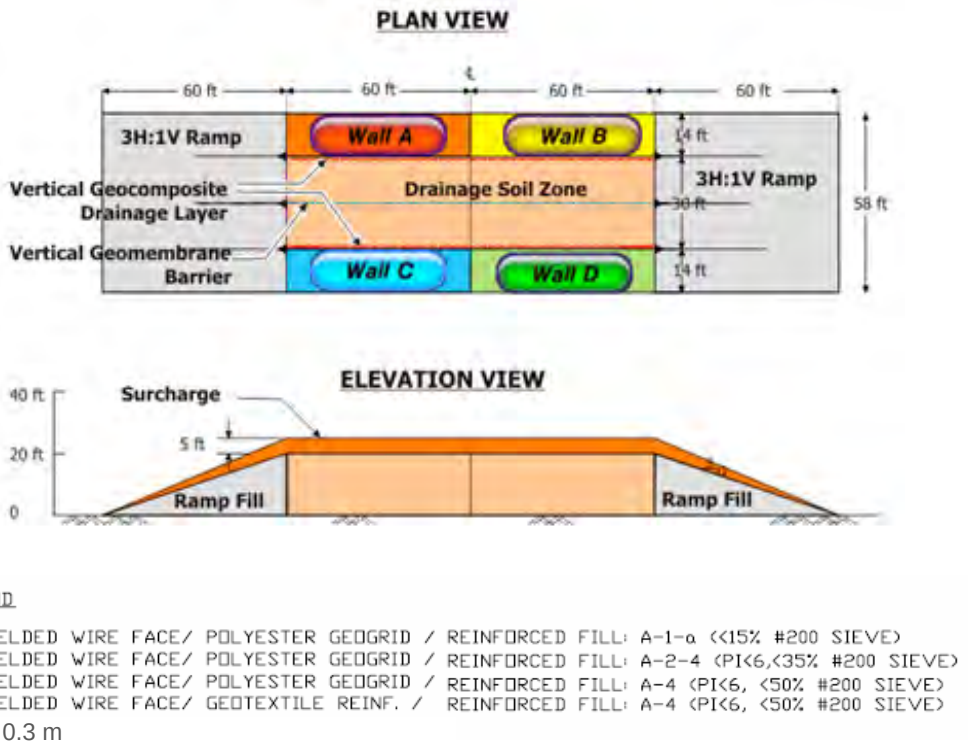

Figure 1: Layout of Field Test for MSE Retaining Walls

Figure 2 shows the typical section through each test wall. The walls were designed with a very low factor of safety. The long term internal factor of safety selected was less than 1.1, without surcharge loading, in order to maximize strains during the field test. The intent was to promote development of a failure plane and maximize load in each reinforcement layer under the extreme load condition (saturation of the reinforced fill combined with soil surcharge load). Designing at low factors of safety requires accurate determination of all input parameters. Three (3) different soil types with varying degrees of fines were selected for the reinforced fill zones of the test walls. The gradation characteristics of these soils are shown in Figure 3.

Processed relatively clean granular soil was available on site through the site operator (P.J. Keating Co.), and was considered a good choice for the A-1-a control section (Reinforced Fill A). Identified as "Keating Graded Base", the material generally has 8 to 10% passing the #200 sieve. While this is less than the maximum 15% allowed by AASHTO, a significant number of DOTs (based on our survey results) would consider this "high fines". Our research team, however, believed that using the "highest fines" material possible, while meeting the AASHTO A-1-a requirements, would better serve the research goals. Therefore, the Keating Graded Base material was "blended" with on-site silty screenings at a ratio of 4:1, to produce an A-1-a soil with a maximum fines content of about 13 percent.

On-site glacial till was selected for Reinforced Soil B. With maximum fines of 23 percent, it is classified as A-1-b (max. allowable 25% passing #200 sieve). While our research team had considered using a reinforced fill soil for Wall B that contained fines up to 35 percent, our goal for this test section was to select a "higher fines" soil representative of a material that realistically DOTs would be comfortable moving to. Our survey indicated that all DOTs consider material with a fines content of 25% as a "high fines" material. Therefore, the till (A-1-b) was considered a good choice for Wall B. From a constructability standpoint, the in-situ moisture content of the till appeared to be relatively close to the ASTM D-698 Optimum Moisture Content, which would allow the till to be placed and compacted directly from the pit without the need for moisture conditioning.

The two remaining test wall sections (C and D) were to be constructed using A-4 soil. The NCHRP Review Panel recommended that the A-4 soil contain a maximum of 50% fines and have a PI < 6. On-site screenings from the Keating construction materials operation were available. Sieve analysis data provided by Keating in 2004 indicated that the fines content was around 40 percent and the material was non-plastic. The screenings material was, therefore, selected for use as the reinforced fill soil in Walls C and D.

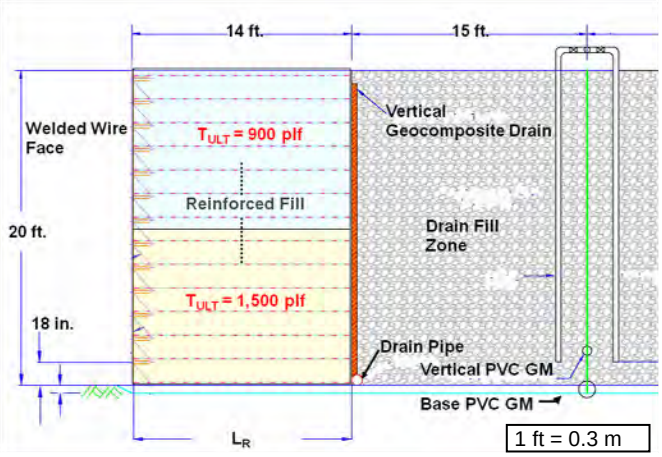

Figure 2: Section Through Test Wall

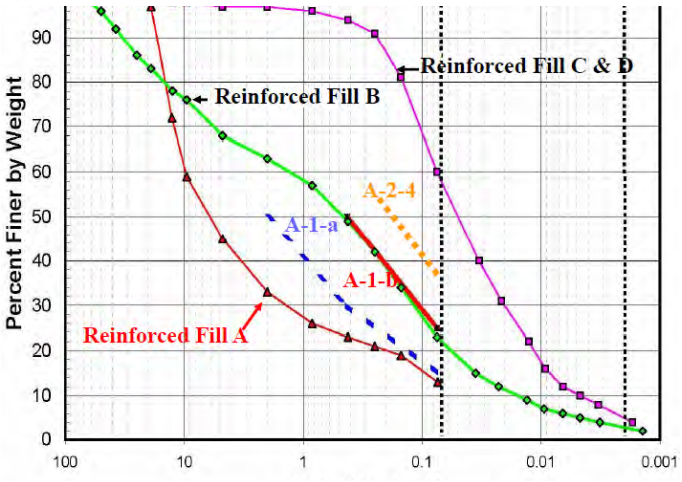

Figure 3: Gradation of the Backfill Soils

Table 1: Engineering Properties of the Backfill Soils

Material	Max. Dry Density $\gamma_{d\,max}$ (pcf)	Optimum Moisture Content (%)	Friction Angle ϕ_{PEAK} (deg.)	Permeability[5] k (cm/sec)
Reinf. Fill A (A-1-a; Keating 4:1 Blend)	134.5 [1] 138 [2]	8.0 [1] 6.0 [2]	50 [3], 37 [4]	2.7×10^{-2}
Reinf. Fill B (A-1-b/A-2-4; Glacial Till)	134.5 [1] 139.5 [2]	6.0 [1] 4.5 [2]	33 [3], 35 [4]	9.3×10^{-5}
Reinf. Fill C & D (A-4; Keating #1 Washings)	112 [1] 119 [2]	13.5 [1] 12.0 [2]	39 [3], 33 [4]	6.1×10^{-5}
Drainage Soil (Local Sand Source)	121.5 [2]	10.5 [2]		7.0×10^{-3}

[1] ASTM D 698 [2] ASTM D 1557 [3] ASTM D 3080 [4] ASTM D 4767 [5] ASTM D 2434 or D 5084

1 pcf= 0.157 kN/m^3

Laboratory tests performed by the research team in 2005 prior to construction indicated that the fines content of the screenings was as great as 60 percent. Pertinent engineering properties of the reinforced fill soils were determined by laboratory testing and are indicated in Table 1.

The foundation conditions beneath the test walls were evaluated by test borings, and consist of very dense natural inorganic soils overlying bedrock, which occurs at relatively shallow depths. Groundwater was not encountered in the test borings.

2.2 Groundwater/Rainfall Simulation and Monitoring Pore Water Pressure Effects

An essential component of an MSE retaining wall that uses reinforced fill with "high fines" soil is aggressive drainage, to prevent the buildup of pore water pressure in the reinforced zone. This pore pressure produces an additional outward force that the wall must resist, and it reduces the strength of the soil that holds the wall in place. Review of case studies indicated that pore water pressures behind the reinforced soil zone invariably played a major role for the serviceability problems, and in some cases complete collapse of walls with unacceptable behavior.

Figure 4 illustrates the proposed test sequence. To simulate groundwater, water was pumped to a feed line at the top of the test sections. A system of valves was used to control the introduction of water from the feed line into the individual drainage soil zones of each test section via slotted, vertical fill pipes. This initiated horizontal flow towards the wall and into the geocomposite drain for the wall. By controlling the head in the drainage soil (with the drain pipe open), the effect of rising groundwater level on the performance of the wall was simulated. We expected little if any effect of pore pressure build up on the test sections, as long as the geocomposite drains function as designed.

This phase of the test was intended to demonstrate that various reinforced fill materials will provide suitable performance, even in areas with high groundwater conditions, as long as they are properly drained.

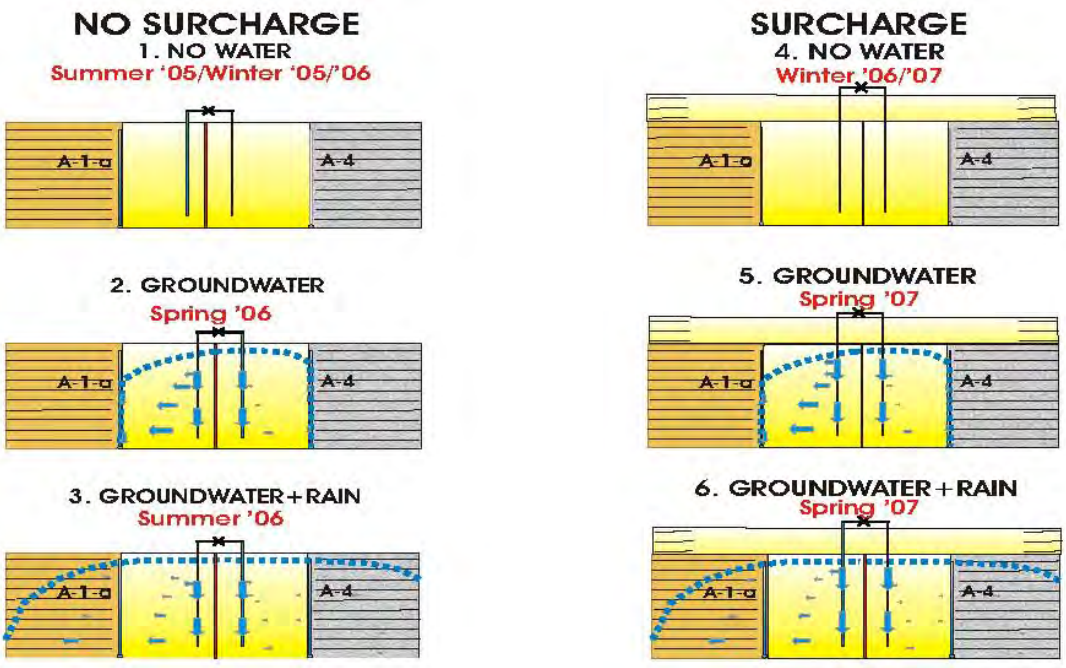

Figure 4: Testing Sequence

By closing a valve on the drain pipe and spraying water on top of the reinforced fill, the effects of poor drainage and heavy rainfall on the performance of MSE walls with the various reinforced fills could be simulated. The pore pressure in the reinforced fill could be increased until the wall experiences noticeable distress. This phase could provide valuable information to evaluate the ability of the numerical models to consider the effects of pore pressure.

Finally, the test areas could be drained, a surcharge added and the test sequence repeated to measure the effects of groundwater and rainfall. The walls were designed so that they should experience considerable distress when subjected to a surcharge and high pore pressures. This allows a factor of safety of essentially 1 to be produced, so that the ability of the numerical models can be checked to predict factor of safety at the only place it can be measured, i.e. at a value of 1.0 (also called incipient failure).

The test sequence consisted of the following steps:

- Construct the MSE wall to 20 ft (6 m) height with a geocomposite drain located at the back of the reinforcing elements.
- Monitor the wall through the winter season with soil at its natural (aka, low) in-situ moisture content, to measure effects of freeze-thaw on wall performance and reinforcing elements.
- In spring raise water level in fill behind the wall to within 1 ft (0.3 m) of ground surface with geocomposite drain open and functioning. This demonstrates that design will work for high groundwater conditions if proper drainage is in place and working.
- Close off geocomposite drain and let pore pressure rise in reinforced fill until some distress is observed in wall or reinforcing elements.
- Drain reinforced fill and monitor response of wall under capillary heads.
- Monitor the wall through the winter season with soil at a high in-situ moisture content.
- Add surcharge.
- Raise water level in fill behind the wall to within 1 ft (0.3 m) of ground surface with geocomposite drain open and functioning. Wall will be designed to support a 5 ft (1.5 m) surcharge under this groundwater condition without unacceptable distress.
- Close off geocomposite drain and let pore pressure rise in reinforced fill until failure of wall occurs. This will provide an important calibration of the ability of the numerical models to predict factor of safety for the only condition where we know the factor of safety, i.e. a value of 1.0.

Construction of the four full-scale test walls commenced in early August 2005, and was completed in approximately two months.

2.3.1 Instrumentation Plan

Each test section was fully instrumented to record data that will be used to evaluate a number of technical questions. Instrumentation consists of strain gages mounted on the geosynthetic reinforcement; piezometers, thermistors, multiple position horizontal extensometers and vertical extensometers positioned throughout the reinforced fill; vertical inclinometers; and an array of high precision prisms mounted on the face of the test walls on which optical survey readings were obtained using Automated Robotic Total Station technology. Figure 5 shows the typical layout.

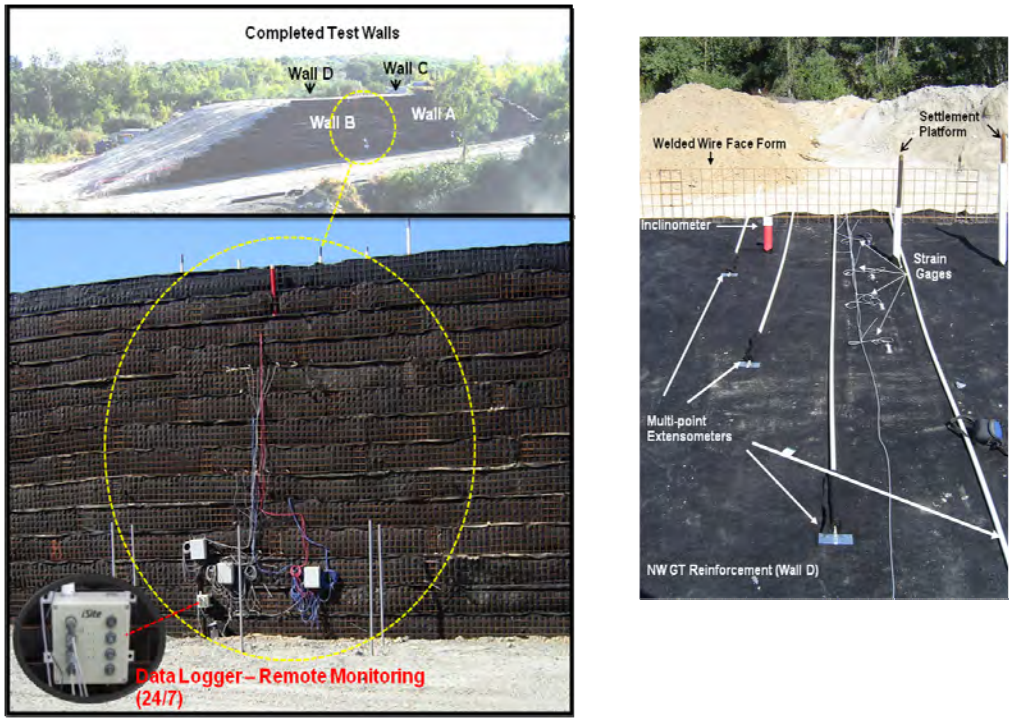

Figure 5: Instrumentation for Each Test Wall

Most instruments were electronic and connected to automatic data logging equipment using the iSite^{TM} system. This system was programmed for each instrument to have a warning level at which an electronic notice was sent to key personnel indicating that some activity was occurring at that instrument. Instruments were read four times each day and stored in the on-site data loggers. These data loggers were connected by cell phone-modem to our web server, which periodically contacted the site and updated its database with the latest readings on all instruments. The database was accessible with a WEB browser and provided up-to-date process readings plotted in engineering units at any time from any location with WEB access. This allowed the field tests to be carried out with far more extensive monitoring than typically possible. The benefit of this more extensive monitoring is to identify the effects of environmental changes, such as temperature and rainfall on the performance of the wall to a degree of detail not previously possible.

The instrumented test walls were monitored 24/7 over a period of approximately 23 months. This allowed observation of seasonal effects on wall performance over a two-year period. While the principle focus of the field test was the behavior of the reinforced fill during the three scheduled test events (i.e. two hydrotest phases and surcharge fill phase), an environmental event that occurred was significant. Specifically, the site experienced record rainfall events in fall 2005 immediately after completion of construction of the test walls. The rainfall that occurred at the site in October 2005 was approximately 15 in. (0.38 m, or almost four times greater than the mean monthly precipitation during the period 1891 – 2000). It caused significant distress to the upper few feet of the wall which moved laterally several inches, settled, and developed tension cracks in the surface of the backfill parallel to the face of the wall as shown in Figure 6. For Walls C and D, over a few weeks cracks appeared further away from the wall eventually reaching to the back of the reinforcement.

Figure 6: Tension Cracks From Heavy Rain

3. MEASURED PERFORMANCE

Overall the test program was very successful in meeting its objectives. The walls were constructed to their intended heights, pore pressures were induced into the backfills and the 5 ft (1.5 m) surcharge was added as planned. The monitoring system worked very well and produced an enormous quantity of data that we are still evaluating. Due to space limitations, we are presenting only a summary of typical measurements and observations.

Figure 7 provides contours of strain measured at the end of the test. Twenty two strain gages were mounted to the reinforcing in each wall. Nineteen of eighty eight gages experienced strains greater than 8% at some point during the test:

Wall A – A23, A32, A42	Wall B – B42
Wall C – C23, C32, C41, C42	Wall D – D12, D21, D22, D24, D31, D32, D33, D34, D42, D43, D45

The numbering code is that the first digit indicates the level of the sensor from bottom to top and the second indicates position behind the wall face. The gages experience mechanical failure at strains above 8%. There is a possibility that some of these high readings could be the result of water entering the strain gage and producing a false reading. All gages were sealed and coated to minimize the opportunity for this to occur, but that is no guarantee. Were the high strains to be a result of water penetration, we would expect a random distribution of gages with high strain readings and a tendency for gages with high readings to be concentrated at the back of the wall where water pressures were higher. On the contrary, the distribution of gages with high strains is concentrated in Wall D, which was the most distressed wall, in the locations where we would expect high strains. While there remains some possibility for some of the high strain readings to be the result of moisture infiltration, we conclude that most of the gages gave accurate indications of true strain in the reinforcement. We have interpreted the data based on the conclusion that all of the gages most likely worked until the strain exceeded 8%.

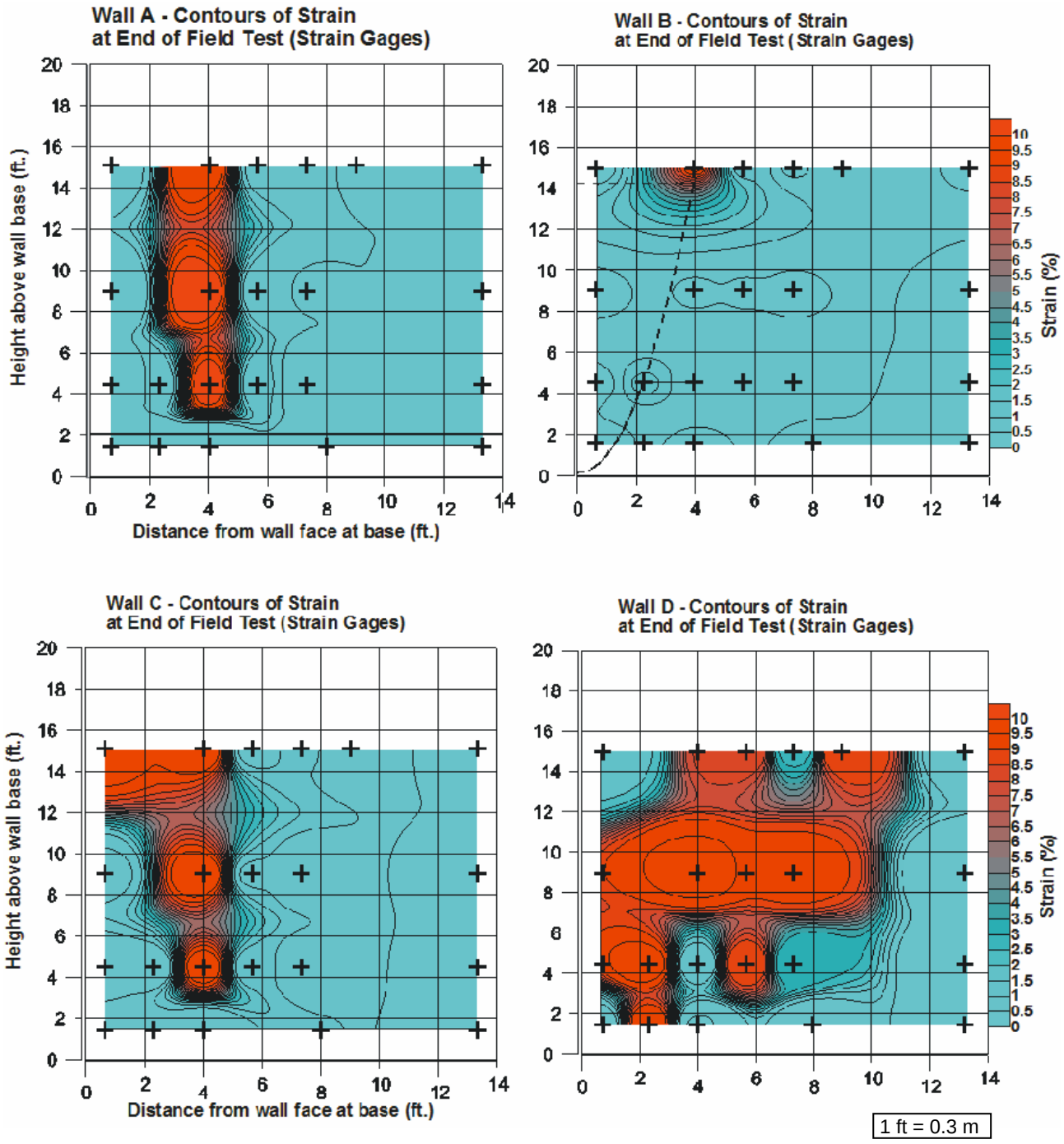

Figure 7: Strain in Reinforcement at End of Test

Figure 8 shows the loads in the reinforcement computed from these strains and the properties of the reinforcement. The maximum loads in lbs/ft (kN/m) relative to ultimate strength of the reinforcement were:

Wall A	Upper Half	200/900	(2.9/13.1)	Lower Half	1300/1500	(19/21.9)
Wall B	Upper Half	800/900	(11.7/13.1)	Lower Half	300/1500	(4.4/21.9)
Wall C	Upper Half	800/900	(11.7/13.1)	Lower Half	1300/1500	(19/21.9)
Wall D	Upper Half	400/1200	(5.8/17.5)	Lower Half	400 /2400	(5.8/35)

At the completion of the tests the reinforcement in Walls A and B had more than 50% reserve strength relative to ultimate strength and Wall C reinforcement had about 15% reserve strength. Wall D had moved outward by about 1 ft (0.3 m), but was still intact. Strains in most of the Wall D gages exceeded 8%, but most likely remained well below the geotextile rupture strain of 20% determined from a confined test. Forces in the geotextile in Wall D were less than ¼ of the ultimate strength.

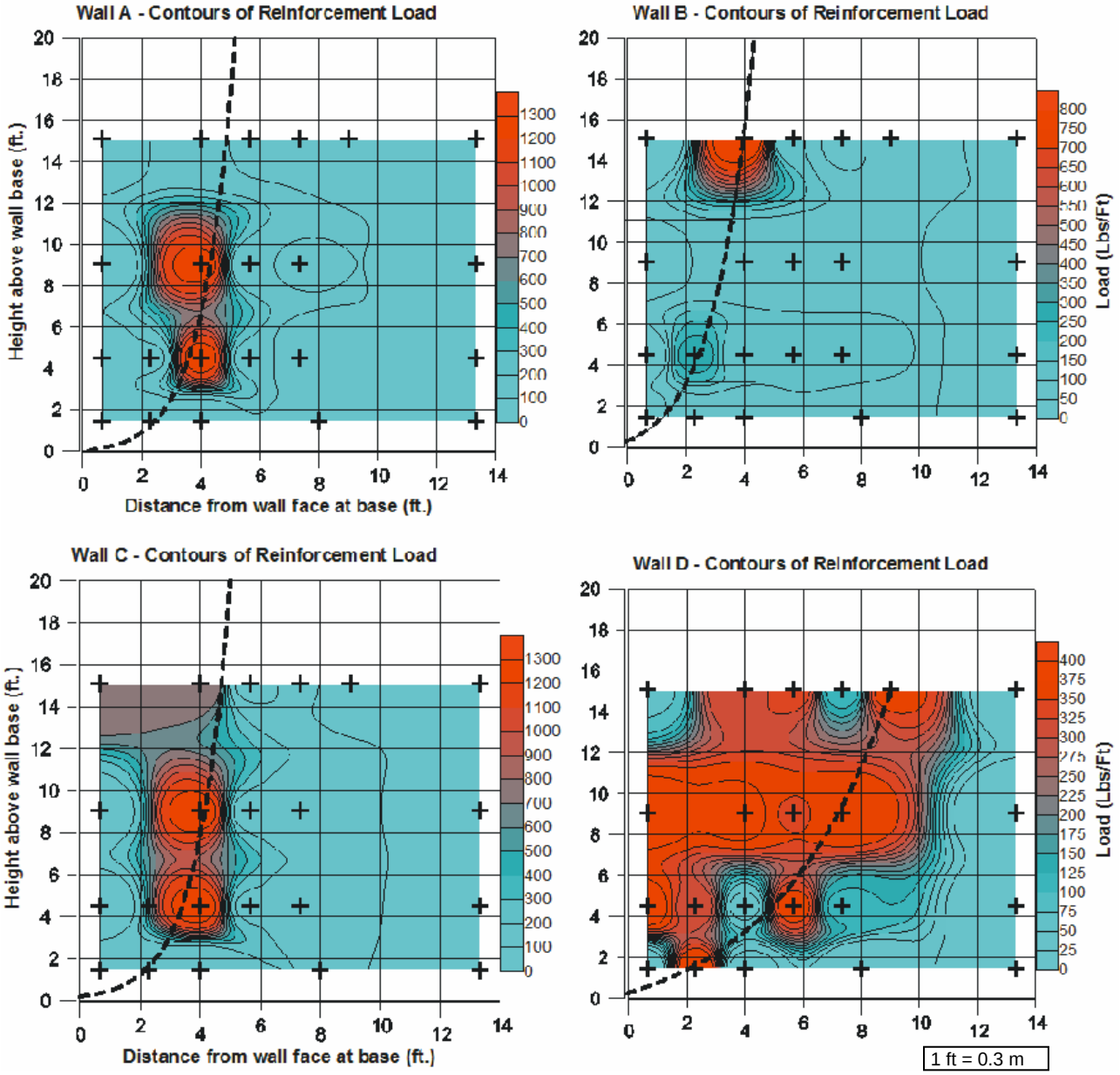

Figure 8: Force in Reinforcement at End of Test

Figure 9 shows the measured horizontal displacement of surveying prisms located on the face of the wall at the center of the loaded area. These movements are continuous from the time the prism could be installed, which was right after placement of the lift of fill in which the prism was anchored. To our knowledge this is the first application of automated total stations to monitor the long term performance of mechanically stabilized earth retaining walls. The system worked very well. The data clearly show the displacements of the wall occurring at the times when additional shear stress was imposed on the soil and reinforcement.

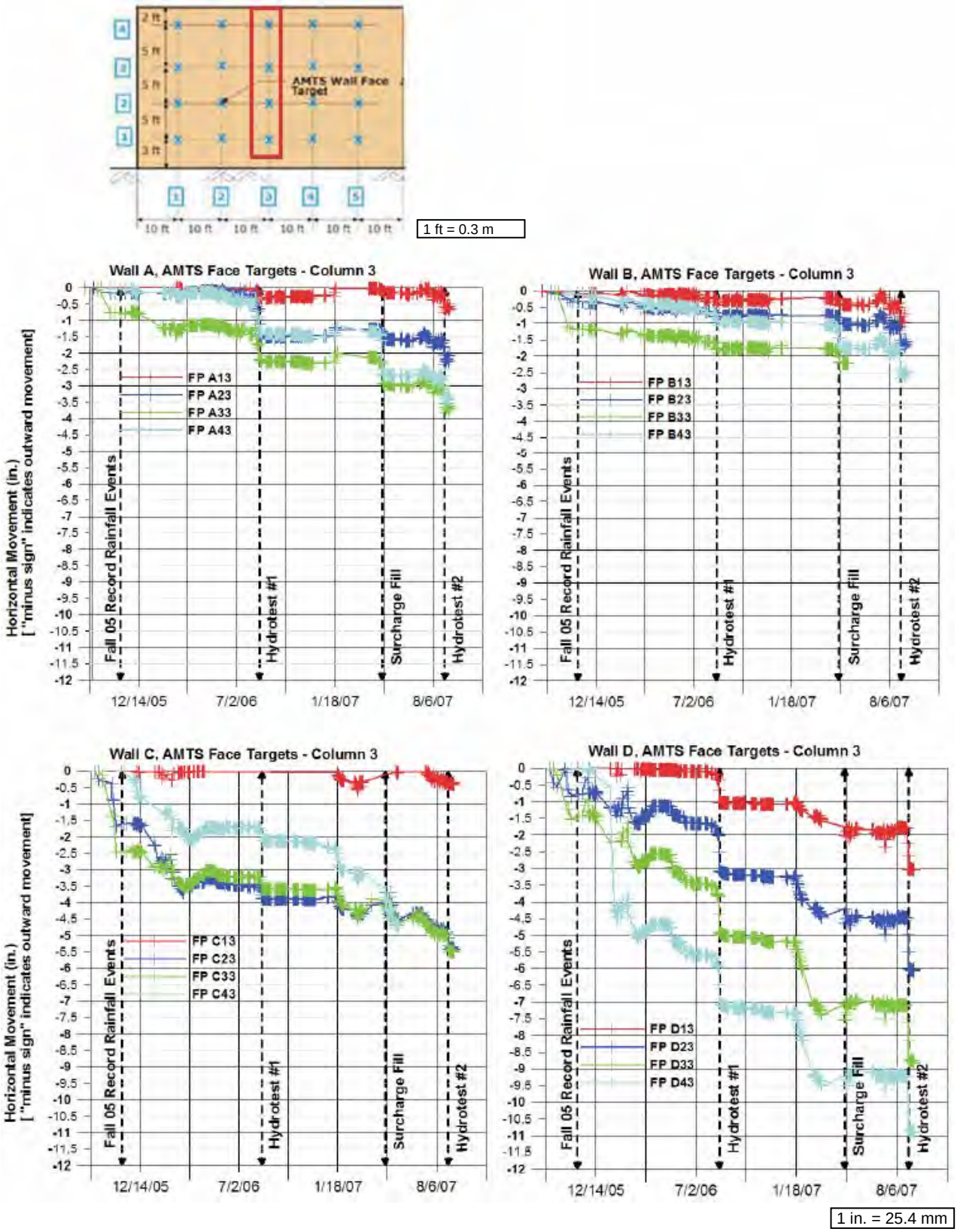

Figure 9: Horizontal Movement of Face at Centerline of Each Wall

Figure 10 shows contour plots of horizontal movement of the face of the walls at the end of the test. There are some variations, but, in general, Wall A displaced outwards by about 4 inches (100 mm), Wall B moved outwards by about 2½ inches (63 mm), Wall C moved out about 5½ inches (140 mm) and Wall D squashed out by 12 inches (300 mm). Typical maximum horizontal movements as a fraction of wall height were approximately 2½ % for Wall A, 1½ % for Wall B, 3% for Wall C, and 6½ % for Wall D.

We were unable to increase the water level in the backfill to the intended height of 18 ft (5.5 m) due to excessive horizontal seepage through the backfills. For Walls B, C and D the flow occurred in zones of concentrated seepage near the vertical geomembrane that was added to the original design to provide hydraulic isolation for each test section. Subsequent evaluation revealed that our field crew had not compacted fill next to the geomembrane for fear of puncturing the membrane. The resulting loose backfill created preferential flow paths and erodible conditions. The maximum height of water achieved was only 14 ft (4.3 m). Consequently the maximum load condition used for a design factor of safety of 1.0 was not reached.

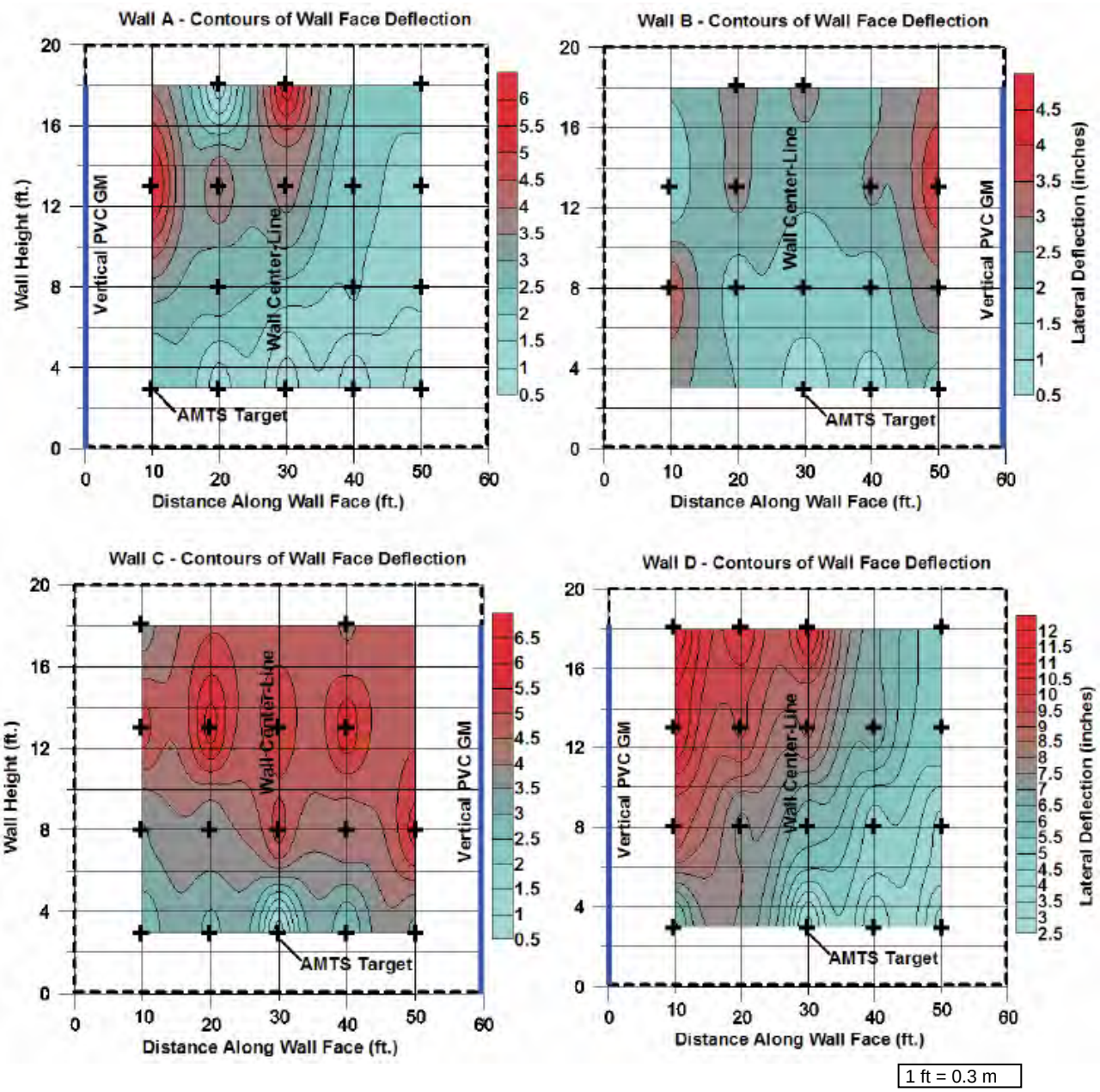

Figure 10: Horizontal Movement of the Face at End of Test

4. CONCLUSIONS

All walls survived the surcharge loading and hydrotests without structural failure. However, because of excessive leakage through uncompacted portions of the backfill, the water level in the hydrotests only reached 14 ft (4.3 m), whereas 18 ft (5.5 m) was used for the design. It appears that the walls behaved as anticipated in the design.

Some of the reinforcement in each wall was strained to near its ultimate strength in Walls A, B and C. The strain gage measurements in Wall D indicate most of the reinforcement was strained more than the mechanical limit of the strain gages. These observations are supported by the independent measurements of lateral movement of the wall which were typically about 2½ % of wall height for Wall A, 1½ % for Wall B, 3% for wall C and 6½ % for Wall D. Despite high strain levels, the walls continued to perform well in terms of structural stability. The monitoring system worked very well and produced an enormous amount of detail about the performance of each wall. The Automated Total Monitoring Station was particularly valuable at providing detailed information on the vertical and horizontal movements of numerous points located on the face of the wall and settlement of plates buried in the retained soil.

The tests show that mechanically stabilized earth retaining walls can withstand substantial positive pore water pressures, provided they are designed to do so. The tests also show that increasing the pore pressure in the backfill causes lateral and vertical deformations of the wall that are as significant as those resulting from adding surcharge loads.

The tests show that soils with as much as 25% fines and a Plasticity Index below 6% can be successfully used as backfill materials in MSE structures, provided the design uses the appropriate material properties and takes into consideration any positive pore pressures that may develop in the backfill over the life of the structure. Based on these results and our professional judgment, soils with up to 50% fines and PI up to 12% may be used in circumstances where the weather conditions permit proper placement of these materials, positive pore pressures are prevented in the backfill, surface water infiltration into the backfill is prevented, and construction is monitored by a qualified professional engineer to ensure that these requirements are fulfilled.

Soils with high fines and some plasticity have lower permeability which creates more difficulty placing the materials to the desired condition. Moisture and density control become more important and more difficult to achieve. Construction with these materials is more weather dependent. Consequently, a higher degree of quality control is necessary to make sure the materials are placed and appropriately compacted to minimize future performance issues.

The lower permeability of soils with high fines and some plasticity also creates the possibility for unintended pore pressures to build up in the backfill and cause adverse performance, if not explicitly considered in the design. This result was clearly demonstrated when the test site experienced 15 inches (0.38 m) of rain over a one month period. Large lateral movements near the face of the wall occurred, which we believe to be the result of a buildup in pore pressure near the face of the wall of sufficient magnitude to cause the wire basket facing elements to slide over the geosynthetic reinforcement. This observation appears to support Terzaghi's 1943 conclusion that resultant pressures on walls can significantly increase during storm events when the soil has a permeability less than 0.002 cm/sec. Due to the potential for such unplanned behavior, it appears that backfills with permeabilities less than 10^{-3} cm/sec should be designed with positive drainage measures at the back of the reinforcing and provisions to prevent surface water from entering the backfill material.

ACKNOWLEDGEMENTS

The authors acknowledge the financial support of the NCHRP program that provided the funding for this work. We also acknowledge the hard work of Geocomp staff, especially John Tripp, to construct the wall and maintain the monitoring system. The authors also acknowledge the major contribution of P.J. Keating Co of Leominster, MA who provided the site for the field test, logistics support and some labor and equipment. Without their generous support our effort would not have been possible.

REFERENCES

Stulgis, R.P. (2005), "FULL-SCALE MSE TEST WALLS", Joint NAGS 2005/GRI-19 Conference, Las Vegas, Nevada, December 2005.

Terzaghi, K. (1943), Theoretical Soil Mechanics. John Wiley and Sons, New York. 510 p.

Geosynthetics 2009
February 25-27 2009, Salt Lake City, Utah

Location of Failure Plane within Narrow GRS Wall Systems

K-H Yang, Dept.of Civil Architectural and Environmental Engineering, Univ.of Texas at Austin, TX, USA
R. Gupta, Dept.of Civil Architectural and Environmental Engineering, Univ.of Texas at Austin, TX, USA
J.G. Zornberg, Dept. of Civil Architectural and Environmental Engineering, Univ. of Texas at Austin, TX, USA

ABSTRACT
The design of a Geosynthetic Reinforced Soil (GRS) wall for internal stability requires computing the reinforcement embedment length against pullout failure. The location of failure plane is important input for this design. The current FHWA design guidelines assume the location of failure plane based on Rankine theory. While this assumption holds true for conventional walls it is unconservative for GRS walls under constrained spaces, also known as "narrow GRS walls". The observations from centrifuge tests suggest that the inclination angle of failure plane is less than that one calculated based on Rankine theory for narrow GRS walls. This paper presents a limit equilibrium study to accurately locate failure planes within narrow GRS walls. The critical failure planes within narrow GRS walls are searched using Spencer's method with a function of noncircular failure plane. The results predicted from limit equilibrium analyses shows a good agreement with the experimental data from centrifuge tests conducted on narrow walls. The results indicate that critical failure plane is bilinear: the failure surface being formed partially through the reinforced soil and partially along the interface between the GRS and stable wall faces. Finally, the effect of wall aspect ratio on the inclination angle of the critical failure plane is computed and depicted in a chart for design purposes.

1. INTRODUCTION

The increase of traffic demands in urban areas has led to widening of existing highways. A possible solution to increase right of way is by constructing Geosynthetic Reinforced Soil (GRS) walls adjacent to previously stabilized walls. The acceptance of GRS walls as a viable solution has been driven by a number of factors, including aesthetics, reliability, cost, construction techniques, seismic performance, and the ability to tolerate large deformations without structural distress. However, due to the high cost of additional right of way and limited space available at job sites, construction of these GRS walls is done under a constrained space. This leads to GRS walls narrower than those recommended in current design guidelines. Narrow GRS wall systems are referred as a geosynthetic reinforced soil wall having an aspect ratio, *L/H*, (ratio of wall width, *L*, to wall height, *H*) less than 0.7 suggested in FHWA MSE wall design guidelines (Elias *et al*., 2001) and placed in front of an existing stable wall (or shored wall). A "narrow" GRS wall systems used for widening of an existing highway is shown in Fig.1.

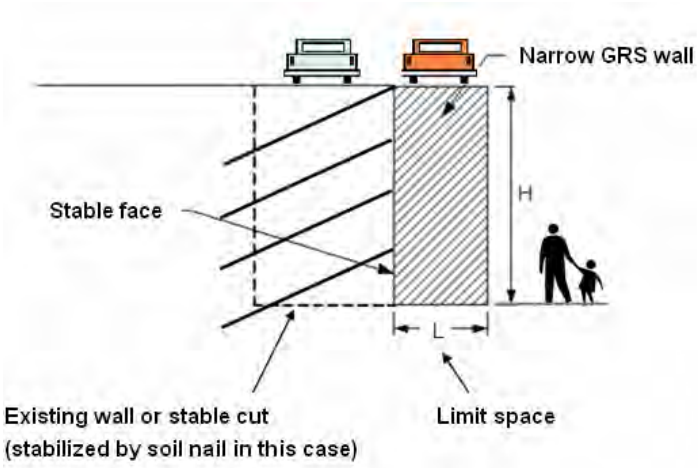

Figure 1: A narrow GRS wall system for widening of existing highway

The behavior of narrow GRS walls differs from those of conventional walls in terms of its interaction with the stable wall face, the magnitude of earth pressures, the location of failure planes and the failure mechanisms. Woodruff (2003) performed a comprehensive series of centrifuge model tests on narrow GRS wall systems. Woodruff (2003) observed that the failure planes of narrow walls was bilinear and had an inclination angle less than that of theoretical Rankine linear failure plane (*i.e.* $45+\phi/2$, ϕ is friction angle of backfill). A detailed description of Woodruff's centrifuge tests and results is presented in Section 2.

Currently, the MSE wall having aspect ratios ranging from 0.3 to 0.7 are designed based on FHWA design guidelines for Shored Mechanically Stabilized Earth (SMSE) wall systems (Morrison *et al*., 2006). These guidelines deals with the uncertainties of narrow wall design by increasing the factor of safety, *FS*, rather than considering the actual characteristics of narrow walls. The FHWA SMSE wall design guidelines suggests to use Rankine failure plane for narrow walls but increase the *FS* against pullout from 1.5 to 2.0 for *L/H*<0.4.

The purpose of this paper is to provide better understanding regarding the behavior of narrow walls in terms of predicting the location of failure plane. The centrifuge tests reported in Woodruff's (2003) are analyzed; then the limit equilibrium modeling centrifuge testing on narrow walls is discussed with emphasis on the method for modeling reinforcement force and searching for nonlinear failure plane; third, the calculated results from limit equilibrium analyses are compared to the experimental data from centrifuge tests; finally, the design charts for variation in inclination angle of failure plane with wall aspect ratio is provided for design purposes.

2. CENTRIFUGE MODEL

A series of centrifuge model tests on reinforced soil walls adjacent to a stable face was performed by Woodruff (2003). A total of 24 different walls with *L/H* ranging from 0.17 to 0.9 were tested. All the reduced-scale walls were 230 mm high and the wall facing batter was 11 vertical to 1 horizontal. Monterey No. 30 sand was used as the backfill material with unit weight of 16 kN/m$^{3.}$ The friction angle was interpolated from a series of triaxial compression tests (Zornberg, 2002) corresponding to the targeted backfill relative density of 70% as 36.7°. The estimated plane strain friction angle was reported as 42.2° using the correlations between triaxial friction angle and plane strain friction angle reported by Zornberg *et al.* (1998). The two different types of reinforcements used in centrifuge study were the commercially available nonwoven geotextiles: Pellon True-grid and Pellon Sew-in. Pellon True-grid was a white 60% polyester and 40% rayon fabric with mass per unit area of 28 g/m^2. The fabric, tested by wide width strip tensile tests (ASTM D4595), had strength of 0.09 kN/m in the machine direction and 1.0 kN/m in the transverse direction and referred as R2 and R4, respectively. Pellon Sew-in was a white 100% polyester fabric with a unit weight of 24.5 g/m^2. The fabric had strength of 0.03 kN/m in the machine direction and 0.1 kN/m in the transverse direction and referred as R1 and R3, respectively. The model walls were placed in front of the wall of aluminum strong box to simulate the stable face.

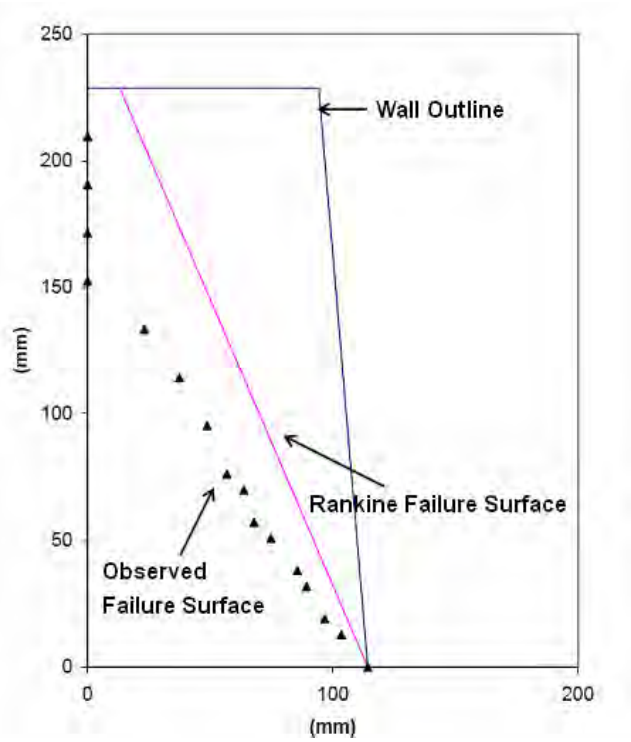

Figure 2. Compound failure at Test 2b, *L/H*=0.4 (Woodruff, 2003)

Tests were performed with above geotextiles involving five different vertical spacing layouts. Each wall was loaded to failure and acceleration (g) required to fail the wall was recorded. High-speed video cameras were used to record the deformations of the wall. The location of the failure surface was determined based on the observed tears (rupture) in each layer of the reinforcement. The tests indicated that the wall would fail internally at *L/H* >0.25 and fail externally in overturning mode at *L/H* < 0.25. For walls with *L/H* >0.6, the internal mode of failure occurred when weaker reinforcement (Pellon Sew-in) was used and no failure occurred with stronger reinforcement (Pellon True-grid). The critical failure planes were linear and the failure surface passed through entire reinforced soil area. When *L/H* ranged between 0.6 and 0.25, the wall failed internally in compound mode. Figure 2 shows the compound failure for a narrow MSE wall with *L/H*=0.4. The critical failure planes in compound failure were bilinear; the failure surface formed partially through the reinforced soil and partially along the interface between the MSE and stable wall faces. The inclination angle of failure plane was less than that predicted by theoretical Rankine failure plane.

3. LIMIT EQUILIBRIUM MODEL

The analyses presented in this section were conducted using limit equilibrium. The UTEXAS4 program developed by Dr. Stephen Wright at University of Texas at Austin (Wright 1999) was used. The primary reason for selecting Limit Equilibrium (LE) was due to their ability to accurately predict failure mechanisms in narrow MSE walls. LE method was used to model three centrifuge tests: Test 2a (L/H=0.6), Test 2b (L/H=0.4) and Test 3a (L/H=0.7). A summary of the condition and result of these tests is listed in Table 1. Since similar procedures are followed in the three tests, only the description of Test 2b is discussed in detail.

Table 1. Summary of centrifuge test conditions for limit equilibrium modeling

Test	Aspect Ratio	Reinforcement Strength	Failure Mode	Failure g-level	Reinforcement Spacing (mm)
2a	0.6	R2	Compound	39	20
2b	0.4	R2	Compound	41	20
3a	0.7	R2	Internal	38	20

3.1 Modeling of GRS and Stable Walls

Figure 3 shows the LE model of wall Test 2b. The geometry of wall model follows the dimension reported by Woodruff (2003), *i.e*, wall height of 230 mm, wall aspect ratio of 0.4 at top of the wall, wall face batter 11 vertical to 1 horizontal, and twelve layers of reinforcement (20 mm vertical spacing).

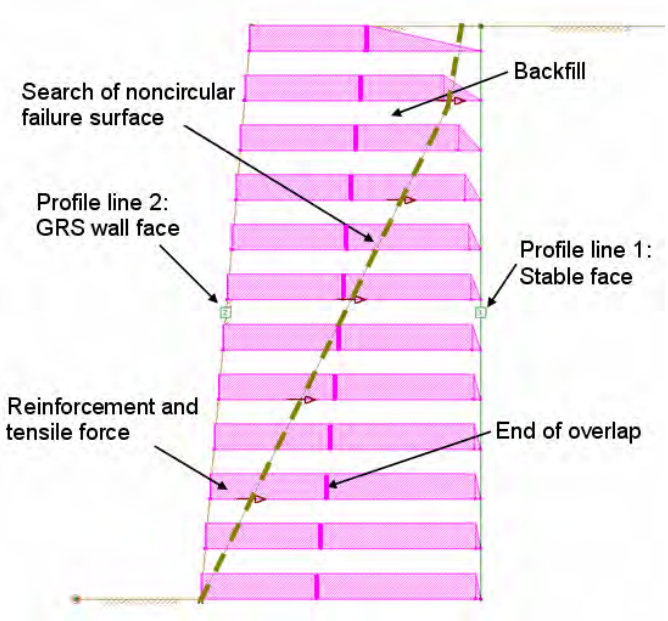

Figure 3. Limit equilibrium model of wall Test 2b

The stable wall face was assigned material properties such that it had theoretically infinite strength (very strong material). Because the existing wall is assumed "stable", the infinite strength of stabilized wall precludes failure surfaces passing through the stable face and constrained the search of the critical failure surface only within the GRS wall. Material model of the backfill in GRS wall was selected following a conventional Mohr-Coulomb model. Monterey No. 30 sand with relative density of 70 was characterized by unit weight of 16.05 kN/m^3, plane strain friction angle of 42.2° and zero cohesion. The centrifugal force was simulated by increasing the unit weight of backfill by N times corresponding to the target g-level.; for example, the unit weight for the modeling of centrifugal force at 41g was computed as 658.05 kN/m^3 (=16.05*41).

3.2 Modeling of Reinforcement

The forces in the reinforcement are limited by its ability to resist failure by rupture and by pullout as shown in Fig. 4. The way of modeling rupture and pullout resistance of the reinforcement is discussed below.

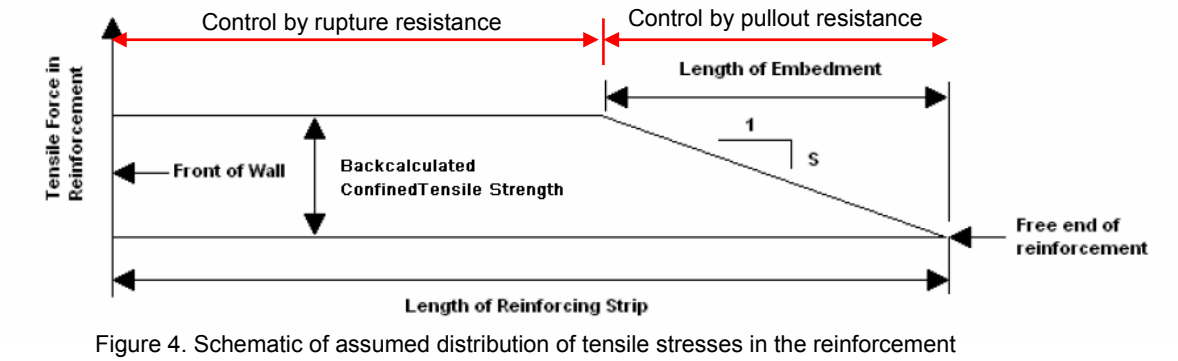

Figure 4. Schematic of assumed distribution of tensile stresses in the reinforcement

3.2.1 Tensile Forces

For the limit equilibrium analyses, the resistance of the reinforcement against failure by rupture was assumed to be the same for all layers of reinforcement as similar reinforcing material was used in each layer. Wide width strip tensile tests (ASTM D4595) showed the unconfined tensile strength of reinforcements used in Test2b was 0.09 kN/m. The reinforcement tensile strength under confinement was back-calculated based on the confined tensile strength for each centrifuge tests by force equilibrium analysis. The average confined tensile strength reported based on this analysis was 2.5 times larger than the unconfined tensile strength of reinforcements. Consequently, a confined tensile force 0.225 kN/m (=0.09*2.5) was used as the tensile strength in each layer of reinforcements.

3.2.2 Pullout Resistance

The pullout resistance of the reinforcement was assumed to increase linearly from zero at the free end of the reinforcement to a value equal to the tensile strength of the reinforcement. Figure 4 illustrates the variation of the longitudinal force in the reinforcement. The rate of change in force with horizontal distance, shown as *S* in Fig. 4 can be evaluated by Eq.[1], which was derived based on FHWA design guidelines (Elias *et al*, 2001).

$$S = F^* C R_c \alpha_v \sigma_{ov} \qquad [1]$$

where: F^* is the pullout resistance factor; C is the reinforcement effective unit perimeter; R_c is the coverage ratio; α_v is a scale correction factor which accounts for nonlinear stress reduction; σ_{ov} is the vertical overburden stress acting on the reinforcement. The recommended equation for the pullout resistance factor F^* for geosynthetic reinforcement is defined in the current FHWA design guidelines for MSE walls as 2/3*tan(ϕ), where ϕ is the backfill friction angle. Based on this recommendation and a friction angle of 42.2° used in Woodruff's centrifuge test, the value of F^* was adopted as 0.60. The effective unit perimeter of the reinforcement, C, was assigned a value of 2 to account for the top and bottom face of the reinforcements. The coverage ratio, R_c, for geosynthetic reinforcement is 1 because the reinforcement is a uniform sheet of material. The correction factor α_v depends primarily upon the strain softening of the compacted granular backfill material, the extensibility and the length of the reinforcement; it can be substantially smaller than 1 for extensible reinforcements. FHWA design guidelines recommends α_v of 0.6 for geotextiles. σ_{ov} is the vertical overburden stress acting on the reinforcement. When the aspect ratio is low, several studies (Frydman and Keissar, 1987; Take and Valsangkar, 2001; Leshchinsky and Hu, 2003; Lawson and Yee, 2005; Kniss *et al.*, 2007; Yang and Liu,2007) have

showed arching effect will reduce the vertical and horizontal earth pressures. This arching effect was included in σ_{ov} as follows:

$$\sigma_{ov} = \gamma z \beta_v \quad [2]$$

where: γ is the unit weight of the reinforced backfill; z is the depth of the layer of reinforcement below the top of the backfill; β_v is the vertical stress influence factor. Kniss *et al.*, 2007 conducted a series of finite element simulations to study the effect of arching effect on the vertical and horizontal stresses. The values of vertical stress influence factors β_v varying with wall aspect ratios are shown in Fig 5. For the case of wall aspect ratio 0.4 in Test 2b, a value of 0.65 was selected based on Fig. 5 to represent the average value of vertical stress influence factor between top and bottom layers. The final distribution of tensile forces of the reinforcements is shown in Fig. 3.

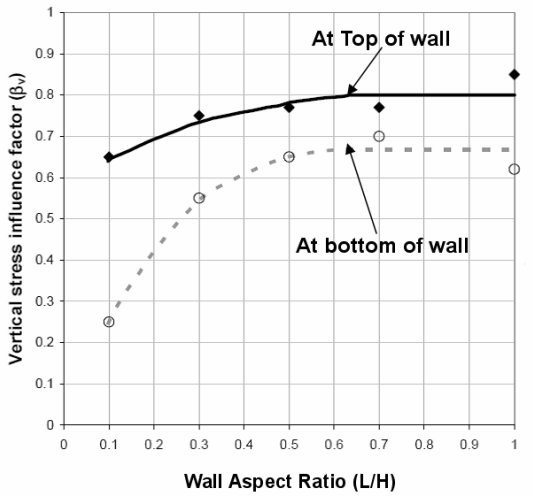

Figure 5. Vertical stress influence factors at the top and bottom of the wall (Kniss *et a*l., 2007)

3.2.3 Overlap Layer of Reinforcement

The reinforcements were wrapped around the wall face. The experimental results showed that this wrap-around (or overlapping) configuration increased the stability of the system. Consequently, the contribution of the geotextile overlap layers to the stability of the models was incorporated in the limit equilibrium models. The tensile force in the overlap layer was modeled using confined tensile force constantly through the entire overlap layer. The length of reinforcement was inputted as 50 mm, which corresponds to the length of the overlap layers in the centrifuge test.

3.2.4 Orientation of Reinforcement Tension

The resistance provided by the reinforcement is characterized in terms of longitudinal and transverse forces at selected points along each layer of reinforcement. The longitudinal force represents the resistance in the reinforcement parallel to the length of the reinforcement and the transverse force represents the resistance in the reinforcement perpendicular to the length of the reinforcement. However, it was assumed that the reinforcement only provides resistance in the longitudinal direction and the resistance in the transverse direction was assumed to be zero.

3.3 Search for Noncircular Failure Surface

Limit equilibrium calculations were performed using Spencer's method (Spencer 1967). This method satisfies all equilibrium conditions, *i.e.*, vertical force, horizontal force and moment equilibrium. The interslice forces were assumed to be parallel to each other. This assumption is required to balance the number of unknown parameters and the number of equilibrium equations. The vertical stress reduction due to arching effect is neglected for calculating the stress on the base of each hypothetical slice in Spencer's method. It is because the arching effect is most influential along the interface between stable face and narrow wall where the soil-structure interaction is most significant. The arching effect becomes less influential toward center line of narrow wall. In addition, it is also to avoid double taking account of the arching effect for both soil and reinforcement.

Limit equilibrium analyses in this study were performed using a search for a noncircular failure surfaces. Kniss *et. Al*. (2007) concluded that the noncircular failure surfaces are more critical than circular failure surfaces. In addition,

Woodruff (2003) also observed that the critical failure surface of a narrow wall showed a bilinear rather than circular shape. The searches for the noncircular failure surfaces were initiated by specifying the initial location of selected points along the failure surface. Kniss *et. al*, (2007) performed a parametric study to find the adequate number of points to define the initial failure surface. The study showed that an initial failure surface defined by from five to nine points is adequate. The seven points, evenly distributed through the height of the wall, were selected to define the initial failure surface. In all analyses, the first point on the initial failure surface was fixed at the toe of the wall. The last point was placed at the crest of the GRS wall. Fixing the first point at toe forced the failure surface to pass through this point, but other points on the initial failure surface were only allowed to move horizontally.

4. RESULTS

The results obtained based on the analyses conducted on the three centrifuge tests are presented in this section. The factor of safety at failure and the location of failure surface are the two most important results obtained from limit equilibrium analysis. In addition, these results are compared to the experimental results from centrifuge testing.

4.1 Factor of Safety versus G-Level

Figure 6 shows the calculated factor of safety as a function of the g-level for Test 2b (L/H =0.4) as obtained using limit equilibrium. The factor of safety decreases with increasing g-level. Figure 6 also shows that the wall is predicted to fail (FS=1) around 41.5g. Centrifuge testing indicated the wall failed at approximately 41g. Consequently, the g-levels at failure from centrifuge testing and limit equilibrium simulation are in a good agreement. Limit equilibrium simulation of Tests 2a (L/H=0.6) and 3a (L/H=0.7) exhibit similar trends. Wall is predicted to fail at 40g for both tests. Centrifuge testing indicated the wall failed at 39g for Test 2a and at 38g for Test3a. Both simulations show a close agreement with the g-levels at failure from centrifuge testing.

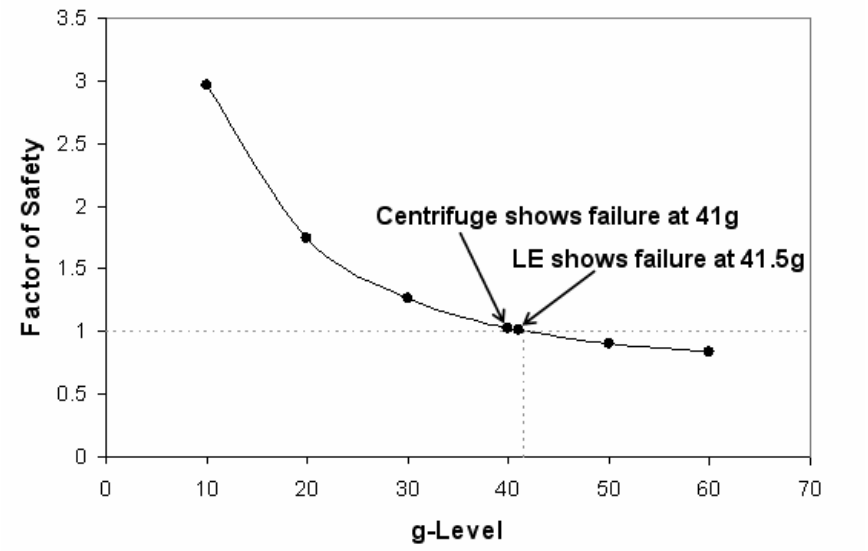

Figure 6. Factor of safety versus g-level for Test 2b

4.2 Location of the Failure Surface

In reinforced soil structures, the portion of the reinforcement that extends beyond the failure surface provides resistance against pullout. Therefore, location of failure surface is important to determine the pullout resistance of the reinforcement and eventually for the design of these structures. Figure 7a shows a comparison between the location of the failure surface obtained experimentally from Test 2b, and the one obtained using limit equilibrium analysis. Both the experimental and predicted results show the failure surface goes partially through the reinforced soil and partially along the interface between the reinforced soil and stable face. Finally, the inclination angle of the failure surface is less than the theoretical value defined by the Rankine failure surface criterion. Figures 7b and 7c show the comparison for Test 2a and Test 3a. Good agreements are also observed. Only a little discrepancy happens at the top of the failure surface in Fig. 7b; the predicted failure surface did not go along the interface near the top of the wall as shown by the experimental results.

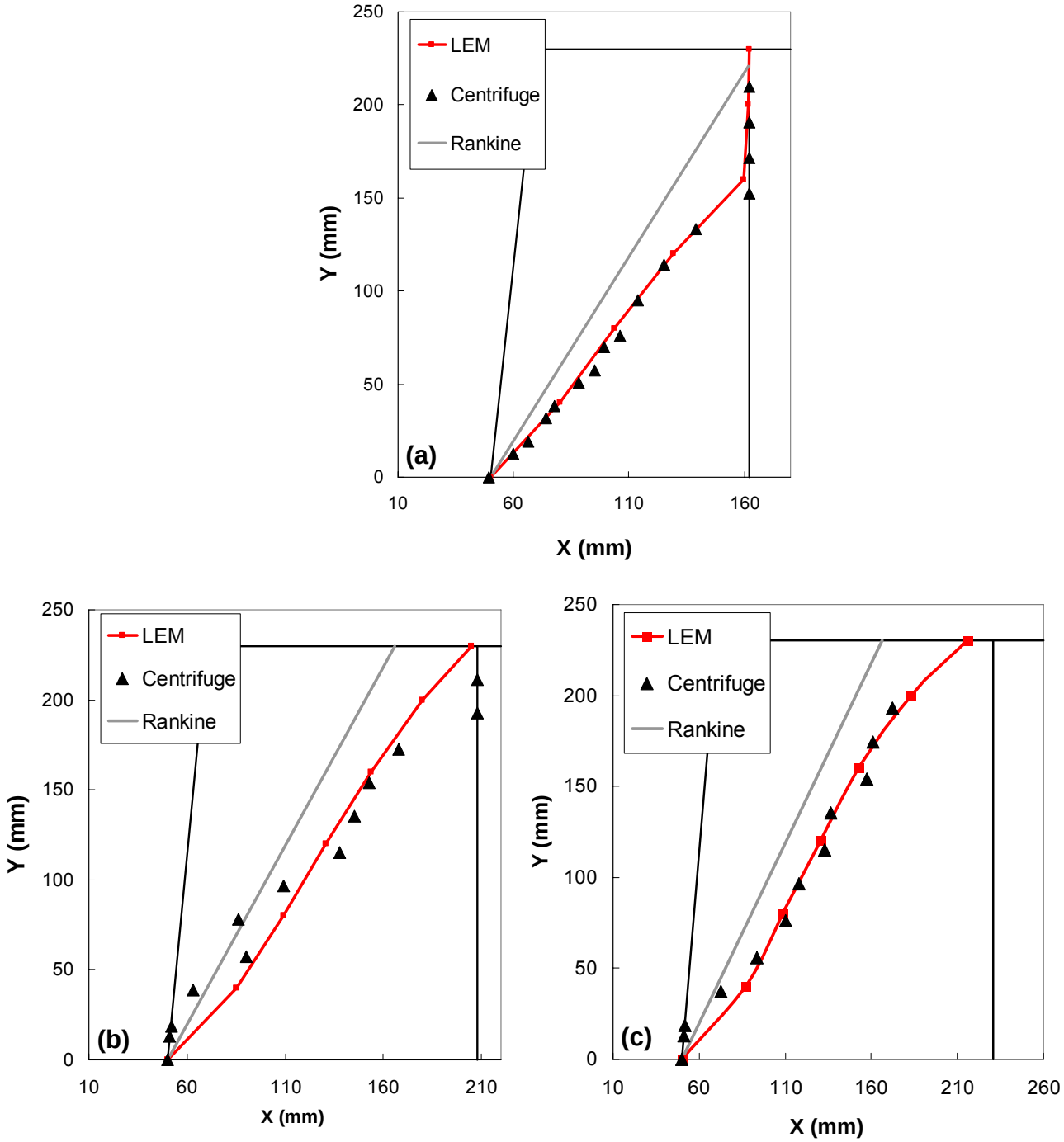

Figure 7. Location of failure surface for (a)Test 2b (*L*/*H*=0.4); (b) Test 2a (*L*/*H*=0.6); (c) Test 3a (*L*/*H*=0.7)

5. Effect of wall aspect ratio on failure plane

5.1 Design Chart: Inclination Angle of Failure Plane versus Wall Aspect Ratio

The inclination angle of the failure plane is an important parameter for calculating the *FS* against pullout. For the case of narrow GRS walls, the inclination angle is denoted as θ_f and illustrated in Fig. 8.

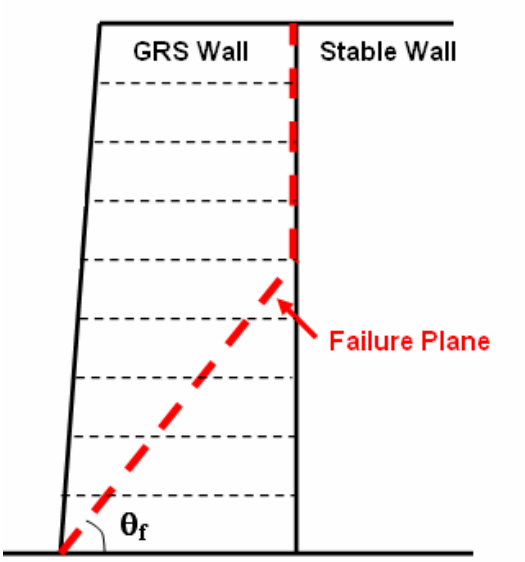

Figure 8. Define inclination angle of failure plane

The inclination angles of failure surfaces from Tests 2a, 2b, and 3b were measured based on the approach described above. Both of the results from centrifuge test and limit equilibrium analysis are shown in Fig. 9. The obtained inclination angles were normalized by the inclination angle of theoretical Rankine failure plane, $45+\phi/2$. A parametric study of the inclination angle of failure surface at L/H=0.3 was conducted. Figure 9 also includes an extra data point of centrifuge test reported by FHWA design guidelines for shored mechanically stabilized earth (SMSE) wall systems (Morrison *et al*., 2006). This data point seems to follow the trend predicted by Woodruff (2003) centrifuge tests and limit equilibrium analyses. In addition, although Woodruff (2003) observed that when the wall aspect ratio decreased below 0.25, the failure mode changed from compound failure to external failure; in some cases, even though wall aspect ratio below 0.25 but the external failure is not going to happen. This may be because the external failure can be prevented by mechanically or frictionally connecting reinforcements to the shored wall. Therefore, the wall aspect ratio (x-axis in Fig. 9) is extended to a value of 0.2. The intension is to include the failure surface of wall aspect ratio from 0.2 to 0.3 for the cases discussed above.

Figure 9 shows a trend of inclination angles decreasing with the decrease of aspect ratios. This trend is characterized by a best-fit regression line using data from limit equilibrium analyses. The dashed horizontal line represents the inclination angle of Rankine failure plane suggested by FHWA SMSE wall design guidelines. The inclination angle suggested by FHWA SMSE wall design guidelines based on Rankine failure plane appears to overestimate the inclination angle of failure surface observed from centrifuge tests and limit equilibrium analyses. This would lead the estimating embedment length of reinforcement and the calculated factor of safety against pullout on unconservative side.

5.2 Possible Factors Affect Inclination Angle of Failure Surface

The reason for the difference in the failure surface from theoretical Rankine failure plane can be attributed to the following three factors:

1. Arching Effect (Interaction with Stable Face)
2. Boundary Constraint (Reduced Aspect Ratio)
3. Presence of Reinforcement

These factors not only constraint the degree of freedom of the soil mass but also interact with soil failure wedge by applying an extra vertical shear force on it (Filz and Duncan, 1997a and 1997b); thereby, the internal failure mechanism of GRS wall can not be easily predicted by Rankine theory (simply based on the Mohr-Column circle with vertical and horizontal principal stresses). For example, as shown in Fig. 9, because of the presence of stable face in narrow GRS wall systems, the normalized inclination angle is less than 1.0 even at L/H=0.7, which has enough space for failure plane to fully develop as Rankine linear failure plane. Moreover, the effect of aforementioned three factors will become amplified as the decrease of aspect ratio; this amplification reflects the decrease of normalized inclination angle as the decrease of aspect ratio shown in Fig. 9.

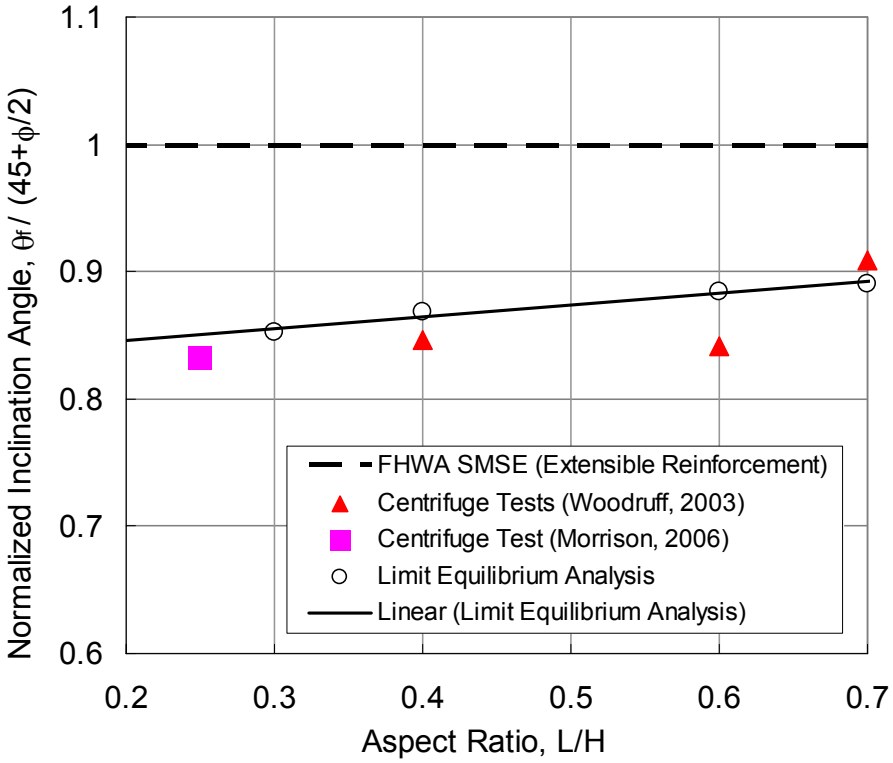

Figure 9. Normalized inclination angles

6. DESIGN IMPLICATION

The wall failure mode is a compound failure for a narrow wall with aspect ratio from 0.6 to 0.3. Due to the nature of compound failure mode (illustrated in Fig. 10a), the failure surface (pink line) will not intersect with upper layer reinforcements (blue dashed lines from reinforcement layer number 7 to 10). The effect of reinforcing backfill through developed tensile force should not be counted for those layers of reinforcements without the intersection with failure surface. One can envision the narrow wall system in Fig. 10a as identically to that in Fig 10b. Only the lower reinforcement layers (*i.e.*, those that extend into the resistant zone) are designed to resist breakage and pullout for the entire "active" MSE mass.

For the situation addressed above, FHWA SMSE wall design guidelines (Morrison *et al*., 2006) recommends to check a overall pullout stability ($FS_{p,,overall}$) in addition to conventional internal stability evaluations (*i.e.* breakage and pullout stability for each individual layer of reinforcement). For the same reason, this study suggests to include a overall breakage stability ($FS_{b,overall}$) into the internal stability evaluations as well . Eq. [3] and Eq. [4] are the formulas used to evaluate the overall stabilities against breakage and pullout, respectively. The idea is to divide the summation of all resistant force by the summation of all driving force.

$$FS_{b,overall} = \frac{\Sigma_{i=1}^{i=j} T_{al,i}}{\Sigma_{i=1}^{i=j} T_{\max,i}} \quad [3]$$

$$FS_{p,overall} = \frac{\Sigma_{i=1}^{i=j} Pr_i}{\Sigma_{i=1}^{i=j} T_{max,i}} \quad [4]$$

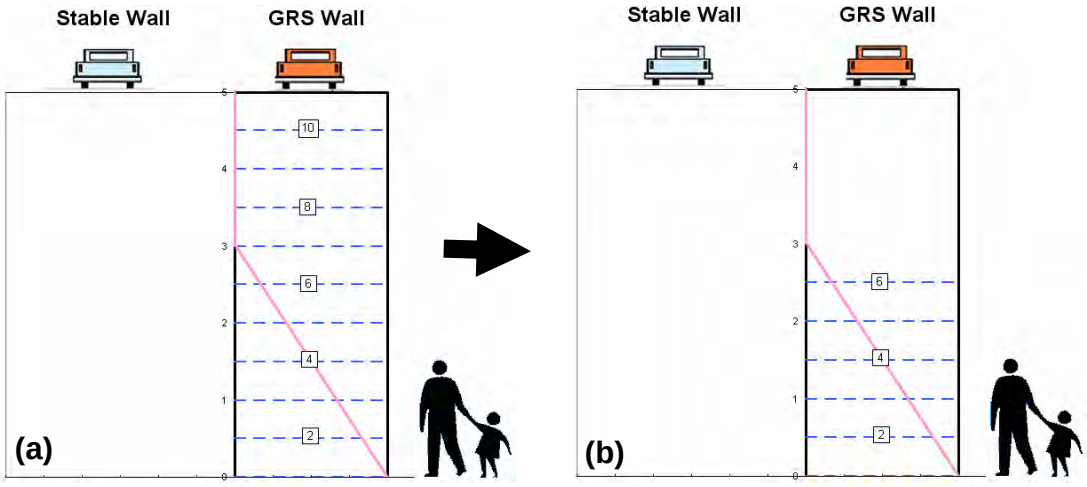

Figure 10. Illustration of two conceptually identical systems:
(a) with upper layer reinforcements; (b) without upper layer reinforcements

where; T_{al} is the allowable reinforcement tensile strength; T_{max} is the maximum tension developed in reinforcement; P_r is the pullout capacity; i is i^{th} layer of reinforcement, $i \in [1,2,3,\ldots j]$; j is the number of reinforcement layer that satisfies pullout criteria ($FS_{p,i}$>1.5) at each reinforcement layer. T_{max} can be calculated as earth pressure times vertical spacing of reinforcements in conventional walls. As for T_{max} in narrow walls, the earth pressure will be reduced due to arching effect and boundary constraint. T_{max} can be estimated as Eq. [5]

$$T_{max} = \gamma z K_a R_d \cdot S_v \quad [5]$$

where: γ is the unit weight of the reinforced backfill; z is the depth of the layer of reinforcement below the top of the backfill; K_a is the active earth pressure coefficient; S_v is vertical spacing of reinforcements; R_d is the reduction factor to account for arching effect and boundary constraint. Readers are referred to Kniss et. al. (2007) and Yang and Liu (2007) for more detail. P_r can be estimated by multiplying S (in Eq. [1]) and reinforcement embedment length L_e together. Note P_r should be less than T_{al}. Reinforcement embedment length L_e can be evaluated as Eq. [6].

$$L_e = L - \frac{h}{\tan\theta_f} \quad [6]$$

where; L is wall width; h is reinforcement elevation, θ_f is the inclination angle of failure surface. θ_f is depended on wall aspect ratio and can be evaluated using Fig. 9.

SUMMARY

This paper presented a limit equilibrium study to locate failure planes within narrow GRS walls. Limit equilibrium analyses were used to model the centrifuge test of narrow GRS walls. The forces in geosynthetic reinforcement for narrow MSE walls were discussed. The predicted results were in agreement with the centrifuge experimental results. The results indicated that critical failure plane was bilinear. The failure surface formed partially through the reinforced soil and partially along the interface between the GRS and stable wall faces. In addition, the inclination angle of the critical failure plane decreased with the decrease in wall aspect ratio. The calibrated limit equilibrium model was then used as the basis for the design of other narrow GRS walls. This study concluded that using the inclination angle as obtained using Rankine failure plane for narrow wall systems results in an overestimation of the actual inclination angle. Thus a new design chart for inclination angle of failure surface versus various wall aspect ratios was proposed. This design chart provided the information on the location of the failure surface and the embedment length of reinforcement needed to calculate the factor of safety against pullout. Finally the design implications related to overall internal stability based on the revised analysis were discussed.

ACKNOWLEDGEMENTS

The work of limit equilibrium analysis was greatly consulted and helped by Dr. Stephen Wright, the author of UTEXAS4 program. The First author is indebted to his Colleague, Ken Kniss, for his preliminary simulations. Comments from reviewers and editors to improve the clarity and quality of paper are appreciated.

REFERENCES

Elias, V., Christopher, B.R., and Berg, R.R., (2001), "Mechanically Stabilized Earth Walls and Reinforced Soil Slopes Design and Construction Guidelines," *Report No. FHWA-NHI-00-043*, Federal Highway Administration.

Filz, G.M., and Duncan, J. M. (1997a). "Vertical Shear Loads on Nonmoving Walls. I: Theory," *Journal of Geotechnical and Geoenvironmental Engineering,* ASCE*,* Vol. 123, No. 9, pp.856-862.

Filz, G.M., and Duncan, J. M. (1997b). "Vertical Shear Loads on Nonmoving Walls. II: Application," *Journal of Geotechnical and Geoenvironmental Engineering,* ASCE*,* Vol. 123, No. 9, pp.863-873.

Frydman, S. and Keissar, I., (1987) "Earth Pressure on Retaining Walls near Rock Faces," *Journal of Geotechnical Engineering,* ASCE*,* Vol. 113, No. 6, June, pp. 586-599

Kniss, K., Wright, S., Zornberg, J.G., and Yang, K.-H., "Design Considerations for MSE Retaining Walls Constructed in Confined Spaces" *Center for Transportation Research (CTR), Report no. 0-5506-1,* Austin, Texas, October 2007.

Lawson, C.R., and Yee, T.W., (2005), "Reinforced Soil Retaining Walls with Constrained Reinforced Fill Zones" *Proceedings*, *GeoFrontiers 2005*, ASCE Geo-Institute Conference, pp. 2721-2734.

Leshchinsky, D., Hu, Y. and Han, J., (2004) "Limited Reinforced Space in Segmental Retaining Wall," *Geotextiles and Geomembranes*, Vol. 22, No. 6, pp. 543-553.

Morrison, K.F., Harrison, F.E., Collin, J.G., Dodds, A., Arndt, B. (2006), "Shored Mechanically Stabilized Earth (SMSE) Wall Systems Design Guidelines," *Report No.FHWA-CFL/TD-06-001,* Federal Highway Administration.

Spencer, E (1967). "A Method of Analysis of the Stability of Embankments Assuming Parallel Inter-Slice Forces". *Geotechnique*, 24(4), p. 661-665.

Take, W.A. and Valsangkar (2001), "Earth Pressures on Unyielding Retaining Walls of Narrow Backfill Width," *Can. Geotech. Journal,* Vol.38, pp.1220-1230.

Woodruff, R. (2003), "Centrifuge Modeling of MSE-Shoring Composite Walls," *Thesis*, the Univ. of Colorado, Boulder.

Wright, S.G. (1999), "UTEXAS4 A Computer Program for Slope Stability Calculations." Shinoak Software, 221p.

Yang, K-H and Liu, C-N (2007), "Finite Element Analysis of Earth Pressures for Narrow Retaining Wall", *Journal of GeoEngineering.*, Taiwan Geotechnical Society, 2(2): 43-52.

Zornberg, J.G., Sitar, N., Mitchell, J.K. (1998). "Limit Equilibrium as Basis for Design of Geosynthetic-Reinforced Slopes." *Journal of Geotechnical Engineering*, 124 (8), p.684-698.

Zornberg, J.G. (2002). "Peak versus Residual Shear Strength in Geosynthetic-Reinforced Soil Design", *Geosynthetic International*, Vol. 9, No. 4, pp 387-389.

Geosynthetics 2009
February 25-27 2009, Salt Lake City, Utah

Interaction between Geogrid and Lightweight Tire Chips-Sand Mixture: Laboratory and Numerical Investigation

T. Tanchaisawat, Kasetsart University CSC Campus, Sakonnakhon, Thailand
D.T. Bergado, Asian Institute of Technology, Bangkok, Thailand
K. Shehzad, University of Engineering and Technology, Lahore, Pakistan
P. Voottipruex, King Mongkut's University of Technology North Bangkok, Thailand

ABSTRACT
This study is aimed to measure and calculate the interaction coefficient between geogrid and sand as well as geogrid and tire chips-sand mixture using laboratory test numerical simulations. Numerical simulation was imperative for the sensitivity analyses of the laboratory test results to find the important parameters. Two types of material were used as backfill, sand and tire chips-sand mixture. The sand and tire chips mixture were in proportion of 70 and 30 % by weight. The index properties of Ayutthaya and tire chips-sand were measured which were similar to previous research. Polyfelt geogrid was used as geosynthetic reinforcement with tensile strength of 97.48 kN/m from in-air tensile test. Pullout and direct shear tests were done on large scale pullout machine. The shear strength parameters of Ayutthaya sand and tire chips-sand mixture were found to be 29.8◦ friction angle with cohesion of 15.6 kPa for sand and 24.4◦ friction angle with 14.3 kPa cohesion for tire chips-sand mixture. The efficiency of the geogrid obtained was larger when calculated by friction angle and lower when calculated by cohesion. The results revealed that interaction coefficient obtained from direct shear tests was approximately 0.9 for both backfill materials. While 0.7 and 0.6 for the sand and tire chips-sand mix, respectively, were assessed from pullout test. Numerical analyses were also performed by using finite element software and finite difference software. The results of the numerical simulation reasonably agreed with the measured laboratory results. As simulation results were similar for the pullout test using both softwares, so simulation of direct shear test was done by finite element software only. Lastly, sensitivity analyses were done for the pullout test by varying the interaction coefficient and axial stiffness of the geogrid. These two important parameters were found to affecting the efficiency of the geogrid reinforcement.

1. INTRODUCTION

In this study, construction of mechanically stabilized earth (MSE) or reinforced soil structure has been proposed by reinforcing the backfill soils with geosynthetic reinforcements. MSE structure does not reduce the subsoil settlements owing to the embankment load. However, the presence of reinforcements can reduce the lateral movements. Subsequently, the settlements, especially the differential settlements, at the top of the embankment are reduced. The use of lightweight geomaterials like rubber tire chips and sand mixture is becoming popular nowadays. The use of lightweight material reduces the amount of the settlement or deformation in the soft clay foundation. Moreover, the recycling of the waste materials such as used rubber tires is good for the environment and sustainable development, they are also good for drainage and in that condition combustion hazard potential is not present (Aydilek et al. 2006).

As sand is having good engineering properties and due to its easy availability, it is used frequently as backfill material for different application such as bridge abutments, reinforced retaining walls, and so on. But the use of the only sand increases the settlement problems during the performance of structures, especially in soft ground areas. Thus, it is advantageous to use lightweight backfill materials such as the tire chips-sand mixtures. The lightweight tire chips-sand mixture is a recycled waste geomaterial. When considering the reinforcing materials used in the field applications, the trend of typical geosynthetic reinforcements has been increasing markedly, especially geogrids. Many researchers are currently studying the basic properties and the stress-strain characteristic of lightweight geomaterials, like tire chips-sand mixture, including the interaction between geogrid reinforcement and those lightweight mixtures by conducting large-scale direct shear tests and pullout tests (Tatlisoz et al. (1998), Prempramote (2005), Tanchaisawat et al. (2007)).

This study comprised on several tests. The study started with sieve analyses and specific gravity tests for Ayutthaya sand and tire chips-sand mixtures. Then, compaction tests were done on sand and tire chips-sand mixtures to determine maximum dry unit weight and optimum moisture content of the materials. Subsequently, in-air tensile, large-scale direct shear, and pullout tests were done to study the interaction between grid reinforcement and backfill materials, silty sand with and without tire chips. Polyfelt geogrid (GX 100/30) was selected as the reinforcing material. Finally, simulation of the pullout and direct shear tests were done by using computer simulation.

2. METHODOLOGY

2.1 Introduction

For the reinforced embankments and walls many backfill and reinforced materials were used like sand, rubber tire chip-sand mixture etc., and reinforcements consist on geogrid, geotextile and so on. For the better design, we need to know the interaction among these materials before constructing reinforced earth structures. The interaction can be investigated by conducting pullout and large-scale direct shear tests on extensible grid reinforcements embedded in sand or rubber tire chip-sand mixture. As a result, the interaction between sand and extensible geogrid reinforcement needs to be investigated thoroughly in this study. Moreover, to conduct pullout and large-scale direct shear tests easily and to interpret results properly, it is imperative to investigate the index and engineering properties of the sand and rubber tire chip-sand mixture.

2.2 Material and Index Tests

The materials used in this study were sand and tire chips. Sand was obtained from local source and tire chips were from shredding process and having steel belts removed (Fig. 1). Backfill materials were of two kinds, sand and tire chips-sand mix with the ratio of 30:70 by weight. Standard test method of specific gravity of material was used for the specific gravity test of sand and tire chips. This test was purposed because results of specific gravity test were necessary for the calculation of other properties of sand and rubber tire chip. The standard procedures of sieve analyses were adopted to investigate the particle-size distribution curve of sand and tire chips. Compaction test was done by using standard Proctor compaction test for both filling materials to obtain the optimum moisture content and maximum dry unit weight. The compaction parameters can be used to determine the degree of compaction effort applied for each fill material throughout the pullout and large-scale direct shear tests.

The backfill material employed in this study consisted of tire chip-sand mixtures composed of tire chips and Ayutthaya sand. The specific gravity test of sand was conducted by ASTM D854-97, “Standard Test method of Specific Gravity of Soil” but for tire chips, the procedures in ASTM C127-01, “Standard Test method for Density, Relative Density (Specific Gravity) and Absorption of Coarse Aggregate” were adopted. The specific gravity of Ayutthaya sand is 2.65 that is in agreement with the previous results while that of tire chips is 1.12.

The procedures of sieve analyses, which are provided in ASTM D422-63, “Test Method for Particle-Size Analysis of Soils” were adopted to investigate the particle-size distribution curves of both Ayutthaya sand and tire chips. For Ayutthaya sand, there was 1.64 % passing through No. 200 sieve with effective diameter D_{10} of 0.22 mm, D_{30} of 0.38 mm, D_{60} of 0.62 mm, the uniformity coefficient (C_u) of 2.82, and the gradation coefficient (C_c) of 1.06. According to the Unified Soil Classification System (USCS), the sand can be classified as poorly graded (SP) (see Table 1). The particle-size distribution curve of the sand is shown in Fig. 2. For tire chips, most of the particle size range between 12 and 50 mm with irregular shape due to the random cutting process. The specific gravity and effective diameter of the tire chips are also tabulated in Table 1. The particle-size distribution curve of the tire chips is also shown in Fig. 2.

Figure 1. Sand, Tire-Chips and Tire Chips-Sand Mixture

2.3 Sample Preparations

As sand with and without tire chip were used, as filling material, it needs to be cured to its respective optimum moisture condition based on the results of standard Proctor compaction test. For the comparison with the sand, tire chip-sand mixture sample were also cured depending upon the optimum moisture content of compaction test, which having proportion of 30(for tire chips):70(for sand) % by weight (recommended by Prempramote 2005). Polyfelt geogrid (GX

100/30) was chosen as reinforcing material for this study which was consisting on highly-molecular, high strength polyester yarns. The yarns were knitted to a stable network and equipped with a polymeric coating protection, in order to achieve a product with high knot stiffness and low material reduction factors (see Fig. 3). The product is suitable for both short-term and long-term soil reinforcement applications. Summary of geogrid properties by manufacture is shown in Table 2.

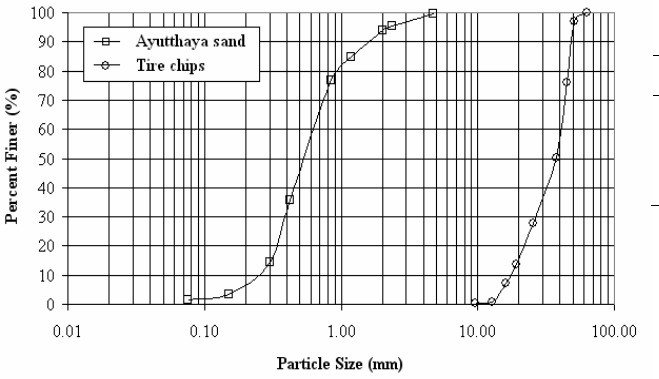

Figure 2. Gradation of tire chips and sand

Table 1. Sand and Tire Chip Properties

Property	Ayutthaya Sand	Tire Chip
Specific Gravity, G_s	2.65	1.12
Effective diameter, D_{10}(mm)	0.22	5.10
Coefficient of Uniformity, C_u	2.82	
Coefficient of Curvature, C_c	1.06	
Classification (USCS)	SP	

Figure 3. Polyfelt Geogrid (GX100/30)

Table 2. GX100/30 Properties

Property (Test Standard)		GX 100/30
Type of product		Knitted Polyester Geogrid
Material		High tenacity Polyester yarns with polymer coating
Characteristic short-term tensile strength (ISO 10319)	MD (kN/m)	100
	CD (kN/m)	30
Elongation at characteristic short-term tensile strength	MD (%)	11
Creep limited strength 120 years (kN/m)		68
Long term design strength for 120 yrs (kN/m)		58
Aperture size (± 5 mm)	MD (mm)	25
	CD (mm)	30
Forms of supply	Width (m)	2.5
	Length (m)	100
	Weight of roll (kg)	108

2.4 In-Soil Pullout Test

Pullout tests conducted in this study were in-soil pullout tests i.e. the clamp was installed in the pullout box confined by the soil. This pullout test program is mainly used for investigating the interaction between geogrid reinforcement and sand, with and without tire chips, and the relationship between pullout resistance and pullout displacement. Both type of filling material were subjected to four normal stresses namely 30, 60, 90, and 120 kPa. The objective of applying these four values was to cover the range of possible reinforcement failures (i.e. slippage and breakage). Since there were four applied normal stresses on geogrid and sand, with and without tire chips, the numbers of pullout tests on the geogrids becomes eight. Since the results obtained from these eight tests were including the results from the clamp with reinforcement; therefore, another eight pullout tests for clamp only (without reinforcements) were also required to subtract from those eight tests. Consequently, the total number of pullout tests were becomes sixteen.

2.5 Large Scale Direct Shear Test

The large-scale direct shear tests were performed to determine the relationship between direct shear force and direct shear displacement, together with determination of shear parameters of the fill materials and shear parameters between fill and reinforcing materials. The direct shear test were performed in two groups, first group was consisting on two types of filling materials with geogrid and second group contain same filling materials but without geogrid. Eight direct shear tests were performed on each group, so in total sixteen tests were conducted.

3. RESULTS AND DISCUSSIONS

3.1 In-Soil Pullout Test

The results of the in-soil pullout test with sand only (Fig. 4) and with tire-chips sand mixture (Fig. 5) shows pullout resistances which increased as normal stress increased because with higher normal stress, the confinement on grid increased. The peak values occurred between 20 to 50 mm pullout displacements for different normal pressures. Afterwards, the peak pullout resistances start to decrease because the geogrid was torn at different places at different normal pressures. The maximum pullout resistances are shown in Fig. 6.

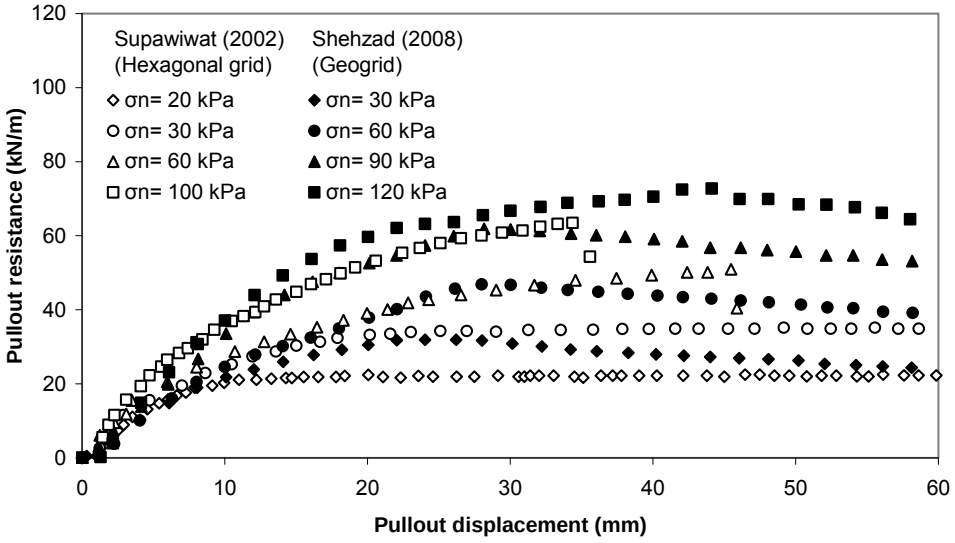

Figure 4. Pullout resistance versus pullout displacement of geogrid with sand only

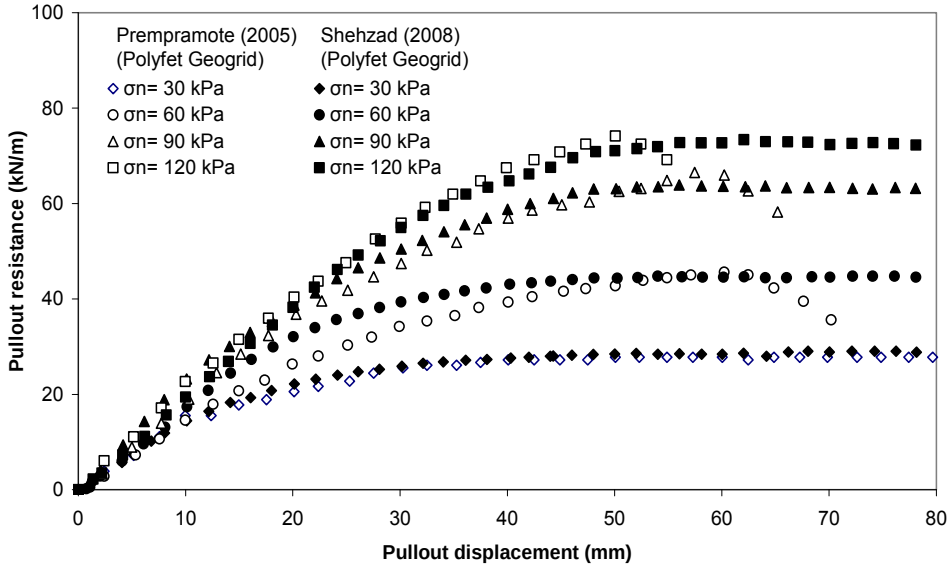

Figure 5. Pullout resistance versus pullout displacement of geogrid with tire chips-sand mixture

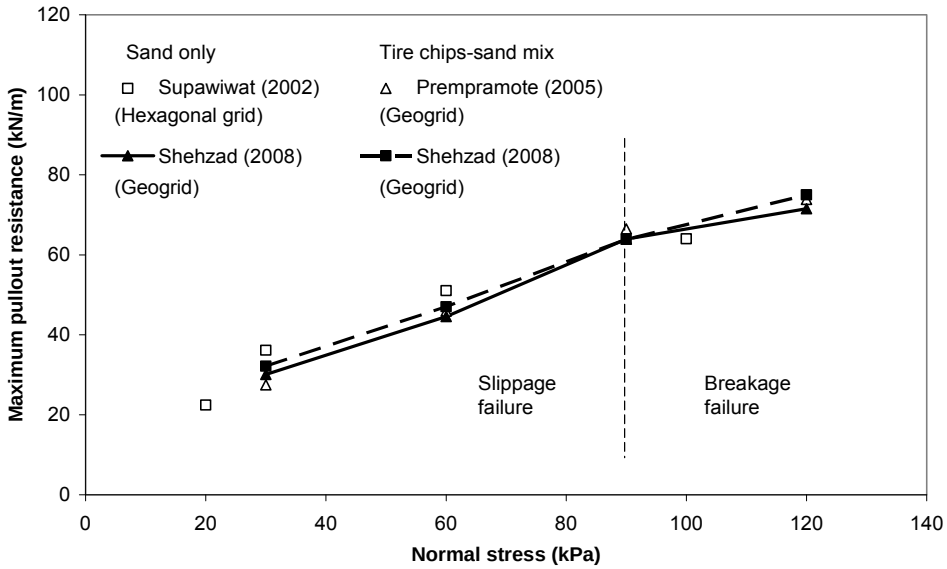

Figure 6. Maximum pullout resistances versus normal stresses for sand and tire chips-sand mixture

On the other hand, the results of the tire chips-sand mixture are quite similar to the previous research. After reaching the maximum pullout resistance, the subsequent values become nearly constant to register the residual strengths. Depending upon the magnitude of the applied normal stress, the failure mode of the geogrid can be divided in two modes, namely: slippage failure and tensile failure. Figure 6 shows that at low normal stresses of 30 and 60 kPa, slippage failures occurred for both sand and tire chips-sand mixture as shown by no tension failure conditions of the geogrid after the test. Moreover, the failure mode is confirmed to be tensile failure at normal stresses of 90 and 120 kPa as indicated in Fig. 6. The tensile failure breakage was observed more in sand as compared to the tire chip-sand mixture.

3.2 Large Scale Direct Shear Test

3.2.1 Backfills Material

In Fig. 7 the direct shear stresses versus direct shear displacements are shown for sand only backfill. For the case of sand only, the direct shear stress increased to maximum and then reduced, and attained an almost constant residual strength at different normal stresses. The displacement required to achieve peak shear stresses varies from 10 to 30 mm. This strain softening behavior is typical of dense sand due to its volume expansion during shear and the consequence interlocking effect.

Figure 8 shows the direct shear test results of the tire chips-sand mixture. The displacement to mobilize the maximum direct shear stresses varies from 30 to 50 mm at different normal stresses. The results show that for tire chips-sand mixture, the results did not exhibit peak shear strength. Instead, the shear strength continued to increase with increasing displacement. However, the maximum displacement was limited due to the limitation of direct shear machine. This finding is consistent with results from previous studies (Prempramote (2005) and Supawiwat (2002)), due to progressive failure in large scale direct shear test.

3.2.2 Backfills Material with Geogrid

The grid reinforcement was placed at failure plane between the upper and lower portion of the shear box. The results of direct shear test with geogrid are plotted in Figs. 9 and 10 for sand and tire chips-sand mixture backfill materials, respectively. The results of direct shear sand and geogrid shows that there is no prominent peak present as compared to the corresponding values without geogrid. The direct shear stresses could be affected by the presence of reinforcement in the failure plane that reduced the contact area between the sand backfill above and below the geogrid. But as the aperture of geogrid was large, it was not very much affecting the shear stresses. In Fig. 10, the results are not very much different from the corresponding results of Prempramote (2005) with similar interaction factor (R=0.92) of the geogrid used in this study (R=0.95). The pullout displacement to attain the maximum shear resistance varied from 5 to 15 mm for sand and 20 to 40 mm for the tire chip-sand backfill.

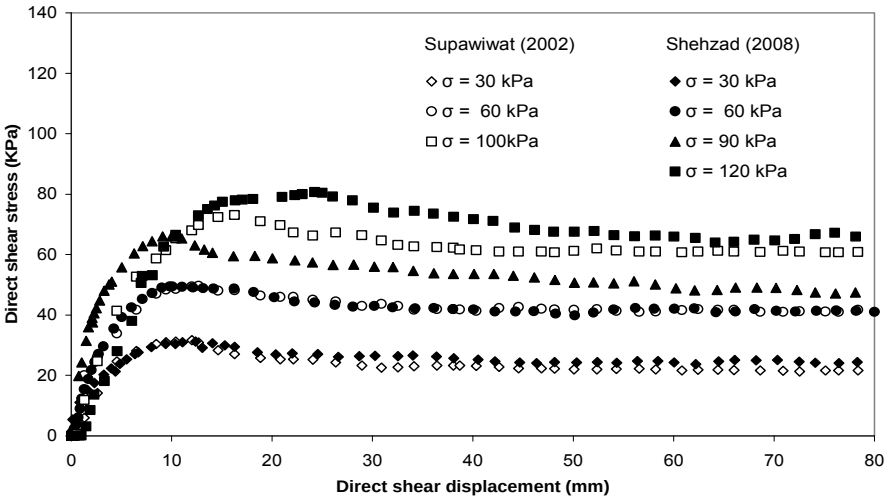

Figure 7. Direct shear stress versus direct shear displacement of sand only

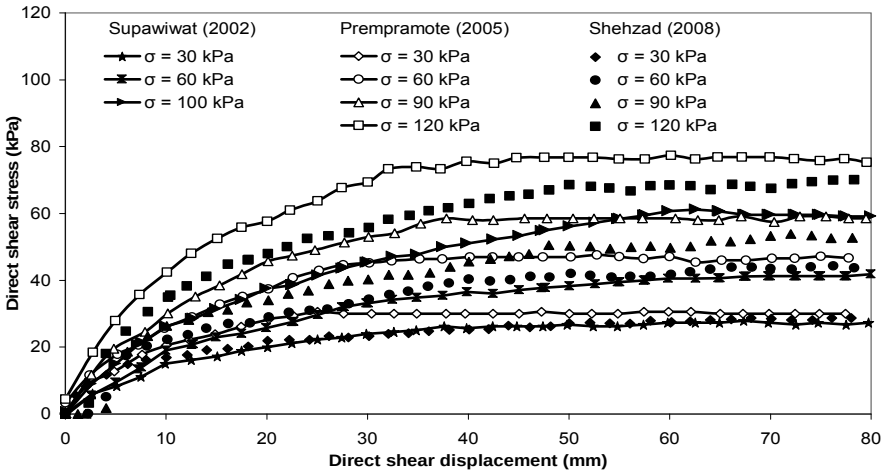

Figure 8. Direct shear stress versus direct shear displacement of tire chips-sand backfill

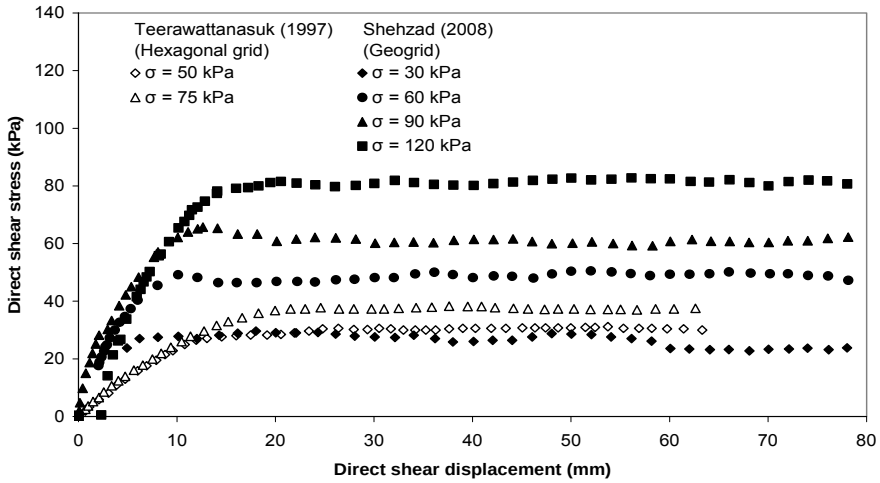

Figure 9. Direct shear stress versus direct shear displacement of geogrid with sand backfill

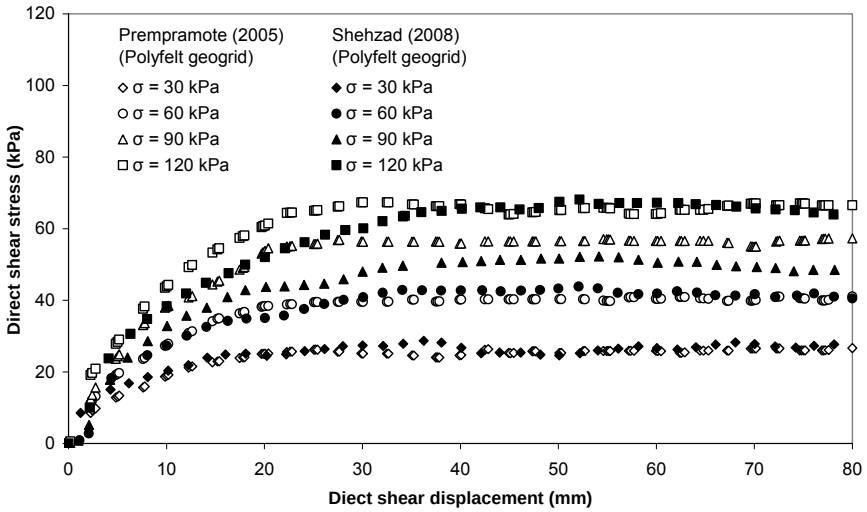

Figure 10. Direct shear stress versus direct shear displacement of geogrid with tire chips-sand backfill

4. NUMERICAL SIMULATIONS

4.1 In-Soil Pullout Test Simulations

In this study, two softwares were used for the numerical simulation of the pullout test. One was the finite element software, PLAXIS 8.2 and second was the finite difference software FLAC V.5. The simulation results of these two softwares were compared.

In case of the finite element software, the model parameters used for the simulation are as follow; elastic model was used for the geogrid element, for sand and tire chips-sand mixture, Mohr-Coulomb elastic perfectly plastic model was used. The modulus of elasticity (E) and poison ratio (v) for both sand and tire chips-sand backfill material were taken from Tanchaisawat et al. (2008). The generated model mesh is shown in Fig. 11.

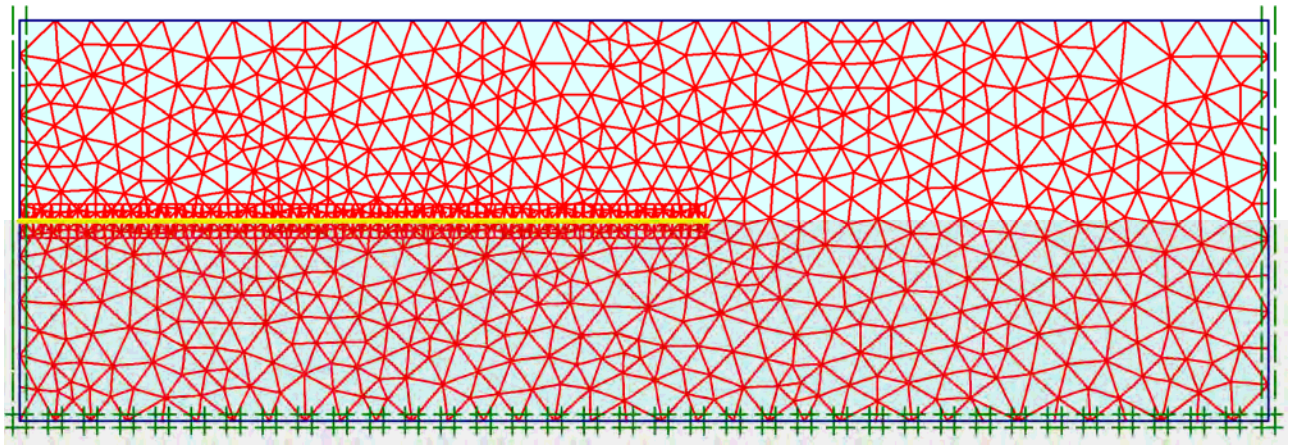

Figure 11. Pullout mesh generated by finite element software (at true scale)

The comparison between laboratory test and predicted results are made in Figs. 12 and 13 for sand only and tire chips-sand mixture, respectively. In case of sand backfill as shown in Fig. 12, the results of simulation captured the overall behavior of the pullout test. The interaction coefficient increased by increasing normal stresses. Another φ-c reduction model was applied on the peak. The function of this model is to make the reduction in φ and c parameters as the stress decreases which is similar to strain softening behavior. After applying the φ-c reduction results improved to some extent.

While prediction of the tire chips-sand mixture (Fig. 13), is quite closer to the measured results including the residual strength.

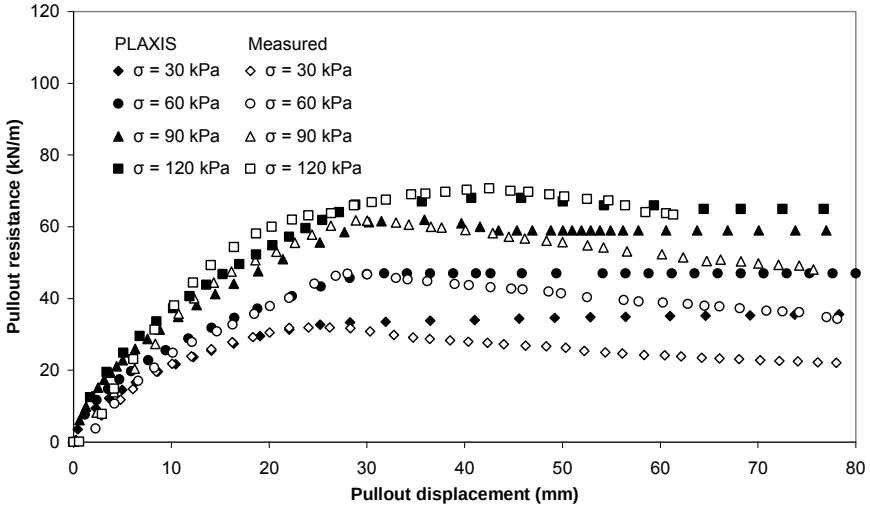

Figure 12. Comparison of measured and predicted pullout resistance from sand backfill using finite element software

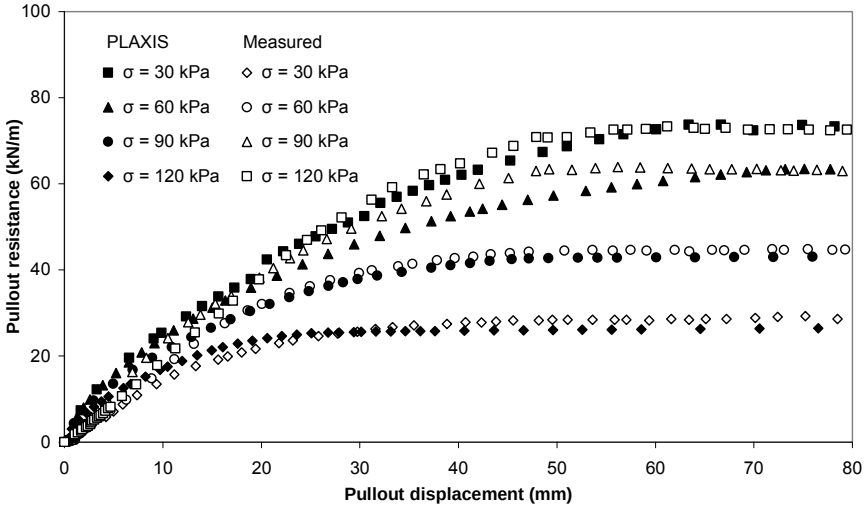

Figure 13. Comparison of measured and predicted pullout resistance from tire chips-sand backfill using finite element software

In case of the finite difference software, pullout test was simulated using the parameters used by the Supawiwat (2002) Mohr-Columb model was used for cable element, simulated the geogrid, with zero bending moment. The hypoplasticity model based on constitutive model proposed by Li and Dafalias (2000) was used for both sand and tire chips-sand mixture. The model mesh of the pullout box was consisted on 26 by 10 elements of perfectly rectangular shape.

From Fig. 14 results shows that the predicted result for the sand only backfill, are describing the behavior of the laboratory test well up to the maximum pullout resistance but after the peak, FLAC results shows only the constant pullout resistance. Because nearly constant was displacement occurred in the reinforcement and did not shows any breakage in the reinforcement as it does in laboratory test, which is similar to previous research by Supawiwat (2002) of the pullout simulation. For tire chips-sand mixture backfill, predicted results by FLAC along with the measured results are plotted in Fig. 15. The predicted results captured the overall behavior of the laboratory test. It is observed that shear stiffness increased by increasing normal stress.

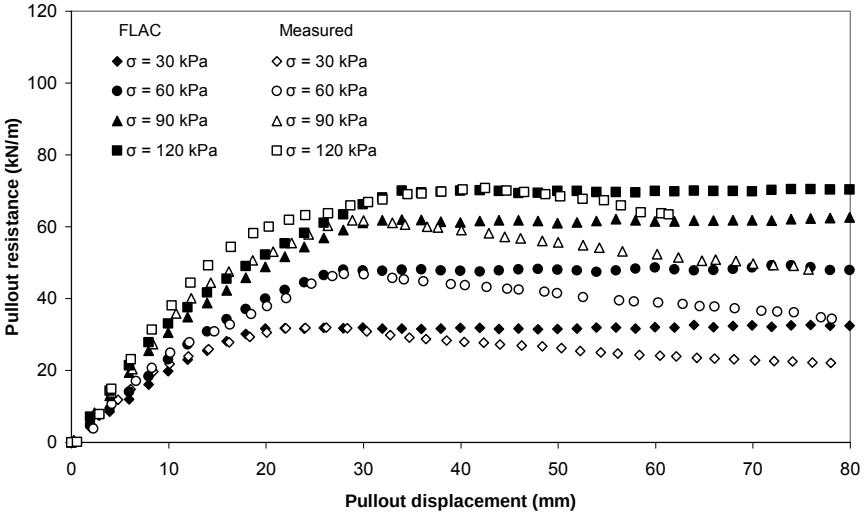

Figure 14. Comparison of measured and predicted pullout resistance from sand backfill using finite difference software

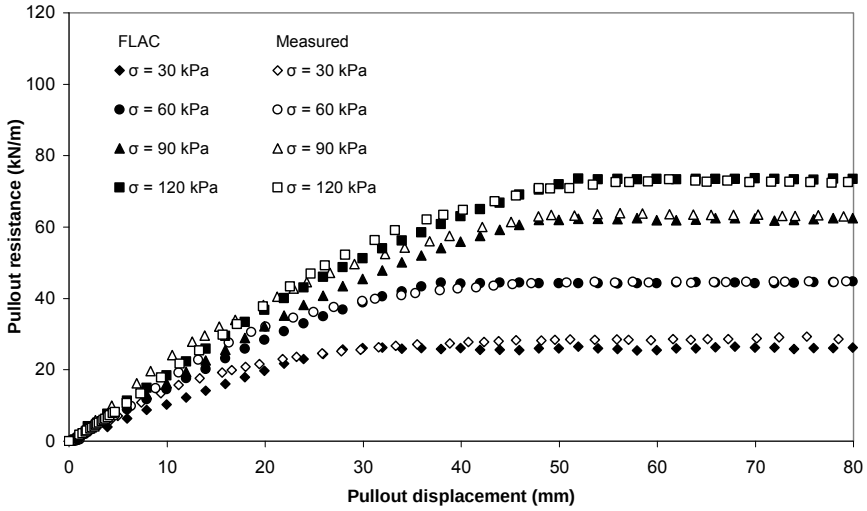

Figure 15. Comparison of measured and predicted pullout resistance from tire chips-sand backfill using finite difference software

5. CONCLUSIONS

Based on the results presented, it can be concluded that; the shear strength parameters of sand and tire chips-sand mixture were determined, have friction angle of 29.8◦ and cohesion of 15.6 kPa. The tire chips-sand mixture was found to have friction angle of 24.4◦ and cohesion 14.3 kPa. The failure envelopes of the pullout resistance show the bilinear behaviour. It was found to be slippage failure at low normal stresses of 30 to 60 kPa and tensile failure at higher normal stresses of 90 to 120 kPa. The interaction coefficients for the pullout test were found to be 0.72 and 0.69 for the sand and tire chips-sand mixture, respectively. For direct shear test, the interaction coefficients were found to be approximately 0.9 for both backfill materials. The results of the numerical simulation reasonably agreed with the measured laboratory results. The simulations from finite element and finite element softwares produced similar predicted results in the pullout tests. The back-calculated from numerical simulations average values of interaction coefficients were found to be similar as to the measured results. The tire chips-sand mixture can be used as lightweight backfill material. As shear strength parameters of the tire chips-sand mixture are only slightly less than the sand and 30% weight reduction can be achieved by replacing sand with tire chips-mixture.

REFERENCES

Aydilek, A. H., Madden, E. T., and Demirkan, M. M., (2006). Field evaluation of lechate collection system costructed with scrap tires, *Journal of Geotechnical and Geoenvironmental Engineering*, ASCE, Vol. 132, No.8, pp. 990-1000.

Li, X. S., and Dafalias, Y. F., (2000). Dilatancy for cohesionless soils, *Geotechnique*, Vol. 50, No.4, pp.449-460.

Prempramote, S., (2005). Interaction between geogrid reinforcement and tire chip-sand mixture, *M. Eng. Thesis No. GE-04-12*, Asian Institute of Technology, Thailand.

Shehzad, K., (2008), Interaction between geogrid and sand with/without tire chips including sensitivity analyses and simulations, *M. Eng. Thesis No. GE-07-04,* Asian Institute of Technology, Thailand

Supawiwat, N., (2002), Behavior of shredded rubber tires with and without sand, its interaction with hexagonal wire reinforcement and their numerical simulation, *M.Eng. Thesis GE-01-14,* Asian Institute of Technology, Thailand.

Tanchaisawat, T., Bergado, D. T., and Voottipruex, P., (2008). Numerical simulation and sensitivity analyses of full scale test embankment with reinforced lightweight geomaterials on soft bangkok clay, *Geotextiles and Geomembranes,* Vol. 26, No. 6, pp. 498-511.

Tanchaisawat, T., Bergado, D. T., and Kanjananak T., (2007). Lightweight geomaterials for bridge appoach utilization, *Proceedings 16th Southeast Asian Geotechnical Conference 2007*, Subang Jaya, Malaysia, pp. 8-11.

Tatlisoz, N., Edil T. B. and Benson, C. H., (1998). Interaction between reinforcing geosynthetics and soil-tire chip mixtures, *Journal of Geotechnical and Geoenvironmental Engineering*, ASCE, Vol. 124, No. 11, pp. 1109-1119.

Geosynthetics 2009
February 25-27 2009, Salt Lake City, Utah

Comparison of Finite Element and Limit Equilibrium Methods in the Stability Analysis of Reinforced and Unreinforced Soil Slopes

A. Farhadi, Tarbiat Moallem University, Tehran, Iran

ABSTRACT

In the stability assessment of reinforced and unreinforced soil slopes, factor of safety is the primary index for determining the failure condition. The limit equilibrium techniques are the most commonly-used analysis methods. Recently the finite element method has gained popularity among geotechnical engineers due to its low cost and significant computing characteristics.

In this paper the stability of a 20m height soil slope is evaluated with both conventional limit equilibrium and finite element methods using ReSSA (2.0) and PLAXIS software's for reinforced and unreinforced soil conditions. The results show an agreement between the two methods of evaluation and also indicate significant increase in the amount of safety factor under reinforced conditions.

1. INTRODUCTION

Soil materials are usually known to be weak in tension. Reinforcement can improve the strength and bearing capacity of soils. Geosynthetics (i.e.,geotextiles, geogrids etc.) are increasingly being used as reinforcing members in construction of earth structures. However in this group, geogrids are more commonly used in practice.

A major requirement in the design of reinforced structures is to assure their stability. There are a few analytical approaches, essentially extended from simplified limit-equilibrium methods (e.g.,Christite and El-Hadi (1977); Ignold (1982)). These methods have been used for safety design of non-reinforced slope. The extension of this method is used for designing of reinforced slope. A number of different techniques are covered by limit equilibrium method. Bishop's simplified method, utilizing a circular arc slip surface, is probably the most popular limit equilibrium method. The basic idea of this method is to find a failure through the slope and then divide the failed mass into slices. Conditions of equilibrium are enforced on the slices and the factor of safety of the slope is determined by taking a ratio of driving forces over the resisting forces. Although Bishop's method is not rigorous in a sense that it does not satisfy horizontal force limit equilibrium, it is simple to apply and, in many practical problems, it yields results close to rigorous limit equilibrium methods.

There are numerous limit equilibrium methods developed to deal with stability of geotextile reinforced slope. Koerner (1990) examined a procedure based on limit equilibrium in reinforced cohesive soils. The strength parameters (C and φ) of soil are considered in analysis. Mechanisms of rotational and transitional failure of reinforced soils were reported by Leshchinsky and Reinschmidt (1985). Leshchinsky and Boedker (1989) proposed a method for stability analysis of reinforced soil, the internal and external stability were considered. Internal stability analyses are based on the limit equilibrium principals and external stability on the basis of spreading the bilinear cone method.

A comprehensive and instructive overview of the many aspects associated with geosynthetics reinforcement is given by Bonaparte et al. (1985). Murray. (1982) developed a method based on simplified limit equilibrium approaches considered the effect of vertical distance between reinforcing elements in slope. Schneider and Holtz. (1986) introduced a designing method for the reinforced slopes using geotextiles and geogrids. The strain compatibility in design of reinforced soil structure was reported by Wallace and Fluet (1987). Schmertmann et al. (1987) examined a design chart for reinforced slopes based on limit equilibrium. Verduin and Holtz (1989), Langston and Williams. (1989) and Jewell. (1982) also proposed designing methods for reinforced earth structure. In this work the stability of un-reinforced and reinforced slope is analyzed based on limit equilibrium and finite element methods. The results are presented and comparison between finite element and limit equilibrium methods in the stability analysis is discussed.

2. MATERIAL PROPERTIES AND SLOPE GEOMETRY

A slope of 20 meters height with upper and lower parts and 6o degrees inclination is considered for stability analysis in both un-reinforced and reinforced conditions. The material properties of embankment, rip-rap layer under the slope's toe and foundation are shown in Tab.1. Properties of geogrids used in this work are shown in Tab. 2.

Tab. 1. Properties of Soil Embankment Slope and Foundation

Parameters / Material	ν	φ (Degree)	C (kN/m^2)	$\gamma_{d(max)}$ (kN/m^3)	γ_{wt} (kN/m^3)	K (m/s)	E (kN/m^2)
Embankment	0.3	32	5	19.5	21.5	1×10^{-5}	40000
Rip-Rap layer under the toe of the slope	0.28	48	0	23	24	1×10^{-4}	65000
Foundation	0.23	45	85	26	27	1×10^{-6}	180000

Tab. 2. Properties of Geogrids

Height (m)	*T_{ult} (kN/m)*	*EA (kN/m)*
0 - 1.8	*160*	*2190*
1.8 - 10.2	*120*	*1640*
10.2 - 16.2	*90*	*1230*
16.2 - 19.6	*60*	*820*

3. METHOD OF APPROACH

In this work an arbitrary slope is considered for stability analysis in reinforced and un-reinforced conditions. First, a computer model of the un-reinforced slope is considered and the limit and initial conditions are defined. Stability analysis is performed in both static and pseudo conditions by ReSSA (2.0) and PLAXIS computer programs. Factor of safety is determined as shown on table 3. In order to determine the effect of reinforcement in the factor of safety, the slope is n reinforced using Jewell (Jewell. 1996) and Schmertmann et al. (1987) methods. The height of the slope is divided into four zone and usage various types of geogrids with different strength properties. The properties of and the arrangement of the geogrids used at different heights is shown in table 2. and Fig1(a) and 1(b). Based on the results given by the mentioned methods, stability analyses are performed in both static and pseudo static conditions by limit equilibrium (LE) and finite element (FE) methods, using ReSSA (2.0) and PLAXIS software's.

.

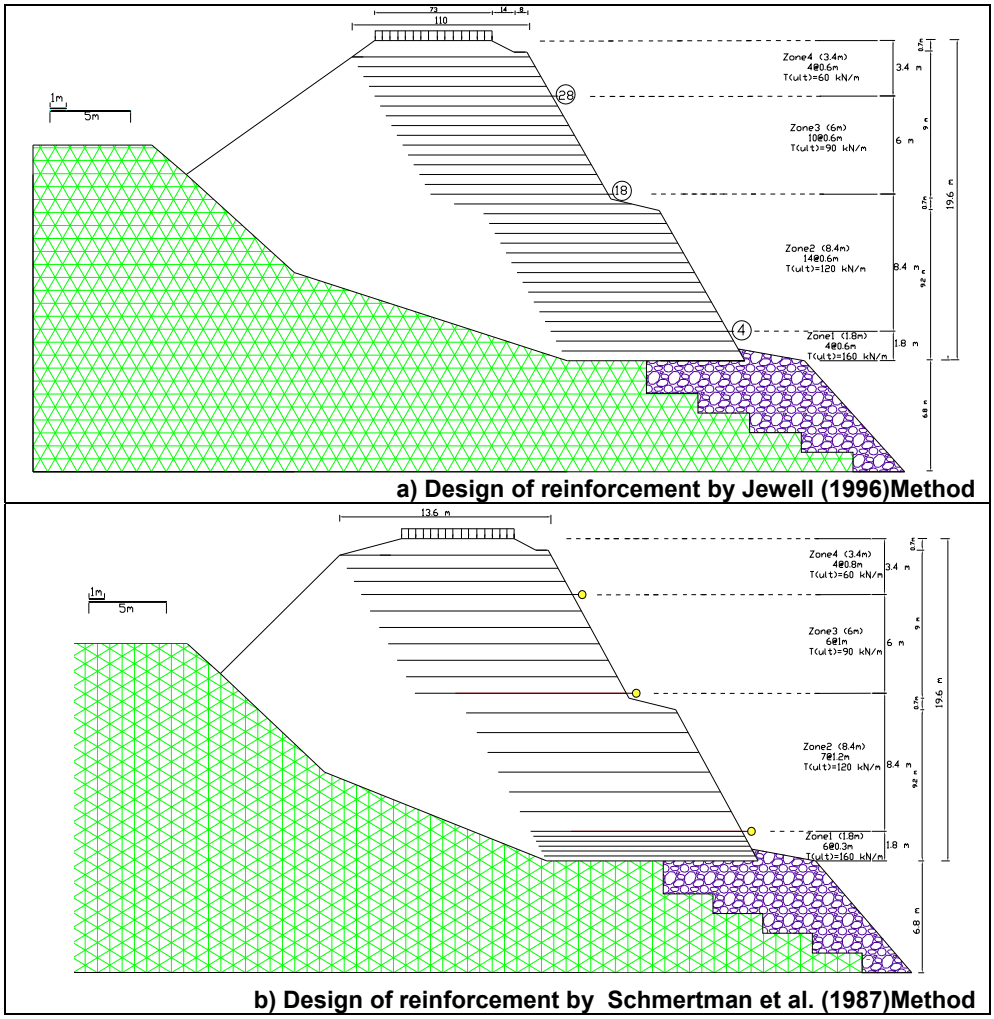

FIG. 1. Design of Reinforcement by Schmertman et al. (1987) and Jewell (1996) Methods

4. ANALYSIS

Two types of analysis were performed. One is based on limit equilibrium (LE) method. The second is based on finite element (FE) method. K_h in both static and pseudo static conditions are assumed to be 2.

4.1 Limit Equilibrium (LE) Method

ReSSA (2.0) software developed by (ADAMA Engineering, 2006), was utilized to generate the results in this work. This software is developed based on the limit equilibrium method and can perform stability analyses for a slope by Bishop, Spencer and definable tri-cone methods. ReSSA has also the capability of performing pseudo static analyses in dynamic conditions by choosing a constant coefficient as an input parameter. Defined discussion of this software can also be finding in the literature by Leshchinsky (2002). The material properties of soil and foundation shown in Tab.1 are chosen as an input data for computer program. The results are presented in Tab.3 and Fig. 2. The results show that the factor of safety is considerably increased in both static and pseudo static conditions in reinforced slope.

Table 1: Results of the Stability Analysis using ReSSA (2.0)

Reinforcement Design by Schmertman et al. Method			Reinforcement Design by Jewell Method			Un-reinforced			Reinforcement Type	
Trilinear Cone	Bilinear Cone	Circular Cone	Trilinear Cone	Bilinear Cone	Circular Cone	Trilinear Cone	Bilinear Cone	Circular Cone	Analysis Method	
1.78	*1.55*	*1.72*	*1.99*	*1.63*	*1.81*	*1.1*	*1.03*	*1.08*	Static Condition	Factor of Safety
1.43	*1.26*	*1.39*	*1.54*	*1.31*	*1.48*	*0.9*	*0.72*	*0.84*	Pseudo Static Condition	

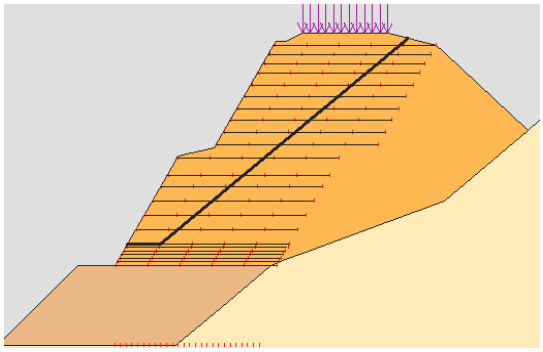

b- Spencer method (bilinear cone)

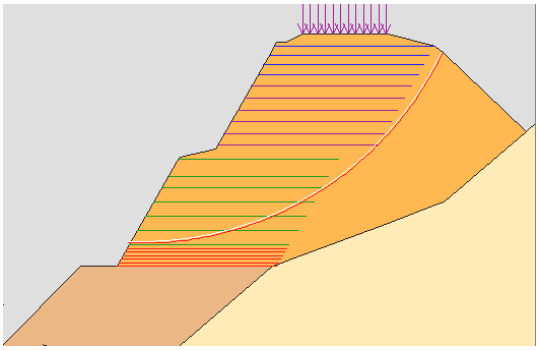

a- Bishop method (circular cone)

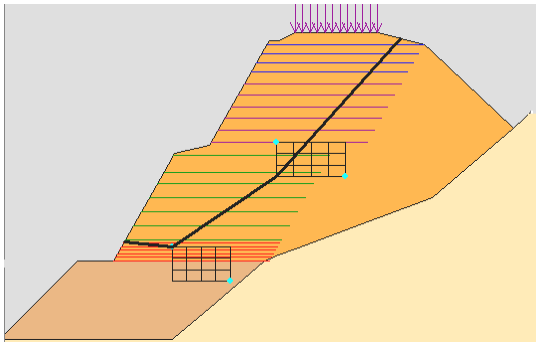

c- Spencer method (trilinear cone)

FIG. 2. Stability Analysis of Reinforced Slope by ReSSA (2.0) using Schmerman Method

4.2 Finite Element (FE) Method

PLAXIS software using finite element approach was adopted in this study. Strength reduction technique is used in PLAXIS to solve factor of safety consistent with limit equilibrium and slope stability. The slope is modeled as shown in Fig. 3. Limit and initial conditions and material properties are defined. The value of 1.25 is assumed for K_h in pseudo static calculation. Stability analysis is performed by software. The results are presented in Tab. 3 and show the increased the factor of safety in reinforced slope in comparison with un-reinforced condition.

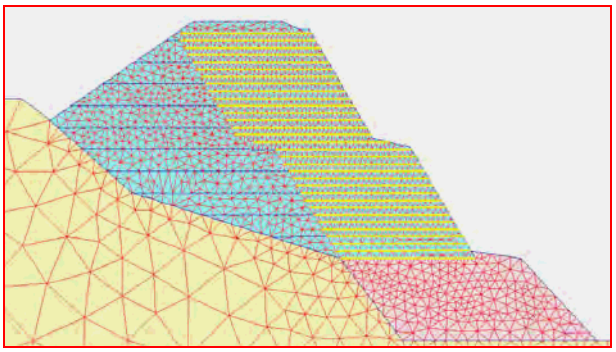

FIG. 3. Finite Element Model of Reinforced Slope in PLAXIS by Jewell Method

Table 4. Results of Stability Analysis by PLAXIS

Reinforcement Designed by Schmertman et al. Method	Reinforcement Designed by Jewell Method	Unreinforced	Reinforcement Type	
1.58	*1.62*	*1.09*	Static Condition	Factor of Safety
1.26	*1.32*	*0.87*	Pseudo Static Condition	

5. CONCLUSION

Limit equilibrium and finite element analysis were performed in this study to investigate the stability of un-reinforced and reinforced slope and also the effect of reinforcement on the factor of safety. The comparative analyses indicate the following.

1- In un-reinforced slope, the factor of safety about 1 is obtained, which shows the necessity of reinforcement.

2- Properly used slope stability limit equilibrium analysis of reinforced slope yields nearly the same factor of safety against failure as the finite element analysis. The observed agreement indicate that the limit equilibrium approach can be used to determined the required tensile strength and the layout of reinforcement for slope.

3- In this work, Bishop's circular arc analysis yield higher factor of safety compare to Spencer method. This difference is due to the assumptions made in each method. Since the Spencer method is more similar to the finite element method, it can be concluded that this method presents more realistic results compare to the other limit equilibrium methods

4- Numerical analysis can be a suitable approach for stability analysis in reinforced and unreinforced slopes. However it must be noted that such an analysis do not indicate the needs of instrumentation for monitoring the behavior of an important earth structures such as embankment dams and slopes.

REFERENCES

ADAMA Engineering Inc. (2006), *ReSSA Version 2.0*, Newark, Delaware, USA.

Chouery, V.E., Watson, C.H. and Berg, R.R. (1989), *Critical failure planes in analysis of reinforced slope*, in Proceedings of Geosynthetics 89 Conference, San Diego, USA: 78-269.

Christie, I. F., and El-Hadi, K. M. (1977), Some aspects of the design of earth dams reinforced with fabric, Proc., Int. Conf. on the Use of Fabrics in Geotechnics, Paris, France, 1, 99-103.

Ingold, T. S. (1982), An analytical study of geotextile reinforced embankment. Proc., 2nd Int. Conf. on Geotextiles, Las Vegas, Nev., Industrial Fabrics Association Int., 3, 683-688.

Jewell, R.A. (1982). *A limit equilibrium design method for reinforced embankments on soft foundations*, in Proceedings of the Second International Conference on Geotextiles, Las Vegas, Nevada, USA, 3: 6-671.

Jewell, R. A. (1996). *Soil Reinforcement with Geotextiles*, Chapter 8, CIRIA ISBN 0 86017 425 5, Thomas Telford ISBN 0 7277 2502 5, 332p.

John, N. W. M. (1987). *Geotextiles*, Blackie and Son, Glasgow.

Jones, C.J.F.R. (1985). Earth *reinforcement and soil structures*, London: Butterworth (Thomas Telford Edition, London, 1996).

Leshchinsky, D. and Boedecker, R.H. (1989). *Geosynthetic reinforced soil structures*, Journal of Geotechnical Engineering, ASCE, 115: 1278-1459.

Leshchinsky,D. and Han,Jie. (2004). *Geosynthetic reinforced* multitiered wall, Journal of Geotechnical and Geoenviromental Engineering, ASCE, 130: 1225-1235.

Leshchinsky, D. and Reinschmidt, A.J. (1985). *Stability of membrane reinforced slopes*, Journal of Geotechnical Engineering, ASCE, 111: 1279-1285.

Long, N.T., Guegan, Y. and Legeay, G. (1972). *Etude de la terre armee a lappareil triaxial*, Rap. De Recherche (17), Paris: LCPC.

Murray, R. (1982). *Fabric reinforcement of embankments and cuttings*, in Proceedings of the Second International Conference on Geotextiles, Las Vegas, Nevada, USA, 3: 13-707.

Rowe, R.K. (1984), *Reinforced embankment: analysis and design*, American Society of Civil Engineers, Journal of Geotechnical Engineering, ASCE, 110: 145-231.

Schmertmann, G.R., Chouery-Curtis, V.E., Johnson, R.D. and Bonaparte, R. (1987). *Design charts for geogrid reinforced soil slopes*, in Proceedings of Geosynthetics '87 Conference, New Orleans, USA: 20-108.

Schneider, H.R. and Holtz, R.D. (1986). *Design of slopes reinforced with geotextile and geogrid*, Geotextiles and Geomembrane, 3: 29-51.

Sharma, H.D. (1991). *Embankment Dams*, Oxford & IBH Publication Co. PVT. LTD., New Delhi, Bombay, Calcutta.

Sherclif, D.A. (1990). *Reinforced Embankments: Theory and Practice*, London, Thomas Telford.

Verduin, J.R. and Holtz, R.D. (1989), *Geosynthetically reinforced slopes: a new procedure*, in Proceedings of Geosynthetics '89 Conference, San Diego, USA: 90-279.

Vidal, H. (1969). *The Principle of Reinforced Earth*, Highway Research Record 282: 1-16.

Wallace, R.B. and Fluet, J.E. (1987), *Slope reinforcement using geogrid*, in Proceedings of Geosynthetics '87 Conference, New Orleans, USA, 32-121.

Geosynthetics 2009
February 25-27 2009, Salt Lake City, Utah

HDPE Geomembranes – Reaching 30 Years, What's Next: or How Much Longer Will My Liner Last?

I.D. Peggs, I-CORP INTERNATIONAL, Inc., Ocean Ridge, FL, USA

ABSTRACT
With the increased use of exposed HDPE geomembrane liners, service lives approaching 30 years, some end-of-lifetimes occurring within 15 years, and increasing regulatory monitoring and auditing required, it becomes advantageous to be able to practically and meaningfully assess any HDPE liner's remaining service lifetime. End-of-lifetime will be a function of HDPE resin used (stress cracking resistance), type of surface texture, formulation of stabilizer additive package (oxidation and UV protection), service temperature range (oxidation and expansion/contraction), and service tensile stress range. A program of liner inspection and periodic sampling, testing, is proposed that will provide a few years warning of end-of-lifetime, thereby facilitating the planning of liner replacement (if necessary) and avoiding potential contamination events and costly remediation works.

1. INTRODUCTION

While there have been many attempts (Hsuan and Koerner, 1998, Sangam and Rowe, 2002, Müller, 2007) to assess the lifetimes of HDPE geomembranes in covered landfill environments there has been only one attempt to assess lifetimes of exposed HDPE (Koerner, 2008). This laboratory research study is, of course, applicable only to the specific HDPE geomembrane(s) tested because lifetime is a function of the HDPE resin used, the specific antioxidant (AO) formulation incorporated in the geomembrane, and the specific environment simulated (Texas, USA). Different resins, different AO formulations (proprietary to each resin and geomembrane manufacturer) and different environments will affect the actual lifetime significantly.

In practice, while it is useful to know the approximate lifetime required of an "HDPE" geomembrane that will be installed in a project, so that one with an appropriate lifetime may be specified, it is probably of more interest to facility owners and their insurance carriers to know what are the remaining lifetimes of the exposed liners that have been installed and that have been providing service for 15, 20, or 35 years already. Best management practice is to get a few years notice of impending end of lifetime (EOL) so that liner replacement can be planned rather than to be faced with a high profile unexpected failure that results in groundwater contamination and extremely costly remediation works.

It is generally agreed (Hsuan and Koerner, 1998, Koch et al., 1988) that EOL will occur when the liner suffers excessive thermal and photo-induced oxidation as a result of high temperatures and ultraviolet radiation (UVR). The liner will then become embrittled and fail by a process of stress cracking (SC) initiated on the exposed surface. Therefore, while the HDPE geomembrane industry successfully resolved the fundamental SC problems of the 1980s by improving resins and additive formulations, a resurgence of SC failures as older HDPE geomembranes reach EOL will inevitably be seen.

For instance, a liner manufactured in 1993 to National Sanitation Foundation (NSF) Standard 54, and with a SC resistance (SCR) in the ASTM D5397 test of over 200 hr failed at EOL in a hot/cold environment by SC at stressed locations after only 15 years (Peggs, 2008). Unquestionably, there were other HDPE geomembranes made in 1993 using other resins and formulations that would still have many years to EOL in the same application. But how many years: 2, 20, or more? Now that HDPE geomembranes are achieving lifetimes of 30 and 35 years such questions are increasingly being asked by many facility owners and regulators. In some jurisdictions leachate pond liners and fuel tank secondary containment liners must be tested every 5 years to ensure they are not damaged.

In another instance a PE cap with many fixed pipe penetrations suffered extensive differential settlement therefore requiring a protocol for assessing the extent of local damage in order to proactively make modifications before large areas of lack of containment occurred. Not only does the rate of degradation depend on the HDPE resin used and the AO formulation, but the reduction of active AO components is also accelerated under stress (Czerny, 1972, Müller 2007). Thus thermal oxidation, UV degradation, and induced stresses act synergistically. Consequently, it is impossible to predict the lifetime of a newly installed HDPE liner.

Therefore, the rate of degradation and the remaining lifetime are a primary function of the project specific environment. A general procedure and a suite of appropriate tests for evaluating the remaining time to EOL of an exposed HDPE geomembrane in any environment are proposed.

2. SITE AND LINER EXAMINATION

For each installation a baseline of material properties must be established from which changes are monitored.

For baseline data it would be ideal to have some archive material that has been stored at room temperature and away from UVR to test, but such is not usually available. Manufacturers often discard retained samples after about 5 years. Facility owners should be encouraged to keep retained as-manufactured samples. The next best option is to use material from the anchor trench or elsewhere in the installation that has not experienced extremes in temperature and that has not been exposed to UVR or to expansion/contraction stresses.

Less satisfactory options are to use the original specifications (perhaps NSF-54), the project specifications, the manufacturer's specifications, or the GRI-GM13 specifications in effect at the time of liner manufacturing. The concern with using these specifications is that while aged material may still meet them, there is no indication of whether or not the measured values have significantly decreased from the actual as-manufactured values that generally significantly exceed the specifications

A final option for obtaining the baseline data would be to use the property values at the time of the first liner sampling and assessment.

The first liner condition assessment consists of a site visit during which a general visual examination is performed together with a mechanical probing of the edges of welds. Welds, particularly extrusion welds, are the primary sites of initial SC due to the added thermal energy input (oxidation), stress concentrating notch geometries, and modified geomembrane microstructures. A visual examination includes the black/grey shades of different panels that might indicate low carbon contents and decreased resistance to SCR. A closer examination is made using a magnifying loupe (eyeglass) on suspect areas such as wrinkle peaks (Figure 1), stone protuberances (Figure 2), the tops and edges of multiple extrusion weld beads, and the apex-down creases of round die manufactured sheet. The last detail is of significance because the combination of oxidizing surface and exposed surface tension when the liner contracts at low temperatures (the fold is pulled flat) can be one of the first locations to crack. Conversely, the apex-up creases do not fail at the same time because the oxidized exposed surface is under compression (or lower tension) when the crease is flattened out (Peggs, 2008).

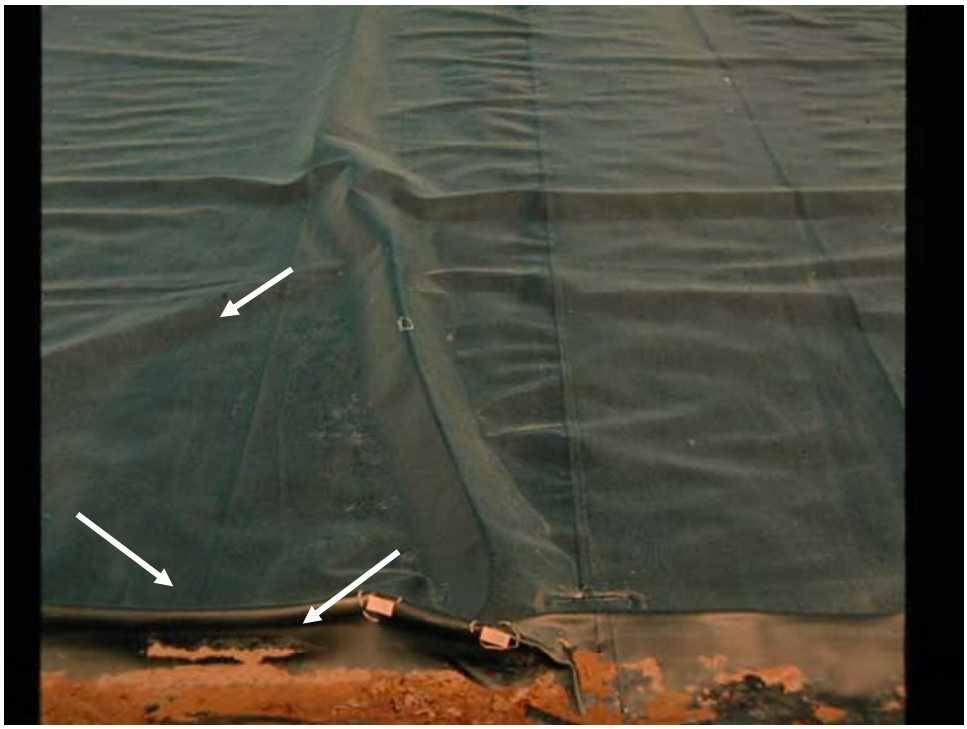

Figure 1 Isolated locations (arrowed) of stress cracking on wrinkles of HDPE liner in black liquor pond

Figure 2 Stress cracks initiated at extrusion die line above protruding subgrade stone

It may be appropriate, but probably not in most cases, to do a water lance electrical integrity survey on the exposed side slopes, but this would only be effective on single liners and double liners made with a composite primary liner with an electrically conductive layer (GCL, conductive geotextile, or integrated conductive layer) immediately under the primary geomembrane. Any leaks that are found would be investigated for their cause.

3. MATERIAL TESTING

A liner lifetime evaluation program should be simple, meaningful, and cost-effective. While it will initially require expert polymer materials science/engineering input to examine and sample the installed liner, to prepare a test program, to analyze the initial test data, and to define the critical parameters, it should ultimately be possible to use an expert system to automatically make predictions using the input test data.

Assuming a lack of original archive material, small samples will be taken from deep down in the anchor trench and from appropriate exposed locations. Potential sites for future removal of samples by the facility owner for future testing will be identified and marked by the expert during the first site visit.

The baseline sample(s) are tested as follows:

- Melt Index (ASTM D1238 (190/2.16)).
- Single point stress cracking resistance [SCR] on a molded plaque by ASTM D5397.
- High pressure oxidative induction time (HP-OIT) by ASTM D5885.
- Fourier transform infrared spectroscopy (FTIR - ATR) on upper surface to determine carbonyl index (CI), on non-archive samples only.
- Oven aging/HP-OIT (GRI-GM13).
- UV resistance/HP-OIT (GRI-GM13).

The exposed samples are tested as follows:

- Melt Index (ASTM D1238 (190/2.16)).
- Carbon content (ASTM D1603).
- Carbon dispersion (ASTM D5596).
- Single point SCR on molded plaque (ASTM D5397).
- Light microscopy of exposed surface, through-thickness cross sections, and thin microsections (~15 µm thick) as necessary.
- HP-OIT on 0.5 mm thick exposed surface layers from basic sheet and from sheet at edge of extruded weld bead preferably at a double weld bead (ASTM D5885).
- FTIR-ATR on exposed surface to determine CI.
- Oven aging/HP-OIT on 0.5 mm surface layer (GRI.GM13).
- UV resistance/HP-OIT on 0.5 mm surface layer (GRI.GM13).

Melt Index is done to assess relative changes in molecular weight (chain scission, cross-linking).

Carbon content is done to assess basic UV protection.

Carbon dispersion is done to assess uniformity of surface UV protection and to check presence of agglomerates that might act as initiation sites for SC.

Stress cracking is performed on plaques to homogenize the geomembrane material and to preclude the situation where the root of the specimen notch is in the as-manufactured oriented microstructure and not in the oxidized surface layer. The latter would not indicate relevant changes (Peggs and Elie, 2008)

HP-OIT is used to assess the remaining amount of stabilizer additives, both in the liner panels and in the sheet adjacent to extrusion welds. Most stress cracking is observed at the edges of extrusion weld beads in the lower sheet where the material is more highly oxidized, where there are stress-concentrating geometries, where there may be grinding damage, and where the melting has locally homogenized the microstructure. It is extremely important to monitor this location. The 0.5 mm surface layer is removed by carefully cutting several small liner samples.

While standard OIT (S-OIT) (ASTM D3895 at 200°C) better assesses the relevant stabilizers effective at processing (melting) and welding temperatures, the relevant changes in effective stabilizer content during continued service (including in the weld zones) will be provided by measurement of HP-OIT. There will be no future high temperature events, except for the occasional repair welds, where knowledge of S-OIT will be useful. Therefore, S-OIT is not considered relevant in this program.

Note that HP-OIT is measured on a thin surface layer because the surface layer may be oxidized while the body of the geomembrane may not. If material from the full thickness of the geomembrane is used it could show a significant value of OIT implying that there is still stabilizer present and that oxidation is far from occurring. However, the surface layer could be fully oxidized with stress cracks already initiated and propagating. For instance, if a surface layer with a thickness of 10% of the geomembrane thickness is fully oxidized, and the remaining 90 % retains 50% of the additive, the overall retained OIT will be 45%. Despite the “high” retained OIT the surface condition is susceptible to SC initiation. A crack will then propagate more easily through unoxidized material than would initiation and propagation occur in unoxidized material. Such performance is implied by Hsuan et al., 2008 and by Boehning et al., 2008. who both showed (Figures 3 and 4) that reductions in break elongations start to occur when HP-OIT retained, or stabilizer remaining, are about 10 - 20% of original.

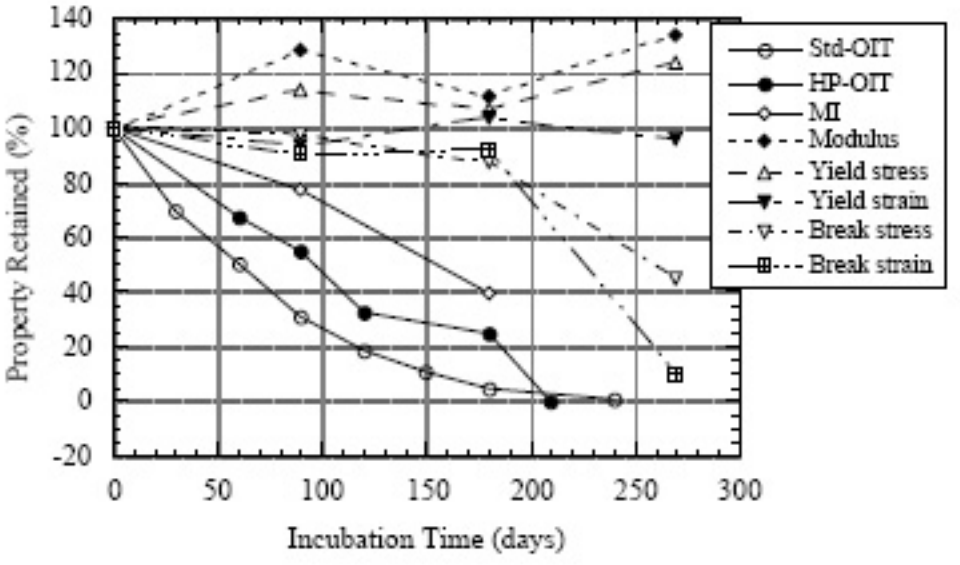

Figure 3. Change in break and OIT properties with exposure time (Hsuan, 2008)

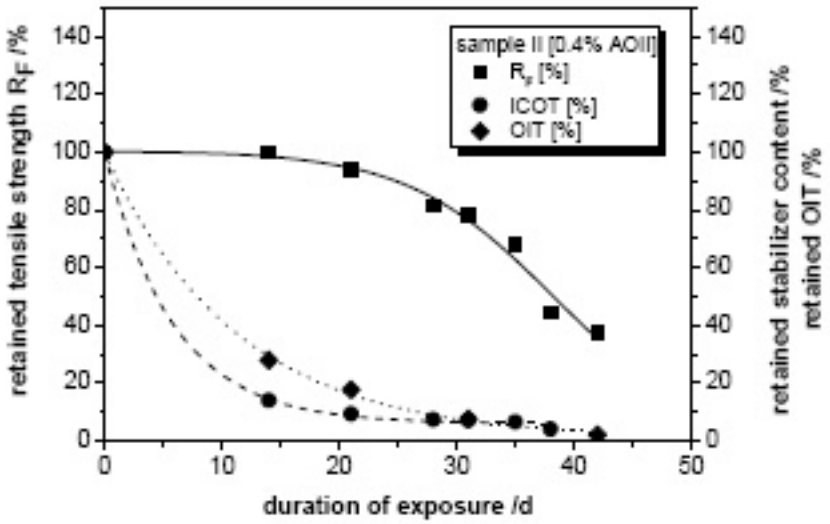

Figure 4. Change in break and AO with exposure time (Boehning et al., 2008)

The fact that the HP-OIT meets a certain specification value in the as-manufactured condition provides no guarantee that thermo- and photo-oxidation protection will be provided for a long time. Stabilizers might be consumed quickly or slowly while providing protection. They may also be consumed quickly to begin with then more slowly, or vice versa. Hence the need for inclusion of oven (thermal) aging and UV resistance tests in the evaluation program. These two parameters, assessed by measuring retained HP- OIT, are critical to the assessment of remaining service life.

Oven (thermal) aging and UV resistance tests performed in this program will provide an extremely valuable data base that relates laboratory testing to in-service performance and that will further aid in more accurately projecting in-service performance from laboratory testing results.

Because we do not know for sure, by OIT measurements alone, whether the surface layer is or is not oxidized (unless OIT is zero), and since we do not yet know at what level of OIT loss there might be an oxidized surface layer (the data base has not

yet been generated), FTIR directly on the surface of the geomembrane is performed using the attenuated total reflectance (ATR) technique to deny or confirm the presence of oxidation products (carbonyl groups).

Following the practice of Broutman and Duvall (1989) and Duvall (2002) on HDPE pipes, if the ratio of the carbonyl stretching peak at wave number ~1740 cm^{-1} and the C-H bending (PE) peak at wave number 1460 cm^{-1} (the Carbonyl Index) is over 0.10 (Figures 5 and 6) there is a sufficiently oxidized surface layer that stress cracking might be initiated.

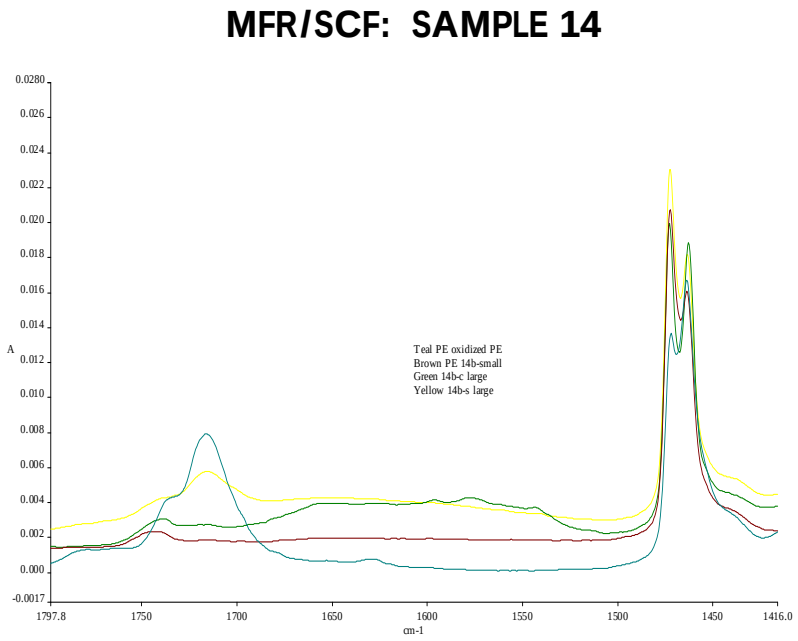

Figure 5. Typical FTIR scan of oxidized (blue) and unoxidized (red/green) HDPE (Tisinger (2008), Peggs, (2008)).

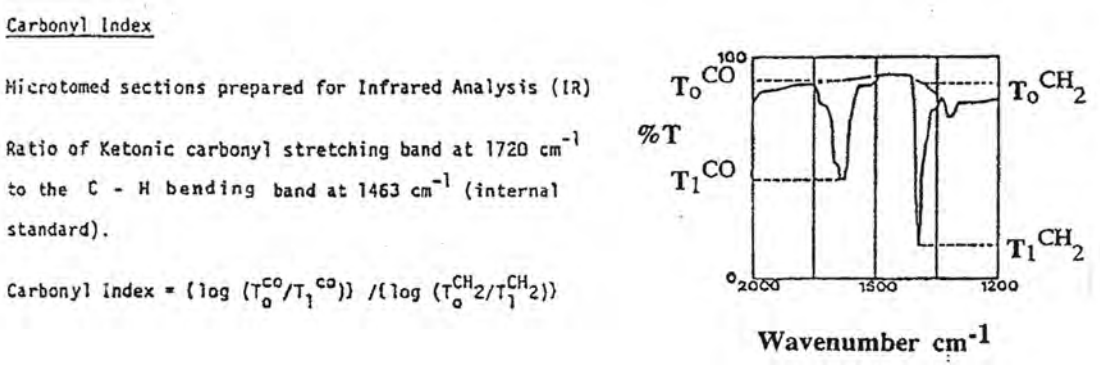

Figure 6. Calculation of Carbonyl Index (Broutman and Duvall, 1989)

Thus the surface microstructural details, where the first indication of EOL will occur, are interrogated in three stages:

1. Has the material lost AO protection?
2. Has enough AO been lost that the surface is oxidized?
3. Has the surface been oxidized to a level that SC has been initiated?

If SC has indeed been initiated EOL is approaching relatively rapidly.

4. LOOKING AHEAD

With the first field assessment test results available, and the extent of changes from the baseline sample known, removal of a second set of samples by the facility owner (at locations previously identified and marked by the initial expert surveyor) will be planned for a future time, probably in two or three years. The extent of changes over two or three sampling and testing procedures will identify the significantly changing parameters on which future assessments may be focused.

It is expected that after two or three test cycles, over periods of 2 to 5 years after the first site visit, it will be possible to get at least 2 to 3 years notice of liner EOL.

5. CONCLUSIONS

The potential end-of-lifetime failure mode, oxidation and stress cracking, of exposed HDPE geomembrane liners has been described.

A site inspection, sampling and testing program for the assessment of remaining service lifetime of HDPE liners in any environment has been outlined.

It is expected that a few year's warning of end-of lifetime will be generated, which will minimize the potential for premature failures and resultant groundwater pollution, loss of valuable product, regulatory attention and fines, undesirable public attention, and very costly remediation work.

REFERENCES

ASTM D1238 (190/2.16), Standard Test Method for Flow Rates of Thermoplastics by Extrusion Plastometer, *American Society for Testing and Materials*, West Conshohocken, Pennsylvania, USA.

ASTM D1603, Standard Test Method for Carbon Black in Olefin Plastics, *American Society for Testing and Materials,* West Conshohocken, Pennsylvania, USA.

ASTM D3895 Standard Test Method for Oxidative Induction Time of Polyolefins by Differential Scanning Calorimetry, *American Society for Testing and Materials,* West Conshohocken, Pennsylvania, USA.

ASTM D5397, Standard Test Method for Evaluation of Stress Crack Resistance of Polyolefin Geomembranes Using Notched Constant Tensile Load Test, *American Society for Testing and Materials,* West Conshohocken, Pennsylvania, USA.

ASTM D5596 Standard Test Method for Microscopic Evaluation of the Dispersion of Carbon Black in Polyolefin Geosynthetics, *American Society for Testing and Materials,* West Conshohocken, Pennsylvania, USA.

ASTM D5885, Standard Test Method for Oxidative Induction Time of Polyolefin Geosynthetics by High-Pressure Differential Scanning Calorimetry, *American Society for Testing and Materials,* West Conshohocken, Pennsylvania, USA.

Boehning, M., Roberts, D. and Schroeder, H.F., (2008). Autoclave Testing: A New Approach for the Evaluation of Oxidative Long-term Resistance of Geosynthetics, *EuroGeo4*, Edinburgh, Scotland, IGS, Paper #143.

Broutman L.J. and Duvall D.E., (1989). Fractographic Study of a Polyethylene Sewer Pipe Failure, ANTEC '89, L.J. Broutman and Associates, Inc., Chicago, IL, USA.

Czerny, J. (1972). Thermo-oxidative and Photo-oxidative Aging of Polypropylene Under Simultaneous Tensile Stress, *Journal of Applied Polymer Science* 16, pp 2623-2632.

Duvall D.E., (2002). Analysis of Large Diameter Polyethylene Piping Failures, Engineering Systems Inc., Aurora, IL, USA.

GRI.GM13, (2006). Test Properties, Testing Frequency and Recommended Warranty for High Density Polyethylene (HDPE) Smooth and Textured Geomembranes, *Geosynthetic Research Institute*, Folsom, PA, USA.

Hsuan et al. (2008). Using Time-Temperature Superposition to Predict Lifetime of Polypropylene Filament Under Elevated Temperature and Pressure, *EuroGeo4*, IGS, Edinburgh, Scotland, Paper #327.

Hsuan, Y.G. and Koerner, R.M., (1998). Antioxidant Depletion Lifetime in High Density Polyethylene Geomembranes, *Journal of Geotechnical and Geoenvironmental Engineering*, June 1998, pp 532-541,

Koch R., Gaube, E., Hessel, J., Gondro, C., Heil, H., (1988). Langzeitfestigkeit von Deponiedichtungsbahnen aus Polyethylene. Müll und Abfall, Hoechst 6316d.

Müller, W., (2007). *HDPE Geomembranes in Geotechnics*, Springer-Verlag, Berlin, Germany, pp 213 - 231.

NSF 54, (1993). Flexible Membrane Liners, *National Sanitation Foundation International*, Ann Arbor, MI, USA.

Peggs, I.D., (1998) private report.

Peggs, I.D., Elie, G., (2008). Factors that Affect the Stress Cracking Resistance of HDPE Geomembrane Liners: Part 1 – What We Know and Might Expect, *EuroGeo4*, Edinburgh, Scotland, IGS, Paper #267.

Peggs, S.J., (2008) private communication.

Sangam, H.P. and Rowe, K.R. (2002). Durability of HDPE Geomembranes, *Geotextiles and Geomembranes 20*, pp 77-95.

Tisinger, L., (2008) private communication.

What the IAGI Approved Installation Contractor and Certified Welding Technician Program Can Do for You

L. Honnigford, International Association of Geosynthetic Installers (IAGI), MN, USA

ABSTRACT
The International Association of Geosynthetic Installers (IAGI) has developed and implemented two programs designed to assist engineers, owners and regulators in improving geosynthetic installations on their job sites. The purpose of the paper is to update the geosynthetic users about the Certified Welding Technician and the Approved Installation Contractor programs. Both of these programs were developed by IAGI to raise the level of professionalism and improve the quality of geosynthetic installations. IAGI 's goal is for engineers and regulators who work with geosynthetic installers on their job sites to embrace these programs and require that Approved Contractors be used on their job sites.

This paper and presentation will discuss the specifics of each program. IAGI's Certified Welding Technicians program tests the skills and knowledge of the geomembrane welders who put liner into landfills, landfill caps and wastewater treatment facilities. The second program, which has been launched by IAGI, is the Approved Installation Contractor program. This program sets a minimum level of standards that installation companies must meet to become an Approved Installer.

The purpose of this paper is to inform engineers, owners and regulators about the advantages of requiring that the installers who work on the containment sites employ Certified Welding Technicians and participate in the Approved Installation Contractor program.

The International Association of Geosynthetic Installers is a group of geosynthetic installers dedicated to advancing the state of the practice in the industry. We welcome all stake holders as members of our organization.

1. OVERVIEW

More than 10 years ago a group of geosynthetic installers got together in Nashville, Tenn. to form what became the International Association of Geosynthetic Installers (IAGI). The purpose of IAGI was to advance the state of the practice in the geosynthetic installation community. Their first project was to write an installation guideline that IAGI continues to use to this day. Another project was to test the welding technicians in the field to determine if they are meeting generally accepted industry standards of welding proficiency. The Certified Welding Technicians program was launched in 1999. Between 1999 and present day more than 400 Certified Welding Technicians worldwide have passed the exam requirements in Polyethylene, PVC and Reinforced geomembrane materials. The IAGI Board of Directors then took up the issue of recognizing companies that meet a minimum level of professionalism in the field. Discussions about defining a program of this magnitude took more than four years to refine. In May of 2006 the Approved Installation Contractor (AIC) program was launched. As of September 2008, there are currently 10 AIC Companies representing companies based on Australia, Canada, Mexico and the United States.

When you think of AIC, think about the Good Housekeeping Seal of Approval®. The Good Housekeeping Seal® designates those products that have met a minimum set or standards. When you see that designation on a product, you know that only a company dedicated to providing excellence would bother to go through the expense and hassle involved in getting the Good Housekeeping Seal of Approval®.

2. BACKGROUND

Forward thinking companies involved in IAGI got together to develop this program in 2002. Much debate and input went into the development. Members were dedicated to achieving a balance between raising the standards of practice with creating a program where small quality companies could achieve this designation.

Based upon focus groups and interviews with member installers, member suppliers, legal council, outside experts in the field, and government officials involved in the geomembrane business, the IAGI began developing a standard of

business practice. Industry professionals involved in AIC program planning had a specific task in mind – to establish a benchmark of business professionalism for installation contractors. Hence, the Approved Installation Contractor (AIC) program was born.

The mission of the AIC program is to establish criteria for recognizing geosynthetic installation companies that meet a minimum level of professionalism, experience and business practices. The goal is to promote growth in the geomembrane installation industry and promote better quality workmanship.

Companies achieving the AIC designation provide documentation that they have made a commitment to implementing a business strategy that strives to get the job done right the first time – from experienced personnel to training programs for their field and supervisory personnel, to having the financial backing to overcome the daily challenges that happen on most construction sites. With any construction site comes Murphy's Law and Mother Nature and they typically have a different set of plans for your job site than those nice ones drawn up and stamped. The experienced contractor knows how to handle those challenges – because they have done it many times before.

Benefits to engineers and owners:

- It gives the user community tools to select experienced professionals for their projects. In project specifications, engineers and owners can require installation companies to have AIC status.
- It raises the level of professionalism for installation companies.

3. REQUIREMENTS

AIC applicants must meet requirements in the following areas: corporate history and business practices, insurance verification, safety training, and professional competence and experience. Below is a list of information required on the AIC submittal form:

- Company history and information
- Minimum 5,000,000 square feet installed annually
- Bonding capability
- General liability insurance
- Worker Compensation insurance
- Automobile liability
- Safety Training
- Health and safety orientation program
- Drug-free work program
- Professional competence/experience
- 15% of their installation force must be Certified Welding Technicians (CWT) required (CWT is an official IAGI certification program for welders.)
- Two letters of reference from engineers that are dated within the past year
- Two letters of reference from contractors/owners that are dated within the past year
- Two letters of reference from geosynthetic manufacturers that are dated within the past year

All of the above information is reviewed and verified by IAGI's third party reviewer. This entire process must be repeated annually. Each company must provide company information and history for the AIC form. General company information is provided including a listing of offices, contacts, company incorporation and registration information. AIC is a dynamic program that is re-evaluated annually. For example, in October 2008, the minimum number of square feet installed by a company was raised to 5,000,000 square feet annually to reflect the generally accepted industry standard for company experience.

In relation to the bonding requirements, AIC designated companies do not have to own a bond at the time of AIC is granted, but they must have a company who is willing to issue a bond to them. The bond company will do due diligence on the company's financial status. Those companies without the financial wherewithal to complete their jobs will not be able to get a bond. Owners and/or engineers may have a minimum level of bonding needed so they might want to designate that an AIC company that meets their internal or their client's minimum bonding requirements.

For most business owners it is only common sense to carry the proper levels and type of insurance coverage. The sad fact is that some do not carry the proper amount or type of insurance. The AIC company must provide evidence of general liability insurance, worker's compensation and automobile liability insurance. The information that is provided is verified by the third party.

4. MEETING ALL REQUIREMENTS

Independently, just one of the above requirements alone does not make an installer good, but when taken together, they are the basis for a company who strives to complete a job on time, accurately and with superior quality as demanded by the project owner. A company can claim to have installed 5,000,000 square feet, but this claim doesn't clarify whether the material was installed well. Each required component of the program serves as a check on another. When a company meets the parameters of the AIC program, the industry can be sure that this company is committed to doing a good job – in every aspect of its business.

5. AIC INTERNATIONAL

AIC International was established after the AIC program began due to the increase in interest from companies outside of the US and Canada. The AIC program was originally established based on the best business practices in the United States and Canada. However, the demand for the AIC program to broaden to the standards accepted in countries around the world was increasing and IAGI has made provisions for these countries. Based on the many different qualifications that the AIC program requires, the AIC International program takes into consideration the best business practices of their specific country. If the company "passes" with their country standards they are granted AIC in their company of origin (e.g. AIC Australia). Therefore, if a company is listed on the AIC Companies list as AIC International, the company may only use AIC when bidding on business in their designated country.

6. HOW TO USE AIC PROPERLY

AIC is not a substitute for engineers or owners to do their own background check or due diligence when planning a new project. If the owner and/or engineering firm has more requirements than are covered by the AIC program, it is the obligation of that party to state those requirements and conduct further investigation of the company to ensure they meet those requirements.

The AIC designation will give the engineer/owner a starting point—knowledge that the companies that have completed the program have a minimum level of industry professionalism and business practices implemented in their companies. IAGI fully expects those hiring an installation company to have other requirements outside the AIC designation based upon the installation company's field of expertise.

7. CWT REQUIREMENT

The Certified Welding Technician Program along with safety training requirements comprises the training component of the AIC program. The CWT program was designed to test the skill and training of those welders who work on geomembrane installations. There are more than 400 CWTs in the industry. Engineers and owners should feel confident specifying that CWTs be on their job site. Since the inception of the CWT program, there are have been many engineering companies that have specified the use of CWTs on a job site which has increased the number of CWTs being tested and successfully passing every year.

Within the past 10 years, IAGI has implemented three different CWT exams; Polyethylene-(which encompasses HDPE and LLDPE materials), Reinforced geomembranes and PVC geomembranes. The first component to be able to qualify to take the exam is that each technician must supply a work resume that shows that they have installed a minimum of 1,000,000 square feet (92,300 square meters) over their work history. This requirement ensures that those that take the exam are experienced installers according to industry standards.

The Polyethylene CWT test consists of two components, a written exam that consists of 77 multiple choice questions and a hands-on welding exam. The hands-on component requires that the technician weld a variety of geomembranes using a wedge and / or extrusion welder. The welds are sent to IAGI Approved third party labs to be tested. The test results are then sent to IAGI's office for grading. The Polyethylene exam allows for technicians to be certified in either wedge (fusion) welding, extrusion welding or both. The PVC and Reinforced exams have only one designation

The Reinforced and PVC exams take both a 71 question multiple choice exam along with a hands-on component. The hands-on requires welding skills for both the seam and patching the respective materials. The Reinforced and PVC exams are currently available in English but will be translated into Spanish in early 2009.

The purpose of IAGI's Certified Welding Technician (CWT) programs is to recognize the knowledge, experience and skill of installers in Polyethylene, PVC and Reinforced geomembrane materials. The programs reward those who qualify with industry resources. This program assists engineers/owners in selecting companies that have CWTs on staff that they have experienced knowledge and skill in the geomembrane installation of particular geomembranes and will provide quality work to the owner.

CONCLUSION

IAGI has established programs such as the AIC and CWT to assist engineers, owners and other industry professionals in selecting and evaluating companies based on the skill level and professionalism of their staff and company standards. IAGI continues to strive to provide a forum for geosynthetics installers to advance installation and construction techniques, and to strengthen the knowledge, image and communication within the industry. For more information about IAGI or the AIC or CWT programs, contact Laurie Honnigford at +1-651-554-1895, e-mail iagi@iagi.com or visit www.iagi.org.

The Importance of Liner Thickness and CQA Implementation in Landfills

M. Marcotte, A.L. Rollin and C. Charpentier, SOLMERS, Canada

ABSTRACT
Leak detection surveys have long proved their usefulness in the domestic waste landfill industry as well as more recently in the mining industry. However, in many projects, the overall liner performance is not documented since few legal measures enforce any control during operation. In this respect, leak detection surveys represent an easy and affordable solution to quantify the integrity of an installation's imperviousness before it gets placed into operation. Leak detection survey methods enable detection of defects that are not readily visible to monitors but are often predictable based on previous experience. Moreover, for an uncovered liner, leak detection surveys may periodically help evaluate the consequences of the site's operation after a certain period.

Based on over 3 000 000 m^2 of geo-electric leak detection surveyed liner, this paper concludes that increasing liner thickness represents an easy solution to improved performance of geosynthetic liners by six fold in some cases. Rigorous Construction Quality Assurance (CQA), can also minimize leaks, reducing their number by as much as 50%, even before implementing a leak detection survey.

1. INTRODUCTION

It is generally recognized by the geosynthetics industry that geomembrane manufacturers produce near-flawless sheets. Appropriate Manufacturing Quality Control (MQC) programs, as well as industry standards, contribute to this desirable result. During their installation, the geomembrane sheets are welded together under variable atmospheric conditions demanding serious on-site monitoring and measurements.

Actually, geomembrane liners are not always as successful as they could be. "Functional impermeability" is always a legitimate goal and the geomembrane choice offers such expectation. But this goal cannot be achieved by just laying a geomembrane liner on the ground and rely on the installer's experience to do the rest. Proper design, appropriate on-site construction quality assurance (CQA) programs and experienced quality assurance monitors are necessary to bring consistency to the field work.

However, material selection process at the design stage sometimes fails to properly take into account the variability of field atmospheric conditions, as well as the different type of equipment and machinery which will then be used on site. Many others factors would also affect the liner integrity such as the sub-grade conditions, the covering procedure with granular material, the expertise (or lack thereof) of the field teams; earthwork contractor, installer as well as CQA monitor.

Thirty years ago, engineers and regulatory agencies designed projects incorporating new synthetic materials as a valuable substitute to compacted clay liner. Nowadays, geomembranes are used extensively as impervious barriers and well recognized for that application.

Because of such recognition, price often becomes the key factor in liner selection. One predicable consequence of that change is strong competition between manufacturers and the installation of thinner liners to get a lower price. Caution is then required since a geomembrane is still a technical material that requires engineering judgment in its selection process.

2. GEOMEMBRANE MATERIAL SELECTION AND THICKNESS CONSIDERATION

In the authors' opinion, the liner selection process must address the expected performance of the facility with regards to its overall imperviousness. Consequently, the nature of the sub-grade should be viewed as the foundation of such an impervious liner. Liner systems, such as single, composite or double lined systems, should then be considered based upon local regulations, availability of granular materials, site conditions at the time of construction as well as the long-term performance of the facility.

The liner thickness selection depends on the nature, density and granular nature of both underlying and covering material. The equipment used on site, the temperature expected during such work, precipitation and water management are also important factors influencing the thickness selection.

Liners in landfill construction, heap leach pads or surface impoundments are used for their imperviousness but selected for their performance's durability (survivability). These liners must be protected against "aggressions" during construction to avoid local failures or perforations. Thickness has been recognized as one of the major factors resisting such "aggressions". Even if localized tension is inevitable, puncture resistance would then be of the utmost importance when overall performance is concerned. The use of a thick geotextile protection (cushion) on both sides logically addresses this concern. Why then is the global cost of the "sandwich" forgotten if thicker membranes used with cheaper textile could better meet the requirement of puncture resistance?

A thin polymeric geomembrane has an extraordinary capacity of maintaining its imperviousness under large strain. It can be estimated that a 1 mm thick membrane expanding in both directions by 150% will lose 56% of its thickness (from 1mm to 0.44mm) without any variation in its permeability. However, in localized areas, it is a serious loss in the factor of safety against puncture, far exceeding any comparable variation for a compacted clay liner.

3. CQA PROGRAMS

In practice, CQA programs deal with documentation issued from QCs and reported corrections of flaws. Documentation, conformity testing, calibrating and trial tests, seam destructive and non-destructive tests are all necessary steps. But a stringent CQA requires the constant presence on site of a certified CQA monitor.

Results of more than a 100 leak detection surveys over the past 14 years analyzed by the authors show that a lower number of leaks were found at the leak detection survey stage in liners installed under stringent CQA program than in the one where no such CQA program existed (see Table 1).

Table 1. Equivalent leak density of different HDPE geomembrane thicknesses

HDPE geomembrane thickness (mm)	Market Share	Leak Density without CQA	Leak Density with stringent CQA
2,0	35%	5.0[(1)]	3.2
1,5	40%	7.5[(1)]	5.1
1,0	25%	31.5	20.5
		12.6	**8.3**
Laine et Mosley (1993)		14	

[(1)] Estimated based on typical data

It can be observed that projects where rigorous CQA programs have been implemented showed more or less 50% less leaks than projects where no such CQA program was applied (Marcotte et al, 2006). However, these results also indicate that the reduction of the liner thickness from 2 mm to 1 mm has increased the leak density by a factor of six (6).

CQA recommended procedures have tremendously improved since the 80's in North America. USEPA publications, as well as numerous technical papers, have addressed the issue in considerable details (Giroud, J.P., (1984), Giroud, J.P., and Fluet, J.E., Jr., (1986), Buranek, D., and Pacey, J., (1987), including USEPA documents showed as references). Fluet (1986) expressed the following statements relative to CQA :

- "In accordance with USA state laws, all QA activities must be conducted under the auspices of a registered Professional Engineer. Similarly, the final report, certification, and record drawings should be signed and sealed by a registered Professional Engineer".
- "QA should be extended to non-construction related activities including during the design and material selection steps. This is especially critical in light of the lack of transmission from senior engineers to junior designers. "
- "QA personnel training and qualifications are now available and need certification. "
- "Non-construction aspects of the lining system such as the manufacturing and assembly of geosynthetics must be included in QA program. "
- "Finally, it is suggested that QA should also extend through the post-construction landfill operation period, and even into post-closure in some cases. In projects where chemical compatibility is in doubt, samples (coupons) of all synthetics materials installed may be immersed in leachate collected from the containment unit and be periodically tested by an independent laboratory for property variation. This permits the owner/operator to receive an advance warning of potential problems, forcing an action to protect the environment. "

4. NON-DESTRUCTIVE SEAM TESTING

Discontinuity in field welded seams can be located using several methods such as pressurized air channel or vacuum (soap) box. These non-destructive techniques have been used, and are still used, extensively in CQA programs to ensure the acceptability of seams as installation progresses. Since faulty seams represent a very small fraction of liner defaults; less than 7% of all failures in the liner as reported by Collucci et Lavagnolo (1995) or 9% from Nosko et al (1996, 2000); most of the leaks created in a liner are ignored using only these methods.

Another interesting finding is that more than 65% of the leaks are located within a one (1) metre strip along the seam (Rollin et al 2002). To evaluate the importance of the covered area of this one meter wide strip, the relationship between the ratio 1m strip area to the total area covered by the liner for a 3 meters deep surface impoundment is presented in the following figure. The lowest ratio, based on a 10 meters wide sheet was found to be at 10% (i.e. ratio is 1/W% where W is the width of a geomembrane roll).

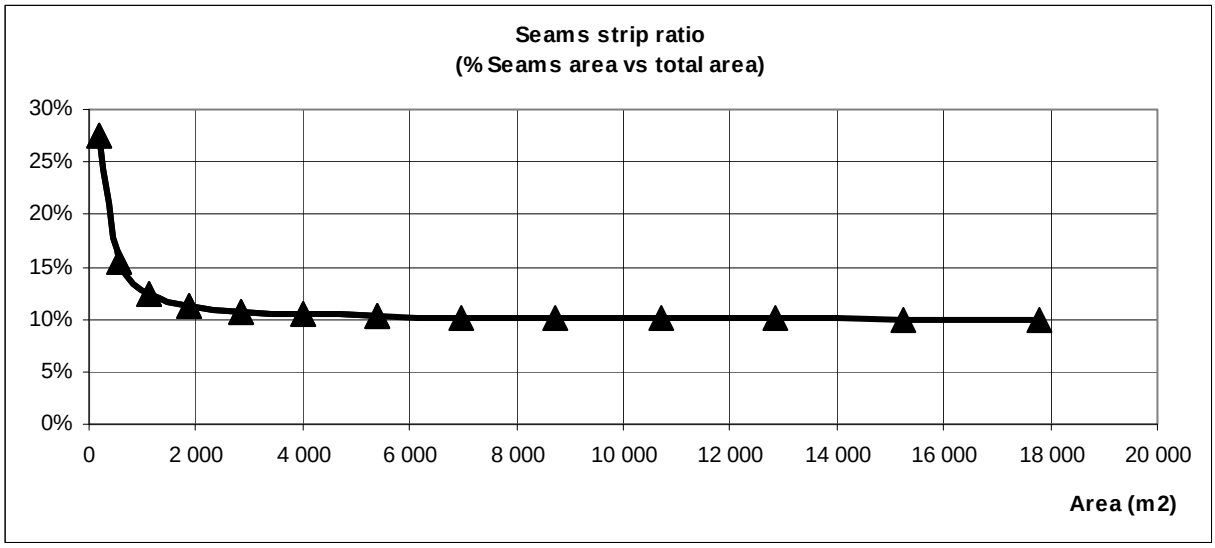

Figure 1. Relationship between the seam strip and the total area of the facility

The plotted curve in Figure 1 indicates that as the cell area increases, the ratio of seam strip area to the total area of the liner reaches a minimum value. This supports the fact that larger leak densities are found in smaller installations as pointed out in the past by Colucci et Lavagnolo (1995), Rollin et al (1999) and Phaneuf et Peggs (2001). The reasons for the greater number of leaks per hectare in liners installed in smaller facilities have been summarized by Colucci et Lavagnolo (1995): smaller installations have proportionally more complex features (corners, sumps, penetrations) per unit area where extrusion welding is used while larger installations, because of their overall budget, tend to have better CQA program and are generally imposed less traffic per unit area.

As one would expect, air pressure tests cannot detect perforations located within the sheet itself since the seam width is less that 1% of this one (1) meter wide seam strip, leaving more or less 64% of this strip untested (35% for the area outside the seam strip). A 100mm wide vacuum box would obviously do better in that respect.

5. LEAK DETECTION ON EXPOSED LINERS

Geoelectric leak detection techniques used on geomembranes have been described in many publications, such as Peggs and Pearson (1989), Peggs (1990, 1993a, 1993b), Darilek and Parra (1988), Darilek et al. (1989), Laine and Miklas (1989), Laine (1991), Laine and Darilek (1993), Laine and Mosley (1993), Rollin et al. (1999, 2002, 2004) and in standards such as ASTM D6747 (Standard Guide for Selection of Techniques for Electrical Detection of Potential Leak Paths in Geomembranes), ASTM D7002 (Standard Practice for Leak Location on Exposed Geomembrane Using the Water Puddle System) and ASTM D7007 (Standard Practices for Electrical Methods for Locating Leaks in Geomembranes Covered with Water or Earth Materials).

The water puddle technique consists in the creation of a difference in potential between the soil under an exposed geomembrane and a puddle of water projected from a diffuser onto its surface. Most geomembranes being highly resistant electrical insulators, as soon as water percolates through a hole and reaches the supporting soil, a “bridge” is created

between these two potentials which generates an electrical current. A detector signals the presence of water infiltration to the operator (via acoustical and visual signals).

As indicated by Caquel et al (2006), the reliability of the method is high, especially for polymeric geomembranes, with a detection rate between 65% and 75%. This method is however dependant on the operator's experience for locating leaks smaller than 3 mm in diameter.

Leak detection techniques can ensure the integrity of an installed liner but it is difficult to assess the virtues of construction quality assurance incorporating such techniques since few comparisons are available between projects. The leak densities obtained in this study can be compared to results presented in other papers in the past. Many of already published results in the field of geoelectrical leak location are related to waste management applications, where the selected geomembranes are thicker (commonly 1,5 mm or 2 mm). In comparison, some of the results used by the authors refer to facilities lined with thinner geomembranes (thickness of 1 mm or less) for very large surface impoundments so that the average leak density is greater than in other published papers (Forget & al. 2005a,b and Forget, 2005).

The relation between leak density and geomembrane thickness has been demonstrated in other publications (Rollin and Marcotte, 2007) but recent data show that leak density could increase by a factor of 4 simply by decreasing the thickness of a PVC liner from 0.75mm down to 0.5mm. (Jacquelin et al 2008).

As an example, geoelectrical leak location surveys are becoming mandatory in the South America mining industry to control the integrity of the geomembranes in their containment applications. Statistics resulting from surveys performed in more than 60 works, in 9 different mine sites with the water puddle technique demonstrate that geoelectrical leak location is a crucial control method that should be perceived as an investment for the mining industry (Jacquelin et al 2008).

In fact, the return on investment is not only related to long term environmental protection, but also by reducing the loss of valuable liquids and therefore increasing the return on investment. Furthermore, Thiel et al (2005) showed that such an advantage could show up as soon as one or two years after installation, specifically if low thickness is contemplated at the design stage.

The relationship between leak density and the absence of a rigorous CQA program has been demonstrated to be crucial (Forget et al 2005a). It was found that most of the perforations happen during geomembrane installation and the afterward covering phase, whether a credible CQA program is implemented or not. However, larger tears and holes are usually created during the geomembrane covering stage by improper placement methods or by the use of too heavy equipment. Common sense would also support that the absence of permanent CQA monitoring on site during the installation and covering work could also have a detrimental effect of the overall quality of the work.

Increasing amounts of data are coming from published leak detection surveys. The prime interest of such data collection is to understand the relationship between installation concerns, CQA procedure and design choices. In that respect, statistics of leak detection surveys must be carefully reported to interested parties if meanings are to be extracted from such results. Leak density value relates to project conditions and average values should be calculated taking that into account based on as many projects as possible.

To improve understanding, data should specifically relate to liner thickness, type of protection and subgrade conditions as well as the covered area, temperature condition and location of leaks with respect to seams position. As a matter of fact, data obtained from one survey should apply to the work done but should not be extended to any other work without extreme caution. On the contrary, data related to well documented works can be used to support choices and better practices for best results.

For instance, data on 25 lined projects totalizing 2 000 000 m^2 of geomembranes are presented in Figure 2. These data are presented in a format where the lower line represents the leak density of only 1 hole for each project area. For instance, one hole over a 500 m^2 project represents a leak density of 20 leaks/ha while 1 hole over an area of 10 000 m^2 gives a density of 1. The upper line shows the variation of leak density with regards to the surveyed area for 5 holes found. It is then easy to find that leak density drops below 10 holes/ha when the surveyed area exceeds 10 000 m^2 which is in conformity with the prediction of Figure 2.

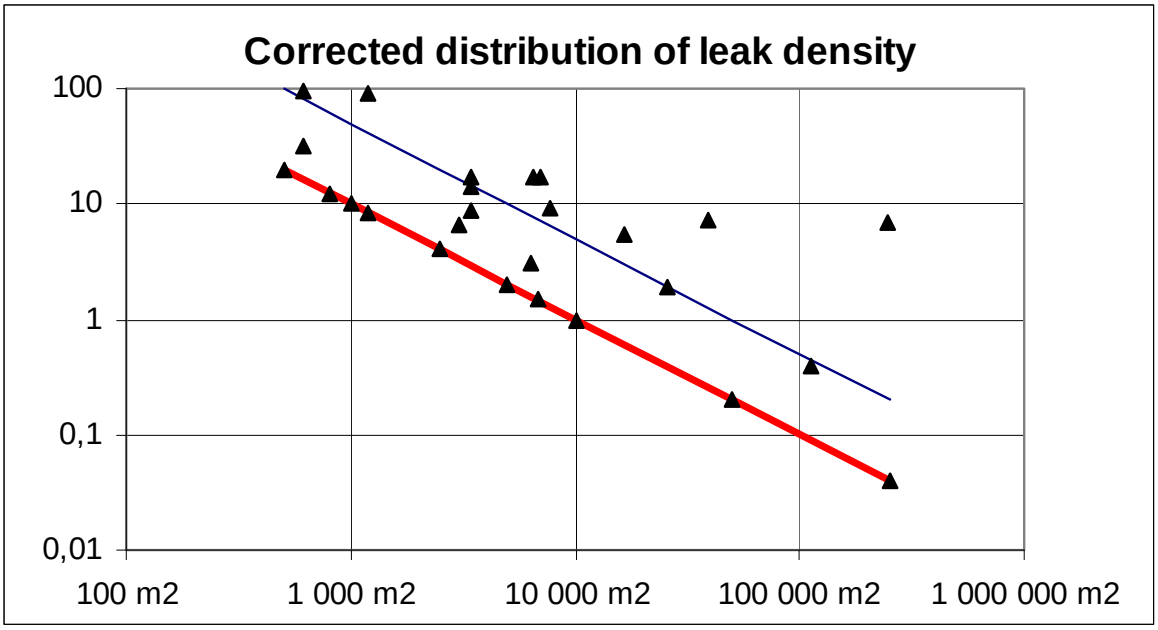

Figure 2. Corrected distribution for leak density versus covered area (m2)

6. CONCLUSIONS

It is a fact that geomembrane liners are not always as successful as they could be. The main reason is that many people, owner, designer and sometimes regulatory offices personnel when they think “geomembranes”, tend to neglect two important aspects of such an application: “educated” design process and on-site quality assurance (CQA). As said before, “functional impermeability” is always a legitimate goal, but this goal cannot be achieved by just laying a geomembrane liner on the ground and expect the installer will do the rest; proper design, appropriate on-site quality assurance and experienced quality assurance monitors are all important.

Based on data collected on over 3 000 000 m^2 of exposed liner with geoelectrically surveys and CQA conducted installation in 200 projects lined with 5 000 000 m^2 of geomembrane, the authors conclude that:

- increasing thickness of polymeric liner is one serious way of reducing leaks occurrence and insure better imperviousness (an increase from 1 mm to 2 mm thick geomembrane, can reduced by 6 fold the number of leaks),
- full time CQA programs improves the actual liner quality on site with respect with its hydraulic performance up to 50%, without any leak detection program, and,
- pressurized air channel testing of HDPE and PVC geomembrane seams can account only for a very small percentage of existing leaks in a project and is not equivalent nor a replacement to proper leak detection survey.

In that respect, from the authors’ point of view, it would be wise as a first step for a designer, to select a thick liner as the best alternate solution to a one (1) meter thick compacted clay layer. Construction cost would then be evaluated for the whole life cycle of the facility according to state of the art guidelines relating to the foreseen consequences of any leaks compared to compacted clay liner’s anticipated performance. Cost and expected performance could then be compared and presented to the client before any final design is performed and a clearer decision made before implementation. Appropriate protection materials, geosynthetic products and natural soils, can then be selected accordingly.

The liner thickness reduction should then be considered when compared to the added security of a specifically more stringent CQA program that would include a leak detection survey. It is believed that permanent monitoring of the field work by an independent third party during construction is the only efficient approach to human negligence and to the control of materials as soon as they are received on site.

This paper suggests that the selection of thicker geomembrane combined with appropriate Construction Quality Assurance programs including leak detection surveys ensure the performance and the durability of confinement works. The presented statistics show a global decrease in the number of leaks found on sites where a thick liner has been installed and where a rigorous CQA program was performed.

REFERENCES

ASTM D6747 Standard Guide for Selection of Techniques for Electrical Detection of Potential Leak Paths in Geomembranes.

ASTM D7002 Standard Practice for Leak Location on Exposed Geomembrane Using the Water Puddle System.

ASTM D7007 Standard Practices for Electrical Methods for Locating Leaks in Geomembranes Covered with Water or Earth Materials.

Buranek, D., and Pacey, J., (1987) "Geomembrane-Soil Composite Lining Systems Design, Construction Problems, and Solutions", Proceedings of the Geosynthetics '87 Conference, New Orleans, (1987).

Caquel, F., Villon, G., Florin, JP. & Marcotte M. (2006). Evaluation of the real performance of a geomembrane electrical leak detection system: full scale experimental study, 8th IGS conference proceeding, Yokohama, Japan.

Colucci P. and Lavagnolo M.C. (1995): Three Years Field Experience in Electrical Control of Synthetic Landfill Liners, *Proceedings of Sardinia'95*, CISA, Cagliari, pp 437-451, October.

Darilek G.T. & Parra J.O. (1988). The Electrical Leak Location Method for Geomembrane Liners, *USEPA/600/S2-88/035*, Sept.

Darilek G.T., Laine D. & Parra J.O. (1989). The Electrical Leak Location Method for Geomembrane Liners, *Proceeding of Geosynthetics' 89*, IFAI, pp 456-462, San Diego.

Fluet, J.E., Jr., (1986) "Geosynthetic Lining Systems: Installation and Quality Assurance", Proceedings of the National Liner/Leachate Conference, St. Louis, 40-49.

Forget B. (2005), "A Case Study Comparing the Impact of the Thickness of Exposed P.V.C. Geomembranes on the Integrity of Containment Systems", *Proceedings Forum on Geosynthetics 2005*, Environmental Works and Roadways Design with Geosynthetics, was held in Edmonton, Canada, on May 4th, 2005.

Forget B, Rollin A.L., Jacquelin T. (2005a). Impacts and limitations of quality assurance on geomembrane integrity : Statistical Study Based on a Decade of Leak Location Surveys. *Proceedings NAGS 2005/GRI-19, Dec. Las Vegas.*

Forget B, Rollin A.L., Jacquelin T. (2005b). Lessons Learned from 10 Years of Leak Detection Surveys on Geomembranes, *Proceed. Sardinia 2005*, Sardinia.

Giroud, J.P., (1984) "Impermeability: The Myth and a Rational Approach", Proceedings of the International Conference on Geomembranes, Denver, 1 (1984).

Giroud, J.P., and Fluet, J.E., Jr., (1986) "Quality Assurance of Geosynthetic Lining Systems", Geotextiles and Geomembranes, 3(4), 249-287.

Jacquelin, T., Bones C.S., Marcotte M. & Rollin A.L. (2008). Recent Results in Geoelectrical Leak Location in the Chilean Mining Industry, *The First Pan American Geosynthetics Conference & Exhibition,* 2-5 March 2008, Cancun, Mexico.

Laine D.L. & Miklas M.P. (1989). Detection and Location of Leaks in Geomembrane Liners Using an Electrical Method, *Proceed. 10th Nat. Conf., Superfund'89*, Washington, Nov.

Laine D.L. (1991), Analysis of Pinhole Seam Leaks Located in Geomembrane Liners Using the Electrical Leak Location Method, *Proceed. Geosynthetics'91*, Atlanta, pp 239-253.

Laine D.L. & Darilek G.T. (1993). Locating Leaks in Geomembrane Liners of Landfills Covered with a Protective Soil, *Proceed. Geosynthetics'93*, vol 3, pp 1403-1412, April.

Laine, D.L. & Mosley, N.G. (1993). Leak Location Survey of a Soil Covered Geomembrane at a Landfill Site in the UK, Green '93 Conference Proceedings, Bolton, United Kingdom, June 28 - July 1,

Marcotte M., Rollin A.L., Jacquelin T. & Forget B., Optimisation de l'intégrité globale d'une géomembrane à l'aide de la détection géoélectrique de fuites, Rencontres 2006, Montpellier (France).

Nosko V. and Touze-Foltz N., 2000: Geomembrane Liner Failure: Modeling of its Influence on Containment Transfer, *Proceedings Second European Geosynthetics Conference*, Bologna, pp 557-560.

Nosko V., Andrezal T., Gregor T. & Garnier P. (1996). Sensor Damage Detection System – The Unique Geomembrane Testing Method, *Proceed. EuroGeo*, Netherlands pp 743-748.

Peggs I.D. & Pearson D.L. (1989). Leak Detection and Location in Geomembrane Lining Systems, *ASCE Annual meeting*, Fort Lauderdale, September.

Peggs I. (1990). Detection and Investigation of Leaks in Geomembrane Liners, *Geosynthetics World*, Vol 1, Issue 2, winter, pp 7-14.

Peggs I.D. (1993)a. Practical Geoelectric Leak Surveys with Hand-Held, Remote and Water Lance Probes, *Proceedings of Geosynthetics' 93*, IFAI, pp 1523-1532, Vancouver.

Peggs I.D. (1993)b. Advances and New Thinking in Landfill Liner Construction Quality Assurance Practices, *Proceedings of Sardinia' 93*, CISA' Cagliari, pp 121-128.

Phaneuf R. & Peggs I.D. (2001). Landfill Construction Quality: Lessons Learned from Electrical Resistivity Testing of Geomembrane Liners, Geotechnical Fabrics Report, vol 19, no 3, April pp 28-35.

Rollin A.L. & Marcotte M. (2007) Impacts of CQA Programs on Geomembrane Integrity in Landfills – Statistical Study Based on a Decade of Leak Location Surveys, *7th French, Japan and Korean Conference*, May, Grenoble (France).

Rollin A.L., Jacquelin T., B. Forget, Saunier P. (2004). A Guide to Detect Leaks on Installed Geomembranes, *Proceedings EuroGEo*, Munich, pp 235-240.

Rollin A.L., Marcotte M., Chaput L., Caquel F. (2002). Lessons Learned from Geo-electrical Leaks Surveys, *Proceedings Geosynthetics 2002*, Nice pp 527-530.

Rollin A.L., Marcotte M., Jacquelin T. and Chaput L., (1999). Leak Location in Exposed Geomembrane Liners Using an Electrical Leak Detection Technique, *Proceedings of Geosynthetics'99*, Boston, pp 615-626.

Thiel, R., Beck A. and Smith, M.E. (2005). The Value of Geolectric Leak Detection Services for the Mining Industry, *Geo-Frontiers 2005 Proceeding*, January 24–26, 2005, Geotechnical special publications 130-142 and GRI-18, Austin, Texas.

USEPA, "Minimum Technology Guidance on Double Liner Systems for Landfills and Surface Impoundments Design, Construction and Operation", EPA/530-SW-85-013 Washington, DC, (1985) 71 pp.

USEPA, "Construction Quality Assurance for Hazardous Waste Land Disposal Facilities", U.S. EPA/ 530-SW-86-031, Washington, DC, (1986) 88 pp

USEPA, "Technical Resource Development: Design, Construction and Operation of Hazardous and Nonhazardous Waste Surface Impoundments." Office of Research and Development, EPA/530/SW-91/054, Cincinnati, Ohio, June 1991.

USEPA, "Technical Guidance Document: Inspection Techniques for the Fabrication of Geomembrane Field Seams." Office of Research and Development, EPA/530/SW-91-051, Cincinnati, Ohio, May 1991.

USEPA, “Technical Guidance Document: Quality Assurance and Quality Control for Waste Containment Facilities.” Office of Research and Development, EPA/600/R-93/182, Cincinnati, Ohio, September 1993.

Geosynthetics 2009
February 25-27 2009, Salt Lake City, Utah

Design of Uranium Mill Facility Liner Systems for the Piñon Ridge Project

K.F. Morrison, P.E., R.G., Golder Associates Inc., Lakewood, Colorado USA
J.D. Elliott, Golder Associates Inc., Lakewood, Colorado USA
J.M. Johnson, P.E., Golder Associates Inc., Lakewood, Colorado USA
R.R. Monok, Energy Fuels Resources Corp., Lakewood, Colorado USA

ABSTRACT
The regulatory environment regarding the processing of uranium ore was altered dramatically in 1992 as a result of major federal regulatory changes, making achieving regulatory compliance a greater challenge for a new facility. One major modification to the regulations is identification of prescriptive liner systems for surface impoundments (i.e., tailings cells and evaporation ponds). Strategically located within the Uravan Mineral Belt District, the Piñon Ridge Project is the first new uranium mill being proposed for construction in the United States in over 25 years. Proposed as a 6.3 million tonne uranium milling operation, the mill will receive uranium ore from a variety of sources. The project includes design and permitting of three 12.3-hectare tailings cells, 16.2 hectares of evaporation ponds, and an ore stockpile pad. This paper will focus on the liner system requirements and designs for the various facilities.

1. INTRODUCTION

Energy Fuels Resources Corporation (EFRC) is in the process of designing and pursuing licensing of a new conventional uranium mill strategically located within the Uravan Mineral Belt District. The proposed Piñon Ridge Mill is located near Naturita, Colorado, and is the first uranium mill being proposed for construction in the United States in over 25 years. With the resurgence of the uranium industry, local interest in the project is high as this area has exhibited slow economic growth since the collapse of the uranium industry nearly 30 years ago. Part of the Piñon Ridge Project involves the design of three 12.3 hectare tailings cells with a combined capacity to store 6.3 million tonnes of tailings, approximately 16.2 hectares of evaporation ponds, and a 2.4-hectare ore stockpile pad.

1.1 Regulatory Background

Under the Uranium Mill Tailings Radiation Control Act (UMTRCA) of 1978, as amended, the Environmental Protection Agency (EPA) has the responsibility of establishing standards for exposure of the public to radioactive materials originating from mill tailings for active uranium extraction facilities licensed by the US Nuclear Regulatory Commission (NRC) or its Agreement State. NRC regulations are issued under the United States Code of Federal Regulations (CFR) Title 10, Chapter 1.

Located in the Agreement State of Colorado, the Piñon Ridge Project is pursuing permitting through the Colorado Department of Public Health and Environment (CDPHE). As an Agreement State, CDPHE has the responsibility for licensing the possession and use of radioactive materials in Colorado under the Radiation Control Act (Title 25, Article 11), and Colorado's Rules and Regulations Pertaining to Radiation Control (6 CCR 1007-1). As of January 2006, thirty-three states have entered into agreements with the NRC, under which regulatory authority has been delegated to the state over most radioactive materials used in non-federal facilities, assuming that the state program is compatible with NRC requirements.

1.2 Key Regulatory Requirements

Regulations pertaining to the design and operation of uranium tailings disposal cells became more stringent in 1992, including the requirement for tailings cells to have a double liner separated by a leak collection layer, with the lower composite liner system comprised of a geomembrane underlain by 0.9 m of low permeability clay. Evaporation pond liner requirements are similar to those for tailings cells, with the exception of the clay underliner. Regulations governing design of uranium ore pads are less specific, stating that "*steps must be taken during stockpiling of ore to minimize penetration of radionuclides into underlying soils; suitable methods include lining and/or compaction of ore storage areas*."

The Colorado state regulations indicate that flexibility is provided in the criteria which allows for optimal tailings disposal on a site-specific basis. Several of the guidelines for uranium tailings disposal include (6 CCR 1007-1, Part 18, Appendix A):

- Consideration of disposal of tailings below grade, either in mines or pits, which is stated as the 'prime option' for disposal of tailings;
- Providing good wind protection to the tailings via topographic features; and
- Employing the groundwater protection standards set forth in 40 CFR Part 192, Subparts D and E.

The groundwater protection standards (40 CFR 264.221) which the uranium tailings disposal cells must meet effectively define the liner system requirements. The prescriptive liner system consists of a double layer liner with the primary and secondary liners separated by a leak collection system, described as follows (from top to bottom):

- Upper primary geomembrane liner;
- Leak collection layer, consisting of drainage gravel or geosynthetic material which meets prescribed minimum permeability or transmissivity values;
- Lower secondary geomembrane liner; and
- A minimum of 0.9 m of low permeability clayey soil underliner with a maximum permeability of 10^{-9} m/s.

When closure includes leaving the liner system in place in perpetuity, which is applicable to the tailings cells, the geosynthetic components are required to be designed of materials which prevent wastes from migrating into the liner during the active life of the facility. When closure of the facility includes removal of the liner system or decontamination of all waste residues, such as the case with the evaporation ponds and ore pads, wastes are permitted to migrate into the liner during the active life of the facility.

1.3 Site Characterization

The project site is located in the Paradox Valley, which is formed by the collapse and subsequent erosion of a well-developed faulted anticline with an intrusive salt and gypsum core. Due to the complex structural geology of the site, the bedrock depths are highly variable, ranging from less than 6 m to greater than 30 m. Near-surface overburden soils consisting primarily of silty sands and sandy silts were indentified to present a risk for collapse upon wetting if left untreated.

At the project site, investigative drilling to depths of up to 180 m below the ground surface did not encounter groundwater under the planned location of the mill facilities. Additionally, a number of aquitards were identified during the geotechnical field program, further limiting any potential impacts to the groundwater regime during the active life of the mill. Despite this site specific characteristic, the tailings cells and evaporation ponds were nevertheless designed with the prescriptive standards applicable to hazardous waste treatment, storage and disposal facilities as outlined in the CFR.

2. TAILINGS LINER SYSTEM DESIGN

2.1 Background

Each of the three proposed tailings cells (Cells A through C) have been designed to provide a minimum capacity to accommodate storage of 2.2 million tonnes of tailings with 0.9 m of freeboard, having liner footprint areas of 12.3 hectares. The tailings cell layouts are illustrated in plan view in Figure 1.

During the course of design, a number of meetings have been held with CDPHE to obtain early feedback on the proposed design concepts, prior to official submittal of the designs as part of the environmental permit. The liner system currently proposed for the tailings cells has evolved as a result of these meetings.

Closure of the tailings cells includes leaving the liner system in-place in perpetuity. Regulations for closure indicate that the liner should remain effective for 1,000 years, to the extent reasonably achievable. Further, the geosynthetic components of the tailings cells are required to be constructed of materials which prevent wastes from migrating into the liner during the active life of the facility. At the design production rate of 450 tonnes per day, the active life of each tailings cell is anticipated as approximately 14 years. Closure of each tailings cell will be initiated once deposition within each cell is completed, including dewatering and construction of an interim cover to limit radiological hazards.

2.2 Liner System Summary

Based on site-specific conditions, and following the guidance of 40 CFR 264.221, the tailings cells were designed with the following liner system for groundwater protection (from top to bottom) (Figure 2):

- 1.5 mm high density polyethylene (HDPE) upper (primary) geomembrane;
- Leak Collection and Recovery System (LCRS) consisting of HDPE geonet on the base of the tailings cells, and a drainage geocomposite on the side slopes;
- 1.5 mm HDPE lower (secondary) geomembrane;
- Reinforced geosynthetic clay liner (GCL) as the low permeability underliner component of the secondary composite liner system; and
- Prepared subgrade consisting of native silty sand and sandy silt soils.

For the tailings cells, the upper geomembrane layer of the liner system was designed to remain uncovered. This is a practical approach for tailings cells because the tailings solids represent little puncture threat to the liner as they are relatively fine-grained, regular equipment access over the liner is not expected, and a soil cover over the liner would be difficult to maintain in the relatively high energy environment associated with hydraulic discharge of slurried tailings. A partial cover has been designed on the gently sloping impoundment floor to prevent damage from wind uplift and to act as a drainage layer for the purposes of reducing the hydraulic gradient on the liner and enhancing tailings densification.

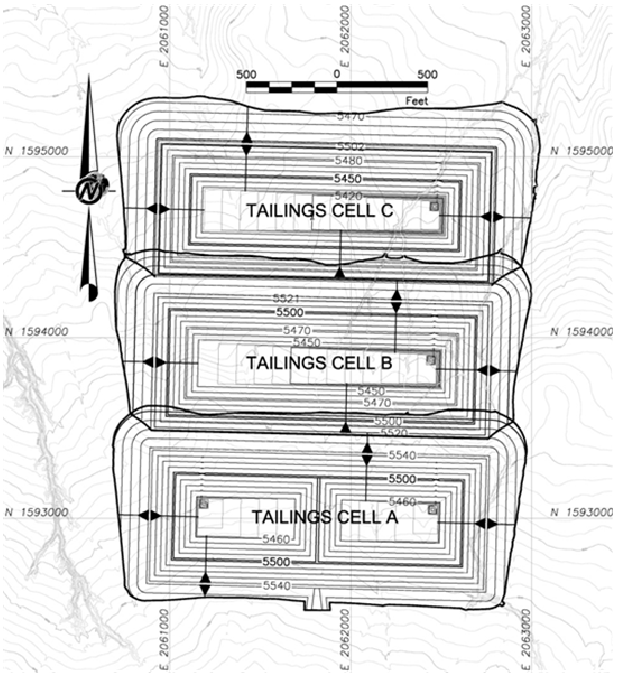

Figure 1. Tailings cell layout.

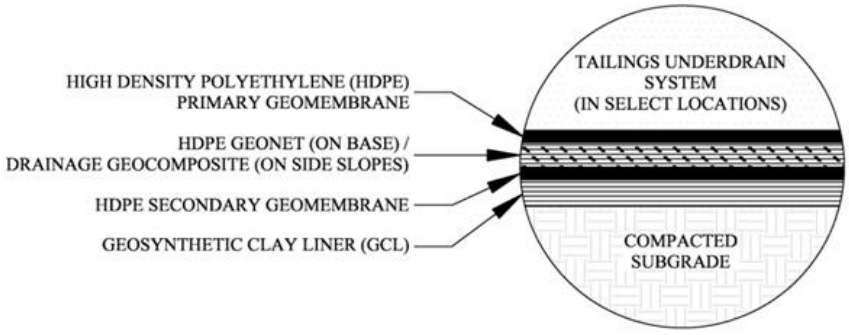

Figure 2. Tailings cell liner system detail.

2.3 Upper Primary Geomembrane Liner

Since the upper primary geomembrane will be exposed to atmospheric conditions as well as a variety of chemicals associated with uranium and thorium processing, including low pH solutions, use of a high density polyethylene (HDPE) liner is proposed. During early meetings, regulators expressed concerns regarding the degradation resistance of HDPE geomembrane, particularly when exposed to ultraviolet (UV) radiation. These concerns were effectively assuaged by reviewing the expected performance requirements for the liner system and summarizing available liner performance data from the engineering literature.

The portions of the tailings cell liner systems that will be exposed to UV radiation for the longest period of time are located near the top of the cells, which are the least critical from a hydraulic containment standpoint (i.e., the hydraulic heads will be low to nonexistent during a short operating life followed by negligible hydraulic loading in the post-closure period). The base of the tailings cells, which will be subjected to the highest hydraulic heads, will be covered with tailings at the on-set of operations and therefore exposed to UV radiation for a very short time.

UV radiation can be expected to cause some deterioration in appearance and mechanical properties with time. A review of available literature investigating the UV resistance of HDPE geomembrane from field performance (Hsuan et al., 1991; Rowe et al., 2003; Ivy, 2002; Adams & Wagner, 2000; Rollin, 2004) and laboratory test data (Koerner et al., 2005; Martin, 2005) provides evidence that exposure of a 1.5 mm HDPE geomembrane to UV for 20 years or more will not result in significant degradation of the geomembrane. Therefore, the amount of deterioration expected will not compromise the performance of the liner system during its anticipated operational life.

Although standard (black) HDPE has been proven to be highly resistant to UV radiation over long periods of time, an additional feature was incorporated into the liner design, which should further reduce the potential for UV damage to the exposed portion of the liner system. The upper primary geomembrane liner will include a light-reflective surface that is resistant to UV radiation and is coextruded with the primary black geomembrane liner. All of the physical properties of a standard black HDPE geomembrane remain the same, but the light-reflective design feature provides added benefits by increasing the weathering resistance by reflecting more solar radiation, while at the same time reducing the range of expansion/contraction resulting from temperature fluctuations, reducing desiccation effects to subgrade soil materials, and improving detection of installation damage. This design enhancement, while not necessary to achieve acceptable system performance, will reduce UV degradation and should also improve constructability, aid quality assurance, and improve system performance.

Single-sided texturing (textured side down) on the upper primary geomembrane is included to increase frictional resistance at the contact with the LCRS layer. Textured rubsheets will be extrusion welded where required by mill operations to facilitate tailings deposition and access during operations.

Additionally, use of conductive liner is proposed for the upper geomembrane to aid in quality assurance testing. This design enhancement was incorporated as a result of meetings with regulators during the facility design. After the liner system is installed, spark testing will be conducted on the conductive liner as a cost-effective and precise way to detect defects in the liner.

2.4 Leak Collection and Recovery System Layer

An important feature of the tailings cell liner system is the Leak Collection and Recovery System (LCRS) layer, designed per 40 CFR 264.221 (by reference from 10 CFR 40 and 6 CCR 1007-1, Part 18). The LCRS is designed to minimize hydraulic head on the lower geomembrane liner. The LCRS has been designed as an HDPE geonet in the base of the tailings cells, and a drainage geocomposite on the side slopes. Geonet was not considered suitable for use on the long side slopes of the tailings cells due to its anticipated low interface shear strength when placed in contact with geomembrane. Instead, a drainage geocomposite, comprised of a geonet laminated on both sides to a nonwoven geotextile filtration media, is proposed to increase frictional resistance with the overlying and underlying textured geomembrane liners.

Per the requirements of 40 CFR 264.221, the transmissivity of the selected LCRS drainage layers exceed the minimum transmissivity requirement of $3x10^{-4}$ square meters per second (m^2/s), and is designed with a minimum grade of one percent. The LCRS layers were designed with transmissivities sufficient to prevent liquid build-up above the secondary geomembrane, per the methods outlined in Giroud et al. (1997b). Leakage collected in the LCRS layer will be routed via gravity flow to a LCRS sump. Collected solution will be recovered via an automated submersible pump installed in one of two HDPE riser pipes, and pumped back to the tailings surface.

2.5 Lower Secondary Composite Liner System

The lower secondary composite liner system underlies the LCRS layer to maximize the amount of solution recovered in the LCRS and act as a final flow barrier, protecting the subgrade. The designed composite liner system consists of a 1.5 mm HDPE double-sided textured geomembrane overlying a geosynthetic clay liner (GCL). HDPE was selected due to its natural resistance to the chemicals in the solution, and the double sided texturing is used to increase the frictional resistance with the overlying and underlying geosynthetic layers.

Due to lack of locally-available clay sources in the vicinity of the project, alternative underliner materials which meet or exceed the prescribed underliner (i.e. 0.9 m of 10^{-9} m/s clayey material) were considered. Alternatives evaluated included bentonite amendment of on-site silty and sandy soils to achieve a low permeability underliner, and use of GCL as the underliner material. The use of GCL was ultimately recommended for this site as soils amended with up to three percent bentonite tested to be nearly one order of magnitude more permeable than the prescriptive clay liner requirement.

Compatibility of the GCL with the anticipated tailings leachate solution was conducted according to the procedure outlined in ASTM D 6766 (Scenario 2, modified) to evaluate the resulting GCL permeability. Testing of the proposed GCL included moistening the GCL samples with tap water to reach an initial moisture content of about 70 percent, and then hydrating with the low-pH synthetic tailings leachate for 48 hours under low effective stress. The GCL samples were then subjected to increased confining pressures, and allowed to consolidate overnight with each effective stress increase. The final confining pressure of 410 kPa is equivalent to approximately 25 m of tailings, which corresponds to the ultimate height of the tailings. Results represent an increase in the reported hydraulic conductivity by nearly half an order of magnitude for a standard GCL sample (from $5x10^{-11}$ m/s to $1.1x10^{-10}$ m/s), and virtually no change in hydraulic conductivity for the polymer-treated sample.

An analysis was conducted using the method proposed by Giroud et al. (1997a) to demonstrate that the secondary liner system consisting of a 1.5 mm HDPE geomembrane overlying a GCL has equivalent or improved fluid migration characteristics when compared to a secondary composite liner system overlying the prescriptive clay liner. Based on this site-specific analysis, which accounts for the loading conditions and anticipated head on the secondary liner system, as well as the potential for an increase in the GCL hydraulic conductivity in the unlikely event that leakage through both the primary and secondary geomembrane liners occurred in sufficient quantity to saturate the GCL with tailings leachate, the amount of flow through the secondary liner system with the prescriptive compacted clay liner was evaluated to be nearly five times greater than the flow through the secondary liner system with a standard GCL underliner. Use of a polymer-treated GCL exhibited improved compatibility with the tailings leachate, further reducing theoretical flow through the liner system. Therefore, the secondary liner system containing a standard GCL performs better than the secondary liner system containing the prescriptive clay liner, and use of a polymer-treated bentonite within the GCL is not warranted. Further, a standard GCL underliner appears to be the most cost-effective and constructible solution to meet (or exceed) the regulatory requirements.

Where geomembrane composite-lined slopes underlain by compacted clay liner materials have been exposed for long periods of time, desiccation and cracking of the clay component often occurs (Giroud 2005). Though use of GCL as the underliner component prevents the issue of clay desiccation, shrinkage has been documented to occur due to long-term exposure of the liner system (Giroud 2005). In addition to the use of white geomembrane to limit the temperature variations in the liner system, other provisions incorporated into the tailings cell design to limit effects of GCL shrinkage include installation of intermediate anchor benches to anchor the GCL layer, and doubling the manufacturer-recommended longitudinal and end-of-roll overlaps. In addition to these construction considerations, pre-hydration of the GCL is provided during the construction process to enhance the permeability characteristics of the GCL (Shackelford et al. 2000; Bonaparte et al. 2002). Immediately prior to GCL placement, water will be applied lightly to the silty subgrade soils which have been compacted to a minimum of 95 percent of the standard Proctor maximum dry density at optimum to plus four percent of the optimum moisture content to facilitate prehydration of the GCL via subgrade moisture adsorption.

2.6 Underdrain System Design

Per Criterion 5E(3) of 6 CCR 1007-1, Part 18, Appendix A, the tailings cells have been designed to facilitate dewatering of the tailings (i.e. lower the phreatic surface and reduce the driving head for seepage) via an underdrain system installed at the base of the impoundment. The tailings are expected to consist of silty sand to sandy silt materials, which are considered amenable to dewatering, particularly if some segregation by particle size results from deposition as dilute slurry.

The tailings underdrain system is comprised of collection pipes at the base of the tailings cell which convey solution to underdrain sumps. The underdrain collection pipes are proposed to consist of perforated corrugated HDPE pipes placed

in trenches, which are backfilled with imported granular drainage materials. The underdrain sump will be constructed above the LCRS sump to provide head for pumping of collected seepage. The underdrain sump is proposed to be backfilled with coarse underdrain fill overlain by fine underdrain fill to ensure filter compatibility with the overlying tailings. Two underdrain riser pipes are proposed within each sump to add redundancy to the system. The lower ends of the risers are slotted in the sump area to provide solution access. Solution is recovered via an automated submersible pump installed in the riser and returned to the mill circuit.

3. EVAPORATION POND LINER SYSTEM DESIGN

3.1 Evaporation Pond Liner System Summary

The evaporation ponds are designed to be constructed as ten inter-connected 1.6-hectare cells, with a total combined area of 16.2 hectares. A second phase of pond construction was designed, including an additional 16.2 hectares of ponds, to provide for an increase in the milling capacity to 900 tonnes per day. The evaporation pond liner design (from top to bottom) consists of (Figure 3):

- 1.5 mm HDPE upper (primary) geomembrane;
- LCRS consisting of HDPE geonet;
- 1.5 mm HDPE lower (secondary) geomembrane;
- Reinforced GCL as the underliner component of the secondary composite liner system; and
- Prepared subgrade.

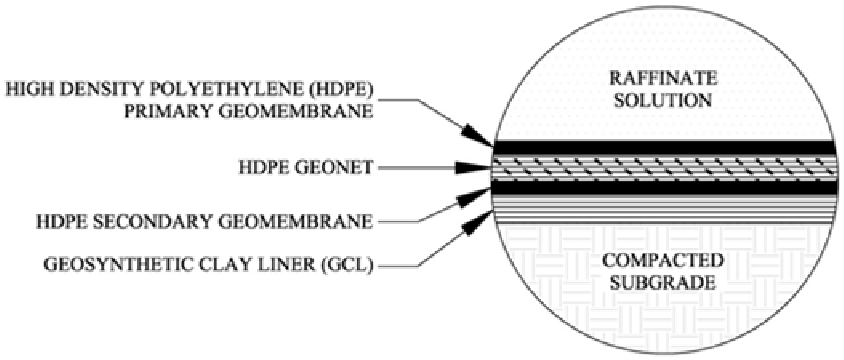

Figure 3. Evaporation pond liner system detail.

3.2 Upper Primary Geomembrane Liner

The upper primary liner will consist of a conductive smooth 1.5 mm HDPE geomembrane. The evaporation pond liner will be exposed for the life of the mill (i.e., up to 40 years), and was therefore designed for long-term solar radiation exposure. At closure, the evaporation pond liner system will be removed and placed in the final tailings cell.

To ensure quality assurance during installation of the liner system, the upper primary geomembrane liner will be conductive to facilitate spark testing of the liner surface upon completion of the installation, similar to the requirements of the tailings cells. A standard black HDPE geomembrane will be employed as the upper (primary) liner for increased evaporation potential.

3.3 Leak Collection and Recovery System

As part of the evaporation pond design, a LCRS has been incorporated to meet the requirements of the regulations. The LCRS is designed to minimize hydraulic heads on the lower geomembrane liner. The LCRS layer has been designed as an HDPE geonet per the methods outlined in Giroud et al. (1997b) with a minimum transmissivity which exceeds the minimum transmissivity requirement of 3×10^{-4} m^2/s (per 40 CFR 264.221).

Leakage through the upper geomembrane liner will be collected in the LCRS layer and routed (via gravity flow) to a LCRS sump located in each evaporation pond cell. The LCRS sump provides capacity for approximately two weeks of anticipated leakage, which facilitates use of a mobile pump for removal of leakage solution. Recovered solutions will be returned to the evaporation pond system.

3.4 Lower Secondary Composite Liner System

The standard of practice for design of evaporation ponds for uranium milling facilities is generally to exclude the low permeability underliner component of the secondary liner. However, the evaporation pond area is underlain by varying thicknesses of collapsible soils and shallow excavation is planned. Therefore the evaporation ponds were conservatively designed applying the same standards as those required for the tailings cells.

4. ORE PAD LINER SYSTEM DESIGN

4.1 Background

The ore pad design consists of a 0.4-hectare reinforced concrete pad surrounded by a 2-hectare lined pad. An elevated ore dumping platform is planned to the east of the 2-hectare lined pad which allows haul trucks to dump ore onto the pad without requiring access onto the pad. This design feature allows ore delivery to site without entrance into the license boundary (a cantilevered retaining wall separates the ore pad from the dumping platform, and also forms part of the license boundary), therefore removing the necessity for mandatory truck decontamination. A stormwater pond is planned to the north of the ore pad to capture surface water flows which are then conveyed to the evaporation ponds, maintaining the ore pad as a zero-discharge facility.

4.2 Ore Pad Liner System Summary

The 0.4-hectare ore pad has been designed as reinforced concrete and designed to minimize infiltration and maximize runoff to the adjacent 2-hectare ore pad. Concrete design for the 0.4-hectare ore pad includes water stops to minimize infiltration at construction joints. The 2-hectare ore pad is sloped gently (approximately two percent) toward the stormwater pond. Little runoff from the ore pad is expected, as direct precipitation is the only water source, aside from occasional dust control spraying.

The liner system considered for the 2-hectare ore stockpile pad includes (from top to bottom) (Figure 4):

- 0.3 m of roadbase gravels;
- 0.75 m of compacted native soils;
- Reinforced geosynthetic clay liner (GCL); and
- Prepared subgrade.

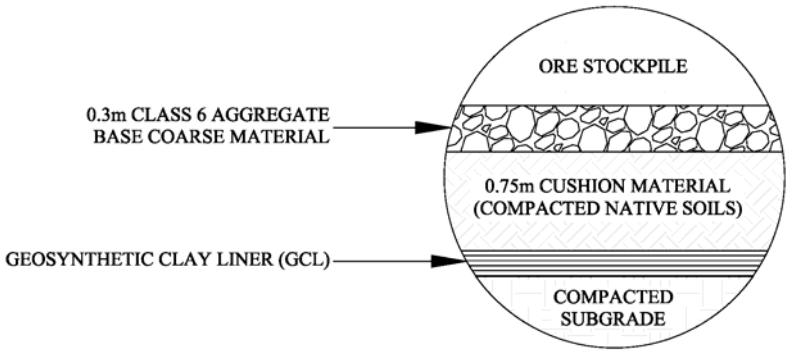

Figure 4. Two-hectare ore pad liner system detail.

4.3 Cover Material

As the GCL serves as the primary flow barrier and the ore pad will be regularly trafficked by construction equipment, a cover was designed to protect the GCL from the maximum anticipated construction traffic loading. The cover consists of 0.3 m of roadbase material, which serves primarily as a wearing surface, and 0.75 m of compacted native soil, which serves primarily as a cushion material to protect the GCL.

4.4 Geosynthetic Clay Liner

The primary liner proposed for the 2-hectare ore stockpile pad is reinforced GCL. The GCL will be placed directly over prepared subgrade. The proposed GCL provides good overall liner system stability at the proposed ore pad base grades, as well as providing a liner system with permeability characteristics appropriate for this application.

5. CONCLUSIONS

Regulations developed in 1992 which govern the design of new uranium mill facilities are currently being applied for the first time at a new facility for the Piñon Ridge Project, located in western Colorado. As an Agreement State, Colorado has the authority to license the possession and use of radioactive materials in Colorado under the Radiation Control Act (Title 25, Article 11), and Colorado's Rules and Regulations Pertaining to Radiation Control (6 CCR 1007-1).

In general, the regulations provide minimum requirements, some prescriptive and some flexible in order to allow for optimization on a site-specific basis. For instance, the tailings cell and evaporation pond liner systems are prescriptive, while the ore pad liner requirements are more flexible, based on general performance standards. The liner system designs described in this paper include adjustments to suit site-specific conditions, while meeting, and sometimes exceeding, the prescriptive and general performance requirements of the applicable regulations.

Early meetings with CDPHE, the responsible regulatory agency, provide a valuable opportunity to adjust the design in response to agency comments prior to actual permit submittal. Formal issue of the permit application for the mill is planned for mid to late 2009, after which point CDPHE has one year to review the application.

ACKNOWLEDGEMENTS

The authors would like to thank Energy Fuels Resources Corporation (EFRC) for allowing this paper to be published. Further, the authors would like to acknowledge the cooperation of the Colorado Department of Public Health and Environment (CDPHE) in providing suggestions which have improved the quality of the proposed facility designs.

REFERENCES

6 CCR 1007-1, Part 18 – State Board of Health Licensing Requirements for Uranium and Thorium Processing, specifically Appendix A (Criteria relating to the operation of mills and the disposition of the tailings or wastes from these operations).

10 CFR Part 40 – Domestic Licensing of Source Material, Appendix A to Part 40 (Criteria Relating to the Operation of Uranium Mills and the Disposition of Tailings or Wastes Produced by the Extraction or Concentration of Source Material from Ores Processed Primarily for their Source Material Content).

40 CFR Part 192 – Health and Environmental Protection Standards for Uranium and Thorium Mill Tailings, Subpart D (Standards for management of uranium byproduct materials pursuant to section 84 of the Atomic Energy Act of 1954, as amended).

40 CFR Part 264 – Standards for Owners and Operators of Hazardous Waste Treatment, Storage, and Disposal Facilities, Subpart K (Surface Impoundments).

Adams, M.W. and Wagner, N. (2000) Forensic study of an HDPE liner – Evaluating physical property integrity of a geomembrane used at a wastewater treatment facility for 11 years. *GFR*. September. Vol. 18., No. 7.

American Society for Testing and Materials (ASTM). ASTM D 6766. Standard test method for evaluation of hydraulic properties of GCLs permeated with potentially incompatible fluids.

Bonaparte, R., Daniel, D.E., and Koerner, R.M. (2002) Assessment and recommendations for optimal performance of waste containment systems. *EPA/600/R-02/099*, December, U.S. EPA.

Giroud, J.P., and Bonaparte, R. (1989) Leakage through liners constructed with geomembranes – Part I. Geomembrane Liners. *Geotextiles and Geomembranes* 8: 27-67.

Giroud, J.P., Badu-Tweneboah, K., and Soderman, K.L. (1997a) Comparison of leachate flow through compacted clay liners and geosynthetic clay liners in landfill liner systems. *Geosynthetics International* 4(3-4): 391-431.

Giroud, J.P., Gross, B.A., Bonaparte, R., and McKelvey, J.A. (1997b) Leachate flow in leakage collection layers due to defects in geomembrane liners. *Geosynthetics International* 4(3-4): 215-292.

Giroud, J.P. (2005) Contribution of the geosynthetics to the geotechnical aspects of waste containment. *The Mercer Lecture, 2005-2006*.

Hsuan, Y.G., Jr., A.E.L., and Koerner, R.M. (1991) Effects of outdoor exposure on a high density polyethylene geomembrane. *Geosynthetics '91 Conference Proceedings*, Atlanta, USA, 287-302.

Ivy, N. (2002) HDPE geomembrane after 20 years of service. *GFR*. June/July.

Koerner, R.M., Hsuan, Y.G., and Koerner, G.R. (2005) Geomembrane lifetime prediction: unexposed and exposed conditions. *GRI White Paper #6*, Geosynthetic Institute, Folsom, PA, 19 pp.

Martin, D. (2005) UV resistance in thin film geomembranes, accelerated and natural weathering studies. Geotechnical Special Publication (GSP) 142, *Proceedings, Geo-Frontiers 2005*, Austin, Texas.

Rollin, A.L. (2004) Long term performance of polymeric geomembranes. *GeoQuebec*, 57th Canadian Geotechnical Conference. 20-24.

Rowe, K., Sangam, H. P., and Lake, C. B. (2003) Evaluation of an HDPE geomembrane after 14 years as a leachate lagoon liner. *Canadian Geotechnical Journal* 40: 536-550.

Shackelford, C.D., Benson, C.H., Katsumi, K., Edil, T., and Lin, L. (2000) Evaluation of the hydraulic conductivity of GCLs permeated with non-standard liquids. *Geotextiles and Geomembranes*, 18, 133-161.

Geosynthetics 2009
February 25-27 2009, Salt Lake City, Utah

Rapid Shear Response of a Needle-Punched GCL

P.J. Fox, PhD, PE, Ohio State University, Columbus, Ohio, USA
J.M. Sura, BSCE, Ohio State University, Columbus, Ohio, USA
J.D. Ross, BSCE, Ohio State University, Columbus, Ohio, USA
J.T. Olsta, MSCE, PE, CETCO, Arlington Heights, Illinois, USA

ABSTRACT
This paper presents rapid internal shear strength data for a needle-punched geosynthetic clay liner (GCL) that was obtained using a large direct shear device. A series of monotonic (i.e., single direction) shear tests illustrate the effect of shear displacement rate *R* on material response at four normal stress levels. The data indicate that peak shear strengths first increased and then decreased as *R* was increased from 0.1 to 28,000 mm/min. The highest peak strengths occurred at *R* = 100 to 10,000 mm/min and were 13 to 23% higher than corresponding static peak strengths (*R* = 0.1 mm/min). Static peak strengths were found to be generally conservative at each normal stress level. Displacements at peak shear strength consistently decreased with increasing *R* and increasing normal stress. Residual shear strengths increased markedly with increasing *R* for *R* ≥ 1 mm/min, whereas the reverse trend was observed for *R* < 1 mm/min.

1. INTRODUCTION

Geosynthetic liner systems are occasionally subjected to earthquakes and other dynamic loads. As such, the characterization of the dynamic shear behavior of these materials is important for prediction of long-term performance. Several studies have been conducted on the dynamic shear response of geosynthetic interfaces, including geotextile/geomembrane, geonet/geomembrane, geonet/geotextile, and geomembrane/geomembrane (Yegian and Lahlaf 1992, Yegian et al. 1995, De and Zimmie 1998, Yegian and Kadakal 1998, Kim et al. 2005). These studies have generally involved low normal stresses, often 15 kPa or less. Very little data exists for high normal stress levels and for certain types of geosynthetics, such as geosynthetic clay liners (GCLs).

GCLs are manufactured hydraulic barriers consisting of bentonite clay bonded to a layer, or layers, of geosynthetic material. These products are widely used in the construction of landfills and other facilities that require hydraulic barriers (e.g., ponds, lagoons, canals). Advantages of GCLs include ease of installation, reduction in liner system volume, and cost savings, especially for facilities where suitable clay is locally unavailable. Particular attention is often given to the shear strength of GCLs and GCL interfaces because bentonite, the essential component of a GCL, is a very weak material after hydration and thus can provide a potential surface for stability failure. Extensive information is now available on the static shear strength of GCLs (e.g., Fox and Stark 2004). By comparison, almost no information is available on the dynamic shear strength of these materials. Lai et al. (1998) presented the initial study in which small specimens of an unreinforced GCL were tested in direct simple shear at low normal stress. Nye and Fox (2007) presented an extensive testing program of monotonic and cyclic direct shear tests on a needle-punched GCL at a single normal stress (141 kPa). Additional data were presented by Fox et al. (2008) for monotonic shear strengths in which shear occurs in a single direction (i.e., single thrust). Information on dynamic GCL strength behavior at higher normal stress levels is needed for the seismic design of bottom liner systems.

A laboratory research program is in progress at Ohio State University to investigate the shear behavior of GCLs and GCL interfaces under dynamic loading conditions. The full testing program is described by Fox et al. (2005). Shear tests are being conducted using a new dynamic direct shear machine that was designed and constructed for the project. Initial data sets presented by Nye and Fox (2007) and Fox et al. (2008) have provided first insights on the internal shear behavior of a needle-punched GCL under monotonic and cyclic loading. This paper presents more recent data on monotonic internal shear strength obtained over a broad range of displacement rates, including tests conducted at higher normal stress levels.

2. PROCEDURES

All tests were performed using a large dynamic direct shear machine that is shown in Figure 1 and described in detail by Fox et al. (2006). The main features of this device include a large specimen size (305 × 1067 mm), large normal stress range (0 to 2000 kPa), large maximum shear displacement (254 mm), large range of displacement rate (0.01 to 60,000

mm/min for zero load), negligible machine friction, and the capability to measure specimen volume change. A GCL specimen is sheared between the underside of a horizontal pullout plate and the floor of the test chamber, each of which

Figure 1. Dynamic direct shear machine.

is covered with an aggressive gripping surface (modified truss plates). The gripping surfaces permit drainage of the specimen on both sides and are sufficiently rough that end-clamping of the geosynthetics is not required. This allows a specimen to fail along the weakest surface and avoids possible progressive failure effects (Fox and Kim 2008). The shearing system is powered by a 245 kN hydraulic actuator that can impart bidirectional (i.e., back-and-forth) motion to the pullout plate. The maximum frequency for sinusoidal loading with a displacement amplitude of 25 mm is 4 Hz. Normal stress is provided by two bellowed air bladders that rest on an overlying stationary load plate. Between the load plate and the pullout plate, a layer of 517 free-rolling stainless steel balls reduce the shear stress due to friction to 0.27% of the applied normal stress. Vertical displacement of the load plate due to specimen volume change is continuously monitored during hydration and shearing using a LVDT. GCL specimens are hydrated from a water reservoir at the rear of the machine through a network of drainage channels in both shearing surfaces. The system has an automated digital servocontroller that provides full control over machine operation and data collection.

An extensive program of rapid internal shear tests has been conducted on Bentomat ST, a woven/nonwoven needle-punched GCL with no thermal bonding manufactured by CETCO (Arlington Heights, Illinois, USA). The average peel strength of the material (ASTM D 6496) was 1580 N/m. Specimens were hydrated using the two-stage procedure described by Fox et al. (1998), in which each specimen is pre-hydrated to the expected final water content prior to placing in the shear machine. Following hydration, 68 GCL specimens were subjected to displacement-controlled monotonic (i.e., single direction) shear tests to evaluate the effect of shear displacement rate R on peak and residual shear strengths and displacements at peak strength. Tests were performed at four shearing normal stress $\sigma_{n,s}$ levels (141, 348, 692, and 1382 kPa) with displacement rates ranging from 0.1 to 28,000 mm/min., the latter of which is the maximum limit of the machine for these loads. Additional specimens have been subjected to displacement-controlled cyclic shear tests with subsequent static shear measurements. The cyclic data obtained at $\sigma_{n,s}$ = 141 kPa is presented by Nye and Fox (2007). This paper presents the monotonic shear results, including new data obtained at high normal stress.

3. RESULTS

Figure 2 shows representative relationships for shear stress τ versus shear displacement Δ that were obtained from the monotonic shear testing program. These curves were obtained for $\sigma_{n,s}$ = 348 kPa and span the full range of displacement rate from 0.1 to 28,000 mm/min. The slowest rate (0.1 mm/min) is the recommended value for conventional static shear testing (Fox and Stark 2004). The curves are generally similar in shape with well-defined peak and residual shear strengths. Large post-peak strength reductions occur at each *R* value due to failure of the reinforcement. Although peak and residual shear strengths show some rate dependency, the general similarity of curves in Figure 2 suggests that the basic mechanism of failure is consistent for all displacement rates.

Values of peak shear strength τ_p are shown in Figure 3 as a function of *R*. As expected, peak strengths increase with increasing normal stress at each displacement rate. At $\sigma_{n,s}$ = 141 kPa, a static peak shear strength of 158 kPa was measured for *R* = 0.1 mm/min. As *R* increased, the average τ_p value increased to 185 kPa at *R* = 1000 mm/min and then decreased to 153 kPa at *R* = 28,000 mm/min. Thus, peak strength increased to a maximum of 17% above the static value and then returned to approximately the same value at the highest displacement rate. Tests conducted at $\sigma_{n,s}$ = 348 kPa yielded a generally similar response. At this normal stress, the highest peak strength (266 kPa) occurred at *R* = 100 to 1000 mm/min and was 13% higher than the static strength (236 kPa). At *R* = 28,000 mm/min, the peak strength (250 kPa) was 6% higher than the static shear strength. For $\sigma_{n,s}$ = 692 kPa, peak strengths increased 14.5% from 352 kPa at *R* = 0.1 mm/min. to 403 kPa at *R* = 10,000 mm/min. and then decreased only slightly thereafter. Peak shear strengths at the highest normal stress level (1382 kPa) again increased with increasing displacement rate. In this case, τ_p reached the highest value (499 kPa) at *R* = 1,000 mm/min, which was 23% above the static strength of 404 kPa. Beyond 1,000 mm/min., τ_p decreased to approximately 469 kPa. At some stress levels (e.g., 1382 kPa) the data display significant scatter, which is attributed to variability of needle-punched reinforcement. The observed trend in peak strengths suggests an increasing and then decreasing resistance of reinforcing fibers as *R* increases. Zornberg et al. (2005) found that τ_p decreased as *R* increased from 0.0015 to 1 mm/min at high normal stress ($\sigma_{n,s}$ = 520 kPa). The slower shear data in Figure 3 are inconclusive with regard to this point (also see discussion by Fox 2006). A key observation with regard to Figure 3 is that, in general, static peak strengths obtained at 0.1 mm/min. are conservative at each normal stress level.

Corresponding displacements at peak shear strength Δ_p are shown in Figure 4. At each displacement rate, the value of Δ_p decreased with increasing normal stress. The data for static shear (*R* = 0.1 mm/min) are somewhat contradictory to the findings of Fox et al. (1998) in which Δ_p for the same GCL product ranged from 21 to 26 mm and did not show a clear trend when $\sigma_{n,s}$ was increased from 38 to 279 kPa. Figure 4 also shows that, at each normal stress, Δ_p generally decreased with increasing *R*. At $\sigma_{n,s}$ = 141 kPa, Δ_p decreased from approximately 31 mm at the slow rates to 21 mm at the fastest rate. Corresponding decreases for the other three normal stresses were 27 mm to 16 mm for $\sigma_{n,s}$ = 348 kPa, 19 mm to 15 mm for $\sigma_{n,s}$ = 692 kPa, and 16 mm to 13 mm for $\sigma_{n,s}$ = 1382 kPa. The explanation for this effect may be that, at higher *R*, the initially loaded reinforcing fibers fail more quickly because there is less time available for load transfer to nearby fibers. If correct, it is interesting that this effect generally produces higher peak shear strengths (Figure 3).

Residual shear strengths τ_r obtained from the same monotonic tests are shown in Figure 5. As expected, residual strengths increased with increasing normal stress at each displacement rate. At each normal stress, τ_r values increased with increasing *R* for *R* ≥ 1 mm/min, which is consistent with most previous studies (e.g., Fox et al. 1998, Eid et al. 1999). This increase is particularly marked for *R* > 1000 mm/min. However, the reverse trend is observed for *R* < 1 mm/min and becomes pronounced at the highest normal stress. A general increase in residual strength with increasing *R* has been attributed to rate-dependent shear resistance of the hydrated bentonite (Fox et al. 1998). The data in Figure 5 indicate that the static shear displacement rate of 0.1 mm/min. may produce unconservative residual strengths for some dynamic applications and that lower values of τ_r can be obtained at *R* = 1 mm/min.

4. CONCLUSIONS

This paper presents data obtained on the rapid internal shear strength of a hydrated needle-punched GCL with no thermal bonding using a large direct shear device. A series of displacement-controlled monotonic (i.e., single direction) shear tests were conducted at four normal stress levels with shear displacement rate *R* ranging from 0.1 to 28,000 mm/min. The data indicate that peak shear strengths first increased and then decreased as *R* was increased from 0.1 to 28,000 mm/min. The highest peak strengths occurred at *R* = 100 to 10,000 mm/min and were 13 to 23% higher than corresponding static peak strengths (*R* = 0.1 mm/min). Static peak strengths were generally conservative at each normal stress level. Displacements at peak shear strength consistently decreased with increasing *R* and increasing normal stress. Residual shear strengths increased with increasing *R* for *R* ≥ 1 mm/min. and particularly for *R* > 1000

mm/min., whereas the reverse trend was observed for R < 1 mm/min. The lowest values of residual strength were obtained at R = 1 mm/min.

ACKNOWLEDGEMENTS

Financial support for this work was provided by a grant from CETCO of Arlington Heights, Illinois, USA. This support is gratefully acknowledged. The writers thank Dr. Jangguen Lee for his assistance with some of the experimental work presented in this paper.

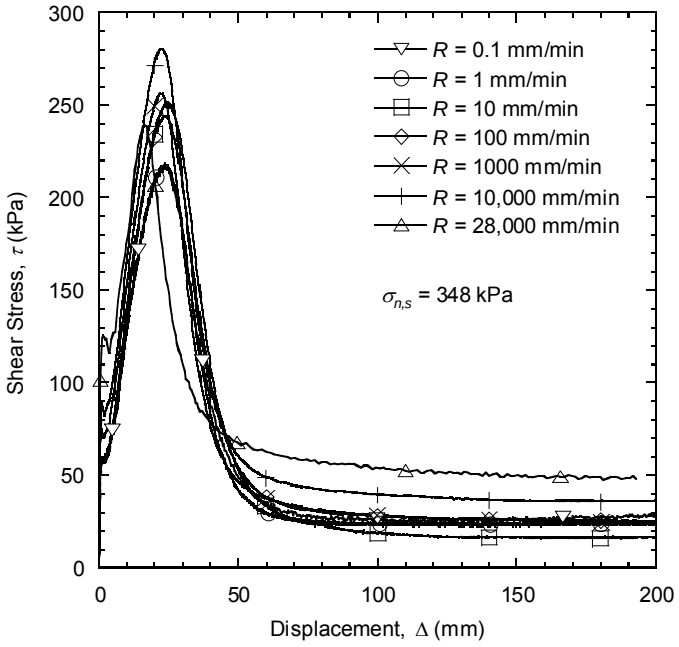

Figure 2. Shear stress-displacement relationships for seven monotonic shear tests at 348 kPa.

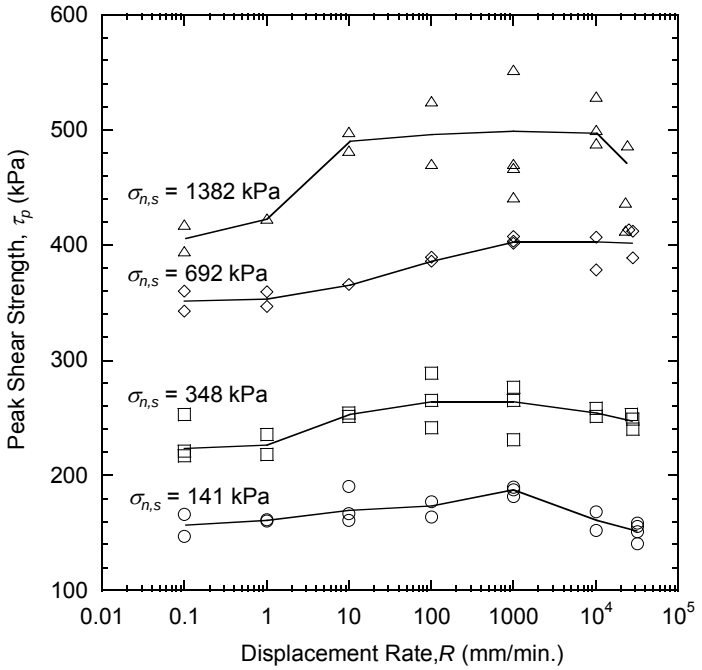

Figure 3. Effect of displacement rate on peak shear strength for monotonic shear.

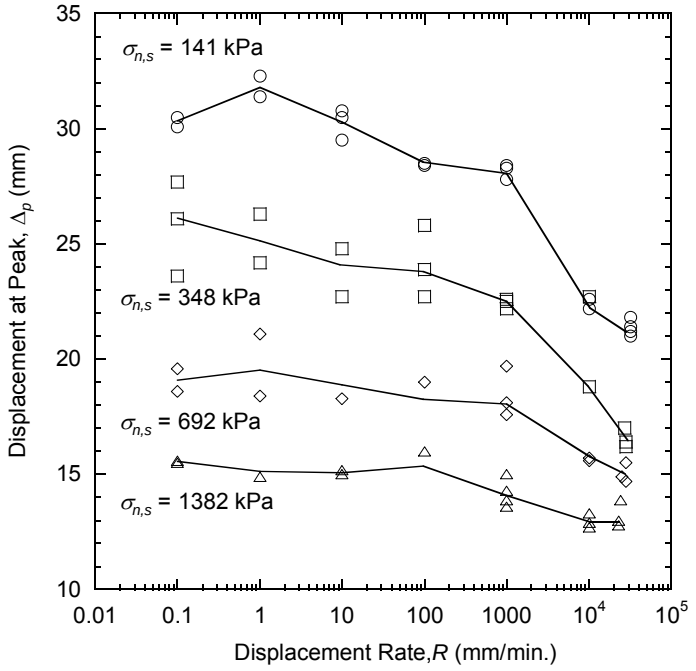

Figure 4. Effect of displacement rate on displacement at peak shear strength for monotonic shear.

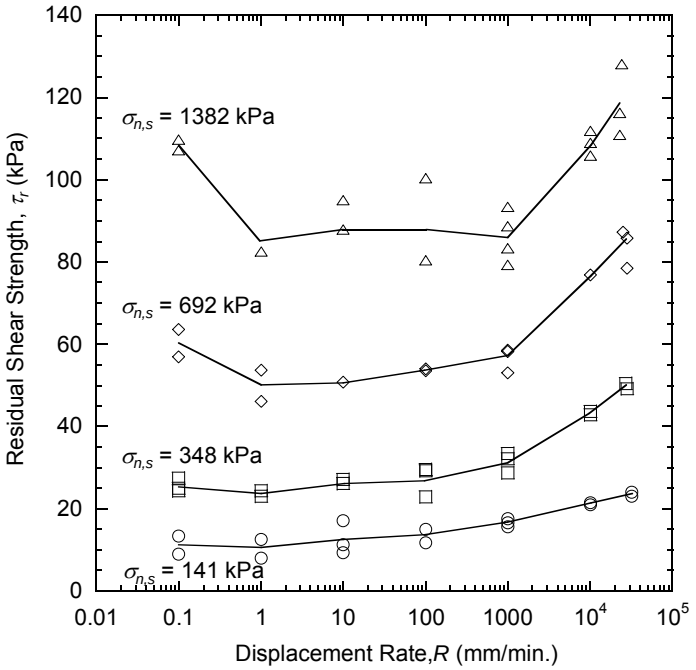

Figure 5. Effect of displacement rate on residual shear strength for monotonic shear.

REFERENCES

ASTM D 6496. Standard Test Method for Determining Average Bonding Peel Strength Between the Top and Bottom Layers of Needle-Punched Geosynthetic Clay Liners, *ASTM International*, West Conshohocken, Pennsylvania, USA.

De, A., and Zimmie, T.F. (1998). Estimation of dynamic interfacial properties of geosynthetics, *Geosynthetics International*, 5(1-2): 17-39.

Eid, H.T., Stark, T.D., and Doerfler, C.K. (1999). Effect of shear displacement rate on internal shear strength of a reinforced geosynthetic clay liner, *Geosynthetics International*, 6(3): 219-239.

Fox, P.J. (2006). Discussion of "Analysis of a large database of GCL internal shear strength results" by J.G. Zornberg, J.S. McCartney and R.H. Swan, Jr., *Journal of Geotechnical and Geoenvironmental Engineering*, 132(10): 1373-1375.

Fox, P.J., and Stark, T.D. (2004). State-of-the-art report: GCL shear strength and its measurement, *Geosynthetics International*, 11(3): 141-175.

Fox, P.J., and Kim, R.H. (2008). Effect of progressive failure on measured shear strength of geomembrane/GCL interface, *Journal of Geotechnical and Geoenvironmental Engineering*, 134(4): 459-469.

Fox, P.J., Rowland, M.G., and Scheithe, J.R. (1998). Internal shear strength of three geosynthetic clay liners, *Journal of Geotechnical and Geoenvironmental Engineering*, 124(10): 933-944.

Fox, P.J., Morrison, T.C., Nye, C.J., Hunter, J.G., and Olsta, J.T. (2005). Current research on dynamic shear behavior of needle-punched geosynthetic clay liners, *Geosynthetics '05,* North American Geosynthetics Society, Las Vegas, Nevada, USA (CD-ROM).

Fox, P.J., Nye, C.J., Morrison, T.C., Hunter, J.G., and Olsta, J.T. (2006). Large dynamic direct shear machine for geosynthetic clay liners, *Geotechnical Testing Journal*, 29(5): 392-400.

Fox, P.J, Sura, J.M., Lee, J., and Olsta, J.T. (2008). Research on dynamic GCL shear strength, *1st Pan American Geosynthetics Conference*, Cancun, Mexico (CD-ROM).

Kim, J., Riemer, M., and Bray, J.D. (2005). Dynamic properties of geosynthetic interfaces, *Geotechnical Testing Journal*, 28(3): 1-9.

Lai, J., Daniel, D.E., and Wright, S.G. (1998). Effects of cyclic loading on internal shear strength of unreinforced geosynthetic clay liner, *Journal of Geotechnical and Geoenvironmental Engineering*, 124(1): 45-52.

Nye, C.J., and Fox, P.J. (2007). Dynamic shear behavior of a needle-punched geosynthetic clay liner, *Journal of Geotechnical and Geoenvironmental Engineering*, 133(8): 973-983.

Yegian, M.K., and Kadakal, U. (1998). Geosynthetic interface behavior under dynamic loading, *Geosynthetics International*, 5(1-2): 1-16.

Yegian, M.K., and Lahlaf, A.M. (1992). Dynamic interface shear strength properties of geomembranes and geotextiles, *Journal of Geotechnical and Geoenvironmental Engineering*, 118(5): 760-779.

Yegian, M.K., Yee, Z.Y., and Harb, J.N. (1995). Seismic response of geosynthetic/soil systems, *Geoenvironment 2000*, Y. B. Acar and D. E. Daniel, eds., Geotechnical Special Publication No. 46, ASCE, 2: 1113-1125.

Zornberg, J.G., McCartney, J.S., and Swan, R.H., Jr. (2005). Analysis of a large database of GCL internal shear strength results, *Journal of Geotechnical and Geoenvironmental Engineering*, 131(3): 367-380.

Safer Levees with Geosynthetic Clay Liners and Erosion Control Mats

G. Heerten, NAUE GmbH & Co. KG, Espelkamp, Germany
J. Klompmaker, BBG Bauberatung Geokunststoffe GmbH & Co. KG, Espelkamp, Germany
C. Lesny, NAUE America, Inc., Atlanta, USA

ABSTRACT
After the past flood disasters in Europe, safe and modern levee cross-sections with geosynthetics have been carried out. The use of filter nonwovens between the levee core and the exposed drainage and ballast berm at the inner levee embankment or the arrangement of geosynthetic clay liners (bentonite mats, GCLs) at the outer levee embankment are included as well-established alternatives in current guidelines. In addition, the efficiency of stabilization measures with geosynthetics integrated in the levee was investigated and a high stability of these construction methods in case of overtopping was documented. Erosion at the inner levee embankment and unexpected levee failures can be prevented and/or be delayed. The potential that such levee breaks by forming a levee gap is minimized, because the levee body cannot be eroded. The approach to improve the safety of levees dramatically by integrating different geosynthetics in the levee cross-section could significantly reduce the danger and potential flooding damages in many other parts of the world.

1. INTRODUCTION

In the aftermath of past high-water events in Germany, a large-scale program to build safe, modern levees of adequate cross-section with geosynthetic materials has been realized. The use of nonwoven filter materials to form a filter-stable, erosion-resistant transition between levee core and the air-side drain and ballast body or the arrangement of geosynthetic clay liners (bentonite mats) as a water-side surface seal have become anchored as established alternatives in current regulations. Beyond the three-zone levee, the effects of geosynthetics integrated into levees as safety measures have been investigated and documented to have a high resistance capability during overflow load conditions. Erosion processes on the inner embankment and the risks of unexpected levee breaches can be minimized with geosynthetic construction techniques; geosynthetics can also be employed as support facilities for emergency reinforcing measures.

2. GEOSYNTHETIC CLAY LINERS (GCL, BENTONITE MATS)

2.1 General

At the end of the 80s, needle-punched shear-resistant bentonite mats were developed as a new geo-engineering construction product. Having only about 1 cm of bentonite – protected against shear force and erosion between geosynthetics – a factory-produced clay sealing material (geosynthetic clay liner, GCL) was introduced as an alternative to conventional clay liners created by on-site earthwork construction. Actually, geosynthetic clay liners are widely used in landfill sealing systems all over the world. In early days the coffer dams to separate the canal section for repair and the secondary seal beneath the asphalt seal of the Bavarian Lech Canal were the first major applications back then to employ this new construction product in water-related construction projects. According to BAW (2002), bentonite mats are classified as mineral sealing systems just like classic clay and loam seals.

Aside from applications for environmental protection against storm damage, there have also been many important water-related structures successfully realized with needle-punched bentonite mats over past years and advanced product developments have been made for underwater installations (BAW 2002). Needle-punched bentonite mats have gained widespread acceptance for levee improvement projects because these products create a simple, effective, economical seal for a levee that simultaneously provides erosion protection for the levee body (Heerten et al. 2002 and Heerten 2003a). Following the Elbe River floods that took place in Germany between 2002 and the end of 2005, about 150 levee reconstruction projects are known in which about 2.2 Mm² of needle-punched nonwovens, about 300 000 m² of geogrids and about 700 000 m² of geosynthetic clay liners (bentonite mats) have been employed (Heerten 2003b and Heerten et al. 2006). One example is shown in Figure 1.

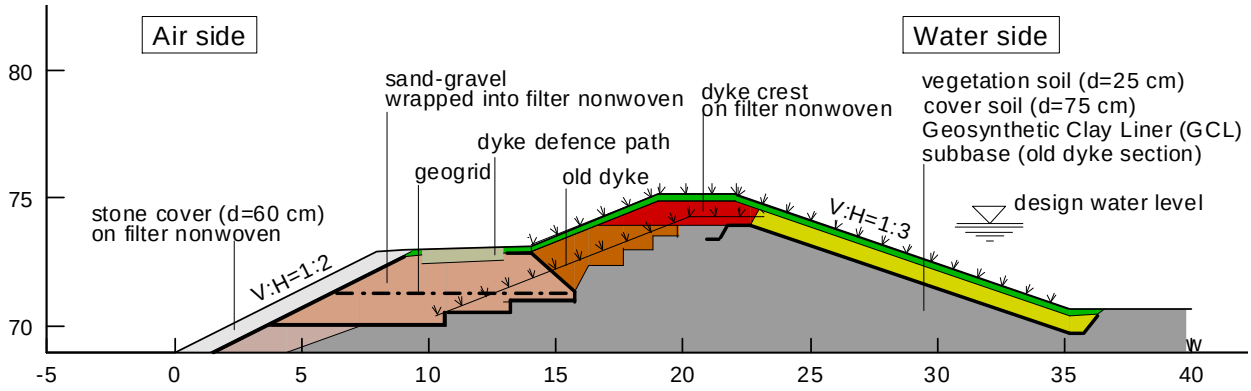

Figure 1. Standard cross-section of a reconstructed Elbe levee near Bösewig / Sachsen-Anhalt (Heerten et al. 2006)

2.2 Levee seal – current excavation results

According to DWA (2005), a cover layer thickness of 80 cm is recommended for both types of mineral sealing system in order to withstand climatic influences. Bentonite mats offer the advantages of low sensitivity to settling without degradation to seal characteristics, consistent quality even after installation, as well as good friction behavior for steeper embankment slopes. However, the potential effects of root penetration and/or rodent infestation must be given attention just the same as with classic seals made of cohesive soil. These effects can be counteracted by the design of the levee's project-oriented cross-section geometry, the use of non-cohesive cover layers unattractive to burrowing animals (Figure 2) or by additional engineering measures. Further information about planning and building with geosynthetic clay liners can be found in BAW (2006), DGGT (2002), Heerten (2007) and Saathoff et al. (2003).

With regard to mineral sealing layers (CCLs and GCLs) in landfill sealing systems, concerns about desiccation for mineral layers and ion exchange for bentonite have been reported and discussed (Heerten & Koerner 2008). In contrast to compacted clay liners (CCLs) needlepunched GCLs show very good "self-healing" performance after desiccation, especially due to the small amount of water needed (approx. 1 l/m²) under a soil confining stress of 15 kN/m². The author also discovered during several excavations in the past years that ion exchange occurred during the first 2 - 3 years (Heerten et al. 2006) and that the self-healing was extremely evident with the excavated GCLs which had powder bentonite sandwiched between the geotextiles.

Excavations of bentonite mats at the German levees Lippe / Haltern-Lippramsdorf (a) in the Ruhr region as well as on the Kinzig near Offenburg (b) at the southern Rhine were carried out recently. The bentonite mats at these locations have been in place for 6 and 12 years respectively. The excavations were performed with the professional accompaniment of ICG Leonhardt - Veith GmbH & Co. KG, geotechnical engineering consultants, as well as representatives of the Karlsruhe office of the BAW. The results of these excavations were presented at the water engineering colloquium 2007 held at the Technical University Dresden (Fleischer et al. 2007). Subsequent laboratory investigations were aimed at assessing possible material changes that may have taken place over the multi-year deployment. In comparison to unused product these excavated samples exhibited no significant quality differences (Fleischer et al. 2007), thus confirming the fully functional condition of the installed bentonite mats. The bentonite mat samples taken exhibited permeability coefficients of $k = 2.5 \times 10^{-11}$ m/s to 8×10^{-11} m/s, even after laboratory proved ion exchange a hydraulic capability corresponding to the suitability tests prior to installation. Geosynthetic clay liners in a levee not being placed between drainage layers as it is a standard for landfill sealing systems show no influence or evidence of changing water content with regard to desiccation or self-healing. The implementations of both old levee improvement measures, (a) and (b), are presented below.

(a) Lippe levees (GCL excavation after 12 years deployment period)

This levee was improved in 1994. It is located in an area of mining subsidence and it is built along both sides of the Lippe River in the vicinity of Haltern-Lippramsdorf and Marl in the Ruhr region. These levees were improved in 1994 for floodwater protection of surrounding residential areas and the nearby Auguste Victoria mine. The improvement raised the levees by 50 cm. The project was commissioned by the Lippe Association who has tailings in the area left over from coal mining activity. A seal on the levee was necessary for both levee stability as well as for ecological reasons (leaching from tailings). The procurement of clay or loam soils was deemed to be uneconomical and would have necessitated extensive installation and monitoring overhead on the 1:n = 1:2 grade embankments during construction. Furthermore, construction time was limited to the months of low rainfall. These prevailing conditions led to an alternative; to lay out a

shear-force transmitting, needle-punched geosynthetic clay liner as a sealing element on surfaces at both sides of the Lippe River then to cover this with a 40 cm thick layer of sand, crushed stone and topsoil (Figure 2). At the southern levee, newly located tail piles were encircled with GCL. Steel sheet piling was installed along the foot of the northern levee to which the GCL was attached. These conditions provided further incentive for a solution with subsidence-insensitive GCL as connections to rigid structures can be accomplished readily and produce a very tight seal.

(b) Kinzig levees (GCL excavation after 6 years deployment period)

As early as 1987, the Southern Upper Rhine / High Rhine Water Authority began work to upgrade the 160 km long levees on the Kinzig (some parts then over 100 years old) to current state-of-the-art conditions. Floodwater events in 1990 and 1991 had already revealed critical levee leakage at several points. An extensive program for Kinzig levee reconstruction was formulated which was to be carried out in 2000 and 2001 that had the objective of creating a state-of-the-art structure. This program included plans to raise defined sections of the levee an average of between 60 cm and 80 cm, a reinforcement of the levee, and to place a needle-punched, shear-force transmitting geosynthetic clay liner on the levee's water side (Santo 2003). On the 1:n = 1:2.8 grade embankment, GCL was laid in sections of 100 m each then covered with a 60 cm thick layer of compacted fine gravel (as an intermediate layer to ward off burrowing animals). These layers were subsequently covered with a final 20 cm layer of topsoil then planted with grass. The gravel was taken directly out of the Kinzig's bed, which also represented an important maintenance function. On the left side near the town of Weier, a total of 36 000 m^2 geosynthetic clay liner was installed as a levee seal (Figure 3). From the standpoint of water authorities, the cost of delivery for a mineral sealing material would have made a loam seal uneconomical. Implementation and quality assurance was done with the consent of a geotechnical expert and the BAW.

Figure 2. Lippe River levee reconstruction (1994): Installing Bentofix® GCL as a levee seal (Saathoff et al. 2003).

Figure 3. Kinzig River levee reconstruction (2001): Covering Bentofix® GCL with locally available fine gravel to ward off burrowing animals (right).

3. OVERFLOW AND EROSION PROTECTION WITH GEOSYNTHETICS

Levee breaches caused by unintentional overflow, and consequential freeboard loss, inevitably represents a form of failure for levees ("unwanted polder") which are not secured. As floodwaters rise to the level of the levee's crown, emergency measures to shore up unsecured levee sections is a high-risk task for anyone involved with such efforts because a sudden breach of the levee must always be considered an imminent possibility. Particularly in areas with major damage potential, protective measures should be demanded which would significantly lower that damage risk.

There are numerous options to retrofit levees and dams with deliberate overflow features. DIN 19712 stipulates, *"Overflow segments are to be carefully planned, implemented and maintained. ... Where potential damage is not too critical, it is sufficient to reduce the grade of the land-side embankment within the range of 1:10 to 1:20 and provide a protected embankment footing."* The risk of a levee breach in combination with sudden flooding of the polder *"can be reduced by protecting the land-side embankment against erosion."* This type of improvement along entire stretches of levee *"was not previously an element of water engineering practice"* (DIN 19712/1997). The standard goes on to state, *"Every levee plan is to be reviewed for catastrophe-reducing potential through the implementation of erosion protected overflow segments at opportune points along the levee."* Under the expression "levee planning" all plans for levees, i.e. also those for levee improvement, are included. However, in practice these requirements are not generally being followed yet (Haselsteiner et al. 2007).

Deliberate overflow segments in levees offer the advantage that water quantities subsequently retained in the polders behind the levee at these points will reduce the floodwater hazard further downstream. But even in endangered areas with high damage potential it is recommended that protective measures be taken to preclude a complete levee breach. Because it is generally uneconomical to create very flat-sloped overflow segments for levees with concrete or grouted revetment – as, for example, is the case in the floodwater relief systems in dam structures (i.e. spillway chutes) – geosynthetics have been gaining acceptance for these applications. In the context of a "ground/geosynthetic composite system" it is possible to develop protective elements that will stabilize endangered inner embankments to prevent levee breaches and maintain levee cross-section integrity in the event of overload conditions. Potential protective methods (which can be combined with one another) employing ground/geosynthetic composite systems are:

(I) surface erosion protection in combination with intact grass cover
(II) near-surface erosion protection (if grass cover should be lost)
(III) integrated erosion protection (protecting the levee's cross-section)

Method (I) is accomplished by reinforcing the inner embankment with an armored grass cover. A three-dimensional erosion protection system is put into the upper layer of the topsoil layer. This protection system is formed by a matting of random array extruded synthetic fiber laid out onto the surface then subsequently filled with a topsoil/seed mixture. The growth of fine roots in the grass cover intertwine with the mat's random array to stabilize the grass cover which is so important for erosion protection. The overhead to realize this method is quite minimal because erosion protection is a consequence of the vegetation measures taken. Model experiments to test the effectiveness of armored grass cover for overflowed dam embankments were performed in Great Britain in 1987. These experiments proved the good functionality of the three-dimensional random array (CIRIA Report 1987). The effectiveness of non-armored grass cover and armored grass cover in comparison to systems with concrete construction are presented in Figure 4.

Method (II) is also an embankment-parallel protective mechanism but it is placed about 20 cm beneath the topsoil layer of the inner embankment. This technique produces a very high degree of protection even if the grass cover should be lost. High-tensile geogrid/nonwoven combinations (2-dimensional) are laid out contiguously over the surface of the levee's core and fixed in place with ground pins (Figure 5). Thus a stabilized overflow bed remains even if the grass cover should be lost. A high degree of protection during overflow can be achieved with relatively low realization overhead (removal of the topsoil layer).

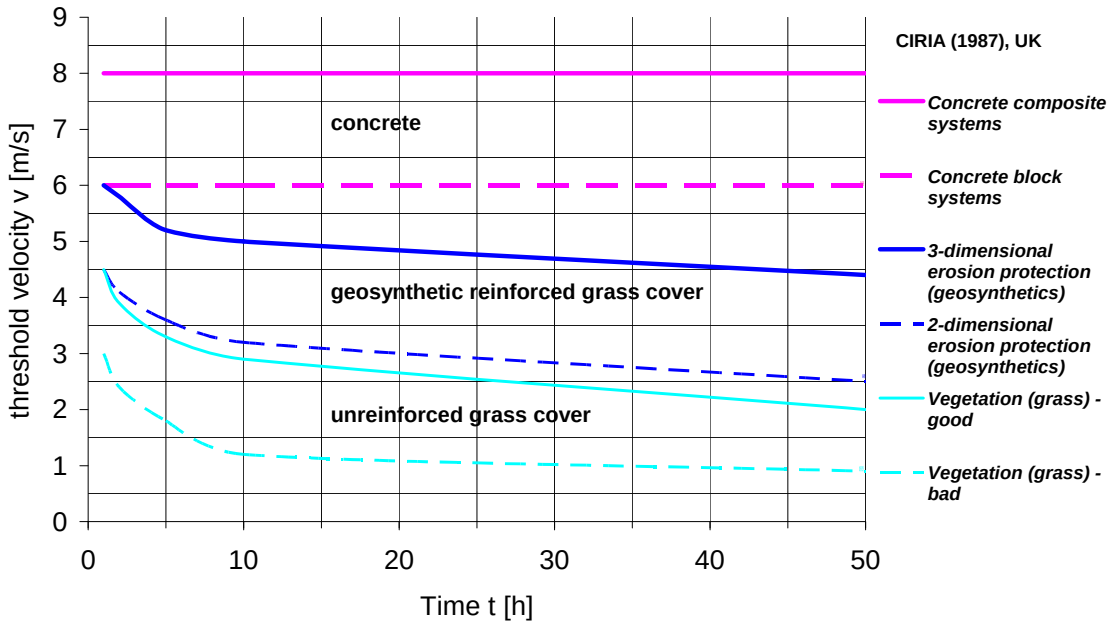

Figure 4. Effectiveness of non-armored and armored grass covers on dam embankments during overflow (CIRIA 1987).

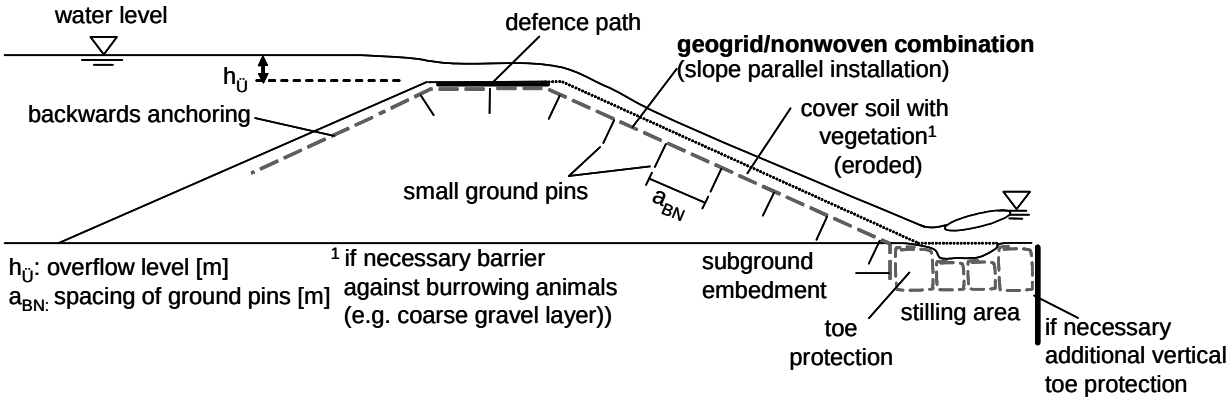

Figure 5. Overflow protection per method (II), embankment parallel with geogrid/nonwoven combinations and ground pins (Haselsteiner et al. 2007)

As a protective measure built into the levee, method (III) offers the greatest protective functionality. A breach failure, as is possible in classic non-reinforced levee bodies, can be excluded entirely. The envelope method (wrap-around method) of layer-oriented encapsulation of earth in nonwovens, or preferably geogrids, is considered a standard procedure for forming earthwork and roadway reinforcement in steep embankments and support structures (slopes of 45° to 90°). Though levees have comparably less embankment slope, this construction technique can be used to handle hydraulic overload conditions even for embankment slopes up to about 33°. Furthermore, when the inner embankment is designed according to Figure 6, a cascaded spill is produced that slows flow speed. The protection afforded by this construction technique can be classified exceptionally high. Implementation is quite simple but does require greater overhead in comparison to methods (I) and (II) due to the dimensioning of horizontal embedded lengths into the area of the levee's core.

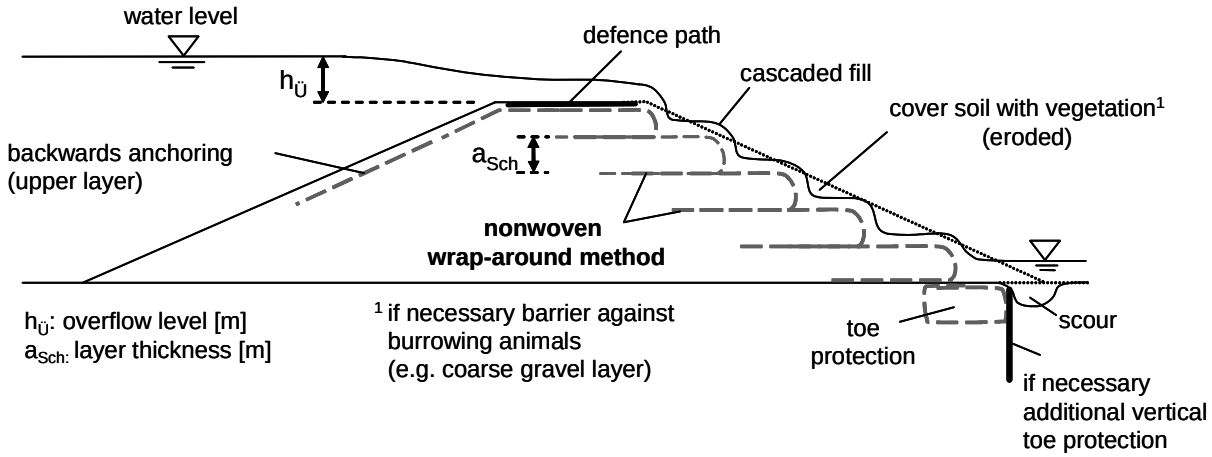

Figure 6. Integrated overflow protection per method (III) in envelope method (Haselsteiner et al 2007).

Model experiments were conducted on the above-referenced methods (I) through (III) in 2006 at Test Institute for Water Engineering and Water Management at the Technical University Munich to evaluate the resistance capability of levee inner embankments with geosynthetic reinforcements under overflow conditions. These investigations were initiated as a part of the "levee reconstruction" research and development program established by the Bavarian State Office for Water Management. The objective of these model experiments was to develop simple, cost-effective construction techniques employing geosynthetics which would inhibit the erosion of levee inner embankments under overflow conditions. Experiments which simulated the loss of vegetation layer (methods (II) and (III)) were carried out and evaluated. Systems with needle-punched nonwovens, sand mats and nonwoven/geogrid combinations were tested in conjunction with inner embankment installation variations: slope parallel, horizontal, with and without envelopes. A levee-integrated with an enveloped ground/geosynthetic composite system on a steep embankment slope of 1:n = 1:1.5 and a near-surface system with needle-punched geogrid/nonwoven combination on a slope of 1:n = 1:2.5 were overflowed. Systems with geosynthetics used in the envelope method (method III, Figure 7) and embankment parallel nonwoven/geogrid combinations or sand mats with structural fixation (method II, Figure 8) proved to be robust. The details of experiments performed are documented in Haselsteiner et al. (2007).

Figure 7. Model experiments at the Technical University Munich, Overflow of the inner embankment per method (III). Left: before overflow, right: in overflow state with up to 130 l/m·s (Haselsteiner et al 2007).

Figure 8. Model experiments at the Technical University Munich, Overflow of the inner embankment per method (II) Left: before overflow, right: in overflow state with up to 300 l/m·s (Haselsteiner et al. 2007).

4. SUMMARY

Figure 9 depicts an improved levee cross-section optimally reinforced with geosynthetics. Its water-side has a surface seal of bentonite mats (preferably needle-punched GCL with powdered sodium bentonite and woven/nonwoven geotextile composite as carrier layer and nonwoven geotextile as cover layer). The levee's core has integrated erosion protection provided by encapsulating levee core material in nonwovens with the envelope method. A filter-effective configuration of air-side drainage is combined with a levee defense roadway. The levee's cross-section was implemented in Poland after the 1997 Oder River floodwater. It offers optimal prerequisites for a long-term, protective, stable and overflow-secure levee. Breach behavior, as would be exhibited by a levee with conventional cross-section consisting only of earthen materials, can be presumed eliminated.

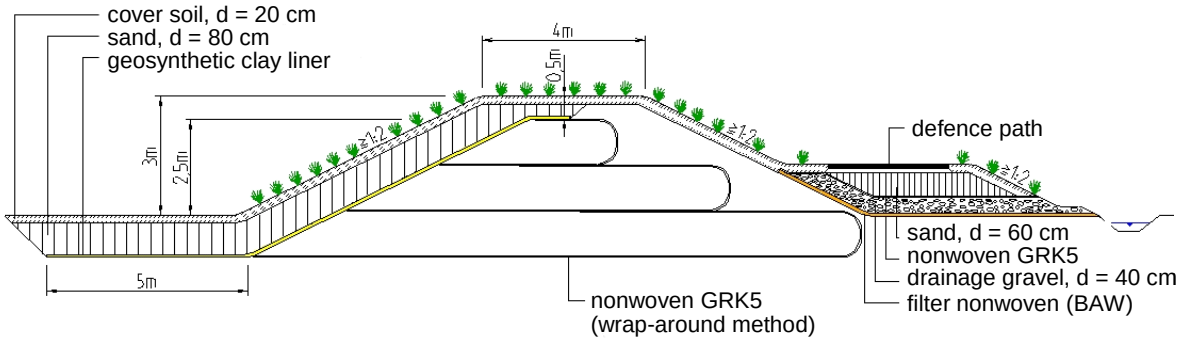

Figure 9. Cross-section of a reconstructed Oder River levee in Poland (Heerten 1999)

REFERENCES

BAW (2002). Recommendations for the use of lining systems on beds and banks of waterways, *Federal Waterway Engineering and Research Institute (Bundesanstalt für Wasserbau – BAW),* Karlsruhe, Germany.

BAW (2006). Richtlinien für die Prüfung von mineralischen Weichdichtungen im Verkehrswasserbau RPW, *Bundesanstalt für Wasserbau*, Karlsruhe, Germany.

CIRIA Report 116 (1987). Design of reinforced grass waterways. *CIRIA Construction Industry Research and Information*

Association, London, UK.

DIN 19712 (1997). German Standard "Flussdeiche" [River dikes], *DIN Deutsches Institut für Normung e.V.*, Berlin, Germany.

DWA (2005). DWA-Themen, DWA-Arbeitsgruppe WW-7.3 "Dichtungssysteme in Deichen", *DWA Deutsche Vereinigung für Wasserwirtschaft, Abwasser und Abfall e.V., [German Association for Water, Wastewater and Waste],* Eigenverlag.

DGGT (2002). Empfehlungen zur Anwendung geosynthetischer Tondichtungsbahnen EAG-GTD, *Deutsche Gesellschaft für Geotechnik e.V.*, *[German Geotechnical Society]*, Essen, Germany, Verlag Ernst & Sohn.

Fleischer, P., Haarer, R. and Heibaum, M. (2007). Bentonitmatten als Damm- und Deichdichtungen – Erkenntnisse aus Aufgrabungen nach unterschiedlich langen Liegezeiten. *Wasserbaukolloquium 2007 "5 Jahre nach der Flut",* Dresden, Germany.

Haselsteiner, R., Mett, M. and Strobl, Th. (2007). Überströmungssicherung von Deichen mit Geokunststoffen. *5. NAUE-Geokunststoffkolloquium*, Bad Lauterberg, Germany.

Heerten, G. (1999). Erhöhung der Deichsicherheit mit Geokunststoffen. *6. Informations- und Vortragstagung über Kunststoffe in der Geotechnik*, Fachsektion Kunststoffe in der Geotechnik der Deutschen Gesellschaft für Geotechnik e. V. (DGGT), München, Germany.

Heerten, G. and Horlacher, H.-B. (2002). Konsequenzen aus den Katastrophenhochwässern an Oder, Donau und Elbe. *Geotechnik* 25, Nr. 4, 231ff, Verlag Glückauf, Essen. Germany.

Heerten, G. (2003a). Der sichere Deich, *Notsicherung von Dämmen und Deichen – Verfahren, Konstruktion und Baustoffe zur Notsicherung,* Symposium der Universität Siegen im Institut für Geotechnik, Germany.

Heerten, G. (2003b). Flussdeiche für lang einstauende Hochwasser. *10. Darmstädter Geotechnik-Kolloquium*, TU Darmstadt, Germany.

Heerten, G. and Reuter, E. (2006). Is the European regulatory capping design of landfills equivalent to geosynthetic alternatives? *Danube-European Conference on Geotechnical Engineering,* Ljubljana, Slovenia.

Heerten, G. and Werth, K. (2006). Anwendung von Geokunststoffen bei der Deichertüchtigung, *Fachtagung Deichertüchtigung und Deichverteidigung in Bayern*, Hrsg. Institut für Wasserbau und Wasserwirtschaft, TU München, Wallgau, Germany.

Heerten, G (2007). Geokunststoffe im Deichbau, *DWA-Tagung: Flussdeiche – Bemessung, Dichtungssysteme und Unterhaltung*, Fulda, Germany.

Heerten, G. and Koerner, R.M. (2008). Oberflächenabdichtungen von Deponien und Altlasten. *24. SKZ-Fachtagung "Die sichere Deponie"*, Würzburg, Germany.

Saathoff, F. and Werth, K. (2003). Geokunststoffe in Dämmen und Deichen. *Sicherung von Dämmen und Deichen: Handbuch für Theorie und Praxis*, S. 221 – 237, Hrsg. Hermann und Jensen, Universitätsverlag Siegen, Germany.

Santo, J. (2003). Deichsanierung an der Kinzig, *3. NAUE-Geokunststoff-Kolloquium*, NAUE GmbH & Co. KG, Adorf/Vogtland, Germany.

High Speed Tear Properties of Geomembranes and Temperature Effects.

G. Kolbasuk and J. Norberg, Raven Industries, Inc., Engineered Films Division, Sioux Falls, SD, USA.

ABSTRACT
Tear tests for geomembranes such as Graves Tear, Tongue Tear and Trapezoidal Tear all utilize relatively slow tear speeds and are typically done at standard laboratory temperatures. Exposed geomembranes need to perform over a wide variety of temperatures including the range of -40ºC to 80ºC. They are also potentially subjected to high speed tear stresses from wind and impact. This paper discusses results utilizing a high speed, high capacity Elmendorf type tear test on both reinforced and unreinforced geomembranes. The tests are performed over a wide range of temperatures and the results compared to a typical, slow speed test. The results demonstrate that testing under standard laboratory conditions does not tell the full story with respect to geomembrane properties under conditions that may exist in the field.

1. INTRODUCTION

The majority of physical property data that is available for geomembranes is generated by the use of standard index tests and performance tests performed under standard laboratory conditions. The index tests that fill specifications and are frequently used to compare different products contain biases (ASTM D4439) and rarely do a good job of duplicating the types of stresses that the geomembranes will be subjected to in service. Almost completely ignored is the influence of temperature on the geomembrane properties, except for a statement of a brittleness temperature.

It is well known that the properties of polymers change with temperature. As temperatures decrease, materials get stiffer, modulus increases and elongation decreases. As temperatures increase, materials get softer, modulus decreases and elongation can increase. Those statements, while giving an intuitive feel for how geomembranes might behave at different temperatures, fail to quantify the changes or shed much light on more complex behaviors.

It is also well known that the speed with which a force is applied to a geomembrane changes the results of physical test properties, particularly those constructed of viscoelastic materials such as polyolefins. Slow strain rates allow the viscous component to be manifested in the form of creep, which tends to lower tensile strength and increase tensile elongation. While many performance tests focus on very slow test speeds to duplicate the effect of long term stresses, geomembranes can also be put in situations where stresses are applied very quickly. This can happen during construction as well as service in applications such as exposed covers and liners.

The research reported in this paper focuses on the effects of temperature and test speed on the tear properties of various geomembranes. It is hoped that this data will provide additional insight for engineers designing exposed geomembrane structures that are subject to possible failure by tearing.

2. TEST PROCEDURES

Since the purpose of this experiment was to compare tear strength over a range of temperatures, only the tear strength in the machine direction was evaluated. Testing was conducted in increments of 10°C, starting at -40°C through +50°C.

2.1 Higher Speed Testing, Elmendorf Tear

Elmendorf tear tests were performed with a Heavy Duty Thwing Albert tear tester using a full scale of 25,600 grams, shown in Figure 1. Testing was conducted according to ASTM D5734. A custom built environmental chamber housed the test apparatus for testing at the various temperatures, shown in Figure 2. Specimens were separated to allow air flow around them and conditioned for a minimum of 15 minutes prior to testing.

2.2 Lower Speed Testing, Tongue Tear

Tongue tear strength was evaluated according to ASTM D5884. An environmental chamber was used on an Instron 3365 to conduct testing at the various chambers, shown in Figure 3. Specimens were individually loaded into the chamber and air at the test temperature was allowed to flow around them and condition for a minimum of 5 minutes prior to testing. Since loading required opening the chamber door, letting in warm, humid air, the specimens were not all placed in the chamber at the same time. Doing so resulted in frost forming on the specimens and slippage in the grips during testing.

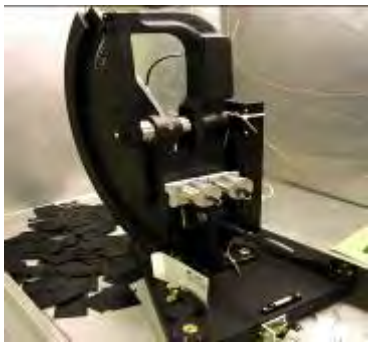

Figure 1, Elmendorf Tear

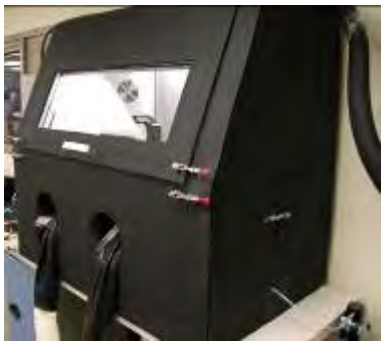

Figure 2, Tear Test Chamber

Figure 3, Instron Chamber

2.3 Materials

Materials were selected to cover a wide range of polymers. Both unreinforced and reinforced where evaluated when available. The geomembranes selected include:

- A relatively pure polyolefin, linear low density polyethylene, unreinforced (LLDPE) and reinforced (R-LLDPE).
- A reactor formed blend of polyolefins, flexible polypropylene, unreinforced (fPP) and two reinforced (RfPP-A and RfPP-B).
- A plasticized polymer, polyvinyl chloride (PVC), unreinforced.
- A cross linked elastomer, ethylene propylene diene monomer (EPDM), unreinforced.
- An alloy, ethylene interpolymer alloy (EIA), reinforced.

The thickness selected for some materials were limited by the maximum test capacity of the higher speed test apparatus.

3. TEST RESULTS

3.1 Elmendorf Tear Test Results

Figure 4 shows the tear strength of the unreinforced LLDPE from -40C to 50C. The tear strength is a maximum at about zero degrees. The decrease below zero is due to the material becoming less elastic and unable to absorb as much energy in the tearing process. At higher temperatures, the material is softening and slowly losing strength.

Figure 5 shows the results for the polyester scrim reinforced LLDPE. At room temperature, the LLDPE stretches to allow the scrim to move and help absorb the tearing force. At higher temperatures, the scrim begins to slip a little more in the small specimen, resulting in lower values. At cold temperatures, it appears that the more rigid polyethylene restrains the polyester, reducing the ability of the reinforcement to absorb energy. The strength steadily decreases from room temperature to a value at -40C that is no more than the unreinforced material.

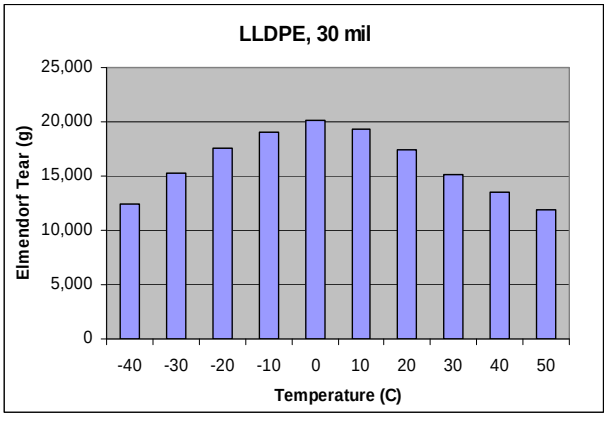

Figure 4, 30 mil LLDPE Elmendorf

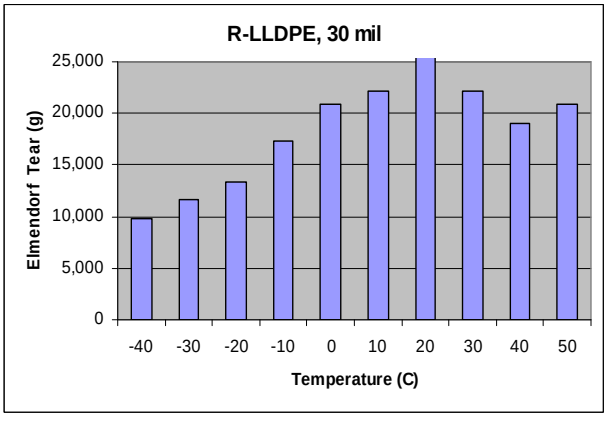

Figure 5, 30 mil R-LLDPE Elmendorf

Figure 6 shows the tear resistance of a 30 mil PVC. As the temperature drops, the plasticizer becomes less effective, resulting in a rapid reduction in the tear strength. Softening at warmer temperatures slowly reduces the tear strength.

Figure 7 shows the EPDM results. The tear strength peaks at about -20C and drops off quickly below -30C. It also loses tear strength fairly quickly as the temperature rises.

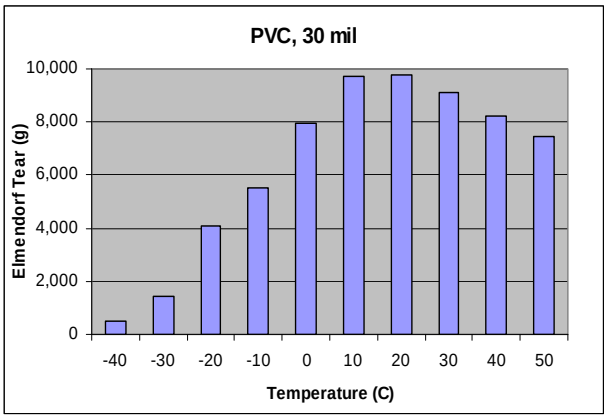

Figure 6, 30 mil PVC Elmendorf

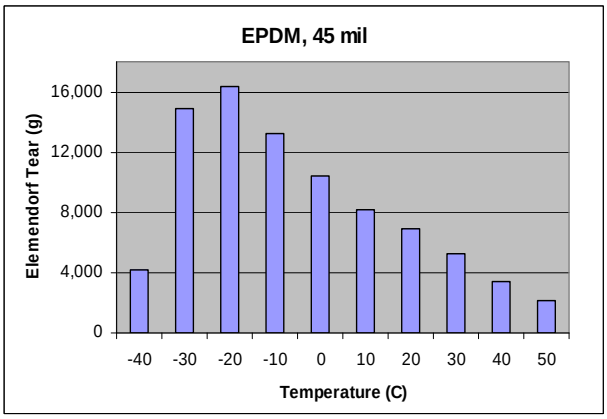

Figure 7, 45 mil EPDM Elmendorf

Figure 8 shows the behavior of the 40 mil fPP. It demonstrates tear properties that are a blend of that shown by the LLDPE and the EPDM. Perhaps not surprising since fPP is a two phase material consisting of both a linear polyolefin and a rubber phase.

Figure 9 is the reinforced EIA. It demonstrates a different behavior, with a minimum tear resistance at 0C. At this temperature, the fabric tears neatly. At both higher and lower temperatures the failure mode transitions from neatly tearing to containing a delamination element that complicates the tear process and increase values.

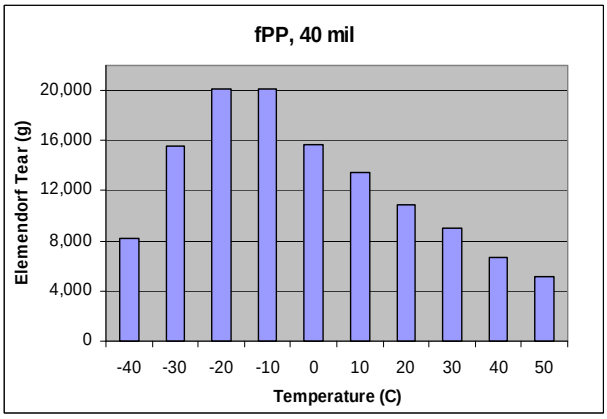

Figure 8, 40 mil fPP Elmendorf

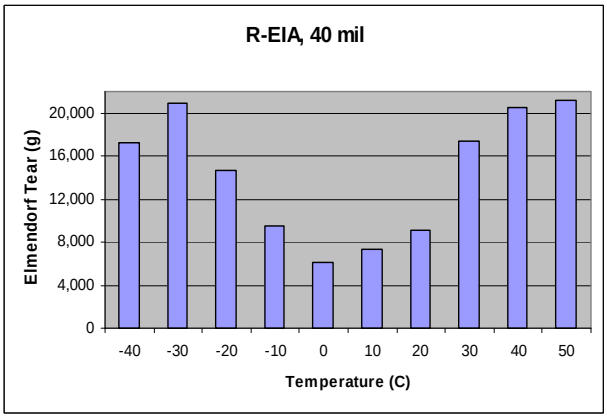

Figure 9, 40 mil R-EIA Elmendorf

Figures 10 and 11 are two different reinforced flexible polypropylene geomembranes. The two membranes look very similar, appear to have a similar reinforcement and are sold to the same market. Yet RfPP-B exhibits twice the 20°C tear resistance as well as a different response to decreasing temperatures. Not knowing what raw materials are used to make these geomembranes, we can not speculate on the reason for the different performance.

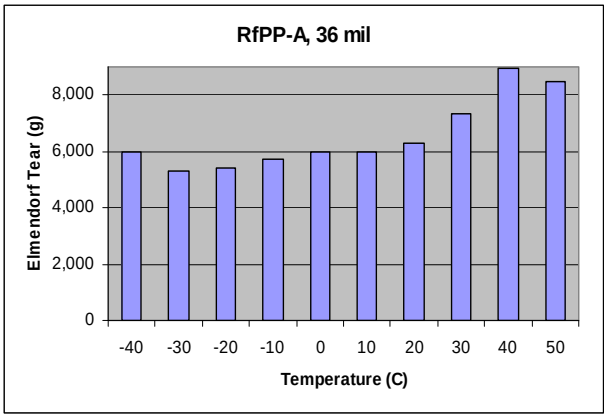

Figure 10, 36 mil RfPP-A Elmendorf

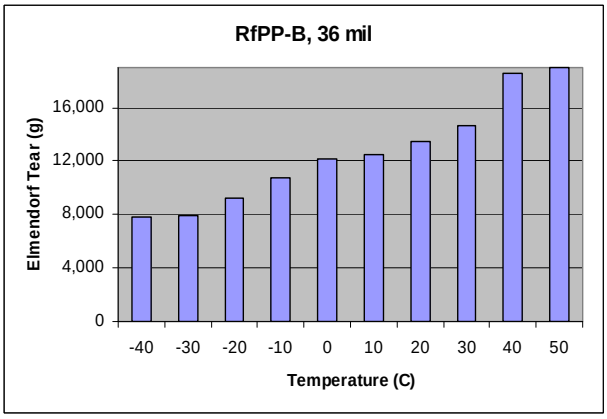

Figure 11, 36 mil RfPP-B Elmendorf

3.2 Tongue Tear Test Results

Figures 12 and 13 show the tongue tear results for the unreinforced and reinforced LLDPE. As with the high speed tear, the reinforced LLDPE shows more of a response to temperature than the unreinforced product. Even though the specimens are much larger, the PET yarns in the reinforced product begin to slip or pull out at higher temperatures, exaggerating the loss of tear strength at higher temperatures. This would probably not be seen in larger specimens or in the field since the yarns would be restrained over a longer length.

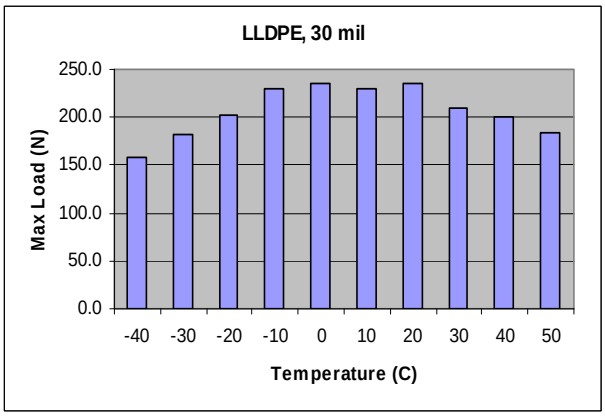

Figure 12, 30 mil LLDPE Tongue Tear

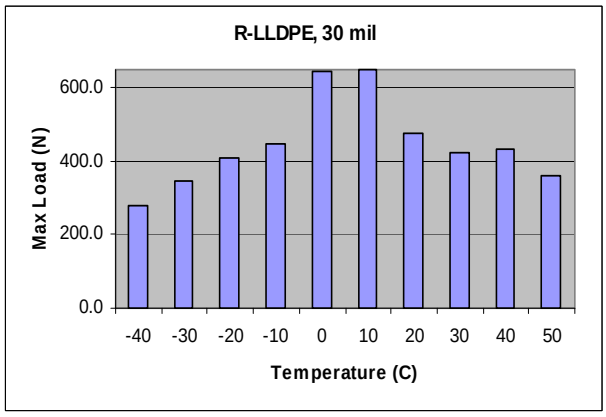

Figure 13, 30 mi R-LLDPE Tongue Tear

Figures 14 and 15 show the tongue tear results for unreinforced and reinforced flexible polypropylene. The unreinforced material has more uniform properties over the temperature range than demonstrated in the higher speed test. The reinforced product has a significant change in properties, increasing by a factor of three going from 0°C to 30°C. The change in strength is accompanied by a change in the failure mode. At less than 20 degrees the yarns are restrained by the fPP and break one at a time in a neat tear. At 20°C and above, the fPP stretches and allows the yarns to bunch up and work together to generate much higher tear strengths. At 50°C, yarn slippage or pull out serves to reduce the tear value.

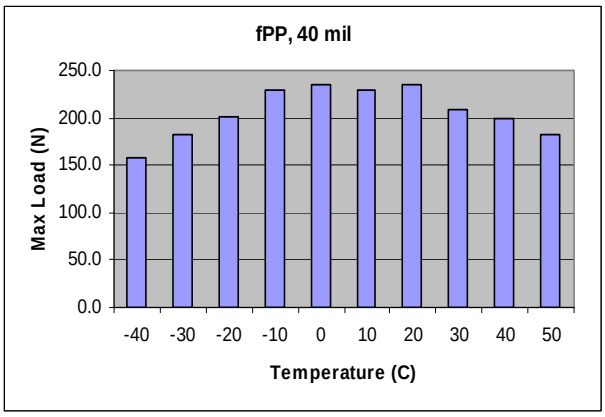

Figure 14, 40 mil fPP Tongue Tear

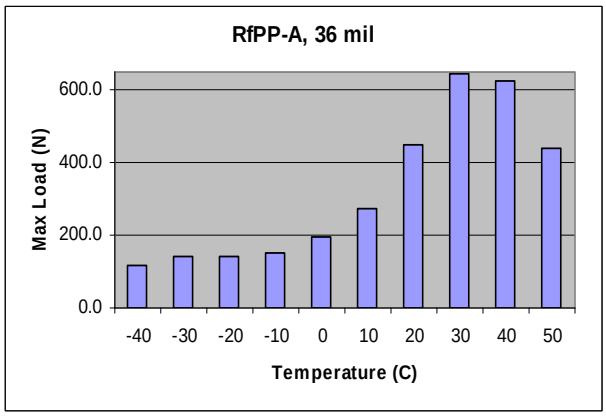

Figure 15, 36 mil RfPP-A Tongue Tear

Figure 16 has the results for the PVC tongue tear. At slow tear speeds, the PVC shows much more uniform performance over the temperature range than it did with the high speed test.

Figure 17 show the results of the EPDM tongue tear. It demonstrates a similar behavior to the Elmendorf test, except that the area of peak tear strength is a little broader and occurs at a slightly warmer temperature.

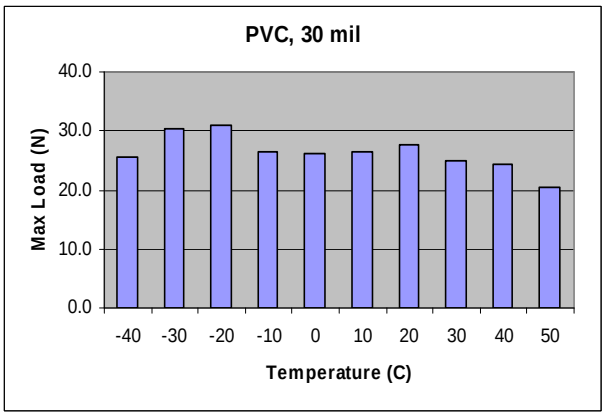

Figure 16, 30 mil PVC Tongue Tear

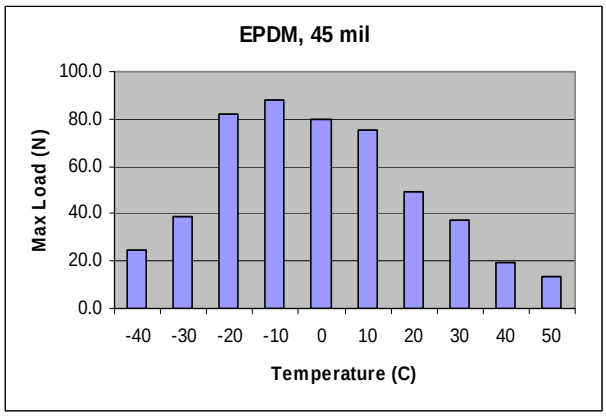

Figure 17, 45 mil EPDM Tongue Tear

At the time of the writing of this paper, the tongue tear results on the rest of the materials was not completed. However, the data presented here is enough for discussion purposes and to draw some conclusions.

4. DISCUSSION

4.1 Effect of Temperature on Performance, Elmendorf Tear.

The first observation from the Elmendorf Tear data in Figure 18 is the lack of correlation of tear strength vs temperature between the various materials. Four different materials have the best tear resistance, depending on the temperature chosen for the comparison. The R-EIA is the highest at -40, -30, +40 and +50 but equal to the lowest at zero degrees. All the unreinforced products have peak tear strengths below room temperature but differ dramatically in how fast the tear strength decreases at lower and higher temperatures. All the reinforced products have peak tear strengths at 20°C or warmer. Rankings of the different materials at each temperature were not evaluated, but it appears positions in a relative tear strength rating would change quite a bit depending on the temperature chose to compare them.

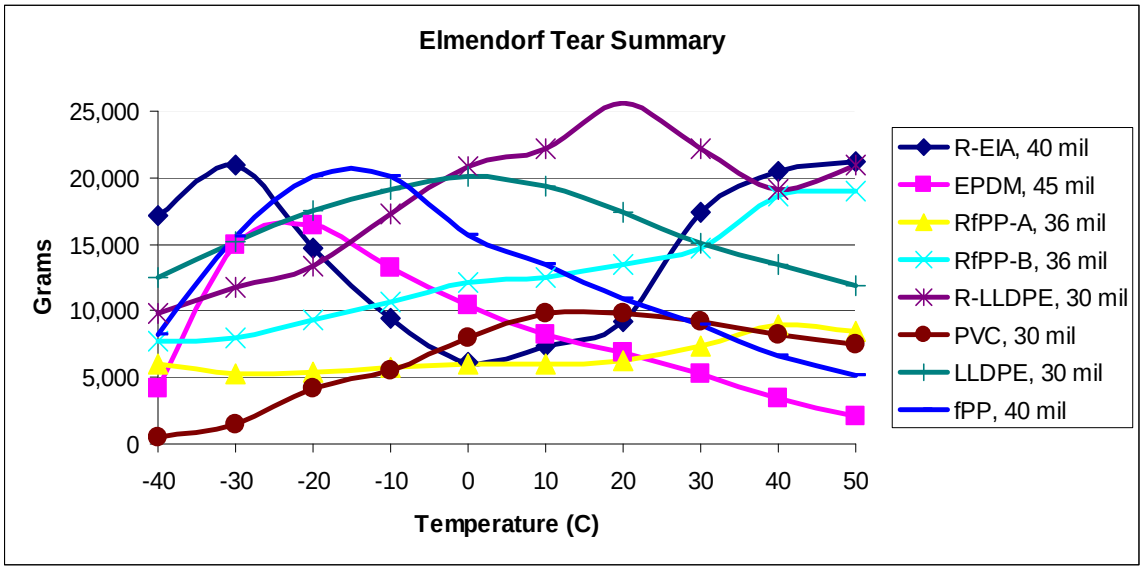

Figure 18, Elmendorf Tear Test Result Summary

4.2 Effect of Temperature on Performance, Tongue Tear.

Figure 19 is less busy than figure 18 partially because fewer materials are plotted. Also, most of the unreinforced materials have much less variation over the temperature range than they do in the high speed test. In the future, we will extend the testing up to 80C to confirm material behavior up to the top end of the temperature range that might normally be expected in exposed field conditions.

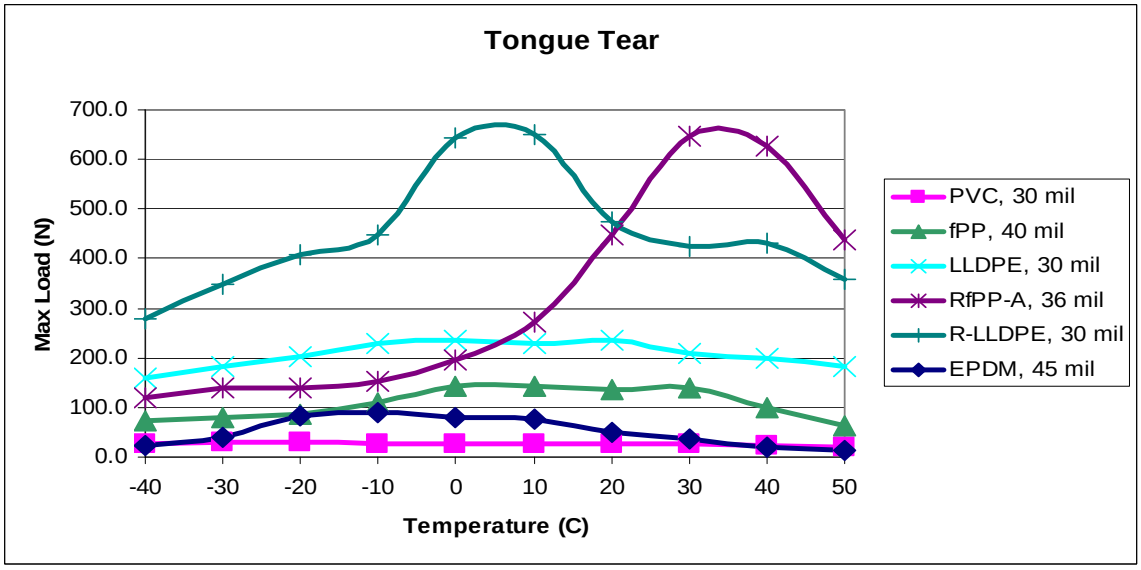

Figure 19, Tongue Tear Test Result Summary

4.3 Effect of Test Speed on Results

Figure 20 plots the tongue tear and Elmendorf tear results at 20°C for six materials on the same graph. There are several observations one could make, but there is only one that will be the focus of this paper. That being that the relative performance of the materials at the two test speeds are not the same. RfPP-A stands out in that it is has almost the highest strength when evaluated at a slow strain rate but has the lowest strength when tested a higher strain rate. The authors also recognize that since the size and shape of the specimens for the Elmendorf and Tongue tear tests are different, that the size and geometry of the specimens may also impact the results. Plans for the future include building larger Elmendorf tear equipment that can handle larger specimens and longer tear lengths.

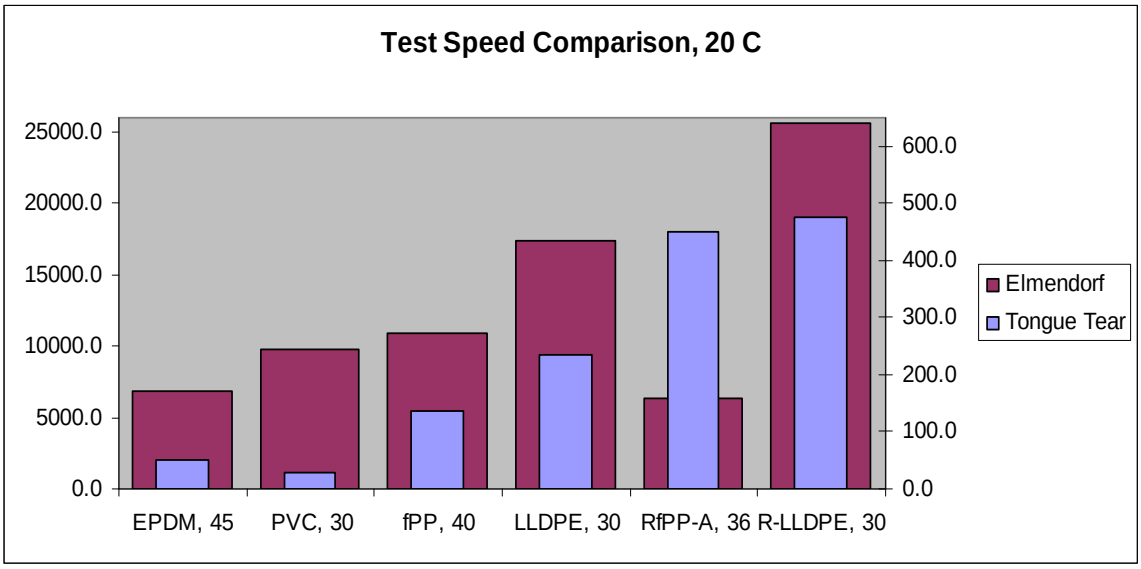

Figure 20, Comparison of Elmendorf and Tongue Tear Results at 20°C

5. CONCLUSIONS

“Room Temperature” is an arbitrary temperature chosen to compare the performance of materials because that is the temperature which is convenient as opposed to it being a temperature that is of special significance to the performance of geomembranes. By focusing on index and performance tests run under standard laboratory conditions, we are ignoring the different performance of geomembranes at other temperatures. We feel being aware of performance at other temperatures is important since geomembranes, particularly exposed geomembranes, spend very little of their life at standard laboratory temperature.

A higher speed tear resistance test demonstrate a difference in performance compared to a slower speed test. Higher speed tear resistance can be significant to geomembrane performance in exposed applications and during construction. Test speeds, particularly for index tests, are selected to give reproducible results in a reasonable amount of time. Testing at very slow speeds and at higher speeds is necessary to understand the range of performance to be expected from geomembranes over the full range of stresses that they may be exposed to in the field.

REFERENCES

ASTM D4439. Standard Terminology for Geosynthetics, *American Society for Testing and Materials*, West Conshohocken, Pennsylvania, USA.

ASTM D5734. Standard Test Method for Tearing Strength of Nonwoven Fabrics by Falling pendulum (Elmendorf) Apparatus, *American Society for Testing and Materials*, West Conshohocken, Pennsylvania, USA.

ASTM D5884. Standard Test Method for Determining Tearing Strength of Internally Reinforced Geomembranes, *American Society for Testing and Materials*, West Conshohocken, Pennsylvania, USA.

Shoreline Protection using Polymer Rope Gabions and Geotextile Tubes

M. Venkatraman, Geosynthetics Division, Garware-Wall Ropes Ltd., Pune, India.

ABSTRACT
India has vast coast line of about 5700 km covering the peninsular portion of the country. There are valuable old monuments, large number of habitations and several industries along the coast. These structures require proper protection from the detrimental effects of sea erosion. Conventional shore protection structures made of masonry or concrete are generally cost prohibitive and also their rigid nature results in undue distressing when subjected to minor ground movements and severe wave actions. In recent times Geosynthetic structures which possess high degree of flexibility and porous nature, have become popular for shore protection works. Geosynthetic structures have also proved to be economical as they use only the locally available soil or dredged material. In India use of such structures are getting impetus. This paper addresses successful case studies of using flexible Polymer rope gabions and Geotextile containers with locally available materials for shore protection works.

1. INTRODUCTION

India has vast coast line of about 5700 km covering the peninsular India. Valuable old monuments, large number of habitations and several industries are located near the coast. These structures are to be protected from sea erosion. The sea erosion is caused mainly by two basic natural forces viz. (i) Tidal level variation, which pushes the reaches of the ocean water further up the slope of the shore and eroding shore while return and (ii) Storms, which disturb state of water body and act as the major catalyst for erosion and shoreline depletion. Commonly adopted structures to impede the actions of waves are seawall, groins or offshore breakwaters which holds the shoreline in place. Conventional structures made of masonry or concrete are generally cost prohibitive. The rigid nature of these structures results in undue distressing of the structures when subjected to slight ground movements or severe wave actions. Use of geosynthetics for hydraulic structures started in 1980s as evidenced from Bogossian et al. (1982) and Harris (1987). Geosynthetic structures constructed using flexible Polymer rope gabions, Geotextile containers etc. which posses high degree of flexibility and porous nature have become popular in recent times. Moreover these structure do not require any expensive foundation systems. Gabions and Geosystems have also proved to be economical as they use only the locally available soil and dredged material.

1.1 Geosynthetics in Shore Protection Works

Commonly built forms of shore protection structures are given in Table 1. The corresponding structural forms of geosynthetics and the geosynthetic products involved are also given in the table.

Table 1. Various forms of Geosynthetics structures for coastal protection

Coastal protection structures	Suitable Geosynthetic structure	Geosynthetic products involved
Sea walls, Spur Dykes, Groynes, Shore revetments	Geotextile containers, Geotextile tubes, Geotextile bags, Geo-mattresses, Polymer rope gabions,	Woven Geotextiles, Polymer rope nets

Geotextile containers are nothing but flexible bags of various sizes and shapes made of suitable geotextiles (permeable but soil tight) and filled with locally available geo-materials, mostly dredged soils. The common forms of Geotextile containers are Geotextile tubes, Geotextile bags, Geomattresses etc. Geotextiles tubes are long tubes made of suitable geotextiles of dimensions in the range of 3 to 5 m diameter and 20 to 40 m length, which are filled with sand slurry through pumping mechanism. Geotextile bags are like pillow bags with size range of 1 to 3 m filled with suitable soils and sealed. Geomattresses are large planar mattress formed with suitable geosynthetic material and filled with soil. These are commonly used as aprons. As these elements are generally made of woven geotextiles and granular soils, they possess high degree of flexibility and water pervious nature as that of filled material. Figure 1 shows the photographs of all these forms of geotextile containers.

Geobags

Geotextile tubes

Geomattress

Figure 1. Various forms Geosystems (Geotextile Containers)

1.2 Geotextile Tubes

Laying large size Geotextile tubes along the shore is a desired alternate to sea walls for prevention of sea erosion. As the dredged sand or easily available local soils are used as fill material, Geotextile tubes are very easy and simple for installation. Geotextile tubes shall be laid in number of patterns and in different configuration according to the wave direction, wave height and purpose of structure. General patterns of laying the Tubes are shown in the Figure 2.

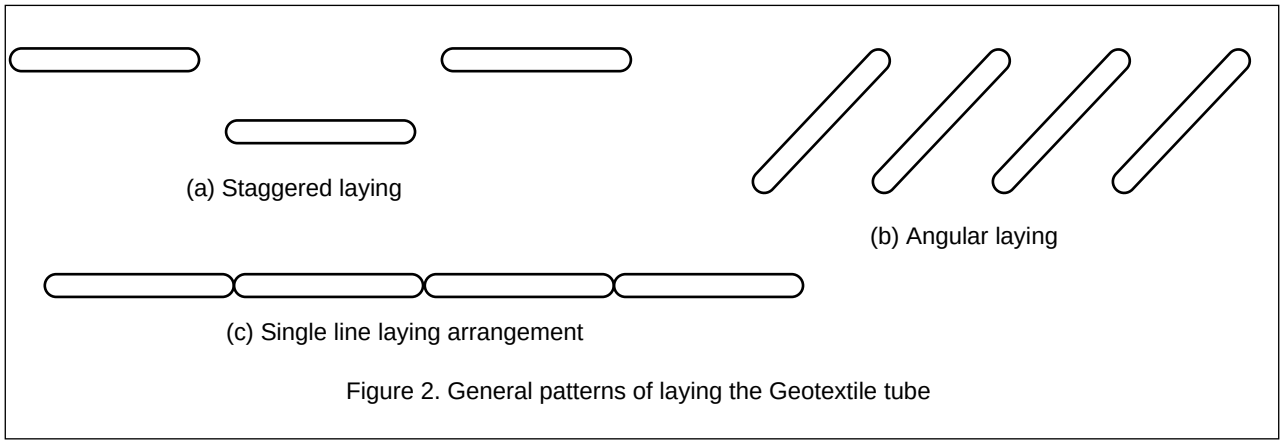

Figure 2. General patterns of laying the Geotextile tube

Mostly woven geotextiles are used for making the tubes, as its tensile strength is normally higher than nonwoven geotextiles. The fill material used for Geotextile Tube (or geocontainer) is checked for fulfilling the criteria for filter, retention, survivability and clogging. General guidelines to this are given in Part VI-4-7 of Geotextile and Plastics of coastal engineering manual of USACE (Unite States Army Corps of Engineers). After filling the geotextile tube with sand slurry the circular cross section of tube will attain elliptical shape. The geotextile in the tube will be subjected to tensile stress in the longitudinal as well as circumferential direction. Along the circumferential direction, maximum stress will be developed at lower side of tube (Lawson, 2006), which is shown in the Figure 3. As the circumferential tensile stress is least at the bottom, the tube is positioned such that the longitudinal seam of the tube lies at the base. Sufficient precautions should be taken against vandalism by any means. Armour layer over the tube structure is always advisable to protect against vandalism. For extra protection against any excess circumferential tensile stresses in the geotextile tube, the entire tube can be wrapped around with one layer of polymer rope net.

1.2.1 Installation of Geotextile Tubes

A number of aspects are to be considered for geotextile tube installations. Since these tubes are made of geotextile, standard guidelines should be followed regarding storage and handling. General installation guidelines are given below.

1. Before the geotextile tubes and scour aprons are deployed to the site, the area is prepared using common grading equipment. The location in which the geotextile tubes are to be placed is usually marked-off with grade stakes.

2. The scour apron is positioned and secured before the geotextile tube is unrolled. It should be unrolled into position with the injection and relief ports (the sand slurry is pumped in to the tube through the injection port and relief port is for pressure relief) facing upwards along the top centerline and it can be secured to the previously installed alignment stakes or anchors.

3. The injection ports are fabricated of the same geotextile that are made of the tube material itself at required spacing. The ports are usually 1.5 m long and 300 mm in diameter. The injection pipe should be inserted approximately 2/3 of the way into the injection port and secured with tension strapping.

4. Prior to filling with any solid material, the tube is to be filled to their desired height with water only. Once the desired height has been achieved, the dredge operator can introduce solids into the geotextile tube. By filling the tube with water initially, the solid materials are allowed to distribute within the tube more evenly.

5. Upon completion of the installation, the injection ports must be secured properly. A commonly practiced method is to simply cut-off the injection port, while allowing enough excess fabric to fold down of the tube. The folded material is then fastened to the tube surface by the use of corrosion resistant lock rings or compression type fittings.

6. Filled and closed geotextile tubes will continue to dewater and the solids will further consolidate for some time. Once the expected amount of dewatering has taken place, the geotextile tubes can be buried and backfilled.

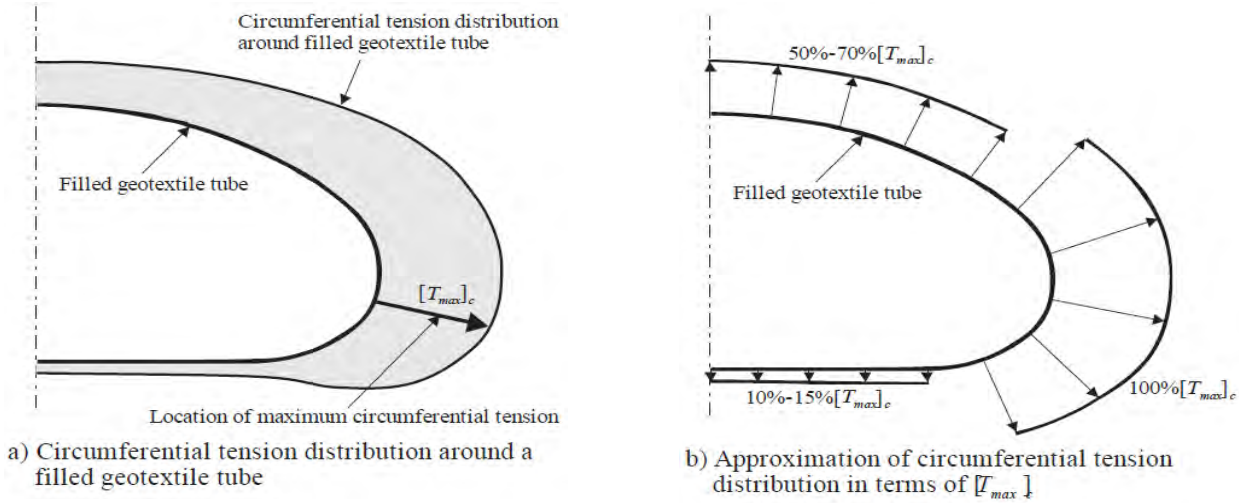

Figure 3. Distribution of tensile force along the circumference of the filled geotextile tubes (Adopted from Lawson 2006)

1.3 Polymer Rope Gabions

Gabions are nothing but boulder filled box type cages formed by nets made of steel wire or polymer ropes. The boxes are properly wired and laced together to form flexible, monolithic, confined building blocks which are called as Gabions. These blocks are porous gravity blocks which stand by its self weight and it does not require any foundation or anchorage. The pervious nature of the gabions allows immediate dissipation of hydrostatic pressure that may cause destabilizing effects. As Gabions promotes growth of natural vegetation, it offers natural aesthetics with decorative landscaping besides maintaining the natural Environment. Gabions can be used effectively and economically in its all applications.

Gabions can be divided into two types based on the netting material, viz. Steel Gabions and Polymer rope Gabions. The steel Gabions are manufactured from heavily galvanized steel wire Nettings. These nettings have a hexagonal mesh with double twisting. For chemically aggressive environment PVC coated galvanized wire netting can be used for better performance. Gabion boxes can be made in various required dimensions.

Polymer rope gabions are fabricated by a unique process in which the ropes are woven into continuous net with square apertures (commonly used aperture sizes are 100 to 150 mm). These are generally available in a prefabricated collapsible form. It was introduced in India by Garware-Wall Ropes Ltd. in the year 2001. Since then this technique has achieved a notable place in coastal engineering. These nets are used to form cages of desired sizes and the cages are filled with boulders. The ropes are manufactured using engineering grade Polypropylene (PP) or High Density Polyethylene (HDPE) and developed with woven joints. As the polymer ropes are inert to most of the chemicals available in coastal environment polymer rope gabions are highly preferred for coastal protection structures. These ropes are of diameter about 9 mm and are stabilised for degradation against ultraviolet radiation. Polymer rope gabions are ideally suited as armour layer in resisting all erodible effects of waves. Photographs of steel gabion as well as boulder filled polymer rope gabions are shown in Figure 4. Boulder fill can be done in-situ or the filled gabion shall be lifted with the help of crane and installed in place.

Steel Gabion boxes

Polymer Rope Gabions

Figure 4. Gabions - Photographs

1.3.1 Polymer Rope Gabions - Installation Techniques

1. Site is prepared to make smooth profile for the arrangement of gabions. Sand filled bags or boulders can be used for the soling work or any filling of weak spots.

2. Over the prepared surface Geotextile or sand mattress is laid with proper over lap and anchorage. Geotextile filter should satisfy design criteria such as tensile strength, permeability and retention criteria etc. General guidelines for these are given in Part VI-4-7, Geotextile and Plastics of coastal engineering manual of USACE.

3. Apron portion and toe wall are installed before setting up the revetment. Over the deployed Geotextile or the sand mattress Polymer rope gabions are stacked and tied with each other. If required steel frames can also be used to keep these gabions in position.

4. Boulders of 100-150 mm size are filled inside the Gabions manually such that the voids spaces within the fill are as least as possible. At places where boulders are not available or incur high cost, geobags filled with suitable dredged material can be used. Stitched bags are filled at site or near by location and filled inside the Gabions manually or by cranes.

2. PRINCIPLE AND DESIGN CONSIDERATIONS FOR SHORE PROTECTION WORKS

The coastal protection structures mainly act as wave energy dissipaters. These are the systems, which help in reducing the erosion of sand along the shore while simultaneously accumulating current-carried sand on the beach. The structure should be safe against all the possible modes of failure. Pilarcyzk (2000) has given comprehensively several failure modes of an offshore structure and are shown in Figure 5. Generally 2-dimensional limit equilibrium method is used to check the stability of the system against expected failures for the calculated wave forces.

Design lives of hydraulic structures are usually taken as 20 years for temporary structures or short-term measures, 50 to 100 years for shore protection structures. However, type of structure and required function decides the return period selection (Pilarcyzk, 2000). Other than above mentioned design criteria, factors such as boat access, navigation, bathymetric characteristics, waves and currents, aquatic and terrestrial habitat, deeper water access, aesthetics, project

expansion, ease of repair, durability, inspection requirements, erosion control, safety, vandalism, ease of construction, and economy in construction are also considered in the designs.

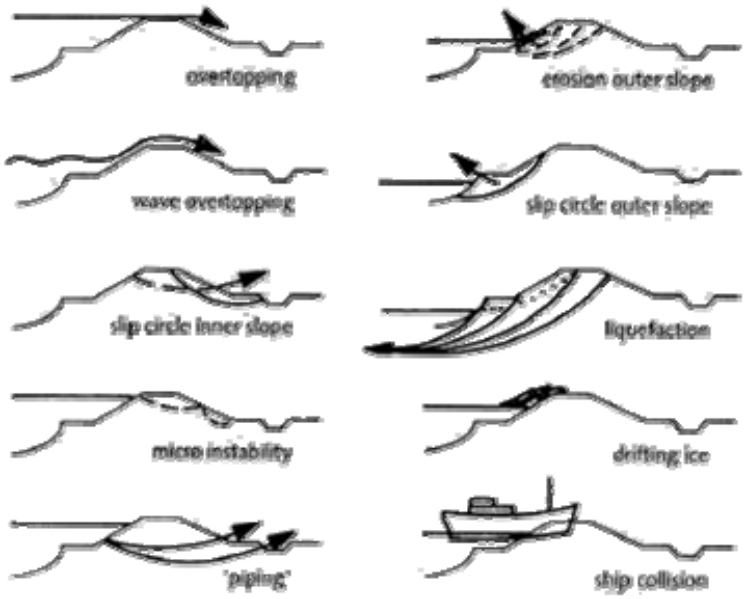

Figure 5. Potential failure modes of coastal structure (adopted from Pilarcyzk, 2000)

3. CASE HISTORIES ON THE USE OF POLYMER ROPE GABIONS FOR SHORE PROTECTION IN INDIA

3.1 Protection against wave erosion near Swaminarayan Temple in the state of Gujarat, India

3.1.1 Problem

The Swaminarayan temple in Tithal, in Gujarat is situated at a distance of around 200-250 m from seashore. The shore suffered extensive erosion due to strong wave action and the formation of eddies contributed by adjacent river and high velocity winds. Seabed erosion had almost reached to the walkway near the temple and posed a threat to the structure in the long run. The problem of erosion is so tremendous that roughly 6 to 7 m of the shore were lost per year. The severity of the erosion can be seen from the photograph shown in Figure 6 (a)

(a) Eroded shoreline of before construction of wall

(b) Sea wall protecting seashore

Figure 6. Status of shore near Swaminarayan temple before and after construction of sea wall

3.1.2 Solution

A shore protection structure using polymer rope gabions with boulder fill was constructed. A layer of Geotextile was laid as a filter media below the gabion at the eroded portion of the beach profile. The design of this wall was carried out by Central Water and Power Research Station (CWPRS), Pune, which is shown schematically in Figure 7. The polymer rope gabions were made of 10 mm diameter rope with aperture size 150 x 150 mm. The total volume of Polymer rope gabion for this work was 6070 m^3. This structure was constructed during May 2001 to October 2001.

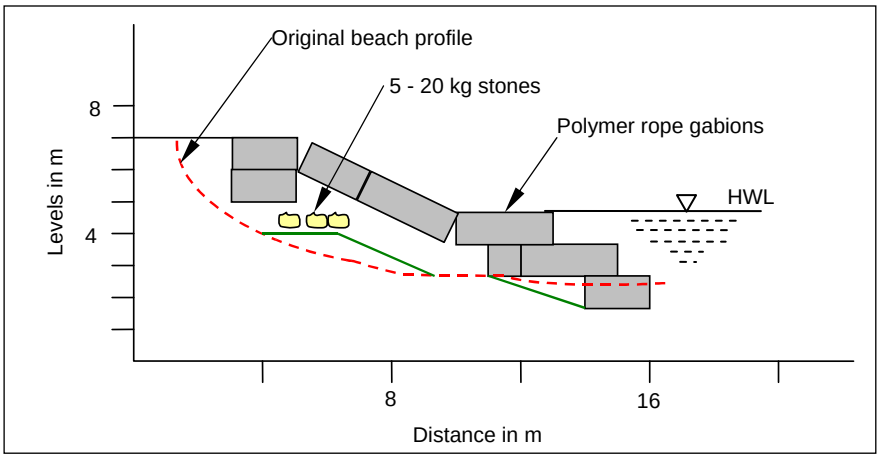

Figure 7. Schematic of the section showing anti-sea erosion bund at Swaminarayan temple.

3.1.3 Current status

After completion of the job, washed out land of about 30 m x 330 m was reclaimed and beautified. The gabion wall is performing very well and about 3 m deep silting has taken place at the toe of the wall. The sea wall after 6 years is absolutely in sound condition even after being subjected to severe cyclonic winds and rainfall. No major maintenance cost has been incurred during the last 7 years. A portion of the wall and silting in front of wall can be seen in the Figure 8.

Figure 8. Swaminarayan temple protection wall after seven years

3.2 Rehabilitation of Sea wall at Moti-danti, in Gujarat state of India

At this site the seawall constructed earlier by conventional materials had failed due to continuous attack of waves and erosion. So it was required to rehabilitate the old structure with the use of Polymer rope gabions. Figure 9(a) shows the

condition of the shore due to the erosion. A sea wall was constructed with boulder mound and Polymer rope gabion as protective cover over them. Figure 9(b) shows the photographs taken during the execution of the seawall. The finished structure is shown in Figure 10. Typical specification adopted for the polymer rope gabion is given in the Appendix-A.

(a) Condition of traditional protection work

(b) Execution of rehabilitation work

Figure 9. Rehabilitation of Sea wall at Moti-danti, Gujarat, India

Figure 10. Completed section of sea wall at Moti-danti, Gujarat, India

4. CASE HISTORY ON COASTAL STURCTURES USING GEOTEXTILE TUBE IN INDIA

4.1 Submerged Geotextile Tube dike at Hooghly Dock Yard, West Bengal, India

4.1.1 Problem

Kolkata Port Trust (KPT) maintains a river line port, which consists of two dock systems i.e. Kolkata Dock System (KDS) and Haldia Dock Complex (HDC). The two dock systems share a common shipping channel from Sandheads to Saugor. The channel bifurcates at this point, one leading to HDC via Auckland & Jellingham and the other leading to KDS via Maragolia crossing, Bedford, Nayachara channel and several other bars. There are 12 bars in the navigational channel between KDS and HDC (upstream of Auckland Bar) and four estuarine bars in the shipping channel leading to HDC. In order to facilitate shipping, the bars and other locations in the shipping channels are dredged throughout the year to maintain navigable depth. The excessive littoral drift and meandering of channel makes movement ships difficult even after dredging. A flexible breakwater system required to be constructed so as to minimize the silt carriage by sea water to the navigational channel.

4.1.2 Solution

Geotextile tube dike was proposed as an alternative to rock dike for constraining the channel movement. Individual geotextile tubes of length 20 m were laid to build the submerged dike. In this project 110 numbers of geotextile tubes of 3m diameter and 20 m length were used. The stitched geotextile tubes were filled by dredged slurry at 30 kN/m^2 pressure with suitable pump. To any prevent failure in geotextile the tubes were filled to about 60 to 70 percent of the theoretical fill volume. The theoretical volume is defined as the cylindrical volume of the container. After filling the geotextile tubes (forming a system of elliptical cross section) were placed at the specific location with the help of splitting barges. Figure 11 shows the photographs taken during the filling and installation of Geotextile tube. Rope net made of 22 mm polypropylene with 250 x 250 mm aperture openings were used for encapsulating tube which is shown in Figure. Enclosed Polymer rope gabion provides additional confinement to the tubes, besides serving as an anchoring unit.

(a) Geotextile tube being unrolled (b) Filling of the tube in barges (c) Installed Geotextile Tube

Figure 11. Geotextile tube at Hooghly Dock Yard, West Bengal, India

4.1.3 Current Status

The construction was carried out during February 2004 to June 2004. The main client of this project was Kolkata Port Trust. National Institute of Ocean Technology has observed the profile of the navigation channel after 6 months of installation. The performance of geotextile tube as a submerged dike is exceptionally well. The movement of shipping channel was found to be restrained.

4.2 Geotextile Tube for Shore protection at Shankarpur to Halda, West Bengal, India

Principle Client: Irrigation and Waterways Directorate, West Bengal, India.

4.2.1 Problem

Coastal line of Bay of Bengal between Shankarpur to Halda had severe erosion due to waves of height 1 m and wave length of 20 m. At some locations vertical cuts of 4m were observed. It was expected to cause severe damage shoreline, scenic views and public property along the coastal line.

4.2.2 Solution

The solution for this issue was proposed by providing geotextile tube in two plus one configuration (two at the bottom and one above that) with toe or Scouring apron and geotextile-Filter Media. Any erosion at the toe and adjacent to the tube

would gradually results in the undercutting of the toe and failure of the slope. Hence Geobags and Geocontainers filled polymer rope gabions were provided as toe protection and covered with Geomattress to stabilize the slope surface. The length of apron is 2.0 m. (which varies with site conditions). Typical arrangement of 2+1 geotextile tube configuration was chosen and the arrangement of geotextile tube varied as per the site conditions and requirement. Geotextile filter media was provided beneath the total system.

4.2.3 Current Status

The project involves the installation of 150 Geotextile tubes of 20 m length and 3 m diameter. The project is still in the construction phase and the completed portion of the Geotextile tube embankment is found to have controlled the erosion to a considerable proportion. There is no loss of sand from the geotextile tube observed as the fabric is tighter and stronger. Completed portion is shown in the Figure 12. Typical specification of Geotextile used for Geotextile tube fabrication is given in the Appendix-B

Figure 12. Protection of seashore with geotextile tube at Shankarpur, West Bengal, India

5. CONCLUSIONS

Geosynthetic materials in shore protection works have come as handy for simpler, faster and economical constructions. This paper discussed the successful case histories on the polymer rope gabions and geotextile tubes for the shore protection works in India. These structures are found to be flexible and were constructed with locally available materials without any enormous foundation works. Apart from technical and economical efficiency these structures are eco-friendly too as they do not use much of the geo-materials hauled from different locations. Hence these techniques have to be extended to all such kinds of projects.

REFERENCES

Bogossian, F., Smith, R.T., Vertimatti, J.C. and Yazbek, O. (1982) Continuous Retaining Dikes by Means of Geotextile. Proceedings of the II International Conference on Geotextiles, Las Vegas, 211-216.

EM 1110 – 2 – 1100, US Army Corps, Coastal Engineering Manual,

Harris, L.E. (1987) Evaluation of Sand-Filled Containers for Beach Erosion Control, An Update of the Technology. Proceedings of Coastal Zone ‘87, ASCE, 2479-2487.

Lawson, C.R., (2006) Geotextile containment for hydraulic and environmental engineering, *Proceedings of the 8th International Conference on Geosynthetics, Yokohama, Japan,* pp 9-48.

Pilarcyzk, K.W. (2000) Geosynthetics and Geosystems in Hydraulic and Coastal Engineering. *A.A.Balekema/ Rotterdam, Netherlands.*

Appendix-A. Specification of polymer rope gabions used in coastal works

Rope and Aperture	10mm rope, Net with 150X150mm aperture size (Varies)
Size of the Gabion	1 m x 1 m x 1 m (may vary depending on site requirement)
Size of the body and border rope	10mm having a weight of 45gm/m with a tolerance of ±10%
Material of the rope	Polypropylene (with ultraviolet stabilizer)
Tensile Strength	Individual rope 1560 Kg (minimum breaking strength) For Rope net 8000 Kg /m width (breaking strength)
Punching shear strength	3000 Kg
Structure of the rope	3 strand
Construction of net	Woven joint at the intersection of ropes
Abrasion resistance	The rope shall have a residual breaking strength of at least of 85% of the stipulated rope strength at the end of 1000 cycles of standard abrasion
Thermal Stability	Minimum residual strength retained = 90%
Resistance to ultraviolet radiation	Material shall be adequately stabilized against ultraviolet radiation to survive for the intended life period.

Appendix-B. Specifications for Geotextile used for tubes

Property		Test Method	Value (MARV)
Polymer		Polypropylene	
Structure		Woven with multifilament yarn in both warp and weft directions	
Mass per unit area		ASTM D 3776	330 g/m^2
Mechanical Properties			
Tensile strength	Warp	Indian Standard: 1969	80 kN/m
	Weft		78 kN/m
Elongation at designated peak tensile load	Warp		25 %
	Weft		25 %
Trapezoid tearing strength	Warp	ASTM D-4533	1600 N
	Weft		1600 N
Puncture strength		ASTM D-4833	600 N
Hydraulic Properties			
Apparent opening size		ASTM D-4751	250 microns
Water flow rate normal to the plane		ASTM D-4491	18 ℓ/m^2/s

(MARV stands for Minimum average roll value)

Geosynthetics 2009
February 25-27 2009, Salt Lake City, Utah

Management of Swine and Dairy Manure with Geotextile Tube Dewatering Containers

B.J. Mastin, WaterSolve, LLC, Grand Rapids, MI, USA
G.E. Lebster, WaterSolve, LLC, Grand Rapids, MI, USA

ABSTRACT
The objective of this study was to evaluate geotextile tube containers, with the aid of dewatering polymers, as a manure management option for both a swine finishing facility and a dairy operation including cost effectiveness, ease of operation, volatile solids and nutrient retention, solids handling time, flow and volume rates, and seasonality compared to land application of anaerobic lagoons. In comparison to an anaerobic lagoon system, geotextile tube containment and dewatering consolidates manure to less than 25% of its original volume, dewatered cake remains dry and protected from precipitation, retains the N and P value of the manure, provides a four season alternative for manure management, decreases methane release to the atmosphere, allows farmers to economically transport manure for distribution in other markets, and dry manure-spreading equipment is less expensive to own and operate than liquid injection equipment.

1. INTRODUCTION

Concerns regarding nutrient losses from the manure of large dairy herds and swine facilities to groundwater or surface runoff have been extremely acute in U.S. watersheds. Nitrogen (N) and phosphorus (P) are the primary nutrients of concern. Manure N can be converted to nitrates in the soil and potentially leach to groundwater. Manure P can potentially move with surface runoff, thus stimulating algae and aquatic plant growth leading to eutrophication of surface waters. Potassium (K) has not been of as much concern environmentally as N and P, but it is of equal concern in fertilizer management strategies. Potassium is important in assessing equivalent commercial fertilizer value of manure. In lieu of dragline land application, manure treatment alternatives currently include composting, solid-liquid separation, anaerobic digestion, and biological treatment lagoons. Advantages of manure management include reduction in mass, nutrient reduction and concentration, pathogen control, and potential by-product sales. Compared to current land application techniques, manure dewatering and subsequent nutrient management increases the land distribution that could economically receive cake solids thus limiting oversaturation of adjacent properties, reduces odors and associated ammonia, hydrogen sulfide, and methane production, and is a four season option without seasonal and weather restrictions.

Large-diameter geotextile tubes have been used to contain and dewater dredge materials from river channels and harbors for decades (Fowler et al. 1995). In these applications, coarse-grain sediments pumped into the geotextile tube settle rapidly and slurry water is discharged through ports in the top of the tube. Geotextile tubes deployed in such settings have been used to form berms and alternative disposal sites to contain additional dredge materials. Sand-filled geotextile tubes are also used to stabilize dunes on beaches, as levees, and as manmade peninsulas to establish harbors. In these applications, confinement of the geotextile fabric adds shear strength to the sediment fill, resulting in a structure that is stable and resistant to erosion. Use of geotextile tubes to thicken and dewater fine grained sediments is a developing field and has had limited application in the agricultural, municipal, industrial, and environmental management markets (Miratech 2005). Technological advances in the use and application of polymers and other chemical conditioning agents for the expedient separation of solids from water have facilitated the use of geotextile tubes for containment, dewatering, and consolidation of hydraulically pumped and excavated materials. This new and innovative technology has been successfully used to dewater fine-grained, contaminated material that contained dioxins, polychlorinated biphenyls (PCBs), polyaromatic hydrocarbons (PAHs), pesticides, metals (with a lithic biogeochemical cycle), and other hydrophobic materials (Fowler et al. 1996, Taylor et al. 2000).

The primary objective of this pilot-scale experiment was to compare the performance and economics of geotextile tube containers for dewatering and consolidating liquid manure (dairy and swine) as well as containing total nitrogen (TKN), ammonia-nitrogen (NH4), volatile solids (TVS), and total phosphorus (TP) compared to current nutrient management practices with an onsite anaerobic lagoon. WaterSolve et al. successfully performed these experiments with the help of two Mercer County Ohio farmers (Ivo Post and Randy Goettemoeller) and Ms. Laura Walker (Mercer County, Ohio Soil and Water Conservation District). In addition, secondary objectives of solids capture and nutrient retention were evaluated for compatibility with current agricultural nitrogen and phosphorus requirements. The data

collected during these pilot trials was used to scale the chemical doses, geotextile tube container dimensions, and equipment required for a full-scale geotextile tube dewatering application.

2. SWINE MANURE – IVO POST FARM, MARIA STEIN, OHIO

2.1 Objective

The objectives of this swine manure management experiment were:

1) Pump manure from a pull-plug swine barn two times per week,
2) Pump the manure through a two-inch discharge pipeline to a dewatering pad constructed adjacent to the onsite anaerobic lagoon,
3) Chemically condition the manure prior to the geotextile tube containers and contain manure solids,
4) Decrease the nitrogen, phosphorus, and solids concentrations discharged to the lagoon,
5) Measure nutrients and solids concentrations over time in the geotextile tube container and filtrate water,
6) Convey the separated water into the anaerobic lagoon, and
7) Land-apply the dried residuals to an approved agricultural field in 2008.

2.2 Geotextile tube container sizing

One 10-yd3 industrial sludge weight geotextile tube container and two 10-yd3 agricultural weight geotextile tube containers were delivered to contain approximately 22,500 gallons of swine manure at two-percent dry weight solids. It was calculated that 30-yd3 of geotextile tube container would be needed to dewater and contain this volume to greater than 20-percent dry weight solids, sufficiently dry to pass a paint filter test, haul off site, and be acceptable for land application with a manure spreader. The resulting volume and mass of residuals at 20-percent dry weight solids would be less than 14 cubic yards and 13 tons, respectively. An operational goal of this project was to hydraulically pump at an average flow rate of 200 gallons per minute.

The residual processing area included a bermed, dewatering pad (gravel area with HDPE-liner) where the water was separated from the solids, manure holding tank for homogenization prior to chemical conditioning, a WSLP-2400 polymer make-down unit, water tank for polymer make-down dilution water, and a discharge culvert where “clean” water was conveyed to the lagoon.

2.3 Chemical conditioning

Sequential application of Solve 10 followed by Solve 9248 was determined to flocculate and dewater Ivo Post’s swine manure most effectively compared to the other polymer combinations. Water release rate and clarity were excellent. However, color remained in the release water. Re-evaluation with 5- to 8-mL polymer doses was used to select Solve 10 (200-ppm) followed by Solve 9248 (266-ppm) as the recommended chemical conditioning program for dewatering this residual during a geotextile tube application.

A 150-mL sludge sample was flocculated and poured through an industrial sludge weight geotextile tube filter apparatus, in order to observe water release volumes and potential drying timelines. Seventy-five milliliters of water were captured in a graduated cylinder within 5-minutes.

2.4 Operations

In the fall of 2007, approximately 22,500 gallons of swine manure were successfully contained and dewatered during this pilot-scale project evaluating hydraulic pumping and subsequent dewatering utilizing geotextile tube technology. The project team was comprised of Mercer County Soil and Water Conservation District, Grand Lake/Wabash Watershed Alliance and several subcontractors, including: Maria Stein Grain, WaterSolve, LLC (chemical conditioning program), AgCert Services, and TenCate Geosynthetics (geotextile tube manufacturer) (Figure 1).

Solve 9248 was used independent of Solve 10 in a single-product conditioning trial for the first two geotextile tube containers. A second agricultural weight geotextile tube container was brought online to compare the previously recommended dual product conditioning program to the single product application. WaterSolve’s LP-2400 polymer make-down unit was used to dilute and activate Solve 9248. A chemical feed pump (10-gph LMI) with a high-viscosity head was used to introduce Solve 10 without dilution. An inline mixing manifold was located between polymer introduction points and downstream of Solve 9248 in the residual line, prior to the geotextile tube containers (Figure 2).

A  B 

Figure 1. Ivo Post site after several pumping events (September 11, 2007). An agricultural weight geotextile tube container (background) was pumped to 32 inches over 10 weeks and an industrial sludge weight geotextile tube container (foreground) was pumped to 29 inches (A). Hogs were grown out from less than 100 pounds to finish at approximately 500 pounds during the experimental period (B).

A  B 

Figure 2. Swine manure was conditioned with Solve 10 followed by Solve 9248 and subsequently pumped into an agricultural weight geotextile tube container (A). WaterSolve's WSLP-2400 polymer make-down unit activated and injected Solve 9248 to the swine residual inline prior to the Geotube containers (B).

2.5 Nutrient Analyses

Influent swine manure and geotextile tube filtrate samples (conditioned with Solve 9248) were collected on 6 September 2007, 11 September 2007, and 20 September 2007 and shipped in coolers at less than 4^{o}C to ALS Laboratories (formerly e-Lab) in Holland, Michigan for TKN, NH4, TVS, TP, total solids, percent moisture, and pH analyses according to Standard Method 4500-N B, Standard Method 4500-NH3 B/C, EPA 160.42, EPA 365.1 R2.0, Standard Method 2540 B, Standard Method 2540 B, and EPA 9045, respectively. After geotextile tube containers were pulse-filled to capacity, core samples were collected over 180-d of dewatering and consolidation (7-d, 14-d, 21-d, 39-d, 67-d and 180-d) and shipped overnight in coolers at less than 4^{o}C to ALS Laboratories for analyses previously described (Figure 3).

Influent swine manure and geotextile tube filtrate samples (conditioned with Solve 10 followed by Solve 9248) were collected on 1 October 2007, 4 October 2007, 8 October 2007, and 11 October 2007 and shipped in coolers at less than 4^{o}C to ALS Laboratories for TKN, NH4, TVS, TP, total solids, percent moisture, and pH analyses according to Standard Method 4500-N B, Standard Method 4500-NH3 B/C, EPA 160.42, EPA 365.1 R2.0, Standard Method 2540 B, Standard Method 2540 B, and EPA 9045, respectively. After geotextile tube containers were pulse-filled to capacity, core samples were collected over 180-d of dewatering and consolidation (18-d, 39-d, 62-d, 39-d, 62-d and 180-d) and shipped in coolers at less than 4^{o}C to ALS Laboratories for analyses previously described.

A  B 

Figure 3. Chemically conditioned (Solve 9248) swine manure (right) and geotextile tube filtrate water (left) collected 06 September 2007 (A). Sample port used for monitoring inline chemical conditioning (B).

2.6 Results

Average (±SD) TKN, NH4, TP, TS, and TVS concentrations of influent swine manure residual chemically conditioned, contained, and dewatered in 10-yd^3 agricultural weight and industrial sludge weight geotextile tube containers was 190,000 mg/kg dry (86,603), 61,667 mg/kg-dry (111,841), 28,000 mg/kg-dry (16,093), 1.56-percent (0.76), and 0.91-percent (0.47), respectively (Table 1). Average (±SD) TKN, NH4, TP, TS, and TVS concentrations of filtrate water released from the agricultural weight geotextile tube container conditioned with Solve 9248 was 2,333 mg/kg-dry (153), 1,520 mg/kg-dry (425), 110.7 mg/kg-dry (19.0), 0.99-percent (0.02), and 0.42-percent (0.02), respectively. Average (±SD) TKN, NH4, TP, TS, and TVS concentrations of filtrate water released from the industrial sludge weight geotextile tube container conditioned with Solve 9248 was 2,000 mg/kg-dry (300), 1,633 mg/kg-dry (231), 112.3 mg/kg-dry (16.6), 0.91-percent (0.07), and 0.38-percent (0.05), respectively. During containment and dewatering, greater than 98-percent of TKN, NH4, and TP were retained within both the agricultural weight geotextile tube and industrial sludge geotextile tube containers. Greater than 38-percent and greater than 53-percent +of TS and TVS were
captured and retained in the Geotube containers, respectively. pH of the raw swine manure, geotextile tube filtrate water, and remaining cake solids over 180-d dewatering remained circumneutral (6.3 to 7.6).

TKN, NH4, TP, TS, and TVS concentrations of core samples collected from the 10-yd^3 agricultural weight geotextile tube container filled with swine manure chemically conditioned with Solve 9248 dewatered for 180-d were 41,000 mg/kg-dry, 20,000 mg/kg-dry, 25,000 mg/kg-dry, 20-percent, and 20-percent, respectively (Table 2). TKN, NH4, TP, TS, and TVS concentrations of core samples collected from the 10-yd^3 industrial sludge weight geotextile tube container filled with swine manure chemically conditioned with Solve 9248 dewatered for 180-d were 16,000 mg/kg-dry, 15,000 mg/kg-dry, 25,000 mg/kg-dry, 19-percent, and 19-percent, respectively (Table 3).

Average (±SD) TKN, NH4, TP, TS, and TVS concentrations of influent swine manure residual chemically conditioned with Solve 10 followed by Solve 9248, contained, and dewatered in a 10-yd^3 agricultural weight geotextile tube container was 121,250 mg/kg-dry (29,545), 89,250 mg/kg-dry (26,625), 12,950 mg/kg-dry (6,523), 2.73-percent (1.03), and 1.77-percent (0.84), respectively (Table 4). Average (±SD) TKN, NH4, TP, TS, and TVS concentrations of filtrate water released from the geotextile tube container conditioned with Solve 10 followed by Solve 9248 was 2,500 mg/kg- dry (115), 1,725 mg/kg-dry (150), 147.5 mg/kg-dry (26.3), 1.17-percent (0.31), and 0.52-percent (0.17), respectively. During containment and dewatering, greater than 97-percent TKN, NH4, and TP were retained within the agricultural weight geotextile tube container. Greater than 56-percent and greater than 70-percent of TS and TVS were captured in the geotextile tube container. pH of the raw swine manure, geotextile tube filtrate water, and remaining cake solids over 180-d dewatering remained circumneutral (6.8 to 7.0).

TKN, NH4, TP, TS, and TVS concentrations of core samples collected from the 10-yd^3 agricultural weight geotextile tube container filled with swine manure chemically conditioned with Solve 10 followed by Solve 9248 dewatered for 180-d were 51,000 mg/kg-dry, 16,000 mg/kg-dry, 29,000 mg/kg-dry, 20-percent, and 19.2-percent, respectively (Table 5).

Table 1. Average (±SD) nitrogen, phosphorus, and solids concentrations of swine manure residual chemically conditioned (Solve 9248), contained, and dewatered in 10-yd^3 agricultural weight and industrial sludge weight geotextile tube containers (06 September 2007, 11 September 2007, 20 September 2007).

Sample	pH	Nitrogen, Ammonia (mg-Kg/dry)	Nitrogen, Total Kjeldahl (mg/Kg-dry)	Phosphorus, Total (mg/Kg-dry)	Total Solids (% of sample)	Volatile Solids (% of sample)
Influent	6.9 (0.2)	161,667 (111,841)	190,000 (86,603)	28,000 (16,093)	1.56 (0.76)	0.91 (0.47)
Agricultural filtrate	6.9 (0.1)	1,520 (425)	2,333 (153)	110.7 (19.0)	0.99 (0.02)	0.42 (0.02)
Industrial sludge filtrate	6.4 (0.9)	1,633 (231)	2,000 (300)	112.3 (16.6)	0.91 (0.07)	0.38 (0.05)

Table 2. Nitrogen, phosphorus, and solids concentrations of core samples collected from a 10-yd^3 agricultural weight geotextile tube container with swine manure chemically conditioned (Solve 9248), contained, and dewatered for 180-d.

Sample	pH	Nitrogen, Ammonia (mg-Kg/dry)	Nitrogen, Total Kjeldahl (mg/Kg-dry)	Phosphorus, Total (mg/Kg-dry)	Total Solids (% of sample)	Volatile Solids (% of sample)
7-d	6.5	19,000	52,000	28,000	12.0	9.8
14-d	6.3	16,000	36,000	20,000	15.0	11.3
67-d					20.0	
180-d	7.3	20,000	41,000	25,000	20.0	20.0

Table 3. Nitrogen, phosphorus, and solids concentrations of core samples collected from a 10-yd^3 industrial sludge weight geotextile tube container with swine manure chemically conditioned (Solve 9248), contained, and dewatered for 189-d.

Sample	pH	Nitrogen, Ammonia (mg-Kg/dry)	Nitrogen, Total Kjeldahl (mg/Kg-dry)	Phosphorus, Total (mg/Kg-dry)	Total Solids (% of sample)	Volatile Solids (% of sample)
7-d	6.3	20,000	43,000	27,000	9.7	8.1
14-d	6.4	15,000	35,000	25,000	17.0	12.8
67-d					23.0	
189-d	7.4	15,000	16,000	25,000	19.0	19.0

Table 4. Average (±SD) nitrogen, phosphorus, and solids concentrations of swine manure residual chemically conditioned (Solve 10 followed by Solve 9248), contained, and dewatered in a 10-yd^3 agricultural geotextile tube container (01 October 2007, 04 October 2007, 08 October 2007, 11 October 2007).

Sample	pH	Nitrogen, Ammonia (mg-Kg/dry)	Nitrogen, Total Kjeldahl (mg/Kg-dry)	Phosphorus, Total (mg/Kg-dry)	Total Solids (% of sample)	Volatile Solids (% of sample)
Influent	6.9 (0.1)	89,250 (26,625)	121,250 (29,545)	12,950 (6,523)	2.73 (1.03)	1.77 (0.84)
Sample Port	6.9 (0.1)	53,500	100,250 (40,467)	37,500 (33,828)	4.10 (0.52)	3.11 (0.45)
	pH	Nitrogen, Ammonia (mg NH_3-N/L)	Nitrogen, Total Kjeldahl (mg/L)	Phosphorus, Total (mg/L)	Total Solids (% of sample)	Volatile Solids (% of sample)
Agricultural filtrate	6.9 (0.1)	1,725 (150)	2,500 (115)	147.5 (26.3)	1.17 (0.31)	0.52 (0.17)

Table 5. Nitrogen, phosphorus, and solids concentrations of core samples collected from a 10-yd^3 agricultural weight geotextile tube container with hog manure chemically conditioned (Solve 10 followed by Solve 9248), contained, and dewatered for 180-d.

Sample	pH	Nitrogen, Ammonia (mg-Kg/dry)	Nitrogen, Total Kjeldahl (mg/Kg-dry)	Phosphorus, Total (mg/Kg-dry)	Total Solids (% of sample)	Volatile Solids (% of sample)
18-d					17.0	
39-d					19.0	
62-d					24.0	
180-d	7.6	16,000	51,000	29,000	20.0	19.2

3. DAIRY MANURE – RANDY GOETTEMOELLER FARM, MARIA STEIN, OHIO

3.1 Objective

The objectives of this dairy manure management experiment were:

1) Pump manure from a scrape-alley barn two times per week,
2) Pump the manure filtrate through a two-inch discharge pipeline after separation with a screw separator to a dewatering pad constructed adjacent to the onsite anaerobic lagoon,
3) Chemically condition the manure prior to the geotextile tube containers and contain manure solids,
4) Decrease the nitrogen, phosphorus, and solids concentrations discharged to the lagoon,
5) Measure nutrients and solids concentrations over time in the geotextile tube container and filtrate water,
6) Convey the separated water into the anaerobic lagoon, and
7) Land-apply the dried residuals to an approved agricultural field in 2008.

3.2 Geotextile tube container sizing

One 10-yd3 industrial sludge weight geotextile tube container and one 10-yd3 agricultural weight geotextile tube containers were delivered to contain approximately 7,500 gallons of dairy manure at four-percent dry weight solids. It was calculated that 20-yd3 of geotextile tube container would be needed to dewater and contain this volume to greater than 20-percent dry weight solids, sufficiently dry to pass a paint filter test, haul off site, and be acceptable for land application with a manure spreader. The resulting volume and mass of residuals at 20-percent dry weight solids would be less than 9 cubic yards and 8 tons, respectively. An operational goal of this project was to hydraulically pump at an average flow rate of 200 gallons per minute.

The residual processing area included a bermed, dewatering pad (gravel area with HDPE-liner) where the water was separated from the solids, manure holding tank for homogenization prior to chemical conditioning, a WSLP-2400 polymer make-down unit, water tank for polymer make-down dilution water, and a discharge culvert where “clean” water was conveyed to the lagoon.

3.3 Chemical conditioning

Sequential application of Solve 10 followed by Solve 9244 was determined to flocculate and dewater Randy Goettemoeller’s dairy manure most effectively compared to the other polymer combinations. Water release rate and clarity were excellent. However, color remained in the release water. Re-evaluation with 5- to 8-mL polymer doses was used to select Solve 10 (400-ppm) followed by Solve 9244 (133-ppm) as the recommended chemical conditioning program for dewatering this residual during a Geotube® application.

A 150-mL sludge sample was flocculated and poured through a industrial sludge weight geotextile tube filter apparatus, in order to observe water release volumes and potential drying timelines. Sixty-five milliliters of water were captured in a graduated cylinder within 5-minutes.

3.4 Operations

In the fall of 2007, approximately 7,500 gallons of dairy manure were successfully contained and dewatered during this pilot-scale project evaluating hydraulic pumping and subsequent dewatering utilizing geotextile tube technology. The project team was comprised of Mercer County Soil and Water Conservation District, Grand Lake/Wabash Watershed Alliance and several subcontractors, including: Maria Stein Grain, WaterSolve, LLC (chemical conditioning program), AgCert Services, and TenCate Geosynthetics (geotextile tube manufacturer) (Figure 6).

Sequential application of Solve 10 followed by Solve 9244 was used in a dual-product conditioning trial for the first two geotextile tube containers. WaterSolve’s LP-2400 polymer make-down unit was used to dilute and activate Solve 9244. A chemical feed pump (10-gph LMI) with a high-viscosity head was used to introduce Solve 10 without dilution. An inline mixing manifold was located between polymer introduction points and downstream of Solve 9244 in the residual line, prior to the geotextile tube containers (Figure 6).

A 

B 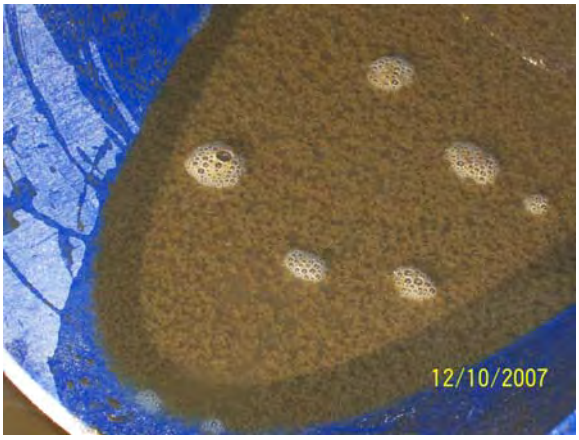

Figure 4. Randy Goettemoeller site after several pumping events (October 12, 2007). An agricultural weight geotextile tube container (background) was pumped to 26 inches over 8 weeks and an industrial weight geotextile tube container (foreground) was pumped to 28 inches (A). Samples collected to verify inline chemical conditioning (B).

3.5 Nutrient Analyses

Influent dairy manure and geotextile tube filtrate samples (conditioned with Solve 10 followed by Solve 9244) were collected on 29 October 2007, 30 October 2007, and 5 November 2007 and shipped in coolers at less than 4^{o}C to ALS Laboratories for TKN, NH4, TVS, TP, total solids, percent moisture, and pH analyses according to Standard Method 4500-N B, Standard Method 4500-NH3 B/C, EPA 160.42, EPA 365.1 R2.0, Standard Method 2540 B, Standard Method 2540 B, and EPA 9045, respectively. After geotextile tube containers were pulse-filled to capacity, core samples were collected over 180-d of dewatering and consolidation (9-d, 14-d, 30-d, 40-d, and 180-d) and shipped overnight in coolers at less than 4^{o}C to ALS Laboratories for analyses previously described.

3.6 Results

Average (±SD) TKN, NH4, TP, TS, and TVS concentrations of influent dairy manure residual chemically conditioned, contained, and dewatered in 10-yd^3 G and industrial sludge weight geotextile tube containers was 58,000 mg/kg-dry (6,928), 24,667 mg/kg-dry (2,082), 5,167 mg/kg-dry (451), 3.50-percent (0.17), and 1.97-percent (0.87), respectively (Table 6). Average (±SD) TKN, NH4, TP, TS, and TVS concentrations of filtrate water released from the agricultural geotextile tube container conditioned with Solve 10 followed by Solve 9244 was 573 mg/kg-dry (77.7), 383 mg/kg-dry (41.6), 21.0 mg/kg-dry (7.9), 0.77-percent (0.05), and 0.38-percent (0.03), respectively. Average (±SD) TKN, NH4, TP, TS, and TVS concentrations of filtrate water released from the industrial sludge geotextile tube container conditioned with Solve 10 followed by Solve 9244 was 637 mg/kg-dry (58.6), 387 mg/kg-dry (30.6), 22.9 mg/kg-dry (18.2), 0.94-percent (0.14), and 0.49-percent (0.10), respectively. During containment and dewatering, greater than 98-percent TKN, NH4, and TP were retained within both the agricultural weight and industrial sludge weight geotextile tube containers. Greater than 73 percent and greater than 75-percent of TS and TVS were captured in the geotextile tube containers, respectively. pH of the raw swine manure, geotextile tube containers swine manure, geotextile tube filtrate water, and remaining cake solids over 180-d dewatering remained circumneutral (6.4 to 7.5).

TKN, NH4, TP, TS, and TVS concentrations of core samples collected from the 10-yd^3 agricultural weight geotextile tube container filled with dairy manure chemically conditioned with Solve 10 followed by Solve 9244 dewatered for 180-d were 36,000 mg/kg-dry, 3,000 mg/kg-dry, 7,200 mg/kg-dry, 25-percent, and 25-percent, respectively (Table 7). TKN, NH4, TP, TS, and TVS concentrations of core samples collected from the 10-yd^3 industrial sludge weight container filled with dairy manure chemically conditioned with Solve 10 followed by Solve 9244 dewatered for 180-d were 38,000 mg/kg-dry, 4,100 mg/kg-dry, 8,200 mg/kg-dry, 21-percent, and 21-percent, respectively (Table 8).

Table 6. Average (±SD) nitrogen, phosphorus, and solids concentrations of dairy manure residual (screw separator pretreatment) chemically conditioned (Solve 10 followed by Solve 9244), contained, and dewatered with 10-yd^3 agricultural and industrial sludge geotextile tube containers (29 October 2007, 30 October 2007, 05 November 2007).

Sample	pH	Nitrogen, Ammonia (mg-Kg/dry)	Nitrogen, Total Kjeldahl (mg/Kg-dry)	Phosphorus, Total (mg/Kg-dry)	Total Solids (% of sample)	Volatile Solids (% of sample)
Influent	6.7 (0.1)	24,667 (2,082)	58,000 (6,928)	5,167 (451)	3.50 (0.17)	1.97 (0.87)
Agricultural filtrate	6.9 (0.1)	383 (41.6)	573 (77.7)	21.0 (7.9)	0.77 (0.05)	0.38 (0.03)
Industrial Sludge filtrate	6.9 (0.1)	387 (30.6)	637 (58.6)	22.9 (18.2)	0.94 (0.14)	0.49 (0.10)

Table 7. Nitrogen, phosphorus, and solids concentrations of core samples collected from a 10-yd^3 agricultural geotextile tube container with dairy manure chemically conditioned (Solve 10 followed by Solve 9244), contained, and dewatered for 180-d.

Sample	pH	Nitrogen, Ammonia (mg-Kg/dry)	Nitrogen, Total Kjeldahl (mg/Kg-dry)	Phosphorus, Total (mg/Kg-dry)	Total Solids (% of sample)	Volatile Solids (% of sample)
9-d	6.4	6,900	35,000	3,400	9.9	1.58
14-d					9.0	
30-d					15.0	
180-d	7.4	3,000	36,000	7,200	25.0	25.0

Table 8. Nitrogen, phosphorus, and solids concentrations of core samples collected from a 10-yd^3 industrial sludge geotextile tube container with dairy manure chemically conditioned (Solve 10 followed by Solve 9244), contained, and dewatered for 180-d.

Sample	pH	Nitrogen, Ammonia (mg-Kg/dry)	Nitrogen, Total Kjeldahl (mg/Kg-dry)	Phosphorus, Total (mg/Kg-dry)	Total Solids (% of sample)	Volatile Solids (% of sample)
9-d	6.4	12,000	75,000	6,900	4.0	0.84
14-d					11.0	
30-d					14.0	
180-d	7.5	4,100	38,000	8,200	21.0	21.0

4. DISCUSSION

In order to initiate these full-scale agricultural geotextile tube projects, project engineers designed the dewatering programs, including estimated geotextile tube container capacity, polymer make-down systems (WSLP-2400/4800), chemical conditioning programs, bench testing, mobilization/demobilization, and technical assistance during start-up for less than $0.0085 and $0.0115 per gallon for to manage swine and dairy manure, respectively. With a shift to a larger polymer shipment(s) and additional geotextile tube containers, subsequent annual costs are expected to decrease overtime to contain, dewater, and consolidate these manures. Excavation, transportation, and disposal of dried solids were not included in calculation of project costs, as these costs would fluctuate depending on the percent solids in the containers and final mass disposed of at the landfills and/or land application.

Start up of these projects required 10 to 30 man hours, including installation of the geotextile tube containers and manifold system, set up of the polymer make-down unit(s), time to initiate solids pumping, and calibration of the inline polymer feed rate. Once the system was calibrated to an optimal solids flow rate and sufficient inline flocculation was observed, the system was monitored once per hour and adjustments made to the polymer feed rate. Throughout the start up process, the solids flow rate to the geotextile tube containers was neither reduced nor stopped. Geotextile tube containers continued to dewater and solids consolidated even as the percent solids of the sludge and strength of flocculation fluctuated during pumping.

Greater than 75 percent of total suspended solids (TSS) were retained within the geotextile tube containers. As pumping of solids was initiated to a new container, a layer of solids covers the inside of the geotextile and decreases the loss of solids due to surface tension. This process typically occurs within one to five minutes of solids flow to the new geotextile tube container and clear filtrate was observed for the rest of the dredging operation. Comparable results were obtained from the belt press and free water was collected and returned to the facility head-works or conveyed for discharge back to the lagoons.

An advantage of using geotextile tube technology was the system was closed loop and solids were only handled one time, during excavation of full containers. A closed loop system eliminates odors, potential for spills, and solids handling, as well as decreases risk(s) of operator(s) exposure to pathogens and other solids contaminants. Also, geotextile tube operations of this magnitude typically occur over days compared to a weeks of continuous operations with a belt press or centrifuge. With a belt press system, solids are open to the atmosphere, potentially release volatiles and associated odors, are excessively noisy, can spill off the belt onto the ground if blinding occurs due to insufficient flocculation, and increases potential risk(s) of operator exposure to solids contaminants.

Flow rates (100 to 2,000 gpm) to geotextile tube containers are dependant on equipment available on site, hiring of a contractor, or by renting from an equipment company. Solids from these projects were pumped with onsite equipment to geotextile tube containers at 100 to 300 gallons per minute. In comparison, a 0.5-m belt press (a typical belt size for a truck mounted rental unit) has a maximum solids flow rate of 150 gpm. There are very few reasons to stop the flow of solids to a Geotube system except potentially changing an empty polymer drum/tote, shifting solids flow from a full container to a new container, and during shut down of operations to make inline design changes. In comparison, belt press operations are typically considered efficient at greater than 75 percent working operations.

Pumping of solids to a new geotextile tube container can occur during any time of the year as long as polymer feed lines and solids lines are freeze protected. Pumping of solids to a partially filled container with frozen solids is not recommended due to inefficient dewatering and filling and the potential for overfilling. However, allowing a full or partially full geotextile tube container to sit outside during a freeze/thaw cycle typically “cracks out” (i.e., releases) additional free water and will not harm the container.

The footprint required for two 60-ft circumference x 100-ft long geotextile tube containers was 555 square meters (6,050 square feet), sufficient to collect filtrate from the geotextile tube containers and channel it back to the facility. Geotextile tube containers were site-specific manufactured to fit the facility’s available footprint. For solids dewatering, containers are manufactured in 30-ft to 120-ft circumferences in 5-ft increments with lengths of 50-ft to 400-ft. standard geotextile tube sizes designed for containment of solids can hold between 20 and 1,750 cubic yards of material.

5. CONCLUSIONS

1) Geotextile tube dewatering technology was successful in treating liquid swine and dairy manure and would improve water quality in the Wabash Watershed.

2) Full-scale hog manure management with geotextile tube technology would cost $0.0085/gallon for greater than 250,000 gallons of manure.
3) Full-scale dairy manure management with geotextile tube technology would cost $0.0115/gallon for greater than 250,000 gallons of manure. Solids separation was required prior to containment and consolidation in the geotextile tube containers. Additional dilution may be required if alley-scrape facilities are to be managed.
4) The secondary gains of geotextile tube containment and dewatering (e.g., nutrient value, dry-storage capacity, four season operations, etc.) have not been quantified as part of these conclusions.
5) Capital costs for equipment and infrastructure modifications would need to be calculated on a case-by-case basis.
6) Greater than 98% of the nitrogen (TKN and NH4) and 99% of the phosphorus (TP) was captured in the geotextile tube containers from the raw swine manure and separated dairy manure.
7) After 180-days dewatering, 75% of the captured nitrogen and 100% of the captured phosphorus was still available in the geotextile tube containers for land application with a manure spreader, etc.
8) In all geotextile tube containers, captured solids dewatered to greater than 20% dry wt solids and passed a Paint Filter Test for subsequent excavation and transport.

REFERENCES

Fowler, J., Bagby, R.M. and Trainer, E. (1995). Dewatering sewage sludge with geotextile tubes, *Environmental Effects of Dredging Technical Notes,* U.S. Army Engineer, Waterways Experiment Station, Vicksburg, MS.

Fowler, J., Duke, M., Schmidt, M.L., Crabtree, B., Bagby, R.M. and Trainer, E. (1996). Dewatering sewage sludge and hazardous sludge with geotextile tubes, *Environmental Effects of Dredging Technical Notes*, U.S. Army Engineer, Waterways Experiment Station, Vicksburg, MS.

Hummer, C.W., Jr. (1998). DOER: A major dredging research programme, *Terra et Aqua*, 72: 13-17.

Taylor, M., Sprague, C.J., Elliot, D. and McGee, S. (2000). *Paper mill sludge dewatering using dredge-filled geotextile tubes,* Internal report, TenCate Nicolon and The Fletcher Group, Greenville, SC.

TenCate Geosynthetics (2005). *Containment and Dewatering*. www.geotube.com.

U.S. Army Corps of Engineers (1987). *Confined Disposal of Dredged Material.* Engineer Manual, 1110-2-5027, Office, Chief of Engineers, Washington, D.C.

U.S. Environmental Protection Agency (1993). *Selecting Remediation Technique for Contaminated Sediments.* Office of Water, EPA-823-b93-001, U.S. Environmental Protection Agency, Washington, D.C.

U.S. Environmental Protection Agency (1994). *Assessment and Remediation of Contaminated Sediments (ARCS) Program.* Remediation Guidance Document, Great Lakes National Program Office, EPA 905-R94-003, U.S. Environmental Protection Agency, Chicago, IL.

Geosynthetics 2009
February 25-27 2009, Salt Lake City, Utah

Evaluation of Geotextile Tube Dewatering Performance of Tailings using Large and Small Scale Tests

R. Satyamurthy, Ph.D., E.I., Ardaman and Associates, Incorporated, Orlando, Florida, USA
M.D. Grzelak, B.S, E.I.T., Syracuse University, Syracuse, New York, USA
T.S. Pullen, B.S, Syracuse University, Syracuse, New York, USA
S.K. Bhatia, Ph.D., Syracuse University, Syracuse, New York, USA
P. Kaye, Ten Cate Geotubes, Phoenixville, Pennsylvania, USA

ABSTRACT
Mining operations typically result in the production of high water content waste products or tailings through the process of extracting the desired mined metal. Tailings usually consist of finely grained material that is discharged into an entrapment area or tailings pond in a slurry form. Successful management of the tailings often involves a dewatering process that can reduce waste volume. Geotextile tubes can and have been used in this application however, without established guidelines. As a means to predict dewatering performance of geotextile tube material in terms of filtration efficiency, the hanging bag test (HBT) is often performed in the field. The HBT requires a large volume of slurry (60 L or more) and greater effort. Small scale tests such as falling head test (FHT) and pressure filtration test (PFT) require smaller slurry volume (0.6 L) and can also be used to determine the dewatering performance of geotextile tube materials. In this paper, test results of HBT, PFT, and FHT conducted to dewater fine sediments representative of mine tailings will be presented. Differences in the test methods and the need for large or small scale tests will be discussed.

1. INTRODUCTION

Mining operations typically result in the production of high water content waste products or tailings through the process of extracting the desired mined metal or mineral. It is often desirable to reduce the volume of tailings by decreasing the water content prior to the disposal or reuse. Tailings usually consist of finely grained material that is discharged into an entrapment area or tailings pond in slurry form. These types of mining activities are common throughout the world and require safe and efficient management of tailings and other high water content refuse. The volume and geotechnical characteristics of mine tailings vary considerably depending on size, nature, techniques and duration of mining operations. Increasing the dewatering capacity is often deemed necessary in order to realize the full potential of the mining operations and increase overall production efficiency. Expansion of existing tailings ponds and the construction of a mechanical dewatering plant are inefficient due to space constraints, cost, and safety concerns. There is an acute need for technologies that can safely and efficiently aid in the disposal of mine tailings.

Geotextile tube dewatering technology promises to have potential of application in dewatering of mine tails and mine wastes. Geotextile tubes are becoming the preferred dewatering method to utilize existing facilities, expedite the dewatering process, reduce slurry volume, contain heavy metals, and reduce processing costs and it also offers advantages over existing dewatering techniques (mechanical and gravity) such as operational ease, reliability, and decreased maintenance costs relative to other dewatering methods. Geotextile tubes can be stacked vertically on top of each other in order to accommodate projects with space constraints and further increase dewatering capacity. Geotextile tubes can be fabricated from 1.5 m to 16 m in diameter and between 10 m to 100 m in length. Although analytical guidance for geotextile tube design is available in literature (Adel et al. 1996, Leshchinsky et al.1996) the lack of guidance for geotextile material selection remains a significant issue (Satyamurthy et al. 2008). Previous studies (Moo-Young et al. 2002, Aydilek and Edil 2002, Kutay and Aydilek 2004, Bhatia and Liao 2004, Liao and Bhatia 2005) have focused on the geotextile suitability when dewatering slurried geomaterials; however, studies focusing on mineral slurries or fine particle slurries are sparse. In addition, limited research has been conducted on the comparison of large scale test (Hanging Bag Test) and small scale test (Falling Head Test and Pressure Filtration Test). This paper describes the comparative evaluation of geotextile dewatering performance using three different test methods (Falling Head Test, Pressure Filtration Test, and Hanging Bag Test). To the writers' knowledge this is the first time that these test methods have been compared, especially for fine sediment slurry.

In geotextile tubes, dewatering or increase in solids concentration is accomplished as the sediment slurry passes through the geotextile tube; particles larger than the geotextile pores are retained and the liquid portion of the slurry passes through. In practical applications, the geotextile tube is filled under pressure, allowed to dewater, and re-filled to repeat the cycle 2-6 times until the throughput is insignificant (Lawson 2006). Specification of geotextile materials for geotextile tube dewatering application has traditionally been based on compatibility between pore size of geotextile (O_g) and particle size of the slurry solids (d_x). Since the compatibility between the pore-size of the geotextile and particle size controls the geotextile selection, the geotextile is the critical component of the geotextile tube dewatering application. Few studies (Huang and Lou 2007, Liao 2008, Moo-Young et al. 2002) have identified the inapplicability of geotextile filter criteria (Giroud 1996, Christopher 1997) for dewatering slurries since conventional soil geotextile retention criteria were not developed for slurry filtration. Thus, there is a great need for researchers to develop design criteria specific to slurry dewatering applications.

The considerations for geotextile selection for dewatering applications include: strength, retention of slurry solids, and geotextile-slurry solids interaction. The lack of an established 'design criteria' for selection of geotextiles used in dewatering high water content slurries necessitates empirical performance evaluation of geotextile with slurry to determine geotextile suitability and need for modification of slurry characteristics. Common methods used for performance evaluation of geotextile-slurry systems are small scale laboratory tests, pilot-scale tests, and full-scale tests. Laboratory bench-scale tests commonly conducted include Falling Head Test (FHT) and Pressure Filtration Test (PFT). Pilot-scale tests and full-scale tests include fabrication of a prototype or actual sized geotextile tube to dewater site specific slurry solids in conditions similar to actual site conditions. The Hanging Bag Test (HBT) is an intermediate type of test which can be conducted either in the laboratory or field and is considered as a laboratory test within the scope of this paper. Among the tests available, the HBT is the only test that is standardized (GRI-GT 14 2004). Laboratory tests are quick, economical, and may not be representative of field conditions whereas pilot-scale and full scale-tests are time consuming, expensive, and more representative of field conditions.

The dewatering of non-plastic slurry solids (uncontaminated) is often observed to be a two stage process consisting of sedimentation and expression. During the sedimentation phase, unflocculated sediment particles settle on the separation medium (geotextile) resulting in growth of a sediment particle deposition commonly termed 'filter cake'; the second phase called 'expression' consists of reduction of the water content of the sediment slurry by percolation through the 'filter cake-geotexile'. The sedimentation rate of the filter cake is primarily influenced by the characteristics of the slurry solids and slurry concentration and the expression rate is primarily influenced by the permeability of the 'filter cake-geotextile'. The factors that influence dewatering include sediment-slurry characteristics (concentration, pH, temperature, and presence of potential contaminants), geotextile characteristics (pore size and its distribution, resistance to clogging, and durability), application of pressure, and test method (Satyamurthy et al. 2008).

Several studies have been conducted to evaluate geotextile dewatering performance of high water content materials using different methods (Moo-Young et al. 2002, Aydilek and Edil 2002, Kutay and Aydilek 2004, Liao and Bhatia 2005, Huang and Luo 2007). The majority of the published studies are based on bench scale tests performed in the laboratory. Only a few studies (Wangensteen et al. 2001, Newman et al. 2003, Lawson 2006, Mastin et al. 2008) report successful field test results and case histories. The lack of established design guidelines particularly regarding the selection of geotextile materials has led to a complete dependence on prior experience of project executives with similar projects. Empirical performance evaluation of candidate geotextile materials are the only available guidelines for geotextile material screening and selection. Methods used for the performance evaluation of geotextile tube materials include: the Falling Head test (FHT), Pressure filtration test (PFT), and the Hanging Bag test, GRI-GT 14 (HBT). Other preliminarily screening tests such as the cone test (Lawson 2006) are also used. Newman et al. (2003) report using the HBT to select geotextile material for dewatering tailings fines and minewater sludge at a mines complex in Greece. They indicate that HBT duration can vary from a few hours to several days. It is interesting to note that the authors recognize that although HBT trials were a good preliminary indicator of geotextile performance, results from field trials varied. This variation was attributed to the differences in the geometric nature and the available dewatering surface area. Some studies (Huang and Luo 2007, Liao 2008) have identified the limitations and non-representativeness of HBTs, but HBTs are being extensively used in practice (Koerner and Koerner 2006). Koerner and Koerner (2006) emphasize the need for development of a standard test method that can be used by engineers to select or approve geotextiles for optimal geotextile tube field dewatering performance. There are no reported studies that compare the utility of the existing test methods with the HBT or field trials and methods to extrapolate empirical findings to predict in situ geotextile tube dewatering are largely unknown.

2. MATERIALS

2.1 Geotextile and Fines

Woven geotextile (W1) made of polypropylene which is commonly used in practice was used in this study. The physical properties are summarized in Table 1. The fine sediment "Tully Silt Fines" used in the laboratory testing was extracted from the aggregate sieving/washing process at a local gravel pit. The geomorphologic origin of the gravel is Pleistocene in age and can be attributed to glacial processes in which localized glacial outwash deposits or moraine deposits are formed. The composition of the fine sediments inferred from scanning electron microscopy (State University of New York College of Environmental Science and Forestry) suggest that the primary geo-chemical constitutes are; silicon, magnesium, calcium, aluminum and iron, with minor amounts of carbon. X-ray diffraction showed that the mineralogic composition of the fine-sediment's parent material is dominated primarily by quartz, carbonates, clay and iron-oxides which are heterogeneous in nature and typical of the glacially derived sediments transported by fluvial processes. Fine fraction of Tully silt termed Tully silt (Fine) was obtained by wet-sieving Tully silt through US Standard Sieve No. 200 and oven drying the passing fraction. The soil is classified as ML in the Unified Soil Classification System (ASTM D 2487). The physical properties of the soil and granulometeric parameters are presented in Table 2.

Table 1. Characteristics of geotextile.

Property	Value
Structure-polymer type	Woven, Monofilament-Polypropylene
Mass/unit area (g/m^2)	585
Thickness (mm)	1.04
Bubble Point[1] (mm)	0.40
AOS[2] (mm)	0.425
Permittivity, ψ (s^{-1})	0.37
Grab tensile strength, MD x CD [3] (kN/m)	96.3 x 70.0

[1]as per as ASTM D 6767; [2] Manufacturer value; and [3]MD: Machine direction and CD: Cross direction.

Table 2. Characteristics of sediment.

Property	Test Method	Value
Specific gravity, Gs	ASTM D 854	2.65
d_{10} (mm)	ASTM D 422	0.001
d_{30} (mm)	ASTM D 422	0.007
d_{60} (mm)	ASTM D 422	0.022
d_{85} (mm)	ASTM D 422	0.05
Coefficient of uniformity, C_u	ASTM D 422	22
Coefficient of curvature, C_c	ASTM D 422	2.2

3. METHODS

As mentioned before, FHT, PFT, and HBT were conducted to determine the dewatering performance of woven geotextile (W1) with fine sediments. The slurry was prepared at a solids content of 33% to be representative of thickened tailings defined by Davies and Rice (2002) as "partially dewatered slurry that has higher solids content by weight as the basic tailings slurry, but is still pumpable; chemical additives are often added to enhance thickening". Performance trials at lower solids concentration indicated failure of the geotextile in dewatering the slurry as all the solids passed through the geotextile. This solids concentration was also deemed optimum for considerations of chemical conditioning. A jar test apparatus was used to simulate in-line mixing conditions for FHT and PFT and a hand held drill fitted with a stirrer was used to mix the slurry for the HBT.

3.1 Falling Head Test

FHTs have been used by researchers (Muthukumaran and Ilamparuthi 2006, Huang and Luo 2007, Liao 2008) to evaluate geotextile dewatering performance. The FHT setup at Syracuse University (SU) consists of a permeameter having an inside diameter of 7.2 cm and a height of 17 cm, a larger FHT device having a height of 35 cm is also available. A schematic of the apparatus is shown in Figure 1. The permeameter consists of a chamber with a top cover plate and a bottom collection section which accommodates a circular geotextile sample having a diameter of 7.2 cm. The acrylic chamber can be fixed to the bottom collection section using a thread assembly to render the permeameter air-tight. The cover plate has an axial inlet port to apply pressure and the effluent is collected using beakers through an axial

port on the bottom section. During a FHT, no additional pressure is applied and the dewatering is accomplished under gravity only.

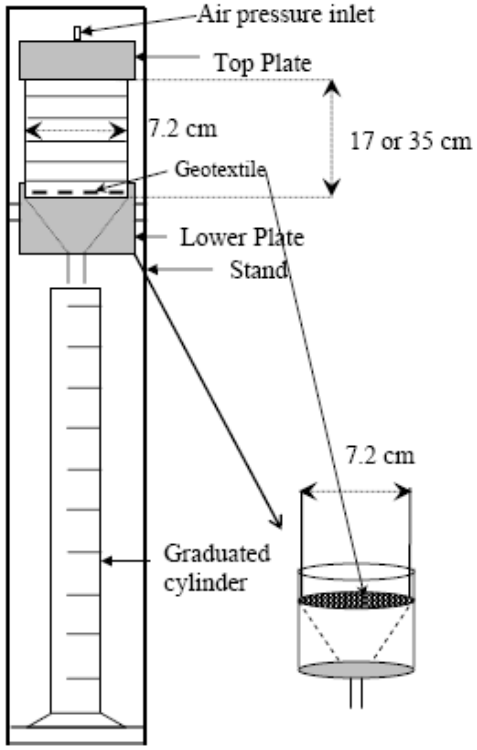

Figure 1. Schematic of Falling Head Test and Pressure Filtration Test Apparatus.

3.2 Pressure Filtration Test

The PFT is an improvisation over the FHT in that it allows application of pressure to accelerate the dewatering rate and more accurately represent field conditions. The PFT has been favoured by researchers as a bench-scale test (Moo Young et al. 2002; Koerner and Koerner 2006; Liao and Bhatia 2005, Satyamurthy et al. 2008) for determination of dewatering performance of geotextiles, although variations exist in the experimental set-ups reported in literature. The PFT at SU utilizes the same setup used for FHT with the only difference being the application of external pressure through the axial port on the top plate. Both the PFT and FHT are not representative of the geotextile tube dewatering process, test a small sized sample, and the scaling up or correlation of test results to predict actual geotextile tube performance is largely unknown. In spite of the limitations, PFT is the preferred alternative as it is a convenient, economical, and rapid test for preliminary comparative evaluation of geotextile alternatives and the role of chemical conditioning.

3.3 Hanging Bag Test

The HBT is an intermediate test between laboratory and pilot scale (prototype test) which has commonly been used in the field before a full scale test (Koerner and Koerner 2003, Newman et al. 2003). The current standard test method for the HBT is Geosynthetic Research Institute GRI-GT 14 (2004), an extension of a test originally proposed by Fowler et al. (1994) for the US Army Corps of Engineers which is further amplified in Koerner and Koerner (2003). A schematic of the test set up is shown in Figure 2. The test uses a standard geotextile bag (40 cm diameter and 150 cm length) suspended from a test frame or scaffold. The bag is filled with about 200 L of slurry to be dewatered and the effluent is collected during the filling stage and subsequently for every 7.6 cm drop in the level of the slurry within the bag. The effluent quality (total suspended solids) and time for dewatering are measured. Completion of test is indicated by no further discharge of effluent from the bag, upon which the standard recommends assessment of the characteristics of the cake formed within the bag although no qualitative or quantitative measures or methods are provided for this purpose.

The experimental procedure used for the tests was in accordance with GRI GT-14 (2004). The following presents a summary of the procedure followed at SU: The bag was hung in the frame with sufficient clearance (the test setup at SU

has a clearance of 0.3 m) to allow easy placement and removal of containers for collecting the effluents from the bag. For the tests performed, clear storage boxes (commercially available of capacity 27 L) were used for collection of effluents. The geotextile bag is pre-wet with water in the laboratory which was accomplished by spraying the bag with the laboratory water supply. The bag was sprayed for 10 minutes. The bag was allowed to drain any excess water that may be present in it from pre-wetting before the slurry is pumped into the bag. The slurry was prepared by transferring the oven dry sediments to the container and adding sufficient water to obtain the required solids content. The slurry was agitated using the mechanical stirrer to obtain uniform slurry and to prevent settlement of heavier particles. For the tests conducted using Tully Silt (fine), the mixing time was generally 5 minutes. A metal rod was used to ensure the slurry was free from clods. Three samples were obtained to verify the slurry solids content prior to pumping. Once the geotextile bag drained all the pre-wetting water, the slurry was pumped into the bag using a standard slurry pump (Manufactured by Zoeller Pump Co, Model: BN 264-A; 0.4 HP) to fill the bag. The effluent from the bag is collected during the filling and the required time for filling is recorded. The time for filling was approximately 1 minute. Upon completion of filling, the volume of effluent collected during the filling stage is measured and recorded. The effluent from the bag was collected at specified time increments and the volume was recorded (GRI GT-14 2004). The total volume of the effluent was oven-dried to obtain the percent solids. GRI GT-14 (2004) recommends obtaining a representative sample from each time increment of at least 100mL. The test is stopped when drainage is no longer observed from the bag. After the test, the bag is cut open to determine the quality of the solids that were retained in the bag. A minimum of nine representative samples were obtained from the inside of the bag for moisture content determination – three each from the top, middle, and bottom. The condition of the filter cake was examined and reported. The cumulative volume of effluent is plotted against time.

The HBT has several inherent limitations including non-representative test method, labour intensive, deceptive measure of slurry level within the bag, and lack of information regarding suitability of test results for correlation to actual geotextile tube performance.

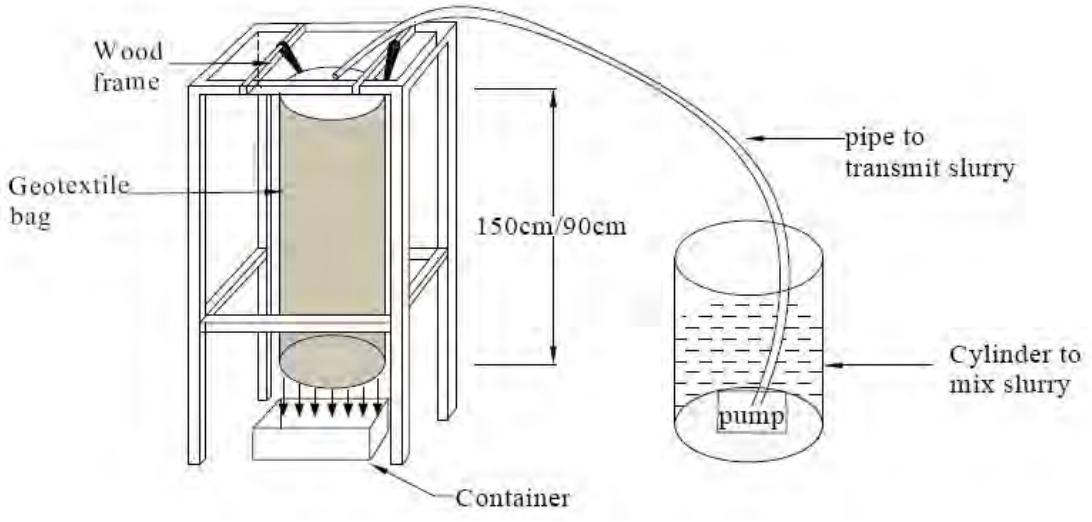

Figure 2. Hanging Bag Test Set-Up.

4. RESULTS

The geotextile dewatering performance was evaluated in terms of two parameters 1) Dewatering Time (flow rate or system permeability) indicative of the geotextile-filter cake void space and amount of geotextile clogging and 2) Solids Percent passing through the geotextile during the test process, indicative of the geotextile retention capacity.

The degree of dewatering was described in terms of dewatering efficiency (DE), defined as:

$$DE\ (\%) = [PSf - PS_i] / PS_i \times 100\ (\%), \qquad [1]$$

where DE is the dewatering efficiency in percent (%), PS_i is the initial percent solids (%), and PS_f is the final average percent solids retained (%).

The permeability of the geotextile-slurry dewatering system, termed system permeability (k_s), was computed using Darcy's law, as shown below:

$$k_s = \left(\frac{\Delta v \cdot h_s}{\Delta t \cdot p \cdot A} \right), \quad [2]$$

where Δv = the filtrate volume collected during the time interval Δt; h_s = the thickness of the soil cake and the geotextile during the collection of filtrate volume; Δv; p = the pressure gradient causing dewatering; and A = the area of the geotextile.

All tests were conducted by allowing drainage of the slurry through the geotextile during the filling process as done in the HBT test. This process is not entirely representative of field dewatering using a geotextile tube, where the geotextile tube rests on relatively impermeable ground which facilitates formation of the filter cake. For all three types of tests conducted, allowing the slurry to drain during the filling stage had an adverse influence on the filter cake formation. This also led to a significant initial slug of fines passing through the geotextile material, similar observations have been reported in literature (Huang and Luo 2007).

4.1 Falling Head Test Results

Three FHTs were conducted to dewater 0.6 L of slurry using geotextile W1. For all the tests conducted, the dewatering pressure was 1.5 kPa and the cumulative volume of filtrate with time (V vs T) was recorded and the results are presented in Figure 3. The dewatering can be observed to occur in two distinct phases, the first phase consists of the initial sedimentation of the filter cake, completion of which is indicated by the point of maximum curvature on the cumulative volume of filtrate with time plot. Upon formation of the filter cake, the second phase commences with the percolation of the remaining slurry through the filter-cake-geotextile system, it is observed that much more time is required relative to the initial sedimentation of the filter cake. At the completion of the test, the filtrate percent solids were determined by oven drying the entire filtrate. The average results of the three FHTs are presented in Table 3.

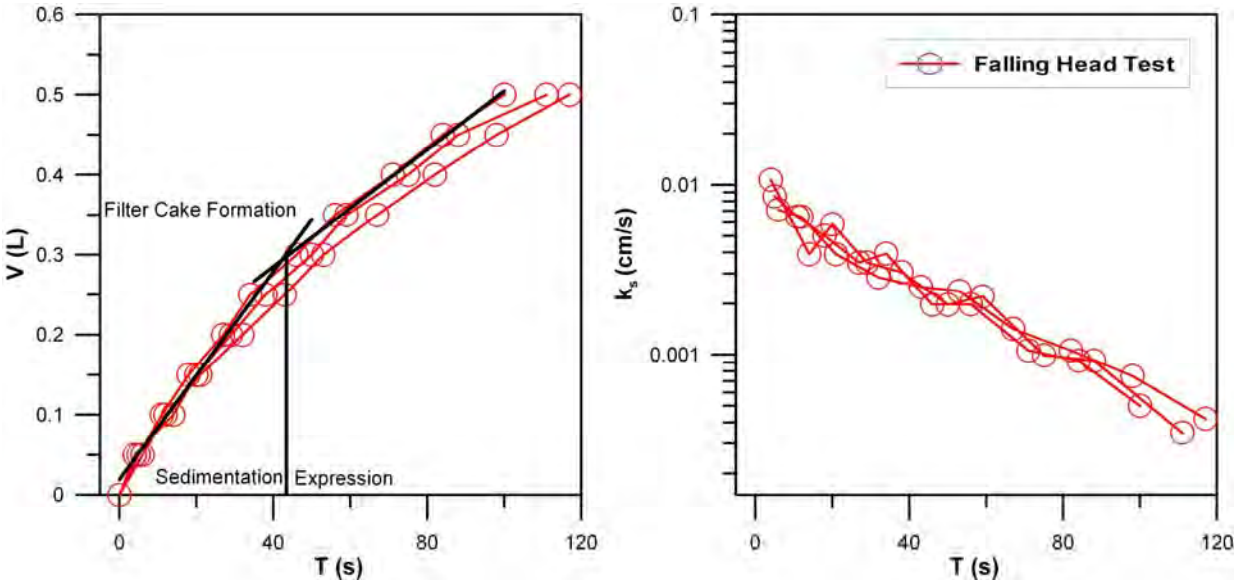

Figure 3. Falling Head Test Results.

Table 3. Comparison of test results.

Parameter	Falling Head Test	Hanging Bag Test	Pressure Filtration Test
Dewatering Efficiency (%)	125.2	127.8	126.0
Percent Piping (%)	75	56	78
Filter Cake Height (mm)	5.3	110	6
Filter Cake Moisture Content (%)	34.63	33.25	34.00
Filtrate Volume / Initial Slurry Volume	0.87	0.73	0.88

4.2 Pressure Filtration Test Results

Results of three PFTs conducted to dewater 0.6 L of slurry using geotextile W1 under a pressure of 34.5 kPa are presented in Figure 4. The dewatering pressure of 34.5 kPa is representative of actual dewatering pressures encountered in geotextile tube dewatering applications. The V vs T plot indicates that the sedimentation of the filter cake and subsequent dewatering occurred much faster relative to the FHT. The application of pressure is the only factor that significantly reduces the dewatering time relative to the FHT. At the completion of the test, the filtrate percent solids were determined by oven drying the entire filtrate. Average results of the three PFTs are presented in Table 3.

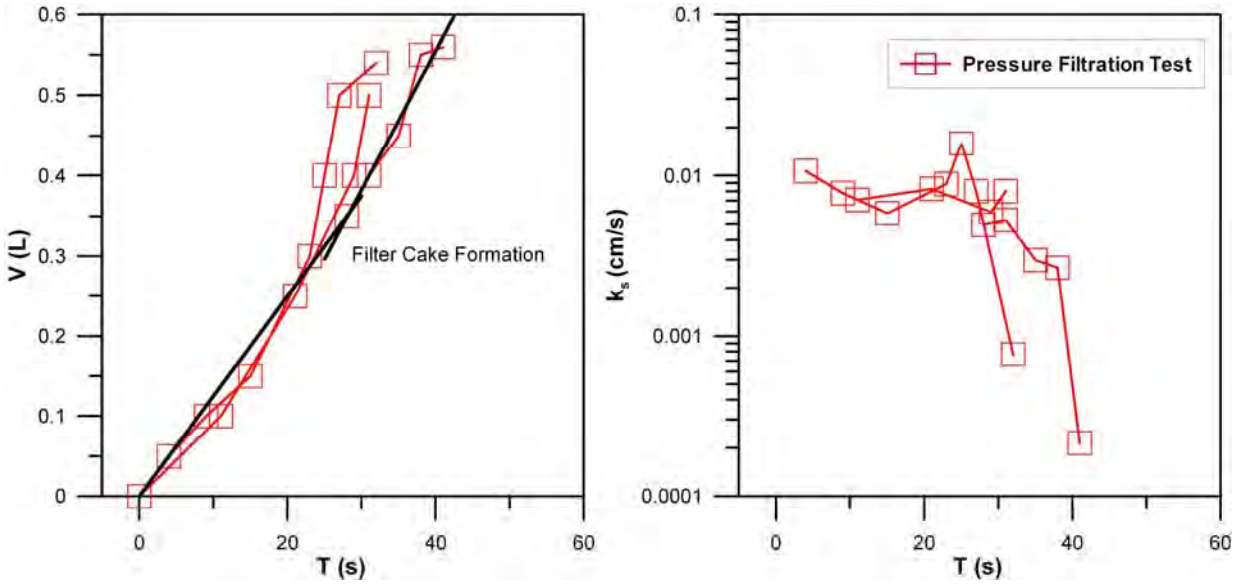

Figure 4. Pressure Filtration Test Results.

4.3 Hanging Bag Test Results

Two hanging bag tests were conducted to dewater 60 L of slurry using geotextile bags having a volume of 200 L. HBTs are laborious (requires 3 personnel) and time consuming (test duration of 24 hours) and therefore only two tests were conducted. Similar to the FHT and PFT, the cumulative volume of filtrate was recorded with time and the variation is shown in Figure 5. Higher flow rates were observed during the initial phases of the test indicated by the initial nearly linear trends of the V vs T. plot. The flow of filtrate stabilized upon formation of the filter cake indicating that the filter cake primarily governs the dewatering rate in the HBT. The total volume of filtrate was oven dried and the filtrate percent solids were determined. The average results of the two HBTs are presented in Table 3.

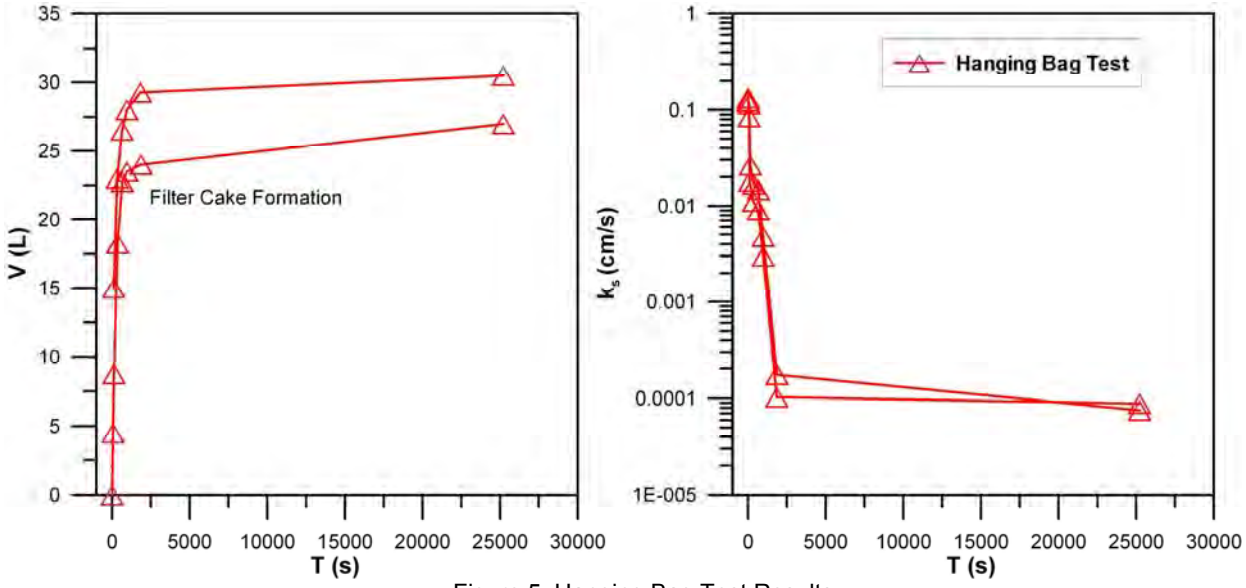

Figure 5. Hanging Bag Test Results.

A comparison of data given in Figures 4, 5, and 6 shows that the progress of dewatering in terms of temporal flow characteristics is very different for these three different types of tests. The point of maximum curvature denotes the completion of the filter cake; for the FHT this was at 35% of the total dewatering time, for the PFT this was at 56% of the total dewatering time, and for the HBT this was at 10% of the total dewatering time. A comparison of the time for filter cake formation suggests that the cake formation was earliest for HBT followed by the FHT and the PFT. To determine the influence of filtrate volume on cake formation, the volume at which the filter cake formed was compared to the total volume of filtrate at the end of the test. The cake formation in the FHT occurred when the filtrate volume was 50% of the final filtrate volume; for the PFT this was at 55%, and for the HBT it was 85%. This observation indicates that, for all the tests, a very significant quantity of the slurry passed through the geotextile before the formation of the filter cake leading to the excessive piping of the fines. The amount of slurry that drained through the HBT was the highest among the tests conducted. The amount of fines passing through was 56% for the HBT, 75% for the FHT and 78% for the PFT; which indicates failure of the geotextile material in dewatering. However, no significant differences in the final filter cake moisture contents were observed in the three tests.

5. DISCUSSION

The volume of slurry dewatered for the bench-scale tests (FHT and PFT) was 600 ml, whereas it was 60,000 ml for the larger HBTs. Also, dewatering was 1-Dimensional (1-D) in the bench-scale tests, whereas it was observed to be 2-D for the HBTs, the dewatering pressure were different for the tests as shown in Figure 6. As shown in Figure 6, the HBT has the largest effective geotextile area available for dewatering. Both the FHT and the PFT have the same area of geotextile for dewatering, whereas the dewatering pressure is much higher for the PFT. Limitations of bench-scale tests are the sample size of the geotextile and small quantity of slurry dewatered. On the other hand, this is a significant advantage when evaluating the influence of test and material variables (pressure, volume, geotextile, slurry concentration, pH, role of additives, flocculants etc). Each of these parameters may have a significant influence on dewatering performance. This poses a vast matrix of possible tests and it can easily be recognized that conducting HBTs for evaluation of the role of test variables requires efforts far greater than the bench-scale tests. It is also important to note that the filling conditions (pumping) for the HBT are significantly different from those for the bench-scale tests (pouring), and similitude does not exist. Thus, there is a significant departure from actual geotextile tube dewatering conditions for the bench-scale and intermediate-scale tests, leading to more difficulties in interpreting the test findings. Therefore, there is an acute need for standard test methods that can accurately model the actual geotextile tube dewatering process.

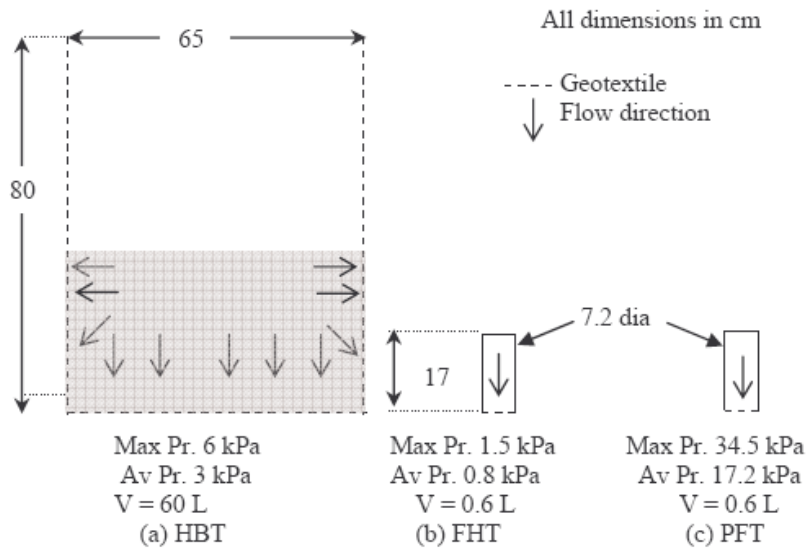

Figure 6. Comparison of Hanging Bag, Falling Head and Pressure Filtration Test Conditions.

Results from the FHT, PFT, and HBT can be scaled up only by comparing pilot scale and actual test results for dewatering the same material. Current bench-scale (FHT and PFT) and intermediate-scale tests (HBT) do not achieve strict similitude for modeling actual geotextile tube dewatering, but can only be used to obtain comparative dewatering parameters. From the current investigation, no recommendations can be made on the usefulness of these tests in predicting actual geotextile tube dewatering. Parameters influence in situ dewatering that cannot be simulated in laboratory bench-scale tests such as pulsating flow conditions, initial filling, and repeated dewatering cycles. Laboratory bench-scale tests can only be recommended for the preliminary evaluation and screening of available material alternatives.

6. CONCLUSIONS

This paper has described a side-by-side comparison of three test methods used to characterize geotextile tube dewatering performance. The tests were conducted to dewater fine slurry using one monofilament woven geotextile that is widely used in practice Based on the results of this study, the following conclusions can be drawn:

1) The dewatering performance obtained from the bench-scale laboratory tests (PFT and FHT) using a small geotextile sample to dewater a small quantity of slurry was similar.
2) All test methods indicated failure of the geotextile to retain the fines, which was primarily due to the excessive amount of fines passing through before the filter cake formation. This strongly indicates the need to modify slurry characteristics or geotextile material properties to ensure adequate retention.
3) Results from the tests conducted show that dewatering efficiency (DE) and water content of the filter cake are similar for all types of tests conducted, therefore, bench-scale tests are recommended instead of larger and laborious HBT for preliminary comparative screening of geotextile alternatives to identify candidate geotextiles for pilot scale tests.

Differences in scale, dewatering conditions, and similitude from field conditions lead to different dewatering conditions. This problem can be best alleviated by comparing actual geotextile tube dewatering performance with bench-scale and HBT.

ACKNOWLEDGEMENTS

The authors are grateful to TenCate™ Geotube® for providing the geotextile used in this study. Ranjan Satyamurthy was supported by the “Wen-Hsiung and Kuan-Ming Li Graduate Fellowship” and was previously supported by the Syracuse University Graduate School (University Fellowship Award). The authors wish to express their gratitude to Richard W. Chave, Experimental Machinist, Department of Civil and Environmental Engineering for his assistance in fabricating the test equipment.

REFERENCES

ASTM Standard D 422. Standard Test Method for Particle-Size Analysis of Soils, *American Society for Testing and Materials*, West Conshohocken, Pennsylvania, USA.

ASTM Standard D 854. Standard Test Methods for Specific Gravity of Soil Solids by Water Pycnometer, *American Society for Testing and Materials*, West Conshohocken, Pennsylvania, USA.

ASTM Standard D 2487. Standard Practice for Classification of Soils for Engineering Purposes (Unified Soil Classification System), *American Society for Testing and Materials*, West Conshohocken, Pennsylvania, USA.

ASTM Standard D 6767. Standard Test Method for Pore Size Characteristics of Geotextiles by Capillary Flow Test, *American Society for Testing and Materials*, West Conshohocken, Pennsylvania, USA.

Adel, H., Hendriskse, S.H. and Pilarczyk, K. W. (1996). Design & Application of Geotextile tubes and Geocontainers, Geosynthetics: Applications, Design & Construction, Balkema, Rotterdam, ISBN 90 5410 8363: 925-931.

Aydilek, A. H. and Edil, T. B. (2002). Filtration performance of woven geotextiles with wastewater treatment sludge, *Geosynthetics International*, 9, No. 1: 41–69.

Bhatia, S.K and Liao, K., (2004), "Overview of Geotextile Tube Applications & Research", *ICGGE-2004*, IIT Bombay, Mumbai, India.

Christopher, B.R. (1997). Geotextiles in filtration applications, *Geosynthetics Asia '97*, Bangalore, India.

Davies, M.P and Rice, S. (2002). Dry stack filter tailings, *Mining Environmental Management*, January: 10-13.

Fowler, J., Sprague, C.J., and Toups, D. (1994). Dredged material-filled geotextile containers, environmental effects of dredging technical note EEDP-05-01, US ARMY Waterways Experiments Station, Vicksburg, Mississippi, USA, 14.

Giroud, J.P. (1996). Granular filters and geotextile filters, *Proceedings of Geofilters '96*, Montreal, Quebec, Canada: 565-680.

GRI Test Method GT14 (2004). Standard Test Method for Hanging Bag Test for Field Assessment of Fabrics Used for Geotextile Tubes and Containers, Geosynthetic Research Institute, GII Publications, Folsom, Pennsylvania, USA: 1-8.

Huang, C.C. and Luo, S.Y. (2007). Dewatering of reservoir sediment slurry using woven geotextiles. Part I: Experimental results, *Geosynthetics International*, 14, No. 5: 253–263.

Koerner, G.R. and Koerner, R.M. (2003). Geotextile tube assessment using a hanging bag test, *Proceedings of the GRI-17 Conference*, GII Publications, Folsom, Pennsylvania, USA: 240-255.

Koerner, G.R. and Koerner, R.M. (2006). Geotextile tube assessment using a hanging bag test, *Geotextiles and Geomembranes*, 24 (2): 129-137.

Kutay, M. E. and Aydilek, A. H. (2004). Retention performance of geotextile containers confining geomaterials, *Geosynthetics International*, 11, No. 2: 100–113.

Lawson, C.R. (2006). Geotextile containment for hydraulic and environmental engineering, *Proceedings of the 8th International Conference on Geosynthetics*, Millpress, Yokohama, Japan (on CD).

Leshchinsky, D., Leshchinsky, O., Ling, H.I., and Gilbert, P.A., (1996), Geosynthetic Tubes for Confining Pressurized Slurry: Some Design Aspects, *Journal of Geotechnical Engineering*, ASCE, 122, No. 8: 682-690.

Liao, K. (2008). Dewatering of natural sediments using geotextile tubes, PhD Dissertation, Syracuse University, Syracuse, NY.

Liao, K. and Bhatia, S.K., (2005), Geotextile tube: Filtration performance of woven geotextiles under pressure, *Proceedings of NAGS 2005/GRI – 19 Cooperative Conference*, Las Vegas, NV, USA.

Mastin, B., Lebster, G.E., and Salley, J.R. (2008), Use Of Geotube® Dewatering Containers in Environmental Dredging, *Proceedings of GeoAmericas 2008*, Cancun, Mexico (on CD).

Muthukumaran, A.E. and Ilamparuthi, K. (2006). Laboratory studies on geotextile filters used in geotextile tube dewatering, *Geotextiles and Geomembranes*, 24: 210-219.

Moo-Young, H.K., Gaffney, D.A., and Mo, X. (2002). Testing procedures to assess the viability of dewatering with geotextile tubes, *Geotextiles and Geomembranes*, 20: 289-303.

Newman, P., Hodgson, M., and Rosselot, E. (2003). The disposal of tailings and minewater sludge using geotextile dewatering techniques, *Minerals Engineering*, 17, no. 2: 115–121.

Satyamurthy, R., Liao, K., and Bhatia, S.K. (2008). Pressure filtration test-assessment based on filtration theory, *Proceedings of 4th European Geosynthetics Conference, EuroGeo4*, Edinburgh, UK, September, 2008 (on CD).

Satyamurthy, R. (2008). Experimental Investigations of Geotextile Tube Dewatering, PhD Dissertation, Syracuse University, Syracuse, NY.

Wangensteen, M., Lafferty, P., and Kobler, J.D., (2001). Innovative dewatering and water treatment techniques for hydraulically dredged sediments, *The First International Conference on Remediation of Contaminated Sediments*, Venice, Italy.

Disposal of Coal Mine Slurry Waste using Geotextile Containers at the North River Mine, Chevron Mining Inc.

M. Watts, Mining Consultant, USA
E. Trainer, TenCate Geosynthetics, USA

ABSTRACT
The processing of raw coal to a saleable clean coal requires many mine operators to wash the run of mine product using a processing plant. The raw coal contains impurities composed of rock and fire clay. Two waste streams are created by this process. Coarse rock and fine rock particles. At the North River Mine the coarse rock is transported to a refuse disposal area by conveyor. The fine rock particles leave the processing plant suspended in water to form slurry. Slurry is normally disposed of via surface impoundments or injected into abandoned underground mine workings. The volume of this waste stream is very significant and expensive to dispose of. In this case approximately 1000 gallons per minute is created on a twenty four hour basis at the North River Mine in Alabama.

With a possible interruption of the primary disposal methods due to available area and construction scheduling, a third method of slurry handling was sought for the interim. The mine needed to continue processing coal for shipment to be able to meet customer commitments. This required slurry disposal. Utilizing geotextile containers for dewatering the slurry waste from the processing plant solved the problem. After a successful test was conducted, and permits obtained, the mine began using the geotextile containers to dewater and contain the solids from the waste stream. Chevron Mining Inc. solicited the help of the Alabama Surface Mine Commission, the Office of Surface Mining, TenCate Geosynthetics, J.F. Brennan Co., Inc., Whittemore Farms Excavation, and PERC Engineering Co., Inc. to develop a unique and successful method to solve the problem.

1. BACKGROUND INFORMATION

North River Mine is an underground coal mine producing over 7 million tons of raw coal per year. The raw coal is processed to yield 3.5 million tons of clean saleable coal. Raw coal is processed at the mine preparation plant at approximately 1000 tons per hour. This yields about 550 tons of clean coal per hour. Refuse is therefore 450 tons per hour of which coarse rock is the primary by-product. At normal operating levels fireclay and fine rock particles suspended in water at a rate of 70 tons per hour in dry weight is also a waste by-product. The slurry waste stream reports to a three million gallon concrete thickener tank adjacent to the preparation plant. Solids in the thickener underflow are increased with the addition of polymers to produce a waste stream of about 1000 gallons per minute. Solids in this pump discharge vary between 25 and 35%. A total of approximately 1.5 million gallons of slurry is produced per day. Particle size analysis of the fireclay and rock slurry reveal that 80% are 400 mesh or smaller. The ultra fine particles tend to stay suspended in the water.

North River Mine began seeking an alternative method of disposal of this slurry waste stream beyond the conventional methods of surface impoundment or injection into abandoned underground mine workings. Since containers made from geosynthetic materials have been used for dewatering various types of sludge wastes, it was thought that they might be able to do the same with coal mine waste slurry. One type available is the Tencate Geotube® Container. The material used for these containers is fabricated from a specially engineered dewatering textile fabricated from high tenacity polypropylene multifilament and monofilament yarns which are woven into a stable network such that the yarns retain their relative position. This provides a sieve to hold the particles and allow the water to run out. The result is a reduction in the retained water and consolidation of the solids. Containers are constructed with PVC fill ports for the attachment of pipes from the pump or dredge through a manifold that allows the filling of several bags at once.

2. PRELIMINARY TESTING

In August of 2007, a test was conducted at the mine to determine if the geosynthetic fabric containers would successfully dewater the slurry waste sufficiently to become a viable option for disposal. (Figure 1) Two one hundred foot long geosynthetic test bags were placed on a pad that had been graded to a 1% slope. In order to facilitate the capturing of the material in the containers and prevent 'blinding' of the fabric, chemical injection was required.

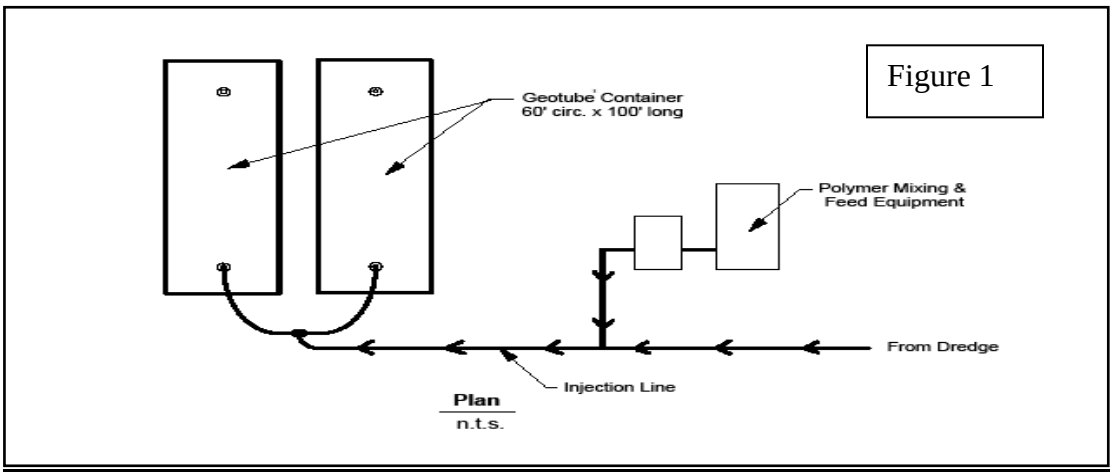

A chemical treatment pump, tanks, and pipe manifold were assembled. (Photo 1)

The treatment plant utilized an anionic flocculation polymer and a cationic coagulant polymer to treat the slurry before it was pumped into the bags. (Photos 2 and 3)

For the test, slurry was pumped directly to the bags from the preparation plant underflow. The bags were filled on August 21st and 22nd. Polymer injection was adjusted when necessary as the changing solids percentage required. As the bags were being filled with the slurry mixture, clear water flowed from them draining into the waste water sediment pond below. The effluent was almost totally clear. For the test, a volume of about 500 gallons per minute was processed alternating between the two containers. After about two days water ceased to flow from the bags and the bags were stable. The test was successful and determined that the system would work on a larger scale.

Once all the needed data was collected from the containers, they were split, the material loaded out with a front end loader into trucks and hauled to the coarse refuse disposal area. The material had a consistency of fine, wet sand.

3. IMPLIMENTATION

In order for the system to be employed on a larger scale the mine had to design the system and seek a permit from the Alabama Surface Mine Commission. Due to the volume of slurry to be processed the mine sought a safe and efficient plan that would allow the containers to be reclaimed in place instead of opening them and transporting the material to the coarse refuse disposal area. The bags are designed to contain, dewater, and consolidate the solid material. A plan was developed to construct bag fields upstream from the existing South Slurry Pond on the mine property. The effluent water would drain to the pond. This pond provided an environmentally safe vessel for the effluent from the process. The Office of Surface Mining provided a technical review of the design and permit as well. This was the first time that the use of geosynthetic bags had been utilized for disposal of slurry waste from a mine washing facility on a large scale. (Figure 2)

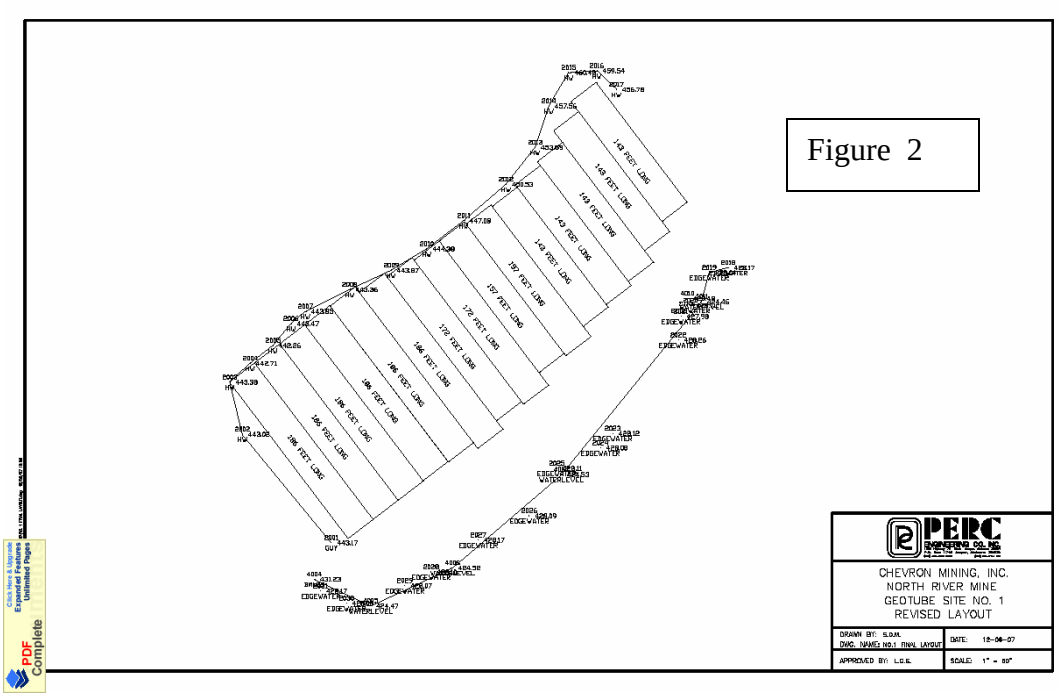

Construction of the pads or bag fields included the following steps:

Removal of vegetation and storage of topsoil
Excavation of earth to construct the pad on grade with 1% slope back to pond
Covering the bag field with 6" inches of drain material (a blend of sandstone 1/3 # 4, 1/3 # 57, and 1/3 # 89).
Covering that with 3" crushed limestone (# 57)
Construction of rock drains and safety berms around perimeter
(Photo 4)

Photo 4

In order to maximize utilization of bag field areas, bags can be stacked on top of each other in a pyramid fashion once the water runs out and the bags have stabilized. Containers were to be placed on top of each other overlapping the line between them. The first field (Bag Field # 1) was approximately two acres in size. The design called for a total of four levels of bags to be filled. Containers were ordered for the field as follows:

11 bags 186-ft long for Level A

9 bags 172-ft long for Level B

8 bags 157-ft long for Level C

7 bags 143-ft long for Level D

The bags used for the field were 60 feet in circumference and could be filled to a height of seven feet. (Figure 3)

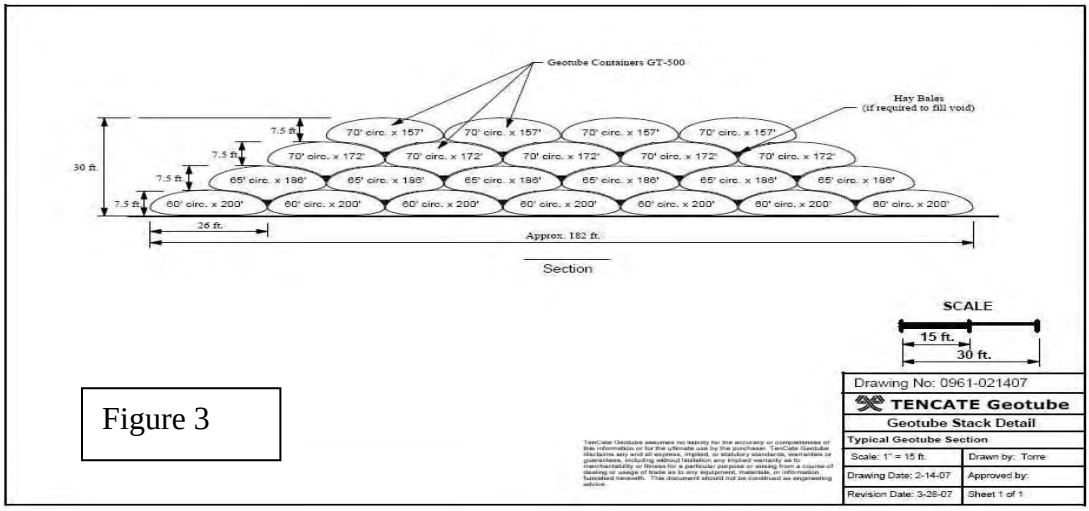

Figure 3

Polymer tanks, pumps, and pipe manifolds were installed on the pad. Other equipment involved included lift truck necessary to unload, maneuver, and stacking of the tubes, light plants, generators, and a field office. Level A bags were then placed on Bag Field # 1 according to the design plan. (Photos 5 and 6)

The original test was conducted by pumping slurry directly from the preparation plant. The operation plan for the project was modified by installing a dredge in the 250 acre foot slurry impoundment to pump to the containers. Removing the material from the impoundment would create capacity in the pond faster than the plant was producing slurry. A Dredge Supply swinging ladder 8 inch dredge was placed into the existing slurry pond to pump the slurry from the pond to the bags. This machine was capable of pumping 1750 gallons per minute to the bags. The bags on Level A were systematically filled from one side to the other allowing Level B bags to be placed on top of Level A safely. This process was then continued to Level C and Level D thus utilizing all of the space designed in Bag Field #1. (Photos 7 and 8)

Photo 7

Photo 8

The pipe manifold allowed the operation to switch from one bag to another, using valves. Once a bag was filled, flow was directed to another bag while dewatering occurred. The containers used were designed for a maximum filled height of 7 feet. The bags were immediately de-watering the slurry and becoming stable quickly. Once the material reached a moisture content of 35% other layers could be added. While filling Bag Field # 1, excavation of Bag Field # 2 began. The second bag field was constructed prior to completion of the first providing two workable layout areas for continuous operation thus eliminating downtime for the dredge and providing time for the containers to drain. Using this method a total of three bag fields were constructed and utilized. The first bag field was modified to allow a second tier of four levels to be added as well.

Productivity was gauged by measuring the height of the filled and retired bags each day. At about the midpoint of the project a physical survey was conducted in the slurry pond to verify the volume pumped. The dredge was initially operated on a twenty four hour basis with two 12 hour shifts per day. A crew of 5 to 6 employees was required to run the dredge, install the piping, maintain the polymer station, position the bags, and monitor the filling operation. Later in the project only one 12 hour shift per day was used. This allowed even more dewatering time for the bags being filled.

Hourly productivity for the project varied slightly with bag field distance from the dredge as well as solids in the slurry. Productivity averaged 1750 cubic yards per twenty-four hour day. A total of 200,000 cubic yards were pumped and disposed of during the project. This yardage was produced from January - August 2008. Since the dredge operation was independent from the preparation plant, the project operated on a different schedule from that of the mine. The completed project utilized 240 bags with a combined total length of 42,000 linear feet. The circumference of the bags ranged from 60 to 70 feet. The containers held an average of 5 cubic yards of material per linear foot of bag. (Photo 9)

Once all the bags in the field were full and dewatered, the site was then ready for reclamation. First a layer of sand was used to cover the sides of the bags to provide a filter medium and then a layer of limestone for drainage. The bags were then covered with earth and finally topsoil. A low ground pressure bulldozer was used to cover the containers. All the bag field sites were very stable and no problems were encountered during the covering operation with the equipment. (Photo 10)

Once this was complete the entire field could then be mulched and seeded using a hydro seeder. The entire project was completed without an accident or environmental incident. (Photo 11)

4. CONCLUSION

Although a relatively new application of this technology for the mining industry, the utilization of geosynthetic textile containers worked extremely well and provided an alternate method of coal mine slurry waste disposal for North River Mine.

ACKNOWLEDGEMENTS

Tim LeBlanc
JF Brennan Co., Inc. – LaCrosse, WI

Mike Windle
Chevron Mining Inc . - Berry, AL

The Use of Geotextile Tube Containers for Dewatering The Restigouche Open Pit Zinc Mine and Settling Pond Basin in, New Brunswick, Canada

J. Douhéret, Terratube inc., Saint-Denis-de-Brompton, Qc, Canada
E. Trainer, TenCate, Commerce, Georgia
A. Lister, TenCate, Oakville, Ont., Canada
S. Hauthier, ASDR Environment inc., Malartic, Qc, Canada

ABSTRACT
Blue Note Mining in New-Brunswick, Canada had been using an open pit mine as tailing pond since 1997. In 2007 they decided to reopen the open pit to extract Zinc.
First challenge was to remove 300,000 m^3 of Zinc contaminated water and 32,000 m^3 of sludge. As discharge water would be pumped into a salmon river, Environmental regulations originally limited the maximum level of Zinc at 90 ppb but raised the limit to 250 ppb considering the situation. Sludge Zinc concentrations were 2,500 ppb.
In all 17 geotextile containers 60ft (18.29m) circumference x 100 ft (30m) long each were used. Sludge was pumped 24 hours a day during 18 days at an average rate of 75 m3/h. Leachate analysis show an average level of Zinc of 125 ppb.
With that success, the mine decided to start using geotextile containers in their wastewater treatment flow process in September 2007. The process is now replacing a conventional settling pond.

1. INTRODUCTION

Restigouche Mine, owned by Blue Note Mining, is located 80 km from the city of Bathurst (North West of New Brunswick, Canada). It was a Zinc and Pb mine.

That site was closed in 1996 and the open pit was used as a tailing pond for the site. As the price of Zinc rose at the stock exchange, Blue Note Mining decided to reopen the open pit to extract the Zinc. 300 000 m^3 of water were accumulated into the open pit. Water was mostly contaminated by Zinc (2100 µg/l). There was also more than 32 000 m^3 of sludge accumulated at the bottom.

Site is located in a mountain area known as windy and rainy. There is no impermeable soil and water has to be discharged into a salmon river where Environmental discharge regulations limit Zinc level at 90 ppb. As the existing Waste Water Treatment Plant (WWTP) of the mine is old, it couldn't be used to handle such volumes.

Mine schedule was also very short to re-start the operation. Works couldn't start before the end of April 2007 after snow and ice melt down. Mine operation was scheduled to start as early as July 2007.

An engineering company did a review of methods and solution to take care of water and sludge removal on time and in the respect of Environmental regulations. They also had to work on solutions to refresh the old WWTP

2. OPEN PIT CLEANING

2.1 Phase 1 – Water Management

Water was highly contaminated by Zinc (2100 µg/l). So it was first decided to precipitate Zinc by adding lime. As lime addition raised the pH, they had to balance pH with CO2 injection.

Works were done by batch. After each lime injection a "mud cat" type of dredge was used to pump water on surface to agitate deep water. A settling time of 4 days was then allowed and surface water was pumped for discharge. A total of 140 metric tons of lime was used. It took 20 days to pump the 300 000 m^3 of water at a flow rate of 550 m^3 per hour.

Considering that particular situation, Environmental authorities increased the discharge criteria at 250 ppb of Zinc. The same criteria applied for sludge leachate.

2.2 Phase 2 – Sludge Management

After phase 1, there was 32 000 m3 of sludge to manage. That volume corresponded to sludge accumulated within the last 10 years and by sludge produced by lime addition into contaminated water.

Sludge was heterogeneous at the bottom of the open pit. There was a first layer of light sludge (0.5 m thick, 2% to 5% solids) above a deep layer of sludge (3 m to 6 m, 6% to 11% solids).

The engineering company evaluated and tested different ways to take care of that sludge. Their conclusions were the following.

Mechanical dewatering (filter-press, centrifuge, etc.) was not adapted considering the chemical and physical parameters of sludge. Leachate concentration in Zinc was high and the existing WWTP was not able to treat it. Also, that solution supposed dewatered sludge transport by trucks to the Caribou site (1000 truckloads @ 34 km) in a relatively short time.

The other solution was to build an on site storage area with an impermeable membrane. That solution solved the problem temporary as sludge and leachate had to be removed some days.

Finally, after local test of sludge dewatering by geotextile containers it was proved that leachate quality was acceptable. Also, as dewatered sludge would be stored, it could be transported out of the site at the dead season without pressure on transport companies and local roads. Also, that solution dramatically reduced the quantity of sludge to be removed compared to other dewatering technologies.

2.2.1 Geotextile Containers Installation and Use

Taking care of 32 000 m3 of such sludge requested 17 geotextile containers 60ft (18.29m) circumference x 100 ft (30m) long each. A lay down area of 34 100 ft2 (3170 m2) was build for 12 geotextile containers. The 5 other geotextile containers were stacked on the 12 already in place. That site was prepared 500 ft from the open pit.

Sludge was pumped at an average flow rate of 75 m³ / hour, 24 hours a day, during 18 days. Sludge was pumped by a “mud cat” type of dredge.

Picture 1: Pad with geotextile containers

2.2.2 Geotextile Containers Performances

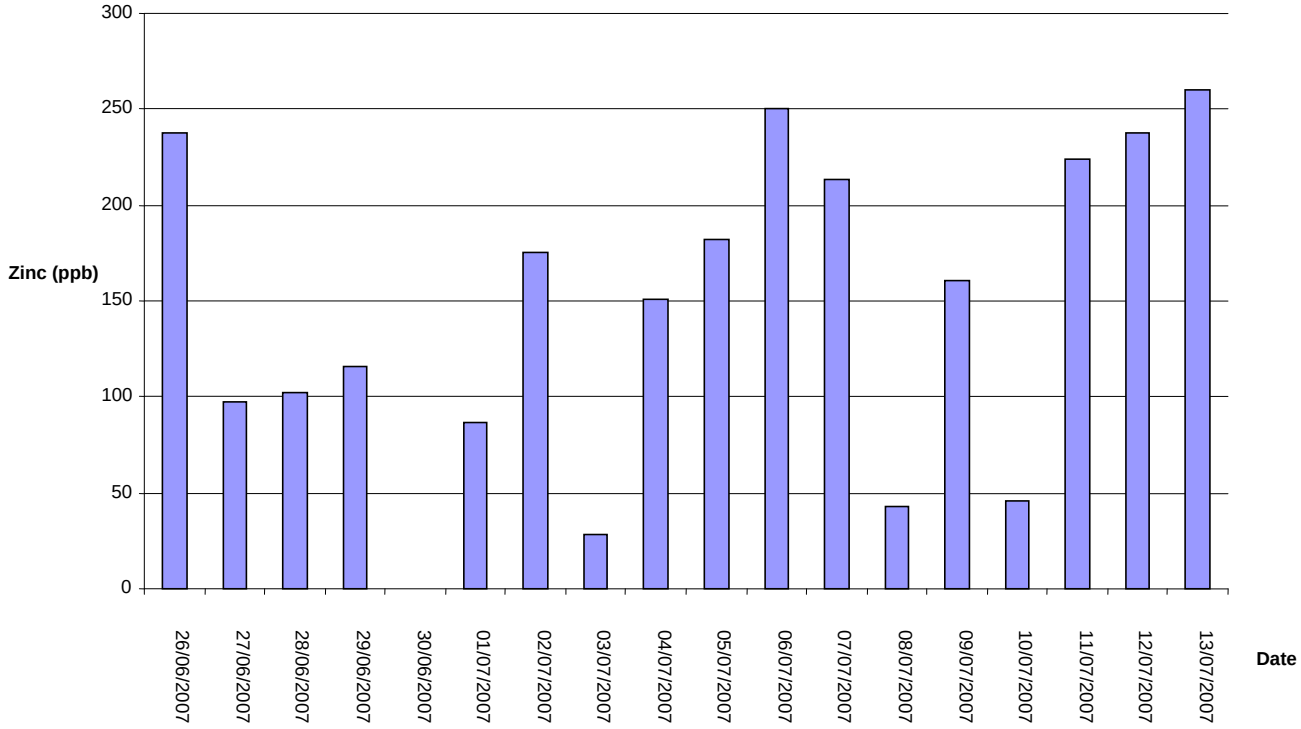

Figure 1: Leachate concentrations in Zinc (ppb) during the 18 days of pumping.

A sample of leachate was taken and analyzed every day by a representative of Environmental authorities. Figure 1 shows the results obtained.

17 days on 18 days, leachate concentration in Zinc was below the discharge objective of 250 ppb determined by Environmental authorities. Zinc concentration was below 150 ppb 50% of the time.

Compared to an initial concentration of 2100 ppb, results show that geotextile container with the proper chemical conditioning kept more than 92% of Zinc.

3. WASTE WATER TREATMENT PLANT REFURBISHMENT

3.1 Initial WWTP process

WWTP is composed by 4 steps.

First step of the process is a sedimentation pond collecting water coming from mining operation and the mine site (hot piles etc.). As second step, supernatant from that pond is treated at the plant itself by adding lime, coagulant (Ferric Chloride) and polymers to collect most of Zinc, other minerals and particles. Lime has two functions: it elevates the pH to make the particles and ions less soluble (when less soluble they will tend to separate from the water). The lime also aggregates to these particles and ions, and thus starts their separation itself from the water. To help the coagulation that the lime started, a solution of ferric chloride is added to the water. Basically, the polymer will cause all gathered particles and ions to be caught and joined together in a chemically inactivated form (the flock). That effluent (treated water and sludge) is then discharged into a settling pond which is the third step of the treatment. On the fourth step, the supernatant from the settling pond is treated by CO2 injection in order to balance pH while pumped into a polishing pond.

Finally, supernatant from polishing pond is discharge into a water stream that goes into a salmon river.

The existing settling pond was not large enough to handle the new expected volumes that would come from mining operation. Also, WWTP performances had to be improved to meet Environmental regulation discharge criteria.

To be environmentally legal, the site's discharge must be within the legal requirements of the federal and provincial Environment Departments.

Metal and solids requirements for the daily samples.

Type of sample	pH	Cu (µg/L)	Pb (µg/L)	Zn (µg/L)	TSS (mg/L)
Minimum in any grab sample	6,5	-	-	-	-
Maximum in any grab sample	9	30	60	250	25
Monthly mean	-	20	30	-	12

Considering geotextile container performances to collect Zinc, the engineering company decided to install geotextile container to take care of sludge produced by the plant itself.

3.2 Geotextile Containers Infrastructure and Operation

Geotextile containers are replacing the settling pond as third step of the WWTP. So, effluent from the plant itself (treated water mixed with sludge) is pumped into the containers. Leachate goes by gravity to the polishing pond.

Flow rate of the plant is between 100 to 500 gallons per minute.

A new lay-down area, close to the plant, was built for 4 geotextile containers of 60ft (18.29m) circumference x 100 ft (30m) long each.

Two (2) geotextile containers are filled while another one is dewatering. One container is only on site in case of any incident.

One geotextile container is changed once every two months. During the summer months, two geotextile containers are changed at the same time.

Picture 2: Geotextile container set up for filtration in a flow process

3.3 Geotextile Container Performances

Geotextile containers proved to be efficient in collecting Zinc. Raw effluent Zinc concentration ranges from 25 000 ppb to 200 000 ppb with an average at 70 000 ppb. Zinc concentration in geocontainer leachate presents an average of 90 ppb on an 8 months survey.

Figure 2 shows detailed performances of geotextile containers during the period.

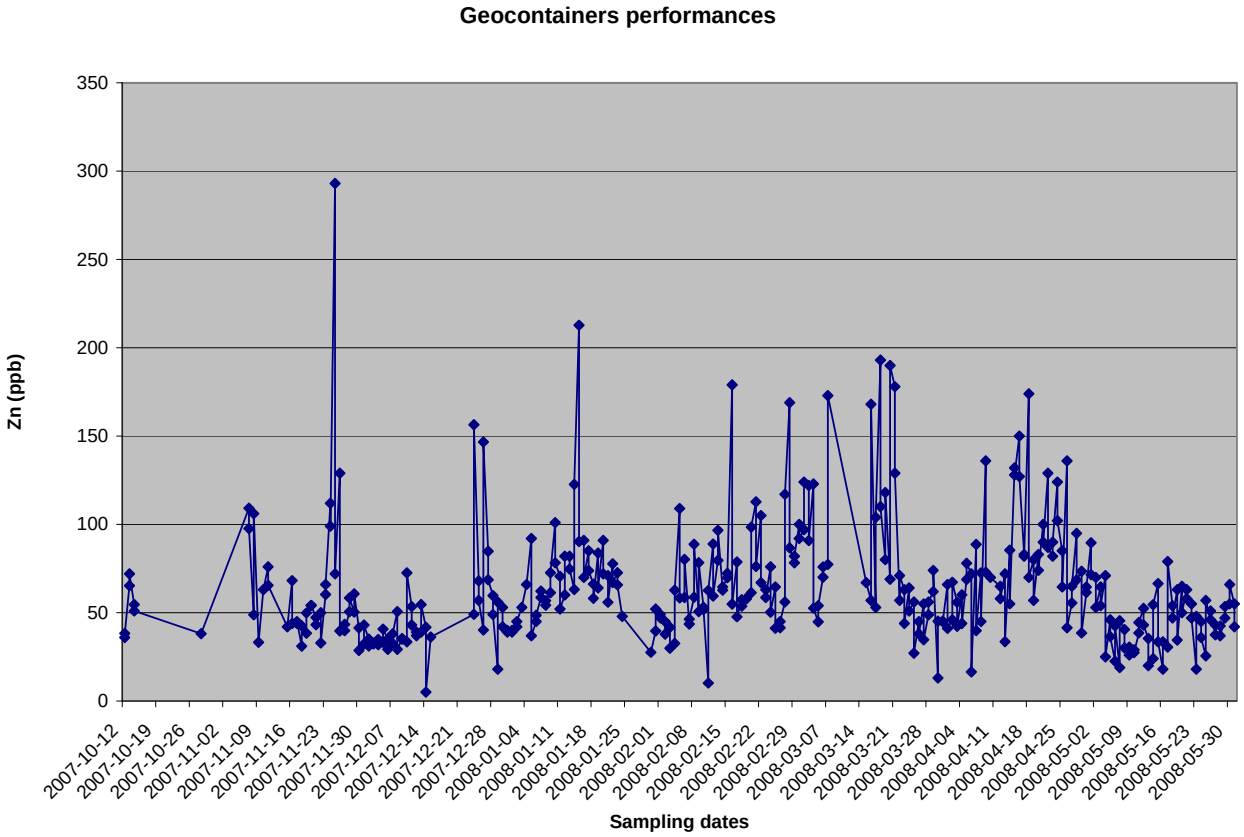

Figure 2: Geotextile container performances – Zinc concentration in geotextile container leachate.
Higher concentrations of Zinc in leachate are observed when pumping starts into a new geotextile container. The geotextile containers are usually pumped for 10 hours before the filtration cake is thick enough to retain fine particles.

Geotextile containers are also used during the winter months even when temperatures are as low as minus 30 Degrees Celsius. During the filling process the high level of salinity in the material prevents freezing and does not reduce the filtration capabilities of the geotextile container.

Picture 3: Geotextile containers in operation during winter

4. CONCLUSION

Both projects at the mine site, proved that geotextile containers are efficient, cost effective and safe for contaminated sludge dewatering and containment.

Geotextile containers are commonly use for lagoon clean out. In this case it was proven that geotextile containers used in the flow process could replace settling ponds and improve the overall performance of the mine Waste Water Treatment Plant.

5. ACKNOWLEDGEMENTS

A special acknowledgement to Restigouche Mine WWTP team and to the engineering company Genivar, for data collection and the pictures of the site,

REFERENCES

Genivar (2008) – Traitement des eaux contaminées – Mine de Restigouche - Maintenance, Engineering and Mining Operators conference, February 24 to 282008, Val d'Or, Québec, CANADA

Geosynthetics 2009
February 25-27 2009, Salt Lake City, Utah

Tests to Evaluate Dewatering and Filtration Efficiency for Geotextile Tubes Design

N.P.B de Castro, MSc, Allonda Geossinteticos Ambientais, São Paulo, São Paulo, Brazil
P.M. Martins, MSc, Allonda Geossinteticos Ambientais, São Paulo, São Paulo, Brazil
T. Stephens, TenCate Geosynthetics, Commerce, Georgia, USA
L.C.Q.C. Melo, Allonda Geossinteticos Ambientais, São Paulo, São Paulo, Brazil

ABSTRACT
Since the 60's, geotextile tubes and bags are used as a geocontainment technology in marine structure applications. More recently, geotextile tubes technology also has been used all over the world to dewater many kinds of sludge and dredged sediments with success regarding safety, volume reduction, efficiency and economy. This process starts with pumping the polymeric coagulates and or flocculated slurry straight to the bags, where the solid part is retained inside and the liquid part flows through the pores of the woven engineered filtration textile. In some cases, depending on chemical and biological analysis, the effluent can return to the original process, be used for agricultural irrigation or even to be discharged in nearby waterways. For a long time it was usual, as a preliminary analysis, to perform a HBT (HBT) to predict the behavior of the engineered filtration textile regarding retention and filtration in a given amount of time. Using time as an important parameter to evaluate the dewatering efficiency, the HBT through the effluent quality and dry mass of the material within the bag provides good and conservative results in comparison to the full scale unit. However, the HBT presents some downside points, such as the manual filling process, the broken flock during filling, and the different position of the hanging bag in comparison to the dewatering tube. These factors imply that the test can be improved and modified to better evaluate the dewatering and filtration performance. This paper presents a comparison between the Hanging Bag Test (HBT) and a Simulated Dewatering Test (SDT) tubes test results using actual samples of contaminated sediments. These results are used to determine the design for full scale dewatering tube designs.

1. INTRODUCTION

Geotextile tubes and bags have been used as a geocontainment system since the 60's in marine structure applications. However, this technology started to be applied as a dewatering process for sludge and contaminated sediments in the mid 1990's, after The US Army Corp of Engineers and TenCate™ Corporation funded research under the CPAR Program to develop innovative technologies for Federal Construction Projects. One of the first projects to utilize this new dewatering technology was the Eagle Lake and Culkin Water Districts, Vicksburg, Mississippi. Here, lime and aluminum sulfate sludges were pumped from disposal lagoons into dewatering tubes. Two dewatering tubes (donated by TenCate™ Corp.) were filled by pumping the sludge into the tubes which were closely monitored for filtration and consolidation testing. Since that time many studies have been conducted about geotextile tubes technology and its benefits for many kinds of waste dewatering all over the world (Fowler et al 2002, Castro 2005, Lawson 2006, Martins 2006).

In some cases, depending on chemical and biological analysis, the effluent can return to the original process, be used for gardening or even be discharged in waterways nearby (Castro et al 2008).
During all phases of dewatering process, (filling, drainage and consolidation), the fabricated woven engineered filtration textile which composes the tubes, must, provide excellent tensile properties, efficient filtration and thorough retention to guarantee an ideal slurry dewatering. Preliminary tests can provide data to design a proper solution that involves the use of fabricated tubes for waste dewatering, once the system efficiency is measured through filtration and retention evaluation (Koerner 1998, Vidal e Urashima 1999, Castro 2005, Martins 2006, Lawson 2006, Melo et al 2007).

The HBT has been used for many years as an important tool in spite of some points that avoid the results of getting much closer to the actual field performance. In order to improve upon this test method, a new field test using a small scale dewatering tube (Simulated Dewatering Test) developed by TenCate™ has been used successfully in many projects, mainly in contaminated dredged sediments, and will be presented in this work (Fowler et al 2002, Lawson 2006, Lundin et al 2006, Mastin et al 2008).

The objective of this paper is to focus on the hydraulic properties required through a discussion of the preliminary tests that provides data to dewatering tube designs, such as, cone test, HBT and an innovative Simulated Dewatering Test tubes.

2. PRELIMINARY TESTS

The main objectives of preliminary tests (it can be in the laboratory or a field procedure) are to:

- visualize and replicate the dewatering methodology,
- verify if it is necessary to us polymeric coagulates and or flocculates that agglomerate suspended solids (polymer),
- evaluate the efficiency of the selected polymer or any other flocculant,
- analyze the clarity of the effluent
- indicate achievable percent solids,

All of this data will be necessary as in put in design methods for dewatering tubes. In addition to this data, the management of effluent after the dewatering process, such as reuse, return to nature or even return to the original process, can be planned according to tests performed before installing an actual tube on a project.

It is important to remember that all tests results are more conservative than actual full scale tubes. Filtration area, weight and filling pressure have great influence on dewatering process (Castro 2005, Martins 2006, Lawson 2006).

2.1 Cone Test

According to Lawson (2006), cone test consists of a 0.3 m diameter geotextile tube sample that is formed into a cone shape. The waste is poured into the cone, in general 500 ml, and the drained liquid is collected in a container below the geotextile sample, as it can be seen in Figure 1. The test is very simple and can be performed in the laboratory or in the field. It is useful for screening chemical accelerants and can give insight into final percent solids concentration, effluent quality and contained volume reduction, besides the polymer dosage.

Figure 1 - Cone test being performed.

2.2 Hanging Bag Test:

According to an ASTM standard proposal (Fowler et al 1994) and GRI GT12: 2004, this test method is used to determine the flow rate of suspended solids through a geotextile bag used to contain slurry material. The results for the sediment that pass through the geotextile bag are shown as the percent total suspended solids in milligrams per liter or parts per million. The flow rate is the average rate of passage of a quantity of slurry and water through the bag over a specific time period. Before performing the HBT it is necessary have the cone test data, approximately 150 liter of flocculated slurry, a frame to support the hanging bag, a hanging bag unit which is shown in Figure 2 and buckets and containers to handle and collect the slurry and effluent.

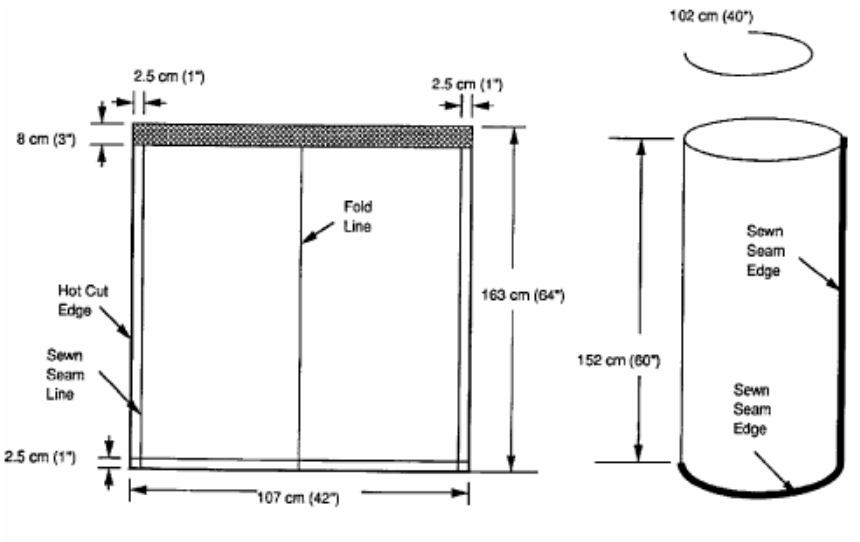

Figure 2 - Geotextile before and after preparation (Koerner & Koerner, R. M., 2006).

This test allows evaluate the slurry properties and the "cake" built within the bag. In general, HBT is a field test, mainly when it is used to dewater specific materials, such as tailings, and shows the efficiency of the used geotextile (Martins et al 2007).

Based on existing references (Fowler et. al 1994, 1997, 2002, Gannett Fleming 2003, Dewatering & Containment Technologies Inc 2003, Kutay e Aydilek 2004, Newman, P. et al 2004, ASTM proposal, GRI GT12: 2004, Koerner e Koerner 2006 e Lawson 2006), this test method is used to determine percent total suspended solids of material passing through the geotextile container over a specified time period. Figure 3 shows the steps and equipments involved.

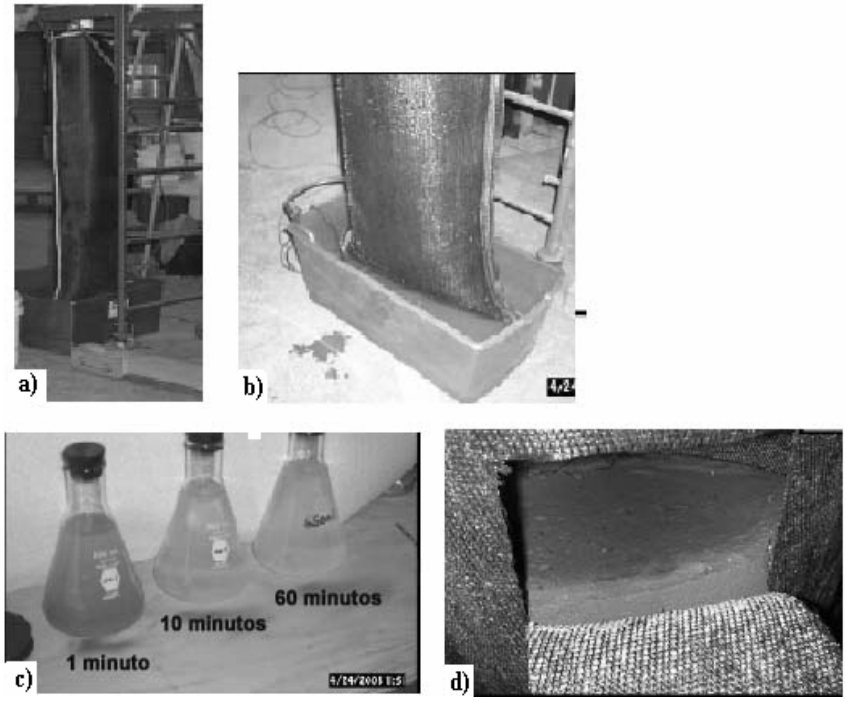

Figure 3 - HBT procedures and equipments: a) Hanging bag unit; b) Filling procedure; c) effluent samples over a specified time period; d) Dewatered material (Gannett Fleming 2003).

2.3 Simulated Dewatering Test:

As an upgrade of the HBT, considering that its results could be more close to the reality, the Simulated Dewatering Test brings an improved operational capacity and neatness to this important phase of the geotextile tubes design process.

The Simulated Dewatering Test, as a field test consists in the following steps, as is recommended by TenCate Nicolon guide line:

- Collect approximately 100 – 150 liters of slurry.
- Mix the samples in a large container to ensure uniformity, such as a 200 liters barrel. If the percent of solids of the slurry is low, a larger sample may be needed.
- Assemble the supporting frame and place a 100 liters plastic container or “tote” under the frame to catch the effluent. Place the Simulated Dewatering Test tube on top of the frame and insert the supplied 70 cm stand-pipe, which represents approximately 7 kPa of head pressure. Figure 4 shows the complete apparatus to perform the test.
- One important point is that the type of polymer, and dosage will have been determined from bench-scale testing, known as the cone test. Make the polymer down into solution. Mix the polymer solution into the slurry sample using a variable speed electric drill or manually mix with a stem until flock is formed. High speed agitation may shear the flock, what is harmful to the dewatering process.
- Fill the bag by pouring the buckets of conditioned slurry into the top of the stand-pipe. A smaller bucket and funnel can be utilized to facilitate this process. Lift the stand-pipe off of the bottom of the bag; otherwise, the introduced slurry may back up in the pipe and overflow. This should no longer be of concern once the Test Bag has accumulated some volume of slurry.
- Continue to fill the bag with conditioned material as rapidly as possible until the sludge rises in the stand pipe to the line indicating 7 kPa, and then stop. Collect effluent samples from the corner of the bag. The effluent should be examined for clarity and samples can be taken for testing if so desired or according to the project demand.

As an optional step, it can be considered that after the test has had ample time to dewater, a sample of dewatered slurry can be collected to determine moisture content and percent dewatered solids. Figure 5 shows the dry mass formed within the bag test.

The findings may be extrapolated to estimate the results of a full scale project. Simulated Dewatering Test can be used to conduct a mass-balance analysis, which also helps to forecast the behavior on full scale.

Figure 4 - Apparatus assembled to perform the Simulated Dewatering Test (TenCate™ Geotube® GDT guideline).

Figure 5 - Simulated Dewatering Test opened to check the dewatering level (TenCate™ Geotube® GDT guideline).

2.4 Available tests and comparisons

As previously mentioned, for a long time it was usual, as a preliminary analysis, to perform a HBT to predict the behavior of the engineered filtration textile regarding retention and filtration in a given time. Using time as an important parameter to evaluate the dewatering efficiency, the HBT through the effluent quality and dry mass of the material within the bag provides good and conservative results in comparison to the full scale unit.

However, the HBT presents some weak points, such as the manual filling process, the broken floc during filling, mainly because of the height of the point from where is dispensed the flocculated slurry, and the different position of the hanging bag in comparison to the reality. Also, the fact that the HBT must be properly closed after perform the test to avoid the material be re-hydrated in case of rain.

These factors imply that the test can be improved and modified to better evaluate the dewatering and filtration performance. The importance of the cone test also can be verified, once all slurry chemical analyses and potential applications start in the laboratory.

In addition, a full scale pilot study can be used as a preliminary test. This is more common in very large projects, but it adds additional costs and extended time to start up the process.

This paper presents a comparison between results from HBTs and results from Simulated Dewatering Tests based on real application using contaminated marine sediments and analyzing the best results to be used as a preliminary test for dewatering tubes design.

3. MATERIALS AND PROCEDURES

The studied material will be called “Sediment A”. It is a natural composite sediment caused by factors involved in its formation. Sediment A is a blend of marine and riverine sediments and it was collected from a harbor site. This place is owned by a Brazilian private port that will increase its capacity by building an embankment and reclaiming this area. Taking this into account, the chemical analyses have shown a lot of compounds and pollutants mixed in the sediments. A thick layer of this material is to be dredged and consolidated in dewatering tubes over an area where structural fill will be placed to form a new container storage area.

Standard Penetration Tests (SPT) were performed around the area where Sediment A was collected and some important geotechnical characteristics were identified. The collected samples presented: clays, recently settled, from mangroves near by, and null SPT values; clay sediments from adjacent rivers and lakes, SPT between zero and 2, low bearing capacity and clays with continental sediments and marine sediments mixed, a very high over consolidation and SPT values higher than 5. Figure 6 shows a typical granulometric curve for Sediment A.

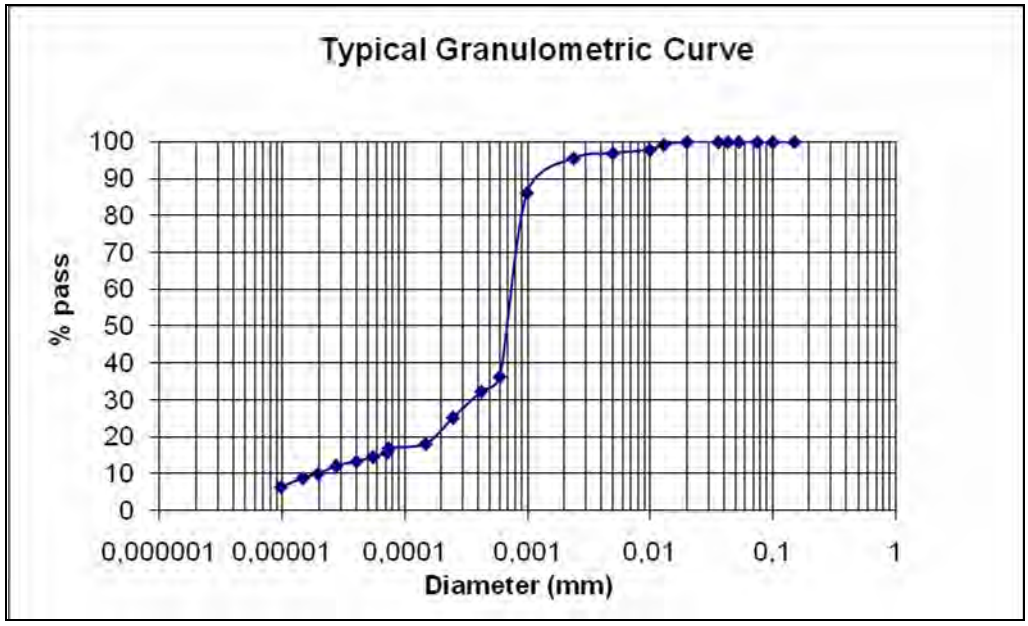

Figure 6 – Typical granulometric curve of Sediment A.

Sediment A was collected from different points around the area and sent to the laboratory, on which Cone Test were performed, followed by HBT's and Simulated Dewatering Test. The sample was diluted in a ratio of 1 part of sediments to 3 parts of salt water in order to simulate a dredged slurry with a moisture content close to the reality during the dredging works and consequently dewatering tube filling. The salt water was also collected from the same area.

Many chemical analyses were conducted to select the optimum polymer based on the dewatering characteristics of Sediment A during Cone Test. The best polymer was a cationic polymer which ensured a cost effective, highly efficient dewatering process, with the lowest possible polymer dosage.

4. RESULTS:

The Cone Tests indicated that final cake solids of approximately 46% was achievable.

Tanking in account, while conduction the HBT and the Simulated Dewatering Test, samples of dewatered slurry would be taken periodically to evaluate the total dewatered solids achieved during given time periods. The samples were taken after 24 hours, 48 hours, 7 days, 15 days, 21 days and 30 days.

Figure 7 shows a summarized result of HBTs. The maximum total solids after 30 days is approximately 54% starting from initial total solids of approximately 7%.

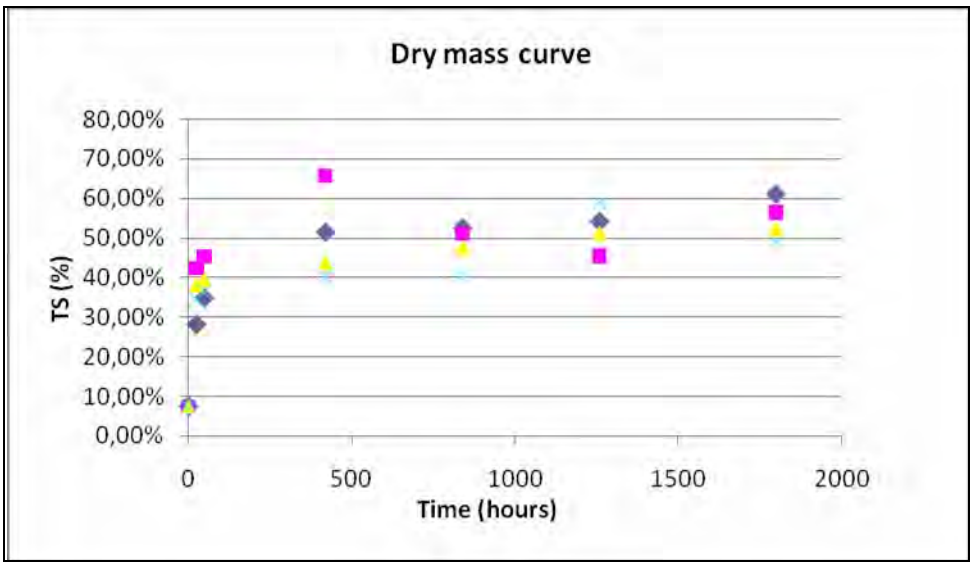

Figure 7 – HBT`s results of Sediment A.

Figure 8 shows the results of the Simulated Dewatering Test tests. The maximum total solids after 30 days is approximately 68% starting from initial total solids of approximately 7%.

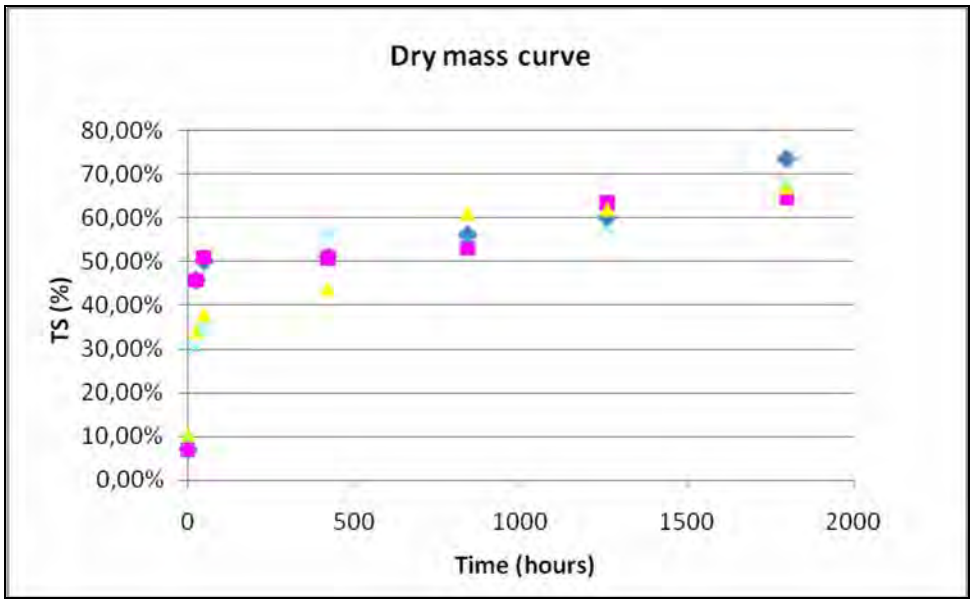

Figure 8 - Simulated Dewatering Test tests results of Sediment A.

5. CONCLUSIONS

There is no doubt that the cone test can be a good indicator to determine the slurry behavior when submitted to a dewatering tube filtration. It also can provide the polymer type and dosage. But field tests can provide more accurate data and use a larger amount of material. Another point is that the material within the bag tests can be analyzed at time intervals, to generate a dry mass curve.

The more field tests are conducted the more accurate the results will be. As it is observed, comparing Simulated Dewatering Test results, the later presented higher values of final total solids, consequently closer to the reality. This is due to a better conception as is listed below:

- Decrease loss of material, because of the confinement of the material slurry injection method
- Decrease flock breakdown due to simulated field conditions
- Total confinement increases dewatering, because slurry can dewater through the bottom sides and the top, which simulates actual full scale operation dewatering
- Once the bag is filled, the material within has no contact with outside elements avoiding re-hydration.

It is very important for dewatering tube design to incorporate the improvements of the preliminary tests, because the better the input data is, the better are the results.

ACKNOWLEDGEMENTS

Acknowledgements are made to Allonda Geossintéticos Ambientais Ltda and TenCate™ Corporation for assistance in providing data and materials.

REFERENCES

CASTRO, N. P. B., Sistemas tubulares para contenção de lodo e sedimentos contaminados. 2005. 103f. Tese de mestrado – Instituto Tecnológico de Aeronáutica, São José dos Campos - SP.

CASTRO, N. P. B., MELO, L. C. Q. C., ESCOBAR, L. B., Environmental integrated solution for septic tank sludge and landfill leachate using geotextile tubes dewatering technology. The first Pan American Geosynthetics Conference & Exhibition, GeoAmericas 2008, March of 2008. Cancun, Mexico.

DEWATERING AND CONTAINMENT TECHNOLOGIES, INC. Lagoon and Ditch Sediment Dewatering Utilizing Geotube Preliminary Pilot Demonstration. Monroe, Michigan: Department of Environmental Quality CPC. (Summary Report, Mar./30/2003)

FOWLER, J.D.T.; SPRAGUE, C.J. E; TOUPS, D. Dredged Material-Filled geotextile Containers, Environmental Effects of Dredging. Vicksburg, MS: U. S. Army Engineer, Waterways Experiment Station, 1994. (Technical Notes)

FOWLER, J.D.T.; BAGBY, R. M.; TRAINER, E., Dewatering sewage sludge with geotextile tubes. Geotechnical Fabrics Report, Set., p 26-30, 1997.

FOWLER, J., DUKE, M., SCHIMIDT, CRABTREE, B., BAGBY, R. M., TRAINER, E., Dewatering sewage sludge and hazardous with geotextile tubes. Geosynthetics. In.: INTERNATIONAL CONFERENCE ON GEOSYNTHETICS, 7, 2002. Anais…[S.n.d]. 6 p.

FOWLER, J. Proposed ASTM standard method: determining the flow rate os suspended solids from geotextile containment system for dregded material. Disponivel em < http:// www.geotube.com.> Acesso em 18/12/2005.

GANNETT FLEMING, HBT final report. Pittsburgh: U.S. Army Corps of Engineers, Gannett Fleming, Inc e Geotechnics, Jul. 2003. Disponivel em < http:// www. geotechnics.net> Acesso em 07/10/2006.

GRI GT12 : 2004. HBT for field assessment of fabrics used for geotextile tubes and containers, Geosynthetics Research Institute, Folsom, USA.

KOERNER, R.M. Design with geosynthetics., Prentice Hall, Englewood Cliffs, NJ., 1998. 761p.

KOERNER, G.R., KOERNER, M.R., Geotextile tube assessment using a HBT. Geotextiles and Geomembranes, v. 24, n. 2, p. 129-137. 2006.

LAWSON, C.R. Geotextile containment for hydraulic and environmental engineering. In. INTERNATIONAL CONFERENCE ON GEOSYNTHETICS ,8th, Yokohama, 2006. Proceedings…, [S.l.: s.n]. 2006. p. 9-48

LUNDIN, G. M., ESCOBAR, L. G. B., STEPHENS, T., Waterways and ponds contaminated with pulp and paper PCB's are contained and dewatered using Geotube® containers, providing an economical environmental solution. Two

location are presented. ABTCP - Vitória 2006, 8° Simpósio da IWA sobre Esgotos de Indústrias Florestais e 6ª Conferencia Internacional sobre o destino e os efeitos dos efluentes de fábricas de polpa de papel. Abril de 2006, Vitória, ES.

MARTINS, P. M., Utilização de tubos geotêxteis para o desaguamento de rejeitos de mineração. 2006. 161. Tese de mestrado – Instituto Tecnológico de Aeronáutica, São José dos Campos - SP.

MARTINS, P. M. ; VIDAL, D. M. ; BITTAR, R.J. . Avaliação do desaguamento de rejeitos de mineração em tubos geotêxteis através de ensaios de bolsa suspensa de geotêxtil.. In: REGEO/GEOSSINTETICOS, 2007, Recife. 6o. congresso brasileiro de geotecnia ambiental e do 5o. simposio brasileiro de geossinteticos, 2007.

MIRAFI Ten Cate Nicolon. Ten Cate Geotube GDT Test – A demonstration of the methodology of geotube dewatering technology, [S.l: s.n], 2007. 4 p.

MASTIN, B. J., LEBSTER, G.E., SALLEY, J. R. Use of geotextile tube dewatering containers in environmental dredging. The first Pan American Geosynthetics Conference & Exhibition, GeoAmericas 2008, March of 2008. Cancun, Mexico.

MELO, L. C. Q. C., ESCOBAR, L. B., CASTRO, N. P. B., Contenção e Desidratação de Lodos Perigosos Através de Tubos de Geotêxtil. XVIII Encontro Técnico AESABESP, FENASAN 2007. Agosto de 2007, São Paulo, SP.

NEWMAN, P; HODGSON, M; ROSSELOT, E. The disposal of tailings and minewater sludge using geotextile dewatering techniques. Minerals Engineering, v. 17, n. 2, p 115-121. 2004.

VIDAL, D., URASHIMA, D. C. Dimensionamento de filtros e drenos em geossintéticos. In: GEOSSINTÉTICOS'99. Outubro de 1999, Rio de Janeiro.

Experimental Evaluation of Geotextile Dewatering Performance

R. Satyamurthy, Ph.D., E.I, Ardaman and Associates, Inc., Orlando, Florida, USA
S.K. Bhatia, Ph.D., Syracuse University, Syracuse, New York, USA

ABSTRACT
Sustained growth of mining and mineral processing around the globe generate enormous amount of tails or fine residue which must be disposed economically and in an environmentally safe manner. The preliminary step in disposal involves separation of the liquid from the fines which has traditionally been done by gravity settling methods. In recent years, geotextile tubes are increasingly being used for dewatering and containment of high water content geomaterials. Several successful applications of woven geotextiles for dewatering fines have been reported throughout the world. Literature on the suitability of geotextile tubes for dewatering fines is sparse. Using appropriate geotextile material dewatering of fines can be optimized. Current state of practice favors woven geotextiles (monofilament or multifilament) despite availability of other types (non-woven and composite). At Syracuse University, experimental studies have been carried out to evaluate the dewatering performance (filtration efficiency and dewatering time) of five different geotextiles [three woven (one monofilament and two multifilaments), one non-woven, and one composite] to dewater fines. Results indicate that the dewatering performance of each geotextile is unique and is primarily influenced by its intrinsic properties. The paper presents a review of pertinent literature, details of experimentation, and findings.

1. INTRODUCTION

Sustained growth of mining and mineral processing around the globe increasingly generates enormous amounts of fine residue which must be disposed in an economical and environmentally safe manner. The mineral industry is one of the most prolific producer of slurry waste, generating an estimated 3.5 billion tones worldwide per year of solid waste, primarily as fine grained slurry called tailings (Newman 2003). The management and storage of mining industry tailings has been recognized as one of the greatest challenges facing mining industry (Fourie 2006). Traditional methods for separation of fines from process liquids are primarily based on the use of gravity settling methods using engineered containment facilities. These methods have significant limitations in terms of the dewatering time and extent, and the need for extensive chemical conditioning to accelerate the process. Recent years have seen the emergence of semi-dry methods that involve pumping the tailings as concentrated slurry to disposal. This is done in order to achieve rapid consolidation of the deposit and to maximize the utilization of the disposal land (Nguyen and Boger 1998). There is an acute need for technologies that can be used to efficiently and economically dewater fine tailings. Among available dewatering technologies, Geotextile tube dewatering applications have been reported to be successful in dewatering low solids content geomaterials in several challenging circumstances (Fowler et al. 1994, Wangensteen et al. 2001, Mori et al.2002, Newman et al. 2004, Lawson 2006). Commercial development of many innovative environmental technologies often stalls at nascent developmental stages. This may be due to a number of factors, including the novelty of the technologies, the need for pilot-scale (compared with bench scale) demonstration projects, potential regulatory or socio-political obstacles, the reluctance of conventional commercial enterprises to handle contaminated materials, and a lack of information about innovative technologies (Hostager and Neil 1998; Krueger 1998). Use of geotextile tubes to thicken and dewater fine-grained sediments is a developing field and has had limited application in the municipal, industrial, and environmental dredging markets (TenCate 2000). Geotextile tubes used for dewatering high water content sediments offer the following advantages: rapid disposal of large volumes of waste, ease of construction, convenient placement, high efficiency, low cost, labor conservation, and low environmental impact (Fowler et al. 1994, Lawson 2006) relative to other existing gravity or mechanical dewatering methods.

1.1 Geotextile tube dewatering

According to ASTM D 4439, a geotextile is defined as “a permeable geosynthetic comprised solely of textiles”, which is used with geotechnical engineering-related materials as an integral part of human-made projects, structures, or systems. Geotextiles are manufactured from polyethylene (PE), polypropylene (PP), polyester (PET), or polyamides (PA), using various manufacturing processes. Depending on the choice of manufacturer, geotextiles are commercially available in either woven or non-woven forms. Woven geotextile types include monofilament, multifilament, and slit filament. They are made by weaving yarns together, they have a relatively higher strength than non-woven products, and they have limited elongation as compared to non-woven geotextiles. Non-woven geotextiles, which can be either needle-punched or heat-bonded, are made by bonding yarns together (Koerner 1999). Composites are innovative geotextiles that are comprised of both woven and non-woven geotextiles, and offer significant advantages over the constituent fabrics. Fourie (2006) describes the use of innovative electrokinetic geotextiles for effective dewatering of deposits of soft clay.

A geotextile tube is constructed by sewing together one or more geotextiles to form a flexible container that can retain saturated materials. The dewatering process consists of pumping high water content slurry through a geotextile tube to bring about separation of the solid and the liquid phases. Lawson (2006) has noted that "Geotextile tubes are part of the system of disposal of slurry like waste and contaminated sediments", and goes on to describe the process as follows: Initially, the slurry is introduced into the system where it is mixed with a dewatering accelerant (if required). The slurry is then pumped into the geotextile tubes where dewatering occurs. Over time, the water passing out of the tubes can be pumped to a water treatment plant for further treatment, be re-circulated to the original slurry ponds, or exit directly to the environment (if it is clean enough). At the end of dewatering, the contained solids may be left in-place, be transported to an off-site disposal facility, or can be recycled for other uses. The overall system includes combinations of pumping equipment and pipelines; geotextile tubes; accelerant additives; water treatment processes; and specific disposal facilities for the final dewatered waste stream. Geotextile tube dewatering has recently gained rapid acceptance as the preferred in-situ technique for separating sediments and water from a dredged suspension using the geotextile as the filter medium. A typical geotextile tube dewatering application for dewatering dredged sediments is shown in Figure 1.

Figure 1 Geotextile dewatering facility

Literature on application of geotextile tube dewatering for low solids containing mine wastes is sparse. Among available literature, Newman et al. (2004) describe the first reported application of geotextile tube dewatering and management of disposal of fine tailings and mine water sludge in Chalkidiki region of Greece. They evaluated the dewatering performance of different geotextiles (polypropylene, polyester, polyester/polyethylene blend and polypropylene blend) to dewater fines/neutralization sludge waste having an initial solids concentration ranging between 5 and 14 % solids (94% passing 44 µm) using Hanging Bag Tests (HBT). HBTs were conducted by suspending geotextile bags on a scaffold and filling the bags with slurry, and monitoring the temporal quantity and quality of slurry. HBTs have been recognized to be laborious and unrepresentative of geotextile tube dewatering process (Huang and Luo 2008, Liao 2008). From conducting an undisclosed number of tests, they selected polyester geotextile and proceeded with large-scale trials which were followed by a successful implementation of geotextile tube dewatering system. The authors note that significant differences in the dewatering performance of other geotextiles were observed when pre-production tests were conducted and some less expensive fabrics could not withstand the variable flows evident by 'catastrophic failures'. Upon completion of the first phase, a second set of tubes were used in a low pH environment and the polyester geotextile experienced no damage whereas the mild steel manifold system was destroyed. Significant limitations of this study include the lack of details regarding the geotextiles and mine waste properties and no information on the preliminary screening techniques for geotextile selection.

The experiences of Newman et al. (2004) strongly suggest that geotextile tubes have the potential for successful applications involving large scale dewatering of slurried mine waste. Their study also highlights the need for simple bench-scale evaluations as opposed to larger HBT to characterize geotextile material dewatering to facilitate screening and selection of geotextile materials for site specific applications. Such evaluations can also be used to justify the need for larger HBT or pilot scale trials. Thus, the need for bench scale tests to facilitate rapid characterization of geotextile dewatering can be recognized to be of practical significance. The use of flocculants or polymers to accelerate dewatering has been reported in literature (Wangensteen et al. 2001, Mori et al. 2005, Lawson 2006) without justifying the need or providing any information regarding the selection methodology used for evaluation of alternatives. The selection of a geotextile for a particular dewatering application requires detailed knowledge of the process in which the geotextile will be used and the properties of both the geotextile and the slurry. Upon obtaining this information, several preliminary performance trials are essential to evaluate the suitability of available geotextile options for dewatering applications. The interaction between geotextile and the slurry governs the success of any dewatering project. Significant savings in cost and time can be realized by using bench-scale tests to screen available geotextile alternatives before proceeding to HBT or performance trials.

The specification of geotextiles for dewatering applications is based on the compatibility between geotextile pore-size and the slurry solids to be dewatered. The use of woven geotextiles for geotextile tube dewatering applications is widespread within the United States and is based on successful past experience. Hardman (1994), for instance, recognized that the "filter fabric," the geotextile for geotextile tube applications, may not be the ideal medium for all process conditions; and in some cases separation (dewatering) has to be assisted, for example, by using aids or body feeds or by polyelectrolyte treatment (commonly termed polymer conditioning). Chemical conditioning of slurries is often essential to accelerate geotextile tube dewatering and empirical evaluations are the only available means to determine optimal chemical treatment considerations. The selection and performance evaluation of aids, body feeds, and polyelectrolytes requires simple and effective evaluation methods. The Pressure Filtration Test (PFT) is ideal for the preliminary screening and the performance evaluation of geotextiles and dewatering enhancers for geotextile tube dewatering applications. This paper presents results of the laboratory PFT to determine dewatering performance (filtration efficiency and dewatering time) of five different geotextiles [three woven (one monofilament and two multifilaments), one non-woven, and one composite] to dewater slurried fines. Considerations of polymer flocculation to optimize the rate and extent of dewatering were also evaluated using these slurried fines, and these findings are presented elsewhere (Satyamurthy 2008, Satyamurthy et al. 2008).

1.2 Pressure Filtration Test

Moo-Young and Ochola (1999) first reported the use of a "modified specific resistance to filtration" test apparatus to perform the pressure filtration test aimed at screening geotextile materials for dewatering high water content materials. Several other studies (Kutay and Aydilek 2004, Bhatia and Liao 2004, Satyamurthy et al. 2008) have used bench-scale pressure filtration test to evaluate geotextile material dewatering performance with different types of high water content materials, as pressure filtration test can be used to characterize the dewatering performance under pressures anticipated in field dewatering. In this test, the geotextile to be evaluated is placed in a specially designed apparatus, slurry of known volume and concentration is poured over the geotextile, and a desired pressure is applied. The test also allows quantification of one-dimensional (1-D) dewatering behavior of slurries with more than one layer of geotextiles under applied pressure. The PFT at Syracuse University (Figure 2) consists of a stand supporting the test chamber consisting of three parts: a lower plate, a middle test chamber, and a top plate. The inside diameter of the test chamber is 7.2 cm and the height is 17 cm; a larger test chamber of 35 cm height is also available. The geotextile sample to be tested is placed on the bottom plate and the middle chamber is fastened using thread fastening assembly over the bottom plate. The top plate is provided with an axial inlet to facilitate the application of air pressure. The bottom plate is provided with a funnel-shaped slope leading to a drainage axial port that drains directly into a calibrated measuring cylinder. The height of the platen is adjustable to facilitate collection using small containers or a single graduated cylinder.

Pressure filtration tests were performed on geotextile specimens of 7.2 cm diameter. The geotextile sample was placed in the apparatus and saturated with water. Once the water drained, 600 ml of slurry of was poured into the test chamber. Drainage of slurry was prevented during this filling stage, and the top plate was fastened. Air pressure was applied to the test chamber from the axial port on the top plate, and drainage was allowed into a graduated cylinder. Visual observations of temporal flow characteristics were recorded as the cumulative volume of filtrate with time. Readings of cumulative volume were recorded at 50 ml increments until the end of the test (indication of no further throughput). Upon completion of the test, the apparatus was disassembled and filter cake height was recorded. The entire filter cake and filtrate was oven dried to determine the solids content and dry solids.

Evaluation of geotextile dewatering performance is evaluated in terms of two parameters 1) Dewatering Time indicative of the geotextile-filter cake void space and amount of geotextile clogging and 2) Solids Percent passing through the geotextile during the test process, indicative of the geotextile retention capacity.

Pressure filtration test results are commonly interpreted in terms of the Filtration Efficiency (%), Piping (g/m^2) and the Dewatering Rate (DR) or Dewatering Time (DT). Moo-Young and Ochola (1999) first reported the use of FE to characterize dewatering and defined FE as:

$$FE = (TS_{initial} - TSS_{final})/ TS_{initial} \times 100 \quad [1]$$

where FE is the filtration efficiency, $TS_{initial}$ and TSS_{final} are the initial total solids concentration and the final total suspended solids concentration, respectively.

Piping is defined as:

$$\text{Piping } (g/m^2) = TSS_{final} / A \quad [2]$$

where A = area of geotextile effective in dewatering.

To quantify the dewatering performance, the Solids Passing (Satyamurthy, 2008) can also be used which is defined as:

$$\text{Solids Passing (\%)} = [TSS_{final} / TS_{initial}] \times 100 \quad [3]$$

Among the parameters used for quantifying geotextile tube dewatering, the Solids Passing (%) appears to be a simple and accurate measure of dewatering performance. During the tests, greater amounts of fines were observed to pass during the initial stages which gradually decreased as the test progressed. This indicates that once the filter cake forms the amount of fines passing reduces significantly.

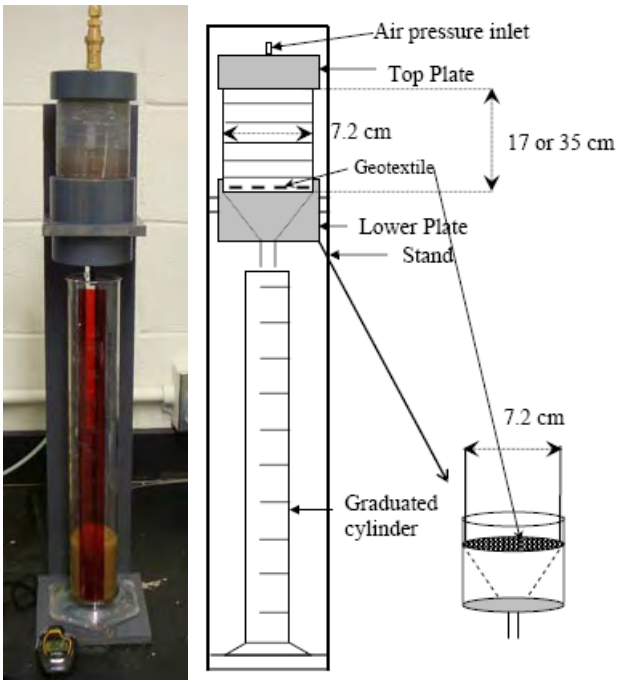

Figure 2. Pressure filtration test apparatus and schematic.

A criticism of the pressure filtration test is that small samples are too small to adequately represent the field geotextile tube dewatering process. Nevertheless, in practice small samples are widely used for assessment and quality control of geosynthetics and soils. Consequently, tests on small tests although economical and rapid, are very useful for screen available material alternatives but cannot be solely used as the basis for design. Pilot scale and full scale tests are recommended to determine actual geotextile tube dewatering performance and operational considerations.

2. MATERIALS

2.1 Geotextiles

The geotextile used for this study were obtained from three different manufacturers. The five geotextiles included three woven (W) geotextiles (one monofilament and two multifilament), which are most commonly used in practice, along with one each of non-woven (NW) and composite (C) types. These geotextiles are representative of the different types of geotextiles available for geotextile tube applications. The woven monofilament geotextile (W1) is made of polypropylene and multifilaments (W2 and W 3) are polyesters of different thickness and characteristic opening sizes. The needle punched non-woven geotextile (NW) is made of polypropylene and the composite geotextile (C) consists of geotextile W2 sandwiched between two layers of polypropylene needle punched geotextile. The geotextile index properties are provided in Table 1.

Table 1. Geotextile index properties.

Properties	W 1	W 2	W 3	C	NW
Polymer Type	PP	PET	PET	PET, PP	PP
Manufacturing Method[1]	MF	MU	MU	MU, NP	NP
Mass per unit area (g/m^2)	585	813	600	906	550
Thickness (mm)	1.04	1.33	1.73	3.27	0.5
Grab Tensile Strength (MD X CD) (kN)	96.3 x 70	175 x 175	175 x 175	175 x 175	100 x 100
Apparent Opening Size (AOS)[2] (mm)	0.425	0.27	0.15	0.045	0.2
O_{100}[3] (mm)	0.40	0.30	0.20	0.12	0.23
Permittivity (s^{-1})	0.37	0.37	0.38	0.41	0.39

Note: [1]NP: Needle Punched, PP: Polypropylene, PET: Polyester, MU: Multifilament, & MF: Monofilament
[2] Manufacturer value [3]Determined from Capillary flow porosimetry

2.2 Fines

Mill ground sediments used in this study were provided by an aggregate manufacturing facility in New York. Fines representative of tailings were obtained by wet-sieving the sediments through US Standard Sieve No.200 (100 % passing 75 µm as per ASTM D 1140). The particle size distribution of the fines is shown in Figure 3 and the fines comprise of a uniform distribution of silt size particles with relatively lower quantity fine clay sized particles. The fines had a uniformity coefficient (C_u) of 22, the coefficient of gradation (C_c) was 2.2, and was classified as ML as per Unified Soil Classification System (ASTM D 2487). The fines ranged in shapes from angular to sub-rounded as revealed by photomicrographs obtained from Scanning Electron Microscope (Figure 4). X-ray diffraction showed that the fines were predominantly comprised of quartz, carbonates, clay and iron-oxides. The specific gravity of the fines was determined to be 2.65.

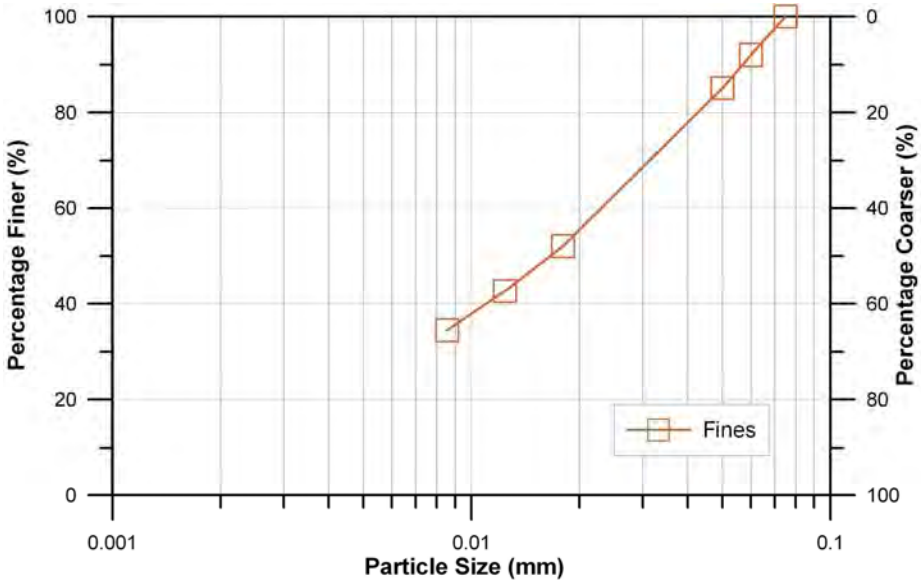

Figure 3. Particle size distribution of fines used in this study.

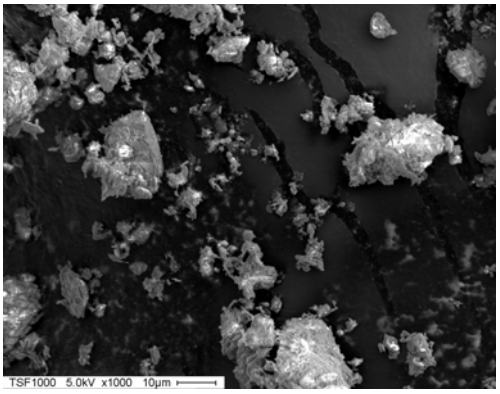

Figure 4. Scanning electron microscope (x1000) image of fines used in this study.

3. EXPERIMENTAL PROCEDURE

The wet-sieved fines were oven dried and pulverized. The dried samples were used to prepare fine slurry of 33 % solids concentration. The slurry was then mixed in a 1-L glass beaker in a Jar Test apparatus (Phipps and Bird PB-700) at a speed of 275 RPM for 300s. The pH of the slurries (supernatant) was determined to range from 7-8 from electrometric measurements using an Oaktron® pH 11 meter at laboratory temperatures between 21-24 ^{o}C. The rapid-mixed slurry was poured manually into the test chamber, and no drainage was allowed during the filling stage to facilitate filter cake formation. Upon completion of the filling, the top plate was fastened, and air pressure of 34.5 kPa was applied and drainage was allowed. In all the tests, the temporal flow characteristics were recorded. The test was carried out until no further discharge of filtrate was observed. At this stage, the pressure was removed and the test set-up disassembled. The filtrate was oven-dried to determine the total solids in the filtrate; water content and the thicknesses of the filter cake were also determined. Three separate tests were conducted to ensure repeatability.

4. RESULTS

The conventional assessment of the PFT results is conducted by evaluating the FE and the DT. In the PFT, filtration is accomplished by depositing solid particles over a geotextile medium, whose purpose is to retain the solids. This process progressively forms a 'filter cake' upstream of the geotextile, which, in turn, functions as the filtration medium for the remaining suspension that is yet to pass through the 'filter cake-geotextile medium'. At the beginning of the cake filtration process, a pressure drop occurs across the geotextile as no cake formation is present, and the flow is governed by Darcy's law. If the suspension was a clean liquid, it would result in a constant flow rate for an imposed pressure gradient resulting in a liner increase in cumulative volume with time. In cake filtration, however, as the deposits progressively make up the cake, a portion of the applied pressure is taken up by the cake, thus, leading to a gradual drop in the filtrate volume over time. The temporal flow characteristics observed during PFT dewatering fines at 33% solids concentration using the five different geotextiles is presented in Figure 5. Three separate tests were conducted using each of the geotextile under identical test conditions to ensure repeatability. Similar dewatering trends are observed for the five different geotextiles except geotextile W2, resulted in the greatest DT. The average results in terms of FE, piping, DT, final cake solids content and cake height are presented in Table 2.

Table 2. Pressure filtration test results.

Properties	W 1	W 2	W 3	C	NW
Filtration Efficiency (%)	94.5	99.3	97.8	99.5	97.2
Dewatering Time (s)	6900	8600	7506	7420	6300
Piping(g/m^2)	1954	227	793	190	1013
Solids Passing (%)	3.3	0.4	1.3	0.3	1.7
Cake solids content (%)	75	78	76	76.3	76.5
Cake height (mm)	50.5	52	50.5	50.5	52.5

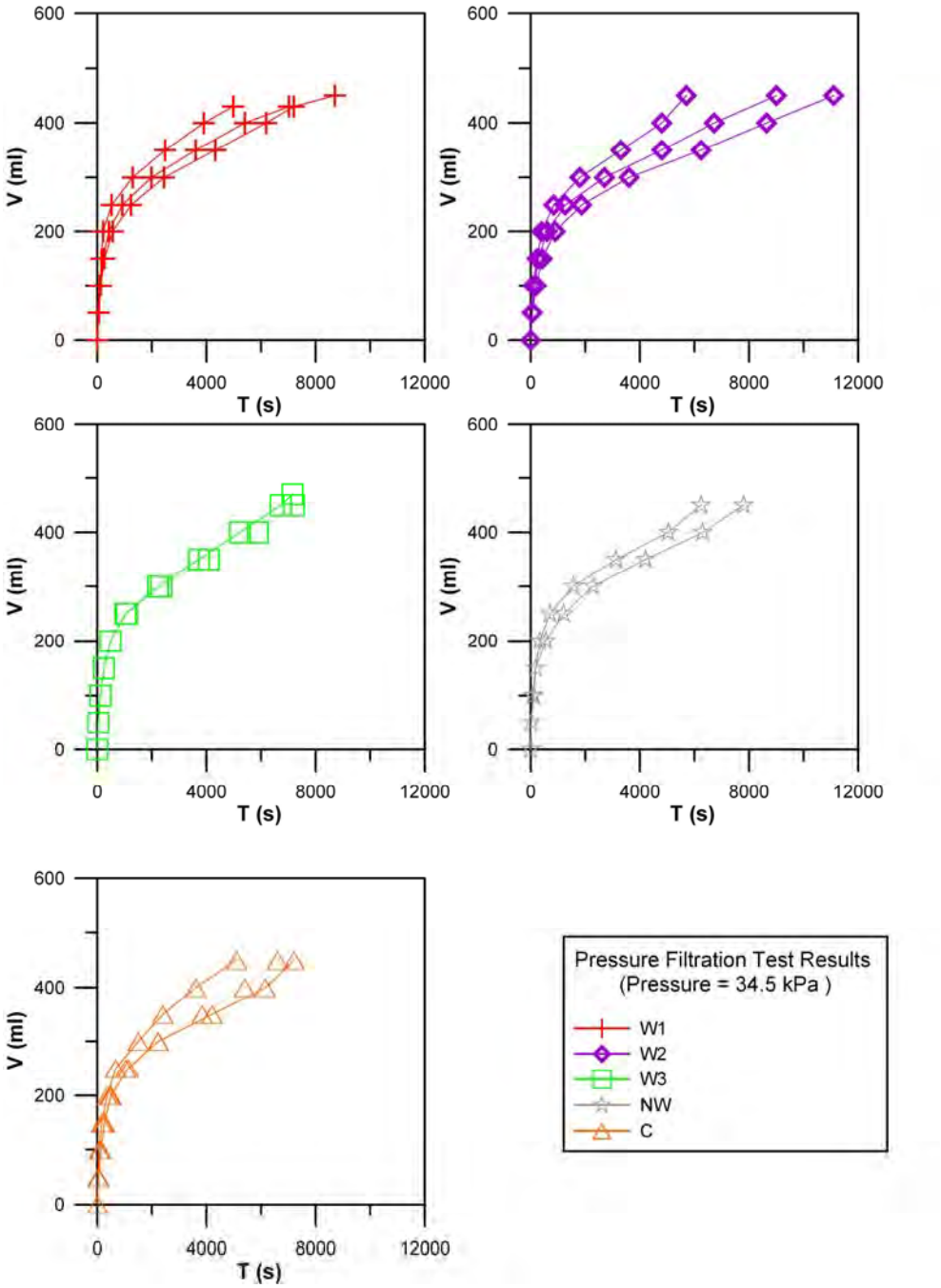

Figure 5. Temporal flow characteristics from pressure filtration tests.

As it can be seen from Table 2, the average FEs for the geotextiles tested ranged between 94.5 (W1) and 99.5 (C), and the corresponding average piping measures for the geotextiles tested were between 1954 g/m^2 (W1) and 190 g/m^2 (C). Geotextiles C and W2 had the best dewatering performance where as geotextile W1 had the lowest FE and greatest average piping. It is interesting to note that both geotextiles C and W2 have significantly different AOS values, that of W2 being 0.27 mm and that of C being 0.045 mm, but the piping values for dewatering under identical test conditions were comparable. No significant differences were observed in the final cake solids content and cake height. The permeabilities of the geotextile-filter cake system were determined and were found to be similar.

5. DISCUSSION AND CONCLUSION

One of the goals of this study was to evaluate correlations between geotextile intrinsic properties and dewatering performance of slurried fines. Koerner (1999) has recognized that from 1972, several direct comparisons of geotextile-opening size (O_g) has been made in ratio form to some granulometric parameter (d_x) of solids to be retained for geotextile soil retention applications. The numerical value of this ratio depends on geotextile type, soil characteristics, flow regime and other factors. The dewatering performance of geotextile used in this study were compared to the geotextile AOS and dimensionless ratio of (AOS/d_{85}) to determine any trends. The geotextile Apparent Opening Size (AOS or O_{95}) is defined as a property that indicates the approximate largest particle that would effectively pass through the geotextile (ASTM D 4751). For the geotextiles considered in this study the O_{95} determined using Capillary Flow Porosimetry (Liao, 2008) and AOS provided by manufacturers were similar and the AOS values are used to explore any relationship between geotextile dewatering performance and this index property. The geotextile performance (retention and time) for dewatering applications can be assessed by comparing the Solids Passing (%) and the Dewatering Time. The experimental observations of Solids Passing and Dewatering Time are plotted against geotextile AOS and (AOS/d_{85}) in Figure 6. The entire range of values determined from three separate pressure filtration tests conducted to dewater slurried fines is shown in Figure 6 although average values were given in Table 2.

From Figure 6(a), given the exception of geotextile W2, there appears to be an increasing trend of Solids Passing with the increase in the geotextile AOS. Geotextile C had the lowest AOS value and was most efficient in retaining the fines as the Solids Passing (%) ranged from 0.17 to 0.42. Geotextile W1, on the other hand, had the highest range and extent of Solids Passing (%). Geotextile W2 is comprised of relatively thinner multifilament fibers which provides for a very complex geometry relative to geotextile W3, which is also a similar type of multifilament. Thus, the complex intrinsic structure of geotextile W2 may have limited the amount of fines passing. Also, it can be observed that an increase in the value of (AOS/d_{85}) beyond six results in significant amount of Solids Passing (%). This indicates that the retention performance of geotextile is influenced by the compatibility of the geotextile opening size (AOS) and the sediment particle size (d_{85}). As mentioned earlier, soil-retention criteria for design of geotextile filters relate geotextile characteristic pore size (O_g) to a representative granulometeric parameter (d_x) [Calhoun, 1972; Rankilor, 1981; Giroud, 1982; Christopher and Holtz, 1985] and from the test results it appears that such a limiting criteria may exist for dewatering slurries. For the fines dewatered in this study, (AOS/d_{85}) < 3 was found to limit Solids Passing (%) to less than 2.5% for geotextiles C and W3 whereas geotextile W2 had (AOS/d_{85}) > 5 but Solids Passing less than 1%. Very different results [Figure 6 (b)] were observed when the Dewatering Time was plotted against the geotextile AOS and (AOS/d_{85}) as the Dewatering Time is expected to decrease with the increase in geotextile AOS. Overlaps in the Dewatering Time can be observed for all five geotextiles which suggests that the geotextile alone does not govern the Dewatering Time. Complex geotextile-filter cake interactions govern the Dewatering Time and results indicate that this may be independent of geotextile AOS. No other significant correlations were observed between the Percentage Passing, Dewatering Time, and geotextile intrinsic properties.

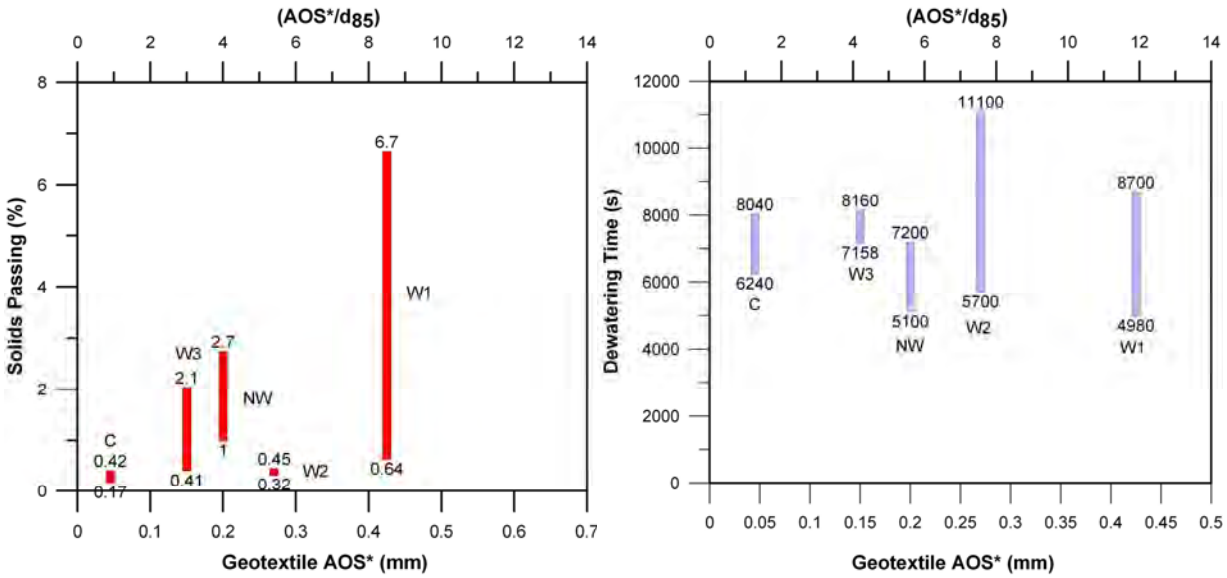

(a) (b)

Figure 6. (a) Solids Passing and (b) Dewatering time versus geotextile AOS and (AOS/d_{85}).
Note:* Manufacturer value

This study demonstrated the practical utility of bench-scale pressure filtration test for preliminary screening and selection of an appropriate geotextile material for geotextile tube dewatering applications. Laboratory bench-scale tests are quick and economical alternatives to facilitate rapid characterization of geotextile tube material dewatering performance. In the present work, experimental studies have been carried out to evaluate the dewatering performance (Filtration Efficiency and Dewatering Time) of five different geotextiles [three woven (one monofilament and two multifilaments), one non-woven, and one composite] to dewater fines. Two multifilament polyethylene geotextiles (W2 and W3) were found to have significantly different dewatering performance. Optimal retention conditions (Filtration Efficiency > 95 %) were observed using one woven multifilament geotextile (W2) and a composite geotextile (C). All geotextiles had Filtration Efficiencies greater than 94% and Solids Passing less than 7 %. Test data did not indicated the presence of a unique limiting value of geotextile AOS or (AOS/d_{85}) at which geotextile retention performance was high. The geotextile intrinsic properties (AOS and geometry) were found to influence the dewatering performance (retention) of geotextile tube materials for dewatering slurried fines. An exception to the existence of a limiting value of the ratio (AOS/d_{85}) indicated that geotextile dewatering is a complex phenomena influenced not only by the geotextile pore characteristics but also its intrinsic geometry. Although further experimental, field and theoretical research is needed, the novel approach presented to compare candidate geotextiles for dewatering applications is a rational and economical procedure.

ACKNOWLEDGEMENTS

The authors are grateful to Huesker Inc, Polyfelt Inc and TenCate Mirafi for providing geotextiles used in this study. Ranjan Satyamurthy was supported by the “Wen-Hsiung and Kuan-Ming Li Graduate Fellowship” and was previously supported by the Syracuse University Graduate School (University Fellowship Award). The authors extend their thanks and appreciation to Richard W. Chave for fabricating the test equipment. The authors acknowledge Ramya Pradhan for assistance with the experiments.
Mention of trade names or commercial products does not constitute endorsement or recommendation for use.

REFERENCES

ASTM D 1140. Standard Test Methods for Amount of Material in Soils Finer than No. 200 (75-µm) Sieve, *American Society for Testing and Materials*, West Conshohocken, Pennsylvania, USA.

ASTM D 2487. Standard Practice for Classification of Soils for Engineering Purposes (Unified Soil Classification System), *American Society for Testing and Materials*, West Conshohocken, Pennsylvania, USA.

ASTM D 4439. Standard Terminology for Geosynthetics, *American Society for Testing and Materials*, West Conshohocken, Pennsylvania, USA.

ASTM D 4751. Standard Test Method for Determining Apparent Opening Size of a Geotextile, *American Society for Testing and Materials*, West Conshohocken, Pennsylvania, USA.

Bhatia, S.K and Liao, K. (2004). Overview of Geotextile Tube Applications & Research, *ICGGE-2004*, IIT Bombay, Mumbai, India.

Hardman. E. (1994). Some aspects of the design of filter fabrics for use in solid/liquid separation processes. *Filtration & Separation*, 31 (10), 813–818

Fourie, A. (2006). Harnessing the Power: Opportunities for electrokinetic dewatering of mine tailings, *Geotechnical news*, 24(2): 27-32.

Fowler, J., Sprague, C.J., and Toups, D. (1994).Dredged Material-filled Geotextile Containers, Environmental Effects of Dredging, Technical Note EEDP-05-01, US ARMY Waterways Experiments Station, Vicksburg, MS, pp14.

Hostager T.J and Neil T.C. (1998). Seeing environmental opportunities: Effects of intrapreneurial ability, efficacy, motivation, and desirability . *J Organizational Change Management*. 11(1): 11-25.

Newman, P. (2003). Geotextile Bags for containment, filtering and decontamination of slurries, In Geosynthetics—Protecting the Environment, Dixon,N., Smith, D. M., Greenwood, J. R. and Jones, D. R. V., (Editors), Thomas Telford, London: 107-120.

Newman, P., Hodgson, M., and Rosselot, E. (2004). The disposal of tailings and minewater sludge using geotextile dewatering techniques, *Minerals Engineering*, 17(2): 115–121.

Nguyen, Q. D. and Boger, D. V. (1998). Application of rheology to solving tailings disposal problems, *International Journal of Mineral Processing*, 54 (3-4): 217-233.

Koerner, R.M. (1999). *Designing with Geosynthetics*, 4th ed., Prentice Hall, NJ.

Krueger N. (1998). Encouraging the identification of environmental opportunities. *Journal of Organization Change Management*. 11(2): 174-183.

Kutay, M. E. and Aydilek, A. H. (2004). Retention performance of geotextile containers confining geomaterials. *Geosynthetics International*, 11(2): 100–113

Satyamurthy, R., Liao, K., and Bhatia, S.K. (2008). Pressure Filtration Test-Assessment based on Filtration Theory, Session for Hydraulic Applications, *EuroGeo4 Conference*, Edinburgh, UK (on CD).

Satyamurthy, R., 2008, Experimental Investigations of Geotextile tube Dewatering, PhD Dissertation Syracuse University, Syracuse, NY, 233 p.

Ten Cate Mirafi. (2000). Geosynthetics in Use, Volume 1, Issue 2.

Lawson, C.R. (2006). Geotextile containment for hydraulic & environmental engineering, *8th International Conferenence on Geosynthetics*, Sep 18-22, Yokohama, Japan., Kuwani & Koseki, J (eds), Millpress, Rotterdam, Netherlands : 9-48 (on CD).

Liao, K. (2008). Dewatering of natural sediments using geotextile tubes, PhD Dissertation, Syracuse University, Syracuse, NY.

Moo-Young, H.K and Ochola, C. (1999). Strain effects on the filtration properties of geotextiles. *Geosynthetics '99*. Boston, MA, Industrial Fabrics Association International, Roseville, MN, 757–768.

Moo-Young, H.K., Douglas, A.G., and Xinghua, Mo. (2002). Testing Procedures to Assess the Viability of Dewatering with Geotextile Tubes, *Geotextiles and Geomemebranes* 20 (5):289-303.

Mori, H., Miki, H., and Tsunekoa, N. (2002). The use of geo-tube method to retard the migration of contaminants in dredged soil, *Geosynthetics - 7 ICG* - Delmas, Gourc & Girard (Eds), Swets & Zeitlinger, Lisse, Nice, France,1017-1020 .

Wangensteen, M., Lafferty, P., and Kobler, J.D. (2001). Innovative dewatering & water treatment techniques for Hydraulically Dredged Sediments, *The First International Conference on Remediation of Contaminated Sediments*, Venice, 10-11 October, 361 (10).

Geosynthetics 2009
February 25-27 2009, Salt Lake City, Utah

Drainage Characteristics through Geotextiles under Tensile Load

D.A. Gaffney, P.E., Ocean & Coastal Consultants Inc., Gibbsboro, New Jersey, USA
G. Hsuan, Ph.D., Drexel University, Pennsylvania, USA
J.R. Weggel, Ph.D., P.E., Drexel University, Pennsylvania, USA
R. Munoz, M.S., E.I.T., Ocean & Coastal Consultants Inc., Gibbsboro, New Jersey, USA

ABSTRACT
Variations in the strain of a geotextile fabric can cause changes in its properties. An understanding of these variations can lead to better selection of geotextile fabrics. Specifically, high strength geotextiles used in large tubes for dewatering rely on the geotextile's ability to retain solids while passing water. By utilizing a newly designed test apparatus, the water flow rates of four high strength geotextiles under strain are observed. Initially, water flow rates of the geotextile fabrics under no strain are correlated with the published data determined by ASTM D4491. The four geotextiles are then subjected to increasing strain by incrementally increasing the tensile load in the either the machine (MD) or cross-machine (XMD) direction. A water flow rate test is then conducted at a specific tensile load. In actual use, geotextile tubes are known to experience the highest loads in the circumferential direction. Depending on how the tube is sewn, the circumferential stress will correspond to either the machine direction or cross machine direction. Experimental trends were observed for all geotextile fabrics in the MD and XMD directions that, if utilized appropriately, can have direct consequences in full scale tube dewatering.

1. INTRODUCTION

Geotextile tubes are becoming an accepted alternative for dewatering high moisture content wastes such as mine tailings, waste water treatment sludge, and dredged slurry. These waste products are similar in that the solid particles tend to be very small, and thus dewatering can be problematic. Geotextile tubes dewater waste materials by encapsulating the slurry, retaining the fine grained solids and allowing water to pass through the porous fabric. Two index properties of the geotextile commonly used to predict performance are Apparent Opening Size (AOS) and Water Flow Rate. The AOS test (ASTM D4751) is performed dry and therefore is only a proxy for how the geotextile will perform when saturated. The water flow rate test (ASTM D4491) is performed using a geotextile sample under zero strain. This is also not representative of dewatering in a tube which subjects the geotextile to variations in the strain.

It has been observed that variations in the strain of a geotextile can cause changes in the behavior of the fabric. Filtration tests conducted by Moo-Young and Ochola (1999) showed an increase in Total Suspended Solids (TSS) in the drainage water with strain for the woven strength layer, while little change was observed in the nonwoven. This implies that the woven polypropylene becomes more open as the tensile load increases. Koerner (1997) reports that under load, nonwovens exhibit a decrease in permittivity while the data for woven slit films is inconclusive due to scatter in the data.

Water flow rate is an important index property for determining the efficacy of dewatering geotextile tubes. It is the author's rule of thumb that during actual field conditions, the geotextile's water flow rate drops one order of magnitude during pumping (e.g. from 20 gpm/ft^2 to 2 gpm/ft^2) and during passive dewatering another order of magnitude (to 0.2 gpm/ft^2). Therefore, even though the published water flow rate is not by itself representative of the flow rate of decant water permeating the geotextile tube, it can still be a proxy for initial predictive purposes.

Commonly used geotextile tube fabrics include high strength woven polypropylene and polyester. These can be woven in a variety of ways using a variety of yarns types, all of which affect the AOS and water flow rate. Less common is the use of nonwoven geotextiles and a newly developed high strength weft insertion knitted fabric. A geotextile tube will experience multiple directions of strain during filling (pumping) and use. The two principle directions of axial and circumferential strain in a geotextile tube correspond to the directions in the geotextile manufacturing process, depending on how it is sewn. For example, if the tube is fabricated by sewing long panels of geotextile together longitudinally, the axial stress will be applied to the MD yarns and the circumferential stress will be applied to the XMD yarns. Most tubes are fabricated by sewing longitudinally. Conversely, some tubes are sewn circumferentially with the result that axial stress is applied to the XMD yarns. Some tubes have also been sewn in a helical fashion, applying the stress on a bias.

This paper will describe the results of water flow rate testing under tensile load conducted at Drexel University using a newly designed test apparatus. These data show changes in flow rate resulting from strain due to load in one direction. Geotextile characteristics, such as the yarn polymer (polyester or polypropylene) and type of construction (woven, weft insertion knitted, non-woven), are shown to impact the strain and flow rate relationship.

In actual use, geotextile tubes are filled with high moisture content slurries. Solids within the slurry, which form a low permeability filter cake on the inside of the tube, also have an effect on flow rate through the geotextile. Results from water flow rate testing will be correlated to a wide variety of actual experiences in the field.

2. GEOTEXTILE WATER FLOW RATE TEST UTILIZING UNI-AXIAL STRAIN

2.1 Test Apparatus and Specimen Configuration

The test apparatus consisted of two parts: 1) tensile loading frame and 2) permittivity device. The geotextile test specimen is situated between the upper and lower components of the permittivity device which are held together by four clamps. The water flows through a 2-inch diameter circular area of the geotextile. The test is performed under a constant head condition. The hydraulic head is controlled by the outlet tube that is free to rotate around the coupling. The hydraulic head is monitored by two hydrometers that are connected to the upper and lower parts of the permittivity device.

For applying tensile loads to the geotextile specimen, a 30-inch long specimen is fixed on one side of the loading frame, passes through and between the upper and lower components of the permittivity device, and then goes over a roller, as illustrated in Figure 1.

Figure 1. Mounting the geotextile test specimen in the tensile loading permittivity apparatus

The end of the specimen is mounted onto a grip that is connected to the load rod, as shown in Figure 2. The loads are gradually added to the specimen, and the amount varies depending on the ultimate tensile strength of the geotextile. Prior to each loading, the upper component of the permittivity device is removed so that the specimen can self-adjust under the applied load for a duration of 15-minutes.

Figure 2. Grips and loading device.

2.2 Test Specimens

The dimensions of the test specimens were 30-in long and 4-in wide. The test specimens were cut from the geotextile using a hot-knife to avoid fiber peeling and fraying. The manufacturing directions (MD and XMD) were clearly marked on each specimen.

3. RESULTS

3.1 Validation of new device

Permittivity (cross-plane permeability) was measured on a variety of low strength geotextiles to compare the values obtained using ASTM D4491 and the new apparatus. The results were very similar indicating that the new apparatus could accurately measure flow rate. Four high strength geotextiles (see Table 1) were used in the water flow rate under tensile strain tests. Table 1 shows the published data as obtained from the manufacturers for the four geotextile fabrics under investigation.

Table 1. Published properties of geotextiles

Geotextile		AOS	Flow Rate	Tensile Strength	
Style	Product	(mm)	(GPM/ft2)	MD (ppi)	XMD (ppi)
A	Weft Insertion Knitted, PET	0.123	129.0	696	635
B	Woven PP	0.425	20.0	400	600
C	Woven PET	0.250	15.0	1000	1000
D	Woven PP (slit tape)	0.180	14.8	447	460

For the Style A geosynthetic fabric, water flow rates were determined utilizing both the new device and ASTM D4491. In the new device, multiple flow rates at a specific head in the MD and XMD direction were recorded and averaged. The

average and standard deviation of all measurements at a specific head was also calculated. Table 2 shows the results obtained by both methods versus those of the manufacturer.

Table 2. Water flow rate from different testing methods at zero load and the manufacturer

Δh	ASTM D4491	New Device				Manufacturer
	Flow Rate	Avg. MD Flow Rate	Avg. XMD Flow Rate	Avg. Flow Rate	Stdv.	Flow Rate
(in.)	(GPM/ft2)	(GPM/ft2)	(GPM/ft2)	(GPM/ft2)	(GPM/ft2)	(GPM/ft2)
0.5	37	41	40	41	1.5	N/A
1.0	64	81	78	80	1.9	N/A
2.0	118	125	128	127	2.7	129

From Table 2, it can be seen that the flow rates produced by the new device closely approximate those listed by the manufacturer. Only minor disagreements exist for those measurements obtained by ASTM D4491 at the higher specific heads of 1 and 2 inches.

3.2 Flow rates for geotextiles under tensile strain

The flow rates for the four types of high strength geotextiles under increasing load were experimentally determined. All experiments began with the flow rate of a sample being determined with no applied load. The load was then incrementally increased and the flow rate once again experimentally determined. The data was then plotted comparing the "flow rate retained" (which is the applied load flow rate divided by the no applied load flow rate) with the applied load in pounds per inch (ppi). Flow Rate Retained greater than 100 percent indicates that the flow rate has increased due to the applied load.

Figures 3 through 6 show the flow rate retained as the load is incrementally increased for each of the four geotextiles. In each case, the increasing load results in a uniaxial strain that directly affects the flow rate of the geotextile. The general trend can be observed as falling into two regions. In the first region, a small increase in the load from 0 to 6 ppi generally leads to a large decrease or increase in the percentage of flow rate retained. In the second region, the increasing load results in less dramatic changes in the percentage of flow rate retained, trending either toward more open or more closed.

Another important observation indicates that load increases in the XMD results in increased flow rate while a load increase in the MD direction has the opposite effect on the percentage of flow rate retained. This result is most pronounced in the three woven geotextiles (Styles B, C and D) and has large implications on their use as geotextile tubes. If the dewatering goal is to retain fines (with dewatering rate being less important), then sewing the tube circumferentially is preferred due to the circumferential stresses being applied to the MD yarns. This will tighten the tube fabric and slow down the dewatering process. In contrast, if rapid dewatering of a coarse material slurry is the goal, then longitudinal sewing will apply the larger stresses on the XMD yarns, thus opening the fabric.

Figure 3. Flow Rate Retained (%) vs. Applied Load (ppi) for Woven, PP, Geotextile (Style B)

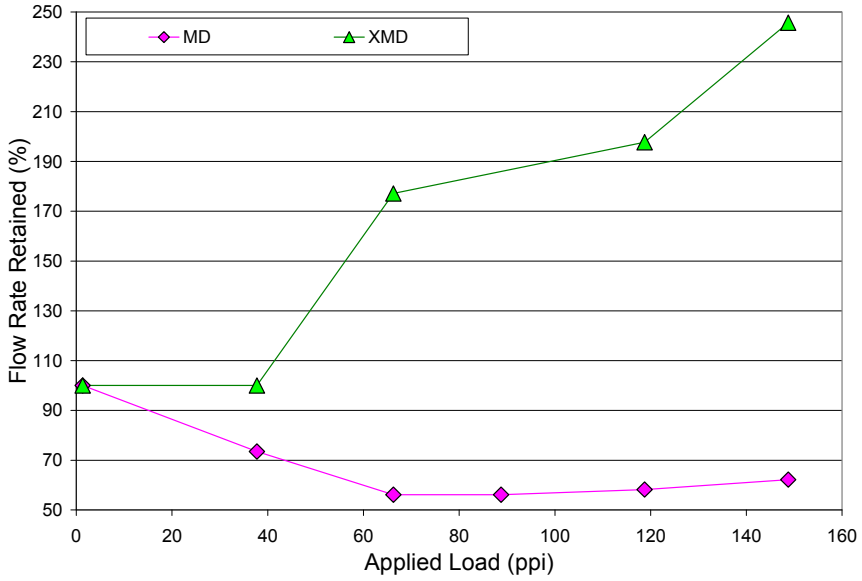

Figure 4. Flow Rate Retained (%) vs. Applied Load (ppi) for Woven, PET, Geotextile (Style C)

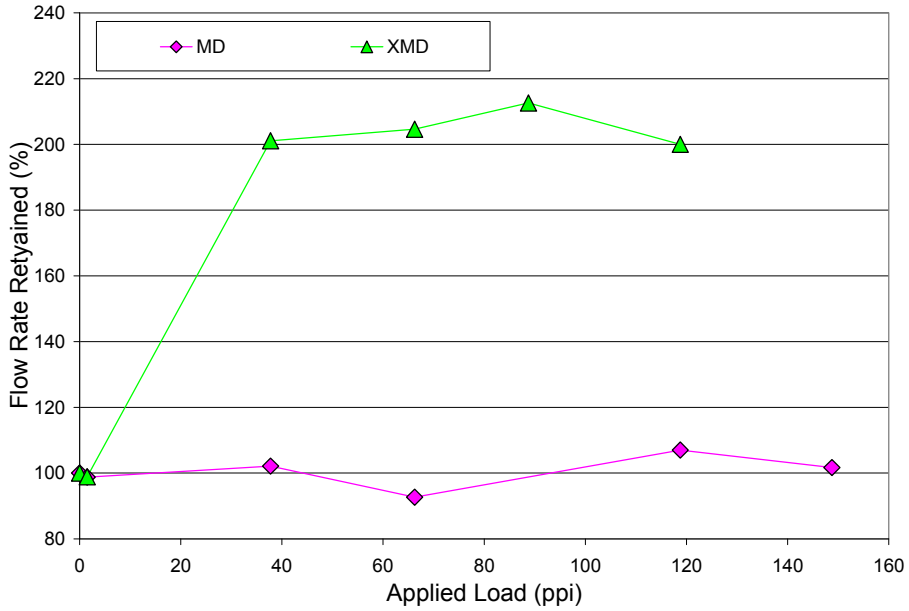

Figure 5. Flow Rate Retained (%) vs. Applied Load (ppi) for Woven, PP (Tape), Geotextile (Style D)

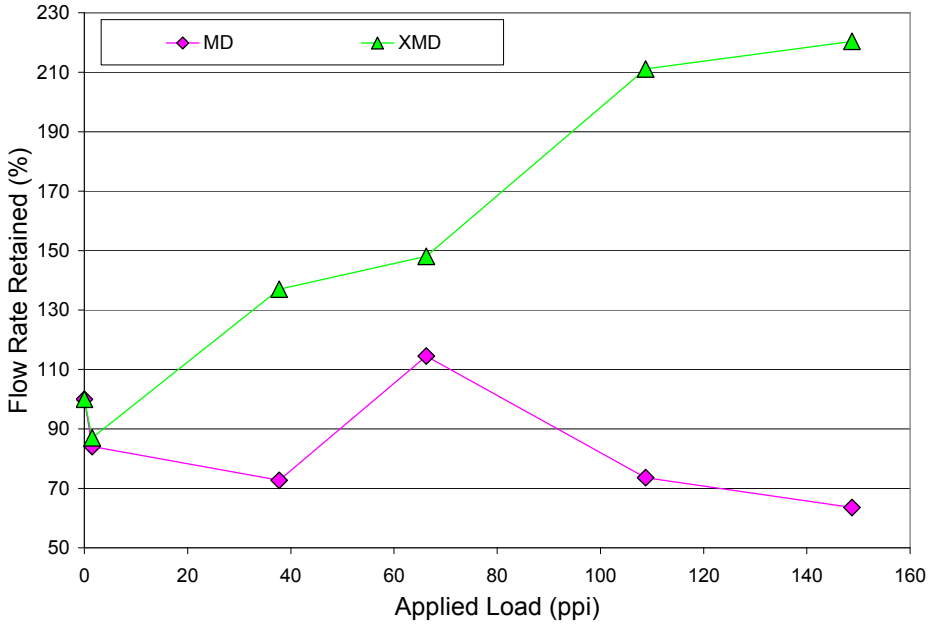

Style A (weft insertion knitted polyester) does not suffer from these variations to the same degree. This geotextile begins with a higher flow rate in comparison and maintains its flow rate through the range of applied loads (see Figure 6). This geotextile was also tested on a bias. The sample was cut at a 45 degree angle and tested in a similar manner. As one might expect, the sample necked down and its water flow rate was dramatically reduced.

Figure 6. Flow Rate Retained (%) vs. Applied Load (ppi) for Weft Insertion Knitted Geotextile (Style A)

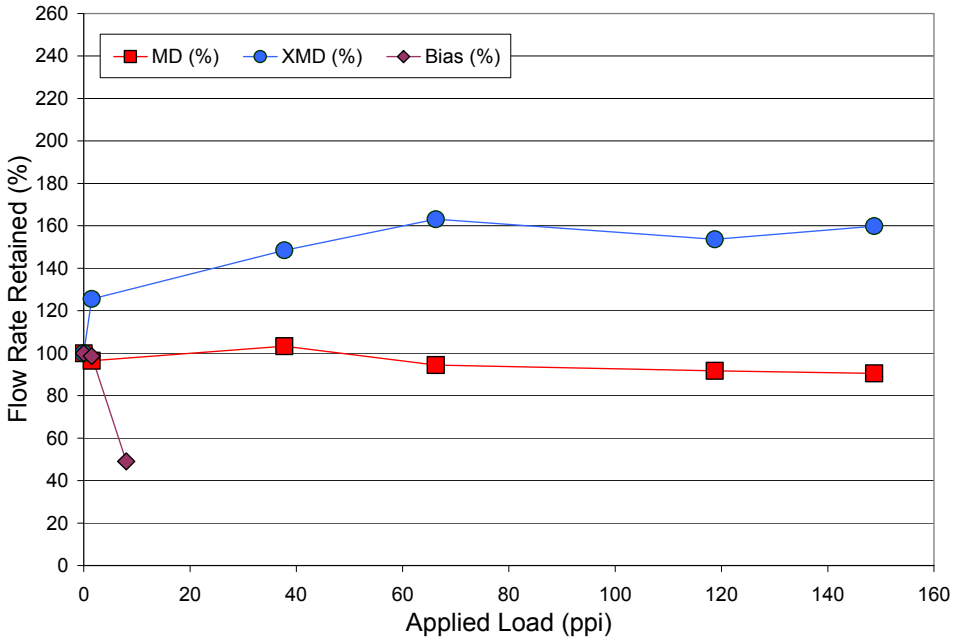

4 FIELD EXPERIENCE

4.1 Geometry of Fabrics

Standard geotextile tube fabrics have wide width tensile strengths greater than or equal to 400 pounds per inch. This is due to the stress placed on the tube during hydraulic filling. Since sewing generally reduces the tensile strength by 40 to 50 percent, many geotextiles designed for use as dewatering tubes have higher strength in the XMD than the MD (i.e. Style B, Table 1). As stated earlier, the highest stresses during filling are in the circumferential direction, and when sewn longitudinally, this corresponds to the XMD yarns. It is interesting to note that for Styles B, C and D, flow rate increased when the loads were increased in the XMD direction. In actual field experience with woven polypropylene fabrics sewn longitudinally, the author has observed that when a geotextile tube reaches a certain height (corresponding to higher circumferential loads) the tubes tend to shed more water.

If these fabrics were sewn into a tube circumferentially, the MD yarns would experience the highest stress, and the flow rate would likely decrease. With this information, the tube manufacturer and project designer can chose the optimal combination of tensile strength and flow rate for a particular dewatering project.

4.2 Comparison of Styles B and D.

Geotextiles B and D are both woven polypropylene with similar published tensile strength and similar published water flow rates. In a side by side test, using the same filling equipment, the same dredged material and the same size tubes, Style B performed better.

Style B is made from fibrillated yarns in the XMD and monofilaments in the MD. Style D is made from heavy slit tape yarns. The tube made from Style D fabric was sewn circumferentially and therefore the circumferential stresses were applied to the MD yarns. This resulted in the flow rate decreasing dramatically. The Style B tube shown in Figure 7 was sewn longitudinally and therefore its water flow rate increased.

Figure 7. Large Geotextile Tube During Filling (Style B on the left and Style D in the lower right corner)

4.3 Longitudinally Sewn and Bias Sewn (Style A)

In another side by side test, geotextile A was tested with coal washing slurry. One tube was sewn longitudinally while the other was sewn on a bias. The difference in dewatering rate was remarkable. As observed in the water flow rate tests, when the geotextile is subjected to tensile loads in a diagonal direction, the water flow rate drops dramatically. The longitudinally sewn tube dewatered well overnight while the tube sewn on a bias was still nearly the same height after two days (see Figure 8).

Figure 8. Comparison of Longitudinal Sewing (right) vs. Diagonal Sewing (left)

5. CONCLUSIONS

The Water Flow Rate apparatus was able to test the permittivity of a variety of high strength geotextiles under load. The test results to date show a general trend that when XMD yarns are subjected to tensile load, the water flow rate increases. When the MD yarns are subjected to tensile load, the water flow rate decreases. Additionally, when a geotextile is subjected to tensile load on a bias, the water flow rate decreases dramatically. These trends are corroborated in the field.

By extension, one can predict that with an increase in water flow rate, the retention of fine grained particles may decrease. This may account for the increase in TSS found by Moo-Young and Ochola (1999).

The weft insertion knitted polyester fabric performed differently than the woven fabric in that the flow rate was initially higher and stayed higher under tensile load. Additionally the relative change in water flow rate was less than the wovens.

The relationships found during this experiment may help the tube designer when evaluating a dewatering project utilizing geotextile tubes. It is unlikely that a tube sewn on a bias would dewater at a satisfactory rate.

It is recommended that more water flow rate tests be performed to add confidence to the data obtained.

ACKNOWLEDGEMENTS

Tensar International is acknowledged for supplying geotextiles and providing a portion of the funds for the study. Drexel University is acknowledged for developing the test equipment and performing the tests.

REFERENCES

Koerner, R.M. (1997). Designing with Geosynthetics, 4th Edition, Prentice Hall, Upper Saddle River, NJ, USA.

Moo-Young, H. and Ochola, C. (1999). Strain Effects on the Filtration Properties of Geotextiles, *Geosynthetics '99*, ASCE, Boston, Massachusetts, USA, 1:123-136.

Geotextile Tube Dewatering Technology Utilized on Massive Scale in Ashtabula River Remediation

W. Cretens, Infrastructure Alternatives, Inc., Rockford, Michigan, USA

ABSTRACT
Accumulated soft sediment of the lower Ashtabula River in Ashtabula, Ohio, was contaminated with organic chemicals such as polychlorinated biphenyls (PCBs) and polycyclic aromatic hydrocarbons (PAHs), heavy metals and some low level radionuclides. The Ashtabula River Remediation, a two phase project which began in 2006 and was completed in 2008, utilized hydraulic dredging in conjunction with geotextile tube dewatering to remove, dewater and dispose of the unwanted sediment. Geotextile tube dewatering technology was very successfully applied in this project, providing an innovative, cost-effective dewatering and disposal option for heavily contaminated soft sediment.

1. INTRODUCTION

Chemical and low-level radiological contaminants present in the sediments of the lower Ashtabula River prevented maintenance dredging in the area for many decades. Disposal in the open waters of Lake Erie (the method used in the past) was not an option because of the contamination in the sediment. A suitable disposal site and method of disposal, as well as funds to cover the increased cost of handling the contaminated sediment could not be found. Without regular maintenance dredging, by 2006, commercial and recreational navigation were severely limited.

In the spring of 2006, contractors began work on a sediment remediation project of great scale. The Ashtabula River Remediation is the largest sediment clean up funded through the Great Lakes Legacy Act to date. Over the course of the entire project, performed in two phases over three dredging seasons, about 640,000 cubic yards of contaminated sediment were removed from the river. Depth in the federally-authorized navigational channel was also restored, returning the river's commercial and recreational potential.

The remedial design incorporated leading edge sediment remediation technologies, including geotextile tube dewatering. Infrastructure Alternatives was contracted by the general contractors of both Phase I & II of the project to design, operate and maintain the sediment dewatering system and was additionally responsible for operation of chemical addition and water treatment processes during Phase II of the project.

2. PROJECT SCALE, DESIGN

Contaminated sediment was removed from the river utilizing a 12 inch diameter hydraulic cutter head dredge. The dredge pumped sediment slurry from the river and into the sediment transfer pipeline. The transfer pipeline was up to four miles long and incorporated four booster pump stations to keep the slurry moving at an adequate velocity and prevent heavy solids such as gravel and sand from settling out in the pipeline.

The sediment transfer pipeline delivered the dredged slurry to the sediment Consolidation Facility (CF), where it was dewatered in geotextile tubes. The CF was a landfill, permitted under the Toxic Substances Control Act (TSCA), and constructed specifically for the Ashtabula River Remediation project. The CF was designed not only to provide a dewatering site, but also a permanent disposal site for the dewatered sediment. At the conclusion of the project, the CF was prepared for capping and closure.

Geotextile tubes were used to dewater the dredged sediment slurry. As the slurry arrived at the CF, flowing at a rate of up to 5,000 gallons per minute, it was directed through a header system to geotextile tubes which were filled in place inside the CF. Weep water (clear water released from the geotextile tubes) drained by gravity to a sump in the CF floor and was processed in an on-site water treatment plant before being discharged back into the Ashtabula River.

2.1 Geotextile Tube Dewatering

Geotextile tube dewatering of contaminated sediment on this magnitude was relatively unknown at project start. There were many unique challenges which had to be addressed in the design of the geotextile tube header system, the construction of the geotextile tubes, as well as in operational plans for the placement and stacking of the tubes inside the CF.

2.1.1 Geotextile Tube Header Systems Design

The header system was comprised of a 12 inch diameter main header which ran along the entire perimeter of the CF and a secondary system of 10 inch diameter "mini-headers." These mini-headers could be described as inverse manifolds, whereby the sediment slurry flowed from the main 12 inch header into a 10 inch header which split to feed several geotextile tubes (an average mini-header fed five geotextile tubes). Flow from the main header to each geotextile tube hooked into a mini-header could be controlled with pinch valves at several points: collectively, at the 12 inch by 10 inch tee which marked the start of the mini-header; and individually, at the 10 inch diameter leg which fed each geotextile tube. Further, flow could be controlled with additional pinch valves to the separate fill ports on each geotextile tube; this gave operators the greatest amount of flexibility and control in filling operations, ensuring that each geotextile tube would be filled as evenly as possible – even filling was absolutely crucial to a stacking plan that called for no less than 10 layers of geotextile tubes to be stacked in the CF by project's end. The header design also allowed operators the ability to quickly stop flow to a group of full tubes and divert it to a group of fresh tubes, a must for such a large system.

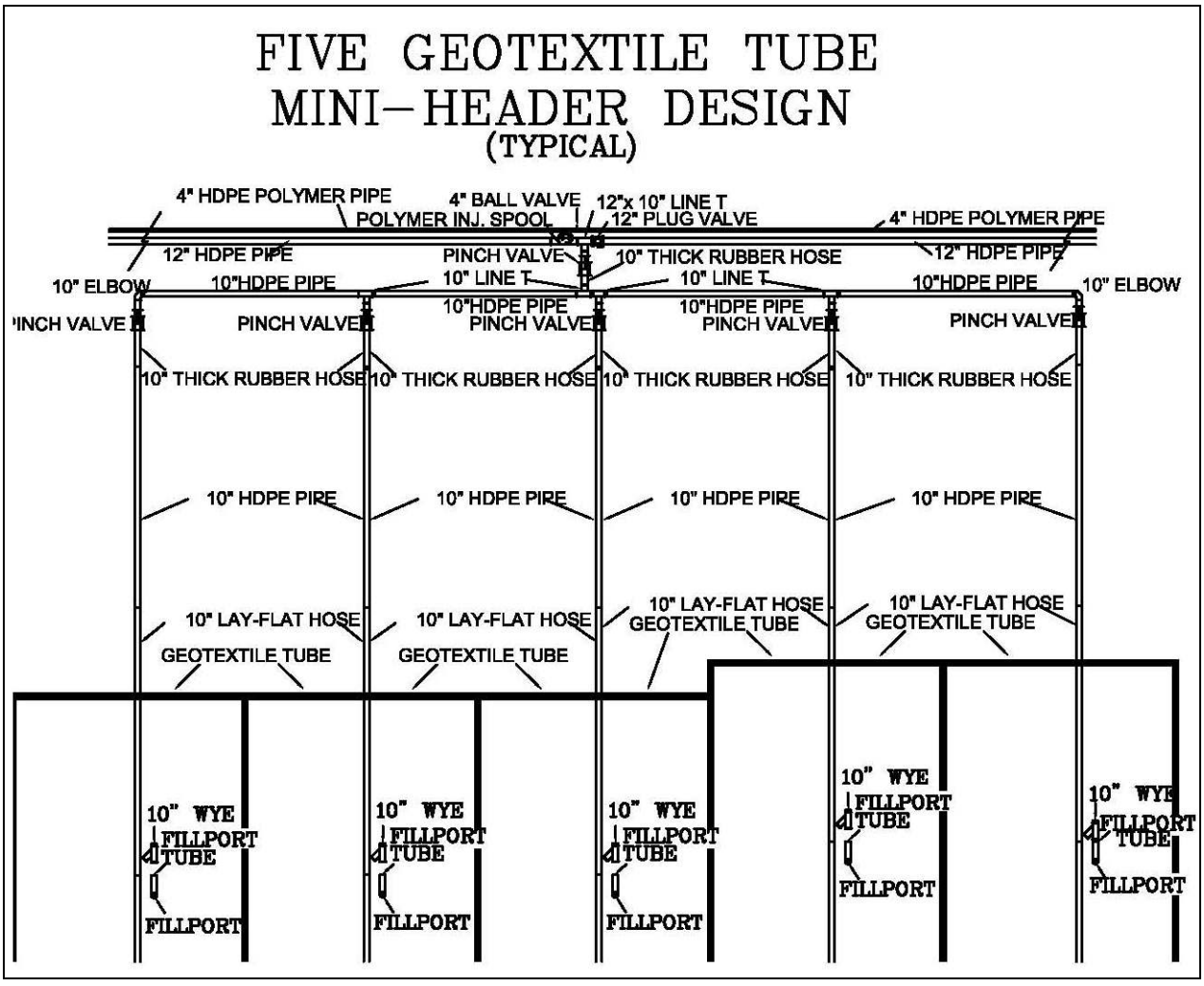

Figure 1. Typical mini-header design.

2.1.2 Geotextile Tube Specifications

Some geotextile tube specifications such as the apparent opening size of the fabric were developed based on the results of preliminary testing performed on core sediment samples from the Ashtabula River. Other specifications were

developed based both on the past project experience of the contractors involved and to accommodate the header system design, geotextile tube layout and stacking plans.

The actual fabric selected for use in the project was chosen based upon the results of hanging bag tests, a proposed ASTM standard for determining a material's potential to dewater in geotextile tubes. Hanging bag tests, performed by Infrastructure Alternatives in the spring of 2006, yielded favorable results for two geotextile fabrics, both of which were determined to be acceptable for use in this application. The tables below summarize the specifications of the two fabrics that were tested. (Geotextile tubes constructed of both fabrics were used in the performance of the project.)

Table 1. Circumferentially Seamed Geotextile Specifications[1]

Mechanical properties	Test method	Units	Minimum average roll value	
			Machine direction	Cross direction
Wide width tensile strength (at ultimate)	ASTM D 4595	lbs/in	400	550
Wide width tensile elongation	ASTM D 4595	%	20 (max.)	20 (max.)
Factory seam strength	ASTM D 4884	lbs/in	400	
Apparent opening size	ASTM D 4751	U.S. sieve #	40	
Water flow rate	ASTM D 4491	gpm/ft^2	20	
Weight/unit area	ASTM D 5261	oz/yd^2	17.3 (Typical value)	
UV resistance (% strength retained after 500 hrs)	ASTM D 4355	%	80	

[1]As provided by the manufacturer

Table 2. Horizontally Seamed Geotextile Specifications[1]

Properties	Test method	Units	Minimum average roll value
Tensile strength (grab)	ASTM D-4632	lbs	600 x 640
Elongation	ASTM D-4632	%	15 x 15
Wide width tensile	ASTM D-4595	lbs/ft	4800 x 7200
Wide width elongation	ASTM D-4595	%	14 x 9
Wide width tensile strength at 5% strain	ASTM D-4595	lbs/ft	1200 x 2640
Puncture	ASTM D-4833	lbs	260
Mullen burst	ASTM D-3786	psi	1200+
Trapezoidal tear	ASTM D-4533	lbs	250 x 300
UV resistance	ASTM D-4355	%	80
Apparent opening size	ASTM D-4751	US std. sieve #	40
Permittivity	ASTM D-4491	sec^{-1}	0.30
Water flow rate	ASTM D-4491	gpm/ft^2	20

[1]As provided by the manufacturer

The construction of the geotextile tubes was also important. Each tube had to have a sufficient number of regularly spaced fill ports to ensure that the tubes could be filled as evenly as possible. The placement of the fill ports also had to accommodate the geotextile tubes that would be stacked over them.

Geotextile tubes used in the project varied in circumference from 70 to 90 feet and had a maximum fill height of 8 feet. These large circumference tubes provide an additional 20 to 25% dewatering and storage capacity when compared to the smaller circumference tubes (45 to 60 feet in circumference) more commonly used in other hydraulic dredging projects. Yet, these large circumference tubes were still light enough to be handled easily by the heavy equipment in use on site. (Dewatering crews utilized an off-road forklift with telescoping boom and 10,000 lb. capacity to lift rolled geotextile tubes; 6-wheeled ATVs were then used to help unroll and slide the tubes into position.) The length of the geotextile tubes used for this project ranged from 80 to 275 feet, placed according to a very specific plan, in order to maximize every available cubic foot of capacity in the CF.

2.1.3 Geotextile Tube Layout Plan

The first objective of the geotextile tube layout plan was to deploy and fill the geotextile tubes of the bottom layer in such a way as to provide a level base for the upper layers. This was crucially important because the CF floor was sloped in order that the geotextile tube weep water would drain freely to the sump. In order to accomplish this objective, a number of specifically sized tubes were deployed in a specific arrangement.

As stated previously, the project plan called for stacking geotextile tubes in 10 layers over the floor of the CF. In order to create a stable base for the stack, the sloped floor of the CF had to be leveled. It was determined that partially filling the first layer of geotextile tubes provided the most cost effective means for accomplishing this objective. Two rows of geotextile tubes were placed parallel to the contour of the floor as Figure 2, below, illustrates. The two rows of tubes were filled with sediment slurry until the fill height at the center of each tube was approximately five feet. These "leveling" tubes were supported at the lowest point in the CF (the weep water sump) by a wedge of gravel, also shown in Figure 2.

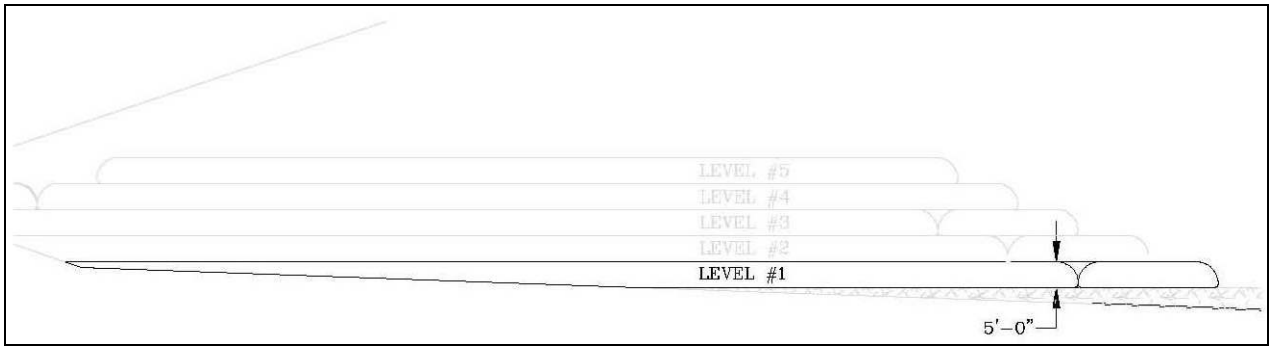

Figure 2. Cross section of the first layer of geotextile tubes, used to level the CF floor (the leveling layer).

Generally, the layout plan for each layer of geotextile tubes began with tubes being placed crosswise on either side of the "haul road," an open strip of real estate, running down the center of the CF. The haul road provided access to the end of geotextile tube farthest from the outer berm of the CF. The tubes were placed first at the end of the CF with the lowest elevation, to prevent the tubes from rolling or shifting out of place. This used gravity to our advantage, pulling each consecutive tube toward a stable, neighboring tube which was already full of dewatered sediment.

After three layers of tubes were filled, tubes were laid lengthwise down the haul road to fill in the space and bring the elevation of the road up to a height equal to that of the topmost layer of crosswise tubes. This pattern of three crosswise and then three lengthwise layers continued through the end of the project.

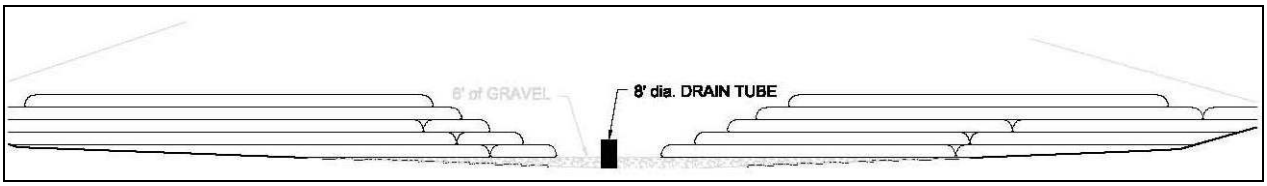

Figure 3. Cross-section of the CF, showing weep water sump (drain tube) and placement of the first five layers of tubes.

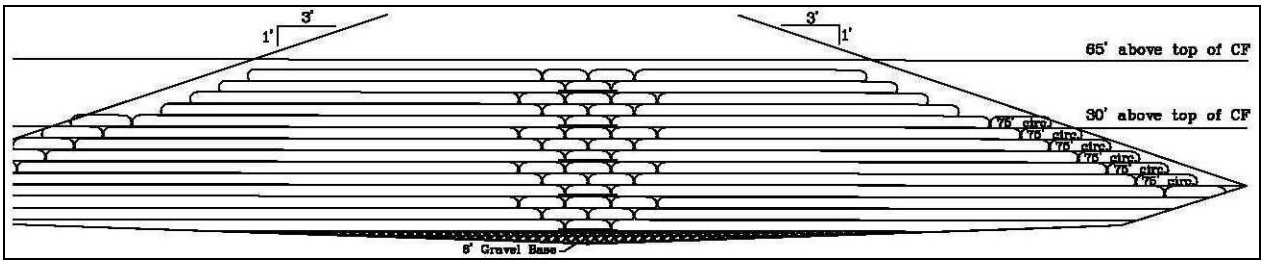

Figure 4. Cross-section of the CF, 140 feet north of the weep water sump, showing the first nine layers of tubes.

Geotextile tubes were also placed lengthwise around the perimeter of the CF; these tubes were referred to as "ring tubes." The purpose of the ring tubes was to contain any spills or sudden releases of contaminated sediment due to the failure of a geotextile tube or a leak in the header system and prevent sediment from flowing out of the CF.

2.1.4 Stacking Geotextile Tubes Ten Layers High

Prior to this project, as far as the contractors were aware, geotextile tubes had only been successfully stacked six layers high. As mentioned previously, the stacking plan devised for this project called for tubes to be stacked in ten layers. Several precautions were taken to ensure that the geotextile tubes in the lower layers did not suffer catastrophic structural failure under the weight of the tubes stacked on top of them. Two individual geotextile tube manufacturers were consulted on this point. It was universally agreed that the overriding control parameter for the stacking operation had to be the consolidation of the material contained in the geotextile tubes (the percent solids concentration of the dewatered material). If the dewatered material was returned to at least in-situ percent solids, the tubes could be stacked on and reasonably assumed to be able to withstand the weight of the upper layers pressing down. Hanging bag tests, an ASTM standard for determining the ability of geotextile tubes to dewater a particular material, confirmed that consolidation reaching in-situ percent solids could be achieved within a reasonable period of time in the geotextile tubes.

The placement of each geotextile tube within the CF and the order in which geotextile tubes were filled was also very important to the success of the stacking plan. Geotextile tubes were to be placed as tightly together as possible, with geotextile tubes placed first at the lowest elevation over the sloped floor of the CF. In this way, pressure would not only be exerted downward on the lower layers, but also from each side, either from a neighboring tube or from the wall of the CF itself.

To increase the stability of the entire stack, geotextile tubes were centered over the place where the sides of the two tubes beneath met and each geotextile tube was approximately 30 feet shorter in length than the tubes in the layer beneath. This gives the stack a pyramid shape.

Adhering to these operational strategies:

- not stacking before material inside the tubes was dewatered to in-situ percent solids,
- placing the tubes as close together as possible,
- centering stacked geotextile tubes over the seam between the two supporting tubes,
- shortening the length of the tubes in each consecutive layer,
- and placing geotextile tubes at the lowest elevation first

proved to be enough to prevent failure of the geotextile tubes of the lowest layers. Ten layers of geotextile tubes were achieved without a single tube failing due to the weight of the upper layers pressing down.

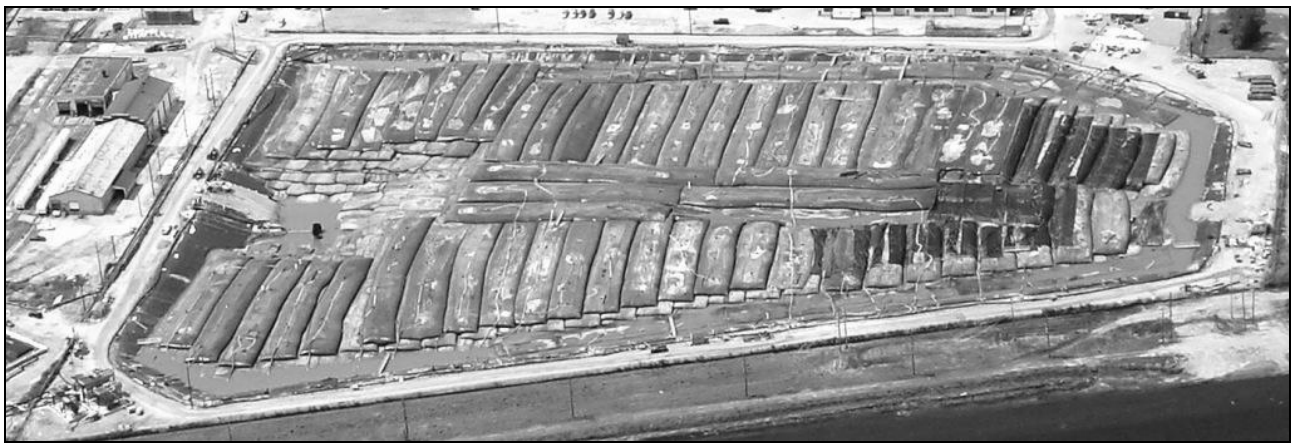

Figure 5. Aerial photograph of stacked geotextile tubes inside the CF (August 2007).

3. FIELD OPERATIONS

Operating a geotextile tube dewatering system of the scale utilized for the Ashtabula River Remediation required that contractors develop specialized operating procedures.

3.1 Chemical Conditioning

Chemical conditioning of the sediment slurry was necessary to ensure optimal solids capture within the geotextile tubes. To accomplish this, a combination of carefully selected primary coagulants and anionic polymers were injected into the sediment slurry as it flowed through the geotextile tube header system. A static mixer in the header system helped to provide the necessary turbulence to properly distribute the polymer throughout the sediment and flocculate the solid material.

Sediment characteristics such as percent solids and grain size changed frequently over the course of the project and required just as frequent adjustments to the dosage rate. Field personnel performed jar tests on site to determine the best chemical dosage for the sediment characteristics present at the time, and then entered the dosage rate into the chemical feed system controller. This controller used real-time flow and density readings from the sediment slurry pipeline to calculate and adjust the speed of the chemical feed pumps, so that the most accurate dose was provided.

3.2 Debris management

To minimize downtime due to plugs in the header system, plug valves and cleanouts were installed in the header system, which allowed sections of the pipeline to be isolated and flushed as needed to remove debris.

3.3 Deploying the geotextile tubes

Ten thousand pound capacity telehandlers with 56 foot vertical reach were used to deploy geotextile tubes on site, the largest of which weighed approximately 3,200 pounds. A telehandler was used to deliver a rolled tube from the staging area to the desired place in the CF. Then, the tube was suspended from the forks of the telehandler using high-tension straps. More straps were used to hook one end of the rolled tube to a 6-wheeled ATV, which then travelled forward, pulling and unrolling the geotextile tube as it went. After the tube had been fully unrolled, but before it was unfolded, dewatering personnel made any adjustments to the placement of the tube, working in teams to pull and slide the tube wherever it needed to go. Lastly, the tube was unfolded and piped into the header system, ready to receive flow.

3.4 Anchoring geotextile tubes to prevent gaps in the stack

Geotextile tubes were anchored in a variety of ways, which helped prevent gaps from forming between neighboring tubes. For example, if two geotextile tubes deployed side by side at the same time, the edges of the tubes closest together could be overlapped. As the first tube was filled, it would trap the edge of the neighboring tube beneath it and prevent that tube from moving when it was filled. This obviously would slightly reduce the capacity of the overlapped tube, but the snug tubes with zero gaps between them prevented further loss of capacity in higher levels. Tubes could also be tied together to keep them close.

If significant gaps or open areas did form in any layer of the stack of geotextile tubes, smaller “filler” tubes, 30 feet in circumference, were deployed in the open area and filled. These “filler” tubes made up for what would have been lost capacity in the CF and also helped make the stack more stable than if the gaps were allowed to remain.

3.5 Active dewatering

Physical means of encouraging the pores of the geotextile fabric to open and release more water quickly were utilized, including: sweeping the surface of the geotextile tubes with stiff-bristled brooms; slapping the tubes with smooth pieces of PVC; and vibrating the surface of the tubes using gas-powered vibratory plate compactors.

3.6 Tracking geotextile tube performance

The performance of individual geotextile tubes was tracked continuously by operators. Initial and final fill height of the each tube was measured using a laser level and the minutes “online” (receiving flow) and minutes “offline” (not receiving flow) were also noted. This information allowed operators on every shift to quickly ascertain the amount of remaining capacity left in each geotextile tube that was in use at that point in time. (As geotextile tubes become filled with dewatered material, their fill cycles become shorter and the period of time required for dewatering gets longer.)

3.7 Weep water drainage and downstream treatment

Weep water from the geotextile tubes flowed by gravity to a sump in the gravel wedge of the CF floor. The primary flow pattern was from around the exposed outer shell of each tube and channels formed by voids between adjacent tubes to the sump at the north end of the CF. Once the stacked tubes approached the perimeter to the CF, a significant amount of filtrate drainage occurred (by design) around the outer perimeter of the "ring" tubes to the sump. In the latter stages of the project, portable submersible pumps were deployed throughout the CF to help move weep water to the sump.

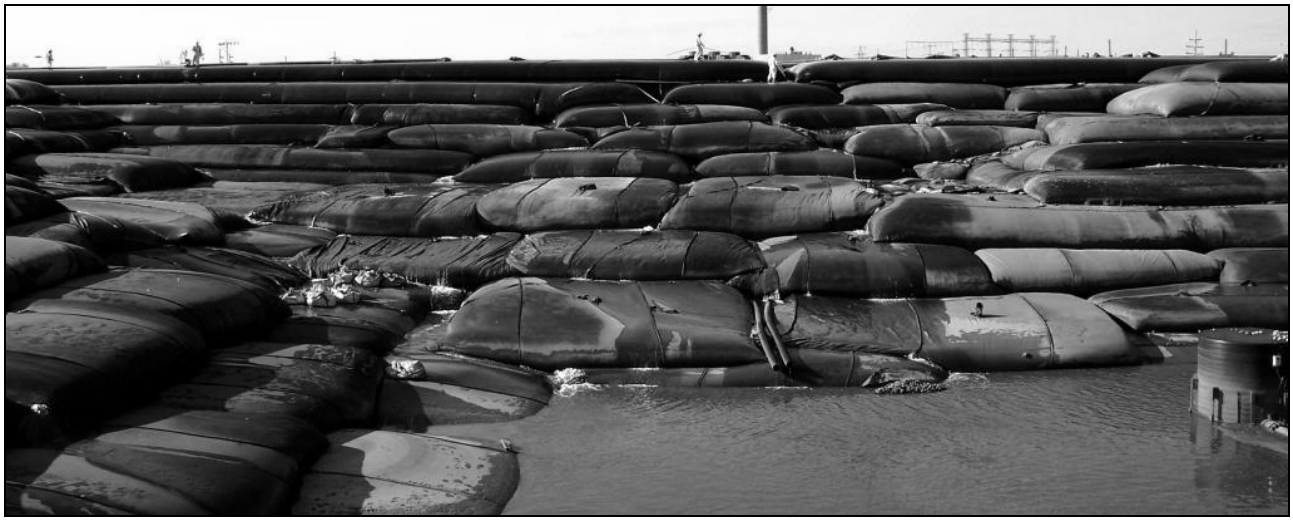

Figure 6. Photo of the CF, with sump in foreground, taken from the top of the surrounding berm (May 2008).

Weep water was pumped with self-priming, variable speed pump at rates of 1,000 to 5,000 gallons per minute (gpm) to the on-site water treatment plant. The first treatment units in the plant were five inclined plate separators, arranged in series, which removed suspended solids from the stream of weep water. The clarified water was then pumped through pressurized sand filters for polishing. Lastly, any remaining organic contaminants in the water were adsorbed in five sets of two Granular Activated Carbon (GAC) units, arranged in series (5 parallel streams with two units treating each stream). A pipeline, approximately three miles in length delivered the treated water back to the Ashtabula River for discharge, which was regulated under a National Pollutant Discharge Elimination System (NPDES) permit issued by Ohio Environmental Protection Agency (OEPA). Accumulated solids from the clarification and filtration processes were transferred back to the CF for final disposal.

3.8 Health and safety concerns

As one might imagine, the CF was full of health and safety hazards that had to be diligently analyzed and controlled to the best of the ability of the crews working there.

3.8.1 Contamination in the sediment slurry

Because of the contamination present in the sediment slurry, CF operations were regulated by OSHA under the Hazardous Waste Operations and Emergency Response (HAZWOPER) standard. All site personnel working inside the CF were required to be 40-hour HAZWOPER certified and also received Radiation Worker Level II training. Environmental monitoring in the CF included airborne dust and PCB monitoring, as well as background radiation level monitoring.

To protect their skin from contacting the PCB-contaminated sediment slurry, personnel were required to wear chemical-resistant coveralls, sealed with duct tape at the ankles to waterproof, steel-toe boots and sealed at the wrists to a double-layer of nitrile gloves. Normal job site personal protective equipment (PPE) such as hard hats, safety glasses, reflective safety vests were also required. And when standing water accumulated in the CF, personnel were required to wear Type V personal floatation devices. This amount of PPE greatly increased the risk of personnel developing heat related illnesses during the warm summer months and generally increased the amount of manpower needed to operate the

system. PPE was also cumbersome to crews who were required to spend their work day lifting and carrying heavy pipes and hoses, assembling and tearing down piping arrangements, and climbing up ramps and scaffolds to reach the top of the geotextile tubes.

3.8.2 Engulfment

Dewatering crews faced the very real risk of being engulfed in contaminated sediment slurry, if a geotextile tube or pipeline should suddenly fail. Several precautions were taken to prevent these situations from occurring:

1. Sediment slurry pipelines were inspected daily for leaks and signs of wear or stress and any leaks were repaired immediately upon discovery.
2. The fabric of each geotextile tube was inspected during initial deployment and daily thereafter; operators searched for flaws, tears, seam separations and weakened areas. Whenever damage to the fabric was found, it was repaired under the direction of the manufacturer or if the damage could not be fixed safely, the tube was taken out of service.
3. Geotextile tubes were also monitored very closely while they were being filled. Standard Operating Procedures for the site called for the tubes to be measured frequently as they approached the manufacturer's recommended maximum fill height. Tubes were never to be filled past the maximum fill height.

3.8.3 Slip, trip and fall hazards

Simple slip, trip and fall hazards were one of the biggest dangers to personal safety in the CF and absolutely, one of the hardest hazards to control because for the most part, they could not be avoided. For example, dewatering geotextile tubes are wet and very slippery to walk on, posing an extreme slip and fall hazard. However, in order for personnel to properly operate the geotextile tubes, they had to be able to observe the entire surface of the geotextile fabric. This required that personnel access the top of the geotextile tubes frequently throughout a work shift. To curb slips and falls from tubes, ramps and scaffolds were installed for personnel to use to access the top surface of the tubes and to walk from the top of one tube to another. In addition, the upper surface of each geotextile tube was flagged around the perimeter, about ten feet from the edge. Personnel were forbidden to walk or work beyond the flags.

Trip hazards and unsure footing were also everywhere in the CF, from the pipelines and hoses running from the perimeter of the CF to every tube inside it, to the sloped, sand-covered walls of the CF. Personnel were asked to paint or flag any places where footing was unsure or places where trip hazards existed. And of course, safety shoes with non-skid soles were also required for all personnel working in the CF. Light plants also helped to make slip/trip/fall hazards easier to see during poor weather and at night.

Figure 7. Ramps and stairways constructed to allow personnel safe access to the top of the stacked tubes (May 2008).

4. CONCLUSIONS

The application of geotextile tube dewatering in the Ashtabula River Remediation must be judged as an overall success. Although the project suffered many challenges, the end result was that the 640,000 cubic yards of contaminated sediment that had been choking the life out of the lower Ashtabula River were removed from the ecosystem and disposed of in a cost effective and environmentally sound way.

ACKNOWLEDGEMENTS

Mr. Stan Baker, Project Manager, de maximis, inc.
Mr. Brent Cardwell, Site Superintendent, Infrastructure Alternatives, Inc.
Ms. Sara Klotz, E.I.T., Infrastructure Alternatives, Inc.
Ms. Amber Wilson, Operations Specialist, Infrastructure Alternatives, Inc.
Mr. Aaron Wright, Dredging Manager, Infrastructure Alternatives, Inc.

REFERENCES

Ptak, et al. "Ashtabula River on Road to Recovery." United States Army Corps of Engineers Buffalo District. 20 Jun. 2008. http://www.lrb.usace.army.mil/

Geosynthetics 2009
February 25-27 2009, Salt Lake City, Utah

Geotextile Permeability Testing - A Primer for Technicians and Engineers

R.S. Lacey, TRI Environmental, Inc., Austin Texas, U.S.A.

ABSTRACT
There are a number of published standard test procedures that are currently in use around the world for determining the permeability of geotextiles perpendicular to their plane of manufacture. These test methods are similar in that they are based on the same principle of fluid flow through a porous media. They differ, however, in their application of this theory to their techniques for defining, measuring and reporting the test results. This paper is a comparative examination of three international testing standards for determining the geotextile permeability.

1. INTRODUCTION

Testing geotextiles for water permeability perpendicular to the plane of the material is both a science and an art. The science is basic fluid mechanics. The art is in harmonizing the science with the perceptions and practices unique both to the guiding standard and the intended use of the test results.

Scientists around the world have developed standard procedures for determining the permeability of geotextiles. These include the ASTM International ASTM D 4491, “Standard Test Methods for Water Permeability of Geotextiles by Permittivity”, the International Organization for Standardization ISO 11058, “Determination of Water Permeability Characteristics Normal to the Plane, Without Load”, and the Standards Australia International AS 3706.9, “Determination of Permittivity, Permeability and Flow Rate”. In addition to having the term “permeability” in the title, these test methods are similar in that they are based on the same principle of fluid flow through a porous media. They are dramatically different however, in their application of this theory to their techniques for defining, measuring and reporting the test parameters.

This paper is a review of the fundamental fluid mechanics theory, followed by an examination of each of the three international testing standards for geotextile permeability and a summary comparison of the various test method attributes.

2. THE SCIENCE OF GEOTEXTILE PERMEABILITY TESTING - DARCY’S LAW

The intent of a permeability test is to define the quantity of water per unit time per unit area that will pass through a material, given the pressure head, in terms of a property of the material. There is a relationship for fluid flow through a porous media, referred to in fluid mechanics references as “Darcy’s Law”. This theory states that, for a saturated porous media, the total discharge, Q_t is equal to the product of the intrinsic permeability of the medium κ, the cross-sectional area of the flow, and the pressure head differential driving the flow, $P_1 - P_2$, all divided by the dynamic viscosity μ, and the length L over which the pressure differential acts:

$$Q_t = \kappa A(P_1 - P_2))/\mu L \qquad [1]$$

Where:
Q_t = Flow rate, m^3/s
κ = Intrinsic Permeability, m^2
$(P_1 - P_2)$ = Pressure Differential, Pa or N/m^2
μ = Dynamic Viscosity, Pa·s
L = Length of flow, m

The pressure head differential, $P_1 - P_2$, can be converted from units of Pa (N/m^2) to an equivalent height in meters of the fluid under test, Δh. This is referred to in all three standards as the “head loss”.

$$\Delta h = (P_1 - P_2)/\gamma \qquad [2]$$

Where:

γ = Unit Weight of fluid, N/m^3

Combining the variable representing the intrinsic permeability, κ, with the dynamic viscosity of water, μ, and with the unit weight of water, γ, results in a single variable "k", commonly referred to in geotechnics as the hydraulic conductivity or coefficient of permeability, the equation becomes:

$$Q_t = kA\Delta h/L \qquad [3]$$

In the context of geotextile permeability testing, the thickness of the geotextile, L, is an additional factor that would unnecessarily complicate the variability of the test results. This factor is removed from the equation by defining the variable referred to as the "permittivity", ψ:

$$\text{Permittivity, } \psi = k/L \qquad [4]$$

The equation for the geotextile permeability test further reduces to:

$$Q_t = \psi \Delta h A \qquad [5]$$

Rearranging:

$$\psi = Q_t/\Delta h A \qquad [6]$$

Inserting these variables into the schematic of a geotextile permeability test:

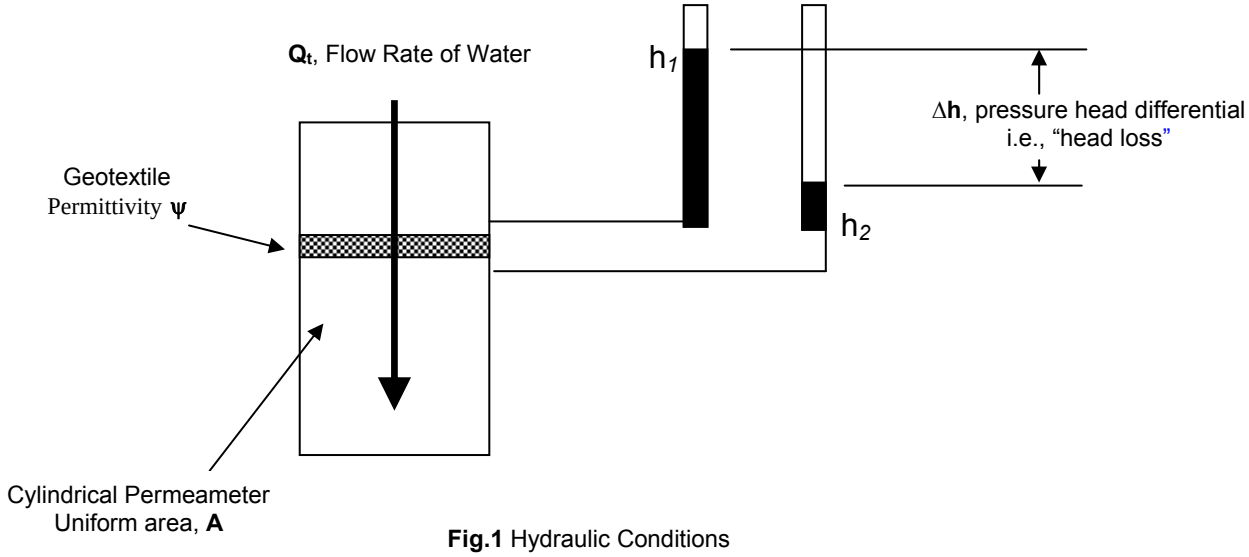

Fig.1 Hydraulic Conditions
Geotextile Permeability Test

These conditions apply to both the constant and falling head test procedures. The equation applies directly to the constant head test, as the head loss remains constant during the test. For the falling head test, the head loss is decreasing with time. The permittivity is calculated from the solution of the integral of the function $d\Delta h = (Q_t/a)\,dt$, where a is the area of the upper standpipe above the specimen. That is, the distance the pressure head differential Δh drops in time dt is equal to the flow rate at that time divided by the area of the upper standpipe, a. Substituting Eg.5 above for Q_t:

$$d\Delta h = (\Delta h \psi A/a)dt \qquad [7]$$

$$d\Delta h/\Delta h = A/a\ \psi\ dt \qquad [8]$$

Integrating: $$\int_{h2}^{h1} d\Delta h / \Delta h = (\psi A/a)\int_{t=t}^{t=0} dt \quad [9]$$

$$\ln(\Delta h_1/\Delta h_2) = (\psi\, A/a)t \quad [10]$$

Rearranging: $$\psi = a\ln(\Delta h_1/\Delta h_2)/At \quad [11]$$

This gives us the equation, Eq.11, for calculating the permittivity for the falling head test conditions.

3. LAMINAR AND TURBULENT FLOW

In order for the theory to remain valid, the equations Eq.6 and 11 should return the same permittivity value for every Q_t and h value during the execution of the tests, that is, the plot of Q versus Δh must be linear. However, if we plot this data for a typical 16 oz/sy nonwoven geotextile material, the following plot is generated during the test.

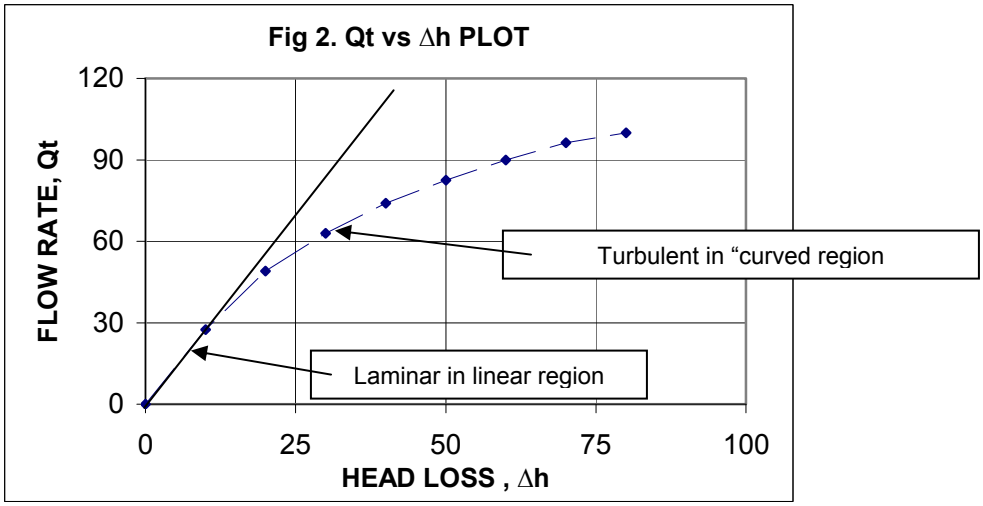

This "curved" flow rate versus head loss behavior is attributed to turbulent flow conditions. In Fig. 2 above, the flow is initially considered laminar. This is where the streamlines, i.e., water trajectory paths, remain approximately parallel with the direction of flow. At a pressure head of approximately 15 mm, the flow rate versus head loss plot curves below the initial straight line segment. This is where the streamlines become chaotic, there are additional energy losses due to mixing, and Darcy's Law is no longer valid.

Theoretically then, the test to determine a geotextile's permittivity should always be performed in the laminar region. While this is clearly addressed in all three standards, each provides a mechanism to test and report data for tests performed outside of the laminar region.

4. ASTM INTERNATIONAL ASTM D 4491

The intent of this standard is to determine the index property defined in the previous section as "Permittivity" at a pressure head of 50-mm. There are two procedures; constant head and falling head. The constant head test is performed with a 50-mm head loss. The permittivity is calculated for the constant head test as follows:

$$\psi, \text{sec}^{-1} = Q_t R_t / \Delta h A \quad [12]$$

Where R_t is the temperature correction factor.

The falling head test is performed with a falling head - constant tail approach, measuring the time for the head loss to fall from 80-mm to 20-mm. The permittivity is calculated for the falling head test as follows:

$$\psi, \sec^{-1} = 1.386 a R_t / At \quad [13]$$

The constant head test procedure includes a step where, after the first specimen is tested a with a 50-mm head loss, the same specimen is then tested starting with a constant head of 10-mm, then increasing the head in 5-mm increments. This data is used to define the laminar region. If the 50-mm results plot outside of the laminar region, the specimen is retested with a head loss value in the mid-region of laminar flow segment. However, the industry practice for routine manufacturing quality control and conformance testing is to determine the permittivity with the 50-mm head loss and explicitly note this on the test report.

The geotextile "nominal coefficient of permeability" is also potentially a result of this test method. The standard states in the "Significance and Use" section, that the nominal geotextile thickness be obtained in accordance with ASTM D 5199 and multiplied by the permittivity test result. The industry practice however, is to measure the thickness of each individual test specimen prior to testing. The thickness gage has a 56-mm diameter (2,462 mm^2 contact area) presser foot applying 2.0 kPa contact pressure. The coefficient of permeability is calculated as follows:

$$k, cm/s = \psi \times t \quad [14]$$

A third result is often requested from this method, although there is no algorithm for it in the standard. This is the frequent practice in the industry to specify a required flow rate per unit area, typically in gpm/ft^2 for a geotextile. This result is calculated from the permittivity result determined with a 50-mm head loss.

$$Q_{\Delta h50}, gpm/\ ft^2 = 74.8\psi \quad [15]$$

INTERNATIONAL ORGANIZATION FOR STANDARDIZATION ISO 11058

The intent of this standard is to determine the property defined as the "Velocity Index", V_{H50}, which is the flow velocity at a head loss of 50-mm. There are two procedures; constant and falling head, both of which include a temperature correction for water at 20° C. The constant head procedure is essentially identical to the ASTM procedure described above and measures the parameter directly with the following algorithm for a constant head loss of 50-mm:

$$V_{H50}, m/s = Q_t R_t / A \quad [16]$$

The falling head procedure is markedly different, employing a falling head – rising tail approach with a "U-tube" type apparatus and measuring water level versus time with a continuous reading, analogue recording device or by computer acquisition. This procedure allows for either a weighing-cell method or a pressure gauge method, both of which measure the change in the height of the water column on the inflow side of the specimen. At least five data points are collected over the duration of the test. The velocity of the flow at each point is calculated based on the following equation:

$$v_{20}, m/s = (h_u - h_l) R_t / t \quad [17]$$

Where:
V_{20} = average flow velocity between two water levels, h_U and h_L
h_U-h_L = distance between the two water levels
R_t = the temperature correction factor
t = the time between the two water levels

The average head loss between the two water level points is calculated with:

$$\text{Ave } \Delta h = h_u + h_l - 2h_0 \quad [18]$$

Where h_0 is the final equilibrium water level, i.e., h at v = 0.

The velocity calculated from Eq.17 is plotted versus the average head loss with a best fit quadratic curve. The velocity at 50 mm of head loss is determined directly from this head loss versus velocity plot.

5. STANDARDS AUSTRALIA INTERNATIONAL AS 3706.9

The intent of this standard is to determine the Permittivity, Permeability and Flow Rate of the geotextile with a series of constant head tests. Each of five specimens are tested using five flow rates each; at least two with velocities less than 0.010 m/s, and at least one between 0.01 m/s and 0.035 m/s. The remaining two can be at convenient flow rates that complete the plot of the flow rate versus head loss.

This test method allows for more than one specimen to be layered together in order to achieve the desired flow velocities at measurable head losses. There is a note, however, cautioning that "significant discrepancies may be observed in some types of woven fabrics".

The equation for calculating the permittivity is:

$$\psi, \sec^{-1} = Q_t n / \Delta h A \tag{19}$$

Where n is the number of layers of geotextile in the test.

The temperature correction factor is not explicitly included in the equation, although there is a note that states; "If temperature corrections are to be made, see AS 1289.6.7.1".

When the flow rate versus head loss plot is non-linear, the desired parameter is determined based on either a 10-mm or a 50-mm head loss. This note suggests that the Australian standard might be addressing the precedence established explicitly in the ISO test method, and implicitly by the industry practice for the ASTM method, to use measurements at a head loss of 50-mm for routine conformance testing.

The coefficient of permeability is calculated based on geotextile thicknesses measured on specimens before testing using AS 3706.1. The thickness gage described in this standard has a required contact area of 2000 mm^2 applying 2.0 kPa contact pressure.

The flow rate results are reported in terms of "Q100", which is the flow rate per unit area, in liters per second per square meter, converted from the data calculated in Eq.17 to a head loss of 100-mm. There is a precautionary note that the Q100 value is only an approximation for tests where the velocity exceeds 0.035 m/s at 100-mm head loss.

$$Q100, liters/s/m^2 = 100\psi \tag{20}$$

6. COMPARATIVE SUMMARY

Occasionally, it is necessary to compare test results obtained with the different standards. For routine conformance testing, the results from the ASTM 4491 and the ISO 11058 should be virtually equivalent. For example, if there is a test results from ASTM D 4491 of 2.0 sec-1, the ISO result would be:

$$V_{H50}, m/s = 0.050\psi \tag{21}$$

$$V_{H50} = 0.10 m/s$$

However, there may not be a direct conversion between the AS test result and either the ASTM or the ISO methods, unless the geotextile under test exhibited laminar behavior at the 50-mm head loss flow rate, which is unlikely, or unless the AS test was performed with the 50-mm head loss condition.

The following table is presented as a comparison of the various testing attributes of the three test methods. The most critical of these, with regard to differences in the test results, is the actual head loss where the values are measured.

COMPARISON OF PERMITTIVITY TEST METHODS

Attribute	ASTM 4491	ISO 11058	AS 3706.9
Method	Constant Head or Falling Head	Constant Head or Falling Head Rising Tail	Constant Head Only
Conventional Test Result, units (Notes)	Permittivity at 50-mm Head, ψ , sec-1 (Measured at 50-mm; laminar region undefined unless explicitly requested)	Velocity Index, V_{H50}, m/s (Measured at 50-mm; laminar region undefined unless explicitly requested)	Flow Rate converted to 100-mm head, Q100, liters/s/m^2 (Calculated based on permittivity determined in laminar region.)
Test Temp	Not specified	18° C- 22° C	Not specified
Temperature Correction	Yes	Yes-Annex A	Yes –Measure and record temp and correct if necessary per AS 1289.6.7.1
Specimens	4	5 –NOTE: Determine number of specimens per ISO 2854 if necessary.	5 - Perform additional tests if coefficient of variation exceeds 20%
No. of Specimens each determination	1	1	More than one specimen can be layered together. Precaution for layering woven geotextiles.
No. Readings per Specimen	5	5 Constant Head 1 Continuous record per specimen for Falling Head	5
De-aired Water	Yes 6 mg/L Dissolved Oxygen Content	Yes 10 mg/L Dissolved Oxygen Content	Yes 6 mg/L Dissolved Oxygen Content
Filtered Water	No	Yes-shall be filtered…	Yes-If de-aired water is not available, filtered water is recommended
Removal of Air Bubbles Accumulating in or on the Specimen	Yes- Apply vacuum just above the specimen before testing.	No –Not explicitly. Precautions regarding air bubbles which can be entrapped in the geotextile	No - Not explicitly. Precautions if bubbles accumulate on specimen and include note in report
Open Manometers used for Head Measurements	Yes – Open manometers.	No- Pressure transducers implied by the 0.2-mm accuracy requirement.	Yes-Inclined alcohol manometer for small head losses
Perform tests in “laminar” region	Yes- Determine the laminar range and retest in mid-region if <50mm. (NOTE: Industry practice is to test and report results for a 50-mm head loss.)	50-mm Head Loss Only - Except when full permeability characteristics are being measured.	Yes – Except when the plot of flow rate versus head loss is curved, then report the permittivity values for either the 10-mm or the 50-mm head loss measurements.
Specimen Support Screen	No	Yes	Yes-Note suggesting a grid may be used for woven textiles
Specimen Pre-soaking	Yes - 2 hours In de-aired water	Yes - 12 hours in wetting agent	Yes – “Wet Conditioned” - wetting agent
Operator Check	Yes - #200 U.S. Sieve screen must have ψ of 5.0±1.3 sec^{-1}.	No	Indirect – statistical review of acceptable limits of error.
Apparatus Head Losses Addressed?	Yes – Calibration curve of flow rate versus head loss is required.	Yes –Apparatus head losses including support screen must be less than 1-mm.	Yes – Subtract head loss inherent in the apparatus including support screen.
Measurement Method for Constant Head tests	The flow rate measurement equipment is not described.	Volumetric – accuracy of ±10 ml. Collect a minimum of 1 liter and the collection time should be 30 s minimum. Alternative- Flow meter with±5% accuracy.	Flow meter is preferred. Alternative - a container, timer and weighing apparatus for water. The required accuracy is not specified for either method.
Test Method Precision Statement	Yes – Precision data indicates wide variation between methods for woven geotextile.	No	No

REFERENCES

ASTM D 4491 (2004) Standard Test Methods for Water Permeability of Geotextiles by Permittivity, *ASTM International*, West Conshohocken, Pennsylvania, USA.

ISO 11058 (1999) Geotextiles and Geotextile-Related Products -- Determination of Water Permeability Characteristics Normal to the Plane, Without Load, *International Organization for Standardization*, Geneva, Switzerland

AS 3706.9 (2001) Geotextiles – Method of Test – Determination of Permittivity, Permeability and Flow Rate, *Standards Australia International, LTD*, Sydney, Australia.

Geosynthetics 2009
February 25-27 2009, Salt Lake City, Utah

Retention Capacity of Geotextile Filters in Cyclic Flow

A. Srikongsri, Univ. of British Columbia, Canada
E.J. Fannin, Univ. of British Columbia, Canada

ABSTRACT
Filtration compatibility data are presented for combinations of five woven and four nonwoven geotextiles tested against six cohesionless soils in a cyclic Gradient Ratio test device. A multistage test procedure was developed to control three test variables, namely the confining stress, the hydraulic gradient and the period of flow reversal. Evaluation of retention capacity of the geotextiles is based primarily on variation of water head across the soil-geotextile interface and mass of soil loss through the geotextile. Implications of the test data are discussed with respect to engineering specification of geotextiles in cyclic flow applications.

1. INTRODUCTION

In contrast to unidirectional seepage flow in routine filter applications, where there is a longstanding body of knowledge on use of geotextiles that is based on considerable field experience and many laboratory studies, the issue of bidirectional, reversing or cyclic flow is one for which our current understanding is very much limited (Fannin, 2006). These flow conditions are involved in provision of filters for protection or control of base soil erosion in estuarine and coastal environments. The performance of a geotextile filter in these applications, and in particular the retention capacity, is typically described with reference to simplified ratios of indicative particle size of the base soil to opening size of the geotextile, which are reported as empirical rules for purposes of design. In the absence of a standardized test method for cyclic flow applications, and given a paucity of appropriate field monitoring and laboratory experimental data, there is uncertainty surrounding the confidence with which the design rules may be used in practice.

Notable laboratory studies on the nature of soil-geotextile compatibility in cyclic flow include those of Cazzuffi et al., 1999; Chew et al., 2000; Hameiri, 2000; Fannin and Pishe, 2001; Hawley, 2001; Hameiri and Fannin, 2002; and Chen et al., 2008. Although our understanding of filtration behavior in cyclic flow has advanced as a result of these studies, it is not yet sufficient to provide for confident recommendations in engineering practice.

Fannin and Srikongsri (2007) provided a critical review of geotextile behavior in cyclic filtration experimental studies, with emphasis on governing factors and design criteria. Three factors, namely wave period, the hydraulic gradient and the confining stress were found to significantly influence compatibility of soil-geotextile filter. Mass loss per unit area and the value of gradient ratio were confirmed as useful indices for interpretation of test results. In this paper, the influence of those factors is examined over a broad variation of AOS/D_{85}, using test data from a newly proposed multistage test procedure. Implications of the laboratory results are then considered for use of empirical design rules in engineering practice.

2. CYCLIC FILTRATION TEST DEVICE

A cyclic Gradient Ratio (CGR) test device was developed at the University of British Columbia (Hameiri, 2000; Hameiri and Fannin, 2002) from experience gained in modifying the ASTM gradient ratio test device (Fannin et al., 1996) to more precisely characterize changes in water head distribution in base soil immediately adjacent to the geotextile. The device comprises a permeameter, collector trough, axial loading system, and hydraulic control system (Fig. 1).

Permeameter: The rigid-wall permeameter is made of Plexiglas to permit observations of the soil specimen during testing. These visual observations prove valuable for interpretation of test behavior, especially for cases of piping or clogging of the geotextile. The permeameter accommodates a cylindrical soil specimen of diameter and length approximately 100 mm. Four ports located on the wall of the permeameter (Port numbers 2, 3, 5, and 6), together with an additional port located above and below the sample (Port numbers 1 and 7), are used to define the distribution of water head. Ports 2, 3, 5 and 6 are located at 88 mm, 75 mm, 25 mm and 8 mm above the geotextile (see Fig. 2). Earlier use of a Port 4 location between that of 5 and 6 is now discontinued, because the measurement provided redundant.

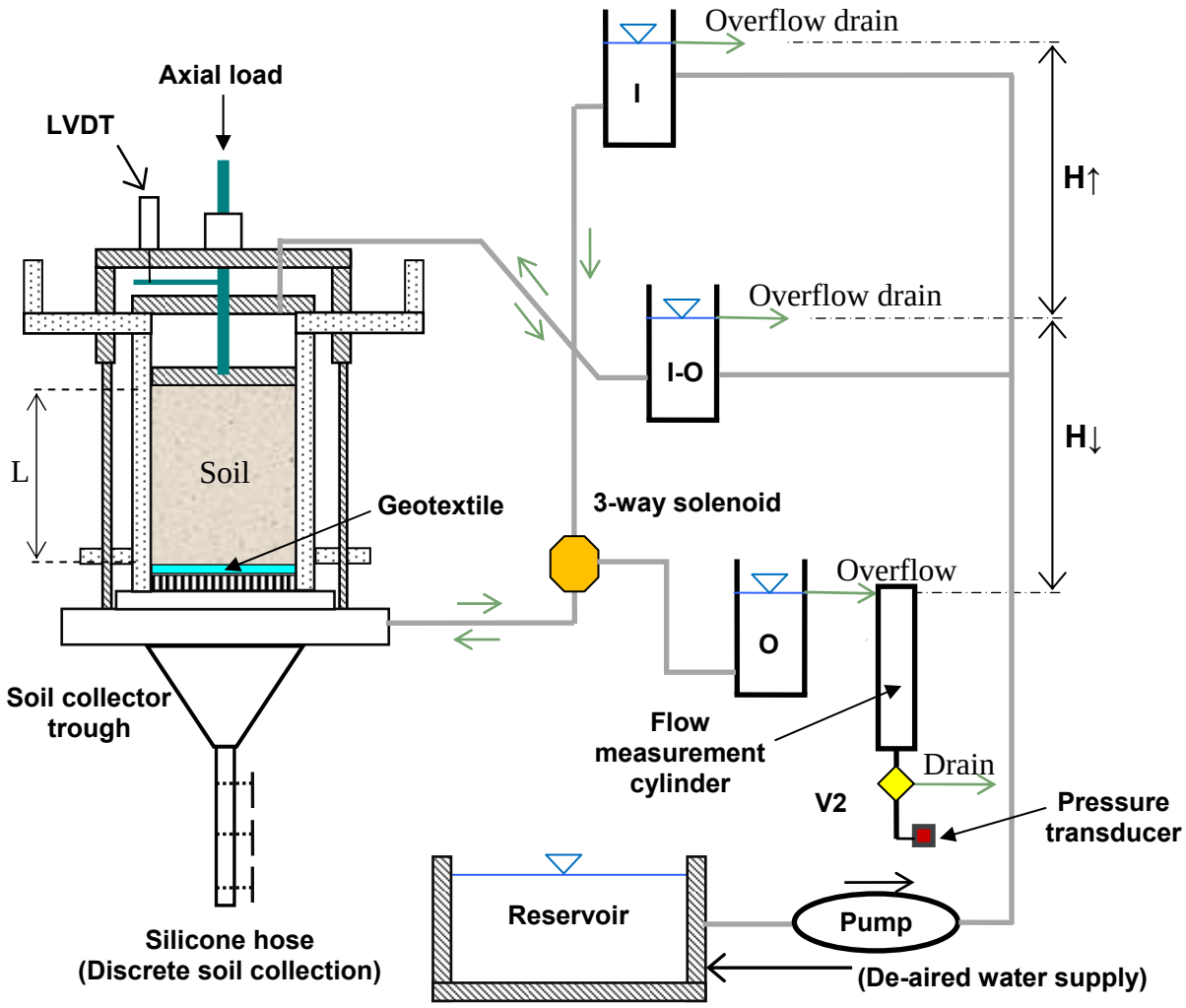

Figure 1. System configuration of Cyclic Gradient Ratio test device

The gradient ratio value is defined by the ratio of the hydraulic gradient in the soil-geotextile composite (i_{sg}) to that in the soil (i_s), where with reference to ports 3, 5, and 7:

$$GR_{ASTM} = i_{sg}/i_s = i_{57}/i_{35} \quad [1]$$

and a modified value based on an additional port number 6, can be expressed as:

$$GR_{MOD} = i_{sg}/i_s = i_{67}/i_{35} \quad [2]$$

Collector Trough: A conical trough mounts below the permeameter and connects to a flexible silicon tube. Particles of soil lost from the specimen that pass through the geotextile are collected in this trough, and settle in the hose. A series of discrete samples may be collected during sample preparation and testing by clamping the hose at various intervals. Upon termination of the test, the tube is removed and the samples extracted for analysis.

Axial Loading System: Vertical stress is applied pneumatically to the top of the sample. The load is transmitted to a loading plate through a piston (see Fig.1). The maximum value of effective stress applied to the specimen in the test program is 50 kPa.

Top and Bottom Boundaries: A geotextile is placed above and below the reconstituted soil specimen. The lower geotextile, which is the test specimen under examination, seats on a wire mesh which in turn is supported by a bottom

plate having 6 mm holes perforated in a triangular pattern with a clearance of 1.5 mm. A double layer nonwoven geotextile specimen is incorporated within the top loading plate, to protect against upward soil migration during periods of reversing flow. The permeameter is sealed by a rigid top plate, on which Port 1 is located.

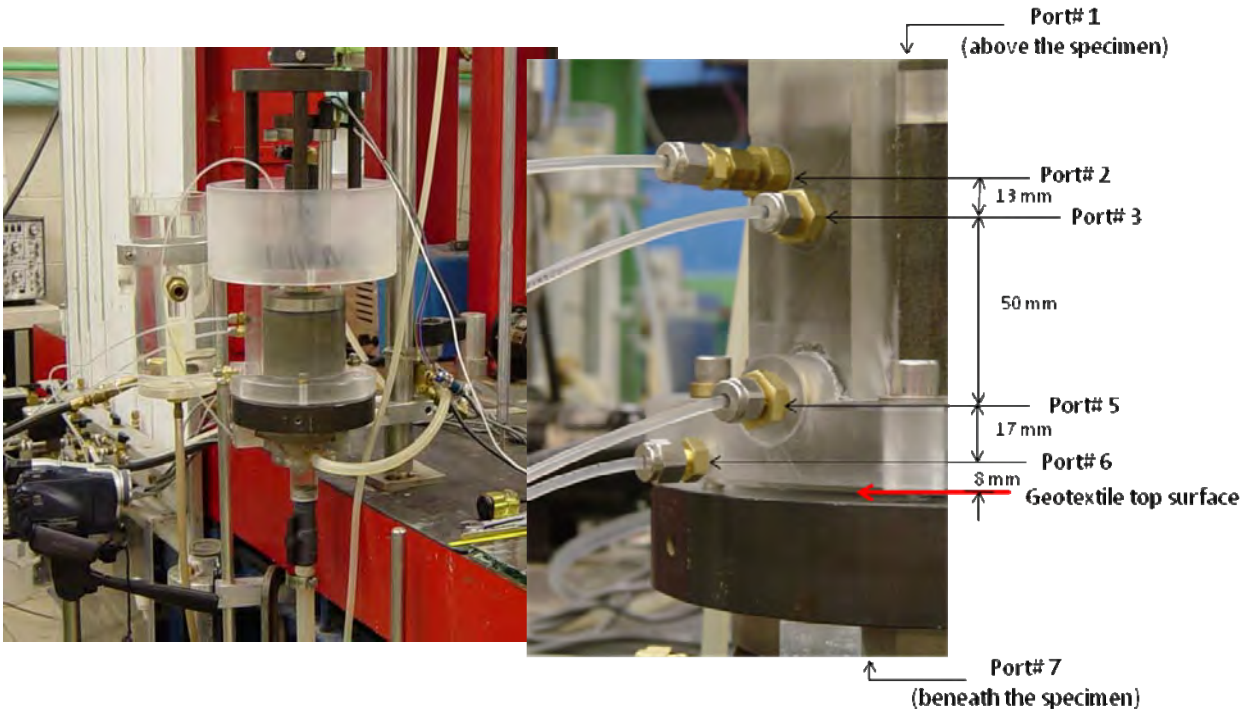

Figure 2. Permeameter cell and port arrangement on the side wall

Hydraulic Control System: The principle of operation is that of head control, by means of three constant-head tanks (see Fig.1), termed the inflow (I) tank, the inflow-outflow (I-O) tank, and the outflow (O) tank. They are supplied directly with de-aired water from a reservoir, by a peristaltic pump. Overflow discharge from all three of these tanks is drained away. Unidirectional downward seepage occurs through the permeameter with flow control from the I-O tank to the O tank. Unidirectional upward seepage occurs with flow control from the I to the I-O tank. A switching operation invokes the reversal of flow, whereby a computer-controlled 3-way solenoid valve is set either to receive flow from the inlet tank or direct flow to the outlet tank. For a given specimen length (L), the imposed hydraulic gradient is controlled by the equidistant spacing (H) of the three tanks.

Instrumentation: Filtration compatibility is evaluated with reference to the distribution of water head across the interface of the reconstituted soil and geotextile specimen. The variation in water head between each port (h12, h23, h35, h56, and h67) is measured with differential pressure transducers. These transducers are better-suited to the measurement of transient pore water pressures than the alternative of manometer tubes. Flow rate is calculated using the volumetric discharge from the outflow (O) tank, which monitors both unidirectional flow and the downward component of reversing flow (I-O tank to O-tank). Discharge is deduced from records of a total pressure transducer mounted below the outflow measurement tank (M). The tank is emptied periodically under the control of a solenoid valve (V2). Additionally, the specimen length is monitored with an LVDT, and the applied normal stress on the top of the specimen is deduced from measurement of axial load.

3. TEST MATERIALS

3.1 Soils

Grain size distribution curves for six soils are reported in Fig. 3. Two soils used by Hawley (2001) are a Fraser River Sand (FRS) and a Mine Waste Tailings (MWT) having a D_{85} of 0.33mm and 0.29 mm, respectively. The FRS is uniform sand with a C_u of 1.8 and the MWT has a C_u of 3.3. The four soils A, B, C and D tested in the current study are produced by sieving: Soil A (D_{85} = 0.18, C_u = 1.6) and soil B (D_{85} = 0.15 mm, C_u = 1.6) are derived from the FRS; soil C (D_{85} = 0.11

mm, C_u = 1.6) and soil D (D_{85} = 0.08 mm, C_u = 1.6) are derived from a naturally occurring silty sand. Soils A, B, and FRS are poorly graded sand (SP). The Mine Waste Tailing is poorly graded sand with silt (SP-SM). The soils C and D are silty sand (SM) and sandy silt (ML), respectively. All gradation curves are internally stable, according to the method of Kenney and Lau (1985), see also Li and Fannin (2008).

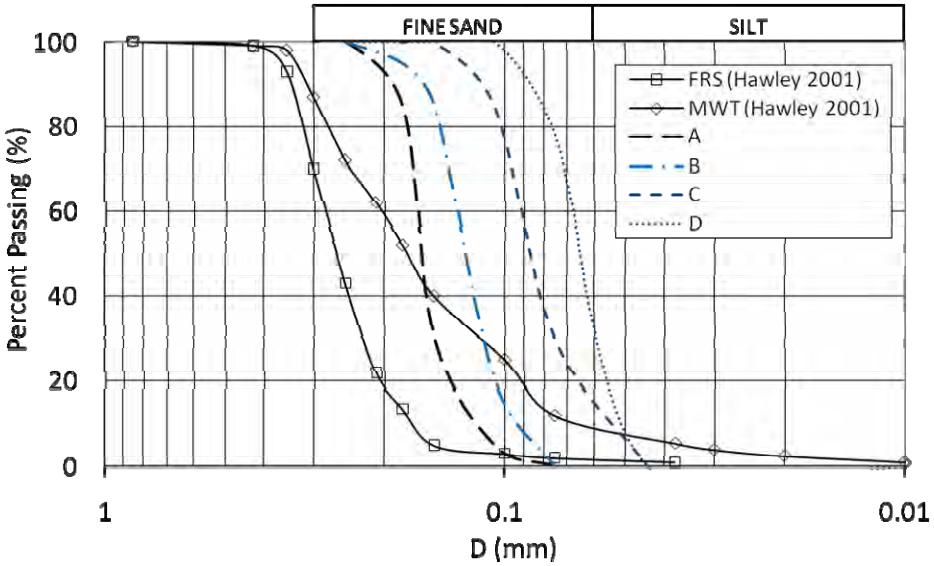

Figure 3. Soil gradations tested in cyclic flow

3.2 Geotextiles

Nine geotextiles have been examined testing: five geotextiles are woven and four are needle-punched nonwoven (see Table 1). The Apparent Opening Size (AOS) varies from 0.18 mm to 0.60 mm.

Table 1 Properties of tested geotextiles

Woven geotextile			Nonwoven geotextile		
Code	Mass/unit area (g/m^2)	AOS (mm)	Code	Mass/unit area (g/m^2)	AOS (mm)
F700	190	0.212	T65	285	0.180
F500	170	0.300	180N	278	0.180
F404	282	0.425	140N	287	0.212
F402	304	0.425	160N	185	0.212
H570	453	0.600			

4. TEST METHODOLOGY

4.1 Test programs

In order to characterize a ratio of indicative particle size to characteristic opening size of the geotextile that governs capacity for soil retention, test combinations of soil and geotextile are selected based on values of AOS/D_{85} that bound those recommended in design guides (for example, Holtz et al. 1997). In the work of Hawley (2001), cyclic Gradient Ratio tests were performed at values of AOS/D_{85} ranging between 0.6 and 2.1, in a total of 15 tests. In the current study, the range was increased to AOS/D_{85} = 2.8, in a total of 17 tests reported herein. A summary of the two companion test programs is given in Table 2.

Table 2 Test combinations of AOS/D_{85} (and number of tests)

UBC (Hawley, 2001)			UBC (Current study)				
Geotextile	Soil		Geotextile	Soil			
	FRS	MWT		A	B	C	D
140N	0.6 (1)	0.7 (1)	T65	1.0 (1)		1.7 (1)	2.25 (2)
160N	0.6 (2)	0.7 (1)	180N			1.7 (1)	
F700	0.6 (1)	0.7 (1)	F700	1.18 (2)	1.4 (2)		2.65 (2)
F500	0.9 (1)	1.0 (1)	F500		2.0 (2)	2.83 (4)	
F404	1.3 (1)	1.5 (1)					
F402	1.3 (1)	1.5 (1)					
H570	1.8 (1)	2.1 (1)					

4.2 Test preparation

Important steps in the preparation for testing involve saturation of the soil and the geotextile, and placement of the soil in the permeameter. The soil and the geotextile are saturated by boiling and allowing them to cool at room temperature, under a vacuum, for a minimum of 12 hr. A water pluviation technique is employed for placement of uniformly graded soils (Fannin et al., 1994).

4.3 Test procedure

A multistage test procedure was developed to examine soil-geotextile compatibility under controlled test variables in cyclic flow test (see Table 3). Of most importance is that each stage of cyclic flow is followed by a companion stage of unidirectional flow stage – this companion stage is used to characterize the post-cyclic nature of the soil-geotextile interface and also to check the specimen integrity before imposing the next stage of cyclic flow.

All test combinations of Hawley (2001), see Table 2, were performed using this multi-stage test procedure at a hydraulic gradient i = 4. In the current phase of study, the multistage test procedure has been revised slightly to examine the influence of three test variables (confining stress, hydraulic gradient and period of flow reversal). The rationale for choosing the magnitudes of each test variable is based on simulation of bank or shore protection structures that experience a low confining stress, and may be subject to a wide range of wave periods. A wave period shorter than T= 10 s is deemed ‘fast’ reversing flow and recommended for simulation of wave action, while longer periods are deemed ‘slow’ reversing flow typical of tidal environments (Fannin and Srikongsri, 2007). Giroud (1996) suggests a typical hydraulic gradient of i = 10 for shoreline protection. Accordingly, each test of the current study examines three confining stresses (σ = 50 kPa, 25 kPa and 5 kPa) two wave periods (T = 6 s and 60 s), and three hydraulic gradients (i = 1, 5 and 9). For a test at any constant wave period in cyclic flow, the test procedure comprises of total of 7 stages (see Table 4), namely 4 stages of unidirectional flow and 3 stages of cyclic flow, which are first imposed at a hydraulic gradient I = 1, and then at i = 5 and finally at 9 across the test specimen.

Therefore, the sequence for one multistage test procedure commences with the first unidirectional flow (UNI 1) for 45 min at a hydraulic gradient of 1 and confining stress of 50 kPa. It is followed by the first cyclic flow (CYC 1) for 90 min, and a subsequent unidirectional flow stage (UNI 2) for 30 min, during which the confining stress is reduced to 25 kPa. The next step is to impose the second cyclic stage (CYC 2) and companion unidirectional flow stage (UNI 3), with the confining stress reduced to 5 kPa during this latter stage. The stage of testing at a hydraulic gradient of 1 is completed by imposing the third cyclic stage (CYC 3) and companion unidirectional stage (UNI 4). Thereafter, the entire sequence (of Table 4) is repeated at a hydraulic gradient of 5, and repeated again at a hydraulic gradient of 9. In the event of filtration incompatibility, the test is stopped if the mass loss becomes excessive.

Table 3 Multistage test procedure (adopted by Hawley, 2001)

Stage	UNI1	CYC1	UNI2	CYC2	UNI3	CYC3	UNI4
Normal Stress (kPa)	0	25	25	25	25	0	0
Wave Period (s)	-	50	-	10	-	10	-
Duration (min)	90	900	30	43	30	43	30

Table 4 Multistage test procedure (current study: test at constant T, sec^{-1}; test sequence at constant i)

Stage Code	1 UNI1	2 CYC1	3 UNI2	4 CYC2	5 UNI3	6 CYC3	7 UNI4
Normal stress (σ)	σ_1	σ_1	σ_1 σ_2	σ_2	σ_2 σ_3	σ_3	σ_3
Duration (min)	45	90	30	90	30	90	30

Remarks: σ_1 = 50 kPa > σ_2 = 25 kPa > σ_3 = 5 kPa

5. TEST RESULTS AND DISCUSSION

5.1 Water head and Gradient Ratio

The typical variation of differential water head measured with time, across selection port locations on the specimen length, is illustrated in Fig. 4 during a change from unidirectional flow (UNI 1) to cyclic flow (CYC 1). The data are for Soil B and geotextile F700, with cyclic flow at a period T = 6 s. Inspection reveals the period of 6 s imposes a very fast flow reversal that does not allow for any steady state condition to establish in the value of differential water head (Fig. 4a). In contrast, testing of the same soil and geotextile combination at a wave period of 60 s yields a very different response (Fig. 4b), most notably the development of a constant value of differential water head. It should be noted that the time required for water head stabilization depends on soil permeability.

Values of Gradient Ratio were calculated from the corresponding values of water head measured in the stages of unidirectional flow imposed before and after the each stage of cyclic flow. The GR values were used to quantify compatibility of the soil-geotextile interface in unidirectional flow, and also to evaluate specimen integrity before imposing the next stage of cyclic flow. All soil-geotextile combinations tested were found stable in unidirectional flow: values of the ASTM Gradient Ratio were in the range 0.9 to 1.5. The modified GR values provide a slightly more sensitive index of compatibility, and were found to vary between 0.8 and 1.9.

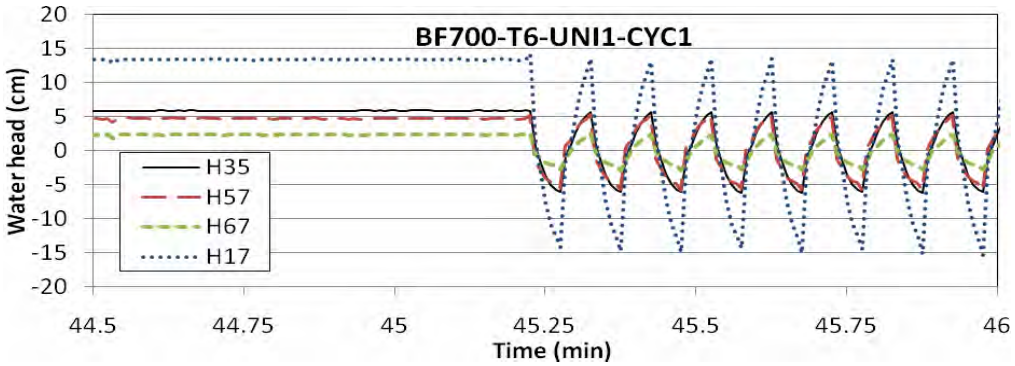

(a)

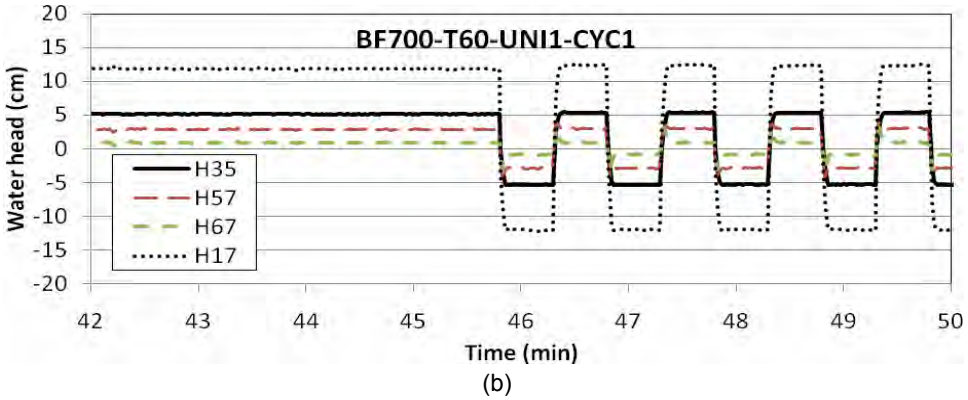

(b)

Figure 4. Illustrative test data for soil B and geotextile F700: (a) T = 6s; (b) T = 60s

5.2 Mass loss

In cyclic flow, mass loss of soil through the geotextile provides a very useful means to characterize soil-geotextile compatibility. In order to determine the rate of mass loss and to examine its variability with elapsed time, soil passing through the geotextile is collected discretely after a given number of flow cycles, by clamping the silicon hose mounted below the collector trough (see Fig. 1). The phenomenon is best reported as a mass loss per unit area over a given number of flow cycles. Accordingly, test data are reported as rate of mass loss (g/m^2 per 100 cycles) in Table 5. The data are for those soil-geotextile combinations in Table 4 with relatively large AOS/D_{85} values, which exhibited a significant mass loss. All five of the geotextiles are woven fabrics, in contact with three different soils.

Results are reported from the current study for cyclic flow at each of the three values of hydraulic gradient (i = 1, 5 and 9) in tests performed a two periods of flow reversal (T = 60 s and 6 s). Additional data are reported from Hawley (2001), which enable direct comparison at a confining stress of 25 kPa. Test C-F500, which has the largest value of AOS/D_{85} examined in the program of testing, was repeated in order to better understand the reproducibility of the results.

Consider the influence of time for flow reversal. In test CF500-T6, mass loss data obtained every 300 cycles over the duration of cyclic flow, at a confining stress of 25 kPa and at a hydraulic gradient of 1 and 9, are presented in Fig. 5. The rate of soil loss appears relatively constant throughout the stage of testing, and does not diminish with elapsed time. Visual observations indicate the soil passed almost continuously through the geotextile during cyclic flow, a behavior that is attributed to the relatively fast period of 6 s between each cycle of flow reversal. Recall the filter ratio AOS/D_{85} = 2.8 for this combination of soil and geotextile, and a similar behavior was evident in testing of soil D and geotextile F700 for which the ratio is AOS/D_{85} = 2.65. Visual observations also indicate the action of soil loss occurred across the entire area of the geotextile specimen, and was not restricted to a few preferential locations.

In contrast, a longer period of flow reversal was imposed in the CF500-T60 test. The relatively slow period of 60 s yielded a different characteristic for the mass loss during in each cycle. In this case, soil particles were seen to pass through the geotextile over an elapsed time of 15 to 20 s, after which the loss diminished quickly to a negligible quantity. The phenomenon expressed itself as a ‘pulse’ of soil loss: visual inspection indicates it to be triggered immediately upon upward flow reversing to downward flow. The behavior is attributed to an arching action in particles of soil at the openings of the geotextile.

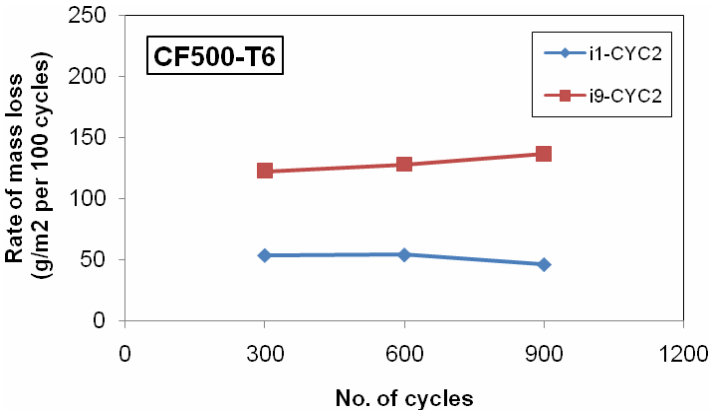

Figure 5. Rate of mass loss versus number of cycles

Table 5 Rate of mass loss in cyclic flow stage (g/m^2 per 100 cycles)

Code & (AOS/D_{85})	Stress (kPa)	T = 60s i = 1	T = 60s i = 5	T = 60s i = 9	T = 6s i = 1	T = 6s i = 5	T = 6s i = 9
MWT-F402 (1.5)	25	-	15.0[1]	-	-	6.5[2]	-
	0	-	-	-	-	20.4[2]	-
MWT-F404 (1.5)	25	-	28.9[1]	-	-	44.2[2]	-
	0	-	-	-	-	49.2[2]	-
MWT-H570 (2.1)	25	-	115.3[1]	-	-	0.0[2]	-
	0	-	-	-	-	33.8[2]	-
C-F500 (2.8)	50	21.3	42.8	84.0	51.7	97.4	116.0
	25	24.2	41.3	75.6	51.0	93.2	128.8
	5	38.4	71.2	146.8	47.9	99.9	164.1
Repeated C-F500 (2.8)	50	6.2	24.2	46.6	35.8	70.9	75.9
	25	14.3	37.9	45.1	61.3	73.5	92.3
	5	19.0	40.8	60.1	71.5	73.8	119.9
D-F700 (2.65)	50	21.3	45.6	96.9	11.3	38.0	75.8
	25	34.1	76.9	104.0	10.8	77.9	78.3
	5	42.7	85.4	131.0	13.2	81.3	91.2

[1] tested at i = 4, T = 50 s, and the values reduced from 1080 cycles
[2] tested at i = 4, T = 10 s, and the values reduced from 260 cycles

The influence of flow reversal on soil passing through the geotextile is further illustrated in Fig. 6, where data for CF500-T60 acquired over a total of 90 cycles are reported as an equivalent rate loss per 100 cycles, together with data for CF500-T6 acquired over a total of 900 cycles as an average rate loss per 100 cycles. The results indicate the mass loss of soil to be greater in cyclic flow at the relatively shorter period of reversal every 6 s rather than every 60 s. The finding is consistent with that of Chew et al. (2000), who report a greater mass loss in laboratory tests at wave periods shorter than 10 s.

Consider now the influence of confining stress, which is reported as the value at the soil-geotextile interface under hydrostatic conditions (Fig. 6). Rate of mass loss appears independent of confining stress in tests at 25 and 50 kPa, particularly at relatively low values of hydraulic gradient. In contrast the rate of loss increased significantly at the very low confining stress of 5 kPa, particularly at the relatively high hydraulic gradient of 9. The behavior is attributed to seepage-induced variations in effective stress yielding very low values at the soil-geotextile interface. The relations quantified in Fig. 6 between mass loss and the combined effects of confining stress and hydraulic gradient in this study are in general agreement with conceptual trends advocated by Cazzuffi et al. (1999).

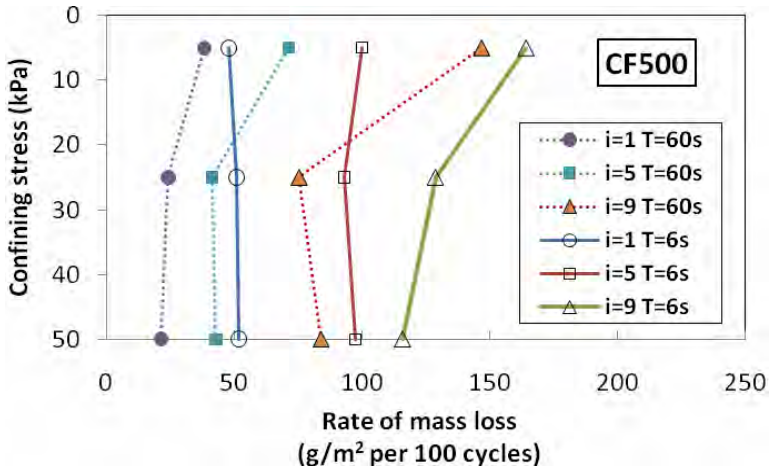

Figure 6. Rate of mass loss versus confining stress

6. RETENTION CAPACITY

The AOS/D_{85} filter ratio describes a characteristic opening size of the geotextile and soil respectively. The variation of rate of mass loss with AOS/D_{85} is presented in Fig. 7 for all of the soil-geotextile combinations examined in testing (Table 2). Accordingly, the results characterize the response of woven and nonwoven geotextiles placed against uniformly graded soils. Data are presented in Fig. 7 for tests at T = 6 s and σ = 5 kPa in the current study, and at T = 10 s and no confining stress in the study of Hawley (2001), which are considered representative of extremely challenging loading conditions in reversing flow. Although the test parameters of each study are strictly not identical, they are believed sufficiently similar to warrant a direct comparison.

Consider the data for nonwoven geotextiles (see Tables 1 and 2). No combination of soil and nonwoven geotextile yielded a mass loss, in tests that included a filter ratio AOS/D_{85} as large as 2.25 (soil D and geotextile T65).

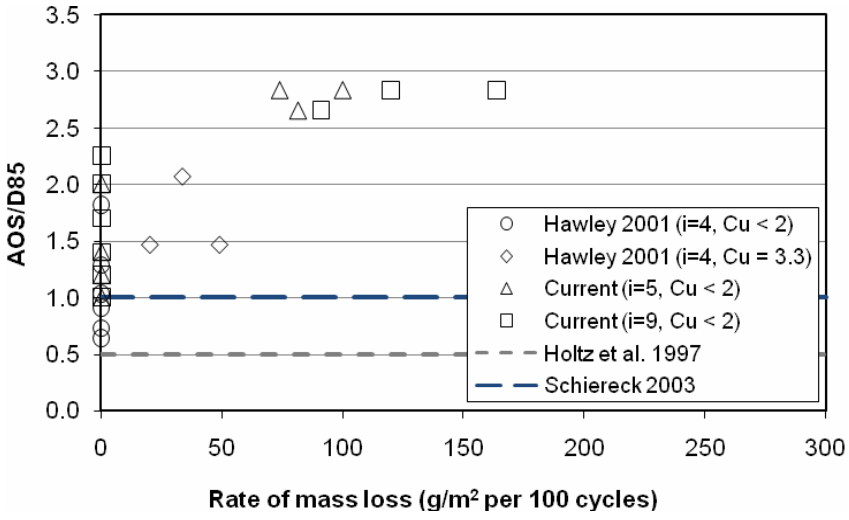

Figure 7. Retention capacity of geotextiles in cyclic flow for severe conditions (T ≤ 10 s and very low confining stress)

Consider the data for woven geotextiles (see Tables 1 and 2). Again, no combination of soil and woven geotextile exhibited a mass loss in tests with soils of $C_u < 2$ and a filter ratio $AOS/D_{85} < 2$. The finding is attributed to a retention capacity that is controlled by a geometric constraint, and development of a stable arrangement of soil particles over the openings of the woven geotextile. In contrast, a significant mass loss was found at values of $AOS/D_{85} > 2.5$ (Fig. 7). Reproducibility of test data appears very reasonable, given the data for the CF500 tests at $AOS/D_{85} = 2.83$. The response implies a significant change in retention capacity occurs for very uniformly graded soils in cyclic flow at 2 <

$AOS/D_{85} < 2.5$. The data of Hawley (2001) obtained for a mine waste tailings (MWT, $C_u = 3.3$) which contain about 10 % silt (see Fig. 3) deserve careful interpretation: the coefficient of uniformity and shape of the grain size curve may also be factors that influence filtration compatibility of this test combination.

Holtz et al. (1997) suggest an acceptance criterion for soil retention of $AOS/D_{85} \leq 0.5$, for conditions of dynamic, pulsating or reversing flow. The empirical criterion is depicted in Fig. 7 for illustrative purposes. The criterion is found consistent with no soil loss, and is therefore deemed appropriate, yet conservative, as a boundary to the findings of the experimental studies reported herein. The conservatism has some practical implications for engineering practice. Shoreline protection works often encounter soils that are predominately fine sand, yet there are few geotextiles with an AOS smaller than 0.05 to 0.075 mm. Therefore, the $AOS/D_{85} \leq 0.5$ rule would eliminate use of a geotextile in soils with a D_{85} less than 0.1 to 0.15 mm, which represents many problematic soils.

In a companion approach, Schiereck (2004) subsequently recommended a criterion for soil retention of $O_{90}/D_{90} < 0.5$ to 1, for cyclic flow conditions. The value of O_{90} is similar, but not identical to AOS. Likewise, the value of D_{90} is similar, but not identical to D_{85}. Accordingly, in the depiction of this empirical filter ratio criterion in Fig. 7, it must be noted the upper limit of the Schiereck criterion is schematically illustrative, but not exact, given the plotting axes. From inspection, this criterion is also well supported by the test data. It too provides a good distinction between soil-geotextile combinations exhibiting soil loss and those with no loss, but with less conservatism than Holtz et al. (1997).

7. SUMMARY REMARKS

Factors controlling soil retention in cyclic flow have been examined with reference to multi-stage tests on uniformly graded soils reconstituted in contact with a woven or a nonwoven geotextile. Interpretation of the test results is based on a relation between the filter ratio AOS/D_{85} and the rate of mass loss (g/m^2 per 100 cycles). The onset of mass loss is attributed to a piping action when the opening size of the geotextile becomes too large in comparison to the base soil. In tests at very low confining stress and relatively fast flow reversal, no loss of soil was found in the nonwoven geotextiles for values of AOS/D_{85} as large as 2.25. Although no loss of soil was found in the woven geotextiles for values of AOS/D_{85} as large as 2 in soils with a $C_u < 2$, some loss occurred in soils with a $C_u = 3.3$ at $1.5 < AOS/D_{85} < 2.1$, and significant loss was evident in woven geotextiles with $AOS/D_{85} > 2.5$.

In all cases the onset of soil loss initiated at AOS/D_{85} ratios larger than the range of 0.5 to 1.0 advocated in design guidance. Indeed the AOS/D_{85} values at which mass loss initiates in these laboratory permeameter tests imply the lower end of the range advocated in design may be unnecessarily conservative. In reporting these test results, it should be noted the findings cannot be extrapolated to widely-graded soils, gap-graded soils and soils with an appreciable fines content.

ACKNOWLEDGEMENTS

The laboratory work has been conducted with financial support from the Natural Sciences and Engineering Research Council of Canada. The provision of geotextile specimens by TC Mirafi, with assistance from Chris Lawson, is greatly appreciated.

REFERENCES

Cazzuffi, D.A., Mazzucato, A., Moraci, N., and Tondello, M. (1999). A new test apparatus for the study of geotextiles behaviour as filters in unsteady flow conditions: relevance and use. *Geotextiles and Geomembranes*, Elsevier, England, Vol. 17, No. 5-6, pp. 313 - 329.

Chen, R.H., Ho, C.C., and Hsu, C.Y. (2008). The effect of fine soil content on the filtration characteristics of geotextile under cyclic flows, *Geosynthetics International*, Vol 15, No. 2, pp. 95 – 106

Chew, S.H., Zhao, Z.K., Karunaratne, G.P., Tan, S.A, Delmas, Ph., and Loke, K.H. (2000). Geotextile filter in revetment subjected to cyclic wave loading, *Advances in Transportation and Geoenvironmental Systems Using Geosynthetics*, *Proc. of Geo-Denver 2000*, August 5-8, Denver, CO, pp. 162 – 175.

Fannin, R.J. (2006). Chapter 6: Filtration, *Geosynthetics* (Ed. R.W. Sarsby), Woodhead Publishing, Cambridge, U.K., pp. 127-147

Fannin, R.J. and Pishe, R. (2001). Testing and specifications for geotextile filters in cyclic flow applications, *Proc. of Geosynthetics 2001*, February 12-14, Portland, OR, pp. 423-435.

Fannin, R.J. and Srikongsri, A. (2007). "Geotextile filters in cyclic flow: test results and design criteria," *Proc. of Geosynthetics 2007*, Washington, D.C., Jan. 16-19, pp. 170-185.

Fannin, R.J., Vaid, Y.P., Palmeira, E.M. and Shi, Y.C. (1996). A Modified Gradient Ratio device. In, Recent developments in geotextile filters and prefabricated drainage geocomposites, *ASTM STP 1281*, S.K Bhatia and L.D. Suits, Eds., ASTM, Philadelphia, pp. 100 – 112.

Fannin, R.J., Vaid, Y.P. and Shi, Y.C., (1994). Observations on the Gradient Ratio Test, ASTM *Geotechnical Testing Journal*, Vol. 17, No. 1, pp. 35-42.

Giroud, J.P. (1996). Granular filters and geotextile filters, *Proceedings of Geofilters'96 Conference*, Montreal, Quebec, Canada, May 39-31, pp. 565-680.

Hameiri, A. (2000). *Soil*-geotextile filtration behavior under dynamic conditions of vibration and cyclic flow. *PhD Thesis*, University of British Columbia, Vancouver.

Hameiri, A. and Fannin, R.J. (2002). A Cyclic Gradient Ratio test Device. *ASTM Geotechnical Testing Journal*, Vol. 39, No.2, pp.266-276

Hawley, R. (2001). Filtration performance of geotextiles in cyclic flow conditions. *MASc Thesis*, University of British Columbia, Vancouver.

Holtz, R.D, Christopher, B.R., and Berg, R.R. (1997). Geosynthetic Engineering, BiTech Publishers, Richmond, BC, pp.29-68.

Kenney, T.C. and Lau, D. (1985). Internal stability of granular filters, *Canadian Geotechnical Journal*, No. 22, pp. 215 – 225.

Palmeria, E.M. and Fannin, R.J. (2002). Soil-geotextile compatibility in filtration, *Proc. of the 7th Int. Conf. on Geosynthetics*, Nice, France, September 22-27, 2001, pp. 853-872.

Li, M. and Fannin, R.J. (2008). A comparison of two criteria for internal stability of granular soil. *Canadian Geotechnical Journal*, Vol. 45, No. 9, pp.1303-1309.

Schiereck, G.J. (2004). Introduction to bed, bank and shore protection. Spon Press, New York, NY, USA.

Geosynthetics 2009
February 25-27 2009, Salt Lake City, Utah

Geosynthetic Aggregate Drainage Systems: Preliminary Large-Scale Laboratory Test Results for Expanded Recycled Polystyrene

D. Arellano, Ph.D., P.E., The University of Memphis, Memphis, Tennessee, USA
M. Zarrabi, Ph.D., The University of Memphis, Memphis, Tennessee, USA
N. H. Jafari, The University of Memphis, Memphis, Tennessee, USA
L.J. Bailey, The University of Memphis, Memphis, Tennessee, USA

ABSTRACT
Preliminary results are presented of the mechanical deformation and the hydraulic behavior of geosynthetic aggregate drainage systems. A full-scale test chamber was developed that would simulate the loading conditions from trench backfill and measure the mechanical deformation and the hydraulic behavior simultaneously. Results for the geosynthetic aggregate drainage systems without pipe indicate that the in-plane flow rate decreases with increase in stress and the associated increase in deformation of the drainage bundle. Therefore, the stress versus flow rate relationship is important for design of drainage systems without pipe. Test results for the drainage systems with pipe indicate that the geosynthetic aggregate may function as a compressible inclusion and may have the benefit of reducing pipe deformation at a given stress level compared with the deformation of the pipe only without geosynthetic aggregate. The cross-plane flow into the pipe was not impacted much by the presence of the surrounding geosynthetic aggregate.

1. INTRODUCTION

Geosynthetic aggregate (GA) are discrete pieces of expanded polystyrene, expanded shale, rubber tire chips, chopped tubular nets, grids, and mats, etc., in the size of large gravel shaped in a manner as to maximize void volume between the individual pieces (Geosynthetic Research Institute 2006a). The GA drainage systems tested as part of this study consist of expanded recycled polystyrene aggregate that is cubical in shape with dimensions of approximately 20 mm by 25 mm by 30 mm as shown in Figure 1. The aggregate is manufactured by melting post-consumer polystyrene, predominantly packaging material, and expanding the recycled polystyrene in a controlled manner into aggregate of a desired shape, size and density. Therefore, a key benefit of GA drainage systems is that their use can contribute to depletion of the current world-wide large quantity of post-consumer polystyrene waste while providing a drainage product that can provide consistent engineering properties. Two engineering properties that are important for design of GA drainage systems include the stress versus deformation and the flow rate versus stress behavior. The objective of this study was to develop a full-scale test chamber and to evaluate the mechanical deformation and hydraulic behavior under vertical stresses that would simulate the loading conditions from trench backfill. A description of the two types of GA drainage systems that were tested and a description of the full-scale test chamber is initially provided. A discussion of the preliminary test results is also provided.

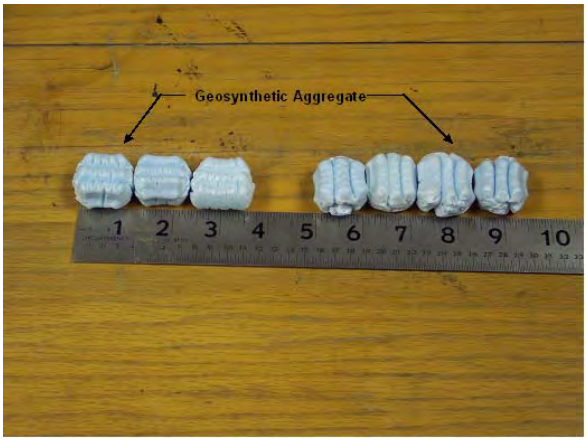

Figure 1. Photo showing a close-up view of typical individual pieces of geosynthetic aggregate.

2. MATERIALS AND METHODS

2.1 Geosynthetic Aggregate Drainage Systems

Two types of prefabricated GA drainage systems were tested. One type consists of 25 cm diameter bundles of GA confined by a polyester net as shown by Figure 2. This type of drainage system is referred to as a GA drainage system without pipe. The second type of GA drainage system tested is similar to the first type except that the 25 cm bundles include a 10 cm diameter corrugated and perforated high-density polyethylene pipe surrounded with 7.5 cm of GA also confined by a polyester net as shown by Figure 2. This second type of drainage system is referred to as a GA drainage system with pipe.

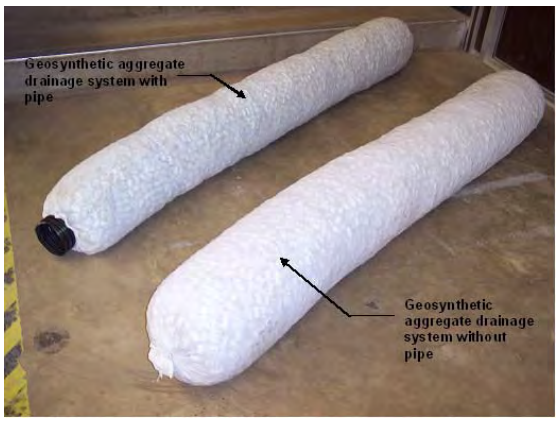

Figure 2. Photo showing the difference between a GA drainage system with pipe and drainage system without pipe.

2.2 Test Apparatus

Based on the experience with testing geopipes, the Geosynthetic Research Institute (GRI) developed a draft test method to measure the mechanical deformation behavior (Geosynthetic Research Institute 2006a) and the hydraulic behavior (Geosynthetic Research Institute 2006b) of GA drainage systems. However, the geometry of the small-scale test chamber included in the GRI standards was modified to minimize the effects of side wall friction between the soil backfill and chamber side walls and arching over the GA drainage systems on the measured mechanical deformation and flow rate. The three-dimensional arching equation, Equation 1, which was presented by Brachman et al. (2000), was used to select an optimal chamber width that would minimize the side wall friction and arching effects when testing 25 cm diameter GA drainage systems.

$$\sigma_v = \frac{\gamma}{2K\mu w}\left(1 - e^{-2K\mu wh}\right) + \sigma_{vo}e^{-2K\mu wh} \qquad [1]$$

This equation provides an estimate of the applied stress that reaches the soil with depth, σ_v. The following are the equation symbol definitions: w is the geometry coefficient and is equal to 1/B+1/L, B is the test chamber width, L is the test chamber length, K is the coefficient of lateral pressure, μ is the coefficient of side wall friction and is equal to tan $ø_{sw}$, $ø_{sw}$ is the angle of side wall friction, γ is the unit weight of the soil, σ_{vo} is the vertical stress applied at the surface of the soil, h is the depth below the surface of the soil where the estimate of vertical stress that accounts for arching and side wall friction is being determined, and σ_v is the vertical stress that reaches the soil at depth h.

To determine an optimal test chamber width that would provide the minimum reduction in the applied vertical stress due to side wall friction and arching effects, various chamber widths were evaluated using Equation 1. The GA drainage systems tested are 1.8 m in length. Therefore, a chamber length of 1.8 m was used. It was initially estimated that the tests would be performed with approximately 75 cm of soil backfill over the GA drainage system. The soil backfill consists of a sand meeting the requirements of a fine concrete aggregate per ASTM C 33 (ASTM C 33). The range of side wall interface friction angle values evaluated was based on the ratio of side wall interface friction to internal friction of the soil ($ø_{sw}/ø$) of 0.5 to 0.7 suggested by Perloff and Baron (1976) and reported by Brachman et al. (2000) for soil and smooth steel interfaces. Thus, for an estimated internal friction angle for the proposed sand backfill of 25 to 35 degrees, the interface friction between the sand and the steel side walls of the chamber was expected to range between 10 and 25 degrees. An estimated sand unit weight of 22 kN/m^3 and a coefficient of lateral pressure of 0.5 were used.

The results of the analysis revealed that the effects of soil arching can be drastically reduced at widths greater than 1 m. The final width of the test chamber selected was 1.2 m.

The height of the chamber that was initially fabricated was 1.2 m based on the draft GRI test standard GC9 (Geosynthetic Research Institute 2006a). However, to further minimize the effects of soil arching, the load was applied directly on top of the drainage system instead of applying the load on soil backfill placed above the drainage system as suggested by the GC9 standard. Therefore, the height of the chamber was decreased to 0.6 m. The load was applied via an aluminum load platen that extended the full width and length of the test chamber. However, after several tests were performed by applying the load across the platen that spanned across the drainage system and the adjacent sand backfill, it was observed that most of the load was being distributed across the sand backfill and not over the drainage system. Thus, the initial test results provided the stress versus deformation behavior predominantly of the sand backfill. This observed behavior is in agreement with Marston's observations of flexible conduits in ditches that the load is spread over the entire width of the ditch if the stiffness of the side fills approach that of the conduit (Handy and Spangler 2007).

Therefore, the platen system was modified by attaching a wood platen that would apply load predominantly over the diameter of the GA drainage system as shown by Figure 3. However, as shown in Figure 3, a wedge of soil backfill remained near the edges of the wood platen between the bundle and the platen. This load application is in agreement with Moser's observations. Moser (1990) indicates that the long-term stress over a flexible conduit may approach the stress imposed by the soil directly over the conduit. The stress of the soil over the conduit can be obtained by projecting a soil prism upwards from the edges of the conduit as shown by Figure 4. The stiffness of GA will typically be less than the soil backfill. Therefore, Moser's prism load concept appears to be applicable for estimating the backfill stress applied by the soil backfill over GA drainage systems. The prism loading condition is simulated in the test system by applying the load predominantly over the drainage system. The application of load predominantly over the drainage system also minimizes the arching effect.

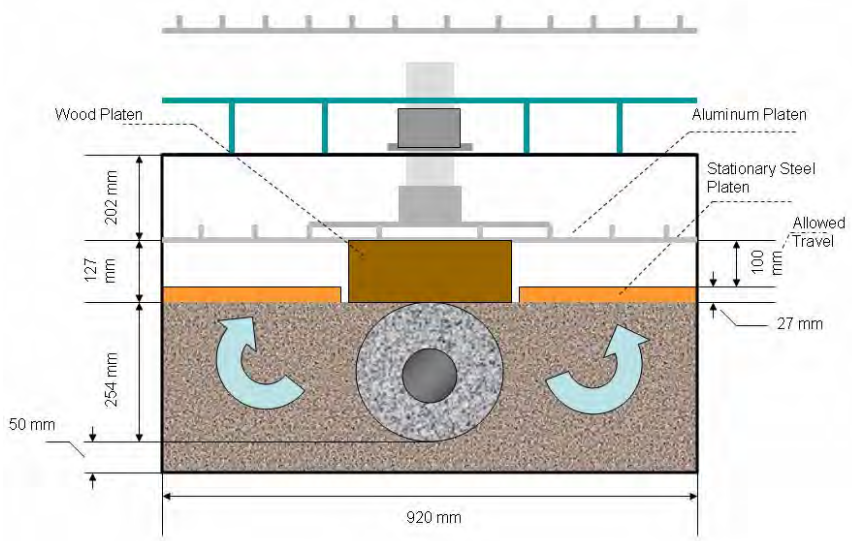

Figure 3. Cross-sectional view of test chamber.

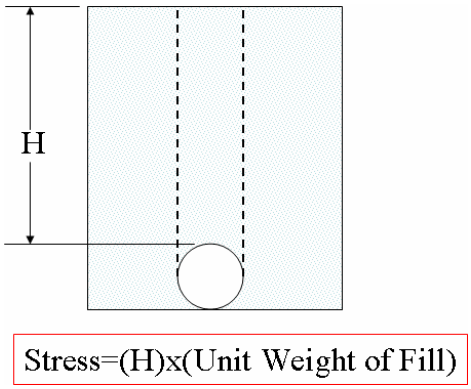

Figure 4. Moser's prism load concept to estimate long-term stress over a flexible conduit (Moser 1990).

Tests were initially performed without the use of the confining stationary steel platens shown in Figure 3. However, it was observed that the unconfined soil backfill was moving laterally and upwards as the load from the wood platen was applied to the drainage system as indicated by the arrows in Figure 3. The stationary steel platens, which are secured to the test chamber, were incorporated in the test system to confine the soil. In practice, soil backfill will typically be placed above the GA drainage systems. Therefore, the adjacent soil backfill below the top level of the GA bundle will be confined by the upper backfill soil. Therefore, the use of the stationary steel plates better simulates the adjacent backfill behavior in the field.

The biggest challenge in designing the test system involved designing a hydraulic system to measure the hydraulic properties of the GA drainage systems. Two different flow scenarios had to be included in the test apparatus. For the GA drainage systems without pipe, the primary flow scenario of interest in design is the flow along the longitudinal length of the bundle. This flow scenario is similar to the in-plane flow (planar flow rate) or transmissivity measured for geonets. For the GA drainage system with pipe, the primary flow scenario of interest in design is the flow into the cross-section of the bundle. This flow regime is similar to the cross-plane permeability or permittivity measured for geotextiles. The hydraulic system is shown in Figure 5.

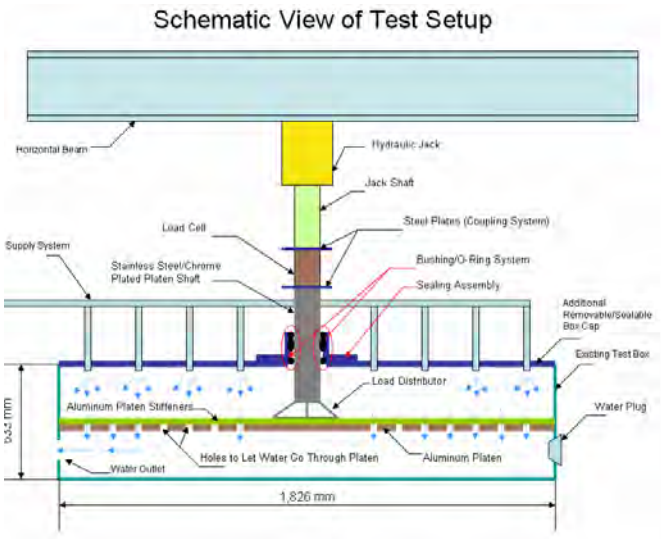

Figure 5. Side view of test chamber.

The key components of the test apparatus include the steel chamber, the water supply reservoir system with pump, the water outflow system with flow meter, the hydraulic jack and aluminum load platen, and the removable chamber box cap with built in water supply system. These components are shown in Figures 6 and 7.

Water is delivered from the external water supply reservoir to the test chamber via a 370 watt (½ horsepower) pump. Upon exit of the test chamber, the flow of water is returned to the external reservoir. This recirculation of water keeps the height of water in the reservoir constant, the energy head supplying the pump constant, and the energy head that the pump supplies to the test chamber constant. At the outlet of the pump, the flow of water can take two separate and distinct paths via a network of valves and pipes. The flow path is dependent on which flow scenario, i.e., in-plane flow or cross-plane flow, is desired.

As shown by Figures 5 and 7, load is applied to the GA drainage system by an overhead hydraulic jack. The piston of this hydraulic jack runs through a sealed opening in the center of the test cap, where it is pinned to an aluminum load platen that spans the entire surface area of the test chamber. As shown in Figure 3, a wooden platen is attached to the center of this aluminum platen to transfer the load directly to the GA drainage systems. The load applied to the platen system is measured by a vibrating wire load cell that measures strain in its cylindrical housing. This load cell sends a voltage signal that is converted in a central data acquisition system into a unit of force. Currently, the hydraulic jack system does not have the capability to sustain load for an extended time. Therefore, each load increment could only be sustained for about 30 to 60 seconds. Also linked to the data acquisition system is a cable extension position extensometer that measures the vertical movement of the hydraulic jack. The measured position of the jack is taken as the measured vertical deflection of the GA drainage system in the test chamber.

1. Water reservoir and water supply pump
2. Main inlet for measuring cross-plane flow
3. Main inlet for measuring in-plane flow

Figure 6. Photo showing the steel test chamber and the water supply reservoir system with pump.

1. Hydraulic jack and load cell
2. Hydraulic jack pump
3. Removable chamber box cap with built in water supply pipe network for measuring cross plane flow.
4. Flow meter and main outlet

Figure 7. Photo showing the steel test chamber, water outflow system with flow meter, the hydraulic jack, and the removable chamber box cap with built-in water supply system.

2.3 Description of Tests Performed

Prior to placement of the GA drainage system in the test chamber, a 5 cm layer of sand backfill is placed and tamped with a hand-held tamper. After the bottom sand layer is placed, the GA drainage system is placed and sand backfill is placed on both sides of the bundle in approximate 5 cm layers. Each layer is tamped prior to the placement of the subsequent layer. Backfill is placed to the top of the bundle. Several tests were also performed by performing extra tamping of each backfill layer to determine the potential impact of compacted effort on the test results. The tests performed with the extra compacted effort are indicated as extra compacted.

After the backfill is placed, the steel platen confining plates are placed on each side of the bundle and secured to the test chamber. The test system is then saturated with water. After saturation of the test chamber, the removable chamber cap is placed, providing a water tight seal. At the start of each test, the pump is engaged and the flow of water from the water supply reservoir enters the test chamber through the appropriate pipe network that is based on the type of GA drainage system being tested.

When testing the GA drainage systems without pipe, the flow of water is through the longitudinal direction of the GA bundle. This requires that the flow of water from the pump be delivered only at the longitudinal end of the GA bundle at the main inlet of the test chamber. An analog pressure gauge is located at the main inlet of the test chamber and at the outlet. These pressure gauges were installed after some of the initial tests were completed. Therefore, inlet and outlet pressure was not measured in some of the early tests that were performed. An ultrasonic flow meter reads the flow rate of the water exiting the test chamber before it is returned to the reservoir.

For GA drainage systems with pipe, the flow of water is in the cross-planar direction. Therefore, the flow of water is no longer delivered at the main inlet of the test chamber, but is instead pumped into the removable chamber cap, where it is channeled through a network of smaller pipes and is pumped into the test chamber via holes in the removable chamber cap. All of the platens below the removable chamber cap have perforations that supply the flow of water from above. An

analog pressure gauge is located at the connection between the pump and the removable chamber cap's network of flow delivery pipes. As with the GA drainage system without pipe test configuration, pressure is read from the pressure gauge located at the outlet of the test chamber and flow is measured by an ultrasonic flow meter.

As load is applied in increments, the corresponding vertical movement that reflects the vertical strain of the GA drainage system and the flow rate at the outlet are measured. While the flow and pressure values are measured directly, the data acquisition system is used to measure the values from the load cell and vertical deflection from the extensometer. The load recorded by the load cell is used to determine the vertical stress exerted on the GA drainage systems. The vertical deflection determined by the extensometer is used to describe the deformation of the GA drainage system being tested.

3. DISCUSSION OF TEST RESULTS

3.1 Geosynthetic Aggregate Systems Without Pipe

Figure 8a shows the stress versus vertical strain behavior of GA drainage systems without pipe. The stress versus strain response appears to be nearly linear to about a strain level of 20 percent then the response is strain-hardening, which is characterized by the nonlinear and increasing stress versus strain curve. As indicated by Figure 3, the maximum displacement that can be obtained with the current test system configuration is 100 mm, which is about a maximum strain of 40 percent for the 25 cm diameter GA drainage system bundles that were tested. As indicated by Figure 8a, the predominant stress at which the maximum allowable strain was achieved is about 70 kPa except for Tests 19, 21, and 23 where an unusually high stress of up to 205 kPa was obtained. It is suspected that in these three tests the initial strain at the start of the test may not have been properly measured and the 100 mm travel allowance of the aluminum platen (See Figure 3) was reached prematurely. Thus, the unusually high stress measured is actually the stress versus strain of the GA drainage system and the full width of the adjacent soil backfill instead of the GA drainage system only. Therefore, one issue that is currently being addressed is how to ensure that the initial strain is consistently measured. The predominant stress of 70 kPa at which the maximum allowable strain was achieved is approximately equivalent to 3.7 m of backfill material with a unit weight of 19 kN/m^3. Therefore, the stresses that are achieved by the current test configuration are reasonable for typical drainage applications that do not involve vehicle loads.

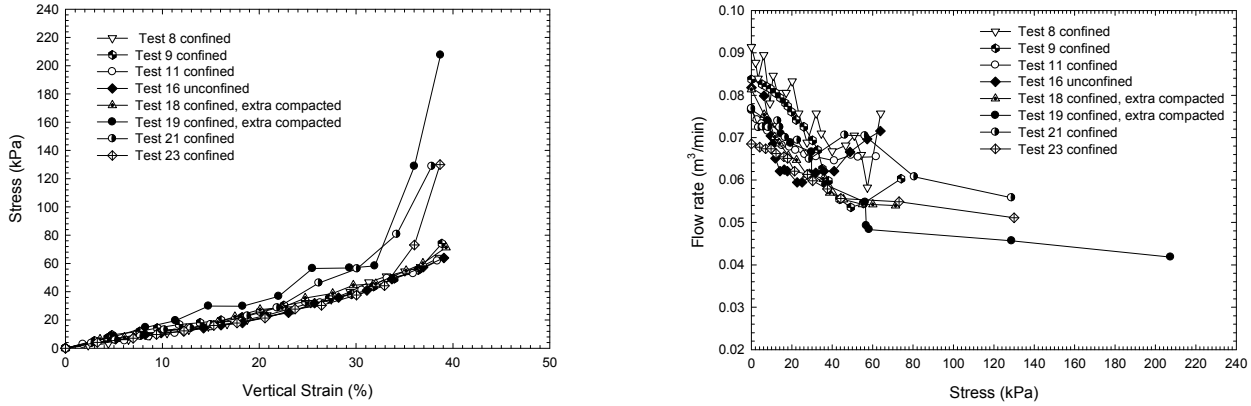

a) Vertical strain b) In-plane flow rate

Figure 8. Test results obtained on GA drainage systems without pipe.

Most tests were performed in a confined state, i.e., with the stationary platens, because as previously indicated the use of the stationary steel plates better simulates the field behavior of the adjacent backfill in a trench. Test 16 was performed in an unconfined state, i.e., without stationary platens. As shown by Figure 8a, no apparent difference in the stress versus strain behavior was observed for this one unconfined test. Extra compacted effort was provided to the soil backfill in Tests 18 and 19. As shown by Figure 8a, no apparent difference in the stress versus strain behavior was observed between the extra compacted backfill in Test 18 and the other tests that were performed with regular compaction. However, Test 19 did reveal that compaction may have an influence on the stress versus strain behavior of GA drainage systems without a pipe. Therefore, a controlled compaction procedure will be implemented in future tests.

Figure 8b shows the flow rate versus stress of the GA systems without pipe. The measured flow scenario represents the in-plane flow (planar flow rate), which is the flow along the longitudinal length of the bundle. As indicated in Figure 8b, the flow rate decreased with increase in applied stress. The flow rate obtained ranged from 0.068 to 0.092 m^3/min prior

to application of stress and decreased to 0.042 to 0.076 m^3/min. The initial hydraulic gradient between the inlet and outlet prior to application of load ranged from 1 to 1.6 and increased up to 3 during load application. The decrease in the flow rate with increase in stress occurs due to the decrease in the void volume between GA pieces. This decrease in void volume occurs because of both compression and rearrangement of the individual GA pieces. The decrease in void volume is also represented by the increase in hydraulic gradient during load application. The flow rate measured is based on the capabilities of the hydraulic system as well as on the flow conditions that the test chamber provides and may not represent the full flow capacity of the GA drainage systems. This issue is currently being addressed.

Figure 9a and 9b shows the results of the stress versus strain and flow rate versus stress behavior, respectively, of a higher density GA system without pipe. The approximate unit weight of regular GA is 0.07 kN/m^3 and the approximate unit weight of the higher density GA is 0.14 kN/m^3. The higher density GA had dimensions of approximately 18 mm by 21 mm by 26 mm, which is slightly smaller in size than the regular density GA. A comparison between Figure 9a and 8a indicates that a higher density GA will result in less strain compared to a regular density GA at a given stress level. Therefore, the use of a higher density GA within a GA drainage system may compress less.

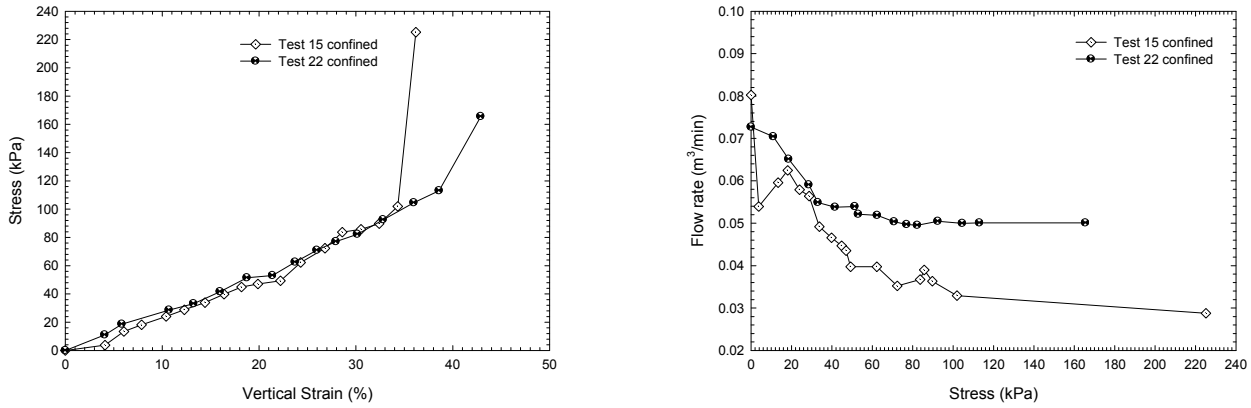

a) Vertical strain b) In-plane flow rate

Figure 9. Test results obtained on high density GA drainage systems without pipe.

However, a comparison of Figure 9b and 8b indicates that a lower flow rate was measured for the higher density GA drainage system. This lower flow rate can be attributed to the smaller particle size of the higher density GA, which provides a lower pore volume than the larger particle size of the regular density GA. The initial hydraulic gradient between the inlet and outlet prior to application of load ranged from 1.2 to 2.1 and increased up to 3.6 during load application. The higher initial hydraulic gradient and the higher increase in hydraulic gradient during application of stress obtained with the higher density GA compared with the regular density GA may also be associated with the lower pore volume of the lower density GA. Thus, a better comparison of flow rate between different GA densities should be made using the same GA particle size between the various densities. It is anticipated that a higher flow rate can be obtained with higher density GA of the same size as lower density GA because higher density GA will compress less as shown by comparing the stress versus strain results in Figures 9a and 8a.

3.2 Geosynthetic Aggregate Systems With Pipe

Figure 10a shows the stress versus vertical strain behavior of GA drainage systems with an internal pipe. A nearly linear stress versus strain response was obtained for the full allowable test system strain limit of 40 percent as shown in Figure 10a except for Test 5. In Test 5 an unusually high stress was obtained at strain levels above 33 percent. As observed in several of the GA drainage systems without pipe test results, it is suspected that in Test 5 the initial strain at the start of the test may not have been properly measured and the 100 mm travel allowance of the aluminum platen (See Figure 3) was reached prematurely. Thus, the unusually high stress measured above 33 percent strain is actually the stress versus strain of the GA drainage system and the full width of the adjacent soil backfill instead of the GA drainage system only. As previously indicated, this issue is currently being addressed to ensure that the initial strain is consistently measured.

Tests 3 through 5 were performed in an unconfined state, i.e., without stationary platens, while the other tests shown in Figure 10a were performed in a confined state, i.e., with the stationary platens. As shown in Figure 10a, the unconfined test results plot at the lower boundary of the stress versus strain plots. Therefore, for a given stress, a higher strain is obtained for GA drainage systems tested in an unconfined state versus the confined state because more displacement

of the soil backfill occurs in an unconfined condition due to the unconfined soil backfill moving laterally and upwards as the load from the wood platen is applied to the drainage system as indicated by the arrows in Figure 3. As previously indicated, the use of the stationary steel plates better simulates the adjacent backfill behavior in the field.

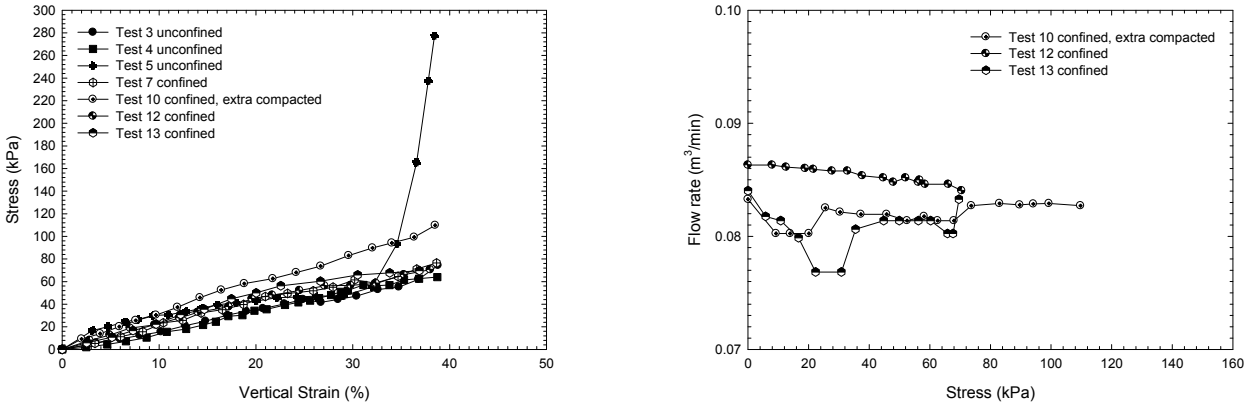

a) Vertical strain

b) Cross-plane flow rate

Figure 10. Test results obtained on GA drainage systems with pipe.

Extra compacted effort was provided to the soil backfill in Test 10. As shown in Figure 10a, Test 10 plots at the upper bound of the stress versus strain plots. Therefore, for a given stress, a lower strain is obtained for GA drainage systems tested with backfill placed with a higher compacted effort. Therefore, a controlled compaction procedure will be implemented in future tests.

Figure 10b shows the flow rate versus stress behavior of the GA systems with an internal pipe. Flow data for Tests 3, 4, 5, and 7, for which stress versus strain data are shown in Figure 10a, is not included in Figure 10b because these tests were performed prior to completion of the test chamber hydraulic system. The measured flow scenario is the cross-plane permeability or permittivity flow into the cross-section of the bundle. The flow rate obtained ranged from 0.083 to 0.086 m^3/min prior to application of stress and predominantly remained in this range during application of stress except for Test 13, which showed a decrease in flow. As previously indicated, pressure gauges were not installed during the initial testing which includes the tests shown in Figure 10. Therefore, the hydraulic gradient could not be determined for the tests included in Figure 10.

Figures 11a and 11b show the results of the stress versus strain and flow rate versus stress behavior, respectively, of a higher density GA system with pipe. The description of regular and higher density GA was previously described in the discussion of the test results for GA drainage systems without pipe. The initial hydraulic gradient between the inlet and outlet prior to application of load was about 1.1 and decreased to 1 during load application. A comparison between Figure 11a and 10a indicates that a higher density GA will result in less strain compared to a regular density GA at a given stress level. Therefore, the use of a higher density GA within a GA drainage system with pipe may compress less. This is the same observation made for higher density GA drainage systems without pipe. However, unlike the observation made for high density GA drainage systems without pipe that a lower in-plane flow rate is obtained for the higher density GA drainage system because of the smaller particle size of the higher density GA tested, the cross-plane flow rate between high density GA drainage systems with pipe shown in Figure 11b is similar to the cross-plane flow rate measured in regular density GA drainage systems with pipe shown in Figure 10b. Therefore, the smaller particle size of the high density GA compared to the regular density GA had only a slight impact on the resulting permittivity of the GA drainage system with pipe probably because the thickness of the GA surrounding the pipe is limited to 7.5 cm. However, GA particle size does have a greater influence on the in-plane flow (planar flow rate) along the longitudinal length of GA drainage systems without pipe.

Figure 12a shows a comparison of the stress versus strain behavior between GA drainage system with an internal pipe and a stand alone bare pipe without GA. The bare pipe that was tested was the same type of 10 cm diameter pipe that is included within the GA drainage systems with pipe. In Figure 12a, the vertical strain of the GA drainage system is based on the 25 cm bundle diameter and the strain of the bare pipe is based on the 10 cm pipe diameter. As indicated in Figure 12a, the test apparatus strain limit is 40 percent for the GA drainage systems but 90 percent for the bare pipe without GA. For the bare pipe, a large vertical strain developed at a stress level of approximately 40 kPa. However, for the GA system with pipe the strain steadily increased with increase in stress. Thus, for a given strain level of 30 percent, the corresponding stress level is 60 kPa and 20 kPa for the GA system and bare pipe, respectively. This is a stress

difference of 40 kPa. Therefore, for a given strain level of 30 percent, the GA system with pipe can tolerate approximately 2.1 m of additional backfill material with a unit weight of 19 kN/m^3 compared to the bare pipe. The stress versus strain behavior observed in GA drainage systems with pipe is similar to the compressible inclusion behavior that is observed in expanded-polystyrene block panels. A compressible inclusion is any material that compresses readily under an applied stress or displacement compared to other materials in contact with, or in the vicinity of, the compressible inclusion (Horvath 1997). The advantage of a compressible inclusion is that the use of a compressible inclusion behind structures such as earth-retaining structures, building walls, and above pipes, culverts, and tunnels, can significantly reduce the earth pressures from both static and dynamic loads (Horvath 1997).

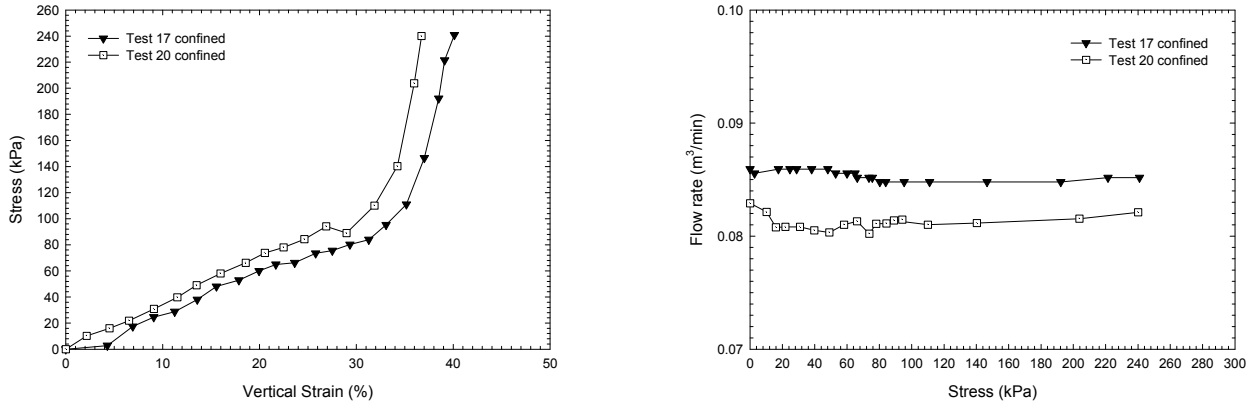

a) Vertical strain b) Cross-plane flow rate

Figure 11. Test results obtained on high density GA drainage systems with pipe.

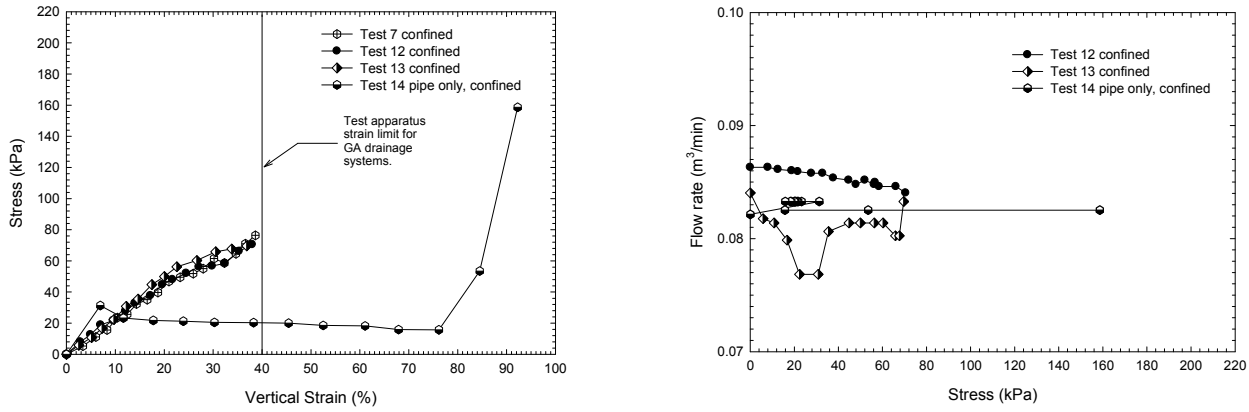

a) Vertical strain b) Cross-plane flow rate

Figure 12. Test results between GA drainage systems with pipe and a stand-alone (bare) pipe.

Figure 12b shows a comparison of the flow rate versus stress behavior between GA systems with an internal pipe and a bare pipe without GA. The measured flow scenario is the cross-plane permeability or permittivity flow into the cross-section of the GA bundle and pipe. The initial and final flow rates of a GA system with pipe is slightly greater than the flow rate of the bare pipe. This difference in the initial and final flow rate measured may be indicative of the higher permittivity of the GA compared to the sand backfill. Thus, even the placement of 7.5 cm of GA around the pipe instead of sand backfill may have the advantage of increasing the flow rate into the pipe.

4. CONCLUSIONS

Two engineering properties that are important for design of GA drainage systems include the stress versus deformation and the flow rate versus stress behavior. This paper presented the preliminary results of a study that was performed to develop a full-scale test chamber and to evaluate the deformation and flow behavior under vertical stresses that would

simulate the loading conditions from trench backfill. The primary components of the test apparatus include the steel chamber, the water supply reservoir system with pump, the water outflow system with flow meter, the hydraulic jack and aluminum load platen, and the removable chamber box cap with built in water supply system. The test system can measure the mechanical deformation and the hydraulic behavior simultaneously. Additionally, the test system can be configured to test either the in-plane flow in the longitudinal direction of GA drainage systems without pipe or the cross-plane flow into the cross-section of GA drainage systems with pipe.

The preliminary testing experience revealed the need to modify the current test apparatus and test procedure. These modifications include reconfiguring the hydraulic jack system so that it sustains load for a longer duration, placing the backfill to a consistent compaction effort such as 90 or 95 percent of the ASTM D 698 laboratory procedure, ensuring that the initial strain at the start of the test is consistently measured, and verifying that full flow of the GA drainage systems is occurring during testing. These modifications are currently being performed.

The preliminary test results on GA drainage systems without pipe indicate that the stress versus strain behavior may be initially linear then the response is strain-hardening and the flow rate decreases with stress increase. The test data obtained on GA drainage systems with pipe indicate that the stress versus strain behavior is nearly linear for the full allowable test system strain limit of 40 percent. The flow rate was less sensitive to stress increase than GA drainage systems without pipe. The use of GA around a pipe instead of sand backfill may have the advantage of increasing the flow rate into the pipe.

Higher density GA drainage systems without a pipe may compress less and, consequently, the flow rate may decrease less than lower density GA. The use of a higher density GA drainage system with a pipe may result in less strain of the overall GA and pipe drainage system. However, the use of a higher density GA may not increase the flow rate into the GA pipe drainage system. The stress versus strain behavior observed in GA drainage systems with pipe appears to be similar to the compressible inclusion behavior that is observed in expanded-polystyrene block panels. The observations presented herein are based on preliminary testing. Supplemental tests are required to validate these observations.

ACKNOWLEDGEMENTS

Post-Doctoral Research Associate, Dr. Morteza Zarrabi, designed the load distribution and the box cap system. His assistance is appreciated.

REFERENCES

ASTM C 33. Standard Specification for Concrete Aggregates, *American Society for Testing and Materials*, West Conshohocken, Pennsylvania, USA.

Brachman, R. W. I., Moore, I. D., and Rowe, R. K. (2000). "The design of a laboratory facility for evaluating the structural response of small-diameter buried pipes." *Canadian Geotechnical Journal*, 37, 281-295.

Geosynthetic Research Institute. (2006a). "GRI Test Method GC9: Mechanical Deformation Behavior of Geosynthetic Aggregate Drainage Systems." GC9, Folsom, PA.

Geosynthetic Research Institute. (2006b). "GRI Test Method GC10: Hydraulic Behavior of Geosynthetic Aggregate Drainage Systems." GC10, Folsom, PA.

Handy, R. L., and Spangler, M. G. (2007). Geotechnical Engineering: Soil and Foundation Principles and Practice, McGraw-Hill, NY.

Horvath, J. S. (1997). "The Compressible Inclusion Function of EPS Geofoam." *Geotextiles and Geomembranes*, 15(1), 77-120.

Moser, A. P. (1990). *Buried Pipe Design*, McGraw-Hill, NY.

Perloff, W. H., and Baron, W. (1976). *Soil mechanics principles and applications*, John Wiley & Sons, New York.

Permittivity of Geotextiles with Uniaxial Tensile Loads

M. Edwards, Department of Civil, Architectural and Environmental Engineering, Drexel University, Philadelphia, PA, USA
J. Kastner, Physics Department, The Richard Stockton College of New Jersey, Pomona, NJ, USA
Y.G. Hsuan, Department of Civil, Architectural and Environmental Engineering, Drexel University, Philadelphia, PA, USA

ABSTRACT
This study evaluates the permittivity of geotextiles, in terms of flow rate, while being subjected to a uniaxial tensile stress, using a newly designed test apparatus. Eight types of geotextiles were used and they included nonwoven, slit film, and, polyester and polypropylene woven geotextiles. The test specimen was 4-in wide and 25-in long. The applied tensile stresses ranged from 10% to 60% of the ultimate tensile strength. A constant 1-in hydraulic head was used to determine the flow behavior.

The results indicate that the flow rate can either increase or decrease as the applied stress increases. The type of geotextile and the orientation of the test sample, with respect to the applied tensile load, are important factors that impact the flow behavior. In general, the flow rate of woven geotextiles increased for samples in the cross-machine direction, and decreased for those in the machine direction, while subject to tensile loading. For the needle-punched nonwoven geotextiles, necking was observed and increased with applied loads, leading to a decrease in the flow rate.

1. INTRODUCTION

Filtration is one of the most common functions of geotextiles. It involves liquid flow across the plane of the geotextile, while retaining the solid on its upstream side. In most geotechnical applications, the geotextile is subjected to a compressive load due to the soil above, while water is being filtered. The current two standard methods for determining permittivity of geotextiles are ASTM D 4491 and ASTM D 5493. ASTM D 4491sepcifies permittivity of geotextiles in an uncompressed state, while, ASTM D 5493 presents the test method for geotextiles subjected to normal compressive loads. None of these two tests, however, consider axial tensile stresses in the geotextiles, as experienced in geotextiles used for filtration in geotextile tube applications, for instance. In the instance of dewatering, a circumferential tensile stress is generated in the geotextile tube during the filling stage. Such stress can have an effect on the water flow rate by changing the opening size of the geotextile. The dewatering behavior can vary significantly due to different orientation of the geotextile with respect to the axial direction of the geotextile tube, as described by Gaffney et al. (2009).

In this paper, a new test apparatus was developed to evaluate the flow behavior of the geotextile while subject to axial tensile loading. Eight different geotextiles were tested; they included two types of nonwoven geotextiles and six types of woven geotextiles. Loads of up to 50% of the tensile strength of the geotextile were applied in the majority of the tests.

2. TEST DESCRIPTION

2.1 Test Apparatus

The new test apparatus, shown in Figures 1a and 1b, was designed for testing geotextiles under axial tensile loads of up to 600 lbs; 150 lb/in (ppi) over a 4-inch wide specimen. The device incorporates a loading system whereby the geotextile can be subjected to axial tensile loading, while measuring the flow rate.

The loading frame consists of a moveable rod across its width to accommodate geotextile samples of lengths 20 to 30 inches (Figure 1b). A constant head permittivity device is positioned between the end of the test frame and the moveable rod. The permittivity device is separated into upper and lower units. A rubber membrane, 0.078 inches in thickness, is attached to the surface of upper and lower units to minimize the transmissivity flow along the geotextile during the test. The upper unit maintains a constant head, while the desired hydraulic head is introduced by rotating the discharge pipe that connects to the lower unit. The hydraulic head is monitored by two piezometers that are connected to the upper and lower units. The flow area is a 2-inch diameter circle (Figure 1b). Water is supplied from a reservoir that is refilled directly with tap water. Once filled, the reservoir tank is left overnight in order to minimize air bubbles generated during the test.

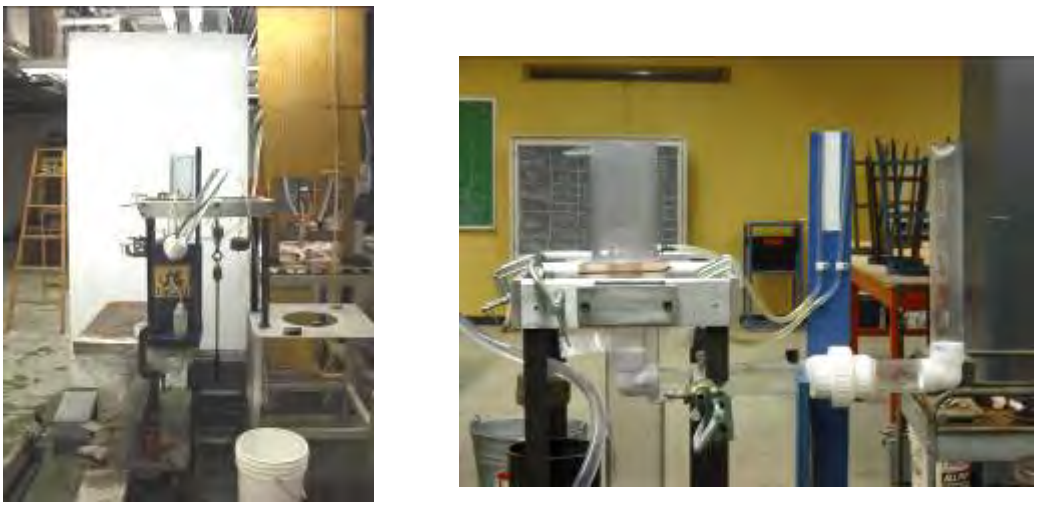

(a) side view (b) front view

Figure 1a. Test apparatus consists of loading frame and constant head permittivity device.

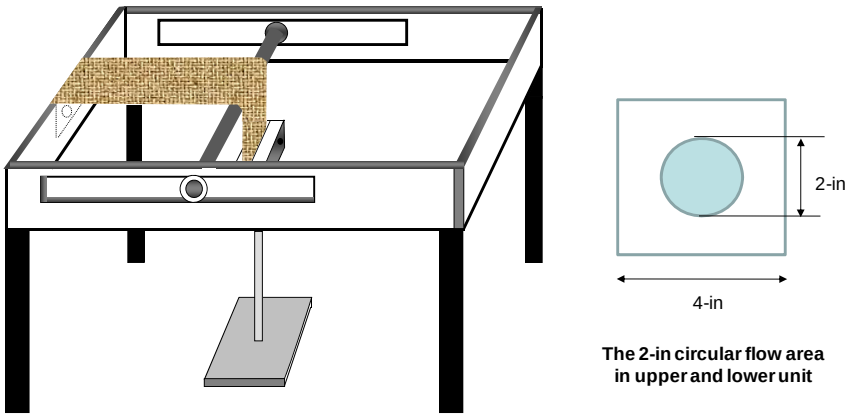

Figure 1b. Loading frame sketch and 2-inch flow area in the upper and lower units.

2.2 Test Procedure

A rectangular shaped specimen with dimensions of 4-in wide and 24-in long is used in this test. The width of 4 inches was chosen because the maximum loading capacity of the frame. Also, to be consistent, the ultimate tensile strength was evaluated using 4-inch wide specimens instead of 8-inch wide as defined in ASTM D4885. The test specimens were soaked overnight in order to ensure saturation and wetting. One end of the specimen was secured to the end of the test frame. The specimen was passed over the lower unit of the permittivity device and laid over the moveable rod. The end of the specimen was clamped with the serrated grip, to which a loading platform was attached (Figure 1b). The moveable rod was locked into a position, so that sufficient clearance between the loading platform and the floor could be assured. The upper permittivity unit was placed on top of the specimen and aligned with the lower unit. Four C-clamps were used to secure the upper and lower units. Water was backfilled through the discharge pipe, up to the top of the lower unit, such that the water level was in contact with geotextile specimen. Bubbles that formed in the pipe were eliminated through the bleed valve.

At each loading, the upper permittivity unit was removed and the desired weight was applied. In order to mobilize the axial tensile stress, the specimen was left with the suspended weight for fifteen (15) minutes during which the specimen was fully saturated with water provided from the lower unit. After that duration, the upper unit was re-secured and water was again backfilled through the discharge pipe.

3. TEST MATERIALS

Eight types of geotextiles were tested. They were needle-punched nonwoven (NW), heatset nonwoven (NW), slit-film woven (SF-woven), polyester woven (PET-woven), and four different types of polypropylene woven geotextiles (PP-woven-1, PP-woven-2, PP-woven-3 and PP-woven-4). The geotextiles were cut into 4-in wide by 25-in long test specimens. Two specimens were cut for each of the woven geotextiles; one in the machine and the other in the cross-machine direction, while one sample was cut for each of the nonwoven geotextiles. It was assumed that the tensile strengths of the nonwoven geotextiles were the same. Two tests were run for each specimen. The hydraulic and mechanical properties of the geotextiles used are shown in Table 1.

Table 1. Properties of tested geotextiles.

Sample	Flow Rate[1]	Ultimate Tensile Strength, (ppi)	
	(gal/min/ft^2)	MD	XMD
Needle-punched NW	109.6	74.6[2]	-
Heat-set NW	10.5	48.0[2]	-
SF-woven	10.9	190[2]	256[2]
PET-woven	23.4	1000[3]	1000[3]
PP-woven-1	30.9	400[3]	600[3]
PP-woven-2	19.9	455[3]	460[3]
PP-woven-3	14.8	447[3]	460[3]
PP-woven-4	15.7	333[3]	333[3]

[1] ASTM D4491 (2-inch hydraulic head)
[2] Measured by ASTM D4885 using 4-inch wide test specimen
[3] Manufacturer's data

4. RESULTS AND DISCUSSION

4.1 Permittivity without Axial Loads

To assure that the new permittivity device was properly designed; the flow behavior of the PET-woven geotextile at different hydraulic heads was evaluated using both the ASTM D 4491 device and the new apparatus. The two sets of data are very similar, as can be seen in Figure 2. However, the slightly lower flow rate obtained from the new apparatus is contributed by the transmissivity, longitudinally, through the rectangular test specimen. As the hydraulic head increases, the amount of transmissivity increases accordingly. In order to minimize the effect of transmissivity on the permittivity flow rate, a 1-inch hydraulic head was selected for this study.

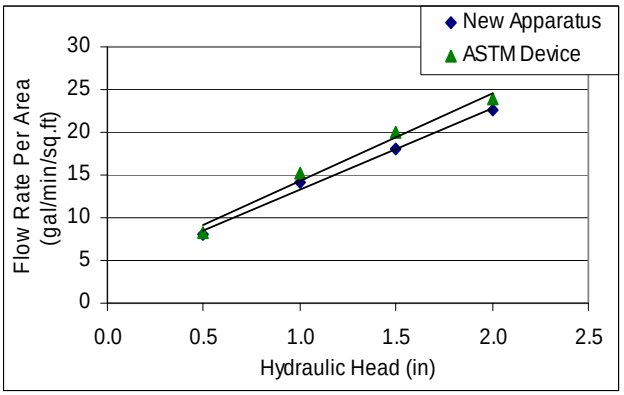

Figure 2. Comparing the flow behavior of ASTM D4491 test device and the new apparatus.

In addition, the flow rate at different hydraulic heads was evaluated for five of the eight geotextile samples using the new apparatus. The tests were performed under zero axial load condition. The objective of this evaluation is to verify the laminar flow occurs within the 2-inch hydraulic head, so that the permittivity test with axial tensile loads can be performed at a hydraulic head of 1-inch.

Figures 3 and 4 respectively show a linear increase of flow rate with hydraulic head for two nonwoven geotextiles and three woven geotextiles, confirming the presence of laminar flow in this range of hydraulic head.

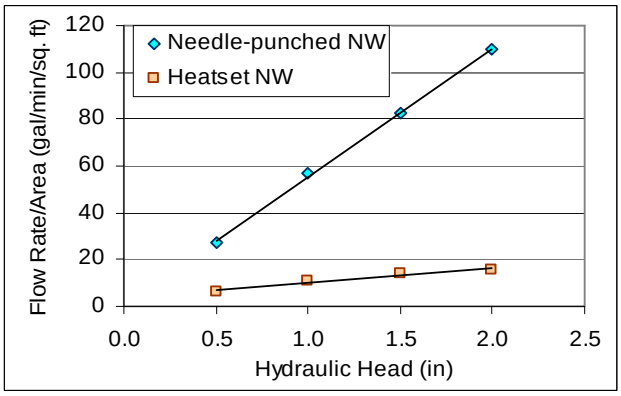

Figure 3. Changes in flow rate per area with hydraulic head for two types of nonwoven geotextiles.

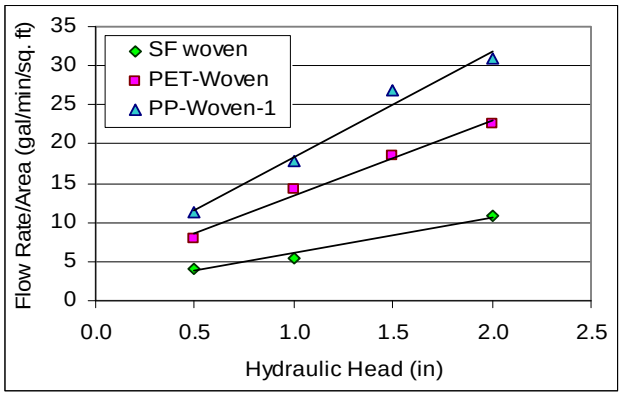

Figure 4. Changes in flow rate per area with hydraulic head for three types of woven geotextiles.

4.2 Permittivity with Axial Loads

4.2.1 Nonwoven geotextiles

Figure 5 and Figure 6 show graphs of the flow rate retained versus applied load for the needle-punched NW and heatset NW geotextiles, respectively. Figure 5 shows a relatively steady decrease in the flow rate through the needle-punched NW geotextile sample. The flow rate retained decreases by 24% when the tensile load increases from 0 to 120 lbs (40% of the ultimate tensile strength). In contrast, the heatset NW exhibits an increase in flow rate by 44% when loaded to 115 1bs (60% of the ultimate tensile strength). The decrease in the flow rate retained for the needle-punched nonwoven can be attributed to the necking that was observed, as the load increased during the test, thus reducing the void sizes of the geotextile. The heatset NW geotextile did not experience the necking phenomenon owing to the thermal bonding. The increase in the flow rate retained was likely caused by the breaking of the thermal bonding as axial loading increased, resulting in the opening up the voids.

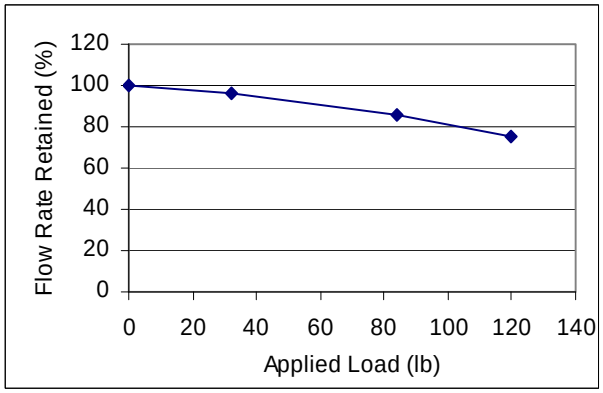

Figure 5. Flow rate retained versus applied load of the needle-punched NW geotextile.

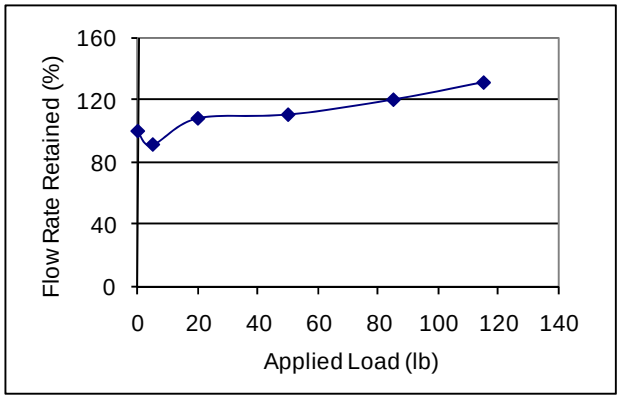

Figure 6. Flow rate retained versus applied load of the heatset NW geotextile.

4.2.2 Woven geotextiles

Figure 7 through Figure 12 illustrate graphs of the flow rate retained versus applied load for the woven geotextile samples. Each figure displays data obtained for each of the woven geotextile samples oriented in the machine (MD) and cross-machine (XMD) directions.

The slit-film geotextile sample exhibits a relatively steady increase in the flow rate retained for both directions. Although the tensile strengths of the MD and XMD of the geotextile are not the same, the flow rate retained profiles are identical in both directions, as the applied load increases from 0 to 415 lbs, as shown in Figure 7.

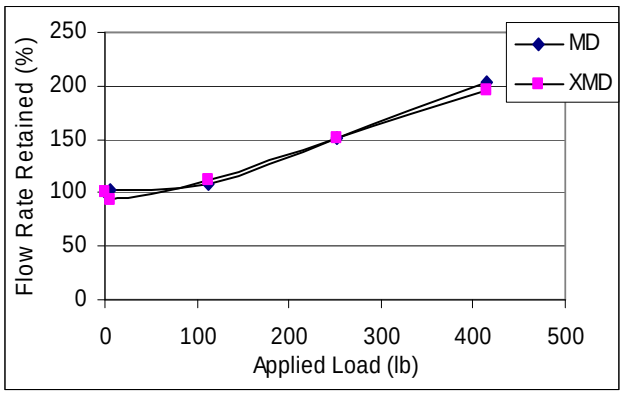

Figure 7. Flow rate retained versus applied load of the SF woven geotextile.

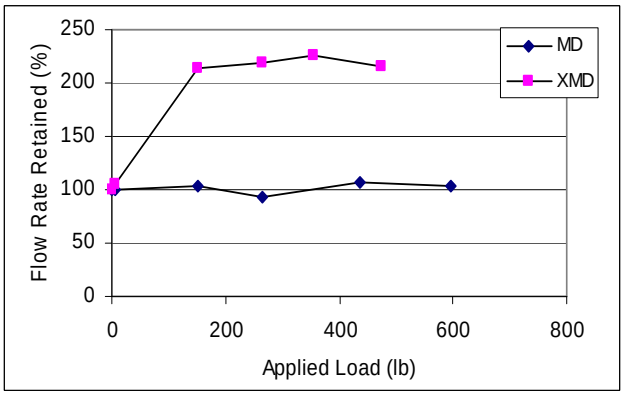

Figure 8. Flow rate retained versus applied load of the PET woven geotextile.

Figure 8 shows that the flow through the PET woven geotextile exhibits different behavior for the MD and XMD samples. In the MD specimen, the flow rate retained essentially remains unchanged, when loading increases from 0 to 595 lbs. On the other hand, the flow rate retained of the XMD specimen increases by 13% at 151 lbs of tensile load. In essence, the flow rate remained the same after that point, even when it was further loaded to 475 lbs. It should be noted that the tensile strengths of the PET geotextile is relatively similar for the MD and XMD samples.

Figure 9 shows the changes in the flow rate retained of the PP-woven-1 geotextile. The flow through the MD specimen decreases by 44% initially, when loaded to 265 lbs and then remains almost unchanged. The XMD sample exhibits the reverse behavior, whereby the flow rate retained is constant at the lower tensile load range, up to 151lbs, and then increases by 76% when loaded from 151 to 595 lbs.

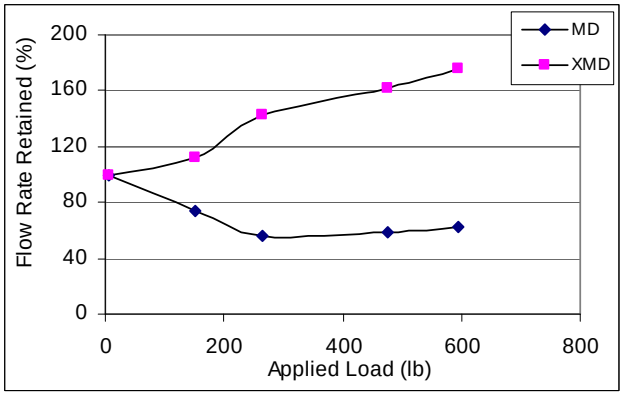

Figure 9. Flow rate retained versus applied load of the PP-woven -1 geotextile.

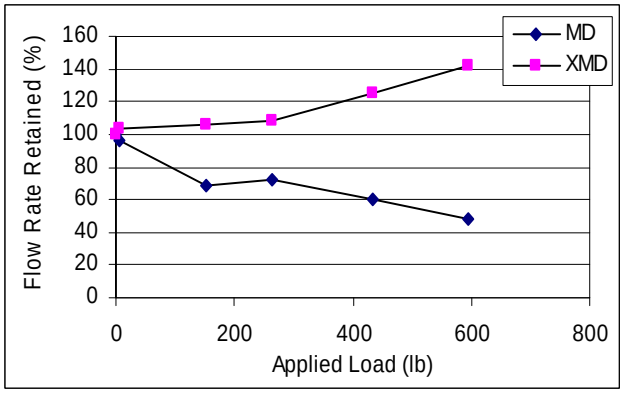

Figure 10. Flow rate retained versus applied load of the PP-woven-2 geotextile.

For the PP-woven-2 geotextile samples, the flow through the MD specimen exhibits a steady decrease in flow rate retained and reaches 52% reduction, when loaded to 595 lbs (Figure 10). In the XMD specimen, the flow rate retained shows a relatively steady increase. Over the same tensile loading as the MD sample, the flow rate retained increases by 42%.

In the PP-woven-3 geotextile samples, a relatively steady decrease in the flow rate retained is experienced for the MD specimen as loading increases (Figure 11). At the tensile load of 595lbs the flow rate retained decreased by 36%. On the contrary, a significant increase in the flow rate retained of the XMD specimen is observed as loading increases. At 595 lbs of applied tensile load, the flow rate is 2.2 times higher than the unloaded value.

The effect of applied load on the flow rate retained of PP-woven-4 geotextile is shown in Figure 12. The flow rate retained decreases approximately 33% as tensile loading increases to 595 lbs, in the MD specimen. A similar amount of increase in flow rate retained was measured, when the same applied tensile load increases, in the XMD specimen.

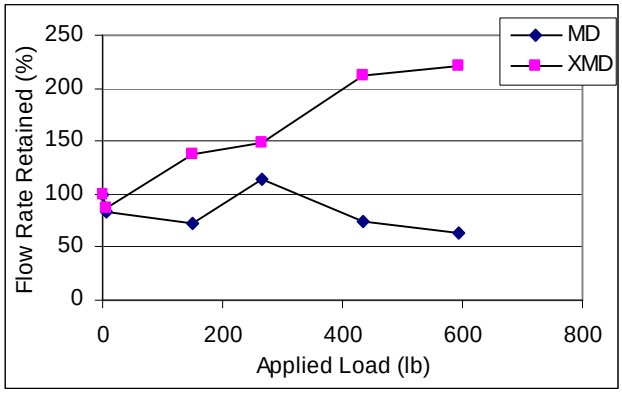

Figure 11. Flow rate retained versus applied load of the PP-woven -3 geotextile.

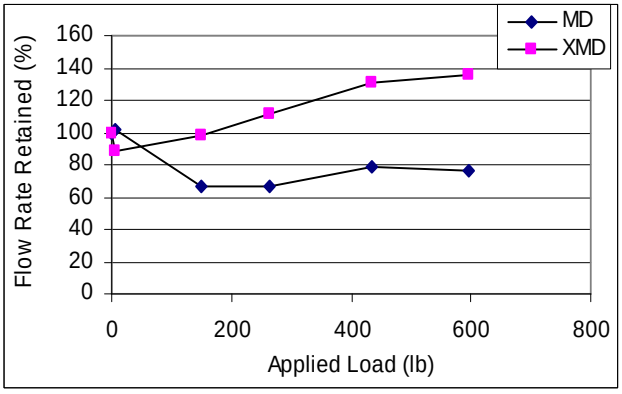

Figure 12. Flow rate retained versus applied load of the PP-woven-4 geotextile.

5. DISCUSSION

The two nonwoven samples exhibited contrasting behavior when subject to tensile loading. The needle-punched nonwoven showed a decrease in flow rate retained whereas, the heatset experienced an increase (Figure 13). The needle-punched NW experienced necking and thus the size of the voids was reduced. Necking was not experienced by the heatset NW, however. Instead, the voids of the heatset NW sample were opened up as the sample was loaded. It should be noted that the heatset NW geotextile is lower in strength by 36% than the needle-punched NW. Thus, the difference in the bonding technique used to produce these materials is one factor that explains the filtration behavior under tensile load, as opposed to the strength of the geotextile.

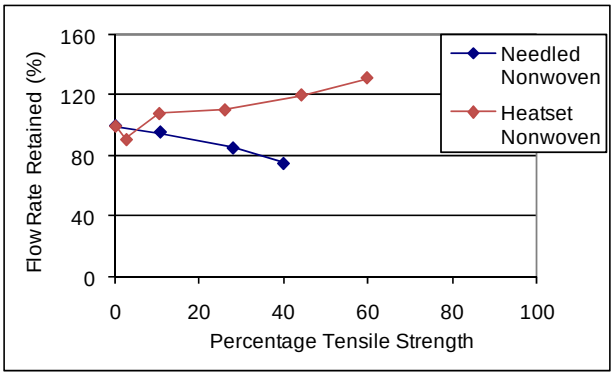

Figure 13. Flow rate retained versus percentage ultimate tensile strength of two nonwoven geotextiles

In the case of the woven geotextile samples, the results indicate that the flow rate can either increase or decrease, as the applied tensile load increases. The flow rate retained increased for all woven geotextile samples in the cross-machine direction, and decreased for all but the SF-woven sample, in the machine direction, while subjected to tensile loading. In the case of the SF-woven, the flow rate retained increases by essentially the same amount in both the cross-machine and machine directions. Figure 14 shows the flow rate retained against the load expressed as % ultimate tensile strength (UTS) of all the woven geotextile samples excluding the SF-woven. All MD specimens, regardless the type of geotextile, behave similarly under axial tensile loading. On the other hand, significant differences can be seen in the XMD specimens. The PET-woven (PET-XMD) sample is the most sensitive to the axial tensile loading; the specimen exhibits an extremely large increase in flow rate retained even though the applied load less than 10% UTS. The PP-woven-1 (W1-XMD) and PP-woven-3 (W3-XMD) samples show similar behavior at applied axial tensile loads less than 15% UTS, after which the flow rate retained of PP-woven-3 increases much more than PP-woven-1, as applied axial tensile load increases. For PP-woven-2 (W2-XMD) and PP-woven-4 (W4-XMD), their flow behavior under axial tensile loading is very similar, and they show the least effect. Their flow rate retained values remained relatively constant until 15% UTS, after which the flow rate increased in general with applied axial tensile loads.

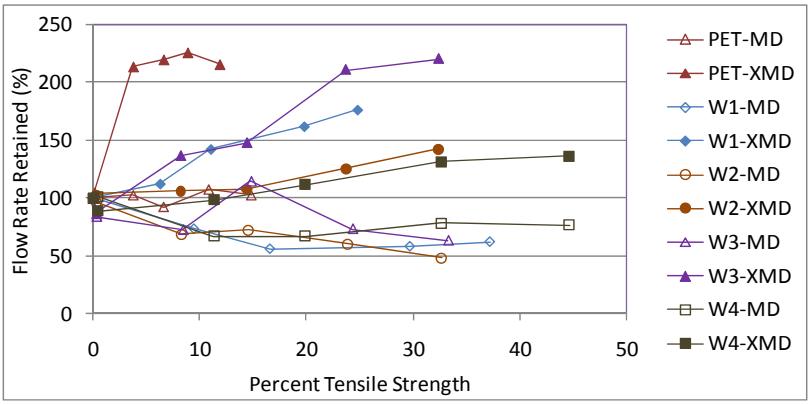

Figure 14. The flow rate retained versus percent ultimate tensile strength of five woven geotextiles.

The data seem to purport that the weaving pattern of the woven geotextiles may play a role in whether the flow rate retained through the geotextile increases or decreases and in which orientation this occurs. Figure 15 shows photos of

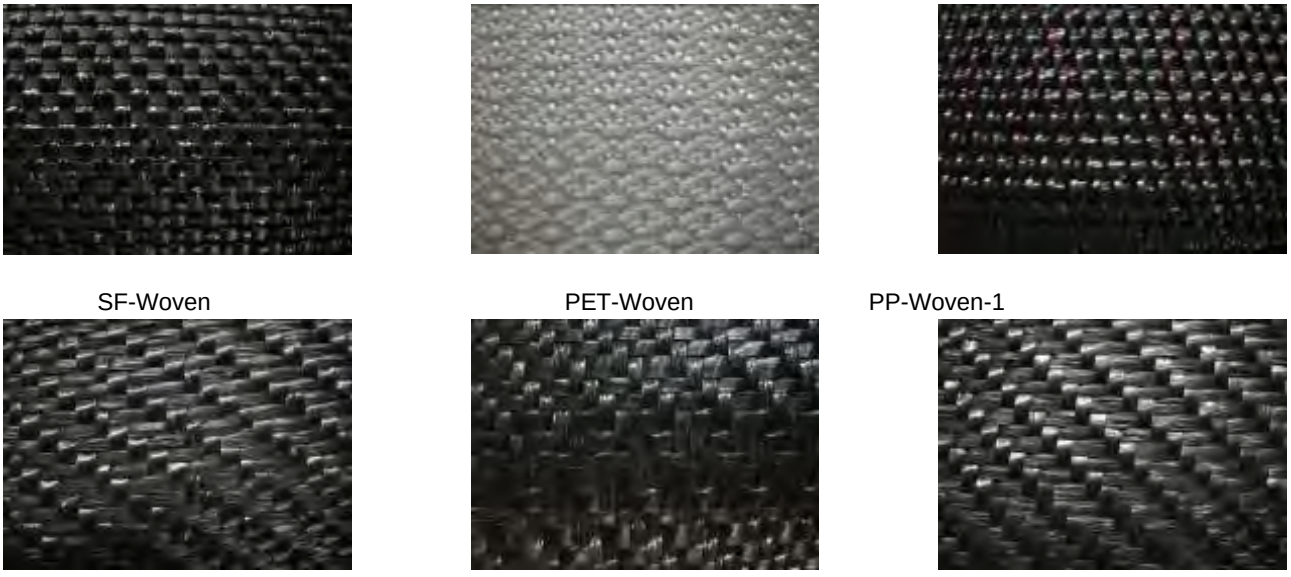

Figure 15. Photos of Woven Geotextile Samples in XMD direction (horizontal direction).

each of the woven geotextile samples. The weaving pattern of PP-woven-2 and PP-woven-4 is apparently the same and that may explain the similarity in their flow behaviors.

Depending on weaving pattern, when loaded in one orientation, the deformation of the geotextile is such that the voids are tightened and when the same geotextile is loaded in the opposite orientation the voids are widened. The degree to which the voids are tightened or widened may depend upon the strain behavior of the geotextile in a given orientation under axial tensile loading. The stress and strain experienced by the geotextile, as the tensile load is applied, needs to be monitored during the test and was not addressed in this study.

The current limitation of this new apparatus is the maximum loading capacity, which is 600 lbs. For very high strength geotextiles, this value can be about 15% of UTS, as in the instance of the PET-Woven sample. Transmissivity is another challenge that was encountered during testing. Some of the geotextile samples experienced in-plane flow, longitudinally, through the geotextile samples. The magnitude of the transmissivity also increased with applied load and was not experienced at zero loading. This phenomenon would introduce error in the measured flow rate but was minimized by using a hydraulic head of 1-inch.

Future research will involve the measurement of the flow rates through geotextiles under bi-axial tensile load, in order to more accurately investigate the effect of tensile stresses generated in geotextile tubes on the flow rate.

6. CONCLUSION

The results indicated that flow rate through the geotextile can increase or decrease under axial tensile loading. The resulting trend is dependent upon various parameters, which include the type of geotextile, the type of bonding and the orientation of the test sample. The applied tensile load, in terms of percentage UTS of the geotextile, does not always predict the changes in the flow behavior. It is purported, however, that the movement of the weaving pattern under axial tensile loading, is more likely to influence the response of the flow behavior of the geotextile.

ACKNOWLEDGEMENTS

The financial support of this project is partially provided by the Ocean-Coastal Company. Mr. Kastner was supported by the National Science Foundation Research Experience for Undergraduate Program and Miss Edwards is supported by the ASEE-GAANN Fellowship. Advice of Dr. Richard Weggel is also appreciated.

REFERENCES

ASTM D 4491. Standard Test Methods for Water Permeability of Geotextiles by Permittivity, *American Society for Testing and Materials*, West Conshohocken, Pennsylvania, USA.

ASTM D 4885. Standard Test Methods for Permittivity of Geotextiles Under Load, *American Society for Testing and Materials*, West Conshohocken, Pennsylvania, USA.

ASTM D 5493. Standard Test Methods for Permittivity of Geotextiles Under Load, *American Society for Testing and Materials*, West Conshohocken, Pennsylvania, USA.

Gaffney, D.A., Hsuan, G., Weggel, J.R., and Munoz, R. (2009), *Drainage Characteristic of Geotextiles under Tensile Loads*, Geosynthetics 2009, Feb. 25-27, Salt Lake City, Utah.

.

Geosynthetics 2009
February 25-27 2009, Salt Lake City, Utah

A Study to Determine the Causes and Effects of Turbulence in Transmissivity Tests

R.E. Belanger, C.B. Queja, C.V. Zantua; Precision Geosynthetic Laboratories, Anaheim, CA, USA

ABSTRACT
This study sought to investigate the nature and quantity of turbulence generated during transmissivity testing of geonets. The turbulence is presented in terms of Flow Rate Loss and Reynolds Number. A method to determine the Flow Rate Loss due to the side walls of the transmissivity apparatus has been developed. Side wall effect pertains to circumstances where the net channels direct the water flow toward the walls of the apparatus thereby creating retardation of the flow. This methodology also enables the possibility of calculating the Storage Capacity of the geonet - the volume of water that can be stored per unit area.

1. INTRODUCTION

Geonets are widely used in civil and environmental engineering applications for planar drainage of various liquids. In some situations it also functions as a passage for movement of gases in waste containment facilities. Geonets are geosynthetics consisting of integrally connected parallel sets of ribs overlying similar sets of various angles. These are so designed primarily for draining liquid purposes (ASTM D4716-08).

Due to high capital outlay for geonet installation, the designed functionality and performance must be cost-efficient. Since transmissivity and flow rate are key parameters in selecting the correct type and thickness of geonet to be used. This information may lead to better decisions affecting engineering and valuing of a project.

It was postulated that the use of the apparatus described in ASTM D4716-08 test method leads to an underestimation of the flow rate due to turbulence caused by the side walls. In the field, the water drains freely in all directions through the flow paths created by the geonet. These flow paths are normally not bounded by walls that are part of the test apparatus. The typical laboratory setup and flow paths, shown for one plane layer of the biplanar geonet, are illustrated in Figure 1 below.

Figure 1 Flow Path of Water

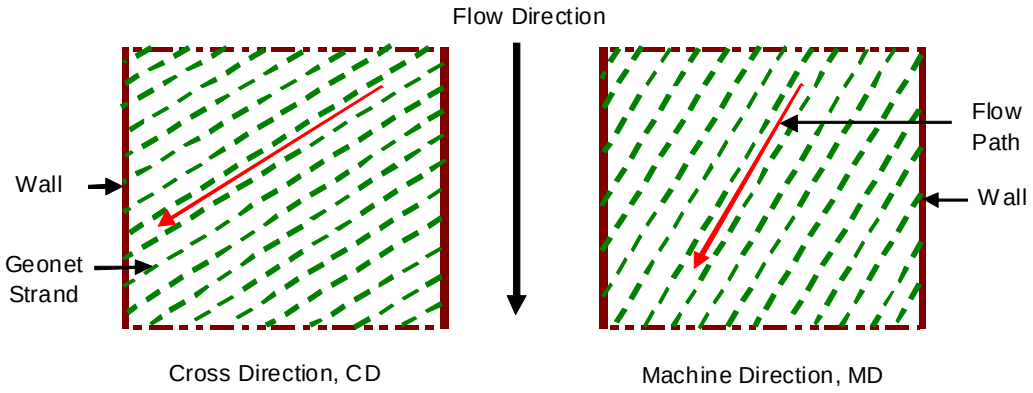

As shown in Figure 1, the CD (Cross Direction) geonet channels, direct the water flow into the wall; whereas the MD (Machine Direction) geonet channels, primarily direct the water flow out of the drainage end of the transmissivity apparatus. This investigative study attempts to estimate the fraction of turbulence contributed by the geonet strands that direct the water flow into the wall of the transmissivity apparatus as measured by flow rate loss caused by the side walls.

Most laboratory procedures produce a high velocity turbulent flow within the geosynthetic, to which Darcy's Law does not apply (Hufenus and Schrade, 2006). Transmissivity is related to laminar flow conditions only and equals the water flow capacity at a hydraulic gradient equal to unity. As non-laminar flow may occur, the term flow capacity is preferred (ISO

12958). Thus, for these investigations the test results will be expressed as Flow Rate and Reynolds Number. Because of the velocities produced during the testing various forms of turbulence are produced that are not well understood.

As part of the methodology, the storage capacity for the geonets is determined. Geonet void space is important because the water flows through the void space between the net strands. This also acts as storage space should the geonet be inundated in excess of its flow rate capacity.

The numbers generated in this paper should be considered estimates to demonstrate trends that can be further refined. It is believed that these estimates will be useful for geonet and geocomposite engineering design, and for the purpose of writing relevant drainage specifications.

2. METHODOLOGY

2.1 Sample Selection and Specimen Preparation

Geonet A with a thickness of approximately 5.65mm and Geonet B with a thickness of approximately 5.80mm; both biplanar sourced from different manufacturers was used for these experiments. They were selected to assess the sensitivity and/or consistency of the test in responding to a relatively slight geonet thickness variation at similar test conditions. The third biplanar geonet, Geonet C, had an approximate thickness of 7.51mm which was chosen to obtain higher flow rates for comparative analyses.

Two specimen widths were used through out the testing; the standard 305mm x 305mm and a narrower half the standard width, of 152mm and a length of 305mm. For testing of the narrower width a closed cell rubber mat was placed next to the 152mm x 305mm geonet specimen to block the water flow (Figure 2). This was done so an estimate of the wall and geonet contributions to the flow rate loss was possible. Because the Wall-To-Width ratio doubles when using the 152mm x 305mm specimen, the wall effect is accentuated. Because there are two 305 mm walls, the Wall-To-Width ratio for the standard setup is 2 (610 mm / 305 mm = 2), and 4 for the narrower specimen (610 mm/ 152 mm = 4).

The testing plan consisted of two sets of tests:

1. The first part tested two different size geonet specimens; 305mm x 305mm and 150mm x 305mm in the Machine and Cross directions for Flow Rate as shown in Figure 3.
2. The second segment tested Flow Rate without the net present that corresponds to the “net-void volume”.

The ‘net-void volume” setup was a laterally unrestricted flow path wherein geonet was not used but the flow path volume corresponded to the comparative net-void volume. The volume of the void space was determined by Equation 2; measuring the specific specimen’s mass per unit area and resin density. . The height separating the top and bottom plates of the transmissivity apparatus for net-void volume testing was carried out by placing a “305mm x 12.7mm x various mm thicknesses” feeler gages” in both sides of the apparatus along the direction of water flow. Depending on the calculated equivalent height determined in Equation 5, various thicknesses feeler gages were stacked on each side to equal the desired gap height. The space occupied by feeler gages was considered in the calculations.

Figure 2. Sample Orientation of 152mm x 305mm Specimen and Rubber Mat In the Transmissivity Apparatus

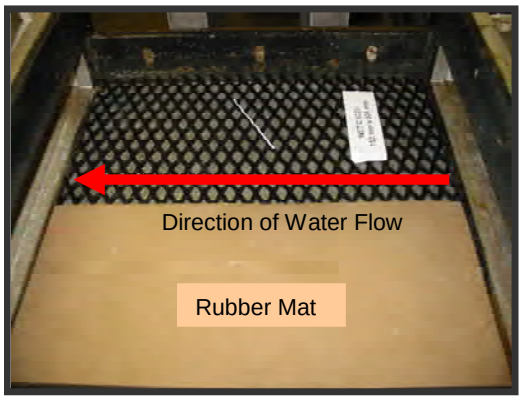

Figure 3. Sample Cut Specimens (305mm x 305mm and 152mm x 305mm)

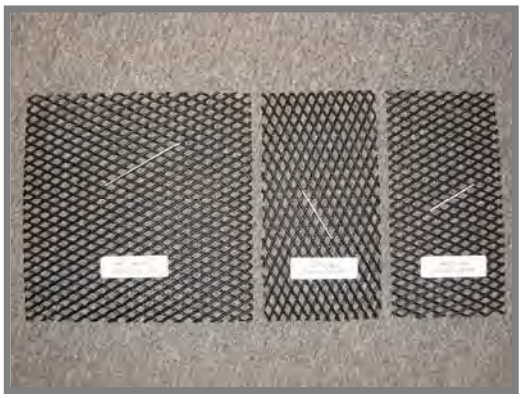

The specimens were carefully die cut to the desired dimensions to ensure visual physical homogeneity. To avoid errors in geonet geometry, only one 305mm x 305mm specimen was prepared to be used for both machine and cross directions (MD and CD) for all three geonet samples. However, one 305mm x 152mm MD and one 305mm x 152mm TD specimens were used. Because the geonets were biplanar, one plane of the geonet was marked so that all tests could be conducted with that plane in the top position for consistency.

2.2 Gradient

Three hydraulic gradients were used: 0.33, 0.10 and 0.025. The 0.33 gradient was the maximum gradient based on the testing apparatus limitation to maintain a consistent gradient with the net-void volume set up. These gradients were also selected with the idea that some of the tests would show Reynolds Numbers (Re) in all three regions:

- laminar if Re < 2300
- transient for 2300 < Re < 4000
- turbulent if Re > 4000

2.3 Normal Load

A normal load of 345 kPa was used for all testing. At this load the geonets exhibited some compression, so for calculating, the reduced thickness was used.

2.4 Testing Procedure

The laboratory experiments were based upon ASTM D4716 Test Method with the noted changes to accomplish the goals of these studies. It was used to determine the in-plane flow rate per unit width and hydraulic transmissivity of the selected geonet specimens using a constant head method. Because the testing was conducted in a primarily turbulent environment, Flow Rate is used rather than Transmissivity.

The first step was to test all geonets according to the described parameters.

The next step carried out was the calculation of the height between the top and bottom plates of the testing apparatus according to the equations that follow; and testing for the flow rates corresponding to the net-void volumes.

2.5 Calculations

The total volume of each geonet specimen was determined by measuring the length, width and “compressed or reduced” thickness by ASTM D5199.

Equation 1

$$V_{\text{total geonet volume}} = L \times W \times T_{\text{reduced}} \quad [1]$$

$V_{\text{total geonet volume}}$ = total volume of geonet specimen including void space
L = Length geonet specimen
W = Width of geonet specimen
T_{reduced} = Thickness of geonet specimen measured after the test at 345 KPa Normal Load

It was necessary to separate the void volume and the geonet volume from Equation 1 in order to calculate the “gap” or height between the upper and lower plates. By measuring the mass per unit area and the density of the geonet resin, the geonet void volume was determined. Having gap height obtained, the transmissivity of the net-void volume or “blank” set up was performed.

Equation 2

$$V_{\text{geonet}} = M / D \quad [2]$$

V_{geonet} = volume of geonet specimen
M = mass of the geonet specimen
D = density of the geonet specimen

The total volume is composed of the geonet plastic volume and the void volume as shown in Equation 3.

Equation 3

$$V_{total\ geonet} = V_{geonet} + V_{void} \quad [3]$$

$V_{total\ geonet}$ = total volume of geonet specimen including void space
V_{geonet} = volume of geonet specimen
V_{vvoid} = void volume

Rearranging Equation 3, the void volume can be determined by Equation 4

Equation 4

$$V_{(void)} = V_{total\ geonet} - V_{geonet} \quad [4]$$

Gap height is derived by substituting the values obtained from the equations above to Equation 5. The length and width of the standard feeler gage used is 305mm and 12.7mm, respectively.

Equation 5

$$V_{total\ geonet} = V_{void} - V_{feeler\ gage} \quad [5]$$

V_{void} = void volume
$V_{feeler\ gage}$ = volume of feeler gage

The measured geonet specimen properties required for this calculation are summarized in Table 1 below together with the determined volumes. The evaluated gap heights were used in the actual test setup in determining "Net-Void Volume Flow Rate" at different gradients.

Table 1. Geonet Properties and Calculated Gap Height for Net-Void Testing

Set-Up No.	Specimen Label	Spicemen Size W (mm)	Spicemen Size L (mm)	Flow Through Sample Along	Thickness (After) (mm)	Density (g/cm^3)	Mass (g)	Volume of Net (cm^3)	Total Volume of the Specimen (cm^3)	Net-Void Volume (cm^3)	Std.Feeler Gage Area (cm^2)	Gap Height, t (see Note 1) (mm)
1	MD Net A	305	305	L	5.60	0.9512	76.20	80.11	520.53	440.42	38.71	5.16
2	CD Net A	305	305	L	5.60	0.9512	76.20	80.11	520.53	440.42	38.71	5.16
3	MD Net A	**152**	305	L	5.66	0.9512	38.90	40.90	262.36	221.46	38.71	5.73
4	CD Net A	**152**	305	L	5.62	0.9512	39.82	41.86	260.47	218.61	38.71	5.66
5	MD Net B	305	305	L	5.71	0.9551	76.59	80.19	531.40	451.21	38.71	5.29
6	CD Net B	305	305	L	5.71	0.9551	76.59	80.19	531.40	451.21	38.71	5.29
7	MD Net B	**152**	305	L	5.66	0.9551	37.86	39.64	262.59	222.95	38.71	5.77
8	CD Net B	**152**	305	L	5.68	0.9551	37.26	39.01	263.30	224.29	38.71	5.81
9	MD Net C	305	305	L	7.40	0.9561	165.31	172.90	688.06	515.16	38.71	6.04
10	CD Net C	305	305	L	7.40	0.9561	165.31	172.90	688.06	515.16	38.71	6.04
11	MD Net C	**152**	305	L	7.29	0.9561	82.73	86.53	338.19	251.66	38.71	6.52
12	CD Net C	**152**	305	L	7.31	0.9561	81.95	85.71	338.90	253.18	38.71	6.56

Measured thicknesses of specimens before testing (ave. of ten readings): Net A=5.65mm, Net B=5.80mm, Net C=7.51mm

3. RESULTS AND DISCUSSIONS

3.1 Geonet Flow Rate

Table 2 lists Geonet flow rates calculated following the actual testing procedures for the 305 mm x 305mm and the 152mm x 305mm specimens at the three gradients specified.

Table 2. Geonet Flowrates

Direction	Dimensions	Net A			Net B			Net C		
	(mm)	G=0.33	G=0.10 *(liter/sec)*	G=0.025	G=0.33	G=0.10 *(liter/sec)*	G=0.025	G=0.33	G=0.10 *(liter/sec)*	G=0.025
MD	305mm X 305mm	0.44	0.22	0.11	0.45	0.22	0.09	0.52	0.24	0.13
MD	152mm X 305mm	0.28	0.13	0.06	0.29	0.12	0.05	0.27	0.14	0.08
CD	305mm X 305mm	0.11	0.06	0.02	0.14	0.08	0.04	0.13	0.07	0.04
CD	152mm X 305mm	0.13	0.05	0.02	0.13	0.06	0.03	0.08	0.04	0.02

MD - Machine direction CD - Cross Direction

3.2. Net-Void Flow Rate (without geonet)

Table 3 lists net-void or blank flow rates calculated without a net in the water path which is proportional to the space vacated by the 305mm x 305mm and the 152mm x 305mm test specimens (see Section 2.5).

Table 3. Net-Void Flowrates

Direction	Dimensions	Net A			Net B			Net C		
	(mm)	G=0.33	G=0.10 *(liter/sec)*	G=0.025	G=0.33	G=0.10 *(liter/sec)*	G=0.025	G=0.33	G=0.10 *(liter/sec)*	G=0.025
MD	305mm X 305mm	1.43	0.75	0.38	1.57	0.85	0.41	1.99	0.93	0.54
MD	152mm X 305mm	0.66	0.38	0.17	0.70	0.39	0.21	0.92	0.45	0.27
CD	305mm X 305mm	1.43	0.75	0.38	1.57	0.85	0.41	1.99	0.93	0.54
CD	152mm X 305mm	0.71	0.37	0.19	0.74	0.41	0.24	0.89	0.48	0.29

MD - Machine direction CD - Cross Direction

3.3. Flow Rate Loss Due to Net

The flow rate is substantially decreased by the presence of the geonet as seen by comparing the flowrates with and without the geonets (Tables 2 and 3). It is theorized that the Total Flow Rate Loss due to net is the sum of geonet, side walls, and other friction losses. However, only geonet and walls effect are considered in this study as the prime causes of turbulent flow and thereby contributes to flow rate loss.

Table 4 below shows the MD and CD flow rate due to net derived by substituting the values from Tables 2 and 3 into Equation 6.

Equation 6

$$\text{Flow Rate Loss Due to Net} = \text{Net-Void Flow Rate} - \text{Geonet Flow Rate} \quad [6]$$

Table 4. Net-Void Flowrates Minus Net Flowrates

Direction	Dimensions	Net A			Net B			Net C		
	(mm)	G=0.33	G=0.10 *(liter/sec)*	G=0.025	G=0.33	G=0.10 *(liter/sec)*	G=0.025	G=0.33	G=0.10 *(liter/sec)*	G=0.025
MD	305mm X 305mm	0.99	0.53	0.27	1.12	0.62	0.32	1.47	0.69	0.41
MD	152mm X 305mm	0.38	0.26	0.11	0.41	0.27	0.16	0.65	0.31	0.19
CD	305mm X 305mm	1.31	0.69	0.36	1.43	0.77	0.38	1.86	0.86	0.50
CD	152mm X 305mm	0.58	0.32	0.18	0.61	0.35	0.21	0.81	0.44	0.27

MD - Machine direction CD - Cross Direction

The values shown above represent the effect that was directly caused by the geonet and its inherent directional flow path with the wall present. These two combined, created varying flow rates, velocities and turbulence. The mechanics of "directional transmissivity" phenomenon in testing geonet and geocomposite is amply explained by M. Minch and M. Li in their Year 2008 paper titled "Effects of Flow Direction on Transmissivity of Biplanar Geonet in…."

3.4. Reynolds Number

Reynolds Numbers for the experimental were calculated to verify if the assumption of turbulent flow was inherent to the testing. Reynolds Number determines the flow characteristic and generally recognized as defining laminar and turbulent flows:

- Laminar if Re <2300
- Transient if 2300 < Re < 4000
- Turbulent if > 4000

The Reynolds Number is important in analyzing any type of flow when there is substantial velocity. It is a non-dimensional quantity associated with the smoothness of flow of a fluid. At low velocities fluid flow is smooth, or laminar, and the fluid can be pictured as a series of parallel layers or lamina moving at different velocities. The fluid friction between these layers gives rise to viscosity. As the fluid flows more rapidly, it reaches a velocity, known as the critical velocity, at which the motion changes from laminar to turbulent, with the formation of eddy currents and vortices that disturb the flow.

The Reynolds Number Equation for Pipe or Duct is shown in Eq. 7

Equation 7

$$Re = 7745.8\ u\ d_h / v \qquad [7]$$

u = velocity (ft/s)
d_h = hydraulic diameter (in)
v = kinematic viscosity (cSt)

The Kinematic Viscosity of water at 68 ^{o}F is for all practical purposes 1.0 cSt.

The velocity u, is in ft/s, so the Hazen-Williams formula was used to convert the gal/min determined from the testing to ft/s as shown in Eq. 8

Equation 8

$$u = 0.4087\ q / d_h^2 \qquad [8]$$

u = flow velocity (ft/s)
q = volume flow (gal/min)
d_h = inside hydraulic diameter (inches)

The hydraulic diameter d_h is not the same as the geometrical diameter in a non-circular duct or pipe and can be calculated with the generic Equation 9.

Equation 9

$$d_h = 4\ A / p \qquad [9]$$

d_h = hydraulic diameter
A = area section of the duct = width x thickness of specimen
p = wetted perimeter of the duct = 2 x width + 2 x Thickness of specimen

Only the Reynolds Number for the standard size specimen of 305mm x 305mm was calculated because it is the condition commonly tested

Table 5. Reynolds Number (305mm x 305mm Geonet Specimen, MD)

	Unit	Net A			Net B			Net C		
		G=0.33	G=0.10	G=0.025	G=0.33	G=0.10	G=0.025	G=0.33	G=0.10	G=0.025
Width, W	in	12	12	12	12	12	12	12	12	12
Thickness, t	in	0.222	0.222	0.222	0.228	0.228	0.228	0.296	0.296	0.296
Area, A	in^2	2.664	2.664	2.664	2.736	2.736	2.736	3.552	3.552	3.552
Wetted Perimeter, P	in	24.444	24.444	24.444	24.456	24.456	24.456	24.592	24.592	24.592
Hydraulic Diameter, d_h	in	0.436	0.436	0.436	0.447	0.447	0.447	0.578	0.578	0.578
Hydraulic Diameter Squared, d_h^2	in^2	0.190	0.190	0.190	0.200	0.200	0.200	0.334	0.334	0.334
Volume Flow, q	gal/min.	6.945	3.423	1.698	7.171	3.535	1.465	8.189	3.845	2.082
Constant, From Equation 8	-	0.4087	0.4087	0.4087	0.4087	0.4087	0.4087	0.4087	0.4087	0.4087
Velocity, u	ft/sec	14.94	7.36	3.65	14.64	7.22	2.99	10.03	4.71	2.55
Constant, From Equation 7	-	7,745.8	7,745.8	7,745.8	7,745.8	7,745.8	7,745.8	7,745.8	7,745.8	7,745.8
Kinematic Viscosity, V	cSt	1.0	1.0	1.0	1.0	1.0	1.0	1.0	1.0	1.0
Reynolds Number, Re	-	50,435	24,858	12,332	50,732	25,010	10,361	44,871	21,068	11,408

Table 6. Reynolds Number (305mm x 305mm Geonet Specimen, CD)

	Unit	Net A			Net B			Net C		
		G=0.33	G=0.10	G=0.025	G=0.33	G=0.10	G=0.025	G=0.33	G=0.10	G=0.025
Width, W	in	12	12	12	12	12	12	12	12	12
Thickness, t	in	0.222	0.222	0.222	0.228	0.228	0.228	0.296	0.296	0.296
Area, A	in^2	2.664	2.664	2.664	2.736	2.736	2.736	3.552	3.552	3.552
Wetted Perimeter, P	in	24.444	24.444	24.444	24.456	24.456	24.456	24.592	24.592	24.592
Hydraulic Diameter, d_h	in	0.436	0.436	0.436	0.447	0.447	0.447	0.578	0.578	0.578
Hydraulic Diameter Squared, d_h^2	in^2	0.190	0.190	0.190	0.200	0.200	0.200	0.334	0.334	0.334
Volume Flow, q	gal/min.	1.809	0.874	0.367	2.224	1.189	0.595	2.139	1.134	0.688
Constant, From Equation 8	-	0.4087	0.4087	0.4087	0.4087	0.4087	0.4087	0.4087	0.4087	0.4087
Velocity, u	ft/sec	3.89	1.88	0.79	4.54	2.43	1.21	2.62	1.39	0.84
Constant, From Equation 7	-	7,745.8	7,745.8	7,745.8	7,745.8	7,745.8	7,745.8	7,745.8	7,745.8	7,745.8
Kinematic Viscosity, V	cSt	1.0	1.0	1.0	1.0	1.0	1.0	1.0	1.0	1.0
Reynolds Number, Re	-	13,133	6,347	2,665	15,730	8,413	4,210	11,720	6,214	3,770

From the Reynolds Numbers shown in Tables 5 and 6, it can be seen that the testing is not a laminar environment with all; but with one point that fell into the Transient region.

3.5 Flow Rate Loss Due To Wall

The direct influence of the geonet was determined by comparing the net flow rates versus the net-void volume flow rates. By subtracting the Net Flow Rate from the Net-Void Volume Flow Rate, the reduction in flow rate due to the Net is determined (Table 4). The net caused reduction in flow rate in two ways: the first is due to the resistance of the net structure itself and the second is due to the geonet flow channels directing the flow into the walls.

At this point the direct net influence has been determined but the direct net influence has two components: net resistance and net flow channels directing flow toward the wall. By using the two different width specimens, an estimate the contribution of the two components can be made.

This has been accomplished by calculating Wall-to-Width Ratio (WWR) for the two different size samples and plotting them against the Flow Rate Loss Due To Net obtained from Section 3.3, as presented in Table 4. Solving for the WWR of the standard specimen yields a numerical value of 2 (i.e., 610mm / 305mm = 2) and calculating the WWR of the 152mm width specimen results to 4 (i.e., 610 / 152 = 4).

By graphing WWR versus Flow Rate Loss due to Net, the Linear Regression Equation for the resultant straight line was determined. This is illustrated by using the data from Table 4 for Geonet B using Flow Rate Loss Due to Net values in MD direction at Gradient 0.33; that is, 1.12 lit./sec for 305mm x 305mm and 0.41 lit./sec for 152mm x 305mm. Figure 4 below is the graph developed by plotting WWR 2 and 4 (*x-axis*) versus Flow Rate Loss Due to Net (*y- axis*).

Figure 4. Flow Rate Loss Due to Net VS. Wall-To-Width Ratio

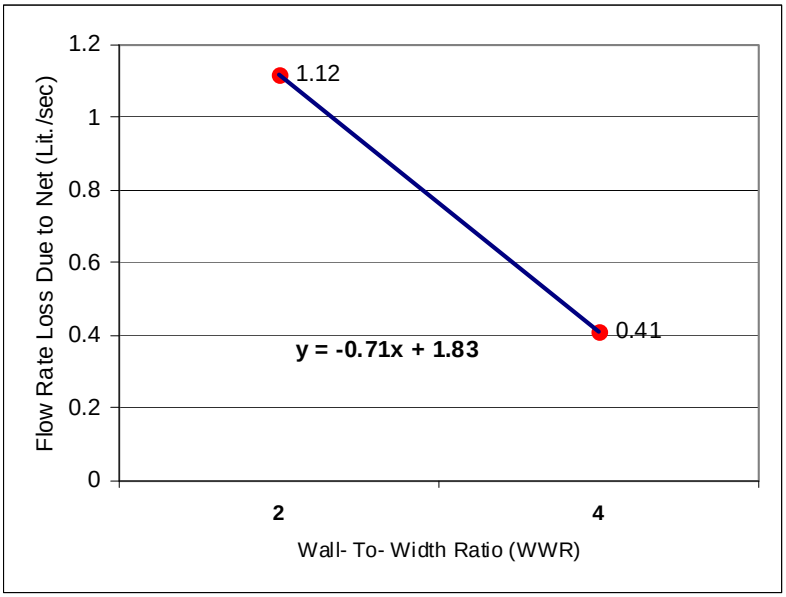

The Linear Regression Equation is: *y =- 0.71x + 1.83*. The constant (1.83) represents the flow rate by setting the wall dimension to zero (WWR=0). Using the same procedure, the other calculated values are listed in Table 6. As determined earlier the Net B flow rate at 0.33 Gradient in the MD direction was 0.45 lit./sec. The 0.45 lit./sec flow rate was the result of the net resistance and the net channels directing flow into the walls.

It was assumed that the actual measured flow rate was an under estimate of the flow rate experienced in the field because in actual condition, the geonet is not bounded by walls as in the test apparatus but rather open ended and free flowing.

Table 6. Flow Rates Summary

MD	NET A			NET B			NET C			
Dimensions	**G=0.33**	**G=0.1**	**G=0.025**	**G=0.33**	**G=0.1**	**G=0.025**	**G=0.33**	**G=0.1**	**G=0.025**	REMARKS
305mm X 305mm net	0.44	0.22	0.11	0.45	0.22	0.09	0.52	0.24	0.13	**[A]** Net Flow Rate (Wall effect present)
305mm X 305mm net-void	1.43	0.75	0.38	1.57	0.85	0.41	1.99	0.93	0.54	**[B]** Net-Void Flow Rate (Wall effect present)
	1.60	0.81	0.43	1.83	0.99	0.48	2.29	1.07	0.63	**[C]** Flow Rate when WWR is set to Zero (X=0)
	0.17	0.06	0.05	0.26	0.14	0.07	0.30	0.14	0.09	**[D=C-B]** Flow Rate Loss Due To Wall
	0.61	0.28	0.16	0.72	0.37	0.16	0.82	0.38	0.22	**[E=A+D]** Hypothetical Flow Rate if Loss due to Wall is eliminated
	28%	22%	31%	37%	39%	42%	37%	37%	41%	**[F=D/Ex100]** % hypothetical Flow Rate unaccounted for due to Wall effect

CD	NET A			NET B			NET C			
Dimensions	G=0.33	G=0.1	G=0.025	G=0.33	G=0.1	G=0.025	G=0.33	G=0.1	G=0.025	REMARKS
305mm X 305mm net	0.11	0.06	0.02	0.14	0.08	0.04	0.13	0.07	0.04	**[A]** Net Flow Rate (Wall effect present)
305mm X 305mm net-void	1.43	0.75	0.38	1.57	0.85	0.41	1.99	0.93	0.54	**[B]** Net-Void Flow Rate (Wall effect present)
	2.06	1.06	0.55	2.25	1.19	0.53	2.91	1.28	0.73	**[C]** Flow Rate when WWR is set to Zero (X=0)
	0.63	0.31	0.17	0.68	0.34	0.12	0.92	0.35	0.19	**[D=C-B]** Flow Rate Loss Due To Wall
	0.75	0.37	0.19	0.82	0.42	0.15	1.05	0.42	0.23	**[E=A+D]** Hypothetical Flow Rate if Loss due to Wall is eliminated
	85%	85%	88%	83%	82%	76%	88%	83%	83%	**[F=D/Ex100]** % hypothetical Flow Rate unaccounted for due to Wall effect

When comparing the net flow rates versus the net-void volume flow rates; the walls were present in both cases so the observed flow rates are attributable to the net and its structure only, not to the walls. The difference between 1.83 lit./sec flow rate loss where the line intercepts the Flow Rate Axis compared to the corresponding 1.57 lit./sec void volume flow rate represents the wall effect, which was calculated to be 0.26 lit./sec. Because the experimental flow rates were determined using an apparatus with walls, the observed flow rates are an underestimate of the actual field flow rates. So, the 0.26 lit./sec can be added to the actual net flow rate value to obtain the actual flow rate that would be observed in the field; that is, 0.72 lit./sec. The 0.26 lit./sec wall effect is 37% of the geonet flow rate for the MD and 2.25 lit./sec or

83% for the cross direction. The higher percentage wall effect in the cross direction is the result of the geonet channels directing more water towards the walls.

4. FINDINGS AND CONCLUSIONS

4.1 Turbulence

Higher Reynolds Numbers were calculated at the 0.025 lowest gradients than anticipated and found to be in the turbulent and transition regions. Though various geonet and test conditions will yield different results; the Reynolds Numbers obtained indicate that gradients lower than 0.025 are required to achieve a laminar flow.

The effect of turbulence can readily be seen when comparing the net-void volume to the flow rate when the geonet is present. However, the total flow rate loss is composed of flow rate loss contributed in part by the net and also by directing the water flow toward the walls of the apparatus.

4.2 Net and Wall Contributions to Flow Rate Loss

Using two different width samples enabled increasing the wall dimension; providing an opportunity to estimate the wall effect. By plotting the Wall to Width Ratio versus Flowrate Loss Due to Net, the line equation permits calculation of the wall effect.

Because in actual use there are no boundary walls, the flow rates and corresponding transmissivities are improved by removing the wall contribution. Knowing the percent flow rate losses due to side wall effect, it can then be converted into a Percent Correction Factor that can be applied to an evaluated laboratory test values to obtain the corrected flow rates. It is hereby concluded that the actual measured flow rate was an under estimate of the flow rate experienced in the field because in actual condition, the geonet is not bounded by walls as in the test apparatus but rather open ended and free

4.3 Void Volume-Storage Capacity

The void volume also represents the storage capacity of the geonet. Therefore, the void volume-storage capacity per acre of the geonets can be calculated by utilizing an area conversion factor.

REFERENCES

Hufenus, Rudolf and Schrade, Ulrich (2006) An optimized method to measure the hydraulic conductivity of geosynthetics under load, Geotextiles and Geomembrane 24;243-253. 244

ASTM D4716 Standard Test Method for determining the (In-plane) Flow Rate per Unit Width and Hydraulic Transmissivity of a Geosynthetic Using a Constant Head., American Society for Testing Materials, West Conshohocken, Pennsylvania, USA

M. Minch and M. Li, Effects of Flow Direction on Transmissivity of Biplanar Geonet in Landfill Drainage Applications, 2008

ISO 12958 Geotextiles and geotextile-related products- Determination of water flow capacity in their plane, ISO, Switzerland

Hazen-Williams Equation – Calculating Friction Head Loss in Water Pipes, The Engineering ToolBox, www.engineeringtoolbox.com

Hydraulic Diameter, The Engineering ToolBox, www.engineeringtoolbox.com

Reynolds Number, The Engineering ToolBox, www.engineeringtoolbox.com

Geosynthetics 2009
February 25-27 2009, Salt Lake City, Utah

Wide-Width Tensile Testing of High Strength Geotextiles - An Inter-Laboratory Study

C.J. Sprague, P.E., TRI/Environmental, Inc., Greenville, SC, USA

ABSTRACT
The wide width tensile test has proven adequate for the testing of certain products, specifically nonwoven and slit tape woven geotextiles. Yet there are issues associated with the wide-width tensile testing of reinforcing geotextiles, particularly very strong geotextiles. Two significant issues associated with testing high-strength geotextiles are the amount of pre-loading of the specimens and the necessary width of the specimens. This paper reports on an interlaboratory study of two high-strength polyester geotextiles with tensile strengths of 160 kN/m (900 lb/in) and 320 kN/m (1800 lb/in). Three different width specimens were tested: 50 mm (2 in), 100 mm (4 in), and 200 mm (8 in). The geotextiles were each tested with 0.5% and 1.0% pre-loads. Duplicate testing was carried out at two different laboratories. The results of this study demonstrate the relative affects of pre-load and specimen width on the ultimate strength and modulus of high-strength geotextiles.

1. INTRODUCTION

High-strength geotextiles (> 17.5 kN/m (100 lb/in) ultimate tensile strength) have become a common element of reinforced soil structures, especially soil embankments built over soft subgrade soils. In these structures, tensile strength is commonly specified at a specific strain level that is compatible with the amount of deformation desired in the soil and subgrade. This strain level is often in the range of 2 to 5 percent. The tensile strength and strain behavior of candidate geotextiles is typically measured using generally accepted standardized testing procedures, such as ASTM D 4595, *Standard Test Method for Tensile Properties of Geotextiles by the Wide-Width Strip Method* and ISO 10319, *Geosynthetics – Wide-width Tensile Test.* These test methods recognize that at low strain levels, the tensile results may be significantly influenced by the width of the tested specimen and the preload applied to the specimen, as well as by grips and rate of strain.

Placing an initial nominal load, or preload, on complex tensile specimens is commonly necessary to facilitate surface mounting of strain gauges and proper alignment of the specimen prior to beginning the test. Once the preload is applied the strain is “zeroed”, and the test is initiated. Thus, preloading eliminates the recording of some initial tensile behavior making it potentially difficult to accurately assess initial modulus characteristics – especially in materials that experience higher elongations. Because of this, the referenced standards – and this paper - focus on strength and relative strain levels rather than the more complex issues surrounding various calculations of modulus.

Another issue is the width of the test specimen. Wider specimens require much larger load cells, grips and support structure than do narrower specimens. While 200 mm (8 in) wide specimens are commonly required in standard test methods, the option to use narrower specimens is usually noted if it can be shown that the specimen width does not affect the results.

In support of further procedural refinements, an interlaboratory testing effort was undertaken to provide data on two of these parameters – specimen width and level of preload. Presented herein is data on the results of two laboratories that tested 320 and 160 kN/m (1800 and 900 lb/in.) geotextiles. The test widths used were 50, 100, and 200 mm (2, 4 and 8 in.) and the testing was carried out using both 0.5 and 1.0 % preloads. One of the laboratories was an independent commercial testing lab, while the other was the quality control laboratory of a geotextile manufacturer. Both labs have extensive experience testing high-strength geotextiles using roller grips and surface mounted extensiometers.

2. TENSILE TESTING PROCEDURES

2. 1 Critical Testing Parameters

ASTM D 4595, *Standard Test Method for Tensile Properties of Geotextiles by the Wide-Width Strip Method* and ISO 10319, *Geosynthetics – Wide-width Tensile Test* both present detailed discussions on test setup and execution. Critical testing parameters are common to both. Table 1 summarizes the most critical parameters detailed in ASTM D 4595, *Standard Test Method for Tensile Properties of Geotextiles by the Wide-Width Strip Method*.

Table 1. Critical Parameters Associated with ASTM D 4595

Critical Parameter	ASTM D 4595
Grips and Gripping Conditions	Sufficient to grip entire specimen width and to prevent slippage
Guage Length	Set the distance between the clamps at the start of the test at 100 ± 3 mm (4 ± 0.1 in.).
Strain Measurement	A measured strain within the specimen can be obtained from jaw to jaw measurements or the center portion of the specimen can be gaged using LVDTs' mechanical guages, or laser devices.
Rate of Cross-head Displacement or Rate-of-Strain in the Specimen	Set machine to 10 ± 3 %/min. strain rate
Specimen Length and Width	200 mm (8 in.) wide x ≥ 200 mm (8 in.) long
Level of Preload to Remove Slack [for ultimate tensile strengths > 17.5 kN/m (100 lb/in)]	A pretension force equal to 1.25% of the expected breaking force should be applied, however in no case should the total pretension force exceed 222 N (50 lbf).

3. SPECIMEN WIDTH AND PERCENT PRELOAD

While the generally preferred specimen width is 200 mm (8 inches), narrower specimens have been used when the testing equipment has insufficient capacity to sufficiently stress the wider specimen. Preload is commonly used to remove any slack that remains after placement of the specimen in the grips. Figures 1 through 13 present the results of testing two different strength geotextiles at varying widths and preloads of 0.5 and 1.0%. Each curve is the average of five specimens. The averaging is done based on test time. Figures 1 through 6 report the test results from laboratory #1. Figures 1, 2, and 3 present the results of testing 2, 4, and 8 inch wide specimens, respectively, of both strength geotextiles. Figures 4 and 5 present the results of testing with 0.5 and 1.0 percent preloads, respectively, on both strength geotextiles. Figure 6 presents all the average results from laboratory #1. Figure 7 presents all the results from laboratory #2. Figures 8 through 13 focus on the low-strain and ultimate strain results from both laboratories. The sample identification code used in the figures is ultimate strength (lb/in) – preload (lbs) – width (inches). Thus, 1800-9-2 is 1800lb/in strength – 9 lb preload (0.5%) – 2 inch wide specimens.

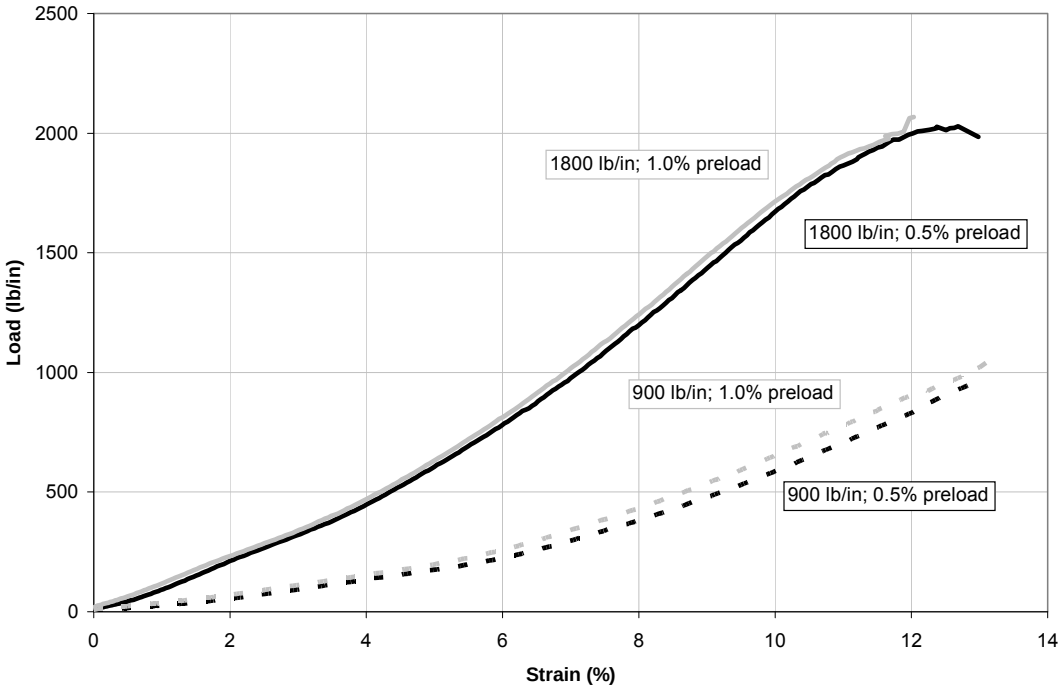

Figure 1. 2-inch Wide, 0.5 and 1.0% Preload, Avg of All Specimens – Lab #1

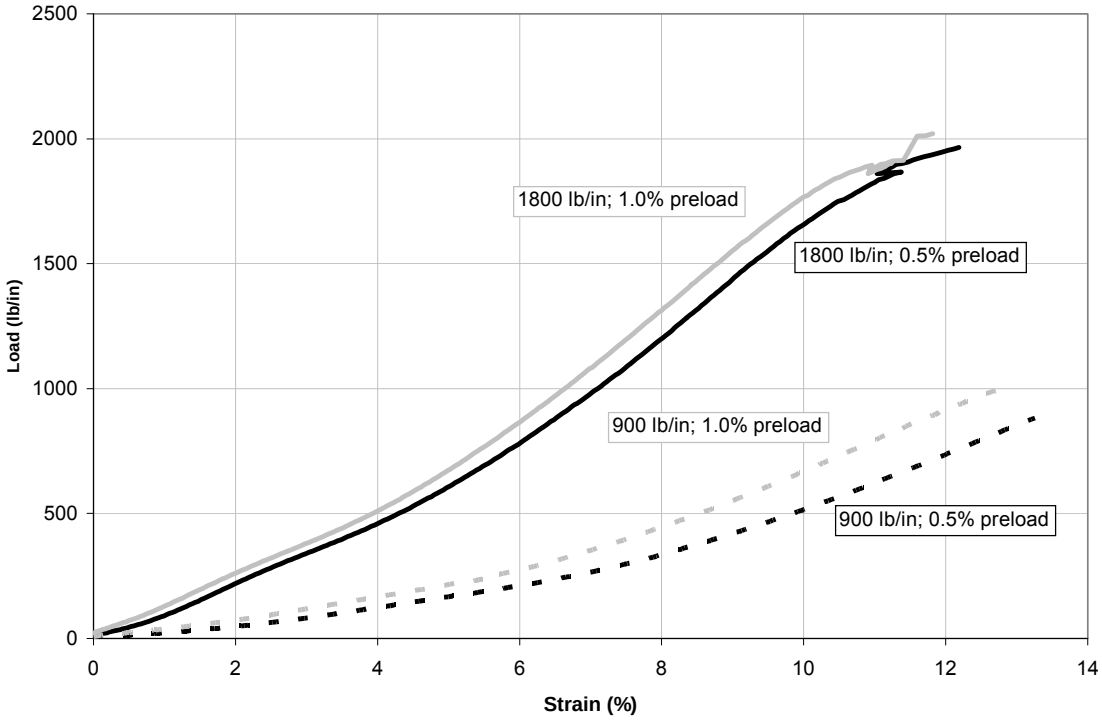

Figure 2. 4-inch Wide, 0.5 and 1.0% Preload, Avg of All Specimens – Lab #1

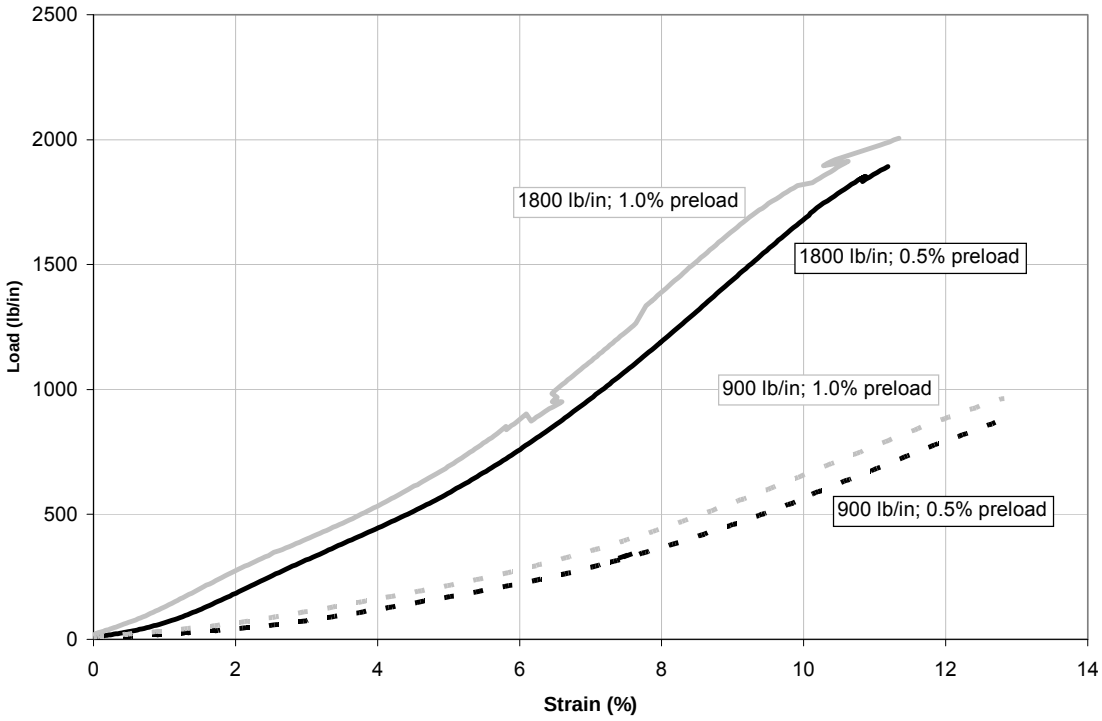

Figure 3. 8-inch Wide, 0.5 and 1.0% Preload, Avg of All Specimens – Lab #1

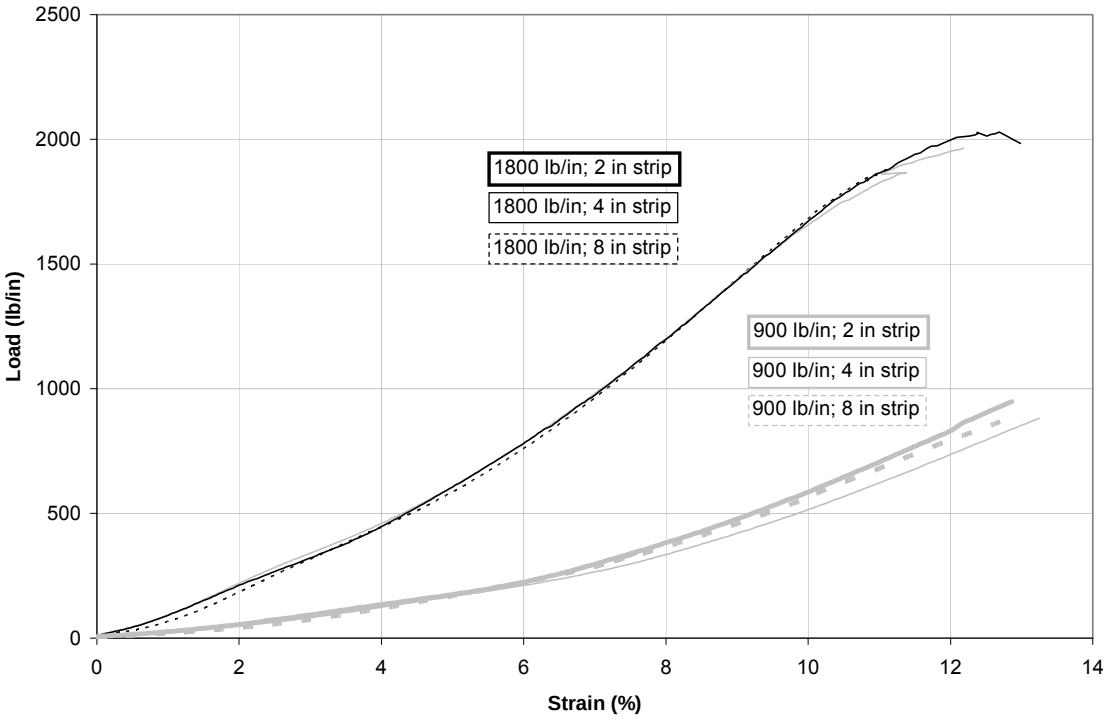

Figure 4. All Widths, 0.5% Preload, Avg of All Specimens – Lab #1

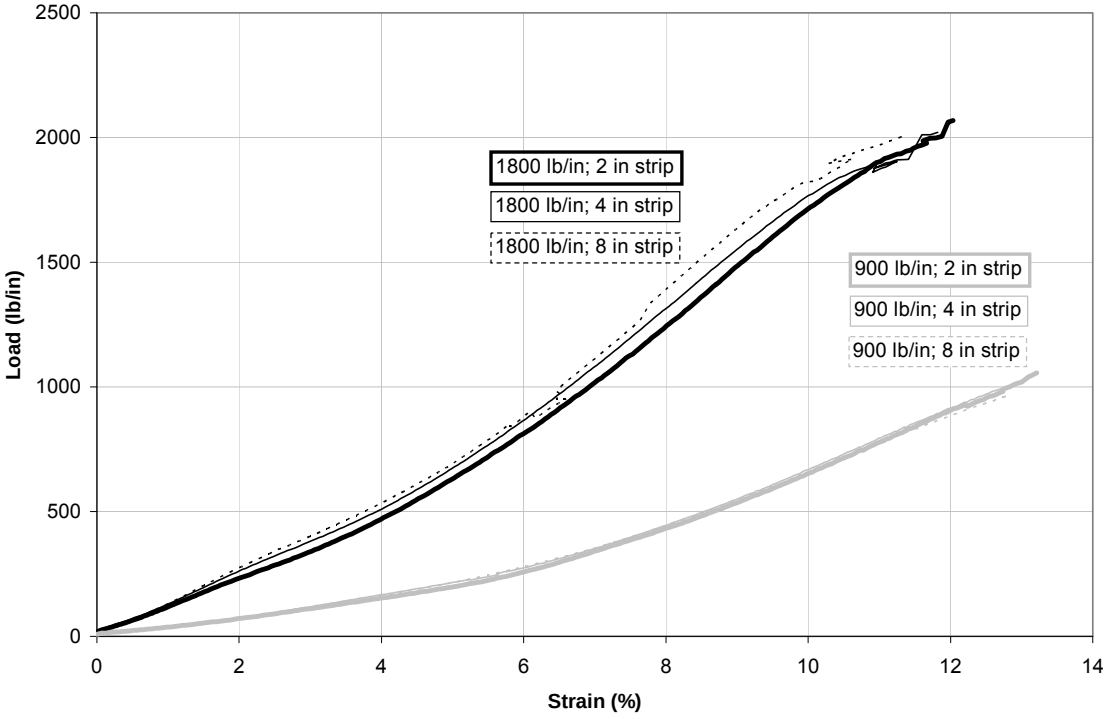

Figure 5. All Widths, 1.0% Preload, Avg of All Specimens – Lab #1

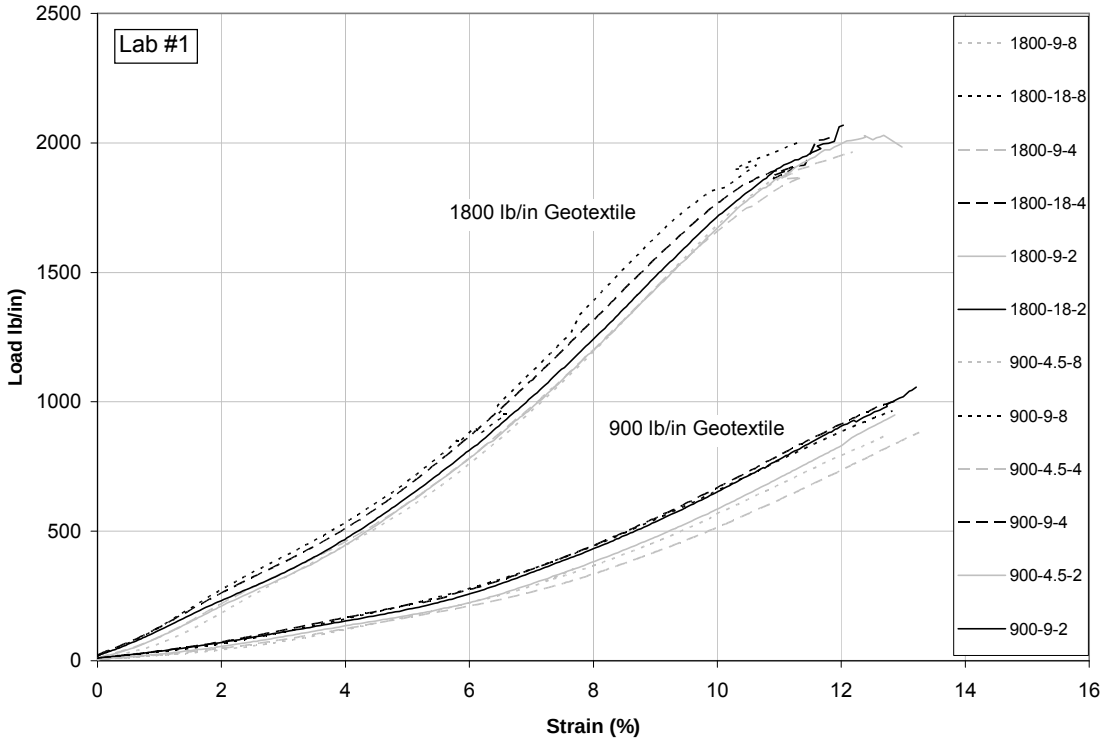

Figure 6. All Widths and Preloads – Avg of All Specimens – Lab #1

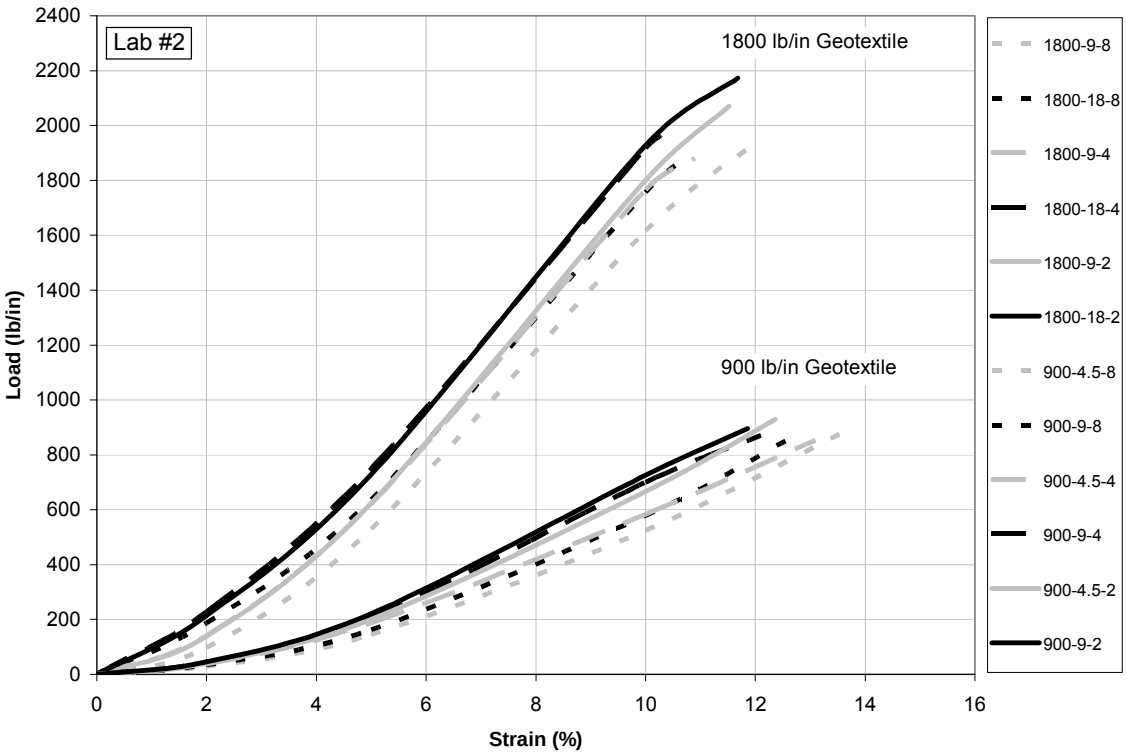

Figure 7. All Widths and Preloads – Avg of All Specimens – Lab #2

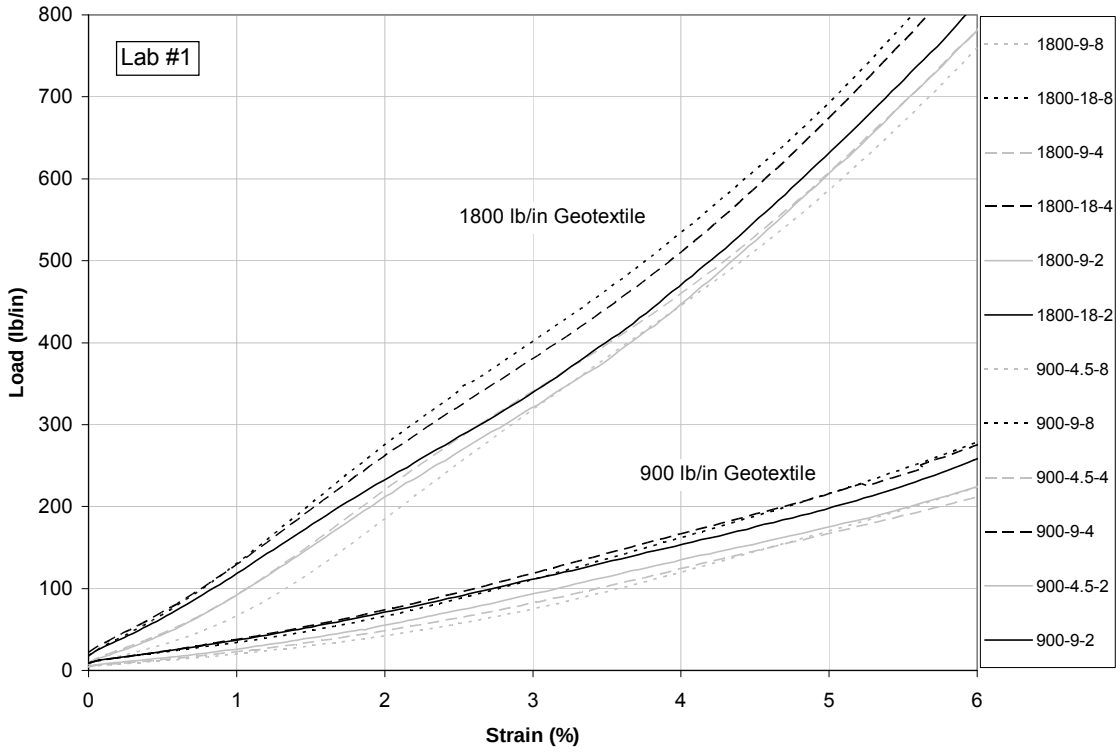

Figure 8. Close-up of Low Strain Region – Avg of All Specimens – Lab #1

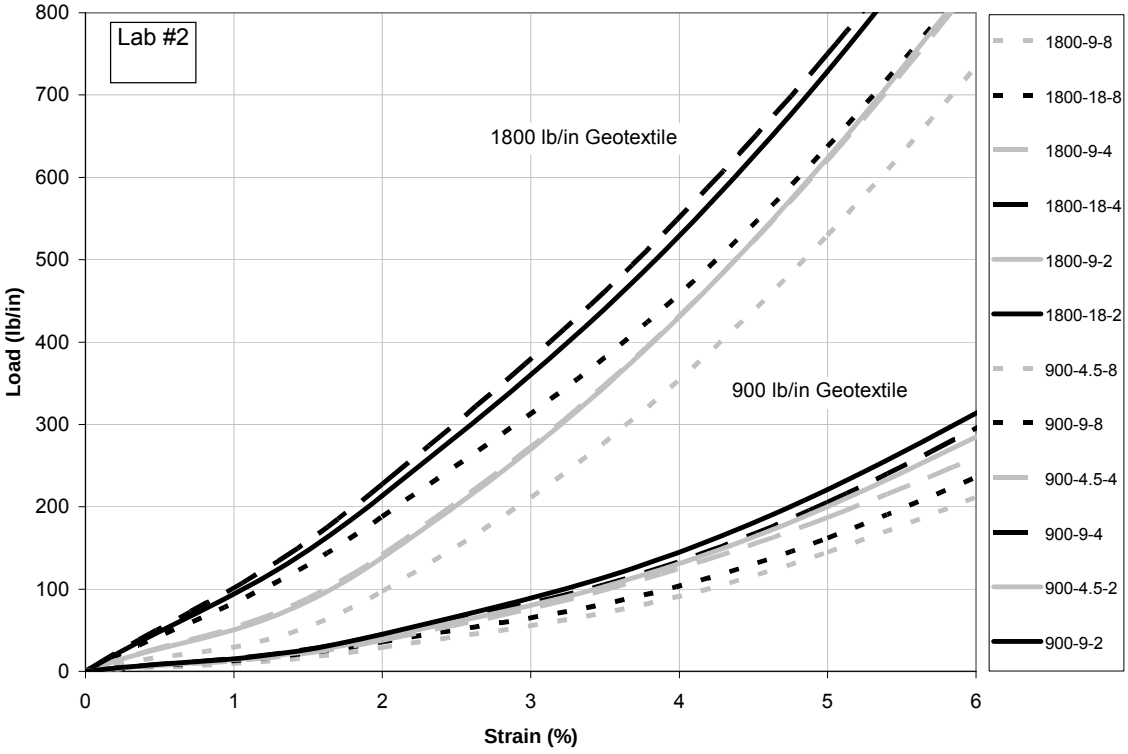

Figure 9. Close-up of Low Strain Region – Avg of All Specimens – Lab #2

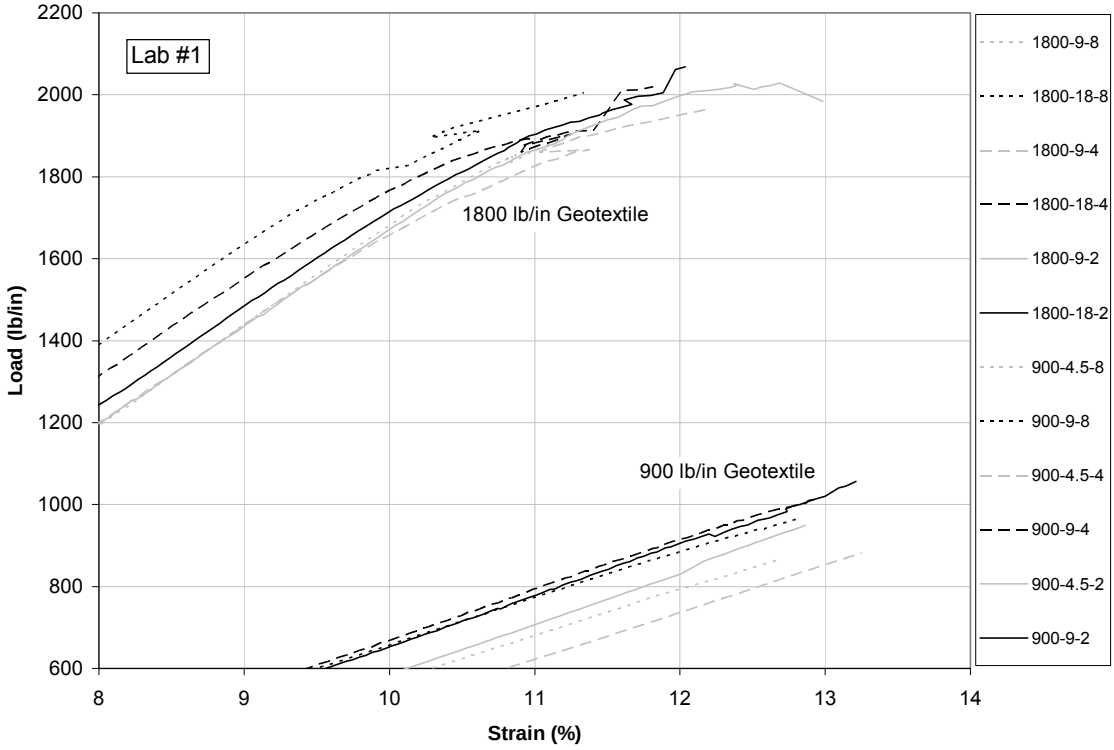

Figure 10. Close-up of Ultimate Strain Region – Avg of All Specimens – Lab #1

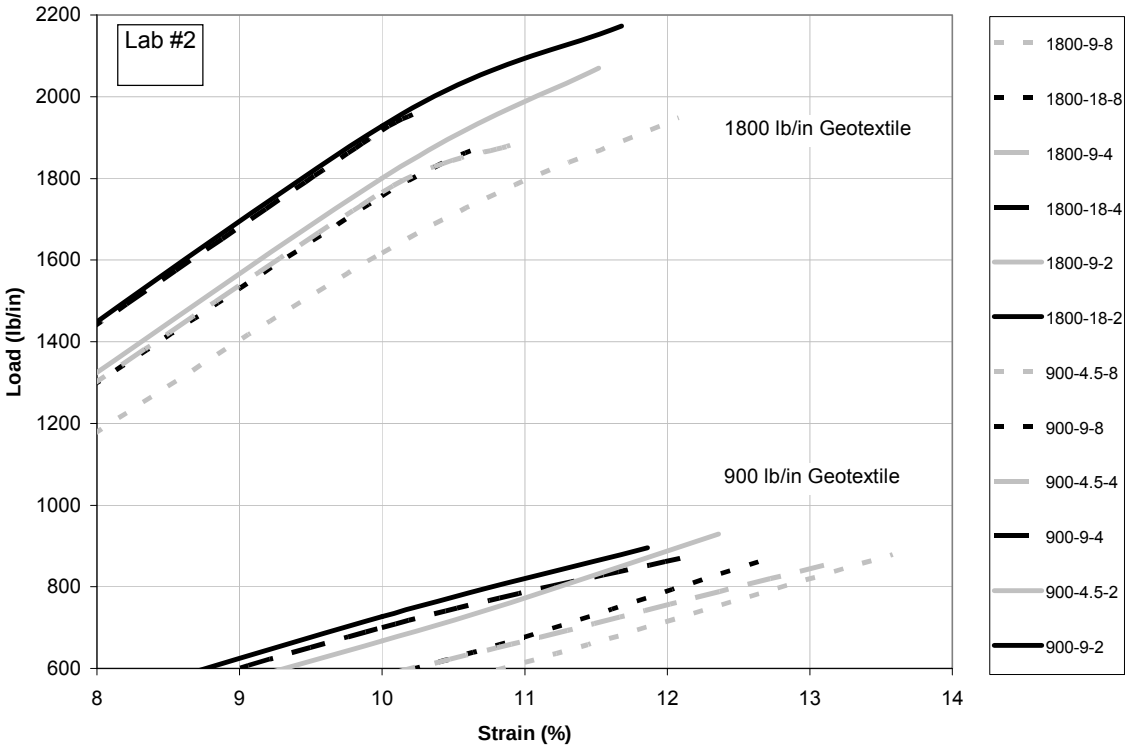

Figure 11. Close-up of Ultimate Strain Region – Avg of All Specimens – Lab #2

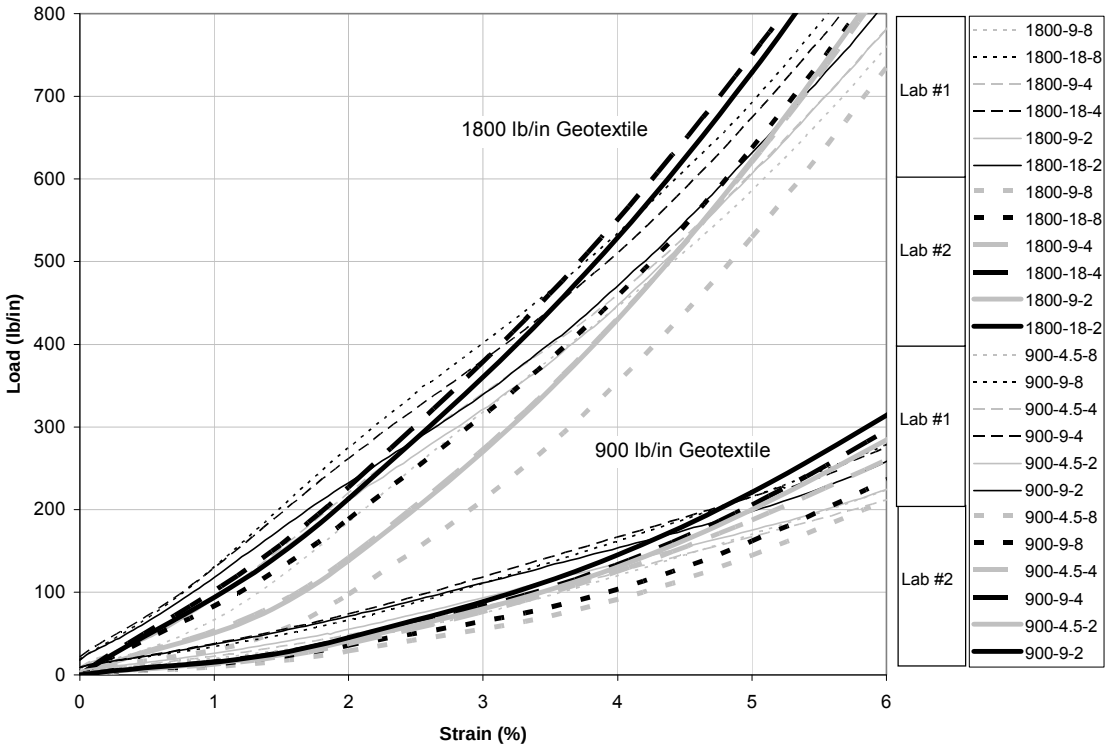

Figure 12. Close-up of Low Strain Region – Avg of All Specimens – Labs #1 & #2

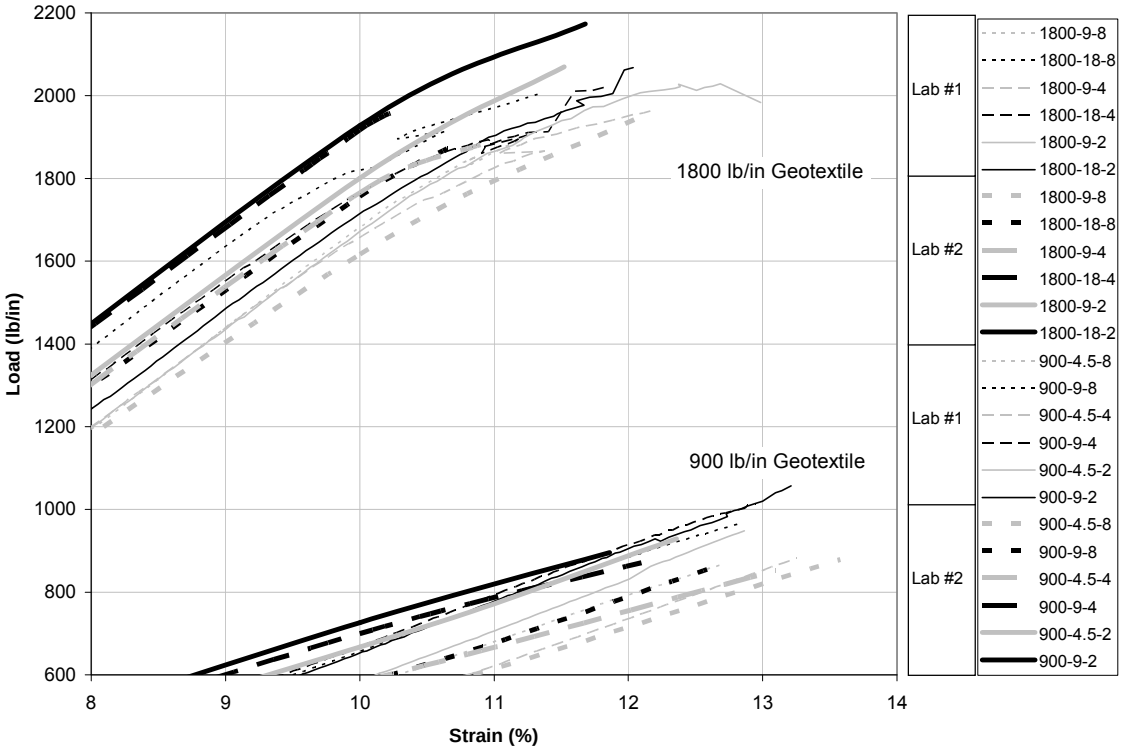

Figure 13. Close-up of Ultimate Strain Region – Avg of All Specimens – Labs #1 & #2

4. OBSERVATIONS AND CONCLUSIONS

From all the figures it appears that width and preload do make a difference in the test results. In general, greater width and lower preload lead to more conservative results, i.e. lower load at a given strain level. Conversely, narrow strips and higher preloads lead to less conservative results, i.e. higher load at a given strain. Figures 1 through 3 support these conclusions and appear to indicate that the preload has the biggest affect. In fact, Figure 4 and 5 appear to indicate that preload may completely mask the effects of specimen width. Yet, when all the results are superimposed in Figure 6, the wider test specimens of the stronger fabric produced the highest loads when using the higher preload suggesting that caution be used in making too general conclusions. Still, Figure 7 shows that the results produced by Laboratory 2 are completely consistent with the conclusion that greater width and higher preloads produce conservative results. Figures 8 and 9 focus on the low-strain portion of the curves and show, rather clearly, that the higher strength geotextile experienced much greater test variability, regardless of preload and specimen width, than did the lower strength geotextile. Specimen width seemed to have the greatest affect on low-strain results in lab #2, while both specimen width and preload affected the results in lab #1. Figures 10 and 11 focus on the ultimate strain portion of the curves. Though no specific relationships between preload or specimen width and ultimate strain are apparent, the ultimate tensile loads are reasonably consistent with the narrowest specimen results generally being somewhat higher that the other widths. Finally, Figures 12 and 13 give a glimpse of the inter-laboratory reproduceability of the test method (ASTM D 4595). While the general shapes and locations of the curves are respectable, the data offers no conclusive evidence relating to the most appropriate specimen width or preload to enhance inter-laboratory reproduceability.

As noted in the introduction, preloading eliminates the recording of some initial tensile behavior making it potentially difficult to accurately assess initial modulus characteristics – especially in materials that experience higher elongations. Because of this, the referenced standards – and this paper - focus on strength and relative strain levels rather than the more complex issues surrounding various calculations of modulus.

ACKNOWLEDGEMENTS

The author would like to acknowledge the two laboratories that participated in this inter-laboratory testing program: Ten Cate Geosynthetics - Melissa Medlin, Lab Manager, and TRI/Environmental - Jarrett Nelson, Special Projects Manager.

REFERENCES

ASTM D 4595, *Standard Test Method for Tensile Properties of Geotextiles by the Wide-Width Strip Method*, ASTM International, Conshohocken, PA.

ISO 10319, *Geosynthetics – Wide-width Tensile Test.* International Standards Organization.

Pull Out Tests on a Geosynthetic Composite: Influence of Soil on Shear Resistance

S-H Lajevardi, PhD, INSA de Lyon, Villeurbanne cedex, FRANCE
A. Couradin, INSAvalor, INSA de Lyon, Villeurbanne cedex, FRANCE
D. Dias, INSA de Lyon, Villeurbanne cedex, FRANCE
A. Herault, COLBOND Geosynthetics, Saint Denis La Plaine cedex, FRANCE

ABSTRACT
The design standard "Stabilisation of fine soil on slope" being drafted within the French Soils and Roads Standardization Office seeks to establish compliance with the Eurocode 7, for the design of geosynthetics ensuring the stability of the overburden soil by placing the geosynthetic composites on such slopes. The major application areas include waste storage facilities, road or rail embankments, reservoirs and dams. The geosynthetic composites function when the soil-geosynthetic interface shear strength is fully mobilized. Therefore , the pull out tests were carried out at the Laboratory of Civil and Environmental Engineering at INSA Lyon to quantify and compare the shear resistance of geocomposite in the presence of two site materials, gravel 0/31,5 and sand 0/5 . The tests were conducted at normal stress of 7 kPa in a tank. The results show that the geosynthetic composite tail begins to move after the head displacement crosses a certain threshold value. The results were further analyzed to obtain values of internal friction of the upper yarn layer of the geosynthetic composite.

1. INTRODUCTION

Pullout tests have been extensively used to study the anchorage behaviour of the reinforcing elements in soil reinforced walls and steep slopes. Various materials have been tested including metallic reinforcement, geotextiles and geogrids (Alimi et al. 1977; Schwab et al. 1977; Juran and Chen 1988; Lentz and Pyatt 1988; Palmeira and Milligan 1989). The interpretation of the test results, however, remains a problem owing to their dependency on soil type and condition, stress level, material extensibility, geometry of the tested specimen and other factors. When dealing with composite materials (geotextile and filament fibre), the problem is further complicated by the fact that pullout resistance is provided by geotextile in the direction of the pullout load and frictional and bearing resistance is provided by filament. The overall performance of geocomposites is, thus, expected to be influenced by various factors such as the extensibility of the longitudinal geotextile, the frictional resistance of filament fibre and the strength of junctions between the geotextile and the filament fibre at the seam.

This paper compares behaviour of a geosynthetic composite when used with the two types of confining soil. The tests were carried out in a three dimensional tank to reproduce the field conditions as closely as possible. Care was taken to maintain consistency during the two tests by providing controlled environment and similar instrumentation. The tests were able to reproduce the influence of the soil dilatancy, which influences the behaviour of reinforcement in field conditions.

2. MATERIAL AND METHODS

2.1 The test tank

The two tests were carried out on geocomposite anchored in a test tank filled with sand and gravel (Fig. 1). The test tank had inner dimensions: 1.10 m width, 1.10 m height and 2.0 m length. To apply a surcharge (~ 7 kPa) on the geocomposite and to check the interface soil resistance, a sand or a gravel layer is used on the geocomposite.

Figure 1. Pull out test (INSA Lyon, LGCIE, Coulomb 3).

2.2 Geosynthetic

The reinforcements are made of geosynthetic containing a flexible lightweight geocomposite, consisting of 4.90 m wide, three-dimensional polyamide grip layer and 5.00 m wide woven reinforcing fabric. Both components are family sewn together with stitches at 3.5 cm centres in seams at 10 cm centres (Fig. 2). The woven fabric extends approximately 0.20 m to one side of the grip layer. This ensures that the joint is covered when lanes of geocomposite are laid adjacent to one another.

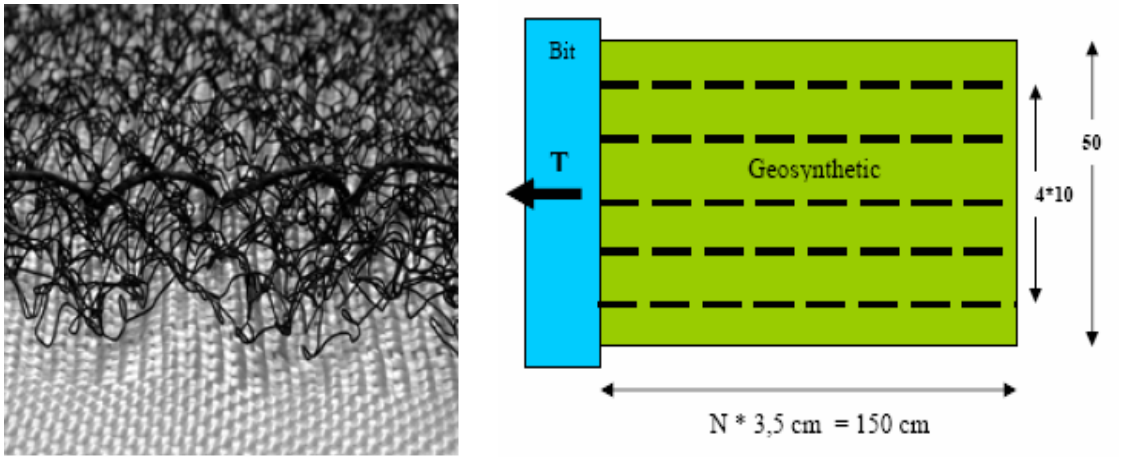

a) Geocomposite Enkamat®. b) Plan view of stitches.

Figure 2. Geosynthetic.

The dimensions of these geocomposite are: 490 mm width and 10 mm thickness and 100 m length. In these tests, one layer of 1.50 m length and 0.50 m wide geocomposite was anchored to the tank.
This type of geocomposite may be used as a reinforced grip layer on geomembrane of landfill capping layers, retention/balancing ponds and lined impounding reservoir. Geomembranes need a soil cover to protect them against UV radiation and mechanical damage and for aesthetic reasons. Where the friction between the soil cover and the geomembrane is too low to achieve an acceptable slope angle, geocomposite can be used to ensure stability. The retention of the soil within the matrix of the grip layer is such that the angle of friction at the soil / grip layer interface is 0.9- 1.0 times the angle of internal friction of the soil itself. The friction at the interface of geomembrane/geocomposite depends on the reinforcing fabric and the type of membrane. To avoid damage caused by UV radiation or wind the geocomposite should be covered immediately after installation. Properties of the composite are in the Table 1.

Table 1. Properties of the geocomposite.

		Mean value	Tolerance value
Polymer		PA/PET	
Mass per unit area	g/m^2	730	-10
Thickness	mm	10	-0,6
Tensile strength MD	kN/m	200	-20
Tensile strength CMD	kN/m	45	-5
Elongation at break MD	%	12	-6, +3
Elongation at break CMD	%	12	-6, +3
Resistance to static puncture	kN	2	-0,6
Resistance dynamic perforation	mm	15	3

2.3 Material Used

The material used in the two tests is a gravel 0/31.5 and a fine dense sand 0/5 known under the name of Hostun RF. The principal characteristics of gravel are: granulometry (mm) 0.08-35, density 1.91 – 2.05 ton/m^3, cohesion 61 kPa and friction angle 36°. The sand principal characteristics are: granulometry (mm) 0.16-0.63, density 1.32 - 1.59 ton/m^3 and friction angle 38°.

2.4 Sensors

The applied pressure is controlled by two sensors. A pressure gauge is used to measure the pressure applied and a total pressure sensor installed at the top of the layers of polyfoam controls the real vertical stress applied. A total pressure sensor is also installed on the wall of the tank to measure the horizontal stress. To follow the geocomposite behaviour in the tank, this one is instrumented by displacement sensors on its entire length and by a force sensor at its head.

Wire sensors were used. Eight of them (A to G) are placed on supports at the tank rear, allowing measurement of displacements of the tail and along the reinforcement (Fig. 3). In order to avoid any friction effect with sand or gravel during the pullout test, these cables are threaded in Teflon sheaths.

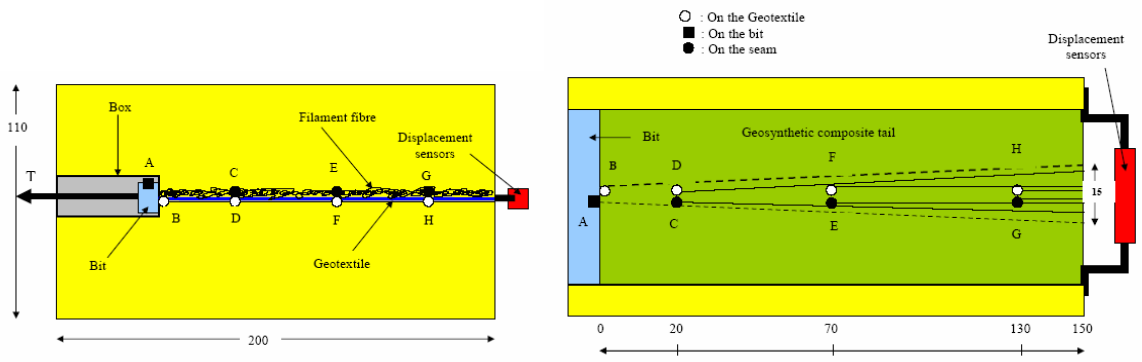

Figure 3. Dimension geocomposite tail (150*50 cm) and sensors positioning.

To measure the tensile force, an annular load sensor is placed at the end of the pull out jack. All of the measurement sensors are connected to a computer.

2.5 Pluviation system

In order to control the density of the sand set up and to simulate the reconstitution of a sandy ground formed by sedimentation, a pluviation method is used in second test (Fig. 4). It is defined as a technique of granular sample reconstitution by material discharge.

An automatic system, double axis, allowing that the whole tank surface was set up. It is controlled by a computer and moves at constant speed in the two direction of the tank. A hopper is placed above the tank and connected by a flexible

pipe to allow mobile carriage on the automatic axis system. Sand runs out of the hopper towards the carriage by the means of a ring of diameter equal to 20 mm. This system makes it possible to control the flow of sand. The speed can be adjusted, making it possible to obtain a density of approximately 1.55 ton/m^3.

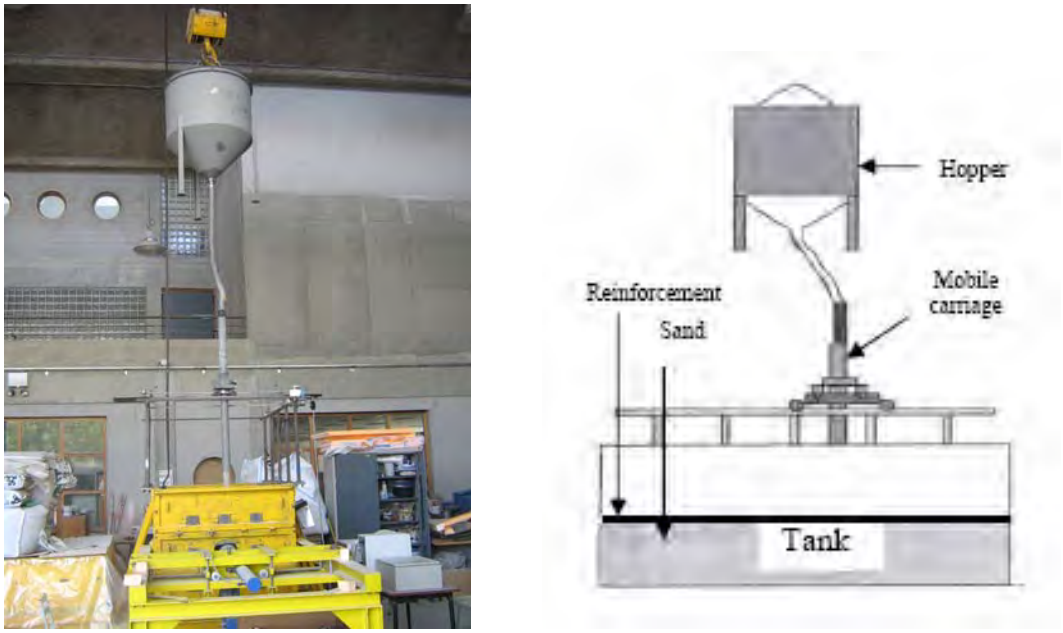

Figure 4. Pluviation system (INSA Lyon, LGCIE, Coulomb 3).

3. EXPERIMENTAL TESTS

The pull-out test consists of a tank, an extraction jack and a data acquisition system (Fig. 5). The principle of operation is to exert a force of traction on the geosynthetic composite tail studied through an extraction jack.

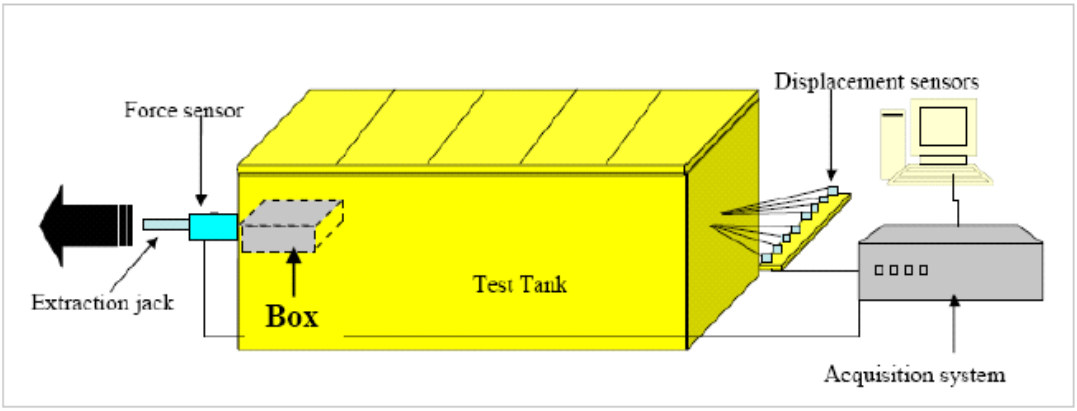

Figure 5. Pull-out test materiel (from Abdelouhab et al. 2008).

3.1 Procedure

The preparation of a test begins with an empty tank in which eight layers of polyfoam plates (60 * 600 * 1250 mm) are set up until the position of the guiding box is reached. Next, a vertical stress sensor is placed on the Polyfoam plates and then, the guiding box is placed in the tank and set on the Polyfoam plates which are tight to the tank wall.

A layer of sand is placed with a thickness of about 4 cm on the Polyfoam plates and the vertical stress sensor is positioned. The level of sand must be controlled to ensure that the surface is plane. Set on the sand is a PVC plate impregnated by a grease, which is deposited on a plastic film only to protect of geotextile (fig. 6).

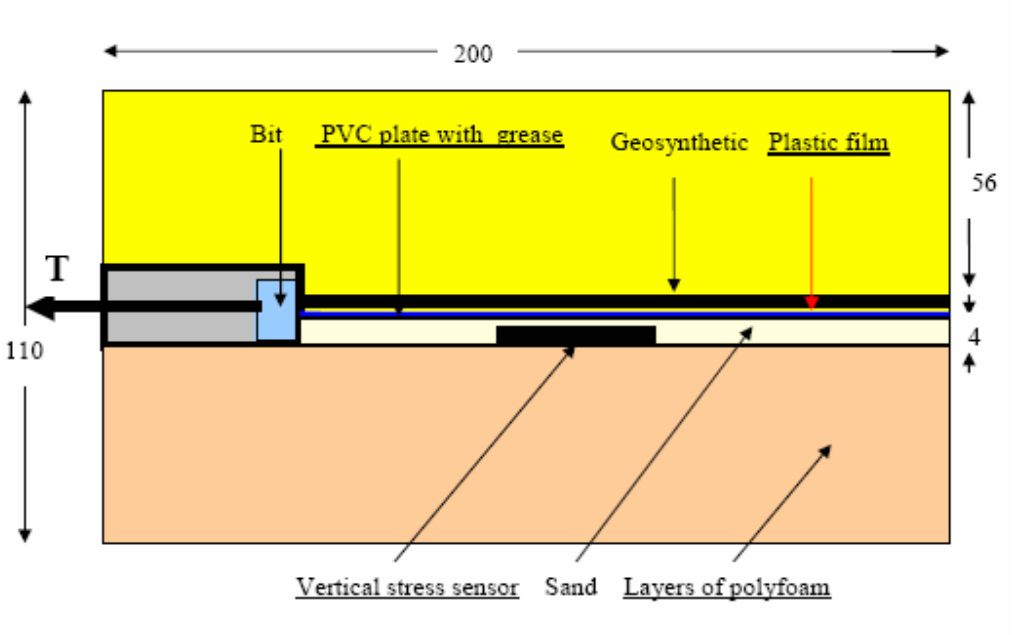

Figure 6. Schematic filling of the tank.

Then, the reinforcement, equipped with the sensors, is installed before the filling of the tank. Into the tank and above the geocomposite sample, there is an empty place of about 56 cm height. For the first test, a layer of gravel (38cm height) is placed above the geocomposite sample to simulate a vertical stress of 7.4 kPa. Then for this test, the vertical stress on the geocomposite sample is 0.38 x 2.0 x 9.8 = 7.4 kPa. Also for the second test, a layer of sand (42cm height) is placed above the geocomposite sample for a vertical stress of about 6.2 kPa (0.42 m x 1.5 x 9.8 = 6.2 kPa). The tests were carried out at an extraction speed of 1 mm per minute.

3.2 Test routine

Two tests were carried out on the two types of material and one at the same level of surcharges. A test with gravel and another test is with sand.

4. ANALYSES AND RESULTS

The tests made it possible to determine the tension load, the maximum tangential shear stress, the maximum and overall strain and the maximum friction angle mobilized as well as displacement in several points of the geocomposite sample.

The maximum tangential shear stress τ_{max}, was calculated with equation 1:

$$\tau_{max} = F_{max} / (W_g \times L_g) \quad [1]$$

Where:
F_{max} = maximum tension (kN)
W_g = width of the geosynthetic, (m)
L_g = length width of the geosynthetic, (m)

Table 2. Summary results.

Test	1 with the Gravel	2 with the Sand
Vertical stress (kPa)	7,4	6,2
Friction angle (°)	64	59
Maximum tension (kN)	11	8
Tail / Head delay (mm)	50	75
Increase of the vertical stress	1,51	1,55
Maximum strain ΔL/L (%) for 150 mm Ut *	10	5,7
Overall strain ΔL/L (%) for 150 mm Ut *	4,6	2
Maximum tangential shear stress (kPa) for 150 mm Ut *	13,6	9,6

Ut*: Head displacement.

Table 2 shows summary of the tests results obtained on the geocomposite sample for the gravel and the sand. These results show that during these two tests with similar stresses, the friction angle and the maximum tensile load for the gravel are higher than the sand. Also, these results show that the maximum and overall strain and the maximum tangential shear stress for the gravel are more important than the sand. Perhaps this phenomenon can be explained by the light compaction of the gravel. In addition, Table 2 shows the phenomenon of dilatancy which is more importantly with sand. The increase in vertical stress with sand is 1.55 times the value of the initial normal stress, however, it is 1.51 times with gravel. The measured geocomposite-sand interface friction angle is higher than the internal friction angle of the sand. Also, the pull-out tests carried out by Abdelouhab A. (2008) on Geosynthetic straps used in Reinforced Earth Walls, show that the friction angle between the sand and the reinforcement (ϕ = 52° under confinement stress of 8 kPa) is higher than the internal friction of the sand (ϕ = 38°).

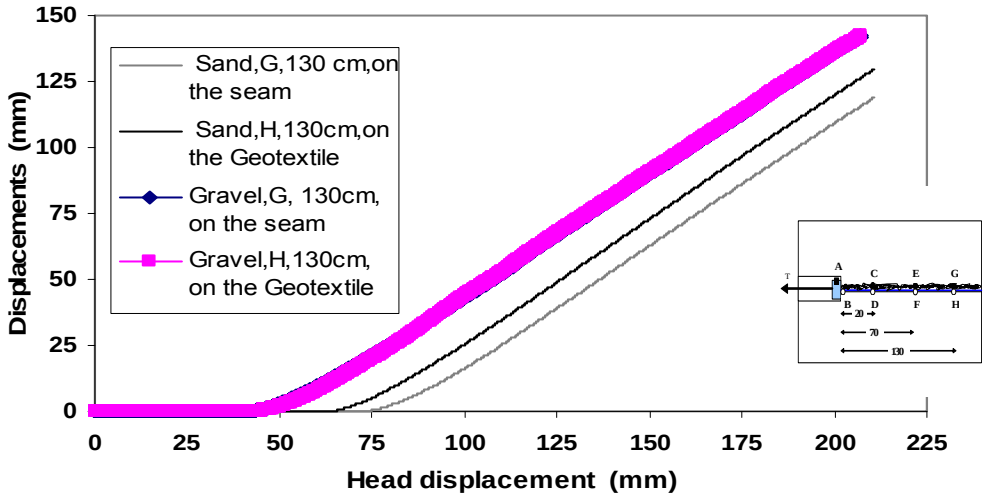

Figure 7. Displacement of the points located at 130 cm length of the geocomposite sample.

The analysis of the behavior of the two type soil shows that the geocomposite sample does not start to move over all their length, as soon as a load is applied at the head. The delay is more important with sand (Fig. 7). These figures (Fig. 7 and 8), show that the tension in the sample is gradually mobilized with the increase of the tension at the head of the sample. Thus, friction is mobilized gradually along the band and displacement at the head is required for low tensile stress.

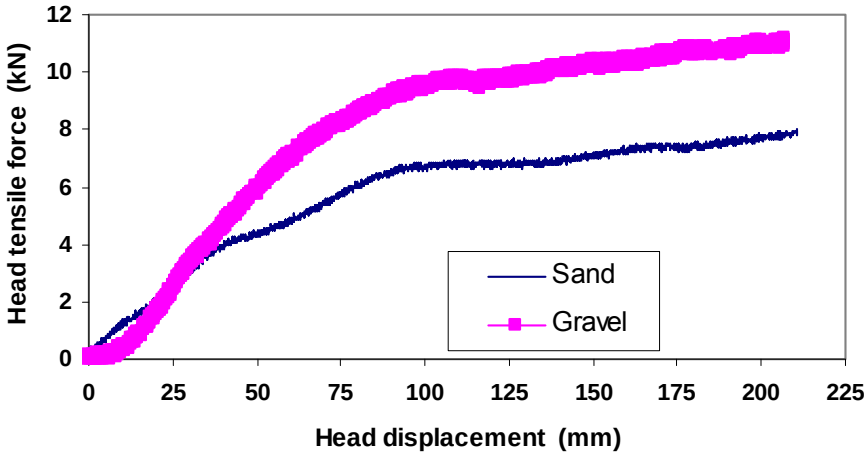

Figure 8. Tensile force at the head of geocomposite sample (vertical stress equal to 7 kPa).

5. CONCLUSIONS

The results seem to have a good accuracy and the instrumentation has functioned properly. However, only one test was performed for each material. During these two tests and similar stress (~ 7 kPa), the geocomposite sample reached levels of strain eligible (less than 12%). In configurations studied, it appears that the shear occurs gradually from the interface geotextile / filament fibre (seam) to the surrounding soil.

The maximum tensile force in the gravel is more important than in the sand (~ 27%). It therefore appears how the soil mass where is placed on geocomposite sample is important. The highest value of shear stress in the gravel reinforces this observation. Indeed, the behaviour of the gravel (friction and cohesion) is different from the one of the sand (only friction).

The delay between the tail and head reflects a progressive mobilization of the sample. The delay is more important with sand (50%). The similar behaviour of the two types of soil with the geosynthetic can be confirmed by an analytical model. The analytical modelling of displacement curves using the test results will make it possible to define the interaction law between the ground and geosynthetics and to develop the knowledge for a new design method.

ACKNOWLEDGEMENTS

This article is a research work of the reinforced earth structures behaviour and which is the subject of collaboration between the LGCIE laboratory of the INSA Lyon and the COLBOND Geosynthetics.

REFERENCES

Abdelouhab, A., Dias, D., Freitag, N., Bourdeau, Y. and Kastner, R. (2008). Analytical modelling of pull-out tests on geosynthetic straps. *The Challenge of Sustainability in the Geoenvironment 'GeoCongress* 2008', New Orleans, USA.

Abdelouhab, A., Dias, D., Freitag, N. and Bennani, Y. (2008). Pull-out tests analytical modelling to deduce the constitutive soil/reinforcement interface behaviour. *4th European Geosynthetics conference Edinburgh UK.*

Abdelouhab, A., Dias, D., Freitag, N. and Bourdeau, Y. (2007). Soil/Reinforcement interface characterization using three-dimensional physical modeling. *The 5th International Symposium on Earth Reinforcement* 'IS Kyushu 2007', Fukuoka, JAPAN.

Alimi, I., Bacot, J., Lareal, P., Long, N. T., and Schlosser, F. (1977). "Etude de l'adherence sol armature." Proc., 9th Int. Conf. Soil Mech. and Found. Engrg., *Japanese Society of Soil Mechanics and Foundation Engineering*, Tokyo, Japan, Vol. 1, 11-14.

Bakeer, R.M. et al. (1998). "Geotextile friction mobilization during field pullout test". *Geotextiles and Geomembranes* 16(1998), 73–85.

Briançon, L.. Girard, H., Poulain, D. and Mazeau, N. (2000). "Design of anchoring at the top of slopes for geomembrane lining systems", *Proceedings of the Second European Geosynthetics Conference*, "EUROGEO 2000". Bologna, Italy, 15-18 October 2000, vol.2, pp 645-650.

Briançon, L. (2001). Stabilité sur pentes des dispositifs géosynthétiques — caractérisation du frottement aux interface et applications*. Ph.D. thesis*, Université Bordeaux I, Talence, France.

Chu, L.M. and Yin, J.H. (2005)." Comparison of Interface Shear Strength of Soil Nails Measured by Both Direct Shear Box Tests and Pullout Tests", *Journal of Geotechnical and Geoenvironmental Engineering*, Vol.131, No 9.

Juran, I., and Chen, C. L. (1988). "Soil-geotextile pull-out interaction properties: testing and interpretation." Transp. Res. Record 1188, Transportation Research Board (TRB), *National Research Council*, Washington, D.C., 37-47.

Lentz, R. W., and Pyatt, J. N. (1988). "Pull-out resistance of geogrids in sand." Transp. Res. Record 1188, TRB, *National Research Coneil*, Washington, D.C., 48-55.

Moraci, N., Romano, G., Montanelli, F. (2004). Factors affecting the interface apparent coefficient of friction mobilised in pullout condition. *Third European Geosynthetics Conference*, vol. 1, Monaco, pp. 313–318.

Murad, Y., Abu-Farsakh, Khalid Farrag, Izzaldin Almoh'd and Ather Mohiuddin, (2004), "Evaluation of interaction between geosynthetics and marginal cohesive soils from pullout tests". *Geo jordan*, 2004, 143, 25.

Palmeira, E. M., and Milligan, W. E. (1989). "Scale and other factors affecting the results of pull-out tests of grids buried in sand." *Geotechnique*, London, England, 39(3), 511-524.

Perkins, S. W. and Edens, M. Q. (2003)."Finite element modelling of a geosynthetic pullout test", *Geotechnical and Geological Engineering*, 21: 357-375, 2003.

Raju, D.M. and Fannin, R.J. (1998)." Load.strain.displacement response of geosynthetics in monotonic and cyclic pullout", *Can. Geotech*. J. 35: 183.193.

Schwab, E.F., Pregl, O., and Broms, B.B. (1977). "Deformation behavior of reinforced sand at model tests measured by the X-ray technique." Proc., Int. Conf. 676 on *Use of Fabrics in Geotechnics*, Association Amicale des Ingenieurs Anciens El6ves de l'E.N.P.C., Paris, France, Vol. 1,105-112.

Sugimoto, M. and Alagiyawanna, A.M. N., A.M.ASCE, (2003)." Pullout Behavior of Geogrid by Test and Numerical Analysis", *Journal of Geotechnical and Geoenvironmental Engineering*, Vol.129, No 4.

Sugimoto, M., Alagiyawanna, A.M.N., Kadoguchi, K. (2001). "Influence of rigid and flexible face on geogrid pullout tests", *Geotextiles and Geomembranes* 19 (2001) 257–277.

Wilson-Fahmy, R.F., Koerner, R,M., Honorary Member, ASCE, and Sansone, L.J. (1994). "Experimental behaviors of polymeric geogrids in pullout", *Journal of Geotechnical Engineering*, Vol.120, No 4.

Wilson-Fahmy, R.F. et al. (1994). "Long-term pullout behavior of polymeric geogrids", *Journal of Geotechnical Engineering*, Vol. 121, No 10.

Geosynthetics 2009
February 25-27 2009, Salt Lake City, Utah

Combined Saturated Soil-Geotextile-Geonet Composite Flow Test

G. R. Koerner, Geosynthetic Institute, Folsom, PA, USA
A. E. Eith, Waste Management Inc., Fairless Hills, PA, USA
R. M. Koerner, Drexel University, Philadelphia, PA, USA

ABSTRACT
This paper presents a flow rate test method for assessing the potential clogging behavior by landfill leachate as it flows vertically through a column of granular soil, then a geotextile filter and then, after turning approximately 90°, through a geonet drainage core. As such, it reasonably simulates conditions at the base of a landfill when leachate moves through the leachate collection layer and then through the removal layer.
The test apparatus and method is described and flow rate results are presented using different soil types and flow times. It suggested as being a performance test in which product-specific materials can be evaluated against site-specific leachate.

1. INTRODUCTION

The leachate collection and removal system (LCRS) at the base of a landfill is meant to limit the maximum hydraulic head on the liner system beneath it. The criteria of 300 mm maximum is used worldwide with essentially little variation among the various national environmental regulations, Koerner and Koerner (2007). That said, the manner of achieving this criterion is rarely regulated and is left to the site-specific landfill designer to achieve. As far as *collection* is concerned the choices are a granular soil (size being a major variable) with or without geotextile filters, or a drainage composite (typically a geonet with geotextiles on top and bottom). As far as *removal* is concerned the drainage composite core, i.e., the geonet, serves this function as well. It should be mentioned that an embedded drainage pipe network within the soil collection layer is often used for removal, but this test does not address that option.

To be sure, many researchers have investigated flow rate behavior of combined soil and geosynthetic systems; Koerner, et al. (1984), Cazzuffi, et al. (1986), Lawrence (1987), Dickson (1990), Berhout (1994), Lacey (1995), Gardoni and Palmeira (1999), Jeon and Jacek (2006), and others. Most, however, have the flow moving vertically throughout the various components involved. In contrast, the flow in this test is vertical through the soil and geotextile filter and then horizontally in the plane of the geonet. Note that in the field the flow is not exactly ninety degrees since the drainage composite is invariably at a slight slope angle.

The test method developed in this study uses a graduated column which contains the candidate soil and is underlain by a composite with an attached geotextile on its upper surface acting as a separator and filter to the soil above. Hence it is indeed a drainage composite and will be referred as such. The drainage composite is open for the exiting in-plane flow on all sides. The leachate flowing in the geonet exits over an outlet weir, so as to keep the entire test system saturated. The system's flow rate is measured from the incrementally calibrated column.

The test is felt to be a performance test where the candidate soil can be evaluated along with a particular drainage composite (geotextile and geonet) under consideration. The variation of the leachate flow rate can be evaluated over time. The test can also be used to compare materials (e.g., having different soil types, geotextiles, and/or cores) as well as for research purposes.

2. DETAILS OF TEST APPARATUS

The recommended type of test apparatus to evaluate soil-filter-geonet combined flow is shown in Figures 1 through 4. The main container used to house the soil and the head of leachate is a transparent plastic column (which is graduated with flow quantities) with an inside diameter of 57 mm. Of course, other sized columns can be used depending upon the type and amount of soil or other particulate material that is involved. Its length depends upon the desired soil column length. It is recommended for this column to be 650 mm or larger so that the flow rate can be measured in the clear column above the soil level.

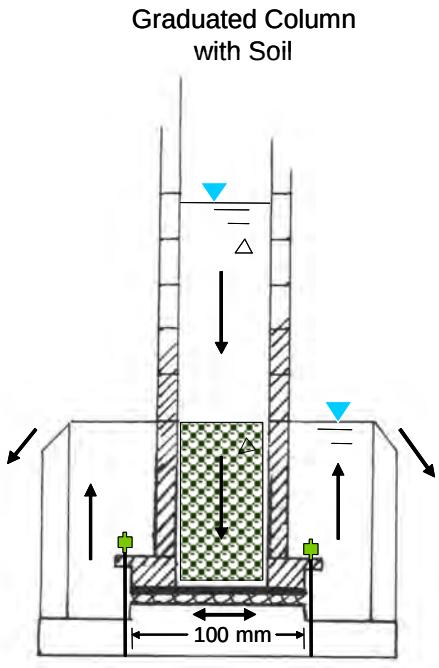

Figure 1. Cross section of testing device. (bold arrows are flow directions)

Figure 2. Disassembled components of recommended testing device.

Figure 3. Base of testing device where flow exits.

Figure 4. Assembled testing device.

The base of apparatus holds the drainage composite (geotextile or geonet) with its geotextile facing upward and supporting the overlying soil layer. Thus the drainage composite forms the bottom of the system. It is required that a support platen be flat and level beneath the drainage composite. An overflow weir extending around the base of the main container is used to assure saturated conditions which is a requirement of the test.

The entire assembly should be placed in a large collection tray where the exiting leachate can be reused or collected and returned to the landfill for proper treatment. One can check for steady-state conditions by comparing inlet and outlet fluid quantities, this would also allow the technician to verify complete saturation.

In regard to using landfill leachate in a laboratory setting, there is always concern over proper health and safety issues. Of course, use of hazardous waste leachates brings to bear an entire set of regulations which must be diligently followed. Even with MSW leachate there is a concern and for this reason the testing being presently conducted is at a landfill site immediately adjacent to the leachate storage reservoir. Thus, fresh leachate is available and plentiful, and discarding of it after passing through the system is easily accomplished.

3. TEST SPECIMEN SIZE

The geonet composite test specimen must be sufficient large so as to cover the entire bottom of the soil containing cylinder and extend beyond the flange so as it can be caulked or glued to the upper platen in a fashion to make a proper seal. For the assembly shown in Figure 5 this requires a 100 mm diameter circular test specimen. Once assembled into the apparatus, the composite and soil should be back saturated from the exit weir. This will allow air to escape out of the soil column. Furthermore the system should be allowed to equilibrate prior to taking aata.

Figure 5. A geocomposite test specimen and its sealant so as to fix it the base of the flow cylinder.

4. PROCEDURE

Upon setting the base, the drainage composite, and the graduated cylinder assembly the setup should appear as in Figure 4. The test soil is now placed and it invariably will be a cohesionless granular drainage soil. Note that if large gravel is being considered, the entire assembly will have to be larger in diameter than the one being described here. In any case, the soil is placed at its targeted density and moisture content. This is not considered as being critical, since the downward flowing leachate will “tune” the soil as testing commences. Leachate is now introduced from the top of the graduated cylinder until it overflows the base container. As mentioned, proper collection and discarding of the leachate are important considerations.

Data collection should start as soon as the system is saturated and the flow rate is stabilized (i.e., inflow equals outflow). Readings should be taken from the calibrated cylinder at gradually increasing time increments depending on the specific soil, geotextile, and geonet types being evaluated. Sheet flow is occurring with the exiting liquid coming from the drainage core into a collection trough at the downstream side. It is not necessary to monitor this exiting flow. Figure 6 shows several of these test setups being used at a local landfill.

In general, the time period for taking data initially is minutes to hours and thereafter (depending mainly on the leachate’s amount of suspended solids and microorganisms) days, week, or months.

(a) Group of test columns incubating in leachate (b) Single column being tested

Figure 6. Test column evaluating leachate flow rate through soil, geotextile, geonet system.

5. CALCULATIONS

While permeability (hydraulic conductivity) of soils, permeability or permittivity of geotextiles, and transmissivity of geonets are the common indicators of hydraulic behavior, this test setup is not amenable to the use of Darcy's Law as is required for each of these parameters. This is due to the change of flow orientation within the test setup. This change is not modeled easily and as a result flow rate through the system is the only parameter that can be offered. In doing so, it is important to note that the resulting flow rate is "test setup dependent". As such, transportability of test results to other devices (due primarily of scale effects) is difficult, if not impossible.

6. TYPICAL RESULTS

Perhaps the main target of the test itself is to obtain an indication of system clogging (soil, geotextile, and/or geonet) by the site-specific leachate being used as the permeant. Figure 7 gives the various possibilities that can result in this regard.

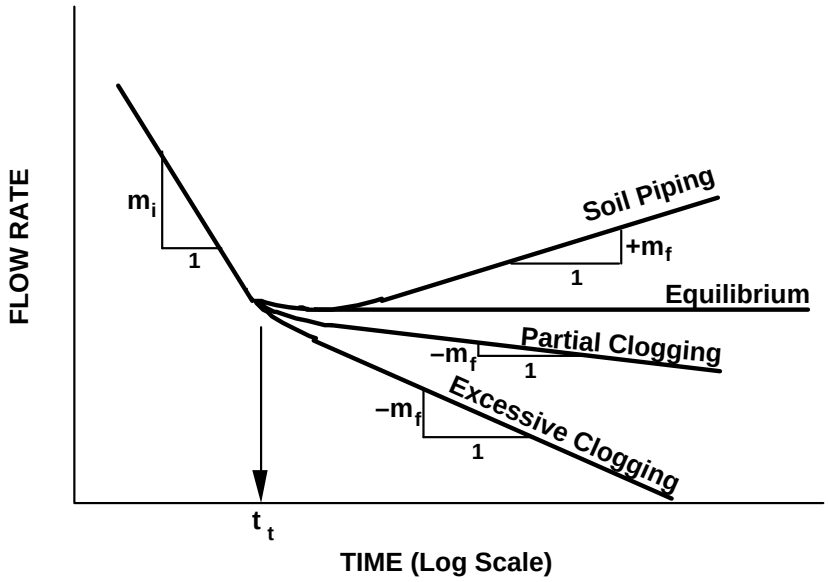

where

t_t = transition time required to begin to investigate long term flow rate phenomenon
m_i = initial slope due in large part to soil densification via downward flowing permeant
m_f = final (terminal) slope which is of primary interest

Figure 7. Various possible long-term flow rate behavioral curves.

The initial series of tests conducted using this test setup varied the type of soil in order to observe the system's behavior. Figure 8a shows the particle size curves of the soils evaluated and Figure 8b gives the flow rate response of each out to 680 hours. In all cases a 150 g/m^2 needle-punched nonwoven geotextile was used along with a 0.51 mm thick HDPE biplanar geonet beneath the soil column. The behavior appears logical in light of the different soils used. Presently, six different granular soils are being evaluated; two sands, two fine gravels, and two mixtures of soil and fine gravel. Results will be forthcoming.

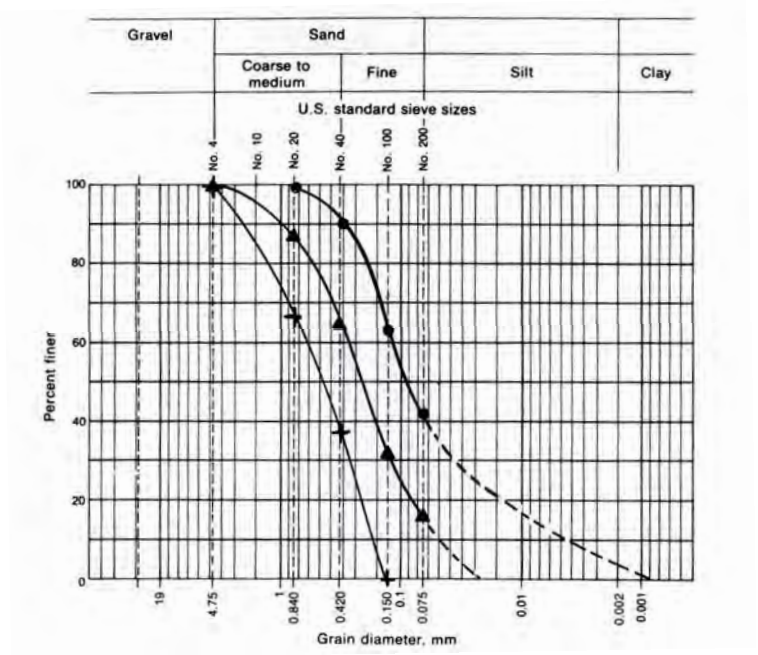

(a) Different soils used for initial tests

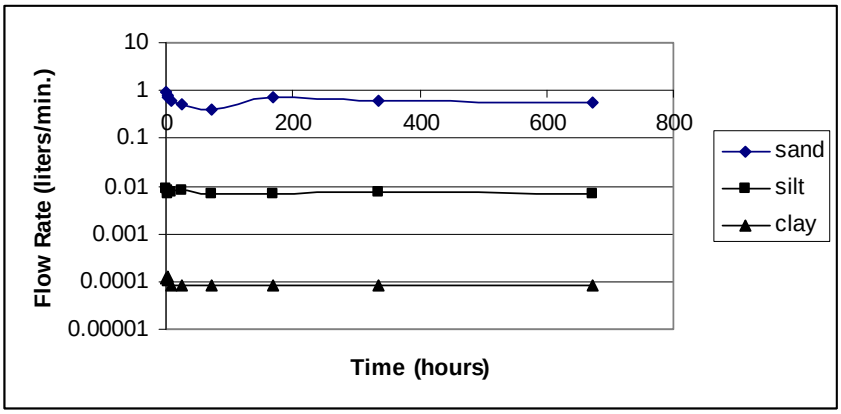

(b) Flow rate responses for above three soils

Figure 8. Flow rate behavior curves.

7. CONCLUSION AND RECOMMENDATIONS

The performance test method presented in this paper has as its goal to evaluate leachate flow vertically through a column of soil and a geotextile, along with that flow turning horizontally and flowing within a geonet core. Thus, soil, geotextile and geonet are evaluated for their flow rate capability. This flow rate is being observed over time to assess if clogging by the leachate occurs, to what degree and in what particular material.

While different soils, geotextiles, geonets and leachate can be evaluated it is important to recognize that the flow rate behavior can only be assessed in light of the specifics of the test setup being used. While this is a limiting condition it is anticipated that insight into the important issue of landfill leachate clogging and removal system (LCRS) assessment will be forthcoming.

REFERENCES

Berkhout, H. C. (1994). In-plane permeability measurement of geosynthetic drains - part I, *Geosynthetics World*, Vol. 4, No. 4, pp. 12-15.

Cazzuffi, D., Ferrara, G., Venesia, S., D'ischia, A. and Silvestri, T., (1986). Transmissivity of geotextiles and related products: laboratory tests and practical applications, *Proc. 3rd IGS Conf.*, Vienna, Austria, pp. 879-884.

Dickson, M. G., (1990), Comparative testing for geotextiles and composite transmissivity, *Proc. 4th IGS Conference*, The Hague, The Netherlands, pg. 364.

Gardoni, M. G. and Palmeira, E. M. (1999). Transmissivity of geosynthetics under high normal stresses, *Proc. Geosynthetics '99*, IFAI Publ., Roseville, MN, pp. 769-782.

Jeon, H.-Y. and Jacek, M. (2006). Drainage performance of composite geotextiles under confined loads, *Proc. 8th Intl. Conf. on Geosynthetics*, Yokohama, Japan, Millpress Publ., Rotterdam, (on CD only).

Koerner, R. M., Bove, J. A. and Martin, J. P., (1984). Water and air transmissivity of geotextiles, *Jour. of Geotextiles and Geomembranes*, Vol. 1, No. 1, Elsevier Publ. Co., pp. 57-74.

Koerner, R. M. and Koerner, J. R. (2008). GRI's second worldwide survey of solid waste landfill liner and cover systems, *GRI Report #34*, October 24, 2008, Folsom, PA, 137 pgs.

Lacey, R. (1995). Transmissivity testing: state-of-the-practice, *GFR*, Vol. 13, No. 3, IFAI, pp. 8-9.

Lawrence, C. A., MSCE Thesis submitted to Drexel University, June 1987.

Geosynthetics 2009
February 25-27 2009, Salt Lake City, Utah

Performance of using PVD with and without Vacuum Preloading

P. Vootipruex, King Mongkut University of Technology, North Bangkok, THAILAND
D.T. Bergado, Asian Institute of Technology, Pathumthani, THAILAND
J. Saowapakpiboon, Asian Institute of Technology, Pathumthani, THAILAND
S. Youwai, King Mongkut University of Technology Thonburi, Bangkok, THAILAND

ABSTRACT
This paper presents the comparison of test results involving prefabricated vertical drain (PVD) with and without vacuum preloading. Laboratory tests were conducted in large scale consolidometer having diameter of 300 mm and height of 500 mm with reconstituted specimens using PVD with and without vacuum. In addition, field data were collected from the site of the Second Bangkok International Airport (SBIA) improved by PVDs with and without vacuum preloading. Analyses were carried out to compare the compressibility parameters by back-calculation of laboratory and field settlements using Asaoka (1978) and Hansbo (1979) methods. From the laboratory tests, the C_h value of reconstituted specimens were 1.05 and 2.20 m^2/yr for PVD without and with vacuum preloading, respectively. In addition, k_h/k_s value of reconstituted specimens for PVD without and with vacuum preloading were 1.50 and 1.45, respectively. The horizontal coefficient of consolidation of PVD with vacuum preloading was higher than PVD without vacuum preloading. After the improvement, the water content was reduced which consequent increase in the undrained shear strength. The field data analysis based from back-calculated results showed that the k_h/k_s amounted to 4 for both PVD with and without vacuum preloading. The C_h values amounted to 4.36 m^2/yr and 6.21 m^2/yr for PVDs without and with vacuum preloading, respectively. The time to reach 90% degree of consolidation for PVD with vacuum preloading was shorter than PVD without vacuum preloading by about one-third because of higher C_h value. The settlement predictions by Asaoka (1978) graphical method agreed with the observed values. Thus, the addition of vacuum pressure leads to the increase of the horizontal coefficient of consolidation which shortened the time of preloading. Moreover, the k_h/k_s values were almost the same with and without vacuum preloading.

1. INTRODUCTION

The main purposes of soft ground improvement are to increase soil strength, reduce soil compressibility and increase soil stiffness of the soft foundation. One of the cheapest soft ground improvement method is by drainage using prefabricated vertical drains (PVDs). PVDs are artificial drainage paths made of geosynthetics that is inserted into the soft ground to shorten the drainage path and, there-by, reduce the consolidation period. Usually, a surcharge load equal to or greater than the expected loading is applied over the soil surface to generate the necessary hydraulic gradient needed for vertical drainage through the PVDs. The instability problem of embankment with prefabricated vertical drains preloading limits the height and slope of embankment. The PVD improvement with surcharge embankment can be combined with vacuum pressure to eliminate the instability problem and to accelerate the rate of consolidation. The vacuum consolidation was proposed in the early 1950 by Kjellman (1952). The studies of vacuum induced consolidation continued up to the present (Holtz, 1975; Choa, 1989; Cognon et al, 1994; Bergado et al, 1998; Tang and Shang, 2000; Chai et al 2006a, b; Bergado et al, 2006; Saowapakpiboon et al, 2008a b). Vacuum consolidation preloads the soil by reducing the pore pressure while maintaining constant total stress instead of increasing the total stress. The effective stress is increased due to the reduced atmospheric pressure in the pores and the soil mass. The net effect is an additional surcharge ensuring early attainment of the required settlement and an increased shear strength resulting in increased embankment stability with subsequent rapid improvement of the soft foundation.

2. LABORATORY TEST USING PVDs WITH AND WITHOUT VACUUM PRELOADING

2.1 Test Specimens

The soil samples were obtained from the site of the Second Bangkok International Airport (SBIA) located at Samut Prakarn province, Thailand which is approximately 30 km southeast of Bangkok. The soft clay samples were collected from 3.0 to 4.0 m depth and placed in covered containers. Table 1 tabulates the physical properties of the soft Bangkok clay. The PVD material used consisted of CeTeau drain (CT-D911). The PVD properties are summarized in Table 2.

2.2 Large Consolidometer

The large scale consolidometer consists of a steel cylindrical chamber made up of 10 mm thick with inner diameter of 300 mm and 500 mm height placed over circle steel base plate. Silicon grease was applied to the insides of the cylinder camber to reduce friction between inner surface of consolidometer chamber and load transfer plate. Geotextile was placed on the top of soil sample to prevent clogging of loading piston. Vertical load was applied through a loading piston at the top of soil by using load transfer plate with thickness of 50 mm connected to a loading arm ratio of 5. The diagram schematic of the apparatus shown in Figure 1.

Table 1. Physical properties of soft Bangkok Clay

Characteristics	
Liquid limit (%)	102.24
Plastic limit (%)	39.55
Water content (%)	112.69
Plasticity index	62.69
Total unit weight (kN/m^3)	14.70
Specific gravity	2.66

Table 2. Summary of CeTeau drain properties (CT-D911)

Characteristics		
Drain Body	configuration	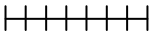
	material	Polypropylene
	channels	44
Filter Jacket	material	Polypropylene
	colour	grey
Weight (g/m)		78
Width (mm)		100
Thickness (mm)		3.5

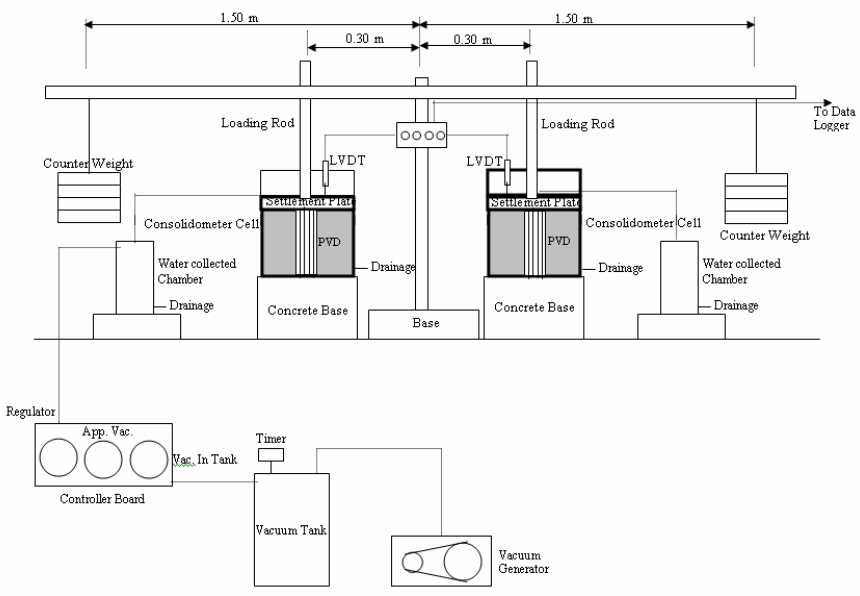

Figure 1. Schematic of large scale consolidometer

2.3 Vacuum Generator

The vacuum pressures that were applied to consolidometer chamber were generated from two vacuum pump and then stored in vacuum tank which has maximum capacity of -120 kPa.

2.4 Consolidometer Test

The reconstituted specimen in the large consolidometer was consolidated with PVD under a vertical stress of 100 kPa, including the 50 kPa reconstitution pressure. Another reconstituted specimen was consolidated with PVD under a vertical stress of 50 kPa combined with -50 kPa in vacuum pressure. The settlement of both specimens were monitored until it reached 90 % degree of consolidation using the method of Asaoka (1978). Afterwards, undrained shear strength and water content were determined.

2.5 Vane shear apparatus

A laboratory vane shear apparatus, capable of measuring shear strengths at different locations and depths, was used to determine the undrained shear strengths before and after the tests. The vane blades, made of stainless steel, were 20 mm in diameter and 40 mm in height. It was attached to an adjustable stainless steel rod and could be adjusted to locate measurement points within the soil specimen. The maximum torques were measured electronically for each test point.

3. FIELD TEST USING PVDs WITH AND WITHOUT VACUUM

3.1 Site Investigations and Field Construction

Both vacuum-PVD and conventional PVD system at Suvarnabhumi Airport, Thailand was reported by COFRA (1996). The soil profile at the site can be divided into 8 sublayers as shown in Table 3 and it consists of a 2.0 m thick weathered clay layer overlying very soft layer which extends from 2.0 m to 10.0 m depth. Underneath the soft clay layer, a 3.0 m thick medium clay layer can be found. The light-brown stiff clay layer can be encountered at 15.0 m to 30.0 m depth. The groundwater level was found at about 0.50 m depth. In Table 4 the pre-overburden pressure (POP) is derived from the given OCR value. The numbers are rounded and taken as an average value of each layer. The soil profiles within the site are relatively uniform with some small variations in the soil thickness. The typical soil properties along with soil parameters are summarized in Figure 2. The consolidation coefficient is estimated from Bergado et al. (2002).

Table 3. The stratigraphy

Present surface	0.00 m	
Water level	-0.50 m	
Type	Top layer(m)	Bottom layer(m)
Top layer, weathered clay	0.00	-2.00
very soft clay1	-2.00	-5.00
very soft clay2	-5.00	-10.00
soft clay	-10.00	-13.00
soft to medium clay	-13.00	-15.00
stiff clay1	-15.00	-17.00
stiff clay2	-17.00	-20.00
stiff clay3	-20.00	-30.00

Table 4. The compressibility consolidation parameters

Type	Unit weight [kN/m^3]	Compressibility			POP (kPa)	C_v theory [m^2/year]
		RR	CR	C_a		
Top layer, weathered clay	18.50	0.035	0.350	0.014	30	-
very soft clay1	13.80	0.050	0.500	0.020	20	0.79
very soft clay2	14.00	0.042	0.420	0.017	30	0.79
soft clay	15.00	0.040	0.400	0.016	60	0.79
soft to medium clay	15.70	0.030	0.300	0.012	80	0.79

stiff clay1	18.50	0.008	0.080	0.003	300	-
stiff clay2	19.00	0.008	0.080	0.003	500	-
stiff clay3	20.40	0.000	0.000	0.000	500	-

The conventional PVD method, the PVD was installed into 10 m depth with a spacing of 1.00 m and arranged in a square pattern. This method had the embankment height in 4.3 m with loading in 2 stages. Typically, a 2:1 side slope was used for low embankment with height less than 2.5 m. However, a 4:1 side slope was adopted for high embankment to reduce the effect from erosion due to rainfall. The high embankment is usually constructed along with counterweight berm for stability purpose. Therefore, the gradient of the side slope was intergrated with the berm as shown in Figure 3. For the vacuum-PVD method, the PVD was installed into 10 m depth with a spacing of 0.85 m and arranged in a triangular pattern as shown in Figure 4. The following boundary conditions used in the design were : installation time of drains of 2 months, maximum pumping time of 4 months. For the vacuum-PVD similar the instrumentation equipments were installed to monitor the field behavior. The readings of the piezometers, the vacuum gauges on the pumps and the settlement are discussed. For the vacuum-PVD, the following boundary conditions were used in the design : installation time of drains of 2 months, maximum pumping time of 4 months, vacuum pressure of -60 kPa, depth of PVD of 10 m below ground surface and 60 % consolidation requirement. The embankment was 2.8 m (18 kN/m^3). Embankment was constructed in two phases, namely: Phase 1 (1.5 m, day 0) and Phase 2 (1.3 m, day 14).

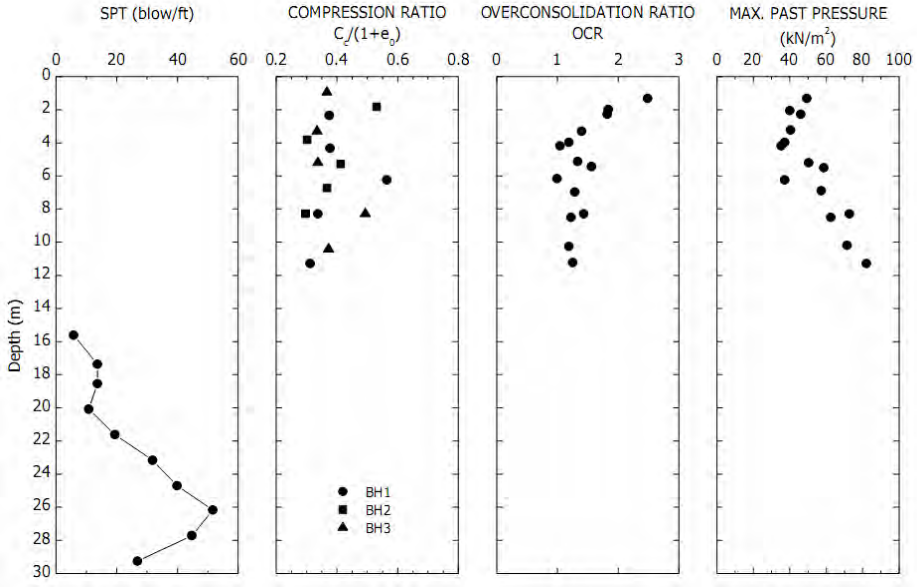

Figure 2. Soil parameters of SBIA project (Bergado et al., 2002)

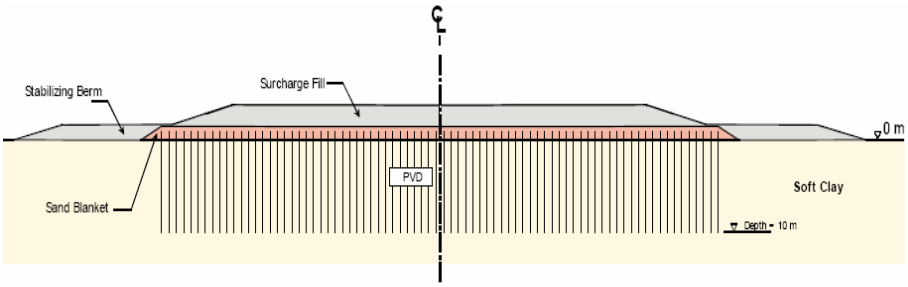

Figure 3. Cross-section of PVDs with embankment method (Seah, 2006)

The final settlement was calculated from using the Asaoka (1978) graphical method. This method is based on the field monitoring data. The horizontal coefficient of consolidation, C_h, can be also back calculated in the different time depend on the time of PVDs installation. Before the PVDs installation, the vertical drainage mainly governed in calculation the

degree of consolidation. After the PVDs installation, the horizontal drainage mainly governed in calculation the degree of consolidation.

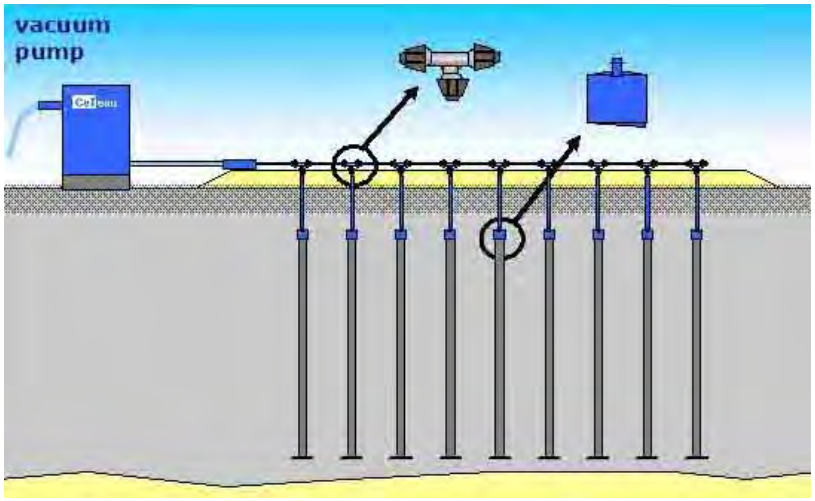

Figure 4. Cross-section of PVDs with vacuum preloading method

4. BACK CALCULATION C_h VALUES

From the settlement observation, Magnan (1983) has modified the observational method proposed by Asaoka (1978) to back calculate the coefficient of consolidation. On the basis of settlement plot, it was possible to evaluate that value. The horizontal coefficients of consolidation have been evaluated from the followings:

$$C_h = \frac{-D_e^{\,2} \cdot F \cdot \ln(\beta_1)}{8 \cdot \Delta t} \quad [1]$$

where:
D_e = diameter of drain influence zone
$F = F(n) + F_s + F_r$
Δt = time interval for settlement plot according to Asaoka (1978) method
β_1 = Slope of the settlement plot in terms of the settlement at time t_i and of time t_{i-1} in an arithmetic scale

On the other hand, by the method of Hansbo (1979), C_h is back calculated from the following relationships when U_h = 90%.

$$U_h(t) = 1 - \exp\left(\frac{-8T_h}{F}\right) \quad [2]$$

where U_h is the degree of consolidation for horizontal drainage; T_h is the time factor for horizontal drainage; F is the factor which expresses the additive effect due to the spacing of the drains, F(n), smear effect, F_s, and well-resistance, F_r. The values of F(n), F_s and F_r are given by the following equations:

$$F(n) = \ln\left[\frac{D_e}{d_w}\right] - \frac{3}{4} \quad [3]$$

$$F_s = \left[\frac{K_h}{K_s} - 1\right] \ln\left[\frac{d_s}{d_w}\right] \quad [4]$$

$$F_r = \pi z(L - z)\frac{K_h}{q_w} \quad [5]$$

where D_e is the diameter of the equivalent soil cylinder, d_w is the equivalent diameter of the drain, K_h is the coefficient of horizontal permeability, K_s is the horizontal permeability of the smear zone, d_s is the diameter of the smear zone, z is the distance from the drainage end of the drain, L is the length of the drain for double drainage and twice the length of the drain for single drainage, q_w is the discharge capacity of the drain at hydraulic gradient of 1 (one). The time factor, T_h, for horizontal drainage can be calculated using:

$$T_h = \frac{C_h t}{D_e^{\,2}} \quad [6]$$

where C_h is the coefficient of horizontal consolidation and t is the time elapsed after the application of the load.

5. RESULTS

The test results were based on the work of Wanthong (2008) under the Supervision of the Authors. The final settlements between the specimen with PVD consolidated with vacuum preloading and the specimen with PVD consolidated with surcharge preloading for reconstituted samples are shown in Figure 5. The settlement of the specimens with PVD under vacuum preloading was considerably faster consolidation rate than the specimens with PVD under surcharge preloading in the early stages of the settlement. But the final settlements of both specimens were same which were approximately 23 mm.

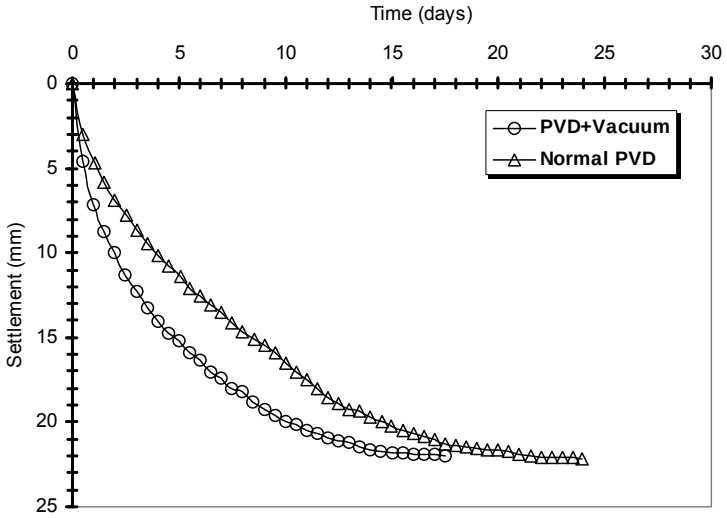

Figure 5. Settlement-time relationship from large consolidometer of reconstituted sample in the laboratory using PVDs with and without vacuum preloading

The measured and the theoretical time settlement curves for the reconstituted specimens are shown in Figure 6a and 6b for PVD with and without vacuum preloading, respectively. The values of C_h and K_h/K_s for the specimen with only PVD are 1.05 m^2/yr and 1.5, respectively. For the specimen with PVD under vacuum preloading, the corresponding values are 2.2 m^2/yr and 1.45, respectively. Consequently, the use of vacuum preloading increased the permeability of the smear zone resulting in the increase in C_h by 100% and decrease in K_h/K_s of about 5%. As expected the horizontal coefficient of consolidation of reconstituted specimen improved by PVD with vacuum pressure was higher than specimen without vacuum pressure due to higher rate of consolidation compared with PVD only improvement. Thus, the construction rate can be faster with reduction in consolidation time. The settlement prediction of laboratory result in the early stages of the

settlement, were underpredicted but after 60% of consolidation, the predicted settlement yielded good agreement with the observed settlements for both improvement by PVD with and without vacuum pressure.

Figures 7a and 7b show that the percentage of water content reductions and percentage of strength increase with the increased distance from PVD after improvement with and without vacuum preloading, respectively. The vane shear strengths after PVD improvement with vacuum pressure were higher than PVD improvement without vacuum preloading.

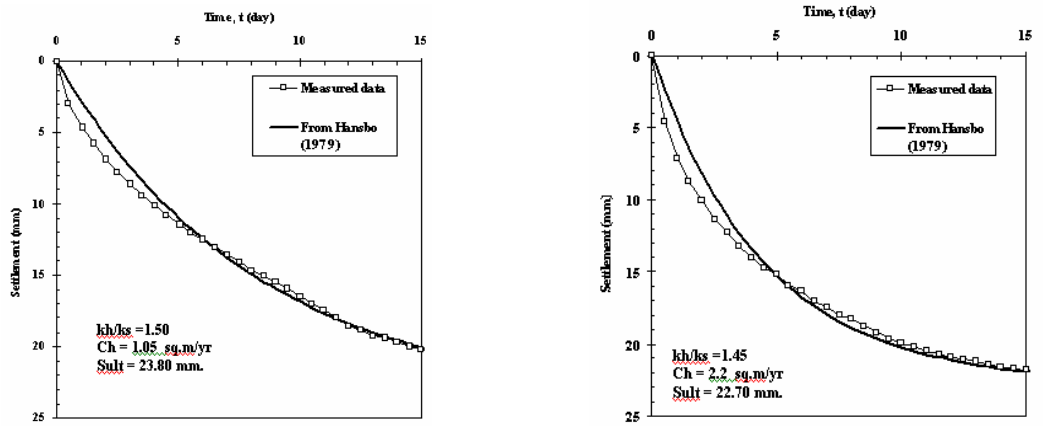

(a) (b)

Figure 6. The observed and fitted curves for settlements to determine C_h values for the reconstituted specimen in large consolidometer (a) PVD with surcharge and (b) PVD with vacuum preloading

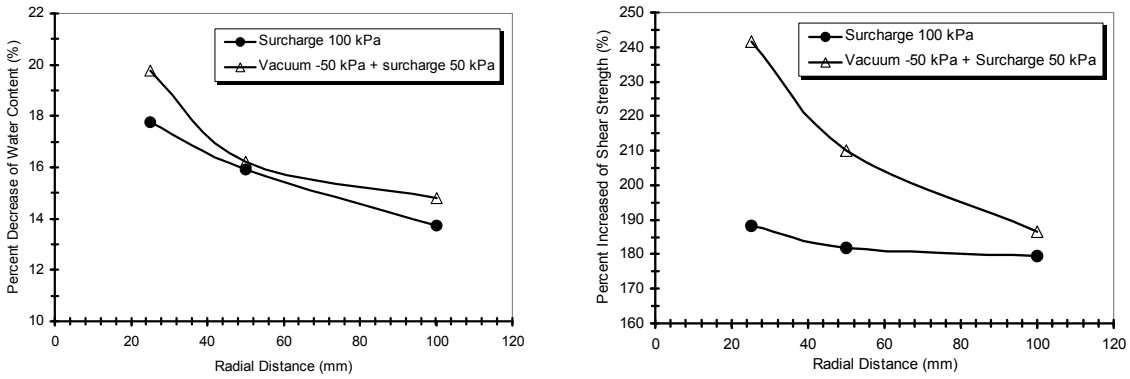

(a) (b)

Figure 7. After consolidation test of the consolidometer using reconstituted samples of PVD with and without vacuum preloading (a) Water content reduction (b) Shear strength increase

The method of Hansbo (1979) were used to analyze the field observation data of two stations of PVD improving by conventional surcharge load and the other two stations of ground improvement by PVD with conventional surcharge load combined with vacuum preloading. The measured settlements of those stations were then compared with the predictions. The comparison of settlement behavior using PVDs without and with vacuum preloading are plotted with time in Figures 8 and 9. The PVD with vacuum clearly indicate faster rates of settlements. The values of C_h and k_h/k_s contributed to the time to reach 90% degree of consolidation of PVD improved soft Bangkok clay. The reduction of time to reach the 90% degree of consolidation using surcharge load combined with vacuum pressure was higher than PVDs without vacuum pressure by about 1.4 to 1.5 times due to the higher rate of horizontal coefficient of consolidation.

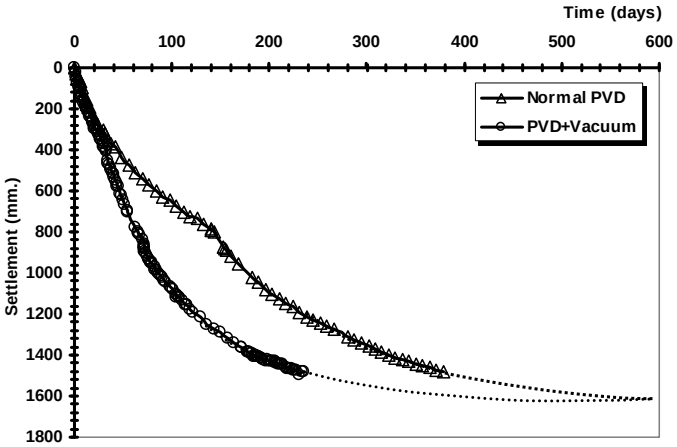

Figure 8. Comparison of settlement of PVD improvement with and without vacuum preloading (Sta. X=13560, Y=12567-12600 for PVDs with embankment and Sta. X=12566.4, Y = 12583.500 for PVDs with vacuum preloading)

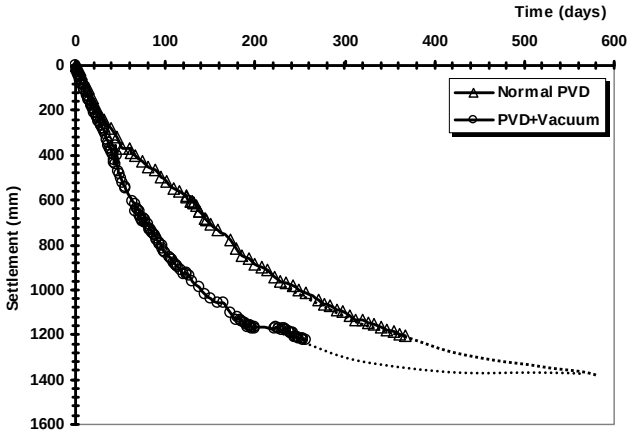

Figure 9. Comparison of settlement of PVD improvement with and without vacuum preloading (Sta. X=14012, Y=12567-12633 for PVD with embankment and Sta. X=12566.4, Y = 12570.000 for PVD with vacuum preloading)

Figure 10a shown the in-situ and back-calculated C_h values at station X = 14012, Y = 11567-12633 by using PVD with surcharge load. The C_h value was 4.22 and 4.15 m^2/yr for Asaoka method and Hansbo method, respectively, with k_h/k_s values of 3.8. The final settlement predicted from Asaoka method was 1356.62 mm. Figure 10b shown the in-situ and back-calculated C_h values at station X = 13560, Y = 11567-12600 by using Asaoka (1978) and Hansbo (1979) method. The C_h value was 4.45 and 4.63 m^2/yr for Asaoka method and Hansbo method, respectively, with k_h/k_s values of 4. The final settlement predicted from Asaoka method was 1678.94 mm.

Figure 11a shown the in-situ and back-calculated of C_h values at station X = 12566.4, Y = 11706.00 by using PVD with vacuum preloading. The C_h value was 5.95 and 6.10 m^2/yr for Asaoka (1978) method and Hansbo (1979) method, respectively, with k_h/k_s values of 4. The final settlement predicted by Asaoka (1978) method was 1356.62 mm. Figure 11b shown the in-situ and back-calculated of C_h values at another station X = 12566.40, Y = 11683.50 by using Hansbo (1979) method. The C_h value was 6.31 and 6.47 m^2/yr for Asaoka (1978) method and Hansbo (1978) method, respectively, with k_h/k_s values of 4. The final settlement predicted by Asaoka (1978) method of the station was 1614.94 mm.

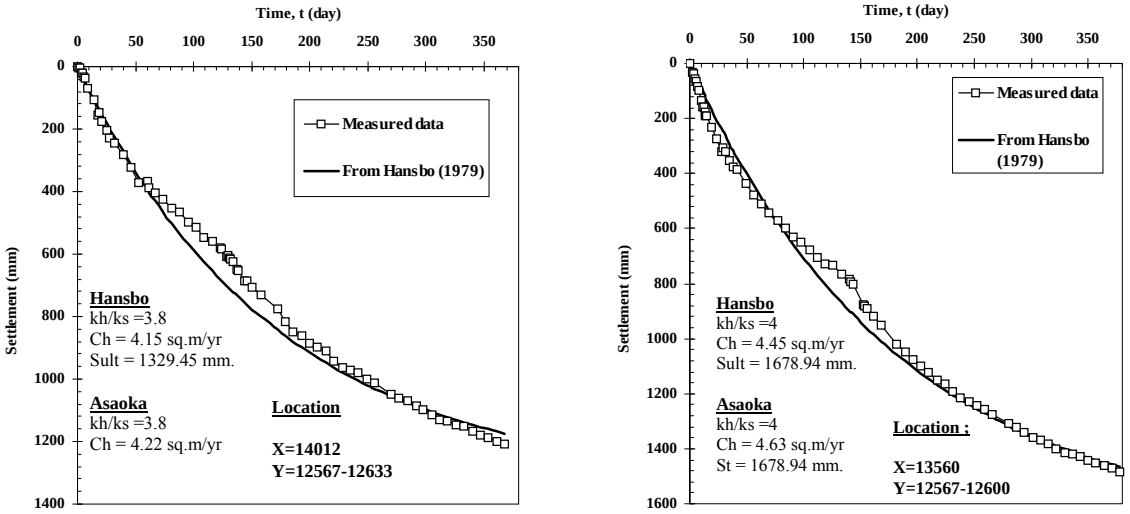

Figure 10. Back-calculated compressibility parameters of field observations of PVDs with embankment (without vacuum preloading) (a) X=14012 Y=12567-12633 (b) X=13560 Y=12567-12600

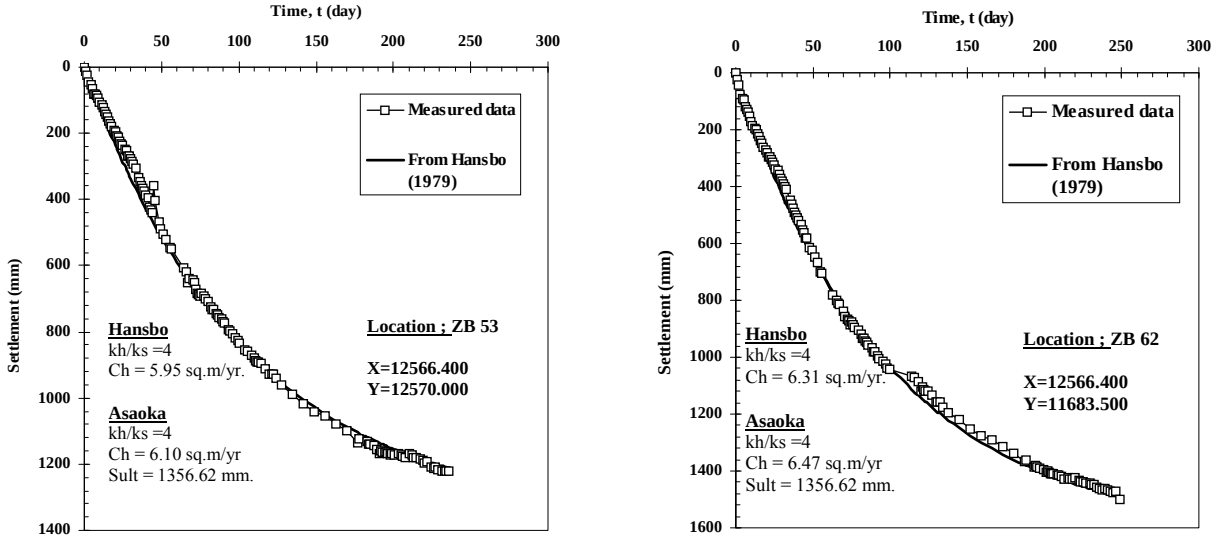

Figure 11. Back-calculated compressibility parameters of field observations of PVDs with vacuum preloading (a) Station ZB 53 (b) Station ZB 62

The surface settlement predicted by Asaoka (1978) graphical method are based on the monitoring record. The predicted surface settlements at different loading stage of PVD improvement with and without vacuum preloading using Asaoka (1978) method. The predicted surface settlement is slightly overestimated compared to the field observation data but the method of Asaoka (1978) yielded very good prediction. The addition of vacuum pressure to PVD seems to increase the coefficient of horizontal consolidation, C_h as expected.

6. CONCLUSION

Based on the data and results of the analyses, the following conclusions can be made:

1) The back-calculated Ch values of reconstituted specimens were 1.05 and 2.20 m^2/yr for normal PVD and vacuum PVD, respectively. The corresponding kh/ks values were 1.50 for normal PVD and 1.45 for vacuum PVD.

2) Based from back-calculated results, the field data showed that the k_h/k_s are 4 for both normal PVD and vacuum PVD. The average C_h values were 4.36 m^2/yr. and 6.21 m^2/yr. from the normal PVD and vacuum PVD, respectively.

3) The surface settlement prediction by Asaoka (1978) graphical method yielded very good predictions for PVD without vacuum preloading but for PVD with vacuum prediction, the predicted settlements were slightly higher than the field observation data.

REFERENCES

Asaoka, A. (1978). Observational procedure of settlement prediction, *Soils and Foundations*, 18(4): 87-101.

Bergado, D.T., Chai, J.C., Miura, N. and Balasudramaniam, A.S. (1998). PVD improvement of soft Bangkok clay with combine vacuum and reduced sand embankment preloading, *Geotechnical Engineering Journal*, 29(1): 95-121.

Bergado, D.T., Balasubramanian, A.S., Fannin, R.J. and Holtz, R.D. (2002). Prefabricated vertical drain (PVD) in soft Bangkok clay: A case of NBIA project, *Canadian Geotechnical Journal*, 39: 304-315.

Bergado, D.T., Saowapakpiboon J., Kovittayanon, N. and De Zwart, T.P. (2006). Ceteau-S PVD vacuum system in soft Bangkok Clay: A case study of the Suvarnabhumi Airport Project, *The 6th Sysposium on Soft Ground Improvement and Geosythetics*, Bangkok, Thailand: 18-27**.**

Chai, J.C., Carter, J.P. and Hayashi, S. (2006a). Vacuum consolidation and its combination with embankment loading, *Canadian Geotechnical Journal*, 43: 985-996.

Chai, J.C., Miura, N. and Bergado, D.T. (2006b). Preloading clayey deposit by vacuum pressure with cap-drain. *Proceeding 21st Japanese Geosynthetic Symposium*, Aomori, Japan: 45-52.

Choa, V. (1989). Drains and vacuum preloading pilot test. *Proceeding 12th International Conference on Soil Mechanics and Foundation Engineering*, Riode Janeiro. Brazil. 1347-1350.

COFRA (Thailand), (1996). Design and Proposal for the Execution of a Test Field: Vacuum Consolidation for the Landslide Road System for Second Bangkok International Airport, Bangkok, Thailand.

Cognon, J.M., Juran, I. and Thevanayagam, S. (1994). Vacuum consolidation technology : Principles and field experience, *Proceedings Vertical and Horizontal Deformations of Embankments (Settlement'94), ASCE Special Publication* 40(2): 1237-1248.

Hansbo, S. (1979). Consolidation of clay by band shaped prefabricated drains, *Ground Engineering*, 12(5): 16-25.

Holtz, R.D. (1975). Preloading by Vacuum: Current Prospects, *Transportation Research Record*, Washington, D.C., U.S.A. 548: 26-69.

Kjellmann, W. (1952). Consolidation of clay soil by Means of Atmospheric Pressure, *Proceedings on Soil Stabilization Conference*, Boston, U.S.A.: 258-263.

Magnan, J. P. (1983). Back analysis of soil consolidation around vertical drains, *Improvement of Grou*nd, 2: 45-52.

Saowapakpiboon, J., Bergado, D.T., Chai J.C., Kovittayanon, N. and De Zwart, T.P (2008a). Vacuum-PVD Combination with Embankment loading Consolidation in soft Bangkok Clay: A case study of the Suvarnabhumi Airport Project. *Proceeding of the 4th Asian Regional Conference on Geosynthetics*, Shanghai, China: 18-27**.**

Saowapakpiboon, J., Bergado, D.T., Hayashi S., Chai J.C., Kovittayanon, N. and De Zwart, T.P (2008b). CeTeau PVD Vacuum System in soft Bangkok Clay: A case study of the Suvarnabhumi Airport Project. *Lowland Technology International*. 10(1): 42-53.

Tang, M. and Shang, J. Q. (2000). Vacuum preloading consolidation of Yaogiang Airport runway. *Geotechnique*, 50(6):613-653.

Wangthong, P. (2008). Prediction and performance using PVD with and without vacuum preloading, *M. Eng. Thesis,* Asian Institute of Technology, Bangkok Thailand.

Improvement of Pond Ash with Prefabricated Vertical Drain

G. Venkatappa Rao, Department of Civil Engineering, University College of Engineering, Osmania University, Hyderabad, India
G. K. Pothal, Department of Civil Engineering, Indian Institute of Technology Delhi, New Delhi, India

ABSTRACT
Thermal power plants using pulverized coal produce large quantities of ash as a by-product. The ash ponds occupy about 30,000 hectares presently and are expected to be doubled by year 2012. This can be restricted by raising the ash pond dykes by upstream method of construction. In the upstream method of raising of ash pond dykes, strengthening or consolidation of the ash pond fill nearer to the starter dyke is required. This paper presents the application of prefabricated vertical drains to accelerate the consolidation process of pond ash deposits.

Model tests under simulated conditions have been carried out on two samples of pond ash collected from an ash pond. The changes in the total settlement and moisture contents at different depths of the tank have been studied, with and without the installation of prefabricated vertical drain. The paper demonstrates the significant improvement shown in both the pond ashes by the use of prefabricated vertical drains.

1. INTRODUCTION

Thermal power plants using pulverized coal produce large quantities of ash as a by-product. A total of about 85 thermal power plants in India with an installed power capacity of around 84,000 MW generate about 120 Million tonnes of ash per year. Consequently the ash generation per year is expected to touch around 170 Million tonnes by the year 2012 and around 225 Million tonnes by 2017. This results in the ash generated by the thermal power plants being disposed off in the vicinity of the plant as a waste material covering several hectares of valuable land. The ash ponds occupy about 24,000 hectares presently. The area is expected to increase up to 60,000 hectares by year 2012. This can be restricted by raising the ash pond dykes by upstream method of construction.

Primarily, there are two types of ash disposal being practiced by the thermal power plants in India – the wet disposal system (more commonly adopted) and the dry disposal system. In the wet disposal system, the ash is mixed with water to make a slurry which is then pumped to the ash disposal lagoons known as ash ponds through pipelines. At the disposal area, the dry ash is dumped to form mounds of ash, using elaborate earth moving machinery. The ash deposit placed in slurry form has a very low density and leads to problems such as liquefaction during earthquake, poor bearing capacity, large settlement, etc.

In this paper, a laboratory study using PVD for the consolidation of pond ash deposit under simulated conditions is presented. The effective use of PVDs in pond ash deposits has been studied by model tank studies with two types of pond ash samples collected from an ash pond. The paper depicts the significant improvements in terms of total settlements and moisture content by the use of prefabricated vertical drains.

2. BACKGROUND

2.1 Spatial Variation of Ash in Ash Ponds

As the slurry is deposited through a pipe near the dyke, at the discharge point, ash is predominantly sand sized possibly with a few lenses of fine material, whereas far away from the slurry disposal point, the ash is more likely to contain predominantly silt sized with few lenses of coarse material. The zone in between these two zones is characterized by extensive horizontal layering of fine and coarse ash. A comprehensive view of the vertical and lateral variation of ash in a typical ash pond is shown Figure 1.

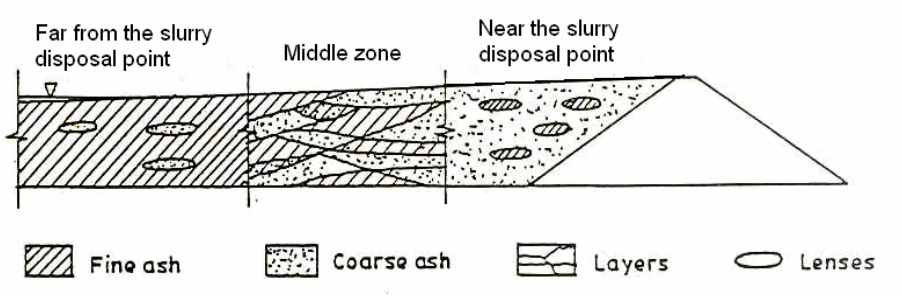

Figure 1 Sorting and layering in an Ash Pond (Modified after Datta, et al., 1996)

2.2 Methods for Raising Ash Dykes

There are three different methods for raising of ash ponds. They are :

- Upstream method of construction
- Downstream method of construction
- Centre-line method of construction

2.2.1 Upstream method of construction

In the upstream method of construction, the starter dyke is constructed at the downstream toe and the ash is discharged to form a beach. The beach adjacent to the starter dyke then becomes the foundation for a first or the second embankments. A typical embankment configuration by the upstream method of construction is depicted in Figure 2. The main advantages of the upstream method are cost and simplicity. Only minimal volumes of mechanically placed fills are necessary for construction of the peripheral embankment and large embankment heights can be attained at very low cost.

Use of upstream raising method, however is limited to very specific conditions and incorporates a number of inherent disadvantages. Factors that constrain the application of the upstream method include phreatic surface control, water storage capacity and seismic liquefaction susceptibility. The dyke can be raised up to a limited height as all stages are built on top of the hydraulically filled ash.

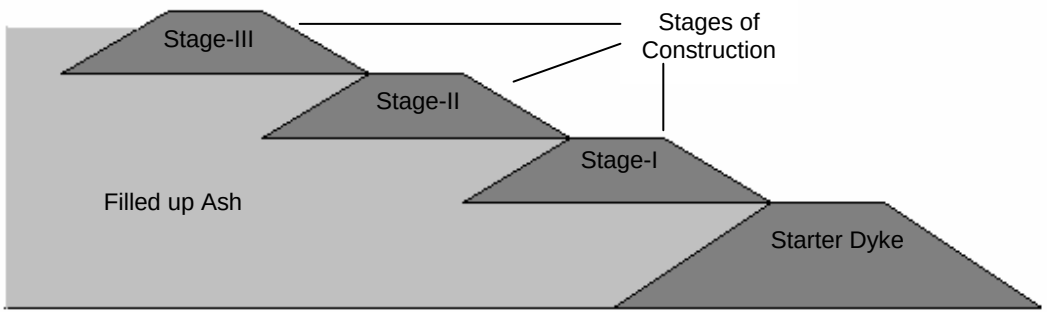

Figure 2 Raising of ash dyke by the upstream method of construction

2.3 Prefabricated Vertical Drain (PVD)

A PVD in general is made of two components, namely, the sheath and the core. The sheath is a non-woven filter fabric used to prevent the entry of the soil particles and allow only the water into the drain. The core is made of different profiles and helps in transporting water vertically through the drain. Both the core and the sheath are either joined together usually at the edges by thermal bonding or the core is inserted separately by folding the sheath over it and subjecting to ultrasonic welding. The entire PVD is approximately 100 mm wide and 4 mm to 6 mm thick and comes in rolls up to 300 m in length. The modem commercial PVDs differ from each other with respect to the method of manufacture, materials used and the geometrical shapes.

Literature on the drains reveals that the core and the sheath are made of either polyester or polypropylene and in some cases polyethylene. These materials used for the manufacture of PVDs have a long life. In the last decade a large

number of PVDs have appeared in the market cutting down their costs appreciably also permitting easier installation even in difficult environment, e.g. water. Presently, more than 50 types of different vertical drains, which may be installed down to depths approaching 60 m, at rates up to 1 m/s, are available in the market.At Indian Institute of Technology Delhi, a PVD, using coir and jute yarns, was developed (Venkatappa Rao et al., 2000) which was shown to be comparable with typical synthetic drains, particularly at kinked conditions.

The design procedures commonly adopted for ground improvement by PVDs are summarized by Sarkar and Venkatappa Rao (1999).

2.4 Field Studies

Gandhi (1999) showed that the low bearing capacity of the ash deposit can be improved by the technique of installation of stone columns by vibroflotation. However, it is difficult to be executed and is an expensive technique for adoption. Nevertheless, improvement of ash near the dyke is a must by the upstream method. Hence, use of PVDs offers a potential technique.

Prefabricated vertical drains (PVDs) have been used successfully in many soil improvement and land reclamation project in Asia and the rest of the world (Hansbo et al., 2005; Bergado et al., 2002). In India, PVDs were installed in Kakinada Port as well as Kandla Port effectively. However, their use in pond ash slurry deposits is not yet attempted. The possible of PVDs for raising of ash dykes by the upstream method of construction is presented in Figure 3.

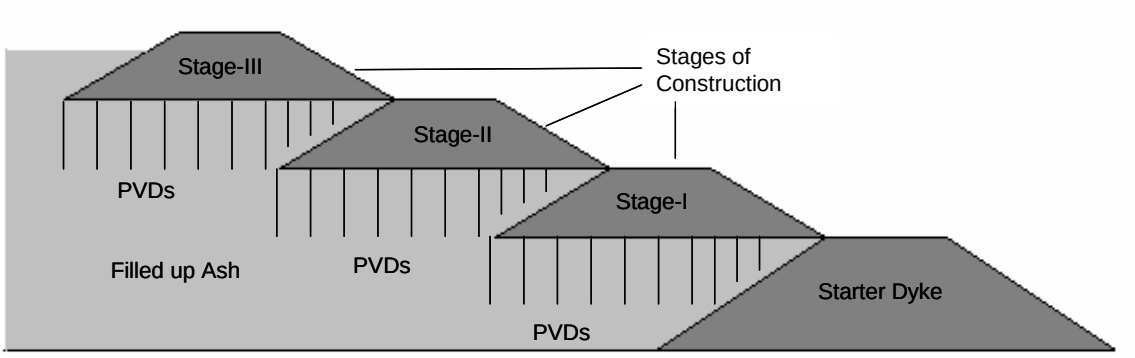

Figure 3 Possible use of PVDs for raising of ash dyke by the upstream method of construction

2.5 Model Tank Studies

The performance of the drain can best be judged by its function in the field condition. However, to simulate these conditions, in the laboratory, experiments are carried out by placing the drain in the soil for a long period and observing its performance. In one such experiment Venkatappa Rao et al. (1994) placed vertically three jute fibre drains of 750 mm long in one tank filled with kaolinite clay and evaluated their performance. Sampath Kumar (2000) also carried out experiments with a braided natural fibre drain in a tank filled with kaolinite clay.

3. EXPERIMENTAL WORK

3.1 Materials

3.1.1 Pond ash

For the current research work, the pond ash samples were collected from the ash ponds of the Captive Power Plants of The National Aluminum Company Limited (NALCO), Angul, Orissa, India. Two types of pond ash samples were collected from two different places from the ash pond, one from near the slurry disposal point, where the particles are generally coarser in nature (designated NC) and the other, far away from the ash disposal point where the particles are finer (designated NF). The physical properties of both the pond ash are given in Table 1.

Table1: Physical properties of pond ash

Physical properties		Values	
		NF	NC
Grain size distribution	Gravel size (> 4.75mm) (%)	0	0
	C.Sand size (4.75 - 0.475mm) (%)	2	4
	F.Sand size (0.475 - 0.075mm) (%)	40	76
	Silt size (0.075 - 0.002mm) (%)	56	19
	Clay size (< 0.002mm) (%)	2	1
Specific gravity		2.02	2.48
Liquid limit (%)		48	33
Plastic limit (%)		Non-plastic	Non-plastic
Maximum dry density (kN/m^3)		10.7	13.6
Optimum moisture content (%)		34.5	25.2
Angle of internal friction (Degrees) at MDD		31	36

3.1.2 Model tank

The tank used in this study and the detailed arrangement is shown in Figure 4. Such an arrangement was previously used by Sampath Kumar (2000) for evaluating braided PVD.

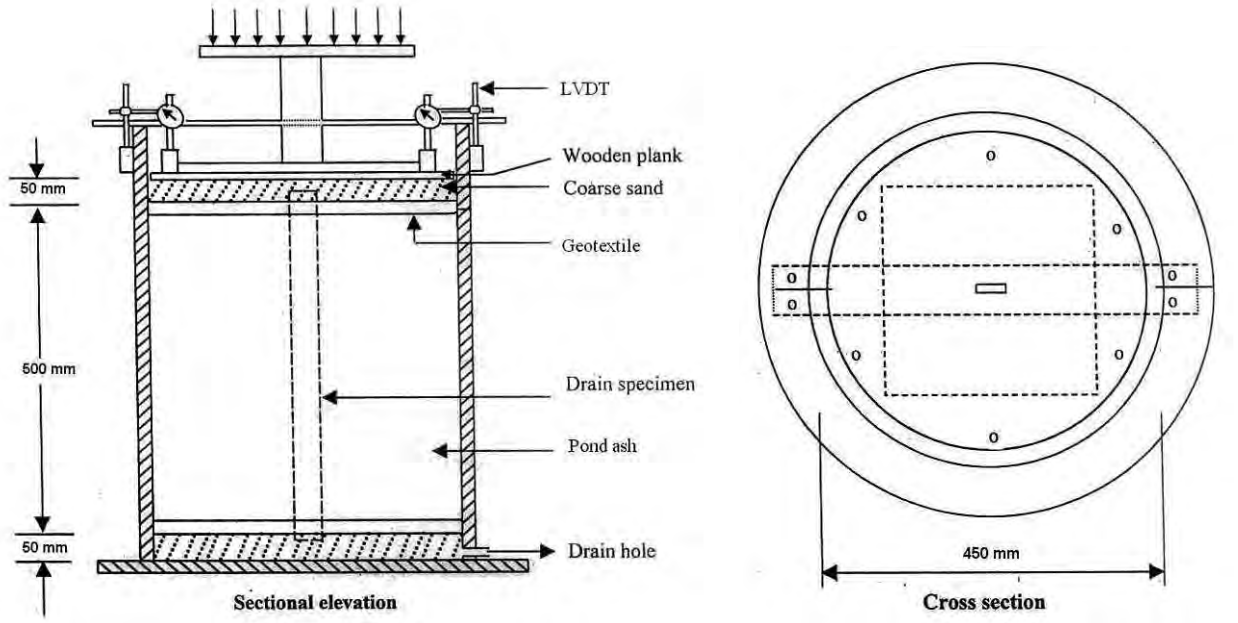

Figure 4 Typical arrangement for model test on pond ash with prefabricated vertical drains (Modified after Sampath Kumar, 2000)

The model tank made up of 10 mm thick plate has 450 mm internal diameter and has a height of 750 mm. A hole of 20 mm diameter is provided at the bottom of the tank in order to freely drain out the water during the consolidation process. The loading was done with dead weights through a guided platform made of steel. Two long travel LVDTs were fixed to record the vertical displacement of pond ash under application of loads. The LVDTs were connected to a data logger with an accuracy of 0.1 mm.

3.1.3 Testing procedure

The inner surface of the tank was cleaned and was made smooth by polishing with fine sand paper. A thin coating of grease was applied to the surface. The tanks were filled with coarse sand up to a height of 50 mm from the bottom. The sand layer was compacted to get the required density. A non-woven geotextile was placed on the sand so as to act as a separator between the sand and the pond ash. The pond ash samples were mixed with water at water content more than their respective liquid limits. The pond ash was mixed thoroughly so that there will be no air bubble present inside the slurry. The pond ash slurry was carefully poured in small quantities at depths of 100 mm at one time and is allowed to

settle down. The same procedure was repeated till the pond ash slurry was filled up to the required height of 500 mm. To fill the tank with PVD; the PVDs were first placed in the tank before pouring the pond ash slurry. The PVD was placed in between two perspex sheets of 10 cm width and was kept to stand vertical in the centre if the tank penetrating into the sand layer. The bottom non-woven geotextile must have a rectangular hole to allow the PVD to pass through it. Then the procedure of filling the tanks were the same as that of without PVDs as described earlier. A circular piece of non-woven geotextile having the diameter of 450 mm was placed on the pond ash. A rectangular hole equal to the size of the PVD was made at the centre so that the PVD can project into the sand layer. Sand was filled on the geotextile layer and was spread over the whole area of the tank. The sand was then compacted to a depth of 50 mm. After the top layer of sand was made smooth and horizontal a wooden plank of 440 mm was placed on it. The loading frame was placed on the wooden plate and was fixed to the tank by fasteners so that there will be no danger during loading. The LVDTs were fixed to the fixed arm of the loading frame and their ends were connected to a six channel data logger. The initial readings were noted and the procedure of loading was started. The total stages of the model test are shown in step by step in Figures 5 and 6.

a) PVD placed vertical

b) Pond ash slurry being poured

c) Slurry being filled

d) slurry after settling down

e) Geotextile separator being placed

f) sand being placed

Figure 5 Photographs showing detailed procedure for preparation of the model

4. RESULTS

Load was applied gradually up to a pressure of 29.4 kPa as shown in Figure 7. It took 45 days for the maximum pressure to be applied and this pressure was maintained upto the 60th day.

For the first 10 days, the settlements of the two tanks were almost equal, as can be observed in Figures 8 and 9 for both the types of pond ash. At higher pressures, the difference in the two curves becomes significant, which is obviously due to the presence of drain in one of the tanks. The difference in settlement eventually reaches to the highest value and then begins to decrease gradually. After about 45 days of the test, the curve without drain eventually becomes straight and approaches towards the curve with drain. It is observed that the total settlement in 60 days was 18.52 mm without the drain whereas it was 21.93 mm with the drain for pond ash type NF and 21.41 mm and 26.17 mm respectively for pond ash type NC.

Figure 6 Photograph of model test in progress

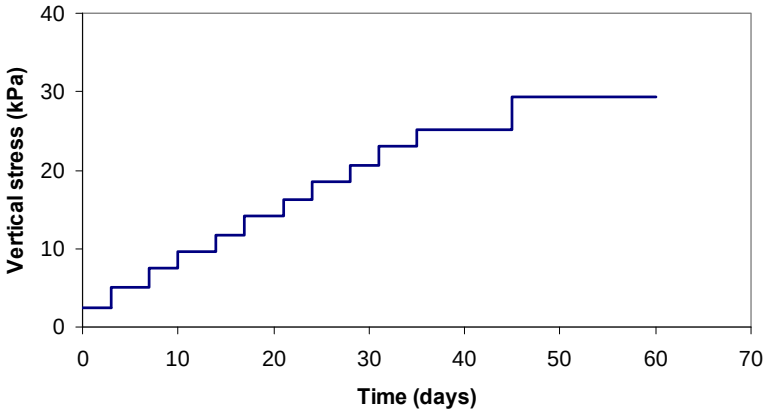

Figure 7 Application of Vertical pressure with time

In a way the above data reflects the performance of the drain. This may also be further reinforced through the data obtained for the moisture content measured before and after consolidation for both the pond ash as presented in Figures 10 and 11. As seen from these figures, the average moisture content of the pond ash was around 52 % and 39 % for NF and NC type of pond ash respectively. At the end of the consolidation, the moisture content of both the tanks was observed to be the least at about 42 % and 28 % respectively. Also the moisture content profile obtained with the drain is nearly vertical, with the moisture content at the center at mid-height being marginally higher indicating the general efficacy of the drain. On the other hand the moisture content profile for the tank without the drain is entirely different and exhibits highest moisture content at mid-height, only marginally lower than the initial moisture content. This is indicative of the fact that the consolidation that is taking place is at a much slower rate than with the drain.

5. CONCLUSIONS

It is a well known fact that ash in a slurry pond remains soft i.e. unconsolidated even when the ash level reaches the dyke crest. (Only drying is found to strengthen the pond ash). In this study, it is shown that pond ash can be consolidated by using PVD under low vertical stresses. Hence the method has great potential for application.

The following conclusions have been made from the present experimental studies

- The consolidation settlement of both the pond ash types significantly increases with application of PVD.

- The distribution of moisture content in a pond ash deposit becomes uniform with the use of PVD.
- PVDs can be suitably used for consolidation of pond ash deposits and the pond ash dykes can be raised above the prepared pond ash deposite.

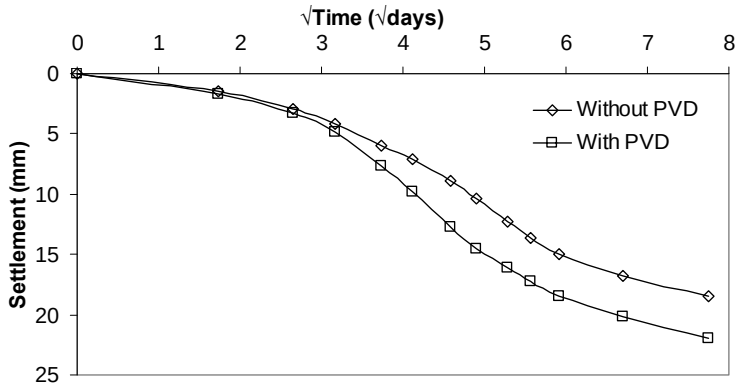

Figure 8 Settlement vs. square root of time for pond ash type NF

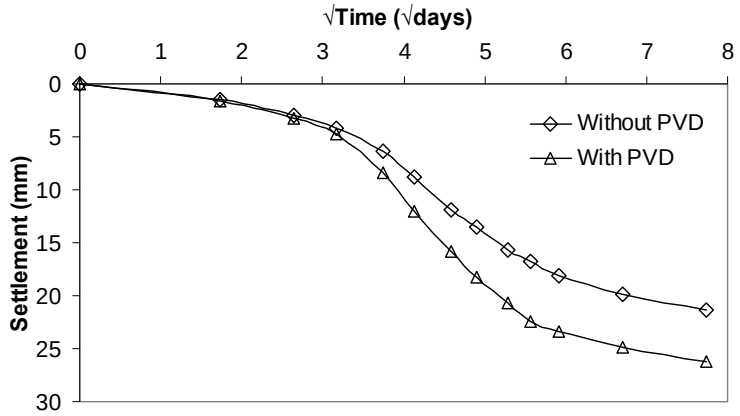

Figure 9 Settlement vs. square root of time for pond ash type NC

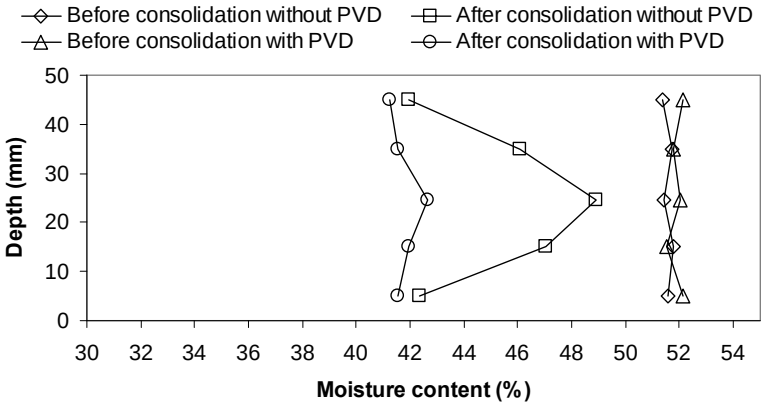

Figure 10 Profiles of moisture contents with and without PVDs for pond ash type NF

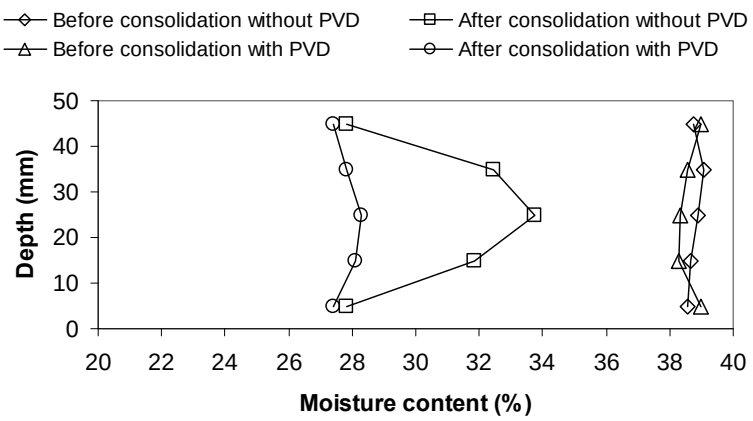

Figure 11 Profiles of moisture contents with and without PVDs for pond ash type NC

ACKNOWLEDGEMENTS

The authors are very grateful to The General Manager, Captive Power Plant, National Aluminium Company Limited (NALCO), Angul, Orissa, India for his help during the collection of the pond ash samples from the ash ponds of NALCO.

REFERENCES

Bergado, D.T., Balasubramaniam, A.S., Fannin, R.J., and Holtz, R.D., 2002. Prefabricated Vertical Drains (PVDs) in Soft Bangkok Clay: A Case Study of the New Bangkok International Airport Project, Canadian Geotechnical Journal, 39: 304 – 315.

Chitra, R., 2006. Pseudo-static and Probabilistic Stability Analyses of Ash Containment Systems, Unpublished Ph.D. Thesis, Indian Institute of Technology Delhi.

Datta, M., Singh, A. and Kaniraj, S. R., 1996. Spatial Variation of Ash Characteristics in an Ash Pond, Ash Ponds and Ash Disposal Systems, Narosa Publishing House, New Delhi: 111 – 119.

Gandhi, S. R., 1996. In-situ Densification of Deposited Ash Slurry, Ash Ponds and Ash Disposal Systems, Narosa Publishing House, New Delhi: 211 – 221.

Hansbo, S., Jamiolkowski, M. B. and Kok, L., 1981. Consolidation by Vertical Drains, Geotechnique, March, V 01.43: 3 – 17.

Sampath Kumar, J. P., 2000. Studies on Braided Prefabricated Vertical Drain, Unpublished Ph.D. Thesis, Indian Institute of Technology Delhi.

Sarkar, S. S. and Venkatappa Rao, G., 1997. Pre-consolidation of Soft Soil by Strip Drains, Geohorizon: State of Art in Geosynthetic Technology, Sarkar, S. S. (Editor), Bangalore: 272 – 282.

Venkatappa Rao, G., Khan, M. A. A. and Narayan Sarma, G. V., 1994. Efficacy of jute fibredrains", 2nd International Workshop on Geotextiles, New Delhi: 86 – 91.

Venkatappa Rao, G., Sampath Kumar, J. P. and Banerjee, P. K., 2000. Characterization of a braided strip drain with coir and jute yarns, Geotextiles and Geomembranes, Vol. 18: 367 – 384.

Geosynthetics 2009
February 25-27 2009, Salt Lake City, Utah

Use of Geosynthetics to Mitigate Frost Heave on Trail Ridge Road

D.E. Alzamora, Federal Highway Administration, Resource Canter, Lakewood, Colorado
K. Haramy, Federal Highway Administration, Central Federal Lands Highway Division, Lakewood, Colorado
S.A. Anderson, Federal Highway Administration, Federal Lands Highway Program, Lakewood, Colorado

ABSTRACT
Trail Ridge Road is the main road through Rocky Mountain National Park in Colorado. The section of roadway above an elevation of 3300-meters is highly susceptible to frost heave and creep which creates subsidence zones and adverse roadway conditions. Conventional recommendations include excavation of existing frost susceptible soils to below the frost depth and replacement with a thick layer of well draining, non-frost susceptible material and/or use of a coarse-granular crushed rock cap. Due to the lack of readily available material, remote location, and tight construction limits, the traditional solutions would add a significant cost to the overall project. In addition, the depth of the excavation was perceived to have a significant impact to the delicate alpine environment and traffic control. An alternate using less excavation, geogrids for stabilization, and a drainage geocomposite as a capillary break was proposed to improve the roadway condition for significantly reduced impact and cost. The construction of this project was completed successfully in the fall of 2007.

1. INTRODUCTION

1.1 General

Rocky Mountain National Park is located in north-central Colorado near the town of Estes Park, approximately 70 miles northwest of Denver, in the eastern Rocky Mountain Range. Trail Ridge Road (also known as Colorado State Highway 34) is the main road through the National Park, connecting the Estes Park Valley on the east and the Kawuneeche Valley on the west. Five roadway failure areas mainly caused by frost heave and solifluction were evaluated along the roadway between the Rock Cut pullout and the Alpine Visitor Center (Figure 1). The roadway surface at the evaluated sites had subsided between 150-mm and 600-mm from the original elevation creating major dips along the roadway. These dips are a significant safety hazard for vehicles, potentially causing loss of contact with the roadway surface and control of vehicles.

Due to the amount of snow received, this route is typically open only between the end of May and the middle of October and is maintained by the National Park Service. The construction of Trail Ridge road was completed through mostly cut and fills in 1941 and was first paved in 1949. The existing roadway is a two-lane thoroughfare with a paved surface width of 7.5 meters with little to no shoulder provided. The highest roadway elevation on Trail Ridge Road is 3,713 meters and it is considered the highest continuously paved road in the United States. Park visitation has seen an annual steady growth which includes traffic volume and vehicle size from about 200,000 annual visits in 1930 to over 3 million annual visits today. This number is projected to further increase to 4.9 million by 2020. Pavement sections and road geometry were not initially designed to accommodate the high stresses caused by neither the number of vehicles nor the weight and size of recreational vehicles, buses, and vehicles pulling trailers.

1.2 Geology and Subsurface Conditions

Trail Ridge Road is located in the heart of Rocky Mountain National Park, which rises to elevations from 2,380 to 4,350 meters and includes Longs Peak, one of Colorado's highest points. These mountains are part of the northern Front Range that lies within the geologic province known as the Southern Rocky Mountains. These north-south trending mountains are characterized as broad-backed uplift, along whose crest erosion has laid bare wide areas of Precambrian rocks. These Precambrian rocks consist of Granite, granitic Gneiss, and biotitic Schist that have been sculpted by several episodes of glaciations. Glacial and periglacial features are present today as U-shaped valleys, hanging valleys, cirques, cirque lakes, lateral moraines, and solifluction lobes. The soils consist mainly of glacial deposits, talus, and residual soils derived from weathering of the granitic basement rocks.

The morphology of adjacent slopes suggests that alpine permafrost is present at the high elevation sites discussed herein. Permafrost is uncommon in the Rocky Mountain Region but does exist at high elevations and varies on the basis of soil texture and degree of induration, water content and lithology, slope aspect and snow cover. The adjacent slopes show lobes that are evidence of solifluction, a process where saturated soil tends to flow down slope like a viscous fluid on top of a relatively impermeable boundary. At the site the conditions for solifluction are observed in the spring when the near surface soils have thawed and are saturated with snowmelt water, and frozen soil forms an apparent boundary at depth. At this time of year the drainage ditch on the upslope shoulder of the road is full of water.

In general, the immediate (overburden) subsurface materials consisted of loose granular soils classified as SM, SW, and SC by the USCS to depths ranging from 2.5 to 5 meters. The overburden soils were underlain by decomposed granite with large granitic boulder core stones. The existing pavement thickness at these sites ranged from 200 to 500 mm. The thick asphalt sections were indications of several attempts to maintain the road surface with overlays.

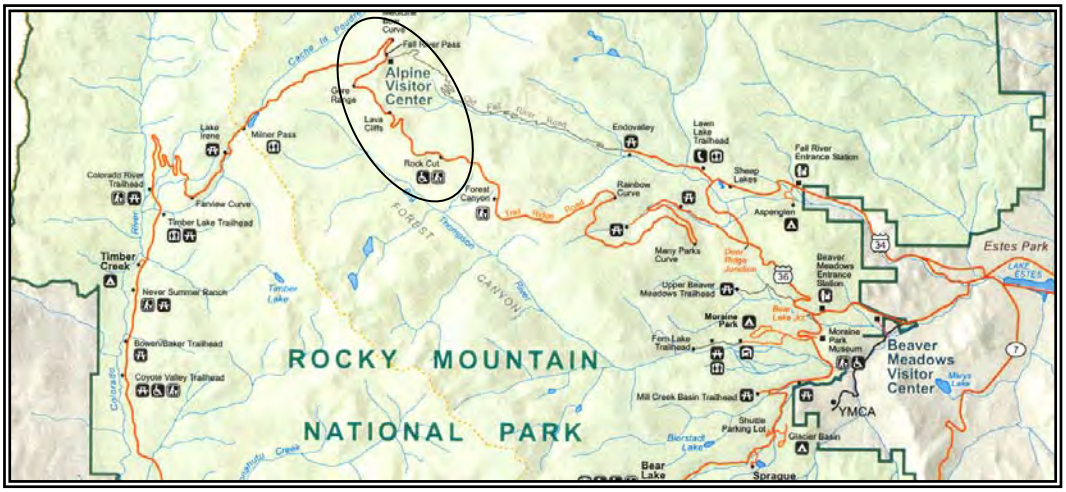

Figure 1. Site map showing Trail Ridge Road

2. PROJECT NEEDS

Several areas along the Trail Ridge Road have experienced significant deformations in the form of subsidence. These subsided areas cover distances between 150 m to 1600 m along the roadway and have subsided as much as 600-mm in certain areas from the original roadway grade creating hazardous dips along the driving path. The subsidence areas are at high elevation, above timberline, located where the road traverses a slope and where snowmelt introduces significant water in the spring. Drifting of snow and management of snow on the road may play a role in where the problem areas are located. The road is not plowed through the winter and is opened in late spring when only a few snow drifts are left to be cut through. Given this setting, the cause of deformation is believed to be primarily due to frost heave, creep and solifluction.

Solifluction is a process that is affecting the road from the slope above the road, outside the roadway prism, and stopping it would be like trying to push a viscous fluid up a slope (Turner et al., 1996). As such, solifluction is a difficult process to deal with, especially if work outside of the roadway prism is not permitted due to the environmental impact of the construction process. Fortunately, solifluction may be only a secondary cause of the distress. If solifluction were dominant it is expected that the deformation of the road would be more lateral than vertical, and that is not the case.

Frost heave and creep occur more in the vertical direction. Frost heave is caused when water around soil particles begin to freeze, causing the soil to dilate, create a vacuum, and attract more water from unfrozen ground. This process begins to create ice lenses within the soil matrix and causes the soil to move up and outward, in a direction generally perpendicular to the ground surface. The frost heave process is highly dependent on the affinity of the soil for water, the availability of water, and ground temperature (Guthrie, et. al., 2003). The Upper part of Trail Ridge Road has all the components essential for frost heave to occur, such as long periods of cold weather, readily available water in the saturated soils, and frost susceptible soils.

Creep occurs when the frozen ground thaws and since settlement is driven by gravity the direction of settlement is mostly vertical. Therefore, a cycle of heave and thaw results in downslope migration of soil; up and out with the heave and straight down with the thaw. If the soil also dries at some point in the season the drying can lead to densification which is also manifest as settlement at the ground surface. Frost heave, creep, and seasonally variable water contents are thought to be the primary causes of settlement and road distress.

For the purpose of this report only two of the evaluated sites will be specifically described here: **Area “A “and Area “B”.** All the other sites have somewhat similar geotechnical and hazard conditions.

Area "A": In this area a segment, about 150 meters, of the roadway was subsided up to 600 mm below the original roadway grade, Although both lanes have settled, most of the subsidence occurred in the outbound lane. Shoulder wash out and drop off were also apparent within this area as shown in Figure 2. Two non functioning small (200 mm) cross draining pipes existed within the subsided area. A drainage ditch with French drain was also installed in the upslope area. The natural slopes on the upside (inbound) are relatively flat about 1V:6H and on the downside (outbound) of the road is 1V:3H. These gentle relatively flat slopes combined with the location of the site in a drainage valley, cause most of snow runoff to either penetrate the granular soil or run over the road surface washing the fines (silt particles) out of the subgrade accelerating the subsidence problems. The soils encountered in the subgrade were classified as SM and the SPT- N values were in the inbound (N=14) were more than two times those in the outbound lane. Although, the N-values were not high, they indicated that most of the problems are caused by the washing of the soil particles beneath the outbound lane.

Figure 2. Shoulder Deformation

Area "B": This area extends a distance of about 1,600m along the roadway. It has experienced various failed (dip) zones to a depth of about 200 mm along the outbound lane, see Figure 3. This portion of Trail Ridge Road consisted of cut and fill slopes. The natural materials found within this site is mostly decomposed granite along the inbound side of this segment, a paved ditch with widths up to 1.8 meters and a 150 mm curb provide drainage for much of this section. A 0.9 meters high wall about 90 m long also existed along the inbound side of this section. A 90 m paved ditch segment approximately 60 m away from the end of the wall controlled the drainage along the outbound lane. Several drop inlets and culverts are in place throughout the ditch line. The subsurface soils in this area were classified as SW-SM with varying SPT-N values attributed to encountering boulders in soft soil matrix. The subsidence problems within this section appeared to be mainly related to snowmelt infiltration and loose fill material. Surface drainage along the roadway seems to be adequate and in working order. The roadway surface along the inbound portion of the roadway appears stable and does not show signs of significant subsidence or structural failures.

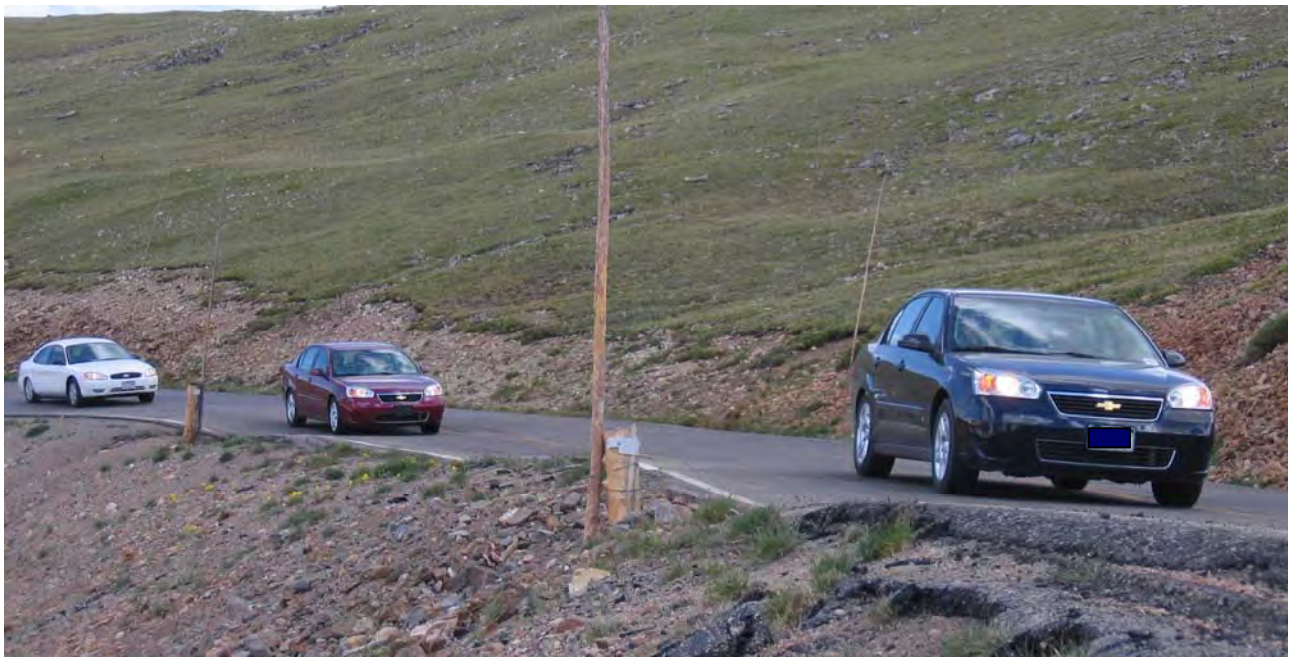

Figure 3. Roadway Dips at Site B

3. ALTERNATIVES

Several alternatives were considered and evaluated for reconstructing these problem areas along Trail Ridge Road taking into account 1) cost, 2) environmental impact, and 3) constructability. The following is a summary of the four alternatives which were considered during project development.

Alternative 1 is considered as the conventional solution and the baseline, see Figure 4. It consists of excavating 3 meters below the roadway elevation extending across the entire cross section of the road and replacing the native excavated materials with imported 25 to 150 mm crushed rock fill material on top of permafrost foundation. This is known as an air convection embankment (ACE) and has been widely used for road construction in Alaska, Maine, and Canada to mitigate frost heave (Saboundjian et al., 2002). Since National Parks do not allow the development of a waste or borrow site, this alternative is very costly for this road due to the cost of hauling materials out and into the Park. The large volume of materials transported for this fix will also cause a safety hazard in the park and additional wear and tear on the existing Trail Ridge Road. This option may also require road closure and/or lengthy delays during construction as traffic is routed through the excavation. Due to restrictions on construction limits due to environmental concerns, traffic maintenance during construction will be extremely difficult. A variation of this method that reduces material handling somewhat is the use of a “cap” of rock fill of about 25% to 50% of the frost depth (Uhlmeyer et al., 2003).

Although this alternative addresses the frost heave problem, it neglects the solifluction issue. To stabilize the slope against movements caused by solifluction, while working within the road prism, large concrete blocks would need to be cast below ground level and anchored in the ditch line above the roadway. This is a solution which to our knowledge has never been deployed for this application. It was decided by the project development team that in addition to being extremely costly, the solifluction problem extends globally through out the region and does not appear to be the primary contributor to distress. Therefore, this structural component was eliminated from all the alternatives. The focus was then aimed at maintaining more constant water content by reducing or eliminating infiltrating surface water, groundwater movement, and capillary action from the roadway prism.

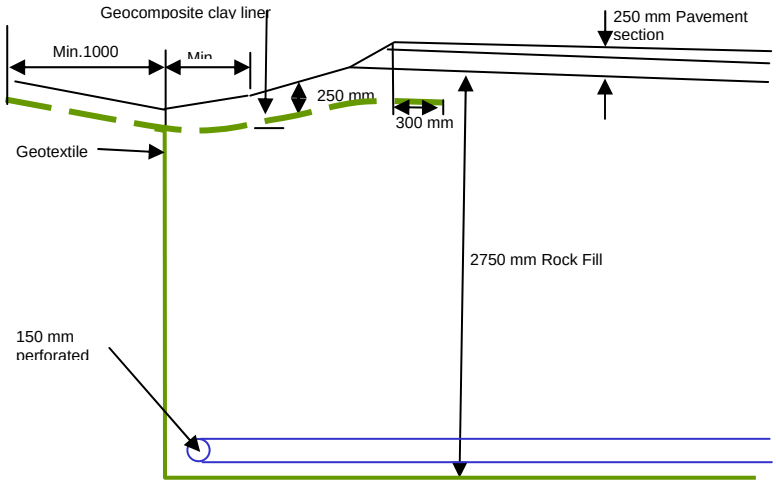

Figure 4. Alternative 1

Alternative 2 also consisted of an excavation of 3 meters below the roadway elevation and replacement. This alternative replaces the lower meter with well graded granular materials and the upper 2 meters with geogrid reinforced native soils, in addition to improved drainage measures. Although this fix reduces some of the material handling issues in Alternative 1, this alternative was not selected. Similar to the first alternative, the large excavation will significantly impact the sensitive alpine environment and could cause road closures and/or lengthy delays. This alternative also does not address the solifluction but the reinforced fill section will provide a stiffer section which would allow deformations to transition more gradually and therefore eliminate the abrupt dip in the roadway.

Alternative 3 combines a structural component and a geotechnical solution. Excavate between 1.5 to 2 meters below the roadway elevation replace materials with reinforced native soils and bridge the roadway surface using concrete slabs or soil reinforcement founded on micropiles embedded to at least 5 meters below the roadway elevation. Although this option improves safety and traffic congestion during construction by reducing the excavation, the cost is much higher than the other alternatives. This alternative somewhat improves the slope instability caused by solifluction by providing improved lateral resistance but it is not very economical.

Alternative 4 incorporates geosynthetic drainage composites to mitigate frost heave in lieu of the granular backfill to provide drainage and a capillary break (Christopher, et. al., 2000). The use of this drainage composite reduces the cost significantly by reducing the excavation depth to approximately 1.5 meters below the road surface, nearly eliminating the need for hauled materials and reusing the native materials with geogrid reinforcement as the fill on top of the drainage composite. As in alternative 2, this alternative does not address the solifluction but the reinforced fill section will provide a stiffer section which will allow deformations to transition more gradually and therefore eliminate the abrupt dip in the roadway. A detailed cross-section is shown in Figure 5.

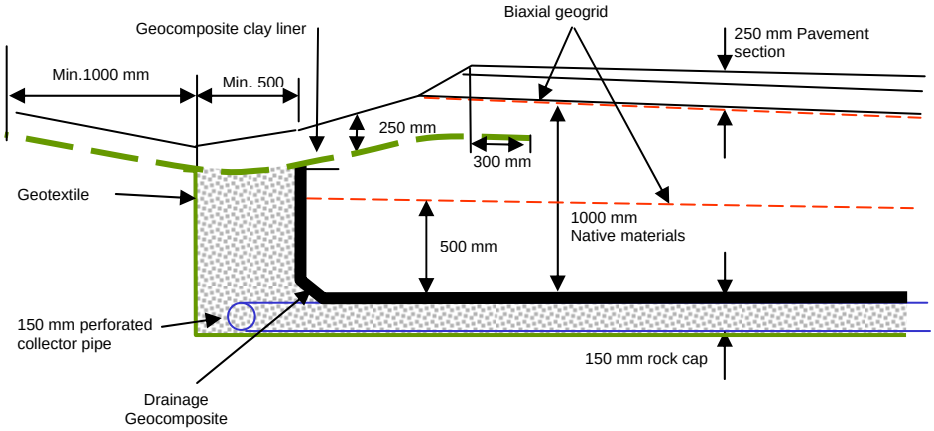

Figure 5. Alternative 4 Cross Section

4. RECOMMENDATIONS

The fourth alternative was selected based on its ability to address most of the project needs at significantly reduced impact to the environmentally sensitive areas, surrounding alpine environment, and traffic during construction. It is the most economical alternative and offers the greatest value. Although this is a new application for the product and there is some uncertainty with the long-term performance when compared to a full depth replacement (Alternative 1) or a structural solutions (Alternative 3). The low cost and low impact of this alternative is believed to have the best value for the project. There are elements of risk with this design in that not all potential modes of distress are addressed (i.e. solifluction), and the functioning of the geocomposite as a capillary break has not been tested in this environment. These are relatively low risks which the stake holders are willing to take.

In general, since most of the problems are caused by water, it is essential to control the water flowing through the roadway section from above ground, near surface soils, and capillary rise. It was recommended that at all sites, the remediation technique incorporate underdrain systems, installed at the edge of the roadway, that intercept and collect ground water and direct its flow to the down slope side of the roadway. The underdrain system is encapsulated in a geotextile filter which will protect the underdrain from being contaminated by the fine grained soils. The drainage composite primarily acts as a capillary break between the natural soil layer and the roadway embankment fill. The capillary break prevents migration of water by making the void large enough within the geonet to stop the effect of capillarity. The surface water is prevented from infiltrating the pavement section by incorporating a geocomposite clay liner under the inside ditch. The water in the drainage ditch is collected and outlet on the downhill side of the slope through drop inlets and culverts. The combination of these geosynthetic materials serve to keep water from infiltrating into the roadway section which helps mitigate the issues related to frost heave and freeze/thaw.

5. CONSTRUCTION CONSIDERATIONS

A key component for the recommended alternative was the geocomposite material and construction specification. The geocomposite specified as the capillary break was composed of a tri-planar geonet core consisting of thick supporting ribs with diagonally placed top and bottom ribs with thermally bonded non-woven geotextiles on both sides. Table 1 summarizes the parameters considered to be most critical for this function.

Table 1. Geocomposite Specifications

PROPERTY	TEST METHOD	UNITS	VALUE
Geocomposite Hydraulic Properties			
Min. thickness	ASTM D5199	mm	7.6
Transmissivity-load of 720 kPa at gradient of 0.1	ASTM D 4716 GRI-GC8	m^3/sec/m	1.8 E-03
Flow rate		lpm/m	10.8
Coefficient of Permeability		m/day	20,500
Nonwoven Geotextile			
U.V. Resistance (500 hrs)	ASTM G 154	%	95
Serviceability Class	AASHTO M-288		Class 1
Grab Tensile	ASTM D 4632	N	900
Tear Strength	ASTM D 4533	N	350
Puncture Resistance	ASTM D 4833	N	350
AOS	ASTM D 4751	mm	0.18
Permittivity	ASTM D 4491 Falling head	Sec^{-1}	0.5

The installation process of the geocomposite is considered critical to the success of the project. The primary objective of the procedures is to maintaining a clean core by protecting the ends of the geocomposite during installation. The

function of the core is to act as a capillary break therefore the gap between the two layers of geotextiles has to be kept clean. The following were some of the key procedures which required to be followed by the construction staff.

- Store geocomposite panels in a clean, dry environment, away from construction equipment pathways and out of direct sunlight, protected from heat, cold, mud, dirt, and dust.
- Place the materials at the elevation and alignment as shown on the plans.
- Secure/seam each component of the geocomposite (geotextile(s) and geonet) to the like component at overlaps (Figure 6).
- Inspect the materials and seams for geotextile and geocomposite damage prior to covering the deployed geocomposite.
- Do not drive heavy equipment directly over geocomposite during fill placement without a minimum fill thickness of 300 mm.

In addition, figure 7 shows the placement of the biaxial geogrid which is specified to reinforce the fill being placed and stiffen the overall section. The geogrid is being rolled out parallel to the roadway alignment and overlapped between rolls. Plastic ties are being used as a construction aid while the fill is being placed.

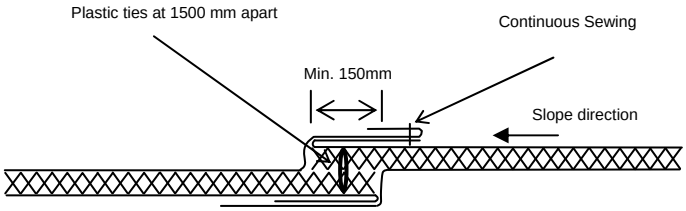

Figure 6. Geocomposite Seam Detail

Figure 7. Placement of Biaxial Geogrid

CONCLUSIONS

The project completed in the fall of 2007 reconstructed the road using a geosynthetic solution to provide drainage and reinforcement of the structural section. The use of the drainage composite as a capillary break or moisture barrier was considered to be a new application for this product and was selected as the preferred alternative due to the reduced environmental impacts, traffic maintenance, and costs. The use of geosynthetics for design of capillary barriers to mitigate frost heave will be evaluated as part of a Central Federal Lands Highway Division technology deployment effort looking at moisture barrier alternatives. This work will result in the development of design guidelines for this application.

ACKNOWLEDGEMENTS

The authors would like to acknowledge the personnel at the Rocky Mountain National Park for their contribution to a successful project. We would also like to acknowledge Dennis Black and his staff of field inspectors, which make it all happen.

REFERENCES

Christopher, B.R., Hayden, S.A., and Zhao, A., 2000. Roadway Base and Subgrade Geocomposite Drainage Layers, Testing and Performance of Geosynthetics in Subsurface Drainage, ASTM STP 1390, J.B. Goddard, L.D. Suits, J.S. Baldwin, Eds., American Society for Testing and Materials, West Conshohocken, PA.

Guthrie, W.S. and Hermansson, A., 2003. Frost Heave and Water Uptake Relations in Variably Saturated Aggregate Base Materials, 82nd Annual Meeting of the Transportation Research Board, Paper No. 03-4391, Washington, DC

Saboundjian, S., Goering, D.J., 2002. Air Convection Embankment for Roadways: A Field Experimental Study in Alaska, 82nd Annual Meeting of the Transportation Research Board, Washington, DC

Turner, K.A. and Schuster, R.L., 1996. Landslides Investigation and Mitigation, Transportation Research Board Special Report No. 247

Uhlmeyer, J.S., Lovejoy, J.S., Mahoney, J.P., Pierce, L.M., Gribner, M.R., and Olson, G.D., 2003. Design and Construction of Rock Cap Roadways – A Case Study in Northeast Washington. Transportation Research Board 2003 Annual Meeting CD-ROM Compendium of Papers

Geogrids as Seismic Reinforcement for Earthen Buildings

D. Torrealva, MsC, Engineering Department, Pontificia Universidad Católica del Perú, Lima, PERU

ABSTRACT
Existing earthen buildings are about half of the housing inventory in the world. In many places were these buildings are located, strong earthquakes are also very frequent, causing every time considerable material damage and irreparable loss of lives and cultural property. In spite of its seismic vulnerability, vernacular earthen houses, however, are still being used by millions of people in many countries because of cultural, climatic and economic reasons. In the search for widely available and compatible materials, biaxial geogrids placed on both surfaces of the adobe wall, connected throughout it and plastered with earthen mortar, appears as a promising solution for reinforcing new and existing earthen buildings without changing its appearance and providing excellent seismic resistance, avoiding collapse. This has been corroborated by static and dynamic simulation test carried out at the Catholic University of Peru.

1. INTRODUCTION

1.1 Seismic Vulnerability of Earthen Buildings.

The main structural elements of earthen building are the walls, and their seismic vulnerability is due to its high mass therefore producing high inertial forces and its very low tensile strength giving as a result a brittle type of failure, with a sudden collapse (Fig. 1).

Figure 1. Destruction of adobe houses Pisco, Peru. 5/08/2007 (Photo: Eric Hulburd)

Inertial forces generated by earthquakes are mainly related to the mass of the walls. Seismic forces perpendicular to the walls produce out-of-plane bending, and cracking starts at the upper corners of the walls. Large vertical cracks separate the walls from one another overturning front walls onto the adjacent street. Lateral seismic forces acting within the plane of the walls generate shear forces that produce diagonal cracks, if the seismic movement continues after the adobe walls have cracked, the pieces may collapse independently.

1.2 Seismic Reinforcement for Earthen Buildings

In the last 30 years, there have been several attempts to solve the problem of the low seismic resistance of vernacular earthen buildings. They have addressed both, the new and the existing earthen buildings using natural (wood and cane) and industrial materials (steel bars, steel mesh and cement). In both cases, the most effective solution found so far, is to provide the building with uniform reinforcement, horizontal and vertical elements placed at a certain distance ranging from 0.40 to 0.70 meters or the use of a steel mesh with or without cement mortar plaster.

For new buildings, the most common solution is to incorporate an internal mesh of vertical whole canes every 50cm and horizontal split canes every 3 or 4 layers firmly tied at the corners and wall intersections and at the crown wooden beam

(Vargas 1978). The main inconvenience of this solution is that natural materials cannot be applied in cases where massive construction is undertaken such as in the aftermath of an earthquake.

For existing buildings two solutions have proven to be effective: completely reinforce the building with an external welded wire mesh anchored to the foundation and top beam (IAEE 1986) and, partially reinforce the buildings with an external steel mesh covering both sides and tying them through the adobe walls (Zegarra et al. 1997), this solution would require a sand cement mortar plaster for the sake of protection of the steel mesh. Both solutions can also be applied to new buildings. There are however some inconveniences in the use of these solutions, first, it implies materials, wire mesh and cement that are much too expensive for their use in vernacular housing, second, the sand cement plaster have the inconvenience of incompatible stiffness with the adobe walls, and third, for buildings of cultural value, a sand cement stucco on an adobe wall, will change its plastic appearance.

Structural interventions in earthen buildings have always had the problem of accomplishing engineering recommendations and at the same time being simple enough to be used by economically depressed people. Therefore, the structural intervention that provides life safety and improves the survival of the building must be executed in a way that produces minimal impact in the original building and its construction materials, the reinforcement used must be compatible with the earth material and simple enough for technical and economical reasons. In other words, the objective is to reach the maximum safety with minimum intervention.

Within this context, an industrial polymer geo-grid was used as external reinforcement for earthen buildings in research projects at Catholic University of Peru carried out since 2004. Earthen model houses scaled ¾ of the original were externally reinforced with biaxial geo-grid at both sides of the wall and connected through it with nylon threads, The models were then subjected to several seismic simulation tests in one direction demonstrating the effectiveness of the polymer reinforcement in maintaining the stability of the building even in strong motions.

2. THE GEOGRID ALTERNATIVE

2.1 Reinforcing Material

In the year 2004, the Catholic University of Peru initiated a systematic experimental work in which several polymer grids were tested as possible seismic reinforcement for earthen buildings. After several static and dynamic tests were the variables were the type of grid and its reinforcement configuration, it was concluded that the biaxial geo-grid placed at both sides of the wall, connected through it with polystyrene threads and plastered with mud mortar, is a highly compatible and efficient reinforcement that eliminates the seismic vulnerability of earthen buildings.

The reinforcing geo-grid requires standard properties of strength and stiffness. The grid tested as reinforcement (Fig. 2) is fabricated from high density extruded sheets punched with a precise and regular pattern of circular holes. The grid is then stretched in both directions at controlled temperature and tensile force in order to obtain a biaxial grid with square like openings, rigid joints and flexible ribs.

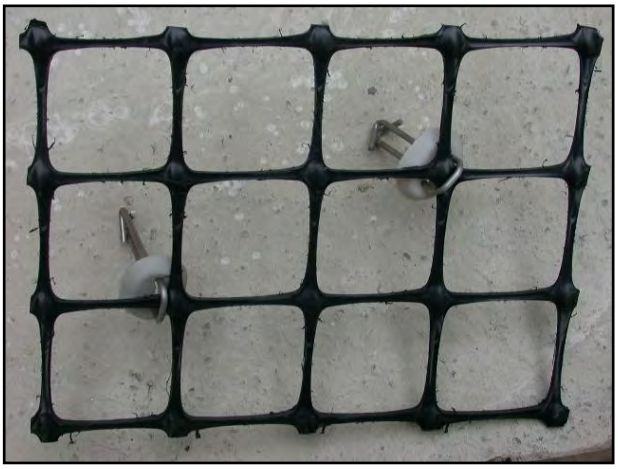

Figure 2. Biaxial geogrid.

2.2 Construction Procedure

For existing buildings, as a first step, the plaster of the wall must be removed before placing the grid on both sides of the wall. To fix the grid to the wall, it is necessary to drill 3/8" holes at vertical and horizontal distances of 40cm and tying both sides with polyester threads, it is not necessary to fill the holes after tying. Commercially available geo-grids come in rolls of 3 to 4m wide by 50 to 75m long, it must be placed on the walls in such a way that cover the wall surface continuously in the horizontal direction. Finally, the grid must be covered with a mud based plaster. For new buildings the polyester threads can be left embedded in the mortar as the wall is built (Figure 3).

Figure 3. Construction process of geogrid reinforcement

3. SEISMIC SIMULATION TEST ON SQUARE HOUSES

In order to compare the influence of the mortar, only half of the model house was plastered (Fig.4).

Figure 4.Model reinforced with geogrid, half plastered

3.1 Experimental results

The model was subjected to seven seismic motions with peak acceleration of 0.15g 0.30g 0.60g 0.80g 1.0g and two motions of 1.2g, the signal was derived from a record of the Peruvian earthquake of May 31st, 1970. The tests demonstrated that placing an external polymer grid on both sides and connected trough the thickness of the adobe wall is an effective way to avoid partial or total collapse of adobe buildings even for severe earthquakes.

If the grid is not covered with mud stucco, the initial strength is the same as the plain unreinforced wall and the tensile strength of grid is mobilized after the wall is cracked. The broken pieces of wall are confined by the grid and by keeping them in place; partial or total collapse was avoided. The mud plaster over the grid greatly increases the initial shear strength and the stiffness of the wall. By controlling the lateral displacements, it prevents the cracking of the wall in great extent (Fig. 5).

Figure 5.Non plastered side and plastered side after testing.

4. SEISMIC SIMULATION TESTS ON NUBIAN VAULT

As a result of a project for the Health Ministry in the rural areas carried out by the non governmental organization Amares, there was the opportunity to test the effectiveness of this reinforcing technique in an earthen building of different architectural typology. Two Nubian Vaults models were subjected to the same series of dynamic simulation tests on the shaking table. Model 1 was a plain model and Model 2 was externally reinforced with the geo-grid but without plaster. The plaster was not placed on the walls surface because of weight limitations. The test series was the same that the one used in the square model house. The direction of shaking was coincident with the transversal section of the vault. The reinforced vault resisted greater seismic intensity motions than the unreinforced vault avoiding the collapse of the vault and providing inelastic deformation capacity to the earthen vault. The unreinforced vault collapsed at moderated seismic motions (Fig. 6).

Figure 6. Reinforced vault and non reinforced vault after test.

5. SHEAR STRENGTH OF ADOBE WALLS

From the earthquake resistant point of view, one of the main properties of the structural walls is the in plane shear strength that can be obtained from cyclic horizontal shear tests by dividing the horizontal force between the net horizontal cross area of the wall. Three walls of the same architectural configuration were tested in different projects, Blondet et al, (2005) reported the comparative tests of a plain wall and a grid reinforced wall without plaster. A third wall was tested in 2007 with grid reinforcement and plastered with mud (Fig 7). The results show that the wall reinforced with geo-grid and plastered with mud, increase the initial strength in 40% and the ultimate strength by 150%. In absence of plaster, the reinforcement only provides displacement capacity regarding the plain wall. Also it was noticed a significant increase in the absorbed and dissipated energy with big capacity of horizontal displacement. At ultimate stages of testing, big portions of the plaster detached from the wall diminishing the horizontal force but nevertheless maintaining the displacement capacity as in the case of no plaster. (Fig. 8)

Figure 7. Cyclic shear test on reinforced adobe wall.

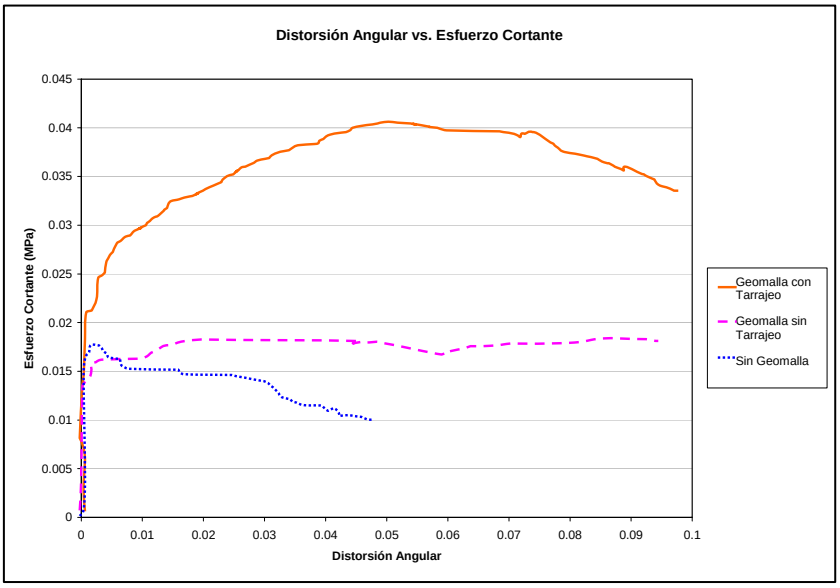

Figure 8. Comparative evolvement curves of plain, reinforced without plaster and reinforced and plastered walls in shear test.

6. OUT OF PLANE BENDING RESISTANCE OF ADOBE WALLS

Another important structural property of the wall is the out of plane bending capacity that can be obtained by out of plane horizontal force tests. Three 0.80 x 1.60m walls with a thickness of 0.25m were subjected to loading and unloading tests. The walls were horizontally supported at the bottom and top creating a simply supported bending type of behavior. The tests corroborated that the grid embedded in the plaster mortar creates a composite material where the adobe wall takes the compression forces and the grid the tension forces (Fig. 9), and that they work jointly until ultimate stages of testing.

The reinforced panel can undergo 25 times more horizontal displacement than the plain panel (Fig. 10) while achieving an important increase in bending capacity.

Usually, adobe dwellings have a wall thickness of 0.40cm however, in almost all static and dynamic tests performed at Catholic University, ¾ scaled models have been used because of weight limit requirements for the shaking table. The intention of previous tests have been always to compare different types of reinforcing techniques.

Figure 9. Out of plane bending test on reinforced adobe wall.

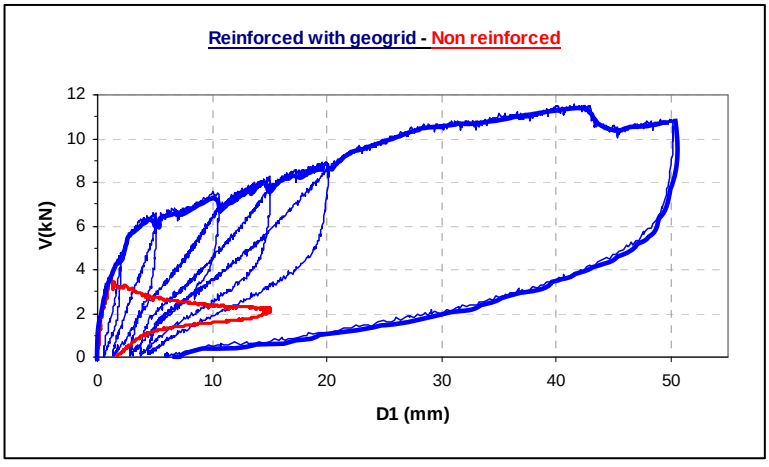

Figure 10. Comparative curves of plain and reinforced walls in bending.

7. CONCLUSIONS

- The geo-grid reinforcement placed externally on the wall surface is very effective in drastically reducing the seismic vulnerability of the earthen buildings with different architectural typologies.
- The biaxial geo-grid by its compatibility with natural soil, high tensile strength, stiffness and durability is suitable to be used as external seismic reinforcement on earthen buildings.
- The geo-grid embedded in the mud plaster creates a composite material providing tensile resistant and displacement capacity to the whole earthen structure. It is now possible to develop mathematical expressions to compute the shear and bending stresses.
- This technique can be applied to both existing and new adobe buildings. In case of existing buildings the plaster has to be removed and placed again after the reinforcing procedure.
- By providing a mean to satisfy the safety conditions of actual construction codes, this technique can help to legitimize earth as a construction material and allow the tradition of building with earth to continue in the future in earthquake prone countries.
- All seismic simulation tests performed, varying the reinforcement configuration, grid type and orientation of the house regarding the direction of shaking, have demonstrated that uniform and compatible external reinforcement placed continuously on the walls drastically reduces the seismic vulnerability of earthen buildings and even eliminates it.

REFERENCES

Bariola J, Vargas J, Torrealva D, Ottazzi G. (1988) Earthquake Resistant Provisions for Adobe Construction in Peru . 9th World Conference on Earthquake Engineering. Tokyo-Kyoto, Japan.

Blondet M, Ginocchio F, Marsh C, Ottazzi G, Villa García G, Yep J. (1988). Shaking Table Test of Improved Adobe Masonry Houses. 9th World Conference on Earthquake Engineering. Tokyo-Kyoto, Japan.

Blondet M, Madueño I, Torrealva D, Villa García G, Ginocchio F. (2004) Reinforced of Adobe Constructions with Industrial Elements Earthbuild2005 New Zeland.

Internacional Association for Earthquake Engineering Guidelines for Earthquake Resistant Non-Engineered Construction. Revised Edition of “Basic Concepts of Seismic Codes” Vol. I, Part 2, (1980), October 1986. Tokyo, Japan.

Leroy E, Kimbro E, Webster F, Ginell W. (2000) Seismic Stabilization of Historic Adobe Structures. The Getty Conservation Institute. Final Report of the Getty Seismic Adobe Proyect, Los Angeles.

Scawthorn C. (1985) Strengthening of Low-Strength Masonry Buildings: Analytical and Shaking Table Test Results. Dames and Moore San Francisco California. Research Supported by the National Science Foundation USA.

Sofronie R, (2004). Performances in Seismic Strengthening of Masonry. (Paper 182) 13th World Conference on Earthquake Engineering. Vancouver, B.C. Canada.

Torrealva D. (1986)A Field and laboratory Tested Technique for Retroffiting Adobe Houses in Seismic Areas. Middle east and Mediterranean Regional Conference on Earthen and Low-Strength Masonry Buodings in Seismic Areas. Ankara, Turkey, 1986

Vargas, J. (1978). Recommendations for Design and Constructions of Adobe Houses. Experimental Study. In Spanish. International Symposium Earthquake, and the Reconstructions Process. Guatemala.

Zegarra L, Quiun D, San Bartolomé A, Giesecke A. (1997). Reinforcement of Existing Adobe Dwellings 2nd part: Seismic Test of Modules. In Spanish. XI National Congress of civil Engineering. Trujillo, Peru.

Zegarra L, Quiun D, San Bartolomé A, Giesecke A. (2001). Behavior of Reinforced Adobe Dwellings in Moquegua, Tacna and Arica during the 23-06-2001Earthquake. In Spanish. XIII National Congress of civil Engineering. Puno, Peru.

Yeager Airport Runway Extension: Tallest Known 1H:1V Slope in U.S.

J. M. Lostumbo, P.E., Region Engineer, TenCate Geosynthetics, East Amherst, New York, USA

ABSTRACT
Yeager Airport was constructed atop mountainous terrain near Charleston, WV in the 1940's. Construction consisted of excavating 7 hill tops and filling surrounding valleys to create a flat site for the runways. Due to this dramatic terrain, development to meet FAA safety regulations was extremely difficult, and some concessions were allowed. However, the airport recently needed to extend Runway 5 approximately 150 meters (500 feet) in order to meet current FAA safety regulations.

Bridges, walls and reinforced slopes were evaluated as construction options to extend the runway. The geosynthetic reinforced slope option provided the most economical alternative; plus, the vegetated green faced system allowed for a more aesthetically pleasing alternative to blend into the surrounding green hills and valleys. The reinforced structure is a 1H:1V (45 degree face batter) geosynthetic reinforced steepened slope, 74 meters (242 feet) high. To our knowledge, this is the highest geosynthetic reinforced green faced 1H:1V slope constructed in the United States.

1. INTRODUCTION

Yeager Airport, formerly known as Kanawha Airport, in Charleston, West Virginia was constructed atop mountainous terrain near the city limits. Completion of the airport in 1947 was the culmination of an almost 20 year evolution in air service in the state of West Virginia.

Air service for the Charleston area began in 1930 with the dedication of Wertz Field in Institute, WV, approximately 6 miles outside the city limits. In 1933, the state of West Virginia was one of only two states that did not have air mail service, until American Airlines opened passenger and mail service routes from Washington to Chicago via Charleston. As larger passenger planes began to be used, Wertz Field became more and more limited for use. The small airfield was not suitable for landing larger planes. In the late 1930's, American Airlines notified the City of Charleston that it would discontinue service to Wertz Field because of these limitations.

Charleston realized that a site for a new airport needed to be found in order to keep up with the needs of the aviation industry and to keep air service viable for the Charleston area. A committee evaluated potential sites in the greater Charleston area and determined that the valley floor offered no suitable site large enough. The committee decided "we must build on the hilltops." A series of semi-connected hill tops know as "Coonskin Ridge" was suggested by the committee as the best site option for an airport, however, significant earthwork would be required to level the site. In 1940, development plans began for the site with many obstacles to overcome. In the meantime, Charleston lost air service as Wertz Field closed in 1942 when the approaches were blocked by the construction of a synthetic rubber plant.

The need for the new site development intensified and construction finally began in October 1944. Construction consisted of excavating 7 hilltops and filing the surrounding valleys to create a flat site large enough for the airport. Earthwork proceeded continuously for 3 years and was finally completed in mid-1947. At the time, this was reported as the second largest earth moving project in history, behind only the Panama Canal. Since the airport was constructed on hilltop ridges, the ground surface slopes steeply down around the airport more than 91 meters (300 feet) to the surrounding Elk and Kanawha rivers. Due to this dramatic terrain, development to met FAA safety regulations was exceptionally difficult and some concessions were made. The airport was completed in 1947 and began operations December 1st as Kanawha Airport. The airport changed names to Yeager Airport in honor of West Virginian Chuck Yeager in 1985. Construction consisted of moving more than 6,881,000 cubic meters (9,000,000 cubic yards) of earth and rock and required more than 907,000 kilograms (2,000,000 pounds) of explosives. Grading along for the project cost approximately $4.5 million, more than 34 times the cost of the site.

In order to comply with current FAA regulations, Yeager Airport was required to upgrade its facilities. Runway 5 required a 150 m (500 ft) extension to meet the FAA requirements. The previous runway did not include the proper airplane safety and emergency stopping area. The challenge was how to extend the runway 150 meters (500 feet) out over a 91 meter (300 foot) high steep slope.

2. ANALYSIS AND DESIGN

2.1 Subsurface Exploration

A geotechnical evaluation of the site was performed to assess the subsurface conditions of the area. Over 100 borings were performed around the airport to evaluate the soil conditions at the slope as well as to identify excavation areas and other site development for the airport. The site soils consisted mostly of weather sandstone underlain by sandstone and some shale.

The borings showed the bearing area consisted mostly of shallow rock consisting of sandstone. The surrounding area and potential borrow sources indicated mostly weather sandstone and rock with some clay seams. Laboratory testing was performed on the site soils and rock for design parameters. Testing included Standard Proctor Compaction tests, grain size analysis, Atterberg Limits, Triaxial Shear Tests and Rock Core Compressive Strength. The results of the soil test borings and laboratory testing showed very favorable subsurface conditions.

The laboratory test results indicated that the maximum dry densities of the weathered sandstone and sand material at the site ranged from 19.2 to 20.9 kN/m^3 (122.1 to 133.1 pounds per cubic foot (pcf)) with an optimum moisture of 8.3 to 11.8 percent. The clay seams with rock fragments had maximum dry densities of 17.9 to 18.8 kN/m^3 (114.3 to 119.5 pcf) with optimum moisture contents of 12.1 to 12.6 percent. The triaxial shear tests indicated internal friction angles of the weather sandstone ranging from 38.9 to 39.6 degrees. Compressive strength testing of the rock cores indicated compressive strength of 30,405 to 97,630 kPa (4,410 to 14,160 psi).

2.2 Design Considerations

Based on the subsurface conditions at the site, the design team looked at options to extend Runway 5 the required 150 meters (500 feet). One of the key constraints was that the runway had to remain open during construction. The ground surface of the existing runway was at elevation 288 meters (946 feet). This limited the construction methods, as cranes or large equipment could not exceed elevation 283 meters (930 feet) as to not infringe on the airport's airspace. Bridge type structures, retaining walls and reinforced steepened slopes were all initially considered. A bridge structure was quickly eliminated as being too expensive, too difficult to build and not aesthetically pleasing. A retaining wall was also eliminated as an option due to expense and aesthetics. Additionally, a bridge or wall structure would have required construction cranes and other equipment that may have exceeded the height restriction for construction. Construction of the reinforced slope could be completed with traditional earthwork equipment and the height restrictions would not be an issue. A reinforced steepened slope was determined to be the best option for the project. It offered an economical solution that would be relatively easy to construct and would blend in to the surrounding green hills of West Virginia.

Several reinforced slope options were evaluated, with varying slope face angles. Ultimately it was determined that a 1H:1V green faced (vegetated) slope was the most economical slope option for the project and site conditions. The high bearing capacity of the sandstone and the high friction angle of the on site soils meant the limits of the structure could be kept to a minimum. A reinforced structure this large might require some type of bearing improvement or staging of construction to allow for settlement if not founded on rock. Since the slope would be founded primarily on rock, consolidation of the bearing strata was not a concern. Also, the high friction angle of the on site soils provided two significant benefits: 1) It eliminated the need to import borrow soil from off site, and 2) It kept the required embedment lengths of the reinforcement material to a minimum.

The design used traditional slope stability analyses and computer program modeling to select the minimum strength requirements, vertical spacing and embedment lengths of the geosynthetic reinforcement. The soil properties used as part of the design are shown below in Table 1.

Table 1. Basic Soil Properties used for Design.

Soil Layer	Unit Weight, γ kN/m^3 (lb/ft^3)	Internal Friction Angle, Φ (degrees)	Cohesion, c (lb/ft^2)
Reinforced Soil Zone	18.1 (115)	36	0
Retained Soil Zone	18.1 (115)	36	0
Bearing Soil Zone	22.0 (140)	40	0

The design of the slope resulted in three types of primary reinforcement strengths being selected. The designed embedment lengths for the tallest slope section ranged from 53 meters (175 feet) at the bottom to 44 meters (145 feet) at the top. Vertical spacing of the primary reinforcement was 0.45 meters (1.5 feet) at the bottom of the slope and 1 meter (3 feet) at the top. The minimum Long Term Design Strength (T_{al}), per Equation 1, for the primary reinforcement are shown in Table 2.

Table 2. Primary Reinforcement Strength Requirements.

Reinforcement Type	Minimum Long Term Design Strength (T_{al}), kN/m (lb/ft)
P-1	56.4 (3,861)
P-2	54.4 (3,725)
P-3	43.4 (2,971)

$$\text{Where } T_{al} = T_{ult} \div (RF_{CR} * RF_{D} * RF_{ID}) \quad [1]$$

T_{ult} – Ultimate Tensile Strength of Reinforcement
RF_{CR} – Reduction Factor for Creep
RF_{D} – Reduction Factor for Durability
RF_{ID} – Reduction Factor for Installation Damage

The high quality structural fill available at the project site proved to be very beneficial in the design aspect of the project. However, it also resulted in the use of a very coarse backfill in the reinforced fill zone. Since the gradation of the fill was slightly outside the typical gradations used, site specific installation damage testing was performed to verify the reduction factors used to calculate the Long term Design Strength of the reinforcement. The Mirafi Miragrid XT Geogrids proposed for the project were tested by a third party testing laboratory to measure the reduction factors for installation damage using the proposed backfill soil for the project. The geogrids proposed were woven polyester uniaxial geogrids coated with PVC. The test results showed the geogrid for was highly resistant to installation damage using the proposed rocky backfill soil. Even though the results indicated lower reduction factors could be used, the initial specified reduction factors were used. Since a lower reduction factor would result in a lower calculated minimum ultimate tensile strength of the reinforcement, the higher reduction factors for installation damage were used for consistency and added conservatism. The specified soil gradation is shown in Table 3.

Table 3. Specified Soil Gradation for Reinforced Backfill.

Sieve Size	Specified Project Backfill, Percent Passing (%)	Typical Backfill Gradation per FHWA, Percent Passing (%)
152 mm (6 in)	100	
20 mm (3/4 in)		100
4.75 mm (No. 4)	30 to 100	20 to 100
0.85 mm (No. 20)	0 to 60	0 to 60
0.075 mm (No. 200)	0 to 50	0 to 50

Based on the results of the laboratory testing and following the project specifications, the minimum ultimate tensile strength required for the geosynthetic reinforcement was determined for each type. Using the appropriate reduction factors for PVC coated polyester geogrids, the minimum ultimate tensile strength was calculated based on the design. The minimum tensile strength is shown in Table 4. As you can see, the required tensile strength for Reinforcement Type P-1 and P-2 are relatively close, so the same reinforcement was used for both Types. This allowed for less handling, easier placement of the reinforcement, and less waste during construction, because only two types of geogrid were used.

Table 4. Primary Reinforcement Ultimate Strength Requirements for Polyester Geogrid.

Reinforcement Type	Minimum Ultimate Tensile Strength Required (T_{ult}), kN/m (lb/ft)	Actual Ultimate Tensile Strength of Geogrid Used, kN/m (lb/ft)
P-1	160.1 (10,968)	187.9 (12,870)
P-2	154.5 (10,581)	187.9 (12,870)
P-3	123.2 (8,439)	145.2 (9,950)

The facing material for the slope is a small aperture mesh type geogrid. Erosion Control Blankets or other type of bio-degradable erosion control products were not used. Typically, 1H:1V slopes are the transition point between using an erosion control blanket on the face or having to use a wrapped face construction with reinforcing elements. Initially it was considered by the design team to use chain link fencing, draped along the face as the face treatment. However, it was realized that for the long term performance of the structure and for aesthetics, the face needed to be vegetated. Erosion control protection that also promoted fast vegetative growth was the right solution. The design team ended up selecting to embed the facing material into the slope at the primary reinforcement locations and then drape the material over the face with 0.75 meter (2.5 foot) overlaps vertically. The product was a green woven polypropylene mesh that provided erosion protection and allowed for fast germination of the vegetation on the slope face.

Figure 1. Green Mesh Slope Facing Prior to Vegetation

3. CONSTRUCTION

Perhaps the most notable thing about the construction of the tallest known 1H:1V slope in the United Sates was that there were no notable issues. Construction proceeded without significant problems or delays. The slope and reinforcement material performed as expected and survived several torrential rain falls during construction. The selection of a reinforced slope allowed the airport to continue operation during construction activities.

Construction of the slope was competed in just under 2 years, starting in the late summer of 2005 and finishing in spring 2007. The flexible polyester geogrid allowed for easy installation; time was not wasted having to anchor or weigh down the material to prevent recoiling. The geogrid used for the project was supplied in 3.6 meter (12 foot) wide rolls that allowed for the use of fewer rolls than if a narrower width geogrid was used. Custom geogrid lengths were supplied to the contractor. This allowed for less waste and reduced the amount of cutting of the geogrid to the required lengths. This sped up construction significantly.

Figure 2. Placement of Geogrid Reinforcement at Bottom Layers of Slope

The borrow source for the reinforced fill material was on the airport property, close to the reinforced slope area. The borrow material was excavated using track hoes and transported using large off road tri-axial dump trucks when possible. Some ripping with large bulldozers and some blasting was also required at the size. After blasting, the material was crushed in order to meet the gradation requirements in the specifications. Some of the approximate material quantities used to construct the slope are shown in Table 5.

Table 5. Approximate Material Quantities for the Project.

Material	Quantity, Square Meters (Sq. Yards)
Primary Geogrid, P-1 & P-2	321,073 (384,000)
Primary Geogrid, P-3	214,049 (256,000)
Secondary Green Mesh Facing	62,710 (75,000)

Figure 3. Reinforced Slope Construction

4. CONCLUSION

The reinforced slope constructed at Yeager Airport in Charleston, WV is the tallest 1H:1V geosynthetic reinforced vegetated slope known in the United States. It was completed in the Spring of 2007 and has been performing as expected. The green mesh facing provided an instantly aesthetically pleasing structure that allowed for quick germination of the slope. Vegetation covered the face within a few months of construction. The reinforced slope option provided fast construction, limited to no interference with airport operations, the most aesthetically pleasing structure and was the most economical. The green structure quickly blended in to the picturesque green mountains surrounding the airport.

This project won the Industrial Fabrics Association International (IFAI) Award of Excellence for Geosynthetic Projects in 2007.

Figure 4. Shortly after completion, already with good vegetation coverage, picture taken at mid-height of slope.

ACKNOWLEDGEMENTS

Special thanks to the design engineer, Mr. Dane Ryan, PE, Triad Engineering, St. Albans, WV and to Cast and Baker Corporation, Canonsburg, PA and JMD Company, Bethel Park, PA.

REFERENCES

Yeager Airport Authority, *Yeager Airport History*, 1997

Earth Dams Project using Structural Geogrids for Tailings Ponds

M. de la Torre, Geoservice Ingeniería SAC, Lima-Peru
B. Torreblanca, Geoservice Ingeniería SAC, Lima -Peru

ABSTRACT
Minera Atacocha S.A Company has developed Cajamarquilla Tailings Pond Project, to store the mining residues product of the metallurgical mineral process. It's located in the central region of Peru. The project consists of 3 ponds conformed by 4 dams. The earth dams have a homogenous section, conformed by borrowed materials. The Cajamarquilla earth dams 2, 3 and 4 have embankments which reinforced with uniaxial geogrids UX1500 HS, to increase the resistance of the embankments and to construct slopes more inclined. The dam's stability was developed into static and seismic conditions. The coefficient of seismic acceleration was 0.15g (according to the seismic analysis).The subsoil foundation of Cajamarquilla dam 2 is formed by soft clay, so the installation of biaxial geogrids was necessary to distribute the embankment's loads.

1. INTRODUCTION

In some places of the central region of Peru, narrow valleys and the rough topography reduce the possibilities of implementation of tailing storage, which are used to store away the residue. Of the metallurgical process of minerals: Under these conditions Cajamarquilla tailing ponds project has established in the high area of the Huallaga valley. Cajamarquilla tailing has tree ponds, with four earth dams of homogeneus material, three concrete retaining walls and a tunnel of 1.0 km length.

To optimize the volumens of storage it was necessary to increase the stream slopes of the embankments; and reinforced with geogrids UX1500 HS. Internal stability analysis was developed considering minimum safety factors.

2. LOCATION OF PROJECT

The project is located at the Central Andes of Peru, in Pasco region, in a high area of Huallaga valley, between km 151+ 954 - km 152 +389 of the main highway Lima – Huánuco.

3. DESCRIPTION OF PROJECT

Cajamarquilla tailings ponds project has 4 dams. Dams 2, 3 and 4 were reinforced with uniaxial geogrids UX1500 HS to raise the slope of the embankment and greatest to store the volume of tailings in the ponds.

Geometry, loads and design requirements

a) Geometry

Cajamarquilla dam nº1
- Height of the dam: 22.0 m
- Downstream slope: 1H:1V
- Upstream slope: 1H:1V

Cajamarquilla dam nº2
- Height of the dam: 27.70 .0 m
- Downstream slope: 1H:1V
- Upstream slope: 0.5H:1V

Cajamarquilla dam nº3
- Height of the dam: 28.0 m
- Downstream slope: 1H:1V
- Upstream slope: 0.5H:1V

Cajamarquilla dam nº4
- Height of the dam: 25.50 m
- Downstream slope: 1.5H:1V
- Upstream slope: 1H:1V

b) Loads

- Horizontal force due tailings

- Seismic Load, considering seismic coefficient of 0.15g

c) Stability of the dams

Minimum safety factors are:

Static condition	1.5
Seismic condition	1.1

4. DAM STABILITY ANALYSES

4.1 Slope Stability

The stabilities of Cajamarquilla dams1, 2, 3 and 4 have been analyzed for the maximum heights.

Properties of soil foundations

Cajamarquilla dams 1, 2, 3 and 4 have the same geological and geotechnical conditions. Right sectors of the ponds are founded on colluvial deposits, central sectors are founded on fluvio alluvial deposits, while left sectors are founded on rocks basement.

Geotechnical conditions of soil foundation are presented in table 1. These geotechnical conditions were obtained by field and Laboratory Tests.

Table 1. Geotechnical parameters of soil foundations materials

Nº	Description	γ_{nat} (t/m^3)	Drained Strength		Undrained Strength	
			C' (t/m^2)	ϕ' (º)	Cu (t/m^2)	ϕu (º)
1	Cajamarquilla 1	1.9	0	38	0	38
2	Cajamarquilla 2	1.85	3	25	5	15
3	Cajamarquilla 3	2.0	0	40	0	40
4	Cajamarquilla 4	1.7	0	33	1.6	25

Properties of the Borrowed Materials

The materials that are used to construct the dams' embankments were obtained from Chicrin quarry and mine waste. Geotechnical parameters of these materials are presented in table 2.

Table 2. Geotechnical parameters of the dam's embankment materials

Nº	Material	γ_{nat} (t/m^3)	Drained Strength		Undrained Strength	
			C' (t/m^2)	ϕ' (º)	Cu (t/m^2)	ϕu (º)
1	Mine waste	2.2	0	40	1.8	36
2	Gravel clay	2.2	0	38	2	34
4	Compacted tailngs	1.6	0	36	1	25
5	Gravel sand	1.8	0	38	0	38

Characteristics of the reinforcement (Uniaxial Geogrids UX1500 HS)

Uniaxial geogrids UX1500 HS are used to reinforce the embankments. The following table shows the physical and Mechanical properties of the geogrids

Table 3. Parameters of the Geogrid UX1500 HS

Load Capacity	Units	MD Values1
True Initial Modulus in Use	kN/m(lb/ft)	1,580 (107,950)
Tensile Strength @5% Strain	kN/m(lb/ft)	52 (3,560)
Ultimate Tensile Strength	kN/m(lb/ft)	114 (7,810)
Long-Term Allowable Load in Sands, Silts & Clay	kN/m(lb/ft)	45.2 (3,100)
Long-Term Allowable Load in Well Graded Sand	kN/m(lb/ft)	49.3 (3,10)
Long-Term Allowable Load in Aggregate	kN/m(lb/ft)	43.1 (2,950)
Integrity of Product Structure		
Junction Strength Flexural Stiffness	kN/m(lb/ft) X1000 mg-cm	105 (7,200) 5,0100
Durability		
Resistance to Installation Damage	%SC / %SW / %GP	95 / 92 / 90
Resistance to Long Term Degradation	%	100

The Ultimate Tensile Strength is 114 Kn/m

$$T_{al} = \frac{T_{ult}}{RF}$$

T_{al} : Allowable tensile strength T_{ult}: Ultimate tensile strength

RF: Reduction factor for installation damage

$$RF = (ID)(CR)(CD)(BD)$$

Reduction factors:

The reduction factors are show in the table 4.

Table 4. Reduction factors

Application Area	RF $_{ID}$	RF $_{CR}$	RF $_{CD}$	RF $_{BD}$
Unpaved roads	1.1 a 1.6	1.5 a 2.5	1.0 a 1.5	1.0 a 1.1
Paved roads	1.2 a 1.5	1.5 a 2.5	1.1 a 1.6	1.0 a 1.1
Embankments	1.1 a 1.4	2.0 a 3.0	1.1 a 1.4	1.0 a 1.2
Slopes	1.1 a 1.4	2.0 a 3.0	1.1 a 1.4	1.0 a 1.2
Walls	1.1 a 1.4	2.0 a 3.0	1.1 a 1.4	1.0 a 1.2
Bearing Capacity	1.2 a 1.5	2.0 a 3.0	1.1 a 1.6	1.0 a 1.2

From: Koerner R.M., Designing with Geosynthetics,

Considering the conditions, that affect the uniaxial geogrids, (from table 4), it would adopt the following values:

DAMAGE INSTALLATION (ID):	1.1	CHEMISTRY DEGRADATION (CD)	1.1
CREEP (CR):	2.0	BIOLOGICAL DEGRADATION (BD):	1.0

From the chart above the reduction factors (RF) can be:

RF = 1D X CR X CD X BD
= 1.1 X 2.0 X 1.1 X 1.0
RF = 2.42

Then, allowable tensile strength

$$T_{al} = \frac{T_{ult}}{RF} \qquad T_{al} = \frac{114}{2.42}$$

$$T_{al} = 47.10 \text{ kN/m}$$

4.2 Stability of the dams without Reinforcement

The minimum safety factors of the Cajamarquilla dams 2, 3 and 4, are obtained from the GEO/SLOPE program. The results are showed in table 5.

Table 5. Safety Factors - Without Reinforcement

Condition	Dam Cajamarquilla	Static	Seismic
Long Term	Nº2	1.09	1.03
	Nº3	1.00	1.17
	Nº4	1.25	1.02

The calculations determine that dams 2, 3 and 4 require reinforced with geogrids to increase their factor of safety.

4.3 Dam stability with Reinforcement materials:

Calculation of Geogrids number

The following equation is used to calculate the number of geogrids:

$$FS = \frac{MR\sum_{i}^{i=n}(Ti)(Yi)}{MD}$$

Where:

MR: Resistant moment without reinforcement
MD: Driving moment without reinforcement (gravity, filtration, earthquake, dead load and live)
Ti: Permissible resistance of reinforcement
Yi: Arm (s) of the moment
n: Number of reinforcement layers
Pullout Factor of safety: 1.5 (granular soils)

Number of geogrids

Cajamarquilla dam nº2
- number of geogrids = 9
- spacing = 2.0 m

Cajamarquilla dam nº3
- number of geogrids = 9
- spacing o = 2.0 m

Cajamarquilla dam nº4
- number of geogrids = 5
- spacing = 2.0 m

Calculus of the embedment length of the geogrids

Embedment length:

$$Le = \frac{(T_{al}) \times (FS_a)}{2 \times (F \times \alpha \times \sigma_v)}$$

Tal = 47.1 kN/m
FSa =(1.5) Pullout Safety Factor
F = Pullout resistance factor for geogrids F=0.8 tan(ϕ)
α = 0.6 a 1.0; Scale effect correction factor to account for a non linear stress reduction a = 0.8
σ_v = Vertical stress at the soil reinforcement interfaces= (21.1) (z); where z is the distance between the crown of the dam and the level of installation of the geogrid

$$Le = \frac{47.1 \times 1.5}{2 \times 0.8 \tan 45^o \times 0.8 \times 21.1 xz} = \frac{2.61}{z}$$

In each case the minimum length of the embedment is 1.00m.

Global Stability Analysis

The next table shows the results of the global stability analysis.

Table 6. Factors of safety - with Reinforcement of Geogrids

Condition	Cajamarquilla Dam	Static	Seismic
Long Term	Nº2	1.56	1.38
	Nº3	1.52	1.12
	Nº4	1.72	1.16

The results indicate, that Cajamarquilla dams are stable according to the static and seismic conditions

The figures 1, 2 and 3 show below the results of the static stability Analysis of the Cajamarquilla dams 2, 3 and 4.

Figure #1 : Static analysis Cajamarquilla Dam nº2

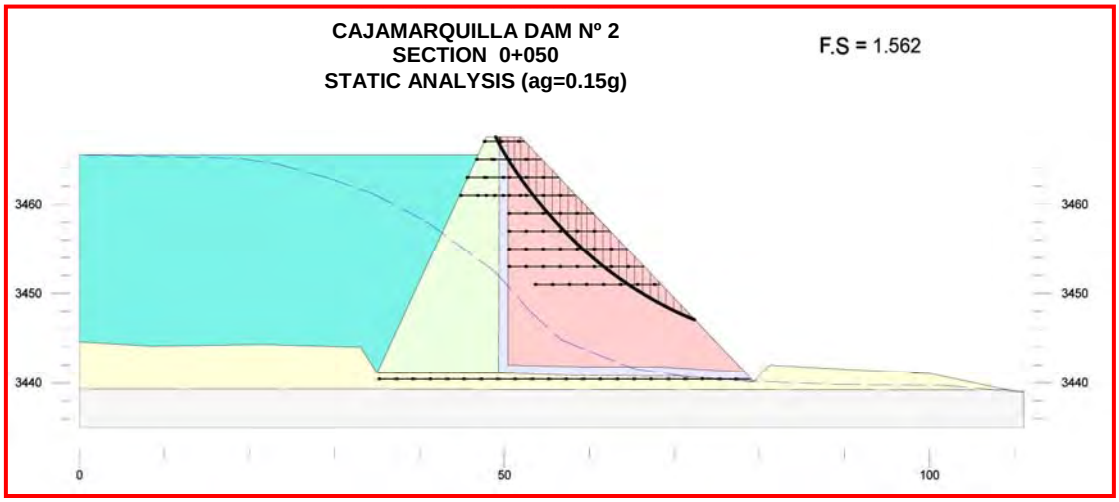

Figure #2: Static analysis Cajamarquilla Dam nº3

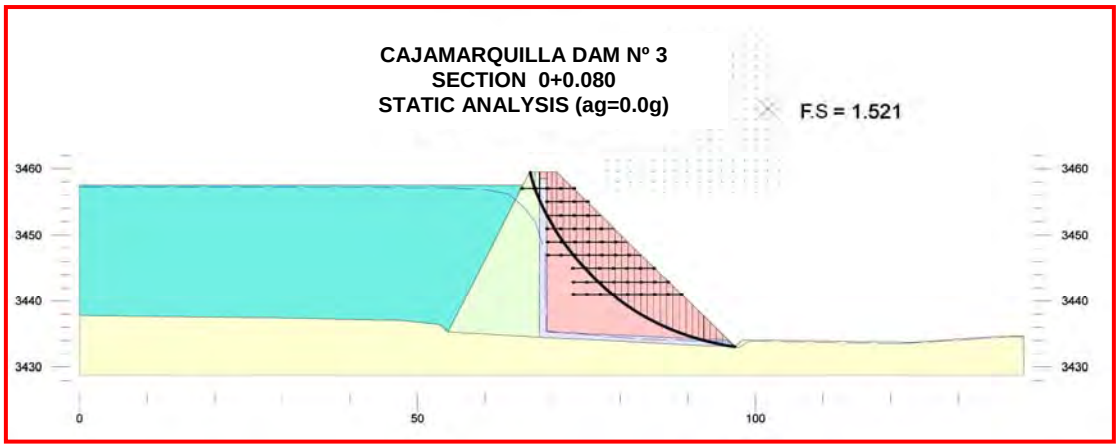

Figure #3: Static analysis Cajamarquilla Dam nº4

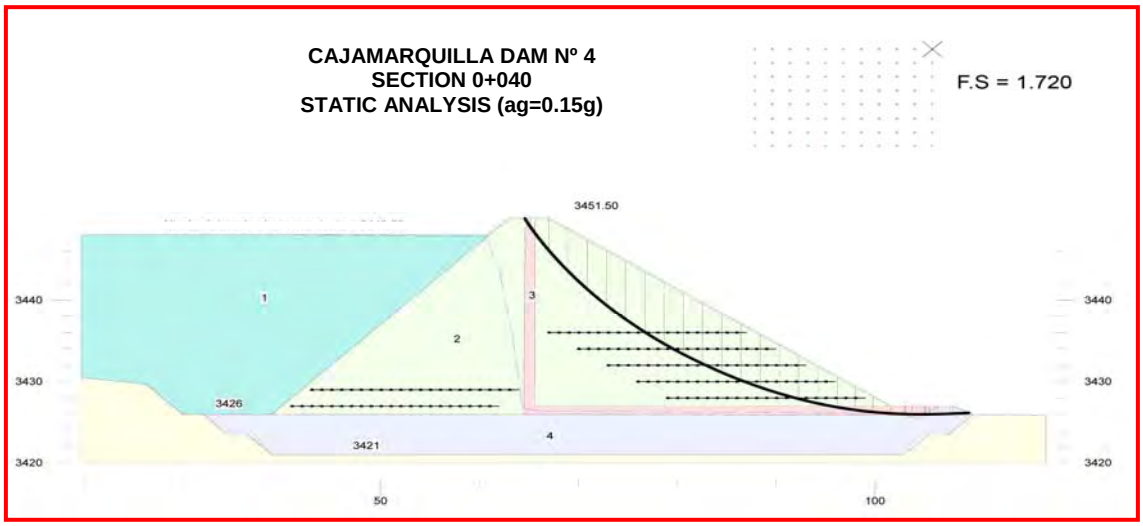

5. CONCLUSIONS

Installing geogrids in the embankment dams allowed construction of downstream slopes as steep as 1H:1V and upstream slopes as steep as 0.5H:1V. Incorporating the geogrids into the embankments significantly decreased embankment volumes while providing global stability factors of safety for both static and seismic conditions that meet minimum factors-of-safety, as summarized in Table 7.

Table 7. Safety factors

Condition	Cajamarquilla Dam	F.S without geogrids reinforcement		F.S With geogrids reinforcement	
		Static	Seismic	Static	Seismic
Long Term	Nº2	1.09	1.03	1.56	1.38
	Nº3	1.00	1.17	1.52	1.12
	Nº4	1.25	1.02	1.72	1.16

ACKNOWLEDGEMENTS

The authors would like to acknowledge Atacocha Mining Company S.A. for the permission provided to publish this paper.

REFERENCES

Geoservice Ingeniería SAC. (2004), Design of the Cajamarquilla slurry ponds 1 and 2, Lima, Perú.

Geoservice Ingeniería SAC. (2005), Design of the Cajamarquilla slurry ponds 3 and 4, Lima, Perú.

Koerner R.M., (1994) Designing with Geosynthetics, fourth Edition, Prentice Hall, New Jersey, USA

Federal Highway Administration (2001), Publication No. FHWA-NHI-00-043, Mechanically Stabilized Earth Walls And Reinforced Soil Slopes Design & Construction Guidelines, USA

Behaviour of Cellular Reinforced Soil Wall

M. S. Khedkar, Department of Civil Engineering, Indian Institute of Technology Bombay, Powai, Mumbai, INDIA

J. N. Mandal, Department of Civil Engineering, Indian Institute of Technology Bombay, Powai, Mumbai, INDIA

ABSTRACT
In the recent past, extensive use of reinforced soil retaining wall systems have been seen for carrying surcharge loads, along with the self weight of the backfill soil. Various reinforcements like strips, rods, sheets and grids with different shapes and sizes are found to be the most common type of reinforcement. Soil reinforcement using of cellular reinforcement (geocell) has been utilized successfully in many other areas of geotechnical engineering; however, there is still need to study the probable use of cellular reinforcement in reinforced soil retaining wall in order to increase performance of wall. In the present paper, deformation behavior of cellular reinforced soil wall is studied and compared with geogrid and geotextile reinforced soil wall. Reduced scaled laboratory experiments are carried out on geogrid reinforced and cellular reinforced soil retaining wall. Effects of vertical spacing, length of reinforcement and surcharge pressure on model soil wall are studied. It is found that under the same surcharge loading, cellular reinforcements perform better than geogrid reinforcements. For the same length and vertical spacing of reinforcements, lesser amount of facing displacement is noted in case of cellular reinforced wall than that of the geogrid reinforced case. A finite element method based compute program 'Plaxis V8' has been used to visualize the behavior of cellular reinforced soil wall.

1. INTRODUCTION

Reinforced soil retaining walls with planar reinforcement like textiles and grids have been used commonly for many applications like flyover abutments and retaining soil in roads and hilly areas. Several researchers have studied the planar reinforced soil wall, e.g. Hatami et al. (2001), Shinde and Mandal (2007), Ma and Wu (2004) and Hatami and Bathurst (2006). Soil reinforcement using of cellular reinforcement (geocell) has been utilized successfully in many areas of geotechnical engineering such as bearing capacity improvement under footing, road and embankments; however, there is still need to study the probable use of cellular reinforcement in reinforced soil retaining wall. Zhang et al. (2006), Khedkar and Mandal (2007), Khedkar et al. (2008), and Khedkar and Mandal (2009) have proposed three dimensional cellular reinforcement for reinforced soil applications with the help of triaxial and pullout tests. However, plane strain model study is more practical to understand the behaviour of reinforced soil retaining wall. Present paper focuses the behaviour of cellular reinforced soil retaining wall.

2. EXPERIMENTAL INVESTIGATIONS

The experimental investigations are planned with reduced scale laboratory model of cellular reinforced soil wall with an objective to study mainly the deformation behaviour of cellular reinforced wall under uniformly distributed loads. Behaviour of the cellular reinforced soil wall was also planned to compare with the geogrid reinforced soil wall. Table 1 demonstrates the details of experimental test program.

2.1 Experimental Test Setup

A laboratory test set up was developed to perform the entire experimentation as per the experimental plan. Considering the modeling laws and laboratory model limitations, the test layout of reinforced soil wall was designed to simulate 2.1 m high wall with a scale factor of 1 (Model): 4 (Prototype). Figure 1 illustrates the laboratory test layout of reinforced soil wall. In order to perform the tests, a custom designed experimental test set up was fabricated. The internal dimensions of test tank were measured as 400 mm wide x 550 mm high x 700 mm long. The test tank was fabricated from 10 mm thick steel sheets in order to ensure minimum deformations. The sidewalls were made from thick perspex sheet in order to allow clear observation of the wall and the backfill. The test tank was facilitated to accommodate the reinforced wall model of size 580 mm (length of wall) by 525 mm (height of wall). The model test wall was positioned at 120 mm from the front face of the tank in order to accommodate the wall deformations, including the failure deformations during the collapse stage. The scope of testing program includes study of cellular reinforced soil retaining wall with full height facing. Therefore, stiff plywood of 7 mm thickness, with 525 mm height and 400 mm in width was used for all the

laboratory experiments, to simulate the independent full height facing. All the potentiometers along with the load cell were connected to data logging system and hence to a computer. All the instrumentation was calibrated before use.

Table 1. Laboratory test layout of reinforced soil wall

Model	Study objective	Reinforcement		
		Type	Length	Spacing
Model-A	Reference test	Unreinforced	0	0
Model-B	Deformation behavior of cellular reinforced wall with different length of reinforcements	Cellular reinforcement (CR)	0.7 H	0.22 H
		Geogrid (GG)	0.7 H	0.22 H
		Cellular reinforcement (CR)	0.6 H	0.22 H
		Geogrid (GG)	0.6 H	0.22 H
		Cellular reinforcement (CR)	0.55 H	0.22 H
		Geogrid (GG)	0.55 H	0.22 H
		Cellular reinforcement (CR)	0.45 H	0.22 H
		Geogrid (GG)	0.45 H	0.22 H
Model-C	Deformation behavior of cellular reinforced wall with different vertical spacing between reinforcements	Cellular reinforcement (CR)	0.7 H	0.17 H
		Geogrid (GG)	0.7 H	0.17 H
		Cellular reinforcement (CR)	0.7 H	0.26 H
		Geogrid (GG)	0.7 H	0.26 H
		Cellular reinforcement (CR)	0.7 H	0.43 H
		Geogrid (GG)	0.7 H	0.43 H

Where, H = height of wall and CR = 10 mm high cellular reinforcements

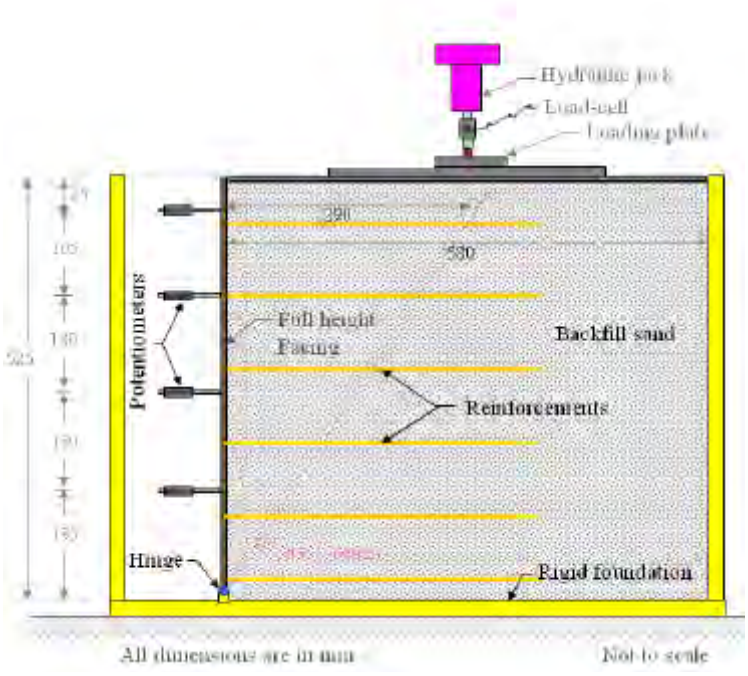

Figure 1. Test layout of reinforced soil wall

2.2 Evaluation of Material Properties

White colored quartz sand with mean particle size of 0.85 mm was used for experimental study. Figure 2 shows the particle size distribution curve for quartz sand. Physical properties of sand includes uniformity coefficient = 1.38; coefficient of curvature = 0.96; minimum dry unit weight = 16 kN/m^3; specific gravity = 2.5; maximum dry unit weight = 18 kN/m^3 and peak friction angle of sand at 47.9 % relative density (from direct shear test) = 34º. The sand can be classified as poorly graded sand, 'SP' according to Indian Standard classification (IS 1498 – 1970). Two types of reinforcement are used in the present study; i.e., the 10 mm high cellular reinforcements and planar grid reinforcement. Model cellular reinforcements have been designed by considering the modeling laws. They were manufactured manually from high

density polyethylene material available locally. The material was made available in the form of porous sheet and then was cut in to longitudinal and transverse members of required

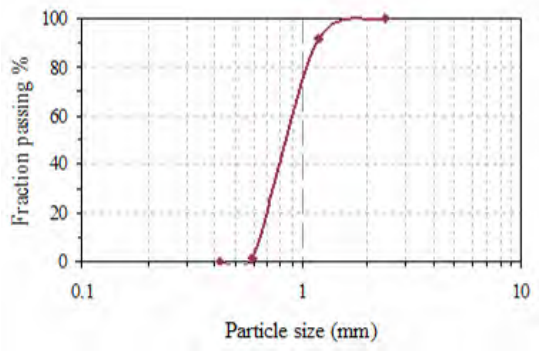

Figure 2 Particle size distribution curve for quartz sand

height to ultimately suture them with the help of cotton thread. While manufacture of reinforcements, extreme care was taken not to damage the material in any way. Figure 3 (a) illustrates the manually manufactured 10 mm high cellular reinforcement. The width of cellular reinforcement was 390 mm and the length was 390 mm 0.7 H. The longitudinal and transverse cell dimensions of all the reinforcements were kept constant i.e., 30 mm x 30 mm.

Aim of the present study includes comparison of behaviour between cellular reinforcements and planar grid reinforcement. In this regard, it was important to select the two reinforcement; ideally, having similar tensile and interface properties. For this purpose extensive material survey was carried out for the tensile strength and interface properties of grid reinforcements; however, the aperture size of geogrid was selected same as that of cellular reinforcements. In order to determine the tensile strength of all the specimens, including 10 mm high cellular reinforcement, the samples were prepared according to ASTM D 6637 (Method B); with size 210 mm wide and three junctions in the direction of testing. Figure 3 (b) shows the tensile strength versus strain curves for different reinforcement samples. It is observed that 'Sample D' failed at 0.91 KN/m strength for a corresponding strain of 4.96%; which is nearly closer to the tensile strength and the corresponding strain of 10 mm high cellular reinforcement (CR10). The numerical values of test results are mentioned in Table 2.

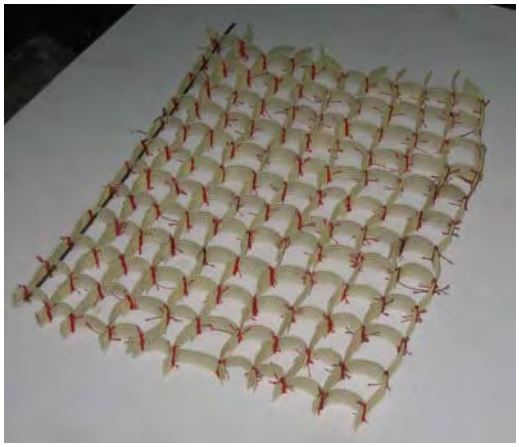

(a) Manually manufactured cellular reinforcements

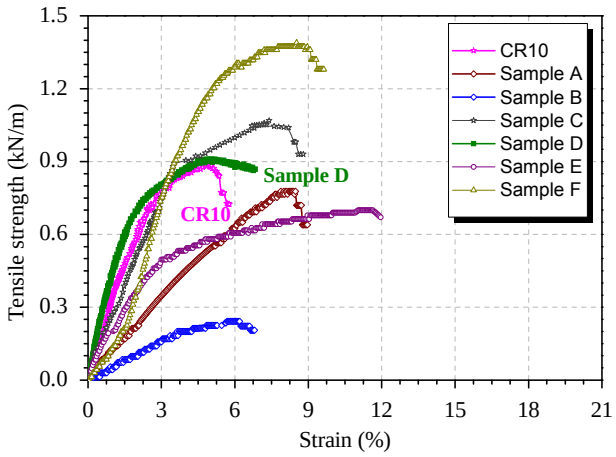

(b) Tensile strength versus strain for different samples

Figure 3. Reinforcement for experimental investigations

Table 2. Properties of reinforcements

Reinforcement properties	Tensile strength (T_f) (kN/m)	Elongation at maximum strength (εf) (%))	Soil - reinforcement interface (Modified direct shear test)
Geogrid (GG)	0.91	4.96	31°
10 mm high cellular reinforcement (CR_{10})	0.89	4.78	31°

2.3 Sample Preparation and Test Procedure

In order to replicate the samples through - out the testing program, the following step by step procedure was adopted to prepare the sample.

1. First the inside walls of the test tank is fully lubricated with grease to reduce side frictions of tank walls. Wall is constructed from bottom to top. A 25 mm layer of sand is placed on the bottom of tank to act as a foundation layer. Full height facing panel is then placed, allowing the rotation of panel on loading. The panel was supported by two struts near the side walls of the tank.
2. The strain points were defined on the reinforcements and strain markers, made of a hard and rigid yet transparent sheet of polyethylene were affixed on the defined points. The reinforcement thus instrumented was then placed directly on the foundation layer and connected to the full height facing panel. A very thin layer of colored sand was placed on the reinforcement to represent reinforcement for deformation analysis.
3. Backfill sand was placed in 25 mm layers by pluvial method on the reinforcement. A height of 900 mm approximately was maintained for this purpose. Also, an electrically operated handy vibrator was used to compact the sand layers to the required relative density of 47.9 %. The density of sand is comparatively low considering the experimental test limitation with cellular reinforcements. Simultaneous layers of sand and reinforcements were placed for entire height of the wall sample.
4. Potentiometers were installed on the facing panel to measure the horizontal displacement of panel also load cell was connected to the loading system to record the surcharge load. All the potentiometers and load cell were connected to the data logger and thus to a personal computer.
5. After completion of sample preparation along with all the instrumentation, a rigid 10 mm thick steel plate was placed on the top of model wall. The instrumentation is kept ‘on’ to record the data. The struts on both the sides were then removed and the initial deformation was measured. The surcharge pressure was applied by using the hydraulic jack, through the loading plate. The load was applied in increments. The ‘failure’ is defined as the decrease in observed load with the progressive increase in lateral displacement of panel.

2.4 Experimental Results and Discussions

Total 22 numbers of tests were conducted in the laboratory, out of which 3 number of test were pilot tests and 4 numbers of tests were conducted to check the repeatability of results. Thus, total 15 numbers of tests are reported in the present paper. All the test results were analysed to study different behaviour parameters of wall. The load was applied in increments to measure the horizontal displacement of panel with the help of potentiometers. The failure is defined as the condition when the measured load can be seen decreasing with increase in horizontal displacement at the potentiometers. Figures 4 (a and b) show the photographic view of the failure patterns for different reinforced walls including unreinforced wall case. Multi-linear failure envelope is observed in both, geogrid and cellular reinforced cases, which may be due to the full height facing panel.

(a) Unreinforced case (b) Reinforced wall under uniformly distributed load

Figure.4. Typical observed failure patterns for cellular reinforced walls

2.4.1 Model A

Model A was with unreinforced sand. A complete collapse failure was seen as soon as the supports were removed.

2.4.2 Model B

In order to study the effect of length variation of cellular reinforcement on behaviour of wall, 10 mm high cellular reinforcement (Model B) was tested with different four lengths of cellular reinforcements; i.e., 0.7, 0.6, 0.55 and 0.45 times the height of wall; for the spacing of 0.22 H. Also, the displacement behaviour of cellular reinforcement is compared with the geogrid reinforced case. Figure 5 (a and b) shows normalized panel displacement for geogrid and cellular reinforcement case for the reinforcement length of 0.7 H. Height of wall is normalized with the vertical distance from wall base and the panel displacement is normalized with the total wall height. Displacements were measured until the failure of wall. It can be observed that for a particular surcharge pressure cellular reinforced soil wall shows lesser normalized panel displacement than that of the geogrid reinforced case; also, increased surcharge pressure can be seen in case of cellular reinforced wall. Greater normalized panel displacements are seen at top wall heights.

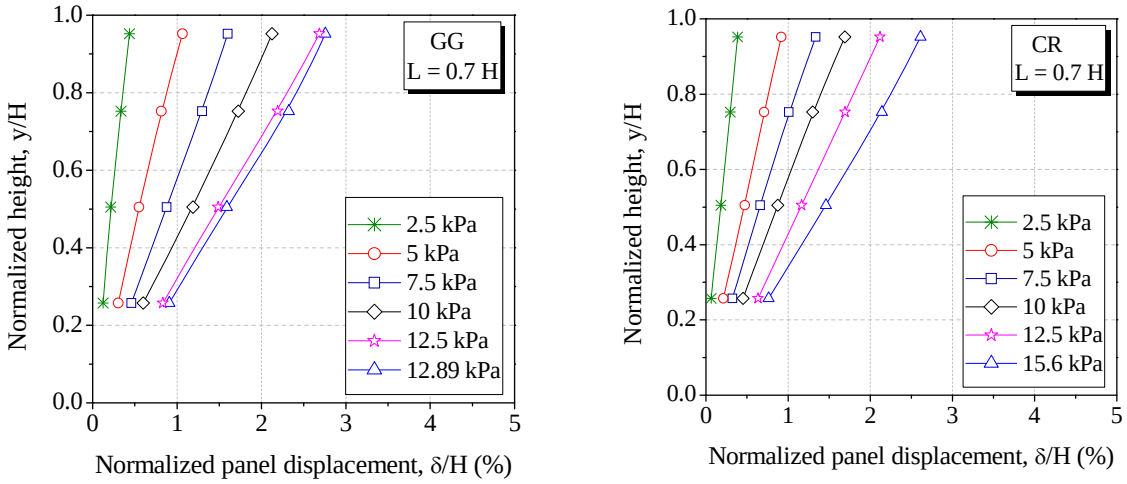

(a) Geogrid reinforced (GG); (b) Cellular reinforced (CR)

Figure 5. Relationship between normalized wall height and normalized panel displacement at various applied surcharge pressures for the reinforcement length of 0.7 times height of wall

Figure 6 (a) represents the comparison in between geogrid reinforced wall and cellular reinforced wall for the varying reinforcement lengths of 0.7 H and 0.55 H. It is observed in both the cases that normalized failure surcharge in the cellular reinforced case is greater than that of the geogrid reinforced case. Also, for a particular surcharge pressure, cellular reinforced wall shows lesser normalized panel displacement as compare to the geogrid reinforced wall. Similar observations are noted with the reinforcement lengths of 0.6 H and 0.45 H, Figure 6 (b); however, maximum displacements as well as surcharge pressures are observed closer for the reinforcement length of 0.45 H.

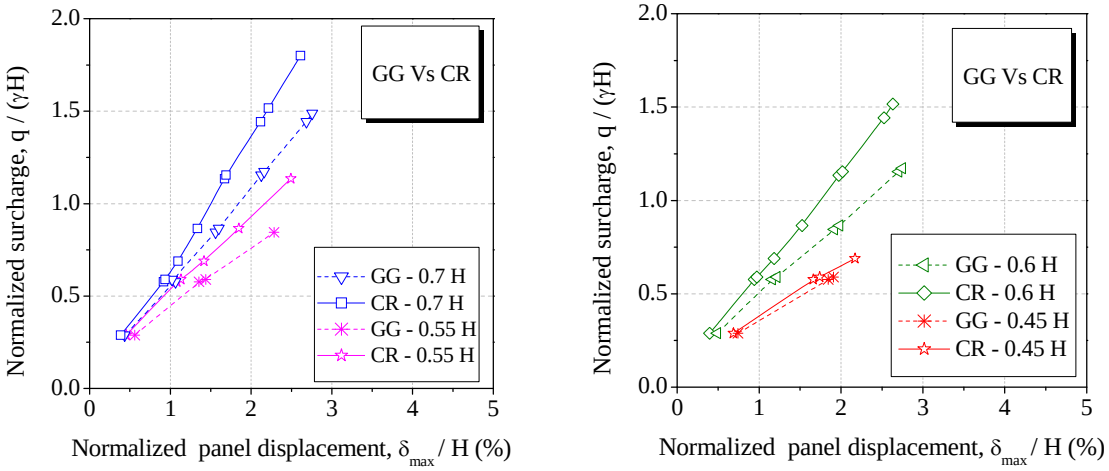

(a) Reinforcement length = 0.7H and 0.55H (b) Reinforcement length = 0.6 H and 0.45 H

Figure 6. Comparison between geogrid (GG) and cellular reinforced (CR) wall for normalized surcharge pressure and normalized panel displacement

2.4.3 Model C

Comparison of normalized panel displacement at the spacing of 0.26 H and 0.17 H for geogrid and cellular reinforcement is shown in Figure 7 (a) where as Figure 7 (b) shows that for the case of 0.43 H and 0.22 H. For a particular normalized surcharge, a reduced normalized panel displacement is observed for the cellular reinforcement case as compare to that of the geogrid case; however, considerable reduction is not observed in case of 0.43 H spacing of reinforcement.

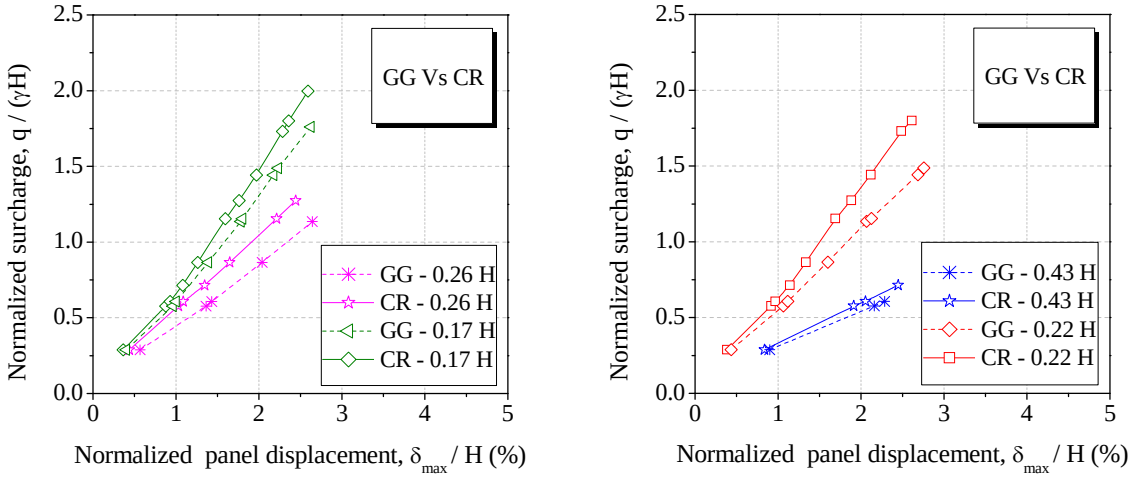

(a) Reinforcement spacing = 0.26 H and 0.17 H

(b) Reinforcement spacing = 0.43 H and 0.22 H

Figure 7. Comparison between geogrid (GG) and cellular reinforced (CR) wall for surcharge pressure versus maximum panel displacement

2.5 Effect of Reinforcement Length on Deformation Behaviour

Experimental results from walls reinforced with various lengths of cellular reinforcements as well as geogrid reinforcements are analysed to study effect the of reinforcement length on the deformation behaviour of wall. Figure 8 (a) compares the maximum deformation for both the reinforcement cases. For better interpretation, maximum displacement (δ_{max}) is normalized with height of wall (H) and the reinforcement length (L) is normalized with wall height.

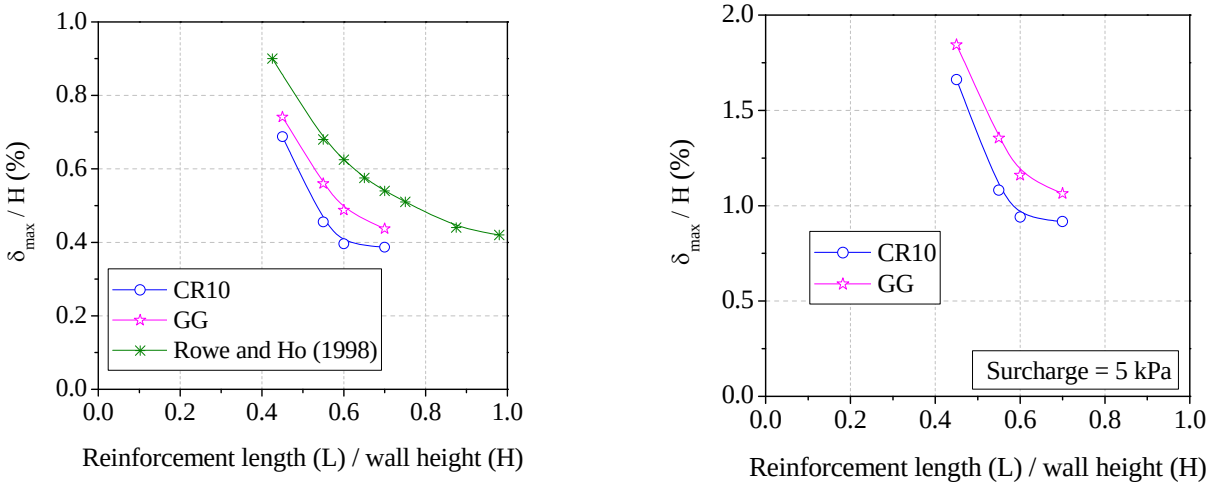

(a) Comparison with Rowe and Ho (1998)

(b) At the surcharge pressure of 5 kPa

Figure 8. Relationship between maximum panel displacement (δ_{max}) /wall height to reinforcement length / wall height for different reinforcements

In case of geogrid reinforced wall it can be observed that the maximum displacement decreases with increase in length of reinforcement. This observation is found consistent with Rowe and Ho (1998). As like in case of geogrid case, cellular reinforced walls also show decrease in the maximum displacement with increase in length of reinforcement. The curve appears steeper up to a particular length to height ratio (L/H) of 0.6 after which it flattens. This indicates that increase in length above the L/H of 0.6 results in very less decrease in wall displacement. Therefore, 0.6 H length of cellular reinforcement can be practically economical for cellular reinforced wall. This length of reinforcement is lesser than the 0.7 H length of planar reinforcements, suggested by literature (Elias et al, 2001; and BS 8006:1995). Maximum displacement versus reinforcement length for geogrid and cellular reinforcement at uniformly distributed load of 5 kPa is shown in Figure 8 (b). For a particular value of normalized displacement (δ_{max}/H), it can be observed that cellular reinforcement gives less the length of reinforcement, as compare to the geogrid case. e.g., from Figure 8 (b), for a δ_{max}/H of 1.15 the reinforcement length for geogrid case is approximately 0.7 H while that for cellular reinforced case is approximately 0.58 H; indicating about 17 % reduction in reinforcement length.

2.6 Effect of Reinforcement Spacing on Deformation Behaviour

Effect of reinforcement spacing on deformation behaviour of wall is studied by analyzing the test carried out with different reinforcement spacing. Figure 9 (a) illustrates the effect of reinforcement spacing on deformation behaviour of wall for geogrid reinforced as well as cellular reinforced case at a surcharge of 2.5 kPa. From geogrid as well as cellular reinforced case, it can be noted that the normalized displacement decreases rapidly with increase in the normalize inverse of reinforcement spacing up to a value of 4.2 after which the rate of decrease is observed reduced. Figure 9 (b) shows the relation between normalized displacement and the inverse of normalized spacing, for both the cases, at a surcharge pressure of 5 kPa. A non-linear decrease is seen in normalized displacement with increase in normalized inverse of spacing. From Figure 9 (b), for a particular value of normalized displacement, the normalized inverse of spacing is found remarkably less for the case of cellular reinforced wall as compare to geogrid case

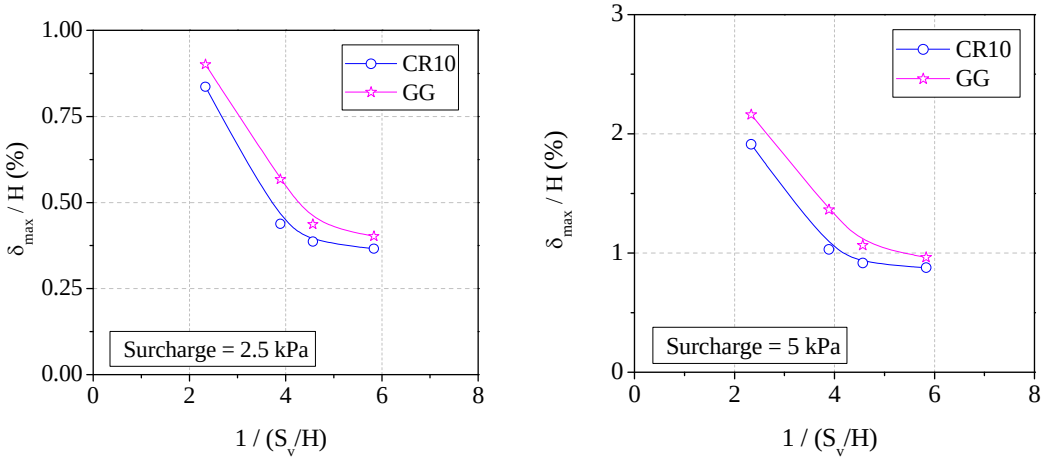

(a) At 2.5 kPa surcharge pressure (b) At 5 kPa surcharge pressure

Figure 9. Relationship between normalized maximum panel displacement and normalized reinforcement spacing for different reinforcements

3. FINITE ELEMENT SIMULATION

In the present study, the laboratory experimentation was scoped up to the deformations study of cellular reinforced wall. However, the probable generation of stresses in the wall along with the probable deformations is studied with the help of finite element method. Input program of Plaxis V8 was used for this purpose. Figure 10 (a and b) demonstrates the geometry for finite element simulation, showing test tank with different reinforcements. Vertical boundary is fixed horizontally, so that the sand cannot move horizontally beyond the boundary yet, the vertical settlement of sand is permitted. Bottom boundary is modeled by total fixity. Facing panel is modeled by plate element. The panel is hinged at the bottom of wall, allowing its rotational movements. The uniformly distributed surcharge pressure was modeled by uniformly distributed load per meter, on top surface of sand cluster. For simulation purpose, the cellular reinforcement is divided in to two parts, i.e., longitudinal members and transverse members. Longitudinal members are modeled by geogrid elements and transverse members are modeled by plate elements, as stiffness is the important parameter for transverse member. Sand was modeled using Mohr-Coulomb model with 15-noded triangular elements. Longitudinal members are modeled by geogrid elements and transverse members are modeled by plate elements.

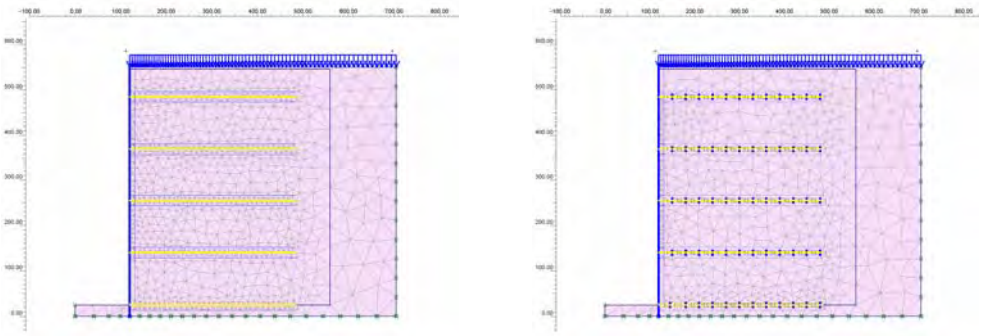

(a) Geogrid reinforcement (b) 10mm high cellular reinforcement

Figure 10. Geometry used in finite element analysis for reinforced soil wall with different reinforcement heights

The geogrid elements were represented with their axial stiffness, EA. While, the plate elements were modeled with flexural rigidity (EI), in addition to the axial stiffness of the reinforcement. The axial stiffness, EA, can be determined from stress strain properties of reinforcement. Axial stiffness of geogrid and 10 mm cellular reinforcement is taken as 18.3 and 18.6 kN/m width of wall. Thus to simulate the stiffness of the transverse member, an equivalent depth (d_{eq}) of 2 mm was specified to the transverse members. The plate element of facing panel was modeled with the flexural rigidity of 325 kN-mm^2/mm and the axial stiffness of plywood was calculated by considering the equivalent depth as 7.5 mm. The interface is modeled by virtual thickness interface element which is calculated as the Virtual thickness factor times the average element size. According to Vermeer and Brinkgreve (1995), for Plaxis program, the interaction coefficient, R, (R_{inter}, in case of Plaxis V8) is defined as the ratio of the shear strength of soil-structure interface to the corresponding shear strength of the soil. To simulate the soil structure interaction (R_{inter}) for planar as well as cellular reinforcements, the test results from modified direct shear tests are used.

3.1 Finite Element Analysis Results and Discussions

Different numerical programs were developed to simulate each wall of Model B as well as Model C and outputs are visualized. The outputs of cellular reinforcement case are also compared with the geogrid case.

3.1.1 Behaviour of Planar versus Cellular Reinforced Wall

The finite element program for both geogrid and 10 mm high cellular reinforced soil wall was developed for different uniformly distributed surcharge pressures. To compare the behaviour of both the cases; here, the results are presented for a particular surcharge value of 12.5 KPa. It is visualized from Figure 11 (a and b) that the extreme total displacement is at the top layers in the both the cases. Also, extreme total displacement for geogrid case is greater than that of the cellular reinforced case.

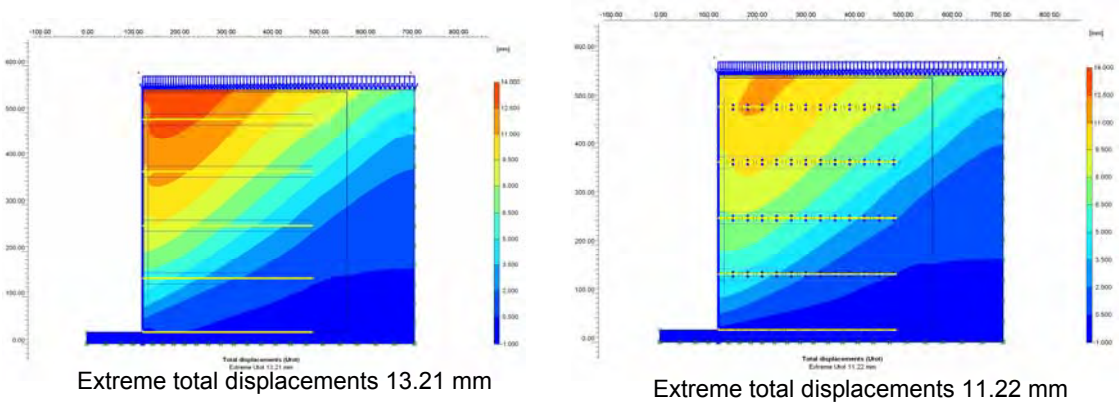

Extreme total displacements 13.21 mm Extreme total displacements 11.22 mm

(a) Geogrid reinforced wall (b) Cellular reinforced wall

Figure 11. Extreme total displacement shedding plot

The extreme horizontal displacements for geogrid and cellular reinforced wall are shown in Figure 12 (a and b). The visualization is exaggerated by a scale factor of three. With consistent to total displacement results for geogrid and cellular reinforcement case, horizontal displacements also visualizes the lesser value for cellular reinforcement case.

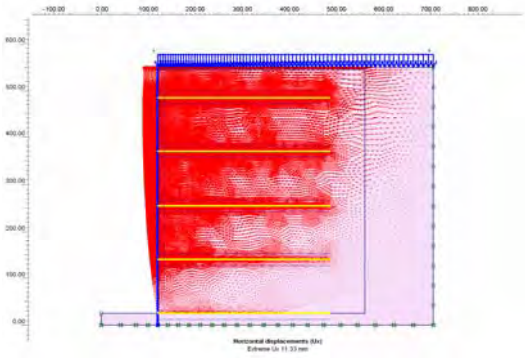

Extreme horizontal displacements 11.33 mm

(a) Geogrid reinforced case

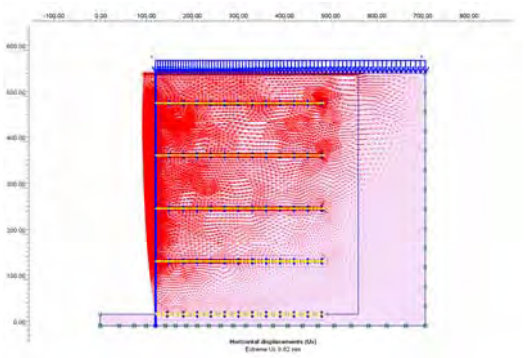

Extreme horizontal displacements 9.62 mm

(b) Cellular reinforced case

Figure 12. Extreme horizontal displacements plot

3.1.2 Behaviour of Reinforced Soil Walls at Laboratory Failure Pressures

In the present study, the laboratory experimentation was scoped to study the deformations behaviour of cellular reinforced wall. However, the probable generation of stresses in the wall along with the probable deformations is studied with the help of finite element analysis. For this purpose, the numerical programs are developed to simulate different reinforcements used in the experimental study. The finite element models are prepared for the incremental surcharge pressures. It is found that all the finite element analysis models were failed at pressures greater than the laboratory failure pressures as shown in Table 3. The behavior of cellular reinforced wall was studied with laboratory failure pressures and the model stresses are reported in Table 3. Total mean stresses as well as total shear stresses are greater for geogrid reinforced wall as compare to cellular reinforced case.

Table 3. Failure pressures, total mean stresses and total shear stress in soil walls reinforced with various reinforcements

Reinforcement	Laboratory failure pressure (kPa)	Failure pressure for finite element analysis (kPa)	Finite element method outputs at laboratory failure loads (Model C: Case -I)	
			Total mean stress ($\times 10^{-6}$) (N/mm^2)	Total shear stress ($\times 10^{-6}$) (N/mm^2)
Geogrid	12.89	13	276.39	210.41
Cellular 10 mm high	15.6	16.5	49.93	35.84

4. CONCLUSIONS

Following major conclusions can be seen from present study:

1. For the tested conditions, multi-linear failure envelope can be seen for the cellular reinforced case.
2. For a particular value of displacement, cellular reinforcement shows lesser reinforcement length as compare to the geogrid case.
3. From the test conditions adopted in the study, cellular reinforced walls shows decrease in the maximum displacement with increase in length of reinforcement. However, increase in length above the L/H of 0.6 results in very less decrease in wall displacement. Therefore, 0.6 H length of cellular reinforcement can be practically economical for cellular reinforced wall. This length of reinforcement is lesser than the 0.7 H length of planar reinforcements, suggested by literature (FHWA, 2001; and BS 8006:1995). For a particular value of displacement, cellular reinforcement shows considerable increase in reinforcement spacing over the planar geogrid case.
4. At a particular load, finite element analysis shows lesser deformation for cellular reinforcement and thus found consistent with the experimental investigations.

REFERENCES

BS 8006: (1995). Strengthened/reinforced soils and other fills, British Standards Institution, London, UK.

Elias, V., E., Christopher, B. R. and Berg, R. R. (2001). Federal High Way Administration (FHWA) "Mechanically stabilized earth walls and reinforced soil slopes design and construction guidelines, Technical Report, FHWA-NHI-00-043, 394 pp.

Hatami, K., Bathurst, R. J. (2006). Numerical model for reinforced soil segmental walls under surcharge loading, *Journal of Geotechnical and Geoenvironmental Engineering,* 132 (6), 673-684.

Hatami, K., Bathurst, R.J., Pietro, P., 2001. Static response of reinforced soil retaining walls with nonuniform reinforcement, International *Journal of Geomechanics* 1 (4), 477–506.

Khedkar, M.S., Mandal, J.N., 2007. Pullout response study for cellular reinforcement. In: proceedings of *5th International Symposium on Earth Reinforcement, IS Kyushu '07,* November 14-16, 2007, Fukuoka, Japan. pp. 293-298.

Khedkar, M.S., Mandal, J.N., 2009. Pullout response of cellular reinforcement under low normal pressures*. International Journal of Geotechnical Engineering* (Accepted for Publication in January, 2009 issue).

Khedkar, M.S., Mandal, J.N., Shinde, A.L., 2008. Reinforced wall with restricted backfill zone in urban areas, *In: proceedings of International Geotechnical Conference on 'Development of urban areas and geotechnical engineering'* June 16–19, 2008, Saint Petersburg, Russia. Volume 1, pp. 239 – 244.

Ma, C. C. and Wu, J. T. H. (2004). Field performance of an independent full-height facing reinforced soil wall, *Journal of performance of constructed facilities,* ASCE, 18 (3), 165- 172.

Rowe R. K. and Ho S. K. (1998). Horizontal deformation in reinforced soil walls, *Can. Geotech. J.,* 35 (2), 312–327.

Shinde, A. and Mandal, J. N. (2007). Behavior of reinforced soil retaining wall with limited fill zone, *International Journal of Geological and Geotechnical Engineering,* 25 (6), 657-672

Vermeer P. A, Brinkgreve R. B. J. (1995). Finite element code for soil and rock analysis, Rotterdam (Netherlands): A.A. Balkema.

Zhang, M. X., Javad, A. A. and Min, X. (2006). Triaxial tests of sand reinforced with 3D inclusions, *Geotextiles and Geomembranes*., (24), 201-209.

Geosynthetics 2009
February 25-27 2009, Salt Lake City, Utah

Geocell Protection against Shallow Failures on Steep Slopes

S.R. Boyle, Ph.D., P.E., Shannon & Wilson, Inc., Seattle, Washington, USA

ABSTRACT
This paper presents case histories of two geocell protected steep slopes in western Washington. Both slopes had experienced shallow slope failures, 300 to 1000 millimeters thick, presenting hazards to downslope transportation corridors. Both slopes were repaired by stripping loose soil, placing geotextile over the ground, anchoring geocells to the slope, and filling the geocells. Site 1 geocells were filled with crushed rock. Site 2 geocells were filled with topsoil and seeded. The geocell protection system was successful at Site 2. At Site 1, slope stability is improved but the geocell system longevity is compromised by soil erosion from beneath the geotextile. The Site 1 project included periodic monitoring of soil weathering below the geocell system and of unprotected control sections. This paper is of interest to those interested in improving stability of shallow failures on steep slopes and soil erosion.

1. INTRODUCTION

Geocell slope protection systems were installed to repair shallow failures of weathered soil from steep slopes at two sites in western Washington. This paper presents conditions at the sites, information on the geocell protection systems, and post-repair slope performance. The first site (Site 1) is located in Castle Rock, Washington, where two parallel BNSF Railroad tracks pass through a 770-meter long cut excavated in the 1930's. The steep cut slopes at Site 1 are typically 40 to 45 degrees, as high as 18 meters, and occur on both sides of the BNSF track. Locally the slopes are steeper than 45 degrees. Site soil consists of cohesionless, lightly cemented silt, which, while able to stand steeply when unweathered, weakens with weathering and saturation. Extended and heavy rainfall and runoff caused failures of weathered soil along the full length of both sides of the cut in February 1996, interrupting train service for 5 days. The 1996 slides were typically about 600 to 1000 millimeters (mm) thick, burying the tracks with 1.5 to 3 meters of soil and an additional 1.5 to 3 meters of trees (Figure 1). Extended and heavy rainfall in December 1998 caused thirteen localized shallow failures along these slopes at locations where soil weathering had occurred subsequent to the 1996 failures. The 1998 failures, with thicknesses less than 600 mm, again interrupted train service (Boyle and Hudak, 2003).

The second site (Site 2) is on a steep slope in northeast Seattle, Washington, adjacent to a popular walking and cycling trail constructed on a former railroad grade. The slope consists of glacially over-ridden, layered, silty sand, cohesive silt, and clayey silt. Several shallow failures occurred along this slope in December 1999, fully or partially blocking the trail at various locations. At Site 2, a 12-meter-long, 12.7-meter-high, 300 to 460 mm thick layer of weathered soil slid off the approximately 35 degree slope (Mann, 2005). The author was not involved in the design or construction of the Site 2 repairs. The author's familiarity with Site 2 is based on observations during frequent trips past the site during and following construction, review of Mann (2005), and personal communications with the Site 2 designer.

At both sites, the shallow failures occurred in weathered colluvium. Soil weathering, by precipitation, oxidation, drying, frost action, and root penetration, weakened the surface soil and allowing the soil to more easily be saturated by precipitation. Unlike the unweathered parent materials, the weathered surficial materials at both sites are unstable at the existing slope angle when they become saturated.

2. REPAIR METHOD

Geocell slope protection systems were installed at Site 1 in 2000 and Site 2 in 2003 to improve slope stability, reduce the rate of future soil weathering at the two sites, and reduce the frequency of slope failures. Both installations were constructed by:

- Stripping loose material from the slope to expose unweathered soil.
- Placing a nonwoven geotextile over the prepared surface.
- Anchoring geocells using tendons tied at the slope crest and stake anchors.
- Filling geocells with crushed rock (Site 1) or topsoil (Site 2).
- Hydroseeding the slope (Site 2 only).

Figure 2 presents the design detail for the geocell slope protection system installed at Site 1. The Site 2 installation was similar to the Site 1 installation. Design and construction information for Sites 1 and 2 are presented in Boyle and

Figure 1. Site 1 slope failures, 1996.

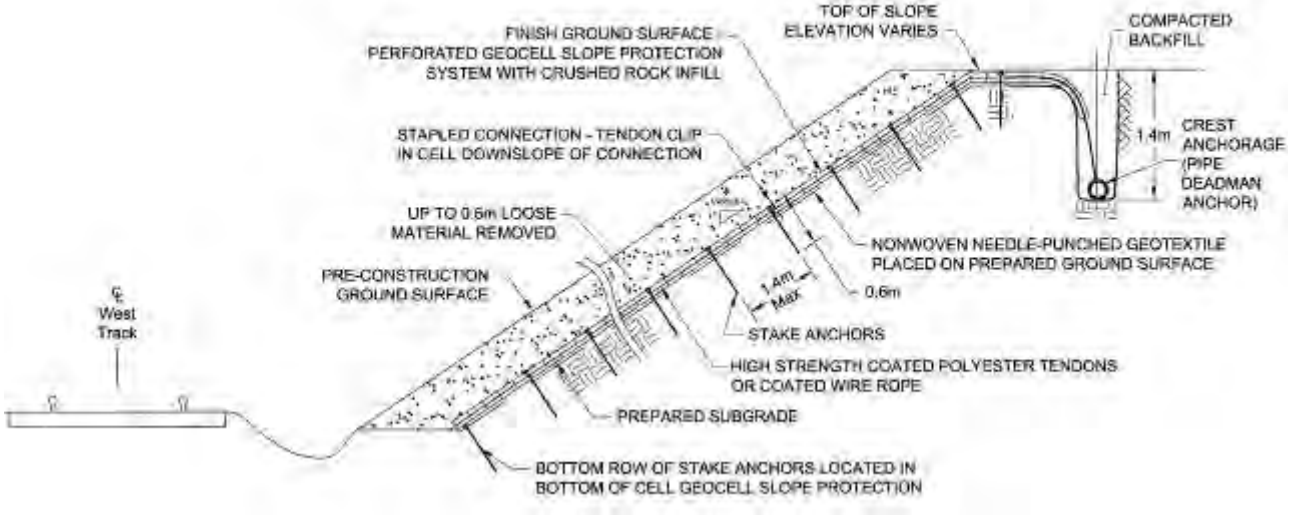

Figure 2. Site 1 geocell slope protection system detail (not to scale) (Boyle and Hudak, 2003).

Table 1. Sites 1 and 2 characteristics and geocell system properties.

Item	Site 1	Site 2
Slope angle	40 to 45 degrees	35 degrees
Slope height	18 m	12.7 m
Slope length	490 m	10 m
Soil	cohesionless silt	silty sand, clayey silt
Geocell product	Presto Geoweb® (perforated)	Presto Geoweb® (perforated)
Geocell cell dimension	200 mm	200 mm
Geocell depth	76 mm	100 mm
Geocell infill	crushed gravel	topsoil
Geotextile	Amoco CEF 4551	Mirafi 180N
Vegetation cover	none	grass
Top of slope anchorage	pipe deadman	vertical 2-inch diameter pipe piles

Hudak (2003) and Mann (2005), respectively. General design and construction procedures for geocell slope protection are presented in Presto Products Company (1999, 2000a, 2000b). Site and geocell system information for Sites 1 and 2 are summarized in Table 1. Construction photos for the two sites are presented in Figures 3 through 5.

The needle-punched, nonwoven geotextile was installed to:

- Limit soil moisture variability by reducing the frequency and depth of wetting and drying.
- Reduce erosion by direct rainfall impact and water flow over the ground.
- Retain soil beneath the geotextile (by filtration).
- Reduce root penetration (to reduce root-growth induced soil weathering, fracturing, and loosening).

At Site 1 the geotextile was also selected to allow infiltration of rainwater falling on the slope during extended light rainfall typical of the area. During heavy rainfall, water exceeding infiltration rates was expected to flow on top of the geotextile and through geocell perforations to the ditch at the slope toe. An impervious material, such as a geomembrane, was not used at Site 1 in part because of regulatory concerns that reducing infiltration would adversely affect the groundwater regime, could increase runoff volumes, and require construction of detention facilities.

3. SITE 1 SLOPE PERFORMANCE

3.1 Soil Weathering

The Site 1 geocell protection system was considered an experimental application because the technology had not been previously applied to a slope as steep, high, or laterally extensive. Nor, to the author's knowledge, had the system been applied primarily to reduce soil weathering, as opposed to principally provide erosion protection. Control sections without geocell slope protection were provided at Site 1 to compare performance of geocell-protected and unprotected slope areas. Unprotected areas at Site 1 include:

- A 23 meter slope segment adjacent to geocell protected slope that was stripped of loose soil and hydroseeded.
- A 30 meter slope segment adjacent to geocell protected slope that was not stripped or otherwise modified.
- A treed east cut slope, opposite the geocell protected west slope.

Post-construction monitoring of Site 1 was performed on five occasions between December 2000 and April 2008 (Shannon & Wilson, Inc., 2008). Slope performance monitoring included observing slope conditions and measuring soil consistency and stiffness at selected locations. We used a T-probe to estimate weathering depth and soil stiffness below the geocell and in untreated control sections. The T-probe consists of a 3-foot-long, ½-inch-diameter steel rod, with an approximately 45 degree conical tip and an integral T-handle. T-probe penetration measurements were conducted near four locations about 20 feet from the toe of the geocell-covered west slope and at multiple locations in untreated control sections. T-probe measurements were made using two methods: (1) by applying a steady firm pressure on the T-probe handle until refusal was achieved, and (2) by applying a number of hard pushes on the probe, pulses, to drive the probe into the ground. Steady push T-probe penetration ranged from about 10 to 125 mm below the geocell and from about 75 to 600 mm in the control section that was stripped of loose soil then hydroseeded. Pulsed T-probe penetration ranged from about 50 to 200 mm below the geocell and from about 75 to 800 mm in the control sections. The ranges of T-probe measurements are presented in Figure 6.

Based on our measurements and observations, little strength loss or weathering has occurred in soil protected by the geocell slope protection system after an initial period of weathering during the first year after installation. During each site visit in which measurements were taken, the soil below the geotextile was observed to be moist but not damp or wet, and medium dense or medium stiff to stiff. T-probe measurements were fairly uniform, with little increase in penetration depth or decrease in soil stiffness between March 2002 and April 2008. T-probe penetration depth varies from about one-third to one-tenth of that measured in unprotected control sections.

Compared to geocell protected areas, substantially greater T-probe penetration and soil strength loss occurred on the unprotected control sections (Figure 6). Near-surface soil in the control sections was generally wet during site visits that occurred during winter months, i.e., the rain season.

3.2 Vegetation Growth

Grasses, ground blackberry (Pacific blackberry), alder, and other vegetation are growing on the geocell-covered slope. The grasses grow in clusters and as widely spaced individual plants. Blackberry, alder and other trees, and bushes are generally widely spaced and in poor health (Figure 7). The geotextile appears to be working as intended as a barrier to

Figure 3. Site 1 slope preparation.

Figure 4. Site 1 geocell anchoring and filling cells with crushed rock.

Figure 5. Site 2 geocell installation and completed slope after hydroseeding.

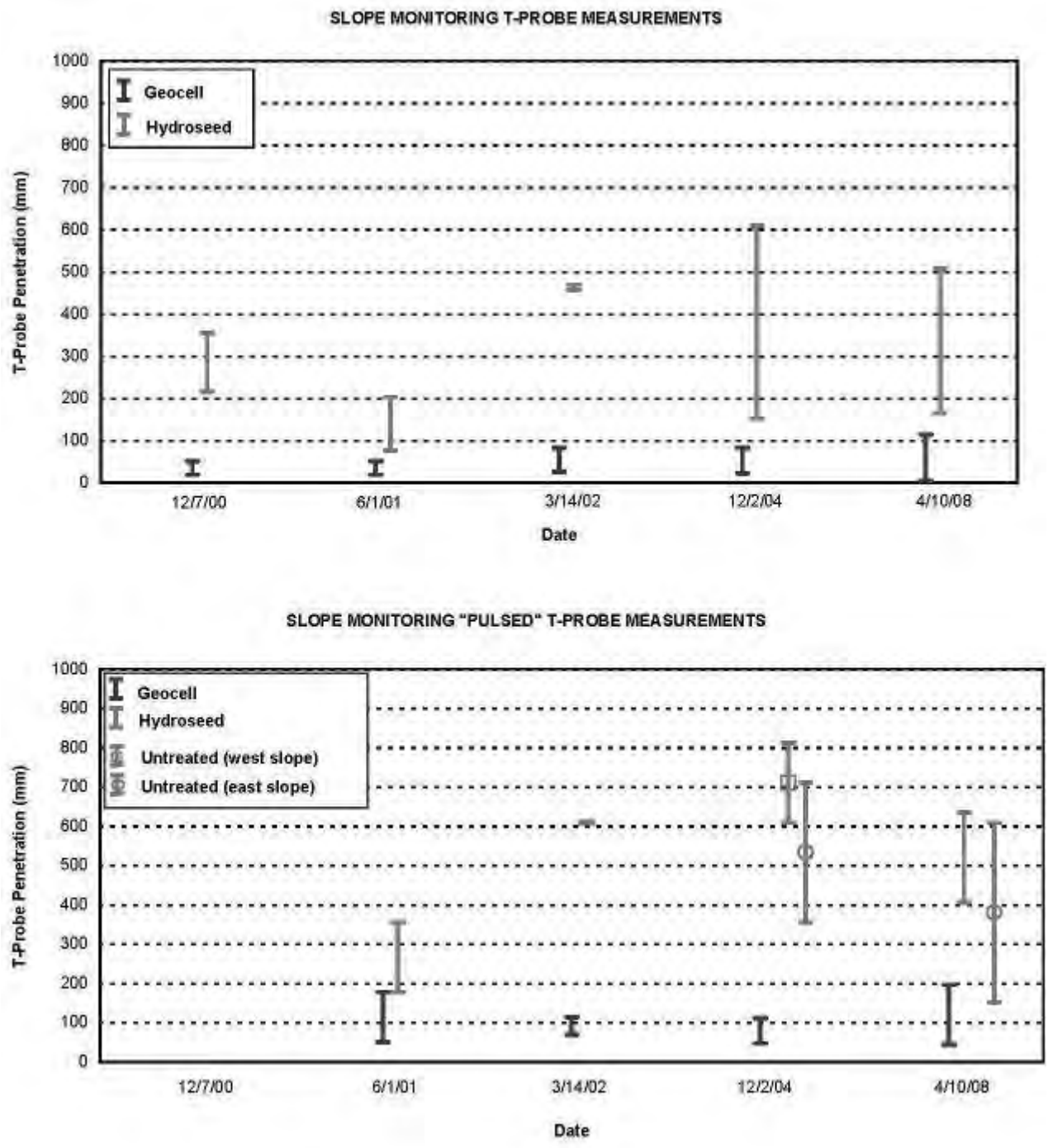

Figure 6. Site 1 T-Probe measurements.

major root penetration, thereby limiting plant growth, root penetration, and root growth-induced loosening of soil below the geotextile and geocell materials.

3.3 Erosion

At multiple locations along the slope, we observed that silt had buried or filled voids in the crushed rock that lines the ditch adjacent to the west track (Figure 8). During our April 2008 site visit we observed widespread loss of crushed rock from geocells (Figure 9). Probing and exposing soil below the geotextile where crushed rock no longer fills the geocells determined that erosion channels are present below the geotextile. The depth of erosion channels ranged from 10s of millimeters to nearly a meter. At two locations, erosion channel bottom widths were about 300 and 450 mm. At two other locations, erosion channel top widths were 2 to 5 meters at the assumed post-construction ground surface elevation. Erosion channels (rills) extended several meters upslope at locations explored. Based on our observations and the pattern of crushed rock loss from geocells, we conclude that concentrated water flow is occurring beneath the geotextile, eroding soil in the process, and depositing the soil in the ditch.

The most likely explanation for sub-geotextile soil erosion is that the erosion initiated where the geotextile was not in direct contact with the soil, and that water infiltrating through the geotextile flows over the ground surface in the void between the ground surface and the geotextile. Where the geotextile is not in contact with the soil, the velocity of water flowing across the soil surface could increase because flow is unrestricted. Eroded silt is likely transported below the geotextile to emerge at the slope toe. Once erosion begins, flow below the geotextile would likely concentrate along the eroded flow paths (i.e., within the rills), increasing and accelerating erosion. Silt erosion may occur because the silt is not cohesive, wetting and weathering readily break the apparently weak interparticle cementation, the silt has near-uniform particle size, and the slope is steep and high. Because the slope is covered with geocell, the full extent of erosion channels could not be observed, and thus their number, depth, shape, and orientation were not determined.

Lack of contact between the geotextile and soil may have occurred where the slope was not sufficiently smooth prior to geotextile placement, the geocell and geotextile system was not sufficiently secured to the ground, or where the geocell and geotextile were stretched over depressions and undulations in the ground surface. The ground surface inclination varies along the slope laterally and vertically. We observed stretched geocell and geotextile not in contact with the ground surface at many locations where slope steepness locally changed, including locations where sub-geotextile erosion was observed.

3.4 Performance Assessment

The geocell slope stability improvement system has performed as intended to reduce weathering rate and depth, thereby reducing hazards to the railroad at the slope toe. Soil below the geotextile was moist but not damp or wet, medium dense or medium stiff to stiff; and significantly firmer and less weathered than soil in unprotected control sections. No slope failures have occurred on the west slope since installation of the geocell slope protection system in 2000. Consequently, there have been no service interruptions since December 2000 related to west cut slope instability. No slope failures have been reported on unprotected portions of the west slope during this same period. Infrequent and relatively small earth slumps, debris flows, and tree fall have occurred on the untreated east slope since December 2000. These events have reportedly occasionally deposited soil and trees on the east railroad track, resulting in slow orders being placed on rail track traffic or diversion of rail traffic to the west track.

Sub-geotextile erosion appears to have occurred in a manner similar to that observed on exposed soil slopes on which vegetation has not become established. Lessons learned include:

- Slope shaping and excavation may not result in uniform slope faces.
- Care should be taken to ensure the geotextile is in contact with underlying soil.
- A crushed rock-filled geocell slope protection system underlain by a geotextile may not be the most appropriate protection for erosion-susceptible, cohesionless soil.

The life expectancy of the Site 1 geocell slope protection system is compromised by erosion that has occurred below it. Erosion will likely continue and accelerate as greater water quantities are channelized, increasing erosive energy. Deposition of eroded silt in the ditch adjacent to the tracks may impair ditch function and increase maintenance costs. If sub-geocell system erosion progresses too extensively, removing the geocell system and repairing the slope may be necessary.

Without partial or complete removal of the Site 1 geocell system, measures to extend the system life and reduce erosion are likely limited to filling of erosion channels and voids below the geotextile. This process may need to be periodically repeated as new erosion channels develop or erosion channels and voids not initially filled increase in size or are discovered. Difficulty with filling the erosion channels and voids, the necessity of working on the steep slope, potential

Figure 7. Sparse vegetation and root system spread across top of geotextile, Site 1.

Figure 8. Silt deposits in ditch at slope toe, Site 1.

Figure 9. Gravel missing from geocells as a result of soil erosion below geocell slope protection system, Site 1.

need for track time to perform the work, and cost would need to be weighed against potential costs and risks of not performing the work and accepting the reduced geocell system life expectancy. Erosion channels and voids below the geotextile could potentially be filled with a high hydraulic conductivity, medium to coarse sand that water could readily infiltrate but would not readily erode. The sand may need to be inserted at multiple locations along each erosion channel. Completely filling erosion channels and voids will likely be difficult. Locally removing the geocell and geotextile to fill erosion channels and voids might be considered.

4. SITE 2 SLOPE PERFORMANCE

The Site 2 slope appears to have performed well (Figure 10). Mann (2005) reported that 13 months after installation grass that was seeded at the end of construction had become established, providing a relatively thick cover. Mann also reported that the underlying soil remained stable and had not degraded by weathering. No evidence of erosion of topsoil from the geocells or of soil erosion from beneath the geocell has been observed. T-probe measurements made in 2008 by the author confirm that the soil beneath the geotextile remains medium dense to stiff or hard. Pulsed T-probe penetration measurements made in September 2008 were able to achieve 200 to 320 mm penetration in silty sand about 2 meters above the slope toe but only 25 mm penetration in cohesive silt about 5 meters above the slope toe. Soil immediately below the geotextile at the locations probed was slightly moist.

September 2008 excavation of soil from within geocells and exposure of the underlying geotextile found that roots of grasses, blackberries, and horsetails that have become established on the slope are distributed throughout the topsoil and through geocell perforations, but have not penetrated the geotextile. The Site 2 slope protection system has met its intended goal of providing slope protection, reducing the rate and depth of weathering, and reducing the frequency of slope failure at the site. Untreated adjacent slopes, including nearby areas where failures occurred in 1999 and subsequently, show that weathering following the slope failures has loosened surface soil, potentially setting the stage for future slope failures in those same locations.

Figure 10. Site 2 slope, September 2008.

5. CONCLUSIONS AND DISCUSSION

Similar geocell slope protection systems were installed on two steep slopes in western Washington. Loose and weathered soil was removed from both slopes prior to geocell system installation, so that the geotextile was installed over medium-dense to hard, undisturbed native soil. Site 1 performance was monitored on 5 occasions. Site 1 monitoring included monitoring of unprotected control sections. Site 2 performance monitoring was less formal and infrequent. Based on observations and measurements, the geocell slope protection systems have reduced both the rate and depth of soil weathering at both sites. Reduced weathering has reduced the potential for slope failures, reducing hazards to downslope improvements, i.e., the Site 1 railroad tracks and Site 2 trail, and users of those systems.

However, Site 1 application of the geotextile-underlain, crushed rock-filled, geocell slope protection system over erodible soil has demonstrated that the design and construction of the system is unsatisfactory at that site for the long-term. Erosion channels and voids have developed below the geocell system. Maintenance of the slope, slope protection system, and ditch will be required. To extend the Site 1 geocell slope protection system life, erosion channels and voids below the geocell system could be filled with sand to the extent practicable. These repairs would likely be difficult. Future erosion may necessitate that erosion channel and void filling occur periodically. The system will have to be repaired or removed should erosion progress to a point where system failure could occur.

No sub-geotextile erosion was observed in at Site 2. Higher soil cohesion, flatter slope angle, and lower slope height are principal contributors to this better performance, relative to Site 1. Precipitation may also be captured by vegetation and in topsoil that fills the geocells. The geocell slope protection system design appears appropriate for Site 2.

Comparison of system performance at the two sites indicates that modifications to the geocell slope protection system design or use of an alternative system(s) is appropriate for future stability improvements at Site 1 and sites with similar soil and slope conditions. One alternative might be to install a geomembrane, or other impervious material, instead of a geotextile below the geocell. A geomembrane would have limited sub-geocell erosion by preventing water from reaching the soil. A geomembrane was considered during design, but was not selected because of concerns about increased runoff, potential modification of the groundwater regime, larger tendon loads, and potential increased right-of-way and costs associated with installing top of slope anchorage sufficient to restrain the larger tendon loads. Alternative systems for retaining shallow weathered soil on slopes could also be explored.

ACKNOWLEDGEMENTS

The Federal Railroad Administration (FRA) and BNSF Railway (BNSF) provided project financing. The author and Shannon & Wilson appreciate the interest in the project by Mr. Donald Plotkin, FRA Program Manager and Mr. Trent Hudak, BNSF. BNSF provided engineering and construction coordination support, as well as access and protection during post-construction slope-monitoring site visits. Wilder Construction, Inc. installed the Site 1 slope protection system, applying creativity and ingenuity throughout construction. Presto Products, the geocell manufacturer and supplier, and their sales and engineering representatives assisted with Site 1 concept development and construction crew training. Glen Mann provided information on Site 2 and the geocell system installation at that site.

REFERENCES

Boyle, S.R. and Hudak, T.M., 2003, Use of geocellular confinement to improve stability of a 480-meter long, 18-meter high, 1H:1V slope, in *Two Rivers Conference, 56th Canadian Geotechnical Conferences*, 4th Joint IAH-CNC/CGS Conference, Winnipeg, Proceedings: Alliston, Ontario, Canadian Geotechnical Society, 7 p.

Mann, G., 2005, Creative repair of a residential landslide, in *36th International Erosion Control Association Conference*, Dallas, TX, Proceedings: Steamboat Springs, CO, International Erosion Control Association, p. 40-48.

Presto Products Company, 1999, *The Geoweg® Slope Protection System Practical Tips & Suggestions*, Appleton, WI, June 3.

Presto Products Company, 2000a, *Geoweb® System Slope Protection Design Package*, Appleton, WI, May 22.

Presto Products Company, 2000b, *Geoweb ® System Slope Protection Construction Package*, Appleton, WI, May 31.

Shannon & Wilson, Inc., 2008, *Performance Analysis and Final Report for Stabilizing Steep Cut and Embankment Slopes, Castle Rock, WA*, Prepared for the Federal Railroad Administration, Washington, D.C., project 21-1-20825, FRA Purchase Order DTFR53-07-P-00453.

Improvement of the Long-Term Trafficability of Container Storage Areas in Harbours with Composite Geogrid Reinforcement

J. Klompmaker, BBG Bauberatung Geokunststoffe GmbH & Co. KG, 32332 Espelkamp-Fiestel, Germany
G. Heerten, NAUE GmbH & Co. KG, 32339 Espelkamp-Fiestel, Germany
C. Lesny, NAUE , 32339 Espelkamp-Fiestel, Germany

ABSTRACT
Due to the globalization of the world economy existing ports are being developed and new ports are being built in order to cope with the increasing volume of goods in transit. New container terminals or port extensions are mostly built on reclaimed land from the sea. As the nourishments with their low or medium density of the fill provide insufficient bearing capacity to take up the final loads of the container terminals, the long-term stability and trafficability of the gained land must be improved. An economic measure to improve the bearing capacity of existing and newly developed terminal areas is the use of geogrid/nonwoven composite material as reinforcement and separation layers. As the geogrid can absorb greater tensile stresses than the base course itself, the tension in the reinforced base course is reduced. This leads to a more efficient load distribution within the base course and thus to less vertical deformation (settlement and rutting) at the pavement surface, which thus significantly increases the serviceability of these intensively used traffic areas.

As shown in laboratory and field tests, a geogrid/nonwoven geotextile composite material can provide a tremendous increase in long-term trafficability compared to areas without reinforcement or only with the use of normal geogrids. This paper will give an overview on the state-of-the-art using geogrid/nonwoven composite materials to increase the bearing capacity of the base course at various international port projects as e.g. in Turkey and the Sultanate of Oman.

1. INTRODUCTION

1.1 General

Container storage areas carry large traffic volumes and typically have concrete or paved surfacing over a base layer of aggregate. The combined surface and base layers act together to support and distribute traffic loading to the subgrade. Problems are usually encountered when the subgrade consists of soft clays, silts and organic soils. These types of soils are often water sensitive and, when wet, unable to adequately support traffic loads. If unimproved, the subgrade will mix with the road base aggregate, which leads to a reduction of strength, stiffness and drainage characteristics, promoting distress and early failure of the roadway. Contamination with fines makes the base course more susceptible to frost heaving.

1.2 Separation of Subgrade and base course

A geotextile which is placed between the subgrade and the base course layer provides physical separation of subgrade and base materials during construction and during operating life of the trafficked area (see Figure 1).

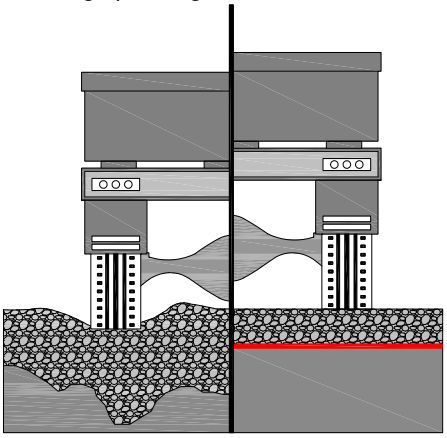

Figure 1. Illustration of geotextile separation function

The separation function of the geotextile is defined by a prevention of mixing, where mixing is caused by mechanical actions. The mechanical actions generally arise from physical forces imposed by construction or operating traffic and may cause the aggregate to be pushed down into the soft subgrade and / or the subgrade to be squeezed up into the base aggregate. A properly designed geotextile separator allows the base aggregate to remain "clean", which preserves its strength and drainage characteristics. The use of geotextile separators ensures that the base course layer in its entirety will contribute and continue to contribute its structural support of vehicular loads; the separator itself is not viewed to contribute structural support to the aggregate layer. Yoder and Witczak (1975) state that as little as 20% by weight of the subgrade mixed in with the base aggregate will reduce the bearing capacity of the aggregate to that of the subgrade. This highlights the importance of a geotextile separator with regard to the performance of base aggregate layers on fine-grained subgrades.

1.3 Reinforcement of base courses using geogrid reinforcement

Vehicular loads applied to the surface of trafficked areas create a lateral spreading motion of the unbound aggregate layers. Tensile lateral strains are created at the interface subgrade/geogrid as the aggregate moves down and sideways due to the applied load. Through shear interaction of the base aggregate with the geogrid, a.k.a. inter-locking, (see Figure 2), the aggregate is laterally restrained or confined (see Figure 3) and tensile forces are transmitted from the aggregate to the geogrid.

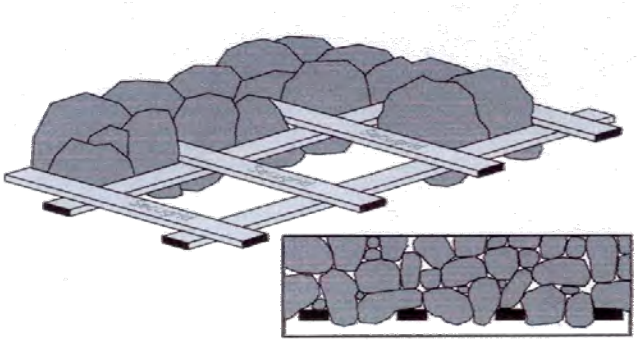

Figure 2. Interaction of aggregate with geogrid

As the geogrid is much stiffer in tension as the aggregate itself, the lateral stress is reduced in the reinforced base aggregate and less vertical deformation at the road surface can be expected. This interaction between geogrid and base course material increases the shear strength and thus the load distribution capacity of the used base course material.

Figure 3. Lateral restraint of aggregate using high modulus laid and welded geogrids

The increased load distribution capacity reduces vertical stresses on the subgrade, which finally reduces the deformation (rutting) on the surface of the aggregate layer. This correlation enables the reduction of reinforced base course thicknesses in comparison to un-reinforced layers (see Figure 4).

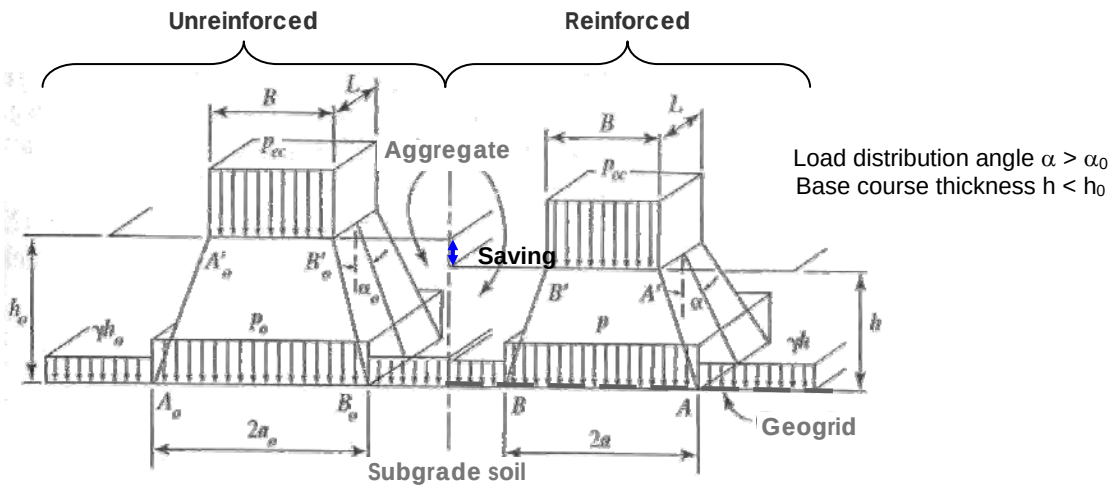

Figure 4. Increase of load distribution capacity with the use of geogrids (Koerner 1998)

In many projects, good quality base course aggregate is not available on site or close to the site. As a result, high transport costs of imported, expensive good quality base aggregate have a great influence on the total project costs. Especially under those conditions geosynthetic reinforcement and separation products can help to save money by reducing the amount of imported fill material needed to achieve the specified bearing capacity for the expected loads on the base course.

To combine the function of reinforcement and separation in one product, so called Geocomposites have been developed. Geocomposites as e.g. Combigrid® (see Figure 5) allow faster construction rates compared to separately installed geogrid and geotextile components.

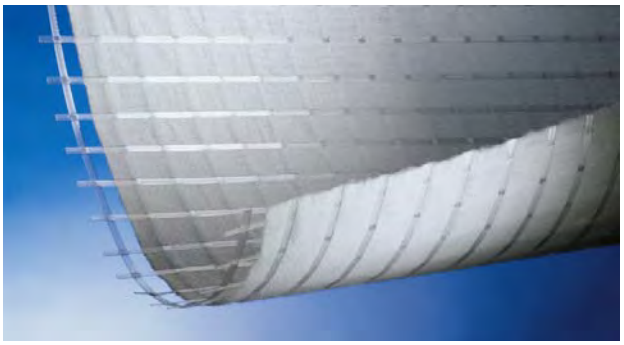

Figure 5. Combigrid® Geocomposite (geogrid reinforcement & needle punched nonwoven geotextile, firmly bonded between the cross laid reinforcement bars)

2. PERFORMANCE OF BASE REINFORCEMENT GEOGRIDS IN ROADWAY STABILIZATION APPLICATIONS

2.1 Large Scale Laboratory Test

The purpose of the study was to evaluate the reinforcement benefit provided by different geogrids. Benefit was defined in terms of the number of load cycles to reach a specific permanent rut depth of 3 inches in the aggregate surface layer for each section and Traffic Benefit Ratio (TBR), which is the number of load cycles for a reinforced section divided by the number of load cycles to reach this same rut depth for a comparable unreinforced test section. The test sections were instrumented to measure geosynthetic deformation and subgrade pore water pressure response.

The pavement test box facility used for the laboratory test was designed and constructed for the purpose of conducting laboratory, full-scale experiments on reinforced and unreinforced pavement sections and it meets the requirements of specifications developed for AASHTO Subcommittee 4E as contained in Berg et al., 2000. The test box facility is

designed to mimic pavement layer materials, geometry and loading conditions encountered in the field as realistically as possible with an indoor, laboratory based facility. This type of test box facility allows a high degree of control to be exercised on the construction and control of pavement layer material properties.
Each roadway test section was constructed with a nominal cross-section consisting of 12 in. (300 mm) of base course aggregate and 40 in. (1.1 m) of subgrade soil with a CBR = 1. The geosynthetic was placed between the base course and subgrade layers. A control test section having the same cross section without a geogrid was used for comparison to the geogrid stabilized sections. A cyclic, non-moving load with a peak load value of 9 kips (40kN) was used to mimic dynamic wheel loads. Sensors were used to measure applied pavement load, pavement surface deformation, and stress and strain in the base aggregate and subgrade soils. At a later state, the results of the dynamic plate loading laboratory tests shall be compared to results from test sections in the field, where moving wheel loads (three axle dump truck) are used to generate the pre-defined deformation rates. In both, the laboratory and the field test, the boundary conditions of the prepared subgrade and base course (as e.g. type, moisture content, gradation & angularity of base) are comparable. Amongst others, the results shall be used to quantify the influence of circular (plate load) versus biaxial loading (wheel load) on the development of rut deformation.

2.2 Test-Box and Loading Apparatus

Test sections were constructed in a 6.5 ft (2 m) by 6.5 ft (2 m) by 5 ft (1.5 m) deep box shown in Figure 6. The walls of the box consist of 6 inch (150 mm) thick reinforced concrete. The front wall is removable in order to facilitate excavation of the test sections.

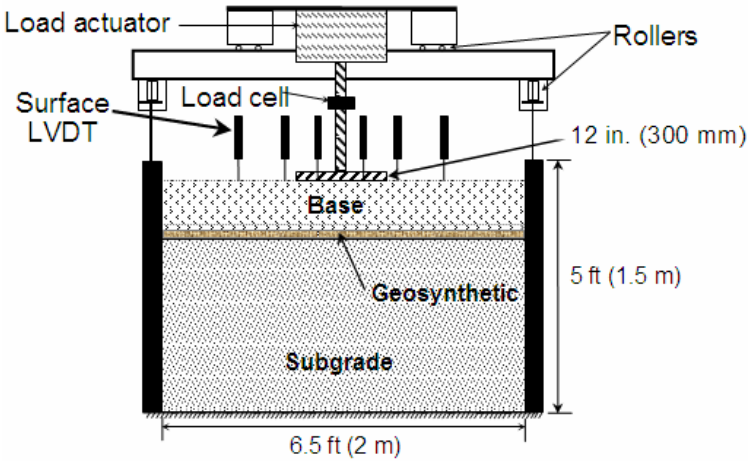

Figure 6. Schematic diagram of the pavement test facility

I-beams set into two of the concrete walls serve as a base for the loading frame. The load frame consists of two additional I-beams that span and react against the I-beams set into the concrete walls of the box. A load actuator, consisting of a pneumatic cylinder with a 12-in. (300-mm) diameter bore and a stroke of 3 in. (75 mm), is placed between the two I-beams of the frame. A 2-in. (50-mm) diameter steel rod extends from the piston of the actuator. The rod is rounded at its tip and fits into a cup welded on top of the load plate that rests on the pavement surface.

The load plate consists of a 12-in. (300-mm) diameter steel plate with a thickness of 1 in. (25 mm). A ¼-inch (6.4 mm) thick, waffled butyl-rubber pad is placed beneath the load plate in order to provide a uniform pressure and avoid stress concentrations along the plate's perimeter. Figure 2 shows an image of the load plate resting on the pavement surface. A binary solenoid regulator attached to a computer controls the load-time history applied to the plate. The software controlling the solenoid is the same software used to collect data from the pavement sensors. The software is set up to provide a linear load increase from zero to 9 kips (20 kN) over a 0.3 second rise time, followed by a 0.2 second period where the load is held constant, followed by a load decrease to zero over a 0.3 second period and finally followed by a 0.5 second period of zero load before the load cycle is repeated, resulting in a load pulse frequency of 0.67 Hz. The maximum applied load of 9 kips (40 kN) resulted in a pavement pressure of 80 psi (550 kPa). This load represents one-half of an axle load from an equivalent single axle load (ESAL).
Instrumentation was included in each test section. The instrumentation is designed to evaluate rutting in the stabilization aggregate, strain distribution in the reinforcement with distance away from the wheel load, and pore water pressure response of the subgrade during placement, compaction and subsequent loading. Instrumentation was included to make the following measurements:

1. Vertical surface deformation in the stabilization aggregate layer.
2. Applied load to the plate using a calibrated load cell.
3. Pore pressure in the subgrade during construction and pavement loading.
4. The geosynthetics were instrumented with wire extensometers, which were connected to LVDTs to measure the transfer of stress away from the wheel loading area.
5. The geosynthetics were extended through the front of the test box and visually monitored to determine if any movement was occurring at the edge of the box during application of the load.

2.3 Geosynthetic Materials

The geosynthetic materials used in these tests were a welded polypropylene biaxial geogrid and a composite geogrid using a welded polypropylene biaxial geogrid where a needle punched nonwoven geotextile is firmly bonded between the cross laid reinforcement bars. Tests were also performed with the welded polypropylene geogrid placed directly over a needlepunched nonwoven polypropylene separation geotextile (NP NW GTX). The used geotextile had a mass per unit area of 4.5 oz/yd^2 (150 g/m^2). The relevant properties of the used materials are shown in Table 1.

Table 1. Geogrid characteristics

Properties	Laid and welded PP geogrid (30 kN/m) (LW GG30)	Laid and welded PP geogrid (60 kN/m) (LW GG60)	Geocomposite material of laid and welded PP geogrid (30 kN/m) + PP nonwoven GTX (GC GG30)
T_{ult} MD lb/ft (kN/m)	1650 (24)	3080 (60)	2060 (30)
T_{ult} XD lb/ft (kN/m)	1650 (24)	3080 (60)	2060 (30)
$T_{2\%}$ XD lb/ft (kN/m)	550 (8)	1850 (36)	690 (13)
$T_{2\%}$ XD lb/ft (kN/m)	550 (8)	1850 (36)	690 (13)

2.4 Subgrade Soil

Piedmont silt (ML-MH) from Georgia was used for the subgrade. The residual soil was selected based on its problematic construction characteristics that include pumping and weaving at near optimum moisture contents, which usually requires chemical or mechanical stabilization, especially when wet of optimum (as is most often the case). Residual soils tend to retain the parent rock structure (e.g., joints and fractures) with additional fractures occurring due to stress relief during excavation. Excess water collected in this structure results in high sensitivity when disturbed. These soils are also often characterized by a relatively fast dissipation of pore water pressure as opposed to more cohesive soils.
The gradation tests (ASTM 422 and ASTM 1140) indicate that the soil is micaeous sandy silt (ML-MH) with 95% passing a 1mm sieve and 65% passing a 0.075 mm sieve. The soil has a maximum dry unit weight of about 109 lb/ft3 (15.2 kN/m3) at an optimum moisture content of 17%.

2.5 Base Course Aggregate

The base course material used in all test section was a graded aggregate base meeting the Georgia Department of Transportation specifications. Standard Proctor compaction test (ASTM D 698) and gradation tests were performed on the aggregate base course and the results are also included in Appendix A. The gradation test results on the aggregate base indicate that it meets the Georgia Department of Transportation specifications for base course materials. The aggregate has a maximum dry density of about 145 lb/ft^3 (22.8 kN/m^3) at an optimum moisture content of 5.4%. The graded aggregate base was estimated to have a friction angle of 43° based on large direct shear tests that have been previously performed on similar materials at GTX.

2.6 Test Results

The primary results of the stabilization test are in terms of the deformation response of the aggregate layer. Figure 7 provides a summary of the permanent deformation response for all test sections constructed with 12 inches of aggregate and a CBR = 1%. Table 2 provides a comparison of the performance characteristics from each test section, including the number of cycles and the corresponding Traffic Benefit Ratio (TBR) for each of the test result at 1 inch (25 mm) and

3 inch (75 mm) of rutting. Rut depths between 1 and 3 inch are acceptable deformation rates for unpaved roads but not for paved roads.
The results clearly show a difference in the performance of the geosynthetics evaluated in the study. The Geocomposite material (laid and welded geogrid (30 kN/m) + nonwoven needlepunched geotextile firmly bonded between the cross laid reinforcement bars) performed the best of all materials tested and reached over 850 cycles of loading before reaching 3 in. (76 mm) of rutting and had a TBR value of over 170. Over 10,000 cycles were required to reach a rut depth of 4 in. (100 mm). Open geogrids may be at a disadvantage with the used type of soil, as no filter stability between the coarse aggregate and the fine grained subgrade is given, so that the soft subgrade can easily be penetrated by gravel particles from the base course layer until interlock is developed. Regardless, both laid and welded geogrids provided significant improvements in deformation response over the control section with TBR values between 11 and 19.

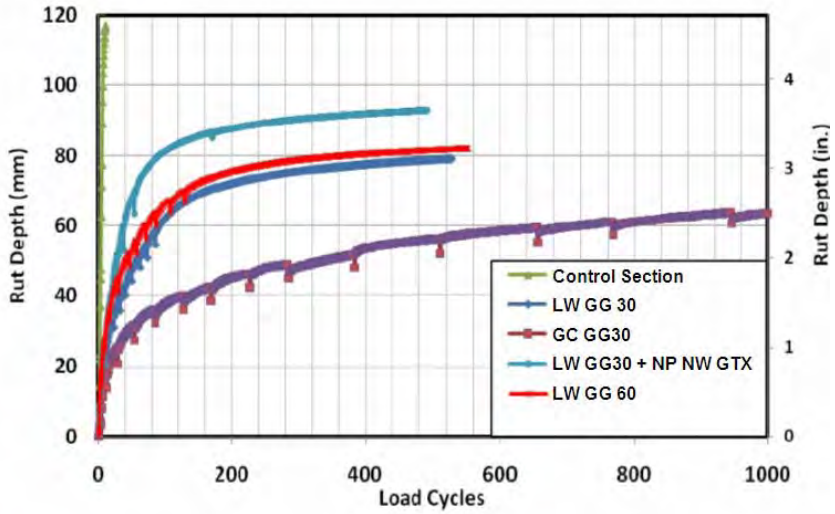

Figure 7. Permanent Deformation Response versus Load Cycles for CBR = 1 Subgrade

Section	Number of Cycles		Traffic Benefit Ratio (TBR)	
	1-in. (25mm) rut	3-in. (75mm) rut	1-in. (25mm) rut	3-in. (75mm) rut
Control	1.5	5	1	1
LW GG30	4.5	97	3	19.4
LW GG 60	1.5	55	1	11
GC GG30	6.5	855	4.3	171
LW GG30 + NP NW GTX	1.2	31	0.8	6.2

Table 2. Performance Characteristics (TBR) of each Test Section

Much of the difference between the two laid and welded geogrids with 30 kN/m and 60 kN/m (LW GG30 & LW GG60) tensile strength can be attributed to the differences in the first few load cycles which are applied a the beginning of the test. As it is not possible to maintain a consistent loading during the application of the first few load cycles movement occurs due to shoving and displacement of aggregate during interlock. In stabilization research performed by the US Army Corps of engineers, these cycles are referred to as "initial seating" (Tingle and Jersey, 2005) and they are removed from the data. If this procedure is followed and the first 3 cycles are removed, the hierarchy of the data remains the same, however then the deformation response of the 60 kN/m laid and welded geogrid is slightly better (less rutting) compared to the 30 kN/m laid and welded geogrid. The laid and welded geogrid placed over the nonwoven needlepunched geotextile (LW GG30 + NP NW GTX). The higher deformation response of the separately installed components is attributed to sliding of the geogrid over the nonwoven geotextile.
A summary of the pore pressure response of each test section is shown in Figure 8. The pore pressure directly corresponds to the results in Figure 7 with the high initial pore pressure developing for test sections where the largest amount of deformation per cycle was measured. The pore water pressure results indicate the disturbance due to

aggregate penetration into the subgrade in the control section and the open geogrid section, which leads to high pore water pressure. The increase in pore water pressure reduces the effective strength of the soil, resulting in an undrained subgrade strength that is actually less than CBR = 1% and correspondingly increased rutting occurs. This rapid pore pressure build up does not occur in the Geocomposite (GC GG30) due to the separation provided by the geotextile.

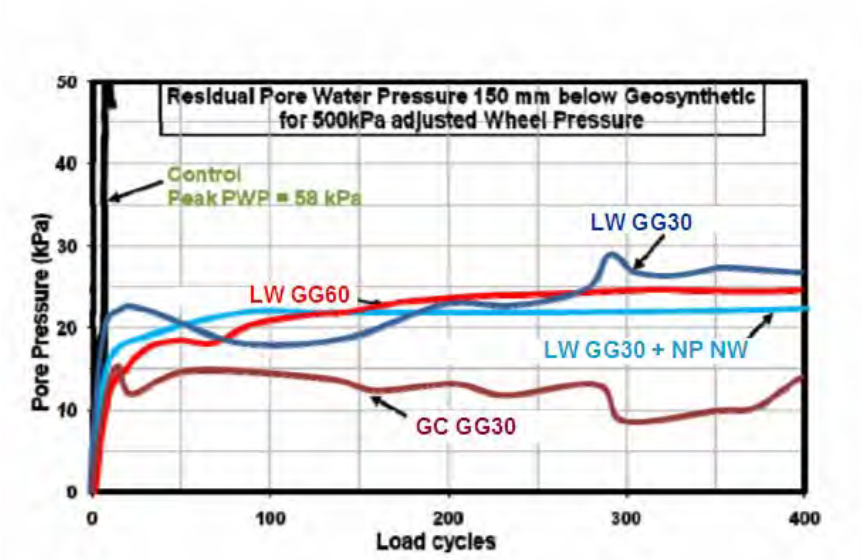

Figure 8. Pore pressure in Subgrade versus Load Cycles for CBR = 1 Subgrade

2. CASE HISTORIES

2.1. MERSIN PORT, TURKEY

Mersin is situated on Mersin Bay, a broad body of water that is open southward to the Mediterranean Sea. Mersin Harbour is close to the extreme north end of the bay and is constructed on a southeast-facing shore line. It is the main port for the Eastern Mediterranean Region's industry and agriculture. The port's rail link and its easy access to the international highway make it an ideal transit port for trade to the Middle East. With its modern infrastructure and equipment, efficient cargo handling, vast storage areas and its proximity to the free trade zone, Mersin is one of the important ports in the East Mediterranean. The facilities at the port handle general cargo, containers, dry and liquid bulk and Ro-Ro Port.

Figure 9. Mersin Port, Turkey

In 2004 it was planned to rehabilitate certain lots of the container terminal because of large rut depths at the pavement surface which had been caused by mobile cranes, trucks and containers. The differential deformations at the pavement surface had a major influence on the traffic safety and even on the safety of the stacked containers. Containers, which were stacked up to 5 high, even fell off, which finally lead to a shortage in the terminals' storage capacities.

As a consequence, the Railway Authority, who was the responsible body for the operation of Mersin Port, decided to take action for rehabilitating the affected lots in the harbor's container storage area.

Figure 10. Installation of composite base course reinforcement

The chosen rehabilitation measure was the use of composite geosynthetic base course reinforcement, because of the easy installation and handling and mainly because of economical advantages. A sample lot of 5,200 m² was realized at first in December 2004. Then an additional lot of 34,000 m² was realized using the same solution till 2006.

The former slab, which was constructed 20 years ago, together with the fill material underneath were removed up to level of the former in-situ subgrade. The thickness of the removed layer was approximately 1.4 m. On the soft in-situ subgrade, a Combigrid® Geocomposite made of a nonwoven needle-punched geotextile and a high modulus laid and welded geogrid, as shown in Figure 5, was installed. On the same day, a well graded aggregate base course with a thickness of 1.0 m was installed on top of the Geocomposite. Finally the new 0.4 m thick concrete slab was installed.

The lack of separation between the original base aggregate and the in-situ subgrade combined with insufficient compaction of the in-situ subgrade had caused the described ruts at the pavement surface over time. With the use of the composite reinforcement, mixing of the fine grained subgrade and the coarse base aggregate is prevented by the geotextile and secondly confinement of the base aggregate is achieved resulting from the installed geogrid component. The geogrid will further reduce differential settlements due to an increased load distribution of the reinforced base aggregate.

2.2 OMAN POLYPROPYLENE LLC PLANT AT SOHAR PORT, SULTANATE OF OMAN

Oman Polypropylene LLC started to build its Polypropylene plant at the end of 2004. For the development of the port at Sohar, which is located at the Gulf of Oman, an area of approx. 24 hectares was artificially created by dredging operations.

The total 2,000-hectare Sohar port and industrial zone will house mega industrial facilities ranging from an oil refinery and aluminium smelter to steel mills. The zone will be one of the world’s biggest greenfield petrochemical and metal-based industrial hubs. Oman Polypropylene LLC is integrated with the refinery. The project will add value to Sohar Refinery’s propylene stream to produce polypropylene that can be used in an array of downstream industries.

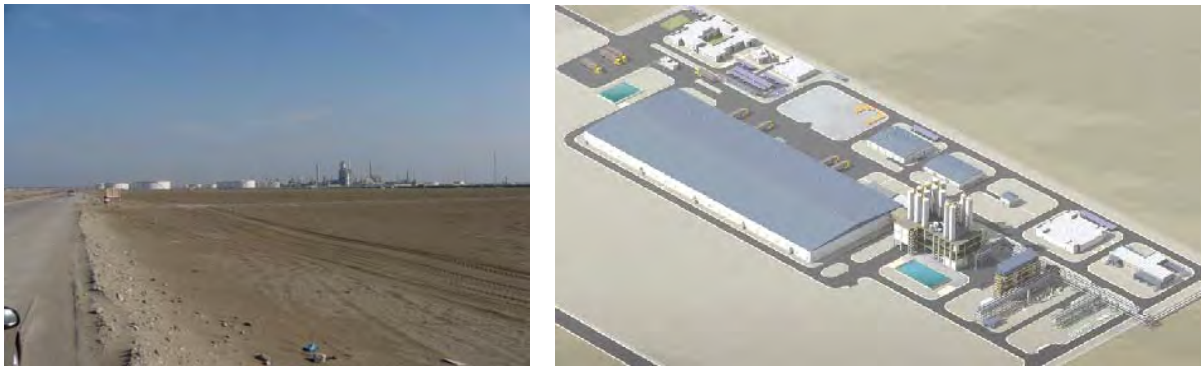

Figure 11 Oman Polypropylene LLC Plant, Sultanate of Oman

Soil investigations have encountered loose to very loose sand and organic silt layers in a depth of approx. 6m. For the development of access roads and storage areas it was therefore required to increase the bearing capacity of the weak subgrade.

As the most economical approach, it was decided to use geogrid reinforcement to provide the required subgrade support for the expected traffic and storage loads. The aggregate base course was installed in two layers of well graded crushed granular material, each 300 mm thick. A base layer of a composite reinforcement layer together with an intermediate laid and welded geogrid reinforcement layer, both having 40 kN/m tensile strength, ensured an increased modulus of the reinforced granular layers and finally a stable platform for the planned roads and storage areas on the originally soft subgrade.

Figure 12 Installation of composite base course reinforcement

The separation geotextile component of the used composite base course reinforcement ensured the integrity of the base course by preventing fines from migrating into the aggregate layer or aggregate from being pushed into the soft subgrade. Altogether approximately 150,000 m^2 of the described composite reinforcement were installed in this project.

3. CONCLUSION

The increase of global trade and transport of goods creates growing demands to handle cargo. To accommodate growing cargo volumes, existing ports are extended and new ports are being built. Soft subgrades are often the basis for the foundation works of new container terminal's pavement systems. As economic construction method geogrids are often used in this case to improve the insufficient bearing capacity for the expected traffic and storage loads. Geogrids first of all allow and secondly improve the compaction of foundation layers on soft soils. The technology of geosynthetic reinforced aggregate layers provides an economic construction method for the development of new container terminals. With the improved structural load-bearing capacity of geogrid reinforced aggregate layers, stress concentrations on soft subrades can be reduced, which minimizes differential settlements at the pavement surface and automatically improves the transport safety of container-handling equipment.

Increasingly so called "Geocomposite" materials are used which consist of a nonwoven geotextile component and a geogrid reinforcement layer. The geotextile with its separation and filtration function ensures that the base course layer in its entirety will contribute and continue to contribute its structural support of vehicular loads as it prevents the aggregate

to be pushed down into the soft subgrade and / or the subgrade to be squeezed up into the base aggregate. The geogrid increases the shear strength and thus the load distribution capacity of the used base course material.

Latest test results from large-scale laboratory testing, which has been presented in this paper, shows the outstanding performance of a specially developed geosynthetic composite material (a welded polypropylene biaxial geogrid with a needle punched nonwoven geotextile firmly bonded between the cross laid reinforcement bars) against individually installed geogrid reinforcement layers or separately installed combinations of geogrid reinforcement and geotextile separators.

The use of the described composite geosynthetic reinforcement in subgrade stabilization projects enables savings with regard to required installation time when compared to separately installed geotextile separator and geogrid components. Secondly a reduction of base course thickness can be achieved compared to unreinforced sections, because of the improved load distribution capacity which is achieved with the use of composite geosynthetic reinforcement. Besides the economical aspect, also the ecological aspect needs to be highlighted. As "good quality" aggregate is often not available close to the construction site or not in the required quantity, the possible reduction of base course thickness with the use of composite geosynthetic reinforcement reduces transport costs and the consequential environmental impact.

REFERENCES

Christopher, B. R. (2008), A Laboratory Evaluation of the Performance of NAUE Secugrid Base Reinforcement Geogrids in Roadway Stabilization Applications, Alpharetta, GA, USA

Giroud, J.P., & Noiray, L. (1981), Design of Geotextile Reinforced Unpaved Roads, J. Geotechnical Eng. Div., ASCE, Vol. 107, No. GT9, 1981, pp 1233 – 1254

Yoder, E.J. & Witcak, M.W. (1975), Principles of Pavement Design, 2nd Edition, John Wiley and Sons, 711

Geosynthetics 2009
February 25-27 2009, Salt Lake City, Utah

Design and Construction of Boulder-Faced MSE Walls (or How Not to Make a Mockery of Rockery)

J.A. Scarborough, P.E., Bunnell-Lammons Engineering, Inc., Asheville, North Carolina, USA
S.C. Interlicchia, Bunnell-Lammons Engineering, Inc., Asheville, North Carolina, USA

ABSTRACT
As growth encroaches on undeveloped, mountainside areas in Western North Carolina, retaining walls are needed to provide level space for construction. A boulder-facing is often perceived as desirable to improve the aesthetics of these walls. Beyond simply stacking boulders themselves for a gravity-type retaining wall, the use of geosynthetic reinforcements can reduce the wall cost as well as the number of boulders required for a stable structure. Current design methods for MSE retaining walls focus on the use of manufactured facing systems, such as segmental blocks or precast panels with known mechanical properties. This paper presents design and construction methods used for boulder walls. Boulders are an irregular natural material. Two contrasting cases are presented: One where a lack of design resulted in failure of the wall, and the other where an engineered design allowed successful construction and performance.

1. INTRODUCTION

Building on sloping terrain often includes the construction of retaining walls to provide grade separation and level ground. In recent decades, the use of mechanically stabilized earth (MSE) technology has been seen as a practical alternative to conventional cast-in-place concrete walls. The impetus for their use seems to be economic, as their construction cost is typically about half of the cost of concrete walls. Guidelines for design and construction of MSE walls are well established by both the National Concrete Masonry Association (NCMA, 1997) and the Federal Highway Administration (Holtz et al., 1995, and Elias and Christopher, 1996). These design methods have been developed for use with manufactured facing systems, such as segmental blocks or precast panels, with regular shapes and known mechanical properties.

In the mountainous areas of Western North Carolina the use of boulders as facing for MSE walls has become common. This trend appears to be driven by the perception of improved aesthetics from the use of a natural material. A significant characteristic of use of boulders as a wall facing are that these natural materials are irregular both in shape and mechanical properties.

Design guidance for boulder walls, as well as for the boulder-facing of MSE walls, has been published by the Federal Highway Administration (Mack et al., 2006). The FHWA publication refers to the use of boulders as “rockery.” The boulder walls described by the Mack et al., (2006) act as a gravity-type retaining wall; the mass of the boulders provides stability.

Unfortunately in Western North Carolina, problems with boulder-faced retaining walls are common. Typical factors contributing to their poor performance include: (1) Inadequate drainage around and within the walls, (2) Substandard compaction of the soils retained by the walls, and (3) A lack of engineered design for these walls. Two case studies are presented; one of a failed, non-engineered boulder-faced wall, and another with a successful, engineered structure.

2. SUMMARY OF BOULDER WALL DESIGN AND CONSTRUCTION METHODS

In addition to providing design and construction guidance, Mack et al., (2006) also provides a literature review of design methods for boulder walls. The design methods presented are described as “prescriptive” or “analytical.” Prescriptive methods are practice-oriented design methods based on what has worked in the past. While analytical methods use engineering principles as a rational basis for wall design.

Prescriptive design methods provide rules-of-thumb for design. Wall characteristics typically determined in this way include: maximum wall height, depth of embedment for the wall toe, wall batter, backslope conditions above/behind the wall, rock sizes needed in the wall, and interior drainage. The maximum wall height presented for walls designed using prescriptive methods was 1.8 m (6 ft). The prescriptive methods presented in Mack et al., (2006) did not include: minimum base widths for the wall, the use of chinking in the wall face, rock shape, and minimum cap rock widths and sizes. Chinking is the use of smaller rocks to fill gaps between larger rocks in the exposed face of the wall.

Analytical design methods for boulder walls evaluate potential failure modes to determine the required size of the wall and of its components. Lateral earth pressures are used as the force acting to create instability. The various methods presented in Mack et al., (2006) require evaluation of potential overturning, sliding, and bearing capacity; typically to determine the height-to-base ratio of the gravity wall. The maximum height recommended for boulder walls was 4.6 m (15 ft). Wall batter and wall embedment were prescriptive, with the need for interior drainage emphasized.

In addition to summarizing previous design methods, Mack et al., (2006) recommends two other potential failure cases be considered: global stability and seismic forces. Soil nails for cut slopes, and reinforcements for fill slopes are suggested as techniques for improving global stability. For MSE walls with a boulder-facing, Mack et al. (2006) suggests detailed analysis of the facing is not required when the facing is primarily for aesthetics and is not a structural component of the wall. Conventional slope stability programs are suggested as appropriate for evaluating the behavior of soil reinforcements.

Sound engineering judgment and sound construction practices for boulder walls and for boulder-faced MSE walls are critical for proper performance. Mack et al., (2006) suggests that the skill with which boulders are placed and fitted in the wall significantly affects the ability of the wall to act as a single mass, the ability of individual boulders to resist overturning and sliding, as well as the overall appearance of the wall. Chinking is suggested at the face of the wall, with the admonition that chinking not provide the primary bearing between boulders. In addition, similar to MSE wall design guidelines, the use of free-draining crushed stone is suggested immediately behind the boulders. However, Mack et al. (2006) suggests it is not appropriate for the crushed stone to be separate the boulder-to-boulder contact. Apparently, the use of crushed stone is believed to create a plane of weakness within an interlocked mass of boulders.

Mack et al., (2006) concludes with recommendations for the evaluation of existing boulder walls, to include a checklist for observations and sample construction specifications for boulder walls. Several items from this checklist are highlighted in the case studies below. The checklist is not reproduced herein, in the interest of brevity. This FHWA publication is a valuable resource for engineers concerned with boulder walls.

3. A TALE OF TWO WALLS – CASE HISTORIES OF BOULDER-FACED WALLS

Two case studies are presented. Wall “A” was constructed without an engineered design and without construction observation – it failed shortly after construction. Wall “B” was an engineered MSE structure. Wall “B” continues to perform well.

3.1 Regional Geology

Both wall sites are located in the Blue Ridge Physiographic Province. The bedrock in this region is a complex crystalline formation that has been faulted and contorted by past tectonic movements. The rock has weathered to residual soils which form the mantle for the hillsides and hilltops. The typical residual soil profile for Walls “A” and “B” include silty sand soils grading downward to partially weathered rock and to the parent rock.

Partially weathered rock is defined, for engineering purposes, as residual material with standard penetration resistances in excess of 100 blows per foot (bpf). Weathering is facilitated by fractures, joints, and the presence of less resistant rock types. Consequently, the profile of the partially weathered rock and hard rock is quite irregular and erratic, even over short horizontal distances. Also, it is not unusual to find lenses and boulders of hard rock and/or zones of partially weathered rock within the soil mantle well above the general bedrock level.

3.2 Wall “A”

Wall “A” was built for grade separation on the downhill side of a new home. It was originally built to a height of 3.7 to 4.6 meters (12 to 15 feet). In North Carolina, the state’s building code requires retaining walls over 1.5 m (5 ft) high to be designed by an engineer. This is often not enforced. Such was the case with Wall “A.”

Construction at the site began in February 2003, and a certificate of occupancy was issued in July 2004. Figure 1 shows a photograph of Wall “A” after its construction, while construction of the house was ongoing. In September 2004, about 165 mm (6½ inches) of rainfall from Hurricane Ivan fell in a three-day period. The rainfall was apparently the trigger for the failure of the wall. Figure 2 shows the remnants of Wall “A” shortly after it failed. Fortunately, the house was unaffected by the failure.

Figure 1. Photograph of Wall “A” (arrows show either apparent poor boulder-to-boulder contact or apparent seams in the wall).

Figure 2. Photograph of a failed Wall “A”

A forensic evaluation of Wall “A,” prepared in October 2004, found three factors directly contributing to the failure:

The wall had been constructed without interior drainage features
The wall had been constructed without proper engineering and due consideration of overall global stability
The soil placed behind the boulders was apparently not well compacted during construction

The forensic report concluded, “… the rock retaining wall would have failed at some time in the future even if the heavy rainfall associated with Hurricane Ivan had not occurred.”

In addition to these factors, it appears construction of the boulder-facing was poor. A close examination of Figure 1 reveals that individual boulders were generally not placed in contact with at least two rocks below, and columns of rocks (i.e., near vertical seams) are apparent. From Figure 2, it appears the boulder wall was constructed as only a thin veneer on the face of a steep soil fill.

The failed Wall “A” was replaced with a soil nailed wall with a segmental block facing during 2005. The replacement wall continues to function well, without apparent distress. The cost of the repair exceeded $200,000.

3.3 Wall “B”

Wall “B” was also built as grade separation below a new home. This boulder-faced MSE wall was designed and built during February to April of 2007. The wall was 4.6 meters (15 feet) high, 5.5 m (18 feet) if including embedment at the toe. A slope inclined at two horizontal to one vertical (2H : 1V) was constructed above the wall. The combined height of the wall and slope was about 12.2 meters (40 feet). Figure 3 shows a portion of the completed Wall “B;” in plan view, the wall was a convex arc (pointing downhill) across a topographic draw.

Figure 3. Photograph of Wall “B”

A conventional boulder wall, such as described by Mack et al., (2006), would create a gravity-type retaining wall using only a mass of boulders. Using geogrid reinforcements to link the boulder facing to a mass of mechanically stabilized earth reduces the quantity of boulders needed for a stable wall. The design of Wall "B" included horizontal layers of geosynthetic reinforcement within the boulder-facing and extending into the silty sand soil fill behind. The silty sand was fine-to-medium grained with about 35 percent fines (i.e., material passing the US No. 200 sieve). The geogrids were placed on a vertical spacing of about 0.6 m (2 ft) with a length no shorter than 8.5 m (28 ft). The geogrid spacing was selected to be compatible with available boulders and with conventional practice for MSE walls. The geogrid length and strength were selected based on the results of conventional slope stability analyses (i.e., to achieve the specified factor-of-safety). The geogrids were required to have a long-term design strength (LTDS) of at least 52 kilo-newtons per meter (3,750 pounds per foot).

Figure 4 shows a critical section for the stability analyses. The darkened lengths at the end of the reinforcement layers model the development length for pullout at the ends of the geogrid. A factor-of-safety of at least 2.0 was used in evaluating pullout capacity at the rear of the geogrid. The soil parameters used in the analyses were conservatively assumed based on a grain-size analysis of the backfill soil. A factor-of-safety of 1.3 was used for the long-term, effective stress, stability analysis. A pseudo-static, seismic, analysis was also conducted using a horizontal coefficient of one-half the expected peak ground acceleration (PGA) for the design earthquake (Kramer, 1996). The pseudo-static analyses were conducted based on a design earthquake with a two percent chance of occurrence in 50 years. The PGA was based on information provided the U.S. Geological Survey (USGS); resulting in a horizontal pseudo-static coefficient of 0.1g. A factor-of-safety of 1.1 was used in the pseudo-static analysis.

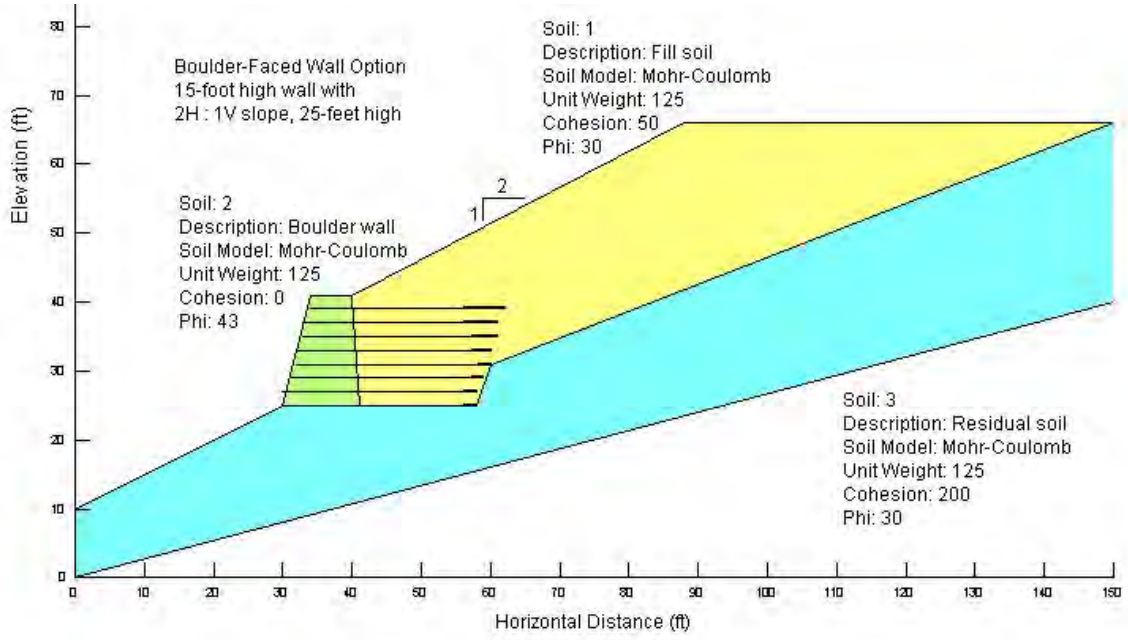

Figure 4. Cross-section of Wall "B"

In addition to the slope stability analysis, the wall design also included a facing stability analysis, similar to NCMA (1997). Lateral earth pressures were applied to the rear of the boulder-facing. Stability for the facing was provided by the strength of the geogrid developed over the width of the boulder facing. To provide consistent contact at this interface, crushed stone was used not only behind the boulders, but between the boulders as well. It should be noted this use of geogrid results in continuous horizontal planes in the boulder wall, as shown in Figure 3, above. An interface coefficient of 0.8 was assumed, and applied to the geogrid-stone interface. Mack et al., (2006) cautions against this; and against the use of crushed stone between the boulders, fearing the development of a potential sliding surface. It is believed the use of crushed stone in the interface allows for more regular development of interface strength. Seismic conditions were not evaluated for the facing connection of Wall "B." Nor was a stability analysis of a potential unreinforeced boulder facing conducted.

Interior drainage for the wall and fill included a 0.3 m (1 ft) thick blanket drain at the base of the reinforced zone, and a French-drain as an underdrain at the base of the fill.

Full-time construction observation services were provided during construction to document compliance with the design. This included verification of the materials used in construction, as well as compaction testing. A moisture-density of at least 95 percent of the soil's maximum dry density with a moisture content within 3 percentage points of the soil's optimum moisture content, as based on the standard Proctor, was consistently achieved. The observed unit weights, for the soil, were consistent with values assumed in design, 125 pounds per cubic foot. Figure 3, above, also illustrates the careful placement and fitting performed during construction of the boulder-facing.

4. CLOSING SUMMARY

A brief review of the literature of boulder walls was presented along with case histories of two boulder-faced walls. The catastrophic failure of Wall "A" was most likely due to: (1) Poor drainage around and within the wall, (2) Poor compaction of the soils retained by the wall, and (3) A lack of engineered design. Wall "B," on the other hand, was constructed in accordance with an engineered design that included the use of geosynthetic reinforcements. Wall "B" has performed well.

The design of Wall "B" included: (1) The use of conventional slope stability analyses to evaluate geogrid placement, and (2) The use of interface and pullout analyses to assess the stabilty of the boulder-facing. It is believed the design method presented above will result in a stable facing for a well-constructed boulder-faced wall.

Mack et al. (2006) presents valuable information for the design and construction of boulder walls. However, it was found several of the construction recommendations conflict with the need for horizontal placement of reinforcements in an MSE structure.

REFERENCES

Elias, V., and Christopher, B.R. (1996). Mechanically Stabilized Earth Walls and Reinforced Soil Slope Design and Construction Guidelines – Participants Manual – FHWA Demonstration Project 82 Ground Improvement, Publication No. FHWA-AS-96-071.

Holtz, R.D., Christopher, B.R., and Berg, R.R., (1995). *Geosynthetic Design and Construction Guidelines – Participants Notebook,* Publication No. FHWA-HI-95-038, revised April 1998.

Kramer, S.L., (1996). *Geotechnical Earthquake Engineering*, Prentice Hall, pg. 653

Mack, D.A., Sanders, S.H., Millhone, W.L., Fippin, R.L., and Kennedy, DG. (2006) *Rockery Design and Construction Guidelines*, FHWA Publication No. FHWA-CFL/TD-06-006.

NCMA (1997). *Design Manual for Segmental Retaining Walls*, Second Edition, National Concrete Masonry Association Publication No. TR-127-A, ISBN 1-881384-07-1.

Geosynthetics 2009
February 25-27 2009, Salt Lake City, Utah

Evaluation of Vegetated RECPs using ECTC's Bench-Scale Test

J.L. Smith, Ph.D., P.E., SUNY College of Environmental Science and Forestry, Syracuse, NY, USA
S.K. Bhatia, Ph.D., Syracuse University, Syracuse, NY, USA

ABSTRACT
The need to provide erosion control on bare soil slopes and channels in hydraulic and environmental applications is a critical issue that spans the globe. The use of ground cover is one of the most effective ways of minimizing soil erosion. Although vegetation is often the ground cover of choice, vegetation is difficult to establish on steep slopes and in high flow areas, and is not always effective. As a result, rolled erosion control products (RECPs) are often used to provide immediate ground cover protection for soils and assist in the growth, establishment, and protection of vegetation. Recently, the Erosion Control Technology Council (ECTC), in conjunction with TRI/Environmental, Inc. (TRI), developed a bench-scale test method for determining the ability of RECPs to encourage seed germination and plant growth. This paper presents the results of a laboratory study of twelve different RECPs, based on this ECTC test method. Attempts are made to evaluate the role of RECPs in enhancing vegetative growth.

1. INTRODUCTION

The need to provide erosion control on bare soil slopes and channels in hydraulic and environmental applications is a critical issue that spans the globe. Typical hydraulic and environmental applications may range from providing stream bank protection along a stream, protecting the side slopes of a landfill, to protecting bare soil slopes in an agricultural field or along a road. Soil erosion strips the land of needed soil and nutrients and negatively impacts the quality of surface waters.

The use of ground cover is one of the most effective ways of minimizing soil erosion. Ground cover intercepts raindrops, dissipating their energy before they can reach the underlying soil particles, thereby minimizing the detachment and transport of soil particles (Gray and Sotir 1996, Toy et al. 2002, et al.) Vegetation has traditionally been a cost effective ground cover method. Vegetation reduces the energy of raindrops by intercepting them; provides soil reinforcement with roots; decreases runoff velocities with its roughness; and maintains the infiltration properties of the soil (Gray and Sotir 1996). Although vegetation is often the ground cover of choice, vegetation is difficult to establish on steep slopes and in high flow areas (Gray and Sotir 1996) and is not always effective (Evans 1980, Fifield et al. 1988, Rickson and Morgan 1988). For example, Evans (1980) found that soil erosion and runoff rapidly increase on soils with less than 70% vegetative cover. Fifield et al. (1988) found that seeding alone on slopes greater than 3 horizontal to 1 vertical (3H:1V) does not significantly reduce soil erosion.

Over the last 15 years, the use of geosynthetic rolled erosion control products (RECPs) for minimizing soil erosion has gained in popularity. RECPs are temporary degradable or long-term non-degradable materials, manufactured or fabricated into rolls designed to reduce soil erosion and assist in the growth, establishment, and protection of vegetation (ECTC 2001). RECPs are able to provide immediate ground cover protection to bare soil slopes and channels, and provide an environment that encourages the germination of seed and the growth of vegetation.

The popularity of RECPs has lead to the development of a number of different RECPs. A recent compilation by the Industrial Fabrics Association International (IFAI) indicates that there are more than 100 different RECPs available in the US alone (IFAI 2007). RECPs are manufactured from a variety of different natural fibers (coir, jute, straw, and wood), synthetic fibers (polypropylene, polyvinyl chloride, and vinyl), and combinations of different natural and/or synthetic fibers. RECPs are also manufactured into a variety of different structures, such as erosion control nets (ECNs), open-weave textiles (OWTs), erosion control blankets (ECBs), and turf reinforcement mats (TRMs) (ECTC 2001). Because of their differences, RECPs can vary significantly in their basic properties and overall field performance.

One aspect of their field performance that is of particular importance is their ability to encourage the germination of seed and the growth of vegetation or biomass. Aboveground biomass refers to the shoots, stems, and leaves of plants. Belowground biomass refers to roots. The ability of RECPs to encourage the germination of seed and the production of both aboveground and belowground biomass (vegetation) is particularly important for natural fiber RECPs, which rely on the establishment of vegetation for their long-term performance. Vegetated RECPs have also been found to further reduce soil erosion in comparison to RECPs alone (Smith 2007). Many field studies have been conducted that document the ability of different RECPs to establish vegetation (Fifield et al. 1988, Fifield 1992, Krenitsky and Carroll 1994, Smith et al. 2003, et al.) Although these studies provide valuable information, one of the difficulties with field

studies is that they are conducted over a wide range of site conditions, such as climate, soil type, vegetation type, and topography. The variability in site conditions makes it difficult to apply the results to other sites, leading researchers to conduct testing under controlled laboratory conditions.

In one laboratory study, Sutherland et al. (1998a) compared the performance of seven different RECPs in the growth of vegetation. The laboratory study focused on measuring differences in the radiative properties (albedo) and soil temperatures developed by different RECPs. It was found that bare soil conditions produced the most hostile climate for vegetation, with the soil surface directly absorbing radiation from the light source. In general, the RECPs were able to moderate soil temperatures by insulating the soil surface, although to varying degrees. The wood fiber ECB tested was the most effective RECP in reducing soil temperatures.

Sutherland et al. (1998b) continued the study by considering the influence of the seven RECPs on soil moisture content and biomass production. Similar to the earlier study (Sutherland et al. 1998a), the wood fiber ECB had the greatest biomass production. It was found that the ability of the RECPs to moderate soil temperatures played a greater role than soil moisture content in biomass production.

Recently, the Erosion Control Technology Council (ECTC), in conjunction with TRI/Environmental, Inc. (TRI), developed several index and bench-scale tests in an effort to standardize and compare different RECPs in the laboratory (Sprague et al. 2002). One of these test methods is a bench-scale test method for determining the ability of RECPs to encourage seed germination and plant growth. This paper presents the results of a laboratory study that compares the seed germination, plant growth, and biomass production of twelve different RECPs using the ECTC test method. Attempts are made to evaluate the role of different RECPs in producing aboveground biomass.

2. MATERIALS AND METHODS

2.1 Materials

Twelve different RECPs from four different manufacturers were selected for the study. Eight of the RECPs are ECBs, temporary degradable RECPs composed of processed natural or polymer fibers mechanically, structurally, or chemically bound to form a continuous matrix (ECTC 2001). W1 and W2 are composed of curled wood excelsior fibers with polypropylene (PP) netting on the top and bottom. WS1 is composed of 92% wood and 8% crimped, interlocking PP fibers with photodegradable PP netting. S1 is composed of straw fiber, SC1 and SC2 are composed of 70% straw fiber and 30% coconut fiber, and C1 and C2 are composed of coconut fibers, with top and bottom nets. Two of the RECPs are OWTs, temporary, degradable RECPs composed of processed natural or polymer yarns woven into a matrix (ECTC 2001). C3 is composed of woven coconut fiber and J1 is composed of woven jute fiber. Two of the RECPs are TRMs, long-term non-degradable RECPs composed of UV-stabilized, non-degradable, synthetic fibers, nettings, and/or filaments processed into 3-D reinforcement matrices (ECTC 2001). T1 is composed of a synthetic netting with a coconut matrix and T2 is composed of a synthetic netting with a PP matrix. A summary of the RECPs and their basic physical properties, as given by the manufacturer, is given in Table 1.

Table 1. RECPs used in this study and their basic physical properties, as given by the manufacturer

RECP	Structure	Fiber	Mass/Area (g/m^2)	Thickness (mm)	Water Holding Capacity (%)	Light Penetration (%)
W1	ECB	Wood	407	9.14	243	50
W2	ECB	Wood	635	14.7	172	22
WS1	ECB	Wood/PP	293	NA	814	59
S1	ECB	Straw	255	8.13	327	11
SC1	ECB	Straw/Coconut	288	7.87	415	4.8
SC2	ECB	Straw/Coconut	391	8.64	200	11.7
C1	ECB	Coconut	282	7.11	317	17.1
C2	ECB	Coconut	271	8.89	110	16.7
C3	OWT	Coconut	700	NA	NA	50
J1	OWT	Jute	499	NA	NA	60-65
T1	TRM	Coconut	429	17.0	NA	9.0
T2	TRM	PP	727	19.3	NA	16

2.2 Vegetation Enhancement Testing

Vegetation enhancement testing was performed in accordance with ECTC Test Method 4, the Standard Index Test Method for Determination of RECP Ability to Encourage Seed Germination and Plant Growth Under Bench-Scale Conditions (ECTC 2004).

Equipment. The equipment used for the testing was designed and constructed at Syracuse University to meet the requirements of ECTC (2004). The testing containers consisted of 10.2-cm diameter by 10.2-cm high containers. This size was modified from the specified diameter of 20.3-cm to decrease the time required to prepare the containers and the amount of soil required for a test. The total area of the smaller 10.2-cm diameter containers was approximately equal to the required area to be randomly sampled from the larger 20.3-cm diameter containers. A guide with 2.5-cm square openings was used to facilitate the placement of seed and the evaluation of plants.

A moist room used for the storage of soil samples was used for the environmental chamber (see Figure 1). Three light fixtures (American Fluorescent Company, Performance Utility Light, High Light Output, Fluorescent, 234SLESW) with lamps (GE Fluorescent, Kitchen & Bath 40, 3400 lumens) were placed above each group of containers. The base of the lamps was set approximately 30.5 cm above the top of the containers to achieve the specified light requirements (900±100 foot-candles) at the soil/canopy surface. A timer was used to turn the lights off and on every 14 hours. A humidistat (Green Air Products Inc., Total Humidity Controller, THC-1) was used to control the relative humidity (RH) in the room to meet the specified requirements (45%±5%). Temperatures in the room were monitored throughout testing and did not significantly vary from the required temperature ($27^{o}C \pm 2^{o}$).

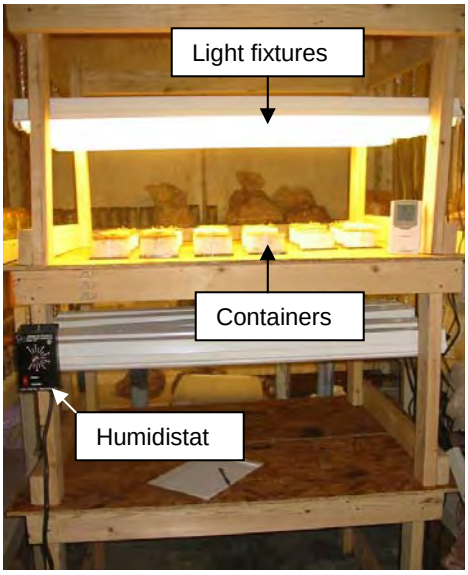

Figure 1. The test setup in the environmental chamber

Materials. Topsoil conforming to ASTM D5268 was used for the tests. The topsoil was classified as a silty sand (SM), in accordance with the Unified Soil Classification System (USCS), and had a soil organic content of 4.66, based on the Loss-On-Ignition (LOI) Method (Nelson and Sommers 1996). Based on ASTM D698, the maximum dry density of the soil was 1670 kg/m^3 at an optimum moisture content of 19.6%.

ECTC (2004) specifies a tall fescue seed mix with 80%±5% of pure live seed (PLS). In this study, certified Kentucky 31 Tall Fescue seed with a PLS of 99.52% was used. ECTC (2004) specifies that each container be sown with 0.50 seeds per cm^2, which equaled 44 seeds or 11 seeds per 2.5-cm quadrant for the 10.2-cm diameter containers. Because of the relatively low germination rates with these tests (between 50% and 75%), the seed rate was doubled so that 22 seeds were sown in each 2.5-cm quadrant for the 10.2-cm diameter containers.

Procedure. In the test, a container is filled level to the surface with topsoil at a moist unit weight of 1360±80 kg/m^3 and moisture content between 35% and 40%. The guide is then placed over the soil to facilitate the sowing of grass seed within each quadrant (see Figure 2a). Once the seed is placed, it is firmly pressed into the soil and covered with a thin layer of soil (see Figure 2b). A thin circular PVC plate (see Figure 2c) is used as a platform so that a circular weight (see Figure 2d) can be used to apply a pressure of 6.9 kPa to compress the seed and the topsoil. A sufficient amount of water is then added to bring the vegetated container to approximately 100% saturation, as evidenced by free water on

the soil surface. The prepared container (see Figure 2e) is then either left bare to be used as a control, or covered with an RECP (see Figure 2f). The container is then placed in the environmental chamber. Each container was watered on days 7 and 14 with a volume of water equal to approximately 1.3 cm over the area of the container, which equaled approximately 102.5 ml.

Figure 2. Steps involved in the preparation of the vegetated containers

The containers were evaluated for plant growth on days 7, 14, and 21. The number of germinated seeds was counted and the lengths of the plants were measured in each quadrant of each container. ECTC (2004) states that the lengths of the plants should be measured by measuring the distance from the table top to the top of the plant, subtracting the height of the soil from the table top. However, this procedure was found to be difficult because of the need to project to different locations across the container. Therefore, measurements were taken from as close to the top of soil as possible, taking into account the thickness of the RECP. At 21 days, the plants were harvested. Root growth was not included in the height or biomass measurements. Only minimal rooting, in the range of a few millimeters, was typically observed. The harvested plants were dried in an oven at 100^{o}C for 24 hours and weighed to obtain a biomass measurement.

Observations. Several observations were made during the test:
1. This method allows for the comparison of the rate of seed germination and plant growth between different RECPs.
2. The test method is time consuming and tedious to set up and evaluate. The smaller 10.2cm diameter containers greatly reduced the time required to set up the test. The guide was also a tremendous help during planting and improving the accuracy of measurements.
3. The evaluation of plant length did not appear to yield results that were significantly different between containers.

4. Attempts were made to normalize the data based on specimen-specific mass per unit area results for each container in comparison to sample roll averages, in accordance with ECTC (2004). The normalization process is used to reduce the variability in the data due to variations in mass per unit area between RECP specimens. However, based on a review of normalized results, it was found that mass per unit area did not play a significant role in the results obtained from the testing. Therefore, actual results are presented.

3. RESULTS AND DISCUSSION

Vegetation enhancement testing was conducted to evaluate the effect of RECPs on the establishment and growth of vegetation. Three containers were tested for each RECP and a total of eight bare soil containers were tested to serve as controls. Bare soil and RECP-covered containers were sown with seeds and evaluated at 7-day, 14-day, and 21-day intervals for number of seeds germinated and plant height, and total biomass at 21 days. Typical photographs of containers at 7-days, 14-days, and 21-days are shown for bare soil conditions and two different RECPs on Figure 3.

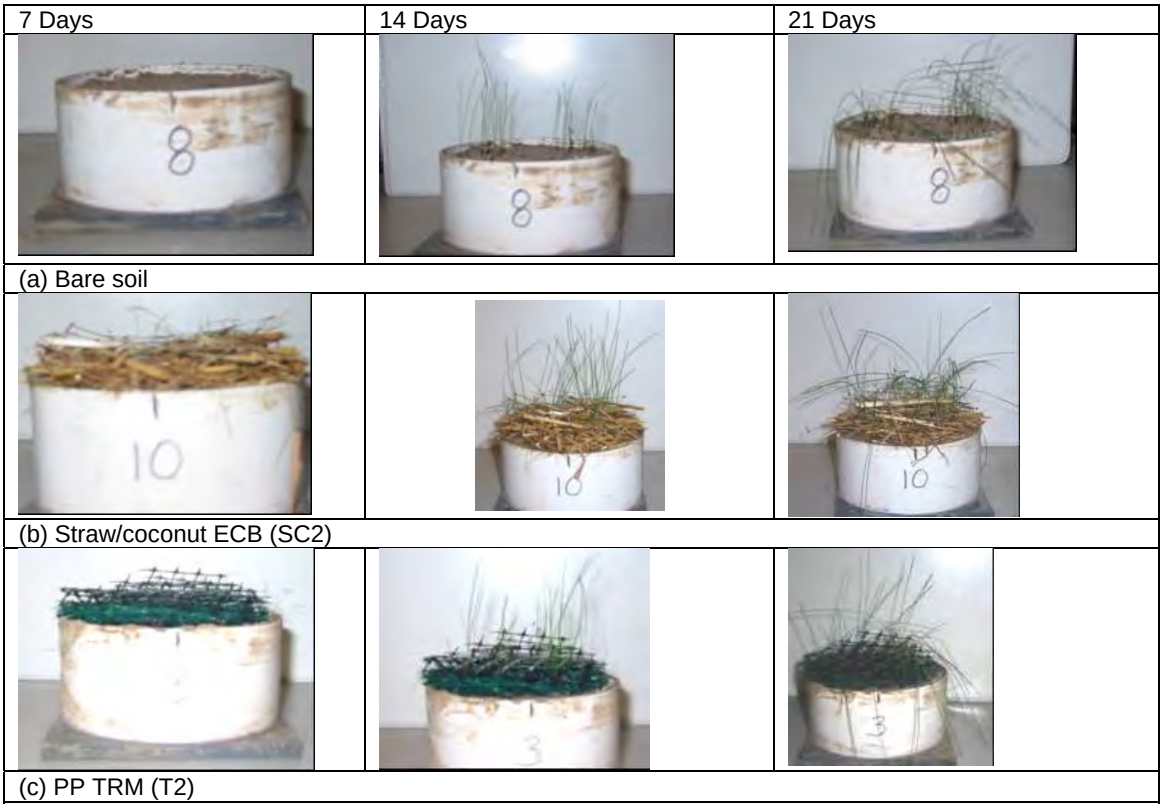

Figure 3. Typical vegetation growth at 7 days, 14 days, and 21 days

A comparison of the range of number of seeds germinated in the RECP-covered and control containers is shown for days 7, 14, and 21 on Figure 4. As shown on Figure 4a, seeds germinated in each RECP-covered container during the first 7 days, but not in the control containers. RECPs C2 (coconut ECB) and SC1 (straw/coconut ECBs) had the best performance, followed by the wood (W2), straw (S1), coconut (C1), and straw/coconut ECBs (SC2) and the coconut (C3) and jute (J1) OWTs. Relatively low seed germination rates were found for the TRMs (T1, T2). It is believed that the netting structure of T1 (coconut) initially prevented the seed from gaining any benefit from the coconut fiber in terms of its ability to moderate soil temperatures, through its moist fibers, or provide moisture to the soil and seed.

As shown on Figure 4b, the numbers of seeds germinated were similar in all of the RECP-covered containers by day 14. Seeds also began to germinate in some of the control containers by day 14, although the numbers were less than in the RECP-covered containers. Increases in seed germination in the RECP-covered containers were also observed at day 21 (see Figure 4c). Modest seed germination increases were observed in only a few control containers at day 21, although to a lower extent than observed in the RECP-covered containers. A few control containers had no seeds germinate at any point during the test. The control plants were also observed to be not as healthy as those in the RECP-covered containers, with the health of vegetation further decreasing by day 21 in the control containers.

Overall, it is believed that the RECPs created more ideal conditions for the germination of seeds in the RECP-covered containers than in the control containers by moderating soil temperatures (in terms of limiting the amount of direct light that reached the seed and through its moist fibers), and by maintaining seed and soil moisture between waterings. Similar observations were made by Sutherland et al. (1998a) and Sutherland et al. (1998b). RECPs play an important role in enhancing the germination of seed during the first 7 days after planting.

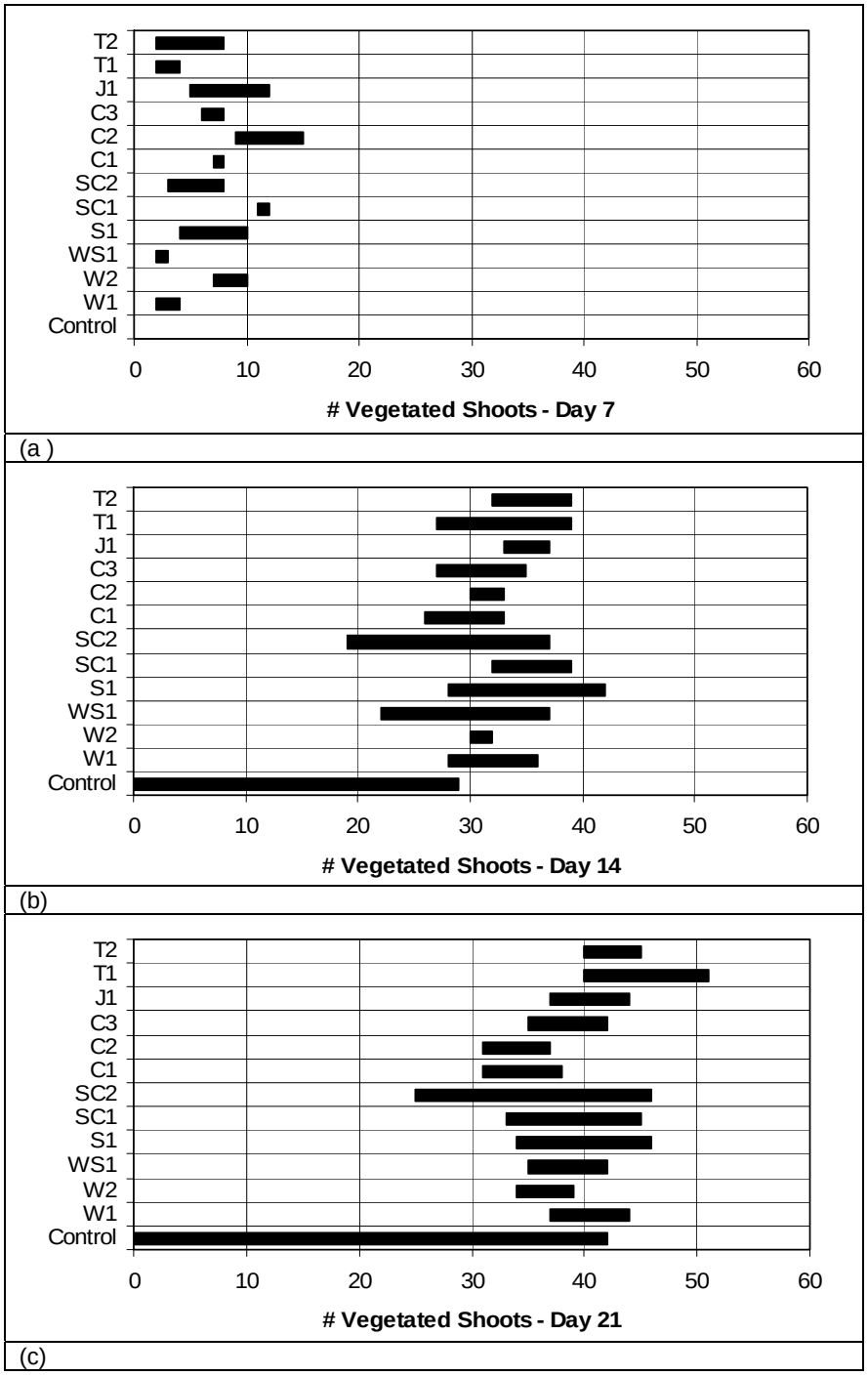

Figure 4. Range of number of seeds germinated

A comparison of the range of plant heights measured in the containers is shown for days 7, 14, and 21 on Figure 5. Similar trends as noted with the number of seeds germinated were found for plant height. For example, a few control

containers had no seeds germinate at any point during the test. Therefore, the range of plant heights for the control containers had a lower limit range of zero. As shown on Figure 5a, a similar range of plant heights was observed for the RECP-covered containers. Plant heights continued to increase by day 14, as shown on Figure 5b. However, by day 14, there was also a wide range in plant height results, possibly due to the comparatively late (later than 7 days) germination of some seeds, and/or to no measureable increases in height for some plant shoots. The relatively wide range of plant height results increased by day 21, as shown on Figure 5c. Overall, plant height varied over a wider range than number of germinated seeds and showed more overlap in results.

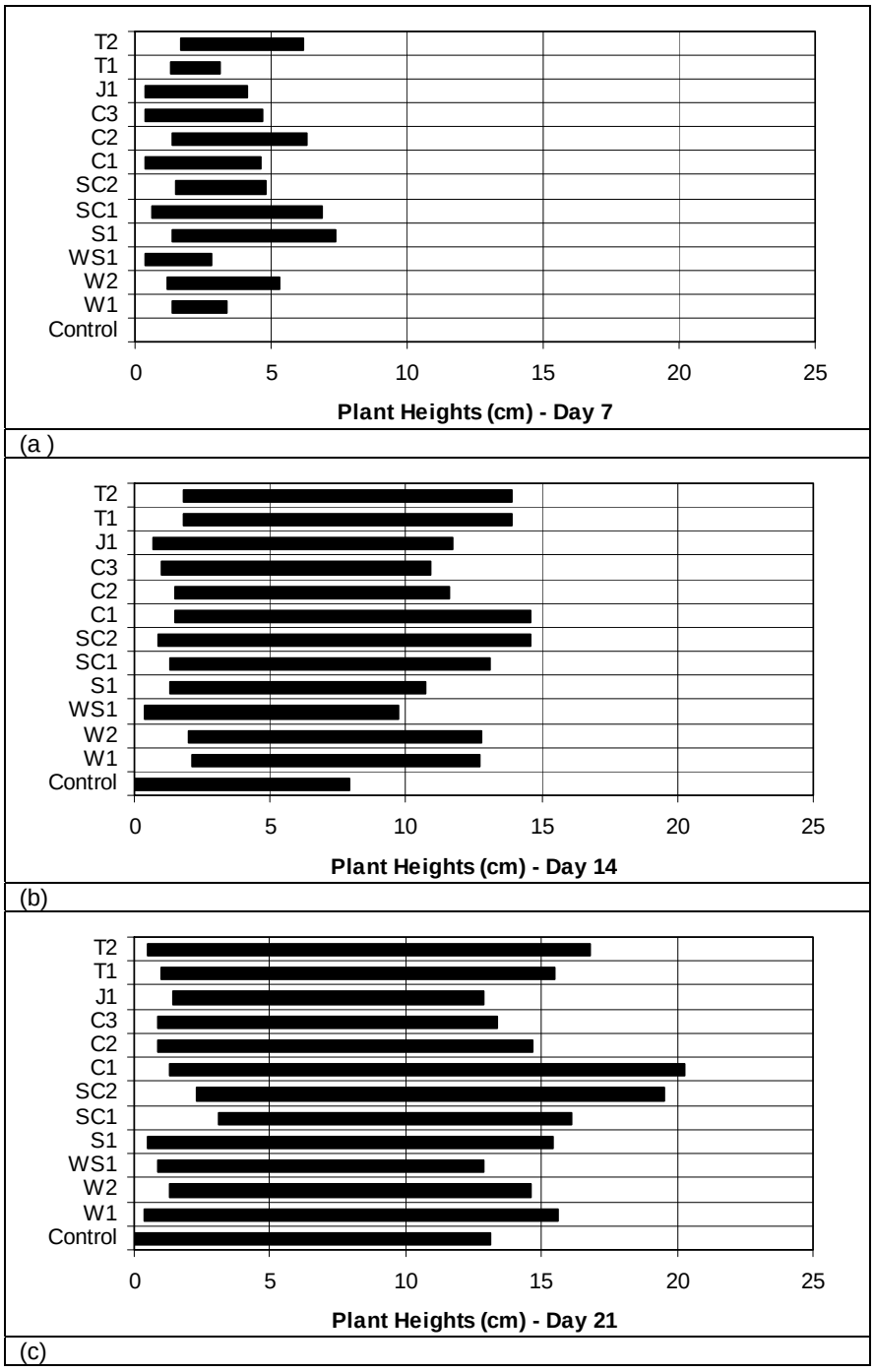

Figure 5. Plant height results

Although the number of seeds germinated and plant height provide valuable information, they do not address the health of the vegetation. For example, the vegetation growing in the control containers was often found to be much thinner and weaker than that growing in the RECP-covered containers. To take the health of the vegetation into account, the vegetation or aboveground biomass (shoots, stems, and leaves) in each container was harvested at 21 days, dried, and weighed to obtain biomass weight.

Average biomass results, along with standard deviations (±1s), are given in Table 2. A comparison of the range of biomass results is given on Figure 6. As shown, biomass production was less for the control containers in comparison to the RECP-covered containers. The RECPs performed similarly in terms of biomass production, with the exception that ECBs SC1 and SC2 (straw/coconut) and OWT J1 (jute) performed more than 1 standard deviation above the average biomass production, and ECB WS1 (wood/PP) and OWT C3 (coconut) performed more than 1 standard deviation less than the average biomass production. There was a moderate degree of scatter for the majority of the RECPs, with J1 (jute OWT) having the largest scatter in results, followed by WS1 (wood/PP ECB) and S1 (straw ECB). There was very little scatter in results for W1 (wood ECB).

Table 2. Average biomass results

RECP	Biomass (mg)
Control	25 ± 21
W1	67 ± 3
W2	60 ± 15
WS1	53 ± 21
S1	55 ± 21
SC1	72 ± 7
SC2	76 ± 18
C1	66 ± 16
C2	57 ± 10
C3	47 ± 9
J1	74 ± 49
T1	67 ± 12
T2	61 ± 13
Average RECP	63 ± 9

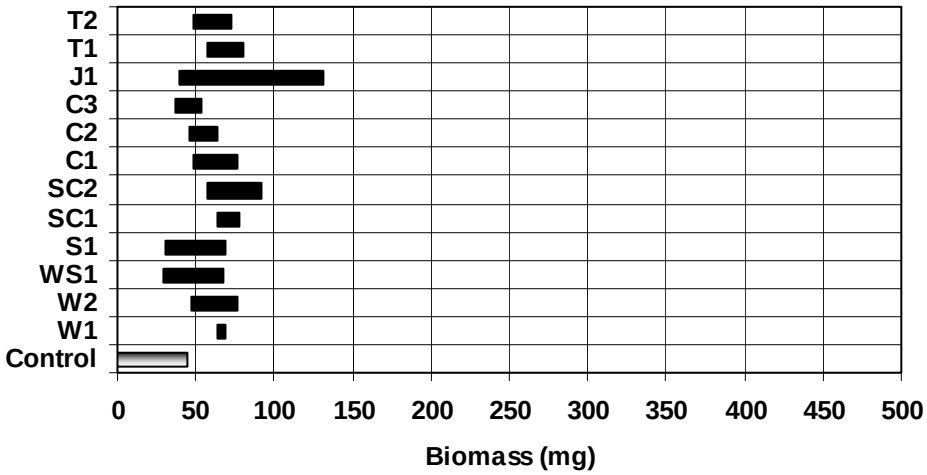

Figure 6. Comparison of the range of biomass results

Although the biomass results showed some differences in the performance of the different types of RECPs, the relatively narrow range of results (between an average of 47 mg and 76 mg) decreased the usefulness of the data in comparing the performance of different RECPs in encouraging vegetative growth. To further evaluate the results, biomass results are compared to results obtained by ECTC (AASHTO 2005) in Figure 7. In comparison with ECTC results, biomass results were similar for the majority of the RECPs tested, with the exception of W2 (wood ECB), S1 (straw ECB), and C1 and C2 (coconut ECBs). The relatively good comparison is surprising because of the number of seeds planted, which were doubled in this study because of the relatively low germination rates. However, the range of data is still in a relatively narrow range (between 46.1 mg and 115.2 mg), making it of limited usefulness in comparing different RECPs.

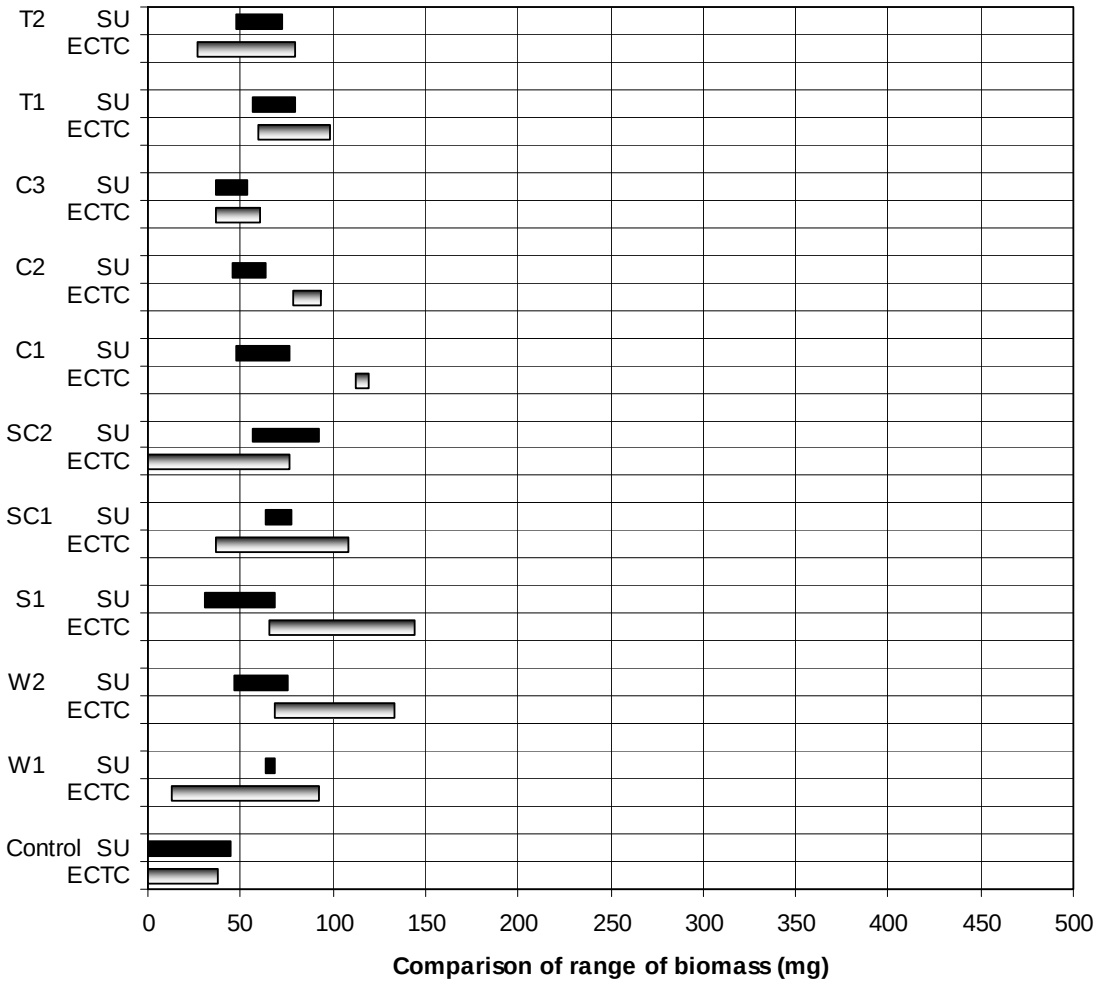

Figure 7. Comparison of the range of biomass results between Syracuse University (SU) and ECTC (AASHTO 2005)

4. CONCLUSION

Field and laboratory studies (Sutherland et al. 1998a, Sutherland et al. 1998b, Smith et al. 2005, Smith and Bhatia 2006) have shown that RECPs vary in their ability to enhance the growth of vegetation. The ECTC method is useful in that it gives an idea as to the ability of an RECP to assist in the germination of seed during the first 7 days. RECPs that were the most successful in germinating seeds during the first 7 days were also the most successful in producing biomass. Although the test does provide some useful information, in its current form, it is limited in its ability to provide an adequate measure to be used for comparing the performance of different RECPs. It is believed that the test could be modified to create harsher conditions (lower humidity ranges and higher temperatures) to provide a greater comparison between different types of RECPs. The current limitations of the test may be that the testing conditions are too conducive to the growth of vegetation for the range of RECP products tested. The test method is also time consuming and tedious. The smaller 10.2-cm diameter containers and the guide greatly reduced the time required to set up and evaluate the test.

5. ACKNOWLEDGEMENTS

The authors would like to thank Mike Davieau for his help with the testing. The authors would also like to acknowledge support received from the National Science Foundation (Award #3535848), the Department of Education (Foreign Language and Area Studies Fellowship in South Asia), and the Syracuse University Graduate School (University Fellowship Award.) The authors would also like to thank Sam Allen and Jarrett Nelson (TRI) for their technical

assistance and Tony Johnson (American Excelsior Company), Bob Moran (Belton Industries), Roy Nelsen (North American Green), and Mark Theisen (Profile Products) for providing materials.

REFERENCES

American Association of State Highway and Transportation Officials (AASHTO) (2005). Laboratory Evaluations of RECPs, *AASHTO's 2004 NTPEP Report Series, Report 12001.3*.

Erosion Control Technology Council (ECTC) (2001). Standard Terminology for RECPs, http://www.ectc.org/guide/chap3.htm> (July 24, 2004).

ECTC (2004). Standard Index Test Method for Determination of RECP Ability to Encourage Seed Germination and Plant Growth Under Bench-Scale Conditions, Approved June 2004.

Evans, R. (1980). Mechanics of Water Erosion and Their Spatial and Temporal Controls: An Empirical Viewpoint, *Soil Erosion*, edited by M.J. Kirkby and R.P.C. Morgan, Wiley.

Fifield, J.S. (1992). How Effective are Erosion Control Products in Assisting with Dry Land Grass Establishment with No Irrigation?, *The Environment is our Future: Proc. Conf. XXIII*, IECA, Reno, NV, 321-333.

Fifield, J.S., Malnor, L.K., Richter, B and Dezman, L.E. (1988). Field Testing Erosion Control Products to Control Sediment and to Establish Dryland Grasses Under Arid Conditions, *Erosion Control - Stay in Tune: Proceedings of XIX IECA Annual Conference*, Louisiana, 327-341.

Gray, D.H., and Sotir, R.B. (1996). Biotechnical and Soil Bioengineering Slope Stabilization – A Practical Guide for Erosion Control, John Wiley & Sons, Inc., New York.

Industrial Fabrics Association International (IFAI) (2006). Erosion Control Product Data, *Geosynthetics*, 24:6, 125-133.

Krenitsky, E.C., and Carroll, M.J. (1994). Use of Erosion Control Materials to Establish Turf, *Proceedings of Conf. XXV*, IECA, Reno, NV, Feb., 81-90.

Nelson, D.W. and Sommers, L.E. (1996). Total Carbon, Organic Carbon, and Organic Matter, *Methods of Soil Analysis, Part 3, Chemical Methods, Soil Science Society of America Book Sec. 5*, D.L. Sparks (ed.), Wisconsin, 961-1010

Rickson, R.J. and Morgan, R.P.C. (1988). Approaches to Modeling the Effects of Vegetation on Soil Erosion by Water, *Geomorphology in Environmental Planning*, J.M. Hooke, ed., Wiley, Chichester, 51-62.

Smith, J.L., (2007). The Use of Rolled Erosion Control Products (RECPs) for Minimizing Soil Erosion, Ph.D. Dissertation.

Smith, J.L., and Bhatia, S.K. (2006). The Use of Index and Bench-Scale Tests for the Characterization of RECPs, *Proceedings of Eighth International Conference on Geosynthetics*, Yokohama, Japan, 2:741-746.

Smith, J.L., Bryz-Gornia, C.J., Bhatia, S.K., and Walowsky, D. (2005) "A Comparative Study of RECPs: Lab Testing and Field Performance," Proceedings of GeoFrontiers 2005, Austin, Texas.

Smith, J.L., Bhatia, S.K., Lake, D., and Walowsky, D. (2003). Evaluation of Vegetative and Root System Growth Through Different Geosynthetic Rolled Erosion Control Products in a Highway Drainage Channel, *Proceedings of 2003 Canadian Geotechnical Society National Conference*, Winnipeg, Canada.

Sprague, C.J., Carver, C.A., and Allen, S. (2002). Development of RECP Performance Test Methods, *Journal of Geotechnical Testing*, 25:4, 1-10.

Sutherland, R.A., Menard, T., Perry, J.L., and Penn, D.C. (1998a). The Influence of Rolled Erosion Control Systems on Soil Temperature and Surface Albedo: Part I. A Greenhouse Experiment, *Land Degradation & Development*, 9, 159-178.

Sutherland, R.A., Menard, T., and Perry, J.L. (1998b). The Influence of Rolled Erosion Control Systems on Soil Moisture Content and Biomass Production: Part II. A Greenhouse Experiment, *Land Degradation & Development*, 9, 159-178.

Toy, T.J., Foster, G.R., and Renard, K.G. (2002). *Soil Erosion: Processes, Prediction, Measurement, and Control*, Wiley, NY.

Geosynthetics 2009
February 25-27 2009, Salt Lake City, Utah

Construction of Subsurface Natural Treatment System Using Geosynthetics

R.S. Johnson, P.E., G.E., Geosyntec Consultants, San Diego, CA, USA
S-S Yeo, Ph.D., Geosyntec Consultants, San Diego, CA, USA
R. Sundberg, P.E., Irvine Ranch Water District, Irvine, CA, USA

ABSTRACT
The subsurface treatment system field demonstration project is to verify and evaluate the field-scale effectiveness and practicality of the system for removal of selenium from dry weather flows in Peters Canyon Channel located in Irvine, California. The concept of this system is to pass dry-weather flows that are diverted from the channel through the box-type media filter cell. The filter cell with dimensions of 65 m (L) x 14 m (W) x 3 m (H) was constructed using a wide variety of geosynthetics such as geotextile, geomembrane, geocomposite, geonet, and geogrid. The filter cell was constructed by encapsulation of a gravel matrix within geomembrane. Mechanically stabilized earth (MSE) concepts were implemented to construct the vertical walls at perimeter of the rectangular media cell. The filter cell included an extensive amount of both perforated and solid piping that is used to operate the demonstration facility in a variety of configurations.

1. INTRODUCTION

For the last 25 years, water quality in San Diego Creek, located in Orange County, California, has been affected by excessive sediments and nutrient levels, including high concentration of selenium. The California State and U.S. Environmental Protection Agency (USEPA) regulations such as the Clean Water Act required the establishment of limits (i.e., Total Maximum Daily Loads, or TMDL) on the amount of pollutants that can be discharged to Newport Bay. San Diego Creek drains approximately 80 percent of the total area tributary to Newport Bay. Due to this need, the Irvine Ranch Water District (IRWD) has developed a Natural Treatment System (NTS) plan to address regional water quality treatment. The NTS plan includes water quality treatment wetlands at 31 sites distributed throughout the watershed. The plan includes facility adjacent to Peters Canyon Channel that is specifically for removing selenium from dry weather low flows. The selenium TMDL is based on meeting the chronic California Toxics Rule (CTR) criterion of 5 parts per billion (ppb) for protection of aquatic health in dry weather flows. Selenium concentrations in dry weather flows in the Peters Canyon Channel typically range from about 30 to 50 ppb, but can be much higher at groundwater seeps and weep holes.

The concept of subsurface treatment system is to pass dry weather flows that are diverted from Peters Canyon Channel through an organically augmented media filter cell, which is composed of a gravel matrix and is constructed using many categories of geosynthetics. The flows are amended with a carbon source to feed bacteria and create anoxic (oxygen-deficient) conditions in the filter cell. Under these conditions, common forms of selenium (i.e., Selenate and Selenite) are converted into an elemental form of selenium and are encapsulated by bacteria growing on the bed materials (e.g., gravel) in the filter cell. The laboratory column test result of this process is shown in Figure 1.

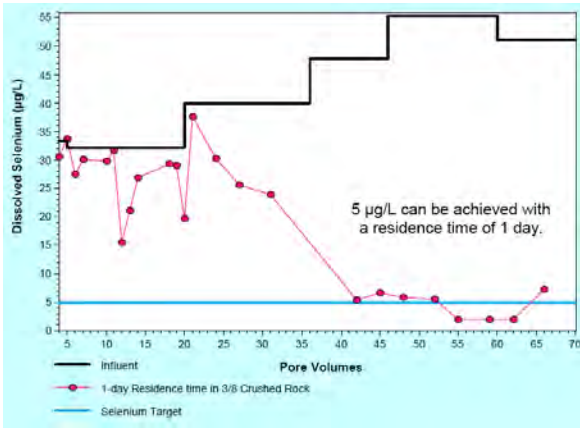

Figure 1. Column test result for selenium concentration decrease

Prior to constructing all of the required filter cells at the site, IRWD decided to install one cell to test and to demonstrate the effectiveness of the proposed treatment technology. This paper focuses on construction of the demonstration filter cell using major types of geosynthetics.

2. SITE INFORMATION

2.1 Site Description

The project site is located near the intersection of Harvard Avenue and Barranca Parkway at Peters Canyon Channel, upstream from the confluence with San Diego Creek in the City of Irvine, California. The site occupies approximately four acres and is an undeveloped open field historically used for agriculture. Figure 2 is vicinity and an aerial photograph of the project site area.

Figure 2. Vicinity and site location map for the field demonstration

2.2 Geotechnical Investigation

A geotechnical investigation was performed using field and laboratory testing. The subsurface condition consists mainly of a massive, firm to very stiff lean clay of low to medium plasticity. Static groundwater was encountered during the geotechnical exploration and was located at 4.2 m (13.6 ft) below ground surface (bgs), which is below the bottom of the designed filter cell. The summary of soil properties measured during the geotechnical investigation is summarized in Table 1. The function of the filter cell required very low loss of water to the adjacent soil. Although the soil has a relatively low permeability, a geomembrane encapsulation was selected to provide a closed environment and isolation from possible chemical interaction with the adjacent soil. The geomembrane also allowed for a means of collecting the gases generated during the filter cell operation.

Table1. Summary of geotechnical investigation

Characteristics	Standard	Value
Dry density	ASTM D 2937	1.7 g/cm^3 (106.3 lb/ft^3)
Maximum dry density	ASTM D 1557	1.9 g/cm^3 (116.5 lb/ft^3)
Optimum moisture content (%)	ASTM D 1557	13
Hydraulic conductivity (cm/sec)	ASTM D 5084	4.5 x 10^{-9}
Soil Classification	ASTM D 2488	CL

2.3 Hydrologic Design Consideration

The required ten filter cells were designed to treat between 8.5 x 10^{-2} to 1.4x 10^{-1} m^3/sec (3 to 5 cubic feet per second (cfs)), which means under dry weather flows and specifically address selenium TMDL concerns. Therefore, the filter cells would not operate during, or immediately after storm events, when flows in Peters Canyon Channel have elevated levels of sediment and/or suspended solids. The design flow range for one demonstration filter cell would be 7.1 x 10^{-3} to 1.4x 10^{-2} m^3/sec (0.25 to 0.5 cfs) with a general design target of 8.5 x 10^{-2} m^3/sec (0.3 cfs).

3. CONCEPT OF SUBSURFACE TREATMENT SYSTEM

3.1 Treatment System

As shown in Figure 3, the subsurface treatment system consists of three major systems: intake and pre-treatment system, media filter cell, and finished water system. The intake and pre-treatment system includes an intake wet well and pump, self-cleaning strainer, bag filter, and electron donor tank. The filter cell was created using geosynthetics and granular media matrix. The finished water system mainly includes oxygenation system, hydrogen peroxide injection system, and finished water pump

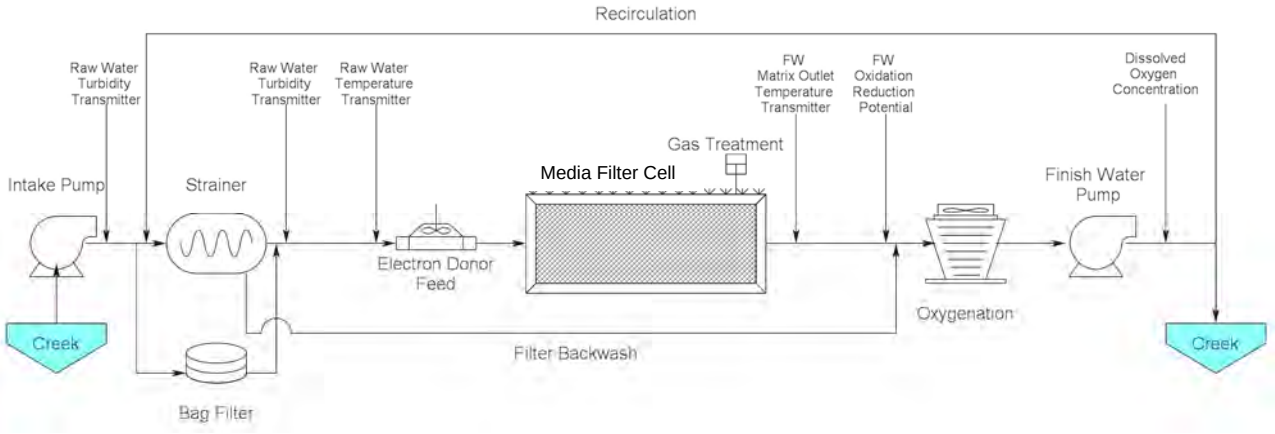

Figure 3. Schematic of subsurface treatment system

3.2 Intake System

The flow water collected using a temporary diversion in Peters Canyon Channel is diverted to the intake pump wetwell. In the wetwell, a pump station provides the necessary lift to supply the treatment system. The water is conveyed using the pump with 100% of the field demonstration design flow (i.e., 8.5 x 10^{-2} m^3/sec (0.3 cfs)). After the pumping, the water flows through a self-cleaning strainer installed on the discharge side of the intake wetwell pump to remove solids (e.g., sediment) from the influent water. The bag filter is manually put on line in lieu of the self-cleaning strainer to periodically gather data on particle size of the raw water.

The electron donor, a readily biodegradable organic liquid chemical, is pumped into the raw water stream to promote microbial growth and regulate the oxidation reduction potential within the filter cell. The rate at which electron donor is pumped into the system is critically important to the operation of the entire system. If the amount of electron donor is too low relative to dissolved oxygen (DO) and nitrate concentrations, then the dissolved selenium will not be reduced. If the amount of electron donor is too high relative to DO and nitrate concentrations then there may be a number of undesirable effects, including higher electron donor costs, hydrogen sulfide and methane gas generation, and incomplete biodegradation of electron donor leading to a high concentration of total organic carbon (TOC) in the effluent.

3.3 Media Filter Cell

The filter cell is the primary treatment component of this project. The filter cell consists of a coarse inert aggregate bed wrapped in an impermeable geosynthetic system. Raw water is pumped from Peters Canyon Channel, amended with electron donor, and injected into the filter cell through a piped header system. Within the filter cell, an active biofilm is grown which attaches to the aggregate. The biological activity helps to create anoxic conditions that are favorable for the conversion of soluble selenium compounds to insoluble colloids and precipitates. The insoluble selenium precipitates are adsorbed to the biofilm and sequestered within the filter cell. Hydraulic retention time and electron donor feed rate are the variables that can be adjusted to maintain the desired environmental conditions. A summary of the filter cell characteristics are presented in Table 2.

Table 2. Summary of Filter Cell Characteristics

Characteristics	SI Unit	English Unit
Length	61 m	200 ft
Width	12 m	40 ft
Depth	3 m	10 ft
Media	¾ minus crushed aggregate	¾ minus crushed aggregate
Volume of Media	2265 m^3	80,000 ft^3
Estimated Effective Porosity	23 %	23 %
Estimated Liquid Capacity	521 m^3	18,400 ft^3
Design Flow	8.5×10^{-3} m^3/sec	0.3 cfs
Containment	Geomembrane composite	Geomembrane composite

3.4 Finished Water System

Since the effluent from the filter cell may be anoxic, an oxygenation system is required to bring the dissolved oxygen (DO) concentration up to an acceptable level for discharge into Peters Canyon Channel. A cascade stair-step oxygenation system was installed because of simple maintenance, underground location, enclosed to allow for capture and treatment of gas that may be generated during the process.

The finished water pump supplies the lift required to convey finished process water from the oxygenation system to Peters Canyon Channel. The location of the finished water pump is within the oxygenation system vault. Flow will be controlled to adjust the speed of the finished water pump.

Although the Field Demonstration is not expected to generate noxious gas at concentrations that would be a nuisance, there is the potential for this to occur if too much electron donor is added or the retention time is too long. Therefore, a gas capture and treatment system was installed. The gas collection and treatment system is included as a precaution to capture and treat H_2S that may accumulate in the filter cell, finished water wetwell and oxygenation system.

4. DESIGN AND CONSTRUCTION OF MEDIA FILTER CELL

4.1 Design and Construction Activities

Construction of the project commenced in August 2007. In summary, construction activities consisted of installing an infiltration gallery in the Peters Canyon Channel, the subsurface filter cell, a process area (pump and equipment housing), and a re-oxygenation system. The filter cell was constructed using geosynthetics and was covered with 0.9 m to 1.2 m (3 to 4 ft) of native soil to allow for the development of a future possible school athletic field. A cross section of the filter cell is presented in Figure 4. A geosynthetic liner system including high density polyethylene (HDPE) geomembrane was installed to keep the filter cell isolated and impermeable. The geosynthetic liner system is summarized in Table 3 and the details are presented in Figure 5. Geomembrane covers the filter cell and functions as

an impermeable envelope. Geotextile is used to provide both separation and cushion for protection of the geomembrane. Gas generated by bacteria from the filter cell is collected using a geocomposite layer over the top of the cell and removed by gas collection pipes. The extensive piping networks allow for this demonstration cell to be operated in a variety of configurations. Inflows and outflows are facilitated by the use of plenums constructed of matrix media modules. In addition, mechanically stabilized earthen (MSE) walls with biaxial geogrid and welded wire fabric (WWF) were constructed to allow for the perimeter vertical walls and for the filter cell to transition into future treatment cells.

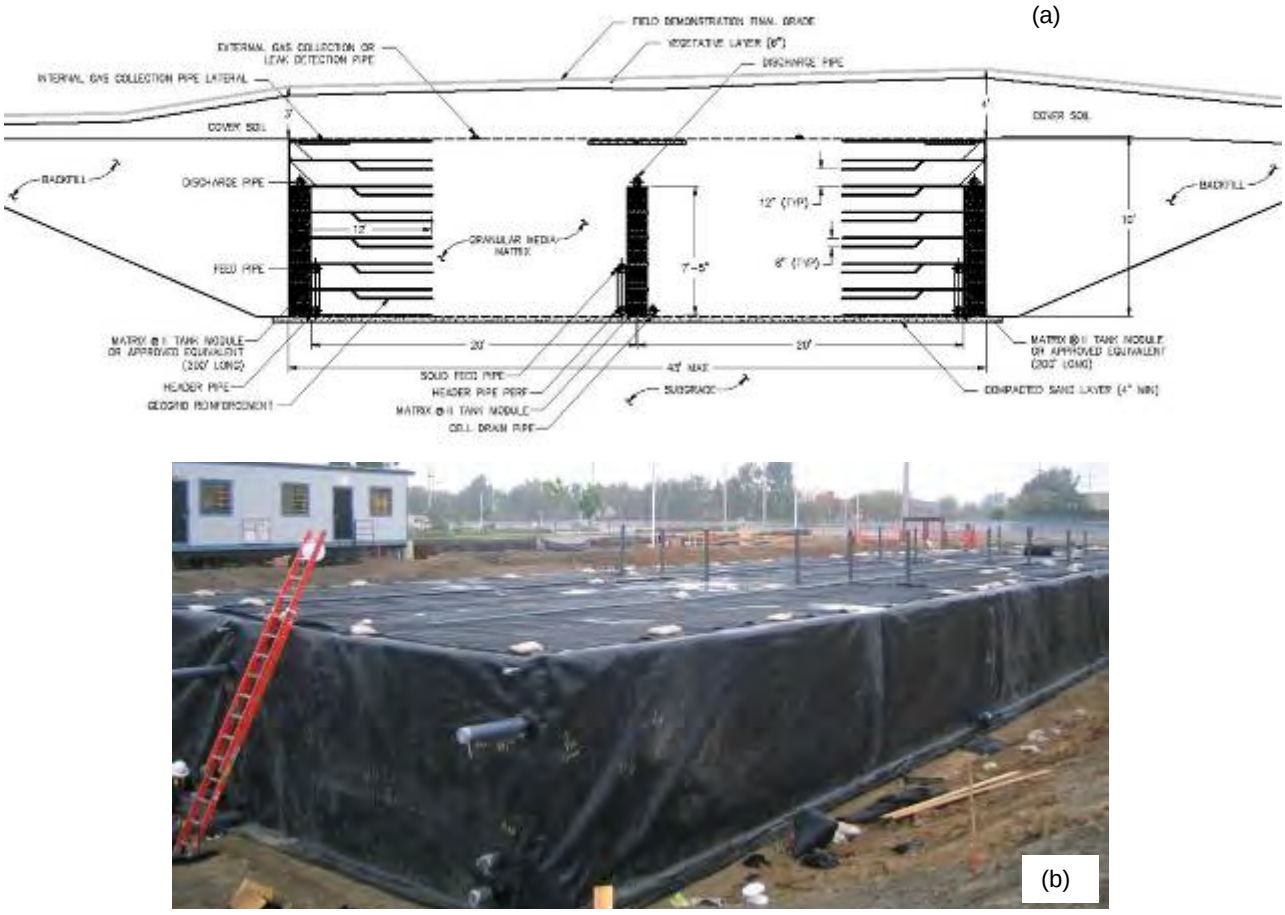

Figure 4. Cross section of the filter cell ((a) construction drawing and (b) photograph during construction)

Table 3. Summary of liner system details onto the filter cell

Location	Liner system detail	Other items
Top liner (from top to bottom, see Figure 5a)	• Top soil including vegetative soil • Geocomposite (geonet sandwiched by geotextile) • Geomembrane (1.0 mm or 40 mil thickness) • Geonet • Geomembrane (1.0 mm or 40 mil thickness) • Geotextile (540 g/m^2 or 16 oz/yd^3) • Granular media matrix (i.e., gravel)	• Perforated pipe was installed for external gas collection on top of geonet. • 18 vertical pipes were installed as monitoring ports
Side wall liner (from inside to outside, see Figure 5b)	• Granular media matrix (i.e., gravel) • Geotextile (540 g/m^2 or 16 oz/yd^3) • Geomembrane (1.0 mm or 40 mil thickness) • Geotextile (540 g/m^2 or 16 oz/yd^3)	• WWF wall units were installed with biaxial geogrid for reinforcement • 12 pipes were installed for inflow, outflow, and gas collection

Bottom liner (from top to bottom)	• Granular media matrix (i.e., gravel) • Geotextile (540 g/m^2 or 16 oz/yd^3) • 60-mil double side textured geomembrane • Geotextile (540 g/m^2 or 16 oz/yd^3) • Compacted sand layer (0.1 m or 4 inches) • Subgrade	-

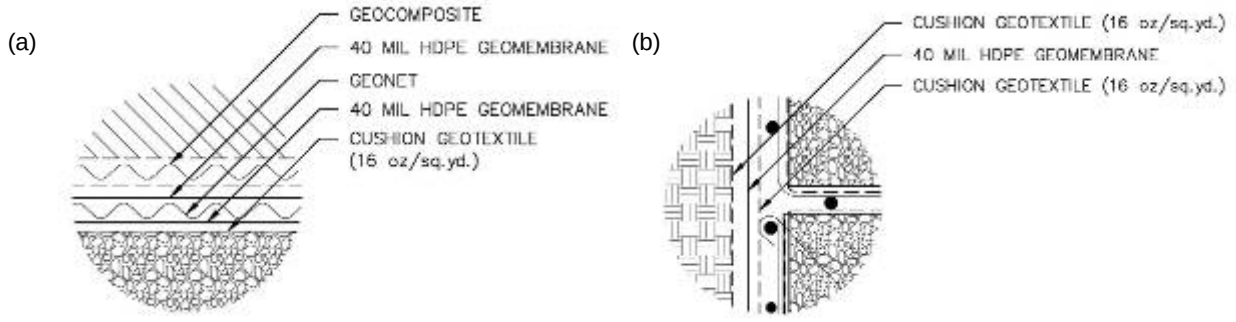

Figure 5. Details of geosynthetic systems: (a) top liner system and (b) liner system on the side

4.2 Practical Significance

4.2.1 Pipe Penetrations

A total of 30 PVC piping penetrations through the liner system of the filter cell were constructed by geosynthetic installer, 18 monitoring ports on top of the filter cell and 12 perforated pipes for inflow, outflow, and gas collection onto the side walls. Pre-manufactured HDPE geomembrane boots were fitted over the PVC perforated pipes and extruded to the geomembrane liner. After the extrusion welding, copper wire spark tests were performed for non-destructive seam testing. In the copper wire spark test, a copper wire is welded into the seam. A probe with a current is passed above the seam with 25 mm (1 inch) distance between the probe and the seam, and any sparks indicate that a hole is present (Sharma and Lewis, 1994). A neoprene gasket and caulking was inserted between the geomembrane boot and PVC geopipe annular space and supported in place with a stainless steel band clamp. The caulking was cured for two to three days after which the stainless steel band clamp was secured to the pipe. After the completion of pipe installation, geotextile was wrapped onto the boot as a cushion material during the backfilling of soil. A design detail and construction pictures of the pipe penetration are presented in Figure 6.

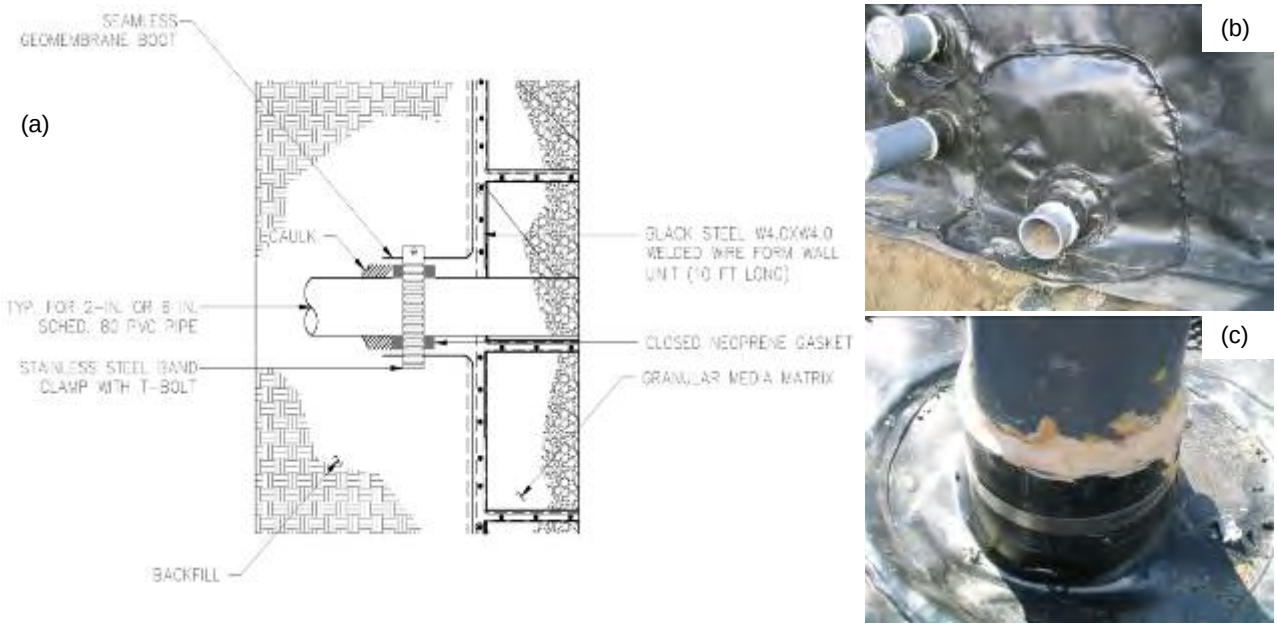

Figure 6. Design and installation of pipe penetrations: (a) design detail for side wall pipe penetration; (b) installation of side wall pipe penetration; and (c) installation of vertical monitoring port

4.2.2 Construction of Side Wall

Geomembrane liner on the side wall is protected by an inside and outside geotextile layer from granular media matrix and backfill. A detail of the vertical side wall is shown in Figure 7(a). The double-track fusion welding was mainly performed for the side wall seaming, as presented in Figure 7(b). The double-track fusion seams were non-destructively tested using the air pressure test (ASTM D 5820) as performed on the top and bottom geomembrane liner systems. Care was taken to fold geomembrane liners at the corners. The folded geomembrane was extrusion welded to the geomembrane liner, as shown in Figure 7(c). Geogrid and WWF were cut to accommodate pipe placement and pipe penetrations were performed with fitted pre-manufactured geomembrane boots as discussed in Section 4.2.1 and as shown in Figure 7(d)

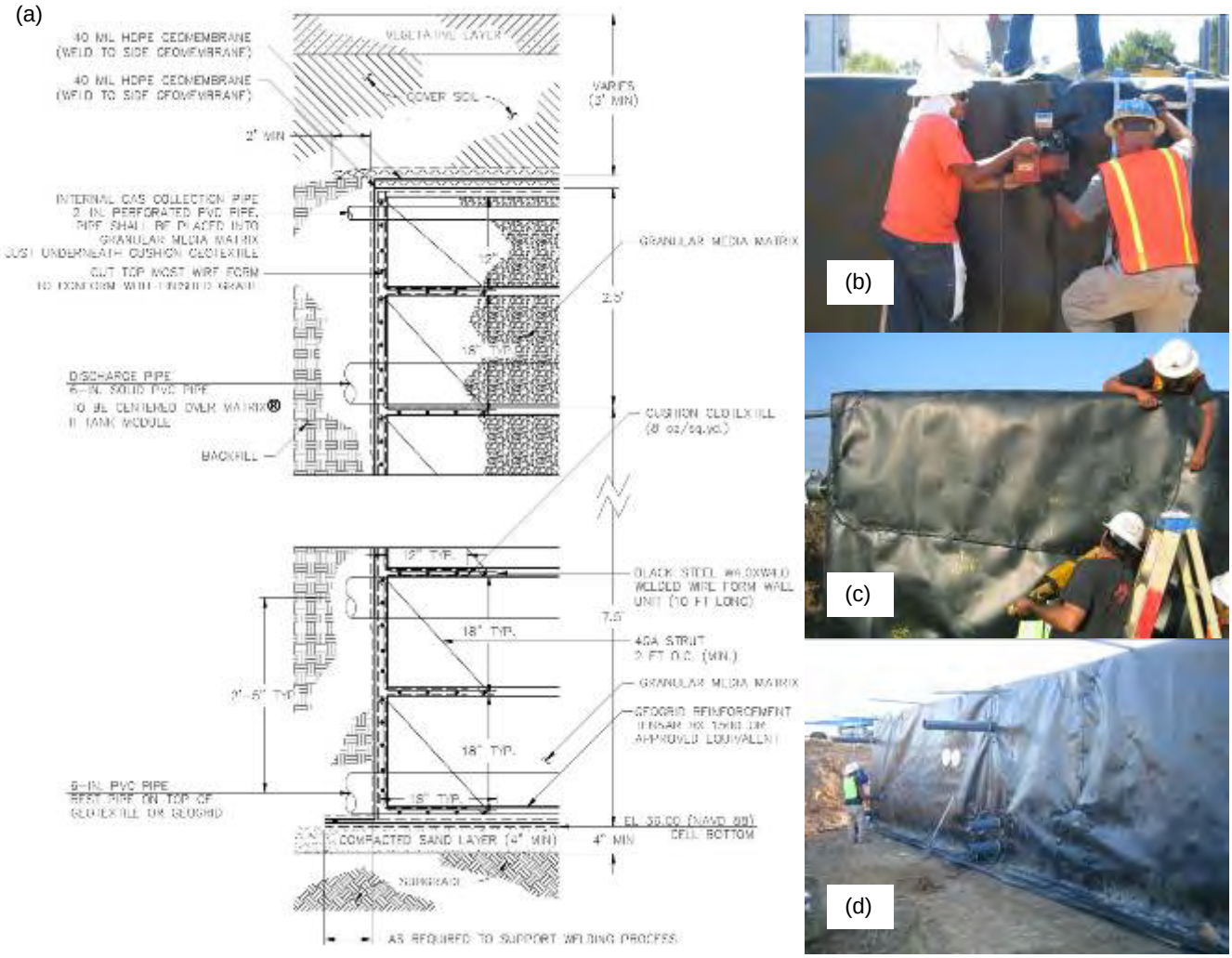

Figure 7. Side wall design detail and construction: (a) design of a side wall; (b) photo of fusion welding on a side wall; (c) extrusion welding for a folding part on a side wall; (d) construction of a side wall

4.2.3 Geomembrane Welding

Two different types of HDPE geomembrane (40-mil smooth geomembrane and 60-mil textured geomembrane) were welded together using extrusion welding techniques, as shown in Figure 8. The extrusion welds were tested with the vacuum test method (ASTM D5641). The test results indicated that these two products could be satisfactorily welded using this technique.

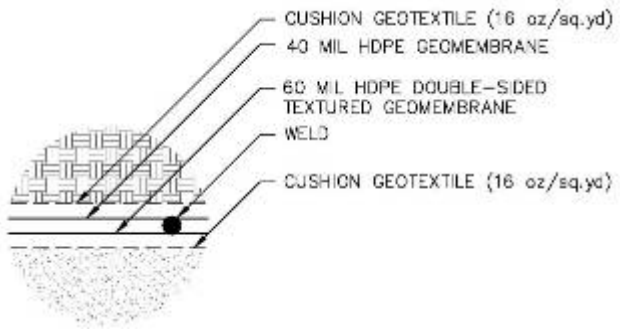

Figure 8. Details of welding with smooth 40-mil and textured 60-mil geomembranes

4.3 Construction Completion of Filter Cell

Construction of the filter cell was performed and was substantially completed in November 2007. The construction sequence was as follows: 1. subgrade preparation (Figure 9(a)), 2. granular media matrix (Figure 9(b)), 3. filter cell wall construction (Figure 9(c)), 4. geosynthetic installation (Figure 9(d)), 5. piping (Figure 9(e)), and 6. backfilling (Figure 9(f)).

Figure 9. Construction procedure of the filter cell

4.4 Trouble Shooting

After the construction completion, a leak was detected during start-up testing of the filter cell. An investigation was conducted to evaluate the source(s) of the leak. A tear was found on the perimiter of sleeve of a liner boot at the west side of the filter cell and was repaired using extrusion welding. In addition, more stainless steel band clamps were added to the pipe penetrations at the east and west sides of the filter cell. Based on the repair process, a time-history leakage rate plot illustrating the leakage rates of the filter cell with respect to the time of the repairs is presented in Figure 10. The plot is complied with the data from Giroud and Bonaparte (1989 (a), (b)). The leakage rate thresholds for large and small holes, included in Figure 10, are based on larger scale applications of liner such as waste containment system and surface ponds. The filter cell is a more complex system than a landfill liner due to the vertical welds and numerous pipe penetrations. The likelihood of holes or perforations in this complex system is much greater than a landfill lining system. The data shows that the leakage rates were significantly reduced after repairs to the liner.

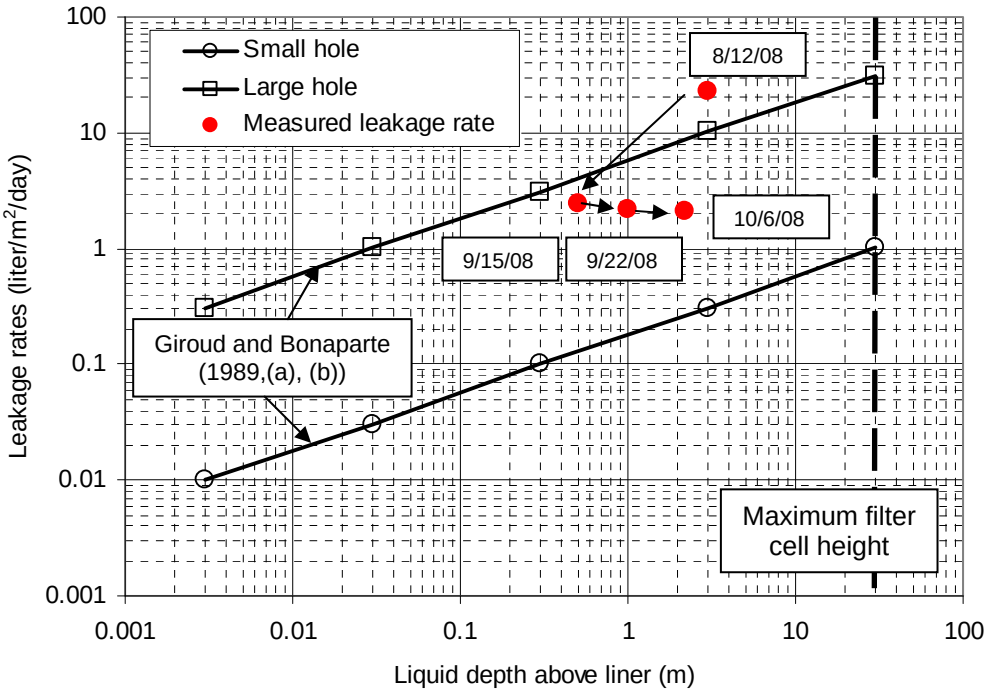

Figure 10. Decrease in leakage rate (8/12/08 to 9/15/08: tear repairs at the west end; 9/15/08 to 10/6/08: clamp repairs)

5. SUMMARY AND CONCLUSIONS

Design and construction of the subsurface NTS was performed using nearly all major categories of geosynthetic materials. The primary benefits of the geosynthetic materials were the flexibility to accommodate a variety of design configurations and the materials provided a non-reactive barrier for environmental isolation of the filter cell. The greatest challenges of this in-ground geomembrane cell was the large number of pipe penetrations and the challenge of both pipe penetrations and panel seam welding on the vertical surfaces. The abundance and variety of specialized geosynthetics provided the designers with a “tool box” of materials, and thus, the flexibility to develop creative solutions to this challenging environmental issue.

ACKNOWLEDGEMENTS

This project was funded by the Irvine Ranch Water District as part of a Natural Treatment System plan to achieve better water quality. The opportunity of writing and presenting this paper is sincerely appreciated.

REFERENCES

ASTM D 1557. Standard Test Methods for Laboratory Compaction Characteristics of Soil Using Modified Effort (56,000 ft-lbf/ft^3(2,700 kN-m/m^3)), *American Society for Testing and Materials*, West Conshohocken, Pennsylvania, USA.

ASTM D 2488. Standard Practice for Description and Identification of Soils (Visual-Manual Procedure), *American Society for Testing and Materials*, West Conshohocken, Pennsylvania, USA.

ASTM D 2937. Standard Test Method for Density of Soil in Place by the Drive-Cylinder Method, *American Society for Testing and Materials*, West Conshohocken, Pennsylvania, USA.

ASTM D 5084. Standard Test Methods for Measurement of Hydraulic Conductivity of Saturated Porous Materials Using a Flexible Wall Permeameter, *American Society for Testing and Materials*, West Conshohocken, Pennsylvania, USA.

ASTM D 5641. Standard Practice for Geomembrane Seam Evaluation by Vacuum Chamber, *American Society for Testing and Materials*, West Conshohocken, Pennsylvania, USA.

ASTM D 5820. Standard Practice for Pressurized Air Channel Evaluation of Dual Seamed Geomembranes

Sharma, H.D. and Lewis, S.P. (1994). *Waste Containment Systems, Waste Stabilization, and Landfills*, John Wiley & Sons, New York, NY, USA.

Giroud, J.P. and Bonaparte, R. (1989 (a)). Leakage through Liners Constructed with Geomembranes – Part I. Geomembrane Liners, *Geotextiles and Geomembranes*, 8, 27-67.

Giroud, J.P. and Bonaparte, R. (1989 (b)). Leakage through Liners Constructed with Geomembranes – Part II. Composite Liners, *Geotextiles and Geomembranes*, 8, 71-111.

The 22nd Annual GRI

Conference Proceedings

"It's All in the Details"

GRI-22 Conference
at the Salt Palace Convention Center
Salt Lake City, Utah – February 27, 2009

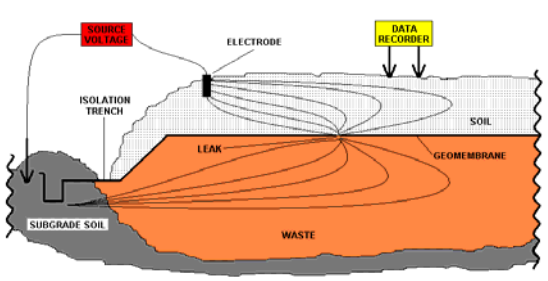

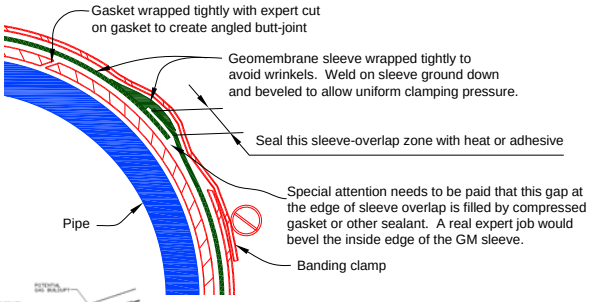

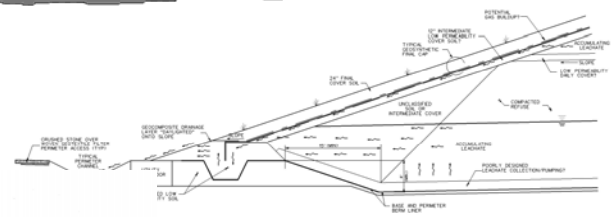

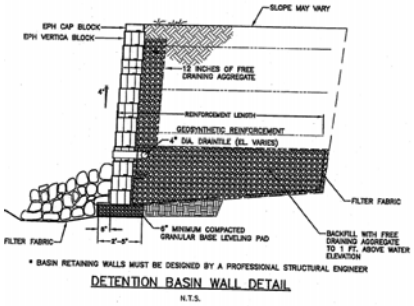

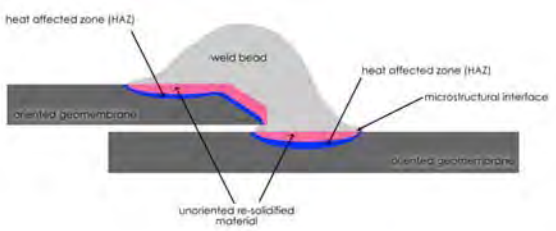

Editors:
Robert M. Koerner
George R. Koerner

GRI
GEI
GII
GSI
GAI
GCI

Y. (Grace) Hsuan
Marilyn V. Ashley

Foreword to the GRI-22 Conference

The Geosynthetic Research Institute (GRI) is the research arm of the Geosynthetic Institute and has organized and hosted annual conferences since 1987. The first conference was one year after the institute's founding on August 12, 1986. As such, it was meant to highlight research conducted internally as well as that of its members insofar as their own in-house R & D activities. The first thirteen conferences were single-theme oriented and thereafter became either 2, 3 or 4 theme events. Having a theme(s) allowed for panel sessions where audience participation in a meaningful and in-depth manner with the speakers was possible. The give-and-take discussions of panel sessions was always a highlight of past GRI-Conferences.

This conference, the twenty-second in the series, is the ultimate in multi-theme topics. In fact, each of the seventeen papers on geosynthetic details are almost completely independent of one another and are only joined together in that each has to do with some aspect of geosynthetics. That said, the individual topics vary tremendously as can be seen in the following summary listing.

- Papers on manufacturing details: (polymer formulations and needle detection)
- Papers on testing details: (textured core thickness, direct shear and transmissivity)
- Papers on field installation procedures: (geomembrane boots and attachments, batten strips, turf reinforcement mat attachments, and drainage geocomposite attachments)
- Papers on field performance issues: (geoelectric surveys, smoke testing, exposed covers, leachate recirculation and segmental retaining wall design and drainage details)
- Papers on totally new devices, concepts and specifications: (profilometers, clay nanoparticle formulations and specification details)

Due to the breadth of the paper topics, audience questions to the speakers will be addressed after each paper is presented.

From a historical perspective it might also be mentioned that the first seventeen GRI conference proceedings were printed and made available to all participants in both soft-bound (at the time of the conference) and hard-bound (shortly after the conference) versions. Beginning with the eighteenth conference proceedings, the papers were only available on CD. This trend, which continues today for all conferences, greatly disturbs the editors (particularly RMK). Retrieval for future reference from traditional printed proceedings in a library is becoming passé. Indeed computer keyword searches are extremely efficient (provided that the indexing and input is accurate and diligent) but the paper must eventually be located, read, and utilized or not as the case may be. We question if citation's are being lost or if accurate literature searches are being conducted. Rest assured at GSI all geosynthetic papers have been downloaded from their original CD's and are available in our library as hard copy!

Conference Organizers and Proceedings Editors
Geosynthetic Institute
475 Kedron Avenue
Folsom, PA 19033 USA

Robert M. Koerner
George R. Koerner
Y. Grace Hsuan
Marilyn V. Ashley

ACKNOWLEDGMENTS

The Geosynthetic Institute (GSI) is an umbrella organization which encompasses all facets of geosynthetic materials. The five sub-institutes focus on research, education, information, accreditation and certification. A conference such as this one contains all of these activities. Clearly, research is being presented. Obviously, the effort is meant to be educational. Additionally, these proceedings form an information outlet which is available to all who are interested. Lastly, all papers directly relate to, or indirectly suggest, the important issues of accreditation and certification.

The institute itself is open to all organizations involved or interested in geosynthetics. This includes government (federal, state and local) agencies, facility owners, designers, consultants, testing laboratories, quality assurance organizations, resin and additive suppliers, manufacturers, manufacturer's representatives, contractors, installers, and research institutes. Recent categories of Affiliated Organizations and Associate Members have been added to facilitate international outreach and to include state regulatory agencies, respectively. Information is available on our Home Page at <www.geosynthetic-institute.org> or from the editors of these proceedings. We wish to acknowledge and thank all of the GSI members and associate members for their support of our endeavors. The current organizations (in the order in which they joined the institute) and their representatives are as follows. Current members of the GSI Board of Directors [BoD] are identified accordingly.

Full Members of the Geosynthetic Institute
GSE Lining Technology, Inc.- *Boyd Ramsey [BoD]*
Earth Tech Consultants, Inc. - *Kevin D. McKeon/Ken Bergschultz*
U.S. Environmental Protection Agency - *David A. Carson*
E. I. duPont de Nemours & Co., Inc. - *John L. Guglielmetti/David W. Timmons*
Federal Highway Administration - *Silas Nichols/Daniel Alzamora*
Golder Associates Inc. - *Mark E. Case/Jeffrey B. Fassett*
Tensar International Corp. - *Joseph Cavanaugh*
Poly-Flex, Inc. - *James Nobert/George Yazdani*
Colbond Geosynthetics - *Joseph Luna/Adrian Dobrat*
Geosyntec Consultants - *Steve Poirier*
Tenax, S.p.A. - *Aigen Zhao/Piergiorgio Recalcati*
LyondellBasell USA, Inc. - *Michael J. Balow/Fabio Caccarani*
TC Nicolon USA - *John Henderson/Chris Lawson*
CETCO - *James T. Olsta*
Huesker, Inc. - *Steven Lothspeich /Dimiter Alexiew*
NAUE GmbH and Co. - *Georg Heerten/Kent von Maubeuge [BoD]*
Propex - *Scott Manning*
STS Consultants - *Jeff Blum/John Trast*
Fiberweb - *Steve Bowlds/William Walmsley*
NTH Consultants, Ltd. - *James J. Parsons/Robert Sabanas*
TRI Environmental Inc. - *Sam R. Allen [BoD]*
U. S. Army Corps of Engineers - *David L. Jaros [BoD]*
Chevron Phillips Co. - *Rex L. Bobsein*
URS Corp. - *John C. Volk*
Solmax Géosynthétiques - *Robert Denis*
EnviroSource, Inc. - *Douglas E. Roberts*

CARPI, Inc. - *Alberto M. Scuero/John A. Wilkes*
Civil & Environmental Consultants, Inc. - *Chris O'Connor*
Agru Americas, Inc. - *Paul W. Barker/Peter Riegl*
Firestone Building Products Co. - *Mark Munley/Paul E. Oliveira [BoD]*
FITI (GSI-Korea) - *Jeongyho Kim/H.-Y. Jeon*
Waste Management Inc. - *Anthony W. Eith [BoD]/Greg Cekander*
NPUST (GSI-Taiwan) - *Chiwan Wayne Hsieh*
GeoTesting Express - *W. Allen Marr/Richard P. Stulgis [BoD]*
GEI Consultants - *Michael A. Yako*
GSE Chile S. A. - *Mauricio Ossa*
Atarfil, S.L. - *Mario Garcia Girones/Emilio Carreras Torres*
Republic Services Inc. - *Clarke M. Lundell*
GSE Europe GmbH - *Stefan Baldauf*
Precision Geosynthetic Laboratories Inc. - *Ronald Belanger/Cora B. Queja*
CETCO Contracting Services - *Archie Filshill*
Raven Industries - *Gary M. Kolbasuk [BoD]*
CTI and Assoc. - *Te-Yang Soong/Steve Wintheiser*
Advanced Earth Sciences - *Kris Khilnani/Suji Somasundaram*
Polytex, Inc. - *Jaime Morales/Elias Jarufe*
Carlisle Syntec, Inc. - *Chris Taylor/Randy Ober*
Ring Industrial Group - *Ben Berteau/Jeffrey Karl*
EPI, The Liner Co. - *Daniel S. Rohe/Mark Wolschon*
Vector Engineering - *Vince Suryasasmita/Richard Thiel*
Weaver Boos Consultants, Inc. - *Mark Sieracke [BoD]*
Aquatan Ply, Ltd. - *Morne Breytenbach/Piet Meyer*
PRS Mediterranean Ltd. - *Arik Nagler*
Jones Edmunds Assoc. Inc. - *Donald E. Hullings*
Intertape Polymer Group (ECP) - *Dohn Berger/Trevor Arthurs*

Affiliated Organizations of the Geosynthetic Institute
GSI Korea (FITI) - *Jeongyho Kim/H.-Y. Jeon*
GSI Taiwan (NPUST) - *Chiwan Wayne Hsieh*

Associate Members of the Geosynthetic Institute
Delaware Solid Waste Authority - *Anne Germain*
Nebraska Department of Environmental Quality - *Gerald Gibson*
New York State Department of Environmental Conservation - *Robert J. Phaneuf*
Maine Department of Environmental Protection - *David E. Burns*
New York State Department of Transportation - *Bob Burnett/James Curtis*
California Water Resources Control Board - *Leslie Graves*
New Jersey Department of Environmental Protection - *Michael Burlingame*
Pennsylvania Department of Environmental Protection - *Steve Socash*
Florida Department of Environmental Protection - *Richard B. Tedder*
U. S. Bureau of Reclamation - *Jay Swihart*
Michigan Department of Environmental Quality - *Xuede (Dan) Qian*
United Kingdom Environment Agency - *Rob Marshall*
Florida Department of Transportation - *Mario Paredes*
National Resource Conservation Service - *Stephen D. Reinsch*
Virginia Department of Environmental Quality - *Donald Brunson*
Massachusetts Department of Environmental Protection - *Paul Emond*

GRI-22 Conference
Salt Palace Convention Center - Salt Lake City, Utah
February 27, 2009

"It's All in the Details"

Needle Prevention, Detection and Removal in Manufacturing Reinforced GCLs

J.T. Olsta, CETCO, USA and M. Phillips, CETCO, USA

ABSTRACT
Geosynthetic clay liners (GCLs) are widely used for containment of liquids or waste in landfills and other applications. For slope stability concerns, if the GCL is placed on slopes then typically a GCL with internal reinforcement is required. North American manufacturers of reinforced GCLs use a needlepunching process. The production of needlepunch-reinforced GCLs sometimes results in the presence of needle fragments during work in progress. There is concern regarding the potential for needle fragments to puncture an overlying geomembrane. This document describes a needle prevention, detection and removal system, which consists not only of metal detectors and magnets, but also includes special operating procedures and a quality management system to ensure that needles in the finished GCL product are minimized to the maximum extent practical.

1. INTRODUCTION

Geosynthetic clay liners (GCLs) are widely used for containment of liquids or waste in landfills and other applications. For slope stability concerns, if the GCL is placed on slopes then typically a GCL with internal reinforcement is required. A common manufacturing practice in North America for internal reinforcement of GCLs is the needle punching process.

2. THE NEEDLEPUNCHING PROCESS

Needlepunching is the process by which loosely laid fibers are entangled to form a continuous nonwoven fabric. A loose layer of fibers is introduced across a needle loom, whose powerful reciprocating motors move a set of needles (often numbering 10,000 or more) mounted on a needle board (Figure 1). Each needle has a barbed shaft which snares fibers on the downstroke and releases them on the upstroke. With thousands of needles moving at hundreds of strokes per minute, the needlepunching process can be used not only for manufacturing geotextiles, but also for reinforcing GCLs. In the GCL manufacturing process a lower geotextile; either woven, nonwoven or woven-nonwoven composite, passes under a hopper. The hopper deposits a layer of bentonite onto the geotextile. A second cap nonwoven geotextile then covers the bentonite and passes through the needle punch loom. Nonwoven fibers from the cap nonwoven geotextile are needle punched through the bentonite clay and the lower geotextile. Significant forces are applied to the needles during this process. A few needles will inevitably break from metal fatigue or entanglement in the geotextiles. While the body of the needle remains in the needle board, a fragment typically ~12 mm long falls onto or is entangled in the GCL.

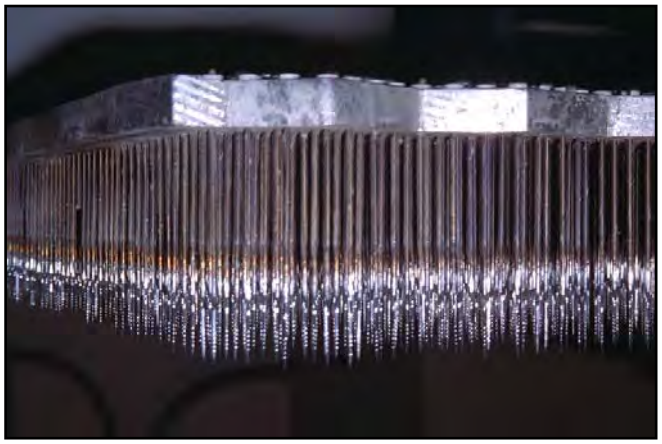

Figure 1. Needle Board

There is a concern regarding the potential for needle fragments from geotextiles and GCLs to puncture a geomembrane that is in contact with the geosynthetic.

3. NEEDLE PREVENTION, DETECTION AND REMOVAL SYSTEM

CETCO's quality assurance plan includes a three-part strategy of prevention, detection and removal. By implementing a variety of procedures relating to the operation of the GCL production line, needle breakage can be largely prevented. At each needle board change the number of broken needles are counted and logged. This data can then be analyzed to determine how factors influence the tendency for needles to break. Modifications to procedures can then control loom maintenance, needle type selection, needle patterns, line speed, stroke rate, stroke depth and other parameters that have been found to have a significant effect. For example, through experimentation, it was found that limiting the stroke depth relative to the GCL reduced the number of broken needles. In a second example, increased frequency of cleaning bentonite from the plates within the loom also reduced the number of broken needles. In a third example, it was found that a certain combination and pattern of needles maximized peel bonding strength while reducing the number of broken needles.

While striving to eliminate breakage, it should be realized that the act of needlepunching through bentonite particles places extreme stress on the needles, and some breakage is inevitable. Therefore, a set of powerful magnets is arranged downstream from the loom, across the width of the GCL (Figure 2). Positioned just above the surface of the geotextiles, the magnets effectively remove most broken needle fragments. Initially, flat magnets were installed. But further experimentation revealed that multiple round magnets were more powerful and effective.

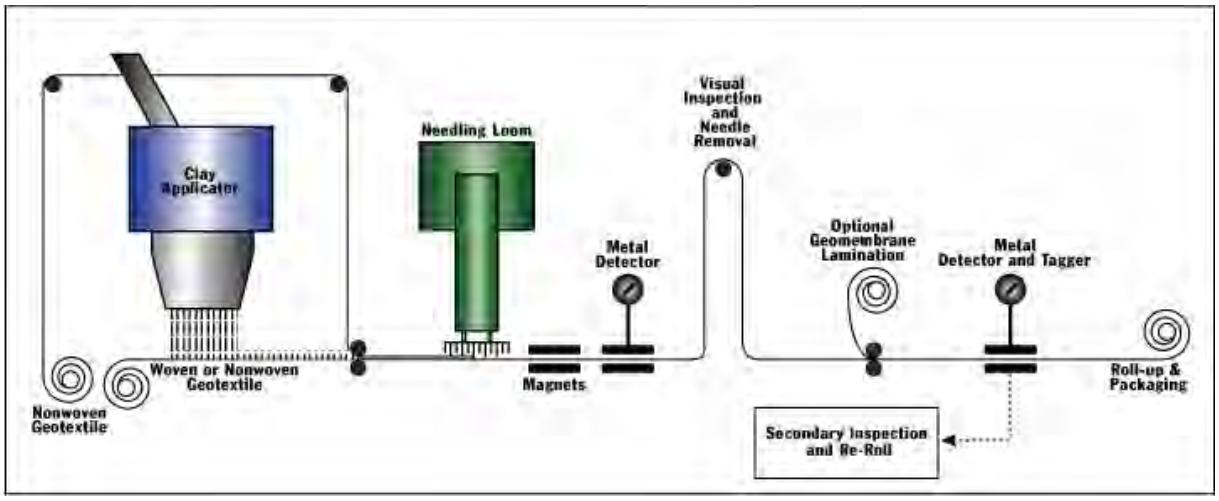

Figure 2. The needlepunched GCL production needle detection and removal system.

Almost all needle fragments are removed by the magnets, but a few do remain in the product and must be detected and removed. Metal detectors are located after the magnets and divide the roll into discrete segments across the roll width. If a needle fragment is detected in one of the segments, then that portion of the GCL on the production line is automatically stopped and a light illuminates the section. A production crewperson stationed on a catwalk then checks for needle fragment(s) in the suspect section (Figure 3). Upstream, the loom continues to operate and that material is collected on a series of accumulator rolls. If the needle is found it is removed with pliers. Then the crewperson resumed movement of that portion of the GCL production line and it passes a second metal detector.

If metal is detected at the second metal detector, a tag is placed on the outside edge of the roll. Flagged rolls are not packaged at end of the line but instead set aside for a secondary off-line detection and removal process. A "re-roll station" is used to unroll the GCL to the spot where the tag was placed. This section of the roll is scanned with a hand-held detector and visually inspected until the needle fragment is found. Protruding needle fragments are removed with pliers and the roll is then completely wound and packaged.

Figure 3. After detection, crewperson on catwalk checks for needle fragment(s).

Occasionally, the crewperson on the catwalk will run out of time when the accumulators have reached capacity. The line resumes movement but the crewperson signals to the roll-up operator to send the roll for secondary inspection even if the second metal detector did not tag the roll.

Initially, analog metal detectors were used. These detectors had several issues. These detectors had to be manually calibrated periodically and were subject to 'noise'. Despite efforts to ground the equipment and move motors away from the detectors some interference persisted. This required at times setting the detectors to a lower sensitivity. Recently both sets of metal detectors were replaced with digital metal detectors. These detectors have data acquisition capability allowing information such as frequency, location and timing of needle detection to be analyzed. The digital metal detectors are automatically self-calibrating. Also, the housing and electronics filter out more noise so the sensitivity can be increased resulting in more accurate detection and fewer false alarms. Fewer false alarms, in turn, give the crewpersons more confidence that a needle is present and keeps them more focused. The sensitivity settings are now locked-out and have restricted access.

In addition, on a weekly basis random rolls are pulled out of inventory and screened on the re-roll station to help verify that the production line metal detection and removal process is effective.

4. CONTINUAL IMPROVEMENT

Another portion of the plan is a quality system that is certified to the International Organization of Standardization (ISO) 9001:2000 standard. A quality management system refers to the activities that a company carries out to satisfy the quality related expectations of its customers. ISO 9001:200 states requirements for quality management systems necessary to demonstrate that a company is capable of effectively meeting customer requirements. As shown in Figure 4, major elements of the system are linked in an iterative process (ISO 2000).

As part of the quality management system, any customer complaints are investigated to determine their root cause. Corrective action measures are then planned and implemented in a timely manner. After the corrective action measures are complete, an internal audit is conducted to verify the effectiveness of the corrective action. Finally, an outside auditor reviews the customer complaints, corrective actions and follow-up. Through this practice and other proactive tasks the goal of continuous improvement in quality is achieved.

A recent customer complaint (the first needle-related customer complaint in three years) highlighted that the human factor, and not just machinery, has to be taken into consideration. The complaint occurred during the peak construction season, when additional shifts are required to keep up with demand. Production logs were

matched to the roll numbers on the complaint investigation and identified that the suspect rolls were produced during the night shift. The following corrective action measures have been implemented. All shifts will be required to have experienced (year-round) personnel at key needle detection and removal locations. Seasonal employees will be given special training designed to increase awareness of the importance of needle detection and removal. Also incentives are being developed for all line personnel, including seasonal employees, which achieve certain quality criteria.

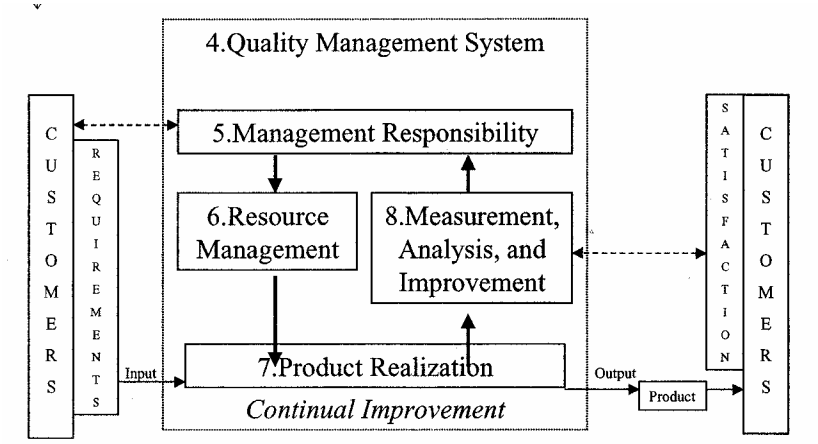

Figue 4. ISO 9001 Process Flow Diagram

5. SUMMARY

In many containment applications reinforced GCLs are required for slope stability. Needle punched GCLs are a common type of reinforced GCL. The needle punch manufacturing process inevitably results in broken needles. There is a concern regarding the potential for needle fragments to puncture a geomembrane in contact with a needle punched GCL. While it is impossible to guarantee that every roll of GCL will be completely needle-free, the implementation of both 1) a needle prevention, detection and removal system, and 2) quality management system results in the best practical quality control of reinforced GCL product.

REFERENCES

ISO (2000), *ISO 9001:2000 Quality management systems – Requirement*, BSI, London, England.

Small Details that Affect Exposed Liner Performance

I. D. Peggs, I-CORP INTERNATIONAL, Inc., Ocean Ridge, FL, USA

ABSTRACT

The influence of small details on the performance of geomembranes is presented. Round die HDPE geomembrane with manufacturing folds placed apex down may stress crack before those placed apex up. Cracking of oxidized PP geomembranes may occur at warp reinforcing yarns before weft yarns. Weld microstructures may include microstructural transition boundaries that act as internal defects. And wires installed for spark testing detail welds, when exposed, can increase the sensitivity of leak detection.

INTRODUCTION

In the early days we sorted out the major details – welding methods, extrusion or chemical welding, fusion or extrusion welding, chemical resistance, expansion/contraction, CCL/GCL, but now we are down to the smaller details, but details that still may have a significant effect on geomembrane performance. The following situations are relevant and will be explained accordingly.

- The two folds in round die extruded HDPE geomembranes.
- Weld cross section microstructures.
- Yarn cross sections in scrim reinforcement.
- Surface die lines.
- Wires installed for seam spark testing.
- Small stone effects.

1. FOLDS

Normally, when evaluated by index test methods, the folds in round die extruded material have little if no adverse effect on the sheet properties. However, in two cases, one in Florida and one in the mid-West they have been seen to be the locations of “premature” cracking failures after about 8 years (Florida) to 15 years (mid-West) of exposed service. Both liners cracked along folds and at other locations such as stones protruding from the subgrade, on patches covering a wrinkled protruding weld burn-through, and alongside extrusion and even fusion welds. All were stress cracks initiated on the exposed surface. The stone protrusion crack (Figure 1), occurred in 2008 and was initiated on an extrusion die line, is a perfect example of a stress crack; straight along its length, straight through the thickness of the geomembrane, and with a ductile fracture at the bottom as the stress in the final ligament rose above the knee in the stress rupture curve (Figure 2).

When examined more closely it was noted that the fold cracks, made up of many small cracks linked together (Figure 3) only occurred on folds with the apex down. No apex-up folds were cracked. At both sites the majority of folds were apex-up. There were also cracks along the edges of extrusion welds in the lower sheet (Figure 4) and in a few fusion welds

Figure 1. Stress cracks on die lines at subgrade stone protrusion.

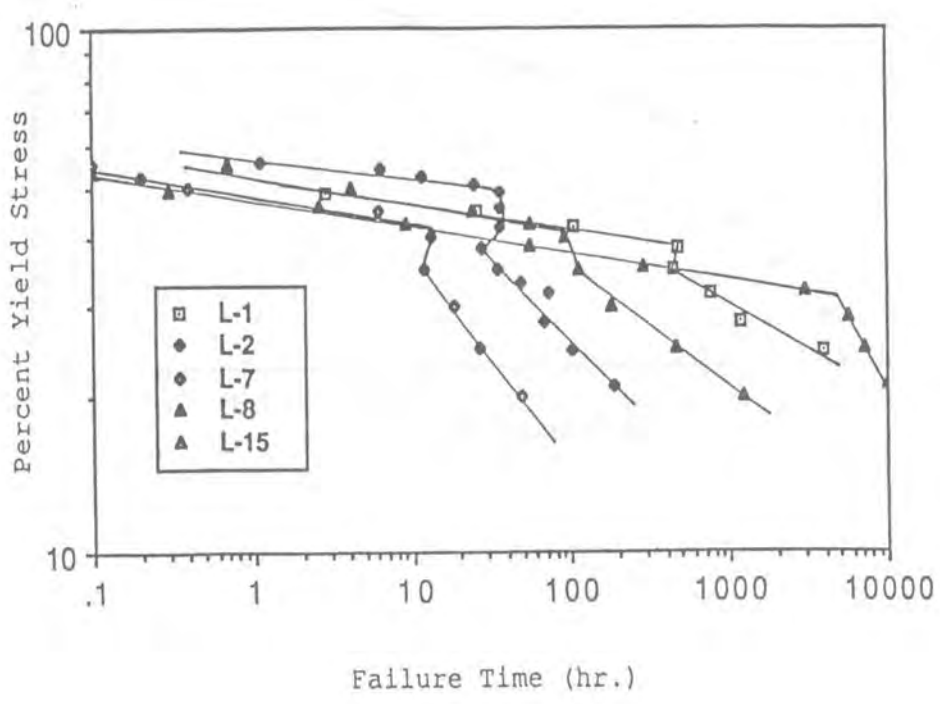

Figure 2. Stress rupture curves for five HDPE geomembranes (Hsuan et al, 1992).

.

Figure 3. Stress cracks in apex-down fold (arrowed).

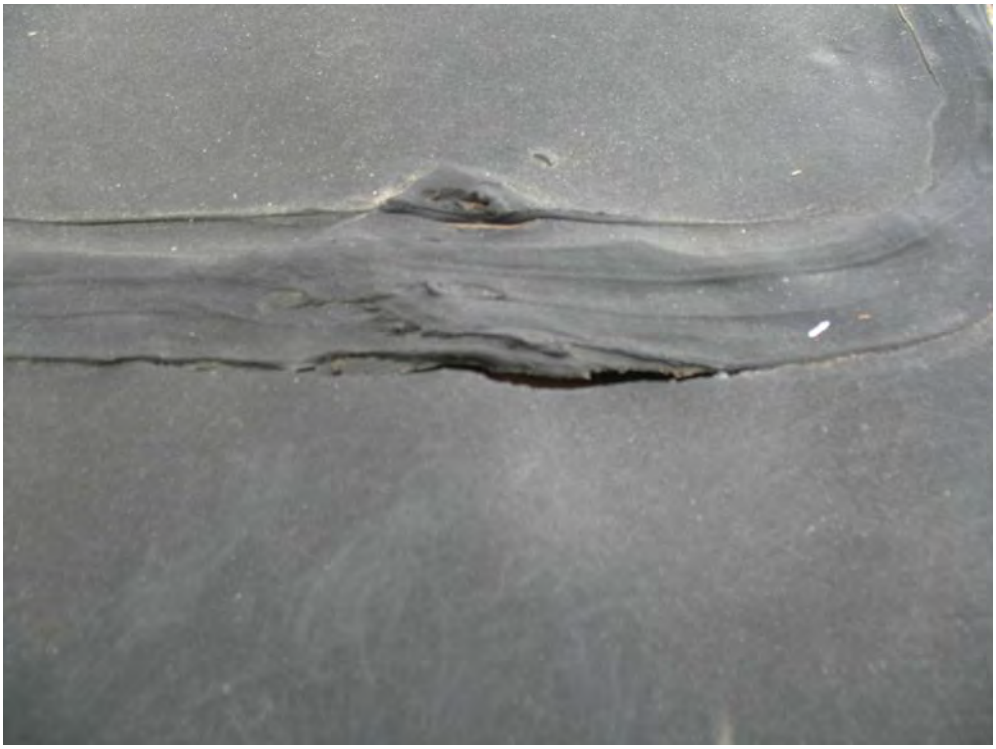

Figure 4. Stress crack (arrowed) along edge of extrusion weld.

When oxidative induction times were measured, and surface carbonyl index determined by FTIR-ATR it was found that while OIT was decreased there was still some AO additive package in the material, but also that significant surface oxidation had occurred. Therefore, it appears that the combination of exposed surface oxidation and tensile stress induced as the liner contracts at low temperatures (and "opens" the fold) reaches the critical level to initiate stress cracking. The many short cracks link together to form longer cracks.

The majority apex-up folds, although oxidized have a compressive, or much lower tensile, stress when they are opened. And the apex-up folds are not oxidized on the underside so cracks are not initiated in the underside surface. So for maximum durability one should install round die geomembrane panels with the folds apex-up.

Both of these specific geomembranes, made by different manufacturers, met NSF 54, manufacturer, and GRI-GM13 specifications at the time of manufacturing and, except for SCR and OIT, at the time of failure. Thus these liners did not prematurely fail, they reached end-of-life (EOL) in the given applications. In other applications they might have lasted longer. And, conversely, HDPE geomembranes made by other manufacturers with different resins and different additive packages might have lasted much longer in the same application. But, how much longer; 1, 15, 40 years?

2. WELD MICROSTRUCTURE

Along the edges of extrusion welds stress cracking typically occurs at an angle of about 15°, not vertically as shown in Figure 5. Why would that be? Figure 6 is a schematic diagram of an extrusion weld cross section.

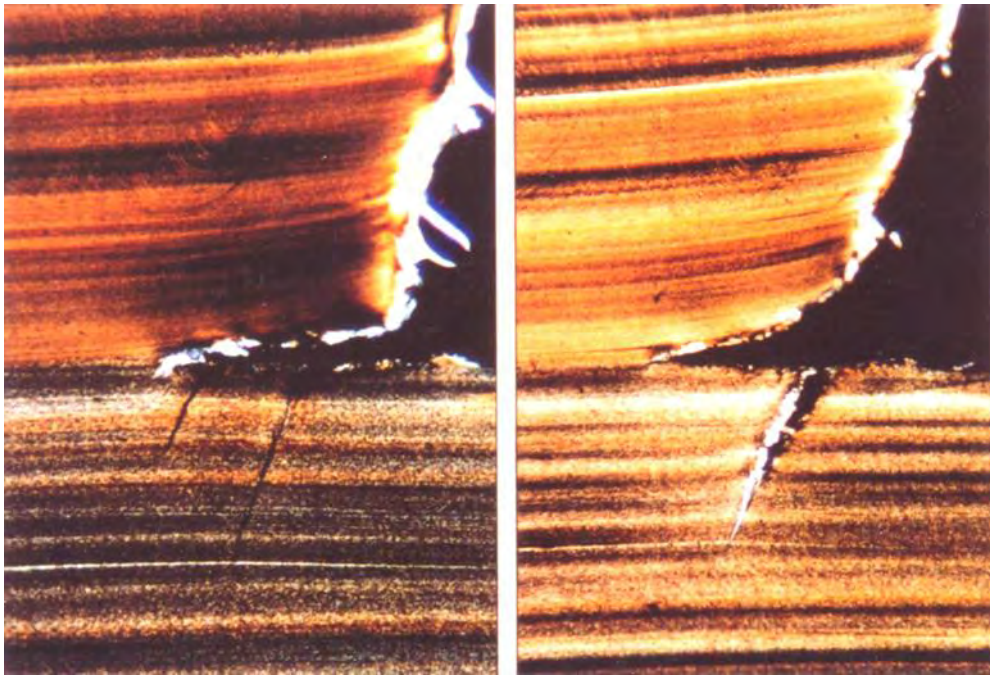

Figure 5. Initial crazing and opened stress crack at edge of weld bead.

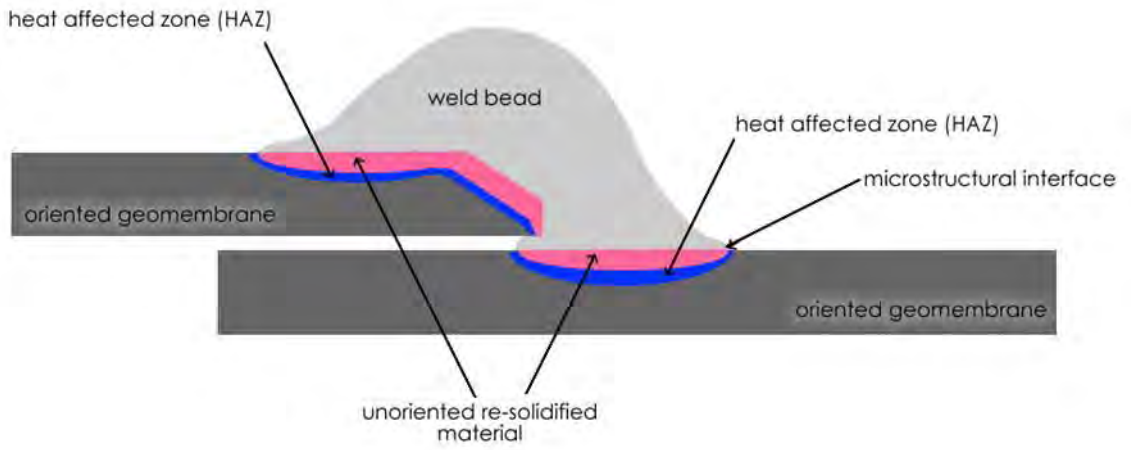

Figure 6. Cross section microstructure of extrusion weld.

When the molten weld bead melts the surface of the bottom sheet it destroys the extrusion-induced oriented microstructure in the plane of the geomembrane. When this molten pool cools and solidifies, having oxidized a little, it does so with a more homogeneous microstructure. In between this unoriented region and the original oriented microstructure there is a heat affected zone (HAZ) of unmelted but heated material in which some small degree of secondary crystallization has occurred. Thus there is a transition boundary between oriented and unoriented material, the sharpness and residual stresses of which are a function of the welding parameters (temperature of material and extrudate, welder speed, and cooling rate). The sharper the boundary (discontinuity) the more likely it is to act as an internal defect at which stress cracking could be initiated.

The same thing occurs in fusion welds but the microstructural gradient and its residual stresses can be controlled by the profile of the wedge edges (sharp-ish corner or rounded) and the application of hot air (annealing). Combined hot-wedge hot-air welds may have some advantage in this respect.

3. SCRIM REINFORCEMENT IN POLYPROPYLENE GEOMEMBRANES

A small feature that has been seen to initiate stress cracking in oxidized reinforced polypropylene (RPP) geomembranes is the difference in cross sectional profiles of warp and weft reinforcing yarns. The higher surface tensile stress in the polymer as it bends around the rounder warp yarns compared to the flatter elliptical weft yarns can make the difference between cracking and no cracking as shown in Figures 7 and 8. It is interesting to note that cracks can occur at 90° to one another in patch and geomembrane. Clearly, the cracks are not initiated by the same principal stress. However in the above polymer, the elliptical yarns soon start to crack (Figure 9). Nevertheless this further demonstrates the synergism of oxidation and stress in accelerating failure and provides fine-tuning possibilities for optimizing geomembrane service lifetimes.

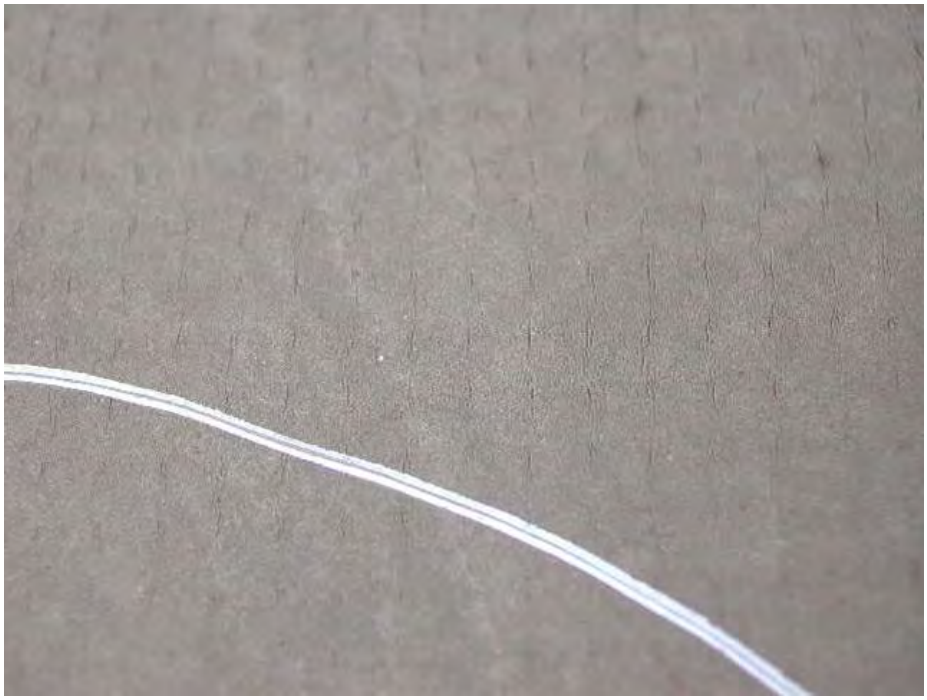

Figure 7. Stress cracking in reinforced polypropylene yarns.

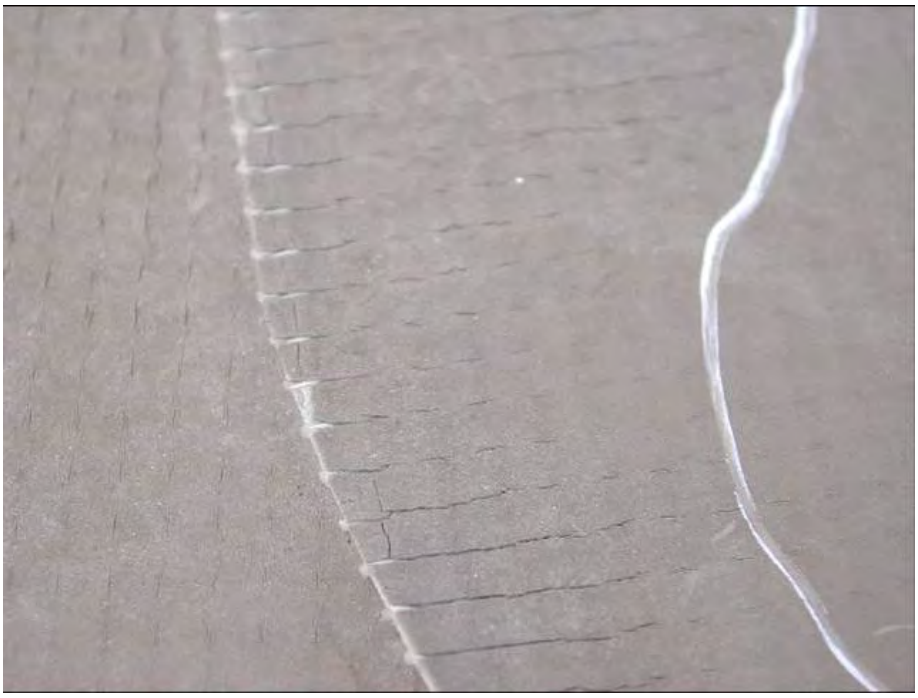

Figure 8. Stress cracking above warp yarns oriented at 90° in liner and patch.

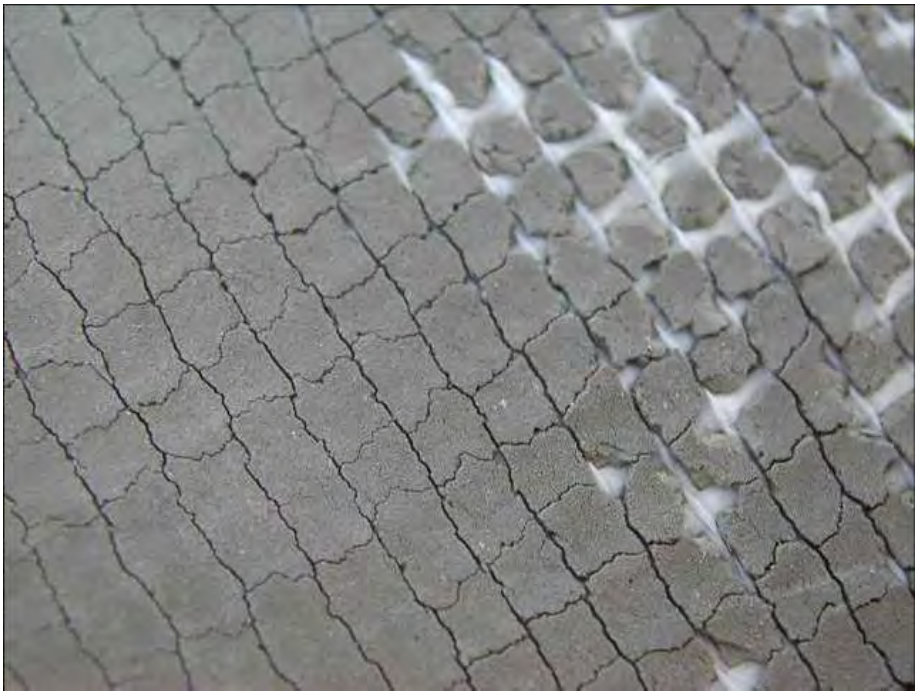

Figure 9. Stress cracking above both warp (vertical) and weft (horizontal) yarns.

4. OIT AND SURFACE CARBONYL INDEX

When HP-OIT is measured a specimen is typically stamped through the thickness of a geomembrane sample, or a plaque is made from small pieces of the geomembrane and a specimen is stamped from the plaque. In both cases material through the full thickness of the geomembrane is tested. Therefore, the HP-OIT evaluates the AO additive through the full thickness of the geomembrane. It is then assumed that at any test result over zero there is still oxidation protection available to the geomembrane. This may not be the case. Oxidation is a surface effect and will consume additives on the surface first, therefore oxidizing the surface first, as demonstrated by many of the failures in reinforced polypropylene floating covers (Peggs, 2008). To determine whether or not surface oxidation has, in fact, occurred the attenuated total reflectance (ATR) method of Fourier Transform InfraRed spectroscopy (FTIR) can be performed on the surface in order to assess the carbonyl products of oxidation; note the peak at 1740 cm^{-1} wave number in Figure 10.

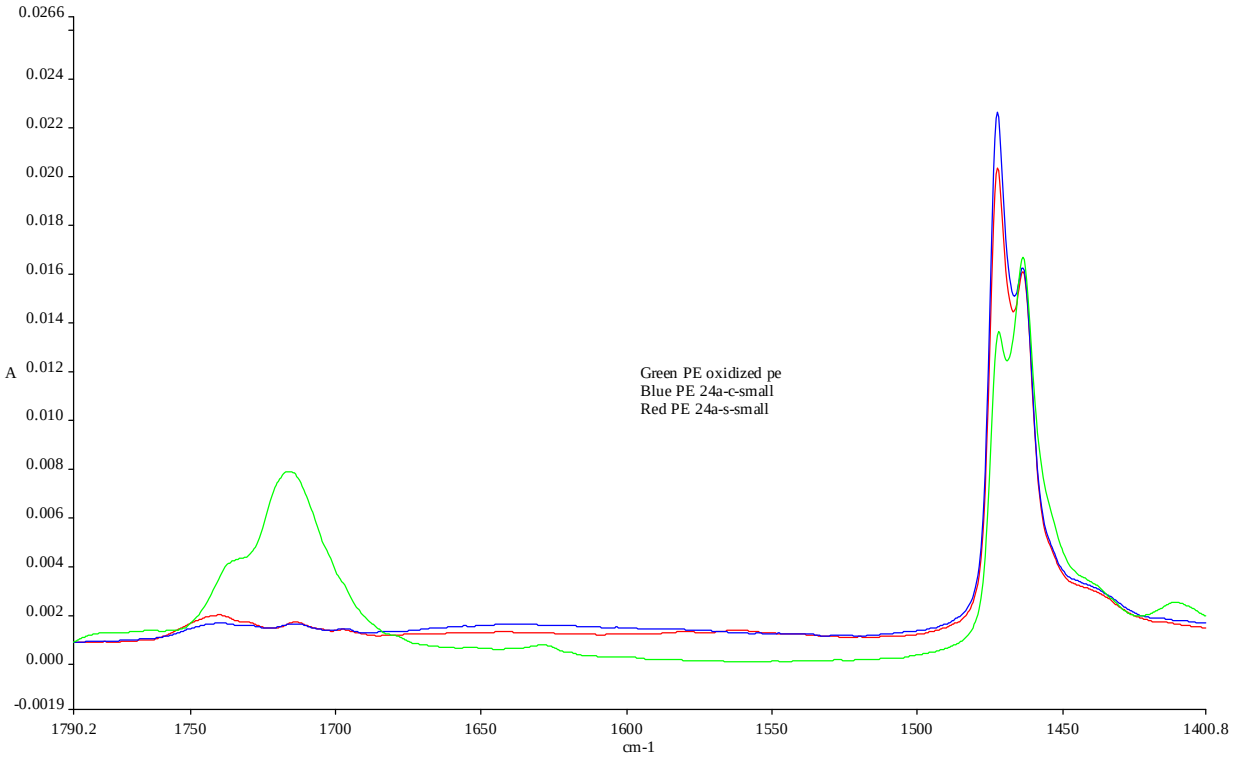

Figure 10. FTIR spectra of oxidized (green) and unoxidized (red/blue) PE.

If the ratio of the height of this peak to the height of the PE peak at 1462 cm^{-1} exceeds 0.1, Broutman and Duvall (1989) and Duvall (2002) consider the surface to be sufficiently oxidized that stress cracks may be initiated. When a stress crack is initiated in oxidized material it will propagate more easily through unoxidized material in the body of the material. Then, of course, when cracks open up, more of the material can be oxidized thus accelerating the process.

A reinforced polypropylene liner that cracked badly had an OIT of 15 min compared to an original value of 133 min. A cracked HDPE surface layer had an HP-OIT of 54 min and a CI of 0.30, while the uncracked surface had an HP-OIT of 215 min and a CI of zero.

5. SPARK TEST WIRES

When conductive wires are included in extrusion welds, such as at pipe boots, for spark testing, a significant benefit can be achieved by the small change of day-lighting the wire at the highest part of the welding (Figure 11). If this wire is then connected to the current return (ground) electrode during a geoelectric water lance survey a much more effective liner integrity survey can be performed. Several times it has been noted that a leak is indicated by the water lance that is not detected by spark testing alone. This is because the leak path may be tortuous and too long for the spark to jump to the wire, but the water lance jet, under pressure, will force water into the leak to make contact with the wire. Such tortuous leak paths have been confirmed by acoustic methods of leak detection that locate the exits of leaks while the conventional applied potential methods locate the entrances of leaks.

Figure 11. Installed (top) and exposed (bottom) conductive wire for water lance testing.

6. SMALL STONES

Leaks can be caused by the smallest of stones, particularly when the stone, such as that shown in Figure 12, is between the geomembrane and concrete. In such cases there should be a geotextile cushion between the two or else the concrete must be very smooth and meticulously clean.

Figure 12. Small stone that penetrated 1.5 mm textured HDPE on concrete.

CONCLUSIONS

Small features such as wires, die lines, stones, burn-throughs, microstructural gradients/interfaces, folds, etc., can have major impacts on liner quality and performance, even appearing to cause premature failure. However, in some cases "premature" failure is actually the end of service lifetime of that specific geomembrane formulation in that specific application.

REFERENCES

Broutman L.J., Duvall, D.E., So, P.K., (1989). Fractographic Study of a Polyethylene Sewer Pipe Failure, *SPE Antec*, pp 1599-1602.

Duvall, D.E., (2002). Analyses of Large Diameter Polyethylene Piping Failures, *Society of Plastics Engineers 60th Annual Technical Conference*, Brookfield, Connecticut, USA.

Hsuan, Y.G., Koerner, R.M., Lord, A.E., Jr., (1992). The Notched Constant Tensile Load (NCTL) Test to Evaluate Stress Cracking Resistance, *6th GRI Seminar*, MQC/MQA and CQC/CQA of Geosynthetics, Folsom, PA, USA, pp 244-256.

Peggs, I.D., (2008). Observations and Thoughts on the Performance of Polypropylene Geomembrane Liners and Floating Covers: Towards Improved Specifications, *EuroGeo4*, IGS, Edinburgh, UK, paper #267.

It's All in the Details; Textured Geomembrane Example

R. E. Belanger, C. B. Queja and C. V. Zantua; Precision Geosynthetic Laboratories, Anaheim, CA, USA

ABSTRACT
Several measurements of the same property of a specific sample by a particular test will not give the same precise results. Values from replicates show variability and it can also be observed from comparing tests results derived from different laboratories that tests performed on the same material will also vary. These variability's have economic consequences when verifying material quality versus a specification.

On the surface, interpretation of test data from geosynthetic testing seems quite straight forward; compare the mean values shown on a test report to the specification requirements. However, a statistical look at the test data presents some interesting issues. These statistical issues can be a problem if not understood or a help when understood.

It can be seen when viewing a geosynthetic test report that values from replicates vary. Sometimes the variation in replicates is large while in other cases it can be relatively small. This variability can also be observed when comparing tests results derived from different laboratories. Thus, there are variations between replicates and between different laboratories. It is obvious that several measurements of the same property of a specific sample by a particular test will not give the same precise results.

This leads to the question of what are the true or reliable results. It is a particular problem when comparing test data between two different laboratories. Is one laboratory correct and the other wrong or are they both either right or wrong? The answer to these questions is critical when one laboratory is a manufacturers' laboratory and the other is an independent or third party laboratory verifying material quality versus a specification.

1. ASTM GUIDANCE

ASTM gives us some insight into the variation between replicates and between laboratories by reporting repeatability and reproducibility for the various test methods.

- Repeatability is defined as a quantitative expression of the random error associated with a single operator in a given laboratory obtaining replicate results with the same apparatus under constant operating conditions on identical test material within a short period of time.

- Reproducibility is a quantitative expression of the random error associated with operators working in different laboratories, each obtaining single results on identical test material when applying the same method.

The variations are obvious but which values are to be used for deciding if a material meets a specification?

Specifications can be set in a variety of ways; some use MARV (Minimum Average Roll Value), others can be minimum, maximum or a range. The MARV is derived statistically as the average roll value determined from long term production less two standard deviations. Such requirement when used in a specification sets a lower limit for the specified property.

2. EXAMPLE USING TEXTURED GEOMEMBRANE CORE THICKNESS

ASTM D5994 Core Thickness of Textured Geomembranes test data are presented below. It should be noted that D5994 will be used but the analyses in this example should apply to most geosynthetic tests. ASTM D5994 was chosen because it is a quite common test that shows a high level of variation due to the irregular surface of some types of textured geomembranes. This is coupled with the inherent limitations of the test apparatus and variation in test procedure itself to render accurate results. It is assumed in this example (Table 1) that the desired specification for the textured geomembrane is 36.0 mils. Laboratory-A has measured Core Thickness in their Laboratory to average 36.0 mils, Laboratory-B has measured 35.3 mils in their laboratory, Laboratory-C has measured 35 mils and Laboratory-D has measured 37.0 mils.

Table 1. D5994 core thickness test data from laboratories A, B, C & D.

Laboratory	**A**	B	C	**D**
Test Replicate	Thickness (mils)	Thickness (mils)	Thickness (mils)	Thickness (mils)
1	30	31.0	40.2	38.0
2	32	36.0	38.7	38.0
3	36	36.5	31.1	36.0
4	38	36.0	37.2	35.0
5	35	37.0	31.9	39.0
6	38	36.5	34.3	35.0
7	37	34.5	36.7	37.0
8	39	38.0	33.7	35.0
9	38	36.0	34.5	38.0
10	37	31.0	31.7	39.0
Sum	360	352.5	350	370
Average	36.0	35.3	35.0	37.0
Mean Difference		0.75	1.00	1.00
SD of Difference		24.9	88.5	51.3
Student-t Calculated		2.77	5.33	4.00
Degrees of Freedom		9	9	9
Alpha		0.05	0.05	0.05
Published Students-t		3.25	3.25	3.25
Assessment		Same	Different	Different

3. ANALYSES OF DATA

Before we consider which of these values meet the specification of a minimum of 36.0 mils there is a “Comparison of Means” mathematical test that will give us insight into whether there is a difference between the values based upon the replicate variation. Laboratory-A shows the desired specification value (36.0 mils) but Laboratory-B is 35.3 and below the specification. The Comparison of Means mathematical test can be used to determine if there is a difference between these two means or if they are possibly the same; see Table 2.

Table 2. Comparison of means between Labs A and B.

Description	**Lab A**	**Lab B**	**d**	**d2**
1	30.0	31.0	-1.0	1.0
2	32.0	36.0	-4.0	16.0
3	36.0	36.5	-0.5	0.3
4	38.0	36.0	2.0	4.0
5	35.0	37.0	-2.0	4.0
6	38.0	36.5	1.5	2.3
7	37.0	34.5	2.5	6.3
8	39.0	38.0	1.0	1.0
9	38.0	36.0	2.0	4.0
10	37.0	31.0	6.0	36.0
Sum	**360.0**	**352.5**	**7.5**	**74.8**
Average	**36.0**	**35.3**		
Mean Difference			**0.75**	
SD of Difference			**24.92**	
Students t Calculated			**2.77**	
Degree of Freedom			**9**	
Alpha			**α=0.05**	
Published Students t			**3.25**	
Comparison			**Same**	

Equations Used in Previous Table Calculations:

Mean Difference $\left(\bar{d}\right)$

$$\bar{d} = \frac{\sum d}{n} \qquad [1]$$

d = difference between replicate measurements
n = number of trials

Standard Deviation of the Difference (S_d)

$$s_d = \sqrt{\frac{\sum d^2 - \frac{\left(\sum d\right)^2}{n}}{n-1}} \qquad [2]$$

Student's t-distribution (t-score)

$$t = \frac{\bar{d}}{\frac{s_d}{\sqrt{n}}} \qquad [3]$$

Degree of Freedom (DF)

$$DF = n - 1 \qquad [4]$$

The Comparison of these two means shows that based upon the variation in test values, we cannot distinguish a difference between them; and they may be the same with 95% confidence. When comparing Laboratory-A (36.0 average) to Laboratory-C that has an average of 35.0 the Comparison of Means shows that 35.0 is different and clearly would not meet the specification.

This leaves the question of whether Laboratory-A and Laboratory-B with Average results of 36.0 and 35.3, respectively, meet the specification because we cannot tell the difference between their test results because of the precision of the testing.

Laboratory D with and average of 37.0 mils is different from Laboratory A with 36.0 mils when tested with the Comparison of Means; however it exceeds the minimum of 36.0. If 36.0 mils were a maximum rather than a minimum and we compared Laboratories A and D; Comparison of Means shows that A and D are clearly different and Laboratory D would exceed the 36.0 maximum.

Statistics from Round Robin test results obtained from several different laboratories leads to some clues as to how these two different laboratory results that appears mathematically the same; one appearing to meet the specification and the other not, can be dealt with.

Table 3 shows some possible Round Robin test results for several laboratories.

Table 3. D5994 core thickness round robin statistics.

Reported Average	Standard Deviation
42	+2.0
41	+1.5
39	+1.0
37	+0.5
36	Mean
34	-0.5
32	-1.0
31	-1.5
29	-2.0

Assuming that Laboratory A, which reported the specification value of 36 mils, was a manufacturer and Laboratory-B was an independent or third party laboratory reporting 35.3 mils; the materials would likely be rejected because the minimum specification was not met. This is in disagreement with what we have learned from previous discussions that mathematically, we could not tell the difference between 36.0 and 35.3.

In this situation, the answer lies in the statistics if well understood. From the statistics shown in Table 2, if the manufacturer measured in their laboratory 36.0 and the material was sent to other laboratories, half of the laboratories would observe a value higher than 36.0 and half of the laboratories would report a value less than 36.0; assuming a normal distribution. So the manufacturers gambling statistic would be a 50/50 chance that the material would fail. The manufacturer can increase his odds of having outside laboratories pass their material by raising the thickness, which has direct economic consequence. To manufacture thicker material would require additional resin, thus, more expensive to produce. However, increasing the thickness would prevent the ambiguous situation where 35.3 mils appear to be the same as 36.0 mils because the additional thickness would raise the 35.3 mils to the minimum thus raising no questions.

In reality, it seems quite demanding to expect the manufacturer to increase the thickness to pass in all laboratories because of test variation. But when it is known that the specification is in terms of minimum the price can reflect the additional thickness to pass in all laboratories.

The example used in this case is over simplified because the manufacturers' laboratory may have round robin test results above or below the average and likewise the other laboratories may show high or low results from round robin testing.

4. CONCLUSIONS

ASTM and participating laboratories are constantly working together to reduce the variations in test results and improve the precision of testing. As can be seen variation in test results has an economic effect. By reducing variation the costs to the manufacturer can be reduced and passed on to the customer.

Though core thickness was used as an example in this paper, the same concepts apply to other geosynthetic tests and the associated materials. As previously noted the specifications may be minimum, maximum, or even a range but the variation in test results will have same adverse effects on cost.

Details to Meet the Test; Direct Shear and Transmissivity Issues

S. R. Allen, R. Lacey and J. Allen, TRI/Environmental, Austin, Texas, USA

ABSTRACT
Geosynthetic laboratories are supporting geosynthetic environmental and transportation applications throughout the world with standardized tests developed by the geosynthetics community. The quality of these tests has been shaped by refinements achieved through continued method development as well as in-the-lab observations of sample test behavior. This has been especially true in the area of geosynthetic-soil interaction testing where the expressed testing goal is to bring field behavior inside the laboratory for characterization and study. While a noble objective, the process of isolating the material or interaction parameter measured, while assuring that site specific conditions are simulated, is rich with details that will dictate whether relative success or failure is realized.

This paper will focus on testing details related directly to geosynthetic design, describing important procedures that are key to successful geosynthetic application design. Geosynthetic-soil interaction tests including interface friction as measured in the direct shear test, and performance transmissivity testing are focused upon.

1. INTRODUCTION

Geosynthetic characterization through laboratory testing has always been a key component to successful design. The waste management industry has learned through slope failures and inconsistent assumptions that site-specific characterization of frictional properties between lining materials assists in confirming a given design, or occasionally, changing a design to assure stability. In the same way, site specific oriented hydraulic flow testing assists the designer in determining available flow rates with selected materials, and modifying designs to achieve the most efficient and cost effective product application.

While test standardization has been robust and has afforded a fairly consistent testing industry service to the designer, there continues to be detail oriented aspects of testing procedures that impact a laboratory's approach to measurement, and the final result obtained. Small differences in measurements may not always be significant in the context of design. However, when approved design supporting test criteria are used to establish product acceptance criteria, these same performance oriented testing activities now support a pass/fail decision making progress on the way towards site specific product acceptance.

This paper evaluates procedural and equipment aspects of two geosynthetic performance tests often used for design confirmation testing. The relevant topic and their respective standards are as follows.

Interface Friction/Direct Shear Testing.

- D5321-08 Standard Test Method for Determining the Coefficient of Soil and Geosynthetic or Geosynthetic and Geosynthetic Friction by the Direct Shear Method
- D6243-08 Standard Test Method for Determining the Internal and Interface Shear Resistance of Geosynthetic Clay Liner by the Direct Shear Method

Hydraulic Performance of Geosynthetic Planar Drains

- D4716-08 Standard Test Method for Determining the (In-plane) Flow Rate per Unit Width and Hydraulic Transmissivity of a Geosynthetic Using a Constant Head

The following sections provide a short description of the test procedures used and the respective parameters most important to consistent and relevant testing.

2. INTERFACE FRICTION / DIRECT SHEAR TESTING

In direct shear testing, the shear resistance between a geosynthetic and a soil, or other material selected by the user, is determined by placing the geosynthetic and one or more contact surfaces, such as soil, within a direct shear box. A constant normal force representative of design stresses is applied to the specimen, and then a tangential (shear) force is applied to the apparatus so that one section of the box moves in relation to the other section. The shear force is

recorded as a function of the horizontal displacement of the moving section of the shear box. The test is often performed at three different normal stresses, selected by the user, to model appropriate field conditions. The limiting values of shear stresses are plotted against the applied normal compressive stresses used for testing.

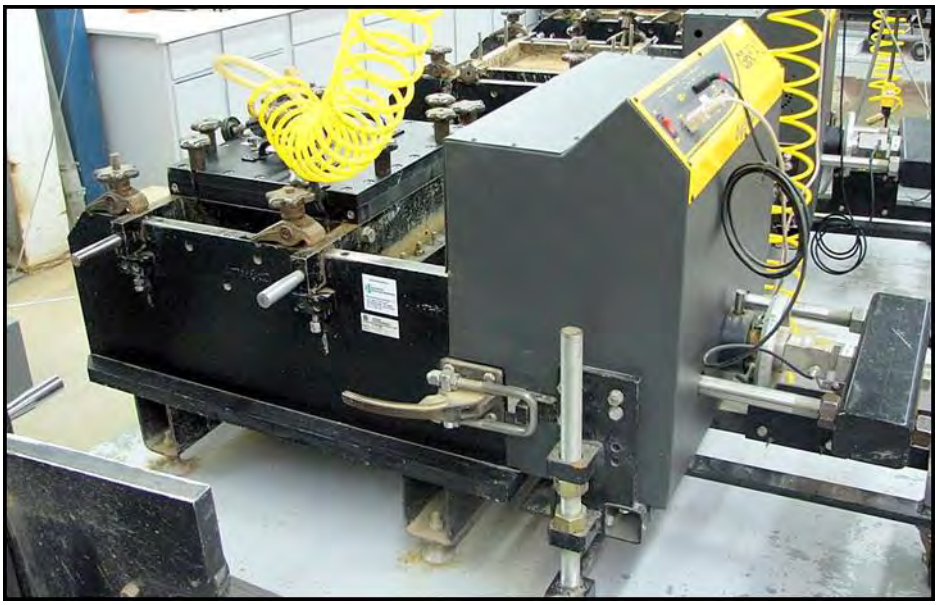

Figure 1. Photograph of a interface friction test apparatus.

2.1 Friction Materials Characterization (Indexing)

As friction testing has been used both to support the design process and to subsequently confirm selected geosynthetic and soil materials, interface friction is both a design and conformance test. Testing in design typically focuses on intended materials and product evaluation for projects. During design testing, the textured geomembrane asperity height, measured in accordance with ASTM D7466-08 *Standard Test Method for Measuring the Asperity Height of Textured Geomembrane*, is often recorded and a physical coupon of tested material archived for subsequent comparison to material shipped to the site. In this way, materials used to confirm design can be "indexed", and directly compared to materials from a specific production run and provided for construction. Similarly, GCL internal peel resistance can be indexed for friction test materials, so that subsequent site specific GCL production material may be compared directly to previously tested material. Some critical attributes to meaningful friction testing will now be discussed.

2.2 Frequency of Testing

As friction testing is generally more expensive and time consuming than routine thickness, density or other index testing, its cost is often the source of rationale for either no testing or minimal testing. The value of slope stability conformation through friction testing is very well established and many have recently used a strategic approach to its implementation in the context of conformance or verification testing. Some have, for example, evaluated the critical interface once over the entire site specific load range and then spot checked this same interface at a single selected normal load.

2.3 Drained Strength Testing

By employing displacement rates that are outside the scope of standard testing, many in the waste and mining industries seem to continue to use undrained friction/direct shear strength results in practice for interfaces involving lean (CL) and fat (CH) clays. Often designers rationalize that this is conservative as the undrained strength will be less than the drained strength. The unavoidable reality is that, if facilitating an undrained test with these materials, the result represents unknown strength due to the unknown value of pore water stress. Results of undrained tests often strain harden over 3 inches of displacement as a result of moving soil from the back of the box to the front through a process called "plowing". This creates a pinch point at the front of the box and a subsequent strain hardening effect. It is well established that clay/geosynthetic interfaces should strain soften if tested in the drained condition (Obermeyer et. al. 2003). In many cases, by committing to the drained, and yes slower, test (by virtue of a much slower displacement rate),

the archived result under drained condition has either allowed the designer to increase air-space or use smooth geomembrane at less cost.

2.4 GCL Hydration

Pre-hydration of GCLs prior to placement in the friction/direct shear box for testing, is an increasing trend. Typically, a GCL is hydrated under a nominal load [i.e. < 24 kPa (500 psf)] prior to mounting in the shear box for subsequent shear testing. The result of hydration of the bentonite under a low normal load leads to the problem of how the GCL is consolidated inside the shear box. If consolidation occurs too rapidly bentonite extrusion through component geotextiles or sealed sides may occur. Fox et. al. (1998) recommends a procedure for hydrating GCLs prior to mounting in the shear box and it is called out as one potential recommendation in the Ohio EPA document on shear strength testing. An alternative approach is to hydrate the specimen under a nominal load of 7 or 14 kPa (1 or 2 psi) for 24 to 48 hours and use constant rate of consolidation to load the specimen slowly enough to the shearing load without forcing bentonite extrusion.

2.5 Testing at High and Low Compressive Loads

In both landfill and leach pad operations it is very common to see normal loads in excess of 950 kPa (~20,000 psf). Almost every friction / direct shear box can receive more compressive load than designed for, usually as a function of customer requests and laboratory urgency. This misuse of equipment is not appropriate and has been a source of errant data. Concurrently, however, some in the testing community have acquired new or modifying existing equipment to accommodate increased loading capacity. Users of direct shear testing apparatus should be aware of equipment requirements generated by high compressive load tests.

Similarly, internal equipment friction or “drag” is a cause of concern when evaluating very low normal compressive loads < 24 kPa (< 500 psf). In an effort to generate more accurate measurement of frictional properties at these loads, some laboratories have established low load shear boxes.

2.6 Remolding of Soils

While establishment of soil test specimens is well defined in many geotechnical test standards, it is not in direct shear test procedures involving geosynthetics. For this and related reasons, friction testing laboratories use a variety, and thus different, methods for remolding soil specimens, especially clay soils for compacted clay liners. A current ballot item in support of a revised friction test procedure is the standardization of soil moisture conditioning prior to remolding in the shear box. This practice along with other geotechnical testing practices are now being implemented at some laboratories though they are not yet specified within ASTM D 5321 and ASTM D 6243. These authors believe it reasonable for laboratories performing soil/geosynthetic interaction testing, such as interface friction testing, to hold credentials for both. That is, these laboratories may hold accreditations from the Geosynthetics Accreditation Institute and the American Materials Research Laboratory or Army Corps of Engineers. The latter readily accredit Proctor tests, moisture contents, and other related soils characterization tests so often of vital importance in the context of interface friction testing.

3. HYDRAULIC FLOW TESTING OF GEOSYNTHETIC PLANAR DRAINS

In this test, also called the transmissivity test, the flow rate per unit width of drain is determined by measuring the quantity of water that passes within a test specimen in a specific time interval under a specific normal stress and a specific hydraulic gradient. The hydraulic gradient(s) and specimen contact surfaces are selected by the user either as an index test or as a performance test to model a given set of field parameters as closely as possible. Measurements may be repeated under increasing normal stresses selected by the user.

3.1 Characterization (Indexing) of Geosynthetic Drains

As hydraulic flow testing has been used both to support the drainage design process and to subsequently confirm selected geosynthetic drainage materials, flow measurement is both a design and conformance test. Testing for design typically focuses on intended site specific materials and product evaluation for projects. During design testing, the geosynthetic design is sometimes characterized for compressive strength in accordance with ASTM D6364-06 *Standard Test Method for Determining Short-Term Compression Behavior of Geosynthetics*, in order to relate observed flow measurements to shorter term resistance to compression. In this way, materials used to confirm flow design can be “indexed”, and subsequently compared to materials from a specific production run and provided for construction. Some critical attributes to meaningful transmissivity testing will now be described.

3.2 Transmissivity Test Equipment

The photograph below shows an example of a hydraulic transmissivity test apparatus. The following items describe critical features of ASTM D 4716 transmissivity test equipment.

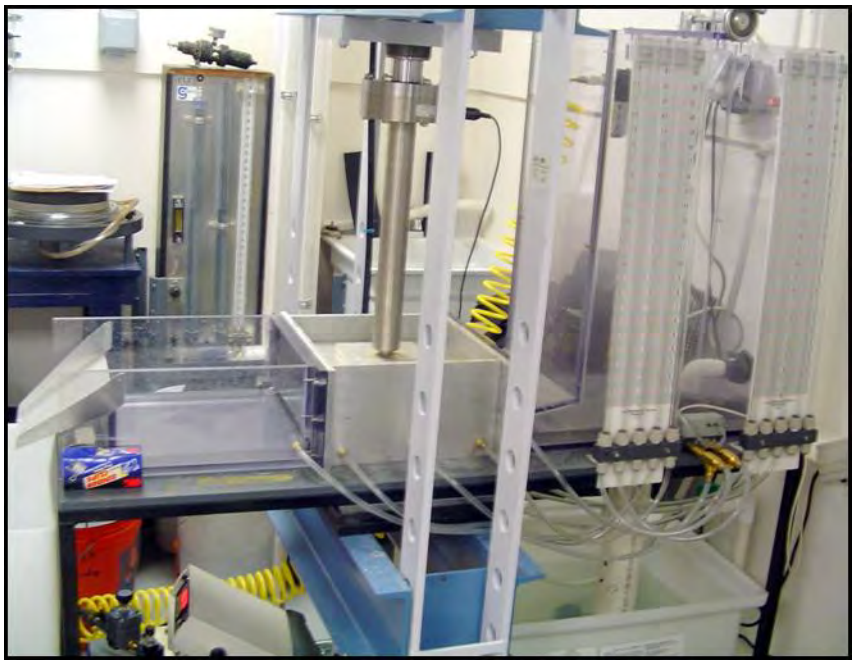

Figure 2. Photograph of a hydraulic transmissivity test apparatus.

- Clear acrylic reservoir box and weir – the clear acrylic allows visual examination of inlet and outlet faces of the test specimens. This is very useful for confirming that air is being forced out of specimens which was initially introduced in the loading tray dry.
- The outlet weir should have a small V-notch or slight "tilt" to allow water to flow continuously at very slow flow rates. Otherwise the water level will cycle up and down with the slight rise necessary to overcome meniscus tension along a wide rectangular weir or around the perimeter edge of a circular overflow riser.
- A loading tray with an upper platen that minimizes sidewall leakage – the geometry of the perimeter seal should prevent water from leaking up around the loading platen while also minimizing the amount of leakage along the platen sidewalls between the perimeter seal and the specimen (referred to as "fugitive flows").
- Specimen Cutting Die Board – the test specimens must be cut so that the sides of the cut specimens fit snugly against the sides of the loading tray.
- Manometers – the perimeters of the drilled and tapped manometer hole surface profiles must be clean and flush with the insides of the reservoir and weir sidewalls. The taps should be located as close to the inlet and outlet faces of the test specimens as possible, i.e., 25 mm (1 in.) from the loading tray faces.
- Pressure transducers should be available for measuring hydraulic gradients less than 0.10 so as to measure the pressure head within an accuracy of ±1 mm of water.
- Several internal taps within the loading tray are preferred to monitor the uniformity and patterns of the head loss within the test specimens. When the sidewall or centerline internal taps indicate a non-uniform head loss regime, the flow is typically being diverted in the direction of one of the two sets of channels formed by the parallel geonet ribs. This is typical of geocomposites tested with a soil superstrate. Occasionally, the onset of geonet compressive roll-over can be detected by observing an abrupt shift in the internal manometer levels as the water is diverted along the ribs that have not lain down.
- Recirculation system – the recirculation port in the recirculation container should be located as far from the return inlet from the weir as possible. This reduces the amount of air bubbles that are re-circulated with the returning water flow. The recirculation pump should be outside of the recirculation tank, connected with a bulkhead fitting. The use of submersible pumps should be avoided as these cause fluctuations in the test water temperature as the pump heats the water.
- Test Water Temperature – the lab ambient temperature should be maintained between 19°C and 23°C. A temperature correction applies within the specified range. Preferred is the use of conditioned water at 20C as this avoids the "correction" due to the use of other test temperatures.

3.3 Transmissivity Testing Procedure

The following describe critical features of ASTM D 4716 transmissivity testing best practice procedure.

- Air Entrapment - for tests without soil in the test section, it is preferred to fill the reservoir-loading tray-weir with water to a level above the elevation of the test specimen before placing the specimen in the apparatus. This gives the technician the opportunity to be sure that no air is trapped in the test specimen.
- For tests where the water must be introduced after placing soil and other materials in the loading tray, pre-flush the specimen before testing by raising the reservoir water elevation to a gradient of at least 0.5 and allow flushing of the air for approximately fifteen minutes. Escaping air should be visible collecting on the weir side of the specimen outlet face.
- Air Entrainment - the water recirculation plumbing should be designed to prevent the flowing water from "free-falling" through air or otherwise mix with air in a turbulent fashion. The amount of water flowing over the reservoir constant head riser should be kept to a minimum. The inlet attached to the reservoir box should direct the water away from the loading tray towards the reservoir box base or sidewall to allow any entrained re-circulation of air bubbles to rise naturally to the surface before being driven towards the specimen inlet face.
- Sampling – additional detail was added to the sampling sections of D 4716 in 2004 to specify that two specimens must be tested to generate a test result. These two specimens should be taken from the "third points" along the roll width sample. The variation of the property along the roll width can be as much as 100%. Therefore, the technician should be vigilant to obtain specimens spaced far enough apart to represent the roll width.
- Underleakage – test sections frequently include a geomembrane under the drainage geosynthetic. Even in clean loading tray bases, these geomembranes often create leakage paths for water to flow through during a test, referred to as "underleakage". Textured geomembrane specimens are the most susceptible to this phenomenon. The bottom surface of these test specimens should be sealed with modeling clay or other impermeable soft sealant, careful to not create new unintended voids and blockages.
- Manometer integrity checks – in order to be certain that there is no air trapped in the manometer tubing or fittings, the manometer levels should be checked after the apparatus is filled with water. Under no-flow conditions, all of the manometers should be the same, measuring the same pressure head level. If the manometer levels are uneven, one or both of the tubes or fittings must have air and should be purged by disconnecting from the site tube and allowing it to drain while watching for escaping air bubbles.
- Maintaining the integrity of GCL test specimens - the inlet and outlet edges of GCL test specimens should be sealed with duct tape to prevent hydrated bentonite from squeezing into the reservoir box and weir. The pre-hydration and loading sequence for test sections involving GCL specimens is critical. If the GCL specimen hydrates under a low compressive stress first, the subsequent loading should be applied slow enough to allow the clay to drain. Otherwise, hydrated bentonite could be forced around the edges of the drainage synthetic which would interfere with the flow.
- Soil superstrates should be confined within the loading tray with narrow strips of very thin polyethylene or rubber that are placed on top of the drainage synthetic and against the inlet and outlet inside faces of the loading tray in an "L" shape. The soil should be in direct contact with the underlying geocomposite or geotextile over at least 250 lineal mm (10 in). This minimizes interference with the intrusion effects. This also allows the soil to drain freely during consolidation.

4. CONCLUSION

In this paper, two performance tests have been evaluated and discussed to demonstrate how equipment and procedural detail may significantly impact the final test result, all within the context of otherwise compliant standardized tests. Of special benefit to the user of the test method, or the practicing testing technician, a robust knowledge and awareness of details significantly improve the testing process while creating more relevant data for the design engineer.

REFERENCES

ASTM D 4716 - 08 Standard Test Method for Determining the (In-plane) Flow Rate per Unit Width and Hydraulic Transmissivity of a Geosynthetic Using a Constant Head

ASTM D 5321 - 08 Standard Test Method for Determining the Coefficient of Soil and Geosynthetic or Geosynthetic and Geosynthetic Friction by the Direct Shear Method

ASTM D 6243 - 08 Standard Test Method for Determining the Internal and Interface Shear Resistance of Geosynthetic Clay Liner by the Direct Shear Method

ASTM D 7466 - 08 Standard Test Method for Measuring the Asperity Height of Textured Geomembrane

ASTM D 6364 -99(2004) Standard Test Method for Determining the Short-Term Compression Behavior of Geosynthetics

Fox, Patrick J, M.G. & Scheithe, J.R. (1998). *Internal Shear Strength of Three Geosynthetic Clay Liners*, Journal of Geotechnical and Geoenvironmental Engineering, 124, No. 10, 933-944.

Obermeyer, Jason E., Gilbert, Robert B., Sebesta, Mark E., Allen, Sam R. (2003). *Drained Shear Testing of Clay-Geomembrane Interfaces*, 56th Canadian Geotechnical Conference

Guidance on the Design and Construction of Leak-Resistant Geomembrane Boots and Attachments to Structures

R. Thiel, Vector Engineering, Grass Valley, CA, USA
G. DeJarnett, Envirocon, Houston, TX, USA

ABSTRACT
Experience in reviewing, designing, performing field inspections, and installing of geomembrane boots and connections to structures has revealed a widely diverse practice of standards and approaches. The execution of these details is very much an art in workmanship, and depends a great deal on the experience and understanding of the installer. There is very little guidance in the literature regarding the fine points of specifying and installing these critical details. The typical manufacturers' details and guidelines are not much more than concepts that have been repeated for two decades. Thus, there is a big difference between what we assume and expect versus what is constructed in terms of leak resistance of geomembrane penetrations and attachments to structures. The goal of this paper is to touch upon some of the detailed and critical aspects that should be addressed when specifying and constructing geomembrane seals around penetrating pipes (referred to as "boots") and attachments to structures.

1. INTRODUCTION

While much attention has been paid in the last 30 years to many other containment issues related to geomembranes (such as chemical compatibility, aging and durability, manufacturing, seaming, subgrade preparation, covering), there is surprisingly little technical discussion related to the design and construction of leak-resistant penetrations and attachments to structures. This subject has largely been relegated to a few simple details, mostly generated by the manufacturers and included in their standard literature.

The content of this paper is derived from the authors' field observations, experience, and deductive reasoning. In addition, a number of other experienced field installers and construction quality assurance (CQA) personnel were interviewed for their opinions related to the subject of this paper. The interviews revealed significant differences in opinions and approaches, sometimes contradictory to one another. There is a large opportunity for more academic studies in this area so that these critical connections can be more definitively engineered, specified, constructed, tested, and maintained.

The subject of this paper relates to those connections that the designer wishes to be leak-resistant, and not simply just a mechanical termination. Many mechanical terminations might have strength as a key design consideration. Most leak-resistance connections should be designed to be as stress-free as possible. For those terminations that need to provide both functions, the design must include provisions for both stress and containment.

When specifying or designing leak-resistant boots or attachments, the lead author finds it more appropriate to think in terms of "leakage impedance" rather than "leak-proof". The reason for this is clear: there is a significant probability that some amount of leakage may develop at these connections. The differences in materials, difficult-to-access geometries, the propensity for creating stress concentrations, the inability to non-destructively test, and the aging and cracking of sealants and gaskets all lead to a higher probability for leakage at these locations than there is in the free-field geomembrane. Thus, one key piece of advice for designers and owners is to be prepared to properly manage the consequences of potential leakage from these locations. Owner-management techniques are beyond the scope of this paper, but could conceptually include such design and operational elements as double liners with leak detection, and enhanced monitoring and response times.

2. BACKGROUND

There is relatively little detailed literature on the subject of designing and constructing leak-resistant geomembrane (GM) seals around pipe penetrations (called "boots") and sealing of geomembrane attachments to structures. What little exists is usually very general and lacking in specificity, with the exception of Wells (1993) and ASTM D6497. A brief review of available literature follows.

Koerner (1994). In the classic *Designing with Geosynthetics* by Koerner (1994) there are less than two pages of text on "connections" and "appurtenances", and some generic figures covering the entire subject. Probably the most well-directed statement in this reference is on page 594 that states "Care and true craftsmanlike work are required for trouble-free and leak-free performance." Other than generally portraying the concepts of penetrations and attachments, there is little substantive guidance on designing and constructing leak-resistant attachments, nor does it point to any references that would make this point.

Daniel and Koerner (2005). In the United States a very useful reference is by Daniel and Koerner (2005) entitled "Guidance for CQA and CQC of Liner and Cover Systems". This work, currently published under the auspices of ASCE, was originally sponsored by the EPA in 1993 with the title "Technical Guidance Document for QA and QC for Waste Containment Facilities". While this document has been of great service to the industry to provide overall support of uniform increased quality in lined installations, it is weak on the subject of boot and attachment details. The brief, less-than-one-page, section on Liner System Penetrations gives very little advice to the goal of constructing a leak-resistant penetration. For example, while the guidance suggests that a pipe-boot skirt should be nondestructively tested with a vacuum box or an air lance, it neglects to mention that the most common type of nondestructive testing in this application is spark testing of an embedded copper wire. The guidance is also misleading in its first recommendation, which suggests that "geomembrane pipe boots are usually factory fabricated" and are only field fabricated in "unique" situations. Quite the opposite is true! The lead and secondary authors have each been a design/CQA practitioner and an installer, respectively, for over 20 years and it is very rare that factory-fabricated boots are utilized. Even when pre-fabricated boots are explicitly specified in the contract documents, it is a very small probability that the installer will provide them, and you could safely bet that most of the boots will be field-fabricated. Furthermore, this guidance document does not provide any discussion of other types of leak-resistant attachments to structures.

Bonaparte et al. (2002) prepared a document for the USEPA's Risk Management Research Laboratory with the goal of evaluating the performance of waste containment design, construction, and operations in the United States, and providing recommendations for improvement. Their study identified a few case histories where pipe penetrations were a problem. Based on these case histories and other general observations, they made the following general statements in various sections of the report:

- "These case histories demonstrate that it is difficult to construct pipe penetrations to be hole free even when extra measures are taken to enhance the integrity of the connections."
- "…all of the design, construction, and operation problems identified in this investigation can be prevented using available design approaches, construction materials and procedures, and operation practices. It is the responsibility of all professionals involved in the design, construction, operation, and closure of waste containment systems to improve the practice of waste containment system engineering"; and also "…the frequency of these problems can be reduced with good design, construction, CQA, and maintenance."
- More specific training of design engineers, CQA personnel, contractors, and operators would reduce the occurrence of problems.
- Development of better construction materials, techniques, and QA/QC procedures to prevent the kinds of construction problems identified in their report.
- It is difficult to construct pipe penetrations of liners to be defect free. A method that was successful for one landfill was to fill the space between the pipe and pipe boot with bentonite slurry. Until new methods for constructing better connections between GMs and ancillary structures have been developed and tested, designs without pipe penetrations (i.e., designs with internal sumps) should be preferred.
- If boots are necessary, use prefabricated boots to minimize extrusion welds.
- Connections between GMs and ancillary structures should be carefully constructed and inspected to decrease the potential for construction-related GM holes.
- Pipe penetrations of liners should be leak tested by ponding tests, leak location surveys, gas tracer tests, or pressure tests of double pipe boots as part of liner system CQA.

Wells (1993). The paper by Wells (1993) is an excellent attempt to define the specifics of the design and construction challenges related to attaching a geomembrane to a concrete structure using a gasketed batten strip. Key elements of a successful leak-resistant connection pointed out in the paper were: (a) smoothness of geomembrane welded seams and the absence of wrinkles under the batten footprint; (b) uniform batten clamping pressure with a controlled strain in the gasket provided by a rigid batten strip, bolts, and nuts; and (c) smooth finish and strength of the concrete substrate. The greatest proportion of the paper is devoted to the education of the reader regarding the allowable compression of rubber gaskets. The paper makes the point that a recommended hardness for gaskets is generally 40 durometer, and that compression of gaskets more than about 10-15% (depending on thickness and shape factor) of their thickness will exceed their elastic limit, cause them to "cold flow" (deform plastically), and lose their resiliency. According to the method presented in the paper, a

typical ¼" thick by 2" wide gasket, which is the most common size used in the industry, should only be compressed about 7% of its thickness. Assuming that the anchor bolts are the common 3/8" dia. by 16 threads per inch, this would only allow the anchor-nuts to be tightened about *one-quarter of a turn* past finger-tight. As recognized by Wells (1993), thin gaskets are often overtightened relative to this design approach. The practical consequences of the paper's conclusions are that designers should specify thicker gaskets (allowing more compression and more turns of the nut) that are relatively lightly compressed by measuring turns of the nut rather than by measuring torque. Although Wells (1993) recognizes that the concrete substrate must be very smooth, and that the ridge formed by the lap joint of the geomembrane seam needs to be very small, the current authors would find that such light compression of 40-durometer material would generally be inadequate to close off the voids commonly caused by uneven substrates and 60-mil geomembrane lap joints.

ASTM D6497. The ASTM Guide D6497 provides a very competent industry standard, and was likely developed with input from Larry Wells. The Guide provides guidance on many critical aspects of geomembrane boots and attachments including the following: (a) the need for a smooth and even substrate; (b) edges and corners of structures should be rounded and cushioned with no voids to protect the approaching geomembrane; (c) precautions against differential settlement of the structure and adjacent ground should be considered; (d) the geomembrane should approach the attachment "in-plane" to avoid bridging; (e) the geomembrane should be cushioned or protected from battens, clamps, and bolts; (f) the area of the attachment should be free of dirt and debris; (g) the rigidity of batten strips should be matched to the bolt spacing to provide uniform clamping pressure; (h) gaskets should have proper chemical resistance and not be over-compressed; (i) pre-fabricated corners, edges, and boots should be considered; (j) shape of penetration is ideally round with no corners, having a minimum size of 50 mm diameter and a minimum 1 m spacing between penetrations; (k) welding sections of embedment strips (which the Guide refers to as "rondels") together before casting in concrete. The figures in the Guide also indicate that for pipe penetrations the free-field GM should be mechanically attached to a concrete pad, using either embed strips or batten bars, and that the pipe boot skirt should then be welded to the free-field geomembrane outside the limits of the mechanical attachment. Although the Guide does not say why that method is recommended, the current authors agree that this is indeed a very good idea for the primary reason that it will reduce stresses on the geomembrane boot. The figures in the Guide also imply that it is a good idea to use a caulk sealant at the edges of gasketed attachments, and provides examples of double-booted penetrations, both of which we believe are good ideas.

Manufacturers' Literature. Often the last resort utilized by designers and specifiers is a requirement to complete the installation "in accordance with the manufacturer's instructions." This common statement would lead one to believe that the manufacturers would have a wealth of information related to the critical details concerning leak-free attachments. In reality what we find are a library of boilerplate CAD details of pipe boots and batten bar attachments, and generic specifications that are general and non-specific. The one exception is that some installation guides for embedment strips are published by some of the manufacturers, such as the "Polyethylene Embed Channel Specification" by PolyFlex (2008).

Installers. While there is almost no literature that is generally produced by installers, per se, they are in fact the greatest resource of experience and understanding in this field. Most of the information presented in this paper can be attributed to the authors' experience and networks with other installers.

3. ORGANIZATION OF THIS PAPER

There are many variations of boots and attachments to structures. The following sections of this paper will focus on the most common types of boots and attachments encountered by the authors, and will go into detail describing common problems and proposed solutions towards the goal of leak-resistance.

Undoubtedly there are many other variations of geomembrane boots and attachments to structures that have been or will be constructed in the field that are not specifically discussed in this paper. Hopefully the concepts discussed in this paper can be used for those variations as well.

4. LEAK-RESISTANT GEOMEMBRANE BOOTS

A diagram of the most typical geomembrane boot is shown in Figure 1. Photographs of typical boots in the field are shown in Figure 2. A boot consists of the following generic elements:

- Sleeve-to-pipe seal (either welded, or caulked-and-clamped, or gasketed-and-clamped)
- Sleeve
- Sleeve-to-skirt connection

- Skirt (sometimes also called the “flange” of the boot)
- Skirt to free-field geomembrane connection

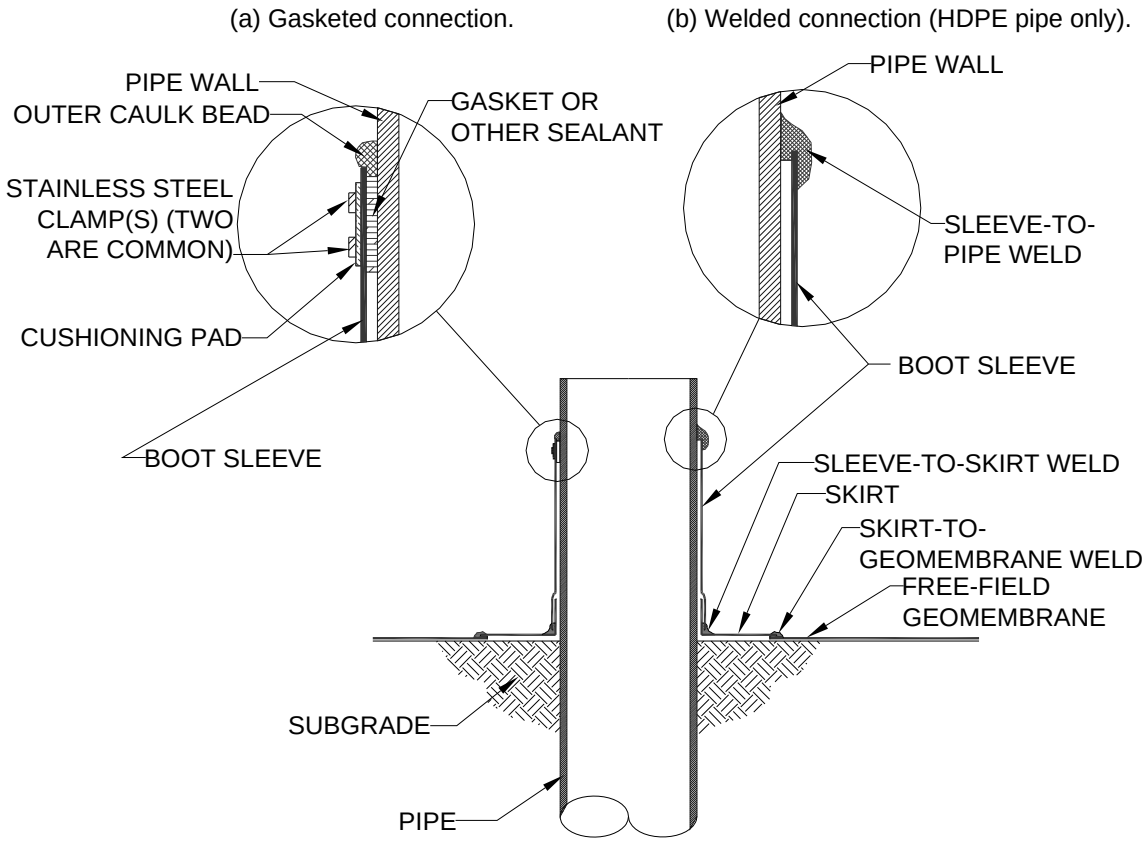

Figure 1. Basic pipe boot elements.

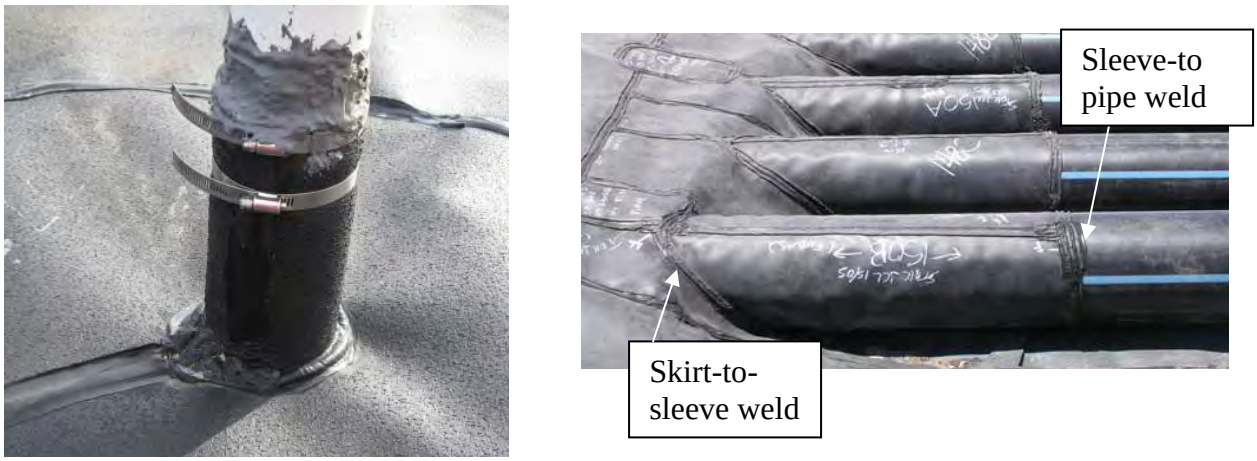

(a) Gasketed and banded boot with polysulfide coating on the end of the boot.

(b) Boot sleeve welded to pipe. This is commonly preferred by many installers for leak resistance.

Figure 2. Typical examples of installed boots.

Prefabricated boots. As suggested by Daniel and Koerner (2005) and by Bonaparte et al. (2002) the use of prefabricated boots is preferable to field-fabricated boots. Prefabricated boots have the sleeve and skirt premanufactured in a single piece, and thus eliminate the sleeve-to-skirt weld, which is often a weak spot. Prefabricated boots made from polyethylene (PE) are often vacuum-formed from base stock material that is substantially thicker than the project-specified geomembrane so that when it is stretched into shape its thinnest spots will have the minimum required thickness. The resulting sleeve will be seamless and will not have a lap joint, which will improve its leak resistance and aid in achieving a uniform clamping pressure. Prefabricated boots from other materials such as EPDM, PVC, or polypropylene can be factory molded or preformed, and sometimes have a stepped-cone or tapered shape where the cone can be cut off at the desired diameter of the pipe.

One of the biggest reasons that the authors have found that prefabricated boots are not used in the industry is because the geometry must be exactly defined ahead of time. The stiffer the geomembrane the more critical this becomes. Often field conditions are slightly different than what is shown on the design drawings. The two most important geometric dimensions that must be accurately defined to order a prefabricated boot are (1) the outside diameter of the pipe, and (2) the angle of the pipe to the subgrade. Having field conditions vary from assumed design conditions is often the "norm" to be expected on construction projects, and even small variations can render a prefabricated boot useless. If the diameter or angle is off, then the integrity of the boot may become compromised due to a poor seal or risking a bridged void at the base of the boot. "It never fits" is a common installer comment regarding prefabricated boots. There is often little incentive for installers to order prefabricated boots because they know the chances of getting the wrong order are high, or waiting to order the boot until the time that the exact field conditions are known will delay a project. Furthermore, there are many instances where the end of the pipe is not accessible and the boot cannot be slipped over the end of the pipe, necessitating a seamed sleeve. And thus the discussion that follows regarding the use field-fabricated boots is most worthwhile.

Clamped and gasketed (or other sealant) connection to pipe. Except in the case of polyethylene geomembranes connected to HDPE pipes, which can have a welded connection, all other boot sleeves will be clamped around the pipe and have either a gasket or other sealant between the pipe wall and the boot sleeve as shown in Figure 1a. The most common problems, and proposed solutions, with these installations are described in the following points, and illustrated in Figures 3 and 4. A checklist of boot issues is provided in Table 1 at the end of this section.

- The gasket material is overlapped and creates a void that may leak at the lap. Solution is to tightly overlap gasket and then cut through both layers of gasket at an angle to obtain a perfect slanted butt-joint.
- The welds are often in difficult geometries and not easily verified for quality. Attempts should be made during design and construction to create good accessibility to all penetrations for good boot construction. All welds should have a copper wire embedded for spark testing (see Figure 4).
- The geomembrane material is overlapped to create the sleeve seam, and creates a void at the edge of the lap that may leak, and also leakage may enter between the two plys of the laps. Solution is to make sure gasket compression fills the void at the edge of the lap, and for very thick geomembrane materials, good craftsmanship would dictate that the edge of the inside of the lap be beveled. Also, provide a seal between the two layers on the lap joint at the outer end of the sleeve to prevent liquid from flowing along that overlap.
- The clamping force from the outer bands or clamps often creates wrinkles in the boot sleeve that may allow leakage. Solution is to have a tight sleeve that will not wrinkle. Start over if it is too loose and there are wrinkles.
- Welds and wrinkles on the boot sleeve cause the clamping force to be uneven which may promote leakage. Solution is to grind and bevel the weld to create a smooth transition so that clamping force is uniform.
- The clamping force on the gaskets is usually not controlled or measured, but is subjectively applied. Clamping with too low or too high of a force may result in a gasket that does not perform properly. There is not a known perfect solution for this issue with gaskets. The best solution is to use a moldable sealant, such as a mastic or a caulk, in lieu of a solid gasket material. Mastics and caulks will fill all of the voids and not be sensitive to compression strain. They generally maintain their elastic-plastic properties for long periods of time, and if chosen properly they will provide some adhesion to the surfaces. Under high-head conditions where there is a concern about plastic-flow of a mastic material, the mastic could be a secondary sealant behind a solid primary gasket.
- Aging and deterioration of the gasket. Solutions are (a) provide a caulk protection bead at the leading edge of the boot to protect the gasket from environmental exposure as much as possible, and (b) periodic inspection and replacement of the caulk beak and the gasket material.
- Most installers believe that permanent-type "band-it" clamps work better than the screw-type clamps because they believe it is difficult to properly tight the screw clamps without stripping them, and they

loosen over time. Clamps become loose over time for other reasons, such as thermal expansion and contraction. Solutions are (a) use multiple clamps; (b) routine inspection; (c) on larger-diameter pipes have special two-piece, three-piece, and even four-piece clamps specially fabricated out of 1/8" thick by 1.5" wide stainless steel to the exact diameter of the pipe (allowing for the thickness of the geomembrane and gasket; see Figure 4).

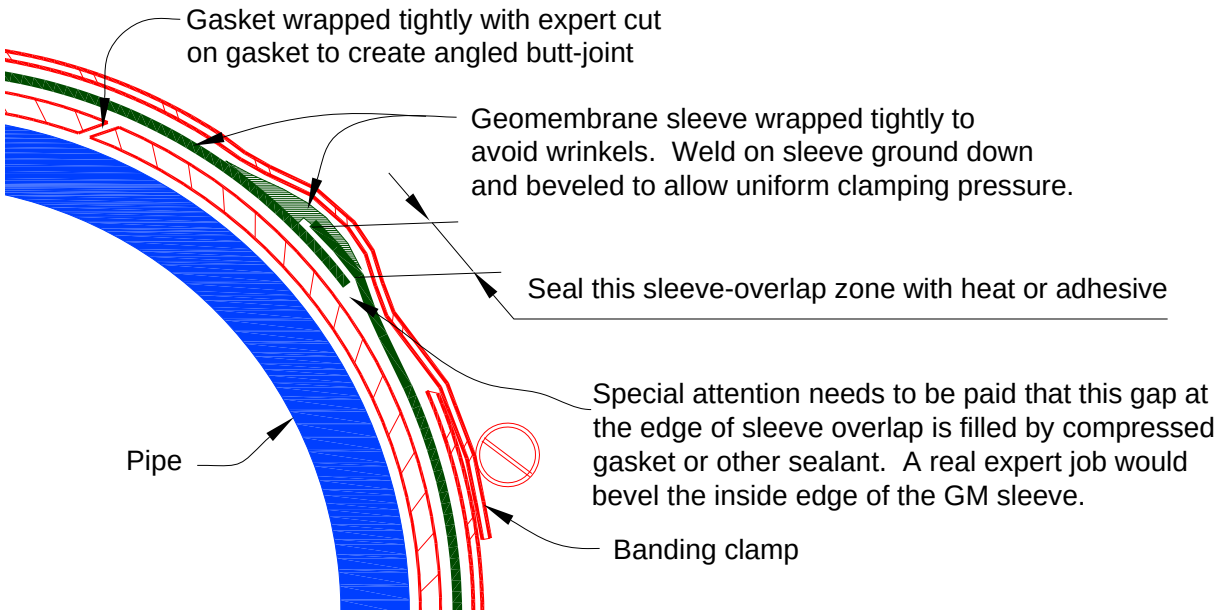

Figure 3. Detail schematic of critical gasketed boot issues.

Note that any gaskets, mastics, or caulks that are used need to be chemically compatible for their intended use. Common mastics are butyl-based (including some that are fuel-resistant) and polyurethane based. Caulks and sealants are most commonly polyurethane, polysulfide, and silicone based, and some may be modified epoxies.

Gaskets are meant to elastically deform and retain resiliency. When they are compressed past their elastic limit, they may loose their resiliency (see Wells, 1993). Gaskets also experience creep over time, and will lose resiliency with time and temperature. The more a gasket is initially compressed, the more accelerated the creep will be. There are differences of opinion regarding gaskets.

Wells (1993) implies that solid pad gaskets should be used. Many designers and installers use "sponge" gaskets, however, which are lighter weight. If they are used, it is essential that they are specified as "closed cell" materials. The sponge-type gaskets experience a great deal of compression when clamped, and are available in pure or blended varieties of neoprene, polyethylene, nitrile, EPDM, and probably some other materials. Their advantage is that they will have a better chance at filling voids and uneven surfaces than the hard gaskets. Their disadvantage is that they are known to lose their resiliency and retain a set after being clamped down or crushed. Another disadvantage is that sponge gaskets may degrade faster than solid pad gaskets, due either to chemical exposure or UV and oxygen.

Solid gaskets require a smooth, hard, even substrate to create a good seal. It is defeating to have a rough substrate or voids and specify a hard gasket. Unfortunately most of the author's experience is that most concrete surfaces are not in good enough shape to receive a solid pad gasket. Even the overlap on a 60-mil liner may cause too much of a ridge for a solid pad gasket to seal, and the seams in that case would need to be butt-joined or expertly tapered. Solid gaskets are available in natural rubber, neoprene, EPDM, nitrile, Teflon, and likely other materials or combinations. Often the gaskets can be manufactured in different stiffnesses, which in the gasket industry is related to hardness or "durometer". A common specification is for "40-durometer" material.

Moldable sealants and mastics are meant to plastically deform and fill voids. They also have an adhesive quality and tend to stick to surfaces. These materials tend to retain their plasticity, although they may age.

(a) Classic example of poorly constructed boot that violates all good construction principles.

(b) Well-constructed boot (before application of caulk bead).

(c) Thin band clamp that has loosened and come off.

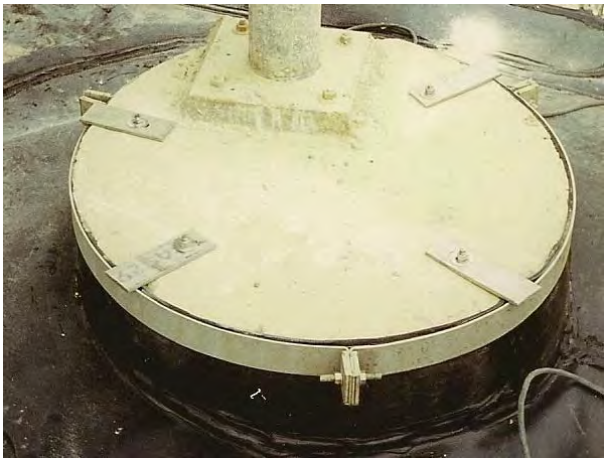

(d) Heavy wide custom clamp around end of a penetration.

(e) Embedding copper wire before weld for spark test.

(f) Conducting hand-held spark test on boot weld.

Figure 4. Examples of poorly- and well-constructed boots.

Caulks, epoxies, and coatings are viscous liquids (some even tend to be plastic-deforming solids) that cure and harden over time, but may retain flexibility for a long period of time depending on the material chosen. If chosen properly these materials will adhere to both surfaces after they cure.

In the case of prefabricated boots from very flexible geomembrane materials such as polypropylene, TPO, or EPDM, where the inner diameter of the premolded pipe sleeve is slightly smaller than the outer diameter of the

pipe, and the pipe wall is smooth and clean, it may be possible to slip the boot over the pipe and clamp it with no gasket. This is common in the roofing industry, but even in these cases, a small amount of caulk-sealant is often used between the boot sleeve and the pipe wall.

Welded Boot Connections. Polyethylene geomembranes have a potentially unique advantage if the penetrating pipe is also a polyethylene material in that the geomembrane can be welded directly to the pipe, as illustrated in Figure 1b. Figure 2 shows a classic welded boot installation. Most polyethylene geomembrane installers prefer welding the boot to the pipe for obtaining a leak resistant boot. Geomembrane welds to pipe walls should be field tested for possible delamination as described in Table 1.

Concrete collar at base of boot. The free-field geomembrane is often mechanically connected to a concrete collar that is constructed on the subgrade around the penetrating pipe. The geomembrane's mechanical connection to the concrete can be provided either by an embedment strip or by a batten bar. The reason for the mechanical connection is to relieve any stresses that are attracted from the free-field geomembrane at the pipe boot connection. For example, Figure 5a shows a tear that occurred in the sleeve-to-skirt connection of a pipe boot at the bottom of a reservoir. Figure 5b shows the sinkhole erosion that occurred as a result of the leaking pipe boot, which eventually resulted in a blowout of the downstream dam. Although designers of ponds should always have design elements that can handle leaks of this sort, this type of leak could perhaps have been prevented if a concrete collar had been constructed around the penetrating pipe, with the free-field geomembrane battened to the concrete, and the pipe-boot skirt welded over the top of the batten connection. This recommended collar-design concept is illustrated in Figure 6, similar to what is presented in ASTM D6497.

(a) Failed pipe boot at skirt-to-sleeve weld.

(b) Sinkhole at bottom of reservoir caused by failed pipe boot.

Figure 5. Example of pipe-boot failure and its implication.

Figure 6 shows the free-field geomembrane being attached to embedment strips that would have been cast into the concrete collar. Some contractors have found it simpler to embed polyethylene "stud liner" into the surface of the wet concrete pad, and that would serve the same purpose for mechanical attachment of the free-field geomembrane. Alternatively, if nothing was installed in the concrete ahead of time, the free-field geomembrane could be quickly attached with powder-driven nail anchor battens. A thick geotextile cushion should be used between the skirt and any underlying batten strips.

Polyethylene material is also available in "plate stock" of various thicknesses, which have also been used advantageously to create leak-resistant pipe penetrations, as well as serve a similar function as the concrete collar. The author has dubbed this a "plate boot". In this case the skirt is made from something like ½" thick polyethylene plate stock, and is directly welded to the HDPE pipe at the desired angle. Figure 7 shows a field-fabricated plate boot where the plate also has electrically-conductive aluminum tape on the bottom inside and outside edges near where the welds will occur so that the final installation can be spark-tested. This type of boot construction requires attention to pre-heating the thicker pipe and plate-stock materials. Added security could be added to this boot by constructing a standard welded skirt-sleeve assembly that would be welded to the pipe, with the limit of the skirt welding outside the limit of the plate stock. In this manner the skirt would be relatively free of potential stresses, and the thick plate-to-pipe weld, which is susceptible to cracks forming in the weld because of the stiffness of this connection. It is also always good to have redundancy around these penetrations.

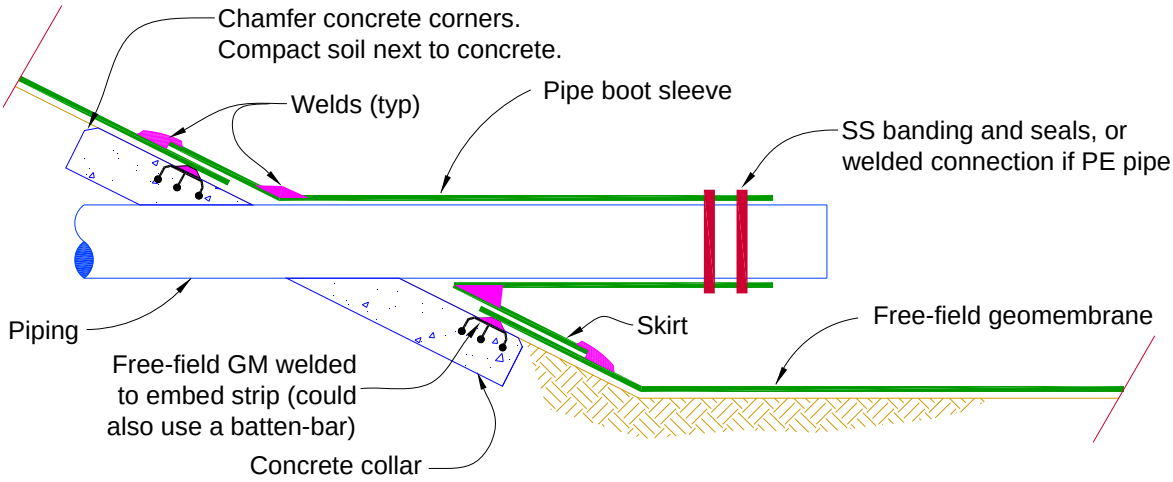

Figure 6. Concrete collar for attachment of free-field geomembrane at base of penetration to keep stress off of skirt-to-sleeve weld (courtesy of GSE Lining Technology).

(a) Fitting plate-skirt.

(b) Applying aluminum tape to bottom of plate for spark test.

(c) Heat-tacking the plate to the free-field geomembrane.

(d) Welding the pipe to the plate. Ideally another welded boot will be installed over this.

Figure 7. Example of “plate-boot” construction.

Figure 8 shows a photograph of another variation on this theme where a small-diameter steel pipe penetrated a concrete wall covered with studliner. In this case a special steel-to-HDPE transition fitting was obtained, a correct-size hole was hole-drilled through the studliner, and installed in the formwork (Figure 8a). After the concrete was placed and the forms were removed, the free-field geomembrane was placed around the pipe and welded to the studliner. A geomembrane skirt was directly welded to the HDPE transition fitting, and the skirt was welded to free-field geomembrane. Note that HDPE-transition fittings are available for different types of metal and PVC pipes in a range of diameters.

(a) Steel-to-HDPE transition fitting in concrete formwork through studliner.

(b) Installed penetration.

Figure 8. Example of welded-boot construction to "studliner" embedded in concrete for a small diameter steel-to-HDPE transition fitting.

Field fabrications of the plate-boot cannot be done if the angle of the slope is too flat or if the pipe penetration is too close to the floor because of the difficulty in getting a weld under the bottom of the pipe. The plate-boot can also be prefabricated in a shop with the plate-skirt shop welded to a pipe section that is delivered to the field. In this case the pipe-and-plate assembly would be set in place in the field (ideally set into a concrete collar, described previously), and the backfill placed behind the plate after it was set. The free-field geomembrane would then be welded to the top of the plate-skirt. Figure 9 shows an example of this with an air-pressure test chamber to verify air-tightness of the penetration. The challenge with these fabrications is getting them to fit the slope in the field, and proper backfilling behind the plate.

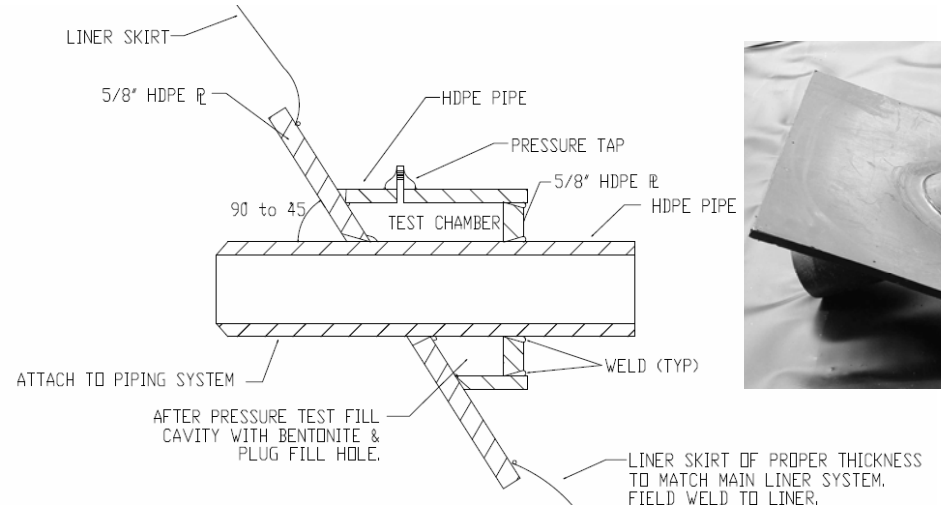

(a) Schematic.

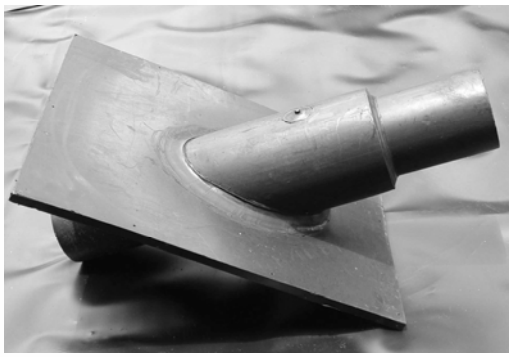

(b) Photo of constructed fitting.

Figure 9. Example of prefabricated "plate-boot" construction (courtesy of GSE Lining Technologies).

Table 1. Checklist of leak-resistant boot issues.

POTENTIAL PROBLEM WITH BOOT	POTENTIAL SOLUTION
General quality	Order prefabricated boots taking care to specify exact OD of pipe and angle to subgrade
Stress concentration at base of boot	(a) Construct concrete collar at base of pipe penetration, fasten free-field geomembrane to concrete, and have boot skirt weld over the top of the attachment. (b) Put weights (e.g. continuous sandbags) around all penetrations to take wind stresses off of exposed penetrations.
Good weld adhesion when welding to pipe wall or other thick-gage polyethylene	Perform adequate pre-heating where thicker material might cause a heat sink and thus prevent a good weld; test the weld using the field-impact method test to check for potential delamination as follows: place a ½" wide blunt metal tip (e.g. large screwdriver head) against the edge of the extrusion weld and hit it with a rubber mallet. If the weld is not properly bonded it will delaminate.
Leaks in boot welds	Spark test all welds associated with the boot by embedding copper wires during construction of the boots. As a supplement, leakage tests can be conducted by pulling a vacuum under the liner and listening with sensitive acoustical equipment for air leakage along the welds.
Long-term concern with leaking gasket on polyethylene installations	Specify HDPE pipe for all penetrations, and use HDPE transition fittings for non-HDPE pipe, to allow all penetrations to be welded.
Leaking gasket	1. Tightly overlap gasket and then cut through both layers of gasket at an angle to obtain a perfect slanted butt-joint. 2. Tightly wrap and clamp the geomembrane sleeve around gasket to avoid wrinkles. Bevel the inside edge of the overlap. Heat tack and weld the sleeve with the clamps in place. After the weld has cooled or cured, remove the clamps, and weld the remainder of the sleeve seam. 3. Seal the overlap on the geomembrane at the end of the lap joint between the two laps (for PE don't just count on the outer extrusion weld) 4. If there is a thick extrusion weld under the location of where the clamp will go, it needs to be ground down and beveled smooth so that the clamp provides a uniform pressure all the way around. 5. Use double clamp, or use an exact premanufactured multi-piece steel clamp that will clamp over a wide area. 6. Provide double (redundant) boot.
Gasket aging and deterioration	Cover the end of the exposed gasket with a caulk. Conduct periodic inspections, caulk maintenance, and replacement as needed. Provide double (redundant) boot.
Plastic flow of moldable or mastic sealant under high-head conditions	(a) Provide best-fit solid gasket or cured caulk ahead of moldable sealant, and caulk the end of the penetration to protect the moldable sealant from high heads and high flows. (b) Provide double boot with standard gasket on outer boot and moldable sealant on inner boot.
Clamps become loose over time	Options are to (a) use multiple clamps; (b) routine inspection; (c) on larger-diameter pipes have special two-piece, three-piece, and even four-piece clamps specially fabricated out of 1/8" thick by 1.5" wide steel to the exact diameter of the pipe (allowing for the thickness of the geomembrane and gasket).
Voids between boot and pipe	Where soil or water pressure will be around the boot it is imperative to have a tight-fitting boot with no voids.
Tight geometry	Leave enough space between multiple boots, and all around each boot, to allow for reasonable installation access for welding and clamping, especially in tight corners and underneath the pipe. Leave enough space and slack material to allow for temperature contraction between boots so that cold conditions do not cause bridging at these stiff locations.
Dynamic forces	Where penetrating pipes will receive hydrodynamic forces from flowing liquids at elbows near the penetration, design and install provisions, such as thrust blocks, to absorb those forces and keep the stresses off of the welds.
Non-circular penetrations	Special problems are created by corners. Band clamps will not work unless they are prebent and there is lots of mastic. Be careful of voids under submerged conditions. Need straight clamps that will exert pressure on each side uniformly. There will need to be extra-care for the wrinkles at the corners. Suggest casting concrete circle around non-circular shapes.

5. LEAK-RESISTANT GEOMEMBRANE BATTEN ATTACHMENTS

A diagram of the most typical geomembrane batten attachments is shown in Figure 10. Photographs of typical battens in the field are shown in Figure 11. A batten attachment consists of the following generic elements:

- Substrate (usually concrete or steel)
- Gasket (or other sealant)
- Geomembrane
- “Rubber” clamping cushion
- Metal (usually SS) batten bar
- Nuts and bolts (usually SS – although brass nuts are sometimes used)

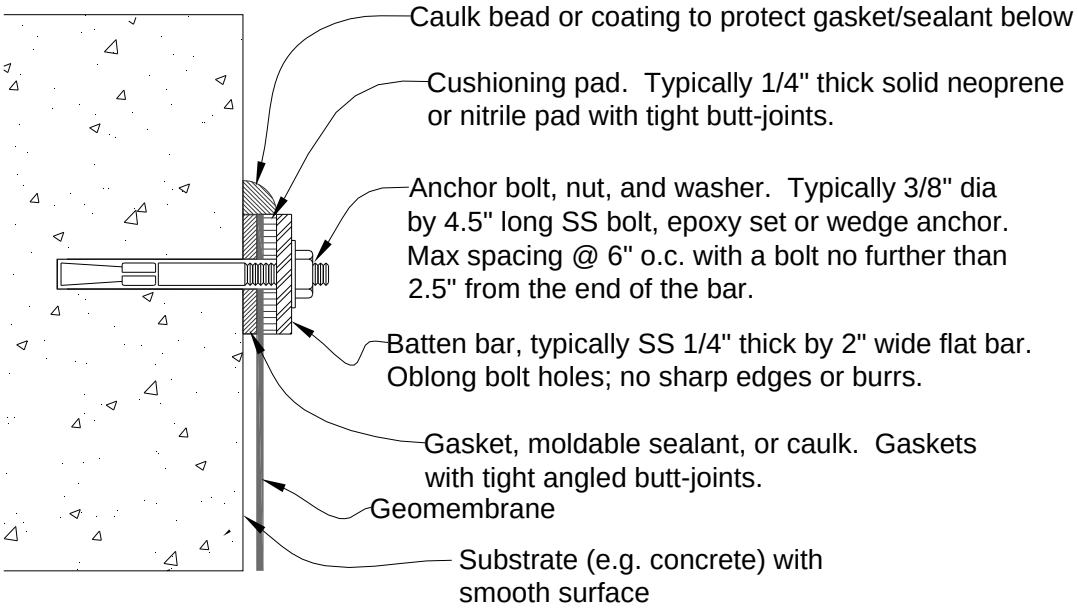

Figure 10. Schematic of typical batten bar elements.

(a) Thick fuel-resistant moldable sealant used to provide leak-resistant seal against rough concrete.

(b) Polysulfide coating over top edge of batten.

Figure 11. Examples of installed batten bars.

When the goal of a batten attachment is not merely as a mechanical connection, but is intended to be leak resistant, then many of the same problems encountered with gasketed pipe boot connections arise with batten attachments. A checklist of batten bar issues is provided in Table 2. Some common problems are illustrated in Figure 12.

(a) Wavy substrate will cause leaks.

(b) Bad concrete joint will defeat batten when submerged.

(c) Hairline crack in concrete will defeat batten when submerged.

(d) Battens at corners need special attention. This one is missing a needed bolt.

(e) Overlapped batten strips are ineffective.

(f) Gasket that was under an overlapped batten showing a section that was crushed past its elastic limit, and a section that was not compressed.

Figure 12. Photos of batten bar problems.

Table 2. Checklist of leak resistant batten bar issues.

POTENTIAL PROBLEM WITH BATTEN	POTENTIAL SOLUTION
Rough substrate	Substrate must be relatively smooth and non-wavy. Rough substrate can be partially compensated with thick moldable sealant. Wavy substrate may require more frequent anchor bolts as well as thick moldable sealant.
Stress concentration at base of batten	Put weights (e.g. continuous sandbags) next to all exposed battens to take wind stresses off of battens.
Leakage under high head or continuous submergence.	These conditions may warrant closer spacing of anchor bolts, and they may get as close as 3" spacing. The required spacing is related to the batten bar stiffness and the substrate smoothness. Detailed engineering is necessary.
Leakage at batten joints	The batten bars must be very closely butted together, but must absolutely not overlap. Anchor bolts should be located within 2" of the end of the batten bar.
Leakage past bolt holes	The solutions are: (a) drill gasket holes slightly smaller than bolts; (b) use moldable sealant that deforms around the bolts as it is compressed; (c) drilling bolt holes leaves dust in the hole that can promote leakage, so it is good to vacuum out the dust ; (d)put caulk in all bolt holes around the bolts before installing the nuts.
Leaking gasket under batten	1. Tightly overlap gasket and then cut through both layers of gasket at an angle to obtain a perfect slanted butt-joint. 2. Tightly fit geomembrane against gasket to avoid wrinkles. Bevel the inside edge of the weld overlaps. 3. Seal the overlap on the geomembrane lap joints between the two laps (for PE don't just count on the outer extrusion weld) 4. If there is a thick extrusion weld under the location of where the batten will go, it needs to be ground down and beveled smooth so that the batten provides a uniform pressure all along its length. Also, a 40-durometer cushioning layer helps distribute the battening force. 5. All of the issues illustrated in Figure 3 for a gasketed boot apply to a batten, where the batten plays the same role as the banding clamp.
Long-term gasket crushing	What really matters is gasket compression and not torque. Clamping with too low or too high of a force may result in a gasket that does not perform properly. The solution for this with batten gaskets is to calculate the allowable compression per the method given by Wells (1993), and determine how many turns of the nut will result in an acceptable amount of compression. If this is deemed unreliable, then the best solution is to use a moldable sealant, such as a mastic or a caulk, in lieu of a solid gasket material. Mastics and caulks will fill all of the voids and not be sensitive to compression strain. They generally maintain their elastic-plastic properties for long periods of time, and if chosen properly they will provide some adhesion to the surfaces. Under high-head conditions where there is a concern about plastic-flow of a mastic material, the mastic could be a secondary sealant behind a solid primary gasket.
Gasket aging and deterioration	Cover the side of the exposed gasket with a caulk. Conduct periodic inspection, caulk maintenance, and replacement as needed.
Plastic flow of moldable or mastic sealant under high-head conditions	Provide best-fit solid gasket and/or cured caulk above a moldable sealant to protect the moldable sealant from high heads and high flows.
Anchor bolt nuts become loose over time	Conduct periodic maintenance. Add more bolts if necessary. *Do not use rivets or powder-driven nails for leak-resistant battens.* You must use nuts and bolts.
Maintenance problems when taking off and reinstalling batten bars because bolt threads are nicked and galled	Solutions are: (a) always apply anti-sieze lubricant on threads before installing nuts; (b) consider using brass nuts on stainless steel bolts. The lead author has had great maintenance success with brass nuts without having negative corrosion consequences.
Corners	Special problems are created by corners. There will need to be extra-care for the wrinkles at the corners. The batten bars must meet precisely at the corner, and have bolts about 2.5" from the corner without weakening the corner.

6. LEAK-RESISTANT GEOMEMBRANE CONCRETE EMBEDMENT ATTACHMENTS

A diagram of the most typical geomembrane concrete embedment attachments is shown in Figure 13. Photographs of typical embedment attachments in the field are shown in Figure 14. An embedment attachment consists of the following generic elements:

- Concrete substrate
- Polymeric embedment strips
- Geomembrane welded to embedment

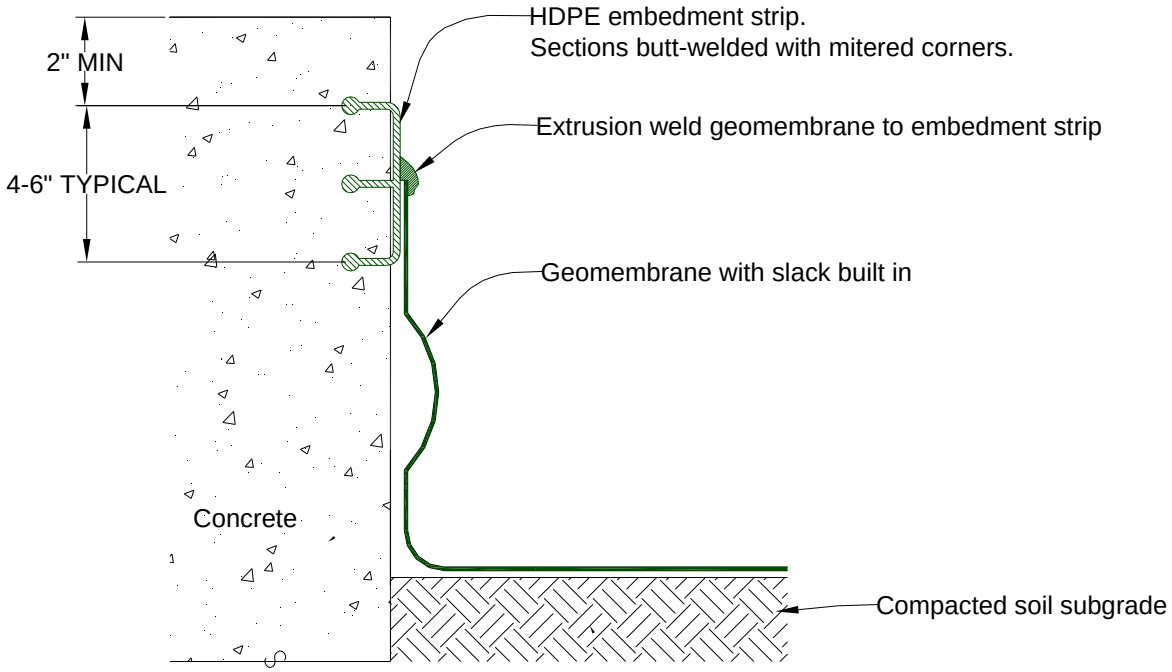

Figure 13. Basic concrete embedment strip elements.

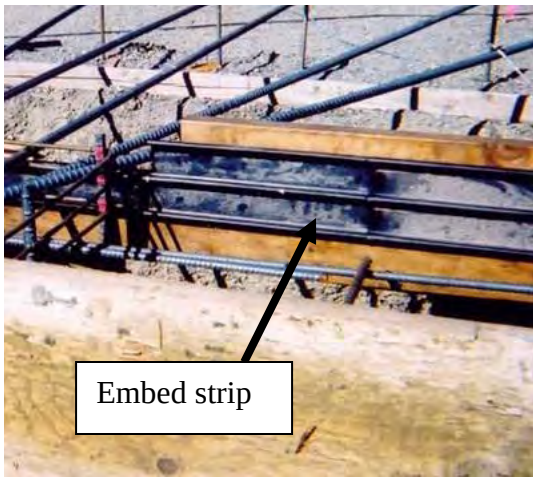

(a) Embedment strip nailed to inside of forms for secondary containment in haz-waste building.

(b) Heat tacking geomembrane to embedment strip after the concrete was placed and forms were removed.

Figure 14. Typical example of embedment strip installation and application.

Embedment strips, called “rondels” in ASTM D6497, are lengths of plastic that are cast into the face of concrete. Embedment strips serve as either simple mechanical attachments where the liner is simply welded to the embedment strip with no other special considerations, or they can serve as a leak-resistant connection that may be submerged.

Some of the first embedment strips were probably PVC “waterstops” that were designed to be cast into the concrete on both sides of a joint, and thus provide a relatively leak-resistant joint. Presumably the PVC waterstop could be embedded in the concrete and be used as an attachment point for a PVC geomembrane, although the lead author would be very suspect of the long-term bond of a geomembrane to a less-plasticized waterstop.

The most popular type of concrete embedment strip that is used for attaching a geomembrane to concrete is made from polyethylene (although the author is aware that similar types of embedment strips are also made from polypropylene and EPDM). The cross sectional shape of the embedment strips varies between manufacturers, but a common cross section is illustrated in Figure 15. A checklist of embedment issues is provided in Table 3.

Figure 15. Cut section through actual concrete embedment strip with welded geomembrane.

Figure 16. Welding geomembrane to embedment strip with preheater on extrusion gun.

Table 3. Checklist of leak-resistant concrete embedment strip issues.

POTENTIAL PROBLEM WITH EMBEDMENT	POTENTIAL SOLUTION
Leakage through concrete or around the embedment	The concrete work must be of a very high quality. It must be properly vibrated. If the concrete is honey-combed, has air voids, or ends up with hairline cracks, then the installation will leak no matter how diligent the welding is performed. Often holes drilled in the embedment strip are advisable to release trapped air. Micofiber reinforcement is recommended. Because of the difference in expansion and contraction between concrete and polyethylene, some amount of leakage can be expected over time. Leakage control is recommended on high-head applications.
Leakage by joints of embedment strips	For leak-resistant installations, it is imperative that the embedment strips be butt-fused at their joints, in a similar fashion to HDPE pipe. All corners must be mitered and butt-fused. Leister sells "mirror plates" designed to heat the embed strips for butt-fusing. If the embedment strips are not butt-welded together, then there will always be a possibility of leakage through the gap. If only the face of the butt-joint is welded, there will always be a possibility for leakage to enter the top of the embedment strip where the face-weld ends.
Nail holes	The embedment strips should be specified to be nailed to the forms using finishing nails. Screws or large-head nails may cause the embedment strips to be ripped out of the concrete when the forms are pulled off. All nail holes should be welded closed. Pulling a vacuum on a double-liner system to check for leaks with both liners welded to the same embed strip can give a false positive leak due to nail holes.
Cold weather welding	Even moderately cold weather can be a problem welding to embedment strips because the concrete is a large heat sink, in addition to the embedment strip being substantially thicker than the geomembrane. Adequate preheating is important. See Figure 16. Check weld bond periodically using field-impact test (see next item)
Welding thin gage material to thick material	Because there is no way to perform a destructive test to check the quality of the weld bond, periodically perform a field-impact test to check for potential delamination as follows: place a ½" wide blunt metal tip (e.g. large screwdriver head) against the edge of the extrusion weld and hit it with a rubber mallet. If the weld is not properly bonded it will delaminate.
Weld leak testing	Always embed a copper wire below the extrusion weld and spark test the weld. As a supplement, leakage tests can be conducted by pulling a vacuum under the liner and listening with sensitive acoustical equipment for air leakage along the welds.
Stress concentration at embedment strip due to wind forces	Put weights (e.g. continuous sandbags) next to all exposed embedments to take wind stresses off of welds.

7. LEAK-RESISTANT PE GEOMEMBRANE TO THICK-WALLED PREFABRICATED HDPE STRUCTURES

Another type of penetration is when a thick-wall HDPE structure, such as a box, sump, or pipe, penetrates into the lined area. The penetration may be through a concrete wall or floor, or through earthen subgrade materials. In this case the geomembrane liner can be welded directly to the structure. There are three considerations that should be taken into account when performing this type of connection:

1. The firmness and evenness of the subgrade immediately adjacent to the structure is important. Specifications should require that the subgrade be flush with the structure so that there is not a sharp discontinuity; and that it be firm and not prone to settlement so that a discontinuity is not formed over time. Even so, it could be a good idea to provide a geotextile cushion strip that bridges the transition from the subgrade to the structure as a preventative measure against potential future settlements.
2. The best designs would have a concrete collar flush around the perimeter of the HDPE structure so that the free-field geomembrane could be bolted (or welded to an embed strip) to the concrete in a purely mechanical fashion. A skirt would then be welded from the free-field geomembrane to the HDPE structure to bridge the gap. The skirt would be largely stress free.
3. Preheat, field-impact test, and spark test procedures as described in Table 3 would be appropriate.

8. RECOMMENDATIONS

In addition to the specific recommendations made in the checklists provided in the main body of this paper, the following general recommendations are suggested as guiding principles for designing and constructing geomembrane penetrations and boots:

- Penetrations and attachments are more susceptible to leakage that the free-field geomembrane liner for many reasons that are discussed in this paper. Owners and designers should always be prepared to manage leakage at these locations. Critical applications should always be designed with redundancy (double liners, double boots, underdrain layers, etc.).
- For exposed and serviceable installations, it is prudent to have a regular inspection and maintenance program for geomembrane penetrations and attachments.
- Penetrations and attachments require a great deal of care and craftsmanship to construct. Designers and CQA personnel should give extra attention to detailing and inspecting these items. Installers should develop in-house standards to assure their own quality of installations.

The discussion provided in this paper should have made it clear that the subject of leak-resistant details is complex and cannot be taken for granted. This situation epitomizes the saying that "the devil is in the details". There are very few technical guidance documents related to these critical aspects of containment construction to aid the specifier and design practitioner, and a lot of faith is usually put on the skill and craftsmanship of the installer. It is hoped that this paper will raise the awareness of the profession to some of the critical issues associated with these details, and that it will lead to higher levels of standardized construction.

ACKNOWLEDGEMENTS

The authors would like to thank Stan Kamienski of NW Linings, Tim Harding of Great Basin Environmental, Bryant Jefferson of Colorado Linings, Andre Harvey of Colorado Linings, Jafer Jaweed from Field Lining Systems, and Dan Murphy, P.E. for their open discussions and providing their opinions as installers.

REFERENCES

ASTM D6497, Standard Guide for Mechanical Attachement of Geomembrane to Penetrations or Structures, American Society for Testing and Materials, West Conshohocken, Pennsylvania, USA.

Daniel,D. and Koerner, R.M. (2005). *Waste Containment Facilities: Guidance for CQA and CQC of Liner and Cover Systems.* 2nd Ed., ASCE Press,354 pgs.

Bonaparte, R. Daniel, D.E. and Koerner, R.M. (2002). *Assessment and Recommendations for Improving the Performance of Waste Containment Systems*. USEPA Report No. EPA/600/R-02/099, Office of Research and Development, Cincinnati, OH, USA.

Koerner, R. M. (1994). *Designing with Geosynthetics*. 3rd Ed., Prentice Hall, Englewood Cliffs, NJ, USA.

PolyFlex (2008). Polyethylene Embed Channel Specification. *Polyflex website,* http://www.poly-flex.com/dropin.html

Wells, L. (1993). Guidance for design of watertight geomembrane attachments to concrete surfaces, *Geosynthetics '93*, IFAI, Vancouver, BC, Canada, pp 1119-1129.

To Batten Or Not, and If So – How?

I. D. Peggs, I-CORP INTERNATIONAL, Inc., United States of America
D. T. Viljoen, Engineered Linings Ltd., South Africa

ABSTRACT
Batten strip water stops cannot be totally avoided in geomembrane lining systems. When they must be used components of batten systems used by an experienced installer and how they are installed are described together with some thoughts on the influences of concrete roughness, gasket dimensions, gasket properties, and compressive forces required. It is evident there is no technically-based standardized procedure for sealing with batten strips but it would be beneficial to the industry to develop one.

1. INTRODUCTION

Batten strip attachments are sometimes a necessary evil, particularly when underwater, which should be avoided wherever possible. In some situations they will never work (Figure 1), in others they can be pulled out (Figure 2) and still others they must be fastened down (Figure 3). Unfortunately there are few quantitative guides to their installation. ASTM D6497 shows a cross section of recommended system (Figure 4) which complements that of Well (1993) as shown in Figure 5. Both of these show gaskets on each side of the geomembrane, which is not often done. Some details that have been generated by one of the authors (Viljoen) through many years of installation in North America and Africa are presented for general consideration and for refinement to specific project applications.

Figure 1. Inadequate sealing of geomembrane beneath batten strip.

Figure 2. Liner pulled from batten strip by adjacent wrinkle.

Figure 3. Improperly fastened batten strip.

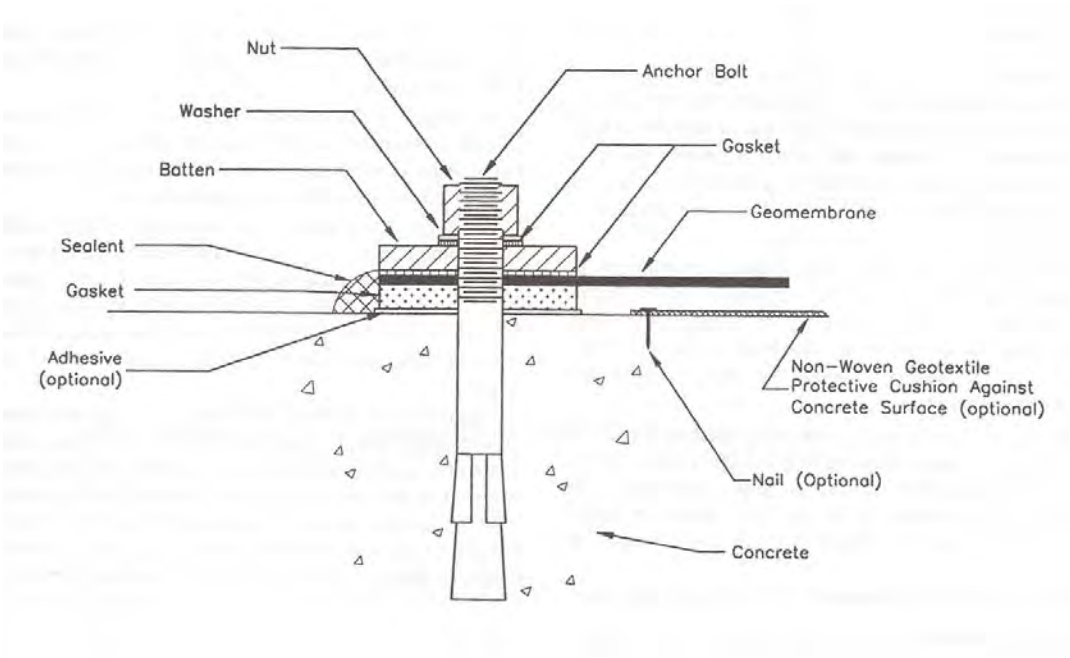

Figure 4. Cross section shown in ASTM D6497.

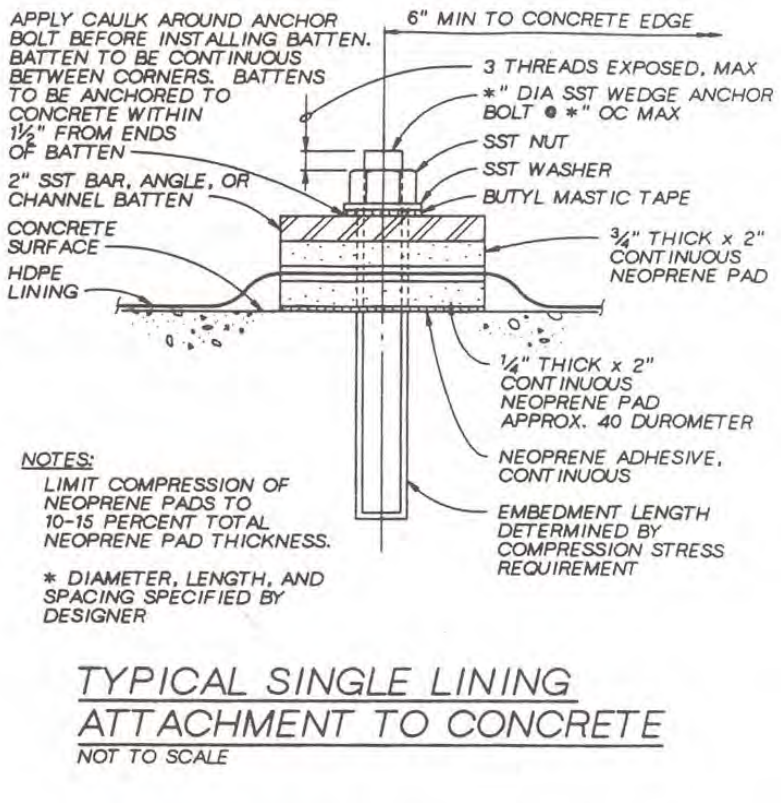

Figure 5. Cross section proposed by Well (1993).

There are six major factors to consider for successful batten strip seals:

- The physical nature of the geomembrane at the fastening – wrinkles, welds, stress, etc.
- Clamping pressure required, along with properties of gaskets
- Surface finish of concrete or other substrate
- Fastener anchorage in concrete or other substrate
- Batten strip material and dimensions
- Chemical resistance of the various components

Ideally, there should be no penetrations through a geomembrane lining system. However, it is not always possible to avoid this, so next best is to minimize the number of these penetrations. It is essential that great attention be paid to these details, as the tendency is to concentrate on geomembrane material specifications and their QC and QA requirements. However, due to a lack of experience and knowledge, many specifiers and engineers tend to overlook the importance of the more complex liner details at penetrations, and simply rely on the installers to do whatever they believe is best.

1.1 Gaskets

There are several types of penetrations through liners, e.g. pipes, manholes, columns, walls, and sumps, and there are many load-bearing concrete structures that require protection and sealing using geomembranes. The second author has found the most reliable sealing detail to be clamping the geomembrane between two pipe flanges using a single or double gasket to provide the necessary sealing effect. But, when it comes to sealing onto concrete surfaces, it is much more difficult to get a good seal. In the mid-1980s the major author used an 8-mm-thick closed-cell neoprene gasket. Its type was R-451-N, made by Rubatex. The density was 0.35 to 0.57 g/cm^3 and it had compression deflection of 117 to 165 kPa. Compression deflection is the force require to reduce the thickness to 25% of the original. This product is still available.

On returning to South Africa in 1989, we could not get the same density gaskets. We tried a Neoprene 25, which had a density of only 160 kg/m^3, but this had inadequate compressive strength and suffered excessive permanent deformation; the 8 mm initial thickness could be compressed down to approx 1 mm. After extensive research we found a 6 mm thick natural gum rubber that produced good results.

It is critically important that the holes through the gasket be pre-punched (and *not* drilled) - typically about 3 - 4 mm smaller than the bolt diameter to ensure a tight fit around the bolt shaft. Also, the gasket should be positioned on the smooth shaft of the bolt—*not* on the threaded section. If this is not possible, some silicone caulking around the bolt and on the concrete surface can help to prevent water from running through the threaded section. But using too much caulking could lubricate the surface of the gasket, and while the nuts are being torqued the gasket may slide/bulge out to one side, leaving a gap between the gasket and the bolt shaft. The ends of the strips of gaskets should be chamfered at ca. 45º, and then glued together. Where a square frame is made around a penetration, the four corners should be glued, and the joints in the steel batten should always be off-set from the joints in the gasket. In other words there should be no unglued joints in the gasket.

Well (1993) states that the important parameters of gaskets are hardness, thickness, shape, and compressive elastic properties. The objective of the compression seal is not to plastically (irreversibly) compress the gasket to force it to conform to the surface profile of the concrete, such that the batten strip is deformed, but rather to deform it elastically and uniformly with minimum required stress such that creep will be a minimum. Therefore, ambient temperature is very important. Thus, the nuts are not torqued to the maximum level possible. Compression force must remain within the elastic range of the gasket material. This usually requires the compression to be within the range of 10 to 15% of the thickness of the gasket with temperature not to exceed about 65°C.

The force required to generate this deformation is a function of the “Shape Factor” (SF) of the gasket, which, for a rectangular cross section is:

$$SF = wl/[(2t)(w+l)] \quad [1]$$

where:

- w = width
- l = length
- t = thickness

A nomograph relating compressive deformation to hardness, shape factor, and compressive stress is shown in Figure 6 (Well, 1993). Shape factors of 2 or 3 are recommended.

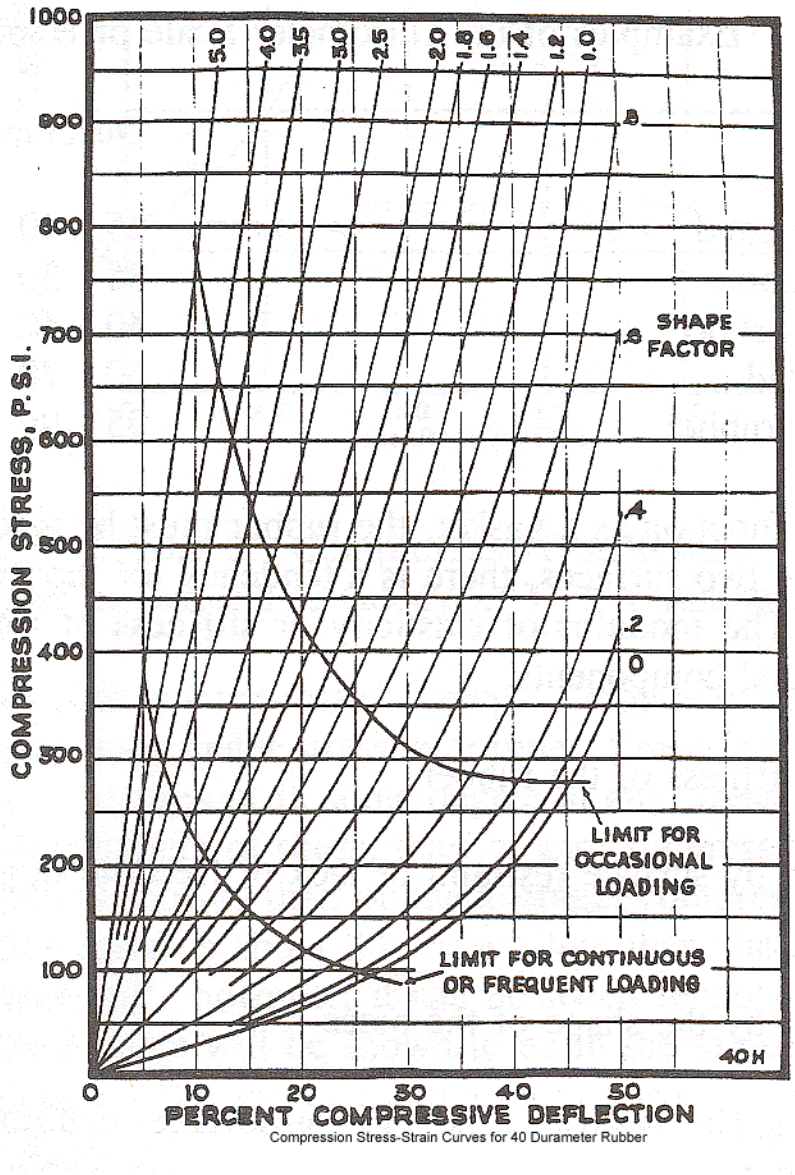

Figure 6. Relation of rubber compression to deflection.

(Reprinted by permission of The Goodyear Tire & Rubber Company, 1959)

Therefore, a typical 10 to 15% compressive deformation of a typical 12.5 mm thick gasket will be approximately 1.5 mm. This will require less than one turn of a nut on a 10 to 12.5 mm diameter bolt with about 6 threads/cm. This is a little impractical, so gasket parameters could be adjusted to require about 2 turns. Well proposes 12.5 mm (0.5 in.) diameter bolts with ~10 threads/cm.

Viljoen finds that appropriate specifications for natural gum rubber gasket material should be as follows:

- Compound reference = NR40
- Hardness = 40 IRDH (± 5 units)
- Specific gravity = 1.12
- Thickness = 6 mm
- Elongation at break = 660% (uniaxial tension)

1.2 Batten strips

Appropriate dimensions of flat steel batten strips and bolt spacing depend on the hydraulic head**.** Under less than one meter head Viljoen suggests 40 x 4.5 mm for stainless steel or 40 x 5 mm if galvanized strip is used, fastened with 8 mm nail plugs or bolts at maximum 160 mm centers. If the hydraulic head is greater than one meter, one should use 40 x 6 mm battens with 10 mm bolts at maximum 160 mm centers.

Bolts should be torqued to 35 Nm, and re-torqued the next day after the gasket has been allowed to equilibrate. This torque, of course, is specific to Viljoen's NR40 gasket material and its shape factor. Stainless steel nuts may tend to weld onto the bolt shafts, so ensure that you can tighten them the next day. An appropriate stainless steel should be used for the liquid being contained. Avoid steels that might pit or are susceptible to crevice corrosion in the liquids of interest. Note that stainless steels are in fact not necessarily "stainless". Rather they more correctly just "stain less" than non-stainless steels.

At the ends of batten strips there should be a bolt that is no further from the end than 50 mm. If the strip is not an underwater seal the distance between bolts may be increased to 300 mm. However, for mechanical performance, this may require a thicker strip since the same requirements for uniform deformation of the gasket and non-deformation of the batten strip still apply.

Viljoen finds that one rubber strip between the concrete surface and the geomembrane is generally adequate, but many projects have been done where a gasket had been specified on both sides of the geomembrane, as proposed by Well (1993) and ASTM. In fact Well (1993) has proposed a 6 mm gasket between geomembrane and concrete together with a 19 mm thick gasket between geomembrane and batten strip.

1.3 Concrete surface

It is essential that the concrete surface has an even, smooth steel trowel finish and be strong enough to hold the anchor bolts in place. While angle iron is sometimes used as a batten strip it is not preferred because the concrete surfaces are not always straight, and it is impossible to bend an angled section to follow the contours of the concrete surface. Note that if the objective is to deform the gasket to only 10 or 15% of its thickness using an essentially non-deforming batten strip, the concrete surface should be smooth to that same 10 to 15% tolerance, otherwise there will be locations where the gasket may not be compressed at all, and where it may be compressed 20 to 30%. Hence, there is an advantage of a double gasket that provides deformation and more uniform confinement from both sides of the geomembrane.

1.4 Geomembrane

A loose skirt of geomembrane, ideally with no welds, folds, or liner overlaps under the gaskets, should be used to ensure proper access to the working face, and to ensure uniform confinement of the geomembrane and gasket between batten strip and concrete. Welds should not be stopped short of the batten strip with overlaps continuing under the batten strip as shown in Figure 7. Welding the skirt to the main lining should then be done after the gasketting has been completed and all bolts fastened. This ensures that the main liner is as stress free as possible.

Figure 7. Extrusion weld stopped short of batten strip allowing liner overlap to leak as indicated by the pointer.

In some cases, a free flap of liner on the outside edge of the batten strip is folded back over the strip and extrusion welded to the main liner, with the expectation that this will act as a back-up (or front-up) to prevent any leakage along the bolts. It will also prevent the batten strips from generating large background signals when contacted by the positively charged water used in water lance and water puddle geoelectric surveys. However, there is always a danger that if the liner is not protected from the anchor bolt ends the hydrostatic pressure will cause the bolt heads to puncture the folded back liner. In any case the geoelectric survey will not identify leaks under the batten strip due to the water making contact with the concrete structure. To avoid this, the concrete structure itself should be covered with geomembrane that extends outwards beyond the batten strips and is welded to the main geomembrane. Here again the geomembrane over the concrete must be protected from puncturing by the protruding anchor bolt ends.

2. SUMMARY

In summary, batten strip attachment of geomembranes to concrete and other structures, is still somewhat of an inexact technology. While good gasket technology is available it typically is not used, with each liner installer following its own standard procedure. This is surprising since underwater batten strip seals can be quite critical. There are potential leakage pathways between concrete and gasket, between gasket and geomembrane, and through other interfaces to and then along the side of the anchor bolt. It is better to cover the batten strip with another layer of geomembrane that covers the concrete so the batten seal is not the active seal. Alternatively, one could raise the batten seal above the maximum operating level. Also, one could use a cast-in extruded profile to which the liner is integrally welded. These options, however, have their own concerns.

Therefore, assuming an appropriate gasket material has been selected with an appropriate shape factor, the sealing procedure might be as follows:

- Remove roughness (> 5% gasket thickness) from concrete surface
- Place batten and mark locations of anchor bolts
- Drill and install anchor bolts
- Use bolts with ~10 threads/cm but with smooth shafts the thickness of the gasket(s) and the geomembrane

- Punch, not drill or cut, holes in gaskets and geomembrane with a diameter about 3 mm less than diameter of bolts.
- Place ~6 mm gasket and adhere to concrete
- Place the geomembrane
- Place ~12 mm gasket
- Place the batten strip
- Apply and tighten nuts to generate about 1.5 mm deformation of gaskets.
- Leave overnight and the following day tighten nuts for another 0.7 mm deformation.
- Apply caulking to outer edges of gaskets, geomembrane, and onto adjacent concrete. This is more important for cut edges of reinforced geomembranes.

In practice the treatment of batten strips is far from standardized, with each installer using his/her own design. Some standardization would be beneficial, such as:

- Gasket material, number of gaskets (one or two), and thicknesses
- Need for and type of gasket/concrete adhesive
- Dimensions of batten strips
- Roughness of batten strip surface on geomembrane or type of interlayer to be used to increase friction to minimize liner pullout and bolt hole tearing
- Diameter and spacing of bolts
- Length of smooth and threaded sections of bolts
- Number of threads/cm
- Diameter and method of making bolt holes in gaskets
- Torque applied to nuts and frequency, or deformation required of the gasket

REFERENCES

ASTM D6497 “Standard Guide for Mechanical Attachment of Geomembrane to Penetrations or Structures”, *American Society for Testing Materials*, West Conshohocken, Pennsylvania, USA.

Viljoen, Du Toit, and Kelsey, C., “Tech Note: Batten Strips and Geomembranes”, www.geosynthetica.net ID#3211, 11/27/07.

Well, L.W., (1993). Guidance for Design of Watertight Geomembrane Attachments to Concrete Surfaces”, Geosynthetics ’93, IFAI, Roseville, MN, USA, pp 1119-1129.

Transition Details for Turf Reinforcement Mats in Storm Water Channels

S. Manning, Propex, Inc., Chattanooga, TN, USA

ABSTRACT
Whoever coined the phrase “the devil is in the details” was onto something. With erosion control products much like any construction product, if they are not installed correctly they simply will not perform correctly. Installation details for turf reinforcement mats (TRMs) and high performance turf reinforcement mats (HPTRMs) are critical for optimum performance. This paper will demonstrate a typical installation and then provide special details when they are used in combination with other systems.

1. TYPICAL CHANNEL/SWALE INSTALLATION

Any project should start with an overall concept of what the project should look like when completed. The concept could come as a plan view, cross-section, or isometric view, the latter being shown in Figure 1.

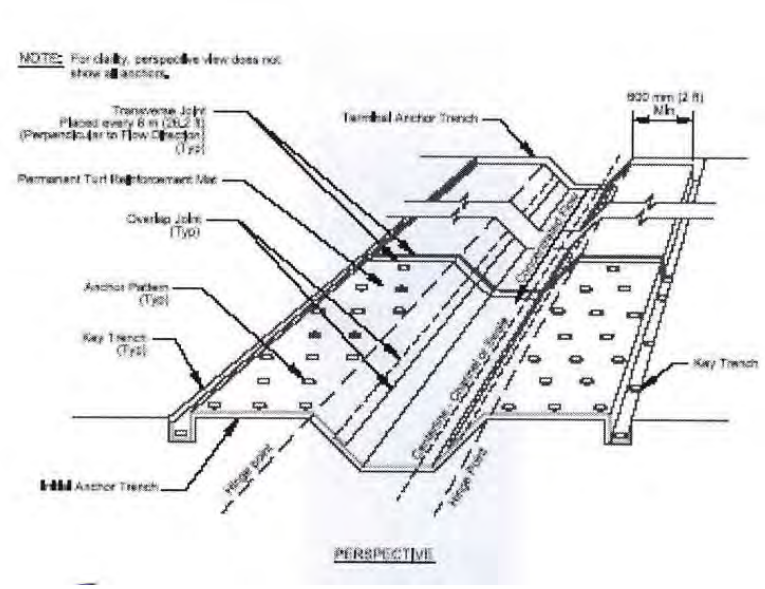

Figure 1. Turf reinforcement mat used in a trapezoidal channel or swale.

The installation concept can be thought of as a jig-saw puzzle with many pieces fitting together in harmony. The pieces, i.e., details, are each designed to provide a specific purpose. Figure 1 above has at least six major details that need to be included just to make the system perform properly.

The details and their respective functions are an upstream trench which minimizes the effect of water coming onto the mat and a downstream trench allowing the water to exit the protected channel without undermining the mat. Other details include longitudinal trenches along the top of the channel that protect the top and sides of the channel from water coming in and undermining the side slopes. Pinning details that inform the installer how often to secure the mat are obviously critical. Overlap details that demonstrate correct spacing and pinning along the sides and roll ends are also important. Finally, unique details including system combinations with hard armor (riprap, concrete, and gabions) and securing TRMs to structures complete the system.

After design but before installation one needs to provide for other details that are not on plans such as site preparation. Site preparation includes grading and compacting the particular area of TRM/HPTRM installation as directed and approved by Engineer. For example, all rocks, clods, vegetation or other objects should be removed so the installed mat will have direct and intimate contact with the soil subgrade. One must prepare the seedbed and incorporate amendments such as lime and fertilizer and/or wet the soil, if needed. Generally, one must apply seed to the soil

subgrade before installing the mat. Disturbed areas must be reseeded. When soil filling, first install the mat, apply seed and then soil-fill per the specification. Project plans and/or specifications must be followed for seed types and application rates.

It is important to remember that installation of TRMs in a channel starts at the downstream section of the project and is installed upstream. This is to insure that overlaps and trenches shingle water correctly. Figure 2 shows the initial trench which is the first trench needed on a project. The trench is excavated across the channel a minimum of 12 in. (300 mm) deep and 12 in. (300 mm) wide at the downstream end of the project.

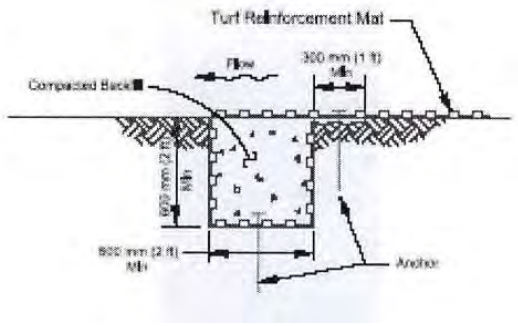

Figure 2. Initial anchor trench downstream detail.

Deeper initial anchor trenches are needed in channels that have the potential for scour. The roll end is placed into the initial anchor trench and secured with anchoring devices at 12 in. (300 mm) minimum intervals. Position adjacent rolls and secure them in the anchor trench in the same manner. Then, backfill and compact the removed soil into the trench. Finally, unroll the mat in the upstream direction over the compacted trench.

Depending on the sequence and geometry of the channel, the next step is to install the longitudinal trenches along the top of the channel side slopes. This is the outside most edges, 2-3 ft. (600-900 mm) over the crest of the slope, of the mat parallel with the channel bottom. The dimensions of trench should be a minimum of 12 in. (300 mm) deep and minimum of 6 in. (150 mm) wide. A detail of the longitudinal trench is shown in Figure 3.

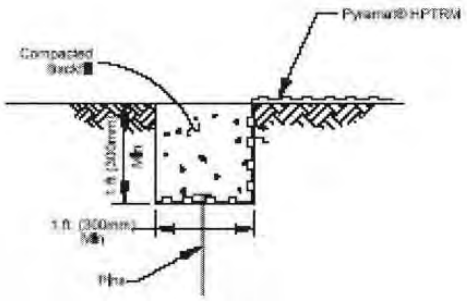

Figure 3. Longitudinal edge trench detail.

Adjacent roll should be overlapped and secured. The installation continues as shown in Figure 4. The roll edge should be 6 in. (150 mm), with the upslope mat on top. They should be secured with one row of ground anchoring devices on 12 in. (300 mm) minimum intervals.

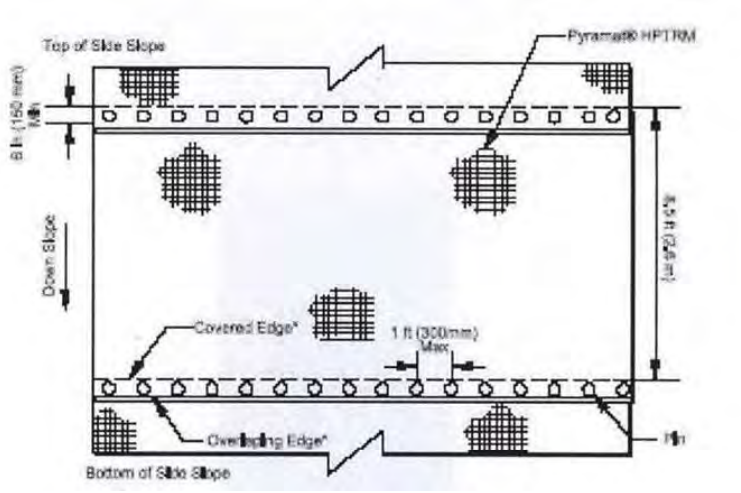

Figure 4. Pyramats® HPTRM overlap at roll edge detail.

The roll end should be 12 in. (300 mm) minimum, with the upstream mat on top. Secure the two rows of ground anchoring devices staggered 12 in. (300 mm) minimum apart on 12 in. (300 mm) minimum intervals, as shown in Figure 5.

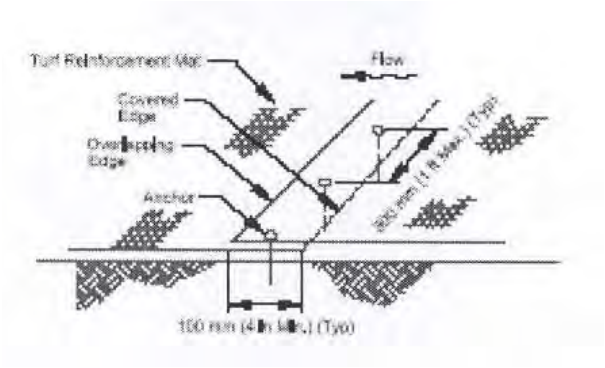

Figure 5. Turf reinforcement mat overlap joint.

As the installation progresses, continue rolling upstream over the prepared subgrade to the next check slot or terminal trench. Check slots are securing locations every 25 to 30 feet (7.6 to 9.1 m). This measure helps control water that might get under the mat and force it back on top. Check slots are placed at 25 to 30 ft. (7.6 t 9.1 m) internals perpendicular to the flow, see Figure 6.

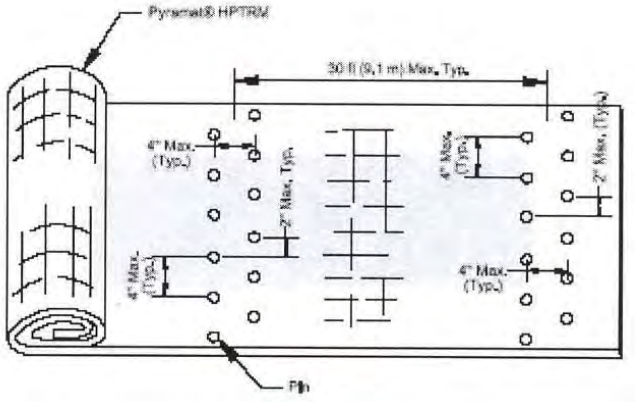

Figure 6. Simulated check slot detail.

The check slot includes placing two staggered rows of anchors on 4 in. (100 mm) centers at 30 ft (9.1 m) intervals.

A terminal trench is used to finish and secure the installation. The terminal trench is located at the upstream most end of the project and is installed by excavating a minimum 12 in. wide × 12 in. deep (300 × 300 mm) trench across the channel. A deeper terminal anchor trench is needed in channels that have higher potential for scour. Place the mat in the trench, anchor, backfill it and compact the soil. Finally, unroll the mat in a downstream direction over a compacted trench with a minimum 1 ft. (300 mm) lap as shown in Figure 7.

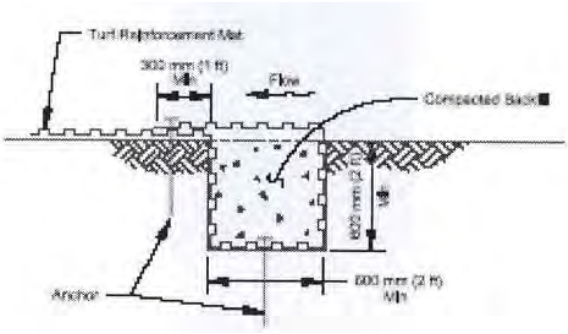

Figure 7. Terminal anchor trench (upstream) detail.

When using a TRM with a geotextile backing, one should seed after installing the mat and then fill it with soil. In all cases, one should irrigate as necessary to establish and maintain vegetation.

2. SPECIAL TRANSITON DETAILS

There are several special transition details that are necessary when using multiple armoring systems in a channel. An example of this would be a channel with continuous water flow in the bottom. In this situation some type of hard armor, like rip riprap, articulated concrete mattresses, placed concrete, or gabions may cover the bottom and a TRM used on the side slopes. This type of system allows for the protection needed on the bottom along with a green solution on the side slopes. These special details may need to be modified specifically for each project. Figure 8 shows a transition detail between concrete on the base and woven TRM or HPTRM on the side slopes.

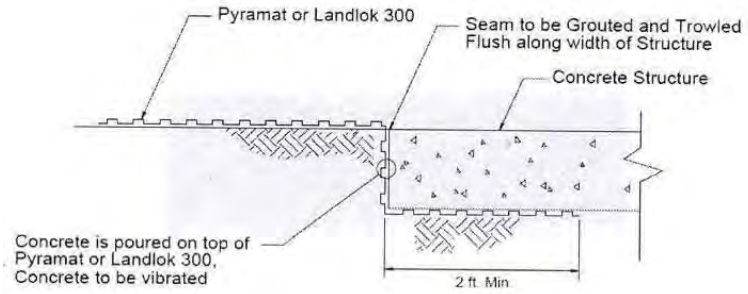

Figure 8. Transition detail between hard armor and TRMs or HPTRMs.

The special detail of Figure 9 illustrates riprap along the lower side slopes transitioning into a TRM or HPTRM up the slopes in a channel situation. It should be noted that HPTRMs and higher tensile strength TRMs should only be used with this particular detail.

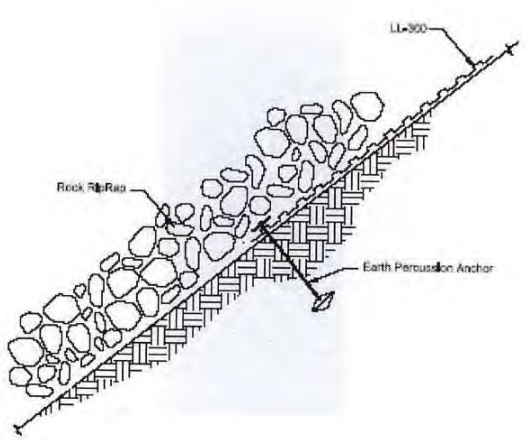

Figure 9. Rip-rap transition details to TRMs or HPTRMs.

Another special detail is attaching TRMs and HPTRMs to structures located with the limits of channels like headwalls and concrete aprons. Figure 10 is a detail of a woven HPTRM and low flow concrete channel being attached with a threaded dowel, washer and hex-nut.

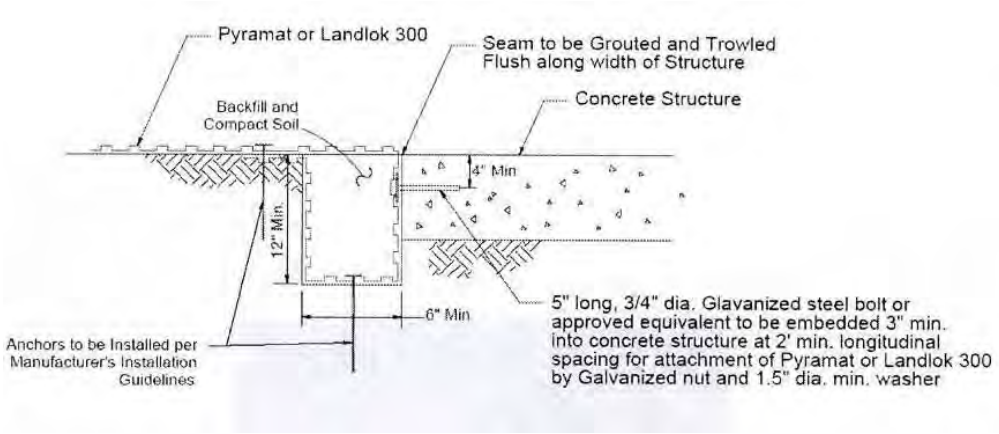

Figure 10. Transition detail of a woven HPTRM to a concrete channel.

3. CONCLUSION

The capability of manufacturing consistent quality turf reinforcement mats (TRMs) and high performance turf reinforcement mats (HPTRMs) is clearly within the state-of-the-practice. The details of installation, however, can circumvent the best quality manufactured materials in all cases. With both TRMs and HPTRMs, details center around connecting like products, e.g., one TRM to the adjacent TRM and dissimilar products, e.g., a TRM to a hard armor system. In this latter situation hard armor like rock rip-rap, articulated concrete mattresses, cast-in-place concrete, and gabions all require special attention.

This paper has attempted to present best installation practice in myriad situations. The eventual performance of TRMs and HPTRMs is critically dependent upon high quality installation practices as described herein.

Geocomposite Drainage Material Connections and Attachments

R. M. Koerner, Drexel University, Philadelphia, PA, USA
G. R. Koerner, Geosynthetic Institute, Folsom, PA, USA

ABSTRACT
Geocomposite drainage materials consist of at least one geotextile attached to a geonet or other type of drainage core. The geotextile serves as both a filter and separator to the adjacent soil so that it allows for liquid flow yet prevents soil intrusion. Oftentimes, geotextiles are on both sides of the drainage core. The geonet or drainage core is the "drain" component which allows for liquid transmission within its plane to a downgradient exit area; be it a outlet pipe, sump, or swale.

Since manufactured rolls of geocomposite drainage materials must cover large areas, field constructed connections along their sides and ends are necessary. This paper addresses such connections. Even further, the ends of the geocomposites must eventually terminate by attachment to pipes, sumps or swales. These are also made in the field by construction personnel. The following situations are presented in this paper illustrating various connections and attachments which the authors currently consider to be best-available-practice;

- connection of overlapping geocomposites on their ends and sides
- geocomposite to horizontal pipe connection
- geocomposite to vertical pipe connection
- geocomposite termination in sumps and swales
- geocomposite termination within landfill anchor trenches

1. INTRODUCTION

There are many different types and configurations of geocomposite drainage materials. All of them, however, are characterized by having a geotextile(s) bonded, attached, or laid upon a drainage core. The geotextile can vary, but for reasons of their versatility and economics, needle-punched nonwoven polypropylene fabrics are the most widely used. Much greater variation is in the drainage core. Biplanar and triplanar geonets are commonly used in waste containment applications; see Figure 1a. They are all made from high density polyethylene. Stiff three-dimensional meshes (made from polypropylene or nylon), and built-up polymer columns, cuspatations, and dimples (made from polystyrene or polyolefins) are also available. They are commonly used in transportation and private development applications; see Figure 1b. The manufacturing of geocomposite drainage materials is very active with new products, and variations of existing products, being developed on a regular basis.

(a) Geonet composite drains (b) Other geocomposite drains

Figure 1. Various types of sheet drainage geocomposites.

Regarding the design of drainage composites there is a wealth of knowledge available. GSI's key word data base indicates that forty-three references are available focusing on the required flow rate or transmissivity in myriad applications. An even greater number of references (seventy-eight in our data base) is available for calculation of the required flow rate or permittivity of the covering geotextile.

Regarding standardized testing of drainage cores for allowable flow rate or transmissivity, one has a choice between ASTM D4716 or ISO 12958. The allowable flow rate or permittivity of geotextiles is addressed in both ASTM D4491 and ISO 11058.

Of course, the issue of a design value counterpointed against a test value is the customary factor-of-safety (FS) upon which each component (drainage core and geotextile) is selected for a particular project. The tacid assumption, however is that field installation is such that the design and testing is representative of the field installation. As such, this paper attempts to present proper field installation of connections and attachments of drainage composites to one another, to various outlet systems such as pipes, sumps and swales, and to anchor trenches.

2. CAVEATS OF THE SUGGESTED CONNECTION AND ATTACHMENT DETAILS

In the suggested installation details to be presented in this paper there is considerable subjectivity taken on the part of the authors. *In fact, this is an opinion paper, pure and simple*. As such, a few caveats regarding our assumptions are in order:

- Butt joining of upgradient-to-downgradient drainage cores is not appropriate for any of these materials. The reason for this is that even a slight separation of the two ends will allow the covering geotextile(s) to intrude into the open space greatly decreasing the allowable flow rate. Overlapping ends of all drainage geocomposites are required in all applications.
- Liquid flow within an upgradient geocomposite core discharging to an overlapped downgradient geocomposite core or drainage pipe cannot have an imbedded geotextile(s) within the flow area. The upgradient core must empty directly into the dowgradient core or pipe without flow passing through an intervening geotextile.
- The upper and/or lower geotextiles must be capable of being hand stripped off of the geocomposite core. This has direct bearing on the adhesion of the geotextile(s) to the drainage core. In this regard, specifications should be limited to a maximum peel strength; perhaps 175 N/m (1.0 lb/in.). There should obviously be a minimum peel strength as well so as to prevent an interface slide from occurring; perhaps 87 N/m (0.5 lb/in.). See Figure 2 for the peel testing of a geotextile from a biplanar geonet core.

Figure 2. Peel testing of a drainage composite per ASTM D7005.

- There can be no exposed drainage core directly against soil, either above or below, at any location. There must be the specified type of geotextile between the drainage core and soil to prevent intrusion of soil into the drainage core. If necessary, the bonding of additional geotextile to the composite's geotextile can be made by heat bonding, adhesive, or sewing.
- The mechanical joining of the sides and ends of rolls of geocomposite drainage materials is usually done with electrical ties; see Figure 3. The main purpose is to provide fixed positioning so as to achieve sheet flow throughout the area to be covered. The spacing of these electrical ties is quite arbitrary but a consensus for biplanar and triplanar geonets appears to be about 220 mm (9.0 in.) at the ends and 1.5 m (60 in.) along the sides. These values also seem reasonable for three-dimensional mesh cores, but not for cores with columns, cuspations and dimples. Manufacturers literature should be followed for these latter products.
- The bonding of geotextiles to other geotextiles has been done by many methods. Heat burnishing use a plate or shoe, use of an adhesive, and actually sewing are all acceptable as long as the bonding is continuous. Strength, per se, is not particularly important.
- The various connections and attachments to follow apply to geonets (biplanar and triplanar, the latter requiring flow orientation to be appropriate) and three dimensional meshes. The built-up polymer sheet cores have unique characteristics insofar as their joining is concerned.

Figure 3. Plastic ties joining sides of a biplanar geonet.

3. GEOCOMPOSITE CONNECTIONS AND ATTACHMENTS

The sketches presented in this main section of the paper are considered to be best-available-technology by the authors. Each situation conforms to the "caveats" presented in the previous section. At the outset, however, we do realize that it is far easier to sketch various situations than it is to fabricate them (continuously under all weather conditions) in the field.

3.1 Connection of Overlapping Geocomposites on Their Ends and Sides

Figure 4 shows an overlapped geocomposite with the upgradient end overlapping the downgradient end. For the sides of the rolls which is placed, upper or lower, is not important. The recommended lengths of overlap ("L") are 300-450 mm (12-18 in.) for ends and 100-150 mm (4.0-6.0 in.) for sides. One other consideration has to do with the roll ends being factory supplied or cut in the field. The manufacturers of geocomposites usually leave an excess of 300 mm (12 in.) of unbonded geotextile for complete coverage purposes. Field cut geocomposites have no such excess geotextile.

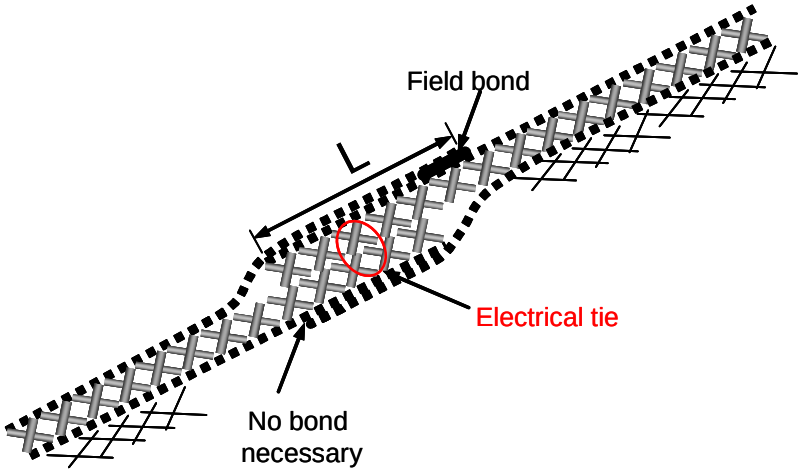

(a) Field cut ends

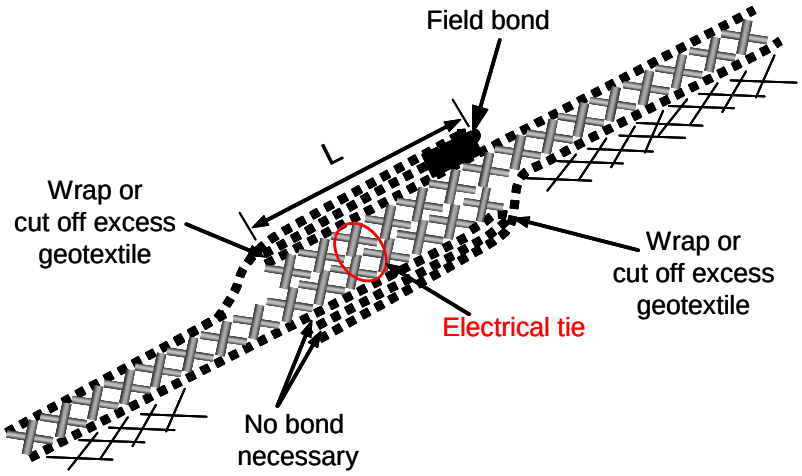

(b) Factory ends with excess geotextile

Figure 4. Recommended overlapping of geocomposite drainage materials.

3.2 Geocomposite to Horizontal Pipe Connection

Geocomposites very often empty their flow into a horizontally placed perforated drainage pipe. The drainage pipe is usually corrugated HDPE with slots in the valleys of the corrugations. However, where external stresses are high, the drainage pipe is often solid wall HDPE or PVC pipe with holes drilled in it at uniform spacings. Whatever the pipe type, the geocomposite drainage core should wrap around the entire pipe with no intervening geotextile in the flow transfer area. Figure 5a gives the desired, but admittedly difficult, preferred detail. The geocomposite's upper geotextile must be stripped off the drainage core, greatly trimmed, and then bonded to the reverse side of the geocomposite with its geotextile intact after wrapping around the pipe. The overlap distance "L" should be approximately three times the encapsulated drainage pipe diameter. Also note that plastic electrical ties are necessary to hold the geonet together particularly for thick biplanar and all triplanar geonet composites. Generally, two ties are necessary to minimize the air space around the encapsulated pipe. This same detail can also be followed if the drainage pipe is located in a trench at a lower elevation than the exiting geocomposite drain; see Figure 5b.

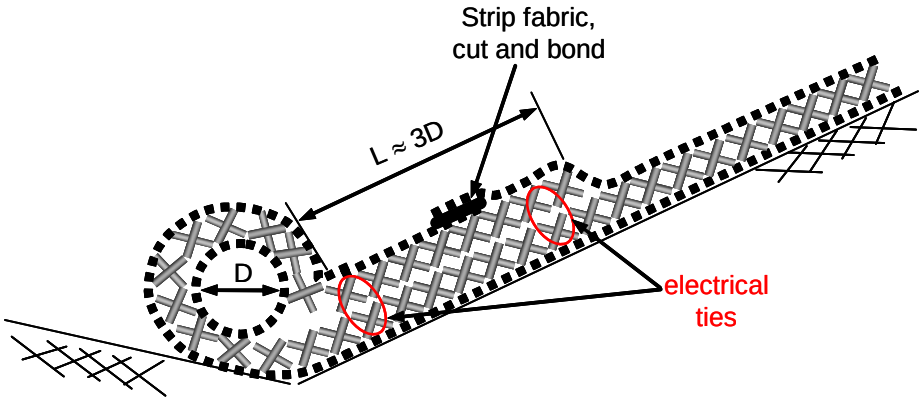

(a) Drainage pipe on a slope

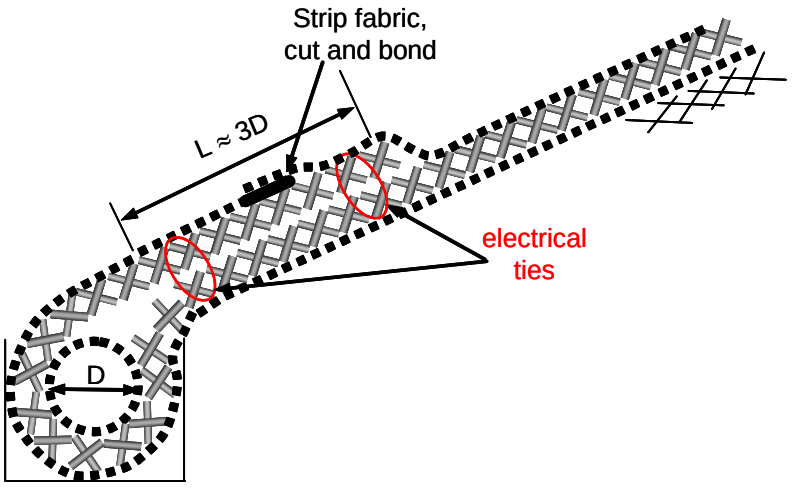

(b) Drainage pipe in a trench

Figure 5. Recommended geocomposite to horizontal drainage pipe connection.

3.3 Geocomposite to Vertical Pipe Connection

A geocomposite drainage system is often used for the collection and transmission of gas under the final covers of solid waste landfills. This drainage composite is located immediately beneath the geomembrane in the cover system. Figure 6a shows the typical situation. Fortunately, commercially available adapters are ideal for these connections; see Figure 6b. A force fit by opposing flanges of the adapter snugs up the geocomposite and allows for full exit of the gases (or liquids). The final extraction is from solid wall pipe (HDPE or PVC) stantions which penetrate the overlying topsoil, cover soil and geomembrane. A geomembrane pipe boot prefabricated to fit over the connection's shaft is necessary for a proper seal of the geomembrane.

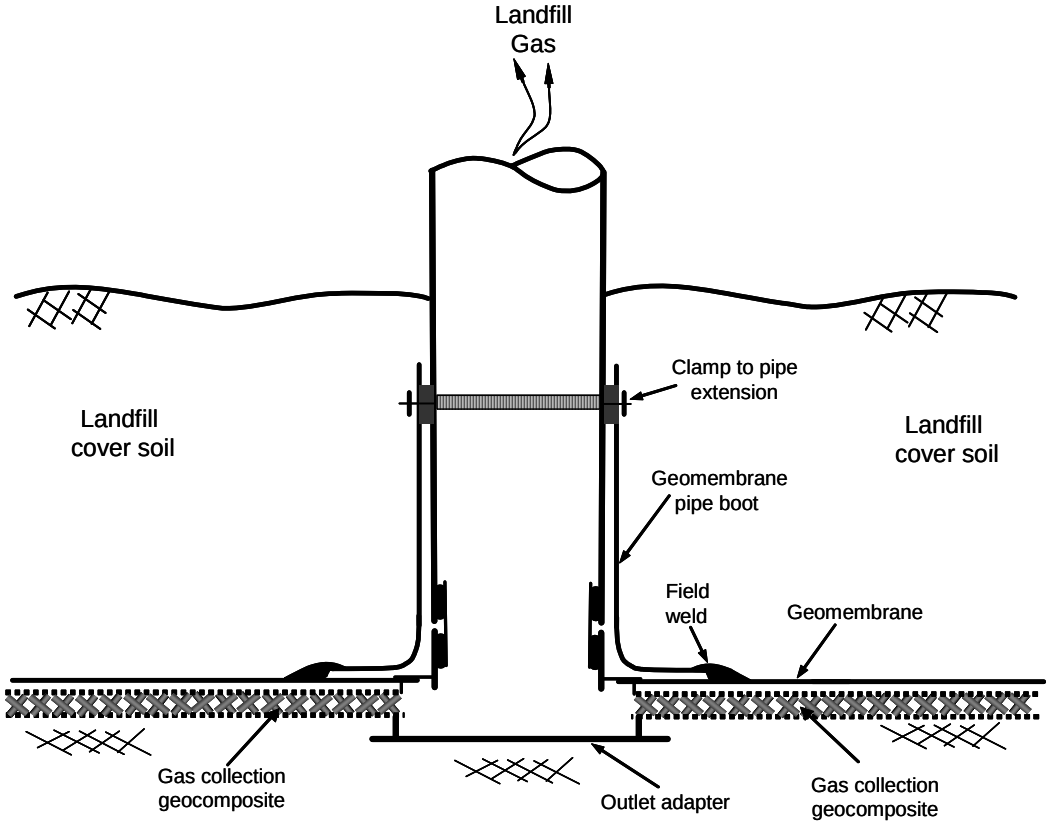

(a) Cross section of adapter and geomembrane pipe boot

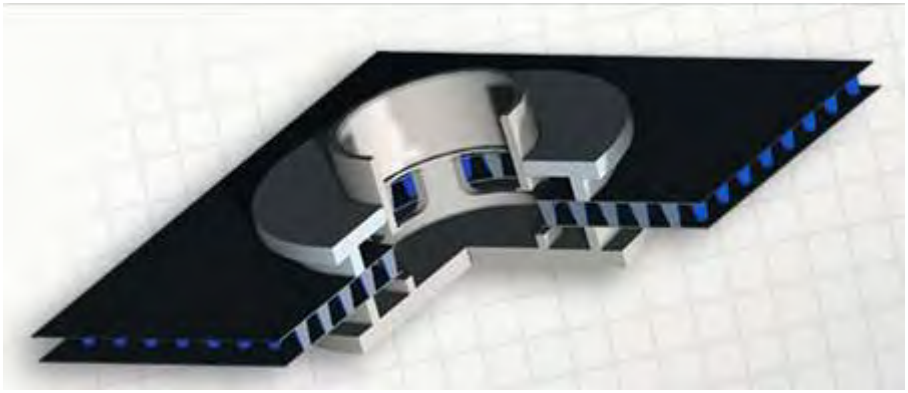

(b) Photograph of a typical adapter without geomembrane boot (compl., Drain Great™)

Figure 6. Recommended geocomposite to vertical pipe connections.

3.4 Geocomposite Termination in Sumps and Swales

Liquid being conveyed by a drainage geocomposite is often emptied in an open area such as a landfill sump or a highway swale. Figure 7a shows the general configuration for leachate removal when exiting into a landfill sump area. Since regulations limit the head on the geomembrane, the leachate must be removed by a submersible pump within a solid wall removal pipe. The drainage geocomposite should cover the entire sump area where it serves a secondary function as a protection for the geomembrane against the coarse gravel generally used as indicated. The geotextile(s) should be left on the drainage core throughout since it will help in filtering out fines leaving the geonet free of sediments.

Figure 7b shows the general configuration for water draining from a slope and emptying into a swale adjacent to a roadway. (Alternatively, it could end by emptying into a drainage pipe as shown in Figure 5). It is important that roadway maintenance operations do not cause a blockage of the exiting core, but otherwise the situation is quite straightforward.

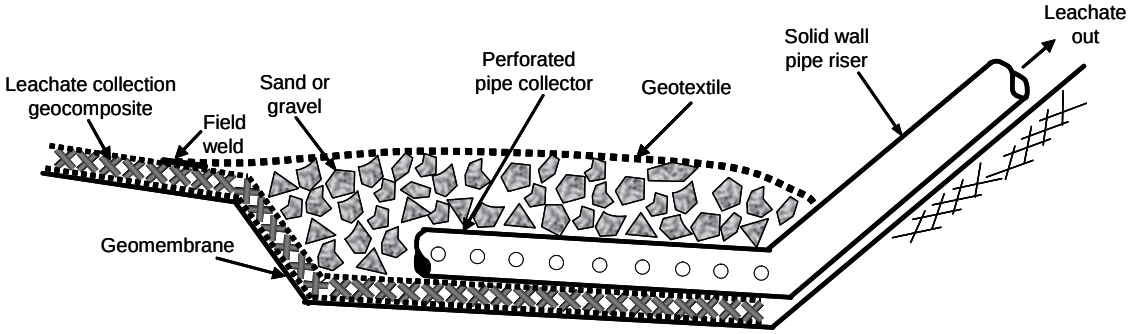

(a) Recommended termination of geocomposite in a landfill sump for subsequent removal

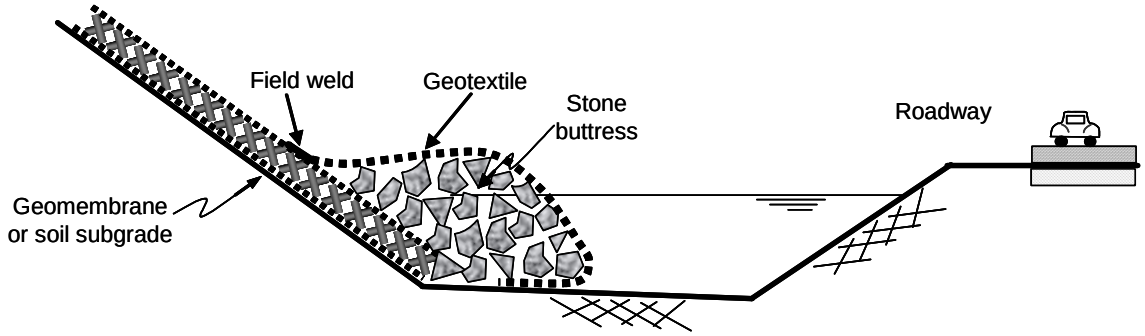

(b) Recommended termination of geocomposite in a swale adjacent to a roadway

Figure 7. Recommended geocomposite terminating into an open collection area.

3.5 Geocomposite Termination Within Landfill Anchor Trenches

Geocomposites are used in three different locations for liquid (water or leachate) drainage purposes in solid waste landfills; (i) surface water drainage above a geomembrane in the final cover, (ii) leachate collection above the primary geomembrane beneath the solid waste, and (iii) leak detection between primary and secondary geomembranes beneath the waste if a double lined system is designed. Note that the gas collection geocomposite shown in Figure 6 is in

addition to the three situations described here. In most cases geotextiles will be bonded to both the upper and lower surfaces of the geonet or drainage core. Figure 8 shows one possible strategy for terminating these three liquid drainage geocomposites in their respective anchor trenches.

For the geocomposite drain in the landfill cover the termination can be in a horizontal pipe (recall Figure 5b) or in a drainage swale (recall Figure 7b). One type of alternative to a pipe could be a geocomposite edge drain, but these are seldomly used by landfill designers. For the geocomposite drain terminations beneath the solid waste mass the entire geocomposite generally enters the anchor trench along with its accompanying geomembrane. This is more for physical anchoring (to prevent the geocomposite from sliding downslope) than for drainage purposes. There is no overriding reason to seal off the ends of the geocomposite since capillary rise of moisture is not possible for these products.

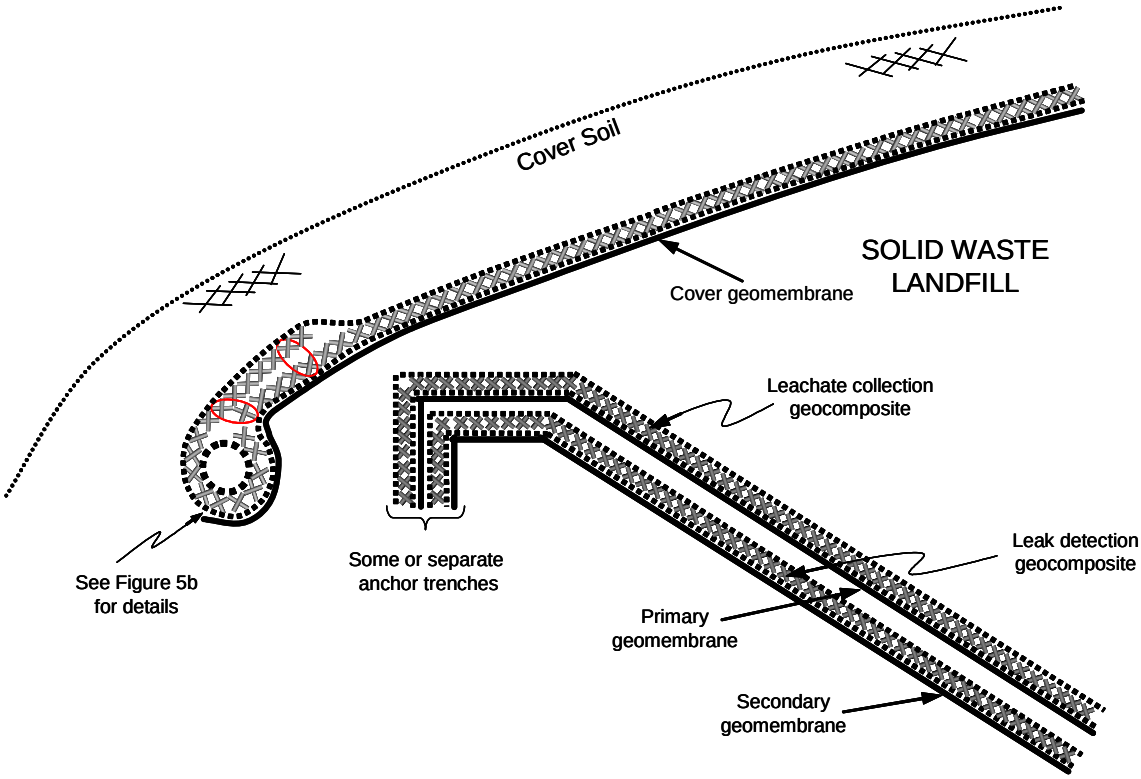

Figure 8. Recommended termination of geocomposites at the boundary and anchor trench of solid waste landfills.

4. SUMMARY AND CONCLUSIONS

This paper has presented recommended details of five different situations encountered with the connections and attachments of geocomposites to one another or to other materials and systems. The geocomposites addressed are all involved with the drainage of liquids or gases. As such, they are indeed drainage geocomposites. The drainage cores are biplanar or triplanar geonets or a myriad of other core types including three-dimensional meshes and built-up polymer columns, cuspations, and dimples. All of these drainage cores are covered with one or two geotextiles usually bonded to the core at the manufacturing facility. The geotextiles are most often needle-punched nonwovens although any other type could be used depending upon the specific design. They are supplied to the job site in rolls of various lengths and widths.

The five situations presented in the paper are the following:

- Connection of overlapping geocomposites on their ends and sides (Figure 4).
- Geocomposite to horizontal pipe connection (Figure 5).
- Geocomposite to vertical pipe connection (Figure 6).
- Geocomposite termination in sumps and swales (Figure 7).

- Geocomposite termination within landfill anchor trenches (Figure 8).

The recommended sketches associated with each situation are not theoretically derived, but are subject to the various caveats given in the paper. They are also based on what the authors feel is best-available-technology as seen over many years of observation.

ACKNOWLEDGEMENTS

This project was sponsored by the Geosynthetic Institute. A list of its members and associate members is available on its website at <geosynthetic-institute.org>.

Maximizing Sensitivities for Geoelectric Surveys on an Existing Final Landfill Cover

T. Bauters and K. G. Haskell, Golder Associates Incorporated, California, USA

ABSTRACT
A geoelectric survey was performed in accordance with ASTM D7007 on a constructed final landfill cover to evaluate the integrity of an in-place geomembrane that was covered with clayey vegetative soil containing over-sized rocks, sticks, and metal debris. The purpose of the survey was to determine the extent of any construction damage to the geomembrane so that appropriate corrective actions could be developed. The detail is truly in the details to execute geoelectric surveys so as to maximize the sensitivity of the geoelectric survey performed and hence pinpoint smaller potential physical defects in the geomembrane. This extends from optimizing soil moisture contents of the vegetative cover materials, to the procedural details of the artificial leak tests, to the potential reduced resolutions due to thicker soil sections and geocomposite drainage layers.

1. INTRODUCTION

A geoelectric survey was performed to evaluate the integrity of a 40-mil linear low density polyethylene (LLDPE) geomembrane that was covered with a 600 mm (2 ft) of clayey vegetative soil containing over-sized rocks, sticks, and metal debris as part of a final landfill cover. The primary purpose of this geoelectric survey was to evaluate the types and frequencies of any defects still present in the geomembrane, and to ascertain the course of corrective actions. A previous geoelectric survey was performed to identify the integrity of the liner two years prior. Geomembrane defects were detected by the original geoelectric survey and were immediately repaired. This original survey was reportedly completed in accordance with ASTM D7007.

The regulatory agencies requested a second independent survey to confirm the results of the original survey. If the second geoelectric survey showed that the geomembrane contained no additional defects or only few defects, then repair of those defects followed by additional surveys in the future might be satisfactory to gain regulatory approval of that final cover. If a large number of defects were found, then complete reconstruction of the entire final cover may be warranted. Therefore, the accuracy of the survey in terms of defect size and completeness was critical for this project. Although ASTM 7007 provides procedures for completing a geoelectric survey, a number of factors are discussed that affect the resolution of the survey.

The geometry of the 52,500 m^2 (13-acre) landfill is an east-west trending prismoidal shaped waste pile with four side-slopes ranging from 4H to 1V to 3H to 1V (horizontal to vertical). The vertical height of the side slopes ranges from 4 m (13 ft) on the eastern side to up to 20 m (65 ft) on the western side of the landfill. While the vegetative cover soil thickness of the landfill was designed to be 600mm (2 ft) thickness, exploratory potholing revealed that the cover thickness above the 40-mil LLDPE geomembrane ranged from 450 mm (1.5 ft) to up to 900 mm (3 ft). The 22,300 m^2 (5.5-acre) flatter section of the landfill (top deck) is graded at 3.5% towards the vegetated drainage swale, with a perimeter berm containing the top deck surface water runoff, and discharging that surface water at a single discharge point. The perimeter berm has a typical width of 3m (10 ft) and a height of 1.2 to 1.8 m (4 to 6 ft) at the eastern end of the site, and is up to 7.6 to 9 m (25 to 30 ft) in width and 1.8 to 3.3 m (6 to 10 ft) in height at the western end of the site.

2. GEOELECTRIC CONCEPT AND SURVEY PROCEDURES

The principle of the geoelectric leak location method is to place a voltage across the earthen material above and below the geomembrane. Geomembranes consist mainly of polymeric materials (HDPE, LLDPE, PVC, etc.) which are all electrically insulative materials. If a “defect” is present in the geomembrane, then current passes through the “defect” and causes an anomaly in the voltage potential field at that location (see Figure 1.) The geoelectric survey consists of measuring this voltage potential along parallel survey lines, covering the entire site of interest. The geoelectric survey sensitivity is affected by the conductivity of the materials within, above, and below the potential defect, and the electrical homogeneity of the materials above the defect, output levels of the electrical power supply, design of the measurement probes and detector electronics, general survey procedures, data interpretation, and skill.

ASTM D7007 provides a detailed practice for completing geoelectric surveys with water or earth materials covering the geomembranes. Prior to performing the actual survey, a leak detection sensitivity test (artificial leak test or actual leak test) needs to be completed to determine the maximum distance between adjacent survey lines. The artificial leak test mimics a current migrating through the geomembrane at that location, with the soil material covering the geomembrane in lieu of actually making a physical hole in the liner. The artificial leak sensitivity test determines the survey line spacing required to detect a certain minimum hole size. Per ASTM D7007, the target diameter of the "artificial leak" is 6 mm (¼ inch) with up to 600 mm (2 ft) of earth materials covering the geomembrane. The following sections discuss the geoelectric survey procedures:

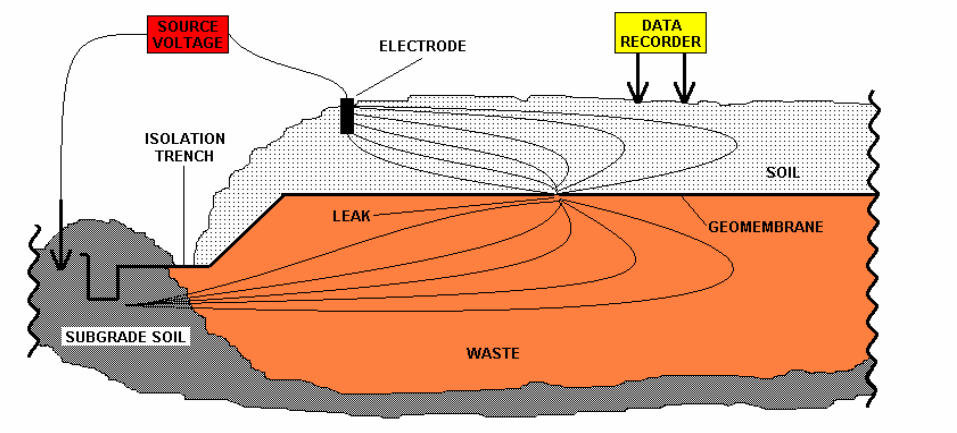

Figure 1. Geoelectric concept.

2.1 Electrical Isolation

Electrical isolation must be achieved around the survey area and other conductive paths (metal pipe penetrations, sump grounds, etc.) to prevent electrical current from traveling from beneath the cover to the ground surface at the edges, and other conductive paths, which will typically cause a large defect signal and potentially mask or interfere with the detection of smaller defects.

Electrical isolation is typically established by performing the geoelectric survey before the edges of the geomembrane are covered (typically left uncovered during the construction process), or can be achieved by removing the earthen materials if already in-place in a narrow path (trench) along the perimeter of the surveyed area and along any other conductive paths.

2.2 Sensitivity Tests

The sensitivity test establishes the defect size in the geomembrane that can be found, and determines the survey line spacing and placement of the current source electrode for the full-scale geoelectric survey. Procedures for this are described in detail in Annex A3 or A4 in ASTM D7007, for an artificial or actual leak, respectively. If the minimum leak size per the ASTM D7007 cannot be achieved, the geoelectric survey will be completed with the largest detectable size and noted in the report.

2.3 Conduct Geoelectric Survey

The application of the electrical charge/current is typically achieved by a generator. Current source electrode access points are created at the distance determined by the location of the artificial leak tests to the current source electrode. This is also the maximum detection distance that can be used during this section of the survey, with resolution or sensitivity readings representative of this artificial leak test. Therefore, additional electrode locations may be needed depending on the resolution achieved during the artificial leak test. The current electrodes are often installed by excavating down to the geomembrane, and if necessary, cutting an access point (that needs to be repaired later) to insert the current electrode under the geomembrane. If geomembrane defects are encountered during the survey, these can serve as electrode access points.

As described in ASTM D7007, a partial, periodic, leak detection sensitivity test is conducted at the beginning and end of each day, and for each set of equipment used to perform the survey. This periodic sensitivity test is performed to assure that the surveyed area was completed with equipment and procedures that achieved the required sensitivity.

2.4 Electrical Anomalies

Areas with electrical anomalies (i.e. potential geomembrane defects) will be flagged and the anomaly excavated around the localized areas creating an exposed geomembrane. Typically the last 100 mm to 150 mm (4 to 6 inches) of soil above the geomembrane will be removed with hand shovels. Once the defect is located, the defect will need to be electrically isolated (by removing conductive earthen materials in proximity of the defect or by being repaired). The geoelectric survey shall than be repeated on the two closest survey lines for an distance of 5 m (15 ft) before and beyond the defect. This to ascertain that that the excavated defect was not masking any other potential defects in close proximity to the initial, now isolated, detected defect. This process will be continued until no further anomalies are detected.

2.5 Defect Documentation

For any physical confirmed defect, the defect will be recorded, which at a minimum typically includes a photograph, a description of the type and size of defect, the location of the defect and the method and details of the repair.

3. MAXIMIZING LEAK DETECTION SENSITIVITIES

In ASTM D7007, Paragraph 4.4.5 it states that; “The leak detection sensitivity depends on the conductivity of the materials with, above, and below the leak, the electrical homogeneity of the material above the leak, the design of the measurement electrodes, the output level of the excitation power supply, the sensitivity of the detector electronics, the survey procedures, and data interpretation methods and skill.” Some of these sensitivity factors are depended upon the equipment quality and the experience and skill of the operators. Those should be optimized by the survey operator such as the design of the measurement probes, sensitivity of the detector electronics, output levels of the excitation power supply, data interpretation methods, and operator’s skill set. The other sensitivity factors depend on the field conditions; a few of those are described in greater detail in the following subsections:

3.1 Soil Moisture Conditions of the Final Cover

In ASTM D7007, Paragraph 6.1.5 it states that; “For surveys with earth materials on the geomembrane the earth material shall have adequate moisture to provide a continuous path for electrical current to flow through the leak. Earth materials usually have sufficient moisture at depth, but sometimes the surface shall be wet with water. The earth materials do not have to be saturated with water. The amount of moisture required depends on the earth material, the equipment, and procedures. Successful leak location surveys have been conducted on earth materials containing as little as 0.5 percent moisture by weight.”

Experience has shown that applying water to a soil surface immediate prior to the survey can reduce “electrical noise” and help increase the sensitivity of the survey. However, the moisture content of the soils between the ground surface and the geomembrane were found to also affect the sensitivity of the survey in the case history being presented. Prior to water application, the initial soil moisture content was determined for this case study, and generally ranged from 8 to 11 percent with localized areas as low as 5 percent and as high as 13 percent. At the start to the geoelectric survey the first artificial leak was placed and it was determined that these existing soil moisture contents were inadequate to detect the target 6 mm diameter defect resolution. Therefore, water was applied to the surface of the landfill to improve electrical potential readings. Moisture contents in the upper 150 mm (6 inches) of the soil were increased to between 9 percent and 19 percent after water was applied.

A total of 97 water truck loads of 15,000 liter (4,000 gallons) each where applied on the cover soil to enhance the conductivity and electrical homogeneity above the geomembrane. Although the water trucks were effective in applying large volumes of water quickly to the ground surface, water trucks do exert significant tire pressures that can potentially induce additional damage, particularly for a thin soil cover containing adverse materials. With advance planning, a temporary irrigation system might achieve increased soil moisture contents while providing less damage potential.

Soil moisture contents were not documented for the original geoelectric survey conducted two years prior to the second geoelectric survey being described here. In addition, eye-witness accounts indicated that no water was applied prior to or during the ground surface during the original geoelectric survey.

3.2 Artificial Leak Tests Procedures

The calibration resolution target for the geoelectric survey at the landfill was set at 6 mm (1/4 inch) diameter artificial leak with typically a 600 mm (2 ft) cover in accordance with ASTM D7007. Artificial leak tests were performed at five locations using simulated leak diameters of between 3 mm (1/8-inch) to 9 mm (3/8-inch) to assure that leak location equipment and survey procedures were capable of detecting a leak with a diameter of at least 6 mm (0.25 inch-diameter) on the majority of the surveyed areas on the landfill cap.

For each artificial test location, the artificial leak was ultimately detected at horizontal distances of more than 2.3 m (7.5 ft), which indicated that survey lines spaced at 4.5 m (15 ft) were adequate to detect the 6 mm (1/4-inch diameter) target. However, the survey crew elected to use a tighter 1.5 m (5 ft) survey line spacing to maximize the sensitivity of the survey.

While the majority of the artificial leaks surveyed were “non-eventful” once water was added to the cover soil, one of the artificial leaks placed on the side slope of the landfill was initially detected despite adding water to the ground surface. Troubleshooting commenced and the procedures were all double checked to assure everything was implemented in accordance with the guidelines set forth in ASTM D7007. Ultimately the artificial leak on the side slope was detected, and the following three sources were pinpointed as the potential culprit for initial non-detection: (i) evaporation of the moisture in the soils adjacent to the artificial leak, (ii) small rocks were backfilled above the artificial leak creating an air void, or (iii) electrical isolation was breached in the perimeter trench by standing water and/or wet soils. Sufficient quantities of water were added to the side-slope to cause some run-off and accumulation of water in the perimeter trench. Ultimately, the artificial leak was excavated and reburied with soil moisture conditioned by adding up 250 ml of water was added to the soil above the artificial leak per ASTM 7007. In addition, care was taken to make sure the soil backfill above the artificial leak was free of rocks and wet soils and standing water were removed from the bottom of the isolation trench.

For the original geoelectric survey, available documentation did not indicate how the artificial leak test was performed to determine survey line spacing. The documentation implied that a single artificial leak location was completed, which probably would be inadequate for a survey covering an area with a variety of cover depths and spanning multiple days.

3.3 Limitations of the Survey Performed

In addition to soil moisture contents, thickness of cover materials will affect the sensitivity of the detectable leaks. While the majority of the landfill cover surveyed is within the detection limits as planned, there were some areas on the landfill where cover thickness affected the sensitivity of the test performed. The top deck perimeter berm has cover soil thickness that could be upwards of 1.8 to 3.3 m (6 to 10 ft). Due to the soil thickness and width of the berm, the sensitivity of the survey in the middle portion of the berm (beyond 7.5 feet on either side) is uncertain and it is not known whether a 6 mm artificial leak would be detected by the survey. However, this uncertainty affects a relatively small portion of the total cover area, which is estimated to be about 1 % of the cover area.

In addition, the side slopes of the final cover had a geocomposite drainage layer installed on top of the geomembrane to prevent positive pore pressures on the side slope and prevent veneer instability. The air void in the drainage geocomposite tends to inhibit electrical conductivity, thus making it more difficult to detect discontinuities in the underlying geomembrane. Nevertheless, when the geocomposite/geomembrane combination of geosynthetics is breached at the same location, those particular defects are detectable in a geoelectric survey.

3.4 General Survey Results

The original geoelectric survey was successful in identifying seven (7) defects ranging from holes 2 mm in diameter to tears several feet in length on the top deck. The second geoelectric leak survey completed for this case study detected ten (10) defects in an area that had been previously surveyed on the top deck. The defects ranged from 3 mm (¼-inch) in diameter up to 12-inches in length. Several of these defects were clearly caused during the initial installation, while at least one defect appeared to be related to the installation of a landfill gas header pipe after the original geoelectric survey was completed. Nonetheless, the results of the second survey raised concerns over the completeness and accuracy of the two surveys that were reportedly completed in

accordance with ASTM D7007. The differences in the survey results could be due to (i) differences in the artificial leak test procedures leading to different sensitivities, (ii) differing soil moisture contents leading to different sensitivities, (iii) differing skill levels of the geoelectric survey teams, and/or (iv) construction related damage occurring between the two surveys.

Both surveys detected defects in the geomembrane along or near the side-slopes where the geomembrane was covered by a geocomposite drainage layer. However, in both cases, the suspected damage causing the defects was grading equipment operating too close to the geosynthetics and creating large tears through both the geomembrane and geocomposite drainage layer. While the geocomposite drainage layer can create difficulties in detecting a potential smaller defect in the geomembrane, it also effectively provides puncture protection for the geomembrane.

4. CONCLUSION

The detail is truly in the details in performing a high resolution geoelectric leak surveys in accordance with ASTM D7007 and to ultimately pinpoint defects in a geomembrane covered with about 600mm of earthen materials. Although the two geoelectric surveys performed were reportedly completed in accordance with ASTM D7007, there were differences in the test procedures that ultimately led to the second survey detecting several significant geomembrane defects that were apparently missed by the original survey.

The leak detection sensitivity of the geoelectric survey was continually checked over the duration of the geoelectric survey by performing artificial leak tests. This procedure is described in detail in Annex 3 of the ASTM D7007 standard. However, understanding the strengths and limitations of the artificial leak process can improve sensitivities for the geoelectric survey and interpretation of the results.

While ASTM D7007 notes that geoelectric surveys can be performed with minimal soil moisture contents successfully, in this case study, increasing soil water contents in a clayey vegetative soil cover led to improved sensitivities. As a result, documenting soil moisture contents during the geoelectric survey could be beneficial in interpreting the difference between two separate surveys of the same area. Furthermore, the results of this case study suggested that soil moisture played a key in the accuracy of the survey and may explain, in part, the differences between the two surveys. Soil moisture contents should be considered in any geoelectric survey.

Potential resolution limitations of the geoelectric survey should be identified early on so as to assure that all involved parties have the same expectations relating to those sections of the geoelectric survey. Thicker sections of vegetative soil cover and geocomposite drainage layers are likely to impact the sensitivity of the survey performed.

ACKNOWLEDGEMENTS

Authors would like to thank Glenn Darilek, P.E., and Daren Laine for providing thoughtful insights to get this survey accomplished in accordance with the ASTM D7007 standard.

REFERENCES

ASTM D7007. Electrical Methods for Locating Leaks in Geomembranes Covered with Water or Earth Materials, American Society for Testing and Materials, West Conshohocken, Pennsylvania, USA.

Smoke Testing of Spray-Applied Geomembranes

G. R. Koerner, Geosynthetic Institute, Folsom, PA, USA
R. M. Koerner, Geosynthetic Institute, Folsom, PA, USA

ABSTRACT
Spray-applied geomembranes are usually associated with the lining of complex foundations and locations were there are many penetrations and appurtenances. Such liner systems can be installed on the inside or outside of walls and in extremely congested areas with pipes, foundations, and materials handling equipment in order to provide a permanent barrier to unwanted gas and/or liquids. Current building code recommendations are to limit vapor barriers to a permeability (diffusion) rate below 0.014 perm. Such barriers, if continuous, can provide not only a barrier but also to regulate temperature and prevent radon, methane, or volatile organic compounds (VOCs) which possibly could leak into a building or other inhabited area. After installation of such a barrier, however, the system should be tested. One such performance test is smoke testing.
This paper will give an overview of spray-applied geomembranes and then discuss smoke testing of such systems. The discussion will outline a testing protocol and give some commentary on the technique. Such a test can evaluate the continuity of spray-applied geomembranes when used in applications like basement waterproofing, secondary containment, holding ponds, tank farms and related facilities.

1. INTRODUCTION AND BACKGROUND

As the name suggests spray-applied geomembranes are field manufactured barrier systems consisting of several liquid components usually sprayed onto a geotextile. They then rapidly cure into a coherent polymeric geomembrane. The original systems were developed and promoted by oil companies (Chevron and Philips, in particular) who used an emulsified asphalt sprayed on a geotextile which cured into a road-like film embedded within and on a fabric substrate. Much more sophisticated systems are currently used. Presently, the components can be organic and/or inorganic and consist of multiple ingredients. The membrane-forming material is a resin (polyurethane, polyvinyl chloride, latex, asphalt, etc.) which contains pigments and is called the “binder”. When the binder is dissolved in a solvent it is called a “vehicle”, and the mixture is capable of being sprayed onto the surface being coated. The solvent then evaporates leaving the binder system coating the intended surface, which is most often a geotextile but can be concrete or soil as well. Drying oils are also used in some formulations and they aid in facilitating the curing process. Other additives are sometimes used to induce specific properties to the final barrier material. After curing, the pigments determine the final geomembrane properties and the color as well. The binder determines the weatherability of the material, its environmental resistance, and the material’s ability to function in a given environment. The required surface preparation or substrate, and often the application equipment and techniques, are dependent upon the particular binder selected.

The principal mechanisms by which binders form geomembranes are reaction with oxygen from the air (oxidation), evaporation of the solvent from the vehicle (solvent evaporation), or chemical crosslinking (polymerization). The geomembrane attained by these mechanisms can be either a thermoplastic or thermoset material. Thermoplastic materials deform and somewhat soften on exposure to extreme heat. Thermoset materials maintain their hardness upon heat exposure.

2. FIELD INSTALLATION

The environmental conditions in which spray-applied geomembranes can be formed are when ambient temperature is 4°C (40°F) or above for a period of 24 hours prior to the application and when there is no ice, frost, surface moisture, or visible dampness on the substrate or ground surface. Materials should be applied when air temperature is expected to remain above 4°C (40°F) during the cure period recommended by the manufacturer. A moisture test for the subgrade can be specified, however, this is generally not a problem when the substrate is a geotextile.

The installer should coordinate work with that of suppliers and other trades to ensure that components to be incorporated into the spray-applied system are available when needed. The surfaces immediately before application of waterproofing materials should be inspected and approved. Loose aggregate, sharp projections, grease, oil, dirt, curing compounds, and other contaminants which could adversely affect the complete bonding of the spray-applied geomembrane to the substrate must be removed or the substrate rejected and replaced.

Each component of the formulation must be protected during transport, mixing and application. Primers and other components should not be diluted unless specifically recommended by the supplier/manufacturer. One should not mix remains of unlike new materials. Residual materials should be thoroughly removed before using application equipment for mixing and spraying materials. Equipment on the project site that has residue of materials used on previous projects should not be allowed. Use cleaners only for cleaning, not for thinning primers or membrane materials. Ensure that workers and others who walk on site wear clean, soft-soled shoes to avoid damaging the waterproofing materials. Figure 1 presents two examples of spray-applied geomembranes using nonwoven geotextiles as substrates.

Some spray-applied geomembranes require application over primed surfaces. When this is the case provide a uniform, wet, monolithic coating material, 1.5 mm (60 mils) thick, by following the manufacturer's instructions. Apply material by trowel, squeegee, roller, brush, spray apparatus, or other method recommended by manufacturer. Usually, however, the material can be applied directly onto a geotextile, or on rigid subgrades. This process can be seen in Figures 1 and 2.

(a) CETCO's Liquid Boot® being applied on a nonwoven heat bonded geotextile in a foundation application

(b) Photograph from Layfield Inc. showing spray applied geomembrane being used in a secondary containment application

Figure 1. Examples of spray-applied geomembranes.

One of the drawbacks with spray-applied geomembranes is thickness control. Thickness is controlled by nozzle speed and distance from the substrate, space between each spray row, pump output, and dwell time. In the best of conditions thickness can be controlled to ± 2 mm for automated system and ± 4 mm for manual systems. Field quality assurance (i.e., inspection) of such a technology is critical to the success of these projects.

There are several applications where spray-applied geomembranes have advantages over factory manufactured geomembranes. They are as follows:

- split-slab construction including foundation walls, plaza decks, balconies, walkways, and parking decks
- beneath piping systems which cannot be readily disconnected and/or removed
- interior walls of tanks which have multiple inlets and outlets
- holding ponds and surface impoundments which have stationary mechanical equipment in the facility for mixing, dispersion, suspension, etc.
- retrofits of secondary containment tanks and tank farms

The final applied materials should be cured according to manufacturer's recommendations. Normal curing time is 24 to 48 hours to achieve a formulation's equilibrium condition. In some conditions such as damp substrates, extremely cold conditions, and/or high humidity, the full adhesion of the membrane will be delayed. The length of delay is also subject to the thickness and severity of local conditions. Table 1 lists several commercially available spray-applied geomembranes.

Table 1. Commercially available spray-applied geomembranes modified from Haxo (1984).

Polymer	Usual Substrate[1]	Cure Time (hours)	Typ. Thickness (mm)	Typ. Thickness (mil)	Water Vapor Pemeance[2] (10^{-2} metric PERM)
polturia	geotextile	24	2.0	80	0.55
polyurethane	geotextile	48	2.0	80	0.5
polyvinyl chloride	geotextile	12	0.75	30	10.4
latex	geotextile	12	0.4	15	30.3
bitumen	geotextile	71	0.75	30	18.4
polymeric asphalt	geotextile	24	1.5	60	2.4
rubber derivatives	geotextile	48	0.75	30	5.3

(1) Substrate can also be masonry, wood, metal or plastic for most formulations as long as the substrate is rigid, clean and dry.
(2) Values were obtained from films tested via ASTM E96 water vapor transmission

3. SMOKE TESTING OF FINAL GEOMEMBRANE

Smoke testing is an effective way to locate and identify the source of an inflow or infiltration problem in a cured spray-applied geomembrane. It is important to find and identify these sources because they may seriously affect the efficiency of the barrier system.

Smoke testing is conducted by placing a blower over a centrally located hole in the cured geomembrane and forcing nontoxic smoke-filled air beneath it; see Figure 2a for the smoke being emitted. Depending on the equipment being used, the smoke can be generated by a smoke bomb (zinc chloride) or liquid smoke (glycol). In both cases the smoke is nontoxic, harmless, and has only a slight odor. It does not create a fire hazard. Commercially available blowers produce excessive volume and pressure for this application. A relatively small blower that produces as little as 2.8 m^3/min (100 ft^3/min) and less than 7 kPa (1.0 lb/$in.^2$) static pressure is sufficient; see Figure 2b. The smoke will fill the interface with the soil beneath the geomembrane, geotextile, or within an underdrain if one is present. It then follows the path of the leak to the ground surface, quickly revealing the source of the leak; see Figures 2c and 2d. Only enough force to overcome atmospheric pressure is required. After filling the interface, geotextile, or underdrain with smoke, staff will have to perform a visual inspection of the area being tested. Typically, one will leave the smoke run until the crew has had ample time to do a thorough inspection. A field crew should consist of a minimum of two people.

One should check all connected pipelines, including abandoned and supposedly disconnected service lines. Minor leaks can easily be overlooked. It is important to carefully check around adjacent structures or houses with close attention given to cleanouts and roof leaders. If smoke is found during the inspection it must be carefully recorded so that it can be corrected after the testing. Mark and paint also help. Cameras make the job easier because a photo or movie will help to relocate the problem after testing so that corrective measures can be taken.

Best results are obtained when the water table is low and on dry days because water is an excellent vapor barrier that can prevent the widespread movement of the smoke. Smoke testing should also be avoided on windy days because even a very light breeze can disperse a wisp of smoke before it is visible at the source of a leak.

Smoke testing may involve many hours of labor and has the potential to affect others on the construction site. It may cause people to summon emergency personnel. Therefore, advance preparation is essential for a successful smoke testing program. One must determine what areas of the barrier system to test and choose a reasonable period of time that can truly be devoted by enough staff to perform the work correctly. One should obtain a comprehensive plan of the site to be tested. Before commencing work, be sure to call the local fire department to inform them of the undertaking. They also need to be informed when work is complete for the day. Table 2 contrasts smoke testing to other more standard geomembrane nondestructive tests.

(a) Smoke emerging from inlet x-cut after tube is removed

(d) Low pressure smoke generator producing liquid smoke from tube

(c) Marked presence of smoke in a defect in a thin section of geomembrane

(d) Smoke plume seen at inadequate geomembrane foundation connection

Figure 2. Photographs of smoke testing spray-applied geomembranes in the field. (compl. of A. Filshill, CETCO Contracting, Inc.)

Table 2. Nondestructive geomembrane seam testing methods, modified from Richardson and Koerner (1998)

Nondestructive Test method	Primary User		General Comments					
	CQC	CQA	Cost of equipment	Speed of tests	Costs of tests	Type of result	Recording method	Operator dependency
1. air lance	yes	-	$200	fast	low	yes-no	manual	high
2. mechanical point (pick) stress	yes	-	nil	fast	nil	yes-no	manual	very high
3. dual seam (positive pressure)	yes	-	$200	fast	moderate	yes-no	manual	low
4. vacuum chamber (negative pressure)	yes	yes	$1000	slow	very high	yes-no	manual	moderate
5. electric wire	yes	yes	$500	fast	nil	yes-no	manual	high
6. ultrasonic impedance	-	yes	$500	moderate	high	yes-no	automatic	moderate
7. ultrasonic impedance -	-	yes	$7000	moderate	high	qualitative	automatic	unknown
8. ultrasonic shadow	-	yes	$5000	moderate	high	qualitative	automatic	moderate
9. smoke testing	yes	yes	$500	moderate	moderate	yes-no	manual	moderate

4. SMOKE TESTING PROTOCOL (MODIFIED FROM LIQUID BOOT®)

A suggested guide for smoke testing of spray-applied geomembranes should consider the following items:

1. The spray-applied geomembrane shall be visually inspected. Any apparent deficiencies and/or installation problems shall be corrected prior to smoke testing (e.g., be IAGI certified).
2. Smoke testing a spray-applied geomembrane should be conducted by an approved applicator and observed by a qualified inspector (e.g., be GCI-ICP certified).
3. The date, time, testing reference area, temperature, wind speed/direction, and cloud cover shall be recorded on the Smoke Testing Record. The ambient air temperature at the time of testing should be in excess of 7°C (45°F) and the wind speed at ground level should be 24 km/hr (15 mi/hr) or less. (Note: visual identification of leaks becomes more difficult with increasing wind speed.)
4. Delineate a maximum smoke testing area of 200-500 m^2 (2,000-5,000 ft^2). Assemble and situate the smoke testing system to inject smoke beneath the geomembrane. Only inert, non-toxic smoke is to be utilized for the smoke test (e.g., a glycol solution works well; recall Figure 2b).
5. Designate testing injection areas by cutting openings in an "X" pattern as shown in Figure 2a in the geomembrane at selected locations. Mark the testing control areas for identification prior to conducting the smoke test.
6. Activate the smoke generator/blower system to a gas rate of approximately 4 to 25 m^3/min (150-950 ft^3/min.). Apply sufficient pressure as to ensure that smoke will permeate the designated testing area. For verification, ensure that smoke is leaking through the testing control areas and correction action by way of an engress port located at the outer perimeter of the smoke testing area.
7. Pump smoke beneath the membrane for approximately two minutes. Observe for leaks in the geomembrane. Reduce pressure and/or flow rate if excessive lifting of the geomembrane occurs.
8. Thoroughly inspect the entire geomembrane surface within the area delineated for testing. Use a marking device to mark or label any leak locations. Mark or label leak locations on floor plan and corresponding testing reference area.
9. Repair leak locations marked in Step #7.
10. Repeat Step's #7 and #8 as necessary to confirm the integrity of the geomembrane.
11. Once the geomembrane has passed the smoke test inspection, the successful completion should be documented and signed off by a qualified inspector as delineated by the engineer, general contractor, or owner.

5. SUMMARY AND CONCLUSIONS

Spray-applied geomembranes indeed have a role to play in the context of the entire gambit of geomembrane application areas. They appear to have a distinct advantage in complicated projects containing numerous penetrations and appurtenances needed for proper functioning of the facility. While these applications tend to be small, this is not necessarily the case.

If one were to develop a benefit/cost ratio for comparison of spray-applied geomembranes to a factory manufactured geomembrane one could easily anticipate material costs being higher for the spray-applied system, while labor costs for installation for a complicated site would be lower. Thus, the denominator of the benefit/cost ratio might (?) be equivalent and the decision would then be based on the short and long-term performance of the material. In this regard, additional information on the specific formulation being used is important. Furthermore, there are no generic specifications available for spray-applied geomembranes and this is considered (by the authors, at least) to be an implement toward further usage of this type of geomembrane at this point in time.

ACKNOWLEDGEMENTS

The authors wish to thank the Geosynthetic Institute (GSI) and its members organizations for their support of the work contained in this paper. The authors would also like to thank the fluid applied geomembrane manufactures for producing such noble products. Special thanks needs to be given to A. Filshill of CETCO Contracting, Inc. for his insight and access to Liquid Boot® installation and smoke testing.

BIBLIOGRAPHY

Bowders, J. J., Deupane, D., Loehr, J. E. and Bouazza, A. (2002). Asphalt – geotextile barriers for waste containment, *Proceedings 7ICG*, Nice, France, A. A. Balkema Publ., pp. 511-514.

Cadwallader, M. (2002). Two case studies of surface-modified HDPE geomembranes, *GFR*, Vol. 20, No. 3, April, pp. 32-35.

Haxo, H. E., Jr., Miedema, J. A. and Nelson, N. A. (1984). Permeability of polymeric membrane lining materials, *Proceedings International Conference on Geomembranes*, Denver, CO, USA, IFAI, pp. 151-156.
Koerner, R. M. (2005). *Designing With Geosynthetics*, Prentice Hall, Englewood Cliffs, NJ, 40 pgs.
Liquid Boot® Membrane Coupon Sampling and Smoke Test Guides, 2006, 20/20 Protocol pdf. Santa Anna, CA, USA pg. 1 of 1.
Richardson, G. N. (1999). Bolted steel tanks with HDPE geomembrane linings, *GFR*, Vol. 17, No. 8, pp. 16-20.
Richardson, G. N. and Koerner, R. M. (1998). *Geosynthetic Design Guidance for Hazardous Waste Landfill Cells and Surface Impoundments*, CN 68-03-3338, U.S. EPA Risk Reduction Lab, Cincinnati, OH, 187 pgs.
Wilson, F. R. (1985). Underground fuel storage secondary containment – early lessons, *Proc. 2nd Canadian Symp. on Geotextiles and Geomembranes*, CGS, Edmonton, Alberta, Canada, pp. 177-182.
www.futuracoatings.com
www.grace.construction.com
www.layfieldgroup.com
www.liquidboot.com
www.specialty-products.com

Exposed Geomembrane Cover Details

D. E. Hullings, Jones Edmunds & Associates, Gainesville, Florida, USA

ABSTRACT

Generally, geomembranes are covered because of the nature of their application or to protect them from damage. They have, however, been used in exposed applications such as roofs, drainage channels, and landfill covers with favorable results for years. In addition to the challenges of exposure to ultraviolet light and potential damage from the elements, exposed geomembrane covers (EGCs) also have the unique challenges of foundation settlement, gas generation pressure, and sheer size, which present difficulties with securing against wind load, shedding stormwater, and access. This paper presents some of the ways these challenges have been overcome in actual applications.

1. INTRODUCTION

An exposed geomembrane cover is an innovative concept that basically does away with the traditional soil cover typically placed over the geomembrane component in landfill final covers. In doing this, EGCs remove one of the biggest problems with traditional covers – soil erosion and slope instability. In addition to the obvious cost savings with not having to obtain and place soil cover and provide vegetation and potential drainage, there is also a savings in maintenance costs such as mowing and channel and basin clearing. These benefits and savings, however, also present some design challenges. Some of the specific challenges for some Florida EGCs and how these challenges were overcome is the topic of this paper.

2. EGC DESIGN

Although only a few EGC designs are well documented, design procedures have actually been well established. The procedures are summarized in this section while the subsequent section describes how these concepts have fared in actual applications.

2.1 Methodology

Design procedures for EGCs focus on the potential for wind-lift and the necessity of providing proper anchorage. Other procedures, such as estimating run-off and accounting for gas pressure, are simple adaptations of methods used in traditional soil-covered designs. Basic design elements are summarized in Table 1 with references provided for more detail. The basic process to address wind loads on EGCs is as follows:

1) Select a wind speed which depends on geography but which, in the United States, is generally in the 70- to 90-mph range except for the hurricane-susceptible southeast and Gulf coastlines where an EGC is not recommended.
2) Calculate uplift pressure, which is directly related to the square of the wind speed and also has a correction factor for slope.
3) Determine the tension in the geomembrane and vary panel length (distance between anchorage points) and geomembrane stress-strain characteristics until the estimated tension in the geomembrane is within acceptable limits for the chosen geomembrane.
4) Calculate anchorage resistance for the anchor trench, ballast, or whatever system is applied.

Table 1. Summary of design calculations.

Design Element	Description	Reference
Wind speeds	Typically 70 to 90+ mph	Wayne and Koerner (1988)
Uplift pressure	S_e (psf) = $0.00124CV^2$ (ft/s)	Wayne and Koerner (1988)
Geomembrane Tension	$T = S_eL$; $T = J\varepsilon_o$	Giroud, et al (1995)
Anchor Trench Resistance	$T_{all} = (0.5\gamma_{AT}d_{AT} + \sigma_n)(d_{AT})(K_p-K_a)/\cos\beta$	Koerner (2005)
Impact Resistance	$I = \pi\rho_h^2 gd^4/9\rho_a c_d$	Gleason, et al. (1998)
Gas Pressure	$U_{max} = \phi_g\gamma_g/\psi_g\ (D^2/8)$	Thiel (1999)
Stormwater runoff	Q = CiA (C=1.0)	Chow (1962)

Richardson (2000) also presents a nice review of these design concepts. In addition to restraining against wind loads, other design elements need to be evaluated that are a little different for EGCs:

1) Resistance to falling objects (including hail and the ever-popular chicken bone).
2) Potential gas buildup and pressure (remember there is little overburden load resisting gas pressure).
3) Stormwater runoff (assuming that 100 percent of precipitation will run off is fairly accurate).

Other design aspects are not readily reduced to equations but must also be addressed with the design:

- Design life
- Access
- Aesthetics

Estimated design lives for exposed geomembrane applications are now pushing 30 years (Koerner, 2008), which bodes well for more exposed applications in the future. For access, trucks cannot be driven over the exposed cover but ATVs with low ground pressure have been used with success and textured geomembrane makes walking up and down slopes much easier. As far as aesthetics is concerned, colored geomembranes are available but no one is going to confuse an EGC with a grassy knoll except at some considerable distance.

2.2 Material Selection

Geomembrane material selection depends on a number of factors:

- Stress/strain characteristics (see computations for tension)
- Survivability (puncture, tearing, etc.)
- Design life
- Cost
- Other site-specific concerns (aesthetics, low temperature performance, etc.)

While a variety of geomembrane types can be used, textured polyethylene and reinforced polypropylene seem to be the materials of choice. Thiel (2003) presents selection criteria that in sum indicate that reinforced polypropylene may have some advantages in physical properties (impact and tear resistance for example) but at a higher cost than the polyethylenes (both HDPE and LLDPE). The three EGCs the author is most familiar with have HDPE and LLDPE covers and have performed quite well. These provide most of the experiences discussed in this paper.

2.3 Anchorage

Providing proper anchorage against wind loads is key to EGC performance, and a number of systems can be used:

- Ballast such as sand bags or tires or water filled tubes
- Anchor trenches
- Soil cover benches
- Roadways
- Vertical anchor attachments to other features such as downchutes and landfill gas collection pipes
- Anchor bolts
- High-strength wire rope
- Vacuum

Ballasting is a straightforward approach – provide enough weight to counteract suction – but when design winds dictate sand bag spacing every five feet, ballasting becomes tedious and expensive. Because most of the EGC is probably sideslope, each bag must be secured to a rope line to stay in place. Anchor trenches are a better option and the systems used successfully in Florida are discussed in the next section. The author has no direct experience with the other options, but attaching the EGC to other features seems suspect given the experience with the stormwater inlet attachment discussed later. The idea of using the landfill gas collection system to pull a vacuum to counteract wind loads is discussed in the section on gas generation.

3. EGC EXPERIENCES

The following experiences are derived from three EGCs in Florida and are summarized in Table 1 with locations shown in Figure 1.

Table 1. EGCs in Florida.

Site	Constructed	Material
Polk County Phase 1	2001	Black HDPE
New River Cells 1 and 2	2001	White LLDPE
Marion Cell III-C	2002	Black LLDPE

Figure 1. Current EGCs in Florida.

All three EGCs are still performing well and are a testament to the above design procedures - and perhaps a little luck. The following details some of the items that have gone right and some items that could be improved.

3.1 Construction

An EGC presents a large surface area susceptible to high winds so that anchorage of the installation is an important perimeter. Simply tucking the geomembrane in an anchor trench at the top of slope is not enough and keeping ballast such as sand bags or tires in place on the side slope can also be problematic. The Jones Edmunds approach is to install the geomembrane in panels approximately 60 feet wide that are anchored in trenches that run up and down the slope. The panel is secured in an anchor trench around its entire perimeter. In addition to providing the additional anchorage strength, securing the panel along its entire length limits creep. The construction sequence is necessarily more complicated than traditional methods and, as shown in Figure 2 includes:

1. Constructing anchor trenches top of slope, bottom of slope, and along the edge of the panel.
2. Constructing a panel by seaming several rolls together over the entire slope length (for typical HDPE, a panel consists of three roll widths).
3. Securing the panel edges in the trench and backfilling (backfill may include bentonite or cement).
4. "Skipping" the next panel and constructing a new panel approximately 60 feet from the first in the same way.
5. Installing the intermediate panel beneath the two secured panels by welding the edges directly to the installed panels. Note that the intermediate panels are not secured directly in anchor trenches.

This method of installing has proved successful in all of our applications.

Figure 2. Construction sequencing illustrating side achorages.

3.2 Stormwater Management

One of the many advantages of an EGC over traditional landfill covers is that soil erosion and instability is not a concern since no soil is placed over the geomembrane. Instead of collecting stormwater in intermediate benches and conveying it to downdrain structures to reduce the impact of sheet flow on soil erosion, stormwater in EGCs can simply sheet flow over the entire length (Figure 3). In addition to the construction cost savings, maintenance is easier since perimeter drainage ditches are not being filled with soil eroded from the sideslopes. Although simplified, there are a couple of details to remember:

- Without soil to store some of the stormwater, nearly all of the stormwater falling on an EGC will run off (a very small amount "wets" the geomembrane or evaporates), so the overall strormwater management system should be designed accordingly.
- Perimeter stormwater trenches should not only be designed for increased run-off but must also provide some energy dissipation and extra freeboard. Note that textured geomembrane does a nice job of slowing stormwater flow and provides a surprising amount of dissipation.
- Securing the EGC directly to stormwater inlets has led to problems as the inlet typically settles more than the surrounding area and stresses the EGC. A seam from the EGC to an inlet at one landfill has required multiple repairs (Figure 4).
- Transition from the EGC to the perimeter trench can be a problem if undermined by flow. Extending the EGC through the back end of the trench is a nice option to consider.
- Landfills do settle, especially with bioreactor operations, and a three percent slope on the topdeck may not be sufficient to maintain positive slope and prevent ponding even on relatively small topdecks.

Figure 3. Stormwater sheet flow off of the EGC and into perimeter ditch.

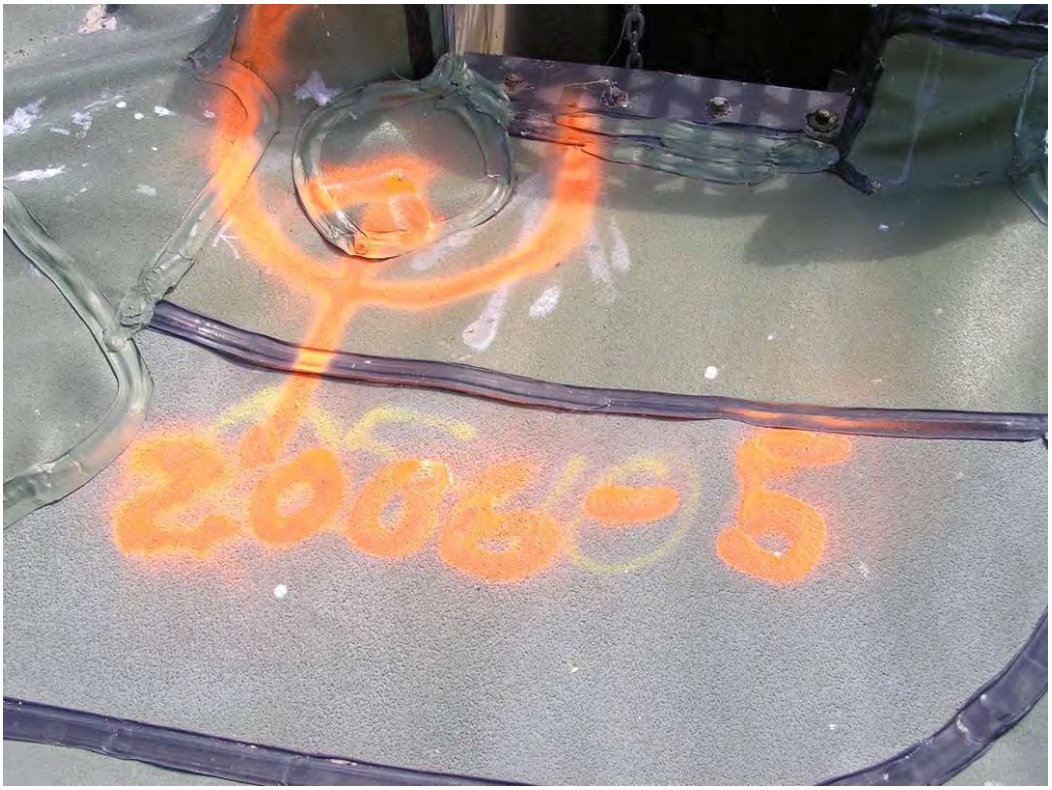

Figure 4. Repairs of an EGC at stormwater inlet.

3.3 Gas Collection

Another unique aspect of EGCs for landfill covers is that gas is being generated beneath the cover. Because EGCs are often used in combination with bioreactors which have enhanced gas generation or on landfills that already have a gas migration issue, landfill gas may be an even greater concern for EGCs than with other covers. As Thiel (1999) discusses, gas build-up beneath traditional covers can have a destabilizing effect, but the potential impact on EGCs is a little different. Without proper gas collection or venting and with no overburden pressure from soil cover, even small amounts of gas may produce gas pockets beneath the EGC. However, without the overburden that can sometimes trap gas migration that ultimately results in large bubbles, known as *whales*, the gas is free to migrate in EGCs. Even so, landfill gas build-up beneath an EGC can result in uplift and is a potential safety concern.

Active gas collection systems are typically found with EGCs covers because EGCs are generally used in applications where gas generation is high. Because the geomembrane forms an "impermeable" layer, the tendency is to push collection pipes farther to the boundary and increase the vacuum since, theoretically, less oxygen will be pulled into the system from the atmosphere. Note, however, that as with any geomembrane, EGCs will have pinholes that allow not only stormwater but air to get through. High oxygen contact at a gas header may indicate a nearby defect in the EGCs. Others have noted that pulling a larger vacuum with the active gas system may pull the EGC down and counteract potential wind loads. Remember, however, that significant wind events also lead to power outages that could take the active gas collection off line. We suggest that a back-up passive vent system be installed to prevent gas-buildup if such an outage were to occur.

Bioreactor operation has also led to a significant amount of leachate being recirculated. At the sixteen-acre Polk County Phase 1, over 20 million gallons of leachate have been recirculated. Seeps are becoming apparent as leachate migrates out of the waste and encounters the underside of the EGC. While the EGC is still performing well, another area with a temporary cover is beginning to trap some seeps at the toe. Future applications will definitely include a toe drain to capture seeps and direct them back down into the leachate collection system.

The final detail to remember is that an active gas collection system, together with a bioreactor, results in much piping. If every vertical well and horizontal line penetrated the EGC, many penetrations would result (Figure 5). Each penetration requires a clamped pipe boot with an extrusion weld around the skirt and thus several potential leaks. Some thought must be given to the underlying pipe network to reduce the number of penetrations through the EGC.

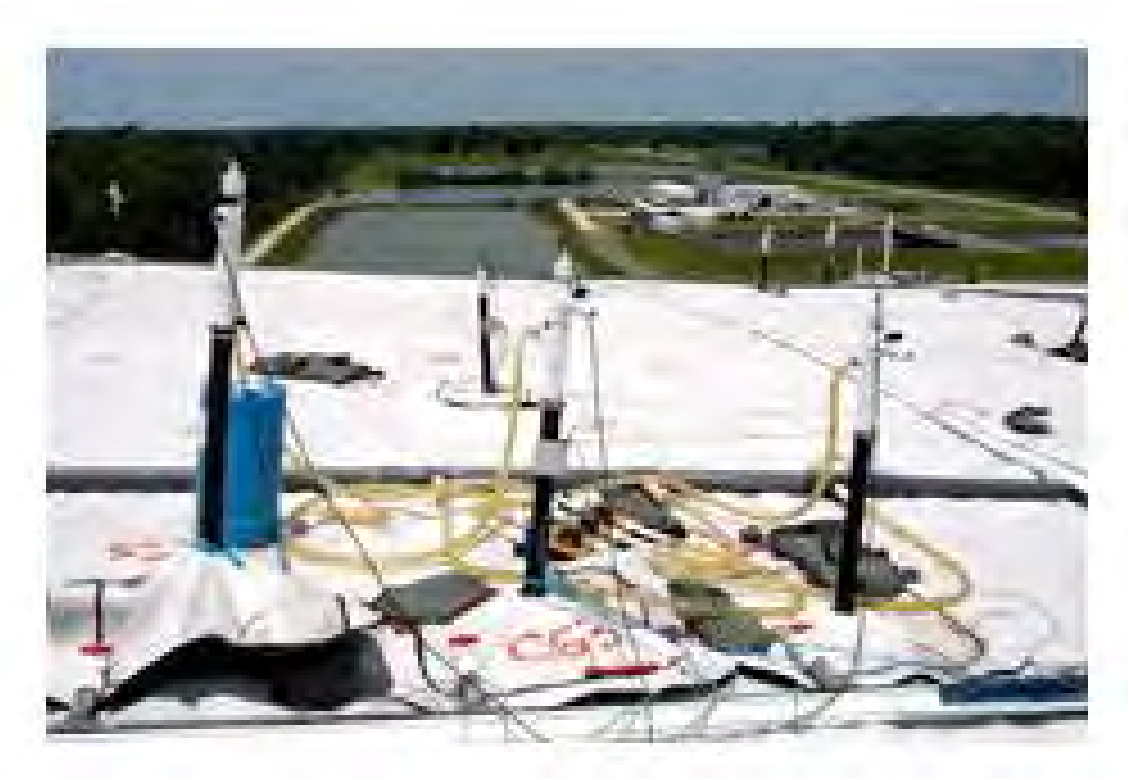

Figure 5. Multiple EGC penetrations.

3.4 Operations and Maintenance

Another benefit of EGSs is that, unlike covered geomembranes, they are easily inspected and can be routinely repaired as necessary. Routine inspections have identified some issues that could be rectified in future designs:

- Differential settlement and daily thermal expansion and contraction have led to some areas where the geomembrane is not in contact with the underlying surface. This "trampoling" is not a permanent situation but changes throughout the day and occurs in different locations. More slack in the system or more flexible geomembranes would address this issue.

- A stormwater inlet at the top of the landfill has settled more than the surrounding EGCs, most likely due to the added weight of the concrete on the underlying solid waste mass. This had led to some tearing of the EGC at the inlet and multiple repairs. Such inlets should be avoided in designs if possible.

- An odd series of holes was identified during the most recent inspection of one of the sites (Figure 6). The source is unclear but speculation is that the holes were made by the litter patrol. Clearly those operating on an EGC must be given directives as to what can occur and what must not occur on the EGC.

- Even with the necessary repairs, average maintenance costs for the Polk EGC has averaged about $3,000 per year – less than the cost of maintaining grass.

Figure 6. Odd holes in EGC.

3.5 Material Performance

Annual laboratory testing on samples of exposed HDPE has been ongoing since 2001 with some of the data presented in Table 2 below. Beginning in 2006, testing on samples that have been covered (no UV coupon) and archived (warehouse) were also included. Tensile properties are still well within specification although there is a

downward trend for elongation at breaks, so the exposed material may be somewhat stiffer after almost seven years. The OIT values are definitely decreasing, indicating that the antioxidants are being consumed as anticipated. The latest data for 2008 are exactly what was expected. High OIT values for archived samples (but somewhat less than original), lower values for field samples not exposed to UV, and lowest values for UV exposed samples. Values from field samples, however, are high enough to indicate that antioxidants are still available in the material and appreciable degradation has not yet occurred in the geomembrane. Note that the HDPE geomembrane used for this EGC application was "off the shelf" with no special additive package for exposed conditions. Although pleased with the performance to date, the author would anticipate even better performance from HDPE manufactured specifically for an exposed application in 2009.

Table 2. Test results from an HDPE EGC.

Property	Const. Spec	2001 Coupon	2006 Coupon	2006 No UV Coupon	2006 Ware-house Coupon	2008 Coupon	2008 No UV Coupon	2008 Ware-house Coupon
I. Tensile Properties (ASTM D 638)								
A. MD Yield Strength (lbs/in-width)	130	167	178	175	179	184	183	176
TD Yield Strength (lbs/in-width)	130	169	183	175	182	185	188	181
B. MD Break Strength (lbs/in-width)	90	194	187	178	202	176	185	189
TD Break Strength (lbs/in-width)	90	179	149	158	164	159	170	188
C. MD Yield Elongation (%)	13	19	18	20	18	21	19	20
TD Yield Elongation (%)	13	18	18	19	17	19	19	21
D. MD Break Elongation (%)	150	498	477	466	515	404	463	465
TD Break Elongation (%)	150	483	271	387	456	344	447	501
II. Wide Width Strip Tensile (ASTM D 4885)								
A. MD Tensile Strength (lbs/in)	-	-	143	157	154	156	158	155
TD Tensile Strength (lbs/in)	-	-	149	161	153	154	157	159
B. MD Elongation at Peak (%)	-	-	20.2	19.3	21.3	19.3	17.2	17.2
TD Elongation at Peak (%)	-	-	18.1	18.6	20.4	17.1	15.8	14.1
III. Standard Oxidative Induction Time (minutes) (ASTM D 3895)								
	125	171.6	37.9	49.4	88.4	29.0	59.0	100
IV. High-Pressure Oxidative Induction Time (minutes) (ASTM D 5885								
	N/A	-	276	278	468	186	258	694
V. Stress Crack Resistance (minutes)(minimum) (ASTM D 5397								
	500	>500	>500	>500	>500	>500	>500	>500

3.6 Field Test

A few years after the Polk County EGC was constructed, it was exposed to three hurricanes that passed through the County. In 2004 Hurricanes Charley, Frances, and Jeanne all passed near the landfill, bringing sustained winds of 75 to 90 mph and wind gusts as high as 115 mph. The three storms brought a total of 20 inches of rainfall and hurricane-force winds originating from all directions. Not only did the EGC not experience a single storm-related problem, no post-storm clean-up in regard to erosion or channel clearing was necessary. Design practices and construction methods have passed the test.

4. CONCLUSIONS

As with any relatively new application, our experience with EGCs has revealed details that have worked and some that could be improved.

4.1 Successful Details

Stormwater management has been greatly improved with EGCs. Without soil to erode, stormwater is clean and maintenance of the stormwater system is almost nonexistent. The textured geomembrane provided to promote access also seems to do a great job in slowing the stormwater run-off and acts as an energy dissipater. Continuing the EGC through the perimeter drainage ditch and anchoring on the other side has removed all transitions and allowed for uninterrupted sheet flow into the perimeter ditch. Also, the wind load design methodology was tested with actual hurricane wind loads that exceeded our design and the EGC not only remained intact but performed admirably.

The anchor trench system performed as expected. Along the same vein, the selection of polyethylene was a good one. Tearing, puncture, and impact resistance have really not been issues and repairs have been limited. The jury is still out, however, on how long the EGCs will last.

4.2 Details That Will Change

The one exception to the great performance of the stormwater system was the one inlet installed at a low point on the top deck. This area has settled more than the surrounding area and has undergone several repairs. Some localized areas of ponding have occurred and in the future the top deck slope will be constructed more steeply, at least five percent and perhaps as much as ten percent slope. EGCs at New River and Polk were part of bioreactor research projects and had numerous penetrations for pipes. In the future, gas collection and leachate distribution piping will be rearranged to limit the number of penetrations through the geomembrane. Differential settlement has led to some areas of trampoling in the HDPE EGC, which has not really resulted in an adverse impact but may be a reason to use something more flexible, such as LLDPE. Because of the bioreactor operations, leachate seeps are beginning to be an issue as leachate collects near the toe of slope. Toe drains within the waste should definitely be built into EGC systems. Overall, the experience with EGCs has been positive and new projects are being discussed. Future applications will be improved as we implement some changes based on what we have learned.

REFERENCES

Chow, V.T. (1962). Hydrologic Determination of Waterway Areas for the Design of Drainage Structures in Small Drainage Basins, *University of Illinois Engineering Experimental Station Bulletin 426.*

Giroud, J.P., Pelte, T. and Bathurst, R.J. (1995). Uplift of Geomembranes by Wind, *Geosynthetics International, Special issue on Design of Geomembrane Applications*, Industrial Fabrics Association International, Vol. 2, No. 6, pp. 897-952.

Gleason, M.H., Houlihan, M.F. and Giroud, J.P. (1998). An Exposed Geomembrane Cover System for a Landfill, Design and Construction of an Exposed Geomembrane Cover System for a Solid Waste Landfill, *Sixth International Conference on Geosynthetics*, pp. 211-218.

Koerner, R.M. (2005). Designing With Geosynthetics, 5th Ed., Pearson Education, Inc., Upper Saddle River, NJ.

Koerner, R.M., Hsuan, Y.G. and Koerner, G.P. (2008). Freshwater and Geosynthetics; A Perfect Marriage, *GeoAmericas 2008*, Cancun, March.

Richardson, G.N. (2000). Exposed Geomembrane Covers: Part 1 – Geomembrane Stresses, *Geotechnical Fabrics Report*, vol. 18, no. 7.

Richardson, G.N. (2000). Exposed Geomembrane Covers: Part 2 – Geomembrane Restraint, *Geotechnical Fabrics Report*, vol. 18, no. 8.

Thiel, R., Purdy, S. and Yazdani, R. (2003). Case History of Exposed Geomembrane Cover for Bioreactor Landfill, *Proceeding for Sardinia '03 Ninth International Landfill Symposium*, October.

Thiel, R.S., (1999). Design of Gas Pressure Relief Layer Below a Geomembrane Cover to Improve Slope Stability, *Geosynthetics '99*, Boston, April.

Wayne, M.H., and Koerner, R.M. (1988). Effect of Wind Uplift on Liner Systems, *Geotechnical Fabrics Report*, July/August.

Zornberg, J.G. and Giroud, J.P. (1997). Uplift of Geomembranes by Wind – Extension of Equations, *Geosynthetics International*, Industrial Fabrics Association International, Vol. 4, No. 2, pp. 187-207.

Challenges at Leachate Recirculation and Bioreactor Landfills

K. McKeon, P.E., AECOM, Trevose, PA
B. Schwartzott, P.E., AECOM, Trevose, PA

ABSTRACT

It is generally agreed that bioreactor status and/or selective recirculation are beneficial to the operator. The technical challenges presented herein are based on the authors' experience in design and issues presented in the field at landfills where leachate recirculation systems have been designed, permitted and constructed. The objective in presenting these technical challenges is to provoke thought concerning potential design, operation and financial impacts of leachate recirculation. This paper does not discuss the specifics of bioreactor design, waste field capacity or leachate chemistry. We understand that specific challenges presented within this paper may vary for each landfill site depending on waste composition, climate, level of commitment to recirculation, and may not be applicable to some facilities.

1. INTRODUCTION

There have been many recent studies, technical papers and demonstration facilities that have documented the theory, mechanisms, and general advantages of aerobic (through controlled injection of air and liquid), anaerobic (through controlled introduction of liquid only), aerobic-anaerobic, and facultative bioreactor landfill operations. As documented within the literature, the main advantages of the controlled recirculation of landfill leachate back into the landfill are the following:

- Storage and treatment of leachate within the waste mass.
- Increased rate of waste settlement and stabilization, and improved waste compaction density allowing for greater waste intake within the same footprint.
- Inducing settlement in overfilled areas.
- Minimizing long-term landfill gas generation as it is accelerated to the near term.
- Reducing the long term "potency" and long-term treatment costs/commitments (closure and post-closure) of landfill leachate.

2. LEACHATE DISTRIBUTION METHODS

2.1 Direct Application

If the permitting hurdle can be overcome, leachate may be directly applied to the working face from trucks similar to water/tanker truck systems used for dust suppression, or from overhead/mobile irrigation equipment.

2.2 Remote Pumping

Leachate may be pumped through solid forcemain piping from landfill perimeter facilities (i.e. storage tanks, lift stations, leachate sumps) and then injected into the waste via subsurface horizontal distribution trenches. The trenches typically consist of a perforated circular pipe within an envelope of porous, free-draining material. Trenches are directed away from finished slopes and are typically plugged with low permeability soil at the injection end to minimize the potential for leachate popouts. A series of trenches may be connected via manifold to a common injection point. The injection point may also be valved and connected in series with solid piping to other injection points. Adjacent horizontal trenches are offset to account for the anticipated zone of influence of leachate percolation from a single trench, and to provide adequate distance from planned vertical gas extraction wells.

2.3 Direct Injection

Leachate may be directly injected into horizontal trenches from tanker trucks through a vertical riser. While the distribution method is similar to remote pumping, solid forcemains and high head pumps are not required.

Figure 1. Leachate injection riser.

Leachate may also be injected into deep wells that may be extended vertically as waste filling progresses, or these wells could be installed prior to capping to induce settlement in overfilled areas. These wells typically consist of piping perforated at the desired recirculation depth interval(s). These wells could also be configured with submersible pumps for emergency evacuation of liquid and may also serve a dual purpose as a vertical gas collection well during periods when liquid is not being actively recirculated. While deep wells typically provide recirculation with a reduced possibility of pop-outs on slopes, they may "short-circuit" to the leachate collection system at the base of the landfill if wells are too deep.

2.4 Leachate Lagoons

Leachate may also be directed (pumped) to larger excavated depressions on plateau areas of the landfill with the intention of allowing downward infiltration into the waste.

3. DESIGN, INSTALLATION AND OPERATIONAL CHALLENGES

There are many technical issues that need to be understood and planned for within the design and permitting process, as well as during installation and operation of these types of liquids management systems. Bioreactor status may be difficult to achieve due to the amount (i.e. volume) of liquids required in addition to landfill leachate and gas condensate to achieve a uniformly wet waste mass. Maier (1998) found absorptive capacity of waste as reported in the literature can vary from 16% to 29%, equating to approximately 148 - 297 liters per cubic meter (30-60 gallons per cubic yard) of waste. Under these estimates, a 1,814 Mg/day (2,000 tpd) landfill and a typical

conversion factor for compaction of 0.83 Mg/m^3 (0.70 $tons/yd^3$) could therefore potentially hold an additional 321,760 to 643,520 liters (85,000 to 170,000 gallons) of liquid per day. However, if waste is wetted too rapidly, a build-up of volatile organic acids may lower leachate pH, inhibiting methane-producing bacteria and the rate of biodegradation (Campman and Yates, 2002). Therefore, complete bioreactor status may prove difficult to attain without applying the rigors of a demonstration facility. However, general recirculation is also beneficial but not without challenges.

3.1 Installation and Shorter Term Issues

- Coordination of wetting efforts for direct application (spray irrigation) between the application truck and landfill compactors must be considered to avoid conflicts and to enable productive use of liquid for compaction efforts. While liquid addition to waste as it is placed would aid in compaction, navigation of an uncompacted waste lift by a leachate application truck could be problematic. Depending on daily tonnage rates and the size of the working face, consideration could be given to applying liquid at the end of the operating day prior to daily cover or at the start of the day after daily cover is removed.

- Leachate application by direct spray irrigation onto the working face should consider weather conditions (i.e. wind). Blowing and misting of leachate is not conducive to controlled application or to maintaining a good relationship with the neighbors. Spray irrigation should be limited to non-windy days. Direct application near the waste surface could be accomplished by draining to a trickling boom mounted beneath a water truck, limiting the potential misting problem and allowing application in windy conditions.

- Cold weather recirculation operations must be considered. Extreme cold may also prove difficult when considering recirculation by direct application at the working face from tanker trucks or portable irrigation equipment as application equipment could freeze. In a pumping scenario, it is likely that re-use of piping is economically preferable. Therefore, temporary solid above-grade recirculation forcemains should be covered with soil or suitable soil-like material (compost, auto-fluff, etc.) to provide insulation against freezing. Forcemains should be configured with a means to evacuate liquid at check valves or low-points in the system to prevent freezing of static liquid.

- Maintaining positive drainage away from slopes to assure liquid drains into waste away from slope after pumping stops can entail deep trench excavation, trench safety and confined space issues. Filling operations personnel should coordinate efforts to provide active areas sloping away from outboard landfill surfaces to minimize trench excavation issues.

- Excessive near-surface recirculation may cause landfill access/traffic problems as the work area and access roads may be more difficult to traverse for hauling vehicles. These issues may be minimized by limiting recirculation activities to a nominal distance of no closer than 30.5 metres (100-ft) to exterior slopes and no closer than 7.6 meters (25-ft) from temporary or permanent access roads in active areas. Using waste tippers may also be an option in keeping hauling vehicles away from the active area.

- Leachate recirculation does not result in less liquid volume and near-term weaker leachate. The designer and operator must consider the treat-ability of concentrated leachate which may arrive at the plant in high concentration and large volumes. For example, the detention time required for effective "pre-treatment" facilities such as aeration of large quantities of leachate should be evaluated. In the planning process, expandable/upgradeable/downgradeable components should be considered as volume and potency will increase in the short term but are expected to weaken over the closure/post-closure period.

3.2 Longer Term Issues

- While controlled recirculation accelerates the decomposition rate of waste, landfill gas production (and odor production) is also accelerated. This requires an earlier deployment of some type of landfill gas collection and control strategy. While a properly designed geosynthetic final cover (with underlying gas relief layer as appropriate and vertical gas wells) can also function to collect and direct generated gas, early capping and well installation would preclude operators and communities from enjoying the benefits of more rapid waste settlement (i.e. airspace re-use). Delay of final capping is desirable until waste has settled and "stabilized". Temporary geosynthetic covers with integrated gas collection or venting, active gas wells and headers, and/or thicker temporary intermediate soil layers could be installed atop over-filled intermediate cover slopes for odor and gas control. Temporary covers could later be removed or trimmed to either claim additional available airspace or to closure cap the area.

- Remote pumping or direct injection into horizontal trenches can lead to saturation at specific elevations during development due to the heterogeneous nature of waste and the application of low permeability materials as cover or fill. Waste filling over areas with ponded leachate can result in horizontal squeeze-out (stepping on a wet sponge) towards the finished slopes of the landfill rather then vertical percolation to the leachate collection system.

- An inadequately designed drainage and pumping system at the base of the landfill will cause build-up of a leachate head on the liner system during normal landfill operations but especially when heavy recirculation is planned. This can effect landfill slope stability, head in excess of the maximum regulated allowance at the sumps, and gas system efficiency. Some conservancy should be built into waste parameters (i.e. higher unit weight, lower shear strength) by the designer for landfill stability analyses based on some knowledge of the owner's level of commitment to recirculation. The base liner system design should incorporate a free-draining protective cover layer and leachate collection lateral and trunks for repetitiveness.

- "Fouling" of horizontal trenches due to clogging could render injection useless and promote back flooding towards the introduction point and subsequent leachate pop-outs (if the introduction point is near a slope) or weak zones along the trench alignment. The designer should carefully select the pipe's hole/slot pattern along the horizontal trench for equitable distribution along its length, and design a free-draining envelope around the perforated pipe with a gradation compatible with the hole/slot size and material type compatible with (i.e. resistant to) leachate. Recirculation should be limited to occur no closer than a nominal distance of 30.5 meters (100-ft) to exterior slopes and/or liner limits. The working face and daily cover applications should be graded away from outer slopes. Keep in mind, a good knowledge of your waste's inherent moisture and the targeted application quantity for a specific application method should be understood. Remote pumping should consider some automation for system shut-off for larger operations or extra personnel may be required for manual operation of larger systems to actively monitor for pop-outs or puddling as they are signs that capacity has been reached.

- Temporary access roads that have become compacted over their useful lives should be removed as they become conduits for leachate. If not feasible due to timing or extensive effort, consideration should be given to commit to cutting out at least 30 meters (100-ft) of the road from its entry point into the active area.

- Low permeability soils (silts and clays) or low permeability alternate daily cover materials (ash, dredge spoils, etc.) that are not designed to be removed for placement of subsequent waste lifts will limit vertical percolation of liquid into the waste mass. This can lead to perched leachate pools in the waste, localized weak zones, leachate pop-outs on landfill intermediate sideslopes as loading is increase from above, watering out of gas wells, leachate between the intermediate soil and geomembrane liner leading to problems at the perimeter anchorage as shown in Figures 2 and 3.

- Problems can arise at benches if seepage relief is not built into the design as shown in Figures 4 and 5.

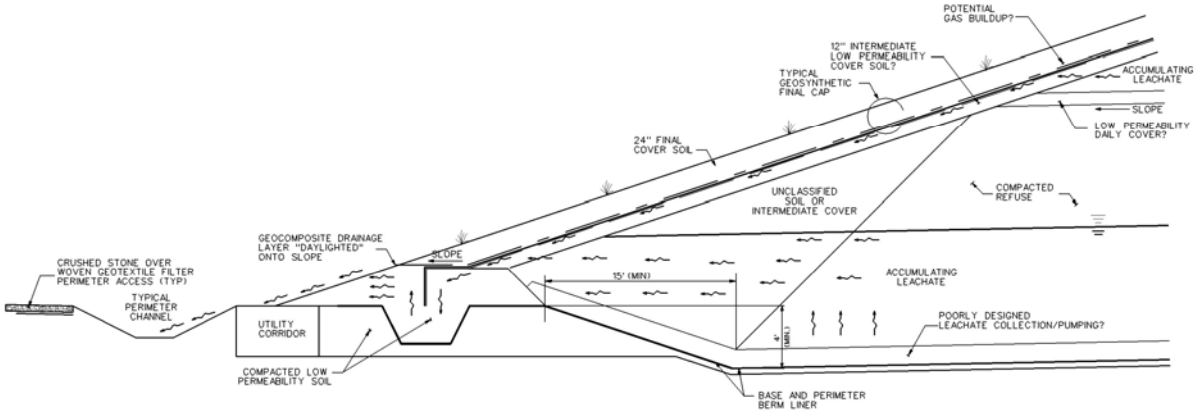

Figure 2. Perimeter anchor trench with some design issues.

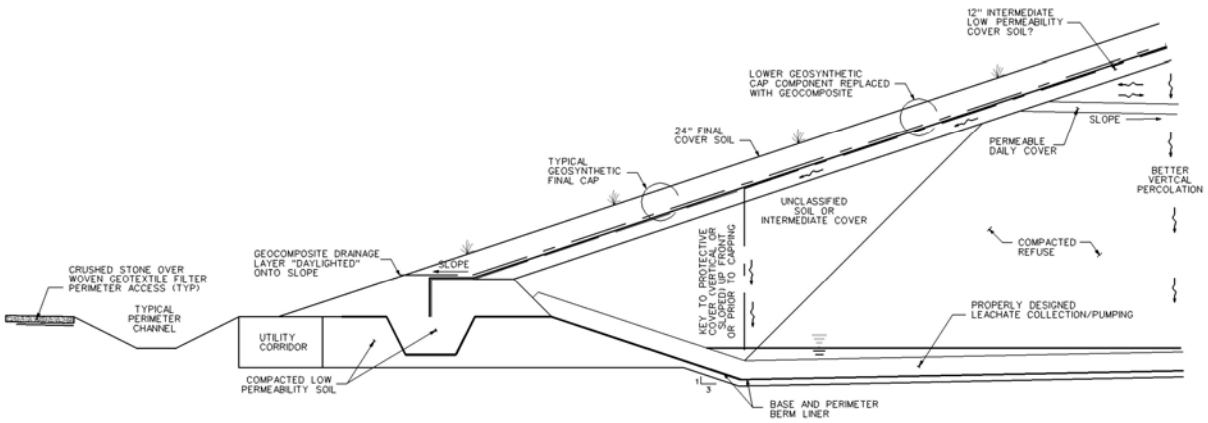

Figure 3. Perimeter anchor trench with some potential solutions.

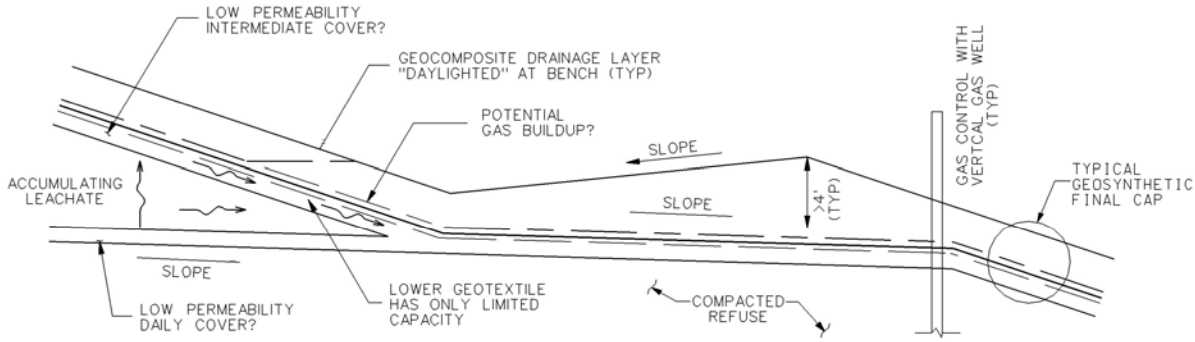

Figure 4. Typical outward sloping landfill bench.

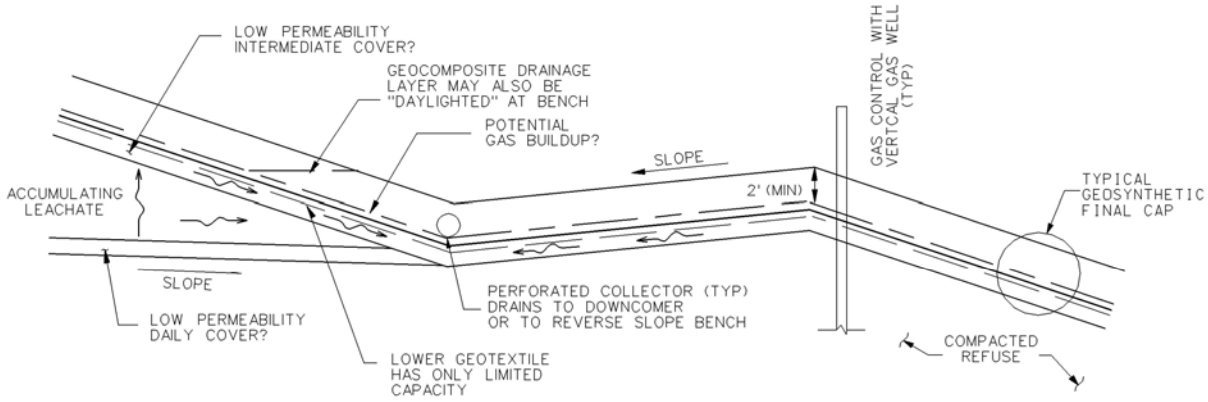

Figure 5. Typical inward sloping landfill bench.

- Incorporation of full or partial blanket geocomposite gas relief layers, strip drains, and vents may be incorporated above the intermediate cover (Thiel 1998, Theil and Narejo 2005) to collect shallow gas and to collect and redirect seepage. There are obvious cost ramifications to the final cover installation (generalized as $5,000 to $15,000 dollars per acre for material full or partial geocomposite relief layer, with additional costs for seepage drains and QA). However, cost of full final cap repair (see Figure 6) is much greater.

Figure 6. Typical removal of final cover system in failure area.

- Excessive recirculation may "water out" vertical and horizontal gas collectors, inhibiting gas collection and leading to excessive odors and slope stability issues related to final cap uplift. These issues may be minimized by limiting leachate application to a target quantity by weight of waste received based on knowledge of site-specific initial water content and absorptive capacity of received waste. Vertical gas/liquid collection wells may be designed with pumping capabilities, or separate wells could be installed to collect perched leachate.

- Offsetting trenches in subsequent recirculation galleries at higher elevations provides additional obstacles for vertical gas well construction. Trench locations should be part of the engineer's planning and design during the permit process.

  While minimizing spacing between adjacent recirculation trenches can provide greater coverage and the greater likelihood of localized uniform wetting and movement towards bioreactor status, oversaturation will provide a barrier against efficient gas collection as screened intervals in gas wells become ineffective when they are watered out. While the design layout for vertical gas collection wells should consider access and adequate spacing for radius of influence (ROI) overlap, it must also account for offsets to horizontal recirculation trenches to prevent damage to piping and to minimize the potential for the watering out of gas wells.

- Pockets of saturated waste from excessive recirculation or from low permeability barriers within the heterogeneous mass can make gas well installation "problematic", see Figure 7. Trying to set a deep gas well to its design depth in these conditions may result in a disappearing gas well. When pockets of leachate are observed during drilling, operations can either coordinate with the designer to backfill and relocate the well to an alternate location or allow for shallow gas well construction for collection of the shallow gas above the leachate pocket.

Figure 7. Landfill gas collection well prior to its disappearance.

5. CONCLUSIONS

Leachate recirculation efforts demand "dollars and sense". Increased equipment and installation costs (blowers, free-draining media, pumps, solid piping, perforated piping, etc.), increased Quality Assurance (pipe pressure testing, as-built survey, etc.) additional monitoring requirements and operational diligence (leachate popout mitigation, final cover inspection for whales and sliding soil, monitor leachate quality as it relates to treatment requirements, etc.) are required. Leachate recirculation should be executed in a controlled manner that must be fully detailed within the construction specifications, landfill operation plan, and environmental monitoring plans. Operations personnel must understand that liquid must be re-introduced in a controlled manner. Waste must not be over-saturated because doing so can affect trafficability in recirculation areas, foul leachate application trenches, lower gas collection efficiency, lower leachate pH and inhibit methane-producing bacteria and rate of biodegradation as partially detailed above.

If soil-like materials (fill dirt, construction and demolition material) are expected to be a large component of the waste stream, it is recommended that these materials be well integrated with municipal waste to minimize the potential for perched leachate. While low permeability covers work for odor control and to limit stormwater inflow (which may be desirable when incoming waste is already near field capacity), they can lead to leachate popouts and effect gas system efficiency as discussed above. These issues could be minimized by using more permeable

soils or alternative soil-like materials, degradable spray-on material such as foam that is designed to be compromised with subsequent traffic, removable temporary covers such as tarp or geomembrane, or requiring removal of or excavation of infiltration windows within placed low permeability soils if they must be utilized when committing to leachate recirculation and bioreactor operations.

The landfill designer must consider appropriate potential impacts to landfill stability (higher unit waste, potential perched leachate, shallow final slopes) incorporate an adequate leachate collection layer above the primary (upper) liner and pumping system to limit the build-up of leachate head, balance the desirability of a uniformly wet waste mass with gas collection system efficiency, consider cost-effective alternatives for interim gas and leachate management, and understand the Owner's goals during the permit process.

REFERENCES

Campman, C. and Yates, A. (2002). Bioreactor Landfills: An Idea Whose Time has Come, *MSW Management* September, October 2002.

Maier, T.B. (1998). Analysis Procedures for Design of Leachate Recirculation Systems, *Proceedings from the SWANA 3rd Annual Landfill Symposium*. Palm Beach Gardens, FL, USA. 1998.

Thiel, R. (1998) Design of a Gas Pressure Relief Layer Below a Geomembrane Cover to Improve Slope Stability. *Geosynthetics International.* Vol.5, No.6, pp. 589-617

Thiel, R. and Narejo, D. (2005).Update on Designing with Geocomposite Drainage Layers in Landfills - Part 2 of 4: Geocomposites on Bioreactor Landfill Sideslopes to Control Seeps and Gas, *GFR Engineering Solutions*, Volume 23, Number 2, 2005.

The Devil is in the Details – Segmental Retaining Wall Design Minutea?

J. N. Paulson, P.E., REDI Engineering, Inc., Alpharetta, GA, USA

ABSTRACT
Segmental retaining wall (SRW) designers are constantly faced with details in both design and construction on every project. While the "major" design details of reinforcement length, strength, and spacing are easily computed (either manually or using readily available software), there are numerous other details that need to be addressed before a detailed package and construction drawings can be completed.
The purpose of this paper is to outline several of the critical details that can make the difference between a complete design or an incomplete one. While these details by themselves may not make or break a project they can, if omitted, cause major problems. This paper addresses seven such details:

1. Site soils information including strength properties
2. Accurate site grading contours showing top and bottom of wall
3. Responsibility of performing global stability
4. Inclusion of a gravel "drainage" layer directly behind the block units and block infill
5. Designing for temporary surcharge above the wall
6. Treatment of surface water behind the top of wall, i.e., "to swale or not to swale"
7. Treatment of surface water during construction

Each of these details will be reviewed, case history examples provided, and author's comments discussed.

1. SITE SOILS INFORMATION INCUDING STRENGTH PROPERTIES

The three soil zones on a SRW project include the reinforced soil, the retained soil, and the foundation soil. Wall designers have the ability to control only one of these zones, the reinforced soil zone. Existing site conditions will dictate the retained and foundation soil zones.

However, before design commences several questions need to be asked. They are as follows:

Was a geotechnical report developed for the site?
Was that engineer asked to qualify these soils, including strength parameters?
What soils are available onsite, and are they acceptable for use in the wall construction?
What does the wall designer do when he is asked to design the wall and this information is not available?

Regarding the last question, the choices for the designer are one of the following; (a) assume soil properties that need to be confirmed by the owner's geotechnical representative before construction to provide assurance that the design is safe, or (b) require a soils investigation by a geotechnical engineer familiar with the site before the design is completed.

This condition occurs frequently in commercial construction and in many cases the soils report, if one was performed at all, only quantifies soil properties for buildings, and in many cases purposely excludes soil parameter recommendations for SRW structures. Yet the wall contractor is supposed to provide a bid to the owner to build the walls.

1.1 Case History

A project was put out to bid. Prior to finalizing his bid the wall contractor spoke to a local geotechnical engineer who had previously designed several walls onsite and had tested stockpiled soils meant for use in the wall construction. The wall designer had used this early wall designers knowledge and recommendations for his design and submittal. The shop drawings were submitted with the proviso that the assumed soil properties were to be confirmed by the site geotechnical engineer.

However, the owner decided to hire another geotechnical testing firm to perform the onsite testing. His was the low bid for this QA soils testing work. This company reviewed the shop drawings and took exception to the paragraph that calls for him to confirm properties and foundation capabilities.

He notified the wall contractor and owner that he was taking exception to the confirmation requirements put on him by the wall designer, claiming he was not able to evaluate the soils onsite without testing. Further, this was a design-build project, so the wall designer and contractor have the obligation to verify the onsite soil suitability.

Additionally, he wanted to drill more borings before he will confirm the bearing capacity of the foundation soils.

Thus, the question becomes; “Who has this confirmation responsibility”? Furthermore, is the “new” geotechnical testing company within their rights to require additional soils testing?

1.2 Author’s Comment

The solution to this situation is to involve the owner in the discussion as early as possible, demonstrating the benefits derived from this site specific information. While he may assume that the onsite soils are acceptable, the early discussion of this issue can eliminate the confrontation that occurs when the wall contractor shows up onsite and no one will confirm the soil properties of the material he is supposed to use. Now a conflict arises at a time critical moment in the project.
For this project, more borings ended up being drilled, and additional soils testing performed.

2. ACCURATE TOPOGRAPHIC INFORMATION WITH WALL LOCATION AND ELEVATIONS THAT SHOW TOP AND BOTTOM OF WALL

Many site topographic surveys that are used to generate site contours are aerial surveys which can be inaccurate, e.g., if the site is heavily vegetated the true soil subgrade elevation will be “masked”. Thus the actual soil elevations may differ significantly from these surveys. The site grading plan provided to the wall designer, and which the site civil engineer uses to lay out the top and bottom of wall elevations may be based on this topographic plan. While this makes little difference if the bottom of wall elevation is higher; the wall will then be shorter that designed.

Unfortunately, the opposite condition can cause problems in that the wall will actually be taller than anticipated, making the submitted wall design inadequate. This condition always seems to occur when the wall contractor mobilizes on the site only to find the wall location has been surveyed and the grades are wrong. Now everyone scrambles to get the accurate top and bottom of wall elevations, feed the information back to the wall designer for redesign, and possibly causing changes in the wall cost and schedule.

2.1 Case History

A retaining wall was located very near a property line with a two lane access roadway directly behind it. The proximity of the property line caused the wall to be designed with high quality stone backfill to minimize the geogrid embedment length. The owner and his excavation contractor were informed that this work needed to be performed when the site was “dry”, and the forecast was for three days of clear skies. The near vertical cutback was also a potential safety concern, so the wall contractor was going to use remote compaction equipment so that his personnel would not be underneath the cut.

The excavation contractor went ahead on a Thursday evening during a rainfall event and excavated the back cut. The cut fell in overnight, undermining a portion of the street above it. He then called the wall contractor to tell him what had happened, and ask him to come to the site and rapidly construct the wall.

Around midnight Friday night the wall contractor realized that the wall was too close to the property line, but decided to finish construction of this section of the wall and shore up the roadway. He used stone and built the wall with a geogrid embedment to height ratio of about 0.6. The wall was completed that weekend, the roadway never collapsed, and the site appears to be stable.

Back calculations showed this section of wall to have minimal safety factors against sliding (FS $\sim$1.5), but appears to be stable. It is not known if the wall construction is too close to the property line, a problem the owner will certainly face when final occupancy permits are requested.

2.2 Author’s Comment

The solution is to get the project surveyor to check wall locations and elevations as soon as possible once he arrives onsite, and notify all parties in a timely manner. This can alleviate the “time crunch” that comes when mobilization has already occurred.

3. RESPONSIBILITY FOR PERFORMING GLOBAL STABILITY

Most wall designers have the capability of performing global stability on the wall(s) they are designing. When significant grade changes occur, which is usually the reason for retaining walls to begin with, or when a slope exists above or below the wall, global stability can control the wall structure design.

However, the site-specific conditions, stratigraphy and soil strength parameters required to perform this analysis will have to come from the site's geotechnical engineer. Thus, there must be a relationship between the owner's geotechnical engineer and the wall designer. This should function in the following manner.

Initially, the site's geotechnical engineer is already reviewing stability of the site's slopes and any structures near the top of a slope or wall. The site's geotechnical engineer has explored the site with borings, performed soils classification and testing, and has made recommendations for the site development activities. He/she has also performed at least an initial assessment of soil strengths for use in bearing capacity and settlement calculations and recommendations. Who better is there to analyze the global stability of the site?

3.1 Case History

A retaining wall was sited adjacent to an entrance roadway to a commercial development project. The retaining wall system provider commissioned the wall designer to design with masonry block units. As the wall designer proceeded, the wall designer realized that the drawings showed a detention pond below and some distance away from the wall. An initial global stability analyses showed the proximity of the pond caused the entire cross section to possess a lower than acceptable factor-of-safety (FS) against rotational stability. He notified the owner, who asked his geotechnical engineer to assess the situation. This geotechnical engineer indicated that this was outside of the scope of his original contract and not his responsibility. He indicated that he needed to drill more borings, and more soils testing to perform this analysis. During this time the construction was stopped.

Some weeks later, the onsite structural engineer performed the calculations using the new soils information and recommended foundation improvement under the pond area as a means to satisfy global stability. This work was performed, and the retaining wall was eventually constructed. It is performing without incident but with a significant time delay in the project.

3.2 Author's Comment

This situation could have been resolved very early in the project if the geotechnical and civil/structural engineers discussed all the structures on the site. A retaining wall is a structure, just like a building and should be treated as such.

4. INCLUSION OF A GRAVEL "DRAINAGE" LAYER BEHIND THE BLOCK UNITS AND FOR INFILL WITHIN THE UNITS

One of the misconceptions in SRW technology is the famous "drainage layer" directly behind the block units. This is shown in all standard wall cross section details, and is actually thought by some to provide a drainage path for the entire wall system. One individual actually had surface water running into the top of this layer, figuring that this open graded stone layer would provide an excellent conduit, eliminating the need for other surface water control features behind the wall!

In reality, little or no water should ever reach this zone. Surface water should run either away from the top of wall, or run over the low permeability soil that is used to cap this drainage layer. Furthermore, there should be little or no seepage coming thru the reinforced soil zone, as these walls are designed assuming no water in this zone.

To answer the question of why such a gravel layer is included in SRW design two points are relevant; (a) assurance of complete block units infill to provide adequate mass, and (b) provide frictional resistance for the geogrid layers that extend out from the back of the block.

Geogrid support is a critical function of this layer. If no competent support is provided, the geogrid has a tendency to slide and then settle directly behind the block. Ripping or tearing of the geogrids at the back edge of the blocks is possible due to the stress concentrations that are generated.

4.1 Case History

Figure 1 shows a geogrid extending out from the back of a block in a dismantled wall. Settlement of several inches directly behind the wall is obvious with the geogrid extending downward at more than a 45 degree angle. Obviously this geogrid block connection is weakened in this condition. The use of a well compacted granular drainage layer directly behind the block units will alleviate this condition from occurring.

Figure 1. Stress concentration of geogrid layer over sharp back-edge of masonry block.

4.2 Author's Comment

Gravel infill is a necessary requirement for many of the block units on the market today. This stone infill provides an interlocking element to the block face. Failure to install this infill layer can result in unit-to-unit movement, distortion of the wall face with gaps, and opening between the blocks. Additionally, the block-to-block shear resistance is based on infill being in place. Drainage zone stone is needed to make sure the geogrid reinforcement is supported at the crucial location just behind the back of the block as well as to provide for any nominal amount of water that may enter at the top of the wall.

5. DESIGNING FOR TEMPORARY SURCHARGE ABOVE THE WALL

A common situation occurs where a retaining wall is needed as part of site development to create sufficient parking spaces for the project. The wall creates sufficient flat space to allow for the required number of car parking spots. Unfortunately this space is also attractive to site contractors for temporary storage of onsite soils and other construction materials. This use is rarely identified ahead of time, and the wall designer is thus rarely notified of this potential use. Unknown surcharges can include the running of heavy construction equipment running directly behind the wall, or temporary surcharges such as stockpiles or staging areas, sometimes for retaining wall block! Too heavy a surcharge loading will penalize the project, adding costs to the project, while the use of too light a surcharge can result in post construction wall movements.

When conditions directly behind the wall are not called out, typical uniform design surcharge loads of 150 to 250 pounds per square foot (psf) is generally used. Likewise, the presence of buildings near the back of the wall can occur but this is

usually known during the design phase. A relevant question is, “Who is responsible for the stability of the building; the wall designer or the project structural engineer”?

5.1 Case History

A wall contractor receives a call from the site; “Your wall has moved; please come and repair it!”. Photos are sent of the failed wall, a 4 ft tall wall, which has obviously moved significantly.

During questioning of site personnel it was revealed that lime stabilization equipment was running behind the wall preparing the subbase for paving. While in itself, this does not sound like a heavy surcharge loading, descriptions from the site revealed that the lime stabilization equipment was a 24,000 lb highway and heavy construction tiller, applying a wheel load of several thousand pounds per square foot directly behind the wall. The four foot tall wall had been designed for a uniform surcharge of 150 lb/sq.ft, nowhere near adequate to resist the actual surcharge loading. The lime stabilization contractor thought he could “make time” using this big machine and had no idea of the limits of the wall. The wall was eventually rebuilt by the contractor, who was compensated for the rebuild time and effort.

5.2 Author’s Comment

It is not uncommon for the upper surface behind a finished wall to be used as a temporary stockpile area, with the corresponding loadings being significant, even thought it is a temporary condition; (see Figure 2). Surcharges need to be identified and designed accordingly, or overloading of the wall can occur. Finally, there are many instances of buildings located directly behind a retaining wall. These are located by the civil engineer, the structure is designed by a structural engineer, and the retaining wall is designed by the wall designer. Does the wall designer now assume responsibility for stability of this building? In many cases the retaining wall is a small design project, and the site may not even have the structures located! This is a major dilemma which must be discussed and suitably addressed by all parties involved.

Figure 2. Top of wall being used for storage thereby applying a surcharge loading.

6. TREATMENT OF SURFACE WATER BEHIND THE TOP OF WALL, i.e., “TO SWALE OR NOT TO SWALE”

Control of surface water behind a retaining wall is a critical aspect of the long term stability of the wall. Does the designer let the water run over the top of the wall? Alternatively, does he provide a swale behind the wall to laterally carry water away? Furthermore, if a swale is used, does it of itself create a location for standing water directly behind the wall? See Figure 3 for this distinction.

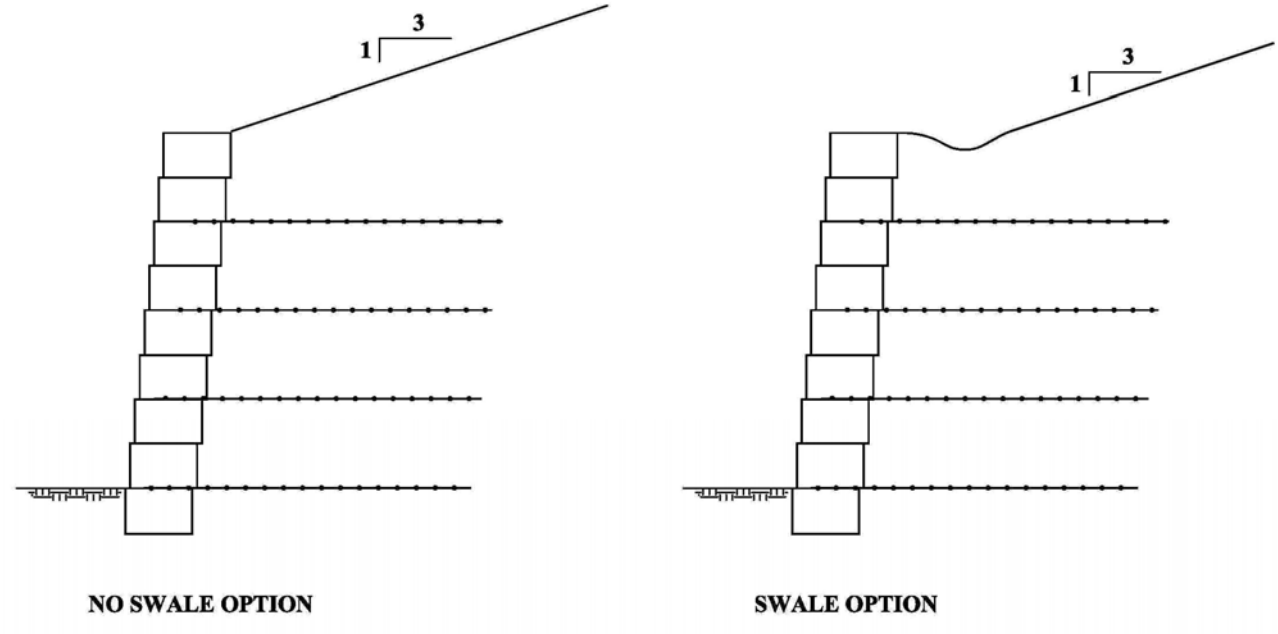

Figure 3. Distinction between no-swale or swale behind masonry blocks.

Ideally, surface water should be directed away from the back of the wall and carried away using controlled surface water control structures. Unfortunately this is rarely the case and many civil engineers use the back of the block units as a sort of “backstop” for surface water. Many runoff structures are actually located right in the reinforced zone, located right behind the back of the wall! While this may work when everything is perfectly constructed, it can be a recipe for problems when everything is not perfect!

6.1 Case History

A wall had been constructed to fill in a ravine with a road running atop it. The top of wall was at the same elevation as the road, and ran several hundred feet in length. No provision was made for the surface water runoff, the assumption being that it would run across the shoulder and over the block, then down the block face.

Should the wall have a swale behind it, and if so, was it the wall designer’s responsibility to show this swale and cause the top of wall to be regraded? Or is it the civil engineers responsibility to address this condition? Note that if a flat swale is to be constructed, provisions need to be made so that this does not result in a collection area for surface water immediately behind the back of the wall.

6.2 Author’s Comment

There is no right or wrong answer to this situation, except to provide as much prevention of water intrusion into the reinforced soil zone as practical. The use of a swale must be accompanied by designing for flow within the swale, and provisions made to assure the swale is lined with impermeable (or relatively impermeable) soils, geomembranes, or geosynthetic clay liners. Even a composite liner should be considered. Alternatively, water over the face of the block, while not aesthetically pleasing, may be a better means of assuring water does not run into the reinforced soil zone.

7. TREATMENT OF SURFACE WATER DURING CONSTRUCTION

Numerous situations occur when a wall under construction experiences problems from a sudden rainfall on the open site. This can apply to the back of the wall, as well as the front. In some cases the use of silt fence in front of a wall to

prevent runoff form leaving the site results in a channel being formed in front of the wall, ultimately washing out the foundation of the very block wall one is trying to protect! Additionally, during construction the back of these walls are open and unprotected. Overnight rains can turn the site into a sloppy mess unless the site is graded away from the back of the wall. Interim progress situations can spell trouble for any wall if surface water grading preventive measures are not taken.

7.1 Case History

The site contractor installed a silt fence directly in front of a wall that was under construction. The site had not been final graded or seeded, but this measure was taken as an interim step to prevent against soil runoff. During a significant rain event the storm water was directed to the front of the wall, with the result that the space between the fence and the wall face formed a channel through which water flowed. This undermined the block units, resulting in the wall facing becoming unstable. This section of the wall had to be de-stacked and rebuilt; see Figure 4.

Figure 4. Uncontrolled rainfall runoff creating undermining and wall instability during construction.

7.2 Author's Comment

Erosion control best management practices should be used on retaining wall construction projects, just as with any other earthwork project. In the vicinity of retaining wall construction care needs to be taken to make sure the structure is not undermined, overloaded, or eroded by these same erosion protection practices.

8. SUMMARY AND CONCLUSIONS

Segmental retaining walls have gained prominence as the grade separation structures of choice within the past twenty years. Their cost efficiency and relative ease of construction makes them attractive to site developers in almost any conceivable situation. However, they must be treated as critical structures, and designed accordingly. The requisite attention to detail applied to all civil engineering structures should be applied to SRW's as well.

This paper has provided only a few examples of details that when overlooked, can (and have) cause problems.

Drainage Details and Stormwater Design Considerations for Mechanically Stabilized Earth Walls

A. S. Filshill, CETCO Contracting Services Company, Trevose, PA, USA

ABSTRACT
The use of Mechanically Stabilized Earth (MSE) walls and slopes has continued to grow over the last 20 years. In many cases these types of walls have offered very cost effective solutions for developers and land owners. Although the amount of problems associated with these walls is minimal, any problems/failures have been associated with three key issues, selection of backfill soil, drainage and installation quality control. The design of stormwater control systems in and around this type of structures raises additional design issues that need consideration. This paper will look at the design details associated with drainage and stormwater management for MSE structures.

1. INTRODUCTION

One of the fastest growing applications in site development has been the use of MSE walls and slopes. Segmental Retaining Walls (SRW) and vegetated welded wire faced walls are the systems used the most; see Figures 1 & 2. This growth has been driven by the rising cost of real estate in the commercial market and the need for additional space to accommodate parking requirements. Site selection now includes land development that previously would not be considered due to the extreme change in grades throughout the site. The right-a-way restrictions facing most highway engineers require retaining walls to be designed for State DOT widening projects. The choice of geosynthetic MSE walls in these designs is the result of them being the most cost competitive of all the current wall systems available.

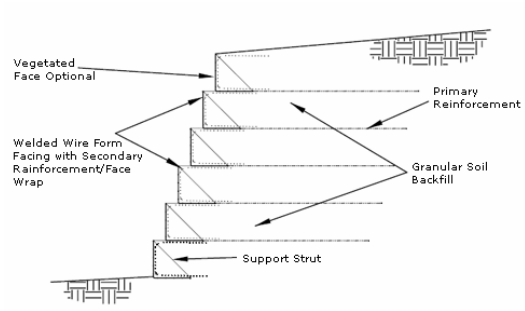

Figure 1. Welded wire vegetated face.

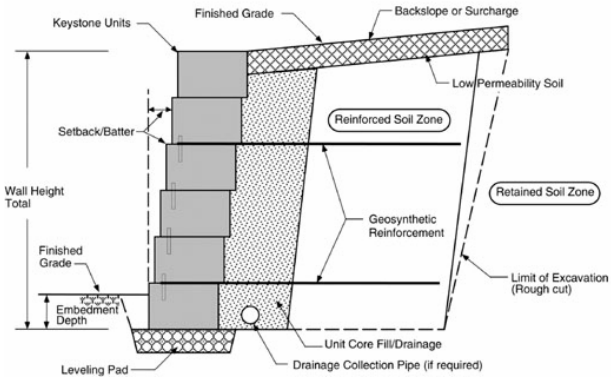

Figure 2. Segmental block retaining wall.

Although the FHWA requires backfill within the reinforced zone to consist of free draining AASHTO A-1-a type material, the commercial/residential markets allows the use of fine grained soil as backfill within the reinforced zone. The Geosynthetic Institute performed a survey of SRW wall failures and found that of the 35,000 wall constructed there was 2 to 5% failures. Of the specific failures they studied 20 of 26 (77%) were due to low permeable soils used in the reinforced zone. None of these walls accounted for drainage in or around the reinforced soil.

2. DRAINAGE DETAILS FOR MSE WALLS

The design of drainage systems within MSE structures is required to reduce or eliminate seepage pressures that can build behind walls and cause excessive deformations or failures. Sources of water behind walls can be from seepage from the retained soil, foundation soil water, or surface stormwater. Retaining walls without adequate drainage can have build up to twice the lateral earth pressure behind the wall in comparison to those with proper drainage.

One of the easiest ways to eliminate the pressure buildup is to use granular backfill within the reinforced zone of the wall. This usually is the most expensive type of backfill and therefore very rarely used by the private sector. The public sector limits fines to 15% and Plasticity Index (PI) <6. Table 1 lists the requirements of the National Concrete Masonry Association (NCMA), the Federal Highway Administration (FHWA) and Dr. Koerner of the Geosynthetic Institute. Existing site soils are used the most and in most of cases consist of fine grained soils. Fine grained soils can be acceptable as long as additional design details are incorporated to allow for proper drainage in and around the wall.

Table 1. Various gradation requirements for soils in the reinforced zone of MSE walls.

Sieve Size	Particle Size	Percent Passing Requirement		
	(mm)	NCMA (1997)	FHWA (1998)	Koerner (1998)
-	100	75-100	-	-
No.4	4.76	20-100	100	100
No.10	2.0	-	0	90-100
No. 40	0.42	0-60	0-50	0-60
No.100	0.15	-	-	0-5
No.200	0.075	0-35	0-15	0

Standard designs always require a stone drainage chimney “front drain” directly behind the segmental block used as the wall fascia. The front drain incorporates a perforated pipe at the bottom of the wall as shown in Figure 2. It is important to make sure the outlets for the drainage pipe are “daylighted” properly. What is not shown in most specifications is some type of filter fabric to separate the fine grained backfill from the stone drainage layer. The use of a filter fabric will prevent piping of the fine grained soil as well as the potential clogging of the stone drainage layer. This detail is difficult to install and there is usually an attempt to eliminate this geotextile in the field. A detail of this is shown in Figure 3.

The vertical stone drainage used behind the segmental blocks will not help walls with fine grained soils used in the reinforced zone. These type of soils required chimney drains or back drain used between the reinforced soil zone and retained soil zone. See figure 4. This type of back drain allows any seepage from the retained soil to escape to the face of the wall where there is adequate drainage. The back drain in figure 3 consists of clean stone with a pipe to convey water to the face of the wall. A geocomposite, sheet drain or heavy weight nonwoven can be used as a drain in place of the stone. Geocomposites are usually selected due to cost and ease of installation.

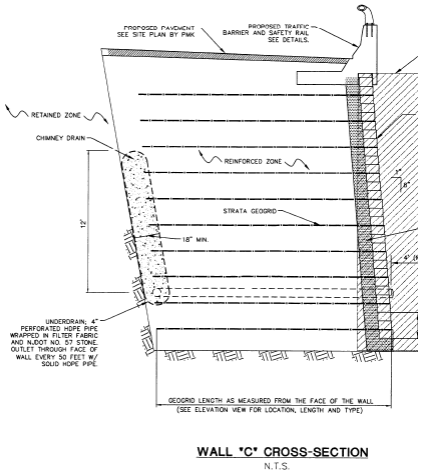

Figure 3. Cross-section of a wall using a stone backdrain.

Geocomposites can also be used in layers within the fine grained material to transfer water to the face as well as commercially available reinforcement products that incorporate drainage media within the reinforcement to allow drainage through the reinforced soil zone.

3. STORMWATER CONSIDERATIONS

The National Pollution Discharge Elimination Systems (NPDES) is the cornerstone of the EPA's Clean Water Act. This Federal requirement mandates that post development levels of a site's stormwater is released from a site at the same rate prior to development. This requires on-site storage and conveyance. In many cases these systems are placed behind the reinforced soil zone of MSE walls. The main areas of concern are as follows:

- Drainage swales in front of the wall (Figure 4)
- Detention basins created by using MSE wall (Figure 4)
- Retention/detention basins used above wall (Figure 5)
- Underground stormwater systems used behind MSE walls (Figure 6)
- Inlet structures during construction (Figure 7)

These stormwater features require the wall designer to account for added factors not always accounted for in wall designs. In many cases the engineer designing the wall is different from the engineer designing the stormwater system. In these cases there is a need for both engineers to evaluate how each design affects the other.

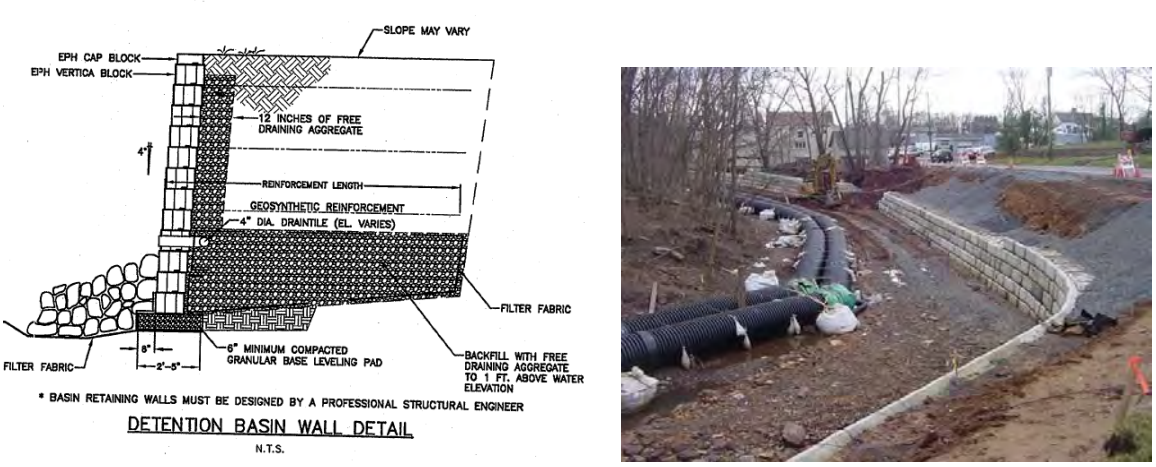

Figure 4. Detention basin wall or wall along drainage channel.

4. DRAINAGE SWALES AND BASIN IN FRONT OF WALLS

Where walls are constructed along active waterways or perimeter walls around detention basins, special attention must be given to the selection of backfill for the reinforced zone up to the maximum height of water. Standard practice is to use backfill consisting of free draining stone 0.3 meters above the maximum water elevation. Pipe outlets for these types of wall should be increased to allow for rapid release of water behind the wall.

In all cases the drainage pipe behind the wall should outlet at an elevation above grade. In many cases the drainage system is designed properly and the outside grading buries the outlet pipe.

5. RETENTION/DETENTION BASINS ABOVE WALLS

In cases where a detention basin is located above a MSE structure, consideration must be give to the spillway location and direction of flow in case of overtopping of the basin. Figure 5 shows a welded wire faced wall that is designed to eliminate hydrostatic pressure behind the face of the wall. This wall failed after a detention basin was

overtopped above the structure. The water from the basin caused the reinforced soil zone to become saturated. Water continued to seep from the face for several days as evidenced by the ice coming from the wall face.

Figure 5. Adverse results arising from a stormwater detention basin above the wall.

6. UNDERGEOUND DETENTION SYSTEMS BEHIND WALLS

A growing concern is the use of underground detention systems behind MSE structures. As stated previously, the value of real estate has caused owners and developers to optimize the footprint of each site they develop. This has created the use of both underground detention and retaining walls on the same site and in many cases adjacent to each other. Figure 6 shows an underground detention system located directly behind the reinforced zone of a vegetated MSE wall. The detention system was 3 meters in height and located behind the top 3 meters of the 10 meter high MSE wall. Although not required, a geomembrane was used to encapsulate the detention system in order to direct the stormwater to the designed outlet and prevent seepage into the reinforced soil zone.

In most cases stormwater detention systems are designed for infiltration and do not require lining. These stormwater systems must be designed to eliminate seepage of stormwater that may effect the design on the MSE structure.

Figure 6. Underground stormwater management system behind 10m high MSE wall

7. INLET STRUCTURES DURING CONSTRUCTION

In many instances inlet structures are constructed to their final elevations prior to the wall backfill being placed. Most site grading plans direct sheet flow towards these inlets and if they are raised above the surrounding grades than water is concentrated behind the wall with nowhere to go. The concentrated water can cause saturation around the structure, soil settlement and erosion; see Figure 7. This can be prevented by using a swale and/or soil berm in front of the inlet to direct stormwater around the wall until construction is completed.

Figure 7. Washouts around inlet structures.

8. SUMMARY AND CONCLUSIONS

This paper provides details on several applications of MSE walls in conjunction with seepage forces and stormwater management. Most problems associated with these types of walls are related to selection of backfill soil, drainage and quality control during installation.

It is known that most commercial sites will use the most cost effective soils as backfill within the reinforced soil zone. Although these soils can be used successfully they create additional design considerations especially as they relate to drainage. Consideration must be given to groundwater, seepage from retained soil, and stormwater in and around these structures. The effectiveness of the stone chimney drain behind the segmental block is minimized if the water cannot get to the drain through the reinforced soil. The use of a back drain and clean stone layers can help to eliminate pore water pressure with the soil.

With the increase of stormwater controls from NPDES permitting requirements, stormwater management is becoming a bigger issue on all sites. How the stormwater is handled on each site, whether above ground or underground, raises several design considerations for MSE structures. Most of the issues can be designed around but it requires coordination between both the MSE wall designer and the stormwater control design.

Characterization of Textured Geomembranes Predictive of Interface Properties: Demonstration of a New Technology

B. J. Ramsey and J. Youngblood; GSE Lining Technology Inc., Houston, Texas, USA

ABSTRACT
GSE is currently developing a new application of technology for textured geomembrane sheet characterization. We believe this method of characterization will demonstrate a strong correlation to interface shear testing with a more rapid testing response time and potentially much greater testing accuracy. The three dimensional characterization technology (see Figure 1) utilizes a larger surface area than current asperity height measurements, and it allows for many other substantial improvements in the measurement and analysis of the topography of the samples. The characterization method will be overviewed and examples of output provided, variables in measurement and mathematical analysis will be reviewed, correlation to interface shear testing performance will be demonstrated and the plans for future research and quality improvements will be discussed.

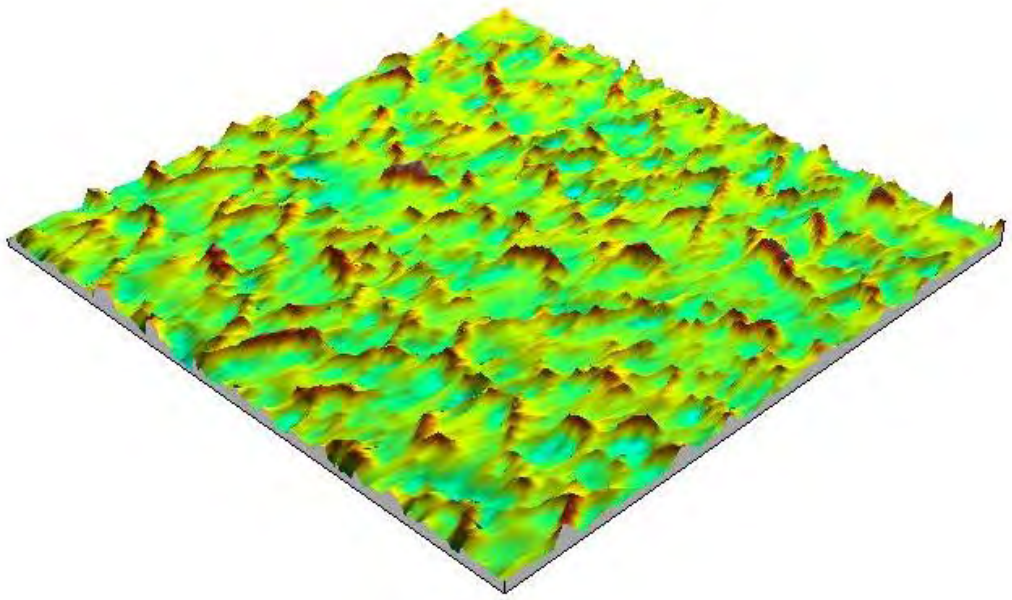

Figure 1. Three dimensional topological characterization of a textured geomembrane.

INTRODUCTION AND BACKGROUND

The prediction of the shear strength/interface properties of geosynthetic materials has been a concern since the beginning of geosynthetic use on various slope angles. As advances have been made in the development of new and improved materials with increasing functionality, some improvements have been made in the characterization of these materials and tests and processes designed to predict and quantify shear strength/interface properties. Unfortunately the standards of practice of testing and materials characterization have not kept pace with the expansion of material performance and engineering rigor. With this paper and the work represented herein, that balance is somewhat adjusted.

The true initiation of this issue, particularly as related to textured geomembrane sheet relates to one of the larger and earliest failures involving geomembrane sheet that occurred in Kettleman Hills, California in 1988 (1)[*]. This failure precipitated a dramatic increase in usage of a new variety of geomembrane sheet; i.e., textured, or surface roughened, geomembrane. The initial version of textured sheet was defined by what it was not; and that was, it wasn't smooth. Time and requirements for more advances have lead to much more definition and characterization. Each further advance in characterization (i.e. tilt table to shear boxes) has lead to more daring engineering, projects with slopes designed to be "as steep as possible" to maximize airspace and improving the cost effectiveness of both the site design and overall project performance. As an industry we have continued to push the envelope of materials performance and design and with any innovative process, in some cases the envelope has been pushed beyond the failure point (2).

The statement of the problem and related issues is relatively simple; Civil engineers want to be able to predict the interface strengths of geosynthetic-to-geosynthetic and of geosynthetics-to-soils Interfaces(3). Manufacturers want to demonstrate the consistency and capabilities of their products in a very timely fashion and in a method the engineering community (4) can utilize. And the Industry as a whole (owners, laboratories, institutes, regulators and others) want these predictions and demonstrations to be consistent, reliable and accurate. Simple right?

As with most complex and multifaceted problems, the execution is extremely complicated. The civil engineer is plagued by a huge variation in his/her predictions; soil type, compaction levels, overburden pressure, moisture levels, seat time, variations in materials performance and many other factors combine to make nearly every project a brand new event requiring "ground-up" calculations(5). The manufacturers test the asperity height of textured sheet(6), but this clearly is not sufficient to satisfy the customer base. The industry cannot make concise and accurate predictions (7).

So what can we do to improve our situation? We have moved from the (overly) simple tilt table to a direct shear box(8). The use of the shear box adds a wider range of test parameters and allows for more control of most of the variables. However, the shear box is still plagued by several problems. One, the overall variability from laboratory to laboratory has not yet reached realistically acceptable levels. Two the test is expensive, e.g., several thousand dollars per test is an average cost. Third, it is not timely; if you do not own a shear box, it is a 2-3 week test from conception to final report. Even if you do own your own box (9), most common test protocols take 4-5 days to complete. All geomembrane manufacturers have made substantial efforts to address and bring progress to these issues; but in the end it is not something they can control.

Thus we have no good (10) correlation between the asperity height, (sheet variety) and the interface /shear properties. In fact, we have seen some cases where the higher asperity heights actually produce interface shear results that are lower that those demonstrated by lower asperity materials. Clearly there is more definition needed that the simple peak/valley measurement generated by asperity height. Not surprisingly, this avenue of thinking has been explored in the past. In the late 1990's GSE supplied partial funding towards a research effort by Dr. Joseph Dove, then of Georgia Tech, now on staff at Virginia Tech (11) to expand the characterization of textured geomembrane sheet into two dimensions. This was accomplished with the aid of a new apparatus which utilized a stylus on a floating arm to track the continuity of asperity heights as a sample was drawn across the apparatus. This process was a significant advancement in the degree of characterization and the results have been published in several papers referenced herein. Unfortunately, there was no direct linkage of the two dimensional characterizations to the interface shear results (12).

[*]The notes accompanying the text appear at the end of the paper immediately preceding the Bibliography.

THE PROPOSED TECHNIQUE OF OPTICAL CHARACTERIZATION

GSE is working to improve both the characterization of the textured geomembrane and the correlation of this characterization to interface shear results. The characterization of the geomembrane has been improved by moving from a one dimensional mechanical methodology (13) to a two and three dimensional optical characterization. This process was developed by improving on the two dimensional stylus profilometry as mentioned above (14).

The equipment utilized to take these measurements is supplied by several manufacturers under the generic type of optical scanning profilometers. Manufacturers include Solarius Development Inc., Fries Research & Technology GmbH, Carl Zeiss Inc., and Micro Photonics Inc. The photograph (Figure 2) illustrates an overview of the device. Figure 3 gives a close-up view of the scanning beam in operation.

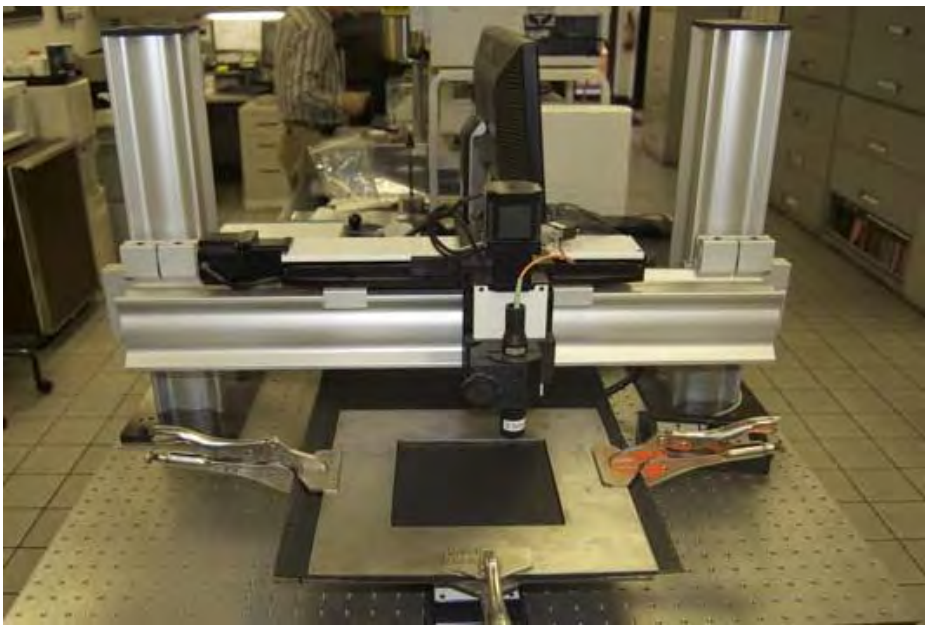

Figure 2. Photograph of an Optical Scanning Apparatus.

Figure 3. Photograph illustrating scanning beam directly downward to a textured geomembrane surface.

This new technology expands the test area, in normal operations providing the asperity height (and much more) characterization of an area up to 300 square millimeters per sample. Most important is the degree of completeness of this characterization; it consists of a non-invasive optical scan of the surface of the material. The data output is then used to generate a topological characterization of the entire tested section of materials. In short, much more than asperity height can now be known about the sample. The shape, size and distribution (density) of the peaks can be known. In an important step, the valleys are also topologically characterized. The "fill volume" can be easily calculated and thus one can understand and isolate the topological characteristics of the portion of the sample above the plane of the sheet.

PRELIMINARY TEST RESULTS

Figures 4 to 9 demonstrate the capability of the software to generate data by altering the threshold of textured surface. Figure 4 is at the base thickness of the geomembrane, and the light blue coloring represents the textured peaks. As the threshold is increased in height, one can see that the area the peaks cover decreases. The software can provide data on the area and volume at different thresholds.

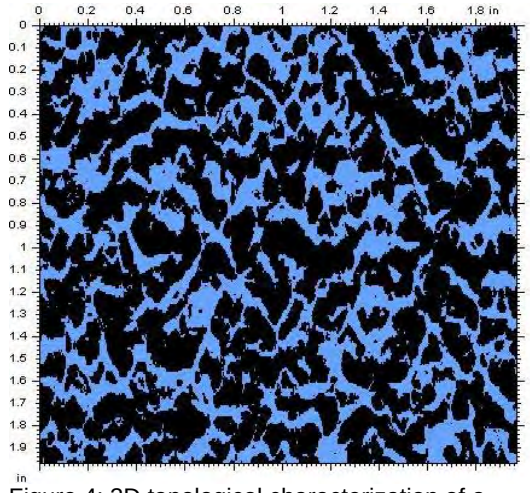

Figure 4: 3D topological characterization of a textured geomembrane (zero plane threshold)

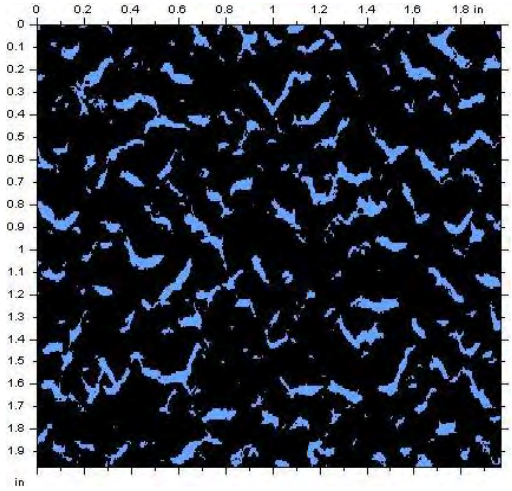

Figure 5: 3D topological characterization of a textured geomembrane (10 mil threshold)

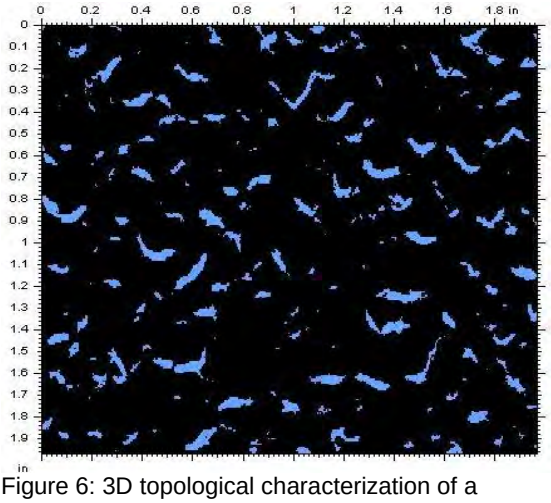

Figure 6: 3D topological characterization of a textured geomembrane (15 mil threshold)

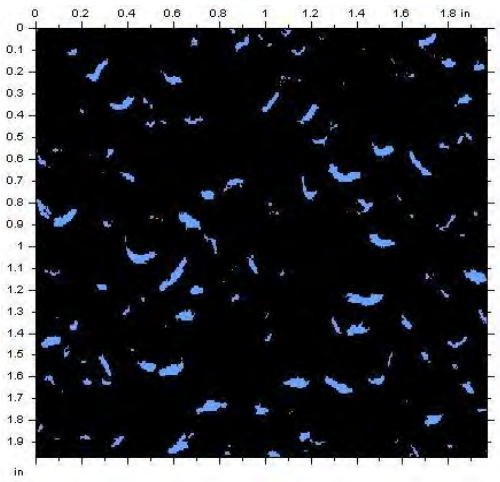

Figure 7: 3D topological characterization of a textured geomembrane (20 mil threshold)

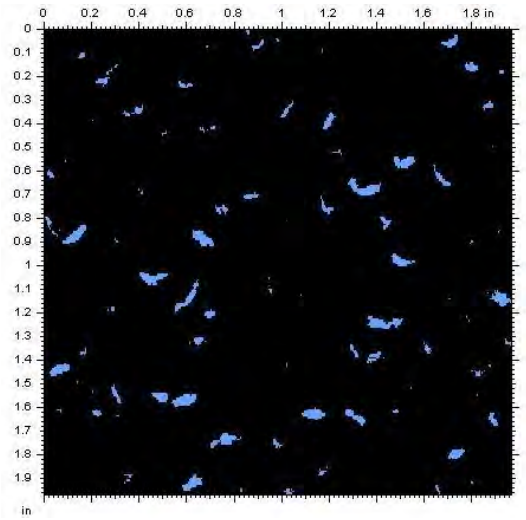

Figure 8: 3D topological characterization of a textured geomembrane (25 mil threshold)

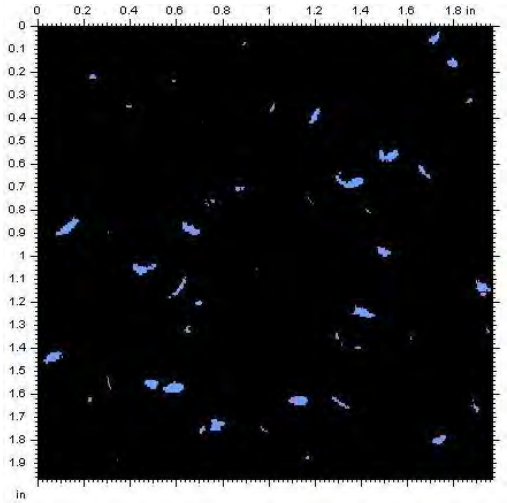

Figure 9: 3D topological characterization of a textured geomembrane (30 mil threshold

GSE has begun initial research regarding parameters such as: height, functional, spatial, hybrid, bearing ratio, and other volume related parameters. There are several hundred parameters which are captured with each scan. A key question is "what are the parameters that correlate most directly with interface shear testing and how exact is the correlation"? To that end we have reviewed several parameters and conducted correlation calculations with a range of direct shear results. A portion of those correlations are illustrated in Figures 10 to 17.

Clearly one of the most studied interfaces is that of a geotextile to a textured geomembrane in a landfill cover application. For that reason, in addition to the large volume of data available, we used that interface as some of the initial, primary correlation schemes. Figures 10 to 13 illustrate some of the work which has been done. In all figures, the x-axis consists of different rolls of textured geomembrane produced on a variety of manufacturing lines over a range of time and raw materials. In all charts the primary y-axis (left hand side) are the results of a direct shear test with a overburden pressure run in accordance with ASTM 5321.

In Figure 10 the secondary y-axis (right hand side) charts the filling quantity (*volume*) of the valleys (15); the empty space below a threshold for a range of thresholds.

In Figure 11 the secondary y-axis (right hand side) charts the bearing *area* of the peaks (16); the area of the peaks above a 0.15mm threshold.

In Figure 12 the secondary y-axis (right hand side) charts the *volume* of the peaks (17); the volume of the peaks above a 0.20mm threshold.

In Figure 13 the secondary y-axis (right hand side) charts a portion of the bearing curve of the peaks (18);

The correlations for each of the comparisons are somewhat self evident, however, a slightly better method (19) is the plotting of the two measured values (20) directly against each other and making a best fit line to demonstrate the consistency. This is done (21) in Figures 14 to 17.

SUMMARY AND RECOMMENDATIONS

Clearly there is more work to be done here. It is our intention to extend this body of work to address an improved and more defined relationship between three dimensional surface topography and the interface shear performance of the characterized samples. Further, to broaden the range of interface shear conditions and characteristics and assure that the presumed correlations extend across as broad a range of interface conditions as possible. And still further, yet more immediate, to utilize this technology to reduce the variation in textured geomembrane sheet and to optimize the structure and performance of textured geomembrane for the requirements of civil engineering usages.

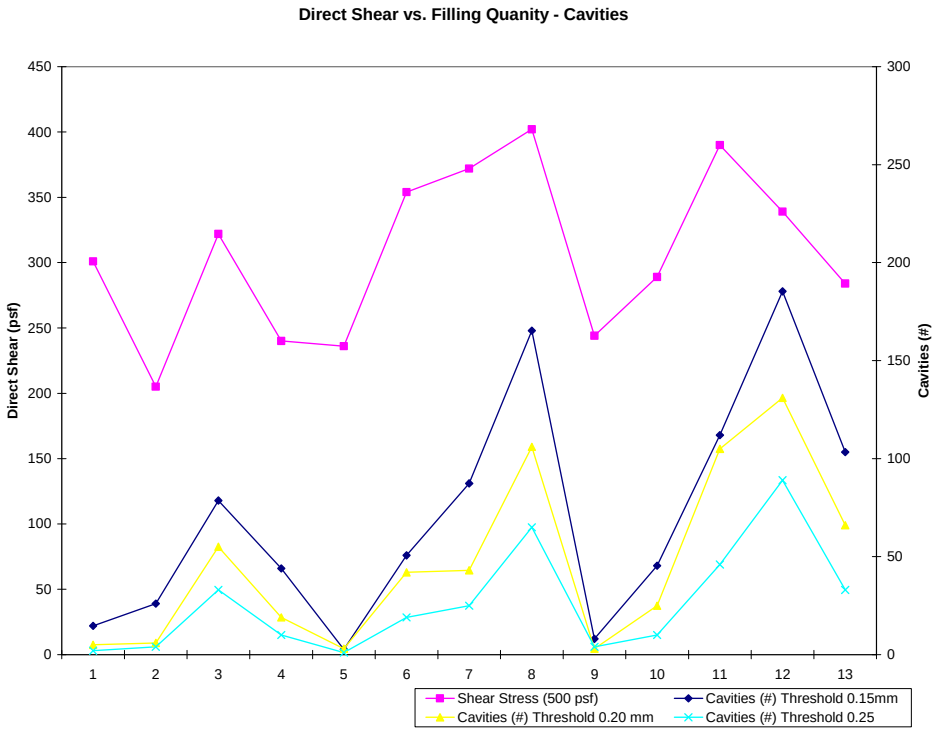

Figure 10. Chart of Direct shear vs. Filling Quantity – Cavities (0.15, 0.20 and 0.25 mm threshold) by sample.

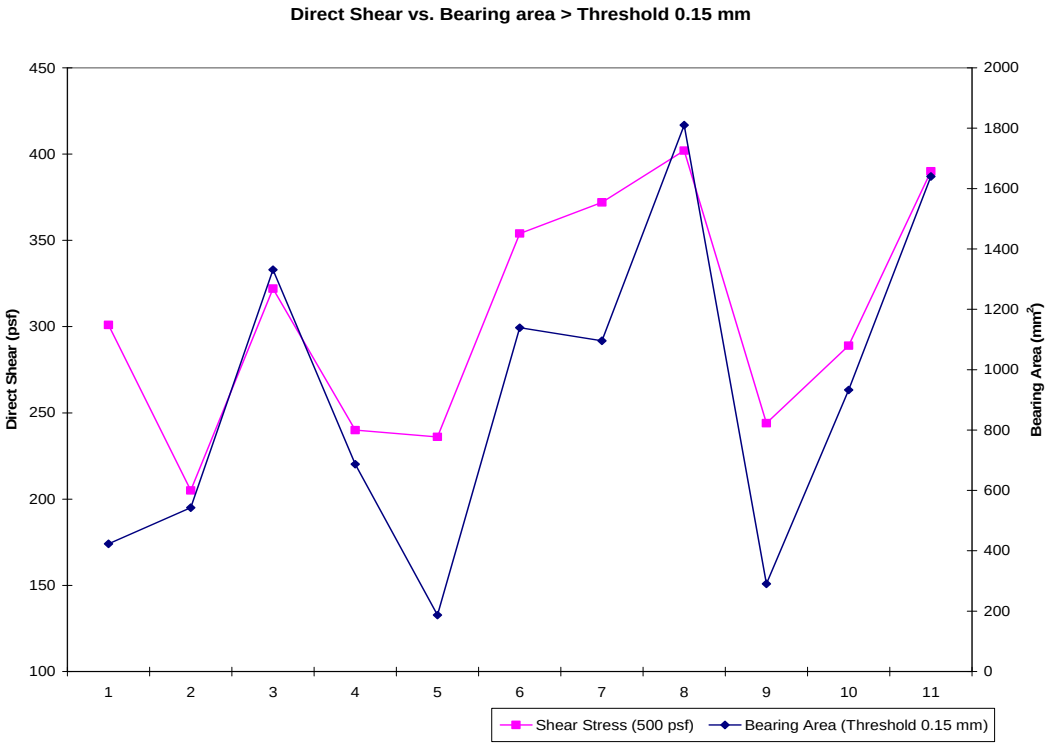

Figure 11. Chart of Direct shear vs. Bearing Area (0.15mm threshold) by sample.

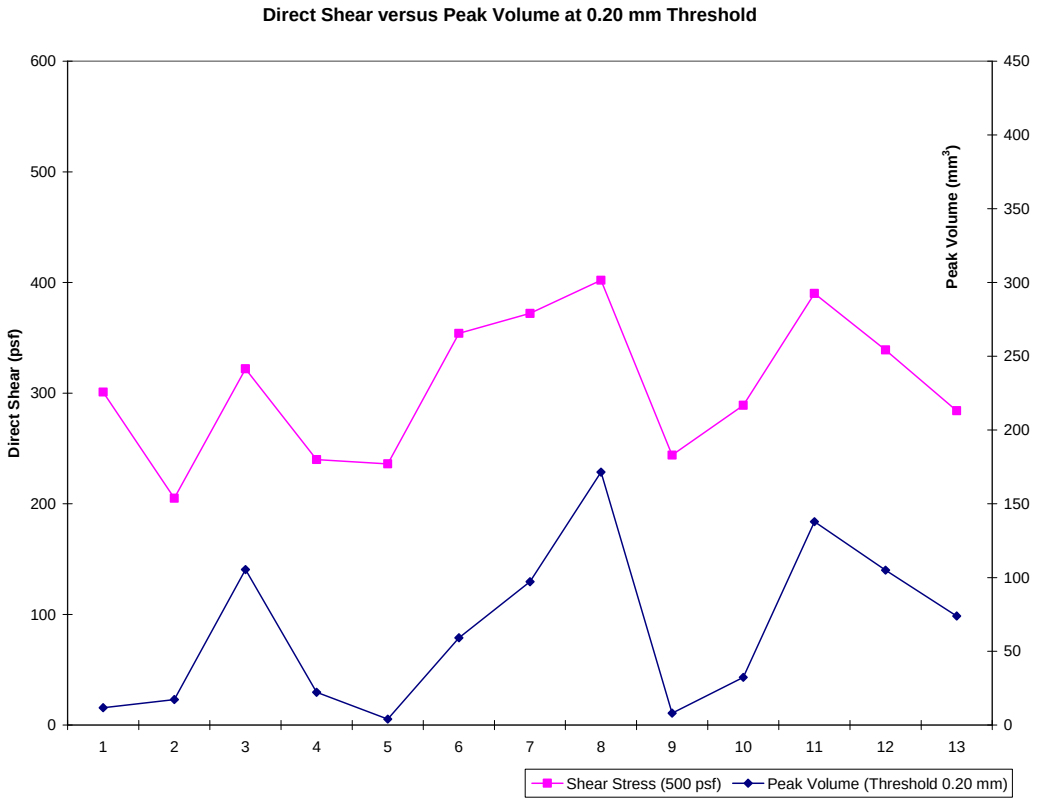

Figure 12. Chart of Direct shear vs. Peak Volume (0.20 mm threshold) by sample.

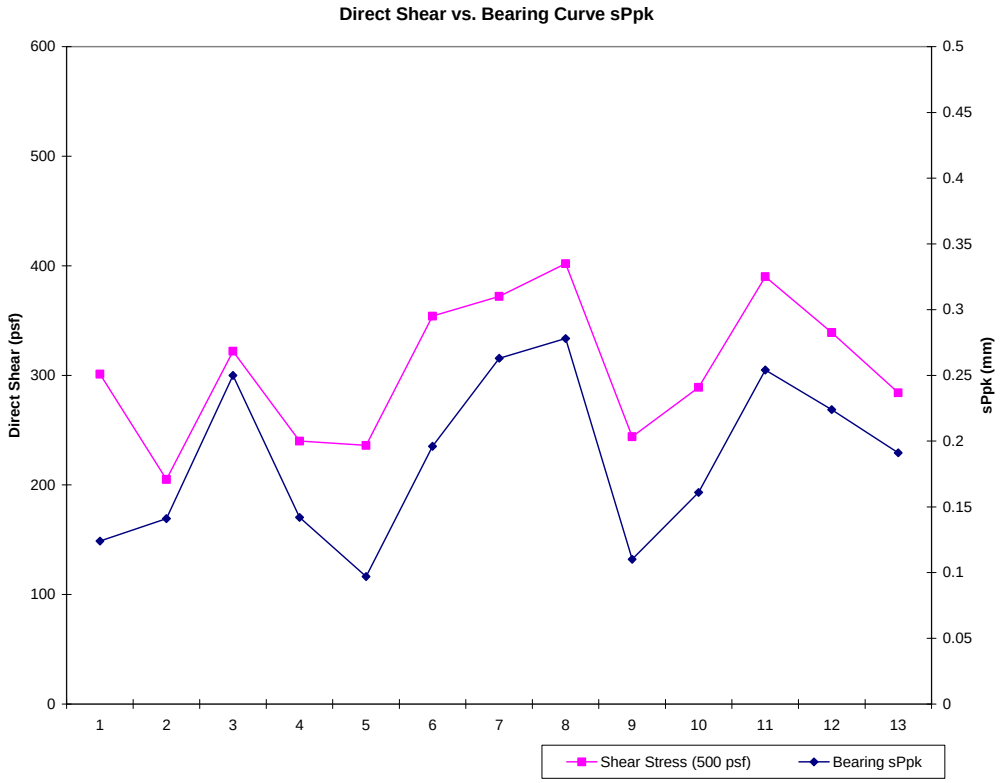

Figure 13. Chart of Direct shear vs. Bearing Curve by sample.

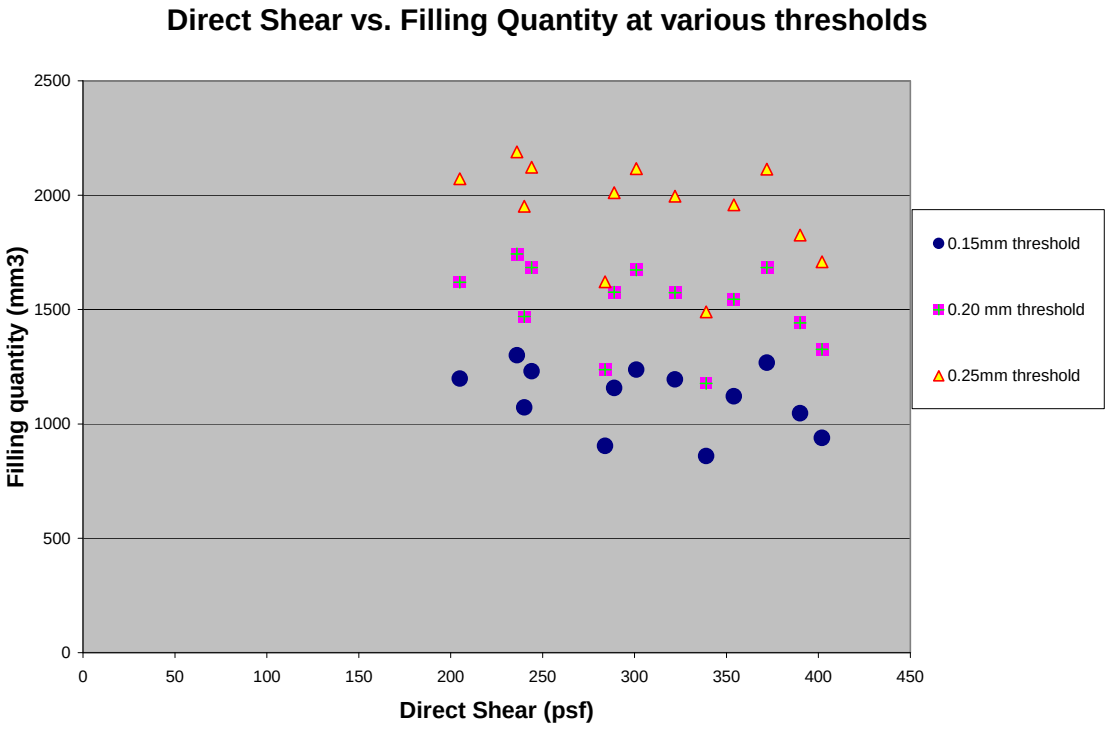

Figure 14. Chart of Direct shear vs. Filling Quantity – Cavities (0.15, 0.20 and 0.25 mm threshold) direct comparison.

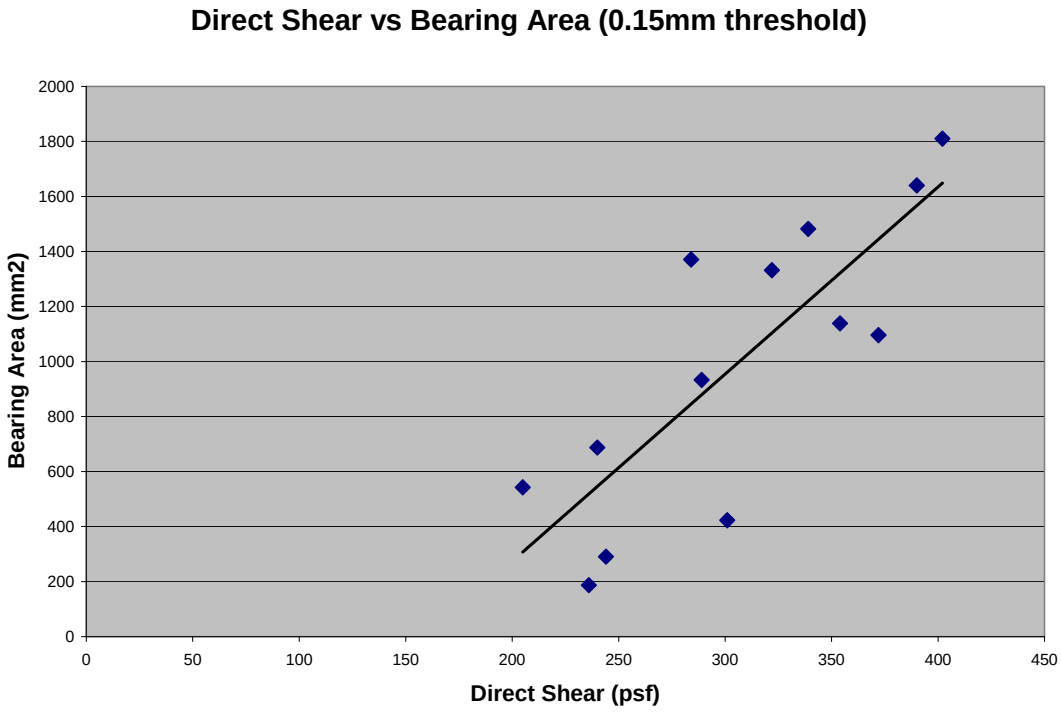

Figure 15. Chart of Direct shear vs. Bearing Area (0.15mm threshold) direct comparison with trend line.

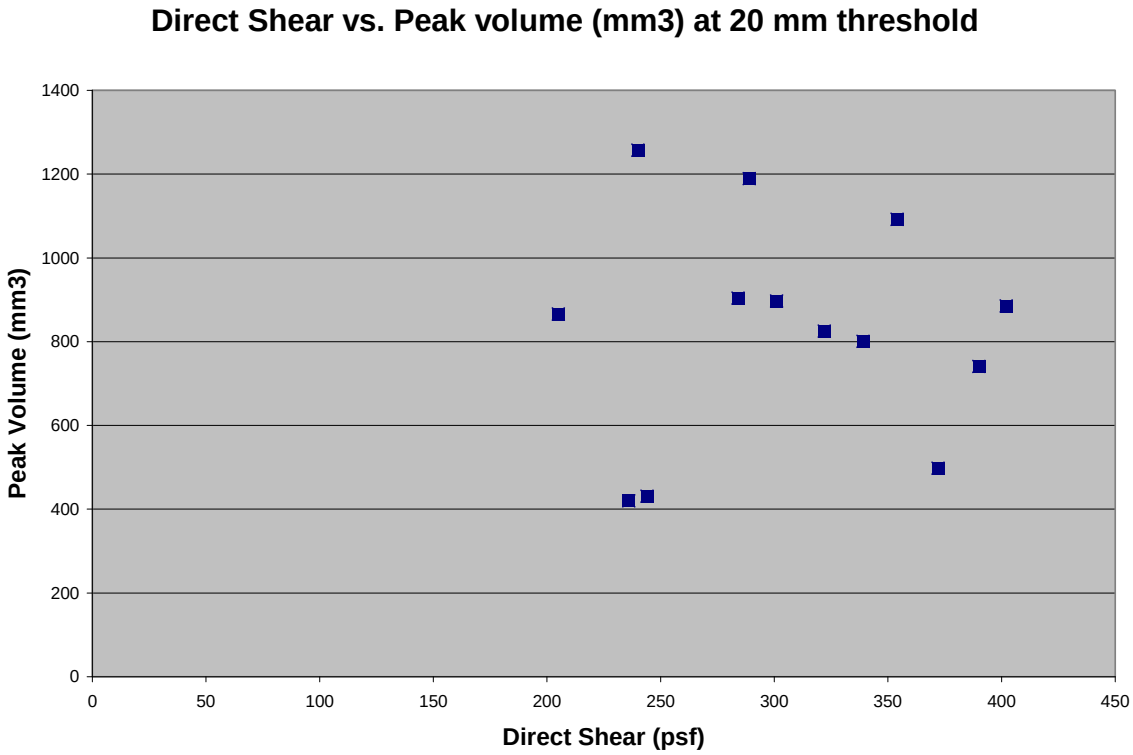

Figure 16. Chart of Direct shear vs. Peak Volume (0.20 mm threshold) direct comparison.

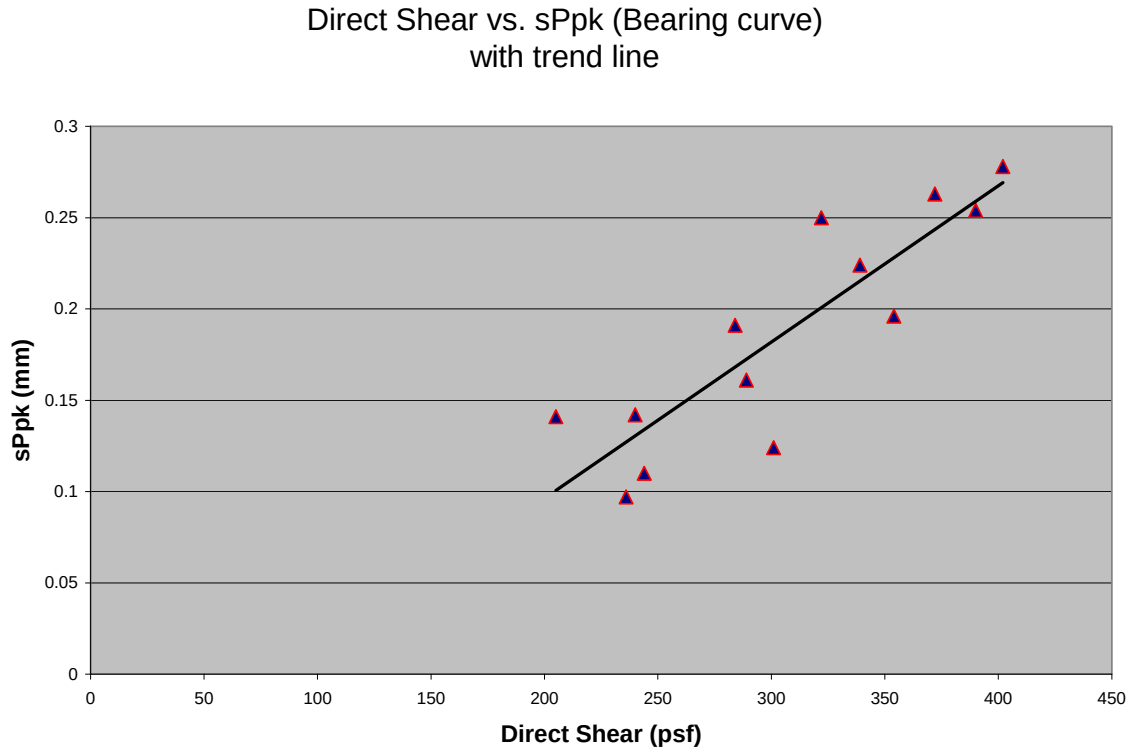

Figure 17. Chart of Direct shear vs. Bearing Curve direct comparison with trend line.

NOTES

(1) http://cedb.asce.org/cgi/WWWdisplay.cgi?9202568 Cause and Mechanism of Failure Kettleman Hills Landfill B-19, Phase IA by R. John Byrne, J. Kendall, and S. Brown

(2) This note, and others, with respect to David Foster Wallace, r.i.p.

(3) The construction of this sentence and its similarity to the title of GRI report #30 reference is not accidental.

(4) Read customers.

(5) The play on words is obvious.

(6) You'all must understand that there is no asperity height knob on the control panel of any geomembrane manufacturer's production lines. Asperity height is an outcome of several factors, all of which affect other performance characteristics of the geomembrane sheet.

(7) Currently the direct shear testing protocol produces variation in excess of 15%; Dr. George Koerner – GAI LAP data.

(8) Not enough can be said about the efforts of Rob Swan in this regard. I have listed a link to a list of papers and documents he has published as well as his master thesis in the references of this paper. He really does deserve credit as one of the "fathers" of this particular niche of civil engineering.

(9) Full disclosure – GSE owns its own shear box; it was originally built by Rob Swan.

(10) "Good" defined as a relationship that works across a wide range of materials and conditions.

(11) Again, some personal credit is due here as well. It is difficult for me to see how this work reaches the current state of progress without the efforts of Dr. Dove.

(12) Despite a sincere effort to do so.

(13) Asperity height

(14) And In fact, the technology is so new that the ISO standards are still being developed for this new topological characterization technology.

(15) This is important! It is the valleys volume (empty space) that is being calculated, not the peaks.

(16) This is again important! It is the *surface area* of the peaks (above threshold) that is being calculated.

(17) This is yet again important! It is the *volume* of the peaks (above threshold) that is being calculated.

(18) A bearing curve is a somewhat abstract mathematical representation of the roughness of the material which discounts the extreme upper and lower portions of the peaks.

(19) Regards to Gary Kolbasuk.

(20) Direct shear values and the corresponding selected texture characterization parameter.

(21) With wide variation in the results (get it! variation in charting the variation!): Valley volume and peak volume appears to be irrelevant to direct shear, Bearing area has some correlation and the Bearing Curve results demonstrate the most consistent trend.

BIBLIOGRAPHY

ASTM D5321, 2008. Standard test method for determining the coefficient of soil and geosynthetic or geosynthetic and geosynthetic friction by the direct shear method. *American Society for testing and Materials*, West Conshohocken, PA, USA.

ASTM D7466, 2008. Standard test method for measuring the asperity height of textured geomembranes. *American Society for testing and Materials*, West Conshohocken, PA, USA.

Dove, J.E. and Frost, J.D., (1996), "A Method for Measuring Geomembrane Surface Roughness", *Geosynthetics International*, Vol. 3, No. 3, pp. 369-392.

Dove, J.E., Frost, J.D. and Dove, P.M., (1996), "Geomembrane Microtopography by Atomic Force Microscopy", Geosynthetics International, Vol. 3, No. 2, pp. 227-245.

Dove, J.E., Frost, J.D., Han, J., and R.C. Bachus. (1997), "The influence of geomembrane surface roughness on interface strength." *Proceedings, Geosynthetics '97*, Long Beach, CA, pp. 863-876.

Dove, J.E., Frost, J.D., Bachus, R.C., Han, J., (1997). The influence of geomembrane surface roughness on interface strength. Proceedings of Geosynthetics'97 Conference, IFAI, Long Beach, CA, USA, vol. 2, pp. 863–876.

Dove, J.E., and Harpring, J.C. (1999), "Geometric and spatial parameters for analysis of geomembrane/soil interface behavior." *Proceedings, Geosynthetics '99*, International Fabrics Association International, Boston, MA, I, pp. 575-588.

Giroud, J.P., (2004). Quantitative analysis of the impact of adhesion between geomembranes and geotextiles on the stability of soil-geosynthetic systems on slopes. JP Giroud, Inc., Ocean Ridge, FL, USA, pp. 14.

GRI REPORT NO. 30, (2005), Direct Shear Database of Geosynthetic-to-Geosynthetic and Geosynthetic-to-Soil Interfaces Geosynthetic Institute, Folsom, PA USA.

GRI Test Method GM12, (Mod. 1: Oct., 1998) Standard Test Method for "Asperity Measurement of Textured Geomembranes Using a Depth Gage" Geosynthetic Institute, Folsom, PA USA

Hsuan, Y. G. and Koerner, R. M., (1999), "Rationale and Background for the GRI-GM13 Specification for HDPE Geomembranes," Proc. Geosynthetics '99, IFAI Publ., St. Paul, MN, pp. 385-400.

Koerner, G.R., "Geosynthetic Institute's Efforts In Accreditation and Certification" Koerner Symposium 2004, Geosynthetic Institute, Folsom, PA USA.

Koerner, R.M., "Designing with Geosynthetics" 5th Edition, 2006, by Prentice Hall Inc. Upper Saddle River, NJ USA.

Koerner, R. M. and Soong, T.-Y., (February 1999) "Assessment of Ten Landfill Failures Using 2-D and 3-D Stability Analysis Procedures," Terzaghi Lecture at Technical University, Vienna, 40 pgs.

Martin, J. P. and Koerner, R. M., (1985) "Geotechnical Design Considerations for Geomembrane Lined Slopes: Part I - Slope Stability," Intl. Journal Geotextiles and Geomembranes, Vol. 2, No. 2, , pp. 299-321.

Ojeshina, Anthony O., "A new high friction HDPE geomembrane" *Geotextiles and Geomembranes Volume 10, Issues 5-6, , Pages 433-441

Richardson, G.N., Thiel, R.S., (2001). Interface shear strength: part I—geomembrane considerations. GeosyntheticFabricReview 14–19.

Swan, R.H. Jr., (1987), "Frictional Behavior of High Performance Geosynthetics", MSCE Thesis, Drexel university, Philadelphia, PA, 175p. Oh, what the hell, we should probably add everything that Rob Swan has ever published; a somewhat aged link /listing is here: http://www.interactionspecialists.com/pdffiles/rhspubs.pdf

Vaid, Y.P., Rinne, N., 1995. Geomembrane coefficients of interface friction. Geosynthetics International 2 (1), 309–325.

Clay Nanoparticle Formulated Geotextiles Used in Geoenvironmental Applications

H.-Y. Jeon, GSI-Korea, Division of Nano-Systems Engineering, Inha University, Korea

ABSTRACT
The general concept of nanotechnology formulations used to manufacture geotextiles are introduced in this paper. Separation and filtration functions using geotextiles from nanoclay formulations are introduced as an important concept. For an example of nanoclay formulations used to manufacture geotextiles, yellow clay as nanoparticles were added to make a polyester formulation in turn to make nonwoven geotextiles to improve the removal effects of toxic and organic components of leachate solutions. Engineering test behavior was evaluated to confirm the effects the of yellow clay addition. Finally, the possibility of nanocomposite formulations for geosynthetics in the future is considered in a number of common situations.

1. INTRODUCTION

Nanotechnology is a new technology which can make a ultimately fine material such as a fiber (see Figure 1) by controlling atoms and molecules down to a 10^{-9} m in size and this technology can be widely used in many industrial situations. Among the many possible nanoproducts, nanofibers could be controlled as far as fiber length, diameter, surface properties, pore distribution, fiber evenness, cross sectional shapes, etc.

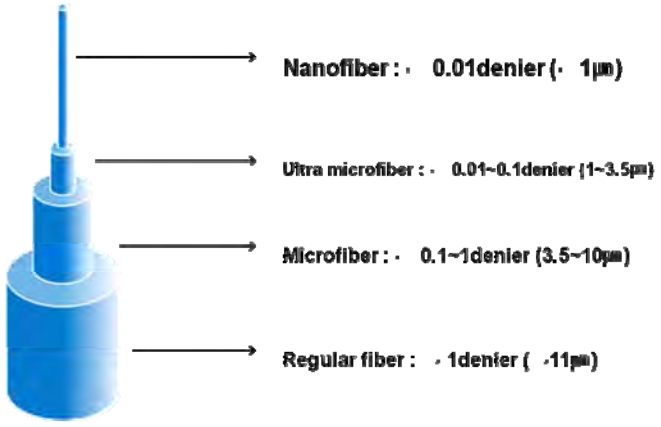

Figure 1. Comparison of nanofibers to conventional standard fibers.

Nanofibers are one of the most advanced materials which can be easily designed with high performance materials having distinctive properties. New geosynthetic materials which have separation, filtration, and absorption functions and are specifically made could be developed in the field of geoenvironmental applications. In addition to fibers, nanoparticles (such as nanoclay) can be used to make unique formulations which can, in turn, be used to make conventional fibers for geotextiles and yarn-type geogrids.

As an example of nanocomposite geosynthetics in geoenvironmental applications, it is very important to eliminate the toxic and organic components of various waste leachate solutions. There is no such capability for the standard manufactured nonwoven geotextiles and needed is to manufacture the functional nonwoven geotextiles which can absorb the toxic and organic components that may be harmful to personal health and the environment.

It is possible to manufacture this type of functional nonwoven geotextile by using nanotechnology. Section 2 will describe nanofiber technology so as to gain insight into extremely small scale manufacturing. The goal of the paper, however, is in Section 3 which will introduce nanoclay into a polymeric formulation so as to manufacture a geotextile for use in geoenvironmental applications. Section 4 will provide commentary for future applications.

2. NANOFIBER APPLICATION METHODS

Figure 2 shows various aspects of nanofiber manufacturing technology and production where it is seen that mass production of nanofibers is possible by modified electro spinning. Electro spinning is the general method used to manufacture nanofibers which is similar to the meltblown method but the current problem is to increase mass productivity.

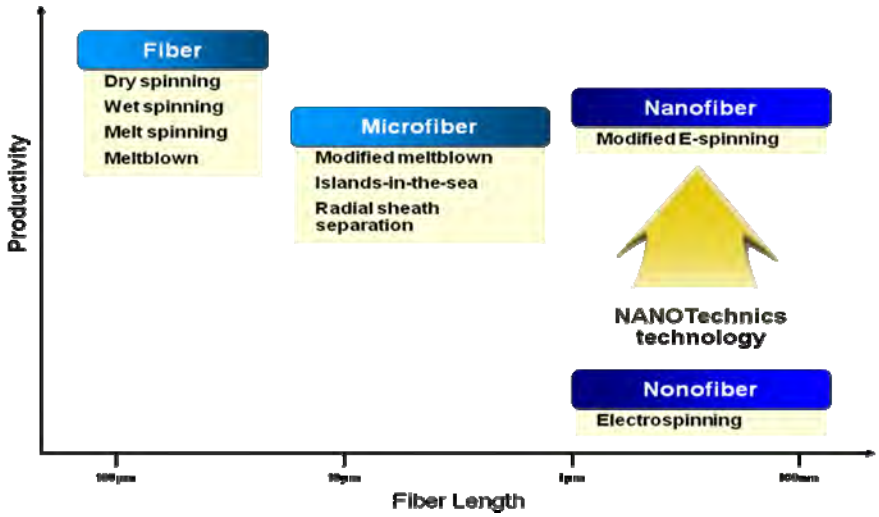

Figure 2. Fiber manufacturing technology and productivity.

In general, regular fibers are widely used to manufacture geotextiles and yarn-type geogrids but filtration efficiency of microfibers and nanofiber geotextiles would be better than the standard fiber used to manufacture conventional geotextiles.

To be considered, it is expected that nanofiber geosynthetics could provide the smart filtration function in geoenvironmental applications by their composition structure as shown in Figure 3. If the numbers of filled fibers per unit area increases, the pore size among nanofibers is decreased.

Therefore, fine pollutants cannot pass through pores made by nanofibers and the filtration efficiency will be improved. This means that ultra thin geosynthetic filters can be manufactured having a high quality filtration function to absorb fine impurities and toxic components in either polluted water and air media; see Figure 4.

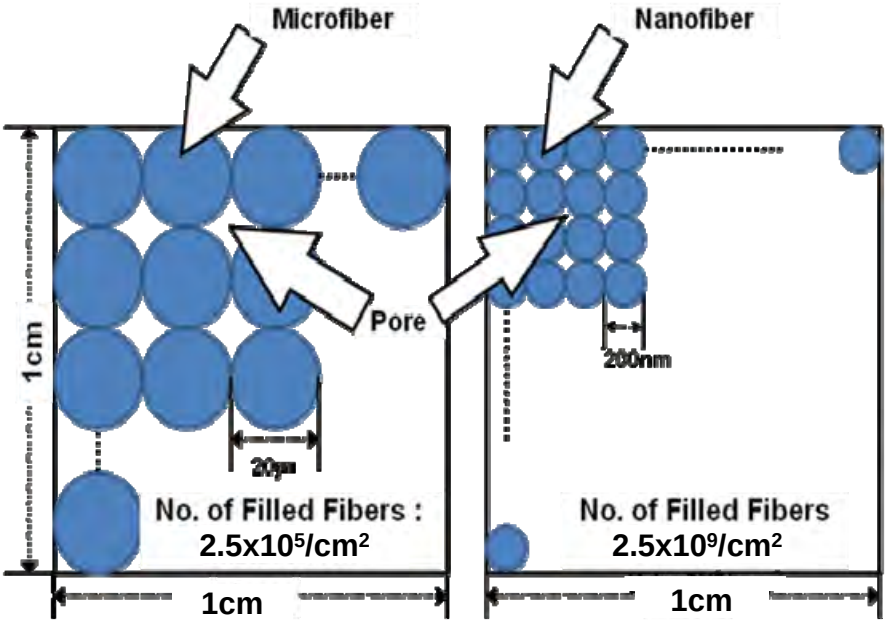

Figure 3. Fiber filling between microfiber and nanofiber per unit area.

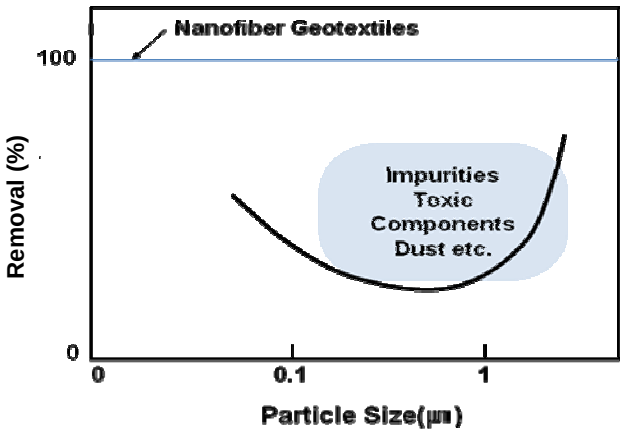

Figure 4. Effect of using a nanofiber geotextile filter.

Figure 5 shows the separation concept of a nanofiber air filter by pressure. To optimize such an air filter, a higher particle collection and dust retention rate should be required.

Therefore, hybrid type air filters must be the optimum and Figure 6 shows such fiber materials versus fiber length. For HMT (hybrid membrane technology) and expanded PTFE materials, nanofiber layers are accumulated above the general fiber materials as a hybrid material. This is the important result of larger specific adsorption area in the surface of geosynthetics.

Figure 7 shows the relationship between separation fields and separation membranes using fiber-related nanotechnology.

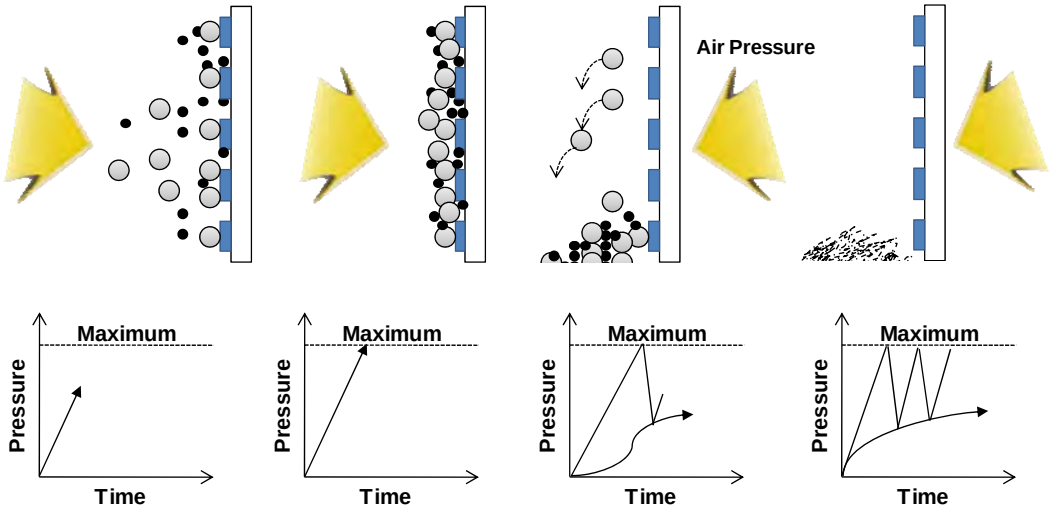

Figure 5. Maintenance of filtration efficiency for nanofiber filters.

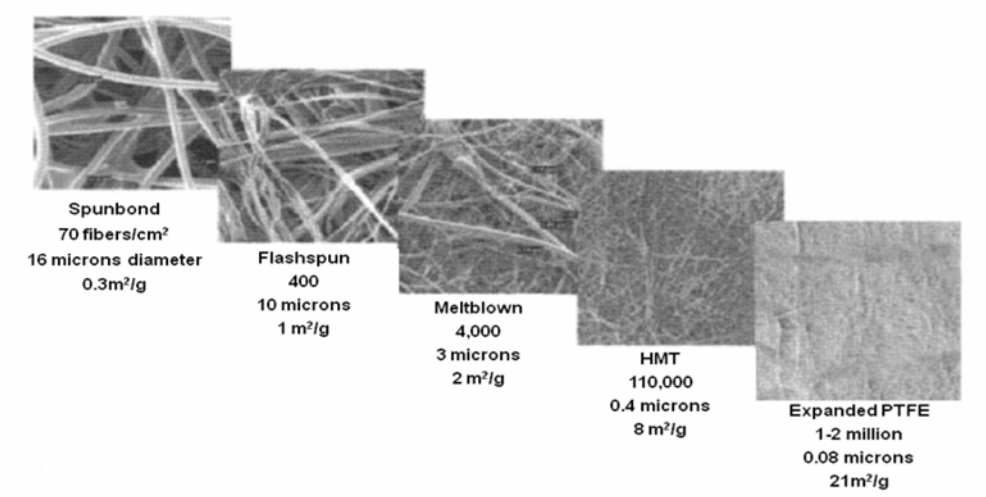

Figure 6. Comparison of fiber diameter and surface area using nanofiber and other fibers.

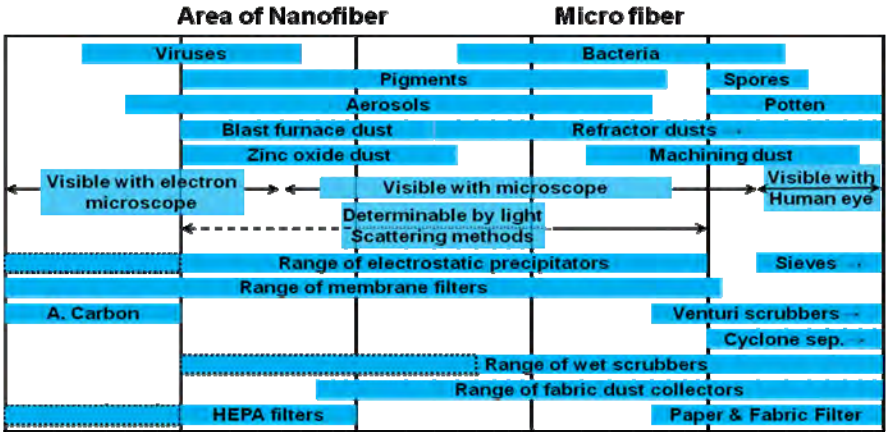

Figure 7. Relationship between separation fields and separation membranes using nanotechnology.

3. FROM NANOFIBERS TO (CLAY) NANOPARTICLES

3.1 Clay Nanoparticles

A related aspect of nanotechnology is to use one or more components of a formulation in the nano-scale so as to create a nanocomposite formulation. Having pellets made from such a formulation, standard manufacturing processes can be used to manufacture any type of geosynthetic material.

The addition of 2~3% yellow clay nanoparticles has been used to make a formulation so as to manufacture polyester geotextiles. Table 1 shows the specifications of the two types of geotextiles in this study; one with nanoclay (the FGT series) and one without (the GT series). The standard polyester geotextiles were used to compare the performance difference against those with the clay nanoparticle fromulation.

Table 1. Specifications two types of polyester geotextiles.

Geotextile Type \ Composition		Weight (g/m²)	Clay Content (%)
Nanoclay Formulated Nonwoven Geotextiles	FGT-1 FGT-2 FGT-3 FGT-4	272 463 784 1514	2~3%
Standard Nonwoven Geotextiles	GT-1 GT-2 GT-3 GT-4	284 480 756 1546	None

Table 2 shows the properties of the nanoclay added to the standard polyester resin formulation. From this it is known that the amount to be added is 2 to 3%.

Table 2. Components of the added yellow clay particles.

Component	Loss	SiO_2	Al_2O_3	Fe_2O_3	TiO_2	CaO	MgO	Na_2O	K_2O
Amount	97.54	1.80	0.07	0.11	0.13	0.01	0.01	0.02	0.01

3.2 Testing Protocols Used to Evaluate Engineering Performance

Tensile properties of nonwoven geotextiles were tested using ISO 10319 to minimize the deviation between index and performance tests.

The modified EPA 9090 Test Method that was proposed by United States Environment Protection Agency was adapted to test the chemical resistance of the geotextiles. The chemical resistance of nonwoven geotextiles in waste leachate solution was evaluated by comparing the strength retention before/after immersion at 25°C, 50°C, 80°C and 180 days using ASTM D 4632.

AATCC 30 was used to estimate the biological resistance in the waste landfill leachate. Similar to chemical resistance, the biological resistance of nonwoven geotextiles was evaluated by comparing the strength retention before/after immersion.

ASTM D4751-99a was used to compare the apparent opening size (AOS) and ASTM D1987-95(2002) was used to examine the permittivity of nonwoven geotextiles before/after immersion in the waste landfill leachate.

Finally, the adsorption efficiency was estimated to obtain the amounts of toxic and organic components that remained within the nonwoven geotextiles through ICP analysis. An actual field leachate was used from the waste landfill site in Gwangju, Korea (Rep.) where food wastes were mainly disposed of. It was seen that the pH value of the leachate solution indicated a weak alkaline state and toxic components, e.g., Cd and Pb, etc., and many kinds of organic components were included.

3.3 Tensile Property Behavior

Figure 8 shows the tensile strength of both the nanoclay formulation and standard nonwoven geotextiles. For the two types (i.e., FGTs and GTs), tensile strengths in the both directions (MD and CMD) increased with weight but tensile strains decreased with weight. This is a very common trend in tensile properties of nonwoven geotextiles.

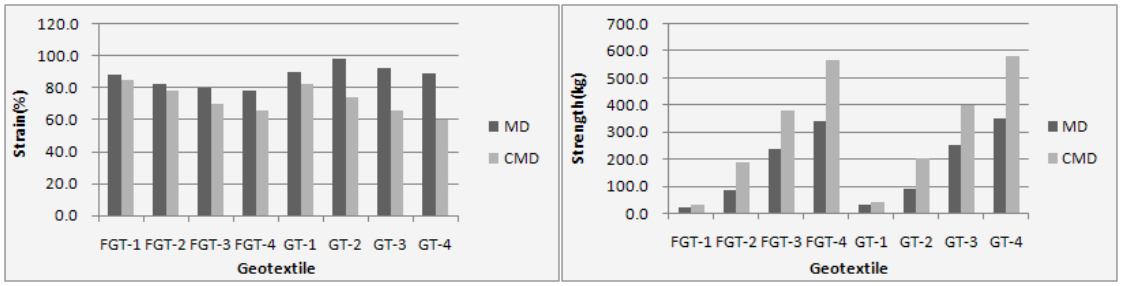

Figure 8. Tensile properties of nanoclay formulated and standard polyester nonwoven geotextiles. (Where MD, CMD mean the machine and cross machine directions, respectively)

3.4 Effects of Chemical and Biological Degradation

Figure 9 shows the tensile strength retention of both the nanoclay formulated and standard polyester nonwoven geotextiles before/after immersion in the leachate solution.

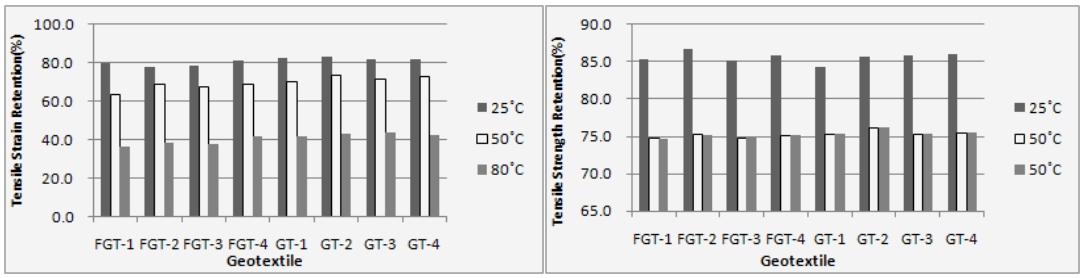

Figure 9. Chemical resistance by tensile property retention of nanoclay formulated and standard polyester nonwoven geotextiles.

Tensile strength and strain retention of both types of polyester nonwoven geotextiles (FGTs and GTs) show the same tendency and this value decreased with increasing temperature. This result is observed very clearly at 80°C and this is due to the hydrolysis effect of polyester under higher temperature and in the alkaline state. Tensile strength retentions of polyester nonwoven geotextiles between before/after immersion in the waste landfill leachate were examined. Figure 10 shows the tensile strength retention so as to explain the biological resistance.

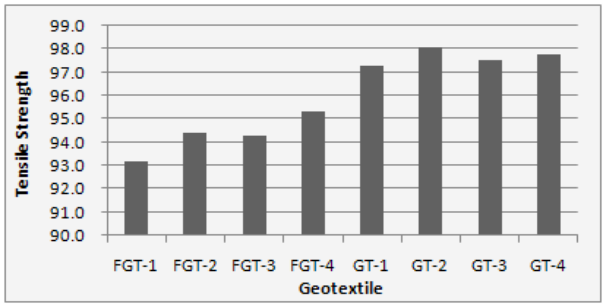

Figure 10. Biological resistance by tensile strength retention of nanoclay formulated and standard polyester nonwoven geotextiles.

The nanoclay formulated polyester nonwoven geotextiles (i.e., the FGTs) show lower tensile strength retention than the standard polyester nonwoven geotextiles (i.e., GTs). It is assumed that this means that the FGTs were influenced by the components of the leachate solutions in a greater or less amount because of the nanoclay component. But this does not mean that fungi and bacteria can attack these geotextiles. Figure 11 shows the values of cumulative reduction factors and the allowable tensile strengths of all of these nonwoven geotextiles.

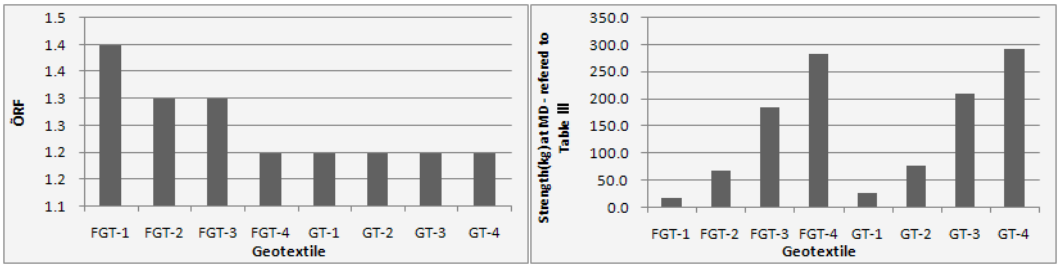

Figure 11. Allowable tensile strength of nanoclay formulated and standard polyester nonwoven geotextiles.

3.5 Hydraulic Properties Due to Clogging Effects

Clogging in nonwoven geotextiles means the tendency to decrease water permeability due to soil particles that have either lodged in the geotextile openings (i.e., lower AOS) or have built up a restrictive layer on the surface of geotextiles. In general, AOS does not decrease if clogging has not occurred within the nonwoven geotextile.

Figure 12 shows AOS values of both types of polyester nonwoven geotextiles before/after burial in the waste landfill site. The nanoclay formulated polyester nonwoven geotextiles (the FGTs) have smaller AOS values than

the typical polyester nonwoven geotextiles and this means more significant clogging occurrence for the FGTs. Therefore, toxic, organic and some floating components in the leachate solution can be easily adsorbed to the nanoclay added polyester fiber surface. After burial, the AOS values of the FGTs decreased due to the increase of adsorption components but some of them were eliminated by a simple washing the nonwoven geotextiles.

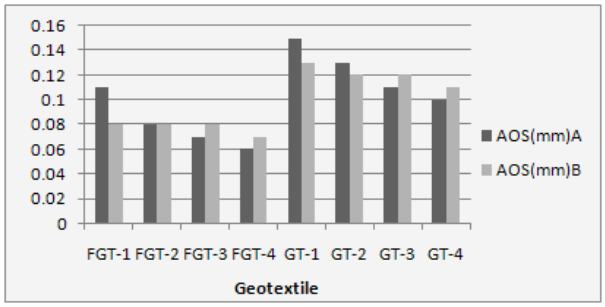

Figure 12. AOS of nanoclay formulated and standard polyester nonwoven geotextiles before/after immersion. (Where A, B mean before and after immersion, respectively)

Figure 13 shows the permittivities of the two types of polyester nonwoven geotextiles before/after immersion in the waste landfill site. As shown in the biological resistance and AOS, permittivities of the nanoclay added polyester nonwoven geotextiles, the FGTs, were smaller than those of the typical polyester nonwoven geotextiles due to the clogging effects of FGTs.

Figure 14 shows the strength retention of the polyester nonwoven geotextiles before/after clogging and the same tendency as considered was observed. The nanoclay formulated polyester nonwoven geotextiles (the FGTs) show smaller tensile strength retention than the typical polyester nonwoven geotextiles (the GTs).

Figure 15 shows the values of cumulative reduction factors and the allowable permittivity of all of these nonwoven geotextiles.

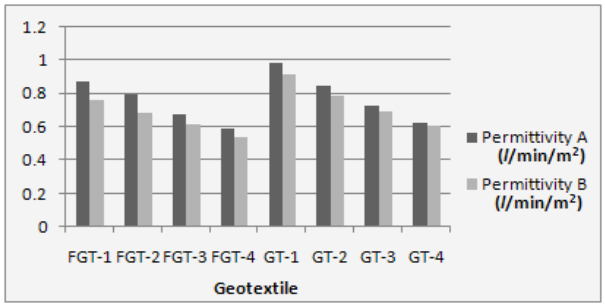

Figure 13. Permittivity of nanoclay formulated and standard polyester nonwoven geotextiles before/after immersion. (Where A, B mean before and after immersion, respectively)

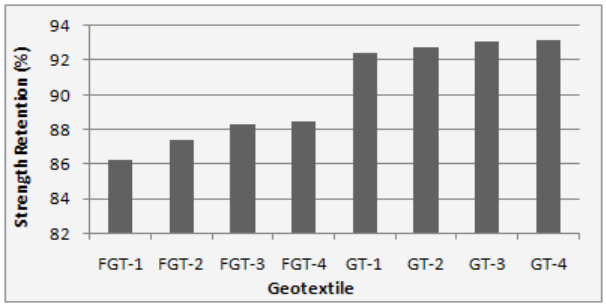

Figure 14. Strength retention of nanoclay formulated and standard polyester nonwoven geotextiles after clogging.

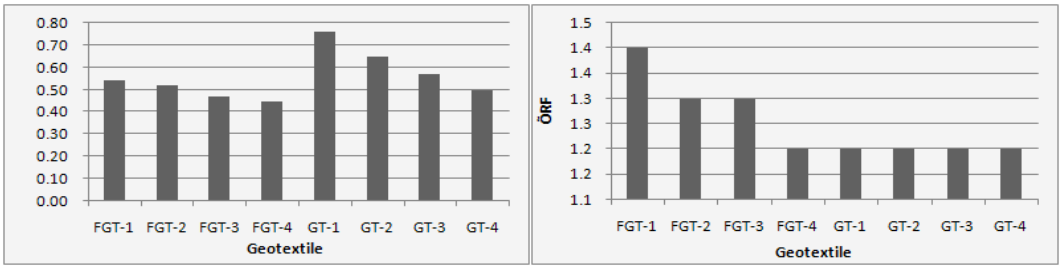

Figure 15. Allowable permittivity of nanoclay formulated and standard polyester nonwoven geotextiles after clogging.

3.6 Adsorption Efficiency

Figure 16 shows the adsorption efficiency of toxic and organic components by both of the polyester nonwoven geotextiles. This value was obtained as the percentage through ICP analysis and nanoclay added polyester nonwoven geotextiles. The FGTs showed excellent adsorption efficiency compared with the standard polyester nonwoven geotextiles (the GTs).

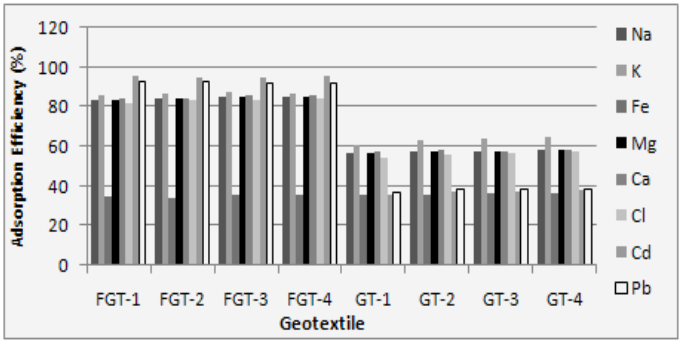

Figure 16. Component adsorption of nanoclay formulated and standard polyester nonwoven geotextiles.

Finally, further study must be continued to generate a detailed, clear and quantitative adsorption effect with various nonwoven geotextiles which have the different fiber composition.

4. FUTURE OF NANOTECHNOLOGY APPLICATIONS IN GEOENVIRONMENTAL ENGINEERING

The following was suggested Dr. Ian D. Peggs in his article, “The Future of Geosynthetics – One Opinion” regarding the manufacturing capabilities for use by the geosynthetics community.

- Nanoclays and nanofibers already exist for use in the geosynthetics technology
- Carbon and graphite are also related to geosynthetics in that they can be generated from polymers

- Geomembrane manufacturers have three layer extruders and a few have five layer extruders suited for the technology
- Multilayer extruded barrier products are not new, so there exists a technology base
- Geogrids can be made stronger
- Geonets can be made less compressible
- Geocells can be made more rigid
- Stress cracking and oxidation resistances can be increased
- New materials will be involved bringing new participants and new applications to the industry
- Five layer geomembranes offer a better opportunity to customize colors (for example) for owners and for better awareness
- Color coding can also be related to performance characteristics
- Color can be marketed – it was done successfully in HDPE gas pipe and PVC water pipe
- The technology presents an opportunity to make a significant step (not just a small one) towards more specialty products that will be accepted and utilized accordingly

Though the above represents a suggestion and recommendation of one geosynthetic expert for nanotechnology geosynthetics in geoenvironmental engineering, it is very important to extend and set up this new application field for advanced geosynthetics. To develop the typical performance of regular geosynthetics, it is very natural and necessary to manufacture nanoparticle formulations and nanofiber geosynthetics as advanced materials and search/extend the new applications to the geoenvironmental engineering fields in the near future.

REFERENCES

1. Koerner, R. M. (2005), *Designing with Geosynthetics* (5th edition), Pearson Prentice Hall, Inc., Upper Saddle River, New Jersey, USA, pp.1-75.
2. Jewell, R. A. (1996), *Soil Reinforcement with Geotextiles*, CIRLA Special Publication, Thomas Telford, Westminster, Chapter 5.
3. Gugumus, F. (1996), Polymer Degradation and Stability, 52, pp.131-159.
4. Holtz, R. D., Christopher B. R. and Berg R. R. (1995), *Geosynthetic Design and Construction Guidelines*, Publication No. FHWA HI-95-038, pp.27-105.
5. Peggs, I. D. (2008), "*The Future of Geosynthetics – One Opinion*", http://www.geosynthetics.net
6. Jeon, H.-Y. et al. (2008), "*Evaluation of Clay Added Nonwovens as Filter in Waste Landfill*", Molecular Crystals and Liquid Crystals, 484, pp185~194.

It's in the Details; Specification Issues

P. E. Oliveira, Firestone Speciality Products, Indianapolis, Indiana, USA

ABSTRACT
It all starts with the specification and request for a proposal providing enough detail to allow for the proper material and system to be bid, to successfully accomplish the intended job. Below is just one example of an RFP/Specification, which makes my point, it all starts with the details. How could anyone really know what is required of the liner for this project? Clarity and specifics are needed to eliminate the misuse and improper material selection for any project. On this one, it appears that anything will work, at least according to the spec writer. I don't think so!

In this presentation, I will describe the details that are needed to give your customers and associates what they need to result in a successful project.

To start this thought process of concentrating on the details, let's look at the example just mentioned.

(*Italicized text in quotation marks was *taken verbatim from an RFP/specification written in 2008, including typos and omissions.)

"Section 1.1 Design Components
Liner Considerations

1. *Liner type, liner thickness and underliner/overliner protection should be based on:*
    - *Puncture protection(includes prevention of slippage from cover fill placement and harvesting equipment)*
    - *Overall cost to construct for operations*
    - *Potential subgrade movement*

2. *For general equivalent liner performance, 60 mil minimum is suggested for HDPE and LLDPE and 45 mil minimum for PP , PVC and EPDM liners.*
3. *With the aggressive 1H;1V side slope, the more flexible liners should have scrim reinforcement to hold temporarily until covered by the salt deposits.*
4. *Black liner is preferred on the sides for added heat as wind blows air across the pond systems. The bottom liner color does not matter since it is buried.*
5. *Omitted*
6. *Surface texturing may offer an advantage if slippage resulting from harvesting equipment is expected.*
7. *The use of a geotextile layer is discouraged due to the potential of increased slippage.*
8. *Liner roll/panel size, manufacturer integrity, seam integrity*
9. *Compatibility with salt solutions and resistance to UV radiation*
10. *Minimum warrantee of 5 years"*

" 4.0 GEOMEMBRANE LINER MATERIAL
4.1 General
The Contractor shall supply and install geomembrane liner materials and miscellaneous materials incident thereto in accordance with the manufacturer's recommendations. Exact locations and lengths may vary to suit conditions encountered in the field, as approved by the Owner. Technical specifications for the selected geomembrane liner shall meet minimum accepted industry standards. The Contractor shall propose a liner system that meets the Owners objectives and may include any of the major liner types (HDPE, LLDPE, PP, PVC and EPDM). Liners shall conform to Geosynthetic Research Institute (GRI) standards. (GM-13 for HDPE, GM-17 for LLDPE and GM-18 for PP (with OIT testing pending), and GM-21 for EPDM) and Geomembrane Institute (PGI) for PVC.
Test methods for synthetic materials shall conform to ASTM and ISO, with GRI and PGI test methods acceptable where ASTM and ISO standards are not yet available."

In addition to the above, when a specification is written, care should be taken that testing procedures are current and are specific to the materials that have been approved and recommended by the spec writer or engineer of record. Obsolete or discontinued specifications and procedures must not be included in specifications.

(An example of this is the following italicized text which appeared in a late 2007 specification for an EPDM liner:)

"1.2 References
C. National Sanitation Foundation (NSF)
1. NSF-54 Flexible Membrane Liners (FML)"

In the above referenced NSF-54 specification (which was discontinued in 1995 and this specification was referenced in 2007) were ASTM plastic film testing requirements and physical property test values, which are simply not applicable to an elastomeric geomembrane. While this seems picky, it is a detail that the professional specification writer must be aware of to eliminate confusion and provide his/her customer a proper specification. Quite often, we see a "cut and paste" table of physicals properties that have incorporated all of the liner types mentioned earlier. ~~D~~rawing a comparison on various polymer types of geomembranes via the physical property numerical values is nearly impossible. How do you compare the grab tensile values of a scrim reinforced product with that of a dumbbell test of an unsupported elastomeric or thermoplastic?

Issues like the inclusion of a carbon black percentage being required in a black loaded geomembrane and or as a requirement on a polymer grade that relies on other forms of stabilization chemistry to accomplish its ability to weathering are just some examples of the lack of education by a specification writer.

In today's atmosphere of multiple product offerings, it is important that those responsible for the material selection and inclusion into the geomembrane specifications be informed regarding the differences of similar polymeric geomembrane construction and manufacturing. The assumption that all products are equal must be challenged and verification of their compliance, to well developed industry standards, is a detail that should not be over looked.

Once established with a specification that is meaningful, concise, and provides the necessary details to manufacture the geomembrane, including the plan drawings, sheet layout and installation details, we can take that specification and move forward.

We all know that this the ability to take that a very detailed plan of attack, called a specification, and convert it into a finished product is sometimes full of good intentions more difficult than it seems. Good intentions are not enough. Research is necessary. Let's look at some "good intentions" or some, of shall I say, "they tried and will be back because they did not pay enough attention to the DETAILS"!

In this presentation I hope that I have stimulated specification writers to do a better job of research and investigation before beginning to develop specific project specification. For those who have to make it real, everyone will be judged by the ability to deal with the details!